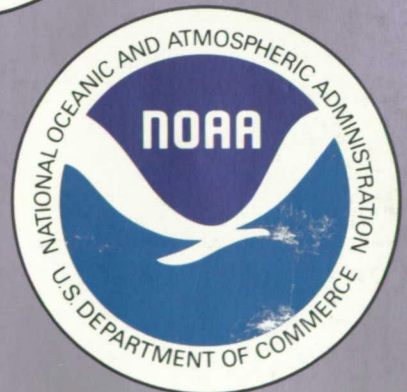


Scientific Assessment of Stratospheric Ozone: 1989

Volume I



(NASA-TM-105442) SCIENTIFIC ASSESSMENT OF
STRATOSPHERIC OZONE: 1989, VOLUME 1 (NASA)
494 p CSCL 13B

N92-15430
--THRU--
N92-15434
Unclass
0053030

548 ps

509303

G3/45

NATIONAL AERONAUTICS AND SPACE ADMINISTRATION
UNITED KINGDOM - DEPARTMENT OF THE ENVIRONMENT
NATIONAL OCEANIC AND ATMOSPHERIC ADMINISTRATION
UNITED NATIONS ENVIRONMENT PROGRAM
WORLD METEOROLOGICAL ORGANIZATION

United Nations Environment Program
United Nations Headquarters
Gigiri
Nairobi, Kenya

World Meteorological Organization
41, Avenue Giuseppe Motta
Case Postale No. 5
CH-1211, Geneva 20, Switzerland

National Aeronautics and Space Administration
Office of Space Science and Applications
Earth Science and Applications Division
600 Independence Avenue, SW
Washington, DC 20546
USA

U.S. Department of Commerce
National Oceanic and Atmospheric Administration
14th Street and Constitution Avenue, NW
Hoover Building, Room 5128
Washington, DC 20230
USA

United Kingdom Department of the Environment
43 Marsham Street
London, SW1P 3PY
United Kingdom

ISBN 92 807 1255 1

WORLD METEOROLOGICAL ORGANIZATION
GLOBAL OZONE RESEARCH AND MONITORING PROJECT – REPORT NO. 20

Scientific Assessment of Stratospheric Ozone: 1989

Volume I

ORIGINAL CONTAINS
COLOR ILLUSTRATIONS

NATIONAL AERONAUTICS AND SPACE ADMINISTRATION
UNITED KINGDOM - DEPARTMENT OF THE ENVIRONMENT
NATIONAL OCEANIC AND ATMOSPHERIC ADMINISTRATION
UNITED NATIONS ENVIRONMENT PROGRAM
WORLD METEOROLOGICAL ORGANIZATION

TABLE OF CONTENTS

	Page
PREFACE	iii
 INTRODUCTION, EXECUTIVE SUMMARY, AND SCIENTIFIC SUMMARIES	
I. INTRODUCTION	v
Background	v
Scientific Scope	v
Relation to Public Policy	vi
II. EXECUTIVE SUMMARY	vii
Recent Findings	vii
Supporting Evidence and Other Results	vii
Implications	xiii
III. SCIENTIFIC SUMMARIES	xv
Chapter 1. Polar Ozone	xv
Chapter 2. Global Trends	xix
Chapter 3. Model Predictions	xxv
Chapter 4. Halocarbon Ozone Depletion and Global Warming Potentials	xxviii
 CHAPTER 1. POLAR OZONE	
1.0 INTRODUCTION	1
1.1 CLIMATOLOGY OF THE OZONE TRENDS IN POLAR REGIONS	1
1.2 CLIMATOLOGY OF POLAR STRATOSPHERIC CLOUDS (PSCs) IN BOTH POLAR REGIONS	23
1.3 PHYSICAL PROPERTIES OF PSCs	38
1.4 HETEROGENEOUS CHEMISTRY	43
1.5 GAS PHASE CHEMISTRY	45
1.6 PHOTOCHEMISTRY OF THE ANTARCTIC SPRING	54
1.7 DYNAMICAL PROCESSES	82
1.8 TEMPERATURE TRENDS—CAUSES AND EFFECTS	115
1.9 CALCULATED AND OBSERVED CHANGES IN ULTRAVIOLET RADIATION AT THE GROUND	127
1.10 ARCTIC PHOTOCHEMISTRY	129

	Page
1.11 CONCLUSIONS AND OUTSTANDING ISSUES	142
REFERENCES	145
 CHAPTER 2. GLOBAL TRENDS	
2.0 INTRODUCTION	163
2.1 OBSERVATIONAL METHODS RELEVANT TO TREND DETECTION	163
2.2 TRENDS IN TOTAL OZONE	194
2.3 TRENDS IN VERTICAL OZONE DISTRIBUTION	219
2.4 TRENDS IN STRATOSPHERIC TEMPERATURES	235
2.5 TRENDS IN TROPOSPHERIC GASES AND OZONE	244
2.6 TRENDS IN STRATOSPHERIC AEROSOLS	261
2.7 SURFACE ULTRAVIOLET RADIATION	263
2.8 OUTSTANDING ISSUES	267
APPENDIX: TRENDS MODELS	268
REFERENCES	271
 CHAPTER 3. THEORETICAL PREDICTIONS	
3.1 MODEL FORMULATION AND RELIABILITY	283
3.2 MODEL PREDICTIONS	317
REFERENCES	395
 CHAPTER 4. HALOCARBON OZONE DEPLETION AND GLOBAL WARMING POTENTIALS	
4.1 INTRODUCTION	401
4.2 HALOCARBON OXIDATION IN THE ATMOSPHERE	401
4.3 OZONE DEPLETION POTENTIALS	424
4.4 HALOCARBON GLOBAL WARMING POTENTIALS	451
REFERENCES	462
APPENDIX A: CONTRIBUTORS AND REVIEWERS	467
APPENDIX B: FIGURES AND TABLES	473

PREFACE

The 1987 Montreal Protocol on Substances that Deplete the Ozone Layer called for convening four assessment panels. This document (Volume I) is the complete report of one of these panels (the Scientific Assessment Panel) convened under the Protocol's review provisions. In the Introduction to this report will be found details concerning the Montreal Protocol assessment and review procedures. This Introduction also contains overviews of the four chapters that comprise this assessment. Chapter 4 on halocarbon ozone depletion and global warming potentials has benefitted extensively from the scientific material and conclusions drawn from the Alternative Fluorocarbon Environmental Acceptability Study (AFEAS).

This latter study was conducted as an international exercise that involved more than 50 scientists during the early part of 1989. The AFEAS was organized and sponsored by fifteen CFC-producing companies from around the world as part of a cooperative effort to study the safety and environmental acceptability of CFC alternatives. Because of the parallelism between the AFEAS study and the analyses performed under Chapter 4, the complete set of research papers prepared under AFEAS has been assembled and is published as the AFEAS Report, an appendix to this scientific assessment. This appendix constitutes Volume II of the World Meteorological Organization Report No. 20.

INTRODUCTION

EXECUTIVE SUMMARY

SCIENTIFIC SUMMARIES

Assessment Co-Chairs

Daniel L. Albritton (USA) • Robert T. Watson (USA)

Chapter Coordinators

Chapter 1. Susan Solomon (USA) Chapter 3. Guy Brasseur (Belgium)
Chapter 2. Gerard Mégie (France) Chapter 4. R.A. Cox (UK) and
Donald J. Wuebbles (USA)

Contributors and Reviewers

J. G. Anderson (USA)
J. K. Angell (USA)
F. Arnold (FRG)
R. Atkinson (Australia)
G. Betteridge (New Zealand)
R. D. Bojkov (Switzerland)
G. Brasseur (Belgium)
J. P. Burrows (FRG)
D. Cariolle (France)
B. Carli (Italy)
G. D. Cartwright (USA)
M.-L. Chanin (France)
A. Charnikov (USSR)
S. Chubachi (Japan)
T. S. Clarkson (New Zealand)
R. A. Cox (UK)
D. Ehhalt (FRG)
D. W. Fahey (USA)
J. C. Farman (UK)
G. Fiocco (Italy)
D. Fisher (USA)
P. J. Fraser (Australia)
J. F. Frederick (USA)
A. Ghazi (Belgium)
J. C. Gille (USA)
L. Gray (UK)
W. J. Hill (USA)
M. Hitchman (USA)
J. S. Hoffman (USA)
A. M. A. Ibrahim (Egypt)
M. Illyas (Malaysia)
Y. Iwasaka (Japan)
P. Johnston (New Zealand)
P. S. Jovanovic (Yugoslavia)
J. B. Kerr (Canada)
J. G. Keys (New Zealand)
V. Khattatov (USSR)
V. Kirchhoff (Brazil)
D. Kley (FRG)
M. J. Kurylo (USA)
Y.-P. Lee (Taiwan)
C. Mateer (Canada)
T. Matsuno (Japan)
W. A. Matthews (New Zealand)
M. P. McCormick (USA)
M. McFarland (USA)
R. McKenzie (New Zealand)
G. Mégie (France)
A. P. Mitra (India)
M. Molina (USA)
J. Moyers (USA)
A. O'Neill (UK)
A. Owino (Kenya)
S. A. Penkett (UK)
L. P. Prahm (Denmark)
M. Prather (USA)
M. Predez (Chile)
M. Proffitt (USA)
J. Pyle (UK)
L. X. Qui (PRC)
V. Ramaswamy (USA)
J. M. Rodriguez (USA)
F. S. Rowland (USA)
J. M. Russell (USA)
Y. Sansano (Japan)
P. C. Simon (Belgium)
S. Solomon (USA)
R. Stolarski (USA)
B. H. Subbaraya (India)
J. Swager (Netherlands)
A. F. Tuck (USA)
P. Usher (Kenya)
D. W. Wei (PRC)
D. Wuebbles (USA)
R. Zellner (FRG)
C. S. Zerefos (Greece)

INTRODUCTION, EXECUTIVE SUMMARY AND SUMMARIES

TABLE OF CONTENTS

I. INTRODUCTION	iii
Background	
Scientific Scope	
Relation to Public Policy	
II. EXECUTIVE SUMMARY	vii
III. SCIENTIFIC SUMMARIES	
CHAPTER 1. Polar Ozone	xv
Polar Ozone Trends	
Polar Stratospheric Chemistry	
Field Observations	
Dynamics	
Future of Polar Ozone	
CHAPTER 2. Global Trends	xix
Introduction	
Trends in Total Ozone	
Trends in Ozone Vertical Distribution	
Trends in Stratospheric Temperature	
Trends in Tropospheric Source Gases and Ozone	
Trends in Stratospheric Aerosols	
Trends in Surface UV Radiation	
CHAPTER 3. Model Predictions	xxv
Stratospheric Models	
Important Issues in Ozone Modeling	
Scenarios for Atmospheric Composition	
Changes in Ultraviolet Radiation at the Surface	
CHAPTER 4. Halocarbon Ozone Depletion and Global Warming Potentials	xxviii
Halocarbon Oxidation of the Atmosphere	
Ozone Depletion Potentials	
Halocarbon Global Warming Potentials	

I. INTRODUCTION

The present document, *Scientific Assessment of Stratospheric Ozone: 1989*, is a scientific review of the current understanding of stratospheric ozone, prepared by international scientific experts who are leaders in their respective fields. This initial chapter is a summary of its major points.

The aims of this summary section are threefold. The Executive Summary (Section II) is a digest of the key points of the *Assessment* and is directed at government officials, the private sector, and the general public. The Scientific Summaries (Section III) of each of the four chapters contain the major research findings of the *Assessment* and are directed to the scientific community.

In the Appendix, which is found at the end of the report, the numerous contributors to the preparation of the *Assessment* are identified. The success of the *Assessment* rests on the prodigious efforts and dedication of these people.

This introductory section briefly gives the background to the *Assessment*, its scientific scope, and its place in the current discussions of public policies regarding the protection of the stratospheric ozone layer.

Background

The goals, scope, contents, authors, and timetable of the *Assessment* were planned at two international meetings:

- The first was part of a two-day meeting, "Scientific Review of Ozone Layer Modification and its Impact," which was held at The Hague, The Netherlands, 17-18 October 1988. There were about 70 international scientific attendees at this first of a series of meetings sponsored by the United Nations Environment Programme (UNEP). About half of these attendees were involved in the subgroup that focused on defining the scope of the *Assessment* and establishing a scientific steering group (see Section IV for the membership).
- The second meeting occurred on 29 November 1988 at the U.K. Department of the Environment in London. Fourteen scientists attended, coming from eight countries, as well as representation from UNEP and the World Meteorological Organization (WMO). The focus of this Steering Committee was on establishing the structure, authors, and timetable of the *Assessment*.

The preparation of the *Assessment* document occurred over the period from January to June, 1989. Numerous scientists from 25 countries were involved either as authors, contributors, or reviewers (see Appendix). Their professional institutions included universities, government laboratories, and the private sector. A review draft was discussed and evaluated at a review meeting at Les Diablerets, Switzerland on 10-14 July 1989, sponsored by WMO. Forty-three scientists from 14 countries were in attendance and many others participated via mail reviews. Those suggestions and comments have been incorporated into the present final version.

Scientific Scope

The focus of the *Assessment* is on four major current aspects of stratospheric ozone: (1) polar ozone, (2) global trends, (3) theoretical predictions, and (4) halocarbon ozone depleting potentials and global warming potentials. Other ozone-related topics are also included: (i) the trends of stratospheric temperature, stratospheric aerosols, source gases, and surface ultraviolet radiation; and (ii) the oxidizing capacity of the

EXECUTIVE SUMMARY

troposphere as it pertains to the lifetimes of ozone-related chemicals (e.g., the partially halogenated compounds that can serve as shorter-lived substitutes for the long-lived, fully halogenated ozone-depleting gases).

The *Assessment* is an update of the comprehensive "Atmospheric Ozone: 1985" (WMO Report No. 16, 1986) and builds upon the recent "International Ozone Trends Panel Report: 1988" (WMO Report No. 18, in press). It focuses on the results of subsequent recent research and the implications for the stratosphere. The ozone research of the past few years has been remarkable. Several major ground-based and airborne field campaigns have explored the recently discovered Antarctic ozone "hole," as well as the Arctic ozone layer. New laboratory studies of gas-phase and surface-induced chemical processes have provided a better characterization of the polar phenomena. Statistical analyses of hemispheric data sets have revealed significant ozone trends for the first time. Theoretical investigations have aided the interpretation of all these findings. The picture contained in the *Assessment* reveals a new and deeper understanding of the influence of human activities on the Earth's protective ozone layer.

Relation to Public Policy

While the *Assessment* is a scientific document, it also will be useful as essential scientific input to policy decisions regarding the safeguarding of the ozone layer, just as were its predecessor documents (e.g., "Atmospheric Ozone: 1985"). In that regard, one of the most noteworthy applications of the *Assessment* will be the forthcoming international review of the Montreal Protocol on Substances that Deplete the Ozone Layer. Indeed, the above timetable was planned such that the international ozone scientific community can provide that service in the form of the *Assessment*. The Executive Summary of the present document has been written with this need to communicate the state of ozone in mind.

At the meeting in October 1988 at The Hague, UNEP established four panels to review the current scientific, environmental, technical, and economic information relative to possible amendments to the Montreal Protocol. The *Scientific Assessment of Stratospheric Ozone: 1989* is the report of the first of these panels. There are corresponding reports from the three other panels. The main findings of all four reports will be presented to a Working Group meeting in Nairobi, Kenya, on 28 August – 5 September 1989, where the reports will be reviewed. Their integration into a single document will be completed, and the resultant integrated report will serve as key input for considerations of possible draft amendments to the Montreal Protocol.

II. EXECUTIVE SUMMARY

Recent Findings

The past few years have been remarkable insofar as stratospheric ozone science is concerned. There have been highly significant advances in the understanding of the impact of human activities on the Earth's protective ozone layer. Since the last international scientific review (1985), there are four major findings that each heighten the concern that chlorine- and bromine-containing chemicals can lead to a significant depletion of stratospheric ozone:

- **Antarctic Ozone Hole:** The weight of scientific evidence strongly indicates that chlorinated (largely man-made) and brominated chemicals are primarily responsible for the recently discovered substantial decreases of stratospheric ozone over Antarctica in springtime.
- **Perturbed Arctic Chemistry:** While at present there is no ozone loss over the Arctic comparable to that over the Antarctic, the same potentially ozone-destroying processes have been identified in the Arctic stratosphere. The degree of any future ozone depletion will likely depend on the particular meteorology of each Arctic winter and future atmospheric levels of chlorine and bromine.
- **Long-Term Ozone Decreases:** The analysis of the total-column ozone data from ground-based Dobson instruments show measurable downward trends from 1969 to 1988 of 3 to 5% (i.e., 1.8–2.7% per decade) in the Northern Hemisphere (30–64°N latitudes) in the winter months that cannot be attributed to known natural processes.
- **Model Limitations:** These findings have led to the recognition of major gaps in theoretical models used for assessment studies. Assessment models do not simulate adequately polar stratospheric cloud (PSC) chemistry or polar meteorology. The impact of these shortcomings for the prediction of ozone depletion at lower latitudes is uncertain.

Supporting Evidence and Other Results

These and other findings are based upon the results from several major ground-based and aircraft field campaigns in the polar regions, a reanalysis of ground-based ozone data from the past thirty-one years, a reanalysis of satellite ozone and PSC data, laboratory studies of gas-phase and surface-induced chemical processes, and model simulations incorporating these new laboratory data and observations. The highlights and conclusions from these activities in four research areas are summarized below.

Polar Ozone

- *There has been a large, rapid, and unexpected decrease in the abundance of springtime Antarctic ozone over the last decade.*

Beginning in the late 1970s, total column ozone decreases (lately reaching 50%) have been observed by both ground-based and satellite techniques, the latter showing that the loss is a continental-scale phenomenon. Ozonesondes at several stations have shown that the ozone loss occurs between 12 and 24 km, reaching as much as 95% at some altitudes.

- *The weight of scientific evidence strongly indicates that man-made chlorine and bromine compounds are primarily responsible for the ozone loss in Antarctica.*

EXECUTIVE SUMMARY

The ozone loss over Antarctica is initiated by chemical reactions that occur on the surfaces of PSCs and that convert the long-lived chlorine into chemically more reactive forms. Laboratory studies have provided important evidence that such chemical reactions can occur on PSC surfaces. Furthermore, reactions can also remove reactive nitrogen species, thereby slowing the reformation of the less reactive chlorine compounds. Satellite data show that the frequency of occurrence of PSCs is the highest in the Antarctic stratosphere. Indeed, the abundance of the reactive chlorine compounds is observed to be elevated by 50–100 times in springtime. The observed reactive chlorine and bromine abundances explain a substantial fraction (60–100%) of the rapid ozone loss observed following the return of sunlight to Antarctica in September, 1987.

- *While the onset of the Antarctic ozone hole is linked to the recent growth in the atmospheric abundance of chlorofluorocarbons (CFCs) and to a lesser extent bromine compounds, many of its features are influenced by meteorological conditions.*

Within the strong circumpolar vortex over Antarctica, temperatures are very low during the winter and spring and there is abundant production of PSCs. These special meteorological conditions set the stage for the occurrence of the ozone hole.

The year-by-year variability in the depth of the ozone hole appears to be related, in part, to the Quasi-Biennial Oscillation (QBO), which is a natural oscillation of equatorial stratospheric winds. For example, there was a very deep ozone hole in 1987, but it was substantially less deep in 1988, possibly influenced by the observed temperature extremes between the years, which modulated the abundance of PSCs. Tropospheric weather systems can also influence stratospheric temperatures and water vapor on regional scales, which would in turn influence PSC abundance and ozone changes.

- *The chemical composition of the Arctic stratosphere was found to be highly perturbed.*

The chemical perturbations in the Arctic were similar to those found in Antarctica, namely, an increase in the abundance of the ozone depleting forms of chlorine in association with PSCs. The studies conducted in January and February in 1989 found that the reactive chlorine abundances were enhanced by a factor of 50–100. No unambiguous evidence for ozone loss has yet been identified for the winter of 1988/1989. Readily detectable ozone reductions would be expected during January and February only if high concentrations of reactive chlorine species were maintained for sufficiently long periods in cold, illuminated air. The degree of Arctic ozone depletion will be influenced by the year-by-year timing of the warming of the polar vortex relative to the arrival of sunlight, as well as future chlorine and bromine abundances. In the Antarctic, the warming of the polar vortex always occurs after the arrival of sunlight (hence, ozone depletion), which contrasts with the Arctic, where warming generally occurs prior to the arrival of sunlight, as in 1989.

Global Trends

- *Several recent analyses of total column ozone data support the conclusion of the 1988 International Ozone Trends Panel (OTP) that there is a downward trend in ozone during winter at mid-to-high latitudes in the Northern Hemisphere over the past two decades.*

The OTP analyzed the re-evaluated data from the ground-based Dobson instruments for the effects of known natural geophysical processes (seasonal variability, the approximately 28-month QBO, and the 11-year solar cycle) and possible human perturbations. After allowing for natural

variability, the analysis showed measurable decreases in the range of 2.3 to 6.2% between 30 and 64°N latitude for the winter months (December - March) between 1969 and 1986, with the larger decreases being at the higher latitudes. This was the first analysis that showed statistically significant downward trends.

The results of model calculations of chlorine-induced ozone loss are broadly consistent with these observed latitudinal and seasonal changes in column ozone, except that the mean values of the observed decreases at mid- and high latitudes in winter are a factor of two to three larger than the mean values of the predicted decreases. This finding suggested that the observed ozone changes may be due, in part, to the increased atmospheric abundances of the CFCs.

Subsequent to the OTP, the results from five new reanalyses of the same OTP data set by three independent analyses, using a variety of statistical models and assumptions, were generally consistent with the earlier result. Zonal mean ozone decreases derived for winter lie in the range 3.2–4.0% over 17 years, when averaged over the latitudes 30–64°N, compared to the value of 4.4% from the OTP analysis. The conclusions were found to be insensitive to the representations used for the QBO and solar cycle, strengthening the belief that the observed trends cannot be attributed to known natural processes.

The extension of the data set beyond that used by the OTP to include 1987 and 1988 does not alter the basic conclusions regarding trends in winter. In addition, no statistically significant zonal trends were found for the summer period (May–August) through 1988. Lastly, within longitudinal sectors, regional differences in the ozone trends were indicated in the Northern Hemisphere, i.e., with the largest changes being observed over North America and Europe and the smallest over Japan.

The present Dobson network and data are inadequate to determine total column ozone changes in the Arctic, tropics, subtropics, or Southern Hemisphere outside of Antarctica. Satellite data can provide the desired global coverage, but the current record is too short to differentiate the effects of natural and human-influenced processes on ozone.

- *Substantial uncertainties remain in defining changes in the vertical distribution of ozone.*

Since the chlorine/ozone theory had predicted that the greatest percentage ozone depletion should occur near 40 km altitude, the OTP looked for indications of such changes in a variety of reanalyzed data sets. The Panel reported that, based on the SAGE satellite data averaged over 20–50°N and S latitudes, ozone near 40 km had decreased by $3 \pm 2\%$ between February 1979–November 1981 and October 1984–September 1987. The SAGE data also indicated a percentage decrease in ozone near 25 km that is comparable in magnitude to that at 40 km. Furthermore, the Panel reported that, based on the Umkehr data from five northern mid-latitude stations, the ozone between 38 and 43 km had decreased by $9 \pm 4\%$ between 1979 and 1986, but this uncertainty range did not account for possible systematic errors. Because the SAGE and Umkehr data records were so short (i.e., less than one solar cycle), no attempt was made to distinguish between solar-induced and human-influenced contributions to these changes.

Adding 15 months of new SAGE data does not change the picture appreciably. Again, no attempt was made to separate the contributions from natural and human-influenced processes. Additionally, a more thorough analysis of data from 10 Umkehr stations in the Northern Hemisphere for the period 1977 to 1987 reports a statistically significant decrease in ozone between 30 and 43 km, the decrease near 40 km being $4.8 \pm 3.1\%$, after allowing for seasonal and solar-cycle effects and correcting the data for aerosol interferences. These losses are somewhat less than those predicted by the chlorine/ozone theory.

EXECUTIVE SUMMARY

Based on SAGE, Umkehr, and ozonesonde data, there are continuing indications of a stratospheric ozone decrease at 25 km and below. Changes at these altitudes are not predicted by global models based only on gas-phase processes. It is not clear whether this points to missing processes in the models or that these sparse measurements are not representative of the global atmosphere. However, such changes are qualitatively consistent with those required for compatibility with the total column measurements.

- *Recent measurements suggest that the rate of growth in atmospheric methane has slowed somewhat.*

It would appear that the rate of methane increase has been slowing down over the last decade, namely, from 16 to 20 ppbv per year in the early 1980s to 12 to 16 ppbv per year in the late 1980s. For the other trace gases that influence stratospheric ozone and climate (CFCs, nitrous oxide, and carbon dioxide), the observed rates of increase have not changed significantly since the time of the OTP report.

Theoretical Predictions

- *Theoretical models do explain many of the general features of the atmosphere, but new limitations have been recognized.*

Many processes control the distribution of trace gases in the atmosphere. To adequately simulate the atmosphere, models must include representations of numerous radiative, chemical, and small- and large-scale dynamical processes. Current models do indeed reproduce many of the patterns observed, for example, in the ozone column: a minimum in the tropics and maxima at high latitudes in the spring of both hemispheres. Furthermore, the north - south and vertical distributions of the ozone concentration are in general agreement with satellite observations, except for Antarctica. On the other hand, a long-standing discrepancy has been the systematic underestimation of ozone concentrations near 40 km.

Several major shortcomings have been identified recently. None of the assessment models adequately represent polar meteorology or attempt to include heterogeneous processes, i.e., chemical reactions on PSCs. The failure to include these processes would likely lead to an underprediction of ozone loss, both directly at polar latitudes and possibly indirectly at mid-latitudes due to dilution arising from large polar ozone losses.

Furthermore, only a few models include the influence of increasing carbon dioxide abundances and decreasing ozone abundances on temperature, which, in turn, lead to a decrease in the destruction of ozone through lower temperatures in the stratosphere. Hence, while there are still open questions regarding the quantitative treatment of the influence of CO₂ (temperature feedback), the predicted ozone depletions from chlorine- and bromine-containing chemicals are less for those global assessment models used in this report (gas-phase chemistry only) that account for CO₂ increases than the predicted ozone depletions from those models that keep temperatures fixed.

- *Current understanding predicts that, if substantial emissions of halocarbons continue, the atmospheric abundances of chlorine and bromine will increase and, as a result, significant ozone decreases, even outside of Antarctica, are highly likely in the future.*

Several scenarios, which represent a spectrum of possible choices regarding man-made emissions of chlorine- and bromine-containing chemicals, have been used to examine the response of

EXECUTIVE SUMMARY

stratospheric ozone to atmospheric chlorine and bromine abundances. The predictions for the year 2060 relative to the year 1980 are discussed below for some of those scenarios. In each scenario, it was assumed that the recent trends continue in the atmospheric abundances of methane, nitrous oxide, and carbon dioxide of 15 ppbv, 0.25%, and 0.4% per year, respectively. The scenarios examined and the results predicted are the following:

SCENARIO (1) A freeze of CFCs 11, 12, 113, 114, 115, halons 1211, 1301, and 2402 at 1985 production levels; CCl₄, CH₃CCl₃, hydrochlorofluorocarbon (HCFC) 22 abundances increase at approximately 1 part per trillion by volume (pptv) (1% of today's level), 4 pptv (3% of today's level), and 6 pptv (7.5% of today's level) per year, respectively.

The chlorine loading of the atmosphere is predicted to reach 9.2 ppbv by the year 2060, about three times today's level, and the bromine loading 31 pptv, about two and one half times today's level. For models that did not include the effect of carbon dioxide (i.e., temperature feedback), predicted column ozone reductions were from 1 to 4% in the tropics, and from 8 to 12% at high latitudes in late winter. For models that did include the effect of carbon dioxide, predicted column ozone reductions were from 0 to 1.5% in the tropics and from 4 to 8% at high latitudes in late winter. These predictions do not include the effects of heterogeneous processes, which would increase the predicted ozone depletions, at least in polar regions. Ozone is predicted to decrease by 35–50% at 40 km in models with no temperature feedback, and about 25–40% in models with temperature feedback, and results in stratospheric temperature decreases of 10 to 20 K.

SCENARIO (2) A 50% cut in emissions of CFCs 11, 12, 113, 114, 115, halons 1211, 1301, and 2402 from 1985 production levels by the year 2000; CCl₄, CH₃CCl₃, HCFC 22 increase at approximately 1 pptv, 4 pptv, and 6 pptv per year, respectively, plus a 50% substitution of CFC reductions augmenting HCFC 22 fluxes (used as a surrogate for other HCFCs).

The chlorine loading of the atmosphere is predicted to reach 7.2 ppbv by the year 2060, and the bromine loading 22 pptv. Only models that did not include the effect of carbon dioxide were used to calculate ozone depletions for this scenario. Predicted column ozone reductions were from 1.5 to 3.0% in the tropics, and from 5 to 8% at high latitudes in late winter. These predictions do not include the effects of heterogeneous processes, which would increase the predicted ozone depletions, at least in polar regions. Ozone is predicted to decrease by 25–40% at 40 km (without temperature feedback). Temperature feedbacks are expected to reduce the predicted ozone depletions as in scenario 1.

SCENARIO (3) A 95% cut in emissions of CFCs 11, 12, 113, 114, 115, halons 1211, 1301, and 2402 from 1985 production levels by the year 2000; CCl₄, CH₃CCl₃, HCFC 22 increase at approximately 1 pptv, 4 pptv, and 6 pptv per year, respectively, plus a 50% substitution of CFC reductions augmenting HCFC 22 fluxes.

The chlorine loading of the atmosphere is predicted to reach 5.4 ppbv by the year 2060, and the bromine loading 14 pptv. For models that did not include the effect of carbon dioxide, there was little change in column ozone in the tropics, and a decrease from 2 to 4% at mid-latitudes. For the one model that did include the effect of carbon dioxide, column ozone was predicted to increase by 0–2% at most latitudes. These predictions do not include the effects of heterogeneous processes, which would increase the predicted ozone depletions, at least in polar regions. Ozone is predicted to decrease by 20–30% at 40 km.

EXECUTIVE SUMMARY

SCENARIO (4) 95% cut in emissions of CFCs 11, 12, 113, 114, 115; halons 1211, 1301, 2402; freeze of CCl_4 and CH_3CCl_3 atmospheric levels constant at 1985; HCFC 22 increase at approximately 6 pptv per year, but no substitution of CFCs with HCFC 22.

The chlorine loading of the atmosphere is predicted to be about 3.6 ppbv by the year 2060, comparable to that of today, and the bromine loading 14 pptv. One model that did not include the effect of carbon dioxide predicted little change of ozone in the tropics and a decrease of up to 4% at high latitudes. These predictions do not include the effects of heterogeneous processes, which would increase the predicted ozone depletions, at least in polar regions.

SCENARIO (5) 100% cut in emissions of CFCs 11, 12, 113, 114, 115; halons 1211, 1301, 2402; and CCl_4 , CH_3CCl_3 , and HCFC 22 by the year 2000.

This calculation was performed to examine the chlorine loading of the atmosphere with time. By the year 2060, the chlorine loading is predicted to be about 1.9 ppbv, significantly less than that of today and approximately the level required to return the Antarctic ozone layer to levels approaching its natural state, assuming that current meteorological conditions continue. Although no model calculations were performed using this scenario, it is likely that all models would predict an increase in global ozone due to the effects of carbon dioxide and methane.

Halocarbon Ozone Depletion and Global Warming Potentials (ODPs and GWPs)

- *The impact on stratospheric ozone of the halocarbons (HCFCs and HFCs) that are proposed as substitutes for the CFCs depends upon their chemical removal processes in the lower atmosphere (troposphere).*

Because they contain hydrogen atoms, the HCFCs and HFCs are primarily removed in the troposphere by reaction with the hydroxyl radicals (OH). Although the photochemical theory of tropospheric OH is well developed, it has not been validated experimentally, and the global OH distributions are based on models. Furthermore, the global abundance of OH is influenced by tropospheric composition, which is changing.

The various estimates of the lifetimes of HCFCs and HFCs in the troposphere have an uncertainty of $\pm 50\%$. This contributes an important source of uncertainty in the prediction of the ODPs and GWPs of the HCFCs and HFCs. The fate of the degradation products of the HCFCs and HFCs and their environmental consequences are inferred from data on analogous compounds and hence the specific degradation processes require further study.

- *The values of the ODPs for the HCFCs are significantly lower than those for the CFCs.*

Theoretical predictions performed by different groups using a variety of models have calculated similar, but not identical, values for the ODPs of the HCFCs, as indicated in Table 1 below.

None of the models used for calculating the ODPs are able to simulate the chemical and dynamical processes causing the Antarctic ozone hole. However, relative to CFC 11, the local Antarctic ODPs of HCFCs 22, 142b, and 124 will be larger, perhaps as much as a factor of two or three times greater than those derived from model calculations that do not include heterogeneous chemistry and that cannot simulate polar dynamical processes. The ramifications of polar ozone depletion for ODPs is not currently clear.

Table 1. Range of Ozone Depletion Potentials (ODPs) and halocarbon Global Warming Potentials (GWPs) determined by one-dimensional and two-dimensional models, assuming scaling for HCFC ODPs and GWPs by CH₃CCl₃ derived lifetime (6.3 years)

Species	ODPs		GWP
	1-D Models	2-D Models	1-D Models
CFC-11	1.0	1.0	1.0
CFC-12	0.9–1.0	0.9	2.8–3.4
CFC-113	0.8–0.9	0.8–0.9	1.3–1.4
CFC-114	0.6–0.8	0.6–0.8	3.7–4.1
CFC-115	0.4–0.5	0.3–0.4	7.4–7.6
HCFC-22	0.04–0.05	0.04–0.06	0.32–0.37
HCFC-123	0.013–0.016	0.013–0.022	0.017–0.020
HCFC-124	0.016–0.018	0.018–0.024	0.092–0.10
HFC-125	0	0	0.51–0.65
HFC-134a	0	0	0.24–0.29
HCFC-141b	0.07–0.08	0.09–0.11	0.084–0.097
HCFC-142b	0.05–0.06	0.05–0.06	0.34–0.39
HFC-143a	0	0	0.72–0.76
HFC-152a	0	0	0.026–0.033
CCl ₄	1.0–1.2	1.0–1.2	0.34–0.35
CH ₃ CCl ₃	0.10–0.12	0.13–0.16	0.022–0.026

The HCFCs all have much larger relative ozone depletion potentials during the first 30 to 50 years after their emission into the atmosphere compared to their steady-state ODP values. The transient values depend upon the atmospheric lifetime and their transport time to the region of destruction of the gas. This transient affect is implicitly taken into account by all models calculating atmospheric chlorine abundances and ozone depletion.

- *The steady-state values of the halocarbon GWPs of the HCFCs and HFCs are lower than those of the CFCs.*

The key factors that establish the halocarbon GWP of a HCFC or HFC are its lifetime in the troposphere and its ability to absorb atmospheric infrared radiation. Halocarbon GWP values differ between species due primarily to differences in their lifetimes, since their abilities to absorb infrared radiation are similar. Hence, one of the the largest sources of uncertainty in the calculation of the halocarbon GWPs of the HCFCs and HFCs is quantifying their rate of removal in the troposphere. Calculations by three groups using different models for the halocarbon GWPs of the CFCs, HCFCs, and HFCs yield similar, but not identical, values, as indicated in Table 1.

The HCFCs all have much larger relative global warming potentials during the first 30 to 50 years after their emission into the atmosphere compared to their steady-state halocarbon GWP values.

Implications

The findings and conclusions from the intensive and extensive ozone research over the past few years have several major implications as input to public policy regarding restrictions on man-made substances that lead to stratospheric ozone depletion:

EXECUTIVE SUMMARY

- The scientific basis for the 1987 Montreal Protocol on Substances that Deplete the Ozone Layer was the theoretical prediction that, should CFC and halon abundances continue to grow, there would eventually be substantial ozone depletion. *The research of the last few years has demonstrated that actual ozone loss due to the CFCs has already occurred, i.e., the Antarctic ozone hole.*
- Even if the control measures of the Montreal Protocol were to be implemented by all nations, today's atmospheric abundance of chlorine (about 3 ppbv) will at least double to triple during the next century. *Assuming that the atmospheric abundance of chlorine reaches about 9 ppbv by 2060, ozone depletions of 0–4% ozone in the tropics and 4–12% at high latitudes would be predicted, even without including the effects of heterogeneous processes.*
- The heterogeneous, PSC-induced chemical reactions that cause the ozone depletion in Antarctica and that also occur in the Arctic represent additional ozone-depleting processes that were not included in the stratospheric ozone assessment models on which the Montreal Protocol was based. Recent laboratory studies suggest that similar reactions involving chlorine compounds may occur on sulfate particles present at lower latitudes, which could be particularly important immediately after a volcanic eruption. *Hence, even with the Montreal Protocol, future global ozone depletions could well be larger than originally predicted.*
- Large-scale ozone depletions in Antarctica appeared to have started in the late 1970s and were initiated by atmospheric chlorine abundances of about 1.5–2 ppbv, compared to today's level of about 3 ppbv. *To return the Antarctic ozone layer to levels approaching its natural state, and hence to avoid the possible ozone dilution effect that the Antarctic ozone hole could have at other latitudes, one of a limited number of approaches is a complete phase-out of all fully halogenated CFCs, halons, carbon tetrachloride, and methyl chloroform, as well as careful consideration of the HCFC substitutes. Otherwise, the Antarctic ozone hole is expected to remain, provided the present meteorological conditions continue.*

III. SCIENTIFIC SUMMARIES

Chapter 1. Polar Ozone

Polar Ozone Trends

The observation of substantial springtime reductions in Antarctic ozone, the Antarctic ozone “hole,” focused world attention on the polar regions. In the few years since the discovery of this phenomenon, a great deal of field and laboratory data have been gathered. Theoretical studies have kept pace with the experimental investigations. This chapter provides a detailed review of the current understanding of the science of polar ozone depletion.

Differences in atmospheric dynamics of the hemispheres cause naturally lower ozone abundances in the Antarctic early spring as compared with the Arctic which should not be confused with the Antarctic ozone hole. Planetary waves are generally weaker in the Southern Hemisphere than in the Northern Hemisphere. The Southern Hemisphere polar winter stratosphere is colder, and the westerly vortex is stronger and more persistent than in the Northern Hemisphere. These factors strongly influence the seasonal and latitudinal variations in ozone in the two hemispheres. The ozone hole is identified not merely with the difference in ozone abundances between the hemispheres or with the latitude gradients, but with a decrease in the ozone abundances found in September and October over the past decade. It is now clear that these decadal trends result from a dramatic drop in total ozone that occurs each September. This unexpected ozone removal results in about a 50% decrease in column abundance by the end of September in recent years, as demonstrated by ground-based measurements from Halley Bay, Syowa, and the South Pole. Ozonesonde and satellite data reveal comparable total column changes, and show that the decreases occur primarily in the height region from about 12 to 24 km, the heart of the polar ozone layer. Further, the satellites demonstrate that the ozone hole extends over broad horizontal scales, at times covering the entire Antarctic continent.

Observed ozone trends in the warmer, winter Northern Hemisphere stratosphere are far smaller than those of Antarctica. Recent analyses suggest that the sub-polar column ozone decreases are largest in the winter and spring, on the order of 5% over the period from 1969 to 1988.

The trend in Antarctic ozone has not been monotonic, but this is not surprising. Inter-annual variations in total ozone occur at all latitudes. One cause of inter-annual variability is the Quasi-Biennial Oscillation (QBO), which is a natural fluctuation of equatorial stratospheric zonal winds and circulation. The mechanisms connecting polar latitude phenomena with the tropical QBO wind oscillation are not well understood.

Polar Stratospheric Chemistry

Hypotheses to explain the ozone hole included halocarbon chemistry, nitrogen chemistry associated with the solar cycle, and dynamical effects. Observations have ruled out the dynamical and solar cycle theories, while a broad range of measurements have been shown to be consistent with the general concepts of the halocarbon theory. The halocarbon theory is based on observations of the widespread occurrence of polar stratospheric clouds (PSCs) in the extremely cold Antarctic lower stratosphere. These provide surfaces on which heterogeneous chemical reactions can take place.

EXECUTIVE SUMMARY

Satellite data from 1978 to the present provide information regarding the vertical, geographical and seasonal extent of the PSCs. Their frequency in the Antarctic stratosphere is about 10 to 100 times greater than in the Arctic. There is an apparent QBO variation in the occurrence of PSCs during both September and October, as well as increasing numbers of PSC sightings during the Octobers of 1985 and 1987 (years of westerly QBO phase). PSCs may also influence the radiative budget of the polar lower stratosphere, hence affecting the mean circulation and ozone distributions.

Laboratory studies suggest that some PSCs are composed of nitric acid and water, condensing at temperatures considerably warmer than the frost point. As the stratosphere cools, these will be the first types of clouds to form, while water ice clouds will form only at colder temperatures. Field studies have demonstrated that the former contain a substantial amount of nitrate. Laboratory studies have also shown that reactions involving nitrogen oxides and relatively long-lived chlorine species (such as ClONO_2 and HCl) can occur on cloud surfaces. These reactions convert relatively inert chlorine reservoirs to reactive species that photolyze readily, releasing chlorine free radicals which can then destroy ozone. The reactions also tie up nitrogen oxides in the long-lived species, HNO_3 , thereby slowing the reformation of chlorine reservoirs such as ClONO_2 . This maintains elevated abundances of chlorine free radicals and the associated rapid ozone destruction over notably longer periods than would be possible if the heterogeneous reactions affected only the composition of chlorine species. Both sunlight and extremely cold temperatures are necessary for accelerated ozone loss.

Once liberated, the chlorine rapidly forms chlorine monoxide (ClO), which can then participate in several ozone-destroying catalytic cycles. These involve formation of the dimer of chlorine monoxide as well as reactions of ClO with bromine monoxide (BrO), hydroperoxyl radicals, and atomic oxygen. Laboratory studies have provided most of the rate coefficients and photochemical parameters needed to characterize these cycles, although there are still significant uncertainties in both homogeneous and heterogeneous chemistry.

Field Observations

Observations of ClO and BrO in Antarctica have provided a critical test of the halocarbon theory of ozone depletion. *In situ* and remote measurements using two independent techniques have demonstrated that the ClO abundances near 20 km are typically about 1 ppbv in the Antarctic vortex during September, about 100 times greater than theoretical predictions that do not include heterogeneous chemistry. However, these elevated ClO abundances are broadly consistent with modeling studies considering the likely PSC chemistry, frequency, and duration. While there are differences in detail among these studies, all show that a substantial fraction of the observed ozone loss (60–100%) can be explained by the observed ClO and BrO abundances using current measurements of kinetic rates. The Antarctic ozone loss is at present believed to be dominated by the dimer cycle during years when depletion is largest, with bromine reactions contributing about 15–35% and reactive hydrogen contributing about 10–15% to the total chemical loss rate. During years of lower Antarctic ozone depletion (e.g., 1988) and in the Arctic, the bromine chemistry is calculated to be more important. Uncertainties in measurements, model formulation and the potential importance of transport processes currently preclude a fully quantitative evaluation of the consistency between observed rates of ozone change and photochemical mechanisms.

A broad range of ancillary measurements in Antarctica supports and extends our confidence in the understanding of changes in gas-phase composition caused by PSCs. These include: *in situ* measurements of H_2O , NO_y (total reactive nitrogen), NO , particle sizes, and particulate nitrate, as well as long-path measurements of OCIO , HCl , HF , ClONO_2 , NO_2 , and HNO_3 . Of particular importance are the observations

of NO_x and H_2O , which show extensive denitrification and dehydration in the Antarctic vortex, believed to result from sedimentation of cloud particles. Denitrification is of particular importance since it controls the amount of nitrogen oxides remaining after PSCs have disappeared, and hence, as mentioned earlier, may strongly affect the rate of reformation of chlorine reservoirs.

Similar chemical measurements have been obtained in the Arctic stratosphere. Satellite and ground-based measurements of steep latitudinal gradients in Arctic NO_2 abundances (the Noxon "cliff") suggest the presence of mechanisms depleting NO_2 in north polar regions. The decrease in NO_2 is qualitatively related to increases in HNO_3 abundances, indicating mechanisms for nitrogen oxides suppression without denitrification (different from that observed in Antarctica). Such an increase could occur, for example, through heterogeneous reactions followed by cloud evaporation. Concentrations of ClO as high as 1 ppbv were observed inside the Arctic polar vortex in the winter of 1989. Enhanced column abundances of ClONO₂ and reduced abundances of HCl and NO_2 also indicated the importance of heterogeneous chemistry similar to that of Antarctica. No unambiguous evidence for ozone loss has yet been identified for the winter of 1989. Readily detectable ozone reductions would be expected to occur only if high concentrations of ClO were maintained for sufficiently long periods in cold, illuminated air. Vortex dynamics during the 1989 winter probably limited these conditions, and are likely to do so in most Northern Hemisphere winter/spring seasons. Thus the Northern Hemisphere ozone trends cannot be unambiguously identified with PSC chemistry, although the observations are qualitatively consistent with such an explanation.

Dynamics

The role of dynamical coupling has been examined in many different studies. Synoptic scale disturbances (tropospheric weather systems) can affect total ozone amounts locally, and may lead to the formation of PSCs. Air may flow through such systems and become chemically perturbed. If there is significant flow of air into and out of the stratospheric polar vortex, ozone amounts may be reduced well outside of the region where heterogeneous chemical reactions on PSCs can occur. Further, some PSCs may be found outside of the denitrified and dehydrated region and may induce chemical perturbations at sub-polar latitudes during winter. Quantitative details are uncertain. Export of air that has undergone ozone depletion may dilute ozone concentrations at lower latitudes when the polar vortex breaks down in the spring. Numerical models indicate that about a 2% change might occur in ozone amounts at mid-latitudes of the Southern Hemisphere due to dilution, and suggest that some fraction of the dilution may remain from one year to the next.

Measurements of the vertical profiles of long-lived tracers such as N_2O and the chlorofluorocarbons in the polar vortices reveal low values compared to those at other latitudes. These apparently result from downward motion and have important implications not only for representations of vortex dynamics but also for chlorine chemical perturbations. For example, measurements indicate only about 0.3 ppbv of total chlorine in the form of chlorofluorocarbons near 20 km at 70°S as compared to 1.0 ppbv at 45°S in about 1987; these imply that the corresponding abundances of reactive chlorine are on the order of 2.2 and 1.5 ppbv, respectively. Thus, the amount of reactive chlorine available for reactions on PSC surfaces in the polar regions is likely to be significantly enhanced compared to lower latitudes.

The stratospheric circulation exhibits variability on a range of time scales. In particular, there is substantial inter-annual variability in the two hemispheres, especially in the Northern Hemisphere. A very deep ozone hole occurred over Antarctica in spring, 1987. The hole was not as deep in 1988, perhaps because dynamics and transport were more vigorous in 1988 than in 1987. Temperatures were also warmer during September 1988 as compared to 1987, which is likely to be the primary cause for a corresponding

EXECUTIVE SUMMARY

decrease in PSC cloud frequencies in the regions sampled by the SAM II satellite between the 2 years. These factors may yield important differences in heterogeneous chemical perturbations and hence may explain qualitatively the difference in the depth of the ozone hole obtained (with 1988 being much less depleted than 1987). The observed behavior fits general expectations based on QBO behavior since the equatorial winds were strongly westerly near 25 km during October 1987, whereas 1988 was characterized by a transition from westerly to easterly winds. If the current QBO cycle has the average period of about 28 months, winds will remain easterly through October 1989, but change to westerly before September 1990. If the past correlation between the QBO and the ozone hole continues and if the current QBO cycle exhibits a period close to the average, then the ozone depletion should be expected to be relatively modest in 1989 and quite deep in 1990 (note, however, that the QBO period can vary by as much as 8 months so that the measured equatorial winds must be examined before any firm comparisons can be made). The next few years should therefore provide an excellent test of the relationship between the QBO and the Antarctic ozone hole.

Minimum temperatures in the high-latitude Northern Hemisphere stratosphere were unusually low in late January/early February, 1989. PSCs were observed as far equatorward as 50°N. A strong, dynamically induced warming occurred at polar latitudes in mid-February and temperatures rose above the threshold values required for PSC formation. Poleward transport of air rich in ozone and nitrogen oxides is likely to have occurred. This warming of the Arctic vortex probably played an important role in limiting ozone loss during 1989.

On the basis of radiosondes and satellite data, a downward trend in lower stratospheric temperatures has been deduced at high southern latitudes from 1979 through 1987 (note, however, that in 1988 temperatures were much warmer than they would have been if this trend had continued monotonically). The largest changes, about 1K/year, were found in the means for October and for November, while no trend was found in September, when most of the Antarctic ozone loss is observed. The observed time lag between the temperature change and the ozone loss, as well as radiative studies with 1-D, 2-D, and 3-D models, suggest that the temperature trend is the result of the ozone trend rather than its cause (i.e., reduced ozone abundances are predicted to yield smaller solar ultraviolet heating rates and hence colder temperatures).

Future of Polar Ozone

The future depletion of polar ozone depends in large part on mankind's use of halocarbons, although other factors may also contribute. In contrast to its behavior at ground level, increased concentrations of carbon dioxide may cool the stratosphere, perhaps affecting the duration and spatial extent of the PSCs in both hemispheres. Possible changes in climate and in the concentrations of atmospheric methane and nitrous oxide may also affect the processes related to the Antarctic ozone hole. The bulk of the chlorine currently in the stratosphere comes from chlorofluorocarbons that have atmospheric removal times on the order of 50 to 100 years, and hence the ozone hole will likely remain over Antarctica for many decades, even if all production were immediately halted. An examination of the Antarctic springtime column ozone record at several locations permits a rough estimate of the atmospheric chlorine content when the Antarctic ozone hole first became apparent. Assuming no changes in temperature, atmospheric dynamics, or photochemical processes, this provides an indication of the total chlorine abundances required to return the Antarctic ozone layer to levels approaching its natural state. A preliminary analysis of trace gas samples indicates an average age of polar lower stratospheric air of about 5 years. Coupled with the onset of detectable ozone reductions in the late 1970s, this suggests that organic chlorine mixing ratios of roughly the mid-1970s are necessary (corresponding to tropospheric total chlorine mixing ratios of about 1.5–2.0 ppbv, including the 0.6–0.7 ppbv of methyl chloride, which is believed to be of natural origin).

Chapter 2. Global Trends

Introduction

This chapter largely builds upon the Ozone Trends Panel (OTP) report by adding new analyses and updating the database.

Since the 1920s, numerous techniques have been developed and applied to determine total ozone and its vertical distribution. Initially, these measurements were not made for the purpose of determining long-term trends. Fortunately, some of these systems, and only the Dobson spectrophotometer for the last 30 years, have the requisite stability to provide data from which such changes may be detected and quantitatively measured.

For trend determination, short-term random noise is not usually a significant factor, since large amounts of data are averaged. The most important characteristic is stability, i.e., the absence of time-dependent systematic errors. Accuracy is desirable, but continuing systematic errors will not obscure the detection of change.

Determination of the global trends in stratospheric ozone has been based on complementary measurements, from the ground and from satellites. Ground-based instruments can be checked and recalibrated as necessary; they are regarded as capable of long-term stable operation, although this depends on some non-technical factors. Their disadvantages are that they are local systems, and provide few observations in oceanic or remote areas. Satellite-borne instruments obtain global data but, once launched, are not available to checking and are subject to drift. It is thus desirable to have these complementary measurements to provide checks on each other.

Trends in Total Ozone

Existing data on total ozone relies heavily on the Dobson instruments and M83/M124 instruments in the Northern Hemisphere mid-latitudes (30–64°N), so that trends can only be determined in this latitude range. Dobson instruments are referenced to the World Standard instrument, whose calibration is reported to have been maintained within $\pm 0.5\%$ over the past 15 years.

Satellite data are provided by the TOMS/SBUV instruments. They have proven to be very useful to verify consistency and identify erroneous readings in ground-based instruments and to confirm the reliability of the World Standard instrument. An important recent result is the development of a method for using the TOMS/SBUV data themselves to remove the effects of long-term instrumental drift. Although such new data are not used in the following analysis, results of initial testing suggest this has been successful, and that the TOMS data can provide in the future a second, independent source of data on global trends.

The main conclusions of the study of total ozone trends are as follows (± 2 standard error limits are shown):

- *New analyses of the total ozone data set used by OTP produce negative trends whose latitudinal and seasonal patterns are consistent with the earlier results (over the 17-year period from December 1969 through 1986).*

EXECUTIVE SUMMARY

Zonal mean decadal changes derived using various statistical assumptions lie in the following ranges during winter (December–March): for 30–39°N or 35°N, $-0.9 \pm 0.9\%$ to $-1.7 \pm 0.9\%$; for 40–52°N or 45°N, $-2.0 \pm 0.8\%$ to $-3.0 \pm 1.7\%$; and for 53–64°N or 55°N, $-2.5 \pm 1.9\%$ to $-3.7 \pm 1.8\%$. Analogous changes during summer (May–August) are: for 30–39°N, $-0.4 \pm 0.9\%$ to $-1.1 \pm 0.9\%$; for 40–52°N, $-0.7 \pm 0.6\%$ to $-1.1 \pm 0.8\%$, and for 53–64°N, $-0.1 \pm 0.9\%$ to $-0.7 \pm 0.9\%$. Results of an independent study performed in the USSR lie within the ranges quoted above.

- *The trends are sensitive to data obtained after October 1982 during periods of anomalies in the ozone patterns.*

If the data are analyzed up to and including October 1982, the summertime trend moves closer to zero by 0.8 to 1.0% per decade. Depending on the details of the statistical model, the analogous change in the wintertime trend is 0.3 to 0.9% per decade less negative.

- *Derived trends for the 17-year period between 1969 and 1986 are insensitive to the statistical treatment of the quasi-biennial oscillation and solar cycle relationships.*

Since the Dobson ozone record approaches 30 years, the trend estimates should be nearly independent of the 11-year solar cycle effect as represented by the F10.7-cm solar flux and the quasi-biennial effect represented by equatorial 50 hPa winds. This is important in that the derived long-term trends are robust to these known natural causes of ozone variability.

- *Extension of the data set into 1988 does not alter the nature of conclusions based on measurements through 1986, although differences in detail exist.*

During winter, derived statistically significant trends are $-1.8 \pm 1.1\%/decade$, $-2.3 \pm 0.9\%/decade$, and $-2.7 \pm 1.2\%/decade$ at latitudes 35°N, 45°N, and 55°N, respectively. Trends derived for summer at 35°N, 45°N, and 55°N are $-0.5 \pm 1.1\%/decade$, $-0.3 \pm 1.0\%/decade$, and $-0.2 \pm 1.2\%/decade$, respectively. None of the summertime trends are statistically significant.

- *Analyses of Dobson measurements from different geographic regions reveal differences in trends.*

Over the period 1969 to 1988, European and North American stations indicate statistically significant wintertime trends of $-2.9 \pm 0.7\%/decade$. Japanese stations indicate a non-significant wintertime trend of $-0.6 \pm 1.0\%$ per decade. Summertime trends vary from $-1.2 \pm 0.7\%$ per decade over North America to $+0.8 \pm 1.2\%$ per decade over Japan.

- *The regional differences in trends derived from the Dobson network are consistent with geographic patterns of ozone change contained in the TOMS/SBUV data sets.*

Data sets now available from satellites are useful in identifying geographic patterns in total ozone changes. However, present satellite data sets have insufficient length for definitive studies of long-term trends.

- *The observed total ozone trends for the winter are more negative than model predictions for the period 1969 through 1986, although there is close agreement between observation and prediction in the summer.*

The observed winter total ozone trends over the latitudes 30 to 60°N ranged from $-1.9 \pm 0.7\%$ per decade to $-2.6 \pm 1.2\%$ per decade among the study groups. Based on the observed trend

uncertainty limits, these changes exceed the theoretical model-calculated winter changes of -0.5 to -1.2% per decade given in the OTP report. The observed summer trends ranged from $-0.6 \pm 0.6\%$ per decade to $-0.8 \pm 0.6\%$ per decade and were consistent within the uncertainty limits with the summer theoretical model calculations of -0.3 to -0.6% per decade.

Trends in Ozone Vertical Distribution

The situation with regard to measurements of the vertical distribution is less satisfactory. Presently, most ground-based observations have been of the Umkehr type, with extensive records at only about 10 stations distributed very non-uniformly over the globe. The observations have a vertical resolution of 11 to 15 km, and are subject to aerosol interference, which can now be corrected for by physical-theoretical methods. The only reliable satellite data are obtained by the SAGE instruments above 25 km. It uses a ratio technique which renders the measurement insensitive to drift. The sampling is 900 profiles a month (two per orbit) with time-varying non-uniform geographical distribution.

The emphasis in the current analysis is first given to the altitude range in the upper stratosphere where the percentage change in ozone concentrations at mid-latitude due to anthropogenic chlorine perturbations is expected to be the largest. The major problem for such an analysis is the scarcity in time and space of the available data base for both satellite and ground-based measurements which precludes any true global evaluation of trends in ozone vertical distributions.

- *Over the regions of maximum density of coincidences (SAGE II minus SAGE I), i.e., 20–50°N and 20–50°S, the comparisons indicate for a 6-year average time period (1980–1986):*
 - an ozone decrease between 35 and 44 km with the maximum ozone change of $-3 \pm 2\%$ occurring at 40 km.*
 - an ozone decrease of $-3 \pm 2\%$ at 25 km and an essentially zero ozone change at 28–33 km and at 45–48 km.*

The only satellite observations that can be used currently for the determination of upper-stratospheric ozone changes are based on the comparison of 33 months (1979–1981) of SAGE I and 3 years (October 1984–December 1988) of SAGE II operations. This analysis constitutes an update of the OTP report by including two more years of SAGE II data, and confirms the previous results. These values represent the changes that occur over this time period and no attempt has been made to correct for solar cycle or any other.

- *Statistically significant negative trends are observed in Umkehr layers 6-7-8 (30–43 km) that correspond to an average ozone change of $-0.4 \pm 0.3\%$ per year at 40 km.*

A trend analysis of Umkehr observations performed at 10 stations in the Northern Hemisphere for the period 1977–1987 has been made on a station-by-station basis using an autoregressive statistical model which accounts for seasonal, solar-cycle and aerosol-induced effects. The latter is of particular importance when considering the high aerosol load in the stratosphere during the year 1982–1983 following the El Chichon volcano eruption.
- *Within the uncertainty limits of SAGE and Umkehr trend results near 40 km, these two independent results are not inconsistent.*

EXECUTIVE SUMMARY

When corrected for the solar effect on ozone over 6 years, the change in ozone from SAGE observations near 40 km is estimated to be $-0.2 \pm 0.4\%$ per year that is not explained by natural and instrumental variation. When compared to the Umkehr trend of $-0.4 \pm 0.3\%$ per year there is no inconsistency within the margins of error.

- *In the lower stratosphere (15–24 km), the estimated change from a limited network of Northern Hemisphere ozonesonde stations is -0.5% per year $\pm 0.4\%$.*

Analysis of ozonesonde data at nine stations (Canada, Europe, and Japan) with records extending for the three longest ones from 1966 to 1986 has been performed to detect possible trends in ozone concentrations in the lower stratosphere. This analysis leads to some differences in the results for the various stations which probably reflect the differences in the system operation and extent of the data bases as well as varying regional effects.

- *Although at the lower edge, the simulation results are within the error bars of the observed changes in the ozone vertical distributions.*

Calculation of changes in the ozone vertical distribution have been performed in the OTP report using 2-D models for the period 1979–1985. The calculated decreases peak at about -6% at mid-latitudes near 40 km.

- *The ozone decrease observed by SAGE instruments and suggested by Umkehr results in the 40 km region contribute very little to explaining the Dobson year-round total ozone trend of -1.1% per decade.*

The SAGE change of $-3\% \pm 0.2\%$ at 25 km over 6 years, when considered together with the negative Umkehr trend in this height range and the statistically significant, but not globally representative, trend of nearly -0.5% per year observed by ozonesondes between 17 and 24 km, seems to suggest that the stratosphere below 25 km is the prime contributor to the observed total ozone trend at mid-latitude.

Trends in Stratospheric Temperature

The update of the previous temperature trend report (OTP) is based on the stratospheric temperature data set already considered, and updated when possible, and the new Rayleigh lidar data. These lidar data have been compared with the SSU (Stratospheric Sounding Unit) data and the NMC (National Meteorological Center) analyses from 1981 to 1987. Substantial differences are observed, accountable in part by changes in the NOAA satellite series.

The recent finding of a statistical relationship between the stratospheric temperature, the QBO and the 11-year solar cycle has a potential implication for trend determination. The zonal asymmetry of the 11-year solar signal, clearly shown by the radiosonde data up to 30 hPa (24 km), and confirmed by the lidar and rocket data at higher altitudes, leads locally to much larger temperature dependence than the one observed in zonal or global means. Caution must be taken when using local or regional data (for T and O₃ as well) unless the data extend over a long enough period to separate trends from solar activity effects.

In the stratosphere, long-term trends can only be obtained from radiosondes at present. Satellite observations are available for less than a solar cycle:

- *In the lower stratosphere (100–30 hPa), the temperature data over the last 20 years suggest a maximum change of -0.4 K/decade at mid- and low latitudes with larger changes occurring at higher latitudes.*
- *In the upper stratosphere, the satellite data for the period (1985/1986) - (1979/1980) indicate a global temperature change of $-1.5 \pm 1^\circ\text{K}$. It is compatible with the $-3 \pm 4\%$ change in ozone concentration around 40 km as observed by SAGE instruments.*

More work is clearly needed to bring data of different sources into agreement and to understand the causes of the large spatial variability, whether or not it is related to solar activity.

Trends in Tropospheric Source Gases and Ozone

- *For most of the tropospheric trace gases, the observed rates of increase up to the end of 1987 have not changed significantly compared to those in the OTP report, which analyzed data up to the end of 1986.*
- *It would appear that the rate of methane increase has been slowing over the last decade, from 16–20 ppbv per year in the 1980s to approximately 12–16 ppbv per year in the late 1980s.*
- *Trend analysis of surface ozone measurements from ozonesonde and ground-based instruments show variable results.*

The 16 Northern Hemispheric sites show a range of trends from -1.1 to $+3.1\%$ per year. Ten of the Northern Hemispheric sites show statistically significant positive trends; one site shows a statistically significant negative trend. The remaining sites show trends that are not significant. The seven European sites all show statistically significant positive trends, ranging from $+1.1$ to $+3.1\%$ per year. All four Canadian sites show negative trends, from -0.1 to -1.1% per year, only one of which is statistically significant. All three Japanese sites show positive trends, ranging from $+0.9$ to $+2.5\%$ per year, two of which are significant. The four Southern Hemispheric sites show trends ranging from -0.5 to $+0.6\%$ per year, only one of which is significant.

Trends in Stratospheric Aerosols

- *Stratospheric aerosols can produce artifacts in ozone measurements by remote-sensing instruments and, in the case of Antarctic PSCs, have been shown to impact ozone destruction through heterogeneous chemistry. In addition, laboratory studies suggest that heterogeneous processes may occur on the surface of sulfuric acid/H₂O aerosols, which are greatly enhanced after volcanic eruptions. The latter effect could be important in providing a mechanism for ozone destruction on a global scale.*
- *From the standpoint of global trends, global stratospheric aerosol loading, which peaked after the eruption of El Chichon, has generally decreased. Although low in 1989, it has not yet reached the lowest values observed in 1978–1979. The 1989 values have little or no effect on ozone measurements.*

Trends in Surface UV Radiation

The Robertson-Berger meters located in the United States showed no increase in surface ultraviolet radiation over the period 1974 through 1985. The measurements do not contradict the observed downward

EXECUTIVE SUMMARY

trend in total ozone. The meter is not sensitive to small changes in ozone, and in addition, the system is strongly influenced by cloudiness and sources of pollution.

Chapter 3. Model Predictions

Stratospheric Models

In order to estimate the impact of man-made chemicals on atmospheric ozone, it is essential to develop models that perform long-term predictions. Current models that are used for these predictions include rather detailed schemes for homogeneous chemistry, and to some extent, account for radiative and dynamical feedbacks. Two-dimensional models predict the latitudinal and seasonal changes in ozone and other trace gases. Among the available models for calculating ozone globally, these 2-D models currently include the best representation of homogeneous physical and chemical processes in the middle atmosphere and have been compared extensively with observations of many stratospheric chemical species. However, none of these models properly account for heterogeneous chemistry and polar dynamics. Because of computational requirements and development time, the recently available 3-D models have had only limited applications in assessment studies, but are important in resolving some issues of model formulation and dynamical feedbacks.

An important prerequisite for prediction models is that they represent with sufficient accuracy the present distributions of trace gases. The 2-D models involved in the present assessment generally reproduce the patterns observed in the ozone column, with a minimum in the tropics and maxima at high latitudes in the spring of both hemispheres. The meridional distribution of local ozone is also in good agreement with the satellite observations. However, important discrepancies have also been noted: in particular, the models systematically underestimate ozone concentrations near 40 km, where they should accurately represent the physical and chemical processes controlling ozone. Calculated and observed distributions and seasonal variations of species such as nitrous oxide, methane, nitric acid, nitrogen oxides, and chlorine monoxide are in qualitative agreement, although substantial quantitative differences are found in certain cases.

The recent intercomparison of stratospheric models (1988, Virginia Beach) has highlighted many specific differences in the models, but has not yet resolved their causes. For example, the photodissociation rates were compared using specified ozone and temperature fields and found to differ among models by a factor of 2 or more in many instances. Follow-up studies examining the detailed radiative transfer in the models are continuing. Tests of the model circulation using synthetic tracers with specified chemistry has revealed substantial differences in the rate of upward motion in the tropical stratosphere. In spite of these individual differences, the calculated distribution of ozone is in good agreement between the models, and may demonstrate the robustness of the ozone photochemistry in these models.

Important Issues in Ozone Modeling

Modeling the polar regions is an especially challenging task because of the difficulty both in simulating the physics and chemistry of polar stratospheric clouds (PSCs) and in modeling the dynamical processes controlling the distribution of tracers and temperature of the high-latitude lower stratosphere in winter. The model predictions in this assessment do not include the effects of heterogeneous processes involving chlorine and nitrogen-containing chemicals on the surface of particles in PSCs. These processes are known to increase the abundance of the chlorine radical, ClO, which plays an important role in reducing ozone in

the Antarctic atmosphere. In several models, exploratory studies including these effects were performed, and showed substantially enhanced ozone depletion at high latitudes during winter and smaller changes in neighboring mid-latitudes for much of the year. Additional studies, including some of these 2-D models and other 3-D models, have shown that the transport of ozone-depleted air from the Antarctic region today can account for ozone reductions at mid-latitudes of several percent.

Laboratory studies suggest that heterogeneous processes on the natural background aerosols (Junge layer, which can be perturbed by volcanic eruptions) could also contribute to enhanced chlorine-catalyzed ozone destruction over much of the globe. Several model studies have examined the effects of parameterized heterogeneous reactions on sulfuric acid aerosols and have shown the potential for additional ozone depletion. Because of uncertainties in the laboratory data on rate constants for these reactions under stratospheric conditions, only sensitivity studies can be made at present.

Stratospheric temperature perturbations resulting from changes in CO₂ or tropospheric climate will in turn affect the photochemistry of ozone. In the upper stratosphere for the scenarios described below, increased CO₂ and reduced ozone both lead to temperature reductions near the stratopause of 10–20 K by the year 2060. This significant cooling is a robust feature of simulations; it leads to a reduced rate of ozone photochemical loss and hence moderates the ozone depletion due to chlorine. In the lower stratosphere, a particularly difficult region to model, smaller temperature changes are predicted. If the lower stratosphere cools significantly (2–4 K) in the future, then reduced chemical loss predicted by the models with homogeneous chemistry would lead to an increase in ozone concentrations that must be considered along with other perturbations. Such changes in stratospheric temperatures could be accompanied by changes in the circulation. A number of the models used in this assessment include radiative feedbacks, and some attempt to account for circulation feedbacks.

Scenarios for Atmospheric Composition

The composition of the atmosphere will depend on the rate at which halocarbons and other trace gases will be emitted in the future. Several scenarios have been considered in this assessment in order to examine the impact of possible control policies. Their details are specified in Table 2. None of the individual scenarios is intended to be a prediction of the future atmospheric composition; the range is only illustrative of different strategies for halocarbon control. They are used to define a range of chlorine and bromine loadings to the atmosphere and to study the consequent response of stratospheric ozone.

The predictions given here should be interpreted with caution in the light of the models' successes and limitations discussed above. Thus, given that the broad features of the present atmosphere are in general reproduced satisfactorily, it is then the broad features of the predictions that should be given most credence. For example, predictions of ozone and temperature changes near 40 km, as well as that of global chlorine loading, are probably more robust than detailed latitudinal behavior, especially in view of the models' lack of PSC chemistry.

1-Reference Scenario. In the reference scenario (A1), the fluxes of the CFCs (11, 12, 113, 114, 115) and halons (1211, 1301, 2402) controlled under the Montreal Protocol were held constant at their estimated 1985 production levels. The concentration of additional halocarbons and other chemically and radiatively important gases were assumed to increase at rates consistent with presently observed trends: CCl₄ at +1 pptv/yr (+1%/yr in 1985); CH₃CCl₃ at +4 pptv/yr (+3%/yr in 1985); CH₄ at +15 ppbv/yr (+0.9%/yr in 1985); N₂O at +0.25%/yr; CO₂ at +0.4%/yr. For HCFC-22 the current estimated emissions (140 Gg/yr in 1985) and growth rate in emissions (5%/yr of the 1985 emission rate) were chosen to be consistent with the

EXECUTIVE SUMMARY

Table 2. Scenarios for halocarbon abundances

1985 Conditions				
Gas	Mixing Ratio (pptv)	Flux (Gg/yr)	Gas	Mixing Ratio
CFC-11	220	350	CCl ₄	100 pptv
CFC-12	375	450	CH ₃ CCl ₃	130 pptv
CFC-113	30	150	CH ₃ Cl	600 pptv
CFC-114	5	15	CH ₃ Br	10 pptv
CFC-115	4	5		
halon 1211	1.5	5	N ₂ O	306 ppbv
halon 1301	1.7	8	CH ₄	1600 ppbv
HCFC-22	80	140	CO ₂	345 ppmv

Scenario Definitions					
Scenario	CFC cut (1996–2000)	CFC-22 Surrogate	CFC-22 Growth	CCl ₄ Growth	CH ₃ CCl ₃ Growth
A1	0%	—	+7 Gg/yr/yr	+1 pptv/yr	+4 pptv/yr
B1	50%	50%	+7 Gg/yr/yr	+1 pptv/yr	+4 pptv/yr
C1	85%	50%	+7 Gg/yr/yr	+1 pptv/yr	+4 pptv/yr
D1	95%	50%	+7 Gg/yr/yr	+1 pptv/yr	+4 pptv/yr
D2	95%	50%	+7 Gg/yr/yr	fix (1985)	fix (1985)
D3	95%	0%	+7 Gg/yr/yr	fix (1985)	fix (1985)
E1	100%	50%	+7 Gg/yr/yr	+1 pptv/yr	+4 pptv/yr
E2	100%	50%	+7 Gg/yr/yr	fix (2000)	fix (2000)
E3	100%	50%	+7 Gg/yr/yr	cut (2000)	fix (2000)
E4	100%	50%	+7 Gg/yr/yr	cut (2000)	cut (2000)
E5	100%	0%	+7 Gg/yr/yr	cut (2000)	cut (2000)
E6	100%	0%	fix (2000)	cut (2000)	cut (2000)
E7	100%	0%	cut (2000)	cut (2000)	cut (2000)
E8	95%	0%	cut (2000)	cut (2000)	cut (2000)
E9	85%	0%	cut (2000)	cut (2000)	cut (2000)
E10	100%	50% cut (2030)	cut (2030)	cut (2000)	cut (2000)

Total Chlorine Abundance, Summed Over All Halocarbons (ppbv)

Year	A1	B1	C1	D1	D2	D3	E1	E2	E3	E4	E5	E6	E7	E8	E9	E10
1985	2.98	2.98	2.98	2.98	2.98	2.98	2.98	2.98	2.98	2.98	2.98	2.98	2.98	2.98	2.98	2.98
2000	4.52	4.41	4.33	4.31	4.07	3.98	4.30	4.30	4.30	4.30	4.21	4.21	4.21	4.22	4.26	4.30
2030	7.09	5.93	5.12	4.89	4.17	3.66	4.77	4.29	4.09	3.52	2.98	2.84	2.58	2.72	3.01	3.38
2060	9.16	7.15	5.75	5.35	4.15	3.55	5.15	4.19	3.87	3.30	2.67	2.27	1.95	2.18	2.64	2.13
2090	10.72	8.09	6.25	5.73	4.05	3.42	5.47	4.03	3.64	3.07	2.41	1.88	1.55	1.84	2.43	1.59

limited atmospheric observations (+6 pptv/yr in 1985). Many of the models used in the assessment had specified temperature distributions and were therefore unable to include the radiative impact on stratospheric temperatures of CO₂ increases or ozone changes.

In this reference scenario (A1), the chlorine loading of the atmosphere increases from 3.0 ppbv in 1985 to 4.5 ppbv in the year 2000, to 7.1 in the year 2030, and to 9.2 in the year 2060. The bromine loading increases from 13 pptv in 1985 (10 pptv CH₃Br; 1.5 pptv halon 1211; 1.7 pptv halon 1301) to 31 pptv in the year 2060 (10 pptv CH₃Br; 3 pptv halon 1211; 18 pptv halon 1301). For models that did not contain the carbon dioxide effect, reductions in column ozone from 1980 to 2060 ranged from 1% to 4% in the tropics and from 8% to 12% at high latitudes in late winter. For models that included the carbon dioxide effect, the corresponding ozone reductions were less: 0% to 1.5% in the tropics and 4% to 8% in high latitudes in late winter. Ozone reductions at 40 km were about 35–50% in models with no temperature feedback and about 25–40% in models with temperature feedback, resulting in temperature decreases of 10–20 K. No heterogeneous chemistry was included in these models. When methane increases are suspended in 1985, ozone column reductions are larger in all latitudes and seasons by about 3%. Methane increases lead to increases in ozone by conversion of active chlorine (Cl, ClO) into inactive chlorine (HCl) and further by contributing to the direct production of ozone by “smog chemistry” in the lower stratosphere and troposphere. Many of the differences in the model results occur in the lower stratosphere where it is more difficult to predict the impacts of radiative and chemical forcing.

2-Scenarios with CFC Reductions. Several scenarios were considered in which emissions of CFCs and halons were reduced between 1995 and the year 2000, with 50% of the total CFC reduction augmenting the HCFC-22 budget. The increase in carbon tetrachloride and methyl chloroform are taken from the reference scenario. When CFC emissions are cut by 50% (B1), the chlorine loading in the year 2060 reaches 7.2 ppbv and the bromine loading is 22 pptv. The corresponding reductions in column ozone by 2060 are about 65% of those calculated for the reference scenario: 1–3% in the tropics and 5–8% at high latitudes in late winter for models without temperature feedback. Ozone reductions at 40 km are also less than in A1, 25–40% (without temperature feedback). No heterogeneous chemistry was included in these models.

When the CFC emissions are reduced by 85% (C1), the chlorine and bromine loadings in 2060 are 5.5 ppbv and 14 pptv, respectively. The reductions in column ozone are approximately 50% of those calculated in the reference scenario. No heterogeneous chemistry was included in these models.

When the CFC emissions are reduced by 95% (D1), the chlorine and bromine loadings in 2060 are 5.4 ppbv and 14 pptv, respectively. The reductions in column ozone at mid- to high latitudes are approximately 40–50% of those calculated in the reference scenario: very little change in the tropics and 2–4% at mid-latitudes for models without temperature feedback. Ozone reductions at 40 km are 20–30%. In the one model that includes the CO₂ effect, modest ozone column increases, 0–2%, are found at most latitudes. No heterogeneous chemistry was included in these models.

Further reductions in chlorine loading were considered by freezing concentrations of methyl chloroform and carbon tetrachloride (D2). When CFC emissions were also cut by 95%, the chlorine loading at 2060 was reduced to 4.2 ppbv. The reductions in column ozone were about 30% of that in the reference scenario, corresponding to about 60% of those calculated in the similar case when CCl₄ and CH₃CCl₃ were assumed to increase. If, in addition, the 95% cutback in CFC emissions is not compensated for by increased emission of HCFC-22 (D3), the chlorine loading at 2060 is reduced further to 3.6 ppbv, but the calculated ozone columns are not significantly different: little change in the tropics and a decrease of up to 4% at high latitudes. This change in chlorine loading, from 4.2 to 3.6 ppbv, has little effect on column ozone because

EXECUTIVE SUMMARY

it is associated with changes in HCFC-22 abundance. In these current assessment models, HCFC-22 does not release a large fraction of its chlorine in the middle stratosphere where chlorine-catalyzed loss of ozone is most important. No heterogeneous chemistry was included in these models.

Examination of chlorine loading. Thus far, in all of the scenarios (A-D) the tropospheric mixing ratio of chlorine, when summed over all halocarbons (i.e., chlorine loading), is well above the 1985 levels of 3 ppbv by the end of the scenarios in 2060. It is interesting to note what different combination of halocarbon reductions could possibly yield a chlorine loading of less than 3 ppbv by 2060, and also whether chlorine levels prior to the onset of the Antarctic ozone hole (at most 2 ppbv) could be achieved by 2060 with any combination of freezes or cuts in halocarbon emissions in the year 2000. Additional scenarios (E) in Table 2 explore the range of chlorine loading assuming that emissions of all halocarbons can be completely eliminated by 2000, except for CH_3Cl . Only a complete cut in emissions of CFCs, HCFC-22, CCl_4 , and CH_2Cl_2 results in chlorine loading less than 2 ppbv by 2060, although a combination of cuts and reductions in emissions (including low levels of CFC emissions) can give values below 3 ppbv. If the time frame is extended to 2090, there is a slightly greater range of emission restrictions that will result in 2 ppbv of atmospheric chlorine. Model assessments of these scenarios were not performed since the ozone perturbations would be dominated by the increases in CH_4 , N_2O , and CO_2 rather than the chlorine abundances.

Changes in Ultraviolet Radiation at the Surface

The changes in UV radiation at the surface have been calculated both for the observed changes in ozone column over the past decade and for the predicted changes in the future. The ultraviolet spectrum has been averaged to account for DNA damage, for plant damage, and for the Robertson-Berger meter's response. The TOMS data normalized to Dobson was used to define the change in the column over the past decade (0 to -4% in the tropics, -4 to -8% in northern high-latitude winter, and -8 to -30% at high southern latitudes from March through December). The calculated UV doses for DNA and plant damage increased by 2-5% in the Northern Hemisphere, by 2-10 % between 30 and 60°, and by 10-60 % under the Antarctic ozone hole. Predictions for 2060 from a model with fixed temperatures and circulation, neglecting heterogeneous chemistry, were used to illustrate future ozone perturbations (reference scenario A1 yielding a chlorine loading of 9.2 ppbv in 2060, 1-4% reduction in tropical total ozone, and 8-12% reduction at high latitudes). The largest absolute increase in average UV dose for the 1960-2060 period is predicted to occur in the springtime at mid-latitudes, and values may be sensitive to systematic latitudinal differences in cloud cover. The greatest relative increase, 20-40 %, occurs at high latitudes in early spring. For the scenario in which CFC emissions are cut by 95% in year 2000 (chlorine loading of 5.4 ppbv), the calculated increases in UV dose are half as large.

Chapter 4. Halocarbon Ozone Depletion and Global Warming Potentials

Concern over global environmental consequences of fully halogenated chlorofluorocarbons (CFCs) has sparked interest in the determination of the potential impacts on stratospheric ozone and climate of halocarbons, both chlorinated and brominated. In particular, the recent search for replacement compounds for the CFCs has primarily focused on several hydrogen-containing halocarbons (HCFCs, HFCs) which need to be closely examined. The kinetics and degradation mechanisms of many of these compounds (CFCs, HCFCs, HFCs, and halons) in the troposphere, their potential relative effects on stratospheric ozone, and their potential relative effects on global climate have been evaluated.

Halocarbon Oxidation in the Atmosphere

The halocarbons containing hydrogen atoms (HFCs and HCFCs), which have been proposed for substitutes for CFCs, react with the OH radical and are primarily removed in the troposphere by this process. The rate constants for attack of OH on these compounds are well defined ($\pm 20\%$ at relevant temperatures) and this reaction is the major loss process for these molecules in the atmosphere.

There are virtually no experimental data available concerning the subsequent reactions occurring in the atmospheric degradation of HFCs and HCFCs. By analogy with similar chemical species, it is predicted that the major products formed from the reactions of the OH radical with HFCs and HCFCs under tropospheric conditions are halogen-substituted carbonyl compounds and hydrogen halides. Based on the available knowledge of gas-phase chemistry, only four of the possible products appear to be potentially significant carriers of chlorine to the stratosphere: CClFO , CF_3CClO , $\text{CClF}_2\text{CO}_3\text{NO}_2$, and $\text{CCl}_2\text{FCO}_3\text{NO}_2$. Physical removal processes (to the liquid phase) will probably reduce this potential, but tropospheric removal pathways for the carbonyl compounds, especially the physical processes, are not well understood and require further study.

The oxidizing efficiency of the troposphere is determined by the abundance of OH radicals. However, quantitative validation of photochemical models by direct experimental measurement of the tropospheric OH concentrations has not been satisfactorily achieved. Global budgets and distributions of methyl chloroform and ^{14}CO have been used to estimate a volume-averaged global OH concentration of $6(\pm 2) \times 10^5$ molecule cm^{-3} . The budget and lifetime of methyl chloroform calculated using OH fields predicted by models is in general agreement with these results.

The calculated lifetimes of HFCs and HCFCs range from 0.25–40 years with an uncertainty of $\pm 50\%$. These are shorter than the lifetimes for the fully halogenated CFCs.

Ozone and ozone precursors (CH_4 , CO , NO_x , and non-methane hydrocarbons) can influence OH concentrations in the troposphere and hence could indirectly influence the lifetime of halocarbons. Model calculations indicate that, if man-made emissions of ozone precursors continue to increase, ozone concentrations are anticipated to grow throughout the Northern Hemisphere. The magnitude of the predicted ozone increase will depend on the detailed assumptions made concerning future emissions of ozone precursors. Model calculations indicating future tropospheric ozone increases as large as 50% also indicate future OH concentrations could decrease by as much as 25%. This would lead to increased lifetimes for many molecules removed by hydroxyl radical chemistry.

Ozone Depletion Potentials

Ozone Depletion Potentials (ODPs) have been defined as the ratio of steady-state calculated ozone column changes for each unit mass of a gas emitted into the atmosphere relative to the depletion for a mass unit emission of CFC-11. This definition provides a single-valued estimate of the cumulative ozone depletion for a gas, relative to CFC-11 on an equal mass basis.

One-dimensional and two-dimensional global atmospheric models have determined ODPs for a number of halocarbons, including CFCs, other chlorinated compounds, several potential replacement hydrohalocarbons, and several brominated compounds. Table 3 gives the range of calculated ODPs from one-dimensional and two-dimensional models for the CFCs, HCFCs, HFCs, plus CCl_4 and CH_3CCl_3 . Although 2-D models have generally a sounder physical basis, there are no real differences between the 1-D and

EXECUTIVE SUMMARY

Table 3. Range of Ozone Depletion Potentials (ODP) determined by one-dimensional and two-dimensional models, assuming scaling for HCFC ODPs by CH_3CCl_3 observed lifetime (6.3 years)

Species	1-D Models ^a	2-D Models ^b
CFC-11	1.0	1.0
CFC-12	0.9–1.0	0.9
CFC-113	0.8–0.9	0.8–0.9
CFC-114	0.6–0.8	0.6–0.8
CFC-115	0.4–0.5	0.3–0.4
HCFC-22	0.04–0.05	0.04–0.06
HCFC-123	0.013–0.016	0.013–0.022
HCFC-124	0.016–0.018	0.018–0.024
HFC-125	0	0
HFC-134a	0	0
HCFC-141b	0.07–0.08	0.09–0.11
HCFC-142b	0.05–0.06	0.05–0.06
HFC-134a	0	0
HFC-152a	0	0
CCl_4	1.0–1.2	1.0–1.2
CH_3CCl_3	0.10–0.12	0.13–0.16

^a1-D models from AER, LLNL, DuPont, and IAS.

^b2-D models from AER, LLNL, University of Oslo, and DuPont.

2-D results. In general, the ODPs for fully halogenated compounds, such as the CFCs, are much larger than those for the hydrogenated halocarbons, which include the potential replacement compounds considered.

Table 4 gives the ODPs determined for several brominated halocarbons from calculations by two models. These compounds should be compared to each other, because of the strong dependence of bromine effects on ozone to background chlorine levels. Bromine Ozone Depletion Potential (BODPs) are used for relative comparisons with Halon-1301, which has the longest lifetime and largest ODP, as the reference.

Although the calculated ODPs agree reasonably well among models, many uncertainties still exist. None of the models used for calculating ODPs include the chemical and dynamical processes causing the seasonal ozone losses over Antarctica. Another uncertainty lies in the model-calculated OH, which is a major source of uncertainty for both lifetimes and ODPs of the HCFCs.

Because of the apparent special chlorine processing and dynamics within the polar winter vortex, local Antarctic ODPs are expected to be larger than those shown in Table 3. Insofar as the observed long-lived tracer distributions, such as CFC-11 in the polar vortex, suggest that much of the total chlorine may be available there, then an upper limit on Antarctic ODPs can be determined by calculating the relative amounts of chlorine transported through the tropopause by the different gases. These chlorine loading potentials (CLPs) determined using assumed reference lifetimes (which generally agree with those in the models used here) can be as large as a factor of two to three times the derived ODP values (c.f., Tables 3 and 5). The ramifications of polar ozone depletion for global ozone depletion potentials (ODPs) are not currently clear.

Table 4. Ozone Depletion Potentials for brominated compounds as calculated in the LLNL one-dimensional model and University of Oslo two-dimensional model

Species	ODP ^a		BODP ^b	
	LLNL	Oslo	LLNL	Oslo
Halon-1301	13.2	7.8	1.0	1.0
Halon-1211	2.2	3.0	0.17	0.38
Halon-1202	0.3		0.02	
Halon-2402	6.2	5.0	0.5	0.64

^aRelative to CFC-11, shown for historical purposes. Values will be underestimates if account is taken of polar effects. Assumed upper stratospheric Cl₂ mixing ratio is 3 ppbv in the LLNL model and 4.5 ppbv in the Oslo model.

^bBromine Ozone Depletion Potentials (BODPs) defined relative to Halon-1301, the longest lived brominated gas.

Table 5. Maximum relative Chlorine Loading Potential (CLP) for examined CFCs, HCFCs, HFCs, and other chlorinated halocarbons based on reference species lifetimes chosen to be compatible with available atmospheric measurements and modeling studies

Species	Reference ^a Lifetime (yrs)	Chlorine Loading Potentials ^b
CFC-11	60.0	1.0
CFC-12	120.0	1.5
CFC-113	90.0	1.11
CFC-114	200.0	1.8
CFC-115	400.0	2.0
HCFC-22	15.3	0.14
HCFC-123	1.6	0.016
HCFC-124	6.6	0.04
HFC-125	28.1	0
HFC-134a	15.5	0
HCFC-141b	7.8	0.10
HCFC-142b	19.1	0.14
HFC-143a	41.0	0
HFC-152a	1.7	0
CCl ₄	50.0	1.0
CH ₃ CCl ₃	6.3	0.11

^aLifetimes (e-folding time) are based on estimates used in scenario development in Chapter 3 summary for the CFCs and from the analysis in Ozone Depletion section for the HCFCs and HFCs.

^bChlorine Loading Potential is defined as the maximum chlorine transported across the tropopause per mass emitted relative to the same for CFC-11. It is proportional to lifetime and the number of chlorine atoms per molecule. It is inversely proportional to molecular weight.

EXECUTIVE SUMMARY

The time-dependent relative ozone depletion values differ from the steady-state ODP values. The time-dependent values depend on the atmospheric lifetime and the transport time to the region of destruction of the gas. The shorter the stratospheric lifetime, the sooner the gas will impact stratospheric ozone and hence the higher the transient relative ozone depletion. An example of this behavior is shown by the HCFC-123 curve in Figure 1. It has a shorter lifetime than CFC-11; its relative ozone depletion is largest soon after emission. Other gases in this category include HCFC-141b and CH_3CCl_3 . Species such as HCFC-22, HCFC-124, and HCFC-142b have somewhat longer time constants in the stratosphere. Their relative ozone depletions build slowly to values (based on their time constants) as large as 0.2 and then decay slowly with time to the derived ODP value. Relative ozone depletion values for HCFCs are greater than ODP values even after 30 to 50 years. Time-dependent relative ozone depletions for CFCs with lifetimes longer than CFC-11 show a monotonic increase to the ODP value. As shown for a pulse injection in Figure 2, the ratio of the cumulative calculated depletion of HCFC-22 or HCFC-123 to the cumulative depletion of CFC-11 is equal to the ODP for these species. Therefore, the ODP is the cumulative response; as discussed above, the transient response of relative ozone depletion may be larger than the ODP value at early times after emission.

Several of the halocarbons indicate a strong latitude dependence in their ODP values and a generally weaker seasonal variation. In particular, ODPs for species such as CFC-12, HCFC-22, HCFC-124, and HCFC-142b, which have greatly different stratospheric loss patterns than CFC-11, produce strong latitudinal gradients in ODPs, with the largest ODPs near summer poles and smallest values in the tropics. The effects of heterogeneous chemistry and polar dynamics could modify these findings.

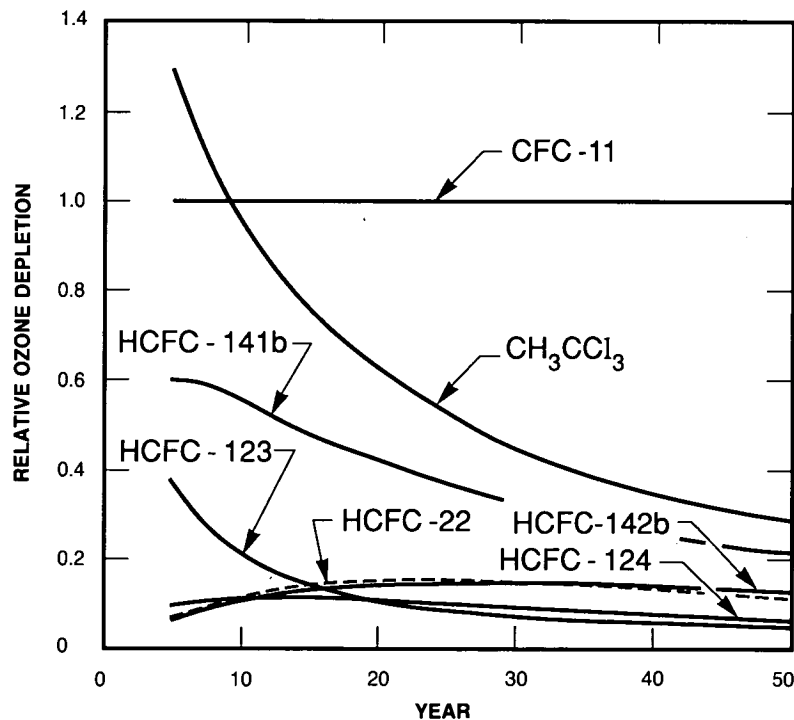


Figure 1. Calculated time-dependent change in relative ozone column depletion following a step change in emission of halocarbons (LLNL 1-D model).

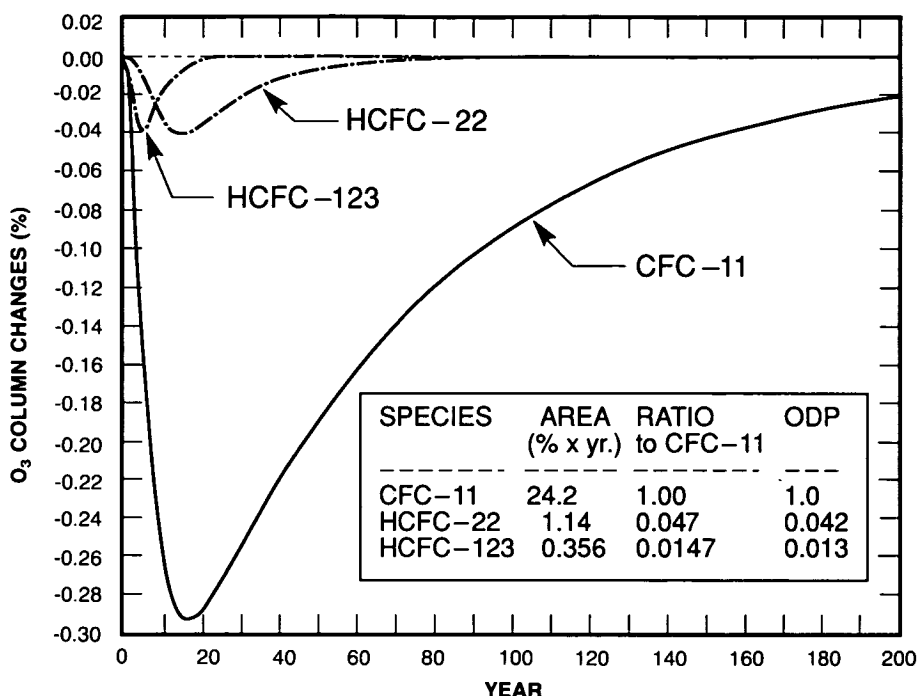


Figure 2. Calculated column ozone change following a pulsed input of 5×10^9 kg (for one year) of specified gas (DuPont 1-D model).

Sensitivity analyses indicate that ODPs are affected to only a minor degree ($\leq 20\%$) by assumed variations in background levels of N_2O , CH_4 , CO_2 , CO , total stratospheric chlorine, and total stratospheric bromine.

Halocarbon Global Warming Potentials

Halocarbon Global Warming Potential (GWP) is defined as the ratio of the calculated steady-state net infrared flux change forcing at the tropopause for any halocarbon for each unit mass emitted relative to the same for CFC-11. This definition quantifies the relative cumulative greenhouse warming per unit mass emitted.

Changes in the infrared fluxes in the surface troposphere system have been calculated for a number of these gases using a line-by-line radiative transfer model (GFDL). In addition, radiative forcing and surface temperature changes for these gases have been calculated using two one-dimensional radiative-convective models (AER and DuPont).

Halocarbon GWPs have been calculated from these results and scaled to a reference set of lifetimes (see Table 6). Agreement of ratio values is good, although direct radiative forcing values for individual gases differ systematically among models (between line-by-line and band models).

Halocarbon GWPs for fully halogenated compounds are larger than those for the hydrogenated halocarbons. Fully halogenated CFCs have halocarbon GWP values ranging from 1.0 to 7.5, whereas HCFCs and HFCs range from 0.02 to 0.7.

EXECUTIVE SUMMARY

Table 6. Halocarbon Global Warming Potentials (Halocarbon GWPs) scaled relative to reference set of halocarbon lifetimes.

Species	Reference ^a Lifetime (Yrs)	AER ^b	DuPont ^b	GFDL ^b
CFC-11	60.0	1.0	1.0	1.0
CFC-12	120.0	3.4	2.8	3.0
CFC-113	90.0	1.4	1.4	1.3
CFC-114	200.0	4.1	3.7	
CFC-115	400.0	7.5	7.6	7.4
HCFC-22	15.3	0.37	0.34	0.32
HCFC-123	1.6	0.020	0.017	0.017
HCFC-124	6.6	0.10	0.092	
HFC-125	28.1	0.65	0.51	
HFC-134a	15.5	0.29	0.25	0.24
HCFC-141b	7.8	0.097	0.087	0.084
HCFC-142b	19.1	0.39	0.34	0.35
HFC-143a	41.0	0.76	0.72	
HFC-152a	1.7	0.033	0.026	0.028
CCl ₄	50.0	0.34	0.35	
CH ₂ Cl ₂	6.3	0.022	0.026	

^aLifetimes are based on estimates used in scenarios development (Chapter 3 summary) for CFCs and from the analysis in the Ozone Depletion section for HCFCs and HFCs.

^bAER and DuPont results are based on surfaced temperature perturbations calculated using radiative-convective models. The GFDL results are based on line-by-line determined radiative forcing.

Halocarbon GWP values differ between species because of differences in infrared absorbances and differences in lifetimes. The range of absorbances is approximately a factor of 4, while the lifetimes vary by a factor of 250. Thus, the range of 600 among the halocarbon GWP values is primarily a result of differences in lifetimes.

Halocarbon GWP values are nearly insensitive to changes in background concentrations of CO₂, CH₄, and N₂O. Minor effects ($\leq 20\%$) do result from influences on chemical lifetimes, but these do not affect the relative radiative forcing.

Calculated time-dependent relative global warmings for halocarbons are initially on order unity, but decrease or increase depending on whether their lifetimes are shorter or longer than that of the reference gas. At long lifetimes the relative global warmings asymptotically approach halocarbon GWP values.

509401
166 PG

chapter **1**

N92-15431

POLAR OZONE

Coordinator

S. Solomon (USA)

Principal Authors

W. L. Grose (USA)

R. L. Jones (UK)

M. P. McCormick (USA)

M. J. Molina (USA)

A. O'Neill (UK)

L. R. Poole (USA)

K. P. Shine (UK)

S. Solomon (USA)

Other Contributors

R.A. Plumb (USA)

V. Pope (UK)

Chapter 1.

POLAR OZONE

TABLE OF CONTENTS

1.0	INTRODUCTION	1
1.1	CLIMATOLOGY OF THE OZONE TRENDS IN POLAR REGIONS	1
1.1.1	Ozone Measurements and Trend Detection	1
1.1.2	The Seasonal and Latitudinal Variability of Total Ozone	2
1.1.3	Observed Trends in the Total Ozone Column Content in Antarctica and Southern Mid-Latitudes	7
1.1.4	Suggested Explanations for the Antarctic Ozone Hole	15
1.1.5	Observed Trends in the Vertical Distribution of Ozone above Antarctica	17
1.1.6	Trends in Northern Hemisphere Ozone	20
1.2	CLIMATOLOGY OF POLAR STRATOSPHERIC CLOUDS (PSCs) IN BOTH POLAR REGIONS	23
1.2.1	Physical Characteristics	23
1.2.2	Seasonal Behavior of PSCs	27
1.2.3	Long-Term Trends in PSC Frequency and Intensity	33
1.2.4	Effect of PSCs on the Radiative Budget	36
1.3	PHYSICAL PROPERTIES OF POLAR STRATOSPHERIC CLOUDS	38
1.3.1	Laboratory Studies	39
1.3.2	Direct Supporting Evidence from Field Experiments	40
1.4	HETEROGENEOUS CHEMISTRY	43
1.5	GAS PHASE CHEMISTRY	45
1.5.1	Photochemical Processes of Importance in Polar Ozone Depletion	46
1.5.2	Laboratory Kinetics and Photochemistry	50
1.6	PHOTOCHEMISTRY OF THE ANTARCTIC SPRING	54
1.6.1	Reactive and Reservoir Chlorine	54
1.6.2	Reactive and Reservoir Nitrogen	62
1.6.3	Other Chemical Species	68
1.6.4	Modeling Studies of the Composition and Photochemistry	74

1.7	DYNAMICAL PROCESSES	82
1.7.1	Differences in Climatology Between the Two Hemispheres and Their Relationship to Observed Ozone Amounts	82
1.7.2	Role of Synoptic-Scale Disturbances	105
1.7.3	Processing of Antarctic Air	108
1.7.4	The Dilution Effect	110
1.8	TEMPERATURE TRENDS—CAUSES AND EFFECTS	117
1.8.1	Resume of Work Discussed by OTP (1989)	117
1.8.2	Other Recent Work	119
1.8.3	Causes of Temperature Trends	124
1.9	CALCULATED AND OBSERVED CHANGES IN ULTRAVIOLET RADIATION AT THE GROUND	127
1.10	ARCTIC PHOTOCHEMISTRY	130
1.10.1	Observations Prior to the 1988-1989 Arctic Winter	131
1.10.2	Conclusions from 1989 Research	138
1.11	PRINCIPAL CONCLUSIONS AND OUTSTANDING ISSUES	142
	REFERENCES AND BIBLIOGRAPHY	145

1.0 INTRODUCTION

The observation and interpretation of an unexpected, large ozone depletion over Antarctica (the ozone hole) has changed the international scientific view of stratospheric chemistry. The observations demonstrating the veracity, seasonal nature, and vertical structure of the Antarctic ozone hole are presented in Section 1.1, along with a brief description of the theoretical ideas first advanced to explain the phenomenon. Evidence for Arctic and mid-latitude ozone loss is also discussed. The chemical theory for Antarctic ozone depletion centers around the widespread occurrence of polar stratospheric clouds (PSCs) in Antarctic winter and spring; the climatology and radiative properties of these clouds represent the subject of Section 1.2. The clouds are believed to be of central importance in Antarctic ozone depletion because they provide a surface upon which important chemical reactions can take place that are not possible in the gas phase, and which greatly perturb the composition of the polar stratosphere. Laboratory studies of the physical properties of PSCs and the chemical reactions that likely take place upon them are described in Sections 1.3 and 1.4. Related gas phase chemical processes that subsequently influence ozone depletion are discussed in Section 1.5. Observations and interpretation of the chemical composition of the Antarctic stratosphere are described in Section 1.6, where it is shown that the observed, greatly enhanced abundances of chlorine monoxide in the Antarctic lower stratosphere are sufficient to explain much if not all of the Antarctic ozone decrease. The dynamic meteorology of both polar regions is the subject of Section 1.7, where important interannual and interhemispheric variations in dynamical processes are outlined and their likely roles in ozone depletion are discussed. Observations and interpretation of temperature trends in polar regions are reviewed in Section 1.8. Observations and calculations of changes in the penetration of ultraviolet radiation due to Antarctic ozone depletion are presented in Section 1.9. The photochemistry of the Arctic stratosphere in spring is described in Section 1.10, where the similarities and differences between the polar regions of the two hemispheres are explored. Finally, in Section 1.11 a summary is given of both the current state of understanding and outstanding issues.

1.1 CLIMATOLOGY OF THE OZONE TRENDS IN POLAR REGIONS

In this Section, ozone trends in polar regions are briefly reviewed; a more detailed and updated review of global ozone trends is the subject of Chapter 2 of this document. The distribution of total ozone deduced prior to the advent of the Antarctic ozone hole is first described and the primary processes that control the distribution of ozone in polar regions are identified. Such an understanding is critical to defining the background against which changes such as those associated with polar ozone trends must be evaluated and understood. Observations of the trends of total ozone in Antarctica are then summarized. It is shown that the Antarctic ozone hole originally detected by Farman et al. (1985a) has been confirmed with a broad range of studies from several international Antarctic stations as well as from satellite data. The observation of a dramatic hole in Antarctic ozone led to several important theories aimed at understanding its origin. These are briefly described in Section 1.1.4. Smaller observed trends at southern mid-latitudes may provide important clues regarding the mechanisms responsible for Antarctic ozone depletion, and are of interest in terms of the possible dilution of polar ozone decreases to lower latitudes (see Section 1.7). Observations of changes in the vertical distribution of Antarctic ozone and possible ozone changes in the Arctic and northern mid-latitudes are also discussed.

1.1.1 Ozone Measurements and Trend Detection

Worldwide ozone monitoring nominally began during the International Geophysical Year (IGY) in 1957, but only a very few stations have continuous records from 1957 to the present day. Ground-based total ozone monitoring is largely carried out using the ultraviolet absorption technique pioneered by Dobson.

POLAR OZONE

Satellite monitoring of total ozone began in 1970, and continuous global coverage dates back only to 1978. Satellite measurements of total ozone are principally based on detection of ultraviolet light backscattered from the troposphere (although research is underway to evaluate total ozone using infrared sensing methods). Thus, both routine ground-based and satellite observations are largely limited to those latitudes and seasons when the sun is above the horizon.

Detection of long-term trends is complicated by many factors including: a) natural variability, which must be estimated based on the available history of measurements and b) characterization of the long-term stability of the calibration of the instruments used. The absolute calibration of ground-based measurements can be tested and checked periodically. However, ground-based data from particular stations can be strongly influenced by natural fluctuations associated with variability in local dynamic conditions; these increase the variance of the data and therefore complicate attempts to deduce trends. In polar regions, local variability is particularly large due to steep latitudinal gradients in total ozone and large amplitudes of atmospheric waves (see Figure 1.1.2-3 below and Section 1.7). The extensive spatial coverage afforded by satellite data alleviates much of the local variability associated with single station measurements, but the absolute calibrations of many of the satellite instruments are subject to drift, which has not been measured while the instruments have been in space (a notable exception is the SAGE measurement technique, which is relatively insensitive to the absolute calibration). The shorter time history of the satellite ozone data as compared to some ground-based records also implies that less extensive temporal variability has been sampled (e.g., the variability associated with the 11-year solar cycle and its fluctuations from one cycle to another cannot be evaluated with a record as brief as 9 years). Use of both satellite and ground-based data sets in concert can greatly strengthen confidence in the trends evaluated from either in isolation, as discussed in detail by the International Ozone Trends Panel report (hereafter referred to as OTP, 1989).

1.1.2 The Seasonal and Latitudinal Variability of Total Ozone

Interest in atmospheric ozone was originally sparked by the work of Dobson and his collaborators, who correctly identified many of the factors that influence the column abundance and vertical distribution of atmospheric ozone. The relative magnitudes and changing roles of photochemical production, loss, and transport processes all play major roles in determining the ozone distribution. Figure 1.1.2-1 displays estimates of the time scale for photochemical destruction of ozone as a function of latitude and height for winter solstice from model calculations including a reasonably complete formulation of gas-phase photochemistry. Heterogeneous reactions and the subsequent photochemistry (see Sections 1.3–1.5) will markedly decrease the photochemical lifetime in polar regions in winter and spring, especially in the presence of polar stratospheric clouds and for anthropogenically perturbed chlorine abundances. Nevertheless, this figure provides useful insight into the behavior of the unperturbed stratosphere. Note the large seasonal differences in photochemical loss rates in polar regions, which are related to the seasonal cycle in solar illumination there.

Stratospheric ozone is produced primarily from photolysis of molecular oxygen, and its mixing ratio maximum occurs near 30–40 km, depending on season and latitude. The ozone concentration maximum is found at lower, denser levels near 15–30 km. In the lower stratosphere (below about 25 km), photochemical production of ozone is very slow due to the limited ultraviolet penetration to these levels, and the ozone densities there are dependent principally on a balance between downward transport from higher levels and local photochemical loss. Natural photochemical destruction of stratospheric ozone takes place mainly through catalytic cycles involving nitrogen and hydrogen free radicals (see for example, Brasseur and Solomon, 1984).

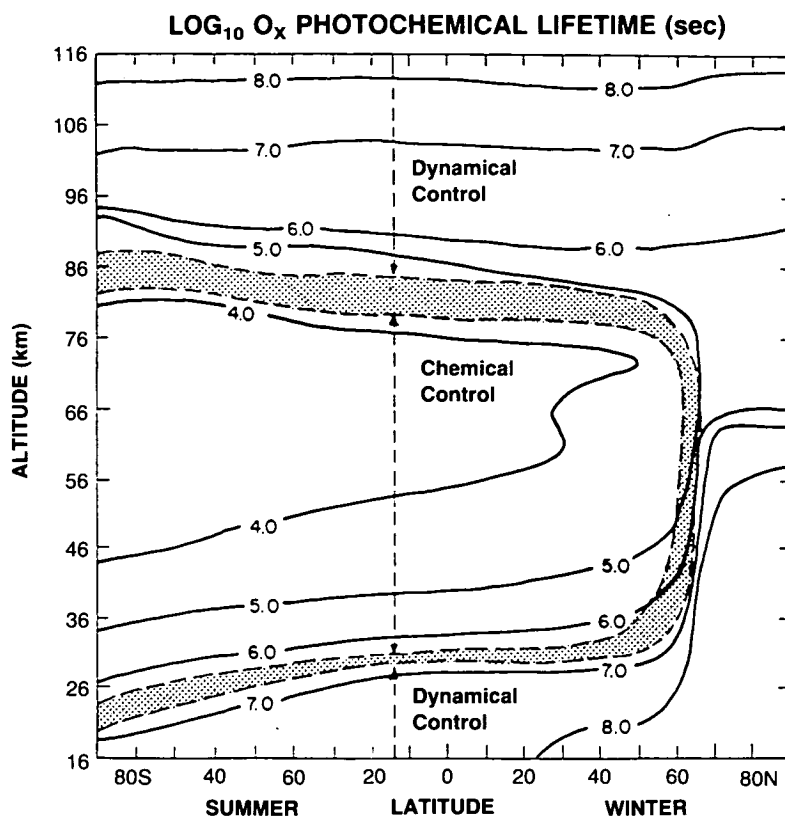


Figure 1.1.2-1 Logarithm of the computed lifetime of the odd oxygen family in Northern Hemisphere winter versus latitude and height, from the Garcia-Solomon two-dimensional model (from Garcia and Solomon, 1985). Regions dominated by chemical and dynamical processes are indicated.

The basic features of the seasonal evolution of total ozone in the northern and southern polar regions were first elucidated by Dobson and co-workers, who compared the earliest ground-based total ozone measurements from Halley Bay, Antarctica, to those from the Arctic station at Spitzbergen. Figure 1.1.2-2 displays the measured annual cycles of total ozone at the two stations. Dobson noted that these differences are indicative of fundamental asymmetries in the atmospheric dynamics of the Northern and Southern Hemispheres, which will be explored below and in more detail in Section 1.7. This natural difference in winter and spring ozone abundances between the two hemispheres should not be confused with the ozone hole.

Dobson et al. (1928) pointed out that total ozone minima are observed at tropical latitudes due largely to upward motion there, while ozone maxima are obtained in polar regions as a result of downward, poleward transport. Figure 1.1.2-3 displays the distribution of total ozone as a function of season and latitude as inferred from observations prior to the 1980s. A fall minimum of about 280–300 Dobson units (DU) is observed in both the northern and southern polar regions. Figure 1.1.2-1 suggests that photochemical destruction of ozone extends to very low altitudes in the summer season at high latitudes (Farman et al., 1985b). Thus, rapid chemical destruction of ozone is the primary cause of the observed fall minimum, and it is therefore not surprising that the two hemispheres exhibit similar values. However, as already noted, the interhemispheric differences in total ozone obtained in winter and spring attest to the important role

POLAR OZONE

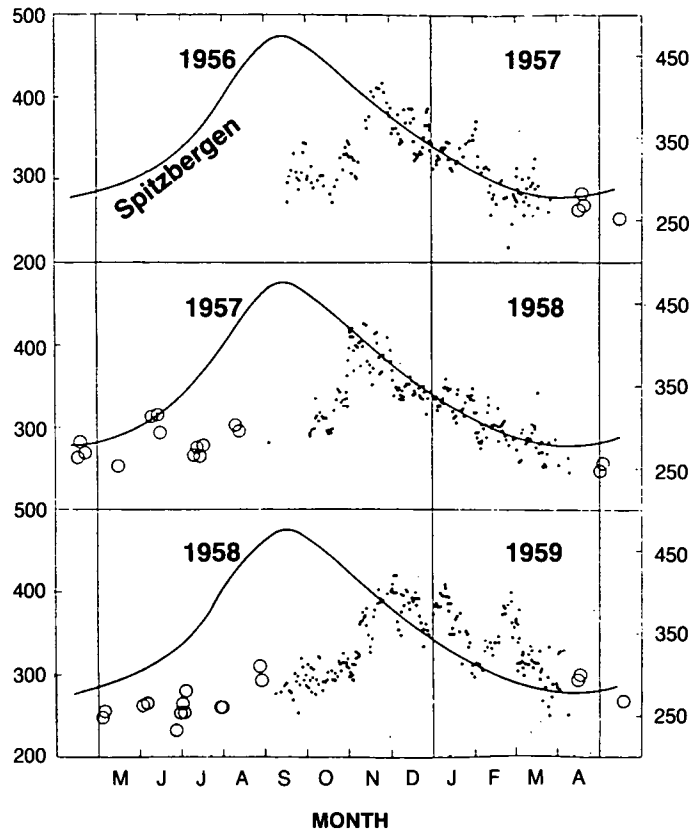


Figure 1.1.2-2. The first 3 years of ozone data from the Dobson instrument at Halley Bay, Antarctica, compared to average values observed at Spitzbergen (shifted by 6 months). Open circles indicate lunar Dobson measurements; closed circles are direct sun measurements (from Dobson, 1968).

played by atmospheric transport processes in determining the abundance of total ozone during those seasons, when photochemical processes are normally slow.

Examination of the temperature structure of the two hemispheres provides useful insights into the origin of the differences in the natural ozone distributions in the north and south polar regions. Figures 1.1.2-4 and 1.1.2-5 display observed seasonal cycles of the monthly and zonally averaged 50-mb temperature and total ozone abundances for 60°N, 60°S, 80°N, and 80°S, based on satellite data (Barnett and Corney, 1985; Keating and Young, 1985). The total ozone values are based on observations from about 1979 to 1982, when the Antarctic ozone hole was beginning to be detectable (see next section). The 50-mb level is located near the region of maximum ozone concentration at these latitudes. The temperatures near 50 mb are influenced by radiative heating and cooling as well as by dynamical heating and cooling associated with the mean meridional circulation. During winter when solar heat sources are absent, temperature increases are related, at least in part, to downward motion and associated warming by compression. Such downward transport will increase the total ozone abundance. The winter and spring dynamics of the two hemispheres (in particular, the observed behavior in 1987–1989) will be discussed in much greater detail in Section 1.7. Detailed reviews are also given by Koshelkov (1987), Koshelkov et al. (1987) and Tarasenko (1988). Here we seek only to establish a very general basis for understanding the natural distribution of total ozone as a framework for discussion of possible trends and their causes.

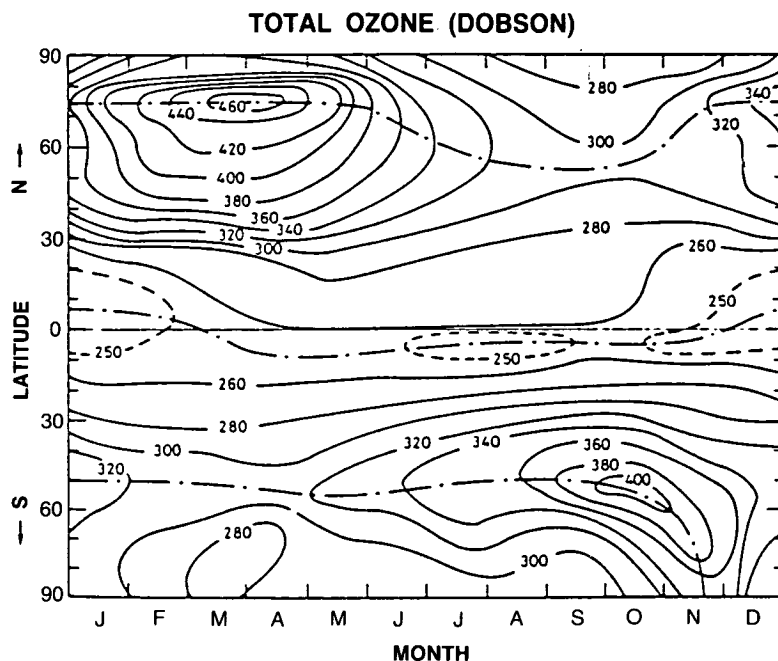


Figure 1.1.2-3. Observed global variation of total ozone with latitude and season, based largely on Dobson data (from London, 1980).

Figure 1.1.2-4 shows that the total ozone abundances observed at 60°N from about May through October are very similar to those observed at 60°S in the conjugate months from November to April. The temperatures are nearly the same in the two hemispheres during these summer and early fall months as well. Temperature and ozone differences begin to increase in early winter (Nov-Dec in the Northern Hemisphere as compared to May-June in the Southern Hemisphere), and very large differences of about 12 K and 50–100 DU, respectively, are obtained by early spring. The differences both in ozone and in temperature reflect the greater planetary wave activity and stronger downward transport characteristic of the Northern Hemisphere winter.

The Southern Hemisphere temperatures remain cold much later in the spring season than those in the Northern Hemisphere. The total ozone increase observed in October at 60°S is associated with a rapid rise in temperature. It is therefore likely to be the result of rapid poleward transport of ozone associated with the final stratospheric warming and should be expected to vary from one year to another in association with the timing and characteristics of stratospheric warmings. The seasonal variations of total ozone and temperature at 80°N and 80°S , and the differences between them, display similar features to those obtained at 60°N and 60°S . Temperatures and total ozone abundances in the two hemispheres are comparable in summer and fall. The total ozone abundance drops to about 300 DU in both hemispheres by fall. In the Southern Hemisphere, zonally averaged winter temperatures drop to a minimum near 185–190 K in winter and spring, and the total ozone remains relatively constant at about 250–300 DU until the temperatures rise dramatically in late spring, when the total ozone also increases. Because of greater wave activity in the Northern Hemisphere, temperatures are on average warmer and ozone levels higher than those of the Southern Hemisphere. Such variations in total ozone are reproduced rather well by three-dimensional models such as the one by Cariolle et al. (1986) and in two-dimensional simulations including for example, that of Stordal et al. (1985).

POLAR OZONE

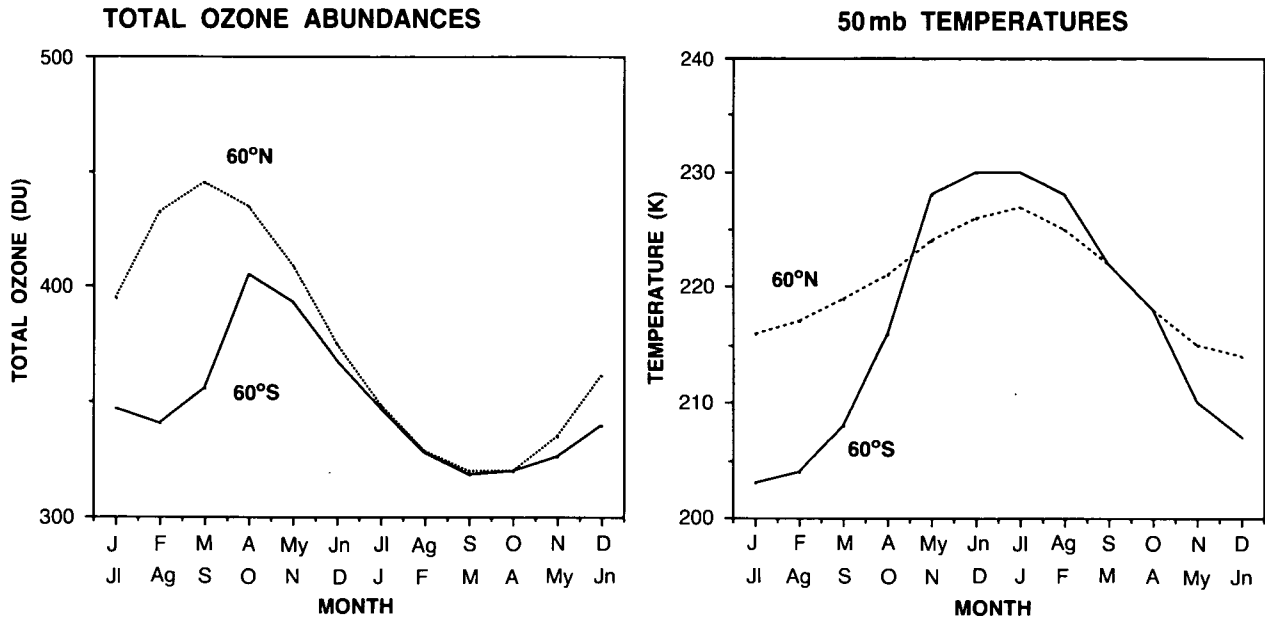


Figure 1.1.2-4. Seasonal cycles of total ozone and 50 mb temperatures at 60°N (January-December) and 60°S (July-June). The total ozone is taken from Keating and Young (1985) and is based upon satellite observations from 1979-1982, while the temperature data are taken from the climatology compiled by Barnett and Corney (1985).

Although the data are limited in the polar night region, Figure 1.1.2-3 suggests that the total ozone abundances in both hemispheres decrease towards the pole. This latitudinal gradient does not necessarily indicate destruction of ozone. Rather, the center of the winter polar vortex should be expected to be very cold in both hemispheres, due in part to slower downward transport than that of the surrounding region.

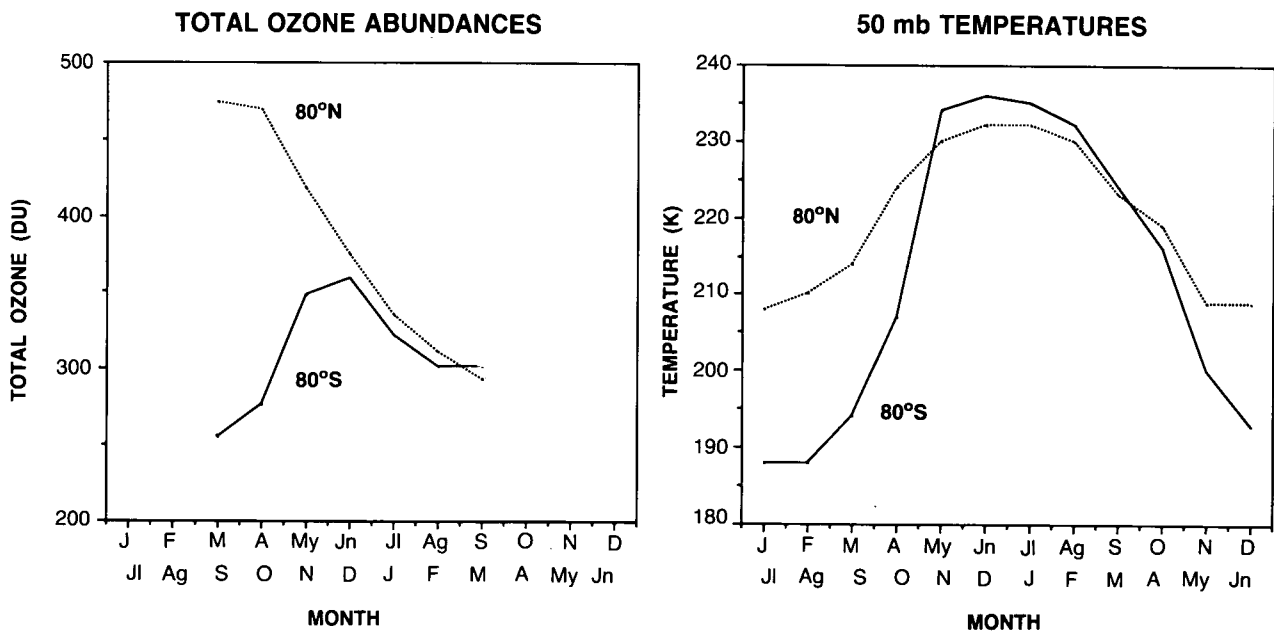


Figure 1.1.2-5. As in Figure 1.1.2-4, but for 80°N (January-December) and 80°S (July-June).

Further, any horizontal transport of ozone from lower latitudes will reach the vortex later than the surrounding sub-polar latitudes. Near the heart of the cold winter polar vortex, ozone levels can therefore remain comparable to the low values obtained in fall (following the chemical destruction obtained in that season), while the surrounding “collar” region is likely to exhibit higher ozone levels due to transport processes. Note that zonally and monthly averaged temperatures and total ozone values may not reflect those of the core of the vortex, especially in the Northern Hemisphere where the vortex is often centered far from the geographic pole.

In summary, polar total ozone in the Southern Hemisphere exhibits the following natural annual cycle: a summer and early fall minimum due primarily to photochemical destruction, then followed by fairly constant low values in winter and early spring associated with very cold temperatures, culminating in a rapid spring increase associated with downward poleward transport during and after the final stratospheric spring warming. In the Northern Hemisphere, warmer winter temperatures indicate greater planetary wave activity and mean descent and hence are associated with larger, increasing total ozone levels through the winter (at least for latitudes equatorward of the heart of the polar vortex). The timing and nature of the spring warming play an important role in determining the springtime ozone increases in both hemispheres.

1.1.3 Observed Trends in the Total Ozone Column Content in Antarctica and Southern Mid-Latitudes

The British Antarctic Survey station at Halley Bay is one of the few worldwide ozone monitoring stations whose record extends back to the late 1950s. Farman et al. (1985a) presented observations of total ozone from Halley Bay (76°S) and the Argentine Islands (66°S) which showed that the total ozone abundance had dropped noticeably over both stations during the period from about the mid-1970s to the mid-1980s, although a small decrease may have occurred even earlier. The changes were much larger at Halley Bay than over the Argentine Islands, and were most pronounced in October, when the total ozone levels above Halley Bay in 1984 were only about 60% as large as those obtained in the late 1950s and early 1960s. A much smaller decrease (5–10%) was also apparent in summer. The strong seasonal asymmetry in the apparent trend suggested that it was unlikely to be a result of calibration errors.

Other observations quickly confirmed the veracity of this remarkable ozone trend. Stolarski et al. (1986) presented total ozone measurements from 1978 through 1986 from the TOMS (Total Ozone Mapping Spectrometer) instrument, displaying the same general trend and seasonal structure. They also pointed out that the ozone changes apparently took place largely in September rather than in October and that the ozone actually decreased rapidly during that month. Thus it was clear that the ozone trend was not due to lower abundances at the end of fall or winter, but was actually characterized by relatively “normal” levels at the end of winter followed by a rapid spring decrease. It is this spring decrease that is now clearly identified with the Antarctic ozone hole. They also noted that polar ozone levels were apparently influenced by the tropical Quasi-Biennial Oscillation (QBO), such that easterly (westerly) phase years exhibited larger (smaller) mean levels of total ozone. The dynamics of the QBO and further discussion of the QBO signal in ozone measurements will be presented in Section 1.7.1.

Chubachi (1984; 1986) and Sekiguchi (1986) showed that the Japanese Antarctic research station at Syowa (69°S) displayed a comparable trend in October, and Komhyr et al. (1986) demonstrated that large October decreases in total ozone had also been obtained at the South Pole.

POLAR OZONE

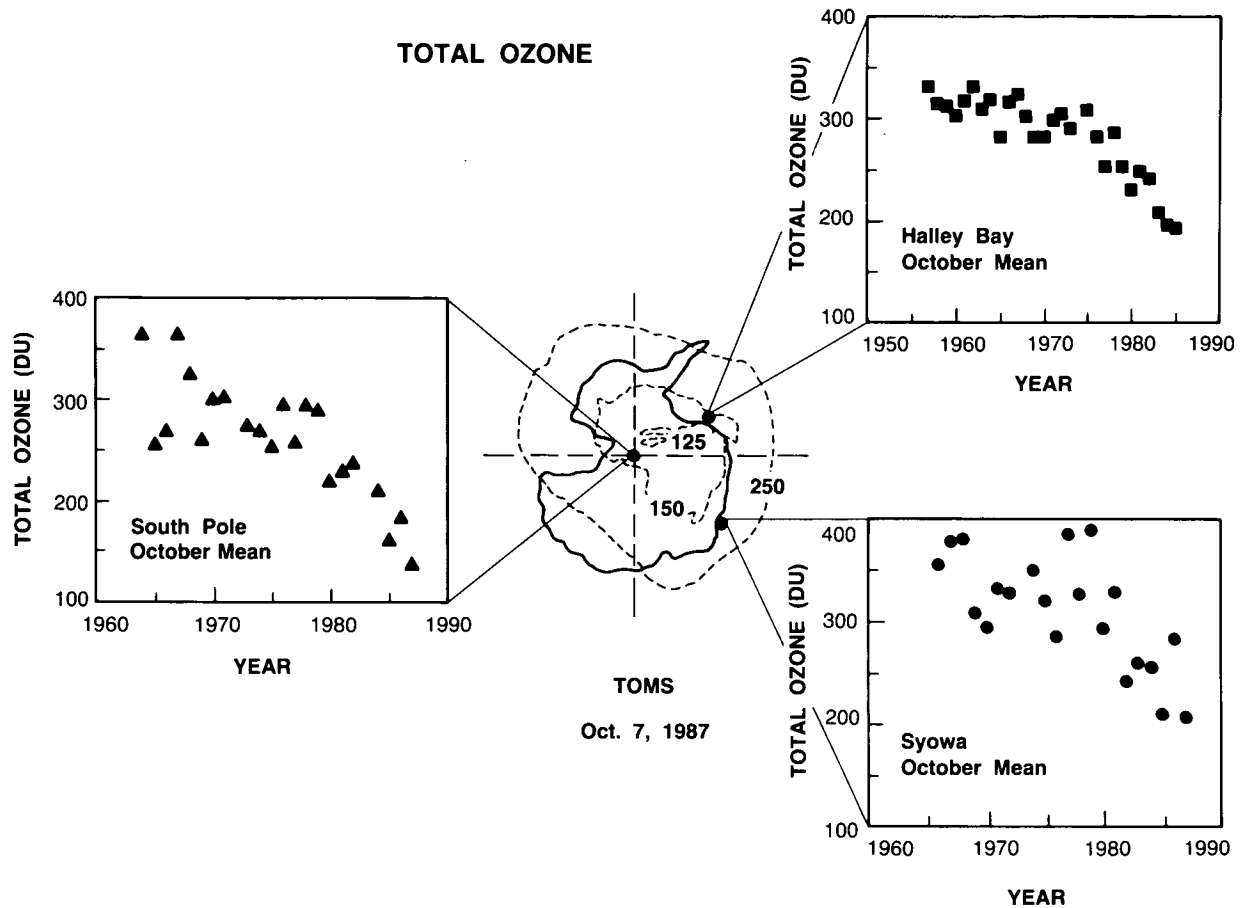


Figure 1.1.3-1. Observed long-term trends in total ozone from the ground-based Antarctic stations at Syowa, Halley Bay, and the South Pole.

Figure 1.1.3-1 is a composite of long-term total column observations in October from Syowa, Halley Bay, and the South Pole. It is clear that all three stations exhibit a substantial decrease in total ozone beginning sometime in the late 1970s or early 1980s. Underlying the station observations is a TOMS map of total ozone obtained in early October 1987, when the Antarctic ozone hole was extremely pronounced. The very low minimum values of total ozone below 125 DU can be compared with levels of about 250 DU observed in 1979, although the data from Halley Bay and later discussion presented here suggest that 300 DU may be more representative of the “undisturbed” value.

Figure 1.1.3-2 displays the monthly mean minimum October total ozone values obtained from TOMS satellite data, along with measurements of the Singapore zonal wind speeds at 30 mb, illustrating the QBO fluctuation. Garcia and Solomon (1987) showed that the minimum temperatures within the polar vortex were strongly modulated by the QBO (with the westerly phase years being colder by some 5–8 K) and summarized evidence for a substantial QBO signal in Antarctic ozone and in the ozone trend. Angell (1988a) showed that the association between the QBO and Antarctic ozone is statistically significant in the long-term record (from the mid-1960s) using ground-based data. Many other authors have also commented on the association between extra-tropical ozone and the QBO. The mechanism is not at all well understood, but the apparent correlation is particularly strong in Antarctica.

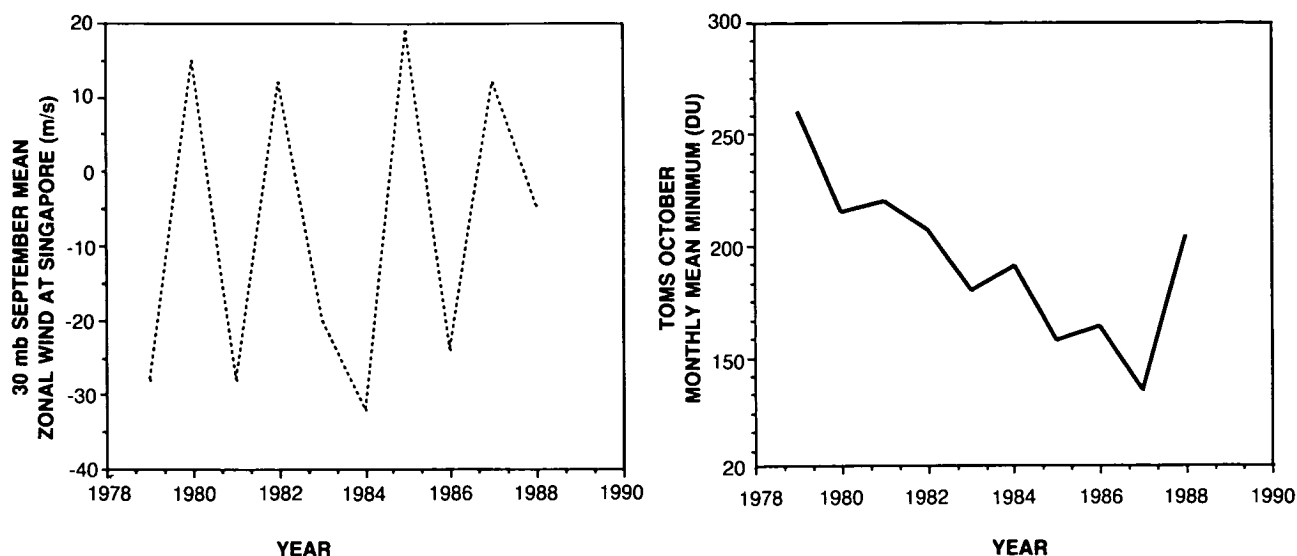


Figure 1.1.3-2. TOMS October monthly mean minimum total ozone measurements along with equatorial zonal wind speeds. Periods of strong westerly QBO phase are indicated (adapted from Garcia and Solomon, 1987).

The association of the QBO with temperature variations suggests that the QBO modulates the meridional circulation and thus the transport of ozone. It is also true that any temperature-dependent destruction processes should be influenced by the observed temperature fluctuations (see Sections 1.3 and 1.4). Regardless of the mechanism, the correlation between ozone and the QBO phase is quite strong and apparently plays a major role in modulating Antarctic ozone abundances in spring. It is worthy of note that the mean period of the QBO is about 28 months (Naujokat, 1986) rather than 24 months, so that the cycle does not necessarily alternate from one austral spring to the next. While October 1987 was an unusually cold month in south polar regions and one of strong westerly QBO phase, 1988 was considerably warmer and the QBO phase was easterly near 10 to 30 mb. The next westerly phase period should be expected to occur after the 1989 austral spring if the mean period of 28 months is followed, so that relatively high ozone levels may also be anticipated in austral spring 1989, with the next cold, westerly phase austral spring likely to occur in 1990. Note that both sets of years of like phase exhibit long-term decreases (i.e., a trend is seen in the easterly phase years of 1979, 1982, 1984, 1986, and 1988, as well as in the westerly phase years of 1980, 1983, 1985, and 1987). If the past correlation between the QBO and the ozone hole continues, then the ozone depletion ought to be relatively modest in 1989 but quite deep in 1990 (note, however, that the QBO period can vary by as much as 8 months). The next few years should therefore provide an excellent test of the relationship between the QBO and the Antarctic ozone hole.

All of the measurements indicated in Figure 1.1.3-1 were obtained with ultraviolet absorption methods, as already noted. While this is the sole historical means of measurement of total ozone, it must also be asked whether there is any possibility that the apparent trends might arise from instrumental effects (e.g., changes in the propagation of ultraviolet radiation associated with enhanced particulate matter or other interfering agents). Observations of the vertical profile of ozone obtained with ozonesondes provide a partial check on the ultraviolet absorption measurements, as will be shown in the Section 1.1.5. However, ozonesondes do not measure the total profile and are sometimes normalized to Dobson measurements of the total column, so that the two methods may not provide independent information. Observations of the rate of decline in total ozone obtained in a particular season in the contemporary Antarctic atmosphere

POLAR OZONE

place a further important check on possible measurement errors, since they have been carried out with a variety of techniques including infrared and visible absorption, as well as ozonesondes. Such measurements also place important constraints on the rates of processes responsible for the ozone hole.

Figure 1.1.3-3 shows observations of the total column abundance above McMurdo Station (78S) in September and October 1986. Large local fluctuations are apparent as noted earlier. These were clearly associated with warm air advected from lower latitudes (Mount et al., 1987). The measurements by TOMS, ozonesondes, infrared and visible absorption are all in fairly good agreement with one another, and display values below 200 DU by late October. Figure 1.1.3-4 shows a similar comparison for 1987, when the dynamical conditions above McMurdo were somewhat less variable, along with measurements of the TOMS minimum ozone within the vortex. These data show that a rapid decline in total ozone is observed in September (days 244 through 273) with four independent methods, eliminating any possibility that its origin is instrumental. It is clear that the overall levels are generally larger at McMurdo than they are at the ozone minimum, but the observed rate of decrease is comparable, about 1%/day, showing that the maximum rate of decline is not confined to the ozone minimum. The observed trends occur over a broad region extending throughout much of the polar region. The latitude dependence of the trends will be discussed quantitatively below. Stolarski et al. (1986) noted that the rate of decline of the ozone minimum in September 1983 was 0.6%/day. This and the more detailed study by Lait et al. (1989) suggest that the rate of ozone loss may have increased, a topic which will be discussed further below.

The observations from Halley Bay suggest that historical levels of springtime total ozone were about 300 DU in October. Gardiner and Shanklin (1986) also noted that the historical total ozone levels averaged from 1957 through 1973 at Halley Bay for September 1-5, 6-10, 11-15, 16-20, 21-25, and 26-30 were 294,

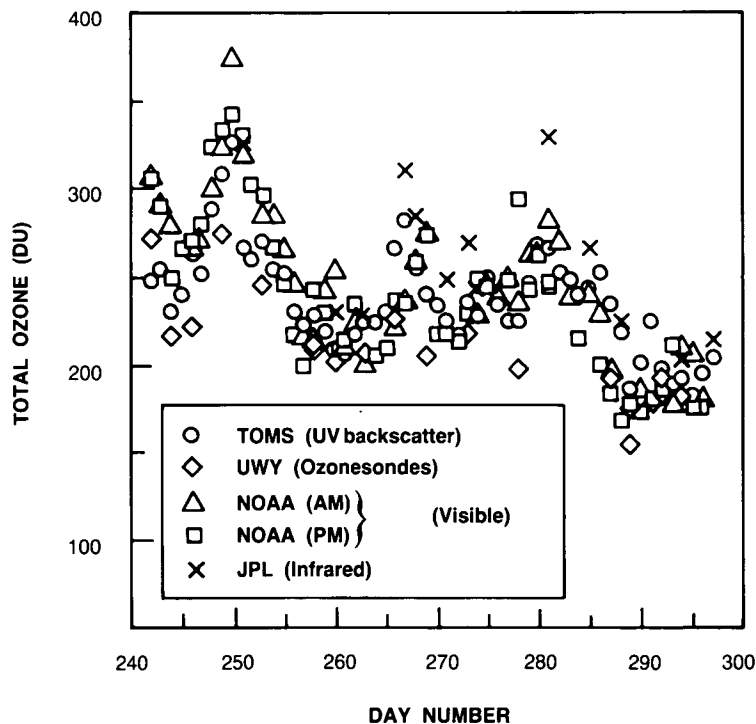


Figure 1.1.3-3. Seasonal decline in total ozone above McMurdo Station in 1986 as deduced by visible, ultraviolet, and infrared spectroscopy, as well as from (unnormalized) ozonesonde observations.

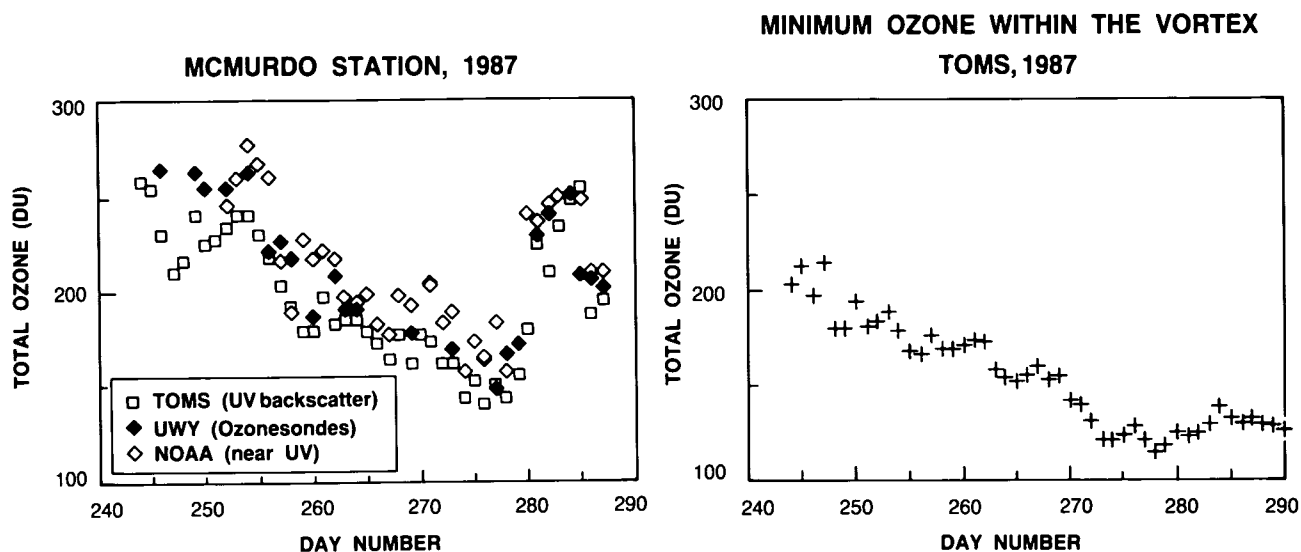


Figure 1.1.3-4. (Left) Same as Figure 1.1.3-3, but for 1987. (Right) Seasonal decline in the daily TOMS ozone minimum during 1987.

282, 306, 299, 299, and 302 DU, respectively. Thus the ozone did not decline during September in historical years. It is therefore critical to note that the ozone hole has been associated with a fundamental change not just in the magnitude of October ozone abundances, but in the character of the ozone seasonal cycle in Antarctica.

The Halley Bay ozone measurements indicate a small decrease in summer compared to historical data, by perhaps 10–20 DU. These data taken together with historical Halley Bay and South Pole ozone measurements in October and September imply that estimation of the depth of the ozone hole in any particular year in the present day atmosphere should be based on comparison to 300 DU, rather than to the contemporary values observed in late August (since these may reflect a partial depletion). It is important to consider whether the smaller summertime Antarctic ozone changes represent a residual of the spring changes or are associated with some other mechanism. This issue will be discussed somewhat further in Sections 1.7 and 1.8.

We now consider the latitude dependence of the ozone trends in somewhat greater detail. The number of ground-based stations in the Southern Hemisphere is quite limited outside Antarctica, and the local dynamics influencing the region of maximum ozone at southern mid-latitudes can influence the trends derived from single-station measurements. The analysis by Bojkov (1986) suggested no apparent trend in Southern Hemisphere total ozone records, but the study of TOMS data presented in the OTP report suggested that this may be due to changes in the location (but not necessarily the magnitude) of the ozone maximum.

Figure 1.1.3-5 presents a contour plot of the percent changes versus month and latitude band from TOMS measurements over the period from 1979 to 1988 based on a linear trend analysis. The TOMS data have been corrected for a long-term drift, based on comparison with ground-based data (OTP, 1989). The correction is about 3.5% from 1978 to 1987. The possibility of latitude dependence in the correction factor is also important, but has not been evaluated quantitatively. Analyses of Northern Hemisphere ground-

POLAR OZONE

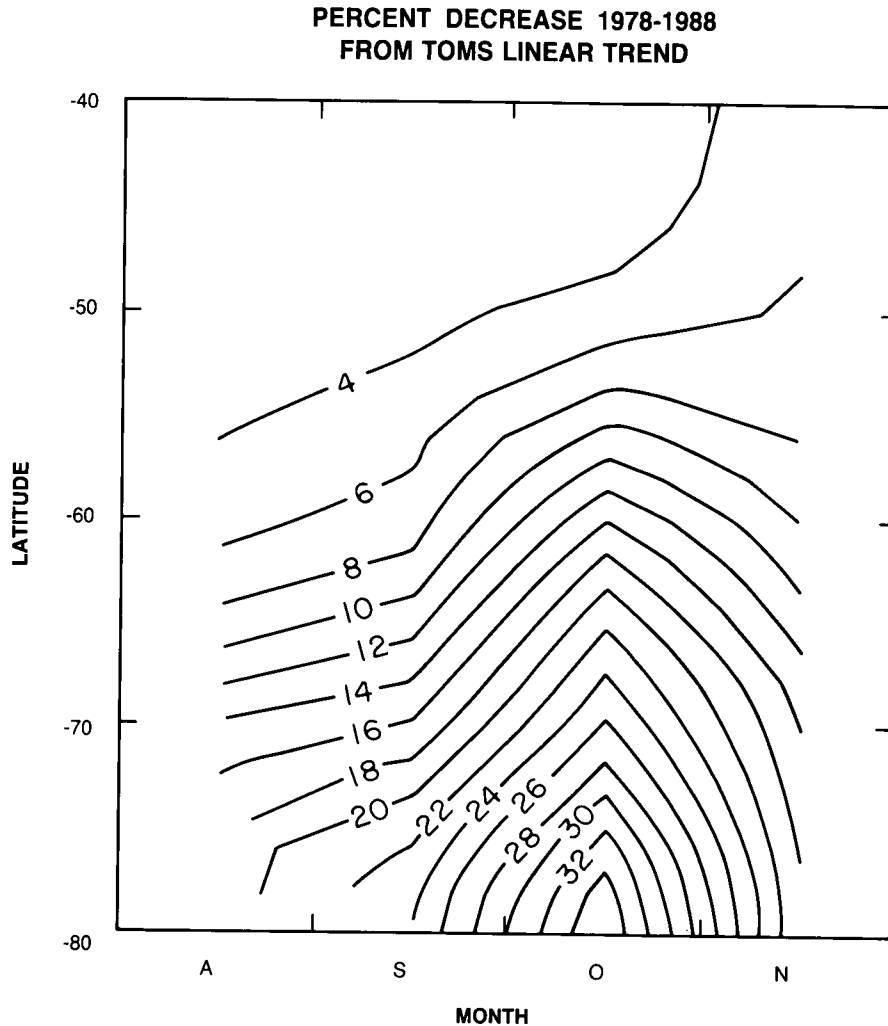


Figure 1.1.3-5. Contour plot of the ozone decrease obtained from 1978-1988 derived from a linear trend analysis of the TOMS measurements (Stolarski, personal communication, 1989).

based data suggest that the 11-year solar cycle is likely to cause a downward trend in total ozone of at most a few percent over this period (Angell, 1988a; OTP, 1989), much smaller than the measured decreases in polar regions. The seasonal variations in these trends are of particular importance with regard to their possible causes. The largest trend of about -34% is deduced near 80°S for the month of October. The magnitude and timing of the trend near 60°S suggests that it may largely be due to spreading, or dilution, of the high latitude depletion. Figure 1.1.3-5 suggests that a good deal of the trend obtained at 50°S in October may also be due to dilution of the polar depletion. Atkinson et al. (1989) pointed out that unusually low ozone abundances obtained over Australia and New Zealand in December 1987 appeared to be linked to transport of air that had been severely depleted in ozone from Antarctica to lower latitudes, especially in association with the final stratospheric warming. It has been suggested that flow of air through the vortex and out to lower latitudes can occur not only in association with vortex breakup, but perhaps throughout the winter and spring (see Section 1.7). Under these circumstances, the ozone trend at latitudes as far equatorward as 50°S could well occur earlier in the spring season than that in the center of the polar vortex

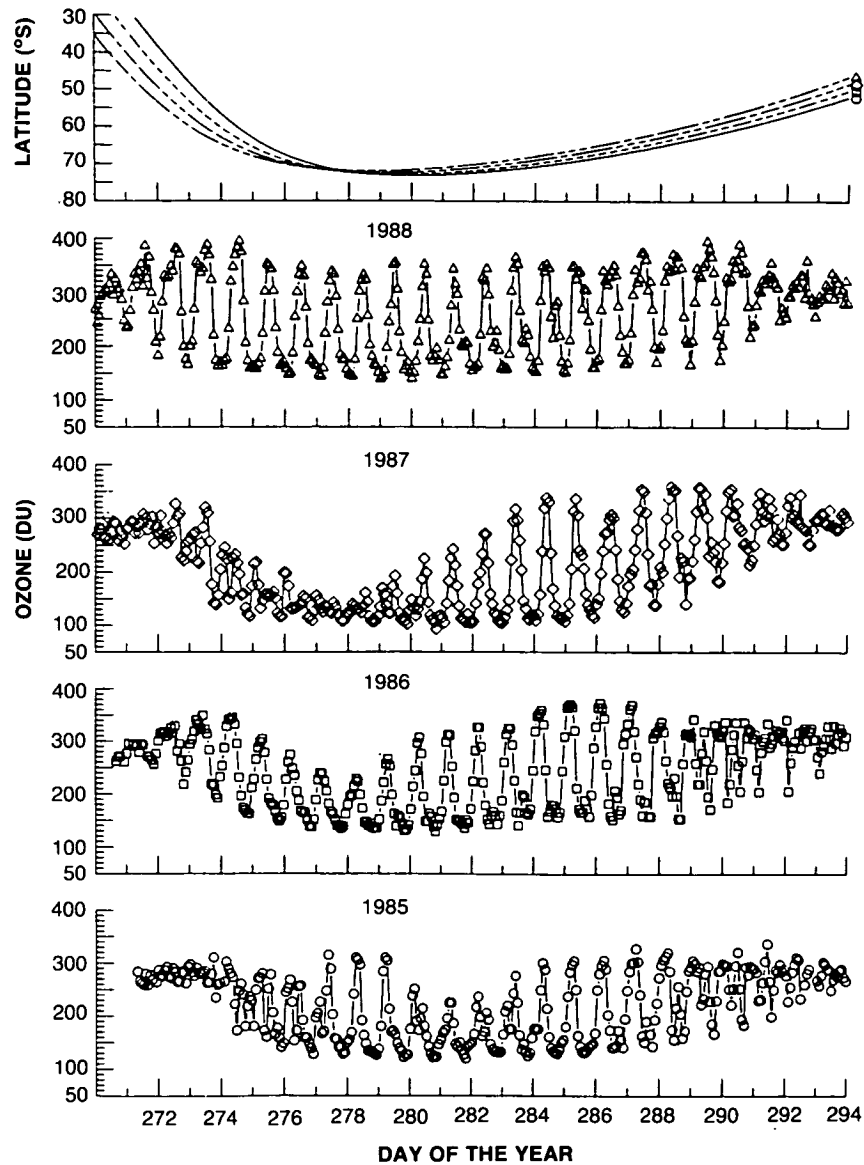


Figure 1.1.3-6. SAGE II total column ozone above 100 mb for all measurement events from day 270 through 293 (September 27- October 20, 1985, 1986, and 1987; September 26-October 19, 1988). Latitude coverage is shown in the top panel for each year. Minimum total ozone ranged from 120 to 126 DU in 1985, 128 to 135 DU in 1986, 101 to 109 DU in 1987, and 140 to 145 DU in 1988 (an update of Figure 2 in McCormick and Larsen, 1988).

and would not necessarily appear as a spreading with a time delay. It is clear, however, that a substantial fraction of the trend at lower latitudes (40°S and 50°S) does not lag those observed in the polar regions; a decrease of the order of 3–4% is indicated even in August and September. Thus, the possible spread of Antarctic ozone depletion to lower latitudes appears difficult to quantify with present observations.

Satellite measurements of ozone have also been obtained by the Stratospheric Aerosol and Gas Experiment II (SAGE II) since October 24, 1984, using a solar occultation technique. Description of the

SAGE II OZONE HOLE OBSERVATIONS
O₃ (DU)

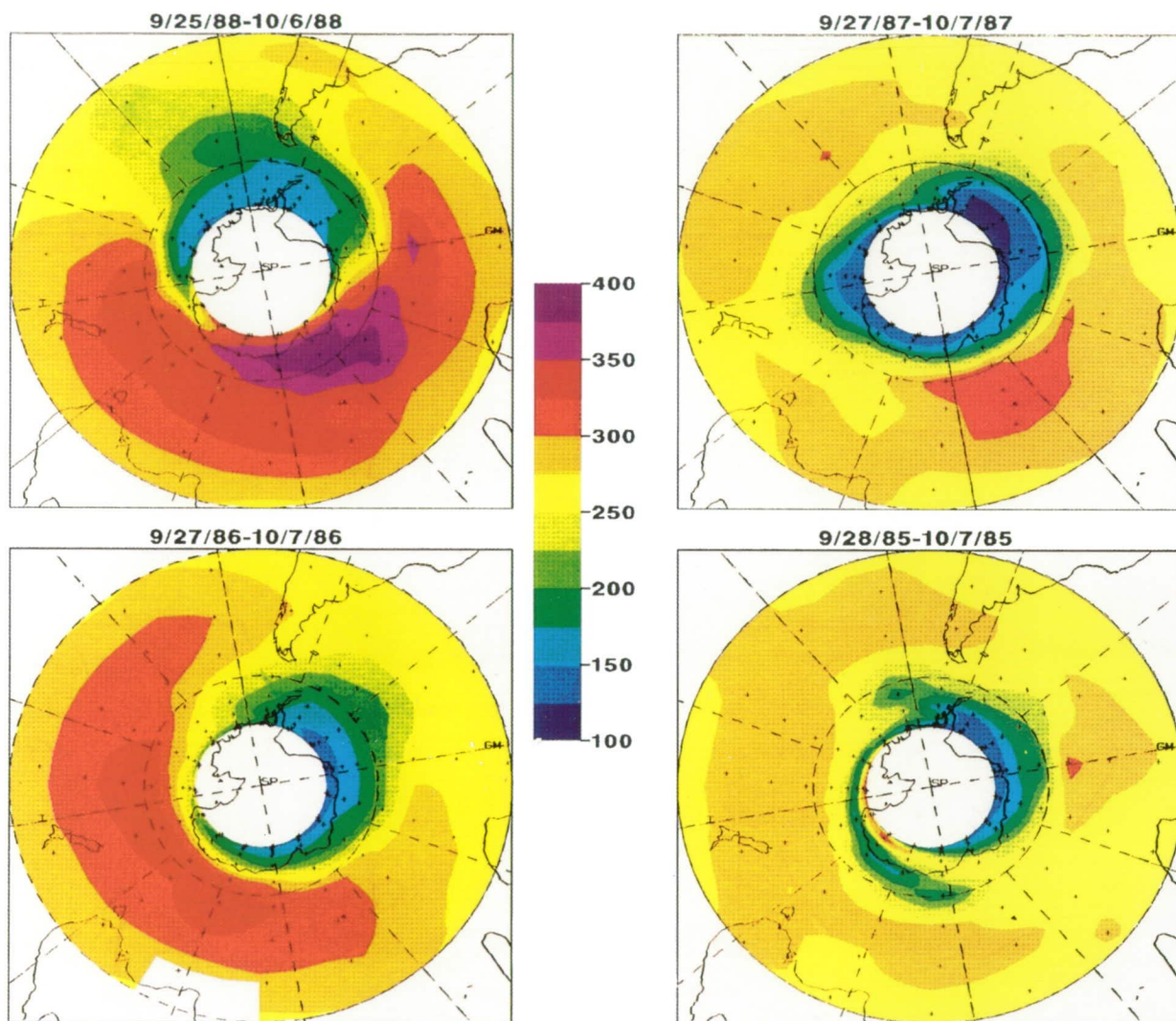


Figure 1.1.3-7. False color images of SAGE II total column ozone above 100 mb for 1985 through 1988. The images are built up as the SAGE II measurement latitude circle moves southward from 30°S in late September to 72°S in the first week of October. The +’s in each figure indicate measurement locations. The ozone ridge and chemical depletion region are quite evident in these images and display a QBO-type response from year to year. Although short-term distortions of the vortex can drastically change the areal extent of the depletion region, the year-to-year trend in ozone depletion minimums and ridge maximums are in agreement with other reported measurements.

ORIGINAL PAGE
COLOR PHOTOGRAPH

instrument, inversion algorithm, and error analysis may be found in Chu et al. (1989) and references therein.

Figure 1.1.3-6, an update of Figure 2 in McCormick and Larsen (1988), shows the variation of total column ozone above 100 mb along a sunset measurement sweep into and out of the Antarctic region for 1985, 1986, 1987, and 1988 in early October. Distortions and displacements of the vortex from the pole allow SAGE II to obtain measurements from the ozone ridge to near the center of the vortex, thus producing the cyclical variations in total ozone apparent in Figure 1.1.3-6. Low total ozone is generally associated with the colder temperatures inside the vortex. Figure 1.1.3-7 shows that in 1985 the minimum total ozone above 100 mb fell in the range of 120 to 126 DU, while in 1986 it ranged from 128 to 135 DU. The greatest ozone depletion to date was for 1987, with most minimum values falling in the 101 to 109 DU range and one profile displaying 93 DU. The 1987 measurements also show the smallest variation from profile to profile, suggesting a depletion region larger areally and more symmetric about the pole. In 1988, however, ozone minima increased to levels of 140 to 145 DU. These data also show the strong depletion of Antarctic ozone, and suggest significant correlation of the depletion with the phase of the QBO as discussed above.

Figure 1.1.3-7 displays gridded SAGE II total column ozone distributions above 100 mb for years 1985 through 1988. The measurements start at 30°S in late September and finish at 72°S in early October. Low levels of total ozone in the region of the polar vortex are produced by ozone depletion occurring from mid-August through the first week of October. The ozone map also displays a ridge of high ozone that is produced by transport from mid-latitudes and minimal horizontal mixing across the vortex edge. The QBO signal is evident in both the minimum level within the chemical depletion region and the ridge values outside the vortex. A long-term trend in Antarctic ozone was also clearly detected by SAGE measurements (OTP, 1989).

In summary, there is no question that a pronounced change in springtime Antarctic ozone has occurred, based on a broad range of satellite and ground-based measurements employing a variety of instrumental techniques. The ozone decrease occurs rapidly during the month of September. Sources of natural variability (such as the QBO) must be considered and do influence year-to-year fluctuations.

1.1.4 Suggested Explanations for the Antarctic Ozone Hole

The discovery and verification of the Antarctic ozone hole quickly prompted theoretical studies aimed at understanding its origin. The fact that the ozone hole was largely confined to Antarctica provided some important guidelines for possible mechanisms, but also meant that the available data to test and verify theoretical notions were sorely lacking. Indeed, apart from the observation that ozone itself had declined precipitously, little else was known about the chemical composition of the Antarctic stratosphere. Meteorological data, while less extensive than those available at other latitudes, did suggest that there had been a significant cooling in the austral spring (Angell, 1986; see Section 1.8 for a detailed discussion). The paucity of detailed observations led to the inception of three very different and, in some respects, contradictory hypotheses to explain the Antarctic ozone decline. In this section, the basic elements of the three theories will be briefly described. The theories will be discussed further in the context of the data that allowed discrimination between them in the later sections of this chapter.

Tung et al. (1986) and Tung (1986) considered the forcing of the Antarctic mean circulation. They noted that the Antarctic stratosphere reaches temperatures approaching radiative equilibrium in late winter and spring. As the lower stratosphere cools, the infrared cooling rate approaches zero, so that the net heating is given by ultraviolet heating alone. They suggested that the return of sunlight to polar regions

POLAR OZONE

could then lead to net upward motion, bringing ozone-poor air from lower altitudes up to the heart of the ozone layer and causing the seasonal decline. Mahlman and Fels (1986) also examined the possibility of upward motion in spring, and pointed out that reduced wintertime planetary scale wave activity might lead to reduced downward transport of ozone during winter and spring. This in turn would be expected to lead to a colder polar stratosphere at the end of the polar night, and thus a greater tendency for springtime upward motion. These dynamical theories thus rested primarily on the extreme coldness of the Antarctic stratosphere to explain the appearance of the ozone hole uniquely in Antarctica, and required a temporal trend in Antarctic dynamics to explain the decadal trend. Possible sources for such a decadal trend included the influence of volcanic aerosols on the radiative balance (Tung et al., 1986) and/or dynamical factors influencing the dynamical forcing of the Antarctic circulation, such as changes in sea surface temperatures or tropospheric dynamics (Mahlman and Fels, 1986; Nagatani and Miller, 1987; Dunkerton, 1988).

It was clear that the seasonal evolution of the ozone depletion and any associated lower stratospheric temperature trends were important elements in these dynamical theories. If the ozone decrease were caused by upward motion, then a temperature decline should be expected to occur before, or simultaneously with, the ozone decline (i.e., if the ozone declines in September then the temperature decline must precede or accompany it). When the dynamical theories were first suggested, little information was available on the temporal evolution of the ozone decline; it was not known whether the observed Halley Bay ozone trend actually occurred during October, or earlier in the spring season. Later studies established that the decline occurs largely in September (Section 1.1.3), providing an important observational constraint against which any theory should be tested.

It is also important to note that ozone provides the primary source of solar heating to the Antarctic lower stratosphere. Thus, a decline in ozone should be expected to result in a decline in temperature somewhat later in the spring season (Shine, 1986). This underscores the importance of identifying not only the existence of any temperature trends, but also their timing relative to the ozone trend. It is the timing (phase lag or phase lead) that is a critical component in distinguishing whether any observed temperature trends constitute a cause or an effect.

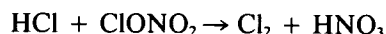
Two fundamentally different chemical theories were also proposed to explain the ozone decline. Figure 1.1.2-1 shows that photochemical processes are expected to take place only very slowly under normal conditions in the polar winter and spring. Therefore, any photochemical means of destroying ozone in this region must rely upon a dramatic change in photochemical time scales.

Callis and Natarajan (1986) considered the production of reactive nitrogen (NO_x) in the upper atmosphere. They noted that the intense solar maximum that occurred near 1980 might have produced large amounts of NO_x in the mesosphere and lower thermosphere. If this NO_x could be transported to the stratosphere, it could potentially deplete ozone photochemically following the spring return of sunlight to polar regions. Such transport would occur primarily in the polar night (since NO_x is rapidly destroyed in the sunlit mesosphere) and might be expected to be most effective in the relatively isolated Antarctic polar vortex as compared to the Arctic. Thus, this theory rested on the importance of solar activity in producing NO_x , its downward transport to the stratosphere in the polar night, and the subsequent destruction of ozone following the return of sunlight to the polar cap. Callis and Natarajan (1986) discussed satellite observations that indicated that a temporal increase in NO_2 might have occurred from about 1979 to 1983.

Several authors considered the possibility that chlorine chemistry and/or the coupling between chlorine and bromine chemistry might be responsible for the ozone decline. As noted by Farman et al. (1985a), the clear increase in chlorine abundances that occurred over the time scale during which the ozone hole

developed (late 1970s to early 1980s) suggests that chlorine chemistry should be considered as a possible mechanism.

Solomon et al. (1986) and McElroy et al. (1986a) noted that the extreme cold temperatures of the Antarctic winter and spring had been shown by McCormick et al. (1982) to lead to greatly enhanced polar stratospheric cloud (PSC) occurrences. They suggested that heterogeneous reactions such as



would both enhance the level of reactive chlorine at the expense of the reservoir species, HCl and ClONO₂, and suppress the abundance of reactive nitrogen (NO_x) in favor of the HNO₃ reservoir. The suppression of reactive nitrogen is quite important, since it impedes the reformation of ClONO₂, allowing the liberated reactive chlorine to remain active (see Section 1.5 for a detailed discussion of the coupling between nitrogen and chlorine chemistry). Ozone depletion could then be expected to occur in the spring, when sunlight is again available to drive photochemical effects following such chemical perturbations due to PSCs. McElroy et al. (1986a) also emphasized the importance of coupled chlorine-bromine chemistry in depleting ozone in such an environment. Molina and Molina (1987) noted that the reaction of ClO with itself to produce the ClO dimer (Cl₂O₂) might be expected to lead to particularly efficient ozone loss under such conditions.

It should be emphasized that both an enhancement in ClO_x and a suppression of NO_x is needed in order for chlorine and/or bromine to effectively destroy ozone in the lower stratosphere. O. B. Toon et al. (1986), Crutzen and Arnold (1986), and McElroy et al. (1986b) noted that the clouds might themselves be composed of nitric acid. Toon et al. (1986) also emphasized that sedimentation of sufficiently large PSC cloud particles could “denitrify” the stratosphere. These processes would further lower the abundance of reactive nitrogen, allowing the chlorine chemistry to destroy ozone still more effectively.

As in the dynamical theory, the extreme cold temperatures of Antarctica and the return of sunlight to the polar regions were essential elements in the chemical hypotheses. The vertical profiles of the ozone changes implied by the three theories were, however, quite different (measured vertical profiles of the ozone change are presented in Section 1.1.5). The solar activity theory suggested large changes in the ozone vertical profile at high altitudes, with decreasing changes below, while the dynamical and halogen chemical theories implied that the ozone profile changes would be largest where temperatures are coldest (around 10–20 km). The halogen chemical theory was also in direct contradiction to the one suggested by Callis and Natarajan insofar as the chemical composition of the Antarctic stratosphere was concerned, since low rather than high levels of reactive nitrogen were hypothesized. Clearly, measurements of reactive nitrogen and chlorine compounds in Antarctica were badly needed. Observations of dynamical tracers and temperature trends were also critical to a fuller understanding of the mechanisms responsible for the ozone decline. Laboratory studies of heterogeneous phase chemistry and thermodynamics of the HNO₃/H₂O/HCl system were key to understanding the possible role of PSC activity in modifying polar chemistry (Sections 1.3 and 1.4).

1.1.5 Observed Trends in the Vertical Distribution of Ozone above Antarctica

The data base of long-term ozonesonde observations from Antarctica is considerably more limited than the total column observations. Historical measurements are only available from Syowa and from the South Pole. More recent data can be used to evaluate the seasonal evolution of the vertical distribution associated with the observed seasonal depletion.

POLAR OZONE

Figure 1.1.5-1 presents observations of the historical change in October total ozone profiles from Syowa and the South Pole, along with the seasonal changes reported at McMurdo and Halley Bay (see original publications of Kondoh et al., 1987; Komhyr et al., 1988; Hofmann et al., 1989c; Gardiner, 1988). Recent observations from the Indian station at Dakshin Gangotri (70°S, 12°E) are also shown (A. P. Mitra, private communication, 1989) as well as measurements from the Soviet station at Molodezhnaya (67°S,

OZONE VERTICAL PROFILES

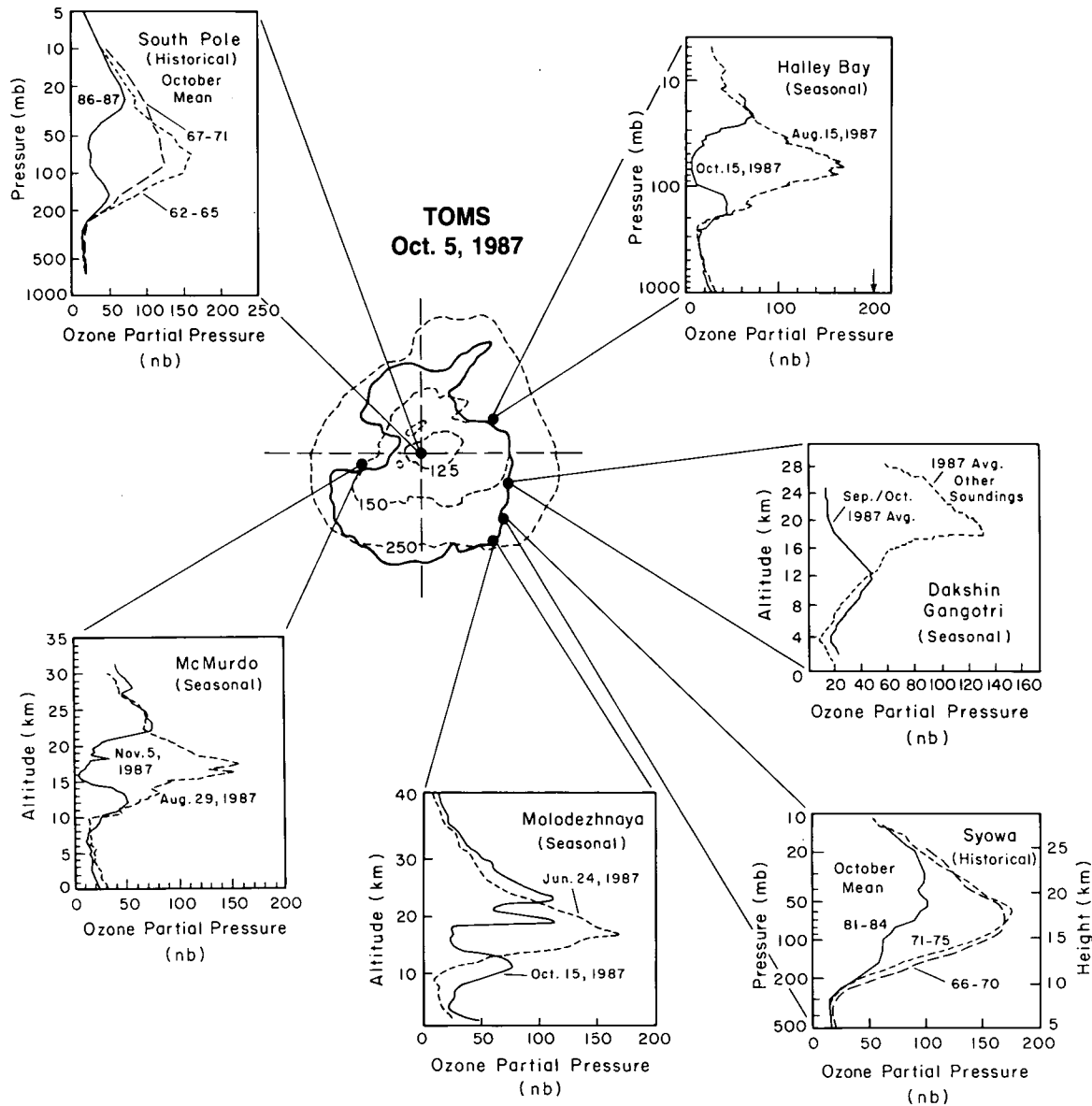


Figure 1.1.5-1. Observations of the change in the vertical profile of ozone as measured by ozone-sondes. At Syowa and the South Pole, historical data show the changes in October mean profiles measured in the 1960s and 1970s as compared to more recent observations. At Halley Bay, McMurdo, Molodezhnaya, and Dakshin Gangotri, similar changes in the vertical profile are revealed in seasonal measurements.

45°E). The Soviet data were obtained with rocketsondes, and hence allow examination of the vertical structure of the ozone profile to levels at and above 35 km, where no ozone depletion is apparent (Kokin et al., 1989). Gernandt (1987) presented evidence for similarly depleted October ozone profiles from the German Democratic Republic's Antarctic research base at 71°S. All of the stations show that the vertical profile of ozone has changed markedly in October. McCormick and Larsen (1986) and McPeters et al. (1986) have shown similar ozone depletions using observations from the SAGE II and SBUV satellite instruments. Figure 1.1.5-2 (left) presents average vertical profiles of summertime ozone from February 1-10 over the latitude region from about 61.5°S to 73°S for various years from SAGE II measurements. These should be contrasted with the right panel in this figure, which depicts the most severely depleted profiles observed in various years from both SAGE I (1981) and SAGE II (1985-1988). Both the ground-based and satellite data show that the ozone decreases are largely limited to the altitude range from 200 to 20 mb (about 10 to 25 km), where local depletions as large as 95% were obtained in 1987. This implies that the maximum local Antarctic ozone depletion cannot get much more severe than it was in 1987 unless the affected altitude range increases. However, the depleted region could expand horizontally, causing larger decreases away from that part of the Antarctic stratosphere suffering the maximum local depletion. Both the ground-based and satellite data reveal the gradual temporal evolution of the profile above Antarctica since about 1980.

Hofmann et al. (1987a) and Hofmann (1989a) noted the occurrence of sharp notches in the ozone profile, and suggested that these may be related to the sharp vertical structure of PSCs that deplete ozone, perhaps through heterogeneous mechanisms beyond those presently understood (see Section 1.4). While the apparent ozone depletion averaged over several kilometers in 1986 was on the order of 50%, the local depletion in such layers appears to be as large as 95%. Thus, the observation of sharply layered depletions places additional constraints on the rates of processes that remove it (see Section 1.6.4). However, it is also important to note that vertical and horizontal wind shear will influence the vertical structure observed at any particular location and may well introduce structure into observed balloon profiles.

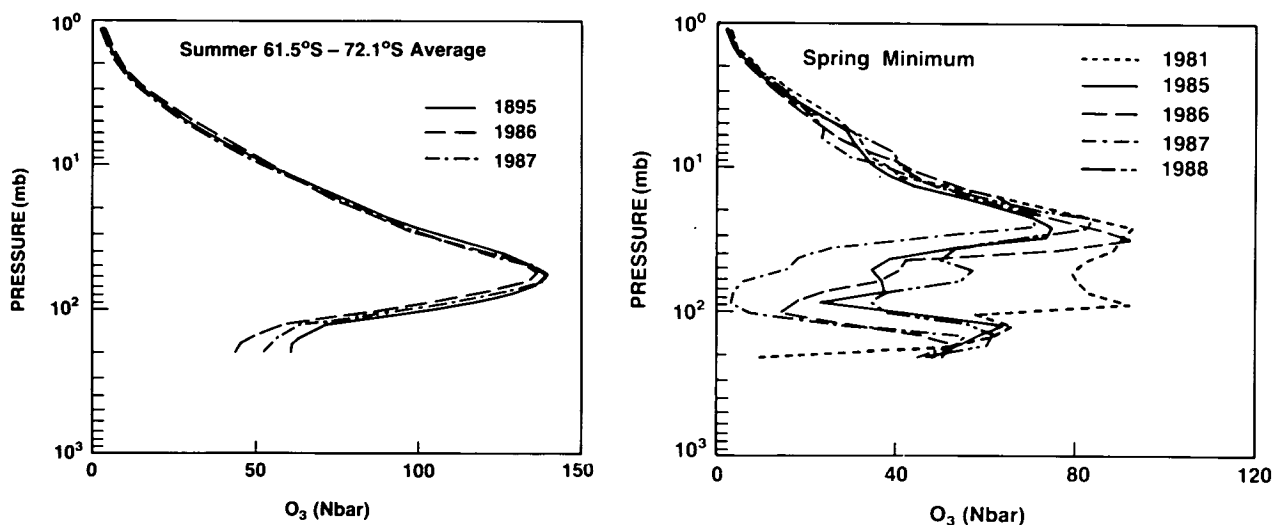


Figure 1.1.5-2. (Left) Average vertical profiles of summertime ozone from February 1-10 over the latitude region from about 61.5°S to 73°S for various years from SAGE II measurements. (Right) The most severely depleted profiles observed in various years from both SAGE I (1981) and SAGE II (1985-1988).

POLAR OZONE

Figure 1.1.5-3 shows the time evolution of ozone at the 18-km level (in the heart of the region of maximum depletion as shown in 1.1.5-1) observed at McMurdo Station in 1986 and 1987 (Hofmann et al., 1989c). Although local fluctuations are evident, a large, systematic decrease is also observed over the months of August and September in both years. It is clear that the rate of decline was appreciably faster in 1987 than that obtained in 1986. A similar increase in the depletion rate near 20 km was measured with South Pole ozonesondes (Komhyr et al., 1989a). Poole et al. (1989) suggest that these differences may be related to observed differences in the frequency of polar stratospheric cloud sightings in the 2 years (see Section 1.2), which in turn are probably a reflection of temperature changes. Differences in the chemistry and dynamics of the Antarctic spring seasons of 1987 and 1986 will be discussed further in Sections 1.6 and 1.7.

1.1.6 Trends in Northern Hemisphere Ozone

The OTP report presented a detailed study of the ozone trends reported in Arctic regions based upon both ground-based and satellite data. The accuracy of calibration procedures at individual total ozone observing stations was carefully considered, and the comparison between TOMS and ground-based data was evaluated at each station. The influence of the 11-year solar cycle and the QBO in modulating total ozone was also evaluated. In this section, the conclusions regarding trends in Arctic ozone that were deduced from the OTP report are briefly summarized. A detailed discussion of Arctic observations of chemical species and dynamical tracers that can provide insight as to the causes of Arctic ozone trends will be the subject of Section 1.10.

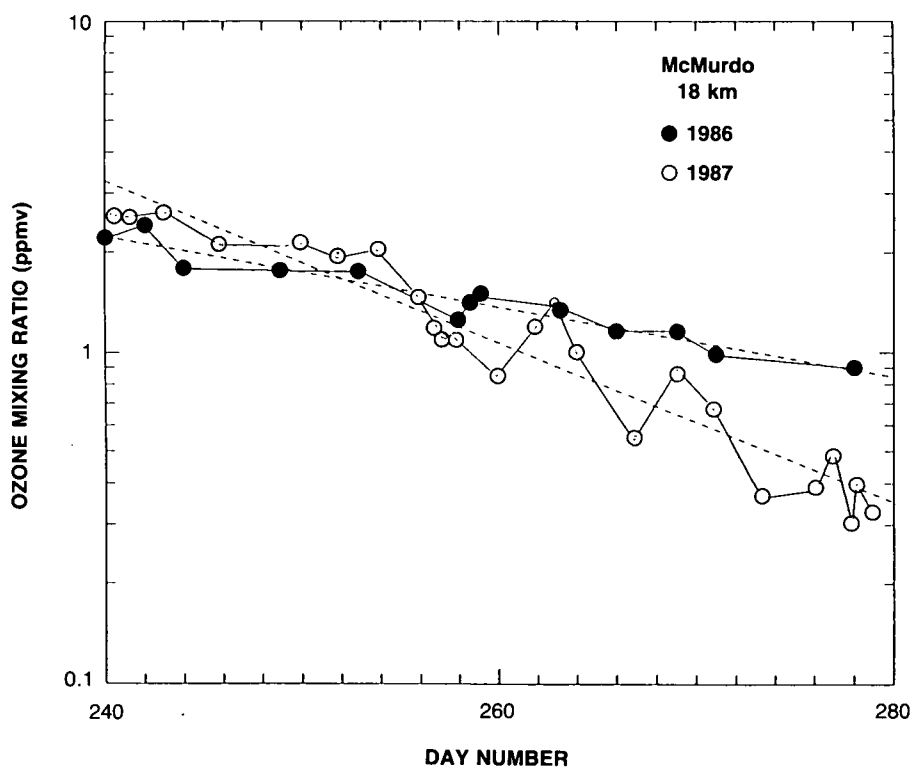


Figure 1.1.5-3. Trend in total ozone at 18 km observed from ozonesondes at McMurdo Station in 1986 and 1987 (from Hofmann et al., 1989a).

One approach taken to evaluating ozone trends using ground-based data was to average over two consecutive solar cycles (1965–1975 as compared to 1976–1986). This approach is expected to alleviate (but probably not eliminate) trends due to the solar cycle and the QBO. Variations between one solar (and/or QBO) cycle and another may still influence the apparent trends, and processes such as the sporadic (approximately 4-year) El Niño Southern Oscillation may also exert an influence. Table 1.1.6-1 displays the results of this analysis for each station considered. The decreases are largest in Arctic latitudes, and are far greater in winter than in summer. Poleward of about 50°N, winter ozone decreases of 2.5–4.7% were reported. These values are larger than model-predicted decreases of 0.9 to 1.1% for 60°N (OTP, 1989).

Table 1.1.6-1. Changes in average total ozone abundances, as measured at individual Dobson stations over the 22-year period, 1965–1986, inclusive (Percentage Differences for 1976–1986 Compared to 1965–1975; from Ozone Trends Panel report, 1989)

North Latitude	Station	Winter ^a	Summer ^b	Annual
74.7	Resolute (Canada)	-1.4 ± 1.8 ^c	-0.8 ± 0.9	-1.6 ± 1.0
64.1	Reykjavik (Iceland)	-2.5 ± 2.2	+1.7 ± 1.3	+0.1 ± 2.4
60.2	Lerwick (Scotland)	-3.8 ± 2.0	-0.9 ± 0.9	-1.6 ± 1.0
58.8	Churchill (Canada)	-4.2 ± 0.9	-1.4 ± 0.8	-2.5 ± 0.7
53.6	Edmonton (Canada)	-4.7 ± 1.3	+0.8 ± 0.9	-1.8 ± 0.8
53.3	Goose Bay (Canada)	-2.4 ± 1.3	-0.1 ± 1.1	-0.8 ± 0.9
51.8	Belsk (Poland)	-3.2 ± 0.8	+1.2 ± 1.0	-1.2 ± 0.9
50.2	Hradec Kralove (Czech.)	-4.7 ± 2.0	±1.1 ± 0.9	-1.8 ± 1.1
47.8	Hohenpeissenberg (FRG)	-1.8 ± 1.7	+0.2 ± 0.9	-1.0 ± 0.9
46.9	Caribou (Maine, U.S.)	-2.8 ± 1.5	-0.6 ± 0.8	-1.8 ± 0.9
46.8	Arosa (Switzerland)	-3.0 ± 1.3	-1.1 ± 1.0	-2.0 ± 0.9
46.8	Bismarck (N. Dak., U.S.)	-3.0 ± 1.2	-1.4 ± 1.0	-2.0 ± 0.7
43.8	Toronto (Canada)	-1.3 ± 1.2	-1.3 ± 0.8	-1.2 ± 0.7
43.1	Sapporo (Japan)	-0.6 ± 1.4	-0.1 ± 0.9	-0.3 ± 0.6
42.1	Vigna di Valle (Italy)	-2.9 ± 1.2	+0.7 ± 0.9	-0.9 ± 0.9
40.0	Boulder (Colorado, U.S.)	-3.9 ± 1.3	-3.1 ± 0.7	-3.3 ± 0.8
39.3	Cagliari (Italy)	-2.5 ± 1.7	-0.7 ± 1.1	-1.1 ± 1.2
36.3	Nashville (Tennessee, U.S.)	-1.8 ± 1.4	-3.3 ± 0.7	-2.4 ± 0.8
36.1	Tateno (Japan)	-0.7 ± 1.6	-0.5 ± 0.8	-0.4 ± 0.7
31.6	Kagoshima (Japan)	+0.9 ± 1.7	+0.5 ± 1.0	+0.9 ± 0.8
30.4	Tallahassee (Florida, U.S.)	-1.7 ± 1.9	-0.2 ± 1.1	-1.3 ± 1.4
30.2	Quetta (Pakistan)	-1.1 ± 1.6	+0.1 ± 0.8	-0.7 ± 0.8
25.5	Varanasi (India)	-0.3 ± 1.4	+0.4 ± 0.9	-0.2 ± 0.9
19.5	Mauna Loa (Hawaii, U.S.)	-1.5 ± 1.7	0.0 ± 0.6	-0.9 ± 0.6
30°N to 60°N		-2.5 ± 1.0	-0.5 ± 0.6	-1.4 ± 0.7
40°N to 60°N		-3.0 ± 0.9	-0.4 ± 0.5	-1.6 ± 0.6
30°N to 39°N		-1.2 ± 1.5	-0.7 ± 1.0	-0.8 ± 1.1

^aWinter = Dec., Jan., Feb., March.

^bSummer = May, June, July, August.

^cResolute is above the Arctic Circle, so that only less accurate moonlight measurements are available during actual winter. These "winter" data are the averages for the months of March and April.

POLAR OZONE

An alternate approach was to attempt to evaluate the magnitude of known sources of variability such as the QBO, solar cycle, etc., using the full record of ground-based ozone data averaged into latitude bands, and then to evaluate any residual long-term trend. Table 1.1.6-2 presents the results of this analysis. While the observed summer decreases are consistent with model estimates including increasing trace gases (chlorofluorocarbons, methane, nitrous oxide, and carbon dioxide), the winter values exceed theoretical expectations. The changes are again largest in winter at high latitudes, where values as large as 8.3% were deduced.

The satellite data were also used in analysis of global ozone trends. The long-term satellite instrument degradation was derived by comparison between satellite and ground-based data, and was estimated at $3.5 \pm 0.5\%$ from October 1978 to October 1987. The TOMS data were then corrected for this drift and the remaining trends were evaluated. Table 1.1.6-3 presents the results of this analysis. It should be noted that an ozone trend of perhaps 1% should be expected over the period from 1978 to 1987 due to the decline in the phase of the 11-year solar cycle during this period. Nevertheless, the TOMS data suggest residual trends of at least 2–3% in the Northern Hemisphere as an annual average.

Table 1.1.6-2. Coefficients of Multiple Regression Statistical Analysis of re-analyzed Dobson measurements of total ozone concentrations collected into latitudinal band averages. (Data are expressed in total percent changes for the period 1969–1986; From Ozone Trends Panel Report, 1989)

Month	Latitude Band		
	53–64°N	40–52°N	30–39°N
January	-8.3 ± 2.2	-2.6 ± 2.1	-2.2 ± 1.5
February	-6.7 ± 2.8	-5.0 ± 2.2	-1.2 ± 1.9
March	-4.0 ± 1.4	-5.6 ± 2.3	-3.5 ± 1.9
April	-2.0 ± 1.4	-2.5 ± 1.7	-1.7 ± 1.3
May	-2.1 ± 1.2	-1.3 ± 1.1	-1.7 ± 0.9
June	$+1.1 \pm 0.9$	-1.8 ± 1.0	-3.3 ± 1.0
July	$+0.0 \pm 1.1$	-2.2 ± 1.0	-1.3 ± 1.0
August	$+0.2 \pm 1.2$	-2.4 ± 1.0	-1.0 ± 1.0
September	$+0.2 \pm 1.1$	-2.9 ± 1.0	-1.0 ± 0.9
October	-1.1 ± 1.2	-1.5 ± 1.5	-0.9 ± 0.8
November	$+1.5 \pm 1.8$	-2.4 ± 1.3	-0.1 ± 0.8
December	-5.8 ± 2.3	-5.5 ± 1.7	-2.1 ± 1.1
Annual Average	-2.3 ± 0.7	-3.0 ± 0.8	-1.7 ± 0.7
Winter Average	-6.2 ± 1.5	-4.7 ± 1.5	-2.3 ± 1.3
Summer Average (a) JJA	$+0.4 \pm 0.8$	-2.1 ± 0.7	-1.9 ± 0.8
(b) MJJA	-0.2 ± 0.8	-1.9 ± 0.7	-1.9 ± 0.8
QBO*	-2.0 ± 0.6	-1.3 ± 0.6	$+1.9 \pm 0.6$
Solar*	$+1.8 \pm 0.6$	$+0.8 \pm 0.7$	$+0.1 \pm 0.6$

*Percent changes per cycle, minimum-to-maximum. All uncertainties are expressed with one statistical significance.

Average of monthly ozone trends in Dobson units per year and percent change in 17 years:

DU/yr:	-0.5 ± 0.16	-0.63 ± 0.17	-0.32 ± 0.14
Percent/17 yrs:	-2.3 ± 0.7	-3.0 ± 0.8	-1.7 ± 0.7

Uniform trend in ozone change assumed throughout the year, in Dobson units per year and percent change in 17 years:

DU/yr:	-0.14 ± 0.13	-0.47 ± 0.13	0.17 ± 0.11
Percent/17 yrs:	-0.7 ± 0.6	-2.3 ± 0.7	-0.9 ± 0.6

Table 1.1.6-3. Percentage changes in total column ozone (measured by TOMS on Nimbus 7, calibrated by comparison with ground-based measurements; from Ozone Trends Panel report, 1989)

Latitude Band	Total Change from 11/1978 to 10/1985	Total Change from 11/1978 to 11/1987
Global, except high latitudes (53°S–53°N)	–2.6 ± 0.5	–2.5 ± 0.6
Hemispheric		
0–53°S	–2.6 ± 0.9	–2.9 ± 0.9
0–53°N	–2.1 ± 1.5	–1.8 ± 1.4
Bands		
53°S–65°S	–0.9 ± 1.8	–10.6 ± 1.6
39°S–53°S	–5.0 ± 1.8	–4.9 ± 1.8
29°S–39°S	–3.2 ± 2.4	–2.7 ± 2.1
19°S–29°S	–2.5 ± 1.9	–2.6 ± 1.5
0–19°S	–1.1 ± 0.8	–2.1 ± 0.8
0–19°N	–1.1 ± 1.5	–1.6 ± 1.3
19°N–29°N	–3.5 ± 2.2	–3.1 ± 1.9
29°N–39°N	–3.7 ± 2.0	–2.5 ± 1.7
39°N–53°N	–2.7 ± 1.7	–1.2 ± 1.5
53°N–65°N	–2.4 ± 1.6	–1.4 ± 1.4

(Linear trends with an autoregressive model through TOMS data, with uncertainties at the one-sigma level of significance.)

In summary, analysis of both ground-based and satellite data has indicated significant (and, more importantly, consistent) trends in Arctic ozone. The trends are far smaller than those obtained in the Antarctic, but exhibit some important common features. Most notably, summer trends were small or zero, while winter trends were much larger, and were greatest at high latitudes (5–10%).

1.2 CLIMATOLOGY OF POLAR STRATOSPHERIC CLOUDS (PSCs) IN BOTH POLAR REGIONS

As noted in Section 1.1.4, several theories advanced to explain the Antarctic ozone hole depend critically on the persistence and characteristics of polar stratospheric clouds. In this section, the physical characteristics of these clouds, their seasonal occurrence frequencies (in both hemispheres) and interannual variability will be discussed. It has also been suggested that radiative effects of the clouds may play a particularly important role in the heat budget of the lower stratosphere and hence in the stratospheric circulation.

1.2.1 Physical Characteristics

Visible sightings of bright clouds in the winter polar lower stratosphere date back to at least the late 1800s (see Stanford and Davis, 1974 for a review). They were dubbed “mother-of-pearl” clouds due to their often very brilliant coloration. Sometimes also referred to as nacreous clouds, it was recognized that these clouds were generally rather localized in extent and tied to surface orography.

McCormick et al. (1982) reported that abnormally high visible extinction values had often been observed in the stratosphere by the SAM II satellite sensor during Arctic and Antarctic winters. While nacreous clouds represent a portion of the cloud population believed to be detected by the satellite sensor,

POLAR OZONE

the satellite observations allow sensitivity far beyond that of the human eye, and thus sample a range of cloud optical depths. Noting that the high extinction events were closely correlated with very cold temperatures, the authors named the phenomenon polar stratospheric clouds (PSCs). Based on a comparison of measured and theoretical extinction coefficient trends by Steele et al. (1983), it was thought that PSCs were H₂O ice particles which formed on frozen stratospheric aerosol nuclei at temperatures below the frost point (≈ 188 K at the 50-mb level assuming 5 ppmv of H₂O). Papers by Solomon et al. (1986) and McElroy et al. (1986a), which suggested that heterogeneous processes involving PSCs might be a major cause of the Antarctic ozone hole, provided the impetus for new studies of the physical characteristics of the clouds. Recent papers that present remote sensing observations of PSCs, balloon-borne particle size and ancillary meteorological measurements, and theoretical PSC microphysics calculations will be discussed in this section. Direct measurements of PSC properties from the airborne and ground-based polar investigations will be discussed briefly below and in Sections 1.3.2 and 1.10.2.

Seminal studies by O. B. Toon et al. (1986), Crutzen and Arnold (1986), and McElroy et al. (1986b) suggested that PSCs might begin to form at temperatures above the frost point as (probably frozen) binary mixtures of HNO₃ and H₂O. Such a mechanism would suppress reactive gaseous nitrogen species (NO_x), which normally counteract chlorine-catalyzed ozone destruction (see Section 1.5). Further, as noted by Toon et al. (1986), such particles might remove reactive nitrogen irreversibly ("denitrify") from the polar stratosphere through sedimentation of large PSC particles containing HNO₃.

Iwasaka et al. (1985a) reported lidar measurements of Antarctic PSCs indicating two distinct cloud particle classes. Alekseev et al. (1988) also presented airborne lidar soundings of lower stratospheric aerosols in the arctic. Poole (1987) and Poole and McCormick (1988a) reported dual-polarization airborne lidar measurements of Arctic PSCs from 1984 and 1986 which support a two-stage PSC formation process. At temperatures from 2–6 K above the frost point, they found that particulate backscatter significantly exceeded that of the background aerosol, but that accompanying depolarization ratios were very small, a signature indicative of (Type 1) PSC particles having radii on the order of the laser wavelength (0.5–0.7 μm). At temperatures near the frost point, they found much larger backscatter enhancements as well as depolarization ratios which were typical of larger, cirrus-like ice crystals (Type 2 PSCs). Clear signatures of Type 1 PSCs were also seen in more recent Arctic PSC lidar measurements by Poole et al. (1988a) and in the analysis of 1987 SAM II Antarctic PSC data by Poole et al. (1988b). The latter study also made the important point that the threshold temperature for Antarctic Type 1 PSC formation was some 5 K colder in October 1987 than in May. The pronounced drop in the temperatures required for PSC formation indicates that irreversible loss of HNO₃ and H₂O vapor occurred during the winter.

Balloon-borne optical particle counter measurements during Antarctic winter and spring were first performed at McMurdo in 1986 and reported by Hofmann et al. (1986, 1987a) and Rosen et al. (1988a). Although conditions were nominally favorable for PSC formation on several occasions, identifiable PSC particles were absent in the two size classes discriminated ($r > 0.15$ μm and $r > 0.25$ μm). This observation led Rosen et al. to speculate that PSCs may be quasi-cirrus clouds composed of large ice particles ($r > 5$ μm) in very low concentrations (< 0.01 cm^{-3}). Balloon-borne particle size measurements were made at McMurdo again in 1987 with an optical counter having additional particle discrimination in the 1–2 μm radius range (Hofmann et al., 1988a). These were supplemented by frost-point hygrometer measurements and ground-based lidar PSC observations (Rosen et al., 1988b). The 1987 measurements showed clear evidence of (Type 1) PSCs at temperatures above the frost point, consistent with the anticipated thermodynamic stability of nitric acid trihydrate (HNO₃/3H₂O). Particle size distributions in these instances were distinctly bimodal, with the larger (1–2 μm) particles having concentrations generally between 0.01 and 0.001 cm^{-3} . Higher concentrations (0.1–2.0 cm^{-3}) of the larger particles were measured in association with

nacreous clouds. Results from McMurdo in September 1988 (Hofmann et al., 1989b) again showed significant particle enhancement at temperatures above the frost point. For example, the concentration of particles with $r > 0.2 \mu\text{m}$ were ten times the normal level at 12 km, and large particles with a modal radius near $0.8 \mu\text{m}$ and a concentration of 0.3 cm^{-3} were also observed. It should be noted, however, that such observations may not represent the particle size distribution characteristic of their formation. Watterson and Tuck (1989) suggest that inflow to the Antarctic vortex occurs preferentially near the Palmer Peninsula, leading to enhanced formation of PSCs in that sector. Adiabatic cooling associated with orographic effects of the peninsula are also likely to play a particularly important role in cloud formation (Watterson and Tuck, 1989; McKenna et al., 1989a; Cariolle et al., 1989a). Watterson and Tuck suggest that sedimentation of large particles in that sector may remove condensables there. This suggests that observations over stations well away from the peninsula (such as McMurdo) may exhibit fewer PSCs in winter and spring due to removal of condensates, and emphasizes the need for general caution in interpreting any locally observed PSC size distribution without detailed consideration of the meteorological conditions.

Recent measurements by Hofmann (1989a) in the Arctic during January 1989 showed in one case a 3-km thick PSC layer near 21 km at temperatures from 186–187 K in which roughly half of the available condensation nuclei grew to radii $> 0.2 \mu\text{m}$, about 1 in 10 grew to radii $> 1.0 \mu\text{m}$, and none grew to radii $> 5.0 \mu\text{m}$. The absence of large ice crystals implied that the observed PSC particles were of the Type 1 class. On a second occasion, thin (300-m thick) PSC layers were observed near 25 km at temperatures near 191 K which consisted predominantly of particles in the $1\text{--}2 \mu\text{m}$ radius range. Further interpretation of these and similar Antarctic data has been presented by Hofmann (1989b), who noted that the small particle mode ($r \leq 0.5 \mu\text{m}$) appeared to be associated with fast cooling events such as those due to mountain lee waves or tropospheric anticyclones. In contrast, the thin layers of larger particles contained only a few percent of the available condensation nuclei and were apparently associated with even more rapid cooling events. Both modes are illustrated in Figure 1.2.1-1. Salawitch et al. (1989) note that sedimentation of the

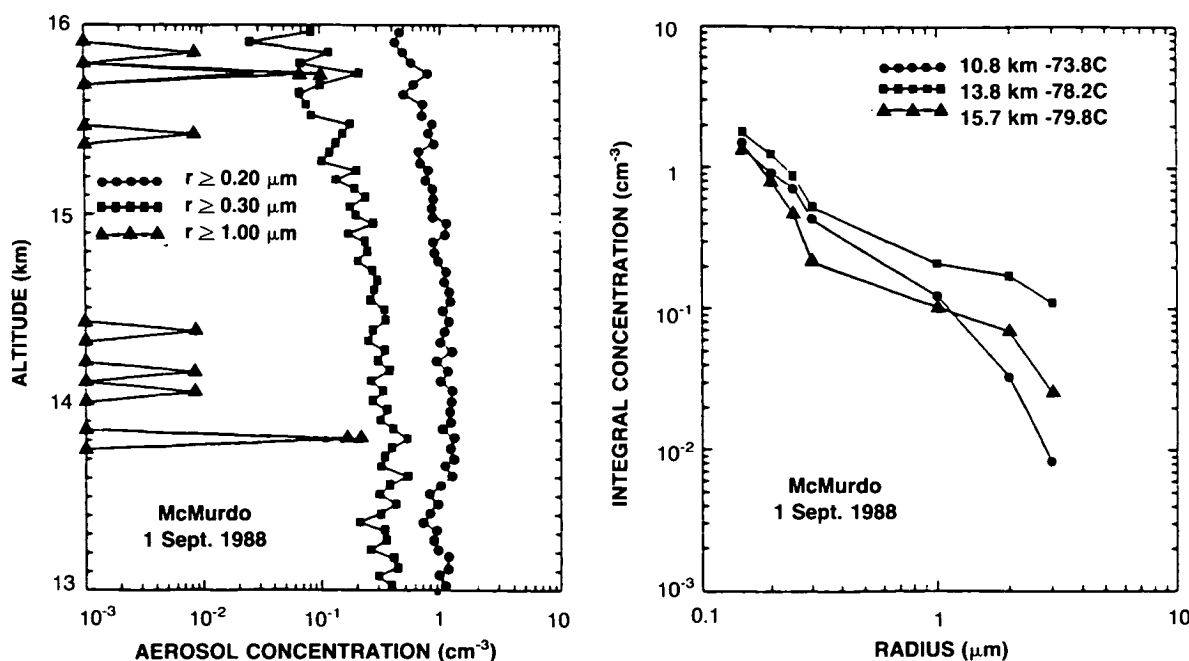


Figure 1.2.1-1. (Left) Vertical profiles of cloud particles observed during balloon soundings at McMurdo Station in September, 1988. Note the thin layers of few large particles observed, for example, near 13.8 km. (Right) Particle size distributions at various altitudes from the same sounding (from Hofmann, 1989b).

POLAR OZONE

large particle mode could significantly denitrify the polar stratosphere without much accompanying dehydration if these particles are composed of nitric acid trihydrate (in contrast to water ice clouds, which could presumably both denitrify and dehydrate the stratosphere). However, Hofmann (1989b) emphasized that such thin layers could not survive long (hours to days) and pointed out that current understanding of cloud microphysics cannot explain their formation. Understanding the formation, composition, and sedimentation of cloud particles is critical to an understanding of the processes responsible for the observed gas-phase composition of the polar stratosphere (see Sections 1.6 and 1.10).

Poole (1987) and Poole and McCormick (1988b) presented calculations from a two-stage PSC microphysics model which assumed that Type 1 PSCs form above the frost point as $\text{HNO}_3/3\text{H}_2\text{O}$ deposited on frozen background aerosol nuclei, and that Type 2 PSCs form subsequently (below the frost point) as H_2O ice deposited on Type 1 nuclei. They used vapor pressure relationships extrapolated from laboratory measurements of liquid $\text{HNO}_3\text{-H}_2\text{O}$ mixtures and assumed that no barrier to cloud particle nucleation existed other than the Kelvin vapor pressure elevation factor. Results showed that for slow cooling conditions (0.5 K/day), only a fraction (5%) of the background aerosol population would be activated as PSC particles, resulting in a bimodal particle size distribution. For typical Antarctic vapor mixing ratios, the authors reported Type 1 modal radii on the order of $1\ \mu\text{m}$ and Type 2 radii near $4\ \mu\text{m}$ and suggested that sedimentation of these larger Type 2 particles might lead to irreversible removal of HNO_3 from the Antarctic stratosphere. Calculated optical properties for Type 1 PSCs generally agreed well with lidar and SAM II observations. Theoretical calculations of the growth of Type 1 PSCs from the background aerosol were also reported by Hamill et al. (1988), who noted that Type 1 particle radii vary inversely (and markedly) with the fraction of aerosol activated into PSC particles.

The formation and growth of Type 2 PSCs has been discussed in recent papers by Ramaswamy (1988) and O. B. Toon et al. (1989). Ramaswamy specifically addressed the role played by Type 2 PSCs in the dehydration of the Antarctic stratosphere during winter, assuming that the particles form by deposition of H_2O ice directly onto the background aerosol and that the Kelvin effect is the only barrier to particle activation. Although not focusing on particle size, Ramaswamy found that Type 2 particles of radii $2\text{-}3\ \mu\text{m}$ formed over the course of several days with temperature decreases below the frost point, and that such a process could lead to extensive irreversible removal of H_2O vapor in the Antarctic. O. B. Toon et al. (1989) presented calculations on the size and lifetime of Type 2 particles forming on Type 1 PSC nuclei assumed to have a modal radius of $0.5\ \mu\text{m}$. The authors found that an energy barrier to ice nucleation (particle activation) akin to that observed in tropospheric cirrus was necessary in order to explain the dependence of observed Type 2 PSC properties on cooling rate. For cooling rates of several degrees K/day, inclusion of the nucleation barrier led to Type 2 particle radii on the order of $20\ \mu\text{m}$, which could rapidly dehydrate the Antarctic stratosphere through sedimentation.

In summary, there is agreement among the various measurements and calculations that Type 1 PSCs do exist at temperatures above the frost point (by as much as $5\text{-}7\ \text{K}$). This temperature regime is consistent with laboratory measurements of the stability of nitric acid trihydrate (Hanson and Mauersberger, 1988a,b), although the presence of super-cooled liquid $\text{HNO}_3\text{-H}_2\text{O}$ solutions, non-stoichiometric solid solutions with compositions near that of the trihydrate, or ternary $\text{H}_2\text{SO}_4\text{-HNO}_3\text{-H}_2\text{O}$ solutions cannot be ruled out. There is little doubt that predominantly water ice Type 2 clouds form at temperatures below the frost point. Recent laboratory vapor pressure measurements (see Section 1.3.1) imply that both PSC classes also likely contain trace amounts of HCl. The notion of a typical particle size for either Type 1 or Type 2 PSCs, on the other hand, appears to be an open question. Theory suggests that PSC particle sizes should depend strongly on the number of nuclei activated into cloud particles, which in turn is a very sensitive function of the physical properties of the nuclei themselves as well as the dynamical environment in which the

clouds form (e.g., the temperature history and the available vapor pressures of condensables). Additional in-situ measurements and more sophisticated modeling calculations are required to address these uncertainties.

1.2.2 Seasonal Behavior of PSCs

In this section, observations of PSC frequency with respect to season and year for both hemispheres will be discussed. This analysis is similar in content to that presented in McCormick et al. (1982) based upon only the first observations of PSCs. Although quantitative details presented herein differ from those of McCormick et al. (1982), the general conclusions regarding the seasonal variation, vertical extent, and hemispheric differences in PSC frequency are largely unchanged from the pioneering study of McCormick et al. The seasonal evolution of PSCs in both hemispheres can be examined by searching the weekly SAM II extinction data base (and ancillary temperature data) for those events which can clearly be distinguished from the background stratospheric aerosol as PSCs. In the study described here, the extinction characteristics of the unperturbed background atmosphere were identified using more detailed information than in previous work (see Poole et al., 1989). The selection criteria employed are likely to allow better discrimination between cloudy and clear conditions, particularly for relatively optically thin cloud events.

It would be desirable to search the SAM II data base for occurrences of Type 2 (predominantly H₂O ice) PSCs. Since the potential for growth to large sizes is much greater for Type 2 particles than for their Type 1 counterparts, Type 2 particles are the more likely to experience rapid sedimentation, which can irreversibly remove condensed HNO₃ from the polar stratosphere. They are therefore likely to play a particularly important role in denitrification. However, there are difficulties in choosing meaningful criteria to identify Type 2 PSCs in the SAM II record:

- (a) SAM II extinction coefficient measurements necessarily represent a spatial average over the instrument's line of sight, a distance on the order of 200 km. Thus, it is impossible to distinguish between patchy Type 2 PSCs and a continuous Type 1 PSC "haze" layer.
- (b) The potential for PSC extinction enhancement relative to that of the background aerosol (the PSC nuclei) depends quite critically on the initial characteristics (size and number density) of the aerosol. Aerosol characteristics are known to vary markedly with height in mid-latitudes, and are not well defined in the winter polar regions.
- (c) Theoretical models of PSC formation and growth have not matured to the stage at which they can provide unambiguous guidelines for differentiation of PSCs by Type.

Due to these unresolved issues in the interpretation of SAM II measurements, only the general trends in cloud occurrence frequency will be discussed here, without regard to intensity or Type.

The latitudinal coverage of SAM II is dependent on the orbit of the satellite and on the position of the sun (since the measurements are carried out by solar occultation; hence, there are no measurements in the polar night region). The latitude of SAM II observations varies from 64° (N or S) at the solstices to 80° (N or S) at the equinoxes. Thus, it is unknown whether seasonal patterns that are discernable from the SAM II data base are representative of actual PSC occurrences over the entire polar region.

The background aerosol population at a given altitude changes over the course of the winter in both polar regions, presumably due to subsidence and particle sedimentation. Therefore, temporally varying

POLAR OZONE

background extinction values were used as the basis for the PSC search described by Poole et al. (1989). These variations are normally quite subtle in the Arctic and are easily quantified, since many SAM II measurements during the winter are of the background aerosol alone (not PSCs). Calculated individual monthly average background extinction ratios and standard deviations were defined for November through February in each winter, while the February values were used as bases for March and April as well. SAM II observations of the Antarctic background aerosol show that a dramatic change occurs between May and October, but the details of the temporal variation are often obscured by the prevalence of very low temperatures and (hence) pervasive PSC sightings during the winter. However, in most years, the background aerosol extinction ratio is believed to remain relatively constant from May through July. Therefore, the temporal trend for each Antarctic winter was approximated by using average background extinction ratios (and standard deviations) from (a) the May monthly ensemble, for May–July; (b) the October monthly ensemble, for October; and (3) a linear interpolation between the May and October monthly ensembles, for August–September.

SAM II PSC observations for altitudes from 14–24 km at 2-km intervals are presented below. All data periods from November 1978 through April 1989 were included, with the exception of observations in 1983, which were omitted due to contamination by El Chichon volcanic aerosols.

Histograms of weekly SAM II PSC sightings in the Antarctic are shown in Figures 1.2.2-1 and 1.2.2-2 for the years 1979–1982 and 1984, at 14, 16, 20, 22, and 24 km. Corresponding figures for 1985–1988 are presented in Figures 1.2.2-3 and 1.2.2-4. Arctic PSC sightings are shown for the 1978–1979 through 1988–1989

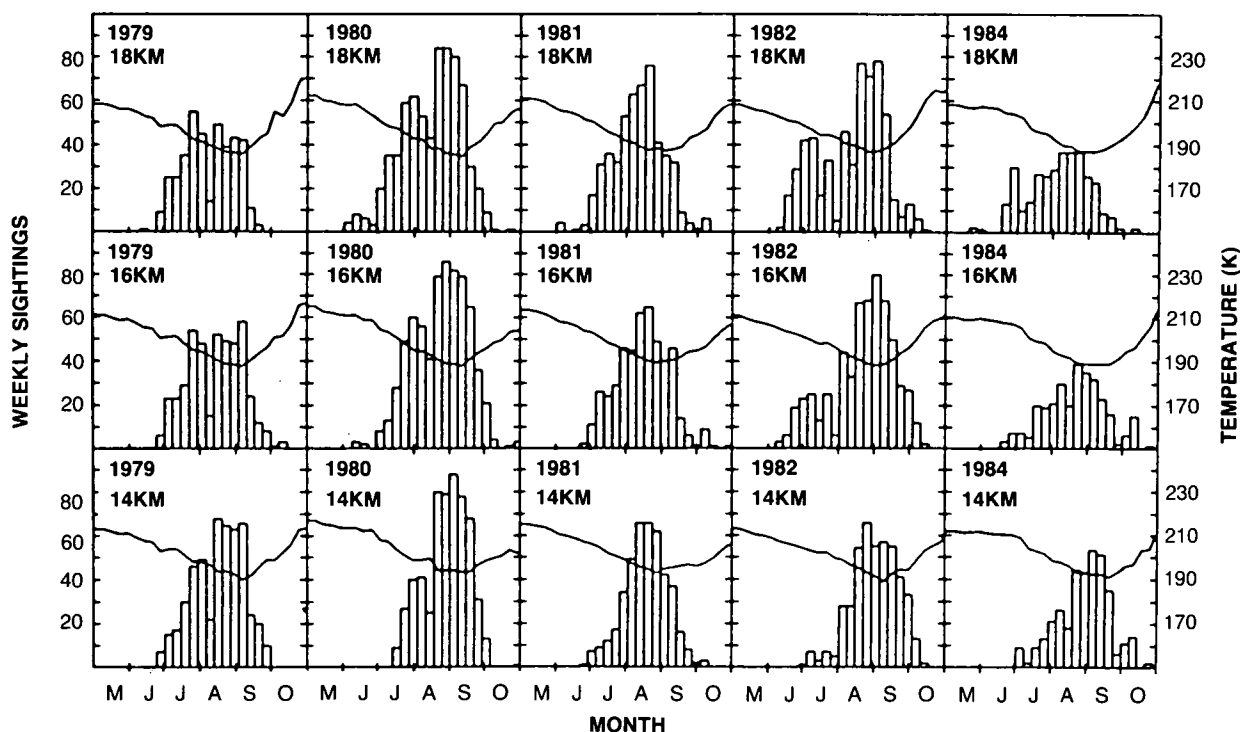


Figure 1.2.2-1. Observations of PSC sightings (per week) from SAM II during 1979, 1980, 1981, 1982, and 1984 for May through October in the Southern Hemisphere vortex (south of the 50 mb polar night jet). Sightings at the 14, 16, and 18 km levels are shown. The solid line indicates the corresponding average temperature for all polar SAM II measurements at each level as a function of time.

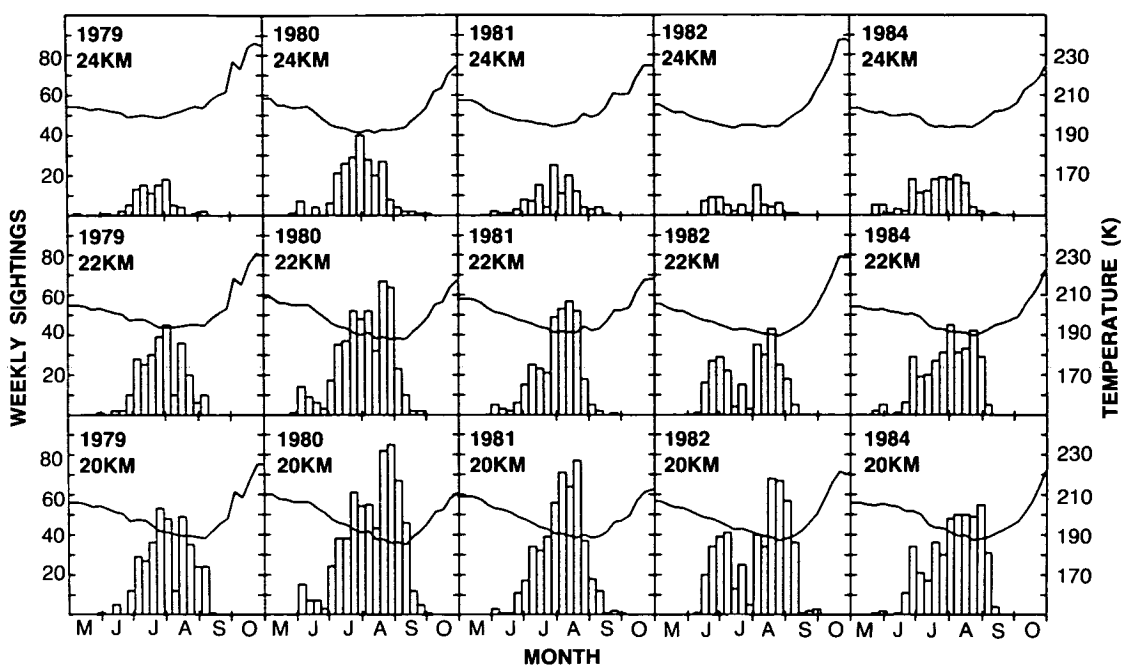


Figure 1.2.2-2. As in figure 1.2.2-1, but for 20, 22, and 24 km.

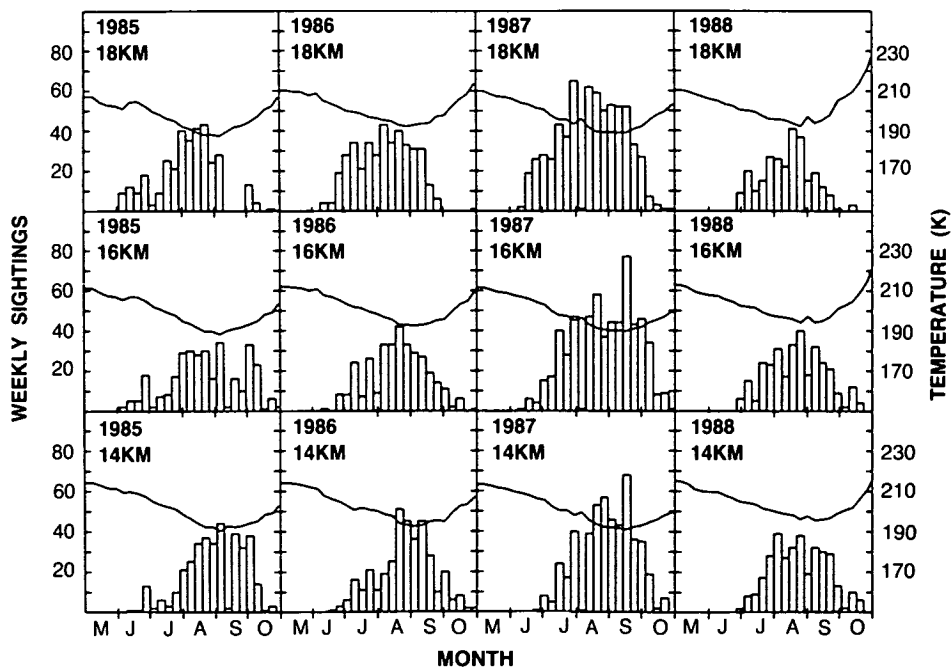


Figure 1.2.2-3. As in Figure 1.2.2-1, but for 1985 through 1988.

POLAR OZONE

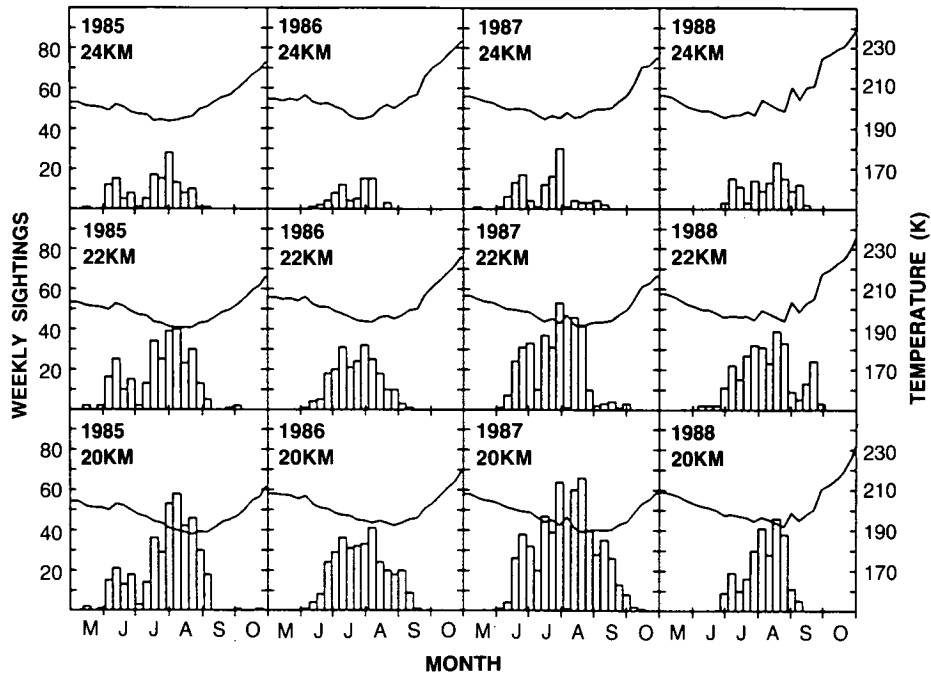


Figure 1.2.2-4. As in Figure 1.2.2-3, but for 20, 22, and 24 km.

winters excluding 1982–1983 in Figures 1.2.2-5 to 1.2.2-8. Also included in each frame is a plot of the weekly average temperature (solid line) for all SAM II measurements (PSC and non-PSC, both inside and outside of the vortex). By inspection and comparison of individual histograms, several general features can be noted:

- (a) At all altitudes and in all years, many more PSCs were observed in the Antarctic than in the Arctic. When totaled over a season, the ratio of Antarctic to Arctic sightings varied considerably with altitude and year, but typically ranged between 10 and 100.
- (b) During a given year in the Antarctic, the maximum number of PSCs was usually seen in the 16–18 km altitude range. The maximum number of Arctic PSCs was usually seen in the 20–22 km altitude range.
- (c) In the Arctic, the vast majority of PSC sightings occurred in January and February. However, there were some sightings in December and even a few in November and March. No Arctic PSCs were sighted in April. As expected, maxima in PSC sightings generally coincided with minimum temperatures. Since the temperatures shown are weekly averages at all SAM II locations including those at which PSCs were not observed, they are somewhat higher than the values at which PSCs are thermodynamically stable, but provide a rough indication of the relationship between the seasonal progression of temperature and PSC formation.
- (d) In the Antarctic, there were occasional PSC sightings in May and quite a few sightings in June, especially at the higher altitudes. The number of sightings generally increased during the winter months at all altitudes, with the temporal peak occurring in late August or early September at altitudes below 18 km and somewhat earlier at higher altitudes. As was seen in the Arctic, maxima in PSC sightings generally coincided with minimum weekly average temperatures. At all altitudes below

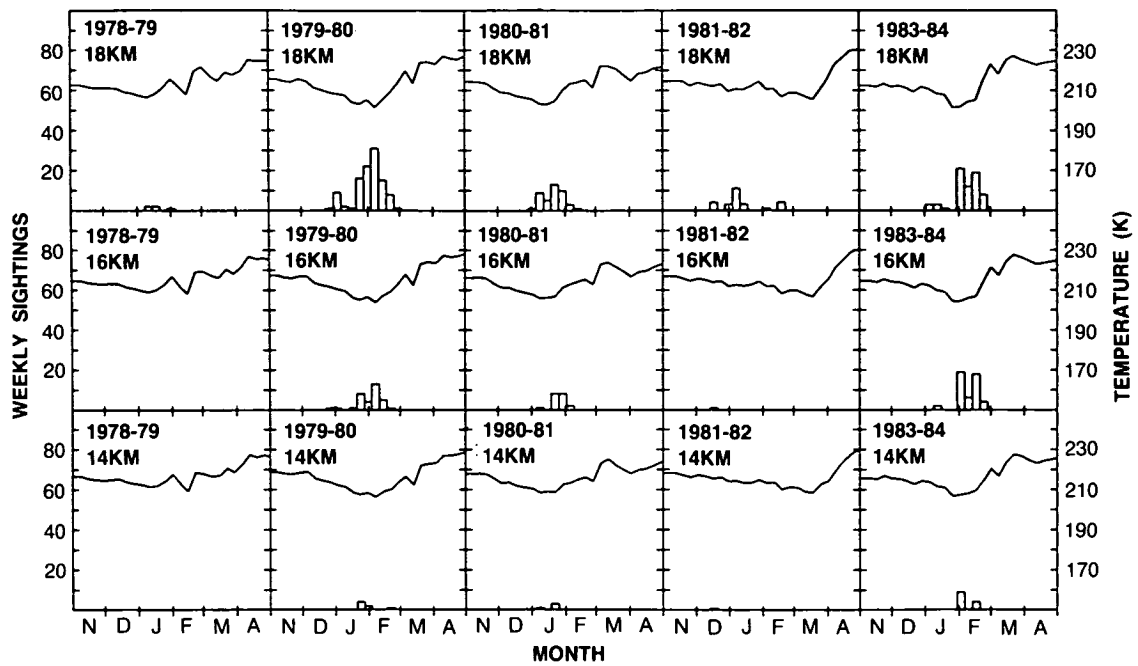


Figure 1.2.2-5. As in Figure 1.2.2-1, but for November through April in the Northern Hemisphere vortex (north of the 50 mb polar night jet) for the 1978-1979, 1979-1980, 1980-1981, 1981-1982, and 1983-1984 winter seasons.

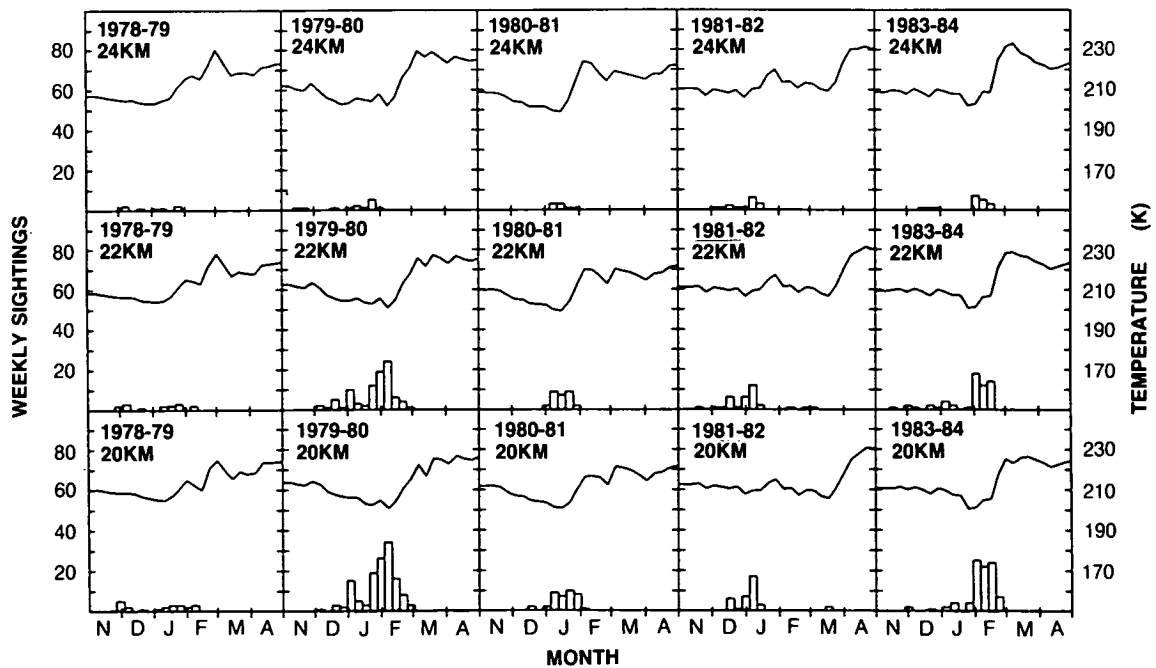


Figure 1.2.2-6. As in Figure 1.2.2-5, but for 20, 22, and 24 km.

POLAR OZONE

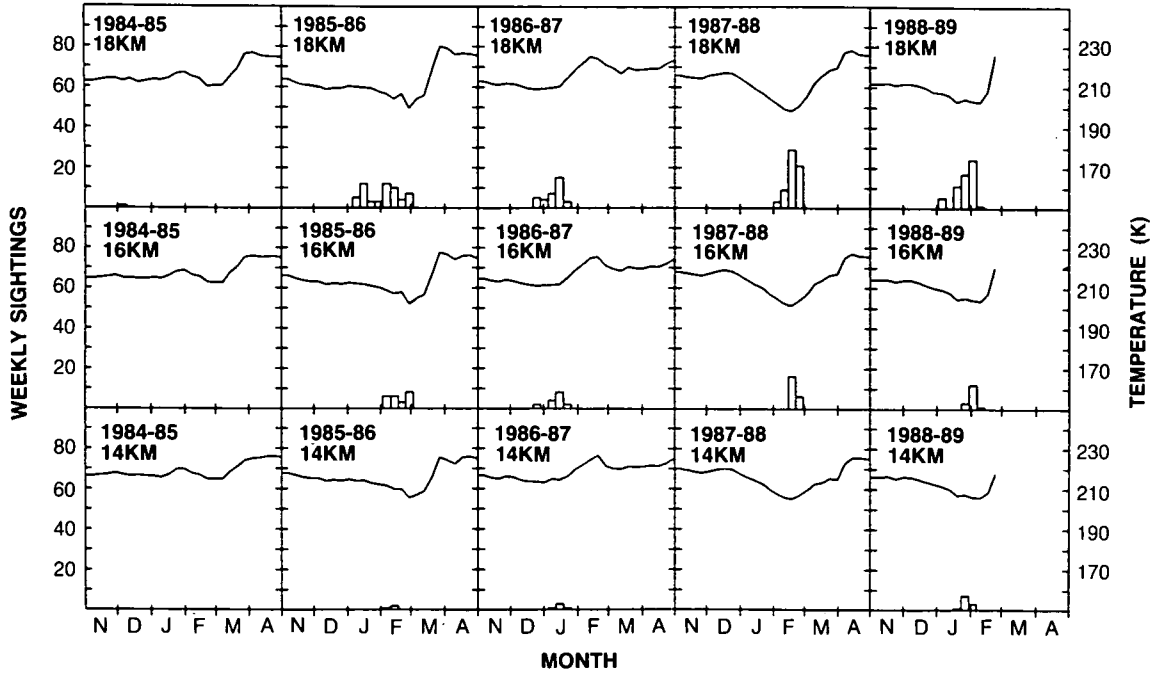


Figure 1.2.2-7. As in Figure 1.2.2-5, but for 1984-1985 through 1988-1989.

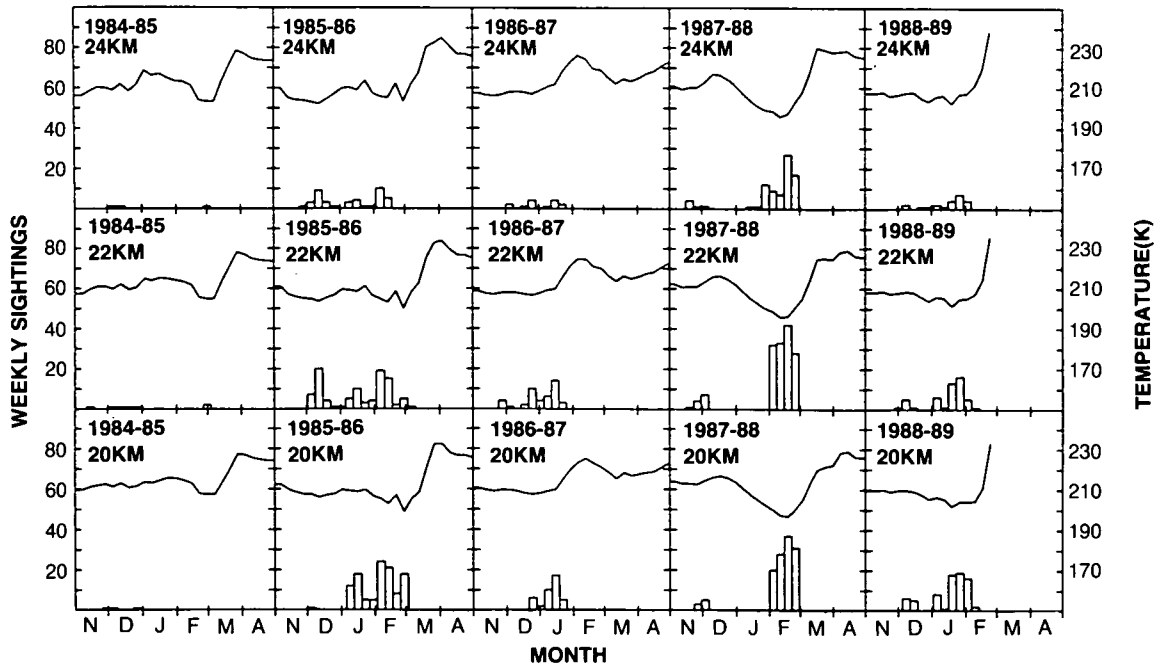


Figure 1.2.2-8. As in Figure 1.2.2-7, but for 20, 22, and 24 km.

20 km, PSCs were generally abundant in September and, in many years, were seen through the middle of October.

The comparison between Arctic and Antarctic PSC sightings thus reveals important differences both in the frequency of PSC sightings and in their duration, especially in spring. PSCs are far more prevalent in the colder Antarctic stratosphere as compared to the Arctic. While PSCs are generally observed in Antarctica in September and often in October, they are only seldom observed in the conjugate Northern Hemisphere Arctic data in March, and never in April in the years for which data are available. The seasonal PSC differences appear related to differences in spring temperatures between the two hemispheres. As discussed in Sections 1.6 and 1.10.2, these hemispheric variations in temperature and PSC duration in early spring months likely lead to large hemispheric differences in ozone depletion.

1.2.3 Long-Term Trends in PSC Frequency and Intensity

The SAM II data base also can be used to examine long-term trends in PSC frequency and intensity. A first-order approach to the entire data base is to integrate weekly averaged extinction coefficient measurements over altitude to form a temporal optical depth record. Observed optical depth records integrated from 2 km above the tropopause to 30 km for both hemispheres for the 1979–87 period are shown in Figure 1.2.3-1. The dates of major volcanic eruptions which injected aerosol into the stratosphere are also indicated.

The occurrence of PSCs in the Antarctic appears every year in the optical depth record as a marked third-quarter maximum, although (as mentioned in Section 1.2.2) the presence of aerosol injected by El Chichon obscures the maxima in 1983–1985. It is also interesting to note that the yearly minimum in

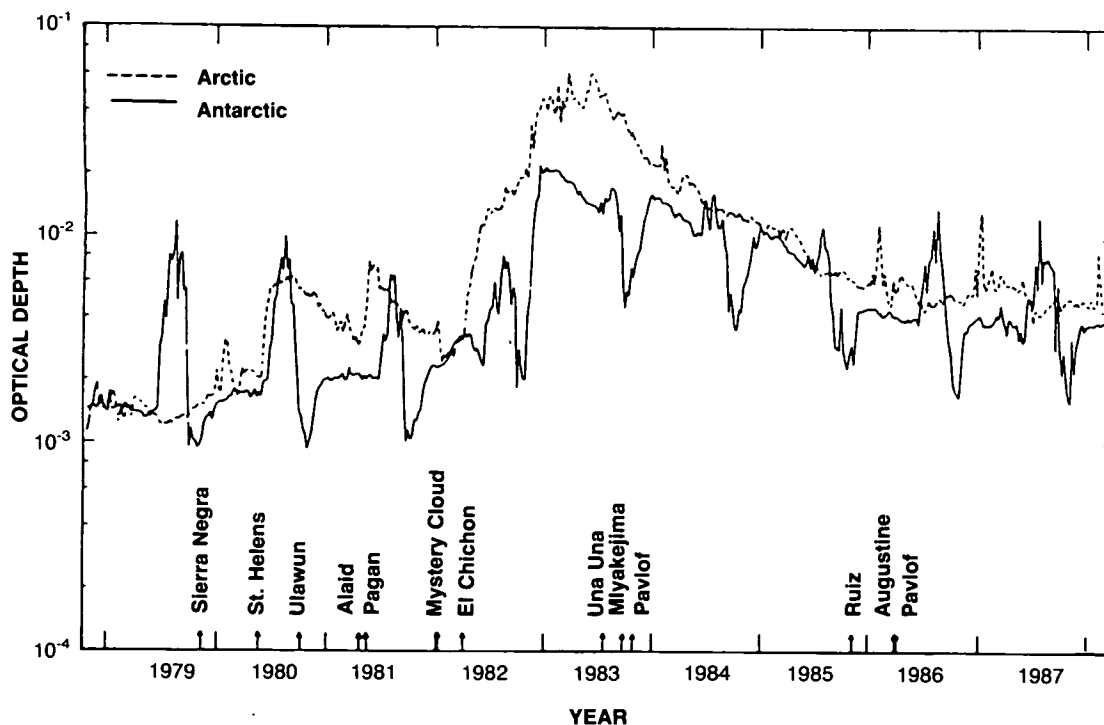


Figure 1.2.3-1. SAM II optical depth integrated from 2 km above the tropopause to 30 km, for the Northern and Southern Hemispheres. Major volcanic eruptions are indicated (after McCormick and Trepte, 1987).

POLAR OZONE

Antarctic optical depth immediately follows the maximum. This may indicate that particulate matter in the Antarctic stratosphere is redistributed downward during winter by subsidence or sedimentation (see Hofmann et al., 1988). The occurrence of PSCs in the Arctic appears (in most years) as a smaller, yet pronounced first-quarter maximum in optical depth. No clear trend for an abrupt minimum in optical depth following the PSC maximum can be seen in the Arctic. Figure 1.2.3-1 certainly establishes that PSCs have been recurrent seasonal phenomenon for the last decade, but reveals no obvious trend in either PSC frequency or intensity.

Another approach to analysis of PSC temporal trends is suggested by the work of Garcia and Solomon (1987), who reported a possible relationship between the quasi-biennial oscillation (QBO) and observed interannual variability in the October minima of mean TOMS total ozone values for Antarctica and of 100-mb temperatures inside the Antarctic vortex. The particular sensitivity of October temperatures to the QBO and the fact that Antarctic vortex temperatures in that month generally lie very close to the expected saturation over the nitric acid trihydrate suggests that the occurrence of PSCs during October might be particularly sensitive to both QBO and longer term trends in Antarctic temperatures. Calculated monthly sums of SAM II Antarctic PSC sightings (defined in Poole et al., 1989) in October for altitudes from 14–24 km (at 2-km intervals) from 1979–1987 are presented in Figure 1.2.3-2, while those for September are shown in Figure 1.2.3-3 (again excluding 1983 due to the masking effects of El Chichon aerosol). The phase of the QBO at 30 mb in tropical regions is also indicated. Results for 14–18 km show pronounced peaks in September and October PSC sightings in 1985 and 1987, with additional peaks in 1980 and 1982 at some

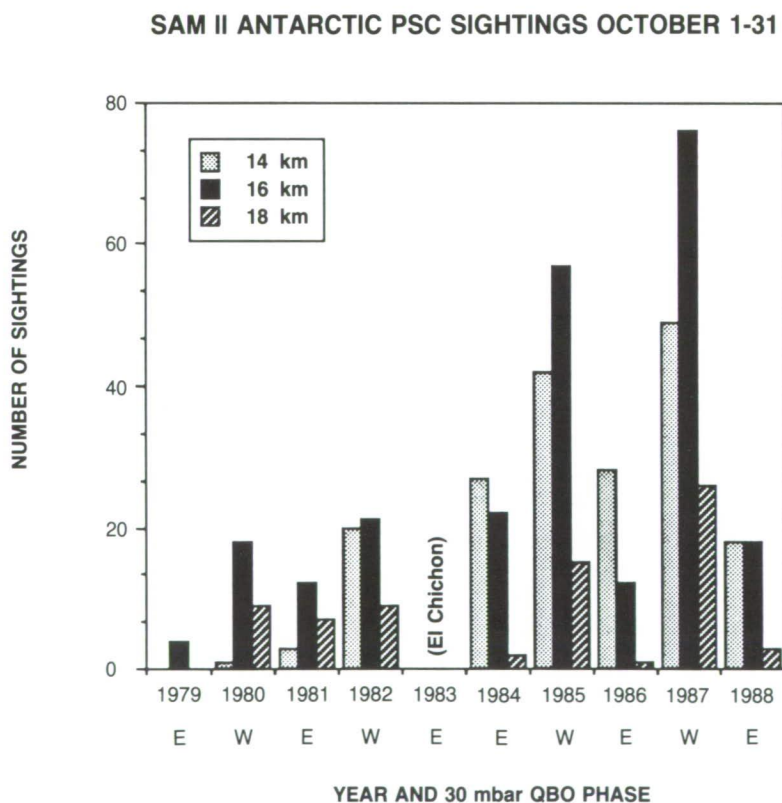


Figure 1.2.3-2. Observations of SAM II PSC sightings for Antarctica from 1979 through 1988 at 14, 16, and 18 km, during the month of October. The QBO phase at 30 mb is also indicated for each year (from Poole et al., 1989).

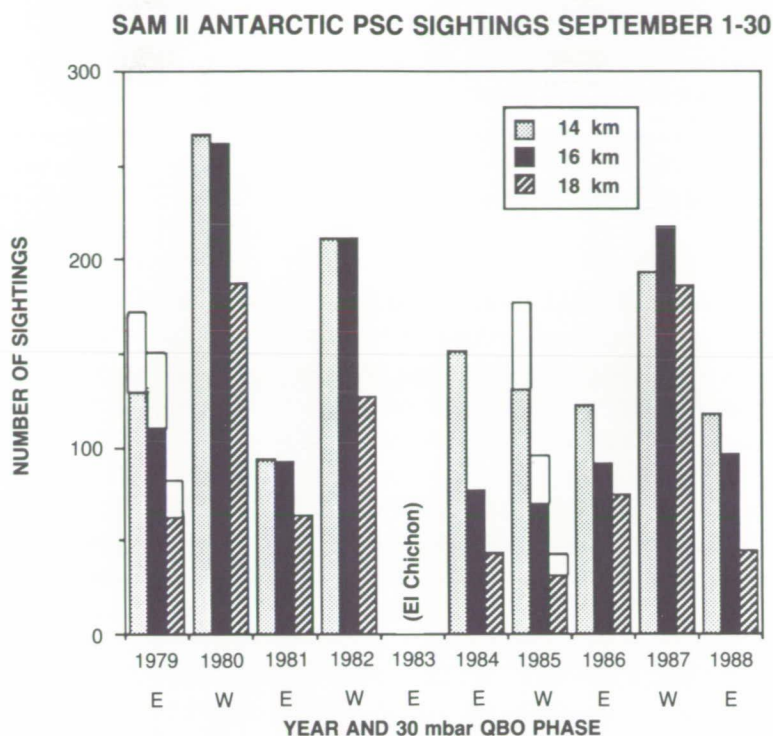


Figure 1.2.3-3. As in Figure 1.2.3-2, but for September.

altitudes. Years in which the Antarctic spring coincides with the strong westerly (easterly) phase of the QBO generally show September and October maxima (minima) in PSC sightings.

Figure 1.2.3-2 also suggests that the trend over the last decade has been towards an increase in PSC sightings at 14 and 16 (and possibly 18) km in the westerly phase years during October but not in September. It is important to emphasize that the determination of the long-term trend is complicated by the strong influence of El Chichon aerosol in 1983. The tallies for 1984–85 are likely low due to the masking influence of El Chichon aerosol remnants. However, Hofmann et al. (1987b) noted that the influence of El Chichon aerosol in the Antarctic vortex was negligible by austral spring of 1986.

The apparent trend is broadly consistent with observed long-term decreases in October temperatures discussed in Section 1.8. The PSC occurrence, temperatures, and ozone loss are expected to be closely interconnected, since ozone provides the source of heat to the stratosphere and the observed changes in temperature probably result in part from the ozone loss (see Section 1.8). Particularly in 1987, for example, the near-complete removal of ozone in the altitude region from about 10 to 24 km during September (Section 1.1) is believed to have substantially decreased temperatures in the lower stratosphere and hence likely played a role in enhancing the time during which PSCs persisted into the spring season.

The QBO and long-term trends in PSC occurrence in October clearly have important implications for heterogeneous chemistry and its effects on ozone. In particular, the apparent QBO modulation of PSCs in September may affect the rates of ozone removal in westerly as compared to easterly years. Further, the long-term trend in PSC frequency in October during westerly phase years should be expected to lengthen the time during which heterogeneous reactions are most effective at suppressing reactive nitrogen levels

POLAR OZONE

and enhancing reactive chlorine, thus leading to subsequent ozone loss (see Poole et al., 1989). The decadal trend in PSCs is likely to feed back into the decadal trend in total ozone and suggests a means of amplifying the expected long-term depletion of total ozone beyond that anticipated from the known growth in total chlorine content. This issue will be discussed further in Section 1.6.

1.2.4 Effect of PSCs on the Radiative Budget

Quantitative calculations of the evolution of the climate of the polar lower stratosphere must consider whether PSCs can significantly alter the radiative budget. As noted for example, by Tung et al. (1986), radiative cooling or heating by PSCs could have a substantial effect on the net radiative heating rate in the lower spring Antarctic stratosphere and hence on the mean meridional circulation and any possible ozone depletion due to uplifting. Further, as discussed in Section 1.7, downwelling may also be of considerable importance in tracer transport in the polar vortex.

The two most detailed studies of the impact of PSCs on the radiation budget (Blanchet, 1985; Pollack and McKay, 1985) were both performed prior to the announcement of the discovery of the ozone hole. Since then, much attention has been focused on the properties of PSCs, both observational and theoretical, and there have been significant changes in our understanding of the clouds (see Section 1.2.1).

Blanchet (1985) and Pollack and McKay (1985) reach fundamentally different conclusions about the sign of the effect of PSC cloud particles on the thermal infrared radiation budget. This is because the impact of the PSCs is critically dependent on the upwelling radiation from the underlying troposphere. Pollack and McKay assume a rather extreme cloudless troposphere with surface temperatures of 195 K; the increase in absorption of the upwelling radiation as a consequence of the PSCs does not balance the increased emission and the cloud particles cause a cooling. Blanchet assumes a rather warmer troposphere, and in this case, the increased absorption dominates, and the clouds cause a warming. Blanchet shows that his results are similar to Pollack and McKay's when similar temperature profiles are used. Hence, while the magnitude of the impact of the clouds is generally determined by such properties as the cloud particle size and number concentration, the net effect is dependent on conditions remote from the clouds.

Another fundamental difference between the two studies is that Pollack and McKay consider the effect of decreased water vapor mixing ratio, as a result of water tied up in the cloud particles. Since water vapor acts to cool the stratosphere by emission in the thermal infrared, its loss leads to a relative warming. For a wide range of conditions, Pollack and McKay show that the effect of loss of water vapor dominates the effect of the cloud particles, and hence the net effect of the particles is to cause a warming. This effect is not considered in Blanchet's work.

Pollack and McKay (1985) calculate the effect of a cloud of extinction coefficient (at a wavelength of 1 μm) of 0.01 km^{-1} , a value based on observations from SAM II. Standard calculations are based on a particle radius of 1 μm , but other radii, ranging from 0.056 to 18 μm are also considered. The effect of the 1 μm particles is very small; they cause a cooling of no more than 0.01 K/day, a value dominated by the relative warming due to loss of water vapor, which can exceed 0.08 K/day. At the extremes of the range of particle sizes used in the calculations, more significant effects are found. For a radius of 0.1 μm , a cooling of about 0.24 K/day is found, while for large particles (10 μm) the cooling reaches 0.12 K/day.

Blanchet (1985) considered the effect of PSC particles growing from 0.0725 μm to 2 μm ; for a case with a number concentration of 6 cm^{-3} , Blanchet considered the effect of increasing particle size (i.e., the extinction coefficient is not held constant as in Pollack and McKay's calculation). Particles with a radius

of $0.5 \mu\text{m}$ (representing an extinction of 0.02 km^{-1} at $1 \mu\text{m}$) give a mild heating of about 0.3 K/day at the cloud base, with smaller coolings towards the cloud top. Particle radii of $1 \mu\text{m}$ cause a peak heating of about 0.2 K/day . Increasing the particle radii to $2.0 \mu\text{m}$ (with a corresponding increase in extinction coefficient of 0.1 km^{-1}) does generate significant heating rates of 1.0 K/day . Blanchet proposed that under normal conditions such particle sizes could not be reached, as such large heating rates would act as a limiting factor in the cloud's development.

Less work has been performed on the effects of PSCs on solar radiation, principally because of the limited sunlight available at times when PSCs are normally presented. Nevertheless, Shi et al. (1986) show that heating rates of about 0.2 K/day are possible in late September and that the solar heating of the particles dominates over effects in the thermal infrared. This is for a case with a total stratospheric optical depth of 0.02 at $1 \mu\text{m}$, a value close to those observed during springtime in the Antarctic. Akiyoshi et al. (1988) performed similar calculations using extinction data derived from SAGE II observations during 1985. These authors do not discuss the extinction coefficients derived from the measurements. They find that the aerosols always act to warm the lower stratosphere in the thermal infrared as well as at solar wavelengths. However, on no occasion is the net heating due to the aerosols greater than 0.1 K/day .

As noted earlier, *in situ* balloonsonde measurements indicate that PSC clouds sometimes consist of particles of radii between $1\text{--}10 \mu\text{m}$, with concentrations of 0.0001 to 0.001 cm^{-3} (Rosen et al., 1988a; Hofmann et al., 1987a,b; Hofmann, 1989a,b). Such low concentrations of particles would, on the basis of the calculations described earlier, have a negligible effect on the diabatic heating.

Kinne and Toon (1989) provide a preliminary report of calculations of the radiative effects of PSCs based on measurements of cloud properties near the Palmer Peninsula from the AAOE experiment. Calculations for PSC Types 1 and 2 were performed for a cold south polar profile for 19 September 1987 (surface temperature about -60°C) both with and without high level ($10\text{--}14 \text{ km}$) cirrus. Their Type 1 PSCs (with an optical thickness of 0.002 and typical particle radii of $0.8 \mu\text{m}$) have an insignificant effect in the absence of cirrus and cause only a slight (-0.09 K/day) cooling with cirrus. The Type 2 PSCs (with an optical thickness of 0.05 and typical particle radius of $15 \mu\text{m}$) have a much larger effect. The thermal infrared cooling (0.3 K/day at cloud top) dominates the solar heating (0.12 K/day at cloud top). In the presence of cirrus the IR cooling rate reaches 1 K/day .

A further set of calculations were performed for optically thick "mountain-PSCs" associated with forced adiabatic ascent such as that present during "mini-hole" episodes (see Section 1.7.2). These calculations are for far warmer Palmer Peninsula profiles (for 21 August 1987 surface temperatures are about -9°C and for 9 September 1987 they are about -3°C). The mountain-PSCs have an optical thickness of 1 and a typical particle radius of $1 \mu\text{m}$. Again the infrared effects dominate over solar heating, although it should be noted that Kinne and Toon use the same solar zenith angle for both days (84°) and do not attempt an integration over daylength. The role of cirrus in modulating the net heating is, however, very dramatic and is shown in Figure 1.2.4-1. In the absence of cirrus, the PSCs cause a strong heating in the thermal infrared, which reaches 8 K/day at cloud base. In the presence of cirrus the net effect is one of cooling, which exceeds 7 K/day at cloud top.

In summary, in the absence of cirrus, thermal infrared radiation reaching the cloud base is principally emitted from the surface and lower troposphere, which are far warmer than the cloud base; hence the cloud base is receiving more radiation than it emits and heats. The addition of the optically thick cirrus blocks the radiation from the lower troposphere; the radiation now reaching the PSC base is from the cold cirrus top, causing the PSC layer above to yield a net cooling. The calculations shown in Figure 1.2.4-1

POLAR OZONE

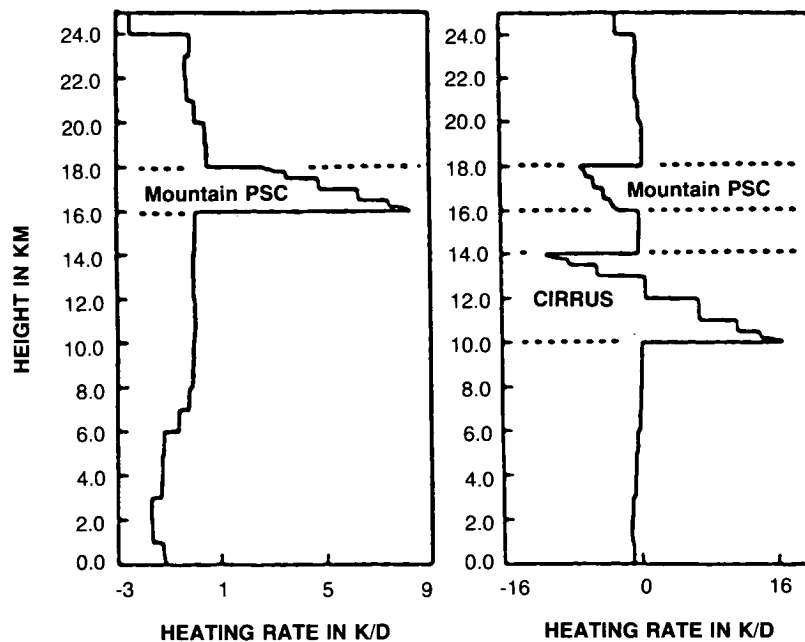


Figure 1.2.4-1. Changes in net heating caused by mountain-PSCs with and without cirrus. The calculations are for a temperature profile from Palmer Peninsula Station for 9 September 1987 (from Kinne and Toon, 1989).

suggest that radiative effects due to clouds may be extremely important under some conditions and clearly demonstrate the importance of accurate specification of the state of the underlying atmosphere.

A full assessment of the impact of PSCs on the radiative budget of the entire polar vortex needs to be performed as considerable uncertainties still remain. Such a calculation would need to include a representative range of tropospheric temperature and cloud conditions, as experienced in the Antarctic during winter and early spring. Clearly the impact of water passing from the vapor to the liquid/ice phase, and possibly out of the lower stratosphere altogether, would need to be incorporated. Perhaps the most important aspect of the radiative properties of PSCs lies in the possibility that some PSCs may lead to very large cooling rates in the lower stratosphere. These in turn could result in substantial downward motion, with attendant effects on the dynamics of the vortex and its ability to work as a “processor” for ozone depletion (see Tuck, 1989, and Section 1.7).

1.3 PHYSICAL PROPERTIES OF POLAR STRATOSPHERIC CLOUDS

The goal of this section is to present laboratory and field studies aimed at understanding the chemical composition of PSCs and their physical properties. In Section 1.3.1, laboratory studies of the co-condensation of HNO_3 and H_2O will be briefly described, and the nature of the interaction of HCl with such surfaces will be summarized. In Section 1.3.2, field observations of chemical species in the particulate phase will be reviewed. It will be shown that both the laboratory and field investigations support the notion that the nitric acid trihydrate is the dominant component of Type 1 PSCs (Toon et al., 1986; Crutzen and Arnold, 1986). Trace amounts of HCl are also expected to be present in such particles based on laboratory and field measurement studies and likely play a particularly important role in heterogeneous chemistry as discussed in Section 1.4.

1.3.1 Laboratory Studies

Co-condensation of HNO_3 with H_2O leads to the formation of PSCs at temperatures above the frost point of water, as concluded by Crutzen and Arnold (1986), McElroy et al. (1986) and Toon et al. (1987) from extrapolations of $\text{HNO}_3/\text{H}_2\text{O}$ vapor pressure data near room temperature.

The physical chemistry of the $\text{H}_2\text{O}-\text{HNO}_3$ system under conditions pertinent to the polar stratosphere has been investigated in the laboratory only very recently (Hanson and Mauersberger, 1988a,b). These authors measured the vapor pressures of both components using high-sensitivity mass spectrometry. The results show that for solids with bulk compositions close to those of the nitric acid trihydrate ($\text{HNO}_3-3\text{H}_2\text{O}$) or the monohydrate ($\text{HNO}_3-\text{H}_2\text{O}$), these crystalline phases can indeed be prepared by co-condensation of gaseous $\text{H}_2\text{O}-\text{HNO}_3$ mixtures with the appropriate composition; bounds on their vapor pressures can be established by extrapolation of vapor pressures of the liquid solutions to the freezing point temperatures, using the Clausius-Clapeyron equation. Furthermore, the results have been shown to agree with the Gibbs-Duhem relationship (Poole, private communication, 1989), which yields the vapor pressure of one of the components in the binary system as a function of the vapor pressure of the other component and of the composition of the condensed phase. These laboratory results corroborate that PSCs consisting of nitric acid trihydrate crystals may form at temperatures several degrees above the frost point of water (see Section 1.2).

The interaction of HCl vapor with water-ice has been studied in the past few years by several groups. Molina et al. (1987) found that HCl has a significant affinity for ice crystals; that it readily diffuses within the surface layers and grain boundaries of such crystals; and that the "sticking" coefficient around 200 K is close to unity, i.e., 0.1 or larger. This coefficient is the probability per collision with the surface that the gas molecule will be incorporated into the condensed phase (assuming a collision frequency given by gas kinetic theory). Similarly high sticking coefficient values were obtained by Tolbert et al. (1987), by M.-T. Leu (1988a) and by Kolb et al. (personal communication, 1988). Molina et al. (1987) and Wofsy et al. (1988) first interpreted their results in terms of a high solubility of HCl in the ice matrix, analogous (but not as large as) that in liquid water. More recent laboratory experiments with a variety of ice substrates, including large single crystals as well as ice frosts, have shown that this affinity of HCl vapor for ice (and the high mobility) are confined to a surface layer that is at least several hundred angstroms deep (Molina et al., 1989). The amounts of HCl absorbed can be orders of magnitude larger than required for the formation of a monolayer at the surface. This behavior is most likely associated with crystal defects, which are known from previous work on ice to be present in layers extending hundreds of angstroms from the surface. Thus, the laboratory observation of a high affinity of HCl vapor for ice frosts is indeed relevant to the behavior of PSCs, since both systems have similarly high surface-to-volume ratios.

In contrast to these results, Wolff et al. (1989) concluded that the solubility of HCl in ice is negligible, and suggested that melting at the surface was responsible for the above observations. Wolff et al. based their conclusions on scanning electron microscopy studies of ice crystals grown by freezing aqueous HCl solutions. It is clear, though, that efficient absorption of HCl vapor by ice can occur readily under conditions where no liquid phase is present, that is, at temperatures below 180 K (Molina et al., 1989).

There is little experimental information on the ternary system $\text{H}_2\text{O}/\text{HNO}_3/\text{HCl}$ at temperatures leading to the formation of solid phases. Tolbert and coworkers (Tolbert, private communication, 1989) have measured a sticking coefficient value of about 0.07 for HCl vapor on nitric acid trihydrate at 190 K. Hanson and Mauersberger (1989a,b) reported vapor pressures of HCl over nitric acid trihydrate at 200 K, with values in the 10^{-8} to 10^{-6} torr range corresponding to compositions in the solid phase in the 0.1 to 2% HCl

POLAR OZONE

range. According to these studies, HCl is significantly more soluble in the trihydrate than in pure water-ice. Work in progress in other laboratories (Molina et al., 1989) corroborates that there is a significant affinity of the trihydrate for HCl. This work indicates that around 180 K, pure water-ice absorbs HCl vapor efficiently only when the HCl partial pressure is above about 10^{-5} torr. The absorption occurs apparently by the growth of HCl hexahydrate crystals, but the hexahydrate is not expected to form at the reduced abundances of HCl present in the stratosphere. Clearly, one of the most difficult aspects of these studies is the proper characterization of the solid substrate, and additional quantitative HCl vapor pressure measurements are clearly needed for various ice substrates.

1.3.2 Direct Supporting Evidence from Field Experiments

Recent field investigations have shed a great deal of light on the composition of polar stratospheric clouds. As noted earlier, a number of studies of PSCs have revealed that the clouds begin to form at temperatures far above the frost point (by as much as 8 K), strongly suggesting condensation of trace species other than water. This was first pointed out by Austin et al. (1986a) based on LIMS observations of anomalous infrared radiance, and studied in detail by Poole and McCormick (1988a,b) using SAM II observations of PSC extinction. Hofmann (1989a,b) and Rosen et al. (1988a) also noted the formation of PSCs at temperatures well above the frost point. Arnold and Knop (1989) reported measurements of HNO_3 in the Arctic that set an upper limit for HNO_3 cloud formation temperatures at 195 K at 23 km, well below the frost point. The optical and physical characteristics of the clouds observed were discussed in Section 1.2. Measurements of particles and gases during the Airborne Antarctic Ozone Experiment (AAOE) and Airborne Arctic Stratosphere Experiment (AASE) provide particularly detailed information on cloud particles and accompanying chemistry.

The observations of total reactive nitrogen (NO_y) by Fahey et al. (1989a,b) also provide important insights into the composition of PSCs. The measurements of NO_y are somewhat difficult to interpret in the presence of PSC particles, because the instrument has a greater sampling efficiency for NO_y in large particulates than for NO_y in the gas phase. This can lead to substantial, particle size-dependent NO_y enhancements when large amounts of NO_y -containing particles are present. These enhancements complicate interpretation of the gas-phase component of the signal but also provide important insights to the particle composition, especially when coupled with concurrent observations of the particle size distribution so that their effects can be quantitatively evaluated (see Fahey et al., 1989b).

Figure 1.3.2-1 shows measurements of NO_y , total water vapor, temperature, pressure, and cloud particles as a function of time on August 17, 1987 from Fahey et al. (1989b). These observations demonstrate that cloud particle formation occurred well above the frost point of water vapor. These observations permit identification of cloud "edges," although it should be emphasized that the past temperature history of air parcels also plays a role in determining the onset of cloud formation and should be examined in a detailed analysis. Nonetheless, it is clear that the observed condensation point was far warmer than the frost point, and in general agreement with expectations based on the thermodynamics of the nitric acid trihydrate as proposed by O. B. Toon et al. (1986) and quantified by the laboratory study of Hanson and Mauersberger (1988a,b). Further, the dramatic NO_y enhancement directly confirms that the particles contain a substantial amount of nitrate. This set of observations therefore provides strong evidence that condensation of HNO_3 plays a critical role in PSC cloud formation.

Observations by Gandrud et al. (1989) support and extend this picture. Gandrud et al. conducted filter sampler measurements of cloud composition during the AAOE experiment. Using a dual filter system,

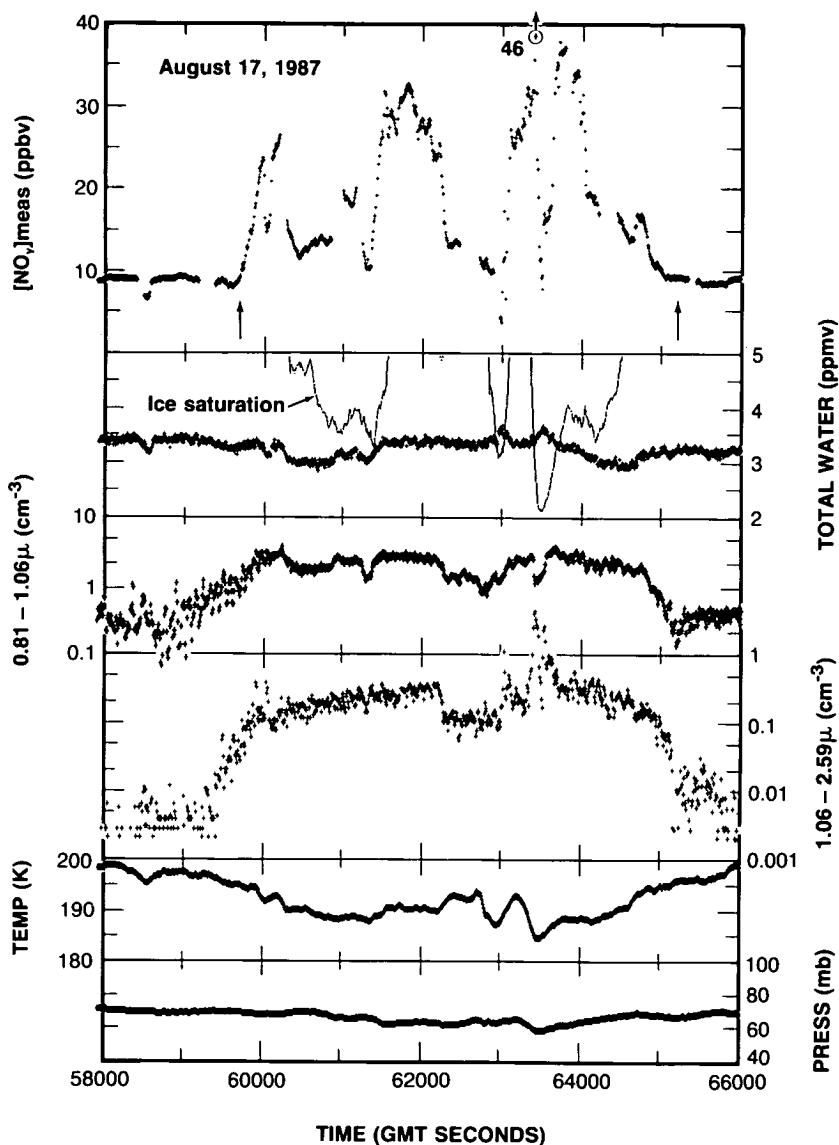


Figure 1.3.2-1. Plot of the flight track data for the encounter with a PSC event on August 17, 1987. The gaps in the NO_y data are caused by instrument calibration checks. The ice saturation mixing ratio is calculated from the observed pressure and temperature using the Smithsonian Meteorological Tables. The cloud edge times are noted by the arrows (from Fahey et al., 1989b).

Gandrud et al. (1989) deduced the amount of nitrate in both the particulate and gas phases. The instrument is sensitive to HNO_3 , ClONO_2 , N_2O_5 , and particulate nitrate. Total acidic chloride (from HCl and ClONO_2) is also observed in both the gas and particulate phases, along with total acidic fluoride. Figure 1.3.2-2 shows the time behavior of the measured percentage of total nitrate in particulates along with other relevant parameters derived for the flight of 4 September, 1987. Note that the most poleward point (about 72°S) was reached at roughly GMT time 61,000 seconds, the temperature at this point was 190 K, and the largest values were obtained during the aircraft "dip" to near 16 km. The data for this flight clearly suggest that a

POLAR OZONE

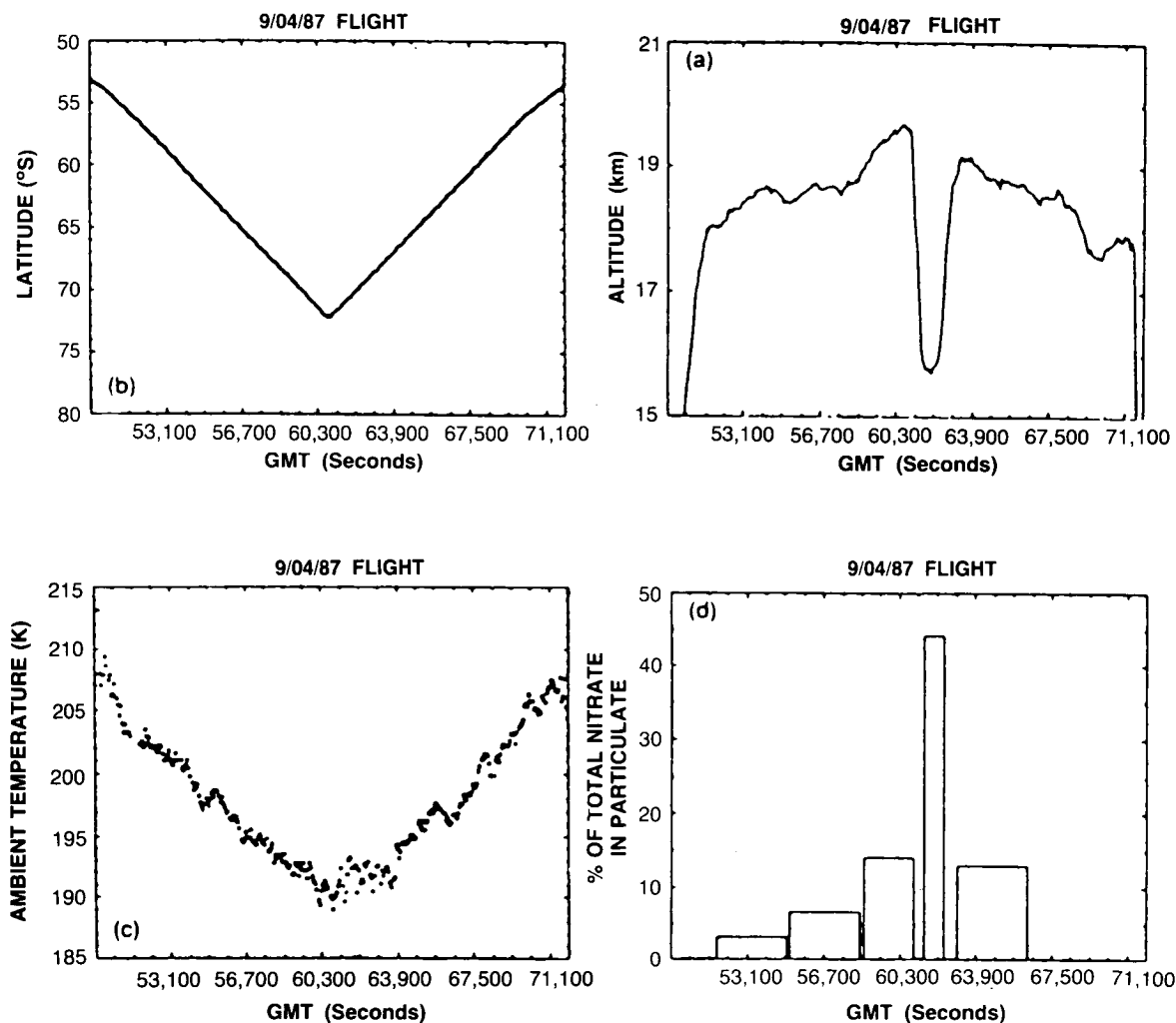


Figure 1.3.2-2. Observations of the percent of total observed nitrate in the particulate phase as a function of time along the AAOE flight track for September 4, 1987 along with observed temperature, latitude and altitude (from Gandrud et al., 1989).

substantial fraction of the available nitrate had been taken up on particles. In contrast, no chloride was observed in the particulate phase on any of the flights, nor were substantial particulate nitrate levels observed outside of the chemically perturbed region. The detection limit for chloride was estimated at 0.08 to 0.16 ppbv Cl. Assuming that the total inorganic chlorine is about 2.5–3.0 ppbv, this corresponds to at most 6.4% of the total chloride, in good agreement with laboratory studies showing that only a few percent of available HCl condenses on ice surfaces (e.g., Molina et al., 1987; Hanson and Mauersberger, 1989a). Similarly, the upper limit for particulate fluoride was only 4–5% of the total acidic fluoride. As discussed in further detail in later sections of this report, the possible removal of nitrate, fluoride, and chloride through sedimentation of large particles can influence the photochemistry of the polar lower stratosphere. The small abundances of chloride and fluoride in the particulate phase strongly suggest that “dechlorination” or “defluorination” will be far less effective than denitrification.

Pueschel et al. (1989) collected aerosol particles during the same aircraft experiments using a wire impactor technique and subsequently analyzed them for nitrate and chloride. Their results revealed a sharp dependence of condensed nitrate on temperature: nitrate-containing aerosols began to form at temperatures below about 193 K, in general agreement with expectations based on the thermodynamics of Type 1 nitric acid trihydrate particles. Pueschel et al. (1989) also concluded that the mass of HCl condensed in the particles was only 3% of the sulfuric acid mass, suggesting that only a small fraction of the available chloride is incorporated into the particles.

As expected from theoretical and laboratory studies, *in situ* measurements of total NO_y and gas and particulate phase nitrate confirm that PSC particles often contain a large amount of nitrate and form at roughly the temperatures expected for the HNO₃/3H₂O system. The formation of nitrate-containing PSC Type 1 clouds is likely to affect the chemistry of the polar lower stratosphere in two important ways: by removing reactive nitrogen from the gas phase (and hence affecting the photochemical balance, at least temporarily), and by allowing for cloud formation at significantly warmer temperatures than the frost point. While the observations are consistent with suggestions regarding irreversible removal of reactive nitrogen via incorporation into particles and subsequent sedimentation, there is no evidence for substantial removal of chloride or fluoride in PSC particles. However, the observations also suggest that a few percent of the available HCl is in the particulate phase (which could drive important heterogeneous processes), consistent with laboratory studies.

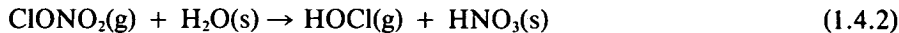
1.4 HETEROGENEOUS CHEMISTRY

Heterogeneous chemical processes in the atmosphere involve a reaction between a gaseous species and a solid or liquid particle. These processes occur in several steps: diffusion of the gaseous molecule to the surface; absorption or adsorption at the surface; diffusion on the surface or into the particle; chemical reaction, etc. For atmospheric systems there is usually not enough information to characterize each of these steps, whose rate may depend not only on the type of particle but also on its temperature, composition, size, shape, etc. On the other hand, the overall reaction rate can be approximated in terms of a single parameter, the "reaction probability *g*," defined as the probability that a collision of a gas molecule with the surface will result in the net chemical reaction in question. This parameter *g* has often been labeled a "sticking coefficient," but this term should be restricted to steps or processes not involving chemical reactions (see Section 1.3).

Molina et al. (1987), using FTIR spectroscopy and gas chromatography, showed that gaseous chlorine nitrate (ClONO₂) reacts efficiently with HCl-doped ice producing molecular chlorine (Cl₂), which is immediately released to the gas phase, and nitric acid (HNO₃), which remains in the solid phase:



These authors measured reaction probability values in the 0.02 to 0.1 range for ice containing HCl at up to 1% mole levels (see Table 1.4-1). Similarly, large reaction probabilities were reported for the same system by Tolbert et al. (1987), who employed a Knudsen cell reactor attached to a mass spectrometer, and by Leu (1988a), who used a fast flow reactor with mass spectrometric detection. In the absence of HCl, the reaction probabilities measured by these groups were somewhat smaller, the gaseous product being HOCl, which has an affinity for ice intermediate between that of Cl₂ and that of HCl:



POLAR OZONE

Table 1.4-1. Reaction probabilities on water-ice

Gaseous Reactant	Temperature (K)	HCl (mole fraction × 100)	Reaction Probability	Reference
ClONO ₂	200	—	0.02	Molina et al. (1987)
ClONO ₂	200	0.03–1.0	0.05–0.1	Molina et al. (1987)
ClONO ₂	185	—	>0.01	Tolbert et al. (1987)
ClONO ₂	185	0–13	>0.01	Tolbert et al. (1987)
ClONO ₂	200	—	0.06	Leu (1988a)
ClONO ₂	200	0.23–7.1	0.11–0.27	Leu (1988a)
N ₂ O ₅	185	—	>0.001	Tolbert et al. (1988a)
N ₂ O ₅	190	—	0.03	Tolbert et al. (1988b)
N ₂ O ₅	190	^a	0.02	Tolbert et al. (1988b)
N ₂ O ₅	190	^b	<0.001	Tolbert et al. (1988b)
N ₂ O ₅	185	7–14	>0.003	Tolbert et al. (1988b)
N ₂ O ₅	195	—	0.028	Leu (1988b)
N ₂ O ₅	195	1.5–4	0.05–0.07	Leu (1988b)

^aOn nitric acid trihydrate.

^bOn nitric acid monohydrate.

Reactions analogous to (1.4.1) and (1.4.2) in which ClONO₂ is replaced by dinitrogen pentoxide (N₂O₅) have been studied in the laboratory by Tolbert et al. (1988b) and by Leu (1988b):



A summary of the reported reaction probabilities is listed in Table 1.4-1. Both because of its apparently large reaction probability and because two chlorine containing reservoir species are affected by it, reaction (1.4.1) is believed to be of particular importance in polar photochemistry (see Section 1.6).

It is likely that nitric acid trihydrate crystals will behave in a manner analogous to water-ice in promoting reactions (1.4.1) to (1.4.4), but this remains to be confirmed in the laboratory. Another issue which requires additional studies involves the competition between water and HCl as heterogeneous reactants, that is, between reactions (1.4.1) or (1.4.3), and (1.4.2) or (1.4.4); the key factor is the concentration of HCl on the surface of the particle. A related question concerns the amount of HCl that will be incorporated into PSCs, and the corresponding concentrations at the surface of the crystals (see Section 1.3.1).

Experiments by Leu (1988b) have indicated a sticking coefficient value greater than about 0.01 for ClO on ice. This system should be studied further to establish whether chemical reactions occur in this process; it might have significant consequences in the polar stratosphere.

The heterogeneous reactions discussed in this section are likely to proceed through an ionic mechanism, without a significant activation energy. The pulsed experiments carried out by Molina et al. (1987) indicated that ClONO₂ remains on the surface of the HCl-doped ice crystals for, at most, a fraction of a second before releasing gaseous Cl₂. Additional studies should be carried out to elucidate the mechanism

of these reactions at a molecular level, particularly considering that there was essentially no precedent in the literature for ice-induced chemistry until its importance in the polar stratosphere became apparent.

For atmospheric modeling purposes (to estimate, for example, the rate at which chlorine is converted to its active form in the polar stratosphere by the reaction between ClONO_2 and HCl on ice), one needs to compute a collision frequency for ClONO_2 vapor with the surface of the PSC particles, to be multiplied by the reaction probability g . The former depends on the abundance and the size of the particles, which can come from atmospheric observations or, in principle, from detailed considerations of cloud microphysics. These considerations, in turn, require information on nucleation rates, vapor pressures, sticking coefficients, etc. The concentration of HCl on the surface of the PSC particles also needs to be estimated, since it affects the reaction probability g . This can be done, assuming complete equilibration in the atmosphere, from laboratory measurements of the HCl surface concentration as a function of temperature, and of the HCl partial pressure in the gas phase (i.e., the thermodynamics of the HCl/ice system). The sticking coefficient for HCl vapor on ice would also be needed if one wants to estimate the time scale for HCl vapor to be absorbed by the PSCs, rather than assuming thermodynamic equilibrium. The desorption rate would then also be needed: it can be obtained from laboratory measurements, or in principle, it can be calculated given the sticking coefficients, the equilibrium vapor pressure, and by taking into account diffusion rates within the particle.

At present even the functional dependencies for many of the relevant parameters are not clear: does the HCl vapor pressure depend linearly on the HCl concentration in the particles? Does the reaction probability for ClONO_2 or N_2O_5 colliding with nitric acid trihydrate crystals depend significantly on whether the crystals are water-rich or nitric acid-rich? How large need the particles be before it matters where the HCl is absorbed, i.e., surface layers vs. bulk solid? Clearly, much additional work remains to be done.

Sulfuric acid aerosols may also promote important heterogeneous chemical reactions in the stratosphere, analogous to those discussed above (Hofmann and Solomon, 1989). However, the chemical reaction rates are uncertain at present. Tolbert et al. (1988a) have shown that ClONO_2 vapor reacts readily with HCl dissolved in aqueous sulfuric acid solutions. For this system, however, measurements of the HCl vapor pressure as a function of temperature and composition are needed, so that the chemical rate experiments can be carried out with a concentration of HCl in the condensed phase that corresponds to stratospheric conditions. Only trace amounts of stratospheric HCl will dissolve in the typical mid-latitude sulfuric acid aerosols (Molina et al., 1989; Watson et al., 1989), which contain less than about 40% by weight of water. In regions at lower temperatures, these aerosols absorb more water (Steele et al., 1983), and may freeze to form sulfuric acid hydrates. As discussed in Section 1.2, at sufficiently low temperature these aerosols grow to form PSCs. It is likely, though, that they become chemically active even before reaching the PSC stage.

1.5 GAS PHASE CHEMISTRY

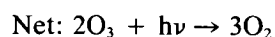
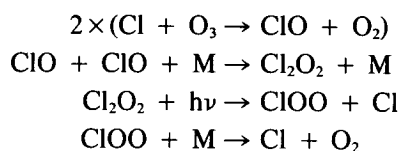
In this section, the gas phase photochemistry relevant to polar ozone depletion will be reviewed. As indicated in Section 1.1.4, it was suggested that heterogeneous reactions on PSCs could lead to enhanced levels of reactive chlorine in the polar lower stratosphere, leading to possible ozone loss through some arguably unusual catalytic cycles. The possible catalytic cycles considered are delineated in Section 1.5.1, and the importance of coupling between reactive nitrogen and reactive chlorine is emphasized. In Section 1.5.2, several aspects of relevant polar photochemistry and their uncertainties are discussed. Finally, photolysis rates for a number of molecules of possible importance in the polar lower stratosphere in winter and spring are presented and their implications for ozone depletion are explored.

POLAR OZONE

1.5.1 Photochemical Processes of Importance in Polar Ozone Depletion

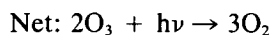
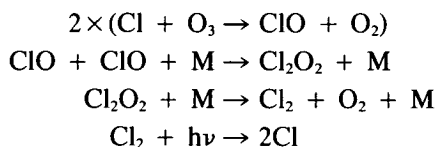
There are several catalytic chemical and photochemical processes that can contribute to Antarctic ozone depletion. Modeling studies that seek to evaluate and compare these cycles insofar as their role in Antarctic ozone depletion is concerned will be discussed in Section 1.6.4.

Molina and Molina (1987) emphasized the importance of ClO dimer formation and photolysis:



The formation of the ClO dimer and its photolysis provides a pathway for ozone loss whose rate is proportional to the square of the ClO abundance, leading to a strong non-linearity in possible ozone depletion. As will be shown in Section 1.6, observations of ClO and detailed modeling studies have shown that this catalytic cycle likely played a dominant role in the intense Antarctic ozone depletion observed during austral spring, 1987.

Molina and Molina (1987) noted that thermal decomposition of the ClO dimer might also lead to ozone loss at cold temperatures:



However, the products of thermal decomposition of the ClO dimer are subject to debate at present. If thermal decomposition of Cl_2O_2 leads to 2ClO rather than to the products indicated above, then significant ozone loss will not occur through ClO dimer formation whenever temperatures are warm enough for thermal decomposition to dominate over photolysis (in effect, a "do-nothing" cycle is obtained rather than ozone destruction). This is a particularly important issue insofar as Northern Hemisphere ozone depletion is considered. Figure 1.5.1-1 illustrates the rate of thermal decomposition of the ClO dimer as a function of temperature based on present best-estimates of kinetic rates, compared to the range of its photolysis rate for solar zenith angles between about 70 and 90 degrees. In examining this figure in order to determine whether photolysis or thermal decomposition is likely to be the dominant fate of any Cl_2O_2 formed, the fraction of the day that is sunlit must be considered along with the local temperatures. During Antarctic late winter and early spring in the lower stratosphere, temperatures generally remain well below 210 K at least until mid-October, so that Cl_2O_2 photolysis is expected to dominate its loss rate. Hence, ozone loss through the photolysis cycle will occur upon formation of the dimer. In the Arctic, stratospheric warmings often raise lower stratospheric temperatures well above 210 K, at least by late February. These warmer temperatures favor thermal decomposition of the dimer and hence are likely to mitigate ozone loss if the products of the thermal decomposition process are 2ClO , even if greatly elevated levels of ClO are present.

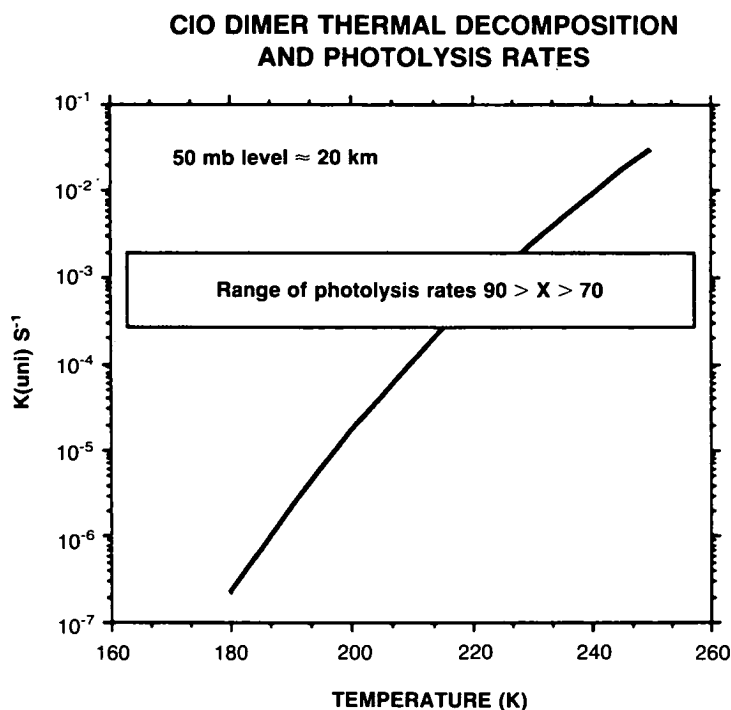
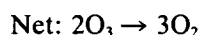
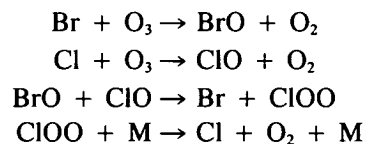


Figure 1.5.1-1. Thermal decomposition rate of Cl_2O_2 near 50 mb (calculated from the equilibrium constant measurements of Hayman and Cox (private communication, 1989) and the forward rate constant of Sander et al. (1989) along with the range of photolysis rates at that level for solar zenith angles from 70 to 90 degrees.

Further studies of the products of Cl_2O_2 thermal decomposition are needed to address this issue, which may represent a significant element in determining inter-hemispheric differences in ozone destruction rates.

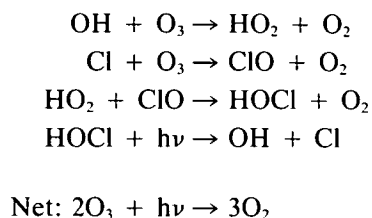
McElroy et al. (1986a), Tung et al. (1986), and Rodriguez et al. (1986) emphasized the catalytic destruction of ozone via the interaction of ClO and BrO:



It is important to note that the reaction between ClO and BrO has three product channels, which influence the diurnal variations of BrO and hence limit its ability to destroy ozone to the sunlit atmosphere. Other channels and their branching ratios are discussed below. The rate of ozone loss due to this catalytic cycle is dependent on the abundances of ClO and BrO in the polar lower stratosphere. Both species have been measured in the Arctic and Antarctic lower stratospheres, as discussed in Sections 1.6 and 1.10. The bromine-catalyzed destruction of ozone can be extremely effective in destroying ozone in the lower stratosphere even at relatively modest enhancements of ClO, leading to a high ozone depletion potential for bromine species (which is believed to play a particularly important role in Arctic ozone depletion due in part to relatively warm temperatures in spring as noted above).

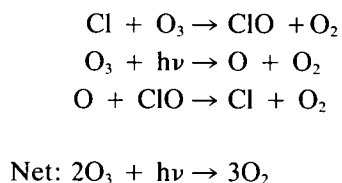
POLAR OZONE

Solomon et al. (1986) and Crutzen and Arnold (1986) also discussed the possibility of the HO_x-ClO_x catalytic destruction of ozone:



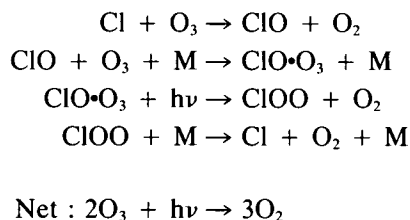
Measurements of HOCl (Toon and Farmer, 1989) in the Antarctic stratosphere discussed in Section 1.6 suggest that this cycle is unlikely to contribute significantly to the observed ozone loss there (but see below for further kinetic studies of relevance).

Finally, the well-known ClO_x-O_x catalytic cycle should be mentioned among currently accepted chemical schemes:

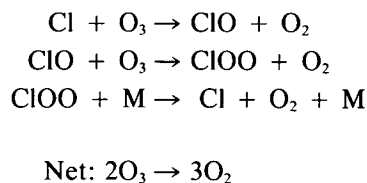


The competition between these cycles in destroying Antarctic ozone depends on the relative abundances of ClO, BrO, reactive hydrogen, atomic oxygen, temperature, the required wavelengths of the indicated photodissociation processes, and the relevant kinetic rate constants.

Some additional potentially important chemical cycles have recently been delineated by Anderson et al. (1989):



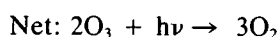
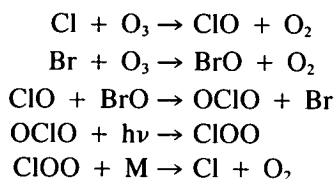
and



Although the current estimated upper limit for the bimolecular reaction between ClO and O₃ is $1.0 \times 10^{-18} \text{ cm}^3 \text{ s}^{-1}$ (DeMore et al., 1987), this reaction could be important if the rate constant is as fast as $1.0 \times 10^{-17} \text{ cm}^3 \text{ s}^{-1}$, and the reaction rate is extremely difficult to determine accurately in the laboratory due to secondary

reactions of the Cl atoms. As will be shown in Section 1.6.4, some studies suggest that additional catalytic cycles such as those indicated by Anderson et al. (1989) may be needed to explain the observed rate of Antarctic ozone depletion, while other studies disagree that any additional losses are needed.

Vaida et al. (1989) propose another possible ozone loss mechanism involving photoisomerization of OCIO. If OCIO photolysis leads to ClO + O, no ozone loss is obtained through OCIO formation. If, on the other hand, OCIO photoisomerizes to ClOO, the following catalytic ozone-destroying cycle is obtained in the sunlit atmosphere:

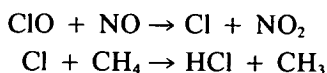


The efficiency of this cycle depends on the rate constant of the reaction between ClO and BrO, the branching ratio for OCIO production, and the quantum yield for OCIO photoisomerization. The latter parameter requires further study in the laboratory.

The interaction between nitrogen- and chlorine-containing species is a critical element in polar ozone depletion. Section 1.4 described heterogeneous reactions that liberate reactive chlorine at the expense of the reservoir species, HCl and ClONO₂. The reactive chlorine can form ClO in the presence of sunlight and go on to participate in the catalytic cycles delineated above. However, the time scale during which the ClO so formed remains available to destroy ozone depends critically on the abundances of the nitrogen oxides, NO and NO₂, which control the rate of reformation of both HCl and ClONO₂ from ClO. In the case of ClONO₂, the reaction leading to its formation is:



so that the rate of reformation of ClONO₂ is directly controlled by the NO₂ abundance. The reactive nitrogen species also play an important role in HCl formation by the more indirect route:



so that nitrogen oxide abundances strongly influence the loss rate of any chlorine radicals liberated by heterogeneous processes. The abundances of gas-phase nitrogen oxide species are reduced by the same heterogeneous reactions responsible for chlorine release (1.4.1–1.4.4). These reactions convert relatively short-lived nitrogen compounds such as N₂O₅ into HNO₃ (a much longer-lived nitrogen reservoir) and hence reduce the abundances of NO and NO₂. Furthermore, the HNO₃ product apparently remains in the particulate phase, and sedimentation of large particles may even remove nitrogen from the stratosphere altogether (denitrification). These processes greatly lengthen the photochemical lifetime of ClO and hence increase the ozone loss rate. Figure 1.5.1-2 illustrates the strong effect of denitrification on the time scale for ClO recovery. In the particular case shown, the abundance of ClO obtained nine days after a notional PSC event is doubled when severe denitrification is assumed as compared to a non-denitrified case.

POLAR OZONE

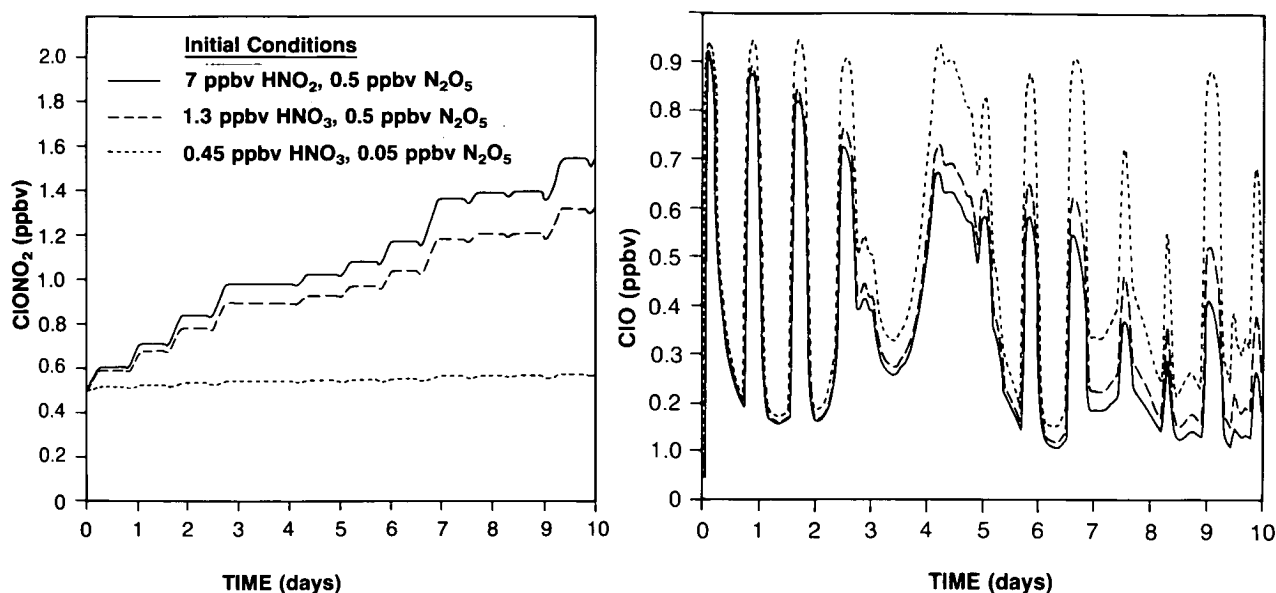


Figure 1.5.1-2. Calculated time behavior of ClONO₂ and ClO during Arctic spring for three different cases, illustrating the importance of the reactive nitrogen content in determining the time scale for photochemical recovery following PSC exposure.

1.5.2 Laboratory Kinetics and Photochemistry

The importance of species such as Cl₂O₂ in the polar stratosphere has been recognized only recently, and the chemistry and photochemistry of this compound had not been investigated earlier. In contrast, the rates of elementary reactions such as Cl + O₃ or ClO + NO₂ had been measured years ago, although not under conditions directly applicable to the polar stratosphere, where they are also important. However, their rates under polar stratospheric conditions can be estimated by extrapolation, for which there exists a theoretical framework (see, e.g., DeMore et al., 1987). In general, though, the uncertainties in the measurements increase at the lower temperatures, and much laboratory work remains to be carried out to ensure the validity of these extrapolations and also to further elucidate polar stratospheric chemistry. This work is challenging, since existing techniques often cannot be readily implemented at the relatively low temperatures and high pressures of interest. Also, there are potentially important reactions—homogeneous and heterogeneous—involving bromine-containing species, higher oxides of chlorine, etc., that should be investigated.

Much progress has been achieved in terms of understanding the physical chemistry of Cl₂O₂, the ClO dimer, since it was first suggested as an intermediate in a catalytic ozone destruction cycle (Molina and Molina, 1987). The infrared and ultraviolet spectra, as well as the structure of this species, which is the symmetrical chlorine peroxide, ClOOC1, are now reasonably well established. The two compounds originally assigned by Molina and Molina (1987) as isomers of Cl₂O₂ are now known to be the symmetric peroxide and Cl₂O₃, which is formed by addition of ClO to OClO, in agreement with the findings of Hayman et al. (1986). These authors reported a measurement of the UV spectrum of ClOOC1, which has subsequently been verified with good agreement by Burkholder et al. (1989), Friedl and Sander (1988), Molina (1989), DeMore and Roux (private communication, 1989), and Vogt, Parmien, and Schindler (private communication, 1989). Figure 1.5.2-1 shows a ClOOC1 spectrum, which is a smoothed average of the results of Hayman et al. (1986), DeMore and Roux (private communication, 1989), and Vogt et al. (private commu-

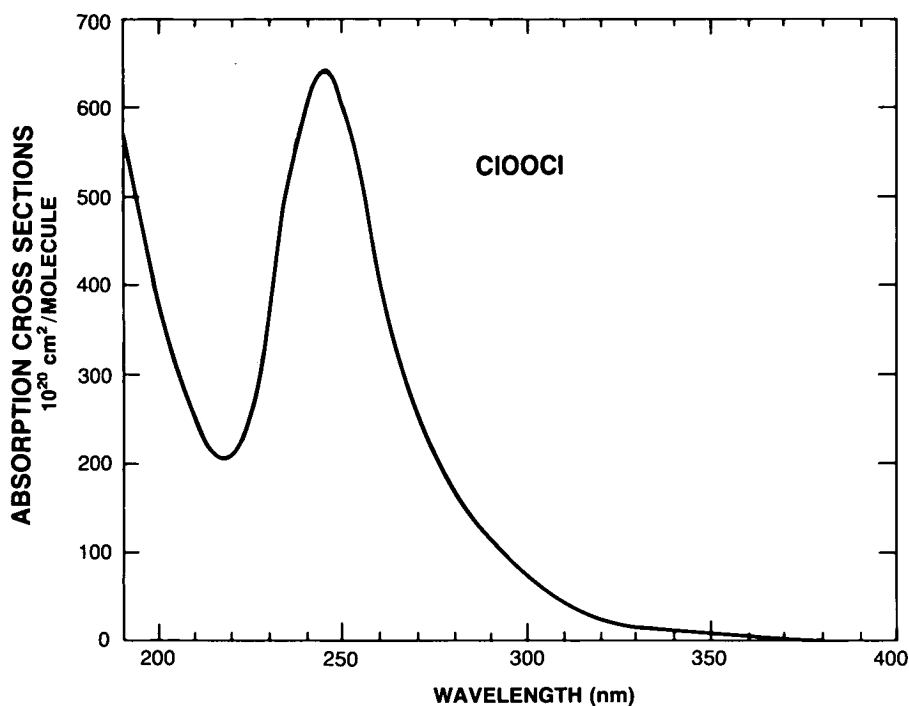


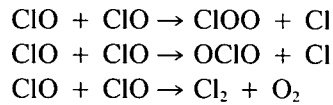
Figure 1.5.2-1. Absorption cross sections of ClOOCl: smoothed average of the results of Hayman et al. (1986), DeMore and Roux (private communication, 1989), and Vogt et al. (private communication, 1989).

nication, 1989). The cross section data of Burkholder et al. are about 35% larger around 280 nm. More accurate data are needed, particularly in the long wavelength tail beyond 300 nm, in order to better estimate the atmospheric photodissociation rates. The long-wavelength tail is of particular importance, since it controls the photolysis rate at the large solar zenith angle characteristic of the polar spring (see the discussion of Figure 1.5.2-3 below). The infrared spectra of ClOOCl and of Cl₂O₃ have also been characterized (Burkholder et al., 1989; Friedl and Sander, 1989; Molina, 1989; Cheng and Lee, 1989). Cheng and Lee noted that their observed infrared spectrum for ClOOCl was in excellent agreement with the predictions of McGrath et al. (1988), and found no evidence for formation of ClOCIO. Furthermore, the thermal stability of these species has been investigated by Cox and Hayman (1988) and Hayman et al. (1986): they conclude that the dimer is bound by 17 kcal/mole, and Cl₂O₃ by about 15 kcal/mole. Ab-initio quantum mechanical calculations have further corroborated the higher stability of ClOOCl relative to that of ClOCIO and ClClO₂, which are other plausible isomeric forms (Toohey et al., 1987; McGrath et al., 1988). More recently, high-resolution microwave spectra of the product of the ClO self reaction have clearly established that it is indeed the non-planar ClOOCl (Birk et al., 1989); furthermore, these authors were able to infer high-accuracy bond lengths and angles for this molecule.

The primary photodissociation products in the photolysis of ClOOCl need to be determined. There are indications from experiments reported by Margitan (1983) that Cl atoms are produced, and this is the channel expected for photolysis at the atmospherically important wavelengths, namely around 310 nm. By analogy with other species such as ClONO₂, absorption of a photon at those wavelengths promotes a non-bonding electron in the Cl atoms to a repulsive electronic state which falls apart by breaking the Cl atom bond. The weaker ClO-OCl peroxide bond is not likely to be affected at those wavelengths.

POLAR OZONE

The self-reaction of the ClO radical has been under investigation since the 1950s: there are three channels for the pressure independent component, which is rather slow:



The pressure-dependent channel yields the dimer, whose existence had been merely postulated in the early studies:



At the temperatures and pressures characteristic of the polar stratosphere, this appears to be the only channel of importance. The rate constant for this pressure-dependent step has been measured by Cox and Hayman (1988), who employed a molecular modulation technique; very recent studies using the more direct flash-photolysis approach have yielded rate constant values that are smaller by up to a factor of two at the temperatures and pressures appropriate to the polar stratosphere (Sander et al., 1989; Trolrier et al., 1989). The 194 K results are shown in Figure 1.5.2-2; the rate increases by a little more than a factor of two between 250 K and 190 K.

The reaction between ClO and BrO also has a complex mechanism with several channels:

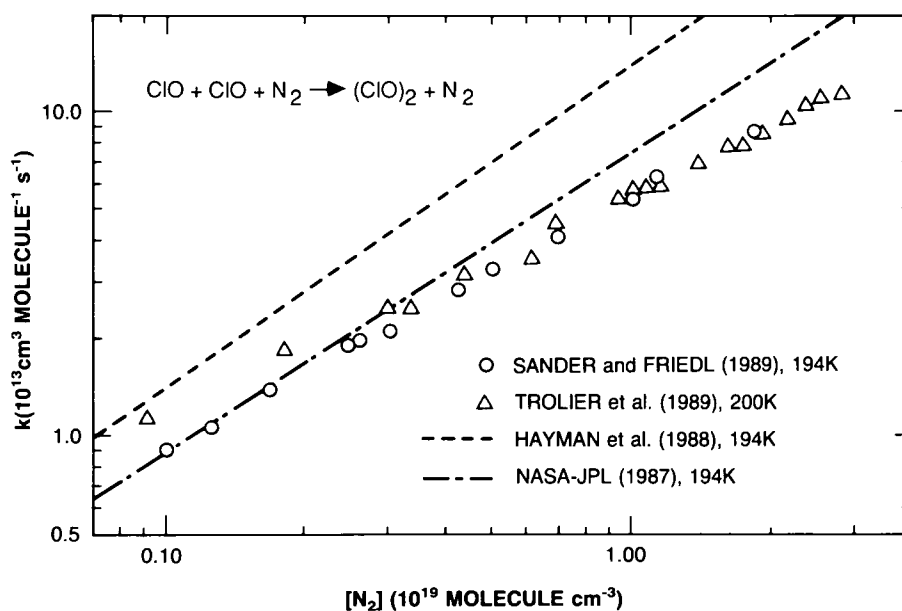
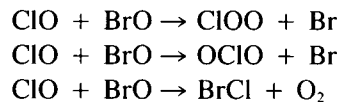


Figure 1.5.2-2. Rate constants for the $\text{ClO} + \text{ClO} + \text{M} \rightarrow \text{Cl}_2\text{O}_2 + \text{M}$ reaction, with N_2 as the third body M.

Several recent studies of this complex reaction have been carried out. The results for the overall rate constant are summarized in Table 1.5.2-1: at room temperature, the older number of Clyne and Watson (1977) is in good agreement with Toohy et al. (1988) and Sander and Friedl (1988), while the value reported by Hills et al. (1987) is about 40% smaller. Also, in this latter work no significant temperature dependence is reported, while Sander and Friedl find that the overall rate constant increases by about a factor of two for a temperature change between 400 K and 220 K.

In terms of the partitioning to the different product channels, all these authors agree that production of ClOO and OCIO are about equally fast; BrCl production appears to be only about 8% of the total, according to Sander and Friedl (1988). This is, however, an important channel, because it provides a means of sequestering BrO during the night, reducing the magnitude of the diurnal OCIO variation. (See Friedl and Sander, 1988; and Sander and Friedl, 1988, for a more detailed description of this work.) As discussed in Section 1.6, OCIO has been measured both at night and during the day in Antarctica.

Although the importance of OCIO as an atmospheric species has only been recognized recently (Rodriguez et al., 1986; McElroy et al., 1986a; S. Solomon et al., 1987), its chemistry and photochemistry had been the subject of many earlier laboratory studies (see, e.g., DeMore et al., 1987). In particular, the absorption spectrum in the near UV, which is highly structured, has been carefully reexamined, since it is needed for the interpretation of atmospheric measurements (Wahner et al., 1987). The upper electronic states are strongly predissociated, and hence the quantum yield for photodissociation is essentially unity.

Simon et al. (1989) have measured a rate constant value at 300 K of about $3 \times 10^{-12} \text{ cm}^3 \text{ molecule}^{-1} \text{ s}^{-1}$ for the reaction

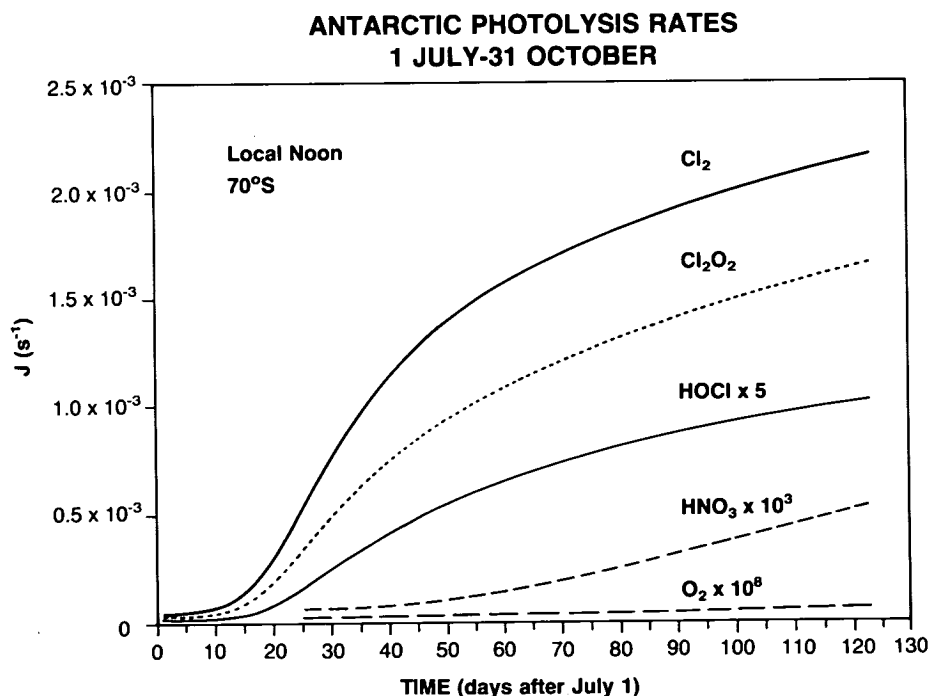


Figure 1.5.2-3. Photolysis rates for Cl₂O₂, HOCl, Cl₂, HNO₃, and O₂ at 70°S at noon as a function of day, at the 50 mb level (approximately 20 km).

POLAR OZONE

The dominant path appears to yield ClOO and CH₃O as products. The authors emphasize that this reaction might lead to enhanced OH levels in the polar stratosphere and hence to ozone depletion through the HO_x/ClO_x catalytic cycle discussed above.

The photolytic properties of many of the molecules considered above are critical to their role in polar ozone depletion. In particular, the products of heterogeneous reactions involving chlorine discussed in Section 1.4 (Cl₂, HOCl, ClONO₂) all have relatively large absorption cross sections in the visible and near-ultraviolet portion of the spectrum. Thus, they photodissociate readily upon exposure to sunlight, even at the exceedingly large solar slant angles typical of polar winter and spring. The photolysis reactions of HNO₃ and O₂ tend to offset the chemical effects of heterogeneous reactions by liberating reactive nitrogen that can reform the ClONO₂ reservoir and by directly producing odd oxygen. These molecules both photolyze at rather short wavelengths in the ultraviolet portion of the spectrum. Hence, their ameliorating influences are likely to be relatively small when solar zenith angles are large and very little ultraviolet penetration is possible. Figure 1.5.2-3 shows the calculated seasonal behavior of the photolysis rates of several of these species, illustrating the fact that chlorine activated by heterogeneous processes can begin to destroy ozone before photochemical processes involving HNO₃ and O₂ can halt or reverse the ozone decline. The points when production of odd oxygen and NO₂ begin to become important will depend not only on the photolysis rates, but also on the HNO₃ abundance.

1.6 PHOTOCHEMISTRY OF THE ANTARCTIC SPRING

Ground-based and aircraft observations, some dating back to the late 1970s, have shown that the chemical composition of the Antarctic spring vortex is highly unusual. The partitioning of both chlorine and nitrogen species has been shown to be dramatically perturbed compared to gas-phase model predictions or measurements at other latitudes, and there is evidence for the removal of substantial quantities of nitrogen oxides and water vapor from the atmosphere. In this section, present understanding of the composition of the lower Antarctic stratosphere will be described. As will be shown, virtually all of the observed perturbations are consistent with the expectation that important heterogeneous reactions take place on the surfaces of polar stratospheric clouds. The implications of these chemical perturbations for ozone depletion are discussed.

The vertical coordinate used for much of the discussion is potential temperature. Approximate equivalent pressures and altitudes for Antarctic spring conditions are given in Table 1.6-1.

1.6.1 Reactive and Reservoir Chlorine

Measurements of ClO coupled with knowledge of the catalytic cycles that destroy ozone (Section 1.5) provide the basis for evaluating the photochemical contribution to Antarctic ozone loss. The primary evidence demonstrating that ClO is responsible for much of the ozone loss in the Antarctic spring is the observation of exceedingly high ClO abundances by two independent techniques. Aircraft and ground-based studies have both shown that the ClO mixing ratios near 18 km inside the Antarctic vortex are on the order of 1 ppbv (deZafra et al., 1987; P. Solomon et al., 1987; Brune et al., 1989a; Anderson et al., 1989). Values expected from measurements at mid-latitudes and from multi-dimensional model studies (neglecting the heterogeneous reactions indicated in Section 1.4) are only about 10 pptv, so that the measured abundances of 1 ppbv are enhanced by a factor of about one hundred. The aircraft studies provide *in-situ* ClO abundances from about 13–20 km using a resonance fluorescence approach, while the ground-based studies employ microwave emission techniques and yield vertical profile information with

Table 1.6-1. Potential temperatures and approximate geometric altitude and pressure equivalents

Potential Temperature (K)	Approximate Geometric Altitude (km)	Approximate Pressure (mb)
428	17.5	55
420	17.0	60
400	16.25	80
380	15.5	100
360	14.25	120
340	12.5	150

about 5 km vertical resolution for the height range from about 15 km to 50 km. Studies using these data (Anderson et al., 1989; Barrett et al., 1988; Ko et al., 1989; Austin et al., 1989; Jones et al., 1989) have shown that such concentrations of ClO can account for much of the observed ozone loss using measured photochemical rates, although there is some debate at present regarding whether the calculated total ozone loss rate is fully consistent with that inferred from observations (see Section 1.6.4).

Proffitt et al. (1989a) have suggested that the latitude at which ClO mixing ratios exceed about 130 pptv is a useful definition of the boundary of the chemically perturbed region (CPR). Figure 1.6.1-1 displays measured ClO abundances as a function of latitude relative to this boundary averaged over the AAOE mission at two different potential temperatures. Within the CPR, ClO mixing ratios are over an order of magnitude greater than outside. The very high ClO mixing ratios observed within the CPR are consistent with calculations employing semi-empirical estimates for the heterogeneous chemistry, likely surface areas, and frequencies of PSCs based on meteorological data, as discussed in greater detail in Section 1.6.4 (Jones et al., 1989). It is also possible that the ClO abundances well outside of the CPR reflect some influence of heterogeneous processes, either through local PSCs that occur occasionally or earlier in the season, or through transport of air out of the polar vortex (see Fahey et al., 1989a; Jones et al., 1989).

Figure 1.6.1-2 displays vertical profiles of ClO mixing ratio obtained over Antarctica in 1987. Data above about 20 km (left) are from ground-based measurements made from McMurdo (Barrett et al. 1988), while those on the right were obtained from aircraft observations (Brune et al. 1989a). The ground-based data show a double-peaked structure, with one mixing ratio maximum near 40 km that is consistent with homogeneous, gas-phase photochemistry, and another near 20 km that is not observed at other latitudes and is thought to be the result of heterogeneous reactions on PSC cloud surfaces in the lower stratosphere. A strong vertical gradient is visible in the aircraft data below 20 km, with rapidly decreasing abundances at lower potential temperatures. This gradient likely reflects in large part the gradient in the abundance of available reactive chlorine as compared to that in organic forms (largely CFCs), as well as altitude variations in the partitioning between the ClO dimer and ClO.

The ground-based data have also provided information on the diurnal variation of ClO. As shown in Figure 1.6.1-3, the ClO observed near 20 km rapidly disappears at night. Such diurnal variation is expected due to formation of nighttime reservoirs such as Cl₂O₂ and OClO (Section 1.5) and supports the identification of ClO. Measurements show that daytime ClO mixing ratios remain high within the vortex for a period of a month or more in the austral spring. Ground-based microwave data (P. Solomon et al., 1987) showed that ClO was greatly elevated in the lower stratosphere throughout September 1986, although little was

POLAR OZONE

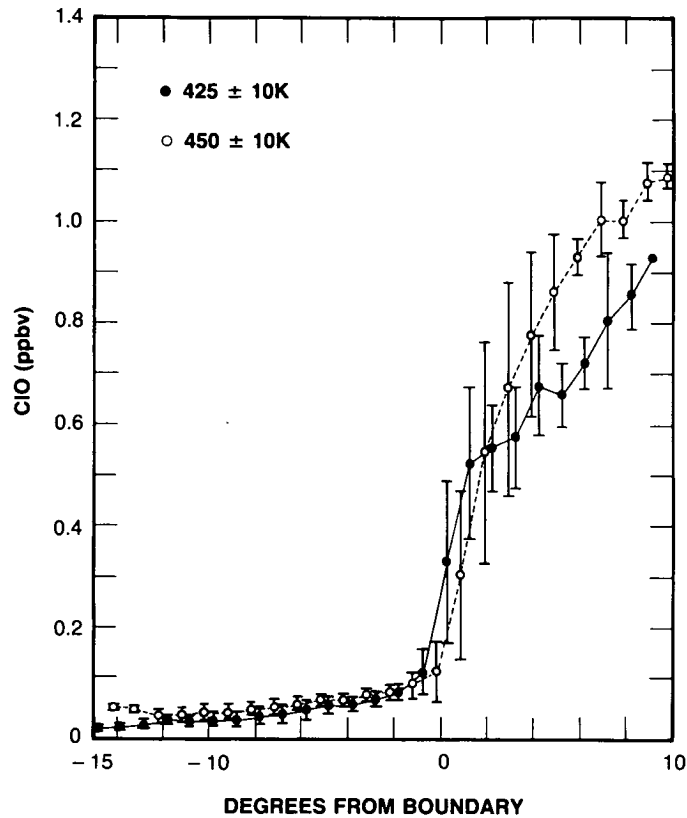


Figure 1.6.1-1. Observed ClO mixing ratio latitude gradients on the 425 and 450 K potential temperature surfaces averaged over the AAOE mission period (Brune et al., 1989a). The latitude averages were performed relative to the boundary of the chemically perturbed region (see Fahey et al., 1989b).

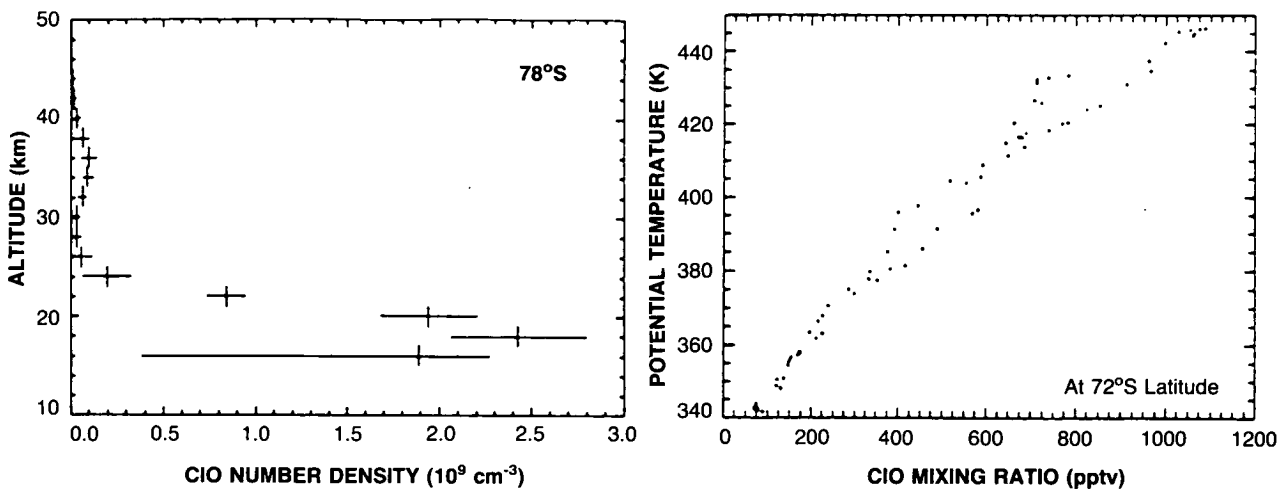


Figure 1.6.1-2. The vertical profile of ClO mixing ratio within the southern polar vortex, from ground-based microwave measurements (left, from Barrett et al., 1988) and from *in situ* measurements at 72°S (right, from Brune et al., 1989a.).

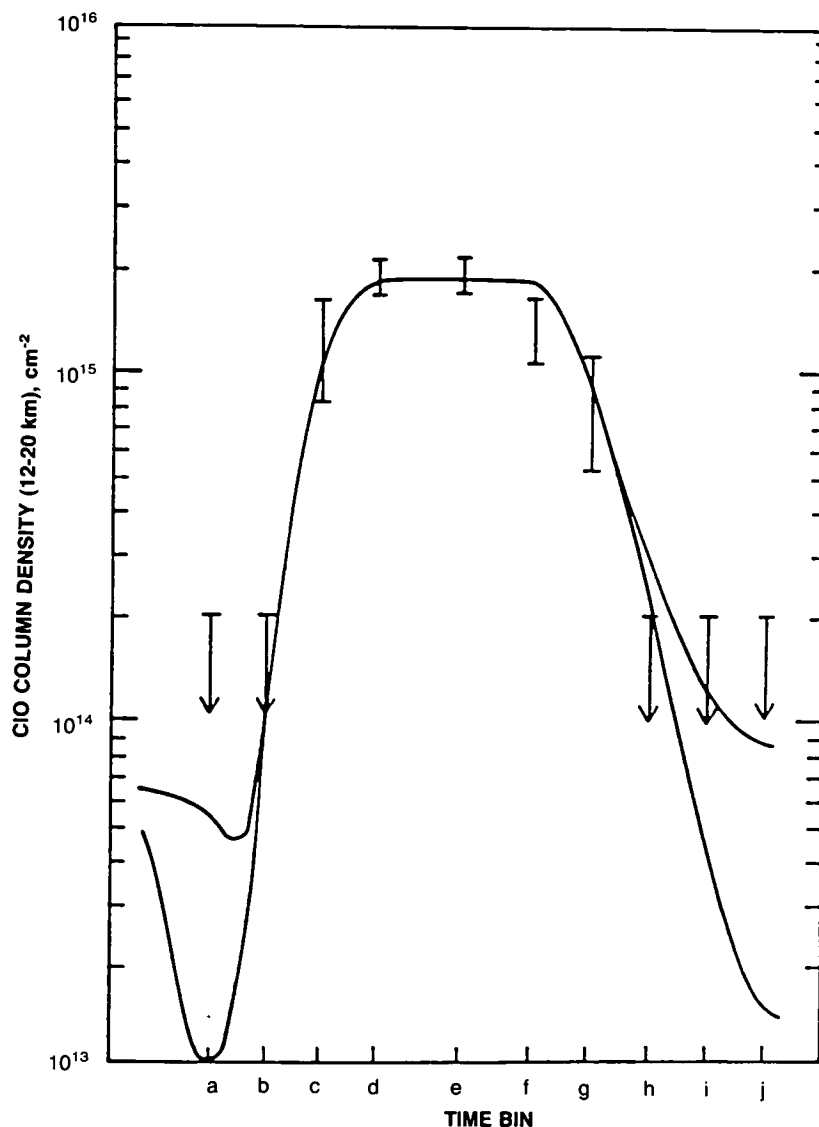


Figure 1.6.1-3. Diurnal variation of the column abundance of CIO below about 25 km at McMurdo Station, Antarctica (from deZafra et al., 1989).

detected in October 1987 (see also, Figure 1.6.1-5). This seasonal trend is broadly consistent with the observed September loss of Antarctic ozone.

Other measurements of chlorine-containing species confirm and support these results. Observations of the column abundance of OCIO have been obtained from ground-based and aircraft-borne spectrometers using many spectral absorption bands in the wavelength range from about 340 to 430 nm (S. Solomon et al., 1987; Wahner et al., 1989b). These have shown that the abundance of OCIO is about 50–100 times greater in the Antarctic polar vortex than can be accounted for without considering heterogeneous chemistry. The enhancement in OCIO is consistent with the observed enhancement in CIO noted above (Solomon

POLAR OZONE

et al., 1989) and provides important, independent confirmation of large perturbations in Antarctic chlorine chemistry.

Figure 1.6.1-4 presents observations of the diurnal variation of OCIO above McMurdo station, showing evidence for rapid formation of OCIO at sunset. Similar diurnal variations were measured by Wahner et al. (1989b). Model calculations predict a pronounced diurnal behavior for OCIO due to rapid formation at sunset, proceeding unhindered by photolysis (Rodriguez et al., 1986; Salawitch et al., 1988). Figure 1.6.1-5 presents observations of the seasonal trend in OCIO in evening twilight from McMurdo Station during 1986

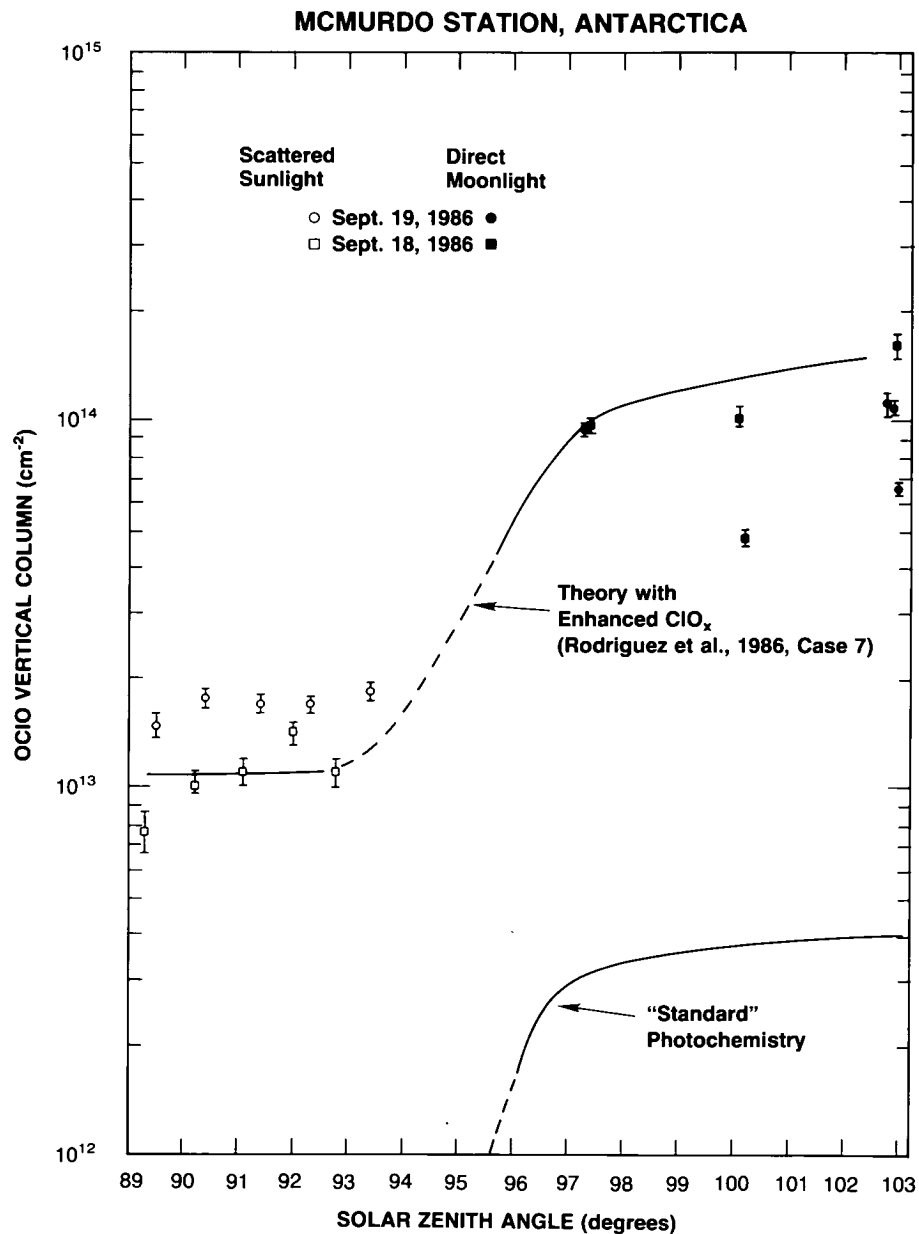


Figure 1.6.1-4. Diurnal variation of the column abundance of OCIO above McMurdo Station, September 18-19, 1986. Twilight and moon measurements are indicated (from S. Solomon et al., 1987).

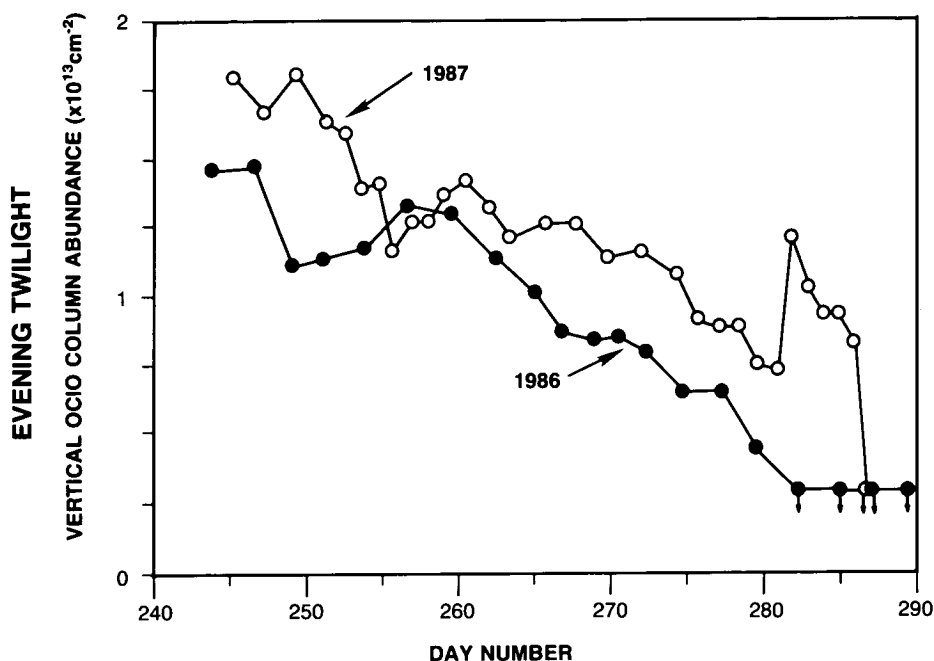


Figure 1.6.1-5. Daily measurements of the sunset OClO column abundances above McMurdo Station in 1986 and 1987 (from Sanders et al., 1989a).

and 1987 (from Sanders et al., 1989). These data show that the abundance of OClO decreases throughout September, falling to zero in early October in both years. This seasonal trend is qualitatively consistent with that in ClO noted above. Poole et al. (1989) have shown a close correspondence between the seasonal evolution of observed OClO abundances and optical depths of PSCs observed in 1986 and 1987. Morning twilight OClO abundances are generally lower than the evening twilight values, and disappear a few weeks earlier (see Section 1.6.4).

Observations of ClONO₂ (Farmer et al., 1987; G. Toon et al., 1989a) and HCl (Farmer et al., 1987; Toon et al., 1989a; Coffey and Mankin, 1989) are also of great importance to understanding the perturbations to chemistry and photochemistry induced by PSCs. Figure 1.6.1-6 presents measurements of the column abundance of ClONO₂ as a function of latitude as indicated by G. Toon et al. (1989a). The abundances of ClONO₂ obtained near the edge of the CPR are a good deal higher than model predictions, and strongly suggest formation of ClONO₂ in those regions where ClO abundances are enhanced by cloud processes or by mixing of processed air, but ClONO₂ is not effectively suppressed by the same cloud chemistry (see Section 1.6.4). As shown for example by Jones et al. (1989), any remaining NO_x will rapidly form ClONO₂ following enhancement of ClO by cloud processing. When stoichiometric considerations limit the amount of NO₂ available for ClONO₂ formation, then the abundance of ClONO₂ drops in clear air after cloud processing.

POLAR OZONE

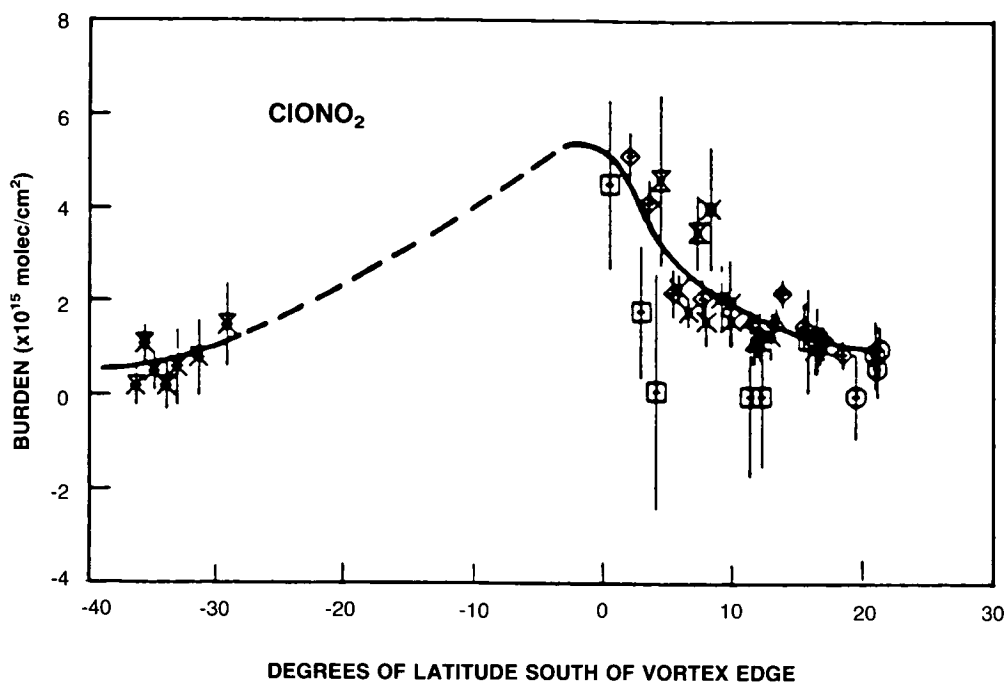


Figure 1.6.1-6. Observed distribution of the ClONO_2 column abundance, plotted as a function of latitude relative to the edge of the vortex in August and September, 1987 (from G. Toon et al., 1989a).

Figure 1.6.1-7 shows observations of the latitude gradients of the HCl and HF column abundances. HF and HCl are both produced by decomposition of chlorofluorocarbons, and are expected to exhibit generally similar latitude gradients, particularly in the winter at high latitudes where chemical loss processes for both are very slow. The ratio between the two quantities provides an important check regarding the contribution of chlorofluorocarbons to the stratospheric chlorine budget, since the relative abundances of fluorine and chlorine released by anthropogenic compounds is well known. The observed mid-latitude column abundances are in agreement with model predictions adopting about 0.6–0.7 ppbv of methyl chloride as the sole significant natural contributor to the stratospheric chlorine budget, with the remainder of stratospheric chlorine and all of the stratospheric fluorine being due to the known release rates of chlorofluorocarbons. In the absence of other processes, one would expect both HCl and HF columns to increase poleward as air with higher concentrations of both compounds moves polewards and downwards. HF exhibits just such a behavior. However, HCl columns decrease sharply with latitude inside the CPR, implying the conversion of virtually all the HCl in the low stratosphere to other forms. This conversion of HCl within the CPR is also clearly evident in the HCl/HF ratio. The observed gradient cannot be explained with homogeneous chemistry, and is consistent with efficient heterogeneous chemistry.

HOCl is of interest since it is believed to be the product of the heterogeneous reaction of ClONO_2 with H_2O . Toon and Farmer (1989) deduced the column abundance of HOCl using about 15 spectral features that occur near $1,227\text{ cm}^{-1}$. By averaging several spectra, they derived a mid-morning measurement for a latitude near 80°S on September 20 of about $1.5 \times 10^{14}\text{ cm}^{-2}$. This value is comparable to estimates from models that include heterogeneous chemistry (see Section 1.6.4).

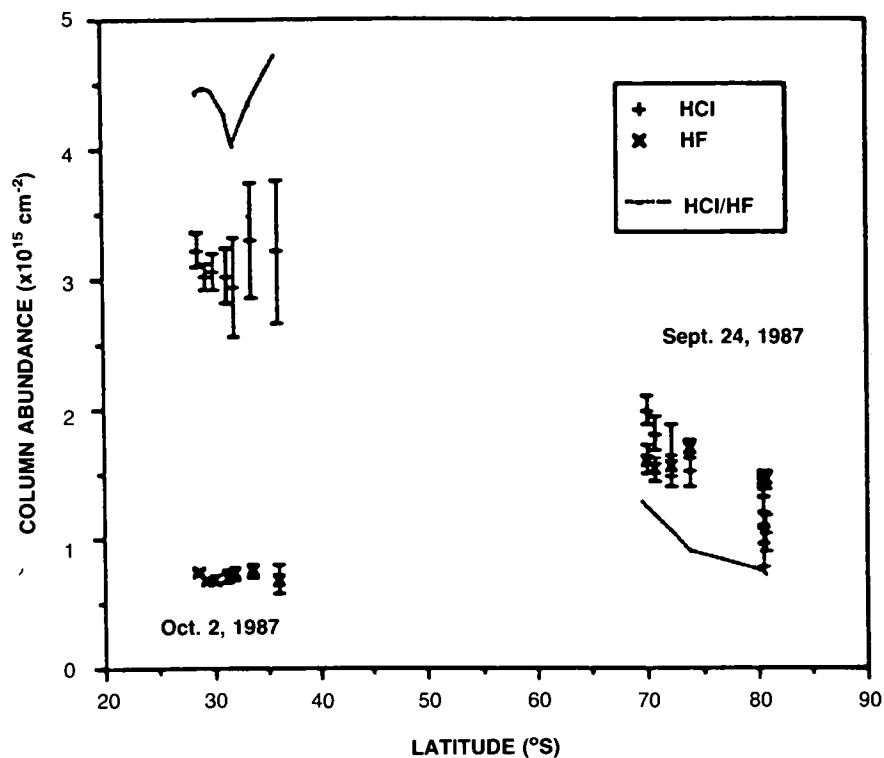


Figure 1.6.1-7. Observed latitude gradients of HCl and HF on the 24th of September and 2nd of October, 1987 (from G. Toon et al., 1989a). The ratio (dashed line) falls from a value of approximately 4 at low latitudes to less than 1 within the polar vortex, indicating conversion of HCl to other forms.

The column measurements of OCIO provide some insight into the photochemical destruction of ozone through the catalytic cycle involving ClO and BrO, while those of HOCl provide indications regarding the column integrated ozone loss rate due to the catalytic cycle involving coupling between HO_x and ClO_x. The photolysis of HOCl is the rate-limiting step in the latter cycle. Assuming a photolysis rate of about $2 \times 10^{-4} \text{ s}^{-1}$ in mid-September throughout much of the sunlit portion of the day, one obtains an ozone loss rate in the sunlit atmosphere of about $3 \times 10^{10} \text{ molec cm}^{-2} \text{ s}^{-1}$, or about $1.3 \times 10^{15} \text{ molec cm}^{-2} \text{ day}^{-1}$ (about 0.02% of the ozone column per day, which is far less than the observed ozone loss rate of roughly 1–2%/day). Neglecting possible ozone loss through OCIO photoisomerization (Vaida et al., 1989), the ozone destruction through bromine/chlorine chemistry occurs through the cycle whose rate-limiting step is $\text{BrO} + \text{ClO} \rightarrow \text{Br} + \text{ClO}_2$. Since the branching ratio for this channel is nearly equal to that for the channel that leads to OCIO production, and since OCIO is very short lived and hence in photochemical equilibrium during the day, we may write:

$$d(\text{O}_3)/dt = -k (\text{ClO}) (\text{BrO}) \approx -J (\text{OCIO})$$

where k is the rate constant for the reaction indicated above and J is the OCIO photolysis rate. The measured twilight OCIO column is about $1 \times 10^{13} \text{ molec cm}^{-2}$ at twilight (90-degree solar zenith angles). Model calculations suggest that the OCIO column abundances present at the smaller solar zenith angles typical of the sunlit period of the day are roughly 0.25–0.5 of these twilight values and that the rate of OCIO photolysis is about $5 \times 10^{-2} \text{ s}^{-1}$ (Solomon et al., 1989). Hence the column integrated loss of ozone

POLAR OZONE

due to the reaction between ClO and BrO is estimated to be about $1.25\text{--}2.5 \times 10^{11}$ molec $\text{cm}^{-2} \text{s}^{-1}$, or about $0.5\text{--}1 \times 10^{16}$ molec $\text{cm}^{-2} \text{day}^{-1}$ (about 0.1–0.2%/day, or about 5–20% of the observed total ozone column loss rate in 1987). The estimates of column ozone loss given here are crude, as they do not include possible effects of atmospheric waves (e.g., zonal asymmetries which influence photolysis processes; see Jones et al., 1989). Seasonal and latitudinal changes in the HOCl and OClO column abundances have also been neglected and the estimates do not include detailed diurnal photochemistry. Nevertheless, such estimates are based directly on observations and, hence, are of use in examining the approximate roles of various photochemical processes. More detailed model calculations based on aircraft and ground-based measurements of ClO suggest that the bulk of the ozone loss rate in Antarctica in 1987 occurred through formation of the ClO dimer (see Section 1.6.4).

1.6.2 Reactive and Reservoir Nitrogen

In retrospect, observations of the column abundance and diurnal cycle of nitrogen dioxide obtained in the late 1970s and early 1980s provided strong indications of perturbed chemistry in the polar winter and spring long before the discovery of the Antarctic ozone hole directed worldwide attention to south polar regions. The NO_2 column abundance in the Arctic winter and spring was found to be significantly lower than theoretical expectations (Noxon, 1979). This phenomenon came to be known as the Noxon “cliff” and was highlighted as a major challenge to our understanding of stratospheric chemistry. Although many of the observations were obtained in the Northern Hemisphere winter, a similar Antarctic “cliff” was found in the only available latitude survey from the Southern Hemisphere (Noxon, 1978). Observations from the New Zealand Antarctic research station (Scott Base at 78°S) published prior to the discovery of the Antarctic ozone hole also displayed remarkably low levels of NO_2 during Antarctic spring (McKenzie and Johnston, 1984), well below those generally found in the Arctic spring. In the high latitude air, both the diurnal variation and absolute abundance of NO_2 were greatly reduced compared to theoretical expectations.

Observations and interpretation of HNO_3 abundances in the Arctic polar night (Wofsy, 1978; Austin et al., 1986b) provided important evidence for an unexplained source of HNO_3 in polar winter, and the possibility of heterogeneous production on atmospheric aerosol was suggested. In particular, the observations showed larger abundances of HNO_3 inside the heart of the polar vortex than found at lower latitudes. These are difficult to reconcile with purely gas-phase production of HNO_3 in the dark polar winter. A few observations of the column abundance of HNO_3 were also available from Antarctica (Williams et al., 1982), confirming that its behavior there was extremely difficult to reconcile with “standard” gas-phase photochemical schemes, and supporting the very low NO_2 column measurements of McKenzie and Johnston (1984). Solomon et al. (1986) compared these observations of the latitude gradient of total HNO_3 column abundance observed in Antarctica to two-dimensional model calculations both including and neglecting heterogeneous production. They suggested that the observed low NO_2 and high HNO_3 column amounts in Antarctica indicated net production of HNO_3 , probably through surface reactions.

Thus, early observations of reactive nitrogen species strongly suggested the possibility that heterogeneous reactions affected the partitioning of nitrogen species in the Antarctic winter and spring. While these observations were very important and strongly suggestive of major gaps in our understanding, it was not until further measurements of reactive nitrogen species were carried out following the discovery of the ozone hole that the mechanisms responsible for them and their significance to ozone chemistry became clearer.

Observations of the NO_2 column abundance in Antarctic spring were obtained with both visible (Keys and Johnston, 1986; Mount et al., 1987; Wahner et al., 1989a) and infrared absorption methods (Farmer et

al., 1987; Coffey and Mankin, 1989; Toon et al., 1989a) from ground-based and aircraft-borne instruments. A detailed comparison between techniques and platforms is beyond the scope of this review, but the measurements are in broad agreement, particularly insofar as the very low column abundances of NO_2 within the Antarctic vortex in the spring are concerned. The ground-based measurements allowed study of the diurnal and seasonal variations at a fixed point, while the aircraft measurements provide important latitude gradient information. Figure 1.6.2-1 shows the observed latitude gradient of NO_2 (from Coffey and Mankin) for two periods before and after 8th September 1987. Also shown are the earlier measurements of Noxon (1979). It is clear that a sharp decrease in NO_2 occurred as the Antarctic polar vortex was approached.

Figure 1.6.2-2 shows observations of the seasonal trend in morning and evening column NO_2 from three different Antarctic sites in 1986 (Keys and Johnston, 1988). Of particular interest is the abrupt onset and end to diurnal variations in NO_2 during the fall season (i.e., on days 53 and 110 at Halley Bay), indicated by the merging of data taken in morning and evening twilight. Farman et al. (1985b) and Keys and Johnston (1986) emphasized the fact that the behavior near day 53 delineates the point in the annual cycle when continuous daytime photolysis of NO_3 ceases, allowing NO_3 to be converted to N_2O_5 during the night and thus introducing NO_2 diurnal variability. These observations also revealed that the spring abundances of NO_2 are far smaller than the autumn levels, and the diurnal variation largely absent in spite of the fact that the diurnal variations apparent in the fall season should be expected to take place in a similar manner during spring. At Arrival Heights, for example, significant NO_2 diurnal variations should be expected from day 240 through day 280, but are nearly absent in the observations. The lower absolute NO_2 abundances and the absence of diurnal variation observed in spring as compared to fall points strongly towards removal of reactive nitrogen or its sequestration in a reservoir whose lifetime exceeds a few days (e.g., HNO_3). Figure 1.6.2-3 presents similar NO_2 observations from the Soviet stations of Molodezhnaya and Mirny (Elokhov and Gruzdev, 1989). The Soviet measurements are taken at a lower latitude (near 67°S) than

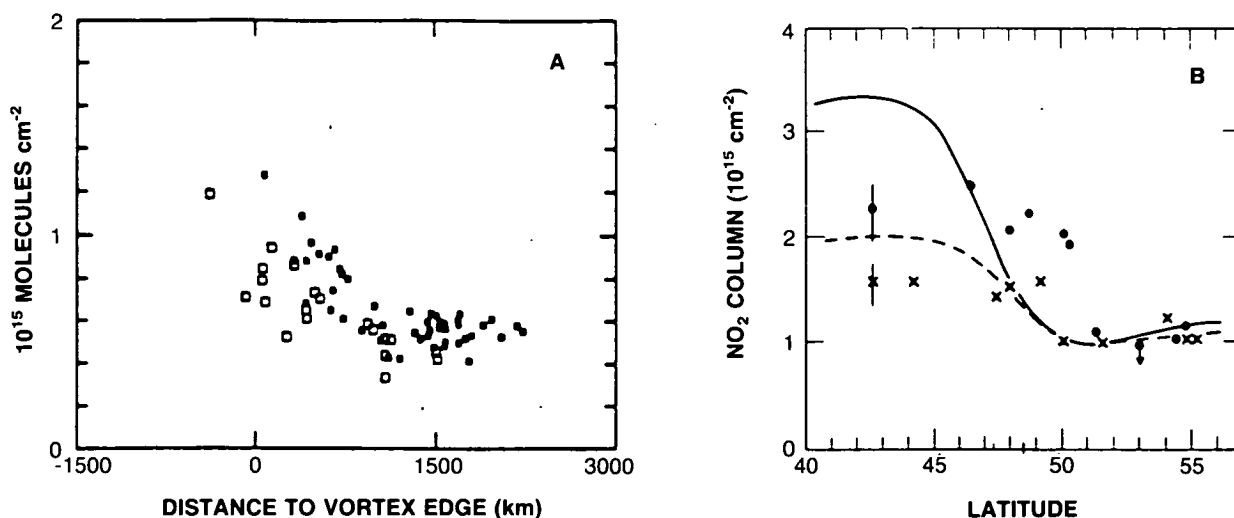


Figure 1.6.2-1. Observations of the latitude gradient of column NO_2 in the Southern Hemisphere. The data from Coffey and Mankin (1989) (A) were obtained with an airborne infrared absorption technique during September 1987, while those of Noxon (1979) (B) were obtained with a shipboard visible spectroscopy instrument.

POLAR OZONE

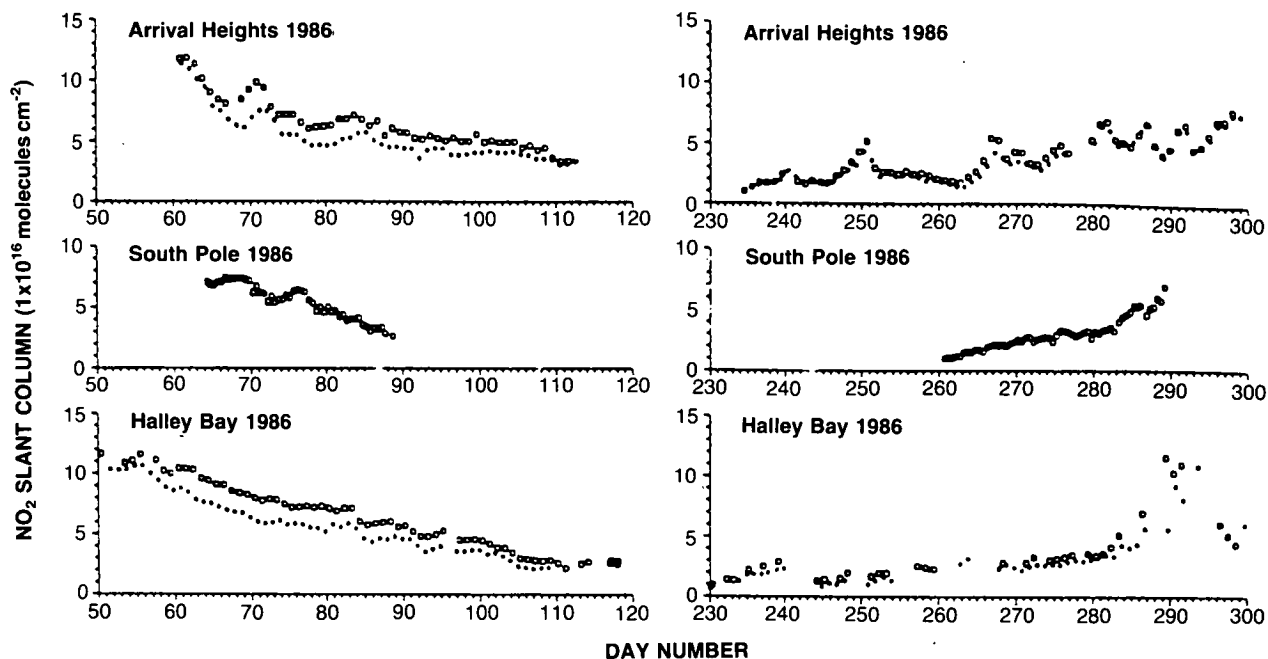


Figure 1.6.2-2. Observations of the seasonal trend in morning and evening twilight slant column NO_2 abundances from three Antarctic sites (from Keys and Johnston, 1988). The vertical column can be deduced by division by about twenty.

those shown in Figure 1.6.2-2, and hence, the diurnal variations of NO_2 persist throughout the fall season there. It is interesting to note that the NO_2 column abundances obtained at Molodezhnaya were very low until late November 1987 (compare Figure 1.6.2-2 for 1986), suggesting limited resupply of nitrogen to the polar vortex until about the time of the stratospheric warming in early December in that particular year (see Section 1.7 for a detailed discussion of the Antarctic vortex dynamics in 1987).

Satellite measurements of NO_2 are also available from the SME, SAGE, and SAGE II experiments. These data reveal sharp reductions in NO_2 in the Antarctic winter, with latitudinal gradients that are qualitatively similar to those obtained from the column measurements discussed above. Thomas et al. (1988) described SME observations of the abundance of NO_2 . The SME observations are restricted to the altitude range above about 28 km. Thomas et al. (1988) compared these data to observations of the total NO_2 column abundance over McMurdo by Mount et al. (1987), and showed that much of the NO_2 normally expected to be located below 28 km was missing. The SAGE and SAGE II satellite observations also provide important information on the altitude profiles of NO_2 within and outside the Antarctic polar vortex. Figure 1.6.2-4 presents a contour plot of NO_2 densities in early October, 1987 from SAGE II, showing evidence for very low average abundances of NO_2 below about 30 mb (approximately the altitude range where polar stratospheric clouds are generally observed, see Section 1.2). The relatively low abundances at higher altitudes in the polar regions as compared to lower latitudes are consistent with other measurements such as LIMS (Russell et al., 1984) and with model calculations. These likely reflect photochemical destruction of reactive nitrogen in the upper stratosphere and mesosphere and subsequent downward transport, and are predicted by multi-dimensional photochemical models employing standard gas-phase photochemistry (see e.g., Garcia and Solomon, 1983).

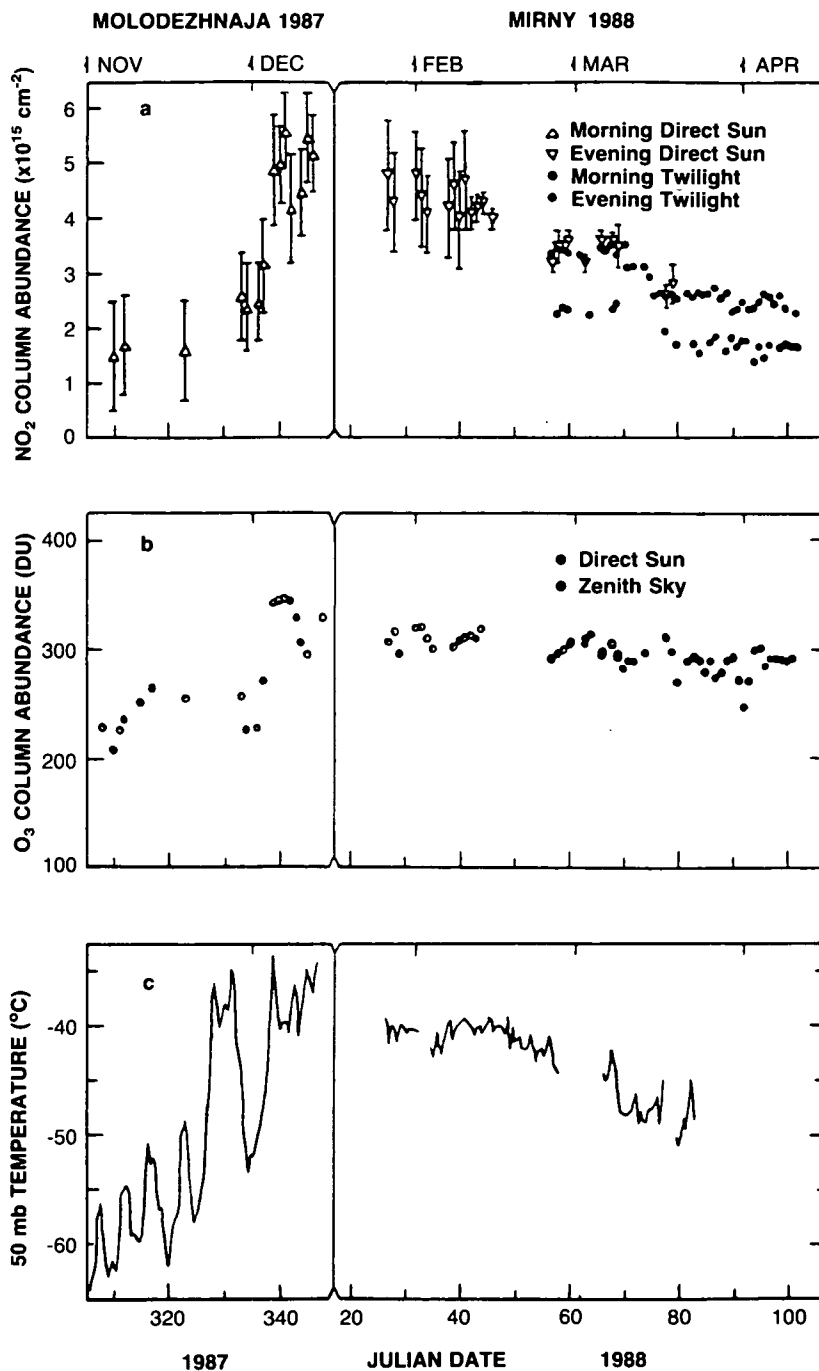


Figure 1.6.2-3 Total NO₂ (a), total O₃ (b), and 50 mb temperature (c) at Molodezhnaya in 1987 and Mirny in 1988 (from Elokhov and Gruzdev, 1989).

HNO₃ column abundances were also measured by infrared absorption methods (Farmer et al., 1987; Coffey and Mankin, 1989; G. Toon et al., 1989a). Figure 1.6.2-5 displays the measured nitric acid column abundance within the Antarctic polar vortex in mid-September. Note the abrupt drop in the HNO₃ column to very low values within the vortex. HNO₃ can be affected by heterogeneous chemistry in several ways.

POLAR OZONE

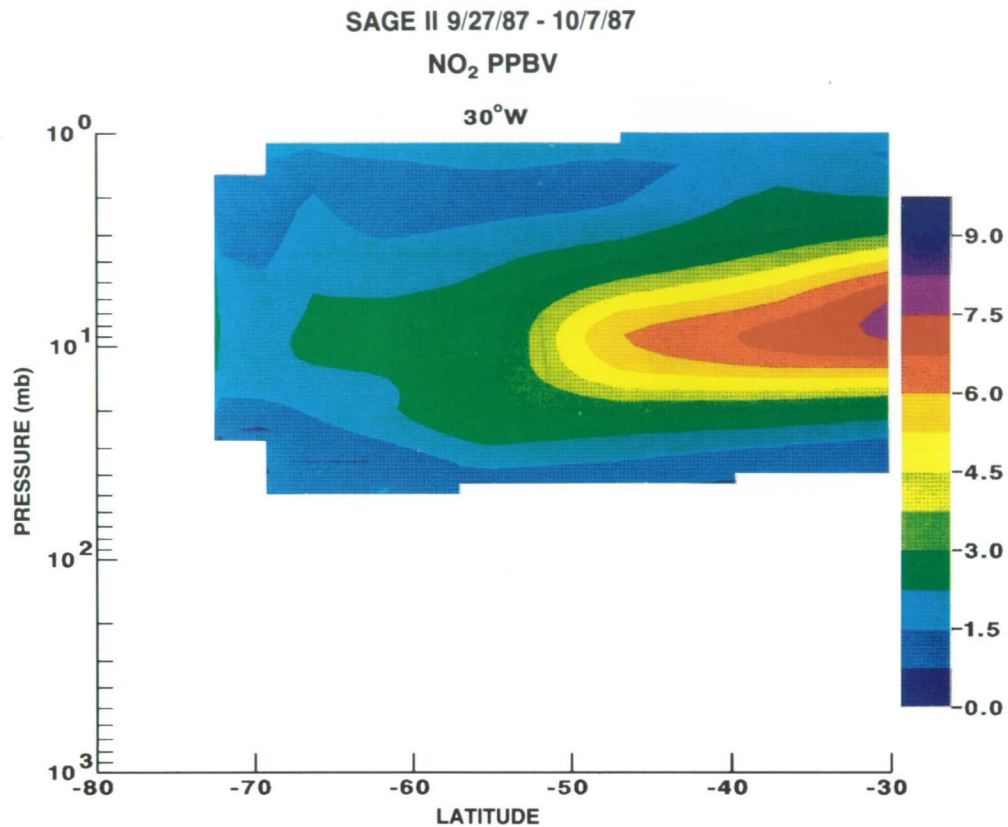


Figure 1.6.2-4. Cross section of NO₂ (ppbv) vs. latitude and pressure for the period from September 27 to October 7, 1987, from SAGE II observations in the Southern Hemisphere (from McCormick, personal communication).

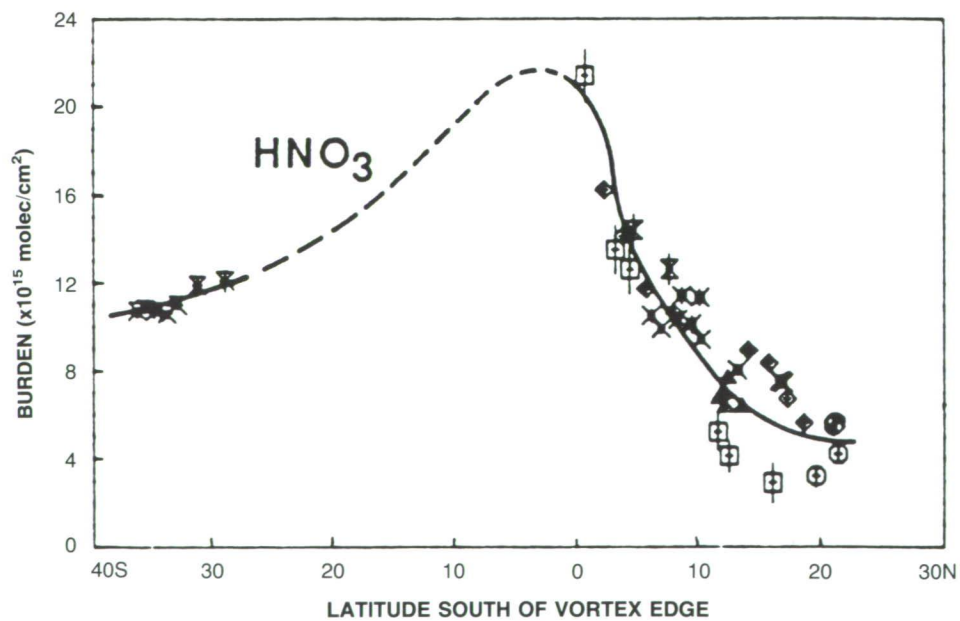


Figure 1.6.2-5. Observed column of HNO₃ plotted as a function of latitude relative to the edge of the polar vortex in August and September, 1987 (from G. Toon et al., 1989a).

If PSC clouds are present, then a substantial amount of the gas-phase HNO_3 can be incorporated into the clouds and abundances of gas-phase HNO_3 will be low. However, the presence of the clouds is believed to lead to conversion of other forms of reactive nitrogen (N_2O_5 , ClONO_2 , see Section 1.4) into particulate HNO_3 . If the cloud particles then evaporate, HNO_3 abundances should be expected to be unusually high. If, on the other hand, the cloud particles sediment out of the stratosphere, then the HNO_3 and NO_y abundances will remain low until transport processes replace or effectively mix with the denitrified air.

In situ measurements of NO_y shown below (Figure 1.6.2-6) demonstrate that substantial, though not complete, denitrification of the Antarctic lower stratosphere (near 18–20 km) occurred in September 1987. The very low column abundances of nitric acid observed in 1987 and the vertical extent of very cold temperatures observed in that particular year indicated that this denitrification extended throughout much of the stratosphere. In contrast, the high values of HNO_3 column observed in November 1978 (Williams et al., 1982) suggest that either a) denitrification was not very extensive in that year (e.g., due to warmer temperatures) or b) that nitric acid was brought in through transport processes, perhaps those associated with the stratospheric warming (but see also, Section 1.7.3). Further observations, particularly of the seasonal trend in HNO_3 throughout the spring season, are needed to understand how transport processes associated with the final stratospheric warming and chemical/microphysical processes associated with formation and evaporation of polar stratospheric clouds influence the abundances of HNO_3 and reactive nitrogen in the Antarctic lower stratosphere.

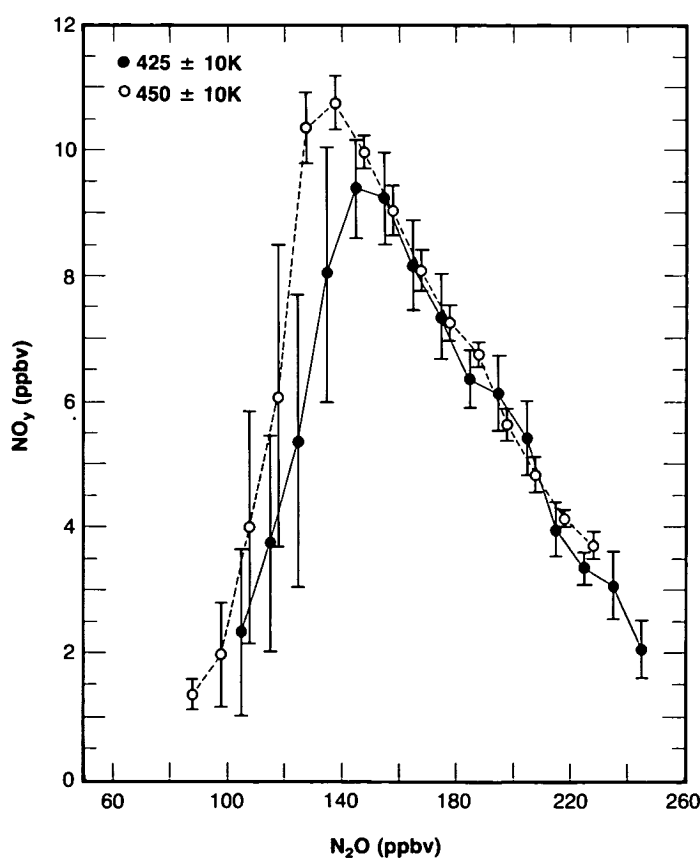


Figure 1.6.2-6. Measurements of total reactive nitrogen (NO_y) versus N_2O obtained from aircraft observations on the 425 and 450 K potential temperature surfaces (from Fahey et al., 1989a).

POLAR OZONE

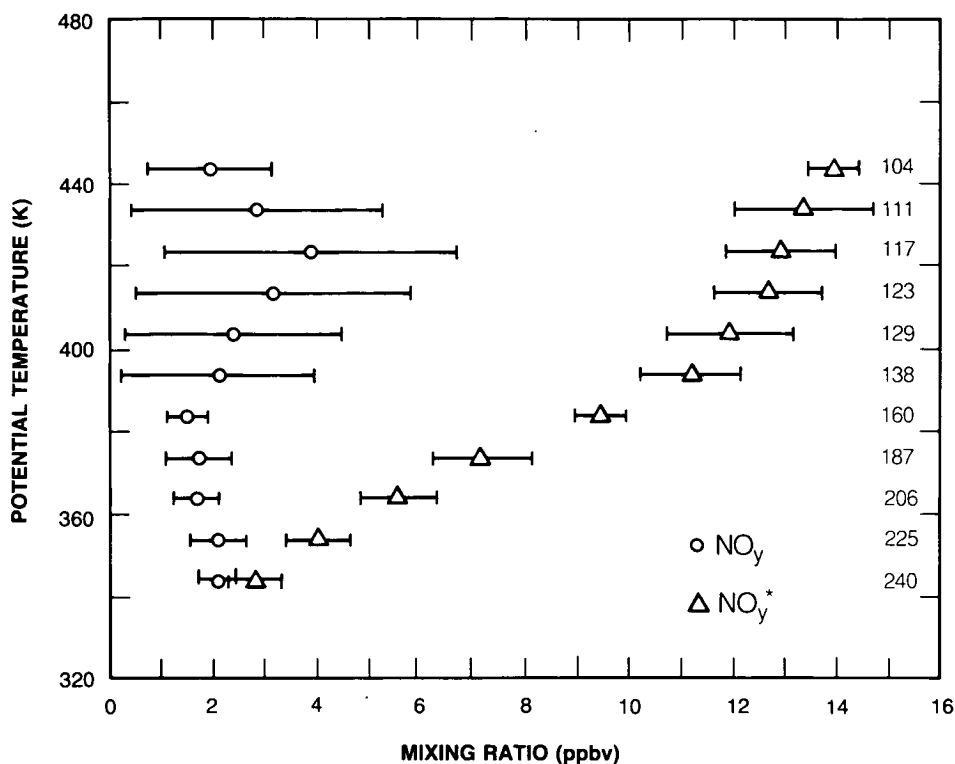


Figure 1.6.2-7. Observed total reactive nitrogen profile (NO_y , circles) and the amount which would be inferred to be present (NO_y^* , triangles) from the N_2O mixing ratios (see right margin), as a function of potential temperature (from Fahey et al., 1989a).

Karcher et al. (1988) report measurements of HNO_3 , NO_2 , HCl , and O_3 column abundances between 64°N and 57°S in June, 1983 and 1984. The latitude gradients obtained and the similarity with measurements from other studies in Antarctic spring led Karcher et al. to conclude that their observations at 57°S revealed significant perturbations due to heterogeneous chemistry. These findings indicate that anomalous chemistry takes place well before springtime and can be evident at latitudes rather far equatorward of the CPR. Such perturbations could have important effects on the seasonal and latitudinal variations in ozone depletion.

In situ measurements of NO and NO_y in the Antarctic vortex were obtained by Fahey et al. (1989a,b). The interpretation of measurements of NO_y can be complicated, since the instrument is more sensitive to the NO_y present in particles than the gas phase. This leads to NO_y "enhancements" when large amounts of NO_y -containing particulate material is present. As discussed in Section 1.3.2, measured NO_y enhancements during PSC events provide strong evidence that Type 1 PSCs contain a substantial fraction of nitrate and begin to form at approximately the temperatures expected for the nitric acid trihydrate (Fahey et al., 1989b).

Fahey et al. (1989a) also studied the behavior of NO_y on occasions when clouds were not present locally (as indicated by the cloud particle counter measurements). Since N_2O is the source of stratospheric NO_y through the reaction $\text{O}(\text{D}) + \text{N}_2\text{O} \rightarrow 2\text{NO}$, the destruction of N_2O is accompanied by a production of NO_y . Thus, one expects increasing concentrations of NO_y as N_2O decreases, and this indeed occurs for N_2O mixing ratios greater than about 140 ppbv at 450 K (about 20 km) as shown in Figure 1.6.2-6. However, for N_2O mixing ratios below about 140 ppbv (in the interior of the Antarctic vortex) this behavior breaks

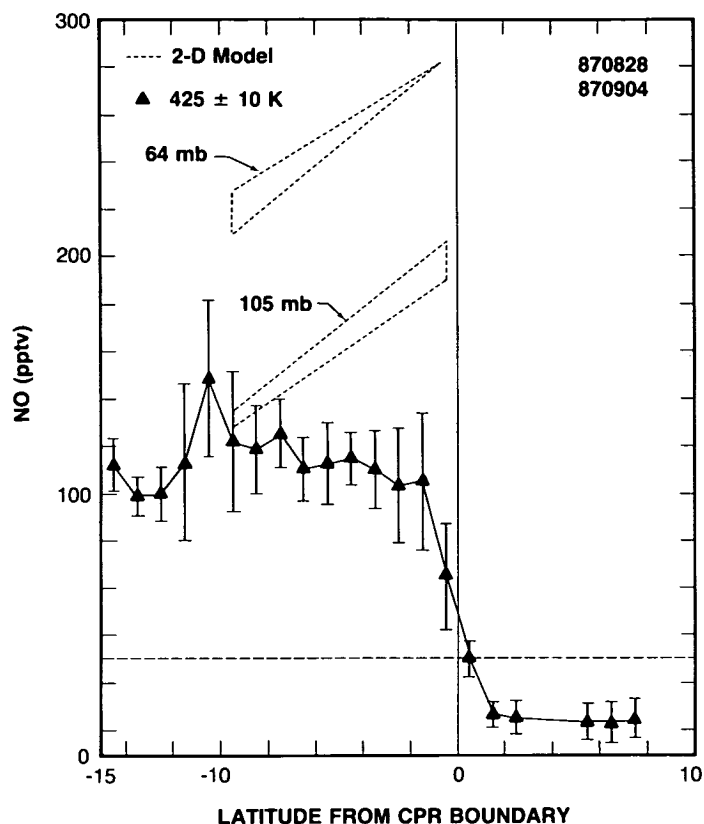


Figure 1.6.2-8. Observed NO mixing ratios versus latitude relative to the chemically perturbed region (from Fahey et al., 1989b).

down, and substantial decreases in NO_y abundances are found. This strongly suggests denitrification processes. Using the correlation between N_2O and NO_y for N_2O mixing ratios above 140 ppbv, a linear expression relating NO_y to N_2O can be derived. From this, the expected NO_y mixing ratio for a given N_2O mixing ratio can be obtained. Figure 1.6.2-7 shows the vertical profile of NO_y^* measured inside the Antarctic vortex and the expected NO_y , referred to here as NO_y^* . The observed N_2O distribution in this region suggests that NO_y values closer to 10 ppbv would be anticipated in the absence of odd nitrogen removal processes. However, NO_y mixing ratios between 1 and 4 ppbv were observed over a wide range of potential temperatures, suggesting that denitrification had occurred over a considerable depth of the low stratosphere. As noted earlier, these results are consistent with the very low HNO_3 columns observed at the same time by G. Toon et al. (1989a) and Coffey and Mankin (1989).

On two Antarctic flights, Fahey et al. (1989a) measured NO rather than NO_y . The results of these observations are summarized in Figure 1.6.2-8. Figure 1.6.2-8 shows that the NO mixing ratios decreased as the polar vortex was approached, in contrast to model calculations that predict increasing abundances in the absence of removal processes (e.g., on PSCs). NO mixing ratios inside the chemically perturbed region were on the order of a few tens of parts per trillion by volume or less. Measurements of the diurnal variations of ClO and BrO reported by Solomon et al. (1989) suggest similar values of 10–100 pptv of NO_2 (see next section). These measurements show that very little NO_x was available within the polar vortex, which is a prime requirement for elevated levels of ClO and attendant ozone loss as emphasized in Section 1.5.

POLAR OZONE

1.6.3 Other Chemical Species

Water vapor is of particular importance in the Antarctic vortex because it plays an active role in the formation of polar stratospheric clouds. The first reported winter Antarctic measurement of water vapor is that of Iwasaka et al. (1985b), who employed a balloon-borne Lyman-alpha hygrometer from Syowa Station. They reported water vapor mixing ratios of only about 1 ppmv just above the tropopause, and argued that dehydration may have occurred through formation and sedimentation of large ice crystals. Iwasaka (1986) also used lidar observations of particles observed above Syowa Station to show that small, non-depolarizing particles formed prior to and at warmer temperatures than ice saturation. Further, Iwasaka (1986) suggested that large, non-spherical particles formed when temperatures dropped below the frost point based on lidar observations of optical depths and depolarization. As discussed in Section 1.2, these observations are consistent with what is now known as Type 1 particles, believed to be largely composed of nitric acid trihydrate, and Type 2 particles believed to contain largely water-ice (see Poole and McCormick, 1988a). The latter are expected to take up much of the available water vapor, thus dehydrating the stratosphere upon sedimentation. Denitrification could also take place through sedimentation of such particles. In the Antarctic in 1987, the region of denitrification corresponded closely to the dehydration (see e.g., Fahey et al., 1989a). Arctic observations display quite different behavior, as will be discussed in Section 1.10.

Rosen et al. (1988b) conducted a series of three balloon observations of water vapor using frost-point hygrometers at McMurdo Station. They also concluded that the mixing ratios of water vapor displayed a minimum near 15–20 km, suggesting vertically localized dehydration through cloud formation.

These conclusions were confirmed and expanded upon by the observations of Kelly et al. (1989). A Lyman-alpha hygrometer was employed on board the ER-2 aircraft to determine the distribution of stratospheric water vapor. Figure 1.6.3-1 shows measurements of the latitude gradient of water vapor

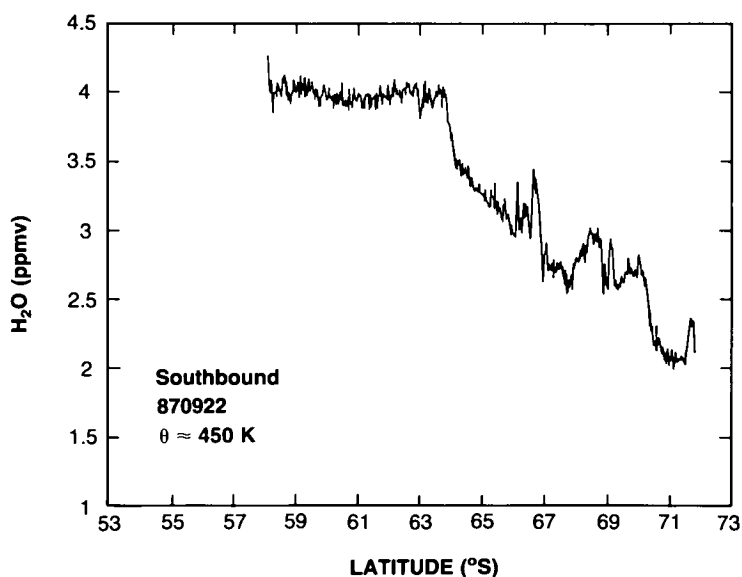


Figure 1.6.3-1. Observed latitude gradient of H₂O on September 22, 1987 near 450 K surface (about 20 km) (from Kelly et al., 1989).

obtained on the 2 September 1987 near 20 km (Kelly et al., 1989). The sharp decreases between 65°S and 67°S provide important evidence of dehydration. Kelly et al. have also argued that the relatively low water vapor abundances obtained at 50–70°S suggest some mixing of air from inside the vortex out to lower latitudes (see Section 1.7).

Figure 1.6.3-2 presents observations of the water vapor distribution in early October 1987 from SAGE II. These data provide a detailed view of the vertical and horizontal structure of the dehydrated region, suggesting that it extends from about 200 to 30 mb (in general agreement with the altitude range where PSCs are observed) and from the polar vortex to perhaps 50°S during the time period of these measurements. This figure was constructed from approximately 10 days of measurements by linear interpolation to an equidistant longitude grid and then to a latitude grid with variable spacing following the density of the measurements for a number of pressure levels. The measurements start at 30°S in late September and finish at 72°S in early October. During this time period the vortex was strongly perturbed along 30°W, allowing SAGE II to obtain a number of observations in the core of the vortex. The water vapor dehydration region overlaps the ozone depletion region to a large extent. Minimum levels of water approach 1 ppmv inside the vortex. Detailed study of such observations is badly needed to determine the extent to which dehydrated air is exported to lower latitudes. Such mixing would also imply transport of denitrified air rich in ClO radicals, and could have important photochemical effects at the lower latitudes (see Fahey et al., 1989a).

Another important chemical species measured in the Antarctic stratosphere is BrO. BrO has been measured both by *in situ* resonance fluorescence on board the ER-2 aircraft (Brune et al., 1989b) and by

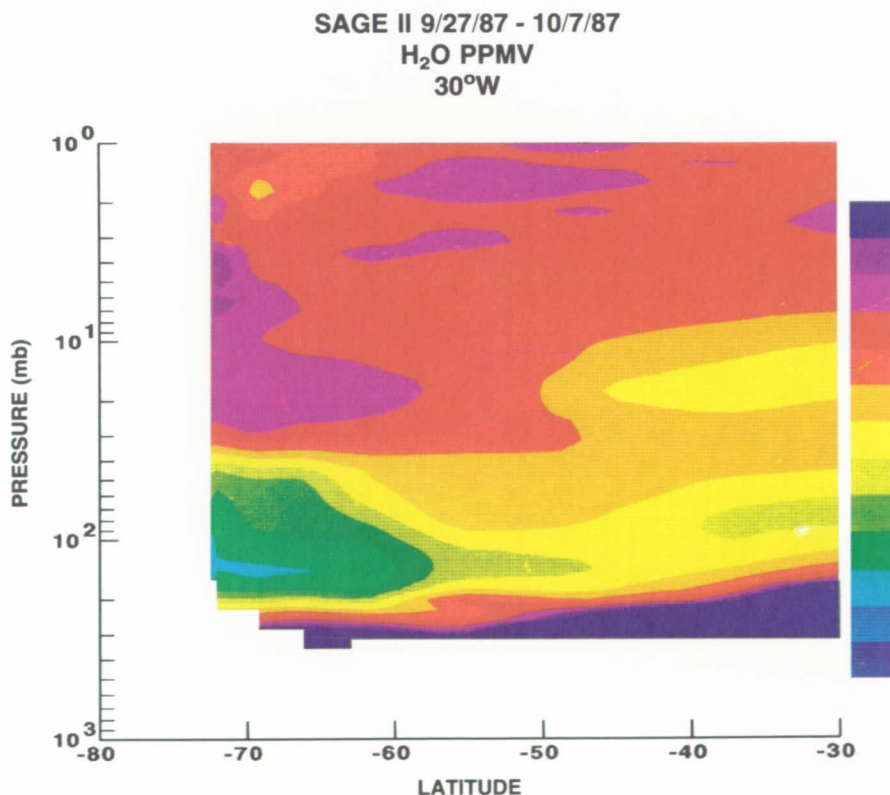


Figure 1.6.3-2. Cross section of H₂O (ppmv) versus latitude and pressure for the period from September 27 to October 7, 1987, measured by the SAGE II instrument (from McCormick, private communication, 1989).

POLAR OZONE

ground-based near-ultraviolet absorption (Carroll et al., 1989). BrO is of particular importance because it participates in a catalytic cycle that can destroy ozone effectively in the lower stratosphere in winter as discussed previously (McElroy et al., 1986a; Rodriguez et al., 1986). The *in situ* measurements of BrO imply mixing ratios of about 2–8 pptv, although it must be noted that the small abundances of BrO lead to greatly reduced signal-to-noise for these measurements as compared, for example, to the resonance fluorescence measurements of ClO. Figure 1.6.3-3 shows the abundances of BrO obtained on several flights as a function of latitude during 1987. As noted in Section 1.5, the balance between ClO and ClONO₂ is critically dependent on the abundance of NO₂, since ClONO₂ photolyzes rather slowly. The sharp gradient in ClO abundances at the edge of the CPR is associated with an inverse behavior for NO and NO₂ believed

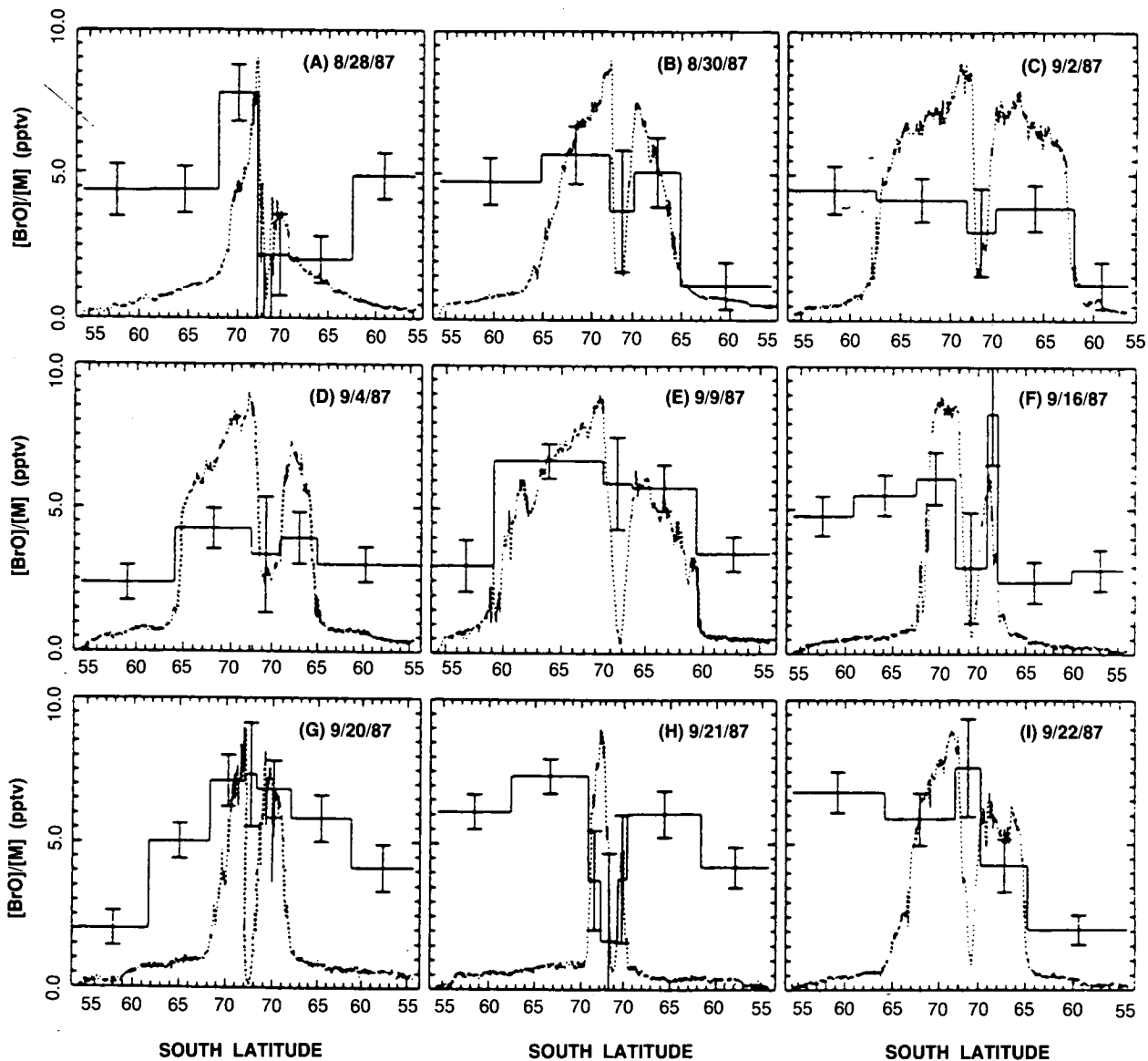


Figure 1.6.3-3. BrO mixing ratios versus latitude for nine flights from about 54 and 72°S, taken between August 28 and September 22, 1987. Horizontal bars represent the distance over which the signals are averaged. ClO mixing ratios are superimposed for comparison, identifying the chemically perturbed region (from Brune et al., 1989b).

to be due to cloud processing (Fahey et al., 1989a). The partitioning between BrO and BrONO₂ is far less sensitive to the abundance of NO₂, since BrONO₂ photolyzes considerably faster than does ClONO₂, and the noontime abundance of BrO is therefore expected to be nearly independent of latitude, consistent with the measurements shown in Figure 1.6.3-3.

Figure 1.6.3-4 depicts the observed vertical profile of BrO at approximately 72°S, showing that it increases with altitude from about 380 to 460 K (about 14 to 20 km). This gradient may reflect the altitude dependence of the bromocarbons and hence the available reactive bromine levels and/or formation of BrONO₂ or other reservoirs at lower altitudes. Figure 1.6.3-5 presents observed diurnal variations of the BrO slant column abundance obtained over McMurdo Station. Carroll et al. (1989) showed that the absolute levels of BrO obtained in the evening twilight measurements were consistent with mixing ratios in the low stratosphere of about 5–15 pptv. Solomon et al. (1989) noted that the much lower morning twilight measurements suggested that BrO levels were reduced at sunrise due to formation of a relatively long-lived reservoir during the night, probably BrONO₂. Both sets of measurements suggest that BrO mixing ratios are large enough to contribute 5–20% of the ozone decline observed in Antarctic spring (see Section 1.6.4).

A broad range of long-lived compounds (e.g., CF₂Cl₂, CFCl₃, CH₃Br) were measured during AAOE by grab sampling and gas chromatographic/mass spectrometric (GC/MS) methods. N₂O was also measured, both by GC/MS and by a tunable diode laser technique (Podolske et al., 1989). The GC/MS technique and an overview of the results are given by Heidt et al. (1989). The implications of these measurements for the chlorine budget and for the dynamics of the polar lower stratosphere are discussed in the next section and in Section 1.7.1.

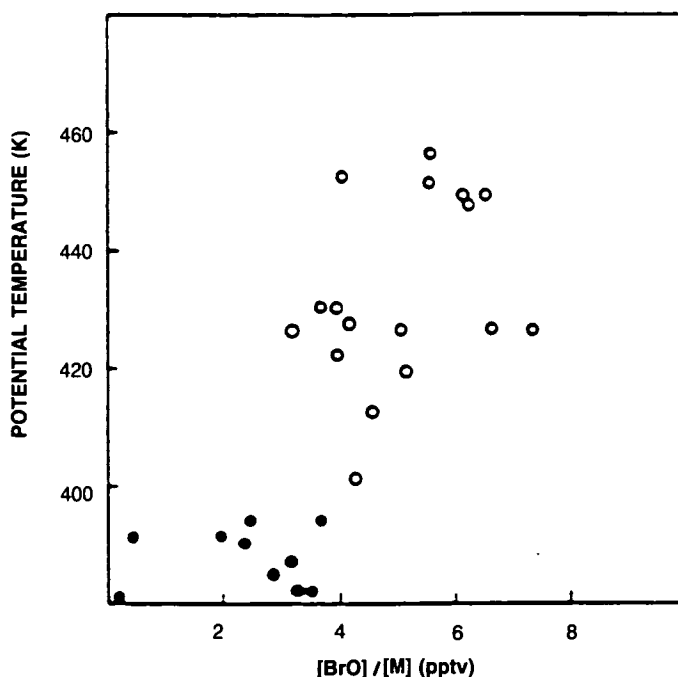


Figure 1.6.3-4. Variation of the BrO mixing ratio with potential temperature. Open circles represent data taken during aircraft flights on constant potential temperature surfaces, closed circles indicate data taken during aircraft ascent and descent at 72°S (from Brune et al., 1989b).

POLAR OZONE

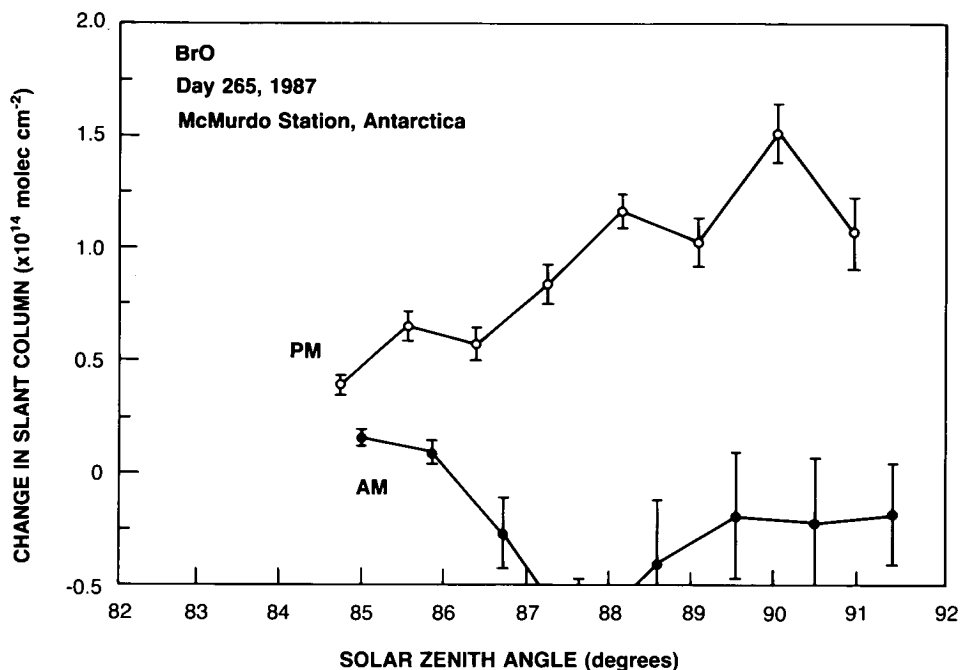


Figure 1.6.3-5. Diurnal variation of the BrO slant column at McMurdo Station (from Solomon et al., 1989).

1.6.4 Modeling Studies of the Composition and Photochemistry

Several of the early chemical modeling studies suggesting mechanisms to understand the Antarctic ozone hole were briefly described in Section 1.1.4. In this section, theoretical studies aimed at interpreting observations of a broad range of chemical species will first be discussed. Specific studies dealing with evaluation of the associated ozone loss rates will then be reviewed.

Rodriguez et al. (1986) and Salawitch et al. (1988) discussed the diurnal chemistry of chlorine compounds such as ClO, OCIO, and Cl_2O_2 under conditions where the chlorine levels are greatly perturbed by the presence of PSCs. Rodriguez et al. (1986) emphasized the important roles of Cl_2O_2 and OCIO as nighttime reservoirs for ClO. Salawitch et al. (1988) emphasized the possible role of BrCl in modulating the diurnal cycle of BrO and thus limiting the nighttime OCIO abundance. Observations of OCIO by S. Solomon et al. (1987), Wahner et al. (1989b) and Solomon et al. (1989) exhibit strong diurnal variations broadly consistent with these predictions. Solomon et al. (1989) also showed that the observed asymmetries in morning and evening twilight OCIO and BrO measurements provided another important element in the diurnal cycle that could be used to infer formation of a relatively long-lived nighttime BrO reservoir, likely BrONO_2 .

McElroy et al. (1988) discussed the ground-based measurements of column abundances of HCl, ClONO_2 , NO, and NO_2 by Farmer et al. (1987). They noted that the low abundance of HCl observed in early September and its subsequent increase during the spring season was qualitatively consistent with the expected recovery of HCl following chemical processing on PSC particles. Their calculations also revealed

general agreement with the observed seasonal trends in HNO₃, NO, and NO₂ abundances and, most important, in the seasonal rate of decline of the ozone column during 1986.

Wofsy et al. (1988) discussed the thermodynamics of mixed HCl/HNO₃/H₂O ices and explored the implications of heterogeneous chemistry for chemical composition and ozone loss. They emphasized that the nonlinear growth in ozone depletion since about 1980 and its rather sudden onset may be related to the titration of reactive chlorine by reactive nitrogen radicals. In particular, they emphasized that dramatic ozone loss might begin when the initial HCl abundance exceeds the sum of 1/2 NO_x (defined as NO + NO₂ + NO₃ + 2 × N₂O₅). The success of such a formulation depends in part on a thorough understanding of the denitrification process, which influences the residual reactive nitrogen available for titration.

Many recent modeling studies have focussed on obtaining a better understanding of observations of the composition of the Antarctic vortex observed in 1987. The broad morphology of the long-lived tracers in the Antarctic spring vortex, in particular the unusually low absolute mixing ratios and the latitude gradients of N₂O and many chlorofluorocarbons is understood in terms of air within the vortex having undergone substantial diabatic descent during the winter months (see, for example Heidt et al., 1989; G. Toon et al., 1989b; Podolske et al., 1989; Parrish et al., 1988; and Section 1.7). These findings have important implications for the understanding of atmospheric dynamics and will be discussed further in Section 1.7.

The appearance of extensive denitrification and dehydration in the Antarctic vortex is understood (at least qualitatively) in terms of the formation of Type 1 nitric acid trihydrate particles that eventually grow to large Type 2 ice crystals and sediment out of the stratosphere. The particle sizes predicted by micro-physical models (e.g., Poole and McCormick, 1988a) are of the order of a few microns, capable of sedimenting at a rate of the order of a few kilometers per week.

Given this basic picture, Heidt et al. (1989) and Jones et al. (1989) have examined the latitude and vertical gradients of chlorofluorocarbons observed within the Antarctic vortex during the 1987 AAOE, and used these data to deduce the abundance of inorganic chlorine available for cloud processing. Such a derivation is dependent upon the measured gradients in chlorofluorocarbons and (to a small extent) upon assumptions regarding the "age of the air" descending within the vortex, since this determines the amount of total chlorine it contains (see Jones et al., 1989 and Section 1.7). Table 1.6.4-1 presents deduced organic

Table 1.6.4-1 Assumed chlorine tracer concentrations and inorganic chlorine content as a function of potential temperature at 72°S. The cases 'A' and 'B' refer to different assumed tropospheric chlorine contents, appropriate to the mid- and late 1980s (see text). The total chlorine contents are 3.15 and 3.5 ppbv

Potential Temperature	420 K	400 K	380 K	360 K	340 K
F11	28.0	53.0	79.0	142.0	200.0
F12	130.0	180.0	220.0	255.0	306.0
F113	9.7	14.0	19.4	27.0	42.0
CH ₃ CCl ₃	6.0	11.5	19.2	30.0	45.7
CCl ₄	7.0	10.0	60.0	90.0	100.0
CH ₃ Cl*	230.0	320.0	390.0	450.0	550.0
net ClO _y (case 'A')	2555.0	2200.0	1750.0	1250.0	750.0
net ClO _y (case 'B')	2970.0	2620.0	2170.0	1670.0	1170.0

*The concentrations of this gas have been inferred using F12 as a proxy (see text).

POLAR OZONE

and likely inorganic chlorine abundances derived from such measurements for one of the studies. The observations suggest that more than 2.5 ppbv of chlorine may be available (i.e., not tied up in chlorofluorocarbons) at the higher altitudes near 420 K (about 18 km) within the vortex. Observations made during the 1986 and 1987 Antarctic springs indicate that a substantial fraction of the available chlorine was present in reactive forms. For models to simulate the latitude and vertical gradients of reactive species within the vortex it was essential to include the effects of heterogeneous reactions taking place primarily on Type 1 nitric acid trihydrate particles (see Section 1.2). In Figure 1.6.4-1 is shown a comparison of observed ClO mixing ratios as a function of latitude with those modeled using an approach that includes a detailed treatment of air flow (Jones et al., 1989). The comparison is for early September on the 428 K potential temperature surface. Poleward of 65°S an abrupt increase in ClO mixing ratio is evident in the observations. In the model, polar stratospheric clouds are predicted to form polewards of 65°S during the relevant period and the modeled ClO mixing ratios increase through the effects of heterogeneous reactions, primarily between HCl and ClONO₂. The same model also simulates well the vertical gradient of ClO within the vortex (see Figure 1.6.4-2), which arises primarily from the vertical gradient in available chlorine. As noted earlier, this and other studies (e.g., Rodriguez, et al., 1989) demonstrate that without heterogeneous reactions on PSCs, modeled ClO mixing ratios in the polar vortex would be about two orders of magnitude lower than observed.

Fahey et al. (1989a) show that chemical processes also play a critical role in establishing the observed NO latitude gradient. NO mixing ratios exhibited a marked fall off for ClO levels above about 70 pptv. Increased ClO due to cloud processing is expected to lead to a faster rate of formation of ClONO₂, higher ClONO₂ levels, and reduced NO and NO₂ abundances. Fahey et al. showed that these considerations are consistent with the observation of a pronounced ClONO₂ "collar" (ring of high ClONO₂ values just inside the chemically perturbed region) by infrared absorption methods (see Section 1.6.1). Clearly, these obser-

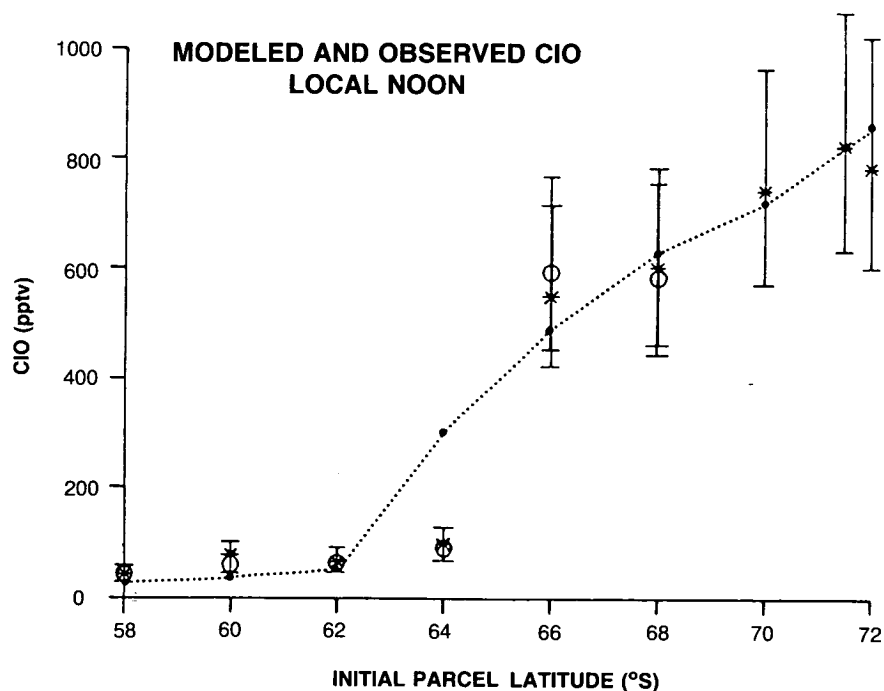


Figure 1.6.4-1. Calculated and observed ClO mixing ratios on the 428 K surface, 4-12 September, 1987 (from Jones et al., 1989).

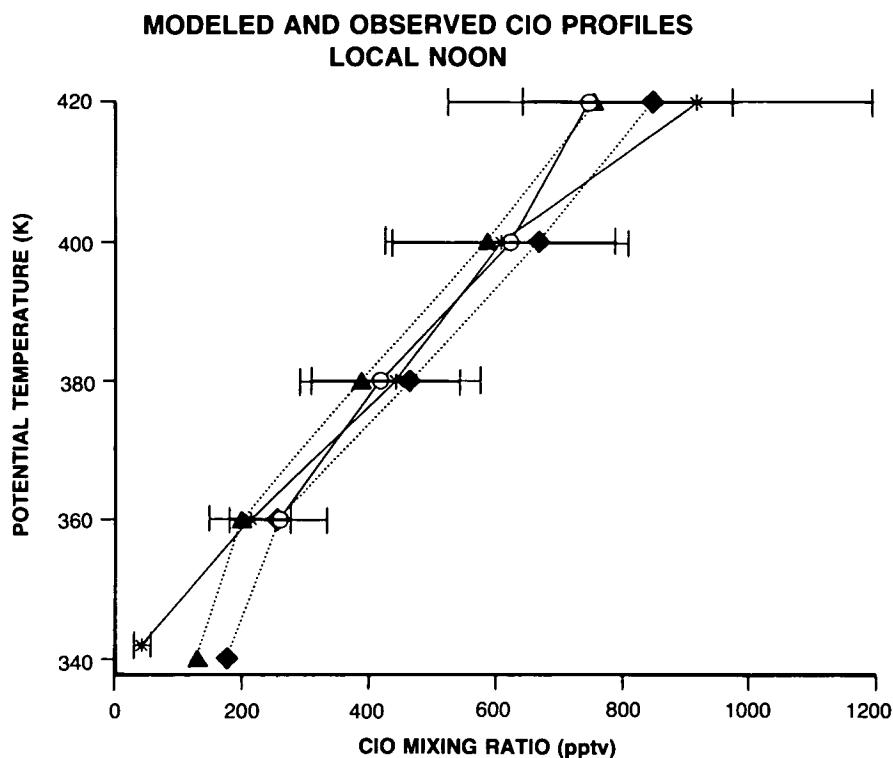


Figure 1.6.4-2. Calculated and observed ClO mixing ratio profiles at 72°S, 4 and 9 September, 1987 (from Jones et al., 1989).

variations and the possibility of rapid formation of ClONO₂ may play an important role in determining the form of the remaining NO_y inside the vortex as shown above.

Jones et al. (1989) noted that the NO abundances and the inferred NO/NO_y ratios observed outside the dehydrated, denitrified region were lower than theoretical predictions, and the ClO mixing ratios higher. They argued that this, and the existence of temperatures outside the denitrified region close to and below the threshold for Type 1 PSC formation, indicate that PSC processes are occurring at latitudes outside of the polar vortex, although mixing of air from within the denitrified region out to lower latitudes may also play an important role in the NO_y and ClO_y partitioning. Airflow through PSC clouds (produced for example, by orographic forcing and/or cyclonic scale weather systems) can process large volumes of stratospheric air, particularly near the edge of the polar vortex where wind speeds are high (see, McKenna et al., 1989a; Cariolle et al., 1989a). Reactions on background sulfate aerosols may also be important. It is worthy of emphasis that perturbations to the NO/NO_y ratio and available chlorine partitioning as far equatorward as 50°S may be of considerable importance to mid-latitude ozone trends.

The observations of high abundances of ClO and OClO throughout September within the vortex, followed by declining values of these reactive species in October are consistent with the picture of heterogeneous release of reactive chlorine on PSCs and the known morphology of the clouds (see Section 1.2). Solomon et al. (1989) have argued that the seasonal cycle of OClO is consistent with an increase in the available NO₂ during September. Using a model including the effects of wind motions but not those of small-scale mixing or diabatic processes, Austin et al. (1989) have suggested that once PSCs vanish, and

POLAR OZONE

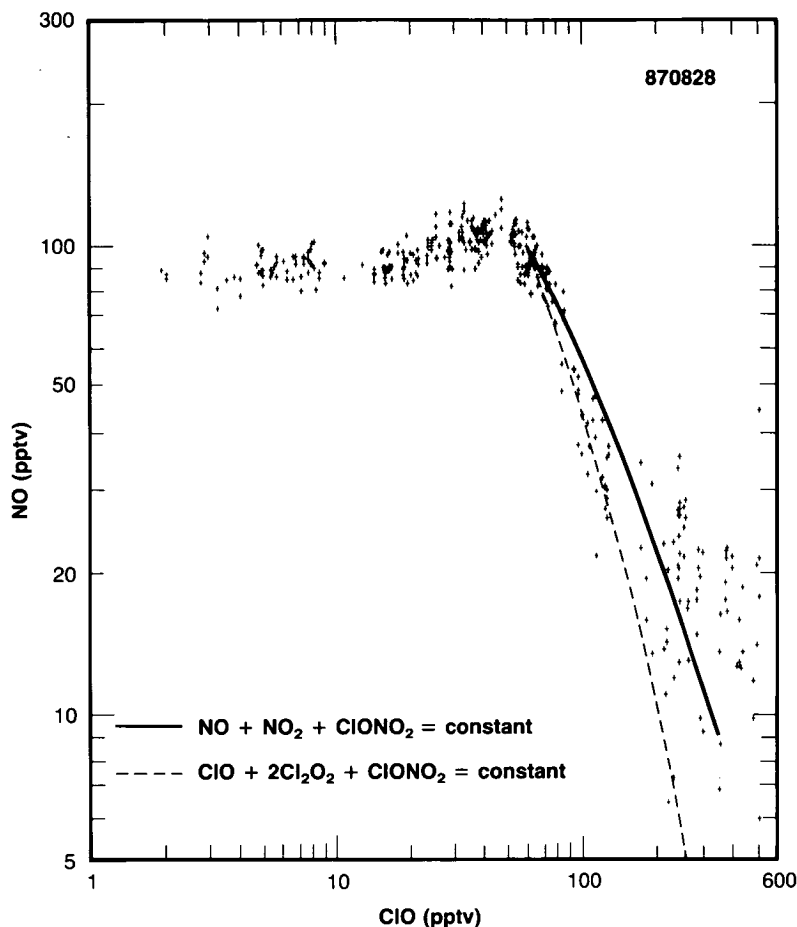


Figure 1.6.4-3. Observed NO and ClO mixing ratios from an aircraft flight on August 28, 1987. The rapid decline of NO at the higher ClO mixing ratios is consistent with $ClONO_2$ formation (from Fahey et al., 1989b).

as sun angles increase, NO and NO_2 abundances begin to rise through increased HNO_3 and $ClONO_2$ destruction (as discussed briefly in Section 1.5). They argue that as a result, atomic Cl abundances rise and HCl begins to be reformed at a significant rate, so tying up reactive chlorine, reducing ClO, and halting further ozone loss. These studies suggest that the onset and termination of photochemical ozone loss (as reflected in ClO and OClO abundances) is closely tied to the availability of reactive nitrogen.

It has been suggested (Tuck, 1989; McKenna et al., 1989b) that significant mixing between vortex air and that from lower latitudes can occur during September. Mixing in of air containing high NO and NO_2 would accelerate photochemical recovery to normal gas phase ClOy partitioning, as discussed in detail in Section 1.5. Further work is needed to determine whether NO and NO_2 do indeed increase (especially in late September) and, if so, to determine the contribution of mixing to the seasonal cycle of the reactive chlorine species.

Several groups have attempted to model the ozone decline observed in 1987 using a variety of approaches. The studies are in general agreement although there are important differences in detail.

Figure 1.6.4-4 shows measured ozone decreases from AAOE aircraft data and computed rates using the dimer formation rates of Hayman et al. (1986) and Sander et al. (1989), along with observed noontime ClO (Anderson et al., 1989). Diurnal variations were computed assuming a zonally symmetric circulation (i.e., constant temperatures equal to those observed at noon along the aircraft flight track and assuming that air parcels circulate along latitude circles as they undergo their diurnal variations). Broad general agreement with the rate of observed ozone decline is obtained for the Hayman et al. rate, but the observed decline is significantly underestimated (by about 35%) if the Sander's et al. rate is used. Anderson et al. adopted the latter, and postulated the existence of an additional termolecular reaction involving ClO and ozone. Hofmann (1989a) suggested that ozone may be destroyed directly on PSC surfaces, based on an observed spatial correlation between ozone loss and particle surface areas. Other possible mechanisms for polar ozone loss were explored in Section 1.5.

Barrett et al. (1988) examined the observed ozone loss over McMurdo Station from ozonesonde observations in 1987 and compared these to calculated values based on their observed ClO observations using the JPL (1987) reaction rate constant for formation of the ClO dimer. They found good agreement between the observed and calculated loss rates. However, Sander et al. (1989) have re-evaluated the same data set using their revised lower reaction rate constant. They concluded that current photochemical mechanisms can quantitatively account for the observed ozone losses from about September 17 through October 7, but noted that additional losses appeared to be required to explain the observed loss earlier in the spring season (August 28 through September 17). Like the calculations of Anderson et al. (1989), these

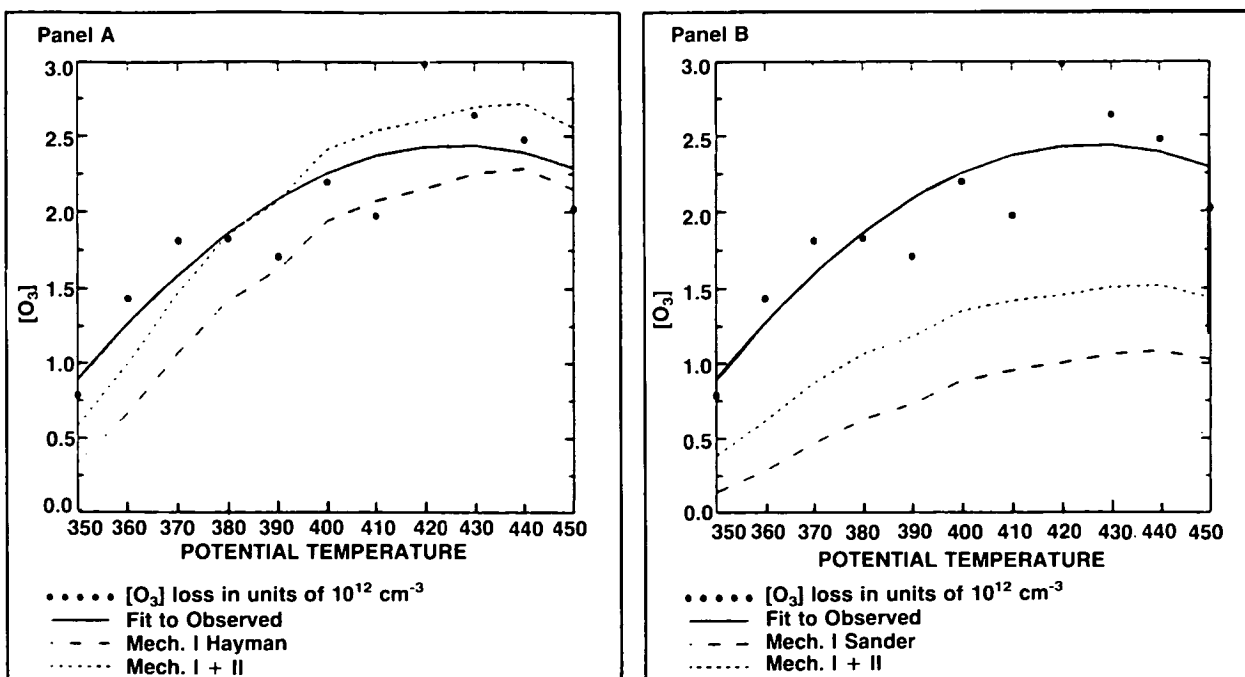


Figure 1.6.4-4. Observed and calculated rates of ozone decline for different ClO dimer formation rates (from Anderson et al., 1989) as a function of potential temperature surface. Panel A displays loss rates for the mechanism involving ClO dimer photolysis (Mechanism I) using the Hayman et al. (1986) rate and for dimer photolysis plus bromine chemistry (Mechanism II). Panel B displays loss rates for the same quantities, employing the Sander et al. (1989) rate for ClO dimer formation.

POLAR OZONE

studies both assumed that observed temperatures and photochemical conditions at a single point were representative of those experienced by air parcels moving around the vortex. A further limitation of these studies was the assumption that ClO measurements obtained during a period of a few days in mid-September applied throughout the month.

The analyses of Jones et al. (1989) included a detailed treatment of airflow along isentropic trajectories appropriate for AAOE observations. Their analysis suggested that the rate of ozone loss in the chemically perturbed region approached 2% per day in early September 1987 using the dimer formation rate of JPL (1987). Of this, about 71% was due to the ClO dimer mechanism, 17% to the reaction of ClO with HO₂, and 12% to the reaction of ClO with BrO. Austin et al. (1989) have shown that when a detailed treatment of air motions is included but mixing is neglected, photochemical ozone losses can exceed 90% at some altitudes by late October, consistent with observations of the vertical profile of the ozone depletion. The calculations by Jones and co-workers suggest that the observed rate of ozone loss remains consistent with model calculations even when the updated rate constants of Sander et al. are considered. This suggests that the effects of zonal asymmetries on the ozone loss rate may be quite significant. Given the sharp gradients in photolysis rates prevalent in the Antarctic spring stratosphere, it is plausible that latitudinal excursions of air parcels may greatly influence photochemical loss rates.

The study of Ko et al. (1989) suggested that while the ozone loss in 1987 could be reproduced, there were some difficulties in simulating the development of the springtime ozone decrease since the 1970s (that is, the seasonal trend in 1987 was found to be consistent with the observed ClO levels, but the decadal trend since the late 1970s could not be entirely resolved solely through consideration of the known increases in chlorofluorocarbon abundances). Measurements of PSCs described in Section 1.2 suggest a trend in PSC abundances during the October months of recent years of westerly QBO phase. Section 1.8 demonstrates that the observed decreases in ozone have caused a trend in October temperatures, which is probably responsible for at least a portion of the observed PSC trend. This suggests that as ozone depletion becomes more pronounced, temperatures may remain unusually low, which in turn can enhance and/or prolong the PSC activity. This is likely to lead to greater ozone depletion and may represent an important mechanism for acceleration of the decadal ozone trend beyond that anticipated solely on the basis of the known increases in chlorofluorocarbon abundances.

In addition to trends in chlorine (and bromine) abundances, non-linear chemical depletion processes, and PSC frequency or intensity, the decadal trend in total ozone should be expected to be influenced by any trends in planetary wave activity, denitrification, the persistence or strength of the polar vortex, and synoptic-scale systems. All of these factors can influence the dynamics, temperatures, and chemical balance of the polar lower stratosphere. Further work is needed to understand the roles played by each.

While there are differences between the individual studies, the observations of sustained high concentrations of ClO throughout the polar spring, coupled with laboratory studies of key reactions (see Section 1.4 and 1.5) provide conclusive evidence that substantial ozone loss is occurring in Antarctica as a result of halogen chemistry, primarily through the formation and destruction of the ClO dimer.

Quantitative uncertainties exist in the absolute rate of the chlorine catalyzed ozone loss. Also, it is not certain whether dynamical mechanisms can contribute a small ozone loss, nor can it be stated that all chemical mechanisms are fully understood. However, it is clear that the available measurements coupled with laboratory rate measurements prove that chlorine chemistry is capable of accounting for at least the major fraction of the total ozone destruction in Antarctic spring in 1987 and can thus account, at least in large part, for the development of the Antarctic spring depletion first noted by Farman et al. (1985a).

Given that chlorine and coupled chlorine/bromine chemistry is responsible for the bulk of the Antarctic ozone reduction observed currently, it is possible to estimate how large a reduction in stratospheric chlorine loading is needed to eliminate the ozone hole. It is assumed that there will be no significant changes in Antarctic meteorology or in PSC frequency due to external processes. Figure 1.6.4-5 displays the October average total ozone abundances at Halley Bay since the late-1950s along with the total tropospheric chlorine content (which is well known, based on worldwide measurements of the CFCs and industrial releases). It is reasonable to expect that the chlorine content of the Antarctic lower stratosphere lags that of the troposphere by a few years due to the time scale for transport to that region. Preliminary analyses of CO_2 measured simultaneously with the CFCs in the Arctic vortex (Heidt, personal communication, 1989) suggest that the average age of air within the polar vortex at about 20 km is 5 years. Figure 1.6.4-5 and measurements at the South Pole and Syowa (see Section 1.1) indicate that ozone abundances were detectably reduced in the late 1970s. Those observations coupled with the above estimate of the age of vortex air imply that it is necessary to return to the CFC levels of the early to mid-1970s in order to eliminate the Antarctic ozone hole. Figure 1.6.4-5 shows that this was a period when atmospheric CFC abundances were rising rapidly. The total tropospheric chlorine abundances then were in the range of 1.4 to 2.0 ppbv, including 0.6–0.7 ppbv of methyl chloride believed to be of natural origin. It would therefore be necessary to achieve a man-made abundance of organic chlorine of about 0.7 to 1.4 ppbv. This analysis assumes no decadal increases in bromine abundances; any long-term trends in the bromine loading of the stratosphere due to halon releases will make this requirement even stricter. It must be emphasized that this is a crude estimate, and that the determination of the average age of air within the polar vortex is a subject of ongoing research.

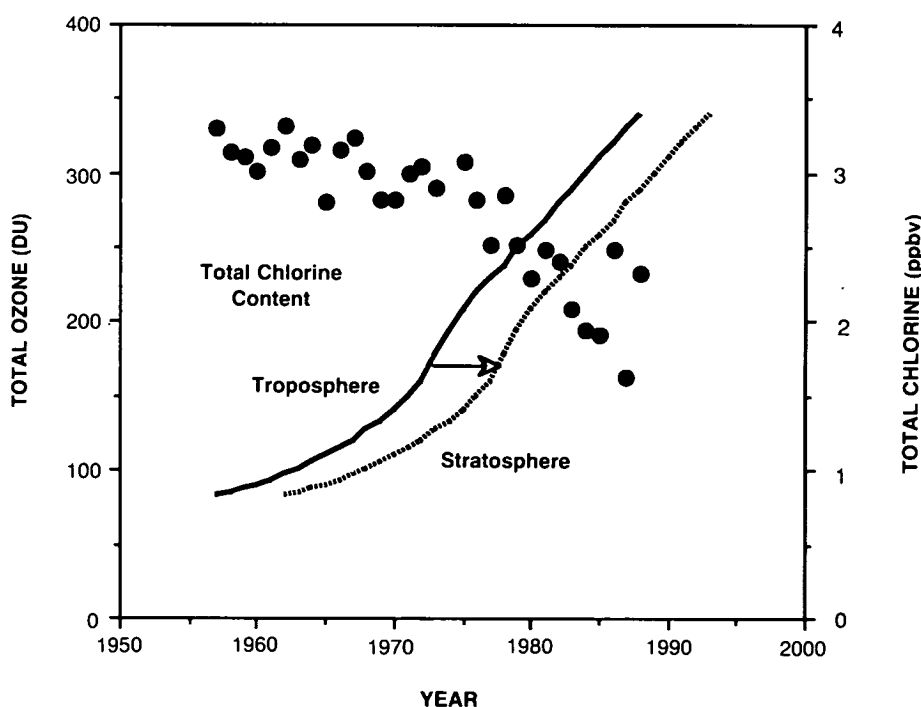


Figure 1.6.4-5. Observed October mean total ozone abundance over Halley Bay, Antarctica, along with the tropospheric total chlorine content, versus year over about the past three decades (from Farman, personal communication, 1989).

POLAR OZONE

1.7 DYNAMICAL PROCESSES

In this section, dynamical processes influencing the ozone distribution and its depletion are summarized. The climatologies of the two hemispheres are compared and contrasted in Section 1.7.1, where particular attention is paid to the observed conditions during recent observational campaigns (Antarctica in 1987 and the Arctic in 1989) as well as to the contrast between the Antarctic springs of 1987 and 1988, in which dramatically different ozone depletions were observed. The inter-annual variations in polar dynamics that appear to be related to the QBO and to the solar cycle are also described, with a view towards gaining a better understanding of their influence on measurements of trends and their cause. Synoptic scale disturbances, known to influence total ozone distributions, particularly the occurrence of mini-holes, are the subject of Section 1.7.2. In Section 1.7.3, different descriptions of the dynamics of the Antarctic vortex are presented and the notion that the vortex may behave as a processor for ozone depletion is described. Finally, Section 1.7.4 is a summary of modeling studies aimed at evaluating the possible ozone depletion effects associated with dilution of the ozone hole.

1.7.1 Differences in Climatology Between the Two Hemispheres and Their Relationship to Observed Ozone Amounts

Measurements of the seasonal and latitudinal variability of total ozone were discussed in Section 1.1, where the large differences between ozone observations made in the Northern and Southern Hemispheres were presented. Some of the chemical and meteorological factors influencing the total ozone distribution were also briefly summarized in Section 1.1. In the following section, factors influencing the transport of ozone are described in more detail, with a particular view towards understanding interannual and inter-hemispheric differences.

The rate of transport of chemical species in the stratosphere (where ozone mixing ratios are largest) is governed mainly by the intensity of planetary-scale disturbances which, in winter, propagate upward from the troposphere, where they are generated by variations in continentality and orography. In the height-latitude plane, such disturbances lead to a poleward and downward overturning of mass in the stratosphere, together with a lateral dispersion of air parcels (see Andrews et al. 1987 for an outline of basic concepts). The result is a poleward and downward transport of ozone during winter, and hence a maximum in the total column in spring.

Interhemispheric differences in total ozone (displayed in Figure 1.1.2-3) stem largely from differences in planetary-wave activity. In winter, disturbances are generally stronger and more persistent in the Northern Hemisphere than in the Southern Hemisphere so transport of ozone is more vigorous and higher values of the total column are reached at polar latitudes. In early spring, however, strong disturbances develop in the Southern Hemisphere during the so-called final warming, transporting ozone and "filling in" the polar ozone hole to some extent.

Planetary-wave activity also displays interannual variability, to which may be attributed at least some of the interannual variability found in the distribution of ozone: the stronger the wave activity, the more rapid the poleward ozone transport, and hence the higher the polar ozone amounts in spring. Such dynamical variations influence temperatures as well as ozone. The variability is especially marked in the Northern Hemisphere. Figure 1.7.1-1 gives an indication of the interannual and interhemispheric differences in lower stratospheric temperatures. For each hemisphere and for the years 1980-88, it shows the envelope of the minimum (brightness) temperatures measured around 90 mb by channel 24 of the Multiwave Sounding Unit (MSU) instrument (see Pick and Brownscombe, 1981, for details of the instrument). Horizontal lines mark

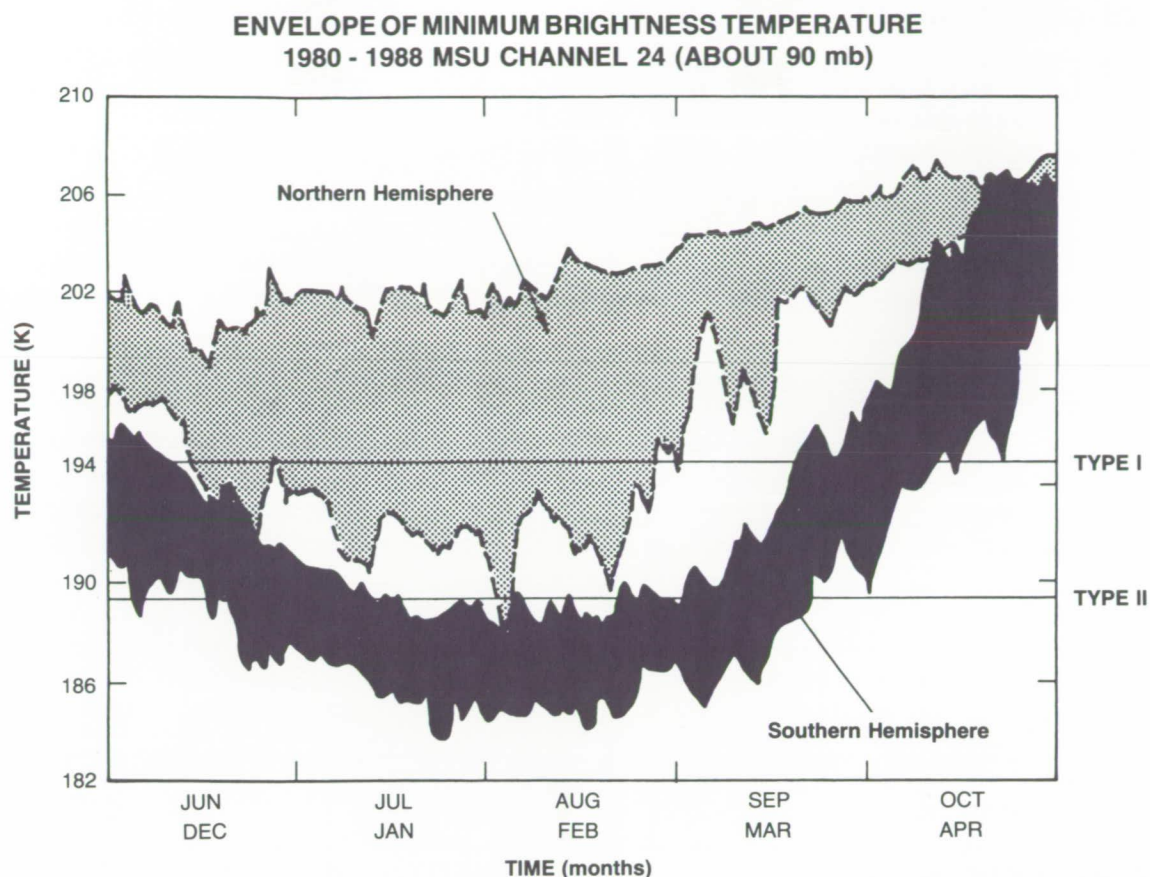


Figure 1.7.1-1 The range, near 90 mb, of minimum brightness temperatures poleward of 20° latitude (deduced from channel 24 of the MSU), computed daily for winter and spring from 1980 to 1988. The location of the minimum temperature is near the pole in winter, but moves to low latitudes during spring. Solid lines and heavy shading correspond to the Southern Hemisphere from June to October (upper labels in the time axis). Dashed lines correspond to the Northern Hemisphere from December to April (lower labels on the time axis). The horizontal lines across the figure represent the temperatures below which type I and type II PSCs can form (from Mechoso et al., 1989).

approximate threshold temperatures for the occurrence of Type 1 and Type 2 PSCs (assuming 5 ppmv H_2O and 7 ppbv HNO_3). Note that the MSU channel 24 measurements represent a weighting over the pressure range from about 200 to 30 mb, so that local temperatures may be considerably colder at some levels if sharp vertical temperature gradients prevail. Several general features can be noted in spite of the averaging. Minimum temperatures are typically 10 K or so warmer in the Northern Hemisphere than in the Southern Hemisphere, seldom falling below the required temperature for Type 2 PSCs. In the Northern Hemisphere in mid-winter, there is a 20-K spread in the minimum temperature. By contrast, in the Southern Hemisphere the minimum temperature is cold enough for Type 2 PSCs for 2 to 3 months, and there is only about a 4-K spread in the mid-winter temperature. Interannual variability is most pronounced in the Southern Hemisphere in October during the transition from winter westerlies to summer easterlies—the final warming. At the corresponding time of year in the Northern Hemisphere (April), there is less variability; the final warming has generally already happened and planetary-waves cannot propagate in the easterly winds.

POLAR OZONE

Measurements of nitrous oxide have provided important insights into the dynamics and transport in the polar regions (Heidt et al., 1989; Podolske et al., 1989). Figure 1.7.1-2 displays observations of the vertical profiles of N_2O observed in the Antarctic vortex during winter (Podolske et al., 1989; note that these values should be scaled upwards by about 9.6% due to recalibration). Summer data are also shown (Schmeltekopf et al., 1977), along with calculations from the GFDL general circulation model. The observed values in winter are far lower than the summer observations, but even the summer data lie well below the winter model predictions. Similar comparisons are found with other three-dimensional models such as the GISS model (Podolske, private communication, 1989). The greatly suppressed wintertime nitrous oxide profile is believed to result from strong downward motion within the Antarctic vortex which is not currently simulated in the model. Such downward motion clearly has important implications for ozone and nitrous oxide abundances. The data suggest that upward motion does not contribute significantly to the observed ozone decline (see Section 1.1.4). Another important finding from measurements of long-lived tracers obtained in both polar regions is the fact that the net effect of diabatic descent coupled with planetary wave disturbances leads to comparable quantities of inorganic chlorine present in the winter vortices of both hemispheres. Figure 1.7.1-3 shows the vertical distributions of the total amount of chlorine bonded in the five most abundant anthropogenic halocarbons obtained from measurements over mid- and high latitudes of both hemispheres during August and September 1987 (Heidt et al., 1989) and February 1988 (Schmidt et al., 1989). The difference between the stratospheric value and the tropospheric value is related to the amount of organic chlorine released to more reactive forms. Note the large differences in inferred available reactive chlorine between polar regions and mid-latitudes, presumably a result of descent within the vortex. The figure suggests that the amount of reactive chlorine available for chemical reactions in the lower stratospheres of both polar vortices is comparable.

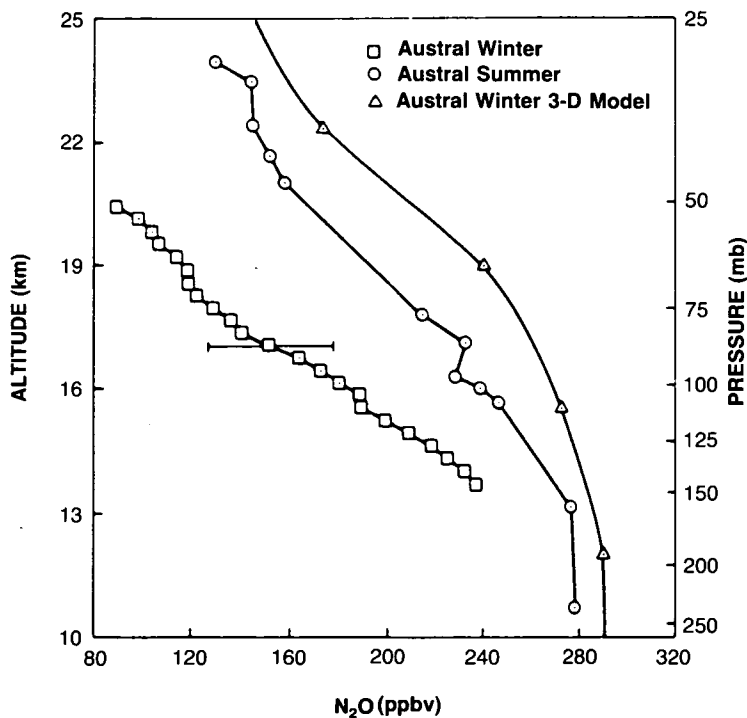


Figure 1.7.1-2. Comparison of N_2O vertical profiles during austral winter-spring from $72^\circ S$, austral summer data from $78^\circ S$ and $90^\circ S$ obtained from the NOAA data set and austral winter three-dimensional model result. Horizontal bars represent range of observed data (2-sigma) (from Podolske et al., 1989).

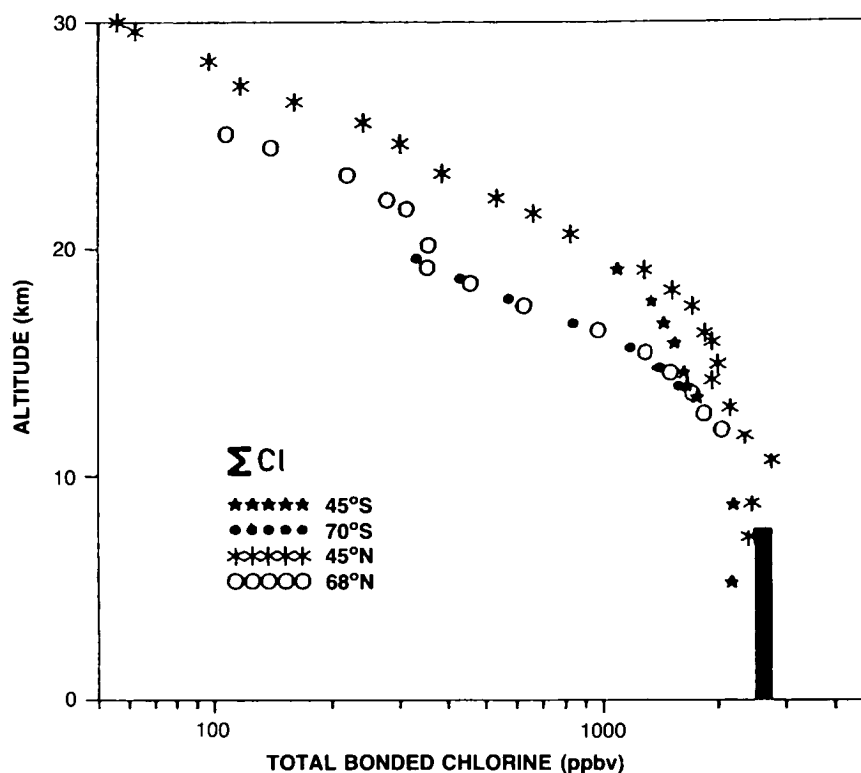


Figure 1.7.1-3. Vertical distributions of the total amount of chlorine bonded in the five most abundant anthropogenic halocarbons. The data are derived from measurements over mid- and high latitudes of both hemispheres during AAOE (Heidt et al., 1989) and CHEOPS (Schmidt et al., 1989). The corresponding tropospheric amount, calculated from the global mean mixing ratios of these species, is given by the vertical bar.

Strong downward motion within the polar vortex may also affect the time scale for exchange of stratospheric air with the troposphere and hence influence the lifetimes for all chemical species within the stratosphere. This may have important implications for calculations of the residence time of chlorofluorocarbons in the stratosphere and thus for ozone depletion potentials (see Chapter 4 of this document).

The stratosphere exhibits substantial variability on time scales longer than 1 year. A quasi-biennial oscillation is found in tropical winds, and in both tropical and extra-tropical ozone amounts (see Section 1.7.3). Longer trends, with a variety of potential causes, have also been identified (see e.g., the summary in OTP, 1989). A long-term trend in planetary-wave activity in the winter troposphere is likely to lead to a trend in the stratosphere of, say, springtime polar temperature and ozone amounts (see Mahlman and Fels, 1986, for a discussion). A putative trend in October temperatures between 1979 and 1985 over Antarctica led Newman and Schoeberl (1986) to suggest that there had been a change in circulation during the period, which may have accounted for all or part of the secular trend in total ozone over Antarctica discovered by Farman et al. (1985a). Even in the Southern Hemisphere, however, there is too much interannual variability to identify dynamical trends clearly in such a short data record (see discussion below of the year 1988). Much longer records of three-dimensional meteorological and chemical fields are needed. Newman and Randel (1988) analyzed a more extensive data set and deduced a much smaller temporal trend in October

POLAR OZONE

temperatures than that presented in Newman and Schoeberl (1986). Section 1.8 describes the observed temperature trends and their causes in much more detail.

1.7.1.1 Outline of the Climatology of the Southern Hemisphere

During the Southern Hemisphere winter, the coldest temperatures occur in the lower stratosphere over the polar region. A strong westerly vortex covers a large fraction of the Southern Hemisphere, extending through the stratosphere (Figure 1.7.1-4[i]). The vortex is nearly axisymmetric about the South Pole; planetary-scale disturbances are weak. After mid-winter, the vortex begins to weaken, at first slowly, because of the evolving field of solar radiative heating. In spring, the weakening is accelerated when planetary-scale disturbances develop. Warm air extends towards middle and high latitudes, and the vortex shrinks (Figure 1.7.1-4[ii]). Typically toward the end of September and during October, the vortex becomes highly distorted as a strong, persistent (though fluctuating) planetary-scale anticyclone develops in a preferred geographical region, 90° E–90° W (Mechoso et al., 1988, give a more detailed description). Warm air extends towards middle and high latitudes, and the vortex shrinks quickly. Finally, it breaks down, first in the upper stratosphere, and then later (and more slowly) in the middle stratosphere (Figure 1.7.1-4[iii]). As the vortex breaks down during this so-called final warming, warm, ozone-rich air spreads from low latitudes over the polar cap. Notice, however, that in the lower stratosphere a remnant of the cold core of the vortex lasts throughout October and generally through November. The maximum in the total column of ozone is held off the pole (Figure 1.1.2-3).

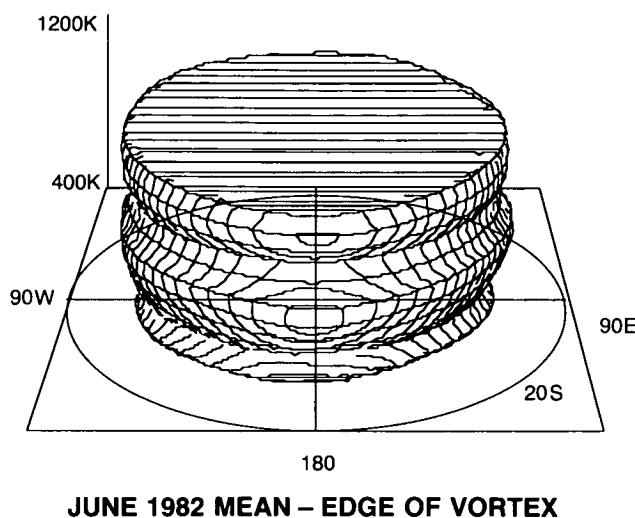


Figure 1.7.1-4(i). Monthly mean perspectives during June 1982 of the three-dimensional structure of the westerly vortex in the Southern Hemisphere from the lower stratosphere (potential temperature surface of 400 K) to the upper stratosphere (potential temperature surface of 1200 K). The edge of the vortex marks the transition from large meridional gradients of potential vorticity at high latitudes to weak gradients at low latitudes, and lies in the transition zone from strong westerly winds at high latitudes to weak westerly or easterly winds at low latitudes. The evolution shown for 1982 is typical of final warmings in the period 1979-1986 (see Mechoso et al., 1988, Figure 13), though the strength of planetary-scale disturbances does vary from year to year.

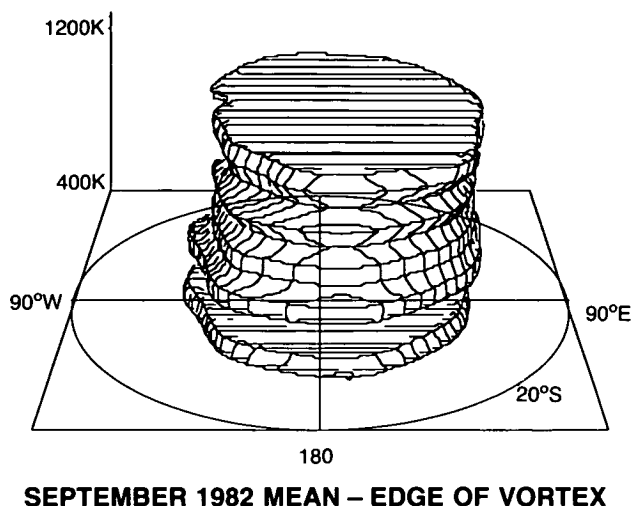


Figure 1.7.1-4(ii). As in Figure 1.7.1-4(i), but for September.

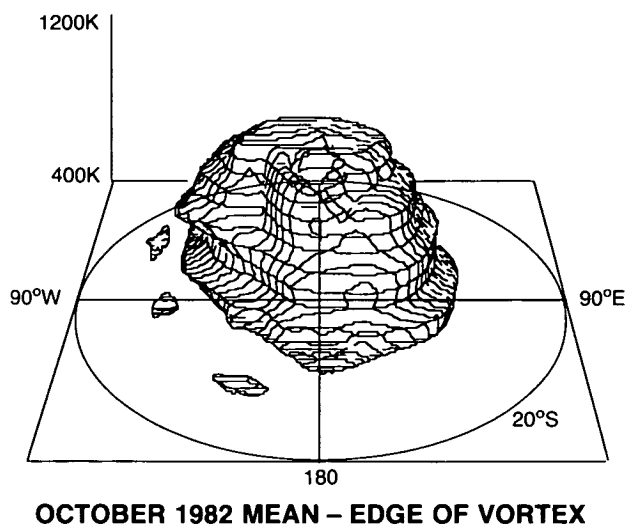


Figure 1.7.1-4(iii). As in Figure 1.7.1-4(i), but for October.

1.7.1.2 Outline of the Climatology of the Northern Hemisphere

The mid-winter circulation of the stratosphere of the Northern Hemisphere is seldom quiescent. Frequent minor warmings occur as planetary-scale disturbances grow and decay. Synoptically, these warmings generally involve (1) an intensification of a climatological anticyclone in the stratosphere (called the Aleutian High), (2) a displacement of the polar vortex over Europe, and (3) a rapid warming of air at polar latitudes where air sinks (and warms adiabatically) at the jet entrance between the anticyclone and the westerly vortex. During some winters, there are major stratospheric warmings: the disturbances are so strong that the normal circumpolar westerly flow is completely broken down, to be replaced by easterlies (in the zonal mean) through a large depth of the stratosphere. Synoptically, the warmings involve the development of either one anticyclone (usually the Aleutian High), when the westerly vortex is displaced

POLAR OZONE

from the pole (see O'Neill and Taylor, 1979), or of a pair of anticyclones, when the vortex splits (see Fairlie and O'Neill, 1988). Air from low latitudes spreads over the polar cap. Polar temperatures rise sharply, often by more than 50 K in a few days. Although rapid radiative cooling in the upper stratosphere can re-establish the westerly flow in a week or two, the longer radiative relaxation times for the lower stratosphere and the persistence of strong disturbances in the upper troposphere may mean that the westerly flow remains weak and polar temperatures high for the rest of the winter and spring. This vertical structure is in marked contrast to the top-down weakening of the westerly vortex in the Southern Hemisphere.

Final warmings in the Northern Hemisphere show much more interannual variability than in the Southern Hemisphere (Yamazaki, 1987), both in the structure of the flow and in the timing of the final breakdown of the westerly vortex (See Figure 1.7.1-5). During some examples, the circulation is highly distorted in the presence of a persistent Aleutian High. The breakdown of the westerlies may happen first in the upper stratosphere, as it does in the Southern Hemisphere, or in the lower stratosphere (in Figure 1.7.1-5, the temperature gradient reversal may precede or succeed the wind reversal). Generally, the breakdown of the westerly vortex is almost complete in the stratosphere; ozone-rich air can spread to higher latitudes in spring than in the Southern Hemisphere (Figure 1.1.2-3). Curiously, some final warmings in the Northern Hemisphere (e.g., that of 1981) are quiescent. The weakening of the westerly vortex proceeds slowly, on a radiative time scale, leading to a late final warming. This may happen after the vortex

TIMING OF FINAL WARMING

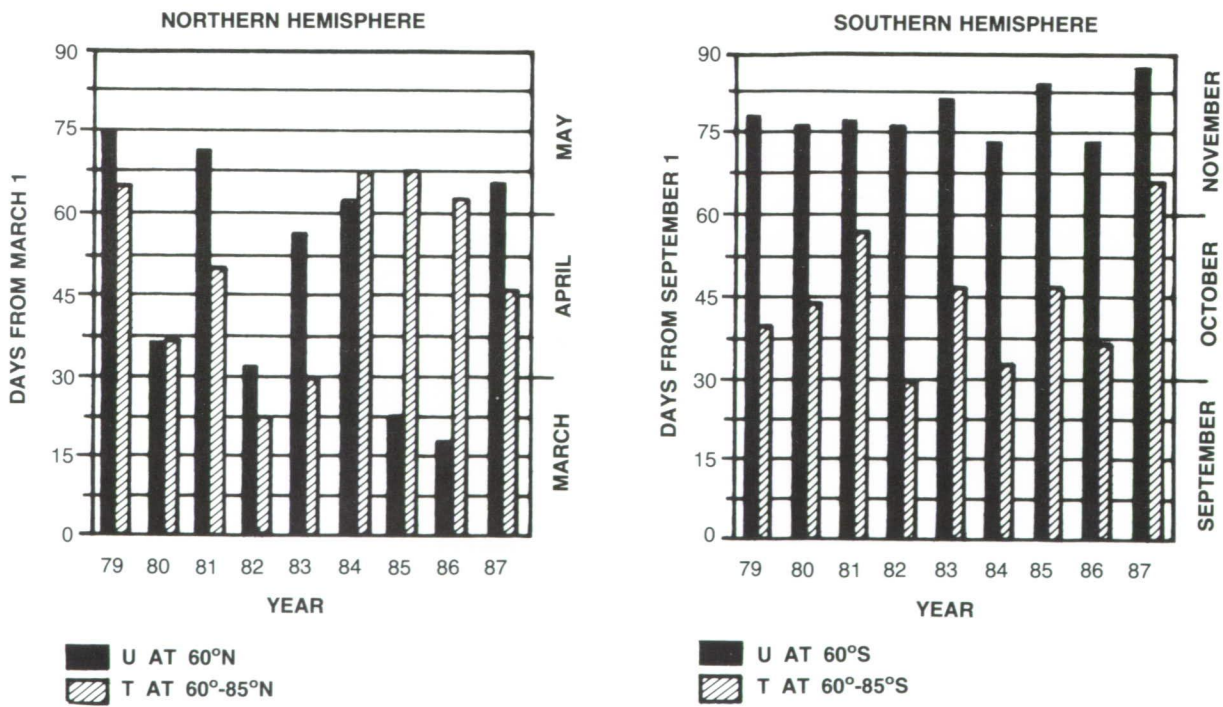


Figure 1.7.1-5. Time of the reversal, at 10 mb, of the zonal wind at latitude 60°, and of the temperature difference between 60° and 85° for the Northern and Southern Hemispheres. Zonal wind is solid; temperature difference is hatched.

has been largely broken down during an earlier major warming (as in 1981). Planetary-scale disturbances of tropospheric origin cannot then penetrate into the stratosphere.

The Southern Hemisphere stratosphere during 1987 and 1988

Total ozone amounts

Knowledge of the circulation in the Southern Hemisphere during 1987 is necessary for a full interpretation of the observations made during an international scientific campaign (the Antarctic Airborne Ozone Experiment) to study the springtime ozone depletion over Antarctica. That year, the ozone hole was the deepest yet recorded (Krueger et al., 1988). The year 1988 is of particular interest because springtime ozone depletion was markedly less pronounced than during the previous several years, and it is important to know whether this presages a long-term recovery of springtime ozone values, or whether 1988 was an unusual year because of natural interannual variability.

Figure 1.7.1-6 shows that there were large differences between 1987 and 1988 in the evolution of total ozone in the Southern Hemisphere, particularly at high latitudes. In 1987, the polar ozone hole was deep, with total ozone amounts falling below 150 DU in October. Polar ozone was eventually replenished, but not until late in the year; the ozone column did not reach 300 DU near the pole until late November. In contrast, in 1988 the ozone hole was not as deep (the ozone column remained above about 200 DU), and the ozone column reached 300 DU near the pole by the end of October. By November, the polar ozone column exceeded that in 1987 by over 200 DU.

As discussed below, the elevated ozone amounts in 1988 are unlikely to signify a long-term recovery of springtime polar ozone in the Southern Hemisphere. It appears that differences in ozone amounts between 1987 and 1988 can be attributed qualitatively to natural variability in the atmospheric circulation, which happens to have mitigated the destruction of ozone to some extent in 1988. In brief, the stratospheric polar vortex was warmer and more disrupted by strong disturbances in 1988 than in 1987. PSCs, and hence heterogeneous chemistry, presumably operated on a smaller volume of air, leading to less ozone depletion. Greater transport into polar latitudes replenished faster the already shallower ozone hole. The following discussion will focus on the lower stratosphere, since processes there have the most effect on the total column of ozone.

Figure 1.7.1-7 shows, for winter and spring 1987 in the Southern Hemisphere, the variation of minimum temperature near 90 mb, as determined from channel 24 of the MSU instrument. Figure 1.7.1-8 shows the fraction of the area of the Southern Hemisphere where temperatures were less than 193 K, a representative value for PSCs to form (ignoring, for simplicity, the distinction between Type 1 and Type 2 PSCs). Solid curves mark the envelope of such curves in the 9-year set, 1980–1988; the vertical separation of these bounding curves represents the inter-annual variability of minimum temperature or area. These figures show that, for most of winter and spring, minimum temperatures in 1987 were low, and that the area where lower stratospheric temperatures were below 193 K was the greatest in the 9-year set. The low temperatures probably result, at least in part, from the decreased solar heating associated with the record minimum in ozone amounts (Shine, 1986; Kiehl et al., 1988) as discussed in Section 1.8. Minimum temperatures rose above 193 K in early October, when PSCs should have mostly disappeared.

Figures 1.7.1-9 and 1.7.1-10 show the corresponding figures for 1988. At the end of August, minimum temperatures rose to their highest values in the 9-year set, and the area below 193 K to its lowest value. By the time sunlight returned to polar regions in September, the chemical make-up of polar air was

POLAR OZONE

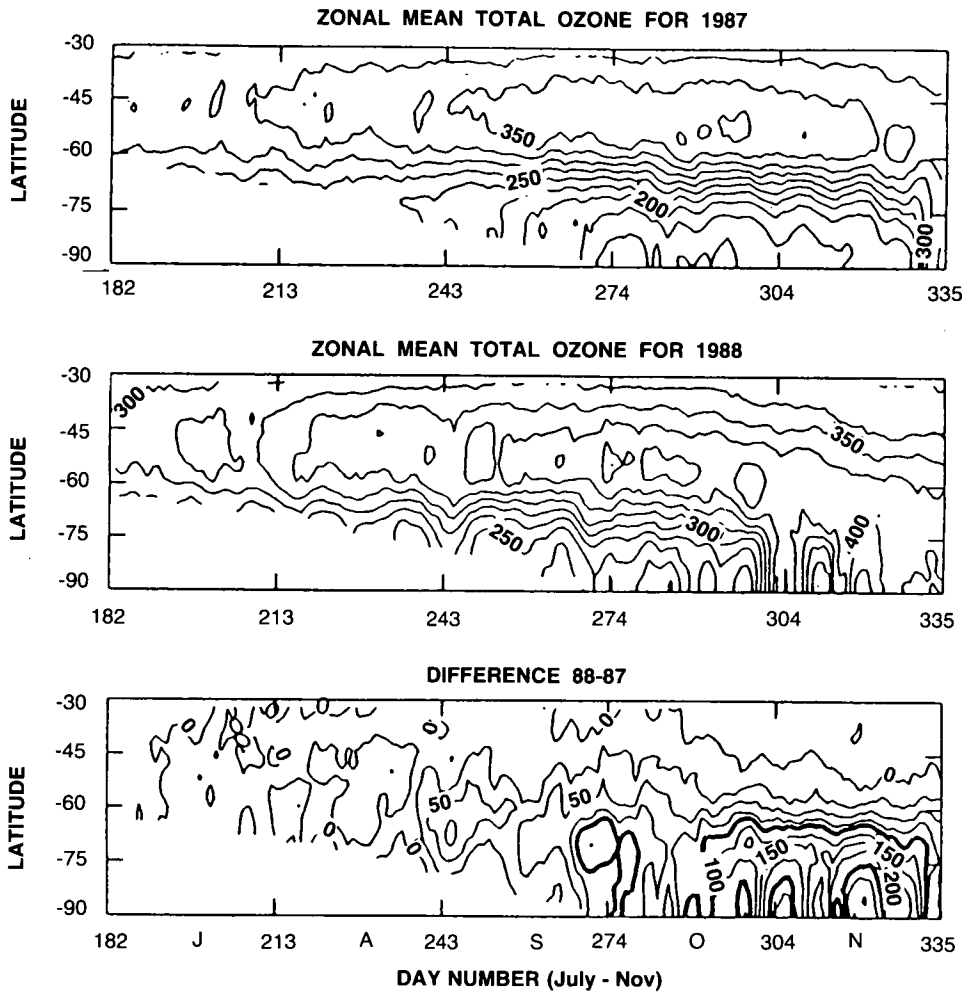


Figure 1.7.1-6. Evolution of zonal-mean total ozone (Dobson units) derived from the TOMS instruments during 1987 and 1988, and of the difference between these two years. Courtesy of M.R. Schoeberl and P.A. Newman.

presumably less anomalous in 1988 than in 1987. Consequently, the decline rate of the total column of ozone was less in 1988.

A slower rate of decline of ozone in 1988 compared with 1987 was followed by an earlier rise in ozone amounts. An explanation for this requires a detailed comparison of the circulations and photochemistry during the 2 years.

The circulation

Figure 1.7.1-11 is the map of Ertel's potential vorticity P and winds on the 500-K isentropic surface near 40 mb in the lower stratosphere for 1 August 1987 (the absolute value of P is plotted). (See Hoskins et al., 1985 for a discussion of the dynamical significance of the quantity P and of its use in interpreting meteorological phenomena.) A strong cyclone coincides with the high values of P over the polar cap. The strong gradients of P marked by the shaded ring resist displacements of air parcels by planetary-scale

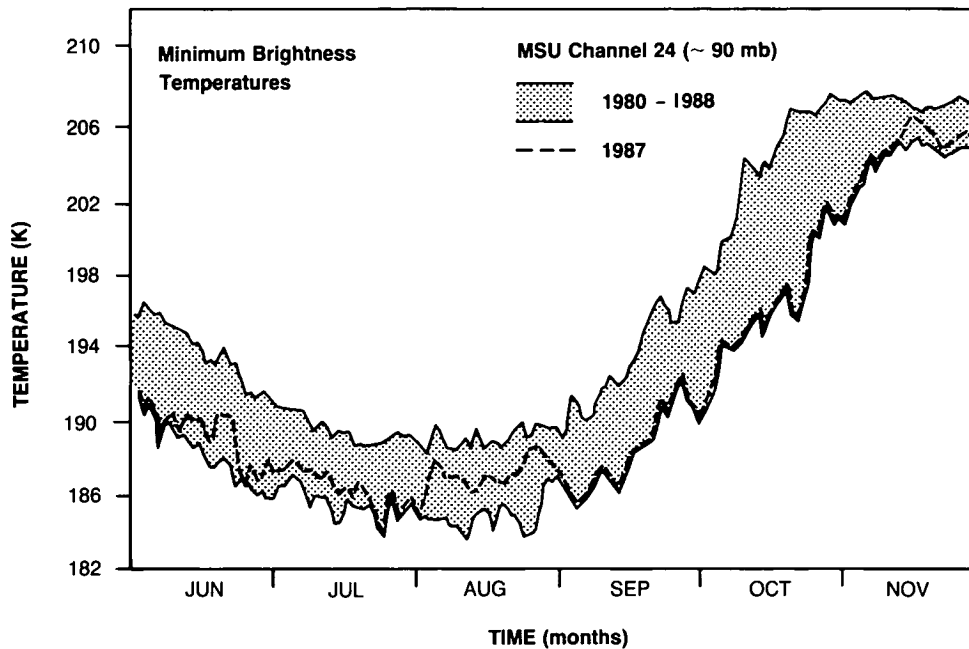


Figure 1.7.1-7. Minimum brightness temperature near 90 mb (derived from channel 24 of the MSU instrument) in the Southern Hemisphere during 1987 (dashed).

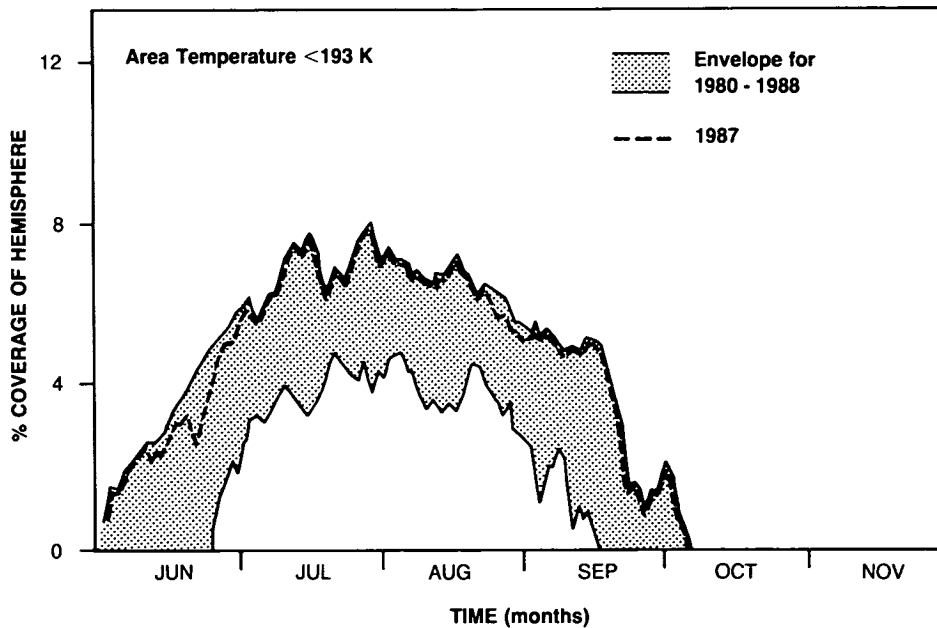


Figure 1.7.1-8. The fractional area (expressed as a percentage) of the Southern Hemisphere over which minimum temperatures near 90 mb in 1987 fell below 193 K, roughly the threshold temperature for formation of polar stratospheric clouds (neglecting the distinction between types of PSC). Solid curves show the envelopes of temperature and area curves for the years 1980-1988.

POLAR OZONE

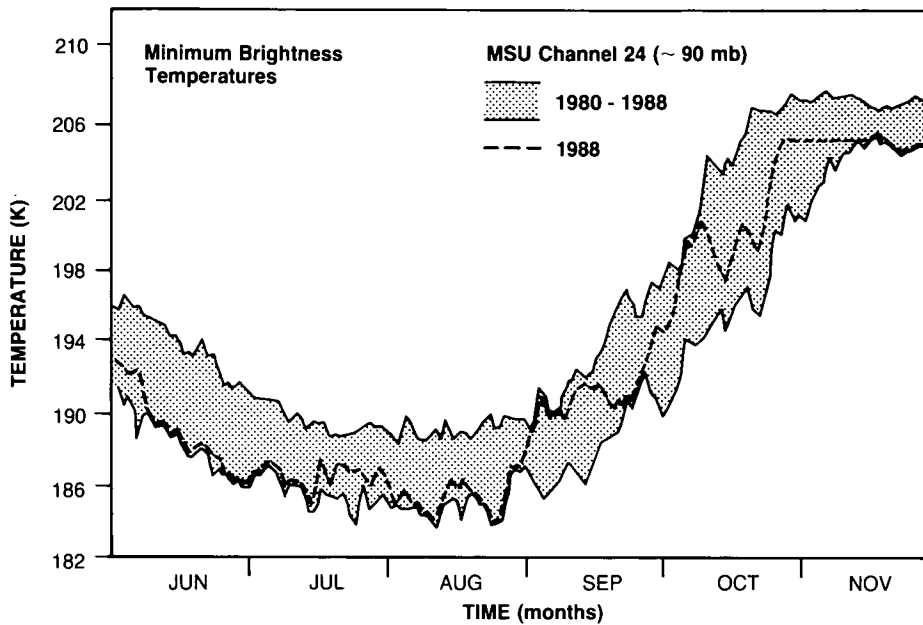


Figure 1.7.1-9. As for Figure 1.7.1-7 but for 1988.

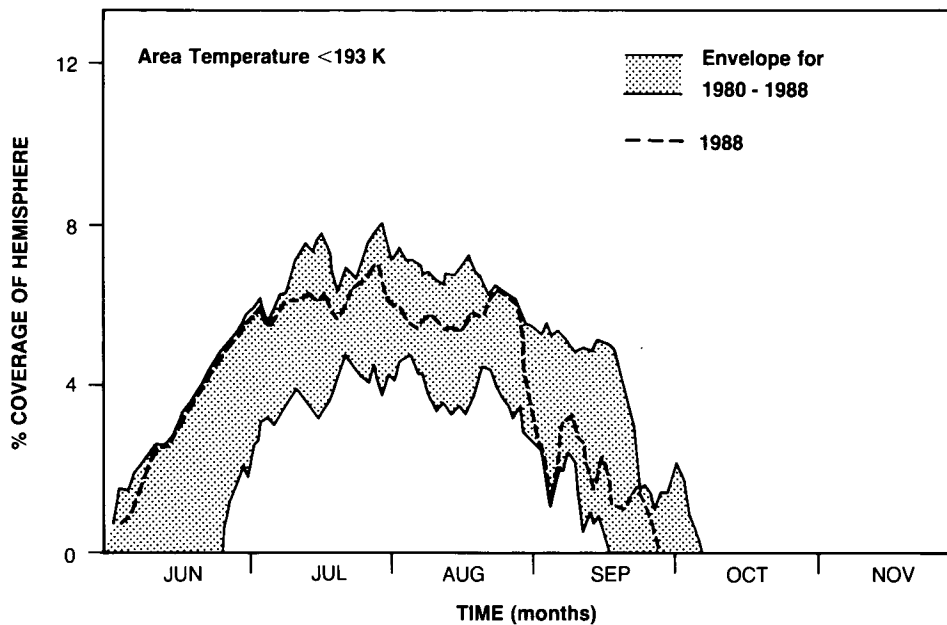


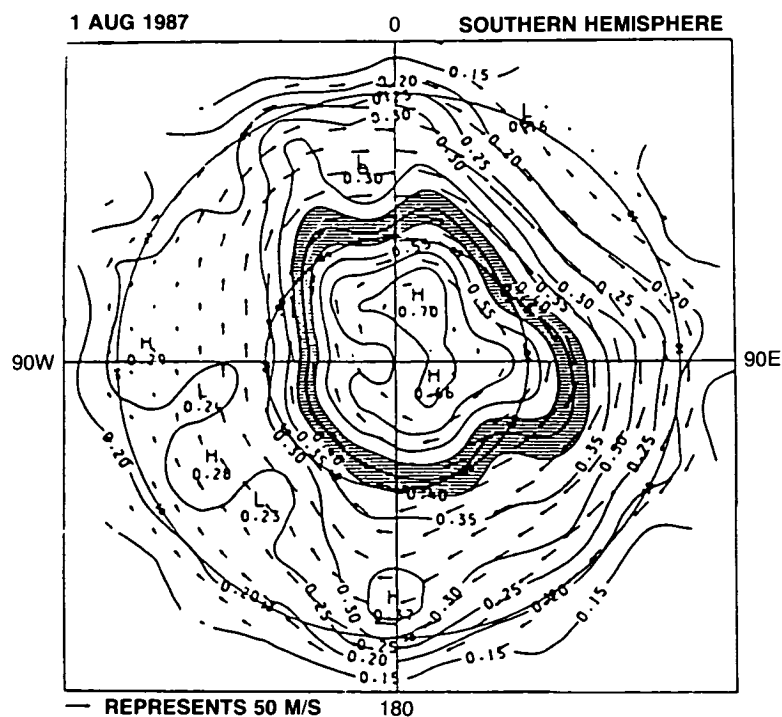
Figure 1.7.1-10. As for Figure 1.7.1-8 but for 1988.

disturbances, and little meridional transport of ozone or other trace chemicals into polar latitudes can occur while strong gradients in the vortex persist. Apart from any slow drift of air parcels due to radiative cooling, air well within the vortex forms an isolated air mass (Jukes and McIntyre, 1987; see also the discussion in Section 1.7.3).

As noted above, planetary-scale disturbances in the stratosphere can accelerate the weakening of the westerly vortex, especially in spring. In terms of the distribution of P , the vortex is broken down as its high- P air is drawn away to lower latitudes around developing anticyclones (see McIntyre and Palmer, 1983). As the vortex shrinks, air can migrate poleward. In addition, disturbances raise the temperature of the air in the vortex, especially near its outside edge. Here, air sinks and warms adiabatically at the entrances to localized jet streams between the westerly vortex and regions of anticyclonic circulation. One would infer that radiative cooling causes air parcels to spiral into the vortex and downward, effecting a corresponding transport of ozone and other trace chemicals. (Note that this picture lacks reliable quantitative details; see Section 1.7.3.)

In winter and spring 1987, however, disturbances to the stratospheric flow were comparatively weak and vortex erosion slow (see also Randel, 1988). Figure 1.7.1-12 shows that by the end of October a strong vortex, associated with strong gradients of P , remained in the lower stratosphere. The maps suggest that, apart from the slow transport due to radiation, the large area of the vortex inside the shaded ring was isolated during winter. In this cold region, heterogeneous reactions in the large volume of air occupied by PSCs could chemically precondition the air for rapid ozone destruction when sunlight returned to polar latitudes.

Figure 1.7.1-13 shows that in early August 1988 the westerly vortex in the lower stratosphere was as strong as in early August 1987. Thereafter, and unlike 1987, the circulation throughout the stratosphere in the Southern Hemisphere was strongly disrupted by planetary-scale disturbances (Kanzawa and



Kawaguchi, 1989). The vortex was displaced from the pole and broken down as it was progressively stripped of its high-P air. In the process, air from lower latitudes migrated polewards. Radiative cooling in the vortex would have contributed to the migration of air parcels into it. By the end of October 1988, only a small remnant of the vortex remained in the lower stratosphere, as shown in Figure 1.7.1-14.

In summary, the following seems the likely explanation for elevated polar ozone amounts in the Southern Hemisphere during spring 1988. There was a comparatively early breakdown of the westerly vortex in the stratosphere of the Southern Hemisphere and an early rise in temperature of most of the air in the vortex above threshold values for the occurrence of PSCs. As the vortex broke down, the ozone-destroying chain of chemical reactions was presumably quenched (1) as PSCs evaporated, bringing heterogeneous reactions to a stop, and (2) as NO_x was transported into polar regions, locking up chlorine radicals in less reactive "reservoir" compounds. The early breakdown of the vortex was also clearly accompanied by poleward transport of ozone-rich air and an early recovery of the total ozone column.

In 1988, natural processes happened to ameliorate, to some extent, the destruction of ozone by man-made pollutants. In view of the importance of heterogeneous chemistry in perturbing chlorine abundances (see Sections 1.3 and 1.6), and the strong dependence of PSC formation on temperature (Section 1.2), it would be surprising if years such as 1987 and 1988 did not exhibit dramatically different ozone depletions.

The Northern Hemisphere winter of 1988/89

During the Northern Hemisphere winter of 1988/89, several measurement campaigns were conducted in Arctic regions (see Section 1.10.2). The goal of those studies was to determine whether the anomalous chemical and meteorological conditions found to favor ozone destruction over Antarctica were also present

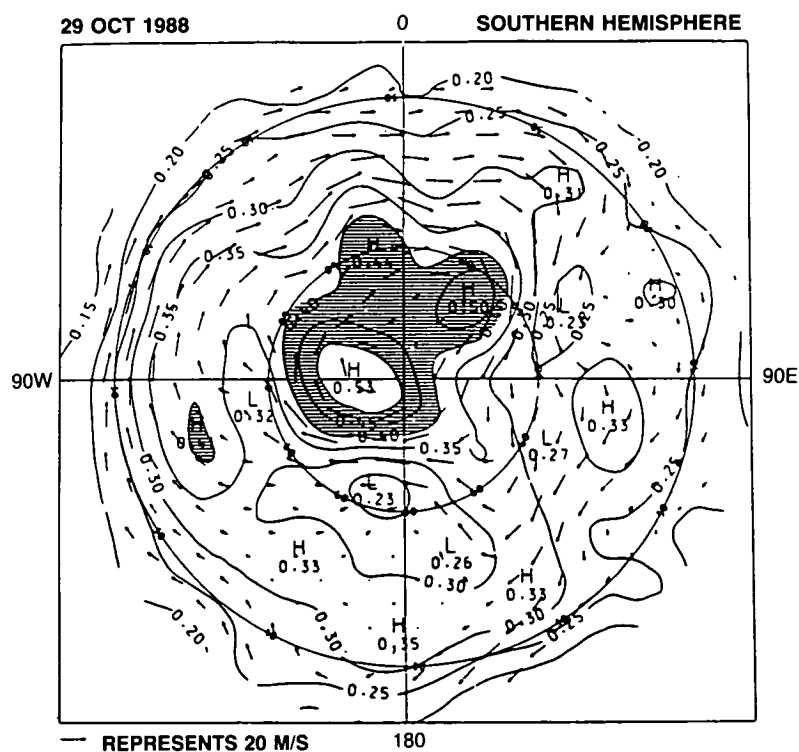


Figure 1.7.1-14. As in Figure 1.7.1-11, but on 29 October 1988.

POLAR OZONE

over the Arctic. In the following, we discuss briefly the dynamical conditions that prevailed in the 1988/89 Northern Hemisphere winter.

The meteorological conditions found during 1988/89 cannot be taken as fully representative of the winter stratosphere in the Northern Hemisphere (indeed, there is so much interannual variability that no one year can be taken as truly representative). January 1989 was the coldest January, at 30 mb in 25 years. Kuhlbarsch and Naujokat (1989) found temperatures as low as 181 K at 30 mb. Associated with these record low temperatures was a strong westerly vortex over the polar cap, as shown in Figure 1.7.1-15.

There followed a dramatic major warming. In the first half of February, temperatures rose sharply through the whole depth of the stratosphere at polar latitudes as a strong planetary-scale disturbance developed (see Fairlie et al., 1989, for details). The westerly vortex elongated as two anticyclones developed, first one over the Pacific and then one over the Atlantic. By mid-February, the vortex was split into two distinct centers of cyclonic circulation (Figure 1.7.1-16). This split extended through most of the stratosphere (the split was incomplete near 100 mb). In the lower stratosphere, the two cyclonic vortices continued to weaken during March. Gradients of potential vorticity were weak at middle and high latitudes; large meanders in the weak flow brought air from subtropical to polar latitudes.

Figure 1.7.1-17 shows the evolution during 1988/89 of the minimum temperature in the lower stratosphere (dashed curve), as derived from channel 24 of an MSU. The shaded region defines an envelope of such curves for the years 1980 through winter 1989. At the end of January, the minimum temperature fell

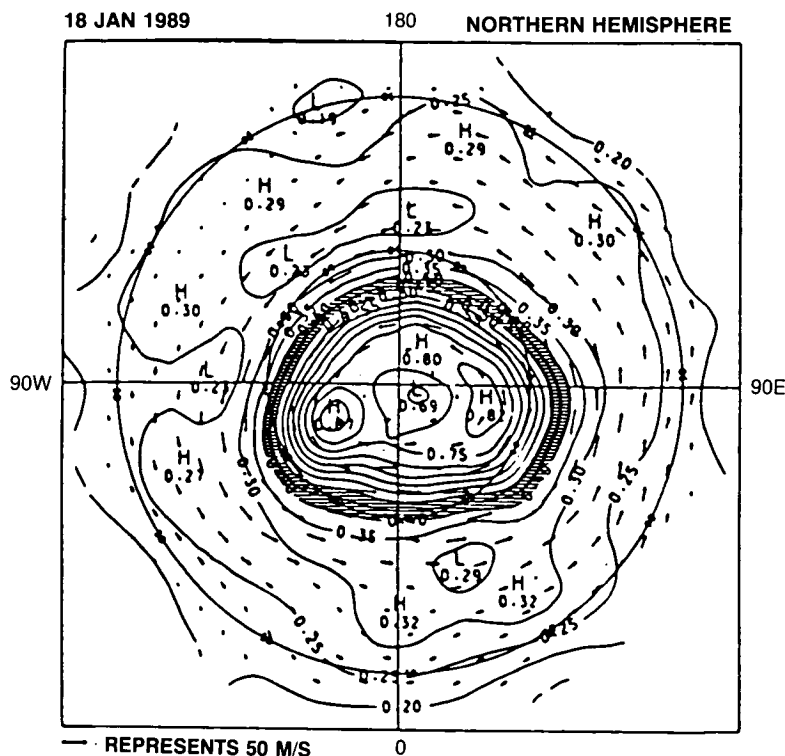


Figure 1.7.1-15. As for Figure 1.7.1-11, but for the Northern Hemisphere on 18 January 1989.

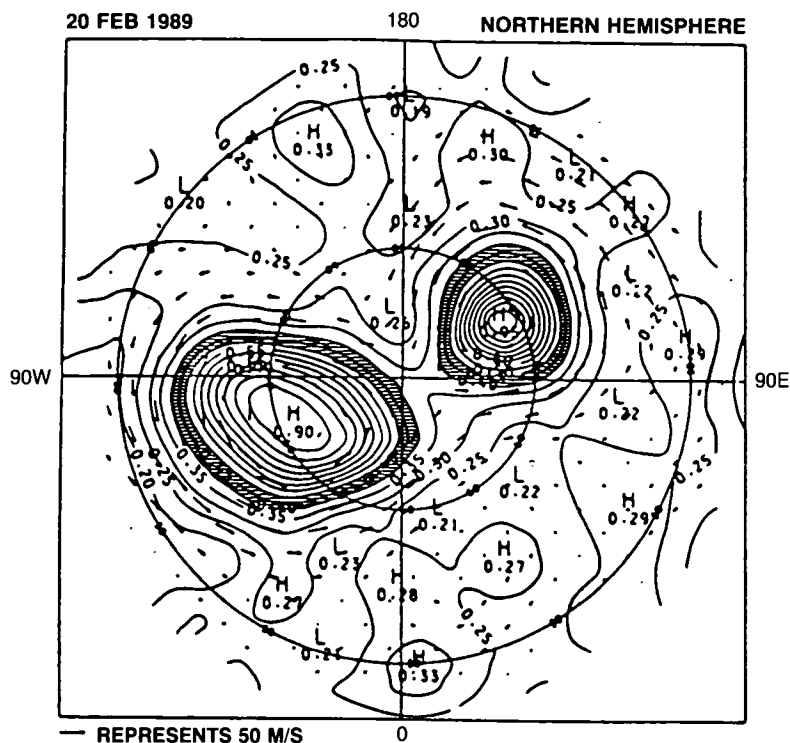


Figure 1.7.1-16. As for Figure 1.7.1-11, but for the Northern Hemisphere on 20 February 1989.

to 190 K, cold enough (less than about 195 K) for Type 1 PSCs to form at these levels, and even for Type 2 PSCs (according to calculations based on the laboratory measurements of Hanson and Mauersberger 1988a,b). MSU temperatures imply that PSCs have covered the polar cap north of about 75° N for about 10 days in mid-January (the presence of local pockets of PSCs farther south is not excluded by the measurements, owing to their limited resolution). Using measurements from the SAM II instrument on board the satellite Nimbus-7 (see McCormick et al., 1979 for details of the instrument), McCormick and Poole (personal communication) inferred the presence of large quantities of PSCs, including Type 2 PSCs, as far south as 50° N in January and early February. Figure 1.7.1-17 shows that, in early February, minimum temperatures rose rapidly above 195 K; SAM II measurements indicate that PSCs disappeared almost everywhere (McCormick and Poole, personal communication).

The MSU temperatures indicate that the area affected by PSCs over the Arctic in winter 1989 was much smaller than over the Antarctic. Taking 193 K as a representative temperature for PSC occurrence (ignoring the distinction between Type 1 and Type 2 PSCs), one infers that the areal coverage is at most one third of that over the Antarctic (although we note that the Antarctic coverage will be overestimated if denitrification or dehydration takes place, altering the abundance of condensables and hence the threshold temperature for PSCs). The duration of PSC activity is much shorter in the Northern as compared with the Southern Hemisphere—the figure of one third applies to a few weeks at most. So far, there have been no reports of dramatic ozone reduction during spring in the Northern Hemisphere (see Section 1.1.6). Note, however, that the MSU measurements span only about 10 years.

POLAR OZONE

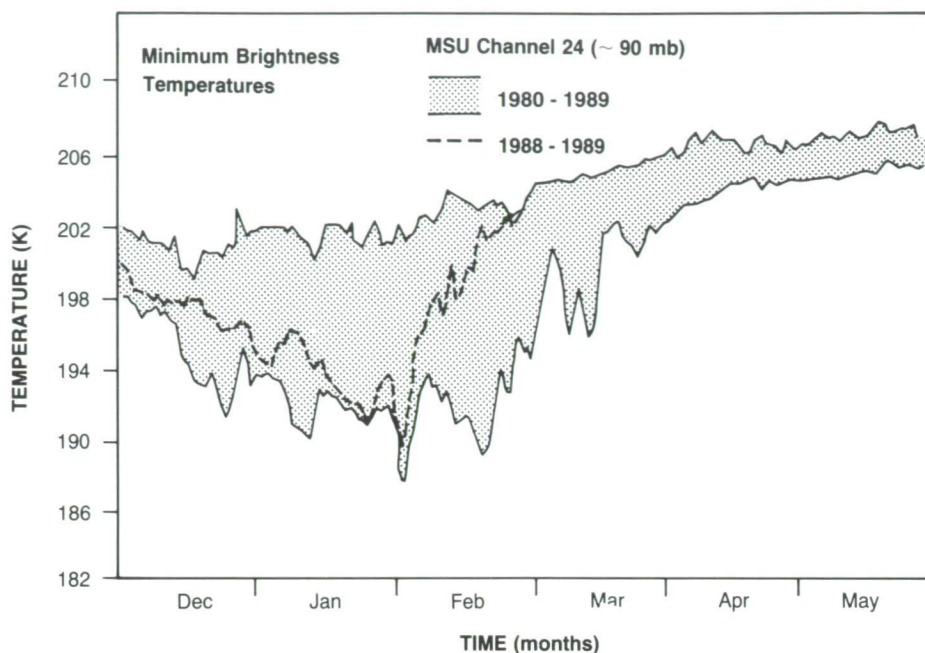


Figure 1.7.1-17. Minimum brightness temperature derived from channel 24 of the MSU (centered near 90 mb) in the Northern Hemisphere for December through May. The dashed curve is for 1988-1989; the full lines form the envelope of such curves for the years 1980 through winter 1989.

1.7.1.3 Effects of the Quasi-Biennial Oscillation and the Solar Cycle

The quasi-biennial oscillation (QBO)

As discussed briefly in Section 1.1, there is evidence that the quasi-biennial oscillation (QBO) in stratospheric tropical winds is linked with QBO oscillations in temperatures, geopotential heights, and total ozone abundances not only in the tropics but at extra-tropical latitudes as well. Observed QBO signals in total ozone and the dynamical factors that influence it will be discussed in more detail in this section. Angell and Korshover (1962, 1964, 1967) detected a quasi-biennial oscillation in temperature at middle and high latitudes of both hemispheres, while Holton and Tan (1980, 1982) and van Loon and Labitzke (1987) found that the winter westerly vortex in the lower stratosphere was weaker during the easterly phase of the QBO. The QBO variability of extra-tropical ozone was recorded by Angell and Korshover (1964, 1967, 1973, 1978), who found that (1) total ozone amounts tended to be low (high) during the westerly (easterly) phase of the QBO; (2) this variation was out of phase with that in the tropics, where ozone amounts vary in phase with the wind; and (3) total ozone changed by about 4% (about 12 Dobson units) between extremes of the QBO. Oltmans and London (1982) and Hasebe (1983) confirmed these findings, as do the recent results derived from the TOMS instrument by Lait et al. (1989), which are shown in Figures 1.7.1-18 and 1.7.1-19. The QBO in total ozone at high latitudes must be allowed for in an explanation of the increasing depletion of ozone in the southern polar spring in the 1980s (Bojkov, 1986; Garcia and Solomon, 1987).

The means by which the tropical QBO is communicated to extra-tropical latitudes is not fully understood. The tropical zonal wind QBO is believed to be driven by the interaction of upward-propagating,

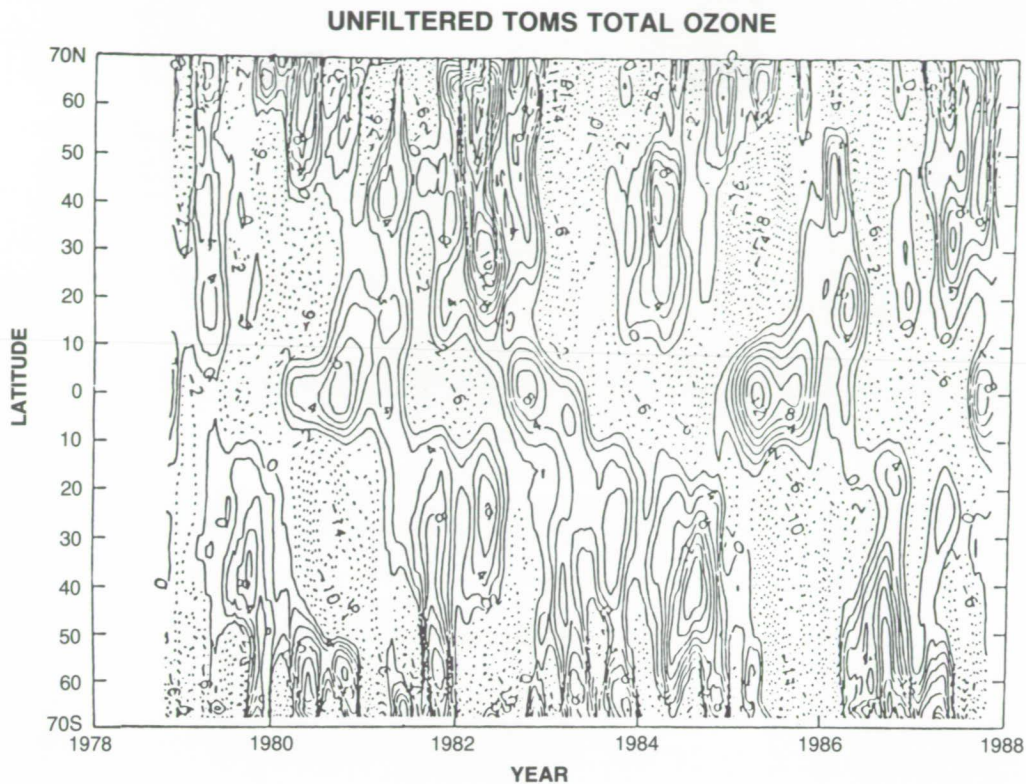


Figure 1.7.1-18. The total ozone fields (in Dobson units) from November 1978 to October 1987 with annual cycle removed.

large-scale tropical waves with the zonal-mean flow. Associated with this forcing is a secondary circulation, which gives rise to a QBO in total ozone and temperature in the tropics, and an oscillation of opposite phase in the subtropics (Plumb and Bell, 1982; Plumb, 1984; Gray and Pyle, 1989). Calculations suggest that this circulation can extend only up to about 15° of latitude from the center of the wave forcing. However, the interaction of this circulation with the global mean circulation may further extend its influence (Gray and Pyle, 1989). Further poleward influence of the QBO may result from a modulation of extratropical planetary-wave activity during winter (Holton and Tan, 1982). These waves can propagate upwards from the troposphere only when winds are westerly. During the easterly phase of the QBO wave activity would be more confined than during the westerly phase, and greater polar warming and poleward transport of ozone would be expected. Evidence for such effects has been given by Labitzke (1982). However, in the first two-dimensional modeling study of the ozone QBO, Gray and Pyle (1989) achieved a realistic latitudinal distribution of the ozone QBO signal without the latter effect, suggesting that it may not represent the dominant mechanism for the ozone QBO.

Concerning the Antarctic ozone hole, Bojkov (1986) first noted an apparent correspondence of the QBO with year-to-year changes in minimum total ozone amounts. Garcia and Solomon (1987) studied variations in total ozone and temperature minima for the October months of 1979–1986, and found that low (high) ozone and temperature were apparently associated with the westerly (easterly) phase of the tropical QBO at 50 mb. Recently, however, Lait et al. (1989) have pointed out that this simple correlation becomes seriously degraded when observations for 1986 are examined carefully and when an extra year, 1987, is included in the series.

POLAR OZONE

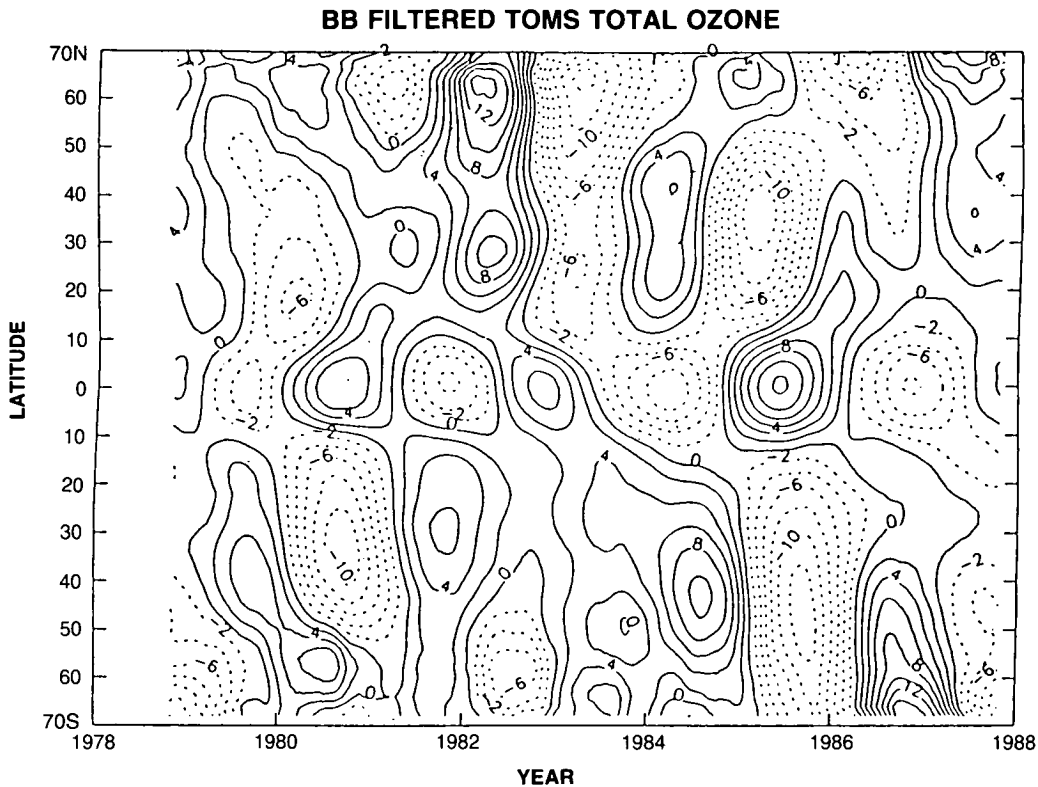


Figure 1.7.1-19. As in Figure 1.7.1-18, but after application of a broad-band filter (taken from Lait et al., 1989).

Figures 1.7.1-20 and 1.7.1-21 show the year-to-year variations over the South and North Poles in October-mean and (correspondingly) April-mean total ozone amounts and 70-mb temperatures for 1979–1988 (note the scale change for ozone between the two hemispheres). Also indicated is the phase of the tropical QBO in 50-mb winds over Singapore for the appropriate month. In the Northern Hemisphere, there is no clear evidence of a correlation between the tropical winds and parameter values at the pole. In the Southern Hemisphere, on the other hand, there appears to be a quasi-biennial modulation of the time series of temperatures and ozone amounts from 1979 through 1985, with minor peaks in temperature and ozone amounts coinciding with the easterly phase of the tropical QBO, and troughs with the westerly phase. In 1986, however, this apparent correlation breaks down if only 50-mb winds are considered: peaks in temperature and ozone coincide with a westerly rather than easterly phase at the 50-mb level. The lowest values of temperature and total ozone occur in 1987. These minima do coincide with the (monthly-mean) westerly phase of the tropical QBO, but winds reversed from easterly to westerly only in October; throughout the austral winter of 1987 tropical winds at 50 mb were easterly. Therefore, it may be fortuitous that the apparent correlation holds up in 1987. In 1988, ozone amounts are about 100 DU higher and 70-mb temperatures almost 20 K warmer in October 1988 than in October 1987, whereas QBO-related increases of no more than about 20 DU and 5 K might have been anticipated from previous years. This discrepancy might be attributable to interannual variability not directly related to the tropical QBO, or it might indicate that different parameters from those used in the figure should be used to establish a more robust correlation.

According to Lait et al. (1989), a much better QBO correlation between tropical winds and polar ozone can be exposed for the Southern Hemisphere by using as a variable the decline rate in September of the minimum value of total ozone (they use the map minimum value of total ozone south of 30°S on daily

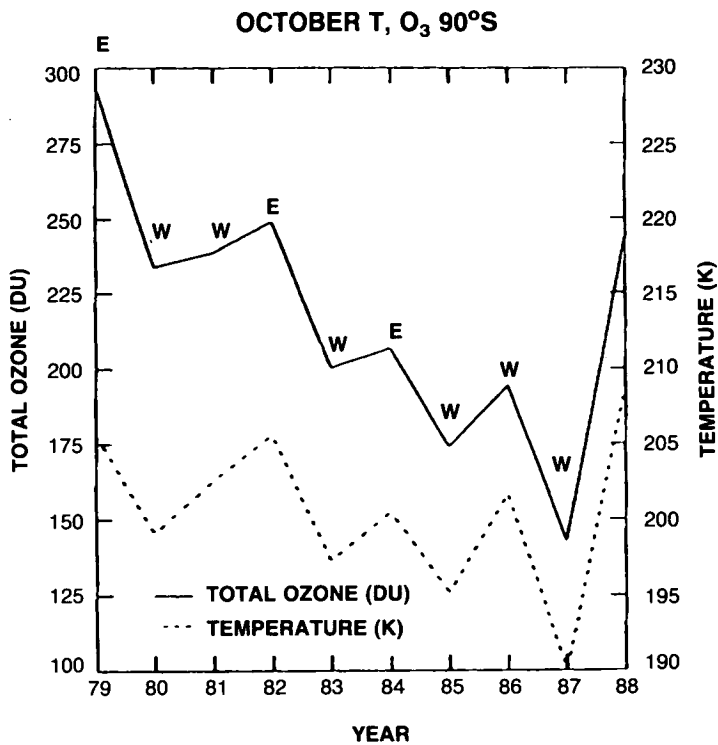


Figure 1.7.1-20. Variation in October mean total ozone and 70 mb temperature over the South Pole. Letters W and E denote the west and east phases of equatorial winds at 50 mb over Singapore.

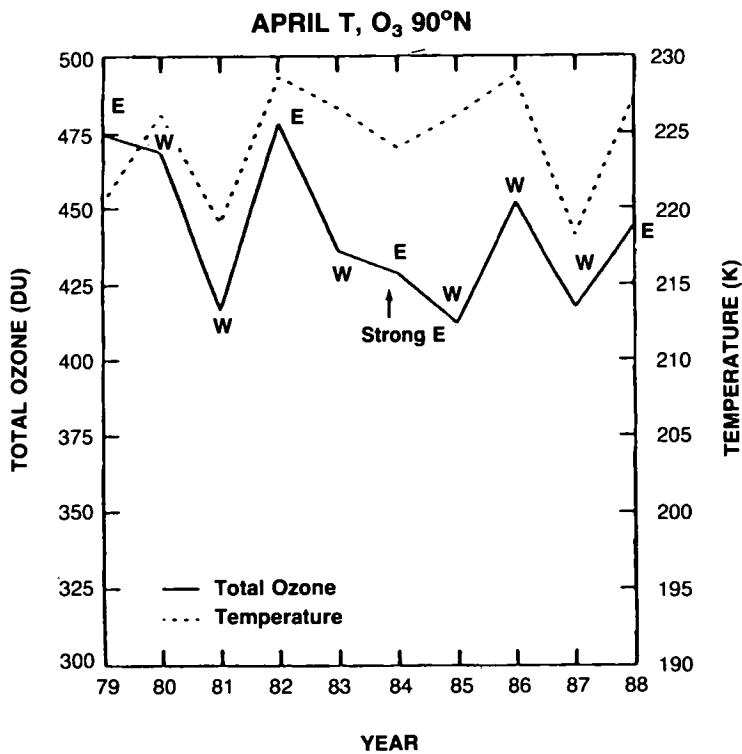


Figure 1.7.1-21. As in Figure 1.7.1-20, but for the April mean in the Northern Hemisphere.

POLAR OZONE

fields derived from the TOMS instrument). This seems reasonable in that any extra-tropical effect of the tropical QBO would presumably modulate the chemical and dynamical processes controlling ozone amounts, and hence the time rate of change of ozone. They found that the correlation is better when tropical winds at 30 mb instead of 50 mb are used. (Why this should be so is not known.) Their results are shown in Figure 1.7.1-22. There appears to be a high degree of correlation between 30-mb tropical winds and the September decline rate of the polar minimum in total ozone (and also between the winds and equatorial total ozone).

It is worthy of note that the QBO oscillation in tropical winds is not coherent at all levels; rather, tropical winds reverse direction first at higher altitudes and progress downwards. In some QBO cycles, the progression below 30 mb can lag considerably that of higher levels (as shown, for example, in Naujokat, 1986). This suggests that a fuller understanding of the correlation between tropical winds and the extra-tropical response may be rather sensitive to the altitude chosen for the correlation, and requires a better understanding of the causal mechanism (especially any relevant time lags) before the appropriate parameters for correlation can be identified. It is particularly important for causal mechanisms to explain the observed discrepancy between the period of the ozone QBO at the Equator (approximately 27 months, corresponding to the period of the zonal wind QBO there) and at higher latitudes, where the period is closer to 2 years. These observations have suggested a strong interaction of the polar ozone QBO with the annual cycle (Gray and Pyle, 1989).

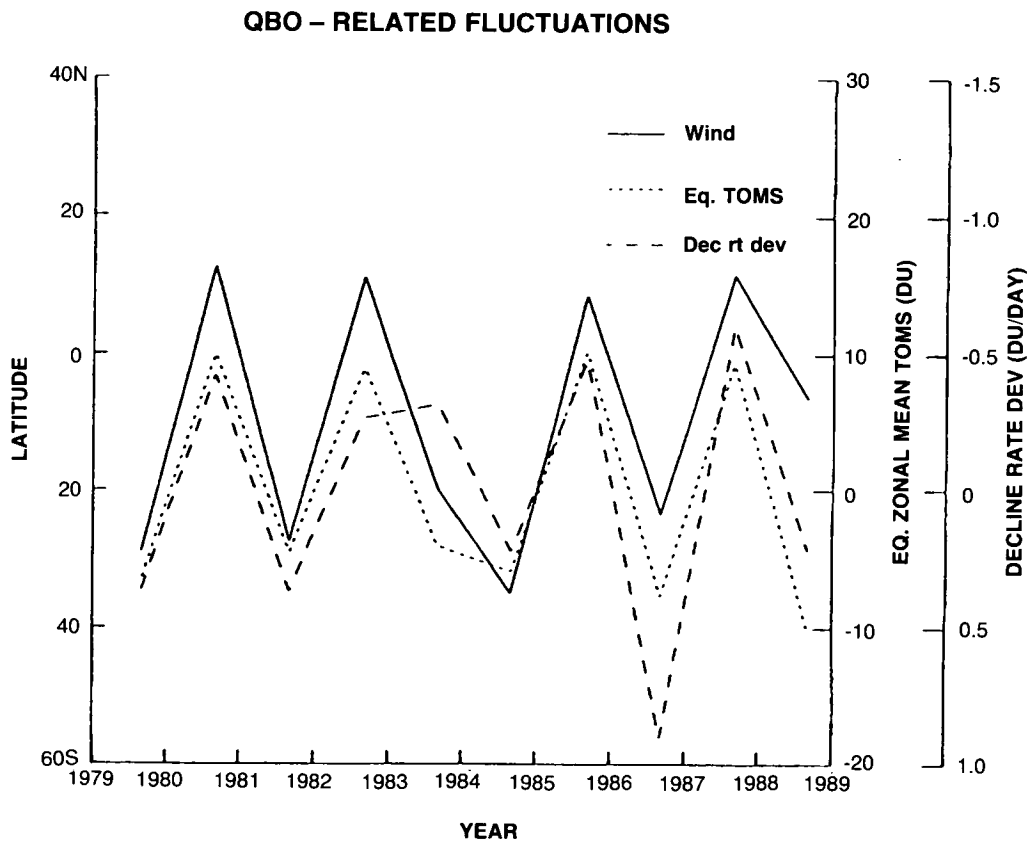


Figure 1.7.1-22. Correlation of August-September winds over Singapore at 30 mb (solid line) with the total ozone decline rate in September (large dashes). A linear trend has been removed from the decline rates. The September-mean values of equatorial total ozone are also shown (short dashes).

Lait et al. (1989) advance the following hypothesis to explain the relation between the tropical QBO and the year-to-year variability in Antarctic ozone depletion. During the easterly phase, increased planetary-wave activity in the stratosphere at middle and high latitudes will (1) increase polar temperatures, thereby reducing the volume and frequency of polar stratospheric clouds, and (2) allow more NO_x to enter the vortex from mid-latitudes, which would reduce the amount of active chlorine.

Numerical experiments and a longer time series of observations is needed to test this hypothesis. Interhemispheric comparisons will surely provide important information. Such work is essential to discriminate between natural variations and anthropogenic changes in ozone amounts.

The solar cycle

The 11-year cycle in the variation of solar UV irradiance (in the wavelength range 175 to 320 nm) produces changes of ozone and temperature in the Earth's atmosphere by changing rates of photolysis and radiative heating (Simon, 1981). These changes must be allowed for when trying to identify anthropogenic effects. Recent theoretical studies of the response of the middle atmosphere to solar UV variability include those of Garcia et al. (1984), Callis et al. (1985), Keating et al. (1985), Eckman (1986), and Brasseur et al. (1987). Figure 1.7.1-23 shows the ozone variation over the course of the 11-year solar cycle as calculated by Garcia et al. (1984).

During high solar activity, increased ozone is predicted at low and mid-latitudes in the upper stratosphere, but large decreases are predicted at high latitudes during local spring (owing to an increase in NO_x). As discussed in Section 1.6, polar observations of reactive nitrogen rule out any large solar fluctuations in

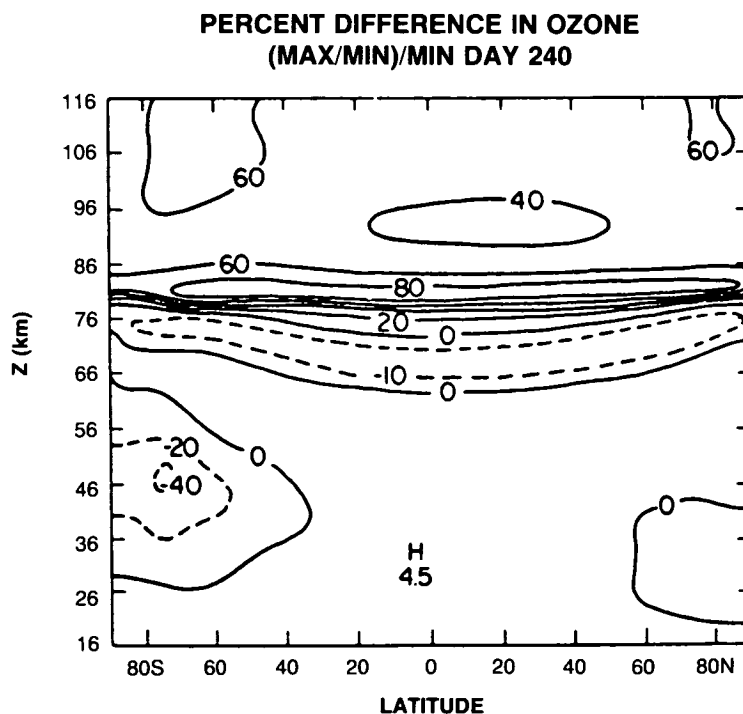


Figure 1.7.1-23. Ozone mixing ratio variation at the maximum of the 11-year solar cycle, as calculated by Garcia et al. (1984).

POLAR OZONE

NO_x at the low altitudes where the bulk of the total ozone column resides. Calculations by Brasseur et al. (1987) indicate that a 10% increase in UV radiation at 205 nm would be accompanied at 5 mb by globally averaged increases of about 3.5% in ozone and 1.5 K in temperature. Calculations of the expected ozone response to solar activity as a function of latitude and season were discussed in OTP (1989).

Recent observational analyses of the possible response of ozone to 11-year solar variations include the works of the OTP (1989), Keating et al. (1981), Chandra (1984), Oehlert (1986), and Reinsel et al. (1987, 1988). Using Umkehr data, Reinsel et al. (1987) detected a 3% variation in ozone at 36 km over the solar cycle. The amplitude of the cycle in total ozone was estimated to be about 2% by Keating et al. (1981), who used data from the Nimbus 4 BUUV instrument. Various investigators have detected a possible relation between stratospheric temperature and the 11-year solar cycle (Schwentek 1971; Angell and Korshover 1978; Quiroz 1979, Nash and Forrester 1987; Labitzke 1987a; Chanin et al. 1987). Using summertime rocketsonde temperatures, Quiroz (1979) found a high correlation between the temperature deviations and sunspot number in the middle and upper stratosphere. Nash and Forrester (1987) found evidence in SSU data of a drop in upper stratospheric temperatures of about 1.5 K from 1980 to 1986, which they attributed to a drop in solar activity.

Recently Labitzke and van Loon (1988a) reported some intriguing results. Linear correlations between three solar cycles in the period 1956–1987 and high-latitude stratospheric temperatures and geopotential heights showed no associations. But when the data were grouped according to the phase of the equatorial quasi-biennial oscillation (QBO), statistically significant correlations resulted: when the QBO is in its west phase, the polar data are positively correlated with the solar cycle, while those in middle and low latitudes are negatively correlated; the converse holds for the east phase. They also found that no major mid-winter warming occurred in the west phase of the QBO during minima in the three solar cycles, though major warmings were found at the minima during the east phase. Because greater poleward transport of ozone occurs during major warmings, one would expect the QBO signal in extra-tropical ozone amounts to be strengthened in solar minima and weakened in solar maxima. Provided the data are divided according to the phase of the QBO, statistically meaningful relationships are also found throughout the troposphere (Labitzke and van Loon, 1988a, b) and in the mesosphere (Labitzke and Chanin, 1988).

As yet no plausible mechanisms have been advanced to explain the correlations in the lower atmosphere; they could be flukes. For example, one could argue that low-frequency variations associated with the dynamics of the coupled ocean/atmosphere system would have, over a limited data sample, apparently significant projections onto a broad range of frequencies, including the 11-year solar cycle. The findings remain a source of debate and speculation.

A major difficulty in assessing atmospheric response to the 11-year solar cycle is the lack of a long-term (many cycles) data base from which statistically significant inferences can be drawn. There may be drifts in instrument sensitivity over extended periods of time, and individual instruments have a limited lifetime (especially those on satellites). One approach has been to investigate the response to short-term variations related to the 27-day solar rotation (Gille et al., 1984a; Hood, 1987; Keating et al., 1987). Results of such studies should be applicable to the 11-year cycle if the main processes controlling ozone amounts respond to solar UV variations on time scales much less than 27 days. Calculations by Brasseur et al. (1987) indicate that ozone changes induced by the 11-year and 27-day cycles are similar in the mesosphere and upper stratosphere, but that there may be appreciable differences in the lower stratosphere.

The analysis of total ozone measurements reported in OTP (1989) and summarized in Section 1.1.6 suggested solar-induced changes in Arctic total ozone of as much as 1.8%. Further, the solar-induced

changes in stratospheric temperatures outlined by Labitzke and Van Loon (1988a,b, 1989) may have appreciable effects on the formation of PSCs and hence on polar ozone depletion. Clearly, such fluctuations must be considered in attempts to deduce ozone and temperature trends, particularly in the Northern Hemisphere where current trends appear to be small (Sections 1.1.6 and 1.7).

1.7.2 Role of Synoptic-Scale Disturbances

It has been known for many years that tropospheric weather systems can have a substantial impact on total ozone amounts by changing the height of the tropopause between the ozone-poor air of the troposphere and the ozone-rich air of the stratosphere, and through horizontal mixing and advection (Dobson et al., 1928). Cyclonic weather systems are usually associated with low tropopause heights and high values of total ozone; anticyclonic systems with high tropopause heights and low values of total ozone.

During the course of the 1987 Airborne Antarctic Ozone Experiment (AAOE), column ozone amounts at southern high latitudes were observed to decline from values near 250 DU to below 150 DU. Particularly rapid reductions in ozone were found to occur on a synoptic scale in so-called mini-holes (Krueger et al., 1988), which last for several days and move slowly from west to east. On several occasions, the total ozone amount measured by the Total Ozone Mapping Spectrometer (TOMS) decreased over a period of 24-48 hours by several tens of DUs. Recently, Newman et al. (1988) noted correlations between low total ozone amounts, low temperatures, and low values of potential vorticity. They concluded that the Antarctic Peninsula is a preferred site for mini-hole intensification. Figure 1.7.2-1 shows an example of a mini-hole

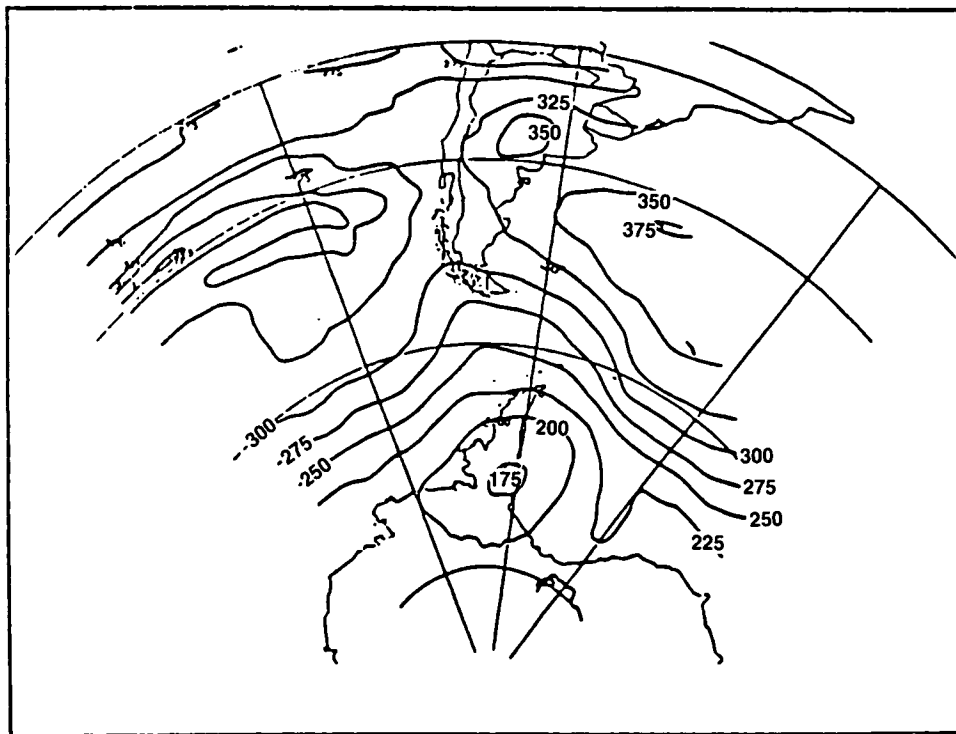


Figure 1.7.2-1. An example of mini-hole over the Antarctic Peninsula on 5 September 1987 (denoted by the bull's eye pattern near the Palmer Peninsula). Data derived from the TOMS instrument (contours labeled in Dobson units). Courtesy of P.A. Newman and M.R. Schoeberl.

POLAR OZONE

over the Antarctic Peninsula on 5 September 1987. Mini-holes are also found in the Northern Hemisphere. A particularly intense mini-hole was observed during the recent Airborne Arctic Stratospheric Expedition (AASE). Total ozone amounts measured by TOMS over Scandinavia fell as low as 125 DU.

Mini-holes are found to be associated with stratospheric clouds (Tuck, 1989). Krueger et al. (1987) pointed out that, as a result of this, total ozone amounts deduced from TOMS measurements could be underestimated in mini-holes because of the effects of high clouds on the ultraviolet radiation measured by the satellite (the problem is particularly acute at high solar zenith angle).

Two possible explanations for the observed rapid reductions in ozone amounts are (1) fast chemical processes and (2) atmospheric motions. On the basis of current photochemical theory, Jones et al. (1989) and Anderson et al. (1989) argued that it is not possible to destroy ozone fast enough to account for the observed transient mini-hole reductions. That atmospheric motions could lead to mini-holes was demonstrated by McKenna et al. (1989a). By calculating air parcel trajectories, they showed that the mini-hole in Figure 1.7.2-1 formed in association with a synoptic-scale anticyclone in the troposphere and lower stratosphere, which concentrated ozone-poor air below the level of the stratospheric polar vortex, thus reducing the column amount. The mini-hole is thus a manifestation of localized dynamical effects rather than irreversible transport of ozone-poor air.

Though of dynamical origin, mini-holes may be associated with important chemical effects, perhaps on spatial scales larger than the holes themselves. The formation of PSCs above synoptic-scale anticyclones provides the mechanism. Isentropic surfaces tend to rise above tropospheric anticyclones, and air cools as it glides upward along these surfaces. If it cools enough to saturate, clouds will form. Figure 1.7.2-2(i) shows cross sections of temperature, and Figure 1.7.2-2(ii) cross sections of potential temperature and saturated mixing ratio of water vapour taken through the mini-hole shown in Figure 1.7.2-1. There is an

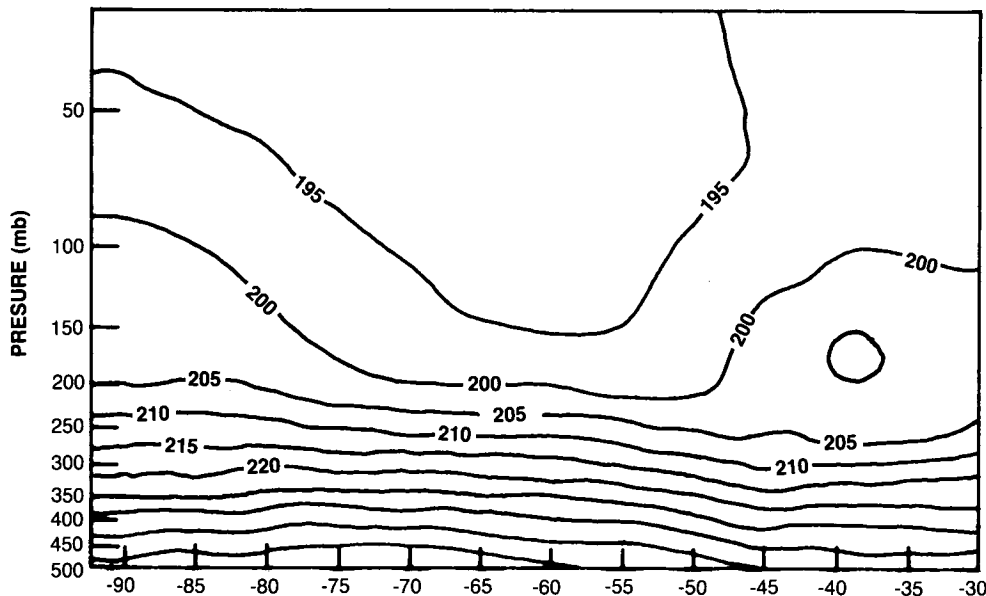


Figure 1.7.2-2(i). Longitude/pressure cross sections on 5 September 1987 at latitude 65°S from 90°W to 30°W, and from 250 to 30 mb (derived from U.K. Meteorological global analysis). (i) Temperature (5 K contour interval).

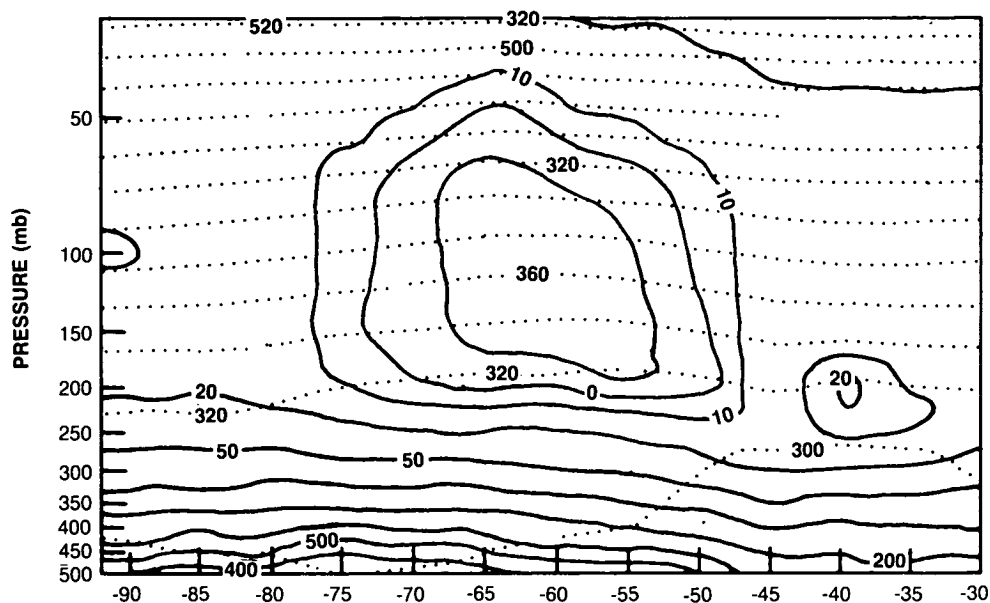


Figure 1.7.2-2(ii). As in Figure 1.7.2-2(i). Saturation water vapor mixing ratios (solid; at 6, 8, 10, and 20 ppmv) and isopleths of potential temperature (broken; contour interval 20 K).

area above 90 mb where temperatures were below 192 K. This local temperature minimum was associated with gently bowed up contours of potential temperature, indicating that air had ascended. The potential for saturation was greatest in the temperature minimum, where saturation mixing ratios were lowest. Type 1 or Type 2 PSCs would form preferentially in such a region.

A cloud deck so formed will remain linked to its generating anticyclone, and will tend to move with the anticyclone. Note, however, that in the lower stratosphere strong winds blow through the localized temperature minimum. Although an air parcel's exposure to PSCs will be short in any one encounter, it may be long enough for heterogeneous chemical reactions to occur to some extent, and thus to perturb the parcel's chemical composition. Tuck (1989) has also postulated that strong radiative cooling above cold polar stratospheric cloud decks causes air to sink, leading to further exposure of air to heterogeneous reactions.

Synoptic-scale disturbances also promote some meridional transport of air in the lower stratosphere (below about 70 mb). The disturbances cannot penetrate much higher because they are trapped by the strong westerly winds in the stratosphere (Charney and Drazin, 1961). Figure 1.7.2-3 shows a sequence of isentropic maps of Ertel's potential vorticity P for the lower stratosphere in late September 1987. Shading marks the edge of the region that was found to be chemically perturbed (Tuck, 1989). Near longitude 180 it appears that air is being peeled off the chemically perturbed region to form an isolated blob of P , which slowly disappears (either because of dissipation or because of inadequate resolution in the synoptic analyses). Murphy et al. (1989) also found evidence for some interchange of air at the edge of the chemically perturbed region.

In summary, synoptic-scale disturbances can increase the amount of air that is subject to heterogeneous chemistry (1) by generating PSCs on a synoptic scale, through which air may flow to give chemical

POLAR OZONE

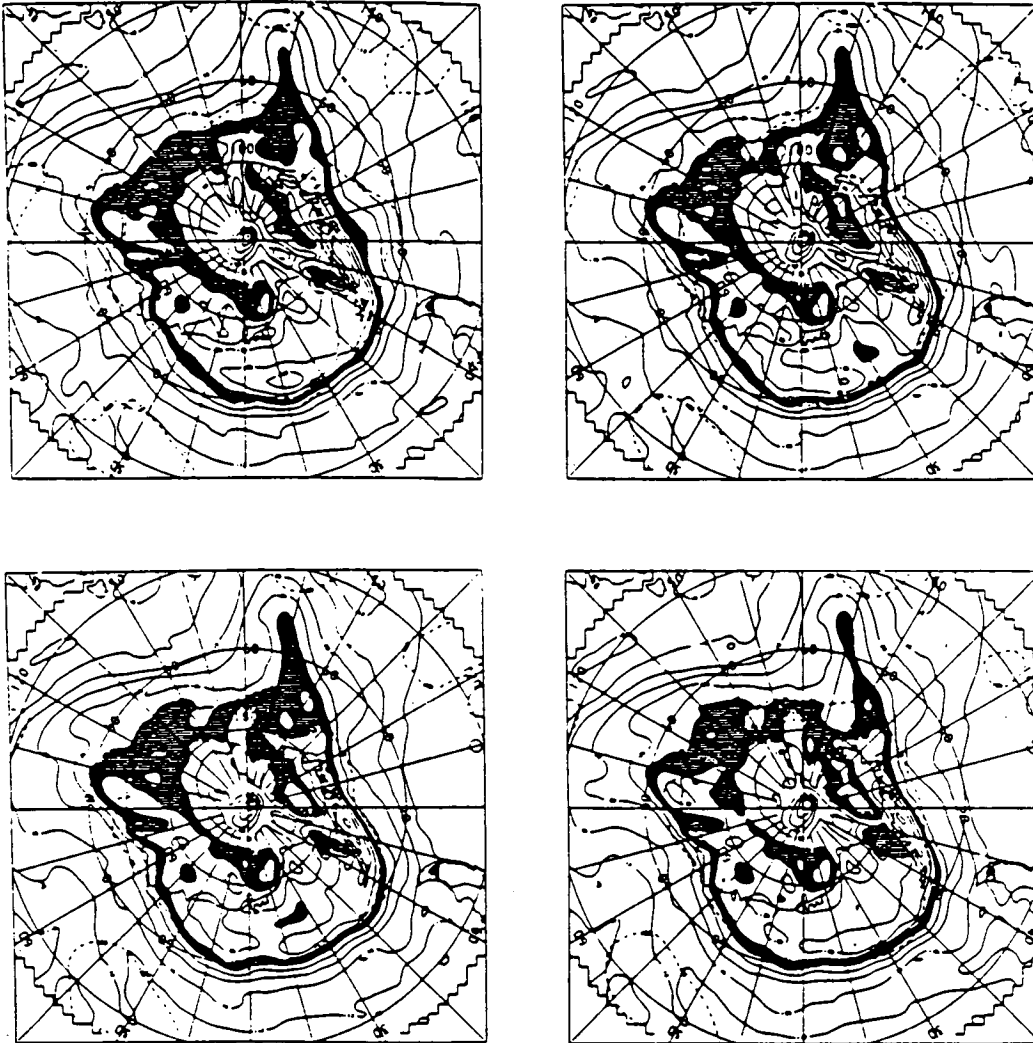


Figure 1.7.2-3. A sequence of potential vorticity distributions on the 428 K surface of potential temperature (from Tuck, 1989).

effects on a larger scale, and (2) by transporting air in and out of large-scale cloud decks (formed by large-scale cooling in the polar night). Quantitative details are uncertain, however.

1.7.3 Processing of Antarctic Air

The heterogeneous chemical reactions that eventually lead to ozone destruction require PSCs, which are found at temperatures below about 193 K within the stratospheric polar vortex. To quantify the amount of ozone that will be destroyed in a given year, one might begin by assuming that the PSC-containing volume is a fixed slug of air. Then the maximum amount of ozone that could be destroyed is the amount in the largest volume of air ever to contain PSCs. Such a calculation would seriously underestimate the amount of ozone destruction if a large amount of air flowed through the PSC-containing volume—that is,

if the PSCs and atmospheric circulation could be viewed as components of a giant “chemical processor.” If that were so, ozone amounts could be affected hemispherically, or even globally, by a sink confined to southern polar latitudes. Some findings relevant to this issue are now outlined.

The PSCs are contained within an intense westerly vortex that is characterized by strong gradients of potential vorticity (see Figure 1.7.1-13). Such gradients resist lateral displacements of air parcels (McIntyre and Palmer, 1983), inhibiting to some extent the mixing of chemically perturbed vortical air with unperturbed extra-vortical air. The term “containment vessel” has been used to describe this situation. There is, of course, no impermeable seal around polar air. Air is stripped from the outer portion of the vortex by planetary-scale waves (Juckes and McIntyre, 1987; Mechoso et al., 1988) and, in the lower stratosphere, by synoptic-scale disturbances (Tuck, 1989; see Figure 1.7.2-3). This air may then mix with extra-vortical air. Moreover, disturbances warm some of the air in the vortex. Increased radiative cooling brings air poleward, downward, and then equatorward in a slow meridional circulation. Thus, air may encounter PSCs, become chemically perturbed, and then move to regions that have remained free from PSCs.

Possible constraints on the putative Antarctic chemical processor have been given by Hartmann et al. (1989a), who used a simplified two-dimensional model, together with data derived from the ER-2 flights during the Airborne Antarctic Ozone Experiment (AAOE) in 1987. By assuming a cooling rate of 0.2 K per day (in agreement with the estimate of Rosenfield and Schoeberl, 1986), they found that the flux of ozone into the region of ozone depletion was only about 20% of the observed decline rate for ozone—that is, the transport effects are much smaller than depletion caused by the local photochemical sink.

Hartmann et al. further argued that a rapid increase in ozone mixing with distance from the center of the ozone hole implies relatively weak meridional dispersion of air parcels. They estimated an upper bound for the effective meridional “diffusion coefficient” in their model, and found it to be rather small: it would take about 125 days to change the ozone mixing ratio by a factor of e . They concluded that only about 20% more ozone could be processed than was in the chemically perturbed region at the beginning of September 1987.

Profitt et al. (1989b) concurred with Hartmann’s et al. estimate of weak lateral dispersion, but argued for much larger subsidence rates. These two views could be reconciled if there were substantial gravity-wave drag, and much more rapid radiative cooling than was used by Hartmann et al. Significant gravity-wave activity has been detected at the altitude of the ozone depletion over Antarctica, but the strength of the associated momentum source is not known (Hartmann et al., 1989b). The required strong cooling could result from the presence of PSCs and cirrus cloud decks, as has been suggested by Kinne and Toon (1989) and Tuck (1989), but cooling rates are uncertain (see Section 1.2). Some evidence that could be viewed as favoring the notion of a chemical processor has been reported.

Tuck used the F11/N₂O ratio at constant potential temperature and potential vorticity to infer a diabatic cooling rate of 4-6 K per day in potential temperature, much larger than the 0.4 K per day used by Hartmann et al. He concluded that the diabatic subsidence was substantial, in broad agreement with the analysis of possible cloud radiative effects presented by Kinne and Toon (1989), as discussed in Section 1.2.4. Murphy et al. (1989) found a positive, small-scale horizontal correlation between N₂O and H₂O in the chemically perturbed region, even though they have oppositely directed vertical gradients. They argued that this was the result of patchy diabatic sinking in regions where air had been dehydrated (i.e., where PSCs had formed), but did not estimate the rate of descent.

POLAR OZONE

Evidence that the containment vessel is not impermeable to lateral air movement comes from several sources.

The distribution of PSCs, as deduced from SAM II data, shows a pronounced longitudinal asymmetry, despite there being no such asymmetry in coldest temperatures. Clouds are found most frequently near the edge of the vortex in the 0-90°W sector; as early as July, the interior of the polar vortex has low incidences of clouds. An interpretation of these observations was given by Watterson and Tuck (1989), who argued that there must be a resupply of condensable material near the edge of the vortex for clouds to persist despite gravitational settling of particulates. They proposed that the clouds recur by adiabatic expansion and cooling of warm, moist air that is injected poleward by upper tropospheric weather systems. Murphy et al. (1989) found evidence for isentropic (quasi-horizontal) mixing at the edge of the polar vortex, while Tuck (1989) suggested that efficient mixing, perhaps by interstitial instability, could account for "flat" regions in N₂O mixing ratios. Kelly et al. (1989) recorded a decrease in the mixing ratio of water vapor on an aircraft flight from Puerto Montt (41°S) to Punta Arenas (53°S) in August 1987. They suggested that this finding was consistent with air being dehydrated over Antarctica and then spreading to mid-latitudes. A tropical origin for the dry air was inconsistent with the measured mixing ratios of other trace chemicals.

On the basis of current modeling and observational studies, no firm judgment can be offered on the degree to which the polar stratosphere may be viewed as a chemical processor. Hartmann's et al. (1989a) model is a considerable idealization of atmospheric transport. It is a co-ordinate based model, and does not recognize explicitly the polar vortex as a physical entity which may move and deform over the polar cap (perhaps not a serious shortcoming for the year 1987, when planetary waves were comparatively weak). Moreover, heating rates used in the model are uncertain, and radiative effects of PSCs (also uncertain) are neglected. On the other hand, the above-cited observational studies do not supply enough quantitative information to estimate the through-put of air in the imagined chemical processor. Local observations (taken from aircraft, say) may lead to erroneous conclusions about large-scale processes. To resolve the issue, simulations with high-resolution general circulation models are called for, backed by parallel studies of both ground-based and satellite data. (Data from the Upper Atmosphere Research Satellite, scheduled for launch in 1990 or 1991, should be of great value.) Some questions requiring attention are:

1. If substantial mass is circulated through the polar region, can temperatures remain below the threshold for PSCs despite dynamical warming?
2. Would the accompanying transport of chemical species limit or enhance the chemical processor?
3. If the notion of a chemical processor is useful, should we expect more ozone to be destroyed in a year with strong dynamical activity and mass circulation (e.g. 1988), or are there complicating factors?
4. Could significant ozone depletion take place in the Northern Hemisphere despite the limited coverage of PSCs?

1.7.4 The Dilution Effect

Initial concern over the observed springtime Antarctic ozone depletion (Farman et al., 1985a) was focused largely upon the high latitude region over the Antarctic continent. As discussed in Section 1.1 and in the above, examination of a number of years of ozone data revealed that a very rapid decline in ozone occurred in the lower stratosphere during the month of September as sunlight returned to the polar region. Reductions in the ozone column of as much as 50% were observed (e.g., references in Solomon, 1988). After reaching a minimum in late September to early October, the ozone column recovered within a few weeks with onset of the final warming and breakup of the polar vortex. Replenishment of the polar ozone

column occurred as the ozone-poor air was exchanged with air masses with relatively higher ozone content from lower latitudes by large-scale, quasi-horizontal transport. This large-scale latitudinal mass exchange apparently occurs throughout austral spring as evidenced by the potential vorticity analyses of Newman (1986) shown on Figure 1.7.4-1. Typically, amplifying anticyclones erode the vortex edge, and air from this region is transported to lower latitudes. Later in spring (usually in November), the vortex breaks up and more extensive lateral mixing takes place.

Export of ozone-poor air from polar regions to middle latitudes produces a deficit in ozone (a "dilution effect," Sze et al., 1989) which might persist for a long period because of the relatively slow chemical replacement time (on order of a month to a year, depending upon latitude) for ozone in the lower stratosphere. Further chemical effects might result from the accompanying export of denitrified and dehydrated

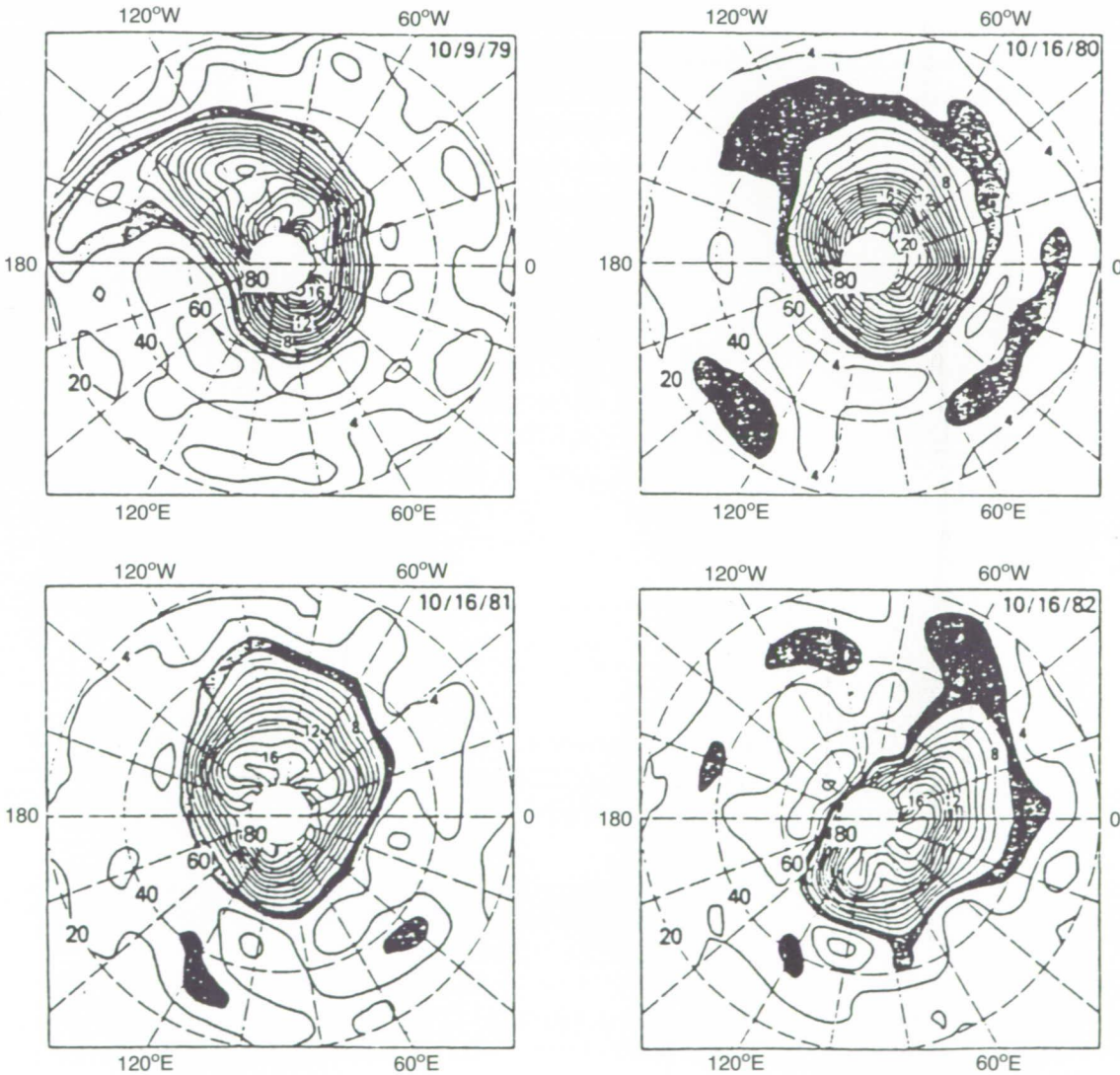


Figure 1.7.4-1. Ertel's potential vorticity on the 600 K isentropic surface. Units $Km^2/kg s$. (from Newman, 1986).

POLAR OZONE

air. If the ozone deficit lasts until the next springtime depletion episode at polar latitudes, the effect may be cumulative with a permanent reduction in the global ozone budget. The data from the Total Ozone Mapping Spectrometer (TOMS) instrument is not inconsistent with such a scenario. Displayed in Figure 1.7.4-2 is the monthly variation of the difference between the 1987-88 TOMS data and that for 1979-80. The 2-year averages for 1987-88 and 1979-80 have been used to reduce the effect of the quasi-biennial oscillation (e.g., Garcia and Solomon, 1987; Lait et al., 1989). Noticeable reductions (4% or greater) for this time period are apparent throughout the year at 50–60°S. The outward bulge toward mid-latitudes is particularly marked in late spring/early summer (November/December) at a time when dynamical considerations suggest that dilution would occur. Moreover, a second bulge toward midlatitudes is seen in April/May coincident with the autumnal peak in wave activity in the Southern Hemisphere noted by Hirota et al. (1983) and Randel (1988). Although the data are supportive of the dilution concept, it should be noted that changes arising from the influence of volcanic aerosols, the 11-year solar cycle, the quasi-biennial oscillation, or other factors cannot be unambiguously separated from changes which might arise from dilution.

Several model simulations have been conducted to study the consequences of dilution. Sze et al. (1989) used a 2-D model (Ko et al., 1985) with an extensive representation of the gas phase chemistry to perform a number of dilution studies. In their simulations, the region from 63°S to the pole was assumed to be an isolated vortex from April to October with no exchange of air permitted across the vortex boundary. An ozone hole was empirically imposed (no heterogeneous chemistry was included) and exchange of extra-vortical air with that from within the vortex was allowed beginning the first of November. In one experiment, the ozone hole (80% reduction from 63°S to the pole from 14 to 22 km) was imposed only in the first year

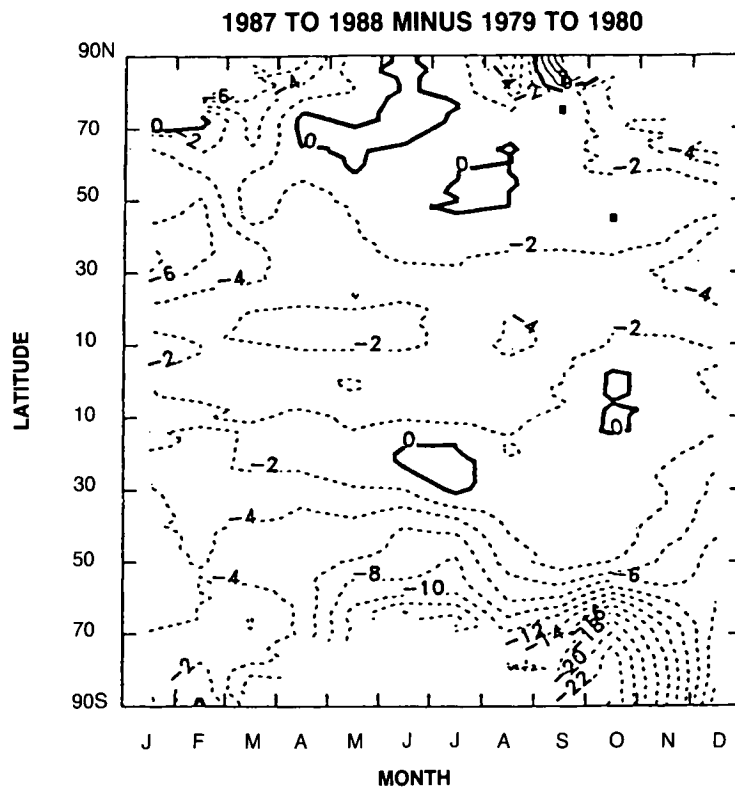


Figure 1.7.4-2. TOMS total ozone. Monthly variation of difference between 1987-1988 average and 1979-1980 average as a function of latitude. Courtesy of R. Stolarski.

with the simulation continued for 3 years. Column ozone reductions of 2 to 6% between 45°–60°S persisted throughout most of the second year with full recovery occurring in the third year. A second experiment was conducted with the simulation lasting 12 years with a prescribed ozone hole occurring each year. The results of that experiment are shown in Figure 1.7.4-3. Steady-state reductions of 3% or larger are evident between 50–60°S throughout the year. Broadly speaking, the results exhibit latitudinal and seasonal variations similar to those seen in the TOMS data (Figure 1.7.4-2). Chipperfield and Pyle (1988) have performed similar studies with their 2-D model. Their results are similar, but smaller in magnitude. The differences in the two studies are most probably a result of differences in the model transport: Sze et al. use the diabatic circulation formulation, while Chipperfield and Pyle use an Eulerian formulation requiring that eddy heat and momentum fluxes be included explicitly.

Prather et al. (1989) have also modeled the dilution effect. Their study differs from that of Sze et al. by using a 3-D off-line tracer model and adopting a simplified, linearized ozone photochemistry. In this study, the ozone hole was imposed instantaneously on October 1 in the region 70.5°S to the pole between 22 and 200 mb. The simulation was then carried out for 2 years (again imposing the ozone hole on October 1). One year later, column reductions of 2% exist as far equatorward at 40°S (see Figure 1.7.4-4). At the end of the second year, the average ozone depletion is about 20% larger than at the end of the first year. These results indicate that most of the ozone deficit existing 1 year after imposition of the hole is in the upper troposphere, south of 40°S. Additional 3-D model studies of the dilution effect have been carried out by Grose et al. (1989), Mahlman (1989) and Cariolle et al. (1989b). The study by Grose et al. used an off-

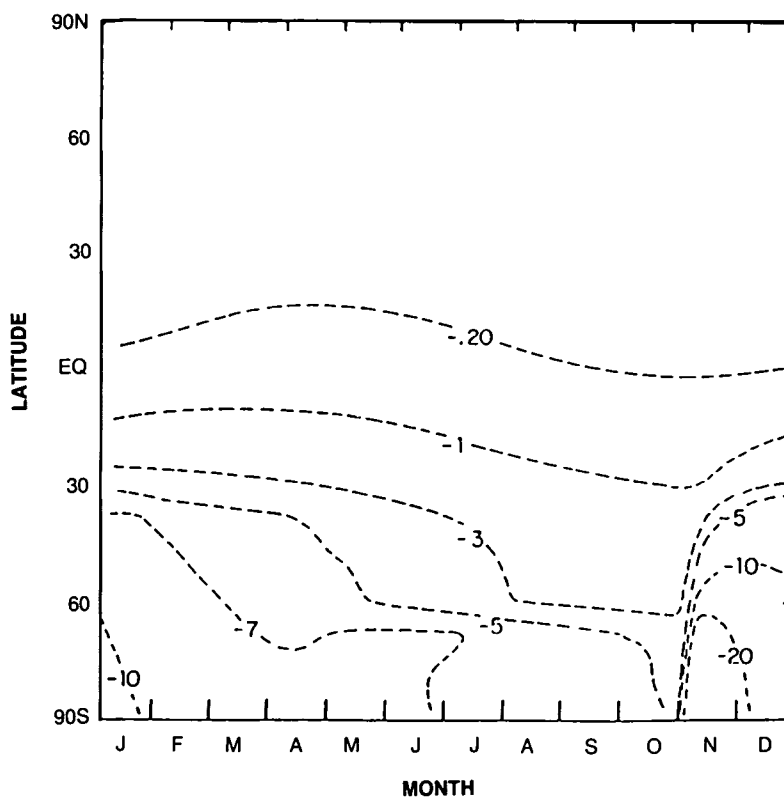


Figure 1.7.4-3. Percent change in the simulated steady-state seasonal and latitudinal distribution of zonal-mean column ozone (from Sze et al. 1989).

POLAR OZONE

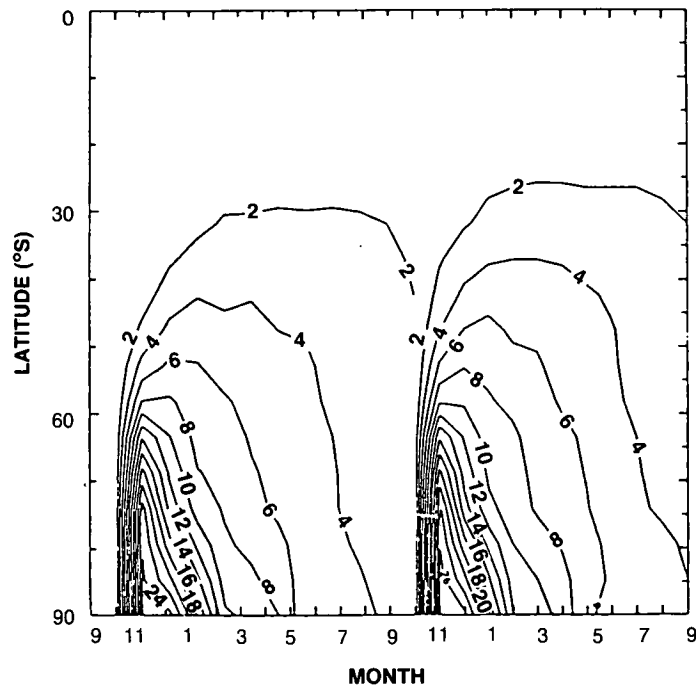


Figure 1.7.4-4. Percent difference in zonal-mean column ozone for Antarctic ozone hole simulation relative to control simulation as a function of season and latitude (from Prather et al., 1989).

line tracer model including comprehensive gas phase chemistry. An ozone hole was imposed in the simulation by specifying a linear loss rate for ozone such that 90% of the ozone in the region from 69°S to the pole between 27 to 112 mb was removed during the month of September (5.75% of the total ozone in the Southern Hemisphere). One year later, a residual deficit of approximately 1.3% persists in the total ozone in the Southern Hemisphere (see Figure 1.7.4-5). Most of the deficit in the ozone exists below the 100-mb level and between 30°S and the pole (approximately 1% of the column at 30°S, 2% of the column from 60°S to the pole). Mahlman (1989) used the GFDL SKYHI model to evaluate the dilution effect (without explicit ozone chemistry but allowing for dynamical feedbacks). Perturbations to an ozone climatology were parameterized as a function of the desiccation of water vapor. The results of this study are similar to those obtained by Prather et al. and by Grose et al. However, an important feature of this study is that the temperature and hence the circulation could change in response to the changing ozone distribution, a feature not possible in the studies with the off-line models. A robust feature of the Mahlman results is a significant temperature decrease (order of 10 K, compared with a simulation with no ozone hole) at polar latitudes in the lower stratosphere which persists approximately 6 months after formation of the ozone hole. Accompanying the decrease in the lower stratosphere is an increase in the middle stratosphere. A similar response was seen both in the study by Kiehl et al. (1988) who studied the response of a general circulation model to reduced polar ozone and in the study by Chipperfield and Pyle (1988) with their 2-D model. These results suggest that a model in which radiative, chemical, and dynamical processes are fully coupled may be required to understand possible feedbacks and their implications over long periods.

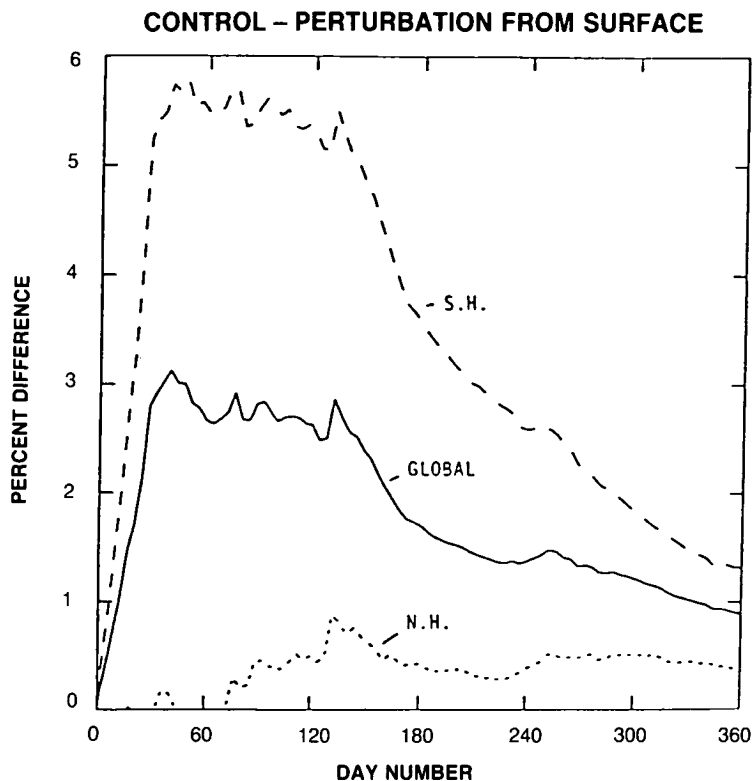


Figure 1.7.4-5. Percent difference in the integrated global and hemispheric column ozone for Antarctic ozone hole simulation relative to control simulation as a function of time (Day 0 is 1 September) (from Grose et al., 1989).

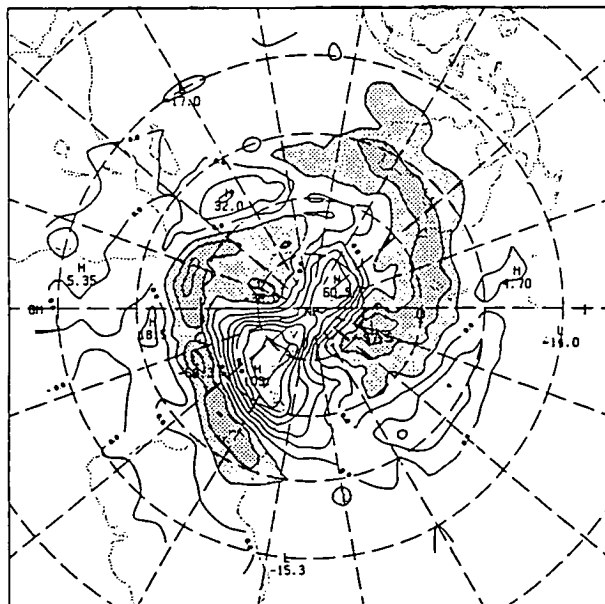


Figure 1.7.4-6. TOMS total ozone for the Southern Hemisphere. Difference (Dobson units) between 8 December and 14 December, 1987. Difference is between three-day means centered about those dates. Shading represents reductions exceeding 15 DU.

POLAR OZONE

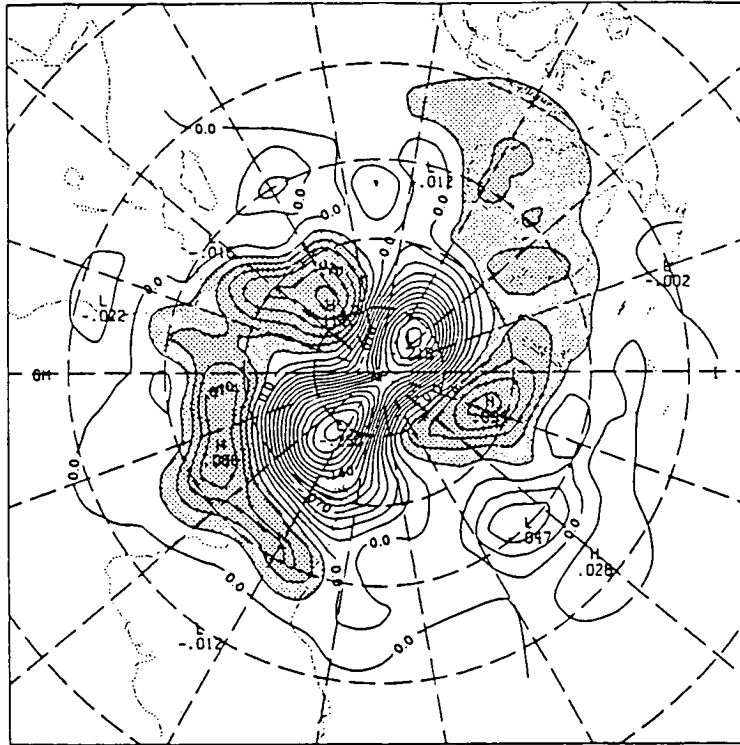


Figure 1.7.4-7. Difference between Ertel's potential vorticity (500 K isentropic surface) for 8 December and 14 December, 1987. Difference is between three-day means centered about those dates. Contour interval of $7.5 \times 10^{-8} \text{ K s}^{-1} \text{ Pa}^{-1}$. Shading represents increases greater than $7.5 \times 10^{-8} \text{ K s}^{-1} \text{ Pa}^{-1}$. (Cyclonic potential vorticity is positive.)

Cariolle et al. (1989b) have also run a comprehensive simulation of the springtime Antarctic ozone depletion with a GCM which allows for an interaction between radiation and ozone mixing ratio. In this study, the ozone loss due to chlorine was represented in a simplified way. Significant ozone decreases were found at Southern Hemisphere mid-latitudes before and after the final warming. In addition, a temperature decrease of about 7 K was found inside the polar vortex in October at 50 mb, and the final warming in November was delayed by about two weeks.

The most remarkable aspect of the model studies cited herein is the degree to which they agree with one another and with the TOMS observations of Figure 1.7.4-2. There are substantial differences among the various models, each model having its own particular shortcomings. Nevertheless, although differences in detail exist, a general conclusion is common to all of these studies. The conclusion is that dilution of mid-latitude ozone by export of ozone-poor air from polar latitudes after breakup of the depleted Antarctic vortex might produce a small residual deficit in ozone which is cumulative from year-to-year. These simulated results should be further qualified by noting that those factors that may also be influencing the ozone data (e.g., volcanic aerosols, solar cycle, QBO) have not been taken into account in the model simulations.

Determining the actual latitudinal extent of the dilution effect is of crucial importance. Inferring the northward limit of the effect from the TOMS data (Figure 1.7.4-2) is difficult for reasons of the limited statistics. Certainly, one cannot categorically deduce the existence of a trend northward of about 50°S from the TOMS data alone. Atkinson and Easson (1988) reported evidence of a significant year-to-year downward trend in ozone at Melbourne (38°S). However, data from a single station is informative, but not definitive. There is some direct evidence that transport of ozone-poor air reached 32°S in the Australia - New Zealand area in December 1987 (Atkinson et al., 1989) following the lowest springtime ozone values ever observed over Antarctica. The Dobson data record exhibited a sudden drop in mid-December across southern Australia and New Zealand to about 10% below normal December values, which lasted for the rest of the month. In fact, the December mean ozone in 1987 was the lowest ever recorded at Melbourne. The timing of this sudden drop coincided with the final breakdown of the polar vortex in the lower stratosphere. Figure 1.7.4-6 depicts the difference in total ozone before and after this event. A corresponding plot of Ertel potential vorticity on the 500 K isentropic surface is shown in Figure 1.7.4-7. The high degree of correlation between these two figures (supported by independent trajectory analyses) suggests that the observed sudden drop in ozone values was a result of the transport of ozone-poor air from the fragmenting vortex. It will require studies from further years to determine whether this was an extraordinary event or a typical example of the dilution effect.

1.8 TEMPERATURE TRENDS—CAUSES AND EFFECTS

The significance of observed changes in temperature in the Antarctic lower stratosphere during springtime remained unclear for some time after the discovery of the ozone hole. Some attributed the changes to dynamical mechanisms that could also be responsible for the ozone hole itself. Other workers believed the temperature changes were an effect of the depletion of ozone rather than related to its cause. It now seems clear that most, if not all, of the year-to-year springtime temperature trend is a result of the diabatic effects of ozone loss; such an effect has been simulated in simple 1-D models (Shine 1986; OTP 1989), 2-D models (Chipperfield and Pyle 1988) and 3-D general circulation models (Kiehl et al. 1988; personal communication Rowntree and Lean, UK Met. Office, 1989). This implies that the radiative effects associated with the near-absence of ozone at some altitudes within the ozone hole have led to a significant change in the climatology of the stratosphere.

Changes in Antarctic lower stratosphere temperatures have assumed particular significance given the central role now thought to be played by polar stratospheric clouds in the chemical mechanisms causing the depletion of ozone. Any long-term trend in temperature, particularly in winter and early spring, might be expected to impact the extent and duration of polar stratospheric clouds.

In the following, measurements of temperature trends and their interpretation will be described. In Section 1.8.1, observations included in the summary of temperature trends measurements in OTP (1989) will be summarized. In Section 1.8.2, more recent studies of temperature trends are described. Section 1.8.3 presents theoretical studies aimed at interpreting the observed trends in temperature and describes their implications for the interpretation of the Antarctic ozone hole.

1.8.1 Resume of Work Discussed by OTP (1989)

Chapter 11 of the Ozone Trends Panel Report (OTP, 1989) contains much detail on observations and modeling of lower stratospheric temperatures in the Antarctic springtime; it is only necessary to give a

POLAR OZONE

brief resume of this report before progressing to more recent studies. The overriding difficulty for trend detection in this region and season is the strong interannual variability in temperature, as discussed in some detail in Section 1.7. Labitzke (1987b) reports October mean temperatures at 50 mbar ranging from -46°C to -69°C at Syowa station (from a sample of 18 years' data) with a standard deviation of 6.2°C . For November a range of -32°C to -50°C is found with a standard deviation of 4.2°C . A similar spread is found at the South Pole, although the variability is slightly greater in November than in October. As discussed in Section 1.7, much of this variability is due to variations in planetary wave activity, perhaps related in part to the QBO, while some is also attributed to the solar cycle by a number of authors.

Sekiguchi (1986) and Chubachi (1986) used radiosonde data from Syowa to deduce temperature trends. Chubachi's analysis showed that the biggest changes in temperature at both 100 and 50 mbar occur during November; over the period from 1974 to 1985 the cooling was found to be about $1.2^{\circ}\text{C}/\text{year}$. Temperature decreases were found in all months except July and September, although the statistical significance of the trends was not discussed. Sekiguchi found strong correlations between interannual variations in ozone and temperature for the period October-December. These were particularly marked in October and November between about 150 and 50 mbar. Angell (1986) used data from 16 radiosonde stations between 60° and 90°S to show strong long-term coolings at 30, 50, and 100 mbar in the austral spring (Sept-Oct-Nov). Angell also showed that the trend varies greatly across the Antarctic continent, with the largest trends occurring along the coast from 30°W to 60°E (including Halley Bay and Syowa).

Other work reported in OTP (1989) concentrates on the more recent NMC data set. From 1,000 to 100 mbar these data are a mixture of radiosonde and satellite data, while from 70 to 0.5 mbar they are based primarily on satellite data. The satellite retrievals are based on a regression with a number of colocated radiosonde and rocketsonde observations; for the layer 70 - 10 mbar the regression coefficients are updated, on average, every 2.5 weeks, while at lower pressures the coefficients are constant. The most complete analysis of these data was performed by Newman and Randel (1988). Their study showed that while there was some offset between radiosonde temperatures and colocated satellite observations, the interannual variation and trends were generally in agreement. A linear trend analysis of satellite observations from 1979 to 1986 (Figure 1.8.1-1) provided support for the radiosonde studies. Of particular importance were the observations showing little or no trend during September. A strong trend exceeding $0.9^{\circ}\text{C}/\text{year}$ was found in the lower stratosphere in October. In order to show the consistency of trends in both radiosonde and NMC data sets, Newman and Randel presented differences in October monthly mean temperatures at 100 and 70 mbar for both sets. The changes are generally in good agreement, although individual radiosonde stations can be as much as 30-40% different. There is certainly no systematic difference in the temperature changes obtained using the two data sets.

Thus, the studies are generally in agreement that a marked downward trend in the springtime temperatures in the Antarctic lower stratosphere has occurred. The trend appears to be restricted to October and November, unlike the change in ozone that occurs predominantly in September. This represents crucial evidence against dynamical theories, as it lags rather than leads the ozone change. Indeed, the change in temperature at pressures greater than 50 mbar, and as importantly its timing, appears to be modeled adequately as a response to reduced diabatic heating resulting from ozone reductions as shown in Section 1.8.3. OTP (1989) presents results from radiatively-determined model calculations, using three different radiation schemes. Calculations with one of the models showed that 80% of the temperature change was due to decreased absorption of solar radiation, while the rest was due to less thermal infrared radiation being absorbed from the warmer troposphere. Hence, most of the cooling would be expected to be observed after the Sun rises.

POLAR OZONE

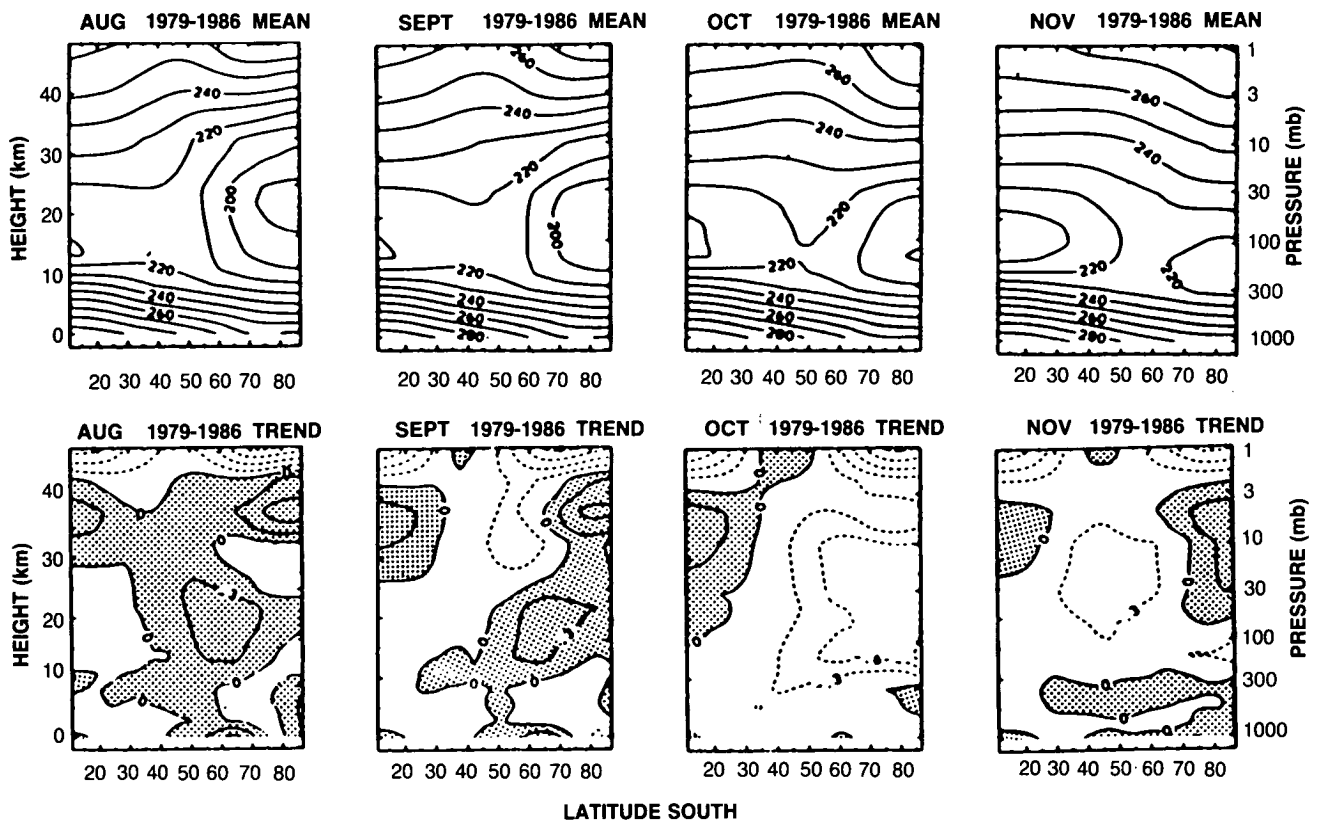


Figure 1.8.1-1. Linear trends calculated from NMC data (in °C/year) for the period 1979-1986, for August, September, November, and December (from Newman and Randel, 1988).

The work reviewed by OTP (1989) leaves a number of unresolved questions. For example, the radiosonde observations indicate that the largest cooling is found in November, whereas the satellite observations indicate that the biggest cooling is in October. Another question stems from the results of the radiatively-determined calculations. All model calculations show an increase in temperature in the upper stratosphere that is related to an increased penetration of thermal infrared radiation from the troposphere due to the decreased ozone amounts in the lower stratosphere. A smaller contribution comes from an increased heating due to solar radiation reflected from the troposphere penetrating to greater heights, for a similar reason. The only slight evidence for such a heating can be seen in the November plots of Newman and Randel (1988) (our Figure 1.8.1-1). More recent developments in this area will be discussed below.

1.8.2 Other Recent Work

The problem of interannual variability has been highlighted by the two most recent austral springs; 1987 and 1988 have been very cold and relatively warm, respectively. This can be seen in temperature data during springtime for the layer 100-50 mbar, shown in Figure 1.8.2-1, which uses data collected from six Antarctic stations as described in Angell (1988b) updated to include 1988 (Angell, personal communication).

POLAR OZONE

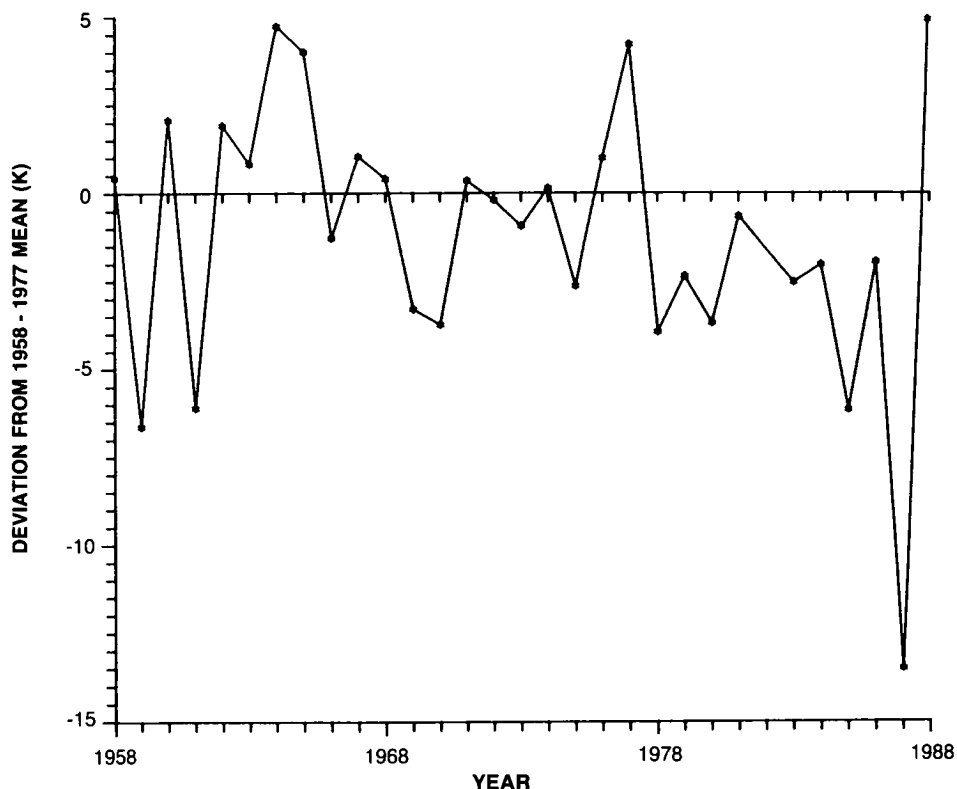


Figure 1.8.2-1. Deviations of temperatures 1958-1988 ($^{\circ}\text{C}$) from the 1958-1977 mean for September to November for Angell's (1988b) six polar stations.

From this figure it can be seen that 1987, in the context of the last 30 years, was exceptionally cold, while 1988 was (narrowly) the warmest on record (see Section 1.7). The difference in measured temperatures between the two springs exceeds 18°C . These data are, however, collected over a broad geographical region (with stations ranging over 24 degrees of latitude) and averaged over the three spring months. The temporal and spatial averaging may disguise, to some extent, the changes in the ozone depleted region, which was far smaller in 1988 than in 1987 (Schoeberl et al., 1989). This view is supported to some extent by other data (see also, the discussion of 1987 and 1988 temperatures and dynamics in Section 1.7). Gardiner (1989) shows that at Halley Bay (this station is one of the six used by Angell for his composite analysis) at 100 mbar, 1987 was indeed the coldest on record in October, November, and December; however 1988, while warm, does not rank as anything like the warmest in the 30-year record (Figure 1.8.2-2). The October mean temperature is about 9°C warmer in 1988 than in 1987, the corresponding figure being 20°C in November. Schoeberl et al. (1989) report that 70-mbar temperatures (from NMC analyses) in late September and October were 5°C warmer in the vortex in 1988 compared to 1987.

Strong evidence of a change in the behavior of the annual cycle of temperature as a result of the ozone depletion can be seen in Figure 1.8.2-3 (Farman, private communication). This figure shows the annual cycle of 100-mbar temperatures at Halley Bay for 1987, together with the mean and extreme values for the period 1957-1975. The severe depletion of ozone within the polar vortex in 1987 was followed by exceedingly low temperatures in October and November, and a delay in the spring warming. Differences

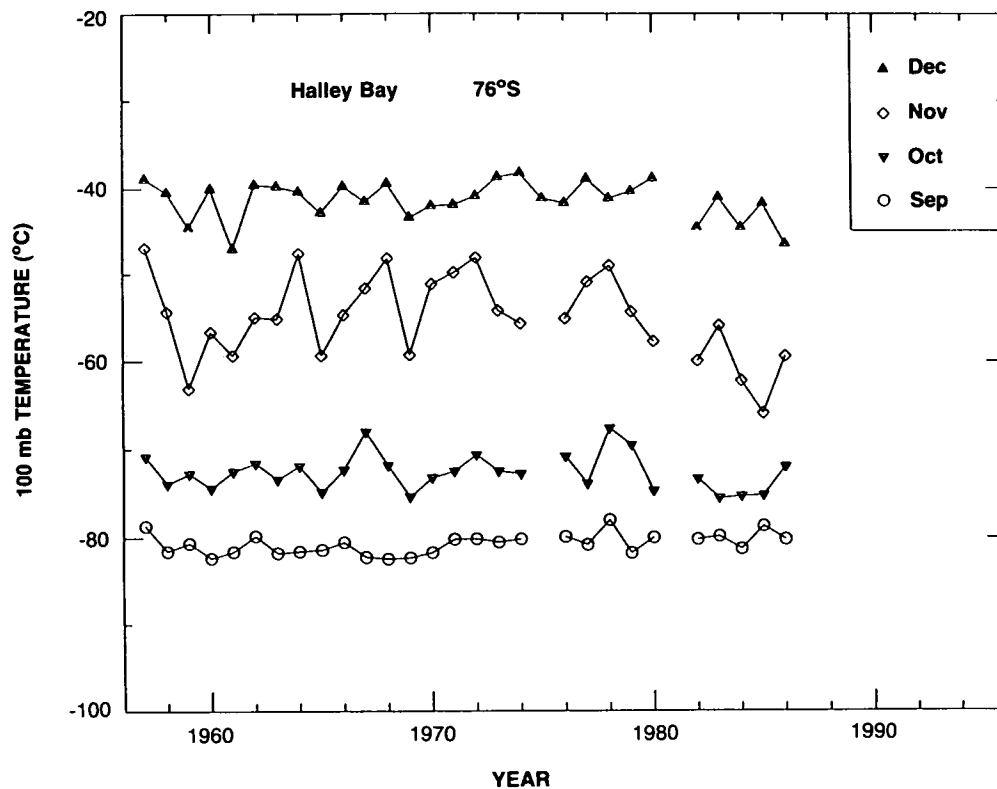


Figure 1.8.2-2. Monthly mean temperatures at 100 mbar for Halley Bay, 1958-1988 (from Gardiner, 1989).

between 1987 and the 1957-1975 extreme minimum exceed 10 K in early November. In 1988, with the less marked ozone depletion, temperatures were found to lie within the envelope of the 1957-1975 extremes.

Randel (1988) has extended the study of Newman and Randel (1988) to look specifically at spring 1987 using NMC data. Figure 1.8.2-4 shows the deviation of temperatures for September to December 1987 from the average for the period 1979 to 1986. The lower stratospheric cooling reached 6°C in October and 14°C in November, a value four standard deviations from the 1979-1986 mean. As with the earlier study, there is little evidence for changes during September. Of some interest is the warming observed in the upper stratosphere; this is qualitatively consistent with the modeling studies mentioned earlier (although Randel cautions that the temperature data at these levels should be considered a qualitative indication only, due to simplifications in the NMC analysis procedure at these levels).

Randel and Newman (1988) rederived linear temperature trends for the period 1979-1987 (compared with 1979 to 1986 in Newman and Randel [1988]). The addition of the single year's data has a substantial impact on the trends; for example, at 50 mbar at the South Pole the trend for 1979 to 1986 is close to zero for November, while including the 1987 data generates a cooling trend in excess of 0.5°C per year. This illustrates the problem of deducing trends from short-period data sets in regions with so much interannual variability.

Angell (1988a) presents temperature trends for four seasons from standard radiosonde observations. His "South Polar" region is the latitude band 60–90°S, and uses data from six stations. Of all the trends

POLAR OZONE

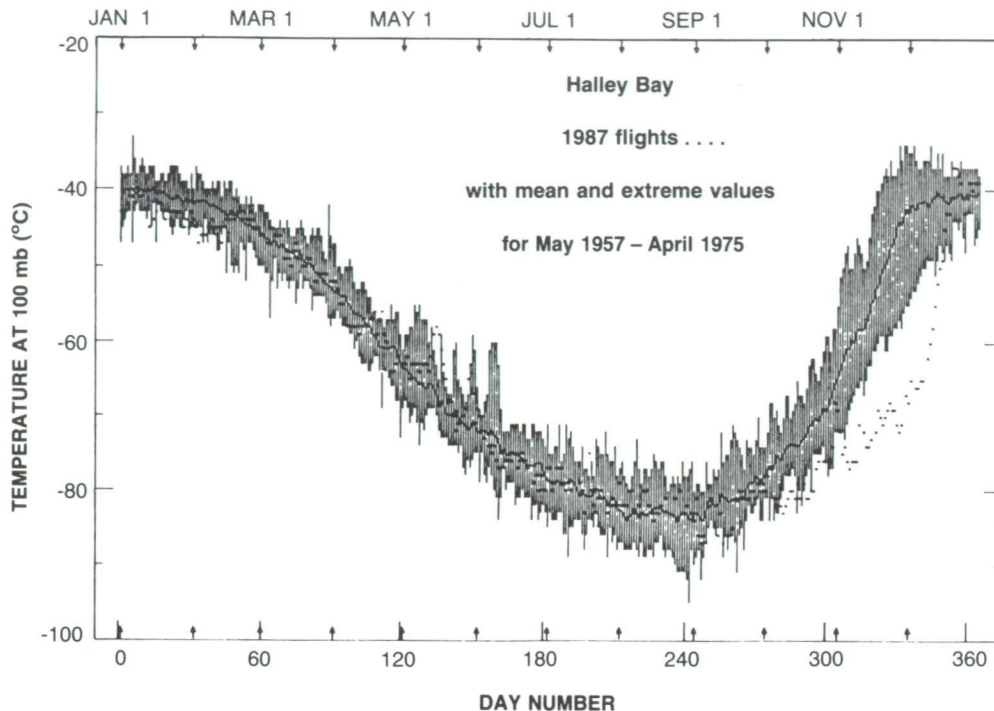


Figure 1.8.2-3. Temperatures at 100 mbar as a function of month from Halley Bay. The dots indicate measurements from 1987. The solid line shows the 1957-1975 mean, with the extremes during this period indicated by the vertical bars.

measured at any altitude or latitude region, the September-October-November trend at 100-50 mbar for the South Polar region is by far the most striking. For the period 1973-1987 the cooling amounts to 5°C per decade and is significant at the 1% level. Some evidence exists for coolings of 2°C per decade for the austral winter, but because of large interannual variations, Angell does not deem them to be statistically significant. For the remaining two seasons, the trends at these levels were found to be small and non-significant.

Temperature trends at the 100-mb level in the Southern Hemisphere were also evaluated by Koshelkov (1989), using data from 1964 to 1985 (two solar cycles). Koshelkov (1989) reported a small trend in the zonal mean temperature at 70°S during September of -0.03 K/yr from 1975 to 1985, while the trends obtained in October and November were considerably larger during this period, -0.25 K/yr and -0.46 K/yr, respectively. Essentially no trend was obtained during the winter months of July and August during the 1975-1985 period, while a slight cooling (-0.22 K/yr) was deduced for the earlier 1964-1974 period.

A different view is presented by Iwasaka et al. (1989) who used radiosonde data from Syowa from 1966 to 1987. Comparing means for the period 1981 to 1987 with means for 1966-1980, it was found that for pressure levels 50 to 100 mbar cooling occurred in all months, except for a short period in mid-winter. The most prominent changes were found in October/November when the later period was found to be up to 9°C cooler than the mean for 1966-1980, with 2°C coolings extending into January. When these changes were scaled by the standard deviations calculated using the 1966-1980 data, the trend was found to be most clear from mid-October to late February; the 1981-1987 temperatures were found to be more than 2 standard deviations from the 1966-1980 mean. From March to October the temperature changes were found to be less than 1 standard deviation from the mean.

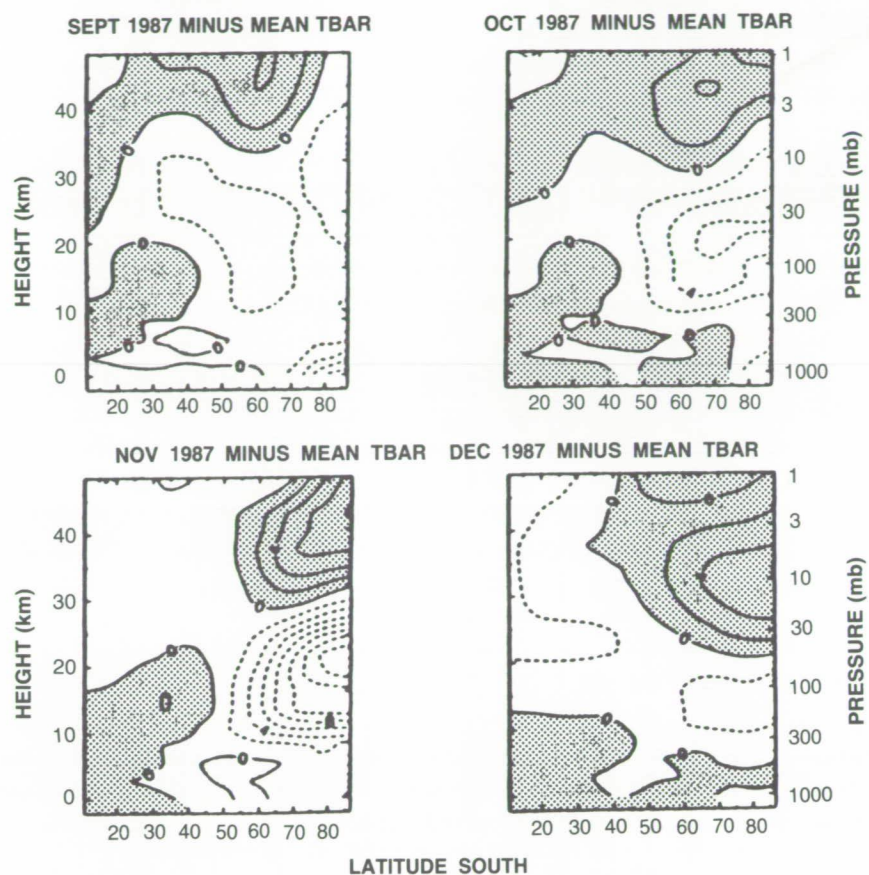


Figure 1.8.2-4. Deviation of NMC zonal mean temperatures for 1987 from the 1979-1986 mean for the period September to December (from Randel, 1988).

Trenberth and Olson (1989) have performed a detailed study of temperature changes at McMurdo and South Pole stations and warn against the dangers of forming monthly average temperatures in regions with irregular observations and large annual cycles. The conventional method of forming monthly-means is to simply average all available observations. Such a procedure is adequate provided that observations are made regularly or there is little change in mean temperature during the month. However, the difference in mean temperature between the first and last day of October at 70 mbar at South Pole is 27°C; a monthly mean formed from a few observations at either the beginning or the end of the month could lead to a biased mean. This is a very real problem, particularly at high altitudes. Trenberth and Olson show that the total number of observations at 100 mbar at McMurdo during October has varied between 2 and 42 over the past decade. Differences between monthly means calculated from a mean of all observations and the average of daily means were found to exceed 2°C on some occasions.

In order to examine recent temperature trends, Trenberth and Olson defined a mean annual cycle at each level at each station, using least squares harmonic fits to daily mean temperatures. Deviations of daily values from this annual cycle were then computed; these deviations were then averaged to produce a monthly anomaly.

POLAR OZONE

At South Pole station, little change of note was found in September, consistent with other studies. In October trends were most evident at 50-100 mbar, and since 1985, temperatures have gone outside the range of observed interannual variability since 1961. The trend is also visible in November, but this month is found more subject to large interannual variation. A significant cooling is also found in Dec-Jan-Feb, and is consistent with changes reported by Iwasaka et al. (1989) from an analysis of observations from Syowa Station. The years 1985-1987 were found to be about 2°C cooler than the long-term mean.

Trenberth and Olson compare their analysis with the NMC analysis. At the South Pole, at 70 mbar, the two analyses display a root-mean square difference of 2.4°C between 1979 and 1987 for October. At McMurdo, the average difference at 100 mbar is 5.8°C and reaches 11.7°C in 1982; they comment that there is little resemblance between the trends and interannual variability from the NMC data and the actual observations from McMurdo.

The question of whether temperature trends are greatest in October or November appears unresolved. Data from Halley Bay show the most noticeable changes in November, in agreement with the Syowa analysis of Chubachi (1986). While the 8-year data set of Newman and Randel (1988) indicates that most the trend is in October, the addition of 1987 to this data set markedly reduces the difference in trends between October and November (Randel and Newman, 1988).

1.8.3 Causes of Temperature Trends

Calculation of the diabatic response of the lower stratosphere to a depletion of ozone is relatively straightforward. As discussed in Section 1.8.2, one-dimensional radiatively determined calculations of the effect of ozone depletion are in relatively good agreement, and can certainly account for a substantial part of observed changes in the lower stratosphere temperatures. Since OTP (1989) a number of studies have performed similar calculations, but using models that allowed for a dynamical response to the temperature changes.

Chipperfield and Pyle (1988) used a 2-D model and imposed a depletion of about 120 DU on a model's predicted Antarctic springtime ozone column of 270 DU. They found temperature decreases exceeding 9 K at 70 mbar by the end of October and, like the 1-D calculations, found substantial warming (reaching 6°C) in the upper stratosphere. Figure 1.8.3-1 shows their predicted temperature change at 39 mbar between the runs with and without the ozone hole. Clear differences in temperature can be seen to persist until late March. These exceed 4°C during January. This indicates that temperature changes outside the springtime may also be due to the after effects of the spring time ozone depletion. This may account for the observations at Syowa (Iwasaka et al. 1989) of a temperature trend in January, given the small decreases in summertime ozone reported in Section 1.1.3. Chipperfield and Pyle's coupled model allows study of the seasonal cycle of ozone as well as temperature following the ozone hole. Although the calculated ozone abundances recovered substantially after the end of October, ozone decreases as large as 15% persisted in January, and remained greater than 5% into early February (Pyle, personal communication, 1989). Chipperfield and Pyle's calculation does not allow us to distinguish between whether the January cooling is due to the lingering ozone depletion or to the long radiative relaxation times delaying the recovery of the temperature. Given radiative relaxation times of the order of 100 days in this region, a 9 K perturbation to temperatures in late October might cause a cooling of 3 K in January.

Two sets of 3-D general circulation calculations have been performed. Kiehl et al. (1988) used the NCAR Community Climate Model. Their imposed ozone hole (which reached a minimum of 160 DU in early October, compared with a control calculation of about 320 DU during springtime) caused coolings of

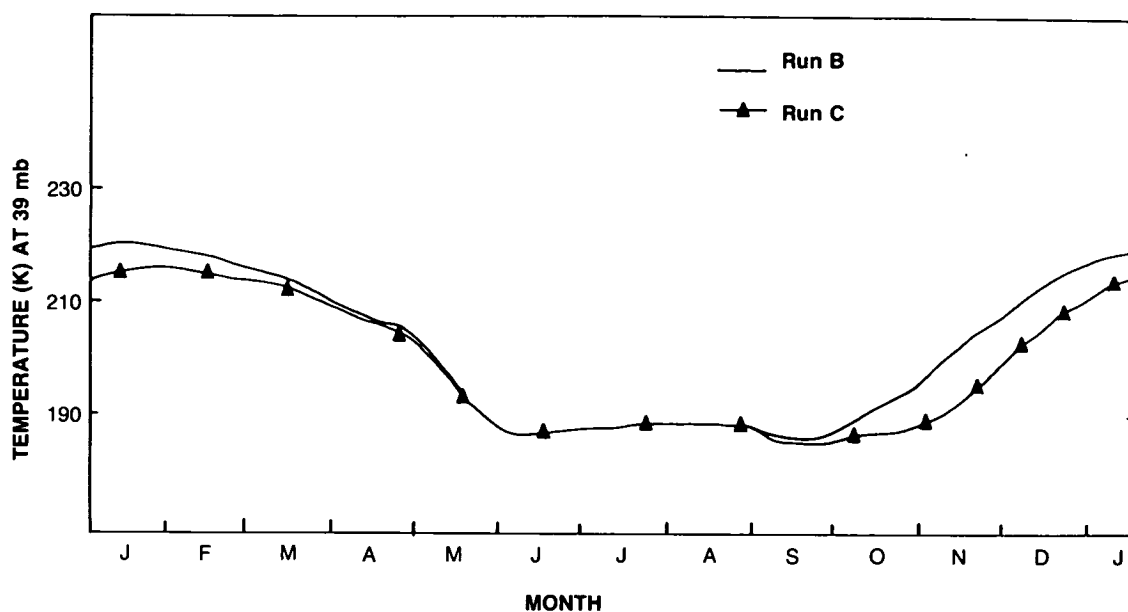


Figure 1.8.3-1. 2-D model temperatures at 39 mb and 76°S with (Run C) and without (Run B) an imposed ozone hole (from Chipperfield and Pyle, 1988).

6°C by the end of October (Figure 1.8.3-2). These authors also found a heating above 10 mbar that exceeded 4°C for some periods. Unlike the simpler model studies, they attributed little of this warming to changes in diabatic forcing. They attributed the difference to the particular vertical profile of the ozone depletion used. The behavior appeared to be closely tied to the model dynamics; in a second experiment with different initial conditions, they found the upper stratospheric temperature changes differed by a factor of two from those found in the first calculation. Rowntree and Lean (personal communication) used the UK Meteorological Office GCM; they imposed a depletion similar to that found in 1987 and, at 90 mbar, obtained coolings of 16 K by the end of November.

A difficult problem concerns the possibility that changes in temperature have altered the dynamical heating in the polar vortex. Some evidence of changes is presented by Kiehl et al. (1988). In their calculations with the imposed ozone hole they found increased downward motion during September and October, which results in a dynamical heating. Further, by the end of November, no final warming had occurred, in contrast to the control simulation. Further work by the same group (Boville, personal communication 1988) shows that an imposed ozone hole can delay the transition to easterlies by 10 to 14 days. Newman and Schoeberl (1988) have presented some observational evidence that years with low ozone are associated with late vortex breakdowns, at least at 100 mbar.

Thus, modeling work performed so far has provided strong evidence that the ozone depletion is likely to lead to a marked temperature trend in the lower stratosphere in October and November, and a smaller warming of the upper stratosphere. The role of dynamics in altering the temperature structure has not yet been studied in great detail, but there is now some evidence that the changes in temperature structure can delay the breakdown of the vortex.

It is important to recognize that these studies do not include a number of potentially important processes. The direct radiative effects of PSCs are ignored and the effects of dehydration (e.g., Ramaswamy

POLAR OZONE

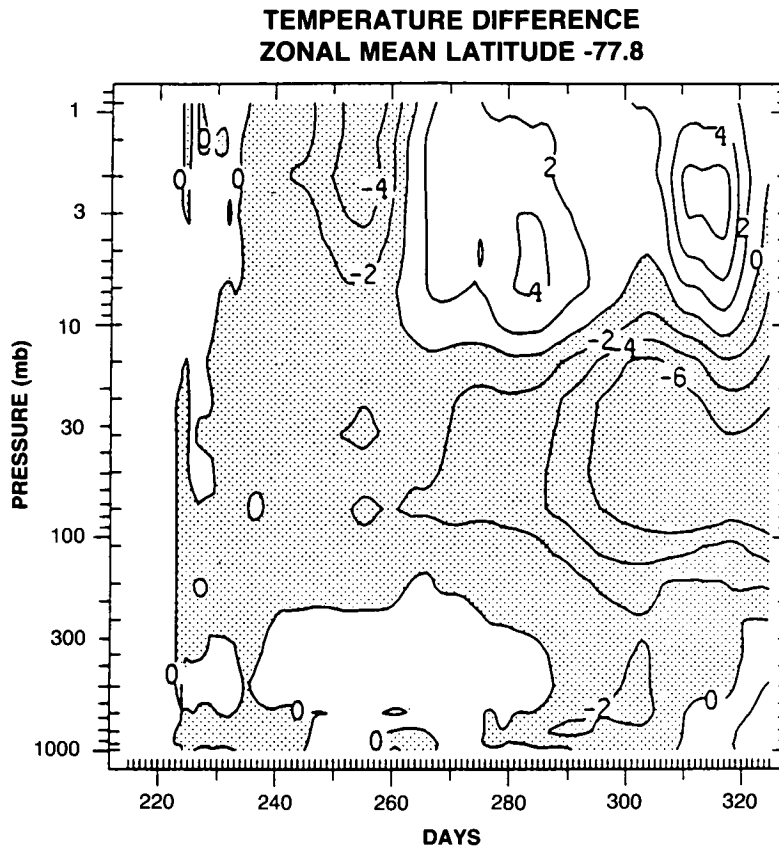


Figure 1.8.3-2. Deviation of zonal mean temperature for a calculation with an imposed ozone hole from a control run without the hole, using the NCAR Community Climate Model (from Kiehl et al., 1988).

1988; O. B. Toon et al. 1988; Kelly et al., 1989) are not considered. The loss of water vapor leads to an effective heating of the Antarctic stratosphere that may amount to several tenths of a K/day (Pollack and McKay, 1985; Shine, 1986); this is a significant perturbation to the radiative budget of the region. Such processes would be important in the prediction of temperature changes if there had been a significant change in dehydration or PSC formation over the period in which the ozone hole had developed; the PSC observations shown in Section 1.2 suggest that a long-term trend in PSC frequency has occurred on average in the month of October, but the likely radiative effects of these trends have not been studied in detail.

A number of workers have suggested mechanisms that may, over the long term, affect the thermal balance of the lower stratosphere. For example, it is well known that increased concentrations of greenhouse gases will lead to a cooling of the stratosphere which may affect the duration and extent of PSCs (Blanchet, 1989; Shine, 1988). Further, Blake and Rowland (1988) have pointed out that likely increases in stratospheric water vapor resulting from increased emissions of methane lead to an increase in the temperature at which PSCs can form (especially Type 1 clouds, which are believed to be particularly sensitive to water content; see Section 1.3 and Hanson and Mauersberger, 1988a,b). However, these effects are unlikely to be as important as changes in temperature, since the formation of PSCs is more sensitive to temperature decreases than to changes in the water vapor mixing ratio. Indeed, the water vapor on its own will lead to a cooling of the lower stratosphere, increasing the probability of PSC formation. The possible coolings could be

balanced by a number of mechanisms. These include the possibility that PSCs warm the lower stratosphere (see Section 1.2.4), the effective warming induced by dehydration and altered dynamics. In the absence of detailed modeling, it is not yet possible to assess the size and importance of the above mechanisms.

1.9 CALCULATED AND OBSERVED CHANGES IN ULTRAVIOLET RADIATION AT THE GROUND

The prime reason for concern about stratospheric ozone depletion is the threat of biological damage due to increased solar ultraviolet radiation reaching the surface. Studies considering the effect of Antarctic ozone depletion on surface ultraviolet irradiances have been performed by Frederick and his colleagues (Frederick and Snell 1988; Frederick et al., 1989; Lubin et al., 1989a, b). The spectral region of most relevance here is the UV-B (280-320 nm). Shorter wavelength radiation (UV-C) is unable to penetrate to the surface, while UV-A (320-400 nm) occupies a region of relatively low absorption by ozone.

Frederick and Snell (1988) presented calculations of the downward solar irradiance at the surface at Miami (chosen as a typical low- to mid-latitude station) and McMurdo Station for both depleted and non-depleted springtime ozone amounts. For all realistic ozone amounts, the UV exposure in the Antarctic spring is lower than typical values at Miami, indicating that visitors to the Antarctic are unlikely to be in danger of excessive doses at this time of year. However, life indigenous to the Antarctic is likely to receive increased doses. To elucidate the danger, Frederick and Snell weight the calculated fluxes by an action spectrum which indicates the relative sensitivity of organisms to UV exposure. One such action spectrum is for erythema, which is believed to be a precursor to skin cancer development. Figure 1.9-1 shows this

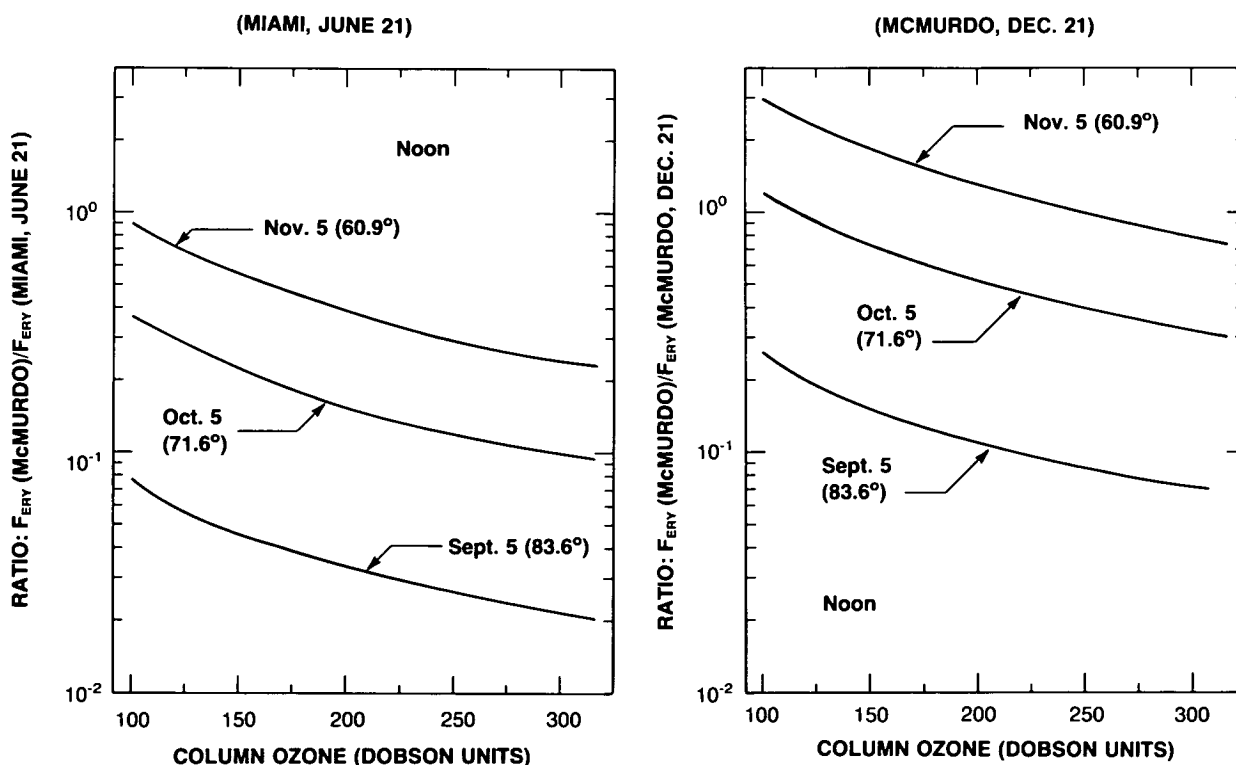


Figure 1.9-1. Ratio of biologically effective downward radiation computed for a range of ozone values at McMurdo during the austral spring to that for McMurdo on 21 December for an ozone column of 350 D.U. All values refer to local noon; solar zenith angles appear in parentheses (from Frederick and Snell, 1988).

POLAR OZONE

Table 1.9-1. Comparison of noontime irradiances computed for McMurdo during October with values for the summer solstice

Spectral Region	Irradiance ratio ^a	
	Day 276/Day 355	Day 300/Day 355
317.5–322.5 nm	0.38	0.83
303.0–307.7 nm	0.96	2.7
298.5–303.0 nm	2.1	8.5
DNA effective	0.85	2.5
R-B effective	0.54	1.1

^aDay 276 is October 3, with a column ozone value equal to 141 DU; day 300 is October 27, with a column ozone equal to 150 DU and Day 355 is December 21 with column ozone equal to 350 DU.

biologically effective downward irradiance at McMurdo for local noon in early October, November, and December as a function of ozone column, expressed as a fraction of the irradiance calculated for McMurdo at the summer solstice with a total ozone column of 350 DU. From this figure it is clear that biologically active irradiances in the springtime can exceed those experienced at the unperturbed Antarctic summer solstice. When averaged over a day, it is found that a 5 November value of 150 DU (as observed in 1987) gives an irradiance 50% greater than the solstice value.

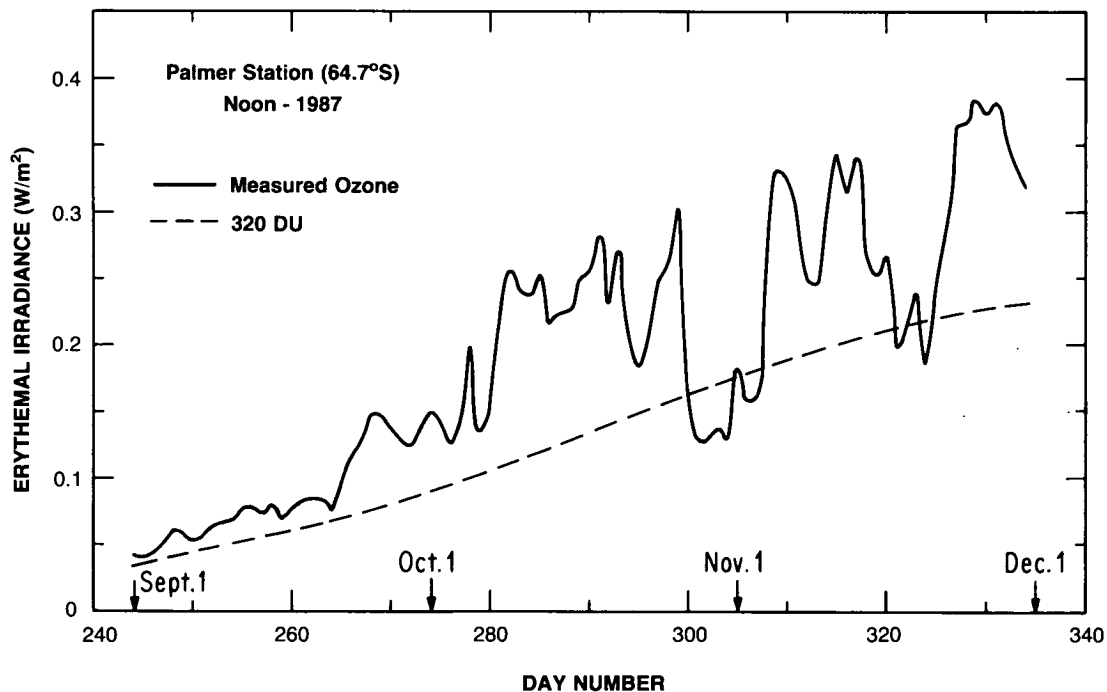


Figure 1.9-2. Computed time history of erythemal irradiance for local noon and clear skies over Palmer Station for September 1 to November 30, 1987 (from Frederick et al., 1989).

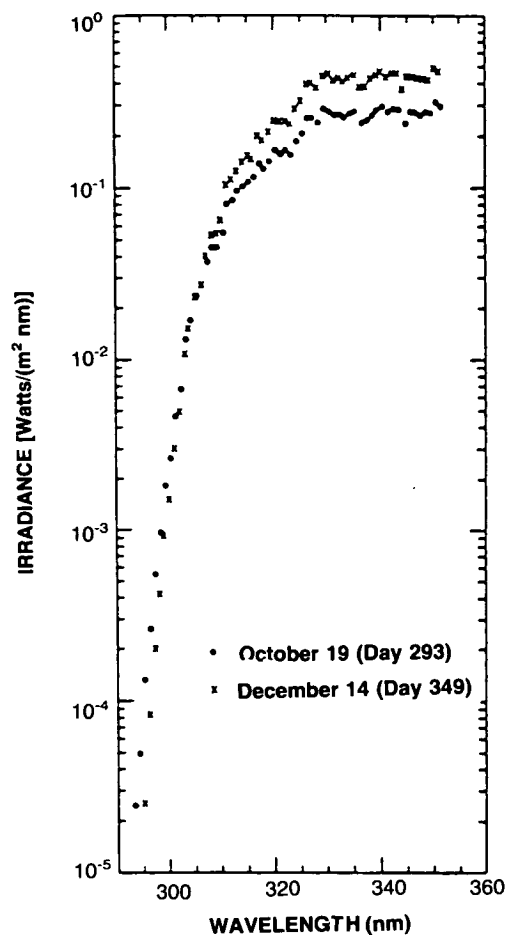


Figure 1.9-3. Spectra of UV solar irradiance measured from Palmer Station at local noon on 19 October and 14 December. The solar zenith angles were 53-54 degrees and 41-42 degrees respectively (from Lubin et al., 1989b).

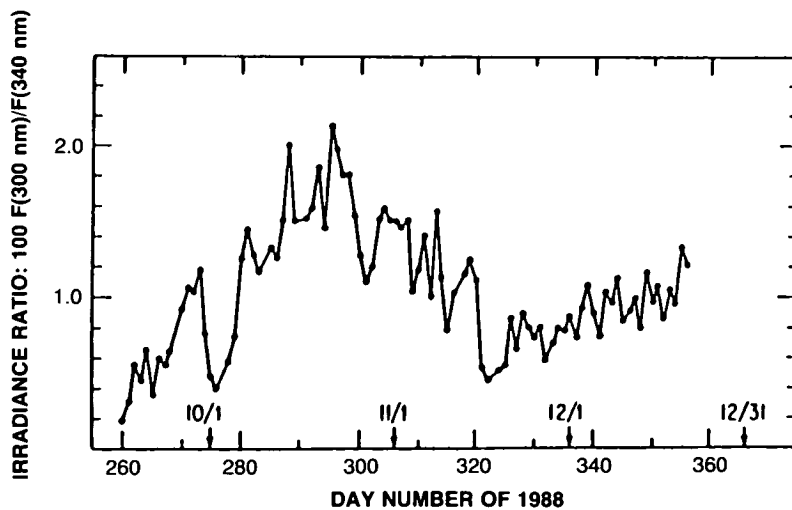


Figure 1.9-4. Ratio of noontime irradiance for 295-305 nm to that for 335-345 nm, for the period 19 September (day 260) and 21 December, 1988 (day 356). The plotted ratios have been multiplied by 100 (from Lubin et al., 1989b).

POLAR OZONE

Lubin et al. (1989a) and Frederick et al. (1989) present calculations of UV radiation in the austral spring for McMurdo Station and Palmer Station, respectively; column ozone amounts are taken from TOMS observations. Table 1.9-1 presents results from Lubin et al. (1989a) for various wavelengths and two alternative action spectra (DNA effective and Robertson-Berger effective). Again the irradiances are expressed as a fraction of the summer solstice values. These model calculations predict a significant perturbation to the UV dose by late October. Frederick et al. (1989) extend the calculation to late November, and choose the latitude of Palmer Station (64.7°S). UV irradiances are compared with those calculated for an ozone column of 320 DU, a typical pre-depletion value. Figure 1.9-2 shows the irradiances, weighted by the erythemal action spectrum for local noon. The increased irradiance is striking, exceeding the reference values by a factor of 2.3 on 5 October and 1.7 on 15 November.

As is pointed out in these studies, the increased day length and decreased solar zenith angle experienced as the summer solstice approaches means that any extension of the depletion into December could cause UV levels to well exceed those normally received.

Observational support for these calculations has been presented by Lubin et al. (1989b). While observations from the unperturbed Antarctic stratosphere are lacking, current observations present strong evidence that ozone depletion (even in the relatively unperturbed austral spring of 1988), caused marked perturbations in surface irradiance in the UV. Lubin et al. measured surface irradiance between 295 and 350 nm using a scanning spectroradiometer at Palmer Station. Figure 1.9-3 shows spectra for 19 October, an ozone-depleted period, and 14 December. Given the increased solar zenith angle at local noon at the later date, it would be expected that the irradiances would be higher in December. While this is true at the longer wavelengths (of which ozone absorbs little), at shorter wavelengths subject to stronger ozone absorption the October value exceeds that observed in December. Figure 1.9-4 shows the ratio of the irradiance at 300 nm and 340 nm for the period 19 September to 21 December. The 340-nm value is little affected by ozone. The purpose of using a ratio is to eliminate changes in irradiance resulting from changes in cloudiness. As can be seen from Figure 1.9-4, the ratio peaks during October, in contrast to the steady rise from solstice to equinox that would be expected in the absence of an ozone depletion.

A discussion of the biological consequences of the ozone depletion is beyond the scope of this report. Nevertheless, the above calculations and observations indicate that the Antarctic ozone depletion has caused a significant perturbation to the biologically effective UV irradiances reaching the surface. Several biological studies are currently examining the possible sensitivity of the spring bloom of phytoplankton to changes in UV radiation incident upon the surface waters surrounding Antarctica. Trodahl and Buckley (1989) emphasized that the radiation dose for organisms in the surface waters beneath Antarctic ice is greatest in spring, when the ice is relatively transparent. Ice turbidity significantly decreases the radiation dose in summer. Further studies of Antarctic biological systems are badly needed to assess possible impacts.

1.10 ARCTIC PHOTOCHEMISTRY

The foregoing discussion has illustrated the important chemical effects induced by polar stratospheric clouds and their relationship to ozone depletion. As shown in Section 1.2, such clouds are far more prevalent in Antarctica than in the Arctic (as first pointed out by McCormick et al., 1982). Further, Section 1.7 illustrated the pronounced differences in dynamical structure and temperature between the two hemispheres. These considerations suggest that the photochemistry of the Arctic winter and spring may be rather different from that of the Antarctic, and is likely to exhibit a greater degree of interannual variability.

In the following, observations of chemical constituents in the Arctic stratosphere will be summarized, with a view towards gaining insight to the possibility of Arctic ozone depletion.

1.10.1 Observations Prior to the 1988-1989 Arctic Winter

As emphasized in Section 1.6, observations of photochemical species in the Arctic polar regions have long provided cause to question purely gas-phase photochemical schemes. Most prominent among these data were the total NO_2 column abundance measurements by Noxon and co-workers. Noxon (1979) emphasized the puzzling occurrence of exceedingly steep latitudinal gradients in NO_2 column amounts in winter. He noted that the steep gradients were associated with stratospheric flow from polar regions. One such Noxon cliff is depicted in Figure 1.10.1-1. Because of the prominent role played by NO_2 and its interaction with chlorine species in ozone depletion (as discussed in Sections 1.3 through 1.6), the characteristics of the Arctic Noxon cliff will next be discussed in some detail.

Noxon noted that not only the absolute amount but also the diurnal variation in NO_2 was unusually small on the poleward side of the cliff, and suggested that this implied conversion of NO_x into a form whose photochemical lifetime exceeds a few days, such as HNO_3 . Noxon et al. (1979) presented observations of the NO_2 column abundance during a wave number 2 sudden warming event in 1979, wherein the arctic polar vortex split in two and one of the low centers moved over western Canada. Observations made near the center of the low indicated NO_2 column abundances of only about $0.5 \times 10^{15} \text{ cm}^{-2}$ in late February,

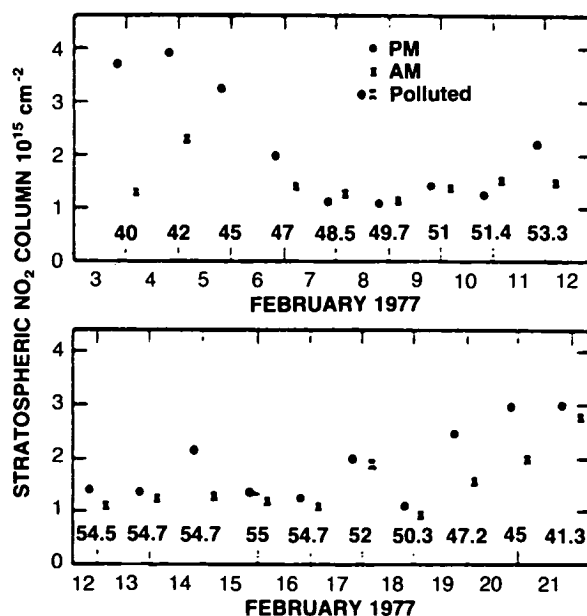


Figure 1.10.1-1. Observation of the Noxon 'cliff' from Noxon (1978). The variation of the column NO_2 is shown as a function of latitude, observed near 110°W longitude. North latitude is shown above the bottom line and the date is shown below it.

POLAR OZONE

lasting for nearly one week. These observations also pointed towards HNO_3 as a likely reservoir for NO_x in high-latitude winter, and, in retrospect, suggest that similar chemical processes to those that lead to ozone depletion in Antarctica could be active in the Arctic.

Noxon et al. (1983) presented a series of observations from various latitudes and emphasized the variable behavior of NO_2 depending upon temperature and flow regime. Figure 1.10.1-2 presents the mean annual cycle of stratospheric NO_2 observed by Noxon et al. (1983) from Point Barrow, Alaska (71°N), while Figure 1.10.1-3 presents the seasonal cycle obtained in three winter-spring observing sequences. These may be compared to observations from 78°S by McKenzie and Johnston (1984), Mount et al. (1987), and Keys and Johnston (1988, see Section 1.6.2). On some occasions in January and February, the NO_2 abundances observed in the Arctic were as low as those obtained in Antarctica, even at latitudes as far equatorward as 50°N (e.g., Noxon et al., 1979). On the other hand, it is evident that the averaged spring NO_2 values over Antarctica are considerably lower than those observed by Noxon et al. (1983) even when account is taken for the differences in the locations of the two sets of measurements relative to the polar vortices. Note that the lowest values obtained in March of the 3 years studied are of the order of $3.5 \times 10^{15} \text{ cm}^{-2}$ even within the polar vortex, while those obtained at McMurdo in the conjugate month of September are often well below $1.0 \times 10^{15} \text{ cm}^{-2}$. This interhemispheric difference in NO_2 is likely to be closely related to the interhemispheric differences in circulation and temperatures noted in Section 1.1 and 1.7. Like ozone, NO_2 is produced in the middle and upper stratosphere at subpolar latitudes; indeed, NO_y and ozone are expected to have similar distributions. This implies that NO_2 column abundances are strongly dependent on downward, poleward transport processes as well as on chemical processes that control the partitioning of NO_y species. The important differences in NO_2 abundances obtained in the Arctic in March as compared to Antarctica in September are likely to reflect at least in part the generally much earlier stratospheric warmings of the Northern Hemisphere and the resulting downward transport of NO_y . Clearly,

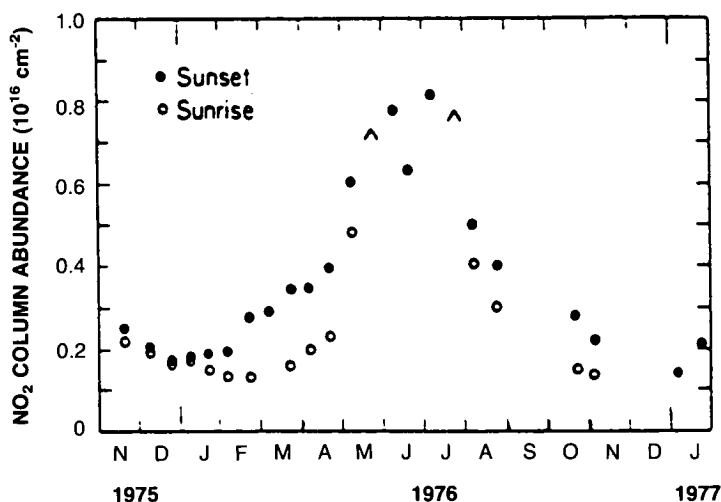


Figure 1.10.1-2. The mean annual cycle of NO_2 at 71°N (Point Barrow, Alaska) from Noxon et al. (1979). Solid circles are sunset measurements, while open circles are measurements taken at sunrise. The arrowheads denote upper limits.

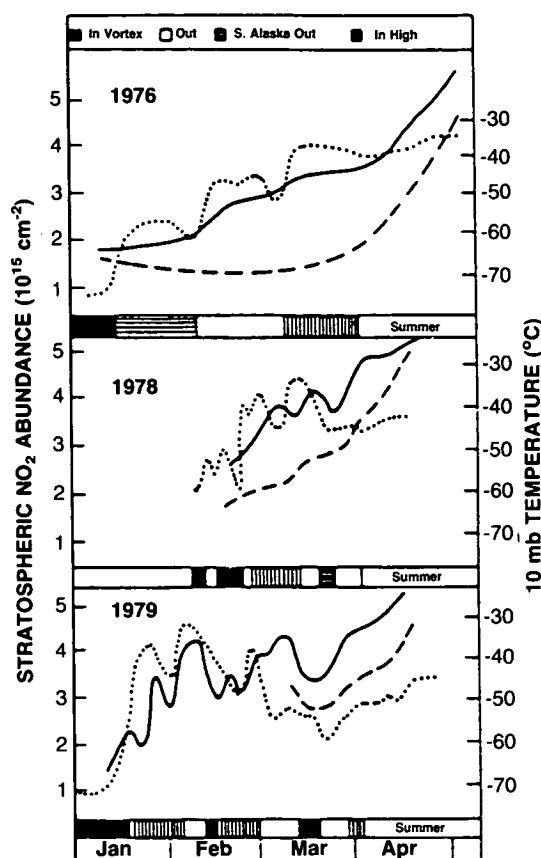


Figure 1.10.1-3. Variation of total NO_2 column abundance over Point Barrow, Alaska (71°N) in three different winter-spring seasons (from Noxon et al., 1983). The solid and dashed lines give the evening and morning NO_2 column abundances, respectively. The dotted line is the 10-mbar temperature over Barrow. The coding at the bottom indicates the position of Barrow relative to the polar vortex at 10 mbar.

this difference suggests that the time period in the spring when NO_2 abundances are suppressed sufficiently to allow effective ozone destruction through chlorine chemistry may be rather more limited in the Arctic than in the Antarctic.

A few measurements of the vertical profiles of reactive nitrogen species are also available from balloon observations. Ridley et al. (1987) presented measurements of NO and NO_2 near 50°N in summer and winter. Those authors emphasized the fact that the sum of NO and NO_2 was apparently reduced by a factor of 10 in winter as compared to summer, as shown in Figure 1.10.1-4. Since NO and NO_2 interchange rapidly with one another in the sunlit atmosphere, it is their sum that is important in considering, for example, the amount of nitrogen oxide available to form ClONO_2 . Thus, the observation of a substantial reduction in nitrogen oxides has important implications for chlorine chemistry. Ridley et al. concluded that the reduction of NO_x was consistent with formation of the N_2O_5 reservoir, based in part on trajectory analyses and observations of the diurnal variation of the total column (which was considerably greater than many of Noxon's observations).

POLAR OZONE

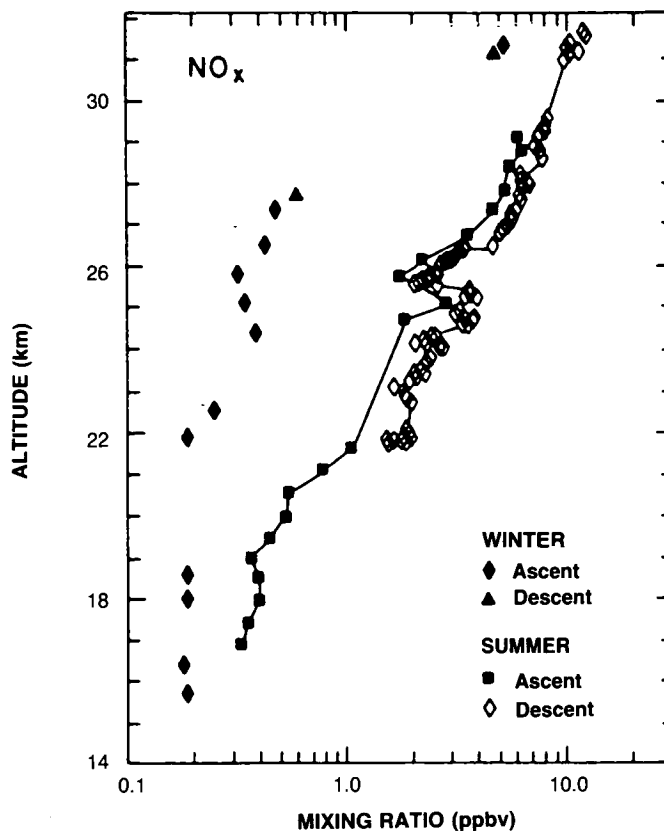


Figure 1.10.1-4. NO_x (NO + NO₂) mixing ratio profiles observed on balloon flights using a chemiluminescent detector launched from Gimli, Canada (50.6°N) on August 10, 1982 and December 15, 1982 (from Ridley et al., 1987).

More recent observations of the NO₂ column abundance in the Arctic winter include those of McCormick and Larsen (1986), Coffey et al. (1981), Mount et al. (1984), Russell et al. (1984), Pommereau and Goutail (1988) and Mount et al. (1988). Pommereau and Goutail examined the diurnal variability of NO_x chemistry and concluded that their data could not be understood without considering conversion into a longer lived storage species (e.g., HNO₃, or removal from the gas phase via particles), and suggested that the observations imply that the removal must be active at temperatures as warm as -45°C. This temperature is far warmer than that appropriate to polar stratospheric cloud formation, suggesting that reactions on background sulfuric acid aerosols may play a role. While these later data have certainly improved the details of our knowledge of Arctic NO₂ abundances and variability, they have not led to major modifications to the general picture delineated by Noxon a decade ago. Indeed, it is worthy of note that while some improvements in our understanding have emerged from recent work, especially insofar as the interplay between NO₂ and N₂O₅ in disturbed conditions is concerned, it is nonetheless the case that recent studies of the importance of heterogeneous chemistry have shown that Noxon's conclusions regarding the origin of the cliff held a great deal of merit.

Solomon and Garcia (1983) pointed out that the relatively long photochemical lifetime of N₂O₅ under cold conditions and the rapid meridional flow induced by displacement and elongation of the Arctic polar

vortex could also make N_2O_5 an important reservoir for NO_2 under some conditions. They emphasized the need to consider the photochemical history of the air parcels, particularly when mid-latitudes receive air from dark polar regions, where NO_x is rapidly converted to N_2O_5 via gas-phase chemistry. Callis et al. (1983) and Zawodny (1986) showed that such processes were likely to be important in understanding satellite observations of NO_2 in polar latitudes. In particular, Zawodny (1986) showed several case studies illustrating that low NO_2 values were associated with flow of air parcels from the polar vortex, but that much higher values were observed when similar air parcels continued their trajectories and were subjected to a day or two of exposure to sunlight at lower latitudes. This observation pointed strongly towards N_2O_5 as an important NO_2 reservoir in those cases.

Observations of the total HNO_3 column abundance in the Arctic include those of Murcray et al. (1975), Coffey et al. (1981), Girard et al. (1982) and Arnold and Knop (1989). A more detailed view of the vertical and seasonal variations of HNO_3 is provided by the LIMS observations (Gille et al., 1984b; Austin et al., 1986b). Figure 1.10.1-5 presents observations of the zonally and monthly averaged HNO_3 distributions from LIMS.

As Austin et al. (1986b) and others have emphasized, the very large abundances of HNO_3 observed in high-latitude winter are difficult to reconcile with gas-phase photochemical schemes. Austin et al. (1986b) noted that the HNO_3 abundances and their temporal variations required a source of HNO_3 in the Arctic polar night. They suggested that the reaction $N_2O_5 + H_2O \rightarrow 2HNO_3$ might explain the observed trends if the reaction probability for N_2O_5 on background aerosol distributions were as little as 1.0×10^{-3} . Recent measurements of reaction probabilities for N_2O_5 on sulfuric acid/ H_2O aerosol by Tolbert et al. (1988a) and Mozurkewich and Calvert (1988) suggest that this process is likely to proceed at least as fast as this requirement; the recent study by Mozurkewich and Calvert suggests that the effective reaction probability may be as large as 0.05-0.09. Hofmann and Solomon (1989) discussed the possible photochemical effects of heterogeneous reactions on background sulfuric acid aerosol, and emphasized the particularly important role of such reactions in middle and high latitudes during winter and spring.

Although N_2O_5 formation and photolysis is likely to play an important role in determining some of the variability of NO_2 in the north polar regions so long as appreciable NO_x is present, insights gained from the understanding of Antarctic ozone photochemistry suggest that the Noxon cliff phenomenon is also certain to be related to the formation of HNO_3 via heterogeneous processes. The relative roles of the two reservoirs probably depend on temperature, flow patterns, and time. It is well known that polar stratospheric clouds are often present in the Arctic winter, if not as persistently as in Antarctica (as discussed by McCormick et al., 1982 and illustrated in Section 1.2). Heterogeneous conversion of N_2O_5 to HNO_3 on any nitric acid trihydrate particles present will augment, and in the winter months is likely to dominate, that due to conversion on background aerosol. Further, the incorporation of HNO_3 into PSC particles, their capacity to perturb the partitioning of ClO_x , and the possibility of denitrification through particle sedimentation are all likely to contribute to the low abundances of NO_2 observed at high latitudes.

In summary, observations of both NO_2 and HNO_3 point towards the importance of heterogeneous reactions in suppressing the abundance of NO_2 in Arctic winter and producing HNO_3 at rates considerably faster than those expected from gas-phase chemistry. These characteristics are clearly similar to those found in Antarctica, and imply that enhanced chlorine radical abundances should be expected in Arctic regions in the late winter and early spring.

Observations of chlorine-containing species were both more limited and more recent than those of the nitrogen species prior to the 1988-1989 Arctic winter. Girard et al. (1982) and Mankin and Coffey (1983)

POLAR OZONE

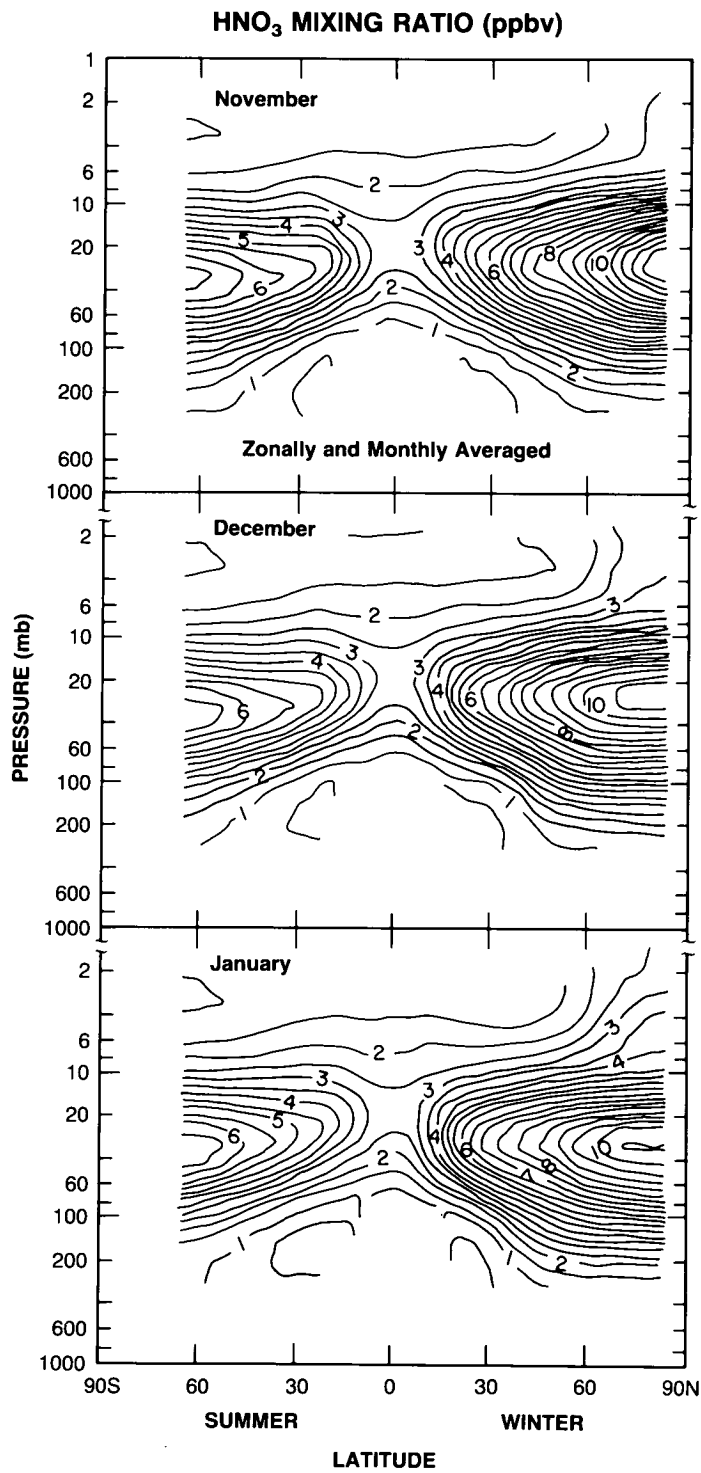


Figure 1.10.1-5. Zonally and monthly averaged HNO₃ mixing ratio distributions for November, December, and January from LIMS observations (from Austin et al., 1986b).

presented latitude surveys of HCl and HF abundances as shown, for example, in Figure 1.10.1-6, but the data were sparse above 50°N and were largely not obtained in winter. It is nevertheless interesting to note in the context of Section 1.6.1 that the HCl and HF abundances observed in the Arctic increase with increasing latitude, and often mirror one another, in contrast to the dramatic depletion of HCl obtained in the Antarctic winter vortex. This suggests that little conversion of HCl to more reactive forms of chlorine had occurred when those particular observations were obtained. Observations of HCl and HF obtained in the Arctic winter vortex in 1989 will be summarized in the next section .

During the winter of 1987-1988, ClO and OClO were both observed in the Arctic. The ClO measurements were carried out in aircraft flights up to about 61°N in western Canada (Brune et al., 1988). Although the ClO observations were obtained rather far from the center of the polar vortex, they were nonetheless of great importance because they revealed ClO mixing ratios of about 60 pptv, in contrast with most photochemical models whose predictions lie around 10-20 pptv for that latitude and time of year. The OClO observations were obtained by visible absorption using the moon as a light source from a latitude of 76.5°N at Thule, Greenland (Solomon et al., 1988). The Arctic polar vortex was centered very near the observing site during this period. Figure 1.10.1-7 presents a comparison of nighttime OClO observations in Antarctica in late August, in Greenland in early February, and at 40°N in Colorado in January. The Arctic measurements of ClO and OClO during the winter of 1987-1988 were thus considerably smaller than those of Antarctica, but were still substantially greater than gas-phase model predictions, suggesting that heterogeneous chemistry had perturbed the chlorine chemistry of the Arctic polar region in winter.

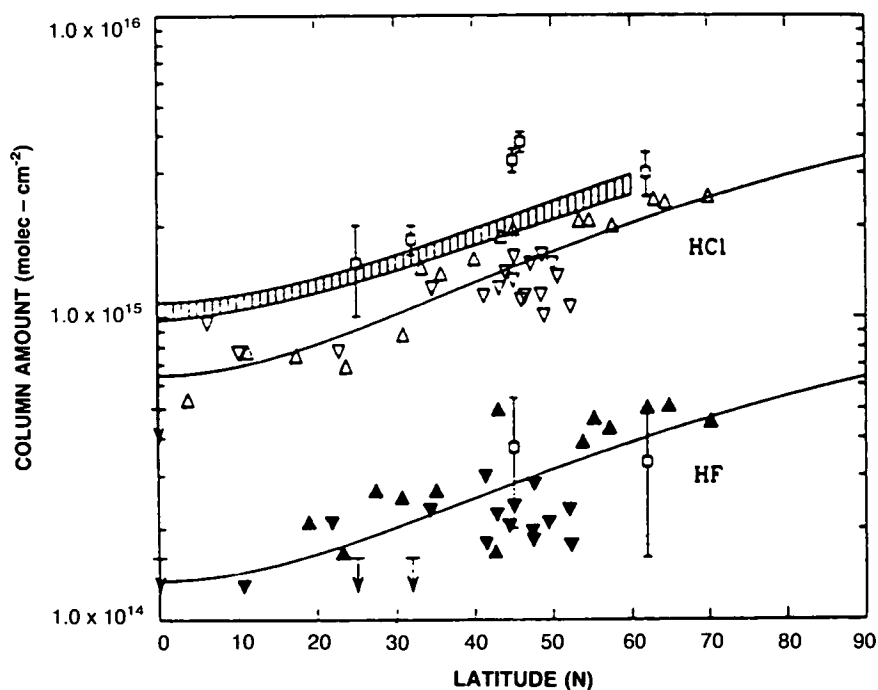


Figure 1.10.1-6. Latitude gradients HCl and HF in the Northern Hemisphere (from Mankin and Coffey, 1983). Upward pointing triangles are summer measurements; downward pointing triangles are winter measurements. The solid curves are least-squares fits to the data. Observations by Girard et al. (1982) are shown as squares with error bars. The hatched band represents model calculations.

POLAR OZONE

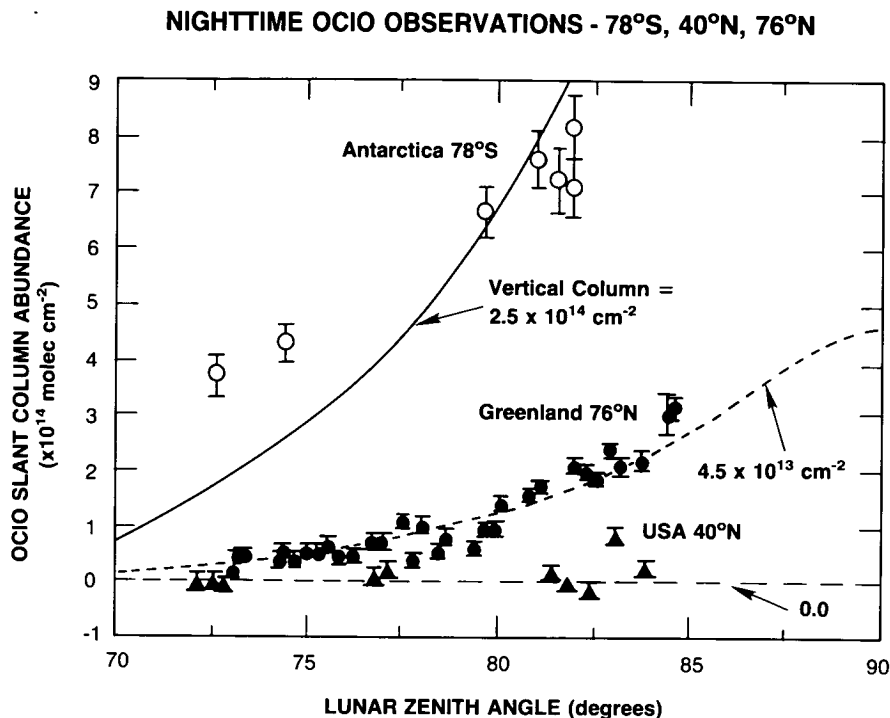


Figure 1.10.1-7. Observations of the nighttime abundance of OCIO versus lunar zenith angle at various locations (from Solomon et al., 1988)

1.10.2 Conclusions from 1989 Research

During January and early February, 1989, several extensive campaigns to probe the composition of the Arctic stratosphere were conducted. The NASA ER-2 and DC-8 aircraft were deployed from Stavanger, Norway, and observations were obtained as far north as the Pole and as far west as western Greenland. *In situ* and long-path instruments probed the composition of the polar stratosphere from these airborne platforms. Other groups of scientists conducted balloon experiments from Kiruna, Sweden and Alert, Canada. Further, measurements were conducted at Heiss Island, USSR, to document the changes in the ozone layer and understand the formation of PSCs. Some of the results from these experiments are currently being analyzed and all will ultimately be presented in peer-reviewed, scientific publications. In the following, we seek only to summarize the major points of these new studies insofar as they are currently available.

In many ways the Arctic Airborne Stratosphere Experiment (AASE) was similar to the Airborne Antarctic Ozone Experiment (AAOE). The major differences between the two campaigns (apart from some differences in instrumentation) were in the timing of the two experiments in relation to the different climatologies of the Arctic and Antarctic (Section 1.7), and their implications for photochemistry and microphysics. In particular, the AAOE experiment was carried out in Antarctica during August and September 1987. The results from that work provided evidence for ozone destruction and allowed measurement of the remarkable perturbations to photochemistry caused by polar stratospheric clouds (summarized in Section 1.6). However, it is quite likely that substantial processing by PSCs had occurred before the AAOE campaign began; thus the end results of PSC activity were clearly observed, but the process was largely not captured in action. The AASE experiment was carried out much earlier in the conjugate

Northern Hemisphere season (January and February). This was the period when widespread PSCs were just beginning to form, allowing study of the conversion of unprocessed to processed air and its subsequent photochemistry. However, substantial ozone loss was not expected during the AASE mission due to the much reduced solar illumination in polar regions at that point in the winter/spring season, and no unambiguous identification of photochemical ozone loss was made.

The observations of PSCs themselves during AASE were carried out by LIDAR, particle spectrometers, satellites, and via the NO_y instrument's enhancement in the presence of clouds. These observations confirmed the presence of both Type 1 and Type 2 clouds and showed that they occur at approximately the expected temperatures based on laboratory studies.

The observed abundance of ClO was far greater than that predicted by gas-phase photochemical models, reaching levels as high as 1100 pptv (enhanced by about a factor of 50 above gas-phase model predictions). Similar enhancements in OClO were also obtained, providing excellent cross-corroboration. ClONO₂ column abundances were elevated near the edge of the vortex, often reaching $3 \times 10^{15} \text{ cm}^{-2}$, but decreased towards the interior of the vortex. These observations are consistent with the observations and interpretation of the ClONO₂ "collar" in Antarctica discussed by G.C. Toon et al. (1989a) and the observed relationship between NO and ClO noted by Fahey et al. (1989b).

The ratio between HCl and HF column abundances was about 3-4 outside the vortex (consistent with the above discussion) but decreased to values ranging between 2.5 and 1 inside the polar vortex (as compared to minimum values of 0.7 found in Antarctica). These observations strongly indicate chemical conversion of HCl to more reactive forms of chlorine. However, since the observed perturbation to the total column was smaller, the data suggest that chemical conversion was either less complete or occurred over a more restricted height range as compared to Antarctica. The combination of the above chemical observations points strongly towards the importance of PSC chemistry. A more direct link was found on some occasions when, in relatively homogeneous air masses (as indicated by atmospheric tracers such as N₂O), abrupt increases in ClO were observed. Those 'edges' in ClO could not be attributed to solar zenith angle effects and were associated in a number of cases with predicted edges in PSCs and hence in cloud processing.

Extremely low column abundances of NO₂ were found inside the vortex, dropping to values as low as $0.3 \times 10^{15} \text{ cm}^{-2}$. As discussed above, these observations are consistent with those obtained by Noxon et al. (1979) and suggest that cloud processing had influenced the abundance of atmospheric NO₂. The observed abundance of NO_y reached a maximum of about 15 ppbv, and little evidence was found for denitrification prior to late January. Flights on January 30 and February 7 and 8 showed extensive denitrification similar to that found in Antarctica near 20 km altitude. *In situ* measurements of NO_y near 12 km suggested enhancements of the local NO_y abundances, very possibly through evaporation of particles sedimented from higher levels. On the other hand, measurements of the column abundance of HNO₃ were as large as $30 \times 10^{15} \text{ cm}^{-2}$, much larger than those found in Antarctica. This suggests that although denitrification had clearly occurred at some altitudes, the PSC particles may have evaporated in the low stratosphere, limiting the column reduction of HNO₃. This view is consistent with the enhanced NO_y levels found at 12 km.

Perhaps the most important issue highlighted by the AASE campaign is the mechanism for denitrification. In contrast to the Antarctic measurements, the Arctic denitrification was associated with modest, if any, dehydration. The detailed mechanism for denitrification is not presently understood. The observation suggests that denitrification and the attendant important effects on chlorine chemistry (as discussed in Section 1.5) may take place at warmer temperatures than previously believed.

POLAR OZONE

The AASE investigators concluded that further studies were required to establish the extent of any ozone loss in 1989 given the highly perturbed photochemistry seen until mid-February. The winter of 1988/89 was somewhat unusual in that temperatures were exceedingly cold until the sudden warming in mid-February, when PSCs disappeared. In other years, the low stratosphere may remain sufficiently cold for PSCs to be present from early December and in some cases (e.g., 1979) from late November until at least the beginning of March (see Section 1.2), extending the period over which significant ozone loss may occur. Such interannual differences likely have a large effect on the net ozone depletion in the northern vortex.

Hofmann et al. (1989a) described some preliminary results from the Kiruna measurements. Particle counter measurements revealed PSCs near 20-25 km on both available flights. Further, as noted in Section 1.2, thin layers of very large particles were sometimes observed. Hofmann et al. emphasized observations of "notches" in the ozone mixing ratio profiles, as shown in Figure 1.10.2-1. The observed notches are qualitatively similar to those identified by Hofmann et al. (1987a) in association with the development of the Antarctic ozone layer, and Hofmann et al. suggest that the same mechanism may be responsible. The implied ozone depletion is about 10-25% near 20-25 km, and only about 3% of the total column. Hofmann et al. emphasize that their study is consistent with but not proof of ozone depletion, since transport processes could conceivably produce similar notches.

Rosen et al. (1989) report preliminary findings from the measurements carried out at Alert, Canada. The optical backscatter instrument clearly detected PSCs on several occasions, and study of the scattering color ratio suggested that the particles fell both into the 0.1-2 μm and 2 μm size ranges. No clear observations of Type 2 PSCs were obtained. The observed altitude range of the PSCs was in fair agreement with

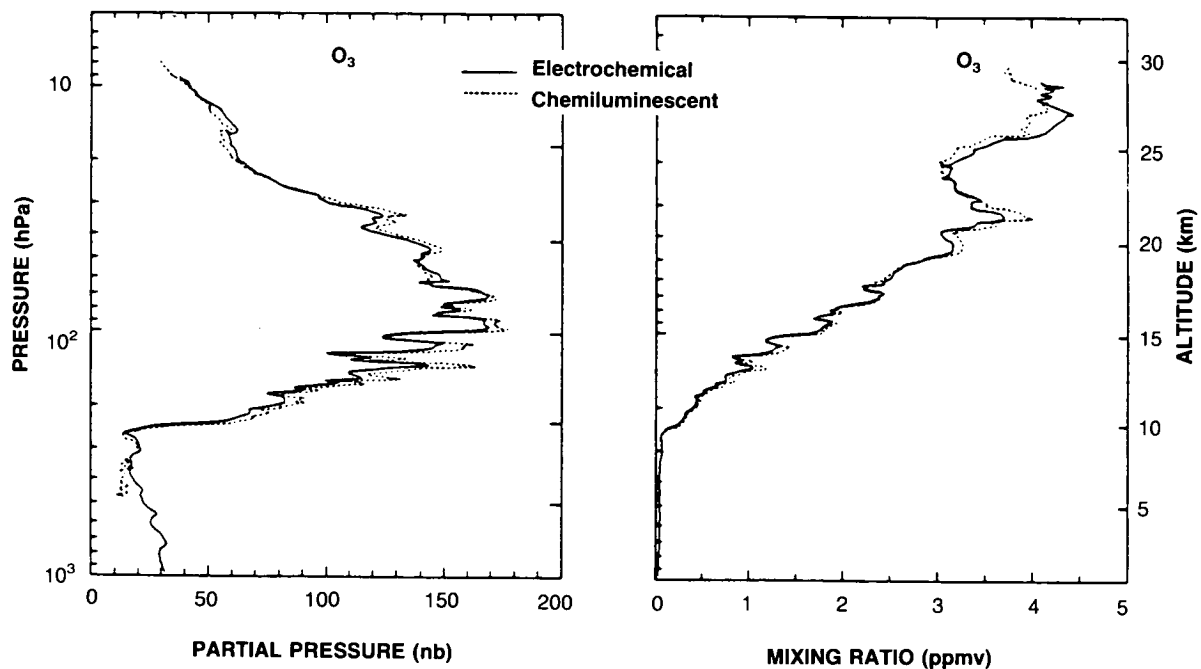


Figure 1.10.2-1. Ozone partial pressure and mixing ratio profiles measured at Kiruna, Sweden, on 23 January, 1989 (from Hofmann et al., 1989b).

predictions based on nitric acid trihydrate thermodynamics. Measurements of HNO_3 suggested that perhaps half of the available HNO_3 had been incorporated into the clouds. On one occasion, nitric acid vapor was almost completely removed near 23.5 km, although no clouds were observed at that level, suggesting possible denitrification.

The Heiss Island study showed that PSCs occurred at temperatures below about -80°C and found no apparent correlation between PSCs and ozone. This important finding suggests that direct removal of ozone on PSCs is unlikely. They also observed a considerable displacement between the temperature minimum and the occurrence of PSCs (by about 5 km altitude). They therefore conclude that denitrification may have occurred, reducing the amount of condensate (HNO_3) available for cloud formation near the temperature minimum. Finally, they noted that there was no convincing evidence for an anomalous ozone decrease similar to that over Antarctica (Khattatov et al., 1989).

Thus, it is clear that a wide range of observational studies conducted in the 1988-1989 boreal winter established perturbations to Arctic photochemistry quite similar to those obtained in Antarctica. However, it was difficult to identify a photochemical ozone loss in association with the observed chemical perturbations. Figure 1.10.2-2 presents the 30-mb temperatures observed during this season. Zonal mean values at 80°N and 60°N are shown, along with the minimum temperature within the polar vortex from NMC analyses (R. Nagatani, personal communication, 1989). As discussed in Section 1.7, a strong major warming occurred around day 65 (mid-February). Therefore, the ozone changes anticipated during this year are considerably smaller than those obtained in Antarctica, in part because air sufficiently cold for rapid ozone loss through ClO dimer photolysis (see Figure 1.5.1-1) was not subject to much solar illumination. Further, mixing of

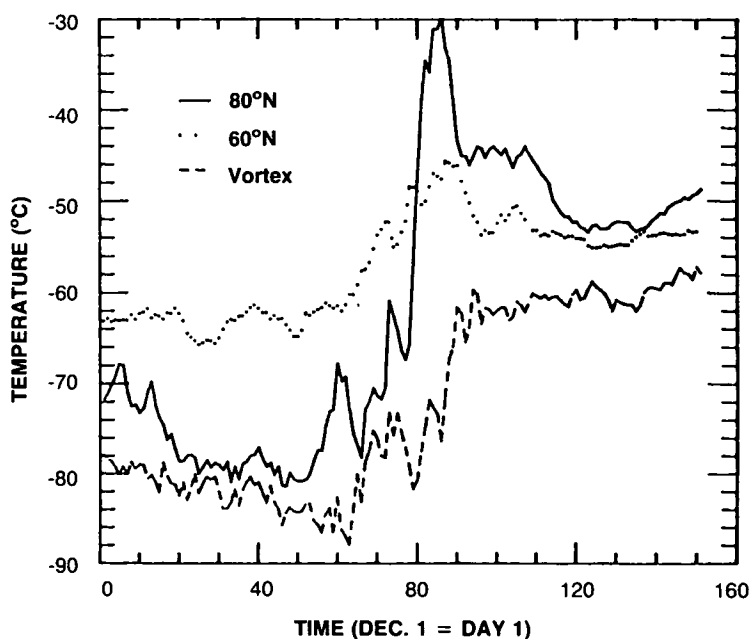


Figure 1.10.2-2. NMC temperatures at 30 mb for the 1988-1989 Northern Hemisphere winter-spring season. Zonal means for 60°N and 80°N are shown, along with the minimum temperatures within the polar vortex (from Nagatani, personal communication, 1989).

POLAR OZONE

air containing high levels of reactive nitrogen in association with the warming may have returned the chlorine partitioning to nearly normal status by about the end of February. Thus, because of warm temperatures or because of mixing associated with the warming (or perhaps both factors) little ozone loss would be expected after about February 15, 1989.

The Antarctic ozone decline occurs largely in September, when the polar cap becomes illuminated and temperatures remain cold. By analogy, one might expect an Arctic ozone depletion in the contemporary atmosphere if temperatures remained cold and the polar vortex relatively isolated as late as the conjugate Northern Hemisphere month of March. Although these conditions were not met during the 1988-1989 Northern Hemisphere winter, other years in the climatological record display different behavior. Figure 1.10.2-3 presents observations of temperatures at 30 mb in the zonal mean for 60°N, 80°N, and the vortex minimum from the NMC analyses for the winter of 1975–1976, one of the coldest Northern Hemisphere spring seasons on record. In that year, the temperatures remained below -70°C until about mid-March. No ozone loss would be expected in 1975–1976, since the chlorine content of the stratosphere was much lower than contemporary levels (Figure 1.6.4-5). However, the studies described in this Section suggest that it is likely that significant Northern Hemisphere ozone loss would occur if a winter-spring season like that of 1975-1976 were to occur in the near future.

1.11 PRINCIPAL CONCLUSIONS AND OUTSTANDING ISSUES

There is now very strong evidence that the ozone depletions observed over Antarctica in spring since the late 1970s are largely the result of chemical reactions with chlorine and bromine compounds, introduced

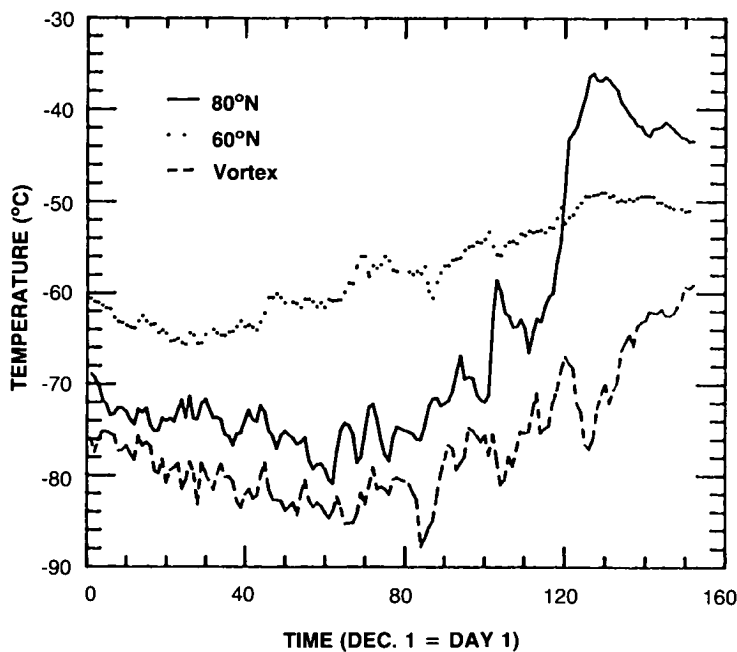


Figure 1.10.2-3. NMC temperatures at 30 mb for the 1975–1976 Northern Hemisphere winter-spring season. Zonal means for 60°N and 80°N are shown, along with the minimum temperatures within the polar vortex (from Nagatani, personal communication, 1989).

into the atmosphere mainly in the form of man-made chlorofluorocarbons and halons. Although some uncertainties remain, in semi-quantitative terms the processes that lead to ozone destruction are well understood. Air containing chlorofluorocarbons (CFCs) and halons enters the stratosphere primarily at equatorial latitudes. In the middle and upper stratosphere the CFCs are broken down by sunlight, releasing chlorine. Much of the available chlorine forms the relatively inert reservoirs, HCl and ClONO₂, particularly as the air descends to low altitudes. The air then moves poleward and downward on seasonal timescales, with some lateral dispersion. In the absence of solar heating, the polar regions cool during the winter months, eventually reaching temperatures at which nitric acid trihydrate and then water ice clouds can form in the low polar stratosphere. On the cloud particles, the HCl and ClONO₂ undergo heterogeneous conversion to highly reactive forms. In sunlight, chemical reactions then release reactive chlorine radicals produced by the heterogeneous chemistry. Chlorine (and bromine) monoxide are observed at levels sufficient to destroy ozone at rates of up to a few percent per day, consistent with observations, leading to a springtime ozone decline.

The effectiveness of this chlorine/bromine catalyzed ozone destruction is enhanced by the heterogeneous conversion of NO_x to nitric acid, which decreases (or even essentially eliminates) the possibility of reformation of the ClONO₂ and HCl reservoirs. Further, sedimentation of cloud particles can remove a substantial fraction of the available NO_x, leading to an even greater and long-lasting suppression of NO_x, ClONO₂ and HCl, and a corresponding enhancement in reactive chlorine. These processes allow high chlorine abundances to be sustained long enough to yield local ozone depletions of over 90% at some levels, and height-integrated depletions on the order of 50%. This picture is based on strong direct evidence from airborne and ground-based measurements made in Antarctica during 1986 and 1987, along with a range of laboratory kinetics and theoretical studies.

The interannual variability of the Antarctic ozone hole, and in particular the correlation between the depth of the ozone hole with the QBO, is not fully understood. However, the magnitude of the ozone depletion observed in 1988 compared to the exceedingly low ozone values of 1987 is qualitatively consistent with the above picture and may be at least partially attributed to the less extensive cold temperatures, fewer PSCs, and more vigorous vortex dynamics and transport in 1988 compared to 1987. It is anticipated that the QBO will likely be in the easterly phase during austral spring, 1989, and return to the westerly phase in 1990. Thus, the 1989 ozone depletion may be expected to be relatively modest, while that in 1990 may be considerably greater if the correlation with the QBO persists. The next few years are therefore likely to provide an excellent test of the QBO-ozone hole correlation. The heterogeneous conversion from reservoir to reactive chlorine on nitric acid trihydrate particles can only occur in the cold winter stratosphere, broadly restricting the geographical extent of the severe ozone depletion to Antarctica and to spring time. There is strong evidence, however, of the impact of the ozone hole at lower latitudes, most notably in the observation of reduced ozone concentrations year round at latitudes well equatorward of the polar vortex. This is attributable in part to the dilution of ozone depleted air as the vortex breaks down in late spring, although the vortex may also act to process a larger volume of air, priming the chemistry for ozone destruction during winter and spring.

In the Northern Hemisphere, while PSCs are frequently observed, they are far less ubiquitous than over Antarctica. Temperatures are generally warmer than in the corresponding season over Antarctica, and frequently temperatures rise dramatically during sudden warmings. The temperature increases can prevent further PSC formation, often well before sunlight returns to the polar cap. Thus, while conditions are in many respects similar to those over Antarctica, in certain important respects they differ, likely resulting in less efficient ozone depletion.

POLAR OZONE

While no comparable Arctic ozone hole has yet been observed, there is evidence of perturbed chemistry in the northern polar vortex. Observations obtained in both 1987/88 and 1988/89 showed that the chemical composition of the polar vortex was perturbed in a way similar to that over Antarctica. At the end of the 1988/89 airborne mission, the vortex was found to be primed to destroy ozone, with ClO mixing ratios exceeding 1 ppbv. However, no unequivocal evidence for ozone depletion was observed by the end of the airborne mission in mid-February. Noting the expected time scale for ozone depletion and the observed evolution of elevated ClO abundances and temperatures, no substantial ozone loss would have been expected in that year. However, years exhibiting colder temperatures later in the season would likely exhibit larger ozone decreases.

An important new finding of the Northern Hemisphere aircraft study was the observation of denitrification with far less evident dehydration than that obtained in Antarctica, implying that removal of substantial amounts of reactive nitrogen (a necessary prerequisite for sustaining high chlorine concentrations) may occur at temperatures above the frost point, and may thus be spatially more extensive than implied by the Antarctic results. This finding is not yet fully understood.

The studies in the Arctic in 1988/89 showed that while exposure to nitric acid trihydrate cloud particles (PSCs) could substantially perturb the partitioning of the chlorine species, an underlying, longer term contribution due to background aerosol could not be ruled out.

There are a number of very specific outstanding issues which significantly limit our ability to understand and predict reliably trends in ozone over both polar regions:

- It is not known whether the ozone trends in the Northern Hemisphere noted in the OTP (1989) are the result of the anomalous chemistry known to be present in the Arctic vortex.
- The detailed mechanism for denitrification, and in particular, the process of denitrification with less severe dehydration than observed in Antarctica, is not adequately understood.
- The rapid appearance of the Antarctic ozone hole, on the time scale of a decade, has not yet been successfully modeled. It is not clear whether the trend can be reproduced by existing models incorporating known changes in reactive chlorine abundances and perhaps in PSC frequency and duration, or whether changes in dynamics and transport also play a role.
- While there is evidence suggesting that heterogeneous reactions on sulfate aerosols can influence ozone concentrations (e.g., immediately after the El Chichon eruption), the importance of normal background aerosol concentrations on gas-phase chemical species is not known.
- The understanding of the role of HO_x species in polar chemistry is constrained only indirectly by HOCl measurements.
- The abundances, partitioning, and stratospheric sources of bromine are uncertain.
- The partitioning of the residual NO_y in the Antarctic vortex is not known.
- The absolute amount of total reactive chlorine and its partitioning among chlorine species (including higher oxides) are uncertain.
- There are significant uncertainties surrounding a number of key reaction rate constants, in particular the rate of the ClO dimer formation at warmer temperatures. It has also been suggested that Cl₂ may be formed during thermal decomposition of the dimer. There are also uncertainties regarding the absolute absorption cross section of Cl₂O₂, particularly at the long wavelengths

that control its photolysis rate at large solar angles. The significance of several suggested additional mechanisms (e.g., $\text{ClO} + \text{O}_3 + \text{M}$) is unclear.

- Additional heterogeneous reactions may be found to influence photochemistry (e.g., $\text{ClO} + \text{ice}$; $\text{HOCl} + \text{ice}$).
- It is possible that Type 1 PSCs may cause ozone loss at the edge of the Antarctic vortex throughout the winter season from May to August. The detailed observations necessary to test this possibility are not presently available.
- The extent to which the polar vortex can process air, destroying ozone prior to breakdown is uncertain. The possible impact of rising chlorine concentrations on the extent of processing is similarly unknown. Other processes (e.g., natural climatic cycles) may also influence the climatology of the stratosphere and hence vortex processing. The implications of these processes for mid-latitude ozone decreases are unknown.
- The effect on the stratospheric circulation of reduced solar heating in spring arising from reduced ozone concentrations is not known.
- The mechanisms causing strong descent in the polar vortex have not been properly explained. The importance of synoptically forced clouds for diabatic processes is not adequately understood.
- The implications of strong descent for the lifetimes of N_2O , CFCl_3 , etc., have not been evaluated quantitatively.
- The “age” and degree of turnover of air within the vortex is of critical importance in determining the availability of reactive chlorine and is a subject of ongoing research.
- The longitudinal variations in PSC formation are not understood quantitatively.
- While marked correlations between polar temperatures and the depth of the Antarctic ozone hole have been observed with the phase of winds in the low equatorial stratosphere (QBO), the detailed mechanism communicating the two regions is not understood.
- The implications of stratospheric cooling associated with greenhouse warming and increases in H_2O due to atmospheric CH_4 increases for the spatial extent and effect of PSCs are unknown. These and other climatic effects that could increase the latitudinal extent of polar ozone depletion are currently under study.
- The origin and significance of summertime temperature trends in Antarctica is not clear. It is as yet unresolved whether these are a result of incomplete radiative or chemical recovery, or reflect dynamical changes.

REFERENCES AND BIBLIOGRAPHY

- Akiyoshi, H., M. Fujiwara, and M. Uryu, Radiative aspects of Antarctic ozone hole in 1985, *Geophys. Res., Lett.*, 15, 919, 1988.
- Alekseev, A. P., V. M. Davidov, V. N. Dosov, S. N. Skuratov, A. E. Tyabotov, and V. U. Khattatov, Airborne lidar sounding of lower stratosphere aerosol in the Arctic, 1988, *Atmospheric Optics*, 1, 8, 1988.

POLAR OZONE

- Anderson, J. G., W. H. Brune, S. A. Lloyd, W. L. Starr, M. Loewenstein, and J. R. Podolske, Kinetics of ozone destruction by ClO and BrO within the Antarctic vortex: an analysis based on in-situ ER-2 data, *J. Geophys. Res.*, *94*, 11480, 1989.
- Andrews, D. G., J. R. Holton, and C.B. Leovy, *Middle Atmosphere Dynamics*, Academic Press, New York, pp. 489, 1987.
- Angell, J. K., The close relation between Antarctic total ozone depletion and cooling of the Antarctic low stratosphere, *Geophys. Res. Lett.*, *13*, 1240, 1986.
- Angell, J. K., Relation of Antarctic 100 mb temperature and total ozone to equatorial QBO, equatorial SST, and sunspot number, 1958–87, *Geophys. Res. Lett.*, *15*, 915–918, 1988a.
- Angell, J. K., Variations and trends in tropospheric and stratospheric temperatures: 1958–87, *J. Climate*, *1*, 1296, 1988b.
- Angell, J. K., and J. Korshover, The biennial wind and temperature oscillations in the equatorial stratosphere and their possible extension to higher latitudes, *Mon. Wea. Rev.*, *90*, 127, 1962.
- Angell, J. K., and J. Korshover, Quasi-biennial variations in temperature, total ozone, and tropopause height, *J. Atmos. Sci.*, *21*, 479, 1964.
- Angell, J. K., and J. Korshover, Biennial variation in springtime temperature and total ozone in extratropical latitudes, *Mon. Wea. Rev.*, *95*, 757, 1967.
- Angell, J. K., and J. Korshover, Quasi-biennial and long-term fluctuations in total ozone, *Mon. Wea. Rev.*, *101*, 426, 1973.
- Angell, J. K., and J. Korshover, Comparison of stratospheric trends in temperature, ozone and water vapor in north temperate latitudes, *J. Appl. Meteorol.*, *17*, 1397, 1978.
- Arnold, F., and G. Knop, Stratospheric nitric acid vapor measurements in the cold arctic vortex - implications for nitric acid condensation, *Nature*, *338*, 746, 1989.
- Atkinson, R. J., and J. Easson, A re-evaluation of the Australian total ozone record, *Proceedings of the International Ozone Symposium*, Eds. R.D. Bojkov and P. Fabian, 1988.
- Atkinson, R. J., W. A. Matthews, P. A. Newman, and R. A. Plumb, Evidence of the mid-latitude impact of Antarctic ozone depletion, *Nature*, *340*, 290, 1989.
- Austin, J., E. E. Remsberg, R. L. Jones, and A. F. Tuck, Polar stratospheric clouds inferred from satellite data, *Geophys. Res. Lett.*, *13*, 1256, 1986a.
- Austin, J., R. R. Garcia, J. M. Russell, S. Solomon, and A. F. Tuck, On the atmospheric photochemistry of nitric acid, *J. Geophys. Res.*, *91*, 5477–5485, 1986b.
- Austin, J., R. C. Pallister, J. A. Pyle, A. F. Tuck, and A. M. Zavody, Photochemical model comparisons with LIMS observations in a stratospheric trajectory coordinate system, *Quart J. Roy Met. Soc.*, *113*, 361–392, 1987.
- Austin, J., R. L. Jones, D. S. McKenna, A. T. Buckland, J. G. Anderson, D. W. Fahey, C. B. Farmer, L. E. Heidt, M. H. Proffitt, A. F. Tuck, and J. F. Vedder, Lagrangian photochemical modelling studies of the 1987 Antarctic spring vortex, Part 2: Seasonal trends in ozone, *J. Geophys. Res.*, *94*, 16717, 1989.
- Barnett, J. J., and M. Corney, Middle atmosphere reference model derived from satellite data, *Handbook for MAP*, vol. 16, SCOSTEP, 1985.
- Barrett, J. W., P. M. Solomon, R. L. DeZafra, M. Jaramillo, L. Emmons, and A. Parrish, Formation of the Antarctic ozone hole by the ClO dimer mechanism, *Nature*, *336*, 455, 1988.
- Birk, M., R. R. Friedl, E. A. Cohen, H. M. Pickett, and S. P. Sander, The rotational spectrum and structure of chlorine peroxide, submitted to *J. Chem. Phys.*, 1989.
- Blake, D. R., and F. S. Rowland, Continuing worldwide increases in tropospheric methane, 1978–1987, *Science*, *239*, 1129–1131, 1988.
- Blanchet, J. P., On radiative heating due to polar stratospheric clouds, *Tellus*, *37B*, 197, 1985.

- Blanchet, J. P., The response of polar stratospheric clouds to increasing carbon dioxide. *Proceedings of the International Radiation Symposium*, Lille, France, August 1988. Deepak Publishing, 1989.
- Bojkov, R. D., The 1979–1985 ozone decline in the Antarctic as reflected in ground-based observations, *Geophys. Res. Lett.*, *13*, 1236, 1986.
- Bowman, K. P., Interannual variability of total ozone during the breakdown of the Antarctic circumpolar vortex, *Geophys. Res. Lett.*, *13*, 1193, 1986.
- Bowman, K. P., and A. J. Krueger, A global climatology of total ozone from the Nimbus-7 Total Ozone Mapping Spectrometer, *J. Geophys. Res.*, *90*, 7967–7976, 1985.
- Brasseur, G., A. De Rudder, G.M. Keating, and M.C. Pitts, Response of the middle atmosphere to short-term solar ultraviolet variations: 2. Theory, *J. Geophys. Res.*, *92*, 903–914, 1987.
- Brasseur, G., and S. Solomon, *Aeronomy of the Middle Atmosphere*, D. Reidel, Dordrecht, 1984.
- Brune, W. H., and J. G. Anderson, In-situ observations of midlatitude stratospheric ClO and BrO, *Geophys. Res. Lett.*, *13*, 1391, 1986.
- Brune, W. H., E. W. Toohey, J. G. Anderson, W. L. Starr, J. F. Vedder, and E. F. Danielsen, In-situ northern mid-latitude observations of ClO, O₃ and BrO in the wintertime lower stratosphere, *Science*, *242*, 558, 1988.
- Brune, W. H., J. G. Anderson, and K. R. Chan, In situ observations of ClO in the Antarctic: ER-2 aircraft results from 54S to 72S latitude, *J. Geophys. Res.*, *94*, 16649, 1989a.
- Brune, W. H., J. G. Anderson, and K. R. Chan, In situ observations of BrO in the Antarctic: ER-2 aircraft results from 54S to 72S latitude, *J. Geophys. Res.*, *94*, 16639, 1989b.
- Burkholder, J. V., J. J. Orlando, and C. J. Howard, Ultraviolet absorption cross sections of Cl₂O₂ between 210 and 410 nm, *J. Phys. Chem.*, in press, 1989.
- Callis, L. B., J. M. Russell III, M. Natarajan, and K. V. Haggard, Examination of wintertime latitudinal gradients in stratospheric NO₂ using theory and LIMS observations, *Geophys. Res. Lett.*, *10*, 945, 1983.
- Callis, L. B., J. C. Alpert, and M. A. Geller, An assessment of thermal, wind and planetary wave changes in the middle and lower atmosphere due to the 11-year UV-flux variation. *J. Geophys. Res.*, *89*, 1373–1379, 1985.
- Callis, L. B., and M. Natarajan, The Antarctic ozone minimum: relationship to odd nitrogen, odd chlorine, the final warming, and the 11-year solar cycle, *J. Geophys. Res.*, *91*, 10771, 1986.
- Cariolle, D., M. Deque, and J. J. Morcrette, A GCM simulation of the ozone seasonal variations at high latitudes in the southern hemisphere, *Geophys. Res. Lett.*, *13*, 1304, 1986.
- Cariolle, D., S. Muller, F. Cayla, and M. P. McCormick, Mountain waves, polar stratospheric clouds, and the ozone depletion over Antarctica, *J. Geophys. Res.*, *94*, 11233, 1989a.
- Cariolle, D., A. Lasserre-Bigorrry, J. F. Royer, and J. F. Geleyn, A GCM simulation of the springtime Antarctic ozone decrease and its impact on midlatitudes, submitted to *J. Geophys. Res.*, 1989b.
- Carroll, M. A., S. Solomon, R. W. Sanders, and A. L. Schmeltekopf, Visible and near-ultraviolet spectroscopy at McMurdo Station, Antarctica, 6, Observations of BrO, *J. Geophys. Res.*, *94*, 16633, 1989.
- Chandra, S. An assessment of possible ozone-solar cycle relationship inferred from NIMBUS 4 BUV data. *J. Geophys. Res.*, *89*, 1373–1379, 1984.
- Chandra, S., and R. D. McPeters, Some observations on the role of planetary waves in determining the spring time ozone distribution in the Antarctic, *Geophys. Res. Lett.*, *13*, 1224, 1986.
- Chanin, M. L. N. Spires, and A. Hauchecorne, Long-term variation of the temperature of the middle atmosphere at mid latitude: dynamical and radiative causes, *J. Geophys. Res.*, *92*, 4201, 1987.
- Charney, J. G., and P. G. Drazin, Propagation of planetary scale disturbances from the lower into the upper atmosphere, *J. Geophys. Res.*, *66*, 83, 1961.

POLAR OZONE

- Cheng, B. M., and Y. P. Lee, Production and trapping of gaseous ClO: The infrared spectrum of chlorine peroxide (ClOOCl) in solid argon, *J. Chem. Phys.*, **90**, 5930, 1989.
- Chipperfield, M. P., and J. A. Pyle, Two-dimensional modelling of the Antarctic lower stratosphere, *Geophys. Res. Lett.*, **15**, 875, 1988.
- Chu, W. P., M. P. McCormick, J. Lenoble, C. Brogniez, and P. Pruvost, SAGE II inversion algorithm, *J. Geophys. Res.*, **94**, 8353, 1989.
- Chubachi, S., Preliminary result of ozone observations at Syowa Station from February, 1982 to January, 1983, *Mem. Natl. Inst. Polar Res.*, spec. issue no. 34, 13, 1984.
- Chubachi, S., On the cooling of stratospheric temperature at Syowa, Antarctica, *Geophys. Res. Lett.*, **13**, 1221, 1986.
- Cicerone, R. J., L. E. Heidt, and W. H. Pollack, Measurements of atmospheric methyl bromide and bromoform, *J. Geophys. Res.*, **93**, 3745, 1988.
- Clyne, M. A. A., and R. T. Waston, Kinetic studies of diatomic free radicals using mass spectrometry, Part 4, The BrO + OCID and BrO + ClO reactions, *J. Chem. Soc. Faraday Trans.*, **1**, **73**, 1169, 1977.
- Coffey, M. T., W. G. Mankin, and A. Goldman, Simultaneous spectroscopic determination of the latitudinal, seasonal, and diurnal variability of stratospheric N₂O, NO, NO₂, and HNO₃, *J. Geophys. Res.*, **86**, 7331, 1981.
- Coffey, M. T., On the temporal change of stratospheric NO₂, *Geophys. Res. Lett.*, **15**, 331, 1988.
- Coffey, M. T., and W. G. Mankin, Airborne measurements of stratospheric constituents over Antarctica in the austral spring 1987, 2, Halogen and nitrogen trace gases, *J. Geophys. Res.*, **94**, 16597, 1989.
- Connor, B. J., J. W. Barrett, A. Parrish, P. M. Solomon, R. L. DeZafra, and M. Jaramillo, Ozone over McMurdo Station, Antarctica, austral spring, 1986: Altitude profiles for the middle and upper stratosphere, *J. Geophys. Res.*, **92**, 13221, 1987.
- Cox, R. A., and G. D. Hayman, The stability and photochemistry of dimers of the ClO radical and implications of Antarctic ozone depletion, *Nature*, **322**, 796–800, 1988.
- Cox, R. A., D. W. Sheppard, and M. P. Stevens, Absorption coefficients and kinetics of the BrO radical using molecular modulation, *J. Photochem.*, **19**, 201, 1982.
- Crutzen, P. J., and F. Arnold, Nitric acid cloud formation in the cold Antarctic stratosphere: a major cause for the springtime "ozone hole," *Nature*, **324**, 651–655, 1986.
- DeMore, W. B., M. J. Molina, S. P. Sander, D. M. Golden, R. F. Hampson, M. J. Kurylo, C. J. Howard, and A. R. Ravishankara, Chemical kinetics and photochemical data for use in stratospheric modeling, evaluation number 8, JPL Publ. 87-41, 1987.
- Deutsch, H. U., Ozone distribution in the atmosphere, *Can. J. Chem.*, **52**, 1491, 1974.
- DeZafra, R. L., M. Jaramillo, A. Parrish, P. Solomon, B. Connor, and J. Barnett, Observation of abnormally high concentrations of chlorine monoxide at low altitudes in the Antarctic spring stratosphere, I. Diurnal variation, *Nature*, **328**, 408, 1987.
- DeZafra, R. L., M. Jaramillo, J. Barrett, L. K. Emmons, P. M. Solomon, and A. Parrish, New observations of a large concentration of ClO in the springtime lower stratosphere over Antarctica and its implications for ozone-depleting chemistry, *J. Geophys. Res.*, **94**, 11423, 1989.
- Dobson, G. M. B., D. N. Harrison, and J. Lawrence, Measurements of the amount of ozone in the earth's atmosphere and its relation to other geophysical conditions. *Proc. Roy. Soc. London, A*, **122**, 456–486, 1928.
- Dobson, G. M. B., Forty year's research on atmospheric ozone at Oxford: A history, *Applied Optics*, **7**, 401, 1968.
- Dobson, G. M. B., The laminated structure of ozone in the atmosphere, *Quart J. Roy. Met. Soc.*, **99**, 599, 1973.
- Dunkerton, T. J., Body force circulation and the Antarctic ozone minimum, *J. Atmos. Sci.*, **45**, 427, 1988.

- Eckman, R. S., Response of ozone to short-term variations in the solar ultraviolet irradiance. 1. A theoretical model, *J. Geophys. Res.*, *91*, 6695–6704, 1986.
- Elokhov, A. S., and A. N. Gruzdev, Total ozone and NO₂ observations at Molodeznaja and Mirny stations, Antarctica, in spring 1987 and in summer and fall, 1988, Middle Atmosphere Symposium, Dushanbe, USSR, 1989.
- Fahey, D. W., D. M. Murphy, C. S. Eubank, K. K. Kelly, M. H. Proffit, G. V. Ferry, M. K. W. Ko, M. Loewenstein, and K. R. Chan, Measurements of nitric oxide and total reactive nitrogen in the Antarctic stratosphere: observations and chemical implications, *J. Geophys. Res.*, *94*, 16437, 1989a.
- Fahey, D. W., K. K. Kelly, G. V. Ferry, L. R. Poole, J. C. Wilson, D. M. Murphy, and K. R. Chan, In situ measurements of total reactive nitrogen, total water and aerosols in polar stratospheric clouds in the Antarctic stratosphere, *J. Geophys. Res.*, *94*, 11299, 1989b.
- Fairlie, T. D. A., and A. O'Neill, The stratospheric major warming of winter 1984/85: observations and dynamical inferences, *Quart. J. Roy. Met. Soc.*, *114*, 557–578, 1988.
- Fairlie, T. D. A., A. O'Neill, and V. D. Pope, The sudden breakdown of an unusually strong cyclone in the stratosphere during winter 1988/89, submitted to *Nature*, 1989.
- Farman, J. C., B. G. Gardiner, and J. D. Shanklin, Large losses of total ozone in Antarctica reveal seasonal ClO_x/NO_x interaction, *Nature*, *315*, 207, 1985a.
- Farman, J. C., R. J. Murgatroyd, A. M. Sinnickas, and B. A. Thrush, Ozone photochemistry in the Antarctic stratosphere in summer, *Quart. J. Roy. Met. Soc.*, *111*, 1013, 1985b.
- Farmer, C. B., G. C. Toon, P. W. Shaper, J. F. Blavier, and L. L. Lowes, Ground-based measurements of the composition of the Antarctic atmosphere during the 1986 spring season, I. Stratospheric trace gases, *Nature*, *329*, 126, 1987.
- Farrara, J. D., and C. R. Mechoso, An observational study of the final warming in the Southern Hemisphere stratosphere, *Geophys. Res. Lett.*, *13*, 1232, 1986.
- Frederick J. E., and H. E. Snell, Ultraviolet radiation levels during Antarctic spring. *Science*, *241*, 438–440, 1988.
- Frederick, J. E., H. E. Snell, and E. K. Haywood, Solar ultraviolet radiation at the Earth's surface, *J. Photochem. Photobiol.*, in press, 1989.
- Friedl, R. R., and S. P. Sander, Studies of ClO and BrO reactions important in the polar stratosphere; kinetics and mechanism of the ClO + BrO and ClO + ClO reactions, Paper presented at the Polar Ozone Workshop, Snowmass, Colorado, May 9–13, 1988.
- Friedl, R. R., and S. P. Sander, Kinetics and product studies of the reaction ClO + BrO using discharge flow-mass spectrometry, *J. Phys. Chem.*, *4756*, 1989.
- Gandrud, B. W., P. D. Sperry, L. Sanford, K. K. Kelly, G. V. Ferry, and K. R. Chan, Filter measurement results from the Airborne Antarctic Ozone Experiment, *J. Geophys. Res.*, *94*, 11285, 1989.
- Garcia, R. R. and S. Solomon, A numerical model of the zonally averaged dynamical and chemical structure of the middle atmosphere, *J. Geophys. Res.*, *88*, 1379, 1983.
- Garcia, R. R., and S. Solomon, The effect of breaking gravity wave on the dynamics and chemical structure of the middle atmosphere, *J. Geophys. Res.*, *90*, 3850, 1985.
- Garcia, R. R., and S. Solomon, Interannual variability in Antarctic ozone and the Quasi-Biennial Oscillation, *Geophys. Res. Lett.*, *14*, 848, 1987.
- Garcia, R., S. Solomon, R. G. Roble, and D. W. Rusch, A numerical study of the response of the middle atmosphere to the 11-year solar cycle, *Planet. Space Sci.*, *32*, 411–421, 1984.
- Gardiner, B. G., and J. D. Shanklin, Recent measurements of Antarctic ozone depletion, *Geophys. Res. Lett.*, *13*, 1199, 1986.
- Gardiner, B. G., Comparative morphology of the vertical ozone profile in the Antarctic spring, *Geophys. Res. Lett.*, *15*, 901, 1988.

POLAR OZONE

- Gardiner, B. G., The Antarctic ozone hole, *Weather*, *44*, 291–298, 1989.
- Gernandt, H., The vertical ozone distribution above the GDR research base, Antarctica in 1985, *Geophys. Res. Lett.*, *14*, 84, 1987.
- Gille, J. C., C. M. Smythe, and D. F. Heath, Observed ozone response to variations in solar ultraviolet radiation, *Science*, *225*, 315–317, 1984a.
- Gille, J. C., J. M. Russell, P. L. Barley, E. E. Remsberg, L. L. Gordley, W. F. J. Evans, H. Fischer, B. W. Gandrud, A. Girard, J. E. Harries, and S. A. Beck, Accuracy and precision of the nitric acid concentrations determined by the limb infrared monitor of the stratosphere experiment on Nimbus 7, *J. Geophys. Res.*, *89*, 5179, 1984b.
- Girard, A., L. Gramont, N. Louisnard, S. LeBoiteux, and G. Fergant, Latitudinal variation of HNO₃, HCl and HF vertical column density above 11.5 km, *Geophys. Res. Lett.*, *9*, 135, 1982.
- Gray, L. J., and J. A. Pyle, A two-dimensional model of the quasi-biennial oscillation of ozone, *J. Atmos. Sci.*, *46*, 203–220, 1989.
- Grose, W. L., R. S. Eckman, R. E. Turner, and W. T. Blackshear, Potential effects of Antarctic ozone depletion upon the global ozone budget, MASH Workshop on Dynamics, Transport and Photochemistry in the Middle Atmosphere of the Southern Hemisphere, San Francisco, CA, April 1989 (to appear in a volume of the NATO Advanced Research Workshop series, 1989).
- Hamill, P., O. B. Toon, and R. P. Turco, Characteristics of polar stratospheric clouds during the formation of the Antarctic ozone hole, *Geophys. Res. Lett.*, *13*, 1288, 1986.
- Hamill, P., R. P. Turco, and O. B. Toon, On the growth of nitric and sulfuric acid aerosol particles under stratospheric conditions, *J. Atmos. Chem.*, *7*, 287–315, 1988.
- Hanson, D. R., and K. Mauersberger, Laboratory studies of the nitric acid trihydrate: Implications for the South Polar stratosphere, *Geophys. Res. Lett.*, *15*, 855–858, 1988a.
- Hanson, D. R., and K. Mauersberger, Vapor Pressures of HNO₃/H₂O solutions at low temperatures, *J. Phys. Chem.*, *92*, 6167–6170, 1988b.
- Hanson, D. R., and K. Mauersberger, Solubility and equilibrium vapor pressures of HCl dissolved in polar stratospheric cloud materials: Ice and the trihydrate of nitric acid, *Geophys. Res. Lett.*, in press, 1989a.
- Hanson, D. R., and K. Mauersberger, HCl/H₂O solid phase vapor pressures and HCl solubility in ice, submitted to *J. Phys. Chem.*, 1989b.
- Hartmann, D. L., L. E. Heidt, M. Loewenstein, J. R. Podolske, J. Vedder, W. L. Starr, and S. E. Strahan, Transport into the south polar vortex in early spring, *J. Geophys. Res.*, *94*, 16779, 1989a.
- Hartmann, D. L., M. R. Schoeberl, P. A. Newman, R. L. Martin, B. L. Gary, K. R. Chan, M. Loewenstein, J. R. Podolske, and S. E. Strahan, Potential vorticity and mixing in the south polar vortex during spring, *J. Geophys. Res.*, *94*, 11625, 1989b.
- Hasebe, F., Interannual variation of global total ozone revealed from Nimbus 4 BUUV and ground-based observations, *J. Geophys. Res.*, *88*, 6819, 1983.
- Hayman, G. D., J. M. Davies, and R. A. Cox, Kinetics of the reaction ClO + ClO → products and its potential relevance to Antarctic ozone, *Geophys. Res. Lett.*, *13*, 1347, 1986.
- Heidt, L. E., J. F. Vedder, W. H. Pollock, B. E. Henry, and R. A. Lueb, Trace gases in the Antarctic atmosphere, *J. Geophys. Res.*, *94*, 11599, 1989.
- Heysfield, A. J., Ice particles observed in a cirriform cloud at -83C and implications for polar stratospheric clouds, *J. Atmos. Sci.*, *43*, 851, 1986.
- Hills, A. J., R. J. Cicerone, J. G. Calvert, and J. W. Birks, Kinetics of the BrO + ClO reaction: implications for stratospheric ozone, *Nature*, *328*, 405, 1987.
- Hills, A. J., R. J. Cicerone, J. G. Calvert, and J. W. Birks, Temperature dependence of the rate constant and product channels for the BrO + ClO reaction, *J. Phys. Chem.*, *92*, 1853–1858, 1988.

- Hirota, I., T. Hirooka, and M. Shiotani, Upper stratosphere circulation in the two hemispheres, *Quart. J. Roy. Met. Soc.*, 109, 443, 1983.
- Hofmann, D. J., Direct ozone depletion in springtime Antarctic lower stratospheric clouds, *Nature*, 337, 447, 1989a.
- Hofmann, D. J., Comparison of stratospheric clouds in the Antarctic and in the Arctic, submitted to *Geophys. Res. Lett.*, 1989b.
- Hofmann, D. J., J. M. Rosen, J. W. Harder, and S. R. Rolf, Ozone and aerosol measurements in the springtime Antarctic stratosphere in 1986, *Geophys. Res. Lett.*, 13, 1252, 1986.
- Hofmann, D. J., J. W. Harder, S. R. Rolf, and J. M. Rosen, Balloonborne observations of the temporal development and vertical structure of the Antarctic ozone hole in 1986, *Nature*, 326, 59, 1987a.
- Hofmann, D. J., J. M. Rosen, J. W. Harder, and S. R. Rolf, Observations of the decay of the El Chichon stratospheric aerosol cloud in Antarctica, *Geophys. Res. Lett.*, 14, 614, 1987b.
- Hofmann, D. J., J. M. Rosen, and J. W. Harder, Aerosol measurements in the winter/spring Antarctic stratosphere: I. Correlative measurements with ozone, *J. Geophys. Res.*, 93, 655, 1988.
- Hofmann, D. J., J. M. Rosen, J. W. Harder, and J. V. Hereford, Balloonborne measurements of aerosol, condensation nuclei, and cloud particles in the stratosphere at McMurdo Station, Antarctica during the spring of 1987, *J. Geophys. Res.*, 94, 11253, 1989a.
- Hofmann, D. J., P. Amedieu, W. A. Matthews, P. V. Johnston, Y. Kondo, W. R. Sheldon, and G. J. Byrne, Stratospheric clouds and ozone depletion in the Arctic during January 1989, *Nature*, 340, 117, 1989b.
- Hofmann, D. J., J. W. Harder, J. M. Rosen, J. V. Hereford, and J. R. Carpenter, Ozone profile measurements at McMurdo Station, Antarctica during the spring of 1987, *J. Geophys. Res.*, 94, 16527, 1989c.
- Hofmann, D. J., and S. Solomon, Ozone destruction through heterogeneous chemistry following the eruption of El Chichon, *J. Geophys. Res.*, 94, 5029, 1989.
- Holton, J. R., and H.-C. Tan, The influence of the equatorial quasi-biennial oscillation on the global circulation at 50 mb, *J. Atmos. Sci.*, 37, 2200, 1980.
- Holton, J. R., and H.-C. Tan, The quasi-biennial oscillation in the Northern Hemisphere lower stratosphere, *J. Meteor. Soc. Japan*, 60, 140, 1982.
- Hood, L. L., Solar ultraviolet induced variations in the stratosphere and mesosphere, *J. Geophys. Res.*, 92, 876-888, 1987.
- Hoskins, B. J., M. E. McIntyre, and A. W. Robertson, On the use and significance of potential vorticity maps, *Quart. J. Roy. Met. Soc.*, 111, 877, 1985.
- Isaksen, I. S. A., and F. Stordal, Antarctic ozone depletion: 2-D model studies, *Geophys. Res. Lett.*, 13, 1327, 1986.
- Iwasaka, Y., Non-spherical particles in the Antarctic polar stratosphere - Increase in particulate content and stratospheric water vapor budget, *Tellus*, 38B, 364, 1986.
- Iwasaka, Y., T. Hirasawa, and H. Fukunishi, Lidar measurement on the Antarctic stratospheric aerosol layer: [I] Winter enhancement, *J. Geomag. Geoelectr.*, 37, 1087, 1985a.
- Iwasaka, Y., A. Ono, and S. Saitoh, Measurement of water vapor content in the polar stratosphere: Syowa station, spring 1983, *Mem. Pol. Res. (Tokyo)*, 39, 51, 1985b.
- Iwasaka, Y., and K. Kondoh, Depletion of antarctic ozone: Height of ozone loss region and its temporal changes, *Geophys. Res. Lett.*, 14, 87, 1987.
- Iwasaka, Y., K. Kondoh, and K. Kawahira, Long term trend in ozone content and temperature in the Antarctic stratosphere - Cooling and ozone decrease tendency, submitted to *Geophys. Res. Lett.*, 1989.
- Jones, R. L., J. Austin, D. S. McKenna, J. G. Anderson, D. W. Fahey, C. B. Farmer, L. E. Heidt, K. K. Kelly, D. M. Murphy, M. H. Proffit, and A. F. Tuck, Lagrangian photochemical modelling studies of the 1987 Antarctic spring vortex: comparison with observations, *J. Geophys. Res.*, 94, 11529, 1989.

POLAR OZONE

- Juckes, M. N., and M. E. McIntyre, A high resolution, one-layer model of breaking planetary waves in the stratosphere, *Nature*, 328, 590, 1987.
- Kanzawa, H., and S. Kawaguchi, Large stratospheric sudden warming in Antarctic late winter and shallow ozone hole in 1988, submitted to *Nature*, 1989.
- Karcher, F., M. Amodei, G. Armand, C. Besson, B. DuFour, G. Froment, and J. P. Meyer, Simultaneous measurements of HNO₃, NO₂, HCl, O₃, N₂O, CH₄, H₂O and CO, and their latitudinal variations as deduced from airborne infrared spectrometry, *Ann. Geophysicae*, 4, 425, 1988.
- Kawahira, K., and T. Hirooka, Interannual temperature changes in the Antarctic lower stratosphere - A relation to the ozone hole, *Geophys. Res. Lett.*, 16, 41-44, 1989.
- Keating G. M., and D. F. Young, Interim reference ozone models for the middle atmosphere, *Handbook for MAP*, vol. 16, SCOSTEP, 1985.
- Keating, G. M., L. R. Lake, J. Y. Nicholson III, and M. Natarajan, Global ozone long-term trends from satellite measurements and the response to solar activity variations, *J. Geophys. Res.*, 86, 9873-9880, 1981.
- Keating, G. M., G. P. Brasseur, J. Y. Nicholson III, and A. DeRudder, Detection of the response of ozone in the middle atmosphere to short-term solar ultraviolet variations, *Geophys. Res. Lett.*, 12, 449, 1985.
- Keating, G. M., M. C. Pitts, G. Brasseur, and A. DeRudder, Response of middle atmosphere to short-term solar ultraviolet variations: 1. Observations, *J. Geophys. Res.*, 92, 889-902; 2. Theory. 903-914, 1987.
- Kelly, K. K., A. F. Tuck, D. M. Murphy, M. H. Proffitt, D. W. Fahey, R. L. Jones, D. S. McKenna, M. Loewenstein, J. R. Podolske, S. E. Strahan, G. V. Ferry, K. R. Chan, J. F. Vedder, G. L. Gregory, W. D. Hypes, M. P. McCormick, E. V. Browell, and L. E. Heidt, Dehydration in the lower Antarctic stratosphere during late winter and early spring, 1987, *J. Geophys. Res.*, 94, 11317, 1989.
- Kent, G. S., C. R. Trepte, U. O. Farruckh, and M. P. McCormick, Variation in the stratospheric aerosol associated with the north cyclonic polar vortex as measured by the SAM II satellite sensor, *J. Atmos. Sci.*, 42, 1536, 1985.
- Keys, J. G., and P. V. Johnston, Stratospheric NO₂ and O₃ in Antarctica: Dynamic and chemically controlled variations, *Geophys. Res. Lett.*, 13, 1260, 1986.
- Keys, J. G., and P. V. Johnston, Stratospheric NO₂ column measurements from three Antarctic sites, *Geophys. Res. Lett.*, 15, 898, 1988.
- Khattatov, V. U., V. U. Rudakov, V. A. Yushkov, and J. M. Rosen, Observations of ozone and polar stratospheric clouds from Heiss Island, 1989, in press, *Meteorologia i Gidrologia*, 1989.
- Kiehl, J. T., B. A. Boville, and B. P. Briegleb, Response of a general circulation model to a prescribed Antarctic ozone hole, *Nature*, 332, 501-504, 1988.
- Kinne, S., and O. B. Toon, Studies of the radiative effects of polar stratospheric clouds, *Proceedings of AMS Conference on Atmospheric Radiation*, in press, 1989.
- Ko, M. K. W., K. K. Tung, D. K. Wenstein, and N. D. Sze, A zonal-mean model of stratospheric tracer transport in isentropic co-ordinates: numerical simulations for nitrous oxide and nitric acid, *J. Geophys. Res.*, 90, 2013, 1985.
- Ko, M. K. W., J. M. Rodriguez, N. D. Sze, M. H. Proffitt, W. L. Starr, A. Krueger, E. V. Browell, and M. P. McCormick, Implications of AAOE observations for proposed chemical explanations of the seasonal and interannual behavior of Antarctic ozone, *J. Geophys. Res.*, 94, 16705, 1989.
- Kokin, G. A., S. P. Perov, D. A. Tarasenko, and A. F. Chizhov, A study of Antarctic ozone anomaly in spring by rocket and ground-based ozonometers, *Meteorologia i Gidrologia*, in press, 1989.
- Komhyr, W. D., R. D. Grass, and R. K. Leonard, Total ozone decrease at South Pole Antarctica, 1964-1985, *Geophys. Res. Lett.*, 13, 1248, 1986.

- Komhyr, W. D., S. J. Oltmans, and R. D. Grass, Atmospheric ozone at South Pole, Antarctica, in 1986, *J. Geophys. Res.*, *93*, 5167, 1988.
- Komhyr, W. D., Oltmans, S. J., Grass, R. D., Franchois, P. R., and R. K. Leonard, Changes in total ozone and ozone vertical distribution at South Pole, Antarctica, 1962–1987, *Proceedings of Quadrennial Ozone Symposium*, Gottingen, FRG, 1989a.
- Komhyr, W. D., R. D. Grass, P. J. Reitelbach, S. E. Kuester, P. R. Franchois, and M. L. Fanning, Total ozone, ozone vertical distributions, and stratospheric temperatures at South Pole, Antarctica, in 1986 and 1987, *J. Geophys. Res.*, *94*, 11429, 1989b.
- Kondoh, K., Y. Iwasaka, T. Suzuki, and S. Kaneto, Ozonesonde measurements at Syowa Station, Proc. NIPR Symp., *Polar Meteorol. Glaciol.*, *1*, 10, 1987.
- Koshelkov, Yu. P., Southern hemisphere reference middle atmosphere, *Adv. Space Res.*, *7*, 83, 1987.
- Koshelkov, Yu. P., Kovshova, E. N., and Fedorov, V. V., Day-to-day variability of temperature and wind speed in the stratosphere of the Southern and Northern Hemisphere, *Antarctica*, *26*, 37, 1987.
- Koshelkov, Yu. P., Temperature trends in the lower stratosphere of the Antarctic and environs, in press, *Meteorologia i Hidrologia*, 1989.
- Krueger, A. J., M. R. Schoeberl, and R. S. Stolarski, TOMS observations of total ozone in the 1986 Antarctic spring, *Geophys. Res. Lett.*, *14*, 527, 1987.
- Krueger, A. J., M. R. Schoeberl, R. S. Stolarski, and F. S. Sechrist, The 1987 ozone hole: A new record low, *Geophys. Res. Lett.*, *15*, 1365, 1988.
- Kruger, B. C., G. Q. Wang, and P. Fabian, The Antarctic ozone depletion caused by heterogeneous photolysis of halogenated hydrocarbons, *Geophys. Res. Lett.*, *14*, 523, 1987.
- Kuhlsbarsch, T., and Naujokat, B., Nordhemispharischer Klimabericht zum Januar 1989, Beilage zur Berliner Wetterkarte, Amsblatt des Instituts für Meteorol., Free University of Berlin, 1989.
- Labitzke, K., On the interannual variability of the middle stratosphere during the northern winters, *J. Met. Soc. Japan*, *60*, 124, 1982.
- Labitzke, K., Sunspots, the QBO and the stratospheric temperature in the north polar region, *Geophys. Res. Lett.*, *14*, 535, 1987a.
- Labitzke, K., The lower stratosphere over the polar regions in winter and spring: relation between meteorological parameters and total ozone, *Annal. Geophys.*, *5A*, 95–102, 1987b.
- Labitzke, K., and M.-L. Chanin, Changes in the middle atmosphere in winter related to the 11-year solar cycle, *Annal. Geophys.*, *6*, 643, 1988.
- Labitzke, K., and H. van Loon, Associations between the 11-year solar cycle, the QBO and the atmosphere, Part I: the troposphere and stratosphere in the Northern Hemisphere in winter, *J. Atmos. Terr. Phys.*, *50*, 197, 1988a.
- Labitzke, K., and H. van Loon, Association between the 11-year solar cycle, the QBO and the atmosphere, Part II: surface and 700 mb in the Northern Hemisphere in winter, *J. Climate*, *1*, 905, 1988b.
- Labitzke, K., and H. van Loon, Association between the 11-year solar cycle, the QBO and the atmosphere, Part III: aspects of the association, *J. Climate*, *2*, 554, 1989.
- Lait, L. R., M. R. Schoeberl, and P. A. Newman, Quasi-biennial modulation of the Antarctic ozone depletion, *J. Geophys. Res.*, in press, 1989.
- Leu, M. T., Laboratory studies of sticking coefficients and heterogeneous reactions important in the Antarctic stratosphere, *Geophys. Res. Lett.*, *15*, 17–20, 1988a.
- Leu, M. T., Heterogeneous reactions of N_2O_5 with H_2O and HCl on ice surfaces: implications for Antarctic ozone depletion, *Geophys. Res. Lett.*, *15*, 855–858, 1988b.
- London, J., R. D. Bojkov, S. Oltmans, and J. I. Kelley, Atlas of the global distribution of total ozone, July 1957–June 1967, National Center for Atmospheric Research, Boulder, CO, 1967.
- London J., Radiative energy sources and sinks in the stratosphere and mesosphere, in Nicolet M., and Aikin, A. C. (eds), *Proceedings of the NATO Advanced Study Institute on Stratospheric Ozone: Its*

POLAR OZONE

- Variation and Human Influences*, pp. 703–721 U. S. Dept. of Transportation, Washington, D. C., 1980.
- Lubin, D., J. E. Frederick, and A. J. Krueger, The ultraviolet radiation environment of Antarctica: McMurdo Station during September-October 1987, *J. Geophys. Res.*, *94*, 8491, 1989a.
- Lubin, D., F. E. Frederick, C. R. Booth, T. Lucas, and D. Neuschuler, Measurements of enhanced springtime ultraviolet radiation at Palmer Station, Antarctica, *Geophys. Res. Lett.*, *16*, 783, 1989b.
- Mahlman, J. D., and S. B. Fels, Antarctic ozone decreases: a dynamical cause, *Geophys. Res. Lett.*, *13*, 1316, 1986.
- Mahlman, J. D., Dynamical effects of the Antarctic ozone hole: A 3-D model experiment, MASH workshop on Dynamics, Transport and Photochemistry in the Middle Atmosphere of the Southern Hemisphere, San Francisco, CA, April 1989, to appear in a volume of the NATO Advanced Research Workshop series, 1989.
- Mankin, W. G., and M. T. Coffey, Latitudinal distributions and temporal changes of stratospheric HCl and HF, *J. Geophys. Res.*, *88*, 10776, 1983.
- Mankin, W. G., and M. T. Coffey, Airborne measurements of stratospheric constituents over Antarctica in the austral spring 1987, 1, Method and ozone observations, *J. Geophys. Res.*, *94*, 11413, 1989.
- Margitan, J. J., Chlorine nitrate: The sole product of the $\text{ClO} + \text{NO}_2 + \text{M}$ recombination, *J. Geophys. Res.*, *88*, 5415–5420, 1983.
- McCormick, M. P., Hamill, T. J. Pepin, W. P. Chu, T. J. Swissler, and L. R. McMaster, Satellite studies of the stratospheric aerosol, *Bull. Am. Met. Soc.*, *60*, 1038, 1979.
- McCormick, M. P., H. M. Steele, P. Hamill, W. P. Chu, and T. J. Swissler, Polar stratospheric cloud sightings by SAM II, *J. Atmos. Sci.*, *39*, 1387, 1982.
- McCormick, M. P., P. Hamill, and U. O. Farrukh, Characteristics of polar stratospheric clouds as observed by SAM II, SAGE, and Lidar, *J. Met. Soc. Japan.*, *63*, 267, 1985.
- McCormick, M. P., and J. C. Larsen, Antarctic springtime measurements of ozone, nitrogen dioxide, and aerosol extinction by SAM II, SAGE, and SAGE II, *Geophys. Res. Lett.*, *13*, 1280, 1986.
- McCormick, M. P., and C. R. Trepte, SAM II measurements of Antarctic PSC's and aerosols, *Geophys. Res. Lett.*, *13*, 1276, 1986.
- McCormick, M. P., and C. R. Trepte, Polar stratospheric optical depth observed between 1978 and 1985, *J. Geophys. Res.*, *92*, 4297, 1987.
- McCormick, M. P., and J. C. Larsen, Antarctic measurements of ozone by SAGE II in the spring of 1985, 1986, 1987, *Geophys. Res. Lett.*, *15*, 907, 1988.
- McCormick, M. P., and C. R. Trepte, Persistence of Antarctic polar stratospheric clouds, *J. Geophys. Res.*, *94*, 11241, 1989.
- McElroy, M. B., R. J. Salawitch, S. C. Wofsy, and J. A. Logan, Antarctic ozone: reductions due to synergistic interactions of chlorine and bromine, *Nature*, *321*, 759, 1986a.
- McElroy, M. B., R. J. Salawitch, and S. C. Wofsy, Antarctic O_3 : Chemical mechanisms for the spring decrease, *Geophys. Res. Lett.*, *13*, 1296, 1986b.
- McElroy, M. B., R. J. Salawitch, and S. C. Wofsy, Chemistry of the Antarctic stratosphere, *Planet. Space Sci.*, *36*, 73, 1988.
- McGrath, M. P., K. C. Clemshaw, F. S. Rowland, and W. J. Hehre, Thermochemical stabilities and vibrational spectra of isomers of the chlorine oxide dimer, *Geophys. Res. Lett.*, *15*, 883–886, 1988.
- McIntyre, M. E., and T. N. Palmer, Breaking planetary waves in the stratosphere, *Nature*, *305*, 593–600, 1983.
- McKenna, D. S., R. L. Jones, J. Austin, E. Browell, M. P. McCormick, A. J. Krueger, and A. F. Tuck, Diagnostic studies of the Antarctic vortex during the 1987 Airborne Antarctic Ozone Experiment: Ozone mini-holes, *J. Geophys. Res.*, *94*, 11641, 1989a.

- McKenna, D. S., R. L. Jones, A. T. Buckland, J. Austin, A. F. Tuck, R. H. Winkler, and R. Chan, The Southern Hemisphere lower stratosphere during August and September 1987: Analyses based on the United Kingdom Meteorological Office global model, *J. Geophys. Res.*, *94*, 16847, 1989b.
- McKenzie, R. L., and P. V. Johnston, Springtime stratospheric NO₂ in Antarctica, *Geophys. Res. Lett.*, *11*, 73, 1984.
- McPeters, R. D., R. D. Hudson, P. K. Bhartia, and S. L. Taylor, The vertical ozone distribution in the Antarctic ozone minimum measured by SBUV, *Geophys. Res. Lett.*, *13*, 1213, 1986.
- Mechoso, C. R., A. O'Neill, V. D. Pope, and J. D. Farrara, A study of the stratospheric warming of 1982 in the Southern Hemisphere, *Quart. J. Roy. Met. Soc.*, *114*, 1365, 1988.
- Mechoso, C. R., A. O'Neill, J. D. Farrara, M. Fisher, V. D. Pope, and B. Kingston, On the breakdown of the Southern Hemisphere stratospheric polar vortex, submitted to *Nature*, 1989.
- Molina, M. J., The chemistry of some reactions believed to be important in ozone depletion over Antarctica, *Proceedings of the International Ozone Symposium 1988*, R. Bojkov and P. Fabian, Eds., Deepak Pub. Co., Hampton, Virginia, 1989.
- Molina, M. J., and F. S. Rowland, Stratospheric sink for chlorofluoromethanes: Chlorine-atom catalyzed destruction of ozone, *Nature*, *249*, 810, 1974.
- Molina, L. T., M. J. Molina, R. A. Stachnik, and R. D. Tom, An upper limit to the rate of the HCl + ClONO₂ reaction, *J. Phys. Chem.*, *89*, 3779, 1985.
- Molina, L. T., and M. J. Molina, Production of Cl₂O₂ from the self-reaction of the ClO radical, *J. Phys. Chem.*, *91*, 433-436, 1987.
- Molina, M. J., T. L. Tso, L. T. Molina, and F. C. Y. Wang, Antarctic stratospheric chemistry of chlorine nitrate, hydrogen chloride, and ice: Release of active chlorine, *Science*, *238*, 1253-1257, 1987.
- Molina, M. J., A. Fucaloro, L. T. Molina, and K. Zahir, Solubility of HCl vapor in various ice substrates, manuscript in preparation, 1989.
- Mount, G. H., D. W. Rusch, J. F. Noxon, J. M. Zawodny, and C. A. Barth, Measurements of stratospheric NO₂ from the Solar Mesosphere Explorer satellite, 1. An overview of the results, *J. Geophys. Res.*, *89*, 1327, 1984.
- Mount, G. H., R. W. Sanders, A. L. Schmeltekopf, and S. Solomon, Visible spectroscopy at McMurdo Station, Antarctica, 1. Overview and daily variations of NO₂ and O₃ during austral spring, 1986, *J. Geophys. Res.*, *92*, 8320, 1987.
- Mount, G. H., S. Solomon, R. W. Sanders, R. O. Jakoubek, and A. L. Schmeltekopf, Observations of stratospheric NO₂ and O₃ at Thule, Greenland, *Science*, *242*, 555, 1988.
- Mozurkewich, M., and J. G. Calvert, Reaction probability on N₂O₅ on aqueous aerosols, *J. Geophys. Res.*, *93*, 15889, 1988.
- Murcray, D. G., D. B. Barker, J. N. Brooks, A. Goldman, and W. J. Williams, Seasonal and latitudinal variation of the stratospheric concentration of HNO₃, *Geophys. Res. Lett.*, *2*, 223, 1975.
- Murcray, F. J., F. H. Murcray, C. P. Rinsland, A. Goldman, and D. G. Murcray, Infrared measurements of several nitrogen species above the South Pole in December, 1980 and November-December, 1986, submitted to *J. Geophys. Res.*, 1987.
- Murphy, D. M., A. F. Tuck, K. K. Kelly, K. R. Chan, M. Loewenstein, J. R. Podolske, M. H. Proffitt, and S. E. Strahan, 1989: Indicators of transport and vertical motion from correlations between in situ measurements in the Airborne Antarctic Ozone Experiment, *J. Geophys. Res.*, *94*, 11669, 1989.
- Nagatani, R. M., and A. J. Miller, The influence of lower stratospheric forcing on the October Antarctic ozone decrease, *Geophys. Res. Lett.*, *14*, 202, 1987.
- Nash, J., and G. F. Forrester, Long-term monitoring of stratospheric temperature trends using radiance measurements obtained by the Tiros-N series of NOAA spacecraft, *Adv. Space Res.*, *6*, 37, 1987.
- Naujokat, B., An update of the observed quasi-biennial oscillation of the stratospheric winds over the tropics, *J. Atmos. Sci.*, *43*, 1873, 1986.

POLAR OZONE

- Newman, P. A., The final warming and polar vortex disappearance during the southern hemisphere spring, *Geophys. Res. Lett.*, 13, 1228, 1986.
- Newman, P. A., and M. R. Schoeberl, October Antarctic temperature and total ozone trends from 1979 to 1985, *Geophys. Res. Lett.*, 13, 1207, 1986.
- Newman, P. A., and W. J. Randel, Coherent ozone-dynamical changes during the Southern Hemisphere spring, 1979–1986, *J. Geophys. Res.*, 93, 12585-12606, 1988.
- Newman, P. A., and M. R. Schoeberl, The break-up of the Southern Hemisphere spring polar ozone and temperature minimum from 1979 to 1987, *Polar Ozone Workshop Abstracts*, NASA Conference Publication 10014, 7, 1988.
- Newman, P. A., L. R. Lait, and M. R. Schoeberl, The morphology and meteorology of Southern Hemisphere spring total ozone mini-holes, *Geophys. Res. Lett.*, 15, 923, 1988.
- Noxon, J. F., Stratospheric NO₂ in the Antarctic winter, *Geophys. Res. Lett.*, 5, 1021, 1978.
- Noxon, J. F., Stratospheric NO₂: 2, Global behavior, *J. Geophys. Res.*, 84, 5067, 1979.
- Noxon, J. F., E. Marovich, and R. B. Norton, Effect of a major warming upon stratospheric NO₂, *J. Geophys. Res.*, 84, 7883, 1979.
- Noxon, J. F., W. R. Henderson, and R. B. Norton, Stratospheric NO₂: 3, The effects of large-scale horizontal transport, *J. Geophys. Res.*, 88, 5240, 1983.
- Oehlert, G.W., Trends in Dobson total ozone: an update through 1983, *J. Geophys. Res.*, 91, 2675, 1986.
- Oltmans, S. J., and J. London, The quasi-biennial oscillation in atmospheric ozone, *J. Geophys. Res.*, 87, 8981, 1982.
- O'Neill, A., and B. F. Taylor, A study of the major stratospheric warming of 1976/77, *Quart. J. Roy. Met. Soc.*, 105, 71, 1979.
- Ozone Trends Panel (R.T. Watson, M.J. Prather, and M.J. Kurylo et al.), *Present State of Knowledge of The Upper Atmosphere 1988: An Assessment Report*. NASA reference publ. 1208, available from the National Technical Information Service, Springfield, VA 22161, 1989.
- Parrish, A., R. L. de Zafra, M. Jaramillo, B. Connor, P.M. Solomon, and J. Barrett, Extremely low N₂O concentrations in the springtime stratosphere at McMurdo Station, Antarctica, *Nature*, 322, 53–55, 1988.
- Pick, D. R., and J. L. Brownscombe, Early results based on the stratospheric channel of TOVS on the TIROS-N series of operational satellites. International Council of Scientific Unions, Comm. Space Res., *Adv. Space Res.*, 1, 247, 1981.
- Plumb, R. A., *The Quasi-Biennial Oscillation, Dynamics of the Middle Atmosphere*, J.R. Holton and T. Matsuno, Eds., Reidel, Dordrecht, 1984.
- Plumb, R. A., and R. C. Bell, A model of the quasi-biennial oscillation on an equatorial beta plane, *Quart. J. Roy. Met. Soc.*, 108, 335, 1982.
- Podolske, J. R., M. Loewenstein, S. E. Strahan, and K. R. Chan, Stratospheric nitrous oxide distribution in the southern hemisphere, *J. Geophys. Res.*, 94, 16767, 1989.
- Pollack, J. B., and C. P. McKay, The impact of polar stratospheric clouds on the heating rates of the winter polar stratosphere, *J. Atmos. Sci.*, 42, 245, 1985.
- Pommereau, J. P., and F. Goutail, O₃ and NO₂ ground-based measurements by visible spectrometry during Arctic winter and spring, 1988, *Geophys. Res. Lett.*, 15, 891, 1988.
- Poole, L. R., Airborne lidar studies of Arctic polar stratospheric clouds, Ph.D. dissertation, University of Arizona, 1987.
- Poole, L. R., and M. P. McCormick, Airborne lidar observations of Arctic polar stratospheric clouds, Indications of two distinct growth stages, *Geophys. Res. Lett.*, 15, 21–23, 1988a.
- Poole, L. R., and M. P. McCormick, Polar stratospheric clouds and the Antarctic ozone hole, *J. Geophys. Res.*, 93, 8423–8430, 1988b.

- Poole, L. R., M. T. Osborn, and W. H. Hunt, Lidar observations of Arctic polar stratospheric clouds: Signature of small, solid particles above the frost point, *Geophys. Res. Lett.*, *15*, 867–870, 1988a.
- Poole, L. R., M. P. McCormick, E. V. Browell, C. T. Trepte, D. W. Fahey, K. K. Kelly, G. V. Ferry, R. Pueschel, and R. L. Jones, Extinction and backscatter measurements of Antarctic PSCs, 1987: Implications for particle and vapor removal, NASA CP-10014, 77–79, 1988b.
- Poole, L. R., S. Solomon, M. P. McCormick, and M. C. Pitts, Interannual variability of polar stratospheric clouds and related parameters in Antarctic during September and October, *Geophys. Res. Lett.*, *16*, 1157, 1989.
- Prather, M., M. M. Garcia, R. Suozzo, and D. Rind, Global impact of the Antarctic ozone hole: dynamical dilution with a 3-D chemical transport model, submitted to *J. Geophys. Res.*, 1989.
- Proffitt, M. H., J. A. Powell, A. F. Tuck, D. W. Fahey, K. K. Kelly, A. J. Krueger, M. R. Schoeberl, B. L. Gary, J. J. Margitan, K. R. Chan, M. Loewenstein, and J. R. Podolske, A chemical definition of the boundary of the Antarctic ozone hole, *J. Geophys. Res.*, *94*, 11437, 1989a.
- Proffitt, M. H., K. K. Kelly, J. A. Powell, M. R. Schoeberl, B. L. Gary, M. Loewenstein, J. R. Podolske, S. E. Strahan, and K. R. Chan, Evidence for diabatic cooling and poleward transport within and around the 1987 Antarctic ozone hole, *J. Geophys. Res.*, *94*, 16797, 1989b.
- Proffitt, M. H., M. J. Steinkamp, J. A. Powell, R. J. McLaughlin, O. A. Mills, A. L. Schmeltekopf, T. L. Thompson, A. F. Tuck, T. Tyler, R. H. Winkler, and K. R. Chan, In-situ ozone measurements within the 1987 Antarctic ozone hole from a high-altitude ER-2 aircraft, *J. Geophys. Res.*, *94*, 16547, 1989c.
- Pueschel, R. F., K. G. Snetsinger, J. K. Goodman, O. B. Toon, G. V. Ferry, V. R. Oberbeck, J. M. Livingston, S. Verma, W. Fong, W. L. Starr, and K. R. Chan, Condensed nitrate, sulfate and chloride in Antarctic stratospheric aerosols, *J. Geophys. Res.*, *94*, 11271, 1989.
- Quiroz, R. S., Stratospheric temperatures during solar cycle 20, *J. Geophys. Res.*, *84*, 2415, 1979.
- Ramaswamy, V., Dehydration mechanism in the Antarctic stratosphere during winter, *Geophys. Res. Lett.*, *15*, 863, 1988.
- Randel, W. J., The anomalous circulation in the Southern Hemisphere stratosphere during spring 1987, *Geophys. Res. Lett.*, *15*, 911–914, 1988.
- Randel, W. J., and P. Newman, Observations of stratospheric temperature changes coincident with the recent Antarctic ozone depletions, *Polar Ozone Workshop Abstracts*, NASA Conference Publications 10014, 10–12, 1988.
- Reinsel, G. C., G. C. Tiao, A. J. Miller, D. J. Wuebbles, P. S. Connell, C. L. Mateer, and J. L. DeLuisi, Statistical analysis of total ozone and stratospheric Umkehr data from trends and solar cycle relationship, *J. Geophys. Res.*, *92*, 2201, 1987.
- Reinsel, G. C., G. C. Tiao, S. K. Ahn, M. Pugh, S. Basu, J. L. DeLuisi, C. L. Mateer, A. J. Miller, P. S. Connell, and D. J. Wuebbles, An analysis of the 7-year record of SBUV satellite ozone data: Global profile features and trends in total ozone, *J. Geophys. Res.*, *93*, 1689, 1988.
- Ridley, B. A., M. McFarland, A. L. Schmeltekopf, M. H. Proffitt, D. L. Albritton, R. H. Winkler, and T. L. Thompson, Seasonal differences in the vertical distributions of NO, NO₂ and O₃ in the stratosphere near 50°N, *J. Geophys. Res.*, *92*, 11919, 1987.
- Rodriguez, J. M., M. K. W. Ko, and N. D. Sze, Chlorine chemistry in the Antarctic stratosphere: Impact of OClO and Cl₂O₂ and implications for observations, *Geophys. Res. Lett.*, *13*, 1292, 1986.
- Rodriguez, J. M., M. K. W. Ko, and N. D. Sze, Antarctic chlorine chemistry: possible global implications, *Geophys. Res. Lett.*, *15*, 257–260, 1988.
- Rodriguez, J. M., M. K. W. Ko, N. D. Sze, S. D. Pierce, J. G. Anderson, D. W. Fahey, K. K. Kelly, C. B. Farmer, G. C. Toon, M. T. Coffey, L. E. Heidt, W. L. Mankin, K. R. Chan, W. L. Starr, J. F. Vedder, and M. P. McCormick, Nitrogen and chlorine species in the spring Antarctic stratosphere: comparison of models with AAOE observations, *J. Geophys. Res.*, *94*, 16683, 1989.
- Rood, R. B., Global ozone minima in the historical record, *Geophys. Res. Lett.*, *13*, 1244, 1986.

POLAR OZONE

- Rosen, J. M., Simultaneous dust and ozone soundings over North and Central America, *J. Geophys. Res.*, **73**, 479, 1968.
- Rosen, J. M., D. J. Hofmann, and J. W. Harder, Aerosol measurements in the winter/spring Antarctic stratosphere, 2, Impact on polar stratospheric cloud theories, *J. Geophys. Res.*, **93**, 677-686, 1988a.
- Rosen, J. M., D. J. Hofmann, J. R. Carpenter, J. W. Harder, and S. J. Oltmans, Balloon-borne Antarctic frost point measurements and their impact on polar stratospheric cloud theories, *Geophys. Res. Lett.*, **15**, 859, 1988b.
- Rosen, J. M., S. J. Oltmans, and W. F. Evans, Balloon-borne observations of PSCs, frost point, ozone and nitric acid in the north polar vortex, *Geophys. Res. Lett.*, **16**, 791, 1989.
- Rosenfield, J. E., and M. R. Schoeberl, A computation of stratospheric heating rates and the diabatic circulation for the Antarctic spring, *Geophys. Res. Lett.*, **13**, 1339, 1986.
- Rossi, M. J., R. Malhotra, and D. M. Golden, Heterogeneous chemical reaction of chlorine nitrate and water on sulfuric acid surfaces at room temperature, *Geophys. Res. Lett.*, **14**, 127, 1987.
- Rowland, F. S., H. Sato, H. Khwaja, and S. M. Elliott, The hydrolysis of chlorine nitrate and its possible atmospheric significance, *J. Phys. Chem.*, **90**, 1985, 1986.
- Russell, J. M., S. Solomon, L. L. Gordley, E. E. Remsberg, and L. B. Callis, The variability of stratospheric and mesospheric NO₂ in the polar winter night observed by LIMS, *J. Geophys. Res.*, **89**, 7267, 1984.
- Salawitch, R. J., S. C. Wofsy, and M. B. McElroy, Chemistry of OClO in the Antarctic stratosphere: implications for bromine, *Planet. Space Sci.*, **36**, 213, 1988.
- Salawitch, R. J., G. P. Gobbi, S. C. Wofsy, and M. B. McElroy, Dentrification in the Antarctic stratosphere, *Nature*, **339**, 525, 1989.
- Sander, S. P., and R. T. Watson, Kinetics and mechanism of the disproportionation of BrO radicals, *J. Phys. Chem.*, **85**, 4000, 1981.
- Sander, S. P., and R. R. Friedl, Kinetics and product studies of ClO + BrO reaction: Implications for Antarctic chemistry, *Geophys. Res. Lett.*, **15**, 887, 1988.
- Sander, S. P., and R. R. Friedl, Kinetics and product studies of the reaction ClO + BrO using flash photolysis-ultraviolet absorption, *J. Phys. Chem.*, **90**, 4764, 1989.
- Sander, S. P., R. R. Friedl, and Y. L. Yung, Role of the ClO dimer in polar stratospheric chemistry: Rate of formation and implications for ozone loss, *Science*, **245**, 1095, 1989.
- Sanders, R. W., S. Solomon, M. A. Carroll, and A. L. Schmeltekopf, Visible and near-ultraviolet spectroscopy at McMurdo Station, Antarctica, 4. Overview and daily measurements of NO₂, O₃, and OClO during 1987, *J. Geophys. Res.*, **94**, 11381, 1989.
- Schmeltekopf, A. L., D. L. Albritton, P. J. Crutzen, P. D. Goldan, W. J. Harrop, W. R. Henderson, J. R. McAfee, M. McFarland, H. I. Schiff, T. L. Thompson, D. J. Hofmann, and N. T. Kjome, Stratospheric nitrous oxide altitude profiles at various latitudes, *J. Atmos. Sci.*, **34**, 729, 1977.
- Schmidt, U., R. Bauer, A. Khedim, E. Klein, G. Kulassa, and B. Schubert, In-situ observations of long-lived trace gases in the arctic stratosphere during winter, in *Proceedings of the Quadrennial Ozone Symposium*, 8-13 Aug, 1988, Gottingen, FRG, 1989.
- Schoeberl, M. R., A. J. Krueger, and P. A. Newman, The morphology of the Antarctic total ozone as seen by TOMS, *Geophys. Res. Lett.*, **13**, 1217, 1986.
- Schoeberl, M. R., R. S. Stolarski, and A. J. Krueger, The 1988 Antarctic ozone depletion. Comparison with previous year depletions, *Geophys. Res. Lett.*, **16**, 377-380, 1989.
- Schwentek, H., The sunspot cycle 1958/70 in ionospheric absorption and stratospheric temperature, *J. Atmos. Terr. Phys.*, **33**, 1829, 1971.
- Sekiguchi, Y., Antarctic ozone change correlated to the stratospheric temperature field, *Geophys. Res. Lett.*, **13**, 1202, 1986.
- Sekiguchi, Y., Ozone and stratospheric temperature change in Antarctica correlated to solar activity, *Proceedings of the Quadrennial Ozone Symposium*, Gottingen, FRG, 1989.

- Shi, G. Y., W. C. Wang, and M. K. W. Ko, Radiative heating due to stratospheric aerosols over Antarctica, *Geophys. Res. Lett.*, *13*, 1335, 1986.
- Shibasaki, K., N. Iwagami, and T. Ogawa, Stratospheric nitrogen dioxide observed by ground-based and balloon borne techniques at Syowa Station, *Geophys. Res. Lett.*, *13*, 1268, 1986.
- Shine, K. P., On the modelled thermal response of the Antarctic stratosphere to a depletion of ozone, *Geophys. Res. Lett.*, *13*, 1331, 1986.
- Shine, K. P., Comment on "Southern hemisphere temperature trends: A possible greenhouse effect," *Geophys. Res. Lett.*, *15*, 843–848, 1988.
- Simon, F. G., J. P. Burrows, W. Schneider, G. K. Moortgat, and P. J. Crutzen, Study of the reaction $\text{ClO} + \text{CH}_3\text{O}_2 \rightarrow \text{products}$ at 300 K, *J. Phys. Chem.*, in press, 1989.
- Simon, P. C., Solar irradiance between 120–400 nm and its variations, *Solar Phys.*, *74*, 273, 1981.
- Solomon, P. M., B. Connor, R. L. de Zafra, A. Parrish, J. Barrett, and M. Jaramillo, High concentrations of chlorine monoxide at low altitudes in the Antarctic spring stratosphere: Secular variation, *Nature*, *328*, 411, 1987.
- Solomon, S., The mystery of the Antarctic ozone hole, *Rev. Geophys.*, *26*, 131, 1988.
- Solomon, S., and R. R. Garcia, Simulation of NO_x partitioning along isobaric parcel trajectories, *J. Geophys. Res.*, *88*, 5497, 1983.
- Solomon, S., R. R. Garcia, F. S. Rowland, and D. J. Wuebbles, On the depletion of Antarctic ozone, *Nature*, *321*, 755, 1986.
- Solomon, S., G. H. Mount, R. W. Sanders, and A. L. Schmeltekopf, Visible spectroscopy at McMurdo Station, Antarctica, 2. Observations of OClO, *J. Geophys. Res.*, *92*, 8329, 1987.
- Solomon, S., G. H. Mount, R. W. Sanders, R. O. Jakoubek, and A. L. Schmeltekopf, Observations of the nighttime abundance of OClO in the winter stratosphere above Thule, Greenland, *Science*, *242*, 550, 1988.
- Solomon, S., R. W. Sanders, M. A. Carroll, and A. L. Schmeltekopf, Visible and near-ultraviolet spectroscopy at McMurdo Station, Antarctica, 5. Observations of the diurnal variations of OClO and BrO, *J. Geophys. Res.*, *94*, 11393, 1989.
- Stanford, J. L., and J. S. Davis, A century of stratospheric cloud reports: 1870–1972, *Bull. Am. Met. Soc.*, *55*, 213, 1974.
- Steele, H. M., P. Hamill, M. P. McCormick, and T. J. Swisler, The formation of polar stratospheric clouds, *J. Atmos. Sci.*, *40*, 2055, 1983.
- Stolarski, R. S., and R. J. Cicerone, Stratospheric chlorine: A possible sink for ozone, *Can. J. Chem.*, *52*, 1610, 1974.
- Stolarski, R. S., A. J. Krueger, M. R. Schoeberl, R. D. McPeters, P. A. Newman, and J. C. Alpert, Nimbus 7 satellite measurements of the springtime Antarctic ozone decrease, *Nature*, *322*, 808, 1986.
- Stolarski, R. S., and M. R. Schoeberl, Further interpretation of satellite measurements of Antarctic total ozone, *Geophys. Res. Lett.*, *13*, 1210, 1986.
- Stordal, F., I. S. A. Isaksen, and K. Hornveth, A diabatic circulation two-dimensional model with photochemistry: Simulations of ozone and long-lived tracers with surface sources, *J. Geophys. Res.*, *90*, 5757, 1985.
- Sze, N. D., M. K. W. Ko, D. K. Weisenstein, J. M. Rodriguez, R. S. Stolarski, and M. R. Schoeberl, Antarctic ozone hole: possible implications for ozone trends in the Southern Hemisphere, *J. Geophys. Res.*, *94*, 11521, 1989.
- Tarasenko, D. A., Structure and circulation of the stratosphere and mesosphere in the Northern Hemisphere, pp. 287, Hydrometizdat, Leningrad, 1988.
- Thomas, R. J., K. H. Rosenlof, R. T. Clancy, and J. M. Zawodny, Stratospheric NO_2 over Antarctica as measured by the Solar Mesosphere Explorer during austral spring, 1986, *J. Geophys. Res.*, *93*, 12561, 1988.

POLAR OZONE

- Tolbert, M. A., M. J. Rossi, R. Malhotra, and D. M. Golden, Reaction of chlorine nitrate with hydrogen chloride and water at Antarctic stratospheric temperatures, *Science*, 238, 1258, 1987.
- Tolbert, M. A., M. J. Rossi, and D. M. Golden, Heterogeneous interactions of ClONO₂, HCl, and HNO₃ with sulfuric acid surfaces at stratospheric temperatures, *Geophys. Res. Lett.*, 15, 851–854, 1988a.
- Tolbert, M. A., M. J. Rossi, and D. M. Golden, Antarctic ozone depletion chemistry: Reactions of N₂O₅ with H₂O and HCl on ice surfaces, *Science*, 240, 1018, 1988b.
- Toohey, D. W., W. H. Brune, and J. G. Anderson, Chemistry of the Antarctic stratosphere: Reactions of ClO and BrO. Paper presented at the Eighteenth International Symposium on Free Radicals, Oxford, England, September 10–15, 1987.
- Toohey, D. W., and J. G. Anderson, On the formation of BrCl in the reaction of BrO with ClO, *J. Phys. Chem.*, 92, 1705, 1988.
- Toon, G. C., and C. B. Farmer, Detection of HOCl in the Antarctic stratosphere, *Geophys. Res. Lett.*, 16, 1375, 1989.
- Toon, G. C., C. B. Farmer, L. L. Lowes, P. W. Schaper, J.-F. Blavier, and R. H. Norton, Infrared measurements of stratospheric composition over Antarctica during September 1987, *J. Geophys. Res.*, 94, 16571, 1989a.
- Toon, G. C., C. B. Farmer, P. W. Schaper, J.-F. Blavier, and L. L. Lowes, Ground-based infrared measurements of tropospheric source gases over Antarctica during 1986 austral spring, *J. Geophys. Res.*, 94, 11613, 1989b.
- Toon, O. B., P. Hamill, R. P. Turco, and J. Pinto, Condensation of HNO₃ and HCl in the winter polar stratosphere, *Geophys. Res. Lett.*, 13, 1284, 1986.
- Toon, O. B., R. Turco, and J. Jordan, Physical processes in polar stratospheric ice clouds. *Polar Ozone Workshop Abstracts*, 90–94, NASA Conference Publications 10014, 1988.
- Toon, O. B., R. P. Turco, J. Jordan, J. Goodman, and G. Ferry, Physical processes in polar stratospheric ice clouds, *J. Geophys. Res.*, 94, 11359, 1989.
- Trenberth, K. E., and J. G. Olson, Temperature trends at the South Pole and McMurdo Sound, in press, *J. Climate*, 1989.
- Trodahl, H. J., and R. G. Buckley, Ultraviolet levels under sea ice during the Antarctic spring, *Science*, 245, 194, 1989.
- Trolier, M., R. L. Mouldin, and A. R. Ravishankara, The rate coefficient for the termolecular channel of the self-reaction of ClO, submitted to *J. Phys. Chem.*, 1989.
- Tuck A. F., Synoptic and chemical evolution of the Antarctic vortex in late winter and early spring, 1987: An ozone processor, *J. Geophys. Res.*, 94, 11687, 1989.
- Tuck, A. F., R. T. Watson, E. P. Condon, and J. J. Margitan, The planning and execution of ER-2 and DC-8 aircraft flights over Antarctica, August and September, 1987, *J. Geophys. Res.*, 94, 11182, 1989.
- Tung, K. K., On the relationship between the thermal structure of the stratosphere and the seasonal distribution of ozone, *Geophys. Res. Lett.*, 13, 1308, 1986.
- Tung, K. K., M. K. W. Ko, J. M. Rodriguez, and N. D. Sze, Are Antarctic ozone variations a manifestation of dynamics or chemistry?, *Nature*, 333, 811, 1986.
- Tung, K. K., and H. Yang, Dynamic variability of column ozone, *J. Geophys. Res.*, 93, 11123, 1988a.
- Tung, K. K., and H. Yang, Dynamical component of seasonal and year-to-year changes in Antarctic and global ozone, *J. Geophys. Res.*, 93, 12537, 1988b.
- Turco, R. P., R. C. Whitten, and O. B. Toon, Stratospheric aerosols: Observations and theory, *Rev. Geophys. Space Phys.*, 20, 233, 1982.
- Turco, R. P., O. B. Toon, and P. Hamill, Heterogeneous physicochemistry of the polar ozone hole, *J. Geophys. Res.*, 94, 16493, 1989.
- Vaida, V., S. Solomon, E. C. Richard, E. Ruehl, and A. Jefferson, Photoisomerisation of OCIO: A polar ozone depletion mechanism, *Nature*, 342, 405, 1989.

- van Loon, H., and K. Labitzke, The southern oscillation, Part V: The anomalies in the lower stratosphere of the Northern Hemisphere in winter and a comparison with the quasi-biennial oscillation, *Mon. Wea. Rev.*, *115*, 357, 1987.
- Wahner, A., G. Tyndall, and A. R. Ravishankara, Absorption cross sections for OCIO as a function of temperature in the wavelength range from 240–480 nm, *J. Chem. Phys.*, *91*, 2734, 1987.
- Wahner, A., R. O. Jakoubek, G. H. Mount, A. R. Ravishankara, and A. L. Schmeltekopf, Remote sensing of daytime column NO₂ during the airborne Antarctic ozone experiment, *J. Geophys. Res.*, *94*, 16619, 1989a.
- Wahner, A., R. O. Jakoubek, G. H. Mount, A. R. Ravishankara, and A. L. Schmeltekopf, Remote sensing observations of nighttime OCIO column during the airborne Antarctic ozone experiment, *J. Geophys. Res.*, *94*, 11405, 1989b.
- Watson, L. R., J. M. Van Doren, P. Davidovits, D. R. Worsnop, M. S. Zahniser, and C. E. Kolb, Uptake of HCl molecules by aqueous sulfuric acid droplets as a function of acid concentration, submitted to *J. Geophys. Res.*, 1989.
- Watterson, I.G., and A.F. Tuck, A comparison of the longitudinal distributions of polar stratospheric clouds, total column ozone and temperatures for the 1987 Antarctic spring, *J. Geophys. Res.*, *94*, 16511, 1989.
- Williams, W. J., J. J. Kusters, and D. G. Murcray, Nitric acid column densities over Antarctica, *J. Geophys. Res.*, *87*, 8976, 1982.
- WMO, Atmospheric Ozone 1985: Assessment of Our Understanding of the Processes Controlling Its Present Distribution and Change, *WMO Report No. 16*, Sponsored by WMO, NASA, NOAA, FAA, UNEP, CEC, and BMFT, Washington, D.C., 1986.
- Wofsy, S. C., Temporal and latitudinal variations of stratospheric trace gases: A critical comparison between theory and experiment, *J. Geophys. Res.*, *83*, 364, 1978.
- Wofsy, S. C., M. J. Molina, R. J. Salawitch, L. E. Fox, and M. B. McElroy, Interactions between HCl, NO_x and H₂O ice in the Antarctic stratosphere: implications for ozone, *J. Geophys. Res.*, *93*, 2442–2450, 1988.
- Wolff, E. W., R. Mulvaney, and K. Oates, Diffusion and location of hydrochloric acid in ice: Implications for polar stratospheric clouds and ozone depletion, *Geophys. Res. Lett.*, *16*, 487, 1989.
- Wuebbles, D. J., F. M. Luther, and J. E. Penner, Effect of coupled anthropogenic perturbations on stratospheric ozone, *J. Geophys. Res.*, *88*, 1444, 1983.
- Yamazaki, K.: Observations of stratospheric final warmings in the two hemispheres, *J. Met. Soc. Japan*, *65*, 51–65, 1987.
- Yung, Y. L., J. P. Pinto, R. T. Watson, and S. P. Sander, Atmospheric bromine and ozone perturbations in the lower stratosphere, *J. Atmos. Sci.*, *37*, 339, 1980.
- Zawodny, J. M., Short-term variability of nitrogen dioxide in the winter stratosphere, *J. Geophys. Res.*, *91*, 5439, 1986.
- Zeller, E. J., G. A. M. Dreschoff, and C. M. Laird, Nitrate flux on the Ross ice shelf, Antarctica, and its relation to solar cosmic rays, *Geophys. Res. Lett.*, *13*, 1264, 1986.

N 9 2 - 1 5 4 3 2

509409

1248

GLOBAL TRENDS

Coordinator

G. Mégie (France)

Principal Authors

M.-L. Chanin (France)

D. Ehhalt (FRG)

P. Fraser (Australia)

J. F. Frederick (USA)

J. C. Gille (USA)

M. P. McCormick (USA)

G. Mégie (France)

M. Schoeberl (USA)

Other Contributors

L. Bishop (USA)

R. D. Bojkov (Switzerland)

W. Chu (USA)

J. J. DeLuisi (USA)

M. Geller (USA)

S. Godin (France)

N. R. P. Harris (USA)

W. J. Hill (USA)

R. D. Hudson (USA)

J. B. Kerr (Canada)

W. D. Komhyr (USA)

K. Kunzi (FRG)

K. Labitzke (FRG)

C. Mateer (Canada)

R. D. McPeters (USA)

A. J. Miller (USA)

R. M. Nagatani (USA)

G. C. Reinsel (USA)

G. C. Tiao (USA)

CHAPTER 2

GLOBAL TRENDS

TABLE OF CONTENTS

2.0	INTRODUCTION	163
2.1	OBSERVATIONAL METHODS RELEVANT TO TREND DETECTION	163
2.1.1	Introduction	163
2.1.2	Measurements Used in Current Trend Analyses	164
2.1.2.1	Total Ozone Measurements	164
2.1.2.2	Profile Measurements	168
2.1.3	Measurements for Future Trend Analyses	174
2.1.3.1	Total Ozone Measurements	175
2.1.3.2	Profile Measurements	177
2.1.4	Comparisons of Errors/Capabilities	181
2.1.4.1	Intercomparisons Relevant to Present Data	181
2.1.4.2	Intercomparisons Relevant to Future Trend Analyses	189
2.1.5	Temporal Sampling Requirements for Total Ozone Trend Detection	191
2.1.6	Concluding Remarks	192
2.2	TRENDS IN TOTAL OZONE	194
2.2.1	Introduction	194
2.2.2	Trend Analysis of Dobson Total Ozone Data	195
2.2.2.1	Result of the 1988 Ozone Trends Panel and Comparison with Other Studies	195
2.2.2.2	Sensitivity Analysis	204
2.2.2.3	Update of Trends into 1988	207
2.2.2.4	Summary of Dobson Analyses and Comparison with Theory	207
2.2.3	Analysis of Satellite-based Data from SBUV/TOMS Beginning in November 1978	210
2.2.3.1	Data Base and Analysis Procedure	210
2.2.3.2	Geographic Patterns of Ozone Change and Comparison with the Dobson Network	214
2.2.3.3	Conclusion of Satellite Data Analyses	219
2.3	TRENDS IN VERTICAL OZONE DISTRIBUTION	219
2.3.1	Introduction	219
2.3.2	Comparison of SAGE I and SAGE II Stratospheric Ozone Measurements	220
2.3.2.1	Zonal Means	221
2.3.2.2	Change in SAGE I and SAGE II Ozone Concentrations	223

GLOBAL TRENDS

2.3.3	Analysis of Umkehr Sonde Data	226
2.3.4	Analysis of Ozonesonde Data	231
2.3.5	Comparisons with Model Calculations	234
2.4	TRENDS IN STRATOSPHERIC TEMPERATURE	235
2.4.1	Introduction	235
2.4.2	Stratospheric Temperature Data Sets	235
2.4.2.1	Radiosondes	235
2.4.2.2	Rocketsondes	236
2.4.2.3	Satellites	236
2.4.2.4	Lidar	236
2.4.3	Intercomparison of Stratospheric Temperature Data Sets	237
2.4.3.1	Radiosonde, Rocketsonde, and Satellite Data	237
2.4.3.2	Comparison of Lidar Data with SSU and NMC	237
2.4.4	Influence of Solar Activity	239
2.4.5	Updating of Previously Used Data Sets	240
2.4.6	Comparison with Trends in Ozone Distribution	243
2.5	TRENDS IN TROPOSPHERIC GASES AND OZONE	244
2.5.1	Introduction	244
2.5.2	Halocarbons	245
2.5.2.1	CCl ₃ F, CCl ₂ F ₂ , CH ₃ CCl ₃ , CCl ₄	247
2.5.2.2	Other Chlorocarbons	247
2.5.2.3	Bromocarbons	250
2.5.3	Nitrous Oxide	250
2.5.4	Methane	252
2.5.5	Carbon Monoxide	253
2.5.6	Carbon Dioxide	256
2.5.7	Tropospheric Ozone	257
2.6	TRENDS IN STRATOSPHERIC AEROSOLS	261
2.6.1	Introduction	261
2.6.2	Stratospheric Aerosols	261
2.6.3	Global Heterogeneous Effects	262
2.7	SURFACE ULTRAVIOLET RADIATION	263
2.7.1	Predicted Trends Related to Column Ozone, 1970-1986	263
2.7.2	Observed Trends in Surface Ultraviolet Radiation	265
2.8	OUTSTANDING ISSUES	267
	APPENDIX 2.A	268
	REFERENCES	271

2.0 INTRODUCTION

Measuring trends in ozone, and most other geophysical variables, requires that a small systematic change with time be determined from signals that have large periodic and aperiodic variations. Their time scales range from the day-to-day changes due to atmospheric motions through seasonal and annual variations to 11-year cycles resulting from changes in the sun ultraviolet output. Aperiodic variations include the irregular quasi-biennial oscillation, with a period of roughly 26–28 months, approximately 4-year variations, and other sources of interannual differences.

Because the magnitude of all of these variations is not well known and highly variable, it is necessary to measure over more than one period of the variations to remove their effects. This means at least 2 or more times the 11-year sunspot cycle. Thus, the first requirement is for a long-term data record. The second related requirement is that the record be consistent; a small effect is being sought, and changes in instrumentation or data analysis method will obscure changes in the atmosphere. A third requirement is for reasonable global sampling, to ensure that the effects are representative of the entire Earth. Therefore, the various observational methods relevant to trend detection are reviewed in Section 2.1 to characterize their quality and time and space coverage. Available data are then examined for long-term trends or recent changes in ozone total content (Section 2.2) and vertical distribution (2.3), as well as in related parameters such as stratospheric temperature (2.4), source gases and tropospheric ozone (2.5), and aerosols (2.6). The relation between trends in total column ozone and variations observed in the solar ultraviolet radiation at the ground are discussed in Section 2.7, and outstanding issues in trends detection are emphasized in Section 2.8.

2.1 OBSERVATIONAL METHODS RELEVANT TO TREND DETECTION

2.1.1 Introduction

This section briefly describes the measurement techniques that have been used in the past or are expected to be used in the future to quantitatively measure trends in total ozone or the ozone vertical distribution. More detailed descriptions of these techniques have been presented elsewhere, in the Ozone Trends Panel Report (WMO, 1989, hereafter denoted OTP) and in previous reports (WMO, 1986; NASA, 1988), earlier ozone assessments, and in scientific journals and reports. The purpose of this section is to describe these observations briefly and to characterize their quality, as well as their time and space coverage.

For the individual measurements, the most critical quantity is stability, or the absence of time-dependent systematic errors. A systematic error, i.e., an error that is consistently present, is the amount by which the mean of a large number of individual observations of the same ozone value could differ from the “true” value. This is also referred to as the accuracy. The relevance of the accuracy to trend determination is further discussed in Section 2.1.6.

In the following sections, the term precision is used to refer to the random variations or spread of values that an instrument would report when observing a constant ozone value. It is sometimes referred to as repeatability, and depends on the random errors of the measuring system. This is important for many studies of atmospheric processes, and could be important for trend studies when only a few observations of a particular kind are available. However, most quantities compared in trend studies involve averaging a large amount of data, reducing the spread, so precision is often not of primary importance.

GLOBAL TRENDS

The section is organized as follows: Section 2.1.2 describes the measurements that have resulted in the data that have been used to derive trends, or closely related observations. The techniques that are expected to add to the trend data for future analyses are presented in Section 2.1.3. Both of these sections are divided into ground-based observations (including balloons or rockets launched from the ground) and satellite observations. Intercomparisons of different types of data, and what they indicate about the capabilities of the different techniques, are described in 2.1.4, which is divided into sections on present and future trend data. This portion of the chapter concludes with brief discussions of the sampling requirements in time and space (2.1.5) and an overview of trend-measuring capabilities (2.1.6).

2.1.2 Measurements Used in Current Trend Analyses

Measurements of ozone in the atmosphere have been made for many years. However, most of the data that have the length of record, accuracy, and stability to allow a search for trends only go back to about the time of the IGY (International Geophysical Year) in 1957. Figure 2.1-1 gives a time-line for the types of measurement that have been used for trend analyses, and the periods involved. These measurements are outlined below.

2.1.2.1 Total Ozone Measurements

Ground-based Measurements

Absorption spectroscopy affords a sensitive means for monitoring the column abundance of ozone from the ground. The attenuation of monochromatic radiation is related to the number of absorbing

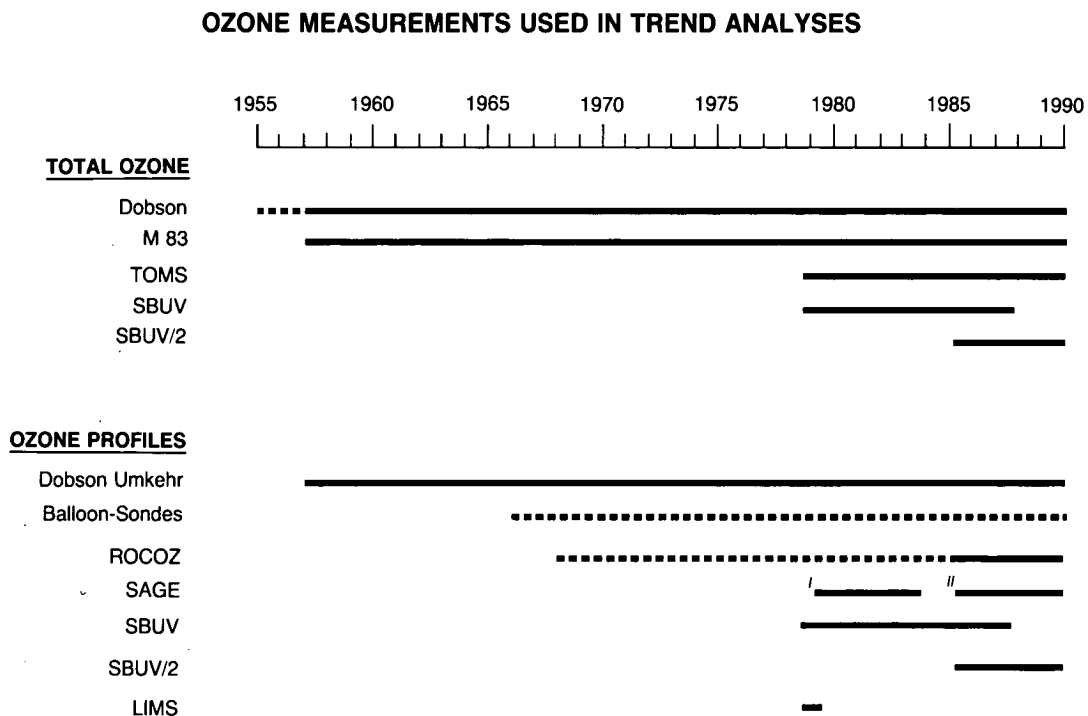


Figure 2.1-1. Time lines of measurements available for use in ozone trend analyses at the present time.

molecules in the optical path as they undergo state transitions that absorb incoming radiation. Absorption features in the ultraviolet and visible regions of the spectrum mainly involve electronic transitions and hence are generally relatively insensitive to temperature and pressure, which is a feature that considerably simplifies the reduction of the data to slant-column abundances.

The source of incoming light may be a celestial body, usually the sun, but also the moon, or a star, or it may be the light scattered from the sunlit zenith sky. Direct-light absorption measurements can be carried out only during clear periods from the ground, since an unobstructed view of the light source is required. Scattered light measurements can be obtained in cloudy weather by some absorption systems.

Dobson Spectrophotometer

The standard instrument in the Global Ozone Observing System is the Dobson spectrophotometer (Dobson, 1957). The instrument is a quartz double monochromator which measures the relative intensities of pair wavelengths in the Huggins ozone absorption band (300–350 nm) from which total ozone in a vertical column of the atmosphere can be deduced. Most precise observations are made on direct sunlight and standard double-pair wavelengths designated AD (305.5/325.4 and 317.6/339.8 nm). Less precise observations are made on clear or cloudy zenith skylight or, infrequently, moonlight. (For a more detailed description of the Dobson spectrophotometer and its operation, see OTP.) Direct sun AD observations generally provide the most precise measurements if the secant of the zenith angle, μ , is less than 3.

Long-term ozone measurement precision for the Dobson spectrophotometer, for annual means, is estimated to be 1% (at the 2σ level), based on the standard deviation σ from analyses of mean data from individual stations (WMO, 1980, 1981, 1982). Attainment of this precision requires that observations at all times be made on correct wavelengths; that changes in spectral characteristics of the instrument be accounted for using data derived from periodic standard lamp tests; that recalibration of the wedge be performed, if evidence suggests it is needed; that periodic recalibrations of the instrument be performed by the Langley method (Dobson and Normand, 1962) or through intercalibration with a primary standard Dobson instrument (Komhyr et al., 1989); that observational errors be minimized; that the temperature dependence of the ozone absorption coefficients be taken into account; and that relations derived empirically between direct sun and clear or cloudy zenith sky observations be adequately quantified. For use of the total ozone data in global trend analyses, it is necessary, furthermore, that observations be made on a sufficient number of days each month in order to obtain representative monthly mean data (see Section 2.1.5), and that the observations not be unduly influenced by local interfering absorbing species, such as sulfur dioxide and nitrogen dioxide or ozone produced photochemically in locally polluted air.

Until 1968, Dobson instrument calibrations at different stations were generally conducted randomly and independently. From 1974 onwards, increasing numbers of instruments have been modernized, refurbished, and calibrated by direct intercomparison with the WMO designated World Primary Standard Dobson Spectrophotometer No. 83, maintained at the World Dobson Spectrophotometer Central Laboratory in Boulder, Colorado. In subsequent intercomparisons, these instruments have shown typical calibration changes of 0–2% for direct sun observations on AD wavelengths. The long-term (1962–1987) ozone measurement stability of Primary Standard Dobson Instrument No. 83 is reported to have been maintained at $\pm 0.5\%$ (Komhyr et al., 1989). Since the mid-1970s, virtually all (90) Dobson instruments of the global Dobson instrument station network have been calibrated several times either directly with instrument No. 83 or indirectly through intercalibrations with Secondary Standard Dobson spectrophotometers calibrated in Boulder in 1977.

GLOBAL TRENDS

The uneven geographical distribution of the existing Dobson spectrophotometer network (Figure 2.1-2) gives rise to a spatial sampling error when attempts are made to determine global ozone content and trends. At most, the Dobson instruments can provide trend information for specific regions of the globe. An important utility of the Dobson instruments is their ability to provide correlative data for satellite instruments that measure ozone on a global scale (Fleig et al., 1986; 1989a; 1989b; Bojkov et al., 1988; McPeters and Komhyr, 1989), but that are subject to calibration drifts and are not highly sensitive to tropospheric ozone.

Filter Ozonometers M-83 and M-124

Since 1957, routine ground-based total column ozone measurements have been made at more than 40 stations in the USSR using a filter ozonometer instrument designated as type M-83 (not to be confused with the Standard Dobson ozone spectrophotometer, which was the 83rd instrument manufactured of the Dobson type). The filter-type instrument is based upon the same principle as the Dobson spectrophotometer in using differential absorption of ultraviolet radiation in the 300–350 nm Huggins band of ozone. The M-83 instrument, however, uses two broadband filters and measures the relative attenuation of the solar ultraviolet radiances either directly from the sun or indirectly from the zenith sky (Gustin, 1963).

Direct intercomparisons between M-83 filter instruments and Dobson spectrophotometers prior to 1971 (Bojkov, 1969) revealed that the M-83 records show 6% less ozone when the observations are restricted to an air mass $\mu < 1.5$, and 20% to 30% more ozone when data are taken for $\mu > 2.0$. A strong dependence

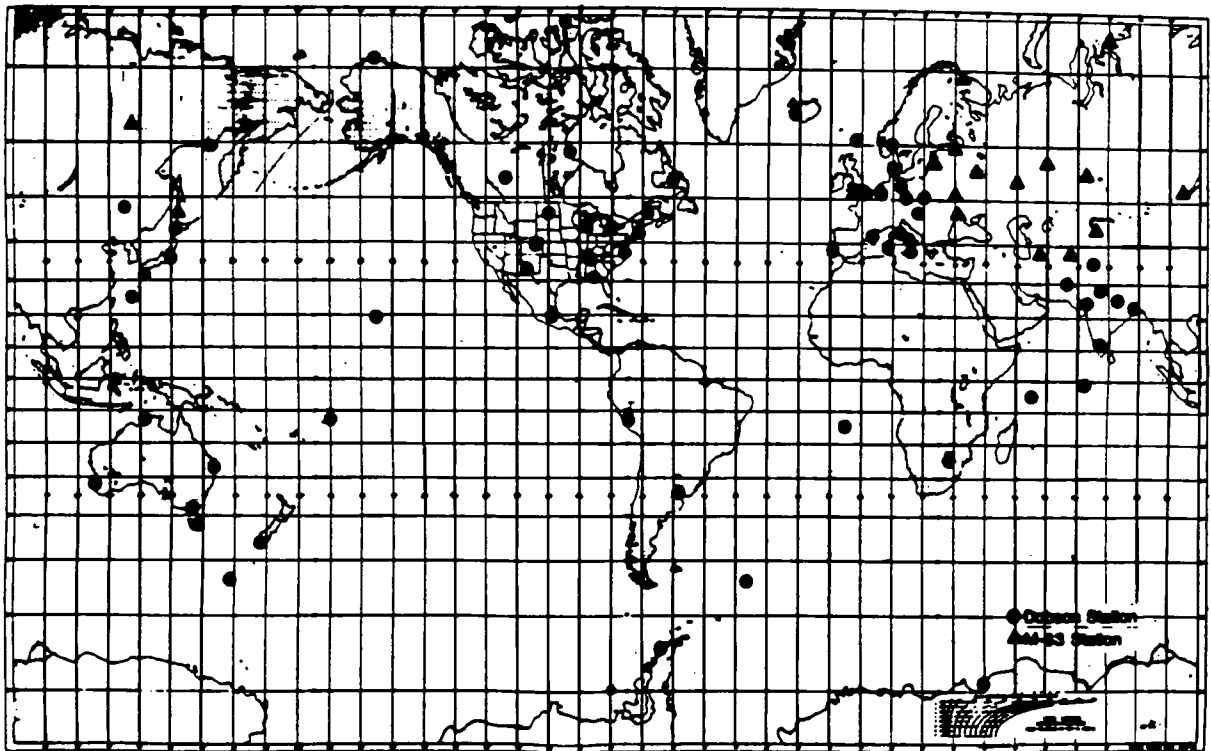


Figure 2.1-2. Location of Dobson (●) and M-83 (▲) stations.

on turbidity was also detected, with 9% to 14% higher ozone readings when the surface visibility was less than 5 km. These strong deviations for $\mu > 2.0$ make many of the high-latitude measurements in the USSR very uncertain, especially for measurements prior to 1972, as described below.

Improved filters were introduced into the M-83 instrument starting in 1972–1973 (Gustin, 1978). The new filters have maximum transmittance at 301 nm and 326 nm, and their band passes are less than those in the earlier version: 22 nm (291–312 nm) and 15 nm (319–334 nm). Comparison of Nimbus-4 BUV satellite overpasses over M-83 stations in the USSR demonstrated a standard deviation of about 50 Dobson Units before 1973, and about 25 DU afterward (WMO, 1980, 1983). The Nimbus-4 BUV overpasses of Dobson stations maintained a standard deviation of about 17 DU during the 1970–1977 lifetime of the satellite.

A much newer, reportedly improved instrument designated as M-124 has been installed in many stations since 1986 (Gustin and Sokolenko, 1985), but no ozone data have been reported yet for this instrument. No trend data with the M-124 can be expected for about a decade unless the data can be satisfactorily cross-calibrated with the M-83 data from the same location.

Satellite observations

Total Ozone Monitoring Spectrometer (TOMS)

The TOMS, launched on the Nimbus-7 spacecraft in 1978, is an instrument (Heath et al., 1975) whose primary measurement goal is to obtain contiguous mapping of the total column ozone amount over the globe (Bowman and Krueger, 1985; Schoeberl et al., 1986). To achieve this, TOMS step scans across the sub-orbital track, sampling radiation backscattered from the underlying surface and atmosphere. Ozone column amounts are inferred by utilizing the wavelength dependence of the Earth's ultraviolet albedo in the Huggins band of the ozone absorption spectrum. The TOMS raw data are measurements of the direct and backscattered solar UV radiation at six fixed wavelength channels (312.5, 317.5, 331.2, 339.8, 360, and 380 nm). Data from the first four channels are used in pairs to provide three estimates of the total column ozone amount by the differential absorption method. The remaining two channels, which are free of ozone absorption, are used to determine the effective background albedo.

It was recognized from the outset that this technique was intrinsically capable of very high accuracy and stability, since the requirement was for a relative measurement of the ratio of Earth's backscattered UV radiance to the solar UV irradiance at the same wavelength. Because both measurements could in principle be made with the same instrument, the determination of albedo as a function of wavelength should not depend on either the absolute calibration of the instrument nor on long-term variations in the sensitivity of the instrument. However, a serious uncertainty is introduced by the use of the diffuser plate, which is not common to both measurements but only used to transform the solar irradiance into a radiance that is comparable in magnitude to the backscattered Earth radiance, and can be measured in the same manner. Observations of the solar irradiance indicated that the diffuser plate was degrading and becoming less reflective with time. Cebula et al. (1988) developed a model of the diffuser and instrument degradation, which was adopted by the Ozone Processing Team (OPT). Application of this model in the reduction of the TOMS data led to a downward drift of the TOMS results compared to those of the ground-based Dobson network (see above) reported by Fleig et al. (1986, 1989a), Bojkov et al. (1988).

Extensive analysis reported by the Trends Panel indicated that the OPT model had large uncertainties and had almost certainly underestimated the true diffuser plate degradation. The errors were large enough to allow agreement with the Dobson data. Subsequently, some results for trends in total ozone in the

GLOBAL TRENDS

Trends Report were based on normalizing the TOMS data to the Dobson values. This allows extension to global coverage, but is at best only an approximation and provides no independent information from TOMS on the trends.

Subsequently, a major advance in the analysis of the TOMS data has been made. Bhartia et al. (1989) pointed out that, for the related Solar Backscatter Ultraviolet (SBUV) experiment, there was a wavelength at 305.8 nm whose data could be used with those from the SBUV 312.5 nm channel to form a new "D pair." Results from this pair are less sensitive to diffuser degradation for two reasons. First, the degradation varies with wavelength, but the D pair wavelengths are only 6.7 nm apart, compared to the 18.7 for the A pair. In addition, because the difference in ozone absorption coefficients is larger for the D pair than for the other pairs, results are estimated to be only 0.22 times as sensitive to diffuser drift than the archived values, which are based on a latitude-dependent weighted sum of the A, B, and C pairs. Because of the large absorption coefficients, D pair values can only be obtained in the tropics, where the total column amount is small, but a comparison showed that they follow the Dobson values much more closely than the archived values do. This provides confirmation that the archived data are in error, as well as strong corroboration that the error mechanism has been identified (Bhartia et al., 1989; Hudson et al., 1989, private communication).

Generalizing from these insights, McPeters et al. (1989, private communication) have developed the "pair justification" method. The basis is that different pairs have different sensitivity to diffuser degradation errors, resulting in a drift between pairs than can be measured accurately. By requiring that all pairs obtain the same total ozone result, and assuming that the uncorrected diffuser degradation is approximately linearly dependent on wavelength, a unique determination of the total ozone is obtained that is independent of diffuser degradation. The implementation makes use of pairs denoted A, B, and C (312.5/331.2; 317.5/339.8; 331.2/339.8 nm). There appears to be a fundamental limit of 0.5–1.0% per decade to the stability that can be obtained. Test results are described in Section 2.1.4.

Solar Backscatter Ultraviolet Spectrometer

The Solar Backscatter Ultraviolet (SBUV) spectrometer (described below in Section 2.1.2.2) also measures the solar ultraviolet radiation that is backscattered by the Earth and atmosphere. Data from four of its wavelength channels, which are the same as four of the TOMS channels, are used in the same way to determine total ozone amounts, but only in the nadir directly below the spacecraft. SBUV ozone values are systematically slightly lower than those from TOMS, but they vary with time in the same way. Because SBUV also relies on the same diffuser plate, its total ozone values have also decreased with time due to diffuser degradation.

2.1.2.2 Profile Measurements

Ground-based Measurements

Standard Dobson Umkehr

The Dobson instrument can also be used to obtain information on the vertical distribution of ozone. Measurements of the downward scattered radiation at two wavelengths are made for solar zenith angles Z from 60–86.5 degrees. From the ratio of these radiances as a function of Z , which reverses for Z near 90 degrees, the vertical profile can be inferred. (The method takes its name from the German word for a reversal.) The solution is usually given in terms of the layer mean ozone partial pressure (nb) of ozone in layers about 5-km thick, but with layer 1, the troposphere, about 10-km thick.

Although the retrieval provides data for Umkehr layers 1 through 9 (0–48 km), the averaging kernels for the present standard algorithm indicate that only data for layers 4 to 8 (19–43 km) should be used for trend analysis, while other layers should be used with caution. The vertical resolution of the retrieval for these layers is from 11 to 14 km. The systematic uncertainty or bias is estimated to be 15–20% in the OTP, and 5–12% by DeLuisi et al. (1989a). Random errors, due to the dependence of the ozone absorption coefficients on the varying temperature, tropospheric and stratospheric aerosols, thin clouds invisible from the surface, and instrumental effects, are of the order of 5–10%, some of which could be reduced by monitoring the clarity of the zenith sky. Neither the systematic nor random errors should seriously affect estimation of long-term trends. Trend estimation will be affected by instrument drifts, by changes in calibration, by stratospheric aerosols, and by real atmospheric temperature trends. Calculations indicate that realistic temperature trends ($< 2^{\circ}\text{C}/\text{decade}$) will induce errors $< 0.2\%/\text{decade}$ in ozone trends for layers 4 through 8 (Figure 3-12, Chapter 3, OTP). Serious errors from stratospheric aerosols are easily recognized in the data and such contaminated data may be edited out before trend estimation. Moderate and smaller errors may be adequately corrected by the methods of DeLuisi et al. (1989a) or by statistical methods using proxy data (Reinsel et al., 1989). Finally, instrumental factors may be handled by statistical methods (e.g., sudden calibration changes as by Reinsel et al., 1989) or by re-evaluation of the observations using new calibration data.

To reduce the time required for an Umkehr measurement, the Short method was developed and tested by Mateer and DeLuisi (1984). This method uses the A-C-D Dobson wavelength pairs in place of the C pair that is used for the Standard Umkehr method. By using the triple pair, ozone profile information is obtained when measurements are made during a solar zenith angle change of 80 to 89 degrees. In contrast, the C pair Standard Umkehr method that has provided most of the past data requires a solar zenith angle change of 60 to 90 degrees. An exploratory ozone profile retrieval algorithm for the Short Umkehr has been developed for testing. An operational algorithm will be developed after the present Standard Umkehr algorithm (Mateer and Duetsch, 1964) has been updated.

Although Umkehr observations date back to the 1930s, the current Umkehr profile archive at the World Ozone Data Centre (viz., retrievals using the present standard C-Umkehr algorithm) begins about the time of the IGY (ca. July 1957). The archive comprises over 35,000 ozone profile retrievals for some 68 stations, uniformly processed using the standard retrieval algorithm (Mateer and Duetsch, 1964). For 26 of these stations, the entire station record consists of fewer than 100 profiles. Reinsel et al. (1984), found only 13 stations with a sufficient number of observations and length of record for use in their trend analyses, while Reinsel et al. (1989) only used 10. One of the stations, Mont Louis, no longer makes observations. The record of Aspendale (the only Southern Hemisphere station in the trend set) ends in 1982. From 1983 onward the record is being continued at Melbourne, 25 km away. The remaining trend stations cover the latitude range from 24 to 53° North.

It appears that additional stations, especially those in the Automated Dobson Network (Komhyr et al., 1985), will have a sufficient number of observations and length of record to be used for trend estimation within the next 5 years. There are presently seven automated Dobson instruments that routinely obtain Standard and Short Umkehr measurements. These instruments were developed by NOAA/GMCC (Komhyr et al., 1985) and are located at Perth (Australia); Lauder (New Zealand); Huancayo (Peru); Mauna Loa (Hawaii); Boulder, Colorado (United States); Haute Provence (France); and Fairbanks, Alaska (United States). The frequency of Umkehr measurements is significantly increased by the automated Dobson because observers are not required, and a shorter observing time (for the Short Umkehr) decreases the chance of cloud interference. Ancillary measurements of sky conditions are also made at the automated Dobson sites. These measurements consist of zenith-sky clouds and turbidity. In addition, lidar measure-

GLOBAL TRENDS

ments of stratospheric aerosols for correcting errors to the Umkehr profiles (DeLuisi et al., 1989a) are routinely made at Mauna Loa, Boulder, and Haute Provence.

Balloon Ozonesondes

Balloon ozonesondes are compact, lightweight, balloon-borne instruments flown with standard meteorological radiosondes for measurement of ozone, air pressure, and air temperature up to altitudes of about 30 km. Regener (1960, 1964) developed a very fast response chemiluminescent ozonesonde, but these instruments often exhibited considerable variations in sensitivity to ozone (which was later corrected). Thus, while an early measurement program provided a great deal of useful information on the ozone climatology over the North American continent, the variable response characteristics associated with the measurements and the relative shortness of the record render the data unsuitable for ozone trend studies in the troposphere and stratosphere.

Brewer and Milford (1960) described an electrochemical ozone detector employing the well-known oxidation of potassium iodide (KI) by ozone as the basic reaction. Subsequently, Griggs (1961) investigated the physical and chemical aspects of a similar balloon-borne instrument commonly referred to as the Brewer "bubbler" ozonesonde. Versions of the instrument are manufactured in the United States, G.D.R., and India. Because the air pumps of the Brewer ozonesondes are lubricated with a thin film of oil that may destroy ozone, they must be conditioned with ozone prior to flight time to minimize the ozone destruction. With proper conditioning, ozone losses can be kept to a few percent, as has been the case at Hohenpeissenberg Observatory (F.R.G.). A few soundings from routine ozone measurement programs conducted in past years, however, have exhibited ozone losses, in extreme cases of up to 50%. Improvement in data quality is achieved through normalization of all soundings to Dobson spectrophotometer total ozone. The normalization factor for any sounding is a constant by which ozone values at all altitudes are multiplied. Use of a constant multiplication factor for normalization may, however, not be justified for soundings that exhibit large ozone losses within the instrument (Hilsenrath et al., 1986). Brewer ozonesonde data having normalization factors that range from 0.95–1.25 are generally acceptable; in an analysis later in this chapter the range 0.9–1.2 is used. The average correction factor for more than 1,000 ozonesondes flown over 20 years at Hohenpeissenberg is 1.07. Other uncertainties associated with ozone measurements with Brewer ozonesondes stem from variations in pump air flow rates above 10 mb, particularly for lightly lubricated pumps that become "dry" after several hours of operation. Build-up of AgI on the platinum anode during operation may also affect sensor performance. The significance of errors due to these effects has not been adequately assessed.

A considerable amount of useful atmospheric ozone vertical distribution data has nevertheless been obtained with the Brewer ozonesondes. The data are suitable for ozone trend analyses, particularly from stations that have maintained unchanged instrument preflight conditioning and test procedures throughout the entire measurement program.

Komhyr (1969) developed an electrochemical concentration cell (ECC) ozonesonde utilizing the reaction of ozone with KI, but with platinum cathode and anode electrodes contained in separate sensor chambers connected by an ion bridge. This sensor evolved from a carbon-iodine (CI) ozonesonde (Komhyr, 1964) that is no longer in use in the United States, but continues to be used in Japan. Because the chemical composition of the electrodes of the ECC sensor remain unchanged during operation, the sensor can be used indefinitely without deterioration of performance. The ECC sonde incorporates a miniature air pump fabricated from Teflon reinforced with glass fibers. The pump is not lubricated, so that minimal conditioning with ozone is required to prevent ozone loss within it. Early versions (type 3A) of the ECC ozonesonde

employed a pump of rectangular cross section. Because of non-uniformity of manufacture, some of the pumps exhibited excessive leakage at pressure altitudes above 15 mb, which in extreme cases have been underestimating the ozone by more than 15%. A newer instrument version (type 4A) employs a Teflon pump of circular cross section with external O-ring seals that is claimed to render the pumps and instruments suitable for use at higher altitudes.

ECC ozonesondes using a 1% KI cathode electrolyte yield measured total ozone amounts that agree closely with Dobson spectrophotometer total ozone. For example, for 525 soundings made by NOAA since 1984 over a wide range of operating conditions, from the tropics to the polar regions, the mean ECC sonde-Dobson spectrophotometer total ozone normalization factor was 1.01 ± 0.05 (1σ) (Komhyr et al., 1989). ECC ozonesondes are, therefore, suitable for use at stations where independent measurements of total ozone are not available, e.g., in polar regions during the polar night.

Ozone measurement uncertainty for ECC sondes is estimated to be $\pm 10\%$ in the troposphere, $\pm 5\%$ in the stratosphere up to 10 mb, with the uncertainty increasing to $20 \pm 5\%$ at 3 mb (Hilsenrath et al., 1986). Two ECC ozonesondes flown with an ozone UV-photometer during the MAP-GLOBUS campaign of 1983 (Aimedieu et al. 1987) gave ozone values that differed from the photometer values by $2.1 \pm 1.1\%$ at 8.1 ± 1.1 mb, and by $-0.6 \pm 3.0\%$ at 3.9 ± 0.4 mb. The low ozone values measured above 10 mb, if real, may stem from application during data processing of inadequate pump efficiency corrections. Variability in the data at these altitudes is attributable at least in part to variations in manufacture of the pump components. It must be pointed out that small, continuing improvements over the years have led to more accurate measurements, but they may also result in spurious indications of trends.

Rocket ozonesondes

Over the last 2 to 3 decades, several groups in various countries have developed and used rocket-sondes. In the USSR, rocket optical ozonesondes (Brezgin et al. 1977) and chemiluminescent sondes (Konkov and Perov, 1976; Perov and Khrgian, 1980; Perov and Tishin, 1985) have been introduced. A solar photometer (Subbaraya and Lal, 1981) and another optical sonde (Somayajulu et al., 1981) have been developed in India. However, the longest data record has been collected in the United States by the ROCOZ and ROCOZ-A systems, which are described here.

The ROCOZ-A ozonesonde is a four-filter, sequential-sampling, ultraviolet radiometer. The instrument was originally developed for stratospheric soundings aboard an ARCAS rocket (Kreuger and McBride, 1968a,b). This instrument was subsequently modified for launch aboard a smaller diameter Super-Loki launch vehicle. In 1982, an instrument improvement program was initiated at NASA's Goddard Space Flight Center/Wallops Flight Facility (WFF). Changes were made to the center wavelengths and spectral shapes of the ultraviolet filters. An integrated calibration facility was established (Holland et al., 1985), and new data reduction procedures were designed (Barnes et al., 1986). A description of the present design of the radiometer has been published by Barnes and Simeth (1986). Because of the short data record of the present instrument, these data are not directly applicable to trend studies at this time.

The ROCOZ-A ozonesonde is propelled aloft by a Super-Loki booster rocket. At rocket burnout, the instrument and its carrier coast to a nominal apogee of 70 km, where the payload is ejected for deployment on a parachute. The radiometer measures the solar ultraviolet irradiance over its filter wavelengths as it descends through the atmosphere. The amount of ozone in the path between the radiometer and the sun is then calculated from the attenuation of solar flux as the instrument falls. In addition, radar from the launch site measures the height of the payload throughout its descent. Finally, knowledge of the solar zenith angle

GLOBAL TRENDS

allows calculation of the fundamental ozone value measured by the radiometer; that is, ozone column amount as a function of geometric altitude. Ozone number density is the derivative of ozone column amount versus altitude. Combined with auxiliary atmospheric soundings for pressure and temperature, ROCOZ-A can duplicate the fundamental ozone values of backscatter ultraviolet (Barnes, 1988) and solar occultation measurements (Cunnold et al., 1989) from satellites. ROCOZ-A comparisons have also been made with the ultraviolet spectrometer on the SME satellite (Barnes et al., 1987b).

Details of the measurements of the precision of ROCOZ-A ozone column amounts and ozone number densities have been published (Holland et al., 1985; Barnes et al., 1986). In addition, there are published results from an equatorial ozone measurement campaign (Barnes et al., 1987a) that found very low variability in stratospheric ozone, temperature, and pressure. From the results of this campaign, it is possible to estimate the precision of the remaining measurements in the ROCOZ-A data set. The full set of precision estimates for ROCOZ-A is given in Barnes et al. (1989). For ozone number densities and mixing ratios, the profile-to-profile repeatability of ROCOZ-A measurements is estimated at 3 to 4%.

The estimates of the accuracy of the ROCOZ-A profiles are also given in Barnes et al. (1989). For ROCOZ-A ozone amount, the accuracy estimates come from an internal, unpublished error analysis. The analysis is based on errors of the effective ozone absorption coefficients used to convert the radiometer readings into ozone profiles, plus the differences between the ozone values at altitudes where two ROCOZ-A channels give simultaneous readings (Barnes et al., 1986). A laboratory flight simulator, based on long pathlength photometry (DeMore and Patapoff, 1976; Torres and Bandy, 1978), has been constructed to measure the accuracy of ROCOZ-A ozone readings. Publication of a detailed error analysis will follow the conclusion of experiments with the simulator. It will complete the primary characterization of the ROCOZ-A ozonesonde. ROCOZ-A ozone number densities and ozone mixing ratios are estimated to be accurate to 5 to 7% and 6 to 8%, respectively.

The vertical resolution of ROCOZ-A ozone profiles is 4 km (Barnes et al., 1986). This resolution comes from the data reduction algorithm for the profiles, since measurements from the instrument are less than 100 meters apart during flight. ROCOZ-A ozone column amounts are smoothed before differentiation for ozone density. The vertical resolution of the smoothed profiles has been adjusted to roughly match the 8-km resolution quoted for the two limb scanning instruments on the Solar Mesospheric Explorer (Rusch et al., 1984), and the 1- to 5-km vertical resolution for SAGE II (Mauldin et al., 1985b).

Satellite Observations

The Stratospheric Aerosol and Gas Experiment (SAGE I and II)

SAGE I and SAGE II are both satellite-borne multi-wavelength radiometers employing solar extinction (occultation) techniques to measure stratospheric aerosols and gases. Ozone profiles are determined from measurements of attenuation of solar radiation by ozone in the most intensely absorbing portion of the Chappuis band, at 600 nm. SAGE I was launched aboard the dedicated Applications Explorer Mission-2 in February 1979 and operated for 34 months until November 1981, when the spacecraft electrical system failed. SAGE II was launched on the Earth Radiation Budget Satellite in October 1984, and has operated continuously since then. Both SAGE I and SAGE II are in approximately 600 km circular orbits with inclination angles of 56 and 57 degrees, respectively, such that the latitudinal coverage is almost identical. Detailed descriptions of the instruments are given by McCormick et al. (1979), and Mauldin et al. (1985a,b).

The capabilities of the two instruments are not identical because of small differences in the instrument configurations and data processing algorithms.

In the solar occultation technique, measurements are made of the solar radiation transmitted through the atmosphere as the sun sets (or rises) behind it relative to the spacecraft. The transmission for a given ray path is the ratio of the signal strength for that ray path to the signal when the sun is above the atmosphere. The vertical distribution of ozone is determined from the changes in the transmission. Other wavelengths allow the concentrations of other gases and aerosols to be determined; the aerosol effects on the ozone transmittance may then be corrected. The retrieval algorithms are described in the OTP, Ch. 3, or in Chu and McCormick (1979), Mauldin and Chu (1982), and by Chu (1986). Because of the high signal-to-noise ratio, a vertical resolution of 1 km is achieved in the stratosphere.

It is important to note that the measurements performed by the SAGE instruments are self-calibrating, in that only relative radiance measurements are required to determine the transmission and, therefore, the distribution of atmospheric species such as ozone. Consequently, no absolute radiance calibration is necessary. The only requirement is that the instrument retain constant responsivity for the duration of each spacecraft sunrise or sunset, usually about 100 seconds. However, the position of the line of sight must be accurately known, which requires very accurate data on the position of the spacecraft during the observing events and a reasonably stable spacecraft. The OTP analysis indicates that absolute accuracy of the ozone values determined by SAGE I and SAGE II is about 6 to 9%, depending on altitude. However, the stability, or ability to detect changes, was 2 to 7% for SAGE I, and 1.3 to 4% for SAGE II. The uncertainty in the difference between SAGE I and SAGE II ozone values allow changes of 2% over the several years between their observing periods to be detected from 25 to 45 km.

A limitation of the occultation technique is the relatively small amount of data obtained, two vertical profiles per orbit, and the changing location of the observed latitudes, rendering comparisons between occultation instruments difficult. The ozone trends detection uncertainty estimated above for the SAGE I and II ozone data do not include errors caused by the undersampling of the natural variability of the ozone distribution in both the spatial and temporal domains.

Ozone data from SAGE II between November 1984 to November 1988 have been archived at the National Space Science Data Center (NSSDC). The SAGE I ozone data have also been archived at NSSDC. Reprocessing of the SAGE I ozone data using the updated temperature correction information from NOAA-NMC has been performed for the ozone trends study, and the data are currently being rearchived at NSSDC. The new temperature data introduce only small differences at high altitudes in the low-latitude regions.

Solar Backscatter Ultraviolet Spectrometer (SBUV)

The SBUV is a downward viewing double monochromator that was launched on the Nimbus-7 spacecraft in 1978 to measure the UV albedo of the atmosphere and surface for the purpose of determining the vertical profile of ozone, in addition to total ozone. Singer and Wentworth (1957) suggested that observations from above the atmosphere, in which the fraction of sunlight reflected back to space (the planetary albedo) is measured as a function of wavelength, could be used to deduce the concentration of ozone as a function of pressure (i.e., altitude). Other experiments utilizing the same principle have flown on Kosmos-65, OGO-4, Nimbus-4, Atmospheric Explorer D, and most recently, NOAA-9 and the Japanese OHZORA satellite.

GLOBAL TRENDS

The SBUV made measurements in 12 wavelength channels, located at (in nm) 255.5, 273.5, 283.0, 287.6, 292.2, 297.5, 301.9, 305.8, 312.5, 317.5, 331.2, and 339.8. Measurements in the channel at 255.5 nm were not used because they were contaminated by NO fluorescence; the next seven were used for extracting profile information, while the last four (which are common with TOMS) are used to determine the total ozone. The solutions are given in terms of ozone amounts within the Umkehr layers. The analysis presented in the OTP shows that only data in layers 6 to 9 (approximately 28 to 48 km) are independent and reliable for trend studies. The vertical resolution of the solutions is 8 to 10 km.

Again, in principle, this technique requires only the measurement of the ratio of the backscattered Earth radiance to the solar irradiance, with the attendant insensitivity to calibration accuracy and stability, but the use of a diffuser plate involves another optical element in the measurement of the solar irradiance which eliminates this advantage. On Nimbus-7, SBUV and TOMS shared the same diffuser plate. SBUV observations of the solar irradiance also showed that the diffuser plate was degrading with time, most rapidly at the shortest wavelengths. The diffuser model of Cebula et al. (1988) was developed from the SBUV observations and used by the OPT for the SBUV data reduction also. The archived results showed very large (25%) downward ozone changes in the upper stratosphere over 8 years, which was the reason for the original appointment of the Ozone Trends Panel. In this case also, it was found that the uncertainties in the diffuser model were much larger than expected, and that the changes in the stratosphere were probably smaller than indicated by the archived data and could even be slightly positive. In this case, the D pair again supports the assertion that the degradation is larger than predicted by the model, but there has been no method developed to date for finding an independent determination of the diffuser degradation at the shorter wavelengths. Thus, at the moment the SBUV data can provide no independent information on long-term trends in the ozone profile (see OTP).

Limb Infrared Monitor of the Stratosphere

The Limb Infrared Monitor of the Stratosphere (LIMS) is a six-channel limb scanning infrared radiometer that also was launched on Nimbus-7 in 1978 (Gille and Russell, 1984; OTP). This type of instrument measures the infrared radiation emitted by atmospheric molecules as the instrument scans across the limb. Because of the geometry, this technique has an inherently high vertical resolution and the ability to sound to high altitudes. Because it measures infrared emission, it can obtain measurements at all local times, resulting in very dense coverage. LIMS obtained ozone data from 15 to 64 km altitude, with a vertical resolution of 2.5 km. The absolute accuracy was about 10%, and the precision a few percent.

Because of the small signals involved, it is necessary to cool the detectors. LIMS life was limited by the technology of that period, which dictated the use of a solid cryogen cooler. This resulted in a 7-month lifetime. Otherwise, it should be useful for trend measurements, especially since it provides a 1978/79 determination. LIMS data were used in the OTP to help evaluate other data.

2.1.3 Measurements for Future Trend Analyses

Many of the methods described previously will continue to be used to obtain data for trend studies. Where these methods are reasonably accurate and stable with time, this is essential, because it extends the length of the data record. However, as technology advances, improvements to old techniques are continually being introduced and new measuring systems are being developed. A number of these are shown in the timelines on Figure 2.1-3, and are described below.

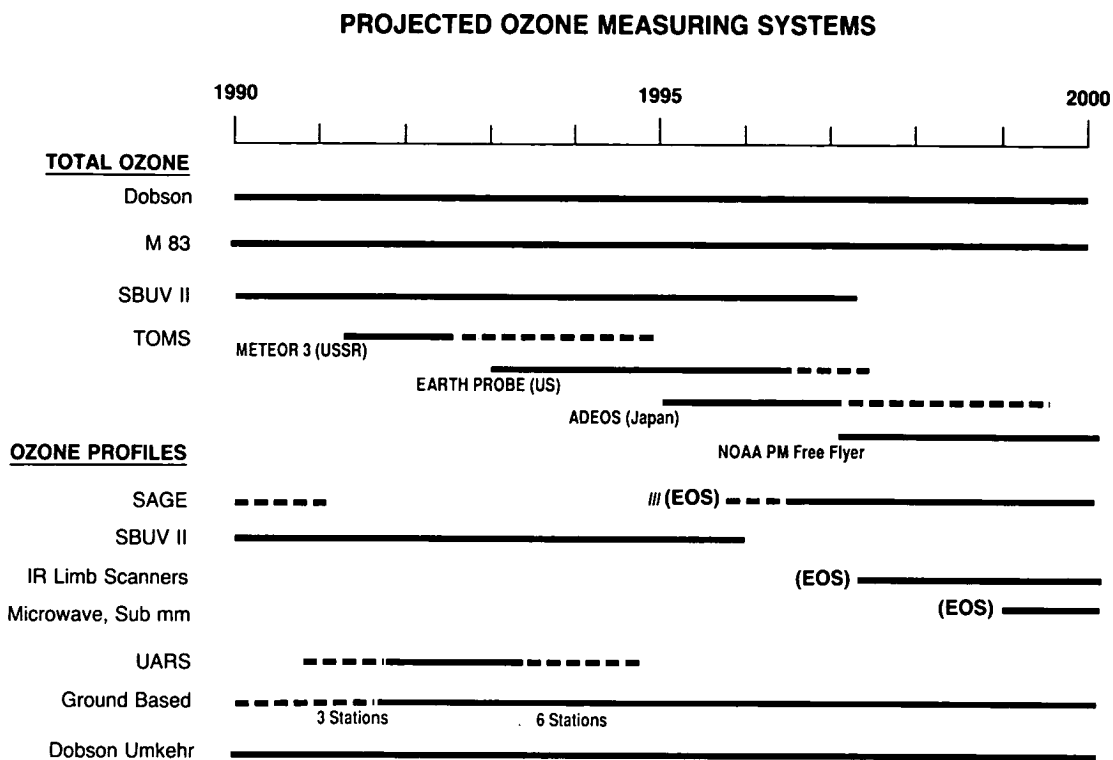


Figure 2.1-3. Time lines for ozone measuring systems that are projected to be operating over the next decade.

2.1.3.1 Total Ozone Measurements

Ground-based Measurements

The Brewer Spectrophotometer

The Atmospheric Environment Service of Canada developed the fully automated Brewer ozone spectrophotometer in the early 1980s. Development of the Brewer instrument was based, in part, on earlier work by Wardle et al. (1963) and Brewer (1973) and was carried out with the goal to replace or supplement the Dobson instrument in the world network. There are presently about 30 instruments operating in 15 countries, including the seven Canadian stations (Kerr et al., 1988). At present, five stations are reporting data to the WODC. The record of routine measurements of total ozone made with the Brewer spectrophotometer started in 1982. These records are presently not of sufficient length to carry out a proper independent trend analysis.

The spectrophotometer is a modified Ebert type with a 1,800-lines/mm holographic grating used in the second order. It simultaneously measures the intensity of light at 5 wavelengths in the ultraviolet absorption spectrum of ozone with a resolution of 0.6 nm. The operational wavelengths are 306.3 nm, 310.0 nm, 313.5 nm, 316.8 nm, and 320.0 nm. Measurements at these wavelengths allow correction for the effects of sulfur dioxide, a potential interferent for Dobson ozone measurements in polluted air. A more complete

GLOBAL TRENDS

description of the automated instrument is given by Kerr et al. (1985). The Brewer instrument has been calibrated on an absolute scale using the ozone absorption coefficients of Bass and Paur (1985). Intercomparison with the Dobson instrument has shown that the Dobson AD direct sun total ozone measurement is about 3% larger than the Brewer measurement. When this bias is removed, the long-term agreement between field Brewer and Dobson instruments at Toronto and Edmonton has been within 1% (Kerr et al., 1988; 1989a).

Although the method to measure total ozone with the Brewer instrument is similar to that for the Dobson instrument, there are differences in sampling and reporting daily data. These differences arise primarily because the Brewer instrument is fully automatic and thereby capable of sampling continuously throughout the day. Measurements are screened and only those of good quality are used to determine the daily mean total ozone value that is reported. In general, good quality direct sun measurements can be made on about 75% of the days at a typical mid-latitude station.

High Resolution Visible/Ultraviolet Absorption Spectroscopy

Absorption spectroscopy affords a sensitive means for monitoring the column abundance of several stratospheric species (e.g., Noxon et al, 1979; McKenzie and Johnston, 1982; Pommereau et al., 1988a, 1988b). A useful approach is to measure the absorption of light scattered by the sunlit zenith sky. An important feature of such measurements is that they can be carried out on cloudy as well as clear days. The optical paths (or air mass factors) relevant to a species in a stratospheric layer become very large at solar zenith angles greater than about 88 degrees, maximizing the slant-column abundance of absorber and hence the observed percent absorption.

Modern optics, electronics, computers, and detectors allow atmospheric absorption spectroscopy to be done with very high precision, typically 0.05% absorption. Multichannel detectors eliminate the uncertainties that scanning optics introduce. Least-squares fitting of the observed spectra to those recorded in the laboratory with the same instrument for several atmospheric gases allows the abundance of more than one atmospheric species to be determined simultaneously. Under favorable spectral conditions, the sensitivity stated above can be enhanced a factor of 50 by such fitting. The stratospheric species that are most amenable to observing with ultraviolet/visible absorption spectroscopy have proven to be O₃, NO₂, NO₃, and OCIO. The characteristics of one instrument that has been applied to these species is used here as an example of the type that is achievable today.

The example (Mount et al, 1987) is a crossed Czerny-Turner spectrometer, with a grating chosen so that the appropriate color filters provide second-order light in the red region of the spectrum, approximately 605–685 nm (for NO₃ observations) and third-order light in the blue region, approximately 400 to 450 nm (for O₃, NO₂, and OCIO observations). The instrument is used at approximately 0.5-nm spectral resolution. The detection system is a Reticon diode array cooled by a refrigerator to about –70°C; the array contains 1,024 independent silicon diodes that simultaneously measure the spectrum over the indicated wavelengths. Eleven diodes cover the full width at half maximum of the instrumental spectral profile. Thus, spectral lines are highly oversampled.

An important advantage of simultaneous measurement of the desired spectral interval (as opposed to scanning) is the elimination of time-dependent changes during the course of a measurement (particularly atmospheric scintillation effects). These can be quite important when the measured species absorb only a few tenths of a percent of the incoming light, as is the case for ozone and OCIO in general and for NO₂ at small zenith angles. After least squares fitting the observed sky data to the reference absorption spectra

measured in the laboratory, the one-sigma standard errors of the fitted column abundances are typically 2–5% for large solar zenith angles for NO₂. Ozone columns can be determined to 10–15% accuracy using the Chappuis bands. Future development is expected to improve this considerably. While most efforts with this technique have been on the measurement of other gases, the technology presumably could be applied to ozone measurements as well.

The largest source of systematic error in the measurements is the evaluation of the air mass factors for scattered light that are used to convert measured slant column abundances to vertical column abundances. These errors largely affect the accuracy but not the precision of the data. Estimated error limits in air mass factors are no more than 10% for solar zenith angles near 90 degrees, and they are substantially less for smaller angles.

Satellite Observations

Future Flights of TOMS Instruments

TOMS data have proven of great value in observing and studying the polar ozone depletions, as well as in providing information on the global decrease of total ozone. With the development of independent techniques for determining the diffuser reflectivity, TOMS data should be able to provide a determination of total ozone decrease over all areas of the globe that is independent of the ground-based Dobson network, although it should agree with the latter in areas where both obtain measurements. For these reasons, it is extremely important to continue TOMS-type measurements. The TOMS instrument on Nimbus-7 is now over 10 years old, and efforts have been made for future flights of TOMS-type instruments on several spacecraft.

First flight of a new, technically upgraded instrument is scheduled for the fall of 1991 on board the Soviet Union's Meteor-3 spacecraft. Unlike the sun-synchronous orbit of Nimbus-7, the Meteor-3 orbit will precess with a period of 225 days. Thus, the coverage will not be as uniform as that obtained with previous data, and adjustments will have to be made for diurnal variations. TOMS has also been selected to fly on a small U.S. Explorer-class satellite in 1993, and on the Japanese ADEOS satellite, scheduled for launch in February 1995. In these cases the orbit will again be sun-synchronous.

An upgraded TOMS will also be part of the Global Ozone Monitoring Radiometer (GOMR), an operational instrument to make long-term ozone measurements. The GOMR, discussed further below, will be included in the complement of operational instruments on the NOAA afternoon free-flier, beginning in about 1997.

2.1.3.2 Profile Measurements

Ground-based Measurements

Brewer Umkehr

Although Umkehr observations have been made with the Brewer Ozone Spectrophotometer for several years (Mateer et al., 1985, Kerr et al., 1989b), this has been a developmental period during which the observational technique and the algorithm have changed. The present body of data is insufficient for trend analysis.

GLOBAL TRENDS

A Brewer Umkehr observation consists of zenith sky intensity ratio measurements for three wavelength pairs over the solar zenith angle range from 60 to 90 degrees. The profile retrieval data cover the altitude range of layers 1 to 10 (0–53 km). The averaging kernels for the present algorithm show that the retrievals for layers 4 to 8 (19–43 km) and marginally layer 9 (43–48 km) are suitable for trend estimation. Until a complete error analysis has been carried out for the Brewer Umkehr system, those for the standard Dobson Umkehr may be considered as only approximately applicable. Results of an intercomparison of Brewer Umkehr, Dobson Umkehr, and ozonesonde data have indicated that the quality of the Brewer Umkehr technique is comparable to that of the Dobson “short” Umkehr method (McElroy et al., 1989).

Lidar

The lidar measurements of the ozone vertical distribution are based on the Differential Absorption Laser technique (DIAL), which requires the simultaneous emission of two laser wavelengths characterized by a different ozone absorption cross section. Part of the laser radiation is scattered back to the surface, where it is collected by a telescope, detected by a photomultiplier and time-sampled to retrieve the altitude resolution of the measurement. The derivative of the logarithm of each signal is computed and the ozone number density is obtained from the difference of the derivatives, divided by the differential ozone cross section. The lidar technique has been described by Mégie et al. (1977), Uchino et al. (1978), Pelon and Mégie (1982), Werner et al. (1983), Pelon et al. (1986), Ancellet et al. (1988), Godin et al. (1989), and McDermid and Godin (1989).

In principle the technique is self-calibrating, and thus particularly suited for the detection of trends. Two types of error affect the ozone lidar measurement. The random or statistical error is related to the signal-to-noise ratio. The systematic error is related on one hand to errors in the value of the ozone absorption cross sections used and their dependence on temperature, and on the other to uncertainties in the different physical processes, such as the Rayleigh and Mie scattering or the absorption by other species (NO_2 , SO_2). The systematic error can be reduced by additional measurements of temperature and aerosol vertical profiles or use of empirical models. The random error which results from this correction is less than 3% in the whole altitude range. The choice of the two wavelengths used in the experiment depends directly on the altitude range monitored. In the troposphere, the limiting factor is the systematic error, which becomes smaller as the difference in wavelength is reduced. A wavelength separation of less than 10 nm is used, and the time necessary to obtain a tropospheric ozone profile is about 10 min for an altitude resolution superior to 1 km and an overall uncertainty less than 5%. In the stratosphere, the separation of the wavelengths needs to be larger (~50 nm) in order to limit the statistical error. Furthermore, the range resolution has to be degraded in the upper range of the measurement (above 30 km) to account for the rapid decrease of the signal-to-noise ratio with altitude. With the present systems, obtaining an ozone profile in the 15–50 km altitude range requires an integration time of 2 to 3 hours for an altitude resolution of 0.5–8 km and a corresponding uncertainty of 2% to 10%.

Microwave Radiometry

Microwave radiometers (MR) are being used increasingly to investigate the middle atmosphere. An MR measures the thermal emission from rotational transitions of the molecule under investigation. The frequency employed is typically below 300 GHz (1 mm wavelength) to reduce the effects of tropospheric opacity (e.g., clouds or aerosols) and local thermodynamic equilibrium (LTE) conditions apply to ~80 km altitude. The sensor operates on the superheterodyne principle that provides a very high spectral resolution, allowing the determination of the exact shape of the emission line. Since the shape of the emission lines are dominated by pressure broadening to 80 km altitude, profiles can be retrieved from an exact measure-

ment of the emission line shape. At low altitudes (~ 15 km) the emission line widths become very large, and this, together with instrumental problems (base line and non-linearities) makes low-altitude retrievals very difficult. The altitude range over which high-quality ozone profiles can be determined from MR measurements is typically 15 to 70 km (Zommerfeld and Kunzi, 1989) with an altitude resolution of ~ 10 km. The accuracy claimed for this sensor is 1 part per million by volume, and the statistical error is of the order of 15%. The measuring time required for a complete profile is approximately 1 hour. Another instrument, developed by De la Noe et al. (1988) has obtained measurements of the ozone distribution with reported random errors from 1 to 5% at 40 km. Connor et al. (1987) present an error analysis for data obtained in Antarctica during 1986; they show measurement accuracies of 15–19% (depending on altitude), supported by intercomparisons with other observations. A detailed study performed recently by Bevilacqua and Olivero (1988) showed that the best vertical resolution attainable is 6 or 7 km.

It should be noted that the accuracy can be improved by using observing sites at high altitudes, thus reducing the attenuation by tropospheric water vapor. For a mid-latitude site at 500 m above sea level (Bern, Switzerland), the observing statistics for favorable conditions are $>80\%$ of the time during fall, winter, and spring, and $\sim 50\%$ of the time for summer. Model calculations (Kunzi and Rubin, 1988) indicate that for $>90\%$ of available observing time the sensor has to be at $\sim 3,000$ m altitude for the tropics, whereas in polar regions the site can be at any altitude.

MR instruments seem particularly well suited to perform long-term trend measurements of total stratospheric and mesospheric ozone and its vertical distribution, since an MR is easily calibrated with black body radiators and thereby has a response that can be made stable over long periods. Furthermore, the operation and data retrieval of an MR can be fully automated and require only little maintenance by skilled operators. However, at present, only little experience is available with MRs in ozone research and more intercomparisons and experience with sites in different climatic regions is needed.

Satellite Observations

Solar Backscatter Ultraviolet Radiometer—Version 2 (SBUV/2)

NOAA is currently flying the Solar Backscatter Ultraviolet Radiometer—Version 2 (SBUV/2) as an operational instrument for measurement of both total ozone and vertical profiles. The first SBUV/2 was launched on NOAA-9 in 1984 and continues to operate in overlap with the instrument launched on NOAA-11 in 1988. This series of instruments is planned to be in orbit through the lifetime of the present afternoon series of NOAA polar orbiting satellites (ca 1996). These satellites sound the atmosphere. Unfortunately, an onboard check of the diffuser plate incorporated in the NOAA-9 SBUV/2 failed to function properly. At the same time, the processed ozone data from this instrument indicate a time-dependent bias with respect to the ground-based information as well as the Nimbus-7 SBUV data that is opposite in sign to our general understanding of diffuser plate degradation. No data from either instrument are now available. This time-dependent bias is still under examination; if the cause for this disparity is discovered, the data will be reprocessed accordingly. An attempt has been made to correct the onboard diffuser plate check on the SBUV/2 follow-on units.

The failure to obtain data from the NOAA-9 SBUV/2 is especially damaging, since the first 2 years overlapped with the last 2 years of the SBUV. The SBUV/2 data could have been used to correct the SBUV diffuser model, allowing a reliable profile trend to be obtained over the 8-year life of SBUV. Alternatively, the differences between the first 2 years of SBUV and SBUV/2 could have been used to get a direct difference, as was done for data from SAGE I and SAGE II.

GLOBAL TRENDS

Upper Atmosphere Research Satellite

The Upper Atmosphere Research Satellite (UARS) is scheduled for launch by the U.S. National Aeronautics and Space Administration (NASA) in late 1991. The instruments have been designed for research purposes and the study of dynamical, chemical, and physical processes in the stratosphere, mesosphere, and lower thermosphere. Although it is not designed to measure ozone trends, a few of the instruments may provide data useful for trend studies.

Ideally, each of the ozone measurements will be sufficiently accurate that it can be compared with the existing body of previous data. However, because of the small trends and the often larger systematic biases between different types of instruments, the clearest indications are likely to occur when similar instruments are used. Some possibilities are: comparisons of ozone measurements among infrared limb-scanners such as UARS IR limb scanners (CLAES and ISAMS) as compared to LIMS and to future EOS instruments (see following); comparisons between measurements made by the UARS Microwave Limb Sounder (MLS) and the future EOS MLS; comparisons between measurements made by the infrared occultation instruments (UARS HALOE, and the later ILAS [see following]); and perhaps also comparisons among the visible occultation observations performed by the successive SAGE instruments.

Infrared Limb Atmospheric Spectrometer (ILAS)

The ILAS is under definition study by the Japanese Environmental Agency for possible launch on the ADEOS satellite, now scheduled for February 1995. It is a solar occultation spectrometer, baselined to use three monochromators in the middle infrared. In addition to the measurement of ozone (9–10 micrometer bands), several other trace species and aerosols will be measured over the 10–60 km altitude range.

Earth Observing System (EOS)

The U.S. National Aeronautics and Space Administration (NASA), the European Space Agency (ESA), and the Japanese Space Agency (NASDA) are developing a co-ordinated international system of polar platforms for remote sensing of the atmosphere, oceans, land surface, biosphere, and solid Earth. The goals are to begin or continue a set of baseline observations of key variables that indicate the state of the entire Earth system, and continue them for at least 15 years. At this time, instrument selection is still underway.

NASA has selected instruments for the definition phase for NASA's polar orbiting platforms (NPOP-1 and -2). It includes, for NPOP-1, an infrared limb sounder and SAGE III occultation instruments that should provide observations of ozone with high vertical resolution, high accuracy, and precision from cloud tops to 80 km. The limb sounder will also be capable of high horizontal resolution. Launch is scheduled for late 1996. In addition, a SAGE III instrument is planned as an attached payload for the Space Station to provide profiles at low to mid-latitudes to complement the NPOP-1 high latitude coverage. The Space Station is scheduled for launch in 1995. For NPOP-2, definition studies are being carried out for limb sounders operating in the infrared, sub-millimeter, and microwave portions of the spectrum, which will make additional measurements of ozone profiles.

The Global Ozone Monitoring Radiometer (GOMR) is planned to be the next in the series of NOAA operational satellite ozone monitoring systems. It is to fly on the satellite series subsequent to the current Advanced TIROS-N with launch about the mid-1990s. The GOMR will supplant the SBUV/2. The GOMR is

currently envisioned as two subsystems: an ultraviolet nadir and side-scan sounder based on Nimbus-7 TOMS technology, as noted above, and an infrared limb sounder based on EOS limb sounding instruments. The nadir sounder will provide total ozone in the sunlit portion of the Earth while the limb sounder will provide stratospheric profiles of ozone and other minor constituents important to ozone photochemistry and climate. The final configuration of the satellite ozone monitoring system is undergoing evaluation.

Three instruments providing ozone measurements in the stratosphere have been selected by the European Space Agency for flight on the first ESA Polar Platform (EPOP-1). GOMOS (Global Ozone Monitoring by Occultation of Stars) is an instrument intended to monitor ozone by stellar occultation, observing the full UV/visible/near-infrared spectrum of stars using a double grating spectrometer. SCIAMACHY (Scanning Imaging Absorption Spectrometer) is a combination of two spectrometers operating also in the UV/visible/near-infrared part of the spectrum to observe transmitted, reflected, and scattered light. It is designed to be used for both nadir and limb sounding plus solar occultation and will provide measurements of tropospheric ozone. MIPAS (Michelson Interferometer for Passive Atmospheric Sounding) is a limb sounder operating in the mid-infrared region of the spectrum. All these instruments are presently in Phase A studies.

2.1.4 Comparisons of Errors/Capabilities

2.1.4.1 Intercomparisons Relevant to Present Data

Total Ozone—Dobson-TOMS-SBUV

TOMS values for total ozone are in good agreement with those from SBUV, being systematically about 1% higher for reasons that are not completely understood. Fleig et al. (1989b), Reinsel et al. (1988), Bojkov et al. (1988), and OTP examined the drift of SBUV relative to an ensemble of 41 Dobson stations and found that there was a roughly linear drift between SBUV and Dobson of -0.38% per year over 6 years. The intercomparison of TOMS data with the network of Dobson stations was also discussed as a function of time in OTP. This shows that TOMS total ozone declined slowly relative to the 41-station ensemble between 1979 and mid-1982—about -0.25% per year—and declined rapidly thereafter, at a rate of about -0.53% per year through October 1986, the end of the period studied. The decline for SBUV was similar. These results are confirmed by a recent study performed by McPeters et al. (private communication, 1989) using a network of 39 stations as shown in Figure 2.1-4a.

While total ozone measured by SBUV/TOMS clearly declined relative to that measured by the Dobson network, further tests were necessary to determine whether the problem is due to degradation of the satellite instruments or to changes in individual Dobson instruments. One such test involved satellite overpass of Mauna Loa, Hawaii, on those days during which the World Primary Standard Dobson instrument, instrument No. 83, was undergoing its regular recalibration at that location. Komhyr et al. (1989) report that the stability of this instrument has been maintained to 0.5–1% since 1962. The trend of TOMS relative to this instrument, also shown in Figure 2.1-4a, is very similar to that obtained relative to the 39-station ensemble—little change from launch through mid-1982 followed by a rapid decline thereafter amounting to approximately -0.7% per year through 1988.

As described above, a purely internal check for instrument degradation is possible for SBUV. The “D” wavelength pair, consisting of wavelengths 305.8–312.5 nm is sensitive to ozone because of its large ozone cross section and is very insensitive to wavelength-dependent degradation errors because of the small wavelength separation. The drift of normal SBUV ozone relative to D pair ozone exhibits the same

GLOBAL TRENDS

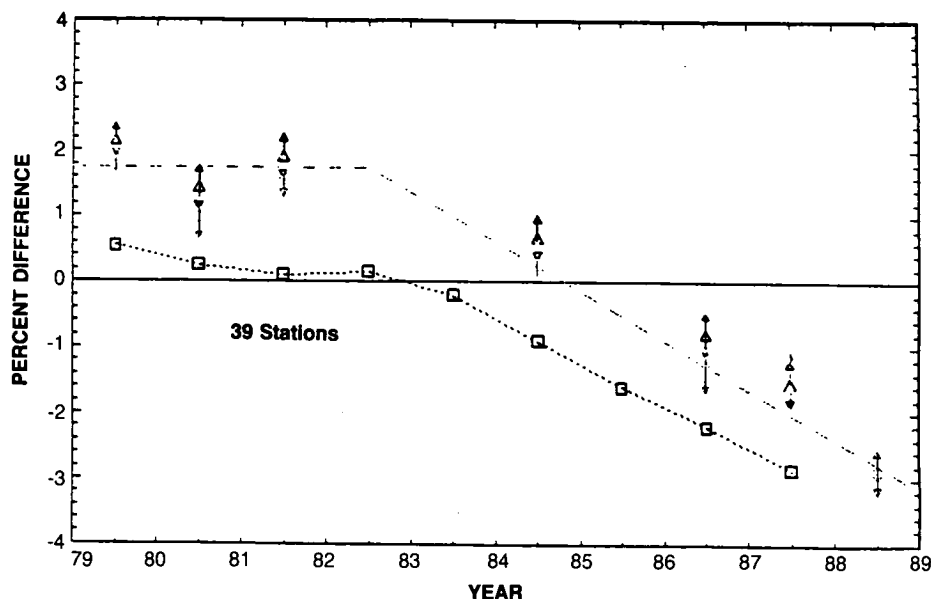


Figure 2.1-4a. Comparison between archived TOMS total ozone data and Dobson data. These TOMS measurements have been corrected for diffuser plate degradation by the method described by Cebula, Park, and Heath (1988) and the Ozone Processing Team (1989). Triangles show the difference between TOMS and the World Primary Dobson Instrument No. 83. (There are reasons to think the 1980 Dobson data are of lower quality than those for other years.) Squares show differences between TOMS and a network of 39 Dobson stations. Both comparisons show a sharp drop of TOMS relative to Dobson ozone, especially since 1982.

pattern as that observed for SBUV/TOMS relative to Dobson and for TOMS relative to instrument No. 83—little change before 1982 followed by rapid change thereafter.

The conclusion that there was about 3.4% drift between SBUV/TOMS and the Dobson network between 1979 and 1987, with much of the drift occurring after 1982, seems inescapable. The fact that the same pattern of relative stability in the TOMS-Dobson comparisons before 1982, followed by a sharp decline between 1982 and 1986, was repeated for so many of the ensemble of 41 independent Dobson stations was strong evidence for SBUV/TOMS instrument degradation, and insufficient correction. The complete confirmation by comparison with the World Standard Dobson instrument and by internal evidence of relative pair drift furnish compelling additional evidence that this trend relative to Dobson is a robust result. As pointed out previously, this drift of SBUV/TOMS is believed to result from degradation of the diffuser plate used to measure solar flux, with incomplete correction.

TOMS data for the ground station overpasses have been reprocessed using the "pair justification" calibration. The comparison of them to the data obtained by Dobson 83 during its calibration at Mauna Loa are shown by the triangles in Figure 2.1-4b, from which it can be seen that there is no large, systematic drift between them greater than a few tenths of a percent over 9 years. Because the techniques are so different, this agreement between the Dobson and TOMS support the conclusion that both are correct. Further confirmation is provided by the squares in Figure 2.1-4b, which presents comparison data between TOMS and a network of 39 stations. They suggest a drift of 0.5% over 8 years, close to the level of calibration stability achievable for this technique (it could also be explained by about a 1%/year increase in tropospheric ozone).

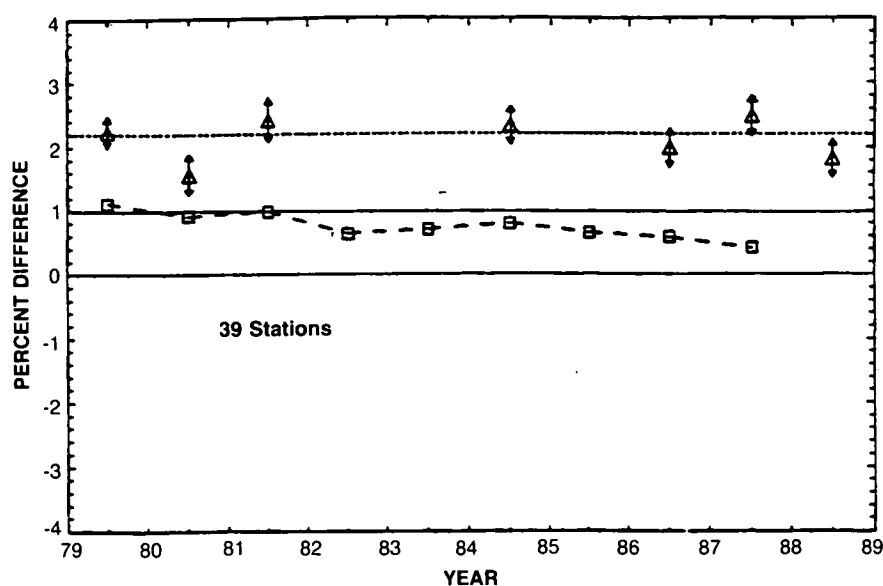


Figure 2.1-4b. Comparison between TOMS total ozone data, where diffuser plate degradation was corrected by the “pair justification” method, and Dobson data. Triangles show the difference between the World Primary Dobson Instrument No. 83 calibration measurements. (There are reasons to think the 1980 Dobson data are of lower quality than those for other years.) The squares show the differences with the network of 39 stations used for Figure 2.1-4a. These results show that once corrected, TOMS has not drifted relative to instrument 83 between 1979 and 1988, and has only changed by about 0.5% relative to the 39 station network between 1979-1987. This may be a real effect (see text).

Vertical Profiles

SAGE I / SAGE II

The accuracy of estimating ozone trends using SAGE I and SAGE II ozone data is discussed in OTP, Chapter 2. It is limited by the systematic errors between the two instruments. These errors range from 5.8% below 25 km to 1.5% at 30 km, 1.6% at 40 km, and 3.0% at 50 km height (see Figure 2.1-3c). This assessment does not include any spatial or temporal sampling error associated with these two data sets.

SAGE I / SAGE II and SBUV

An intercomparison of SAGE I/II and SBUV ozone measurements was performed for the periods February 1979 through November 1981 and October 1984 through December 1986. It is described in detail in OTP. For this comparison, the SAGE I/II profiles were integrated, from concentration as a function of geometric altitude, the primary SAGE product, into Umkehr-layer amounts. In Umkehr layers 7, 8, and 9, SAGE I ozone layer amounts were consistently lower than SBUV in 1979-1981 by 4 or 5%, but SAGE II ozone layer amounts were consistently higher than SBUV in 1984-1986 by $10 \pm 2\%$. The results in Umkehr layer 6 consistently showed SAGE I about 4% higher than SBUV in 1979-1981 and SAGE II about 10% higher than SBUV in 1984-1986. The 1980-1985 offset between SAGE and SBUV increased

GLOBAL TRENDS

monotonically with altitude between Umkehr layers 6 and 9. Coupled with the other information on degradation of the SBUV diffuser plate and the self-calibrating nature of the SAGE instruments, this comparison supports the conclusion that the large ozone changes reported by SBUV at high altitudes are due to larger diffuser degradation at the shorter wavelengths that allowed in the SBUV data reduction.

SBUV, SAGE I, and LIMS Ozone Intercomparisons

In OTP (Chapter 5) the ozone observations during March and April 1979 from three simultaneous satellite instruments, namely the SBUV, SAGE I, and LIMS, were examined. (For a discussion of LIMS, see OTP or Gille and Russell, 1984 and Remsberg et al., 1984.) The analysis is an intercomparison of the ozone data from these instruments in terms of ozone column abundance in four Umkehr layers (layers 6 to 9). In the case of SAGE I and LIMS, it was necessary to convert their primary measured ozone quantities to ozone Umkehr layer amounts for comparison purposes. Since the sampling locations of the SAGE instrument are distributed in a narrow latitudinal belt for a 24-hour period, as opposed to the nearly global observations of the SBUV and LIMS for the same period, the comparison analysis is carried out by following the SAGE I latitudinal sampling progression. Because the three satellite instruments never sampled at the same locations and times, the comparison was made in terms of the zonally averaged ozone layer amount in these Umkehr layers.

For the case of April 1979 and SAGE I sunset, the standard deviation of the SAGE I instrument about its zonal means is less than 10% except at high latitudes. The standard deviation for LIMS about its zonal mean is about 4%, and that for SBUV is about 2%. All three satellite systems show the same pattern with latitude. The results show that SBUV data are about 3% systematically lower than the mean of the three instruments in layer 6 but not systematically different from the other instruments in layers 7, 8, and 9. For each of the three satellites, for each of the four Umkehr layers, and for each of the four times, the root-mean-square deviation from the average of the three instruments is given in Table 2.1-1. For 15 out of 48 entries in Table 2.1-1, the deviations are less than 3%; for 23 out of 48 entries the deviations are between 3 and 5%; and for 10 out of 48 entries the deviations are greater than 5% but less than 10%. This set of data

Table 2.1-1. Estimated overall percentage differences of the calculated zonal mean ozone layer amount of SBUV, SAGE, and LIMS with respect to the average of these three instruments

	UMKEHR LAYER					
	Layer 6			Layer 7		
	SBUV	SAGE	LIMS	SBUV	SAGE	LIMS
1 Sunrise (March 79)	4.5	6.3	2.6	2.4	4.2	4.6
2 Sunrise (March 79)	2.8	3.1	1.6	3.8	2.8	4.0
3 Sunrise (April 79)	5.1	3.7	1.3	2.9	1.5	3.7
4 Sunrise (April 79)	3.8	3.6	2.1	2.8	1.4	3.4
	Layer 8			Layer 9		
	SBUV	SAGE	LIMS	SBUV	SAGE	LIMS
	1 Sunrise (March 79)	1.6	3.6	4.4	4.2	6.1
2 Sunrise (March 79)	3.0	4.1	4.2	3.3	7.7	8.6
3 Sunrise (April 79)	1.6	3.2	3.9	3.0	7.3	9.5
4 Sunrise (April 79)	2.6	1.7	3.3	6.2	1.8	6.9

shows that three totally different satellite systems agree with each other to about 4% in measuring zonal mean ozone amounts in the four Umkehr layers in the middle to upper stratosphere in April, 1979. The conclusion is that this is the level of agreement that has been demonstrated between different measuring techniques as of this time. The differences are probably due in part to differences in systematic errors, such as the absorption coefficients, as well as to effects of the individual techniques. A further inference is that when one is looking for small changes, at this time it is probably necessary to use instruments of the same or closely related types, with the same systematic errors.

SAGE I and SAGE II Comparisons with Ozonesondes

As a further step in understanding data quality, electrochemical concentration cell (ECC) and Mast ozonesonde profiles from the World Ozone Data Center (WODC) data base have been compared with SAGE I and SAGE II ozone profiles, and discussed in OTP (Chapter 5). SAGE I and SAGE II data sets, composed of six profile pairs each, were chosen for comparison at the following six stations: Edmonton (53N,113W), Churchill (58N,94W), Hohenpeissenberg (47N,11E), Wallops Island (38N,75W), Lindenberg (52N,14E) and Praha (50N,14E).

SAGE I and SAGE II measurements over these stations occurred at regular intervals as either of these instruments sampled the latitude band containing any particular station. The six profile pairs representing the SAGE I period are shown in the top six panels of Figure 2.1-5. The WODC profiles were converted to ozone number density, the fundamental unit of ozone measured by both SAGE I and SAGE II. The ozone number density profiles are plotted as a function of pressure from approximately 250 to 5 mb. The SAGE I profiles are plotted as the thin curve bounded by two dashed curves, the dashed curves representing 1σ uncertainties on the SAGE I measurement. The dates of each measurement, the SAGE I event type (sunrise or sunset measurement), the spatial and temporal separation of the station-to-SAGE measurement tangent point, and the correction factor for the ozonesonde are provided on each graph. Typically, SAGE averages over a cylinder of diameter 1 km and length 200 km. The ozonesonde correction factor represents the ratio between the total ozone as measured by the Dobson instrument at the station and the total ozone derived by integration of the ozonesonde profile. Correction factors deviating greatly from unity are indicative, generally, of ozonesonde profiles of questionable reliability. In the analysis done here, ozonesonde profiles were not selectively screened out by rejecting those with correction factors outside of the intervals mentioned above.

The WODC and SAGE I profile pairs in Figure 2.1-5 had a maximum spatial separation of 481 km at Praha and a minimum separation of 71 km at Lindenberg. The maximum and minimum temporal separation between the profile pairs occurred at Hohenpeissenberg and at Lindenberg, respectively. Thus the profile pair at Lindenberg is the closest coincidence between the *in situ* ozone measurement and the remote sensing ozone measurement. This ozonesonde profile is almost entirely contained within the uncertainties of the SAGE I measurement. The precision of an ozonesonde measurement, which is not provided by WODC, has been estimated at 5–10% from ground to tropopause, and at 5% from tropopause to 25 km (Barnes et al., 1985; Hilsenrath et al., 1986). Similar results are shown on Figure 2.1-6 for the SAGE II instrument.

Estimates of the differences between the ozonesonde and satellite ozone measurements are given in the lower panels of Figures 2.1-5 and 2.1.6 over the altitude range from 15.5 to 30.5 km. Each difference profile was calculated by first interpolating the six ozonesonde profiles to the altitudes at which SAGE I and SAGE II measure ozone. For each altitude, the six ozonesonde values were averaged as were the six SAGE I or SAGE II values. The mean values were used to compute the percentage difference between the ozonesonde and the satellite measurements relative to the mean of the ozonesondes. The mean

GLOBAL TRENDS

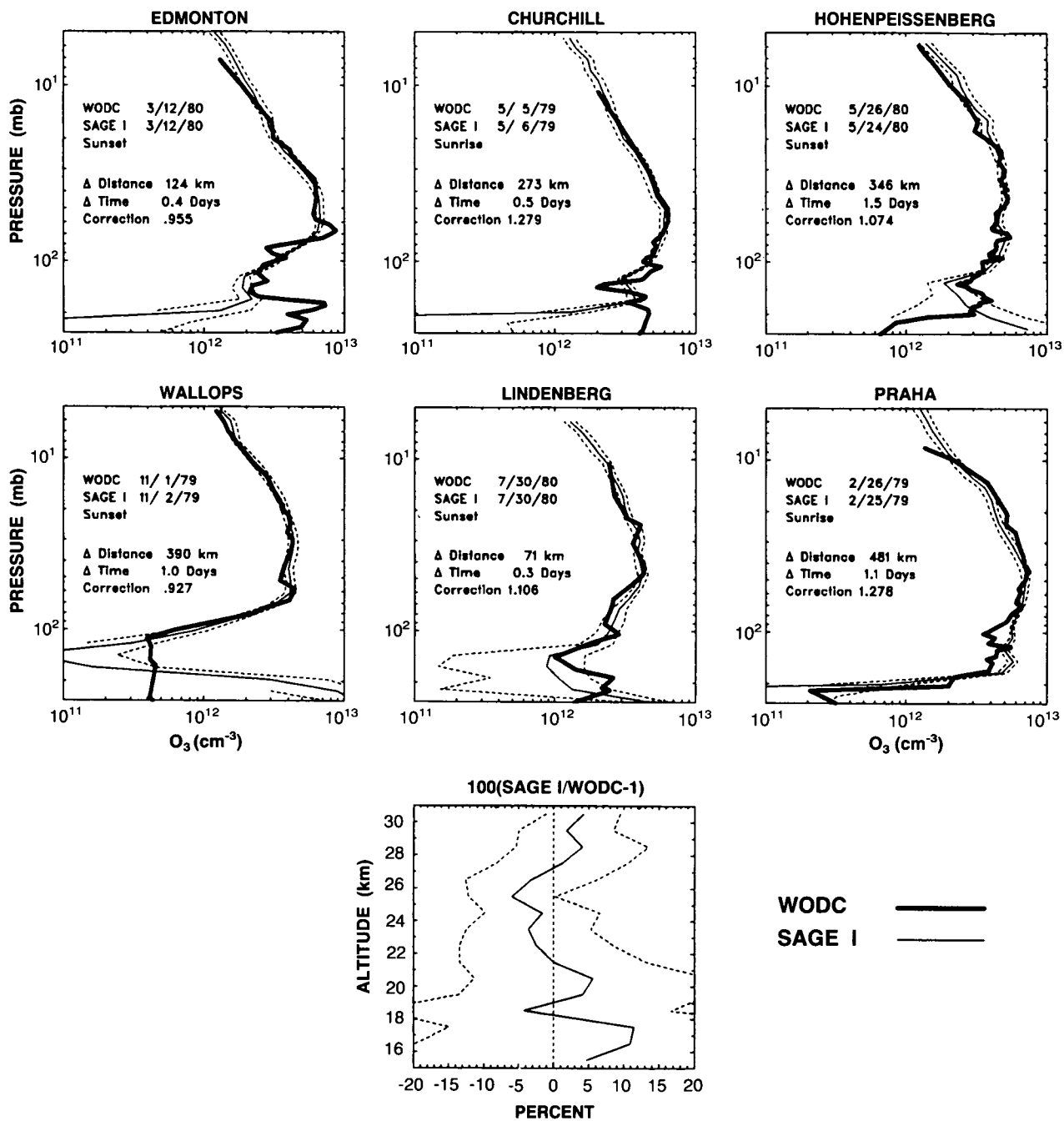


Figure 2.1-5. Samples of profile pairs measured by ozonesondes and the SAGE I instrument appear in the upper six panels. The lower panel is the mean percentage difference between the ozonesondes and the SAGE I ozone. Ozonesonde profiles were interpolated to the altitudes 15.5, 16.5, ..., 30.5 km. The dashed curves represent one standard error.

GLOBAL TRENDS

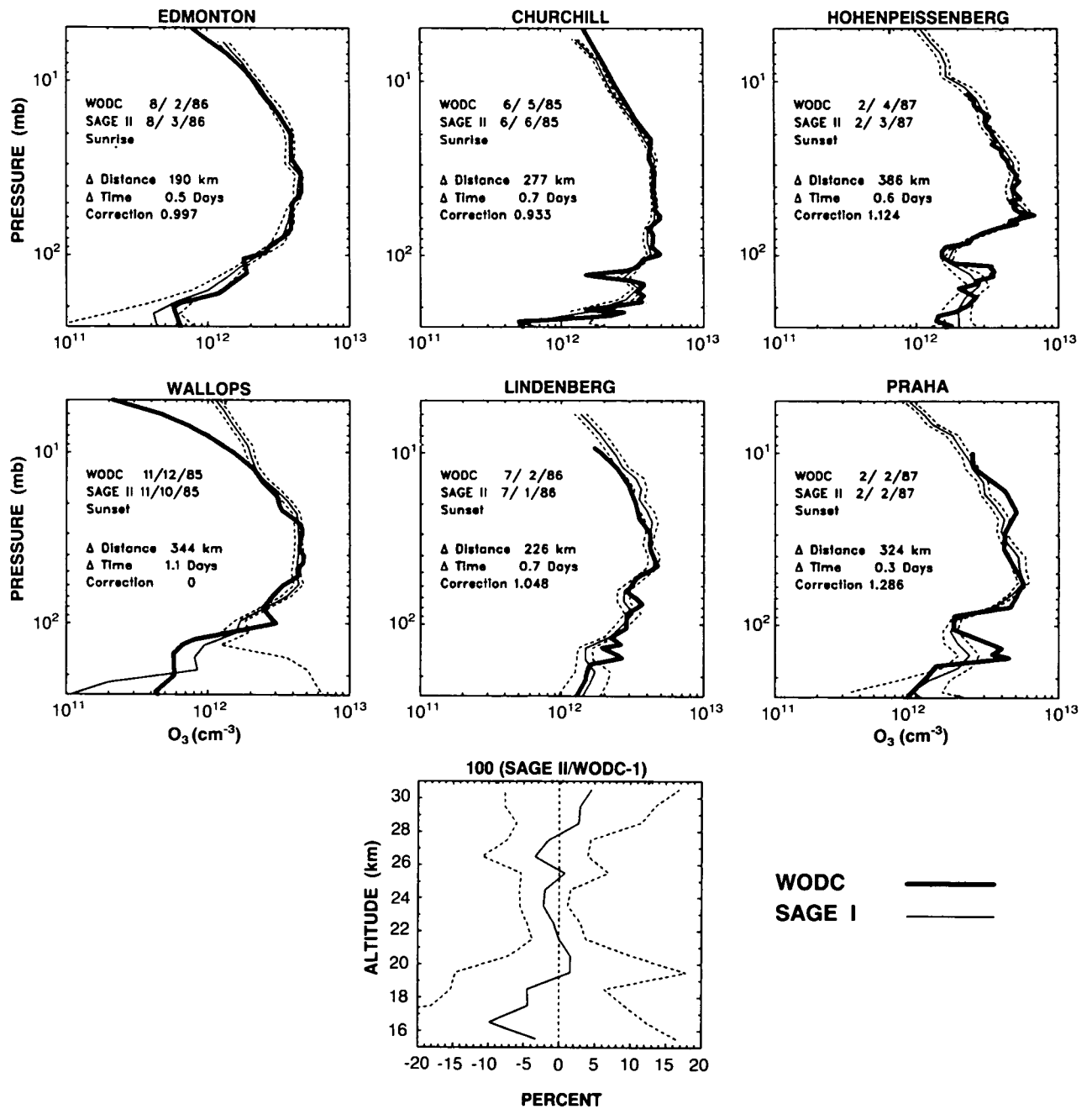


Figure 2.1-6. Samples of profile pairs measured by ozonesondes and the SAGE II instrument appear in the upper six panels. The lower panel is the mean percentage difference between the ozonesondes and the SAGE II ozone. Ozonesonde profiles were interpolated to the altitudes 15.5, 16.5, ..., 30.5 km. The dashed curves represent one standard error.

GLOBAL TRENDS

percentage difference is plotted as the solid curve in the lower panels of Figures 2.1-5 and 2.1-6 with the dashed curves representing the standard error of the mean percentage difference. Using these relatively small samples, the differences between the satellite and the ozonesonde measurements are on the order of 5–10%.

A similar analysis to that described above was performed on a larger sample of ozonesonde and satellite pairs from the same set of stations listed above. An ozonesonde profile and a satellite profile were considered a pair if the satellite measurement location was within 1,000 km of the sonde launch station and within 5 days of the launch time. This criterion yielded 2,306 SAGE I-WODC pairs and 1,474 SAGE II-WODC profile pairs. These sets of pairs had a mean temporal separation of 2.4 ± 1.4 days and a mean spatial separation of 700 ± 200 km. The results of averaging, to form the percentage differences relative to the ozonesondes, are shown in Figure 2.1-7, with the horizontal bars representing the 95% confidence interval of the mean percentage difference. Between 20.5 and 27.5 km, the differences are mostly negative and centered at approximately -6% . Above 27.5 km, the differences computed using both SAGE I and SAGE II ozone are consistently tending toward higher values, a possible indication of ozonesonde pump inefficiency at high altitudes. Below 20.5 km, the SAGE II comparisons with the ozonesondes show an essentially constant difference with magnitude less than 5%, but with increasing uncertainties owing to the spatial and temporal ozone gradients below the ozone concentration peak.

The conclusion is that comparisons of SAGE I and SAGE II profiles, colocated in time and space with ozonesonde profiles archived in the WODC data base, reveal that both the SAGE I and SAGE II satellite measurements consistently agree to within $\pm 7\%$ above approximately 20.5 km.

SAGE-Umkehr

The results of the trends analysis performed on the SAGE I/II data and Umkehr are discussed in Chapter 5 of OTP. At present, a direct comparison between the two data sets, as far as ozone trend is

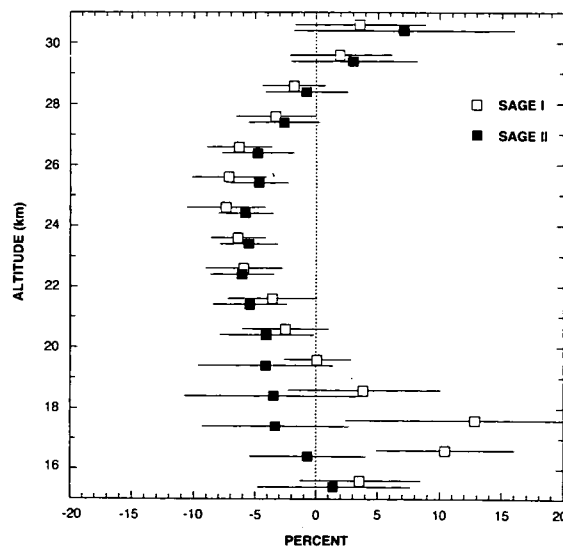


Figure 2.1-7. Mean differences between SAGE I and ozonesondes (open squares) and SAGE II (solid squares) and ozonesondes. Error bars are the 95% confidence interval on the mean ($\pm 2\sigma$).

concerned, has not been performed. The reprocessed SAGE I data that were used for the ozone trends study are being archived at NSSDC. Comparisons between Umkehr data and the previously archived version of the SAGE I ozone data showed some biases between the two data sets within the time period from 1979 to 1981 (Newchurch et al., 1987). An updated comparison with the revised SAGE I ozone data has not been performed. No comparison between the SAGE II ozone data and the Umkehr data has been performed. The changes derived from SAGE I-SAGE II differences and the Umkehr data are discussed in Section 2.3.

2.1.4.2 Intercomparisons Relevant to Future Trend Analyses

Total Ozone—Dobson Versus Brewer and TOMS

The Brewer data have been used in a number of intercomparisons which are of importance to present trend analyses and will be relevant to future trend studies. A number of sites, including five stations in Canada, have been making ground-based total ozone measurements on a routine basis with both the Brewer and Dobson instruments. These data, plus the TOMS measurements, provide three independent sets of routine field measurements of the same atmospheric constituent over a time period of a few years. Intercomparison between these data sets has been useful in evaluating monitoring performance and capabilities. Results of comparisons between Brewer and Dobson data at Toronto and Edmonton have shown an agreement within 1% and a statistically insignificant long-term drift (Kerr et al., 1989a; 1989b). Comparison between TOMS data and Brewer data has shown that the TOMS total ozone has been decreasing relative to that of the Brewer at a rate of 0.6% per year at Toronto between 1983 and 1987, and 0.61% per year at Edmonton between 1984 and 1987 (Evans and Kerr, 1989). These values are similar to the 0.64% per year decrease of TOMS data relative to the ensemble of Dobson data for the same time period (Figure 2.1-4).

Vertical Profiles

Microwave-Umkehr

Only one long-term (greater than 1 year) intercomparison of ozone profiles obtained from Umkehr observations and microwave measurements has been published (Lobsiger, 1987). From April 1984 to April 1985, 334 daytime ozone profiles were obtained with a microwave sensor operated at the University of Bern, Switzerland. For Umkehr layers 6 through 9, simultaneous data were available for 211 days from the Arosa Umkehr station at a distance of approximately 200 km. The seasonal variations observed by both instruments are very similar and the corresponding correlation coefficients for layers 6–8 are 0.87, 0.87, and 0.74, respectively.

SBUV—Microwave

A comparison was carried out between ozone profiles derived from microwave data obtained at the University of Bern, Switzerland and SBUV data. For the latter, archived data (i.e., with no allowance for SBUV instrument drift) were mapped using the Kalman filter technique and evaluated at Bern. Daily data were calculated at pressure levels between 30 and 0.7 mb; when plotted as time series they showed regular variations with season. The Bern data were available for four periods between December 1981 and June 1987. All data were smoothed with a gaussian filter 10-days wide, to reduce short-term fluctuations.

GLOBAL TRENDS

In all periods, there were appreciable biases. Averaged over altitude, the mean differences ranged from 30% to -15%. The level showing the least bias was at 7 mb, where differences ranged from -3% to -13%. The standard deviations around these biases between 10 and 1 mb are 7-10% in the last three periods, with correlations of about 0.5. Because there were changes in the instrument, observational method, and data reduction, it is likely that the changes between the first and second periods, and between the third and fourth, are due to instrumental effects. (During these observational periods, differences between SBUV and the Arosa Umkehr observations showed differences of 0 to -6%, with standard deviations of about 7% and correlations of about 0.5.) The results are not appreciably changed if the comparisons are carried out for ozone amounts integrated over Umkehr layers. The shapes of the vertical profiles were also compared. There were occasions when the agreement was reasonably good, but other situations when there were large differences. There was no obvious correlation of these differences with season.

In conclusion, these microwave observations, while somewhat noisy, and the SBUV observations appear to follow ozone variations and obtain roughly similar results for the day-to-day changes. However, there are large biases which are not entirely understood, and which appear to be rather sensitive to the details of the observations. In order to look for trends, the observing and data reduction will need to be standardized and held constant. As absorption by tropospheric water vapor is a major interference, observing from high, dry sites should reduce some of the observational problems, as noted previously.

De la Noe et al. (1988) reported an intercomparison between microwave ozone profiles and profiles obtained by the BUUV instrument on the OHZORA satellite during September 1985. Over the altitude range 37-55 km, they found an average rms difference of less than 10% for distances between satellite and microwave soundings below 1,500 km, and in general less than 20% for larger distances. They also report comparisons with SAGE II, and find average rms differences of 18% during 1985. Connor et al. (1987) report approximately 10% agreement in microwave-ozonsonde comparisons.

LIDAR—Umkehr—Satellite

Recently, the capability to make lidar measurements of the ozone number density has been demonstrated in France, the Federal Republic of Germany, Japan, and the United States. Two systems are presently operational for systematic stratospheric measurements. The first one is located at the Observatoire de Haute-Provence (OHP), France and has been operating since October 1986. The second one, located at Table Mountain Observatory (TMO), California, USA began systematic measurements in February 1988. Comparisons have been performed with other instruments such as the Umkehr, SBUV, and SAGE II. Concerning the short Umkehr method, a comparison based on 43 profiles at OHP indicated that lidar was about 3% higher than Umkehr in layers 5 and 6, but with the Umkehr values larger than the lidar values by about 7% in layer 7. Concerning SBUV, the comparisons have involved 12 measurements performed in July 1985 and 1986. The lidar values are generally higher than SBUV, with an average difference of about 10%. The comparison with SAGE is more direct in that it does not require conversion to mixing ratios and pressure coordinates, but there are fewer matchups. In general, the difference is less than 15% for each profile. Finally, a comparison of the ozone seasonal variation at different altitudes as determined by the lidar, SBUV, and Umkehr instruments has also been performed at OHP and shows that the shapes are very similar, but that the lidar data show a significantly larger amplitude (Godin et al., 1989).

An intercomparison campaign involving the TMO lidar, the mobile lidar station recently developed by the Goddard Space Flight Center, SAGE II, rocket- and balloon-borne instruments (i. e., ROCOZ-A and ECC sondes) was organized at Table Mountain Observatory in October-November 1988. The com-

parison between the two lidars, which could not be operated at the same time because of interferences between the two systems (located 600 meters apart), shows a day-to-day agreement within 10% in the 20 km–40 km altitude range. This is somewhat greater than the error bars of the two systems, but it can be explained by the fact that the instruments didn't observe exactly the same air masses at a period when the day-to-day variability of ozone was quite high. The comparison with the other instruments involved in the campaign is based on 3 days of observation. The results show an agreement within the instruments' error bars in most cases. However, it is clear that the agreement depends strongly on local meteorological conditions, because the different measurements are not simultaneous. In particular, the agreement was less satisfactory during the passage of an airmass of tropical origin characterized by a lower ozone content.

2.1.5 Temporal Sampling Requirements for Total Ozone Trend Detection

Total ozone measurements are made on a routine basis at many stations around the world. The data are then reported to the WMO World Ozone Data Center in Toronto, Canada and printed regularly in a series of publications entitled *Ozone Data for the World*. Ideally a station takes several readings each day, with the times at which these readings are taken centered around local noon. These measurements are combined to form daily means which are then reported to *Ozone Data for the World* for publication. The daily means are averaged to form monthly means, and it is the monthly means that have been used in all statistical trend analyses. In practice, however, problems such as local weather, funding, and operator availability ensure that total ozone readings are not made every day. Understanding the effects of such missing data on the calculated trends is important in assessing the results of trend analyses and in designing future monitoring networks. A recent study by Tiao et al. (1989) examined the consequences of a reduction in the daily sampling frequency on trend estimates using data from *Ozone Data for the World*. The stations with the most complete daily records were chosen and year-round trends were estimated from data sets where the monthly total ozone means were calculated by using first all the data (1/1), then every other daily value (1/2), next one in four daily values (1/4), and so on down to one in sixteen daily values (1/16): in the last case just two daily values were thus used to calculate each monthly mean. The results are shown in Table 2.1.2. The trend estimates and their standard errors do not vary very much as the sampling rate is reduced to the 1/4 rate, although some differences are found at Mauna Loa and Hohenpeissenberg. These results seem to indicate that for the period 1970–1985 the precision of the long-term trend estimates will not be appreciably different at stations that sampled every other day than they would have been if that station had sampled every day. The reason for this insensitivity is the high day-to-day autocorrelation found in total ozone readings: the larger the day-to-day autocorrelation, the less sensitive the monthly mean (and hence the trend estimate) is to missing daily values. It should be noted that Tiao et al. eliminated the daily values *systematically* and spaced the remaining daily observations evenly through the month. These results are in agreement with the observation that for any particular calendar month, at a particular station, the ratio of the standard deviation of the daily total ozone measurements within the month to the

Table 2.1-2 Summary of Ozone Trend Estimates (in % per year) in total ozone and associated standard error

Sampling rate	Tateno	Hohenpeissenberg	Mauna Loa
1/1	–.002 ± .082	–.078 ± .061	–.382 ± .090
1/2	–.022 ± .082	–.099 ± .066	–.370 ± .091
1/4	–.010 ± .080	–.136 ± .080	–.300 ± .095
1/8	–.046 ± .073	–.103 ± .083	–.348 ± .092
1/16	–.009 ± .082	–.187 ± .084	–.322 ± .093

GLOBAL TRENDS

standard deviation of the monthly means from year to year is typically found to be about 2, indicating that there are about 4 truly independent observations each month.

Tiao et al. (1989) addressed a related issue which concerns estimating relationship between variables in two neighboring locations. Employing total ozone data from two European stations (Arosa and Hoheneissenberg) and those from three Japanese stations (Sapporo, Tateno, and Kagoshima), they have found that the correlation estimates based on monthly averages of daily measurements are insensitive to temporal sampling rate when the measurements are taken on the same days across the locations. On the other hand, the estimates deteriorate as the time lag between measurements taken at the two locations is increased. The main reason for this phenomenon is likely to be that relations on a monthly scale are primarily due to short-term contemporaneous correlations on a daily basis. Although their empirical findings are based on the same variable (total ozone) at two different locations, similar phenomenon is likely to occur between different atmospheric parameters at the same location. Thus, in designing a measurement program when relations between variables are of interest, it is important to exercise care in arranging the timings of different measurements both across and within stations.

Tiao et al. (1989) also investigated how different lengths of record and differing degrees of month-to-month autocorrelation within the data record affect the trend estimate and its standard error, and concluded that the precision of the trend estimates depends critically on the degree of the month-to-month autocorrelation in the measurements. If the month-to-month autocorrelation is large, it is indicative of unexplained medium to long-term variations in the data, and the standard error of the trend estimate is consequently large. It will be most difficult to provide early warning of a trend in total ozone in an area where the month-to-month autocorrelation is naturally high. In practice this means the tropics, and unfortunately there are not many long-term series of measurements in this region.

2.1.6 Concluding Remarks

In the previous sections, numerous past and emerging techniques for the measurement of ozone have been described. Where possible their accuracies and precisions have been presented. A few further remarks on the application of these techniques to the detection of trends are in order.

Following the definitions given in the introduction, if the systematic errors are truly consistent (as, for example, if they are dependent on a poorly known absorption coefficient), the changes or trends that can be detected may be smaller than the absolute error of a system's measurements. This is often the case; applicability then depends on how stable the system or instrument remains over time.

Ground-based instruments can be checked and recalibrated as necessary. These are generally regarded as being capable of long-term stable operation. This is technically true; actual results may depend on funding, the importance attached to the measurements, the skill of the observer, and other non-technical factors. An advantage is that the same instrument is used repeatedly for the observations, so instrument-to-instrument variations do not come into play at a single location.

Balloon and rocket measurements may be calibrated immediately before flight, but only rarely afterward. In addition, the conditions under which observations are made are generally different from those in which the calibrations are carried out. Perhaps most seriously, small instrument-to-instrument variations add an additional source of noise to attempts to look for trends. Because there is usually a relatively limited number of such observations, they have been of limited use for trend studies to date.

The features of satellite instruments are in some ways the converse of ground-based instruments. They cannot be checked in orbit, although they usually have a capability for in-flight calibration of at least some of the critical features of their designs. However, again it is the same instrument used at all locations as well as all times, so gradients and changes may be detected, depending on instrument stability. There is probably not enough experience to say much about instrument-to-instrument differences; the experience with SAGE I and II is encouraging that these effects can be small, but the SBUV-SBUV/2 problems are a cause for concern. Comparisons between different techniques are often illuminating. In principle the differences could be large, but the differences less than ~4% found among SAGE, SBUV, and LIMS in 1979 is an indication of the present level of agreement between different techniques that can be achieved. As noted above, these differences are probably due in part to differences in systematic errors, implying that at the present time, when one is looking for small changes, it is necessary to use very similar if not identical techniques, including instruments and data reduction algorithms, to keep the systematic errors constant. In future it may be possible, with a great deal of care, to reduce the systematic errors to the point that data from different instruments can be combined in trend analyses. This will require further laboratory measurements of the ozone absorption coefficients and their temperature and pressure dependences, comparisons of the retrieval algorithms, and field intercomparisons under as many conditions as possible.

A large amount of data has been collected over many years by instruments whose characteristics are known reasonably well. Initially, few of these measurements were made for the purpose of determining long-term changes. Fortunately, some of these data have the requisite accuracy and stability to provide a reasonable data base for efforts to detect and quantitatively measure changes in the ozone overburden and its vertical distribution, such as those reported by the OTP and later in this chapter.

Looking to the future, the measurement situation for total ozone is moderately satisfactory. The present network of Dobson stations is continuing for the most part, and provides a reasonable network for detecting regional and probably zonal trends in the middle latitudes of the Northern Hemisphere. New ground-based instrumentation appears to provide compatible data, allowing a continuation of the measurement series.

For global observations, the TOMS instrument continues to operate, having already provided almost one solar cycle (11 years) of data. A new technique for internal calibration appears to allow the TOMS to provide an entirely separate data record for total ozone that can be compared and checked against the ground-based network. Additional TOMS instruments are planned for flight on a variety of spacecraft during the 1990s, eventually reaching operational status late in the century. In the interim, if the problems with the instrument and data reduction are solved, the operational SBUV/2 could potentially provide another very valuable data record from the mid-1980s until the operational TOMS is launched.

The situation for the measurement of trends in vertical profiles is somewhat less satisfactory. In the past the ground-based Umkehr techniques were subject to interference by aerosols. It is believed that these may now be corrected, using new techniques and independent measurements of aerosol distributions, but further testing and validation is necessary. The new lidar and microwave methods also require further work to fully understand and characterize them. In addition there are sampling problems; the number of stations taking regular Umkehr observations is limited, and most of them are in the mid-latitudes of the Northern Hemisphere. At present, there are very few stations employing the new technology.

For the present, only data from the SAGE instruments appear to have the long-term stability to allow trend detection. SAGE II (and its spacecraft) are already over 5 years old, and there is not a planned successor until 1996. A failure could result in a lengthy gap. In addition, these data are subject to the

GLOBAL TRENDS

limitations of the sampling of the occultation technique and the attendant uncertainties in comparing different years (see OTP, Chapter 5). Again, if the problems with the SBUV/2 can be successfully resolved, they could potentially make an extremely valuable contribution. Other profile measurements will be obtained by research instruments on UARS, but it is unclear how well they will be able to extend the previous data records. An infrared limb scanner is scheduled to become available in 1996.

Present planning for ozone trend measurements suggests a systems approach, based on complementary ground-based and satellite observations. In this, satellite measurements can be checked for unexpected drifts through comparison with a network of carefully calibrated, maintained, and operated ground-based instruments. In turn, the satellite instruments act as transfer standards, indicating whether any of the ground instruments are drifting relative to the others. This will be especially challenging with respect to the measurement of vertical profiles. The stations in the Network for the Detection of Stratospheric Change (NDSC), which will include new instruments (lidar, UV, IR, and microwave spectrometers), are being planned with this function in mind.

2.2 TRENDS IN TOTAL OZONE

2.2.1 Introduction

This section summarizes the current understanding of trends in total column ozone. The objective of the analyses reported here are: (1) to re-examine the data set used by the Ozone Trends Panel (OTP) using several different statistical models which make varying assumptions in their treatment of the measurements, (2) to update trends derived from the Dobson network using the most recent data available, and (3) to examine the regional behavior of changes in total ozone using both ground-based and satellite-based measurements.

It is essential to recognize the merits and limitations of both the Dobson network and orbiting remote sensors. The Dobson network provides a long-term data record whose duration is suitable for detailed statistical analysis. The deficiency is a limited geographic coverage, with a bias toward middle latitudes of the Northern Hemisphere. The data record obtained by satellites has global coverage, although at present the length of record is inadequate for derivation of long-term trends. In addition, the trends that exist in data sets obtained by satellites contain drifts of instrumental origin. A correction is therefore required, and at present this must be done in an approximate way by comparison with the Dobson network. However, new approaches to data processing may minimize this problem in the future. Nonetheless, satellite measurements are useful in identifying geographic variations in ozone change.

A major effort in the Ozone Trends Panel Report centered on developing a provisionally revised Dobson data set. This made use of ozone measurements from nearby stations, temperatures measured at 50 mb, and detailed studies of the records from each instrument to identify problems in the Dobson data set. In addition, comparison of co-located ozone measurements made by the Nimbus-7 TOMS instrument and the Dobson network allowed identification and correction of inconsistencies in the latter data base. Further information appears in Chapter 4 of the Ozone Trends Panel Report. The updated trend analyses reported here adopt the provisionally revised data base for each Dobson station through December 1986, the latest information available to the Ozone Trends Panel in early 1988. As of this writing, available data after 1986 have received a screening similar to that performed for the provisionally revised Dobson data set, and a number of adjustments have been made to data from 1987 and 1988 to smooth erratic variations.

2.2.2 Trend Analysis of Dobson Total Ozone Data

2.2.2.1 Result of the 1988 Ozone Trends Panel and Comparison with Other Studies

In 1988, the Ozone Trends Panel completed a statistical analysis of Dobson data from a network of stations, most of which were located between 30 and 64 degrees North latitude. The Panel focused on data over the period 1965–1986 for three reasons: It contained two complete solar cycles; effects of the atmospheric nuclear bomb tests should have subsided by 1965; and many more Dobson stations were operating in 1965 than in 1957–1958, thereby providing a more substantial data base than was available in earlier years. The percent changes in total ozone over the 17-year period 1970–1986 were reported by season and latitude zone. These results appear in the first column of Table 2.2-1, labeled as OTP. This work built on statistical studies of ozone performed over the last decade (e.g., Bloomfield et al., 1983; Hill et al., 1986; St John et al., 1981; Reinsel et al., 1987b). Over the Northern Hemispheric latitude band 30–64 degrees North, there was a wintertime change of about –4% for this period (ranging from –2% to –6%

Table 2.2-1. Comparison of trend results by season and latitude (17 years % change between 1970 and 1986 with one standard error in parentheses)

Zone/ Latitude	Year Round				
	OTP	AS1	UW&C1	UW&C2	AS2
53–64°N/55°N	–2.3(0.7)	–1.6(0.8)	–2.1(0.7)	–2.0(0.7)	–1.8(1.0)
40–52°N/45°N	–3.0(0.8)	–2.6(0.7)	–1.9(0.6)	–1.6(0.6)	–1.9(0.8)
30–39°N/35°N	–1.7(0.7)	–0.8(0.8)	–1.0(0.7)	–1.3(0.6)	–1.9(0.9)
Average	–2.3(0.5)	–1.7(0.5)	–1.7(0.5)	–1.6(0.6)	–1.9(0.8)
Zone/ Latitude	Winter				
	OTP	AS1	UW&C1	UW&C2	AS2
53–64°N/55°N	–6.2(1.5)	–4.2(1.6)	–4.7(0.8)	–5.1(0.8)	–5.1(1.0)
40–52°N/45°N	–4.7(1.5)	–5.1(1.4)	–3.4(0.7)	–3.6(0.6)	–4.0(0.7)
30–39°N/35°N	–2.3(1.3)	–1.7(1.3)	–1.5(0.8)	–2.1(0.7)	–2.8(0.8)
Average	–4.4(1.0)	–3.7(1.0)	–3.2(0.6)	–3.6(0.6)	–4.0(0.7)
Zone/ Latitude	Summer				
	OTP	AS1	UW&C1	UW&C2	AS2
53–64°N/55°N	–0.2(0.8)	–1.1(0.8)	–0.7(0.7)	–0.9(0.7)	–0.6(1.0)
40–52°N/45°N	–1.9(0.7)	–1.2(0.7)	–1.5(0.7)	–1.1(0.5)	–1.2(0.8)
30–39°N/35°N	–1.9(0.8)	–0.6(0.8)	–1.2(0.8)	–1.2(0.6)	–1.2(0.9)
Average	–1.3(0.5)	–1.0(0.5)	–1.1(0.5)	–1.1(0.5)	–1.2(0.8)

Notes:

- OTP = Ozone Trends Panel result based on zonal series.
- AS1 = Allied-Signal results using zonal series.
- UW&C1 = Universities of Wisconsin and Chicago results using regional/latitudinal analysis where the same trend is assumed to apply to all stations in a single region.
- UW&C2 = Universities of Wisconsin and Chicago results using regional/latitudinal analysis with a linear trend in latitude.
- AS2 = Allied-Signal results using regional/latitudinal analysis of individual stations including a nuclear weapons correction. The text describes additional differences between the AS2 and UW&C1 and UW&C2 models.

GLOBAL TRENDS

with increasing latitude), a summertime change of about -1% , and a year-round change of about -2% . The statistical model included terms to account for changes in ozone related to the quasi-biennial oscillation (QBO) cycle in winds and the 11-year solar cycle. The long-term trends that remained, as reported in Table 2.2-1, could not be explained by these known natural variations.

Recent analyses by scientists at Allied-Signal, Inc. and the Universities of Wisconsin and Chicago have subsequently verified the findings of the Ozone Trends Panel, including a new analysis of the sensitivity of derived trends to (1) the length of data records, (2) regional differences, and (3) the statistical techniques applied. Of particular interest were the major perturbations in ozone before 1965 and after 1982 and their effects on derived trends, as well as the differences observed among different geographical regions (e.g., North America, Europe, and Japan). The nuclear weapons tests in the early 1960s and natural phenomena, such as the El Chichon volcanic eruption and El Niño events in the 1980s, may be related to these ozone fluctuations. Figure 2.2-1 is a time history of residual zonal mean total ozone in Dobson Units (DU) with most known natural and man-made variations subtracted out. This shows some large perturbations in the post-1982 period following, but not necessarily related to, the El Chichon volcanic eruption. With respect to regional differences, Figure 2.2-2 (a)-(c) shows larger decreases over North America and Europe than over Japan after allowing for known variability. The nonrandom fluctuations that remain in Figure 2.2-2 arise from sources of variation not included in the statistical model, for example the El Niño oscillation, and an incomplete subtraction of known sources such as the QBO. However, these nonrandom fluctuations are removed by the autoregressive filter. The European wintertime dip in 1982–1983 is particularly noticeable.

Table 2.2-1 presents a comparison of five separate sets of trend results, including the Ozone Trends Panel findings, over the 17-year period 1970 through 1986. In these and all subsequent Dobson analyses, the statistical models account for variations in ozone related to the solar cycle, the QBO, and, where applicable, nuclear weapons tests during the 1960s. The derived long-term trends cannot be explained by any of these mechanisms. The time dependence of ozone changes related to nuclear weapons tests is based on calculations by the Lawrence Livermore Laboratory chemical-transport model (Wuebbles and Kinnison, 1989). However, the magnitude of the ozone change is determined from the statistical analysis and is allowed to vary with latitude.

The choice of the period 1970–1986 for the trend assessment corresponds to the period during which theory predicts the onset of effects on the ozone layer related to chlorofluorocarbon (CFC) release. The trend is assumed to start in January 1970 and be zero prior to this time. Sensitivity to the starting date is discussed later. The form of the trend model used in all of the studies is described in Appendix 2.A.

The results in the second column of Table 2.2-1, labeled AS1, were developed by Allied-Signal researchers with the same zonal mean series of total ozone data used by the Ozone Trends Panel for latitude belts 30–39°N, 40–52°N and 53–64°N. Results in the third and fourth columns were obtained by researchers from the Universities of Wisconsin and Chicago (designated UW&C). Unlike the first two sets of results, which analyzed the data after it was pooled into the zonal mean series shown in Figure 2.2-3, the UW&C studies derived a separate trend of each of the 25 stations within the 26–60°N latitude band (see Table 2.2-2, excluding Reykjavik and Uccle). The trends were then fitted (or regressed) against latitude using two different methods. In the first method, labeled UW&C1, all stations within each of three different latitude zones, 30–39°N, 39–50°N and 50–64°N, were assumed to have a common average trend. In the second method, labeled UW&C2, the trends were regressed as a linear function of latitude (Bojkov et al., 1989). Both UW&C methods allow for apparent regional differences over North America, Europe, Japan, and the Middle East. The first method more closely corresponds to the OTP and AS1 analyses based on the

GLOBAL TRENDS

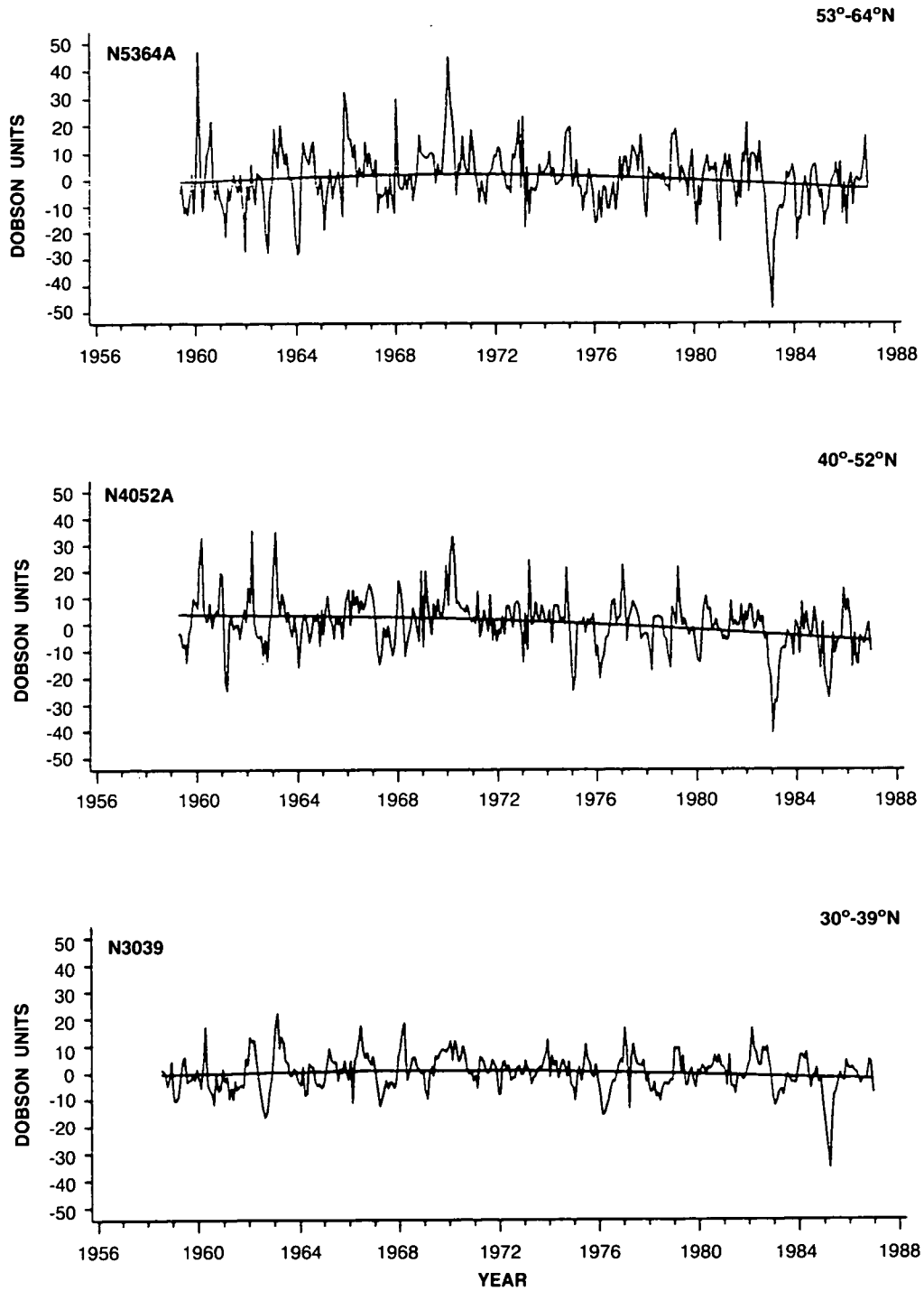


Figure 2.2-1. Monthly and zonally averaged Dobson total ozone values versus time after removal of seasonal, quasi-biennial oscillation (QBO), solar cycle, and nuclear test effects. A smooth line is shown for each of the three latitude zones 53-64°N, 40-52°N, and 30-39° N.

GLOBAL TRENDS

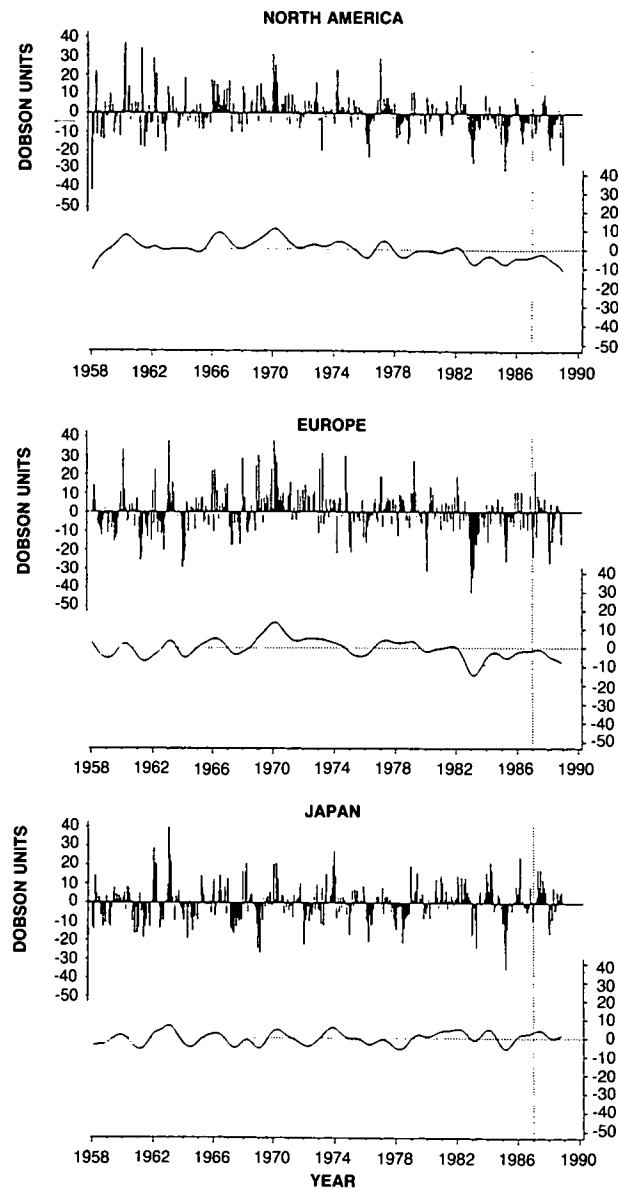


Figure 2.2-2a. Regional plots of Dobson total ozone after removal of seasonal, solar, QBO, and nuclear test effects for North America (top), Europe (center), and Japan (bottom), all months. The deviations are plotted in Dobson units where the upper panels give monthly values and the lower panels are smoothed. Nonrandom fluctuations are removed from the trend analysis by an autoregressive filter. Vertical lines at the end of 1986 denote the end of the data set available to the Ozone Trends Panel.

zonal mean series, while the second method provides a capability for estimating trends as a function of latitude. Overall the second method uses more information contained in the data than does analysis of a zonal series, but it also makes a stronger assumption concerning the relationship of trends to latitude, namely that they are linear. In Table 2.2-1 the trend estimates are given for three latitude zones based on UW&C method 1, and the predicted changes are given for latitudes 55°N, 45°N, and 35°N based on UW&C

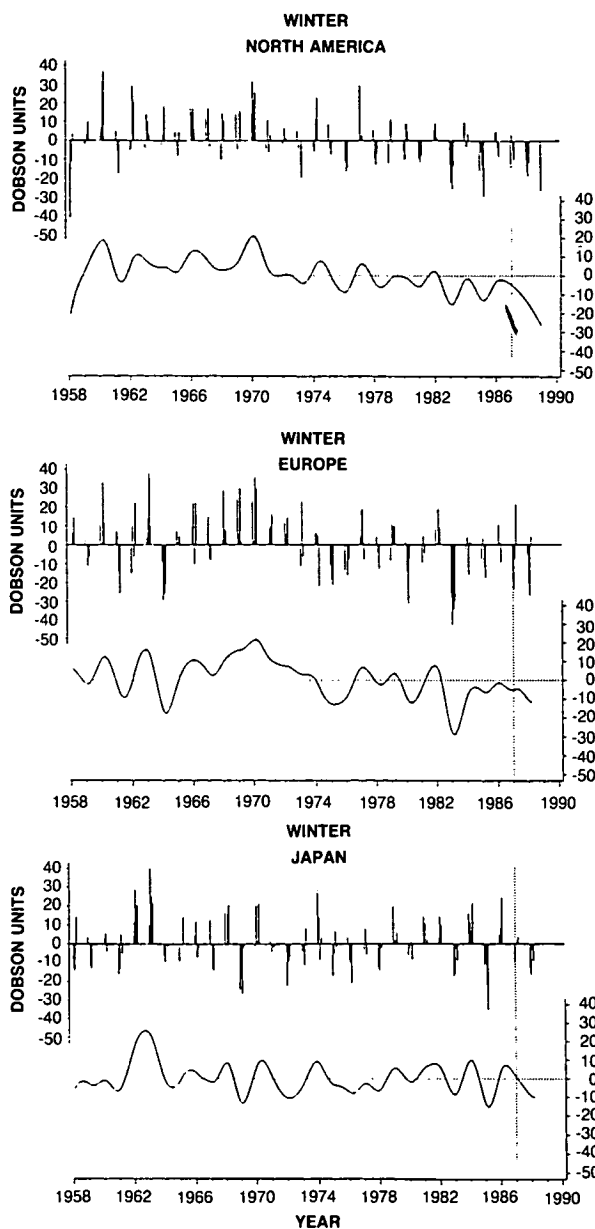


Figure 2.2-2b. Same as 2.2-2a for winter months (December-March).

method 2. Separate trends are derived for year-round, winter (December-March), and summer (May-August), respectively.

The last column in Table 2.2-1, labeled AS2, presents results obtained by Allied-Signal researchers using a technique similar to method 2 in the UW&C study but which includes adjustments for nuclear weapons tests in the 1960s. Results are based on only the 25 stations located at latitudes between 26°N and 64°N (Table 2.2-2). The AS2 results do not use the two stations from Egypt and Pakistan to form a separate

GLOBAL TRENDS

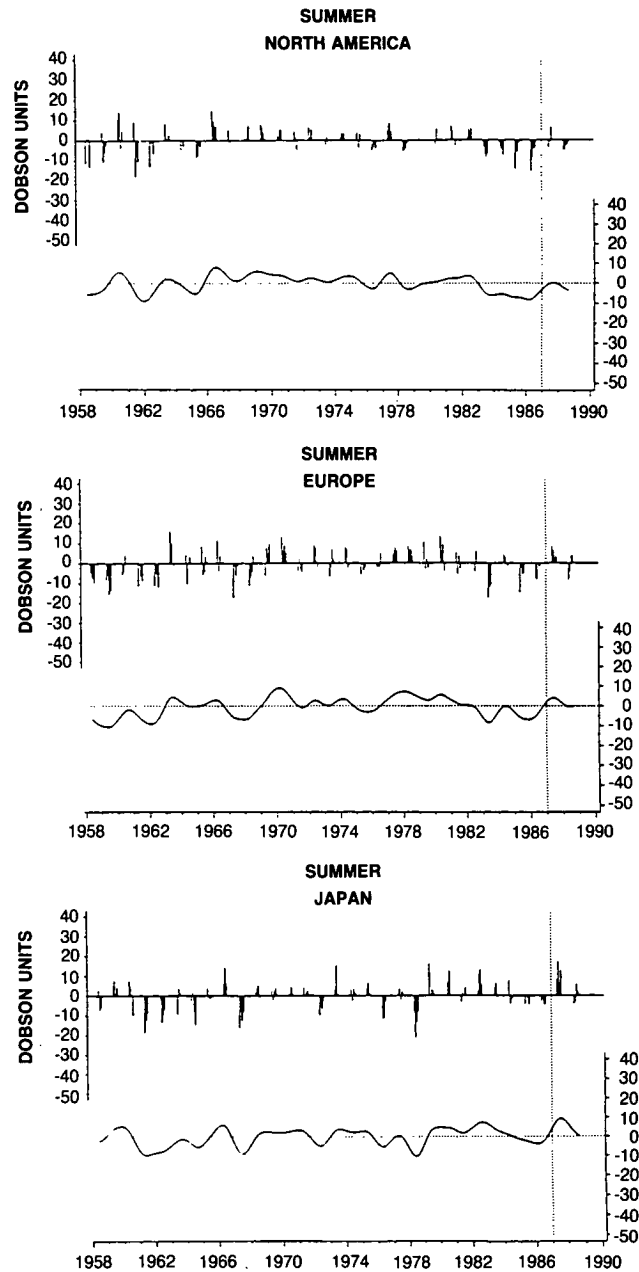


Figure 2.2-2c. Same as 2.2-2a for summer months (May-August).

Mid-East region because of the disproportionate influence these two stations can have on the summary results.

Overall, the five sets of results show a consistent pattern. They indicate a wintertime (December-March) change ranging from -2% to -6% between 1970 and 1986 which correlates with latitude, that is, the wintertime trends become more negative with increasing latitude. The value derived by the Ozone Trends Panel for winter near 55°N latitude tends to be 1–2% more negative than found in the other studies. Also, standard errors associated with the wintertime trends are smaller in those studies that accounted for the additional regional and latitudinal information.

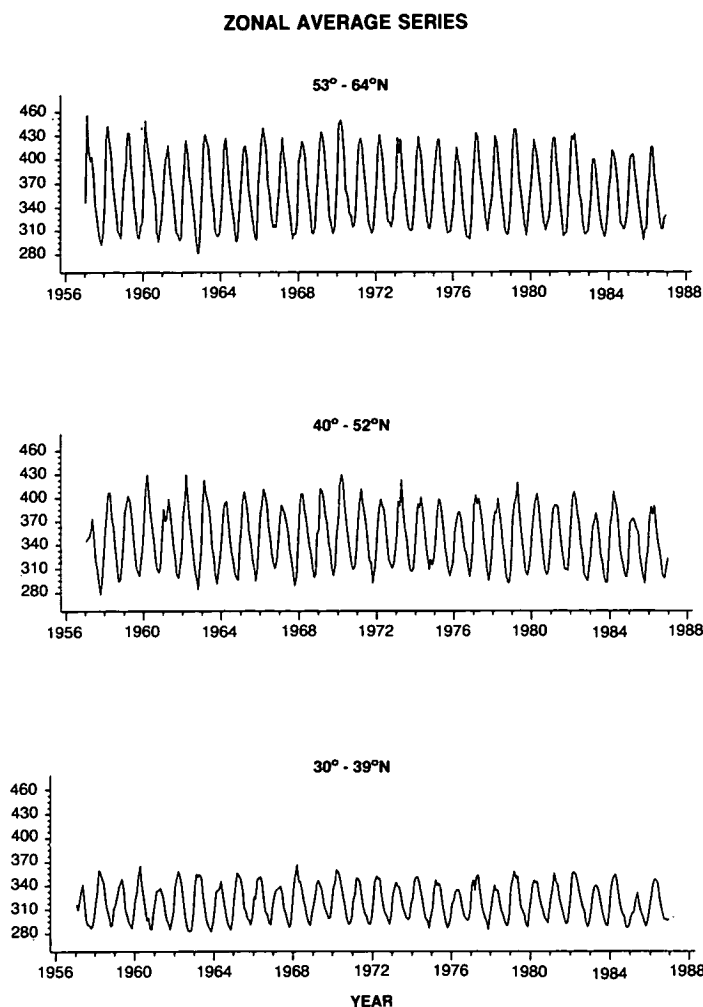


Figure 2.2-3. Plots of Dobson total ozone monthly averages combined into time series for each latitudinal zone 53-64°N, 40-52°N, and 30-39°N. The vertical scale is in Dobson units.

Although for a given latitude, the five sets of summertime trend estimates may differ by as much as about 1%, the change in summertime averaged over all latitudes was about -1% in each study. No significant latitudinal pattern appears in the summertime trends. Similarly, in the year-round trends, no significant latitudinal pattern appears. The concept of “significance” here refers to the statistical sense of exceeding two standard errors. For each study, the average year-round change is approximately -2% over 17 years.

The difference between the two studies which used zonal series (labeled OTP and AS1 in Table 2.2-1) arise mostly from the differing lengths of record. For example, if the pre-1965 data and nuclear test adjustment are excluded from the AS1 analysis, as was done in the Ozone Trends Panel study, then the revised AS1 results would be close to the OTP trends. Other differences among the groups of results in Table 2.2-1 can be ascribed to the inclusion of a nuclear weapons adjustment, which was used in the columns marked AS1 and AS2, the use of four versus three regions and slightly different groups of stations

GLOBAL TRENDS

Table 2.2-2. List of Dobson total ozone stations at latitudes between 26°N and 64°N (data from these stations were revised by the Ozone Trends Panel through 1986)

Region	Station	Latitude	Start Date	End Date	Now available
N. America	Churchill	59°N	1/65	12/86	9/88
	Edmonton	54°N	1/58	11/86	3/88
	Goose	53°N	1/62	11/86	9/88
	Caribou	47°N	5/58	12/86	10/88
	Bismarck	47°N	1/58	12/86	10/87
	Toronto	44°N	1/60	11/86	9/88
	Boulder	40°N	1/64	12/86	10/88
	Wallops Island	38°N	1/70	12/86	10/88
	Nashville	36°N	1/63	12/86	10/88
	Tallahassee	30°N	5/64	11/86	4/88
Europe	Reykjavik	64°N	1/58	10/86	10/88
	Lerwick	60°N	1/58	11/86	10/88
	Leningrad	60°N	8/68	12/85	12/85
	Belsk	52°N	1/63	12/86	8/88
	Bracknell	51°N	1/69	12/86	10/88
	Hradec Kralove	50°N	1/62	6/86	10/88
	Uccle	50°N	7/71	12/86	8/88
	Hohenpeissenberg	48°N	1/67	12/86	11/88
	Arosa	47°N	1/58	12/86	10/88
	Vigna DiValle	42°N	1/58	12/86	11/87
Cagliari	39°N	1/58	12/86	6/88	
Japan	Sapporo	43°N	1/58	12/86	10/88
	Tateno	36°N	1/58	12/86	10/88
	Kagoshima	32°N	1/58	12/86	10/88
	Naha	26°N	4/74	12/86	10/88
Mid East	Cairo	30°N	11/74	10/86	10/88
	Quetta	30°N	1/58	12/86	10/88

(UW&C1 and UW&C2 versus AS2), the analysis of averaged zonal data versus the analysis of individual stations (OTP and AS1 versus UW&C2 and AS2), and small effects due to the choice of solar cycle and QBO adjustments. The essential information in Table 2.2-1 is that all of the analysis techniques produce similar latitudinal and seasonal patterns.

Trends derived from the AS2 model are shown on a station-by-station basis in Figures 2.2-4(a)-(c). Throughout the remainder of this section, trends will be expressed in percent per decade. This allows for easy comparison of trends derived from data records of differing lengths. For the year-round case, all the North American (N) trends are negative, all the European (E) trends are negative except Reykjavik at 64°N, and the four Japanese (J) trends are balanced on either side of zero change. The most northerly Japanese station, Sapporo, lies at 43°N. For the wintertime period, a strong latitudinal pattern emerges with the most negative trends appearing at the most northern latitudes. Only the Japanese stations show little or no wintertime change. In the summertime, the trends, although tending toward the negative side, show no latitudinal gradient.

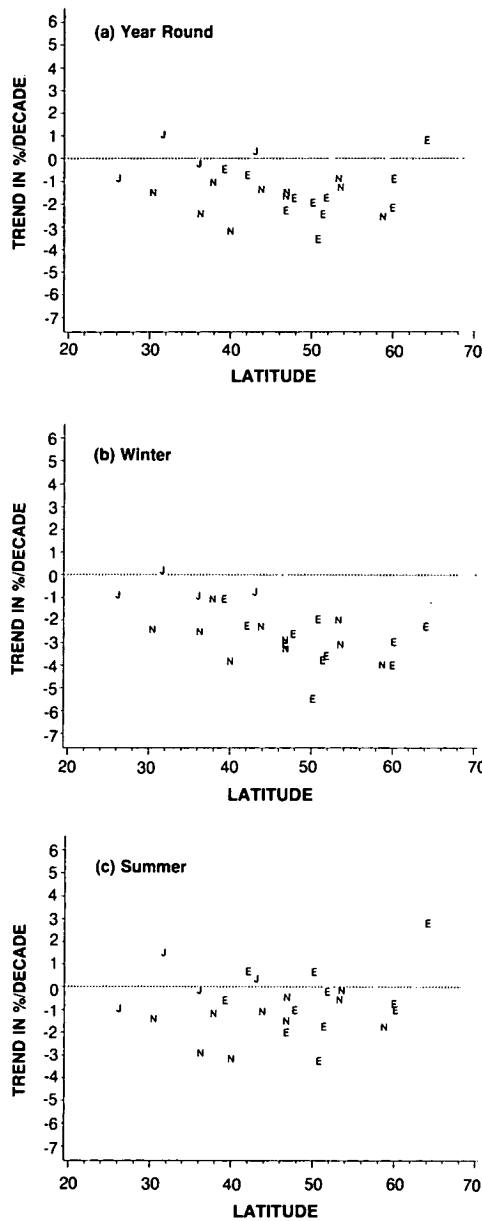


Figure 2.2-4. Individual trend estimates for the period 1970-1986 using the AS2 model of Allied-Signal, Inc. Trends appear versus latitude and are expressed in % per decade for (a) year-round, (b) winter (December-March), and (c) summer (May-August) periods. The plotting symbol is E = Europe, N = North America, and J = Japan.

Fisletov (1989) performed an independent trend analysis of the provisionally revised data from 30 Dobson stations and, in addition, examined the effect of including measurements from the 22 most reliable M-83 instruments in the USSR network. Trends based only on the Dobson record through 1986 lie in the range defined in Table 2.2-1 and show the same latitudinal and seasonal pattern.

GLOBAL TRENDS

2.2.2.2 Sensitivity Analysis

To quantify the dependence of the derived trends on factors such as data length, nuclear weapons adjustment, type of solar adjustment, inclusion of data from Soviet instruments, and nonseasonal versus seasonal trend models, a sensitivity analysis was done. The effects on the trends are summarized in Table 2.2-3 using the Allied-Signal models as baselines. The sensitivities are expressed as the change in trend, in % per decade, due to the factors considered. The results are similar to those obtained by the Ozone Trends Panel.

The exclusion of post-1982 data has a large effect as shown by item 1 in Table 2.2-3 and Figure 2.2-5 (a)-(c). The trends are noticeably less negative or more positive when only data through October 1982 are used. This date corresponds approximately to the arrival of the El Chichon aerosol at middle latitude. Interestingly, the effect on the trends from eliminating post-October 1982 data is larger in summer than in the winter. This is particularly evident when the data are analyzed using a regional/latitudinal model where the effect of dropping post-October 1982 data is to produce a summertime trend 0.8% per decade less negative and a wintertime trend 0.3% per decade less negative. The effects in summer and winter are both about 1% per decade using the zonal analysis. After 1982, summertime ozone in all three regions (North America, Europe, and Japan) went down and stayed down until 1987, whereas wintertime ozone showed some degree of recovery in all three regions (see Figure 2.2-2). Comparison of Figure 2.2-5(a)-(c) with Figure 2.2-4 (a)-(c) shows how the trend patterns change when the post-October 1982 data are dropped. This behavior may be a chemical response to volcanic aerosol from the El Chichon eruption or to a true change in the nature of the long-term trend in ozone. Since derived trends are highly influenced by extreme values or sustained dips at or near the end of the record, the addition of extra data from 1987 and 1988 is important to see if this nonlinear pattern is continuing (see Sections 2.2.2.3 and 2.2.3.2.).

Table 2.2-3. Summary of sensitivity analysis (% per decade effect on trends)

Sensitivity Scenario	Zonal Analysis ^a			Regional/Latitudinal Analysis ^b		
	Year-Round	Winter	Summer	Year-Round	Winter	Summer
1. Exclude Post 10/82 Data	+0.8	+0.9	+1.0	+0.3	+0.3	+0.8
2. Uniform Model	+0.6	—	—	+0.4	—	—
3. Exclude Pre-1965 Data	-0.6	-0.6	-0.5	-0.3	-0.1	-0.4
4. Exclude Nuclear Term	+0.2	+0.2	+0.1	+0.1	0.0	0.0
5. Add Russian Stations	-0.1	+0.4	-0.6	NA	NA	NA
6. Smooth Solar Term	0.0	0.0	0.0	0.0	0.0	0.0
7. Remove Solar Term	-0.1	-0.1	-0.1	-0.1	-0.2	-0.1
8. Remove QBO	+0.1	0.0	+0.1	0.0	-0.1	+0.1
9. Start Trend in 1/65 vs. 1/70	+0.4	+0.7	+0.3	+0.2	+0.5	+0.2
10. Start Trend in 1/75 vs. 1/70	-0.5	-0.9	-0.4	-0.4	-0.6	-0.4
11. Add 1987 and 1988 Data	NA	NA	NA	+0.2	+0.1	+0.3

^aSensitivity effect averaged across three zones 30–39°N, 40–52°N, 53–64°N using AS1 model.

^bSensitivity effect predicted at 45°N using AS2 model.

Note: Rounding is to nearest 0.1% decade.

The table entry indicates the amount (in % decade) to add to the trend from the standard scenario to obtain the trend for the sensitivity scenario.

Example: if data after 10/82 are omitted from the AS1 standard calculation, the zonal year-round trend increases in a positive direction by +0.8% decade; i.e., from -1.0 (standard) to -0.2 (sensitivity calculation).

Winter = December–March; Summer = May–August.

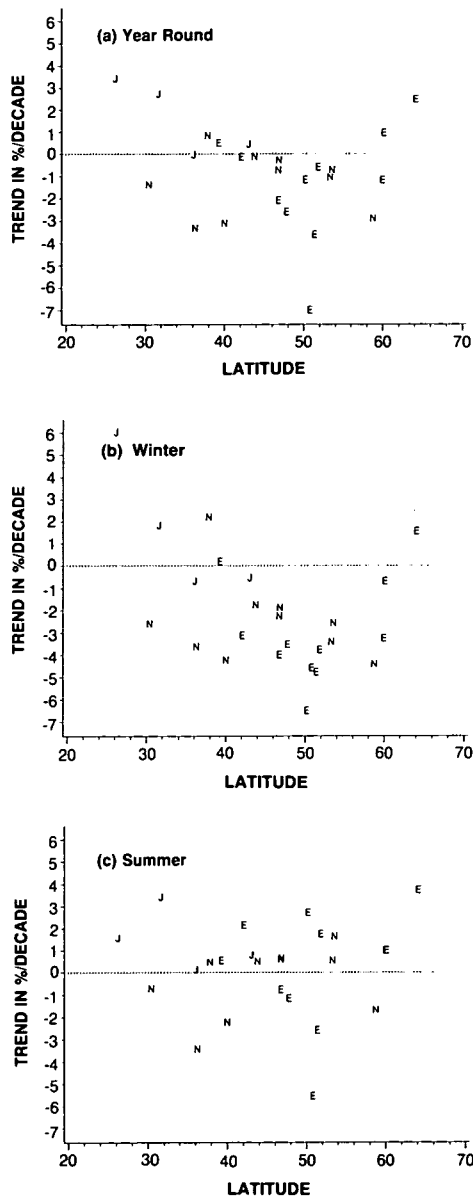


Figure 2.2-5. Individual trend estimates for the period 1970-1986 using the AS2 model of Allied-Signal, Inc. Same as Figure 2.2-4 except trends are fitted only through October 1982. Trends appear versus latitude and are expressed in % per decade for (a) year-round, (b) winter (December-March), and (c) summer (May-August) periods. The plotting symbol is E = Europe, N = North America, and J = Japan.

If the statistical model assumes that trends are the same for all months (i.e., a uniform trend), then the trends are closer to zero by about 0.5% per decade. Analyses suggest that the uniform trend model is not appropriate for use on data poleward of 40°N, since there are statistically significant winter versus summer differences in the trends.

GLOBAL TRENDS

As mentioned earlier, exclusion of pre-1965 data because of possible nuclear effects and the paucity of data leads to more negative trends. In a regional latitudinal analysis, the effect on the winter trends is small. However, in a zonal analysis like that done by the Ozone Trends Panel, the wintertime change is made more negative by about 0.6% per decade when the pre-1965 data are excluded. So, depending on the formulation of the model and the way data are handled, the wintertime trend can be quite sensitive to the re-1965 data.

An analysis by Allied-Signal researchers shows that inclusion of data from Soviet instruments in the zones poleward of 40°N makes the winter trend less negative or more positive by about 0.4% per decade when averaged across the latitude belt 30–64°N, but enhances the summer reduction, with little effect on the year-round trend.

Exclusion of the nuclear adjustment makes the trends less negative by about 0.2% per decade. The treatment of the solar cycle and the QBO in winds has little or no effect on the trends.

The sensitivity of the derived trend to the start date has interest because of issues related to (1) the trends being larger after October 1982 than in the earlier period, and (2) the trend start point being at or near extremes of the solar cycle. As pointed out above, the trend estimates are relatively insensitive to the solar cycle. However, as seen in Table 2.2-3, the trend estimates are sensitive to the start date. For example, in the zonal analysis, the derived winter trend is less negative by 0.7% per decade when the trend is started 5 years earlier (i.e., January 1965) and more negative by 0.9% per decade when the trend is started 5 years later (i.e., January 1975). This could be due in large part to influence of the post-October 1982 data. That is, the influence of the post-October 1982 data becomes larger when the trend period is taken to be shorter relative to the baseline period.

In the sensitivity analysis shown in Table 2.2-3, it should be noted that, in most cases, the regional/latitudinal analysis is less sensitive to the factors considered than is the zonal series analysis. Hence, the former approach is more robust and is currently the analysis of choice for the Allied-Signal and Wisconsin-Chicago research groups. Another reason for its preference is that variability within and across regions can be taken into account along with the latitudinal relationship.

In a separate regional sensitivity analysis (Table 2.2-4) using the Wisconsin-Chicago model, a comparison of trends was made using both the “provisionally revised” Dobson data set and the Dobson data as originally published. This showed that over Europe the “provisionally revised” data gave trends that were about 1% per decade more negative in all seasons than did the original data. Much smaller differences between trends in the two data sets resulted over North America and Japan. The differences in trends caused by the data revisions and especially by the seasonal versus uniform trend model explain why earlier published studies (Hill et al., 1986; Reinsel and Tiao, 1987a) show no significant trends, since the previous

Table 2.2-4. Regional sensitivity analysis comparing trends from the “Provisionally Revised” Dobson data set with the original published data

	Trend Difference = (Revised – Original) in % per Decade		
	Japan (26°N–43°N)	North America (30°–59°N)	Europe (39°N–60°N)
Year-Round	0.2	0.0	– 1.0
Winter	0.2	0.4	– 1.2
Summer	0.2	– 0.2	– 0.8

studies used a uniform trend model on the original Dobson data. Additional discussion of this issue appears in Chapter 4 of the Ozone Trends Panel Report.

In summary, the choice of model (seasonal versus uniform, and zonal versus regional/latitudinal), timing of the trend starting date, and the record length have the largest effects on the derived trends. However, the general pattern of significant wintertime changes at the middle and higher latitudes remains intact under different scenarios.

2.2.2.3 Update of Trends into 1988

As of this writing, data were available into 1987–1988 from all but one of the Dobson stations in Table 2.2-2 (Leningrad). In most cases, data were available through August 1988 or later (see last column of Table 2.2-2). When these data were included in the trend analysis, most of the year-round, winter, and summer trends became slightly less negative. The effects of the additional data are shown in Table 2.2-3 based on the AS2 model, and the individual station trends appear in Figure 2.2-6 (a)-(c) for year-round, winter, and summer, respectively. At 45°N, the winter trends are less negative by 0.1% per decade. At 55°N (not listed in Table 2.2-3), the winter trend is less negative by 0.2%. The biggest change was seen in the summer, where the trend at 35°N is calculated to be 0.5% per decade less negative.

Trends in total ozone tend to be less negative in all seasons when the 1987 and 1988 data are added. Table 2.2-5 summarizes the trend estimates updated into 1988 by latitude alongside the estimates through December 1986, using the AS2 model. Figures 2.2-7(a) through (c) show the differences between trends estimated into 1988 versus those through December 1986 at each station. Notice that at most sites the trend differences are positive with the addition of the new data. Overall, the year-round trend estimates predicted at 35°N and 45°N are no longer statistically significant. The winter trend estimates updated into 1988 at the latitudes 45°N and 55°N are significant but closer to zero than those through December 1986, while the trend at 35°N is slightly more negative. Table 2.2-5 shows that the addition of data into 1988 does not alter the general conclusions of the Ozone Trends Panel, although differences in detail exist.

Table 2.2-6 summarizes the regional effects of including the 1987 and 1988 data by tabulating the AS2 model trends using data through 1986, together with the results using all data available into 1988. In both situations, the Japanese region shows no significant trend year-round, winter or summer. In both cases the year-round and winter trends are significant over North America and Europe, and the summer change is significant over North America. In most cases the changes are slightly smaller when the data set is updated into 1988 as compared to changes derived through 1986.

Although including or excluding the solar cycle term in the statistical model has little effect on the estimated linear trend in ozone (see Table 2.2-3), there appears to be a measurable solar effect on ozone itself. This effect has no apparent relationship to latitude as demonstrated in Figure 2.2-8. The average solar coefficient over the 25 Northern Hemisphere stations is 0.03 Dobson units per unit of 10.7 cm flux (standard error 0.005). This corresponds to a change in ozone of approximately 1.2% from a typical solar maximum to solar minimum, a range taken of 140 units as measured by the 10.7 cm flux.

2.2.2.4 Summary of Dobson Analyses and Comparison with Theory

Recent studies have both verified the findings of the Ozone Trends Panel regarding changes in Northern Hemisphere total ozone over the period 1970 through 1986 and extended the analyses using data through

GLOBAL TRENDS

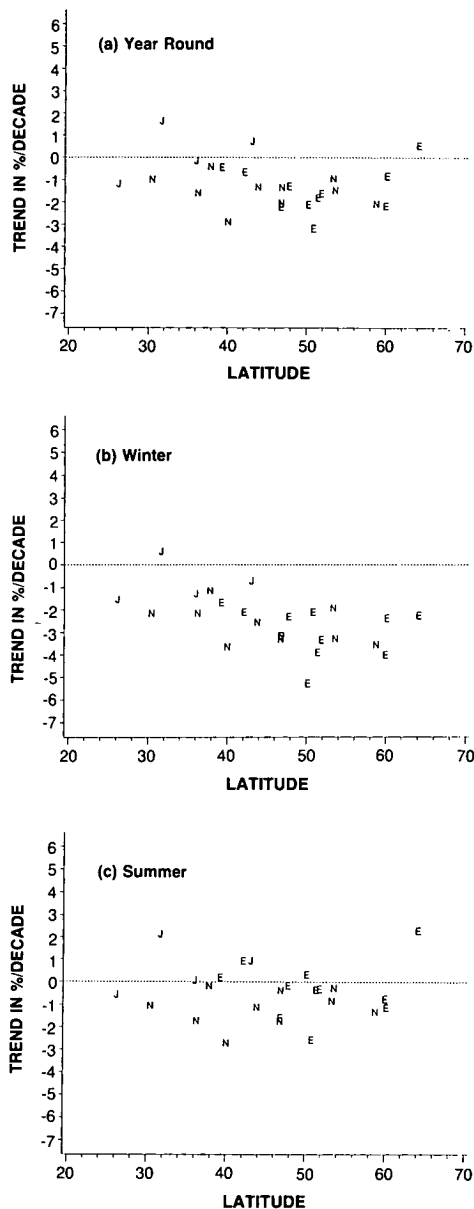


Figure 2.2-6. Individual trend estimates for the period 1970-1988 using the AS2 model of Allied-Signal, Inc. Same as Figure 2.2-4 except trends are fitted using updated data into 1988. Trends appear versus latitude and are expressed in % per decade for (a) year-round, (b) winter (December-March), and (c) summer (May-August) periods. The plotting symbol is E = Europe, N = North America, and J = Japan.

late 1988. Over the latitude band 26–64°N, the new analyses (see Table 2.2-6) found a wintertime trend averaging about -2.2% per decade for the period 1970–1986, with summertime and year-round trends averaging about -0.7% and -1.1% per decade, respectively. These results are slightly less negative than those of the Ozone Trends Panel. The winter reductions become larger with increasing latitude, varying from -1.7% per decade near 35°N to -3.0% per decade near 55°N.

Table 2.2-5. Trends in total ozone derived from Dobson data updated into 1988 compared with trends derived through 1986 (trends are in % per decade with one standard error in parentheses). Winter = December–March; Summer = May–August

Year Round			
Latitude	1986	1988	Diff.
55°N	– 1.08(.56)	– .99(.58)	.1
45°N	– 1.10(.49)	– .94(.50)	.2
35°N	– 1.11(.53)	– .88(.54)	.2
Winter			
Latitude	1986	1988	Diff.
55°N	– 3.02(.59)	– 2.70(.58)	.3
45°N	– 2.34(.41)	– 2.26(.47)	.1
35°N	– 1.66(.48)	– 1.81(.53)	.2
Summer			
Latitude	1986	1988	Diff.
55°N	– .35(.60)	– .21(.59)	.1
45°N	– .68(.45)	– .34(.48)	.3
35°N	– 1.01(.51)	– .47(.54)	.5

A variety of sensitivity studies were performed to determine which features of the ozone data and the analysis techniques most affected the derived trends. The choice of model (seasonal versus uniform and zonal versus regional/latitudinal), timing of the trend starting date, and the record length have the largest influences on the derived trends. However, regardless of the model or the particular treatment of the data, significant negative trends appear in winter at middle to high latitudes.

At the time of this writing, total ozone data are available through late 1988 at many stations. Year-round and winter trends computed using the most recent data (middle to late 1988) are slightly less negative than the trends derived through 1986, while summer trends were noticeably less negative at latitude 35°N. Winter trends based on the updated data continue to show an increase with latitude, from about –1.0% per decade near 35°N to –2.7% per decade near 55°N.

The executive summary of the OTP report presented predicted change in total column ozone based on two-dimensional models for summer (May–August) and winter (December–March). Results appeared as the difference between computed column ozone averaged over the 11-year period 1976–86 and that for 1965–75. For summer the computed difference imply a trend of –0.4 to –0.6% per decade over the latitude range 35°N to 55°N. These values lie within one standard error of the derived summer trends in Table 2.2-5. Predicted trends during winter are more negative than those in summer, being approximately –0.5, –0.8, and –1.1% per decade at 35°N, 45°N, and 55°N, respectively. The corresponding observed trends in Table 2.2-5 are -1.8 ± 1.0 , -2.3 ± 1.0 , and $-2.7 \pm 1.2\%$ per decade, where the error bars are 2σ , 95% confidence limits. Theory and observation both yield trends which become more negative as one moves poleward. However, in all cases the models produce trends that are less negative than the observations and lie outside of the 2σ error bars.

GLOBAL TRENDS

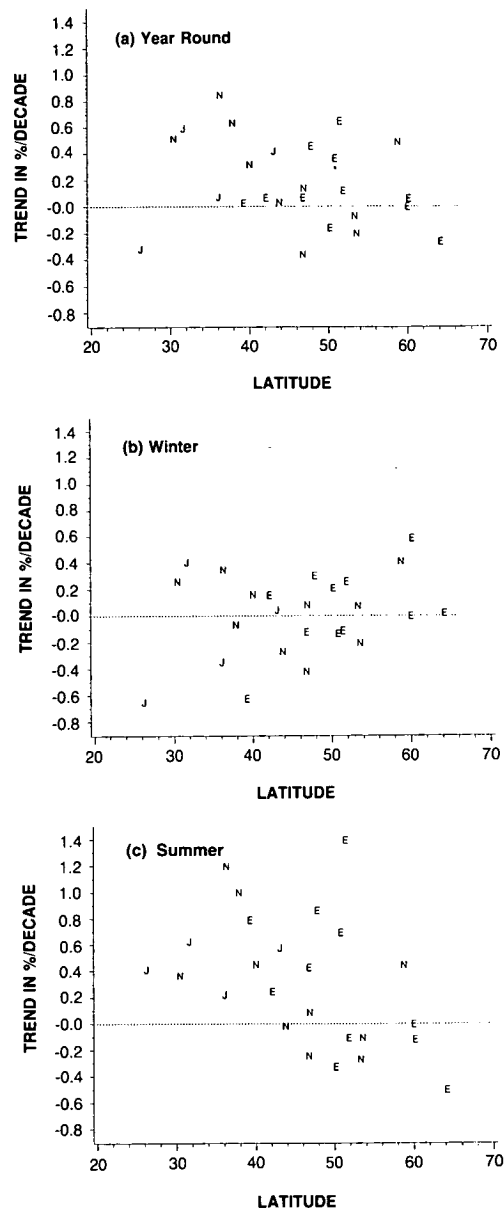


Figure 2.2-7. Differences between estimated trends into 1988 versus trends through 1986. The difference is calculated as the trend including data into 1988 minus the trend through 1986, expressed in % per decade at each Dobson station between 26°N and 64°N (a) year-round, (b) winter (December-March), and (c) summer (May-August).

2.2.3 Analysis of Satellite-Based Data from SBUV and TOMS Beginning in November 1978

2.2.3.1 Data Base and Analysis Procedure

The SBUV and TOMS sensors on the Nimbus-7 satellite began operation in November 1978. Given the short length of these data bases and other problems discussed below, it is not feasible to derive true

Table 2.2-6. Trends in total ozone derived by region based on data through 1986 and data updated through October 1988 (trends are in % per decade with one standard error in parentheses). Winter = December–March, Summer = May–August

Region	Number of Stations	Year Round		Winter		Summer	
		1986	1988	1986	1988	1986	1988
N. America	10	-1.7(.3)	-1.6(.3)	-2.8(.4)	-2.9(.3)	-1.4(.4)	-1.2(.4)
Europe	11	-1.5(.3)	-1.4(.3)	-3.0(.4)	-2.9(.4)	-0.6(.4)	-0.3(.3)
Japan	4	+0.2(.5)	+0.5(.5)	-0.5(.6)	-0.6(.5)	+0.3(.7)	+0.8(.6)
26–64°N	25	-1.1(.5)	-0.9(.5)	-2.2(.6)	-2.2(.6)	-0.7(.4)	-0.3(.5)

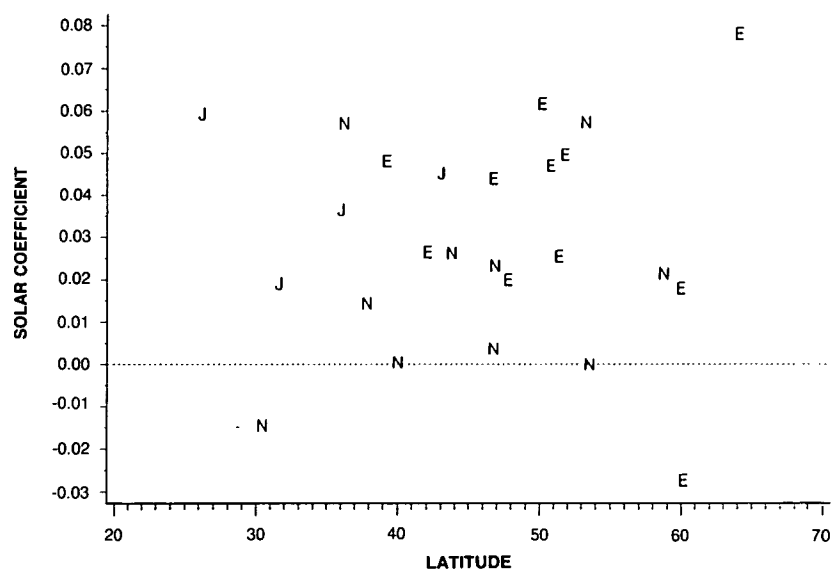


Figure 2.2-8. Solar coefficient (Dobson units per unit of 10.7 cm flux) computed for 25 Northern Hemisphere stations from the AS2 model of Allied-Signal, Inc. The plotting symbol is E = Europe, N = North America, and J = Japan. The average solar coefficient is 0.030, with a standard error of 0.005.

long-term trends from the satellite record. However, satellite data cover the entire sunlit portion of the globe and, subject to the constraint of a short duration, provide valuable information on the geographic patterns of ozone change. Here the satellite data complement the Dobson record, which indicates regional variability in ozone trends but has insufficient geographic coverage to allow detailed analysis of this structure. Figure 2.2-9 (a)-(b) illustrates the geographic variation in ozone changes based on TOMS results normalized to the Dobson network to remove instrument drifts. The plots give the percent differences between annual mean ozone over the period 1987–88 and over 1979–80. Decreases appear in almost all regions. On the Northern Hemisphere (Figure 2.2-9a) the largest ozone decreases, -4.5 to -7.5%, appear at mid-latitudes, especially over the Pacific Ocean. The most prominent feature in the Southern Hemisphere is the ozone decrease which becomes more pronounced as one moves toward the polar region.

The remainder of this section examines the spectral variability of changes in ozone over an 8-year period beginning in 1978 based on SBUV, TOMS, and the Dobson network. The results should be used

YEARLY AVERAGE TOMS 1987 - 1988 MINUS 1979 - 1980

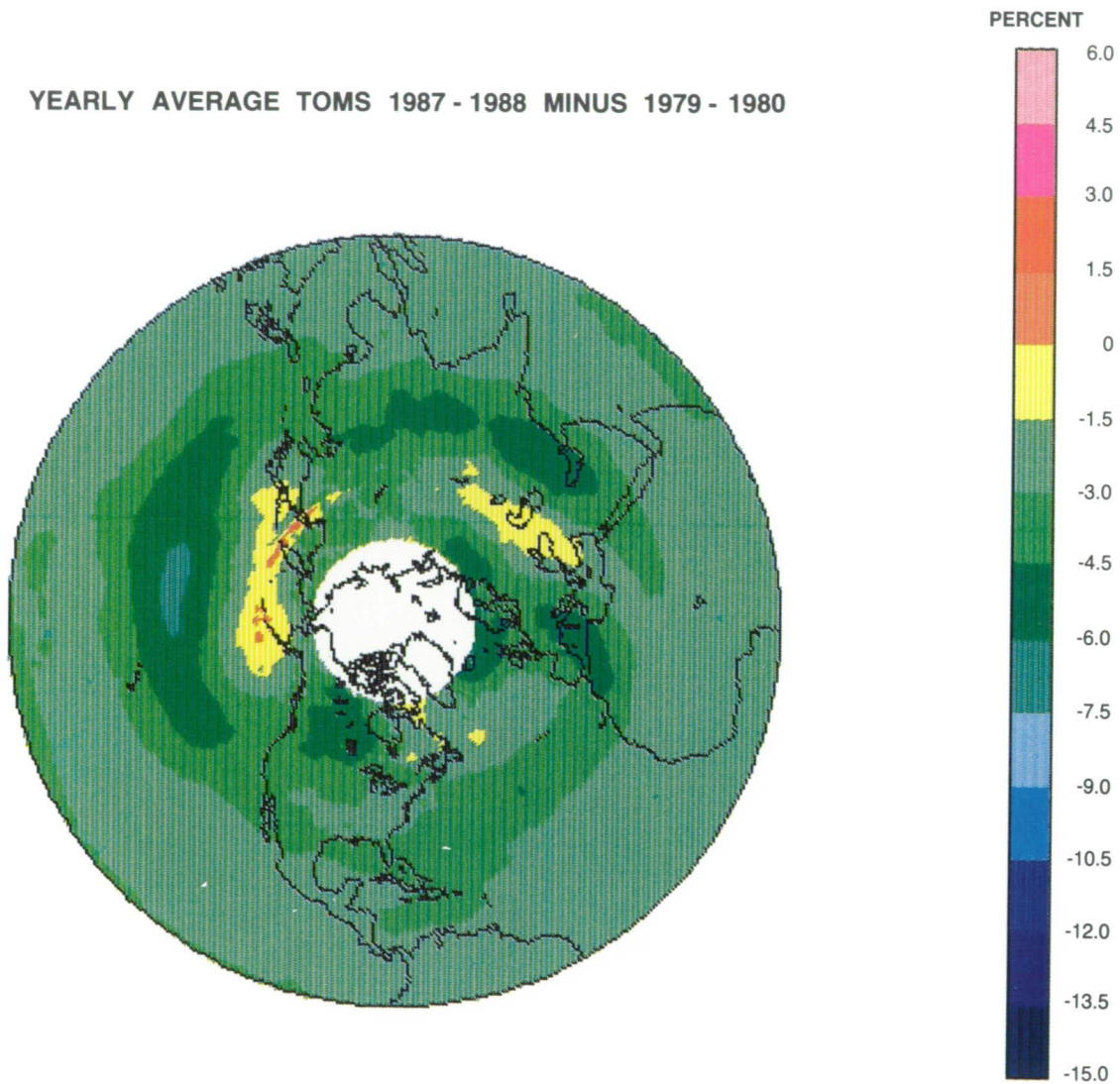


Figure 2.2-9a. Geographic structure in total ozone changes based on TOMS. Results are percent difference in annual mean ozone for 1987-1988 and 1979-1980 for Northern Hemisphere.

only as a measure of geographic structure in ozone changes, not as trends in the same sense derived from the entire long-term Dobson record.

Instrument degradation is a major issue in the analysis of satellite data sets over multi-year periods. Fleig et al. (1986), McPeters and Komhyr (1989b), and Bojkov et al. (1988) have performed a similar analysis for TOMS. Although drifts in the satellite data sets have been removed by comparison to the Dobson network, the correction involves a degree of uncertainty. For this analysis, the SBUV data were normalized to the Dobson record by fitting a single linear trend to all coincident measurements over the 8-year observing period. The TOMS data were normalized to Dobson by comparing coincident measurements during single

YEARLY AVERAGE TOMS 1987 - 1988 MINUS 1979 - 1980

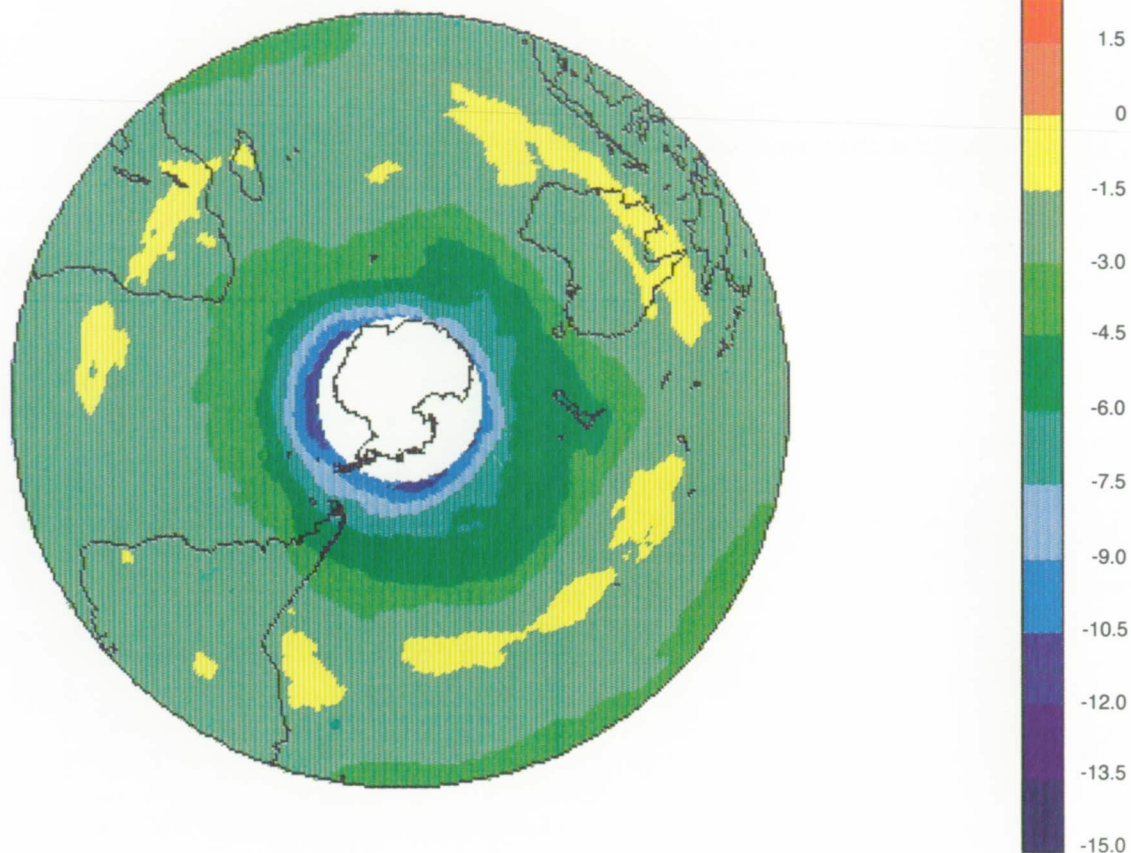


Figure 2.2-9b. Same as Figure 2.2-9a for Southern Hemisphere.

months and deriving a linear trend for each month of the year (R.S. Stolarski, private communication, 1989).

The information of interest is the geographic pattern of changes in total ozone over 8 or 10 years, corrected for solar cycle dependence. A problem arises here in that the data records are less than one solar cycle in length. In particular, the 10.7 cm flux ($F_{10.7}$) decreases markedly during the period 1978 through 1986. As a result, initial test calculations showed unacceptably high correlations between total ozone and $F_{10.7}$. To circumvent this situation, the long-term Dobson record was used to determine the historical relationship between $F_{10.7}$ and total ozone (see Figure 2.2-8). This correlation provided a basis for removing the solar cycle effect from the SBUV and TOMS data sets. The changes in ozone over 8 years, corrected in this way, were compared to those in which the $F_{10.7}$ correlation was removed from the satellite time

GLOBAL TRENDS

series directly. The geographic pattern of ozone change was the same in both cases. This arises from the absence of a clear latitudinal dependence in the solar cycle effect, as shown in Figure 2.2-8. The absolute values of the changes in total ozone, however, depend on the treatment of the solar cycle correlation. This result again demonstrates that the available satellite data are most useful for examining geographic patterns of ozone change. As the data base grows to span more than one solar cycle, studies of true long-term trends will become feasible.

For analysis of the SBUV and TOMS data, the statistical model described in Appendix 2.A was revised so that total ozone, adjusted for the solar cycle, was the dependent variable. In addition, the analysis omitted autoregressive structure in the noise and the term related to the QBO. To account for different variances in a given month of different years, the model was fitted by a weighted estimation procedure with weights for each month inversely proportional to the monthly variances. Finally, the monthly trends were combined into seasonal values by taking the simple averages of December through March as winter and May through August as summer.

2.2.3.2 Geographic Patterns of Ozone Change and Comparison with the Dobson Network

As part of the NOAA/National Weather Service (NWS) continuing Stratospheric Monitoring Program, the Climate Analysis Center has produced monthly global analyses of the SBUV total ozone data (Nagatani et al., 1988). These use the NWS standard rectangular grid array on a polar stereographic projection where the grid size is approximately 3 degrees latitude by 3 degrees longitude at middle latitudes. For each hemisphere the grid is composed of 4,225 points total.

Analyses of total ozone from SBUV were done utilizing the statistical model outlined above for each grid point in each hemisphere. The monthly ozone changes, corrected for solar cycle dependence, were then combined into four winter/summer categories. Results for the Northern Hemisphere appear in Figure 2.2-10 (a)-(b). All contours have the units of percent change per decade, although the data base encompasses only an 8-year period. Note that the analysis ceases at 60°N. This is because the SBUV sensor can acquire data only in daylight. Since the solar terminator moves in latitude with the seasons, 60°N is generally the highest latitude at which data are available during all months.

Figure 2.2-10 (a) and (b) show that changes in ozone deduced in winter tend to be more pronounced and have more regional variability than those in summer, although substantial variations in space exist in both seasons. During winter in the Northern Hemisphere, the changes vary from about -4% per decade over northwest U.S.S.R. to +4% per decade over northeastern North America, with positive changes over the northwest Pacific Ocean and eastern Asia. Note also, the substantial negative changes in the mid-latitude ocean areas where no ground-based observations exist. Summertime values also show a variance around the hemisphere, but with a reduced range. A problem that arises with a short data set is that the derived patterns can be influenced significantly by movement of wave structure in ozone. Derived changes may represent a geographic redistribution of ozone, rather than a net increase or decrease.

Results for the Southern Hemisphere appear in Figure 2.2-11 (a)-(b). While spatial variability around latitude circles is reduced compared to the Northern Hemisphere, many of the statements for the north apply to the Southern Hemisphere as well. One item of particular note is that the largest changes in ozone are over the ocean areas. This demonstrates the value of the extensive coverage obtained by a satellite-borne instrument.

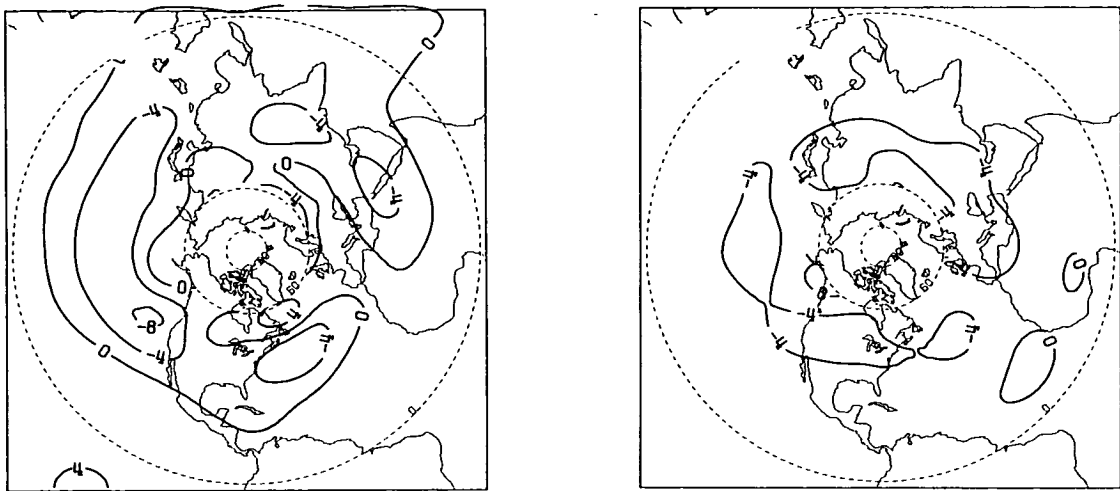


Figure 2.2-10. Geographic pattern of change in total ozone derived from SBUV for the Northern Hemisphere, November 1978-October 1986 for (a) winter (December-March) and (b) summer (May-August). Results are expressed in percent per decade, although the data set covers only an eight-year period. The SBUV ozone values have been adjusted by comparison to the Dobson network to remove instrument artifacts and correlation to the solar cycle.

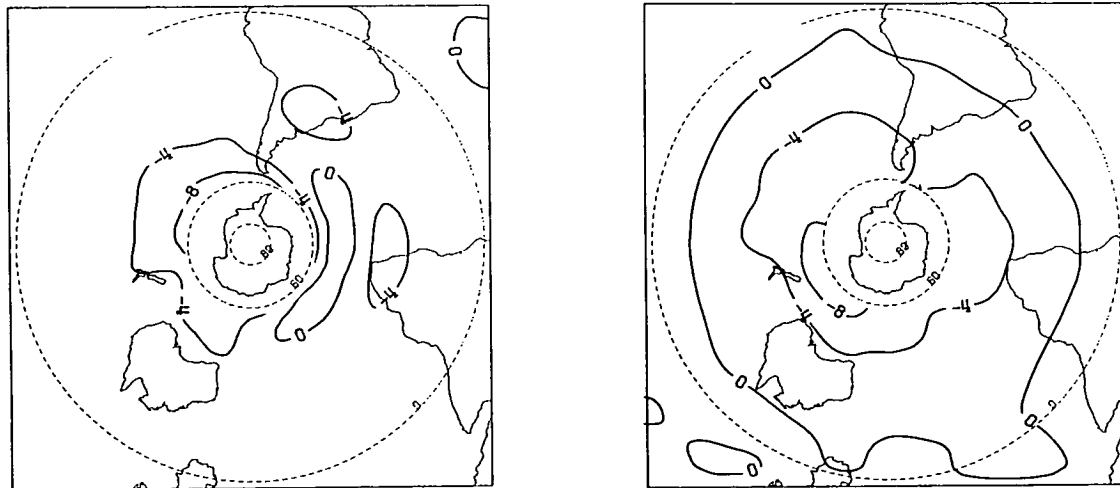


Figure 2.2-11. Geographic pattern of change in total ozone derived from SBUV for the Southern Hemisphere, November 1978-October 1986 for (a) winter (December-March) and (b) summer (May-August). Results are expressed in percent per decade, although the data set covers only an eight-year period. The SBUV ozone values have been adjusted by comparison to the Dobson network to remove instrument artifacts and correlation to the solar cycle.

GLOBAL TRENDS

The geographic structure in Figures 2.2-10 and 2.2-11 implies that zonal mean changes in ozone can represent small differences between larger positive and negative quantities. The zonal mean results based on 8 years of SBUV measurements indicate decreases in summertime ozone over the Northern Hemisphere which exceed those in winter. This result, which appears contrary to the trends in Table 2.2-5, arises from the short duration of the data set. Reference to Figure 2.2-2 (c) reveals a dip in ozone beginning in 1982, which lasts into 1986 over North America and Japan. This period coincides with the final 4 years of the SBUV data set. A recovery in summertime ozone occurs in all regions after the end of the SBUV record.

An analysis similar to that presented above is possible using data from the TOMS instrument. However, for the purpose of this section it is sufficient to show that both SBUV and TOMS detect consistent changes in ozone at selected points on the globe. The TOMS data used in this analysis were provided by R.S. Stolarski and R.D. Hudson (1989, private communication) and have been adjusted by reference to the Dobson network as mentioned previously. These data were placed on a two degree latitude by five degree longitude grid. Comparisons between ozone changes deduced from SBUV and TOMS were done at 14 geographic locations, eight in the Northern Hemisphere and six in the Southern Hemisphere, as listed in Table 2.2-7. For each of the 14 grid points the regression model was applied as for SBUV.

Figure 2.2-12 presents the results derived from both SBUV and TOMS at each of the 14 locations over the 8-year period November 1978 through October 1986. The two sets of results track each other very well, with the largest difference being about 3% per decade at point number 9 (latitude 60°S, longitude 150°E). This discrepancy may arise from the better horizontal resolution and coverage of TOMS in cases where tight gradients exist. The similarity between curves in Figure 2.2-12 supports the reality of the global patterns in column ozone change derived from SBUV. The TOMS data set extends later in time than that from SBUV. An analysis of the 10-year TOMS record, through October 1988, produced a pattern which is generally consistent with that in Figure 2.2-12.

Although both the SBUV and TOMS data sets have been adjusted to conform in a general sense with the Dobson network, this procedure does not force agreement by individual region. It is therefore of interest

Table 2.2-7. Latitudes and longitudes of the 14 grid points selected for comparison of changes in ozone derived from SBUV and TOMS

Point Number	Latitude	Longitude	Season
1	54°N	50°W	winter
2	34°N	55°W	winter
3	34°N	130°W	winter
4	34°N	80°E	winter
5	14°N	25°W	summer
6	40°N	120°E	summer
7	44°N	100°W	summer
8	40°N	20°E	summer
9	60°S	150°E	summer
10	44°S	100°W	summer
11	10°S	40°W	summer
12	44°S	120°W	winter
13	24°S	50°W	winter
14	44°S	20°W	winter

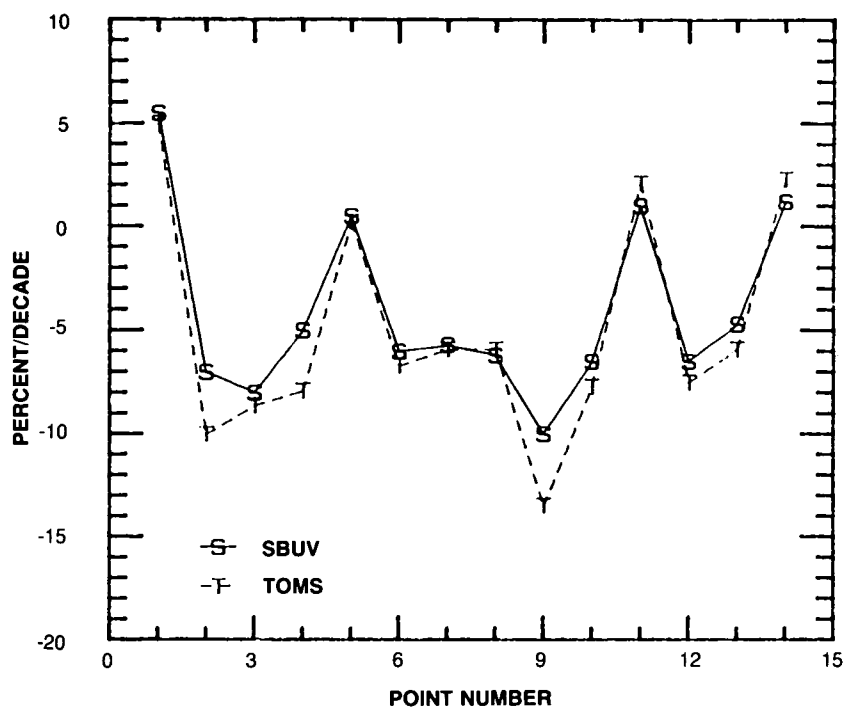


Figure 2.2-12. Changes in total ozone based on eight-year data sets from the SBUV and TOMS instruments. Values refer to the 14 sites listed in Table 2.2-7 and are expressed in percent per decade, although the data sets cover only the eight-year period November 1978 through October 1986.

to examine the compatibility of the ground-based and satellite results over the short time period encompassed by the latter data set. The investigation uses Dobson ozone measurements only over an 8-year period (November 1978-October 1986). As such, the concept of a long-term trend should not be applied. The focus here is on the consistency of geographic patterns in ozone change derived from independent measurement systems. This analysis applies a statistical regression model described in Appendix 2.A to the 25 Dobson stations listed in Table 2.2-2 which are located in Japan (J), Europe (E), and North America (N).

Figure 2.2-13 (a)-(b) presents results for winter and summer over the 8-year period, where the change in percent per decade for each station appears at the appropriate latitude. Comparison of the winter map of Figure 2.2-10 (a) with its Dobson counterpart shows several interesting features. The Japanese stations indicate a change which becomes less negative with increasing latitude. This corresponds well with the latitudinal variation derived from SBUV over this region, with an increase in ozone appearing northwest of Japan. European Dobson data generally indicate the reverse, with a strong negative change with increasing latitude. Changes derived from the Dobson instruments are somewhat larger in magnitude, but reveal a latitudinal pattern in agreement with SBUV. Finally, over North America ozone changes derived from Dobson instruments show no obvious pattern. Based on the map from SBUV, this may arise from the fact that this region is divided into a positive northeast sector and a negative western region.

For the summer season, Figure 2.2-13 (b) shows ozone changes over Japan which are virtually independent of latitude. The result from SBUV in Figure 2.2-9 (b) shows the -4% per decade contour

GLOBAL TRENDS

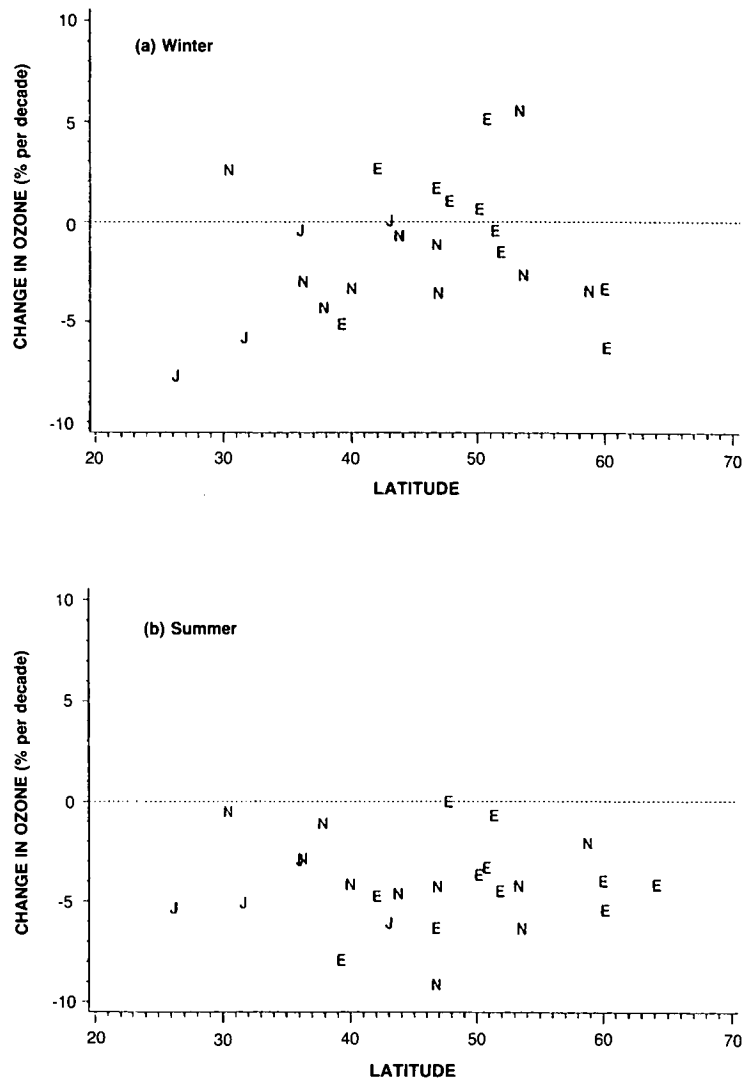


Figure 2.2-13. Changes in total ozone derived from Dobson data for the eight-year period over which SBUV measurements are available, November 1978-October 1986 for (a) winter and (b) summer. The plotting symbol is E = Europe, N = North America, and J = Japan. Results are expressed in percent per decade.

running parallel to the country. Europe also shows a much flatter gradient in summer than in winter, and this is substantiated by SBUV which gives a uniform change of about -4% per decade over this region. Over North America SBUV indicates a very weak gradient, and Figure 2.2-13 (b) reveals ozone changes which depend on the specific location with no obvious latitudinal pattern.

In view of the behavior shown in Figure 2.2-2 and in the SBUV data set, it is of interest to compute the changes in ozone after November 1978 contained in the Dobson record. Table 2.2-8 presents results from the AS2 model, expressed in percent per decade, based only on 8- and 10-year periods beginning in November 1978. Values appear for winter and summer at latitudes 55°N , 45°N , and 35°N and should be

Table 2.2.8. Changes in total ozone derived from the Dobson Network for periods coincident with the SBUV and TOMS data sets (changes in the 8 and 10 years data sets are expressed in equivalent % per decade to facilitate comparisons; one standard error appears in parentheses)

Latitude	Winter ^a		Summer ^a	
	8 Years	10 Years	8 Years	10 Years
55 N	-1.8 (1.5)	-2.2 (1.1)	-4.0 (0.8)	-2.4 (0.7)
45 N	-2.0 (1.0)	-2.7 (0.7)	-4.0 (0.8)	-1.6 (0.5)
35 N	-2.2 (1.5)	-3.3 (1.0)	-3.9 (0.8)	-0.8 (0.7)

^aThe 8 and 10 year records cover November 1978–October 1986 and November 1978–October 1988, respectively. Due to the short duration of these data sets, the derived changes should not be interpreted as long-term trends in the sense presented in previous tables. Winter = December–March, Summer = May–August.

compared with results in Table 2.2-5. As expected, standard errors derived for the shorter data set are larger than those in Table 2.2-5, but the trends still remain significant at the one sigma level. With an adopted uncertainty of one standard error, the wintertime changes derived from the short and long-term Dobson data sets agree. However, a very different picture emerges in summer. Here the ozone changes expressed in percent per decade derived over a 10-year period are very different from those based on 8 years of data. Furthermore, both sets of summer results in Table 2.2-8 imply larger changes in ozone per unit time than does Table 2.2-5. The difference between the 8 and 10-year results arises from the upturn in summertime ozone after 1986 as shown in Figure 2.2-2 (c). The results in Table 2.2-8 should not be interpreted as long-term trends, but they are nonetheless important. In particular, they show that after statistical correction for known sources of variability, atmospheric ozone still displays a temporal behavior which is more complex than a long-term linear trend. This underscores the difficulty in interpreting derived trends in terms of cause and effect.

2.2.3.3 Conclusion of Satellite Data Analyses

The analyses described above yield the following conclusions. (1) For an 8-year record beginning in November 1978 the patterns of ozone change derived from SBUV and TOMS at the 14 selected sites are generally consistent. This suggests that SBUV and TOMS are compatible for detecting geographic patterns in ozone change. In specific regions of very tight gradients, however, the high horizontal resolution of TOMS may provide a more realistic result. (2) Maps of changes in total ozone based on SBUV show significant variability around latitude circles, and a zonal average ozone change can represent the small difference between highly variable quantities. (3) Seasonal changes in total ozone observed by SBUV from November 1978 through October 1986 differ from expectations based solely on the long-term Dobson record. A separate analysis of Dobson measurements beginning in November 1978 supports this conclusion. However, the rate of change of summertime ozone derived from the short Dobson data set is very sensitive to the addition of measurements made after 1986.

2.3 TRENDS IN VERTICAL OZONE DISTRIBUTION

2.3.1 Introduction

This section summarizes present understanding of trends in the vertical ozone distribution. Emphasis is given to the altitude range in the upper stratosphere where the percentage change in ozone concentration

GLOBAL TRENDS

at mid-latitude due to anthropogenic chlorine perturbation is expected to be the largest. The major problem in such an analysis is the scarcity in space and time of the data available from both satellite and ground-based measurements.

As the Ozone Trends Panel (OTP) evaluation has shown that measurements performed by the SBUV instrument on the Nimbus-7 satellite cannot be used for trend analysis, the satellite section (2.3.2) is based only on the measurements of the SAGE I (February 1979–November 1981) and SAGE II (October 1984–December 1988) instruments. As far as ground-based measurements are concerned, only 10 stations in the Northern Hemisphere have a long and reliable enough record of Dobson spectrophotometer Umkehr measurements to be used for trend analysis. In addition, such data are affected by the very high aerosol load in the stratosphere from 1982 to 1984 following the major eruption of the El Chichon volcano. Finally, when considering the available stations performing regular balloon-borne ozonesonde measurements, the situation is even worse with regard to data reliability, especially at the uppermost level.

Therefore, the same merits and limitations of both orbiting remote sensors and the ground-based network, as emphasized in Section 2.2.1 for total column ozone trends analysis, are also relevant in this section. The limitations are even more stringent here, because the biases due to the limited geographic coverage and length of record may be larger due to the restricted data base which can be used. The objectives of the present analysis are thus limited. They are: (1) to update the SAGE II data set through 1988 as compared to the 1986 limitation of the Ozone Trends Panel Report, (2) to perform a detailed statistical analysis of both Umkehr and balloonsonde measurements to evaluate the usefulness of the available ground-based data for the detection of trends in the vertical ozone distribution throughout the stratosphere. As for the total column ozone study performed in the Ozone Trends Panel Report, a trend analysis has been made for each station in order to derive on a station-by-station basis the various natural (solar cycle, aerosols) and man-made variations in the ozone concentration at various altitude levels. It thus constitutes a completely new data evaluation.

2.3.2 Comparison of SAGE I and SAGE II Stratospheric Ozone Measurements

SAGE I and II use the solar occultation technique to measure aerosol extinction and trace gas concentration in the atmosphere (McCormick et al., 1979; Mauldin et al., 1985 a,b, see Section 2.1.1.2). The retrieved ozone profiles have a vertical resolution of 1 km, and their range extends from cloud top up to an altitude limited by the signal-to-noise ratio; for SAGE I the upper limit is about 55 km, and for SAGE II it is approximately 65 km. Profiles are smoothed over a 5-km layer at heights above approximately 48 km to increase signal-to-noise ratio at these altitudes. SAGE I and II instruments utilize essentially the same design with similar optical components. Differences between the two instruments include the number of spectral channels (7 for SAGE II and 4 for SAGE I), the use of narrower spectral bandwidths on SAGE II, and the use of a rectangular field-of-view on SAGE II versus a circular one on SAGE I. These differences do not introduce any significant systematic errors between SAGE I and II ozone measurements as will be discussed below.

The principal sources of error in the measurement of an individual ozone profile are radiometric imprecision, digitizer truncation, and scan mirror pointing errors. These random errors are approximately uncorrelated vertically, and their combined effect on an individual retrieved ozone profile is estimated at each point on the profile from the variance of the measurements from approximately 4–5 scans of the SAGE mirror across the viewing altitude. Each SAGE profile, however, also possesses an uncertainty in reference altitude of approximately 0.25 km which contributes to uncertainties in profile repeatability (Cunnold et al., 1989). The principal systematic errors between SAGE I and SAGE II arise from instrument

scan mirror calibration and the uncertainty in our knowledge of the absorption cross-section of ozone at 600 nm convolved with instrument bandpass and solar spectrum. Aerosols can also produce biases in the ozone retrievals, but only at those altitudes where aerosol concentrations are large (i.e., mostly below 25 km altitude). The relative systematic error between the SAGE instruments is estimated to be approximately 2% (Cunnold et al., 1989). The random error components for both instruments are less than 10% for a vertical resolution of 1 km.

2.3.2.1 Zonal Means

SAGE I and II scan the atmosphere over the Earth's limb at the terminator twice on each of 15 daily orbits. The orbital inclination causes the observation latitude to periodically vary from approximately 75°S to 75°N dependent on season. The latitudes of the SAGE I and SAGE II measurement locations for February 1979 to November 1981, and October 1984 to November 1987, respectively, are displayed for sunset measurements in Figure 2.3-1. Due to the SAGE I orbital elements, the coverage does not repeat from one year to the next as it does for the SAGE II measurement location latitudes. Any gaps in the curves of Figure 2.3-1 are periods of time during which no satellite occultations occurred. Because of power problems on the spacecraft, only sunset data were taken by SAGE I after July 1979, and additional gaps are observed in the SAGE I curves due to this problem. A complete set of sunrise measurements for SAGE II, however, is available.

For analysis purposes, the SAGE I and II data were spatially grouped into 11 latitude bands. The equatorial latitude band was 15°S to 15°N, and the midlatitude bands were 10° wide centered at 20°, 30°, 40°, 50°, and 60° north and south. As the SAGE I or SAGE II observations passed into and subsequently out of one of the latitude bands above, the ozone measurements were averaged to form a zonal mean. In addition, the temporal duration defining a zonal mean was limited to a maximum of 1 week. Thus, a given latitude band contains more than one zonal mean if SAGE I or SAGE II sampled the latitude band for a continuous period of greater than 1 week duration. These typically occur when the measurement location latitude changes from increasing with time to decreasing with time.

Time series of SAGE I and II ozone zonal means at 30 km altitude are shown in Figure 2.3-2a for selected latitude bands. For comparison purposes, they have been time shifted to a common origin. Each time series was analyzed with a three-component linear regression model containing semiannual, annual, and 27-month period terms. The 27-month period term was chosen to model a quasi-biennial oscillation (QBO) in the ozone. The model fits to the data, which are intended as a visual aid, are shown as the continuous curves. At 30 km these time series display the expected features of seasonal ozone variability, namely the strong annual variation in the midlatitudes and the semiannual oscillation in the equatorial region. From Figure 2.3-2a, it is observed in the midlatitudes that both instruments agree in amplitude and phase with no apparent consistent bias. The largest differences occur at the Equator and are due to the fact that the QBO terms in the model are not in phase between the two data sets.

The vertical distribution of the annual and semiannual component amplitudes between 25 km and 50 km were computed and are shown in Figure 2.3-2b. The continuous curves on the plots represent the amplitudes in percentage from the model mean. Squares, either filled-in or open, mark those amplitudes which are statistically significant at the $\pm 2\sigma$ confidence level. A comparison between the SAGE I and SAGE II annual and semiannual component amplitudes shows the similarity in the vertical distribution of amplitude. Both instruments agree on the altitudes at which the midlatitude annual amplitudes effectively vanish, i.e., at 25 km in both hemispheres and at 38 km in the Southern Hemisphere. At 25 km, a phase change occurs between the zonal mean time series below and above this altitude (Wang et al., 1989).

GLOBAL TRENDS

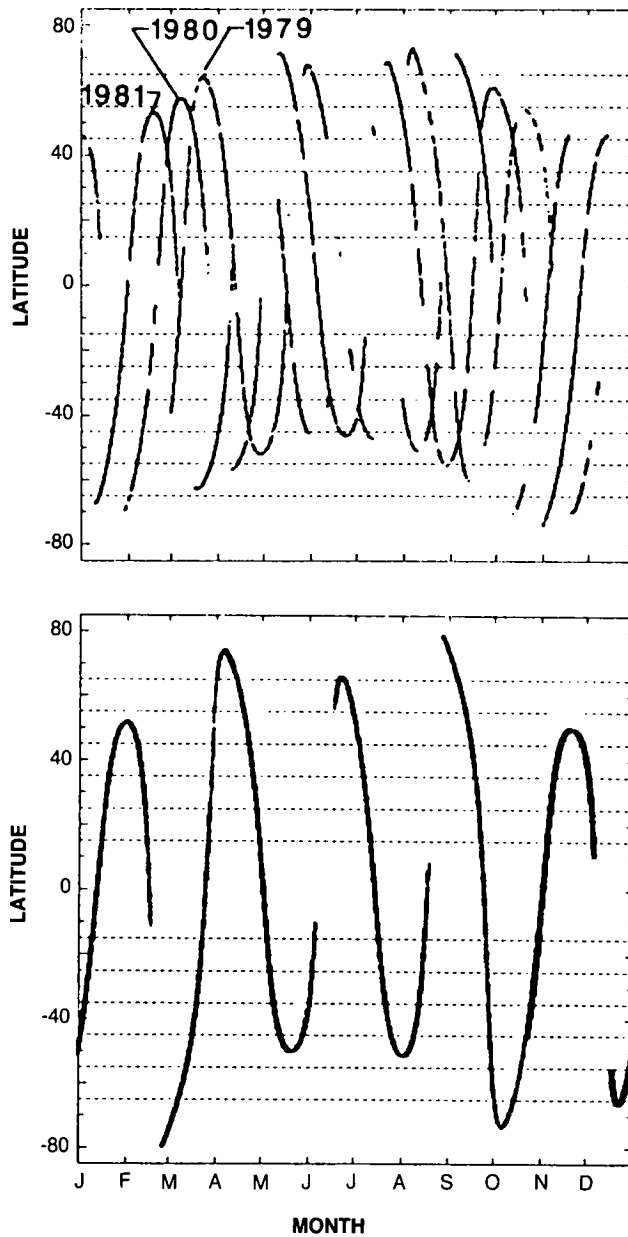


Figure 2.3-1. (a) Latitudes of the SAGE I sampling locations for sunset. (b) Latitudes of the SAGE II sampling locations for sunset. Because of the SAGE II orbital characteristics, the latitude coverage appears as a single curve even though 3 years are plotted.

As of this writing, SAGE II has been in operation for over 4 years. The daily averages of ozone concentration sampled within 10°-wide latitude bands symmetrically placed about the equator were modeled using the analysis previously described. The results for 35 km are shown in Figure 2.3-3. The regressions adequately represent the seasonal and semiannual variability observed in the ozone time series. In addition, near the Equator, the QBO in ozone becomes clearly defined. The high vertical resolution of the SAGE II ozone measurements significantly improves our knowledge of vertical structure of the ozone QBO. Also evident in Figure 2.3-3, the semiannual oscillation appears as a significant component in the ozone vari-

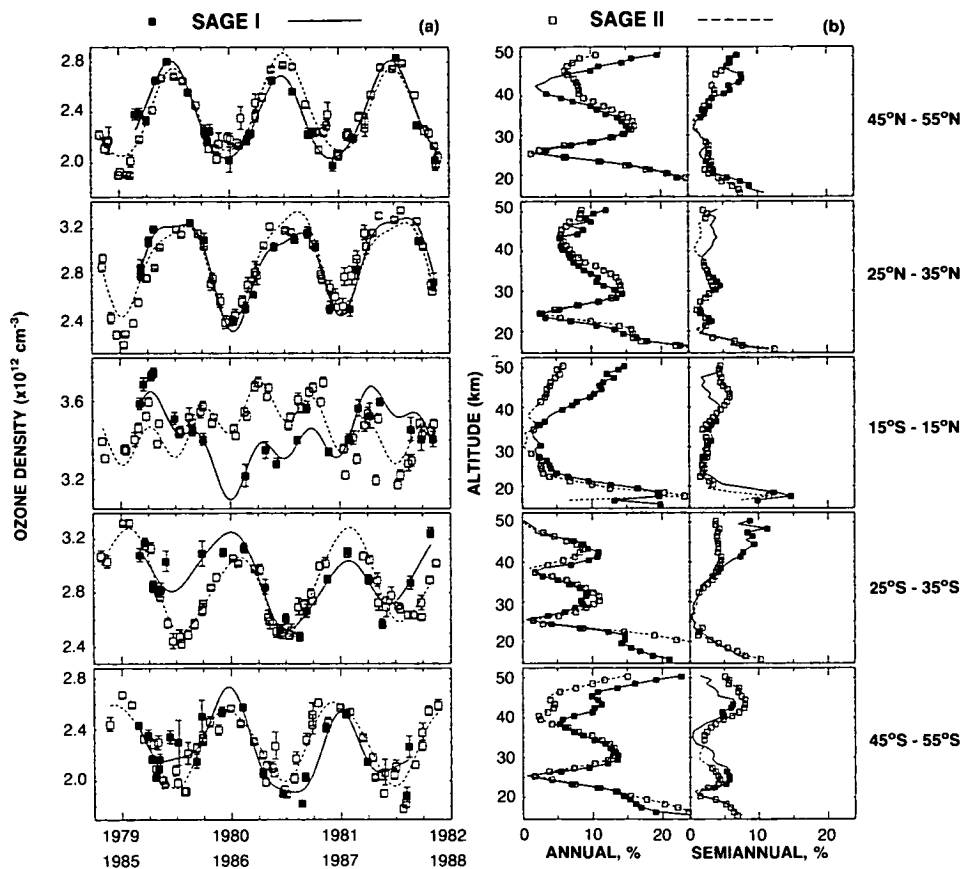


Figure 2.3-2. (a) Zonal mean ozone number density at 30 km for SAGE I during the period February 1979 - November 1981 and SAGE II during the period October 1984 - November 1987 for the five latitude bands of 45°S-55°S, 25°S-35°S, 15°S-15°N, 25°N-35°N, and 45°N-55°N. The vertical bars are the 95% confidence interval on the zonal mean. Smooth curves are the regression estimates. The data have been time shifted for comparison as indicated on the abscissa. (b) Amplitudes of the seasonal and semiannual components of the SAGE I and SAGE II zonal mean time series as derived from the regression coefficients. Units are in percent relative to the model mean.

ability, especially at 5°S. Marching poleward of the Equator, it is observed that the seasonal oscillation gains in amplitude with the semiannual oscillation decreasing in strength.

2.3.2.2 Change in SAGE I and SAGE II Ozone Concentrations

The change in stratospheric ozone concentration that occurred between the 33-month lifetime of SAGE I and the first 4 years of SAGE II was estimated in three ways over an altitude range from 25 to 50 km, the region of the atmosphere essentially free of aerosols that could have any effect on the SAGE II ozone retrieval.

The first method of estimating the ozone change, which minimizes the effects of seasonal and spatial sampling biases, is to select sets of profiles where SAGE I and II sampled the same month of the year within the same latitude band. Such a period of time is defined as an intersection and corresponds to a

GLOBAL TRENDS

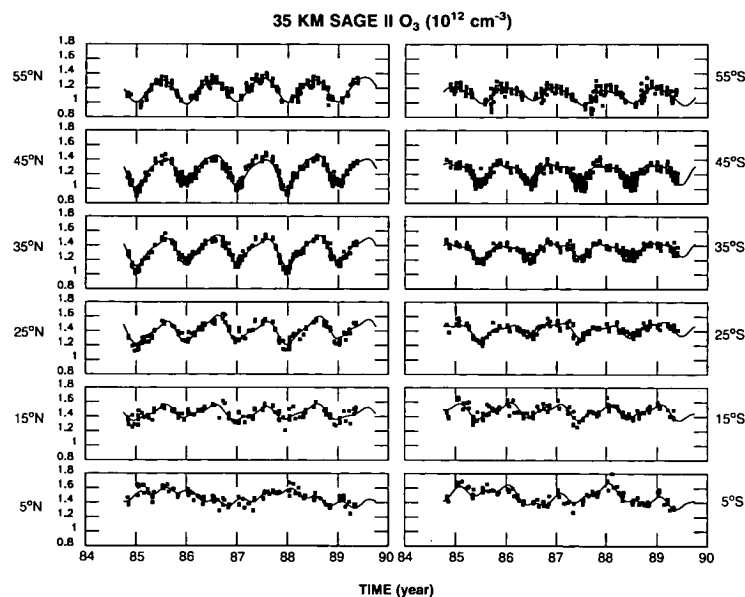


Figure 2.3-3. Daily mean ozone number density at 35 km for SAGE II for twelve latitude bands, each 10° wide-centered on the latitudes listed. The continuous curves represent regressions using a model containing components with periods of 30 months, 12 months, and 6 months.

period of time in the year, of approximate duration 1 month, during which both SAGE I and II sampled the same latitude band. Note that an intersection is independent of the actual year during which measurements were made. The intersection is defined strictly in terms of the month within the year. Within the 11 latitude bands considered, 105 intersections were isolated containing a total of approximately 7,300 SAGE I profiles and 25,000 SAGE II profiles. For each intersection, the SAGE I and II profiles were averaged separately.

The second method of estimating the ozone change is to simply compute the zonal mean time series averages and form the percentage difference. This method has the possible disadvantage that seasonal sampling biases may be introduced.

The third method of estimating the ozone change is to use the regression coefficients derived from the zonal mean time series and compute the mean value of the series over the time period of the data. This method's disadvantage is the empirical nature of the model.

Using all three methods described above, the percentage difference between the SAGE II mean and the SAGE I mean was computed at each altitude using the SAGE I mean as the reference. The intersection (method 1) percentage differences and their corresponding standard errors are displayed in the upper six panels of Figure 2.3-4. For all latitude bands, excluding 60°N and 60°S, methods 2 and 3 gave very similar results to those of method 1. Throughout the 11 latitude bands considered, except for 60°S, the ozone changes from SAGE I to SAGE II are within the range of -4% to +4%. The larger decreases observed in the Southern Hemisphere near 60°S are heavily driven by the intersection in the austral springtime and are likely due to vortex dynamics.

Identical analysis (method 1) was performed using two wider latitude bands: 20°N to 50°N and 20°S to 50°S, areas over which there is relatively dense sampling by both instruments. The mean percentage

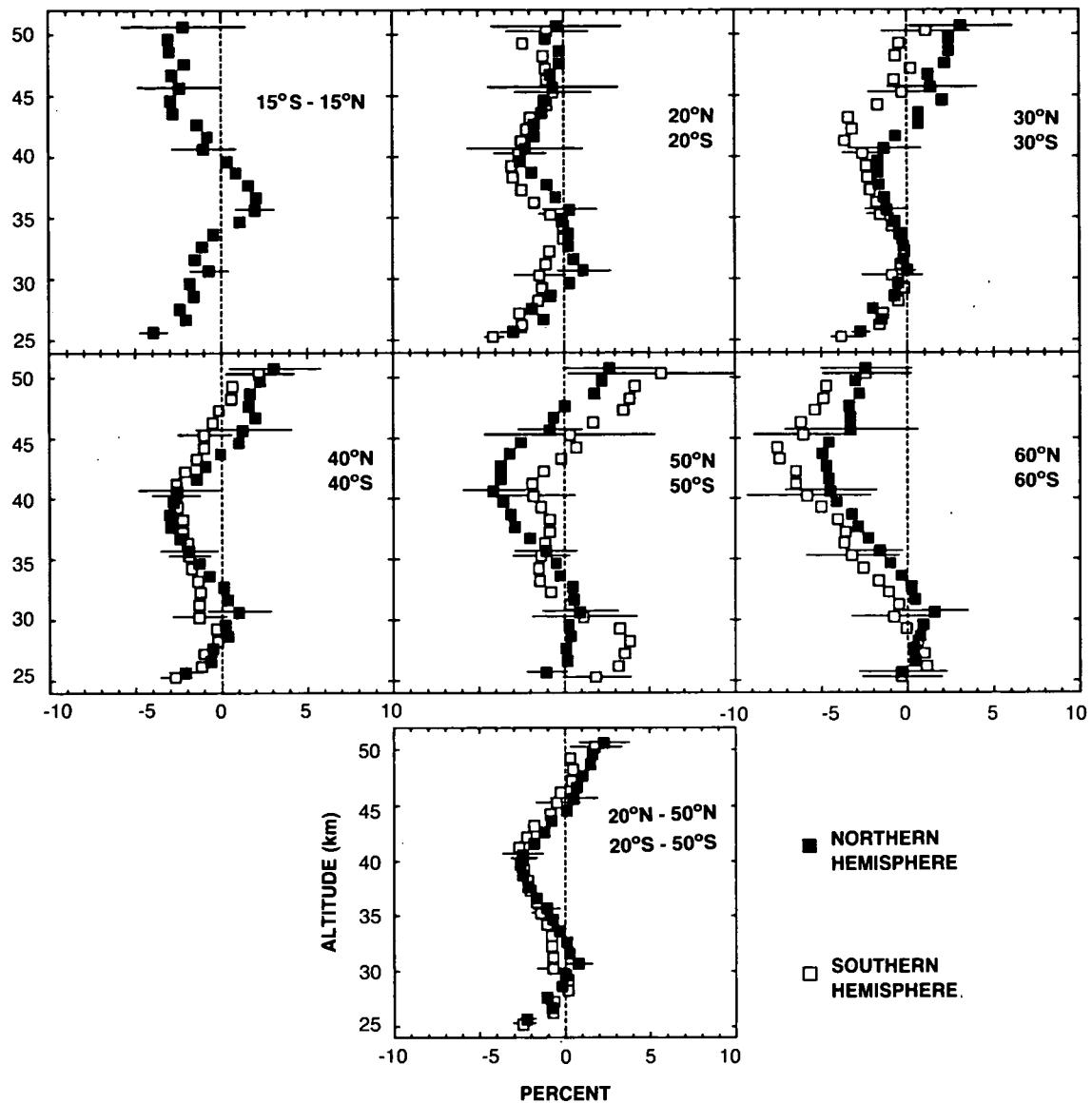


Figure 2.3-4. Mean percentage difference between SAGE II and SAGE I versus altitude computed from the intersection of SAGE I and SAGE II. All intersections occurring between 15°N to 55°N or 15°S to 55°S were combined into one sample to produce the results in the lower panel. The horizontal bars, placed at 5 km intervals, represent the standard error of the mean percentage difference. SAGE I is the reference in all percentage calculations.

differences appear in the lower panel of Figure 2.3-4. The agreement between the two hemispheres is apparent, and indicate for the 6-year period between 1980 (SAGE I) and 1986 (SAGE II):

- an ozone decrease between 35 and 44 km with the maximum ozone change of $-3\% \pm 2\%$ occurring at 40 km,
- an ozone decrease of $-3\% \pm 2\%$ at 25 km and an essentially zero ozone change at 28–33 km and 45–48 km.

GLOBAL TRENDS

These values represent the changes that occur over this time period and no attempt has been made to separate out natural and man-induced variability.

2.3.3 Analysis of Umkehr Data

A trend analysis of stratospheric Umkehr profiles of ozone from 10 stations in the Northern Hemisphere is considered over the period 1977–1987. It constitutes an update of the analysis by Reinsel et al. (1987). The stations are Belsk, Arosa, Lisbon, Sapporo, Tateno, Kagoshima, Boulder, Edmonton, New Delhi, and Poona. Umkehr profile ozone data in the highest 5 Umkehr layers (4–9) are considered in the trend study, which covers an altitude range of approximately 19–45 km. A detailed analysis of the interdependence of the various Umkehr layers and resulting vertical resolution has been performed in the Ozone Trends Panel Report. It shows that ozone retrievals for Umkehr layers 4 to 8 are suitable for trend studies and that the effective vertical resolution for these layers varies from 15 to 11 km. Trends derived in layer 9, where the retrieval is more sensitive to real ozone changes in layer 8—and has greater sensitivity to such changes than the layer 8 retrieval—are of limited interest.

One of the major problems in Umkehr measurements is related to the impact of stratospheric aerosols from volcanic activities. This problem has become even more acute during the period following the eruption of the El Chichon volcano. A comprehensive theoretical examination of aerosol effects on Umkehr measurements was presented by Dave et al. (1979) and DeLuisi (1979) and the problem has been addressed by Reinsel et al. (1984) and DeLuisi et al. (1989a,b). The results of these studies indicate that accounting for the effects of aerosols on the Umkehr data measurements is critical in any trend analysis of these data. The major volcanic eruption of El Chichon in April of 1982 produced significantly larger amounts of atmospheric aerosols than at any time in the previous 25 years. This, in turn, has produced a much more severe impact on Umkehr measurements from stratospheric aerosols from El Chichon than earlier periods. For illustration, deseasonalized monthly averages of Umkehr data in layers 4 through 9 at Arosa are plotted for the period 1977–1987 in Figure 2.3-5. The effects of aerosols on the Umkehr data, starting towards the end of 1982, are apparent. We note that low Umkehr values occur during 1982–1983 not only in the upper layers 7–8 but also in layers 4, 5, and 6. This is in contrast to the earlier theoretical calculations of Dave et al. (1979), which indicate that little error in Umkehr measurements should occur in the middle layers 4, 5, and 6 due to volcanic aerosols. This, in turn, suggests the possibility that real decreases in ozone occurred in these middle layers during 1982–1983 as a result of El Chichon and other natural events of that time period. Hence, large empirical adjustments of these data in layers 4, 5, and 6 for aerosol error effects during this period may not be appropriate.

Because of this severe impact on the Umkehr data, considerable caution needs to be exercised when performing a trend analysis using Umkehr data over the period 1982–1987. In particular, the techniques of the previous analysis (Reinsel and Tiao, 1987) need to be modified to account for the possibility of differences in the aerosols' effects on Umkehr data during the El Chichon period relative to earlier effects—especially any possible nonlinearity in the effects on Umkehr data as a function of optical thickness because of the much larger range of observed optical thickness values during El Chichon than in earlier periods. Because of this, in present trend analysis of both empirically corrected and theoretical model-corrected Umkehr data, two different procedures were considered to treat Umkehr data during a portion of 1982–1983. In the first one (i), all available Umkehr data were used. In the second one (ii), Umkehr data during the portions of 1982–1983 most affected by aerosols were omitted from the analysis. This resulted in the omission of, at most, 8 months of data at each station, generally for the period from November 1982 through June 1983. Procedure (ii) is motivated by the fact that errors in Umkehr data appeared to follow a somewhat different relation to optical thickness for these extreme cases. Also in an empirical adjustment approach, these

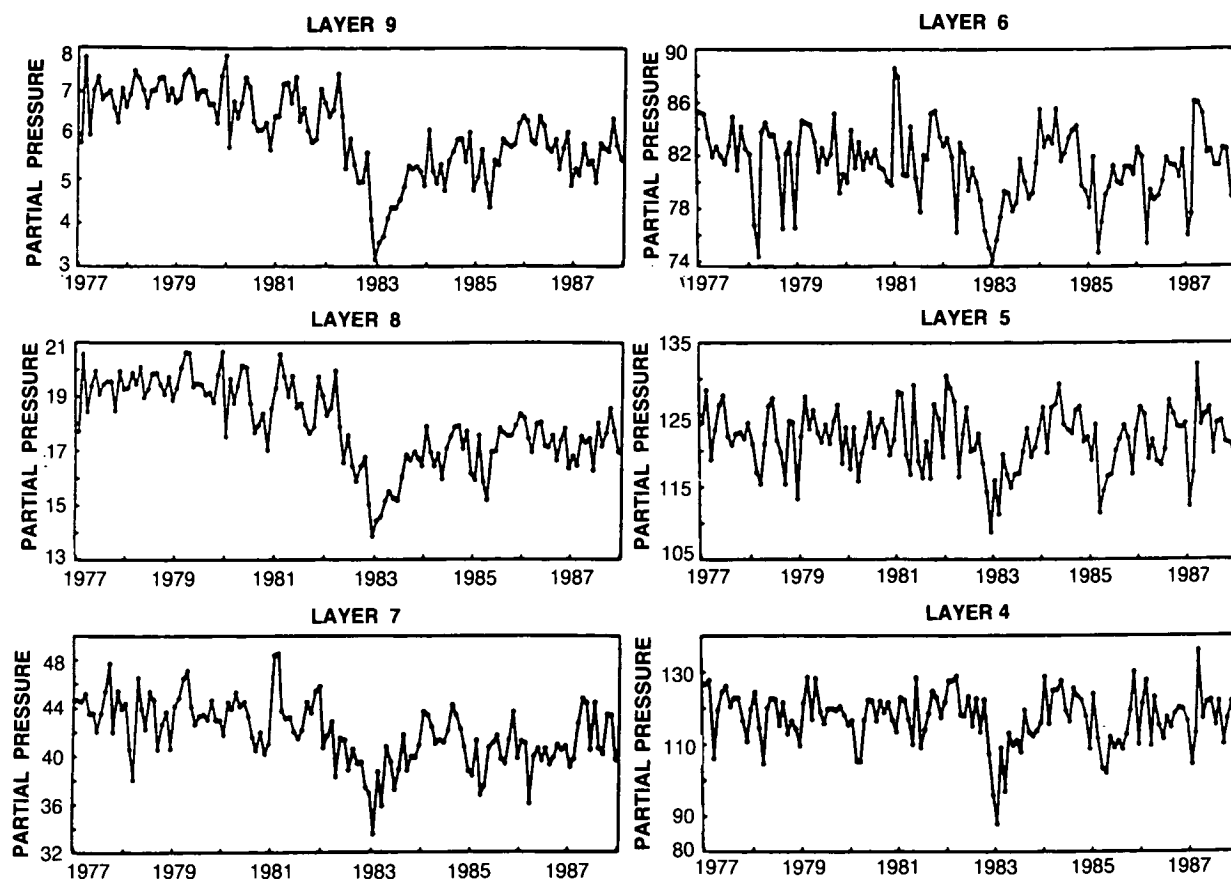


Figure 2.3-5. Deseasonalized Umkehr data at Arosa for layers 4-9, unadjusted for aerosols, for the period January 1977 through December 1987.

extreme cases might exert a substantial influence on the overall estimation results for the aerosol effects, and hence on estimation results for other parameters. In addition, it is rather clear that Umkehr data during this period would be the most sensitive and most difficult to accurately correct in the theoretical model calculations.

The trend analysis has been performed for each of the 10 stations using two statistical models which differ in the approaches of the aerosol effects. These models are described in Appendix 2.A. They include an $F_{10.7}$ solar flux term to account for solar cycle variations, although large uncertainties remain in this evaluation due to the shortness—10 years—of the period analyzed relative to the 11-year solar cycle. The empirical adjustments for the effects of aerosols on the Umkehr data have previously involved the use of monthly averages of measurements on atmospheric transmission of solar radiation available at Mauna Loa, Hawaii (Reinsel et al., 1984, 1987). More recently, lidar aerosol data from several locations in the north temperate latitudes, including Hampton, USA, Garmish, FRG, and Observatoire de Haute-Provence, France, became also available for the last several years since around 1977. It is expected that these data will be more representative of aerosols at the Umkehr station locations than the Mauna Loa data. These lidar data have been used in a detailed study by DeLuisi et al. (1989a) to obtain stratospheric aerosol optical thickness derived from the lidar data for the period 1977–1987 as shown in Figure 2.3-6. DeLuisi et al.

GLOBAL TRENDS

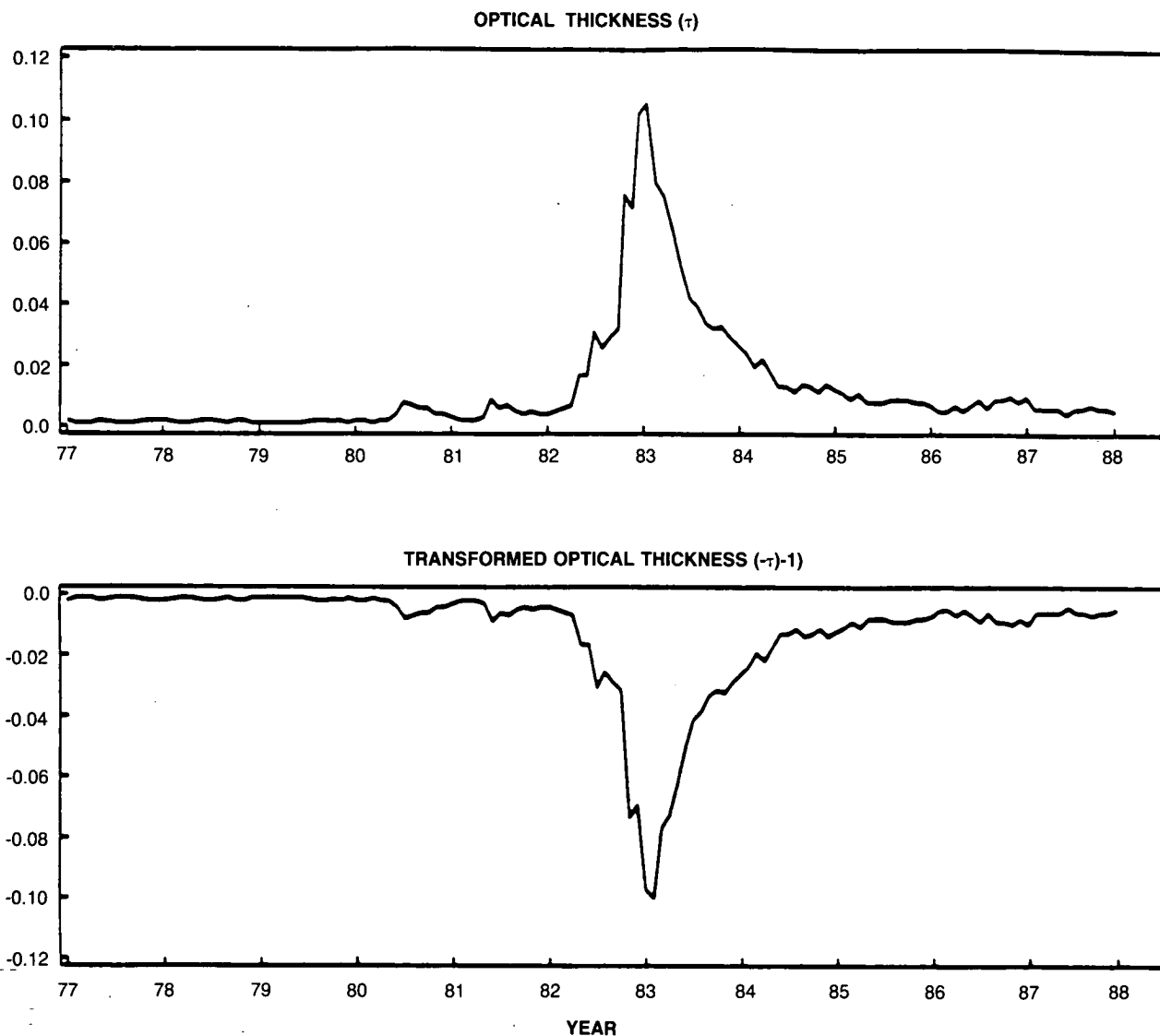
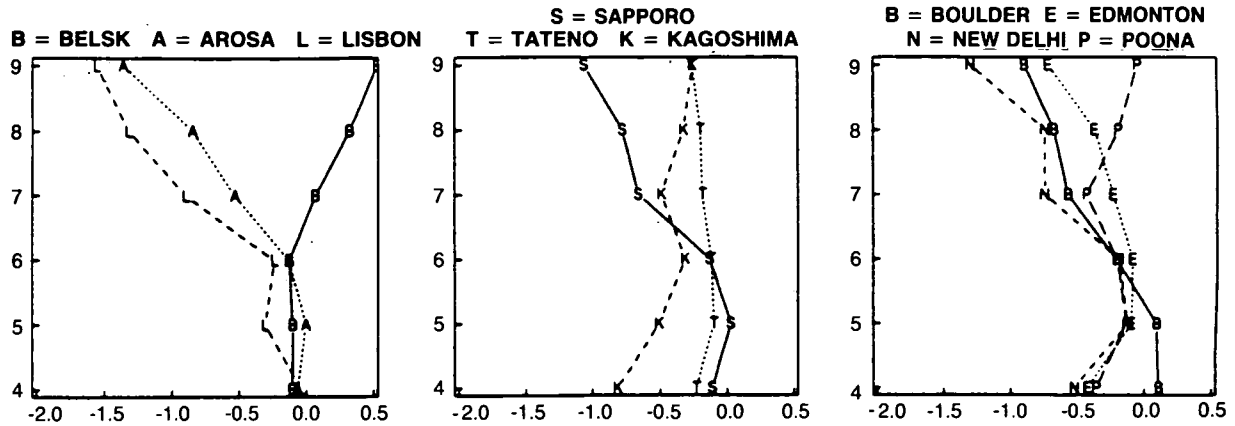


Figure 2.3-6. Stratospheric aerosol optical thickness derived from lidar data (Hampton, Va; Garmish, FRG; Observatoire de Haute-Provence, France) for the period 1977-1987.

(1989a) also used the lidar data in a radiative transfer model to calculate theoretical model estimates of the errors in Umkehr data due to volcanic aerosols, and thus provide theoretical corrections for the Umkehr data during 1978–1986. A detailed description of the correction methods are given by De Luisi et al. (1989a).

Parameter values for both time series models (1) and (2) were estimated for each of the 10 Umkehr stations and each of the five Umkehr layers, 4 through 8, using both procedures (i) and (ii) mentioned previously. (For comparison, a model of the form (2), which does not include any empirical aerosol adjustment, was also estimated for the uncorrected Umkehr data.) Therefore, two distinct sets of estimation results have been obtained for both the empirical aerosol adjustment model (1) and the model (2), where Umkehr data have been corrected for aerosol errors using theoretical model-based calculations (DeLuisi et al., 1989a). The results will be referred to as “empirical corrections” (model 1) and “theoretical

A. EMPIRICAL CORRECTIONS MODEL



B. THEORETICAL CORRECTIONS MODEL

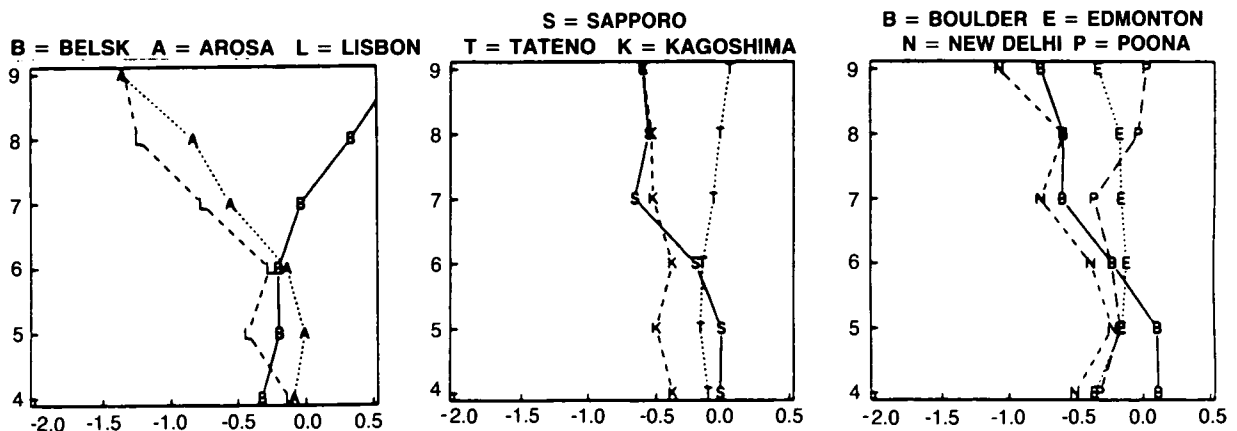


Figure 2.3-7. Umkehr data trend estimates (% per year) from 10 individual Umkehr stations for layers 4-9, for the period January 1977 through December 1987. (Portions of the data, approximately from November 1982 to June 1982 were deleted in the analysis.) (a) Trend estimates based on empirical aerosol corrections model, (b) Trend estimates based on theoretical aerosol corrections model.

corrections” (model 2), and for the two procedures as “no deletions” (method i) and “with deletions” (method ii). The individual station estimates of trend and solar cycle coefficients from both models are plotted in Figure 2.3-7 a-b for each Umkehr layer, for the method (ii), when data were deleted during a portion of 1982–1983.

Estimates of the overall trend in ozone for each layer, as well as reasonable estimates of the uncertainty in the overall estimates, have also been computed by using random-effects models for individual station estimates as in Reinsel et al. (1987). The resultant $\pm 2 \sigma$ confidence interval estimates of trends during 1977–1987 from both the empirical and the theoretical adjustment models (1) and (2) for both procedures are given in Table 2.3-1, together with the solar flux coefficient estimates in % per 100 $F_{10.7}$ solar flux units.

The results of the above analysis indicate statistically significant decreases in ozone during 1977–1987 in Umkehr layers 7 and 8 using either method of correction for aerosol errors, and using either procedure (i) or (ii) for the treatment of data during a portion of 1982–1983. The deletion procedure yields slightly less negative trend estimates in layer 8 for the empirical adjustment technique, and has little effect in this layer

GLOBAL TRENDS

Table 2.3.1. Overall trend estimates (in % per year) from 10 Umkehr Stations for the period 1977–1987 with associated standard errors ($\pm 2\sigma$)

Layer	Empirical Correction Model (1)		Theoretical Correction Model (2)	
	No Deletions	Deletions in 1982–83	No Deletions	Deletions in 1982–83
8	(-0.59 ± .27)	(-0.51 ± .26)	(-0.43 ± .28)	(-0.42 ± .27)
7	(-0.45 ± .17)	(-0.45 ± .16)	(-0.43 ± .19)	(-0.43 ± .18)
6	(-0.16 ± .11)	(-0.17 ± .11)	(-0.26 ± .13)	(-0.22 ± .11)
5	(-0.08 ± .11)	(-0.10 ± .11)	(-0.21 ± .12)	(-0.14 ± .11)
4	(-0.08 ± .20)	(-0.18 ± .20)	(-0.21 ± .20)	(-0.15 ± .20)

Overall Solar flux estimates (in % per 100 units of $F_{10.7}$ flux) from the period 1977–1987				
8	(1.41 ± 0.81)	(1.48 ± 0.81)	(1.47 ± 0.94)	(1.61 ± 0.85)
7	(1.25 ± 0.89)	(1.28 ± 0.97)	(1.20 ± 0.93)	(1.38 ± 0.97)
6	(0.71 ± 0.63)	(0.81 ± 0.68)	(0.38 ± 0.74)	(0.72 ± 0.66)
5	(0.73 ± 0.61)	(0.90 ± 0.62)	(0.47 ± 0.68)	(0.79 ± 0.61)
4	(2.66 ± 1.15)	(2.87 ± 1.20)	(2.49 ± 1.18)	(2.82 ± 1.15)

for the theoretical model adjustment technique. The trend results for layer 7 are essentially the same for all methods. In the middle layers (4 and 5), the deletion procedure has more effect in the theoretical adjustment model, with less negative trend estimates occurring when data are deleted, but the reverse is true for the empirical model. For the most part, when the deletion procedure is used, the two correction methods yield fairly similar trend results overall. By contrast, the corresponding trend estimates obtained from a model such as (2) but with uncorrected Umkehr data are -0.87 ± 0.28 , -0.71 ± 0.19 , -0.31 ± 0.14 , -0.23 ± 0.14 , and $-0.26 \pm 0.22\%$ per year, respectively, for layers 8 through 4. Hence it is seen that failure to incorporate corrections for aerosol errors in the Umkehr data leads to highly distorted trend results, especially for layers 8 and 7.

The trend estimates obtained in this analysis for the period 1977–1987 are generally more negative in layers 7 and 8 than previous trend estimates obtained using data for the period 1970–1981 (Reinsel et al., 1987). Note also, that these estimates are substantially less negative than those obtained by DeLuisi et al. (1989a), which were based on a composite series of five Umkehr stations over the shorter period of 1979–1986 and which did not include an effect for solar flux variations. These trend results must be interpreted cautiously because of the shortness of the time period considered and because of the partial confounding between estimates of trend and solar flux effects over this relatively short period. As an illustration of the dependence of the trend results on the particular time period considered and on the effects of solar variations, a similar trend analysis for data over the period 1978–1987 was also performed. It yielded trend estimates in layers 4–6 that were generally positive and approximately 0.2% per year more positive than the trend estimates in Table 2.3-1 for those layers.

Finally one should note that the trends reported here take into account the effects of the solar cycle. They thus lead to an average decrease in ozone of about $-4.8 \pm 3.1\%$ at 40 km for the 10-year period between 1977 and 1987. When compared to the changes observed by the SAGE instruments, and within the uncertainty limits of SAGE and Umkehr trend results near 40 km, these two independent results are not inconsistent.

2.3.4 Analysis of Ozonesonde Data

A trend analysis using ozonesonde data collected at 13 stations over the period June 1965 through December 1982 has been previously reported (Tiao et al., 1986). This study has been updated for 9 of the 13 stations (Table 2.3-2) using all available data through December 1986. Individual ozonesonde readings in units of partial pressure at various pressure levels were first integrated into ozone amounts in 15 "fractional" Umkehr layers, shown in Table 2.3-3. The readings were screened to meet the following criteria: (1) the correction factor was between 0.9 and 1.2 for the Brewer-Mast (BM) sondes and between 0.9 and 1.15 for the ECC sondes, (2) the burst level was above the top of Umkehr layer 5B, (3) the corresponding daily total column ozone reading was available, and (4) readings with zero partial pressure were removed. In the earlier study, the correction factor in the screening procedure was set between 0.8 and 1.4 for the BM method and between 0.8 and 1.3 for the ECC method. The regression model used in the analysis is described in the appendix.

Employing available data through 1986, Table 2.3-4 gives the trend estimates and their associated estimated standard errors for each of the 15 layers of each of the 9 stations. The estimates are given in percent change per year. Figure 2.3-8 shows profiles of the trend estimates against the layers for each station. Broadly speaking over the majority of the stations, the noticeable features are a positive trend in the lower layers 1A-1D, a negative trend in the middle layers from 2A to 4B, and little or no trend for the layers 5A and above. An overall trend profile across the nine stations can be constructed by considering

Table 2.3.2. Ozonesonde stations, data spans, and measurement methods

Station	Latitude	Data Span	Method of Measurement
Kagoshima	32N	1/70-10/86	Japan
Tateno	36N	3/68-11/86	Japan
Sapporo	43N	3/68-4/86	Japan
Payerne	47N	9/68-12/85	Brewer-Mast
Hohenpeissenberg	48N	1/70-12/85	Brewer-Mast
Goose	53N	6/69-8/80	Brewer-Mast
		9/80-12/86	ECC
Edmonton	54N	10/70-8/79	Brewer-Mast
		9/79-11/86	ECC
Churchill	59N	10/73-8/79	Brewer-Mast
		9/79-10/86	ECC
Resolute	75N	3/66-11/79	Brewer-Mast
		12/79-10/86	ECC

Table 2.3.3. Fractional Umkehr Layers

Layer	1A	1B	1C	1D	2A	2B	3A	3B
Upper Boundary (km)	2.9	5.5	8.0	10.3	12.5	14.7	16.9	19.1
Layer	4A	4B	5A	5B	6A	6B	7	
Upper Boundary (km)	21.3	23.6	25.8	28.1	30.5	32.8	35.1	

GLOBAL TRENDS

Table 2.3-4. Trend estimates for nine stations (in % per year; data through December 1986 when available)

Layer	Kagoshima 32°N		Tateno 36°N		Sapporo 43°N	
	Trend	S.E.	Trend	S.E.	Trend	S.E.
7	-0.0949	0.2570	-0.0288	0.2271	-0.2936	0.3331
6B	0.1168	0.2442	0.0820	0.2188	-0.3130	0.3102
6A	0.4450	0.2336	-0.0172	0.1501	-0.1553	0.2239
5B	0.1386	0.1486	0.0939	0.1213	0.0103	0.1554
5A	0.2157	0.1678	-0.0913	0.1057	0.2996	0.1272
4B	-0.0326	0.2033	0.0892	0.1281	0.0902	0.1821
4A	-0.9895	0.1871	-0.3791	0.1656	0.2923	0.2171
3B	-0.5869	0.4582	0.0672	0.1659	0.8617	0.3700
3A	-0.6076	0.5495	0.3598	0.3561	0.7556	0.5651
2B	-0.7148	0.6638	0.3021	0.3872	1.5540	0.6151
2A	1.5634	0.6002	0.4971	0.4650	2.0444	0.6631
1D	0.3251	0.6275	0.6034	0.4874	3.0894	0.6804
1C	0.8453	0.3820	0.3247	0.2446	-0.2249	0.2728
1B	1.1980	0.4418	0.5309	0.1842	0.2234	0.2888
1A	2.5065	0.4815	1.2485	0.2877	0.9364	0.5446

Layer	Payerne 47°N		Hohenpeissenberg 48°N		Goose Bay 53°N	
	Trend	S.E.	Trend	S.E.	Trend	S.E.
7	-0.3927	0.1189	-0.4774	0.1266	1.1010	0.3989
6B	-0.2419	0.1011	-0.4549	0.1129	1.3753	0.3700
6A	0.0246	0.0872	-0.2564	0.0898	1.1855	0.2995
5B	-0.1226	0.0708	0.0377	0.0671	0.4013	0.2530
5A	-0.2046	0.0691	-0.0928	0.0731	0.0728	0.2075
4B	-0.4088	0.0680	-0.2457	0.0749	-0.0806	0.2150
4A	-0.5021	0.0831	-0.6372	0.0832	-0.6877	0.2600
3B	-0.8211	0.1518	-0.5486	0.1399	-0.9480	0.3735
3A	-0.6697	0.2427	-0.3854	0.1817	-0.8932	0.5202
2B	-0.9774	0.2857	-0.4241	0.2292	-1.5639	0.4874
2A	-0.2042	0.4118	0.0130	0.3712	-1.5020	0.8146
1D	0.3671	0.8308	2.3613	0.3648	-3.1778	0.9368
1C	1.6038	0.4287	2.6830	0.2150	-1.6966	0.5074
1B	2.1197	0.3390	2.2850	0.1762	-0.9935	0.4527
1A	2.4457	0.4170	2.3078	0.2487	-1.0987	0.4945

Layer	Edmonton 54°N		Churchill 59°N		Resolute 75°N	
	Trend	S.E.	Trend	S.E.	Trend	S.E.
7	3.0180	0.3989	3.3806	0.7391	-0.2466	0.3452
6B	2.9733	0.3887	2.7236	0.6748	-0.3685	0.3263
6A	2.2304	0.3403	1.0688	0.4455	-0.3610	0.1761
5B	1.0258	0.2485	-0.1247	0.3595	-0.0532	0.2658
5A	0.2672	0.2021	-0.9767	0.3092	-0.1598	0.0977
4B	-0.3388	0.2735	-1.4080	0.2847	-0.2328	0.0769
4A	-0.2767	0.2503	-1.9890	0.0995	-0.6220	0.0658
3B	-0.9817	0.3416	-0.9869	0.4493	-0.8826	0.1834
3A	-0.4881	0.5318	-1.1097	0.5889	-0.4674	0.1976
2B	-0.5528	0.7432	0.0407	0.3122	-0.3612	0.2293
2A	-2.1986	1.1197	-0.8426	0.8610	-0.5911	0.4114
1D	-1.6091	1.2641	-0.3072	1.4824	1.7975	0.0067
1C	-1.6674	0.4212	-1.0678	0.6925	1.4531	0.6260
1B	-0.7987	0.5065	-1.3955	0.5185	0.6997	0.4748
1A	-0.0882	0.6898	-0.7152	0.6638	-0.0624	0.0204

GLOBAL TRENDS

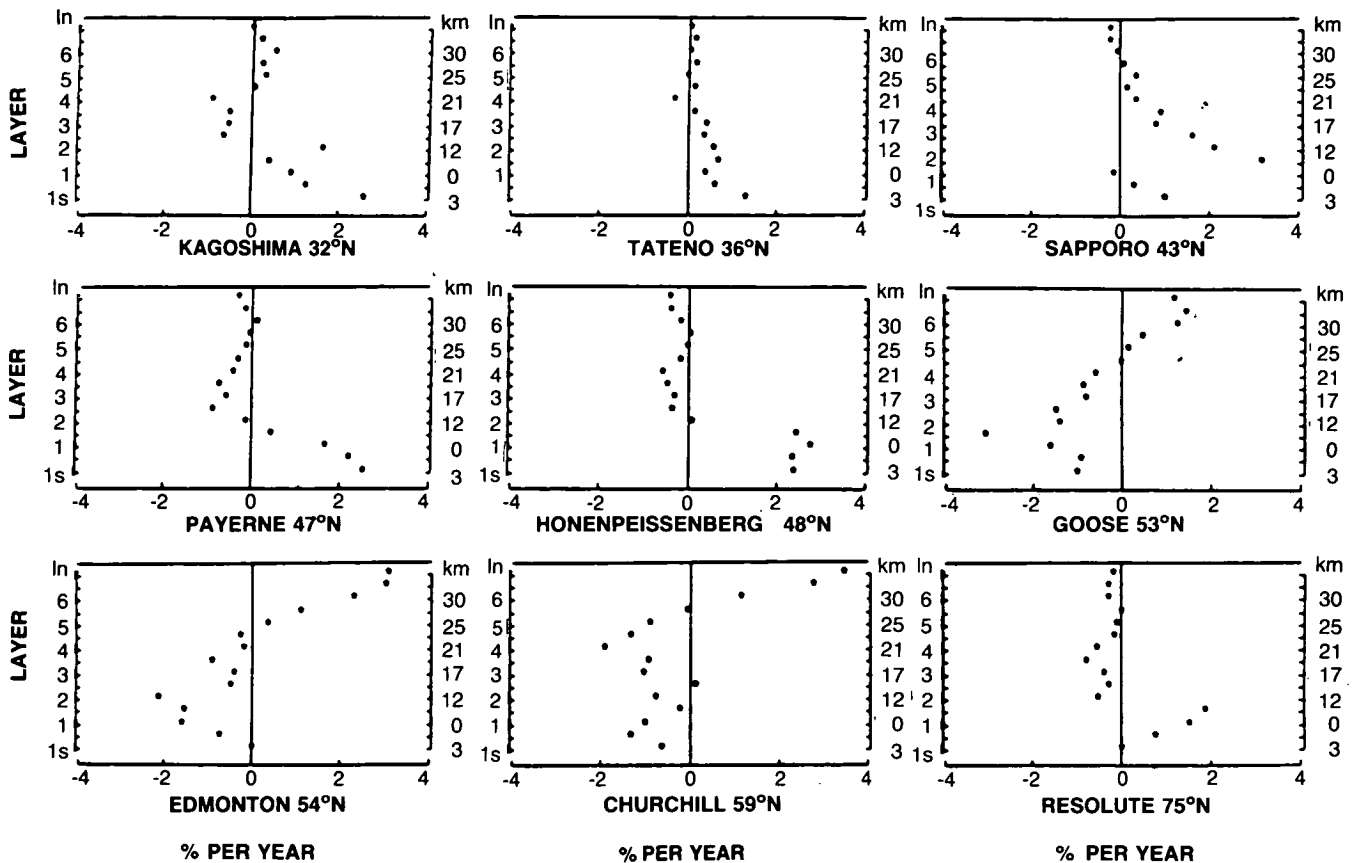


Figure 2.3-8. Trend estimates derived from ozonesondes measurements at 9 stations for 15 fractional Umkehr layers (% per year).

the nine estimates for each layer as a random sample from a normal population and compute the sample average and its estimated standard error. The results are given in Table 2.3-5. Statistically significant trend is observed in layers 3 and 4 (17–24 km). It corresponds to an average ozone concentration decrease of 0.46% per year.

One should be extremely cautious to draw conclusions on a global scale based on the analysis of the ozonesonde data. Figure 2.3-8 shows that considerable differences exist in the trend profiles across the stations, especially in the lower (1 and 2) and the upper (6 and 7) layers. This is also reflected by the width of the confidence intervals in Table 2.3-5. For example, the tropospheric trends derived for Payerne are probably too high because of an improvement in pre-launch procedure beginning in late 1983, not reflected by a level shift term in the statistical analysis. Otherwise, the two European mid-latitude stations do show a rather coherent behavior with similar trends in the lower stratosphere. The situation is rather confusing in the troposphere: although the three Japanese stations have generally positive trends, the three mid-latitude Canadian stations have negative trends, and large positive trends are observed at Resolute (75°N). In addition, while statistically significant ozone decreases are observed in layers 3 and 4, consideration of Table 2.3-4 shows that the decrease in layer 4 is mainly due to the period 1982–1986, as no significant trend is observed when the data through 1982 only are considered (see Table 2.3-5b). Such a picture is rather

GLOBAL TRENDS

Table 2.3-5. Summary of averages of trend estimates (% per year) and standard errors (S.E. $\pm 2\sigma$)

Layer	(a) Data thru 12/86		(b) Data thru 12/82	
	Average	S.E.	Average	S.E.
7	0.6620	0.5041	0.7875	0.6482
6B	0.6547	0.4536	0.6712	0.4933
6A	0.4627	0.2890	0.3669	0.4490
5B	0.1480	0.1224	0.1368	0.2132
5A	-0.0744	0.1292	0.0208	0.1331
4B	-0.2853	0.1523	0.0164	0.0973
4A	-0.6434	0.2052	0.1989	0.5425
3B	-0.5363	0.2073	-0.1615	0.1851
3A	-0.3895	0.1967	-0.4970	0.1998
2B	-0.2997	0.2941	-0.3090	0.4330
2A	-0.1356	0.4549	-0.0158	0.6358
1D	0.3833	0.6499	0.3940	1.1613
1C	0.2504	0.5135	0.1978	0.4633
1B	0.4301	0.4391	0.5121	0.2638
1A	0.8312	0.4646	0.6670	0.4538

consistent with the SAGE observations as it might expand the ozone decrease observed between 28 and 25 km towards lower altitude. However, in the SAGE data the maximum effect is observed at low latitudes in contrast with the sonde data where, except for Kagoshima, the decrease occurred at a number of mid-latitude stations. Thus, apart from the decrease in layer 3 observed consistently over most of the stations, it seems rather difficult to draw any definitive conclusion on a semi-global scale from this data set.

2.3.5 Comparisons with Model Calculations

Adding 15 months of new SAGE data to the analysis performed in the Ozone Trends Panel Report has not changed appreciably the observed change of $-3 \pm 2\%$ in ozone concentration near 40 km over the 6-year period 1980–1986. The more thorough analysis of data from 10 Umkehr stations in the Northern Hemisphere for the period 1977 to 1987 reports also a statistically significant decrease in ozone between 30 and 43 km, the decrease near 40 km being $4.8 \pm 3.1\%$ after allowing for seasonal and solar-cycle effects and correcting the data for aerosol interferences. The mean values of the observed decreases at 40 km are less than the mean values predicted by theoretical calculations performed in the OTP and taking into account both chlorine and solar influences. These are in the range of -6 to -8% over the period 1979–1985. However the large experimental uncertainties prevent a critical test of the theory.

The SAGE change of $-3 \pm 2\%$ at 25 km over 6 years when considered together with the negative Umkehr trend in this height range and the statistically significant, but not globally representative trend of nearly -0.5% per year observed by ozonesondes between 17 and 24 km, seems to suggest that the stratosphere below 25 km is the prime contributor to the total ozone loss at mid-latitude. Changes below 25 km are not predicted by global models based only on gas phase processes. It is not clear whether this points to missing processes in the models of the lower stratosphere or that the sparse measurements are not representative of the global atmosphere.

2.4 TRENDS IN STRATOSPHERIC TEMPERATURE

2.4.1 Introduction

The purpose of this section is to reiterate and update the Ozone Trends Panel Report (OTP) temperature trend analysis. The objective of the OTP analysis was threefold: (1) to establish the quality of a variety of stratospheric temperature data sets; (2) to discuss temperature trend mechanisms, and (3) to determine the consistency of temperature changes with observed ozone changes. This last objective is particularly difficult to reach, since it requires data analyses that minimize the influences of other processes contributing to temperature trends.

Global temperature data sets for the region above 30 hPa (~22 km) are only available after late 1978. For trend analysis, any data set covering such a relatively short period can be strongly influenced by short period anomalies and multi-year cycles such as the Quasi-Biennial Oscillation (QBO), the solar cycle, and even significant interannual variability. In particular, the OTP noted the strong thermal perturbation associated with the El Chichon eruption which occurred near the middle of the analysis period (1979–1986). Thus, rather than trying to estimate a trend, the differences between annual averages at the beginning and the end of the data period were calculated in the OTP. The annual averaging minimizes the QBO effect, and the calculation of changes minimizes the thermal perturbation associated with El Chichon, since it avoids using explicitly the years 1981 through 1984. The effect of the change in the solar flux over this period was estimated using model simulations. Finally, the OTP tried to minimize interannual variability associated with extratropical dynamics by focusing on temperature trends near the tropics to estimate the consistency of ozone and temperature changes.

The update of the previous temperature analysis performed in the OTP report, is based on the temperature data set already available and updated when possible, and the recently available data from Rayleigh lidar observations. The possible implication for trend determination of the recent finding of a statistical relationship between the stratospheric temperature, the QBO, and the 11-year solar cycle is also discussed.

2.4.2 Stratospheric Temperature Data Sets

The stratospheric temperature data sets used in the OTP report were obtained from radiosondes, rocketsondes and satellite radiances. Recently lidar temperature data have become available. In this section, the three data sets used in OTP are briefly summarized and the new lidar data are discussed.

2.4.2.1 Radiosondes

Radiosondes are balloon-borne instruments launched frequently at regular intervals. The density of radiosonde sites is relatively high over most continental regions. However, few measurements are available over the oceans, particularly in the Southern Hemisphere. Radiosondes can measure temperatures above 10 hPa (30 km), but due primarily to the inaccuracy in the pressure measuring, the uncertainty in the temperature measurement above 30 hPa is large. Additional uncertainties arise from the lack of a radiosonde standard, and the variety of instrument types in use worldwide from different manufacturers. Also, for trend analysis, problems arise from the lack of documentation on instrumentation changes which have been introduced over the years, and application of corrections for solar short wave and long wave radiation errors. Although a number of authors report radiosonde temperature trends above 30 hPa, the OTP felt that the uncertainties of the measurements were too large above 30 hPa for trend determination.

GLOBAL TRENDS

2.4.2.2 Rocketsondes

Rocketsondes are rocket-borne instruments, usually thermistors, which can be carried into the mesosphere and lower thermosphere. Due to their larger cost and complex ground station requirements, rocketsonde stations are rather few and the number of sites has significantly decreased in the last few years. Temperature trends obtained from rocketsondes are also influenced by changes in instrument design in the early 1970s, nonstandard data recording procedures prior to 1969, and the estimate of aerodynamic and radiation corrections. The OTP used only high quality rocketsonde data subset accounting for problems, and eliminated rocketsonde measurements that presented temperature differences of 3 K or more with simultaneously launched radiosondes.

2.4.2.3 Satellites

Beginning with the launch of the TOVS (TIROS-N Operational Vertical Sounder) instrument aboard the NOAA polar orbiter series in late 1978, regular temperature soundings of the stratosphere became available on an operational basis (the Stratospheric Sounding Unit [SSU] and Microwave Sounding Unit [MSU] instruments). Satellite temperature measurements prior to this period lack sufficient accuracy or record length.

Trend determination from radiance measurements from the TOVS series is complicated by calibration drift and differences between the performance of instruments in the series. Two approaches for the determination of satellite temperature trends were discussed by OTP. National Meteorological Center [NMC] analyses use temperature retrievals from TOVS radiances and Gelman et al. (1986, 1988) estimated corrections to the operational analysis temperatures for trends calculations. These corrections were derived from comparison with rocketsonde temperatures. Nash and Forrester (1986) also estimated temperature trends from TOVS radiances by intercalibrating the different TOVS instruments using the operational overlap of NOAA-6's SSU and MSU. Thus they were able to estimate the change in the measured radiances in the subsequent SSU and MSU instruments and establish the stability of the measurements over the 1980-1986 period.

2.4.2.4 Lidar

Rayleigh lidars provide density, and therefore, temperature information in the stratosphere and mesosphere. The Rayleigh lidar operates by detecting the Rayleigh backscattered signal from ground-based laser (for a description of the method see Hauchecorne and Chanin [1981] and Chanin and Hauchecorne [1984]). Due to the recent development of the lidar technique and the limited number of operational sites, data from this source were not used in the previous OTP report. To this date, two Rayleigh lidars located in France have been used on an operational basis: Observatoire de Haute-Provence (OHP) (44 N, 6 E) since 1981 and Biscarosse (44 N, 1W) since 1986. The total number of profiles averaged over a nighttime period and defined hereafter as a sequence, exceeds 1000, with an average of two sequences a week. Since the lidar profile is determined by averaging several hours of data, the variability due to gravity waves, which appears in the instantaneous soundings, is reduced.

The Rayleigh lidar temperature precision is height dependent and better than 1 K below 50 Km. However the accuracy of the temperature measurement may be affected by a number of factors: the presence of aerosols, the saturation of the pulse counters from low-altitude returns, and parallax effects between the emission and reception axis. These uncertainties can however be partly corrected. Aerosols

can be determined by simultaneous measurements at different wavelengths and a second channel with reduced efficiency can be used for the low-altitudes returns. Parallax effects can be avoided by using a co-axial system. To estimate the accuracy of the Rayleigh lidar, intercomparisons have been performed with rocketsondes. In 1986, rocketsonde and lidar measurements showed temperature differences between 1 K and 2 K from 30 to 70 km. This difference was smaller than the difference between the two thermistors on the same payload. Furthermore, intercomparison of the OHP and Biscarosse systems (located within 500 km) over 66 simultaneous profiles showed a difference between the two systems of less than 2 K below 80 km.

2.4.3 Intercomparison of Stratospheric Temperature Data Sets

2.4.3.1 Radiosonde, Rocketsonde, and Satellite Data

The temperatures determined independently by Nash and Forrester (1986), NMC, radiosondes (Labitzke et al., 1985), and rocketsondes (Angell and Korshover, 1983) were compared in the OTP report. Generally the analyses agreed, although there were periods of significant disagreement especially in 1982–1983. Figure 2.4-1 (a,b,c,d) from OTP shows the results of these comparisons in the 100–30 hPa (16–22 km), 30–10 hPa (22–30 km), 5–1 hPa (36–48 km), and 2 hPa level (40 km).

2.4.3.2 Comparison of Lidar Data with SSU and NMC

A comparison was performed for the period 1981–1987 between the temperature obtained by lidar and the SSU and the NMC data. The data have been selected to be within 5 degrees of latitude and 10 degrees of longitude of the OHP lidar site. It is however also important to note that both the SSU and NMC data used here are different from those used in the OTP report. The SSU data used in the OTP report were zonal means corrected for instrument changes as described in OTP Section 6.2.2.1 (see Nash, 1988). The SSU data used here are the standard gridded radiances provided by the British Meteorological Office and have not been corrected, and the NMC data used have been adjusted as described by Gelman et al. (1986).

Figure 2.4-2 shows the brightness temperature for the SSU channel 27 (approximately 1.5 hPa) and the lidar temperature convolved with the SSU weighting function given in Barnett and Corney (1984). Figure 2.4-3 shows over the same period the NMC data at 42 km (2.0 hPa) and the lidar data. The average lidar-SSU difference is of 4 K, with a maximum difference of 6.5 K. The average lidar-NMC difference is 3 K at 42 km and varies from –5 K to 7 K.

The lidar-SSU and lidar-NMC differences are generally similar. They can be divided into four periods, which correspond to changes in the biases between the data sets. The first period beginning in 1981 and extending to early 1982 is characterized by larger values of the lidar temperatures. The second period, from early 1982 to mid-1983, is characterized by a close match up of the lidar SSU and NMC data. The third period, from mid-1983 to mid-1985, is characterized again by larger values of the lidar temperatures. The last period, extending from mid-1985 onward, shows smaller differences. Although the reasons for these differences are not readily apparent, it seems that the September 1983 satellite change from NOAA-7 to NOAA-8 resulted in the introduction of large bias between the lidar and SSU/NMC data sets. This

GLOBAL TRENDS

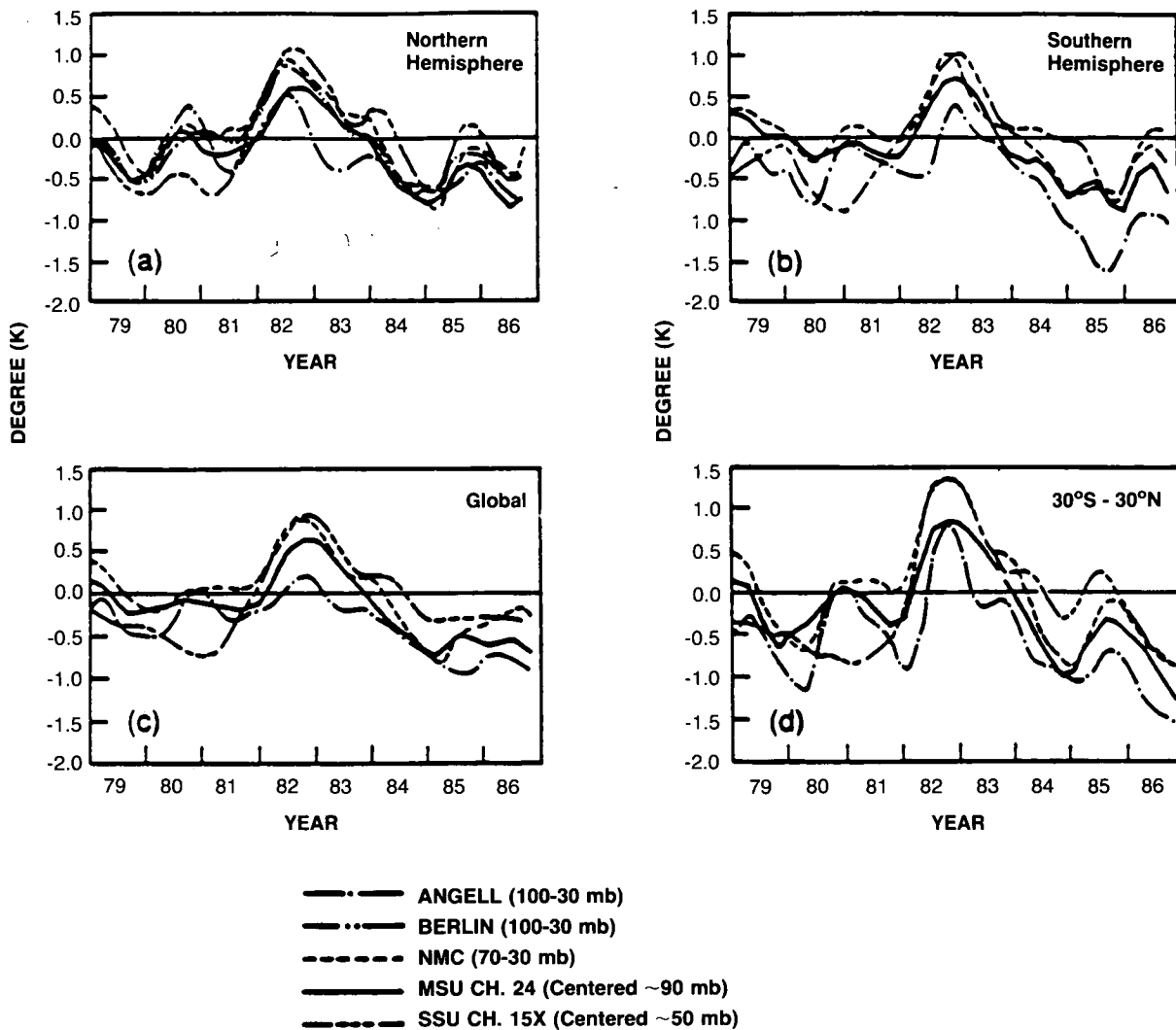


Figure 2.4-1a. Seasonal temperatures with the long-term seasonal averages removed and smoothed 1-2-1 in time: Angell 100-30 mb radiosonde thickness (solid dot); Berlin 100-30 mb thickness (long dash); NMC 70-30 mb thickness (short dash); MSU channel 24 centered at approximately 90 mb (solid); and SSU channel 15X centered at approximately 50 mb (solid dot) for (a) Northern Hemisphere average, (b) Southern Hemisphere average, (c) global average, and (d) 30°S-30°N average. Berlin data were available only for the Northern Hemisphere. Tick marks on the abscissa correspond to the D-J-F seasons.

effect is illustrated by the unadjusted data in OTP Figures 6.2.2.3 and 6.2.2.4, where the change from NOAA-7 to NOAA-8 is approximately accompanied by a 4-K cooling.

Comparisons were also performed between the lidar at 36 km and the SSU channel 26, and the lidar with NMC temperatures at 30 km (10 hPa), 36 km (5hPa), 48 km (1 hPa) and 55km (0.4 hPa) although this comparison relies on the downward extension of the lidar data by radiosondes, and is less germane to lidar-satellite comparisons. The best agreement between the lidar and NMC is obtained at 48 km with a maximum difference of 3 K. The causes of these differences will have to be studied further.

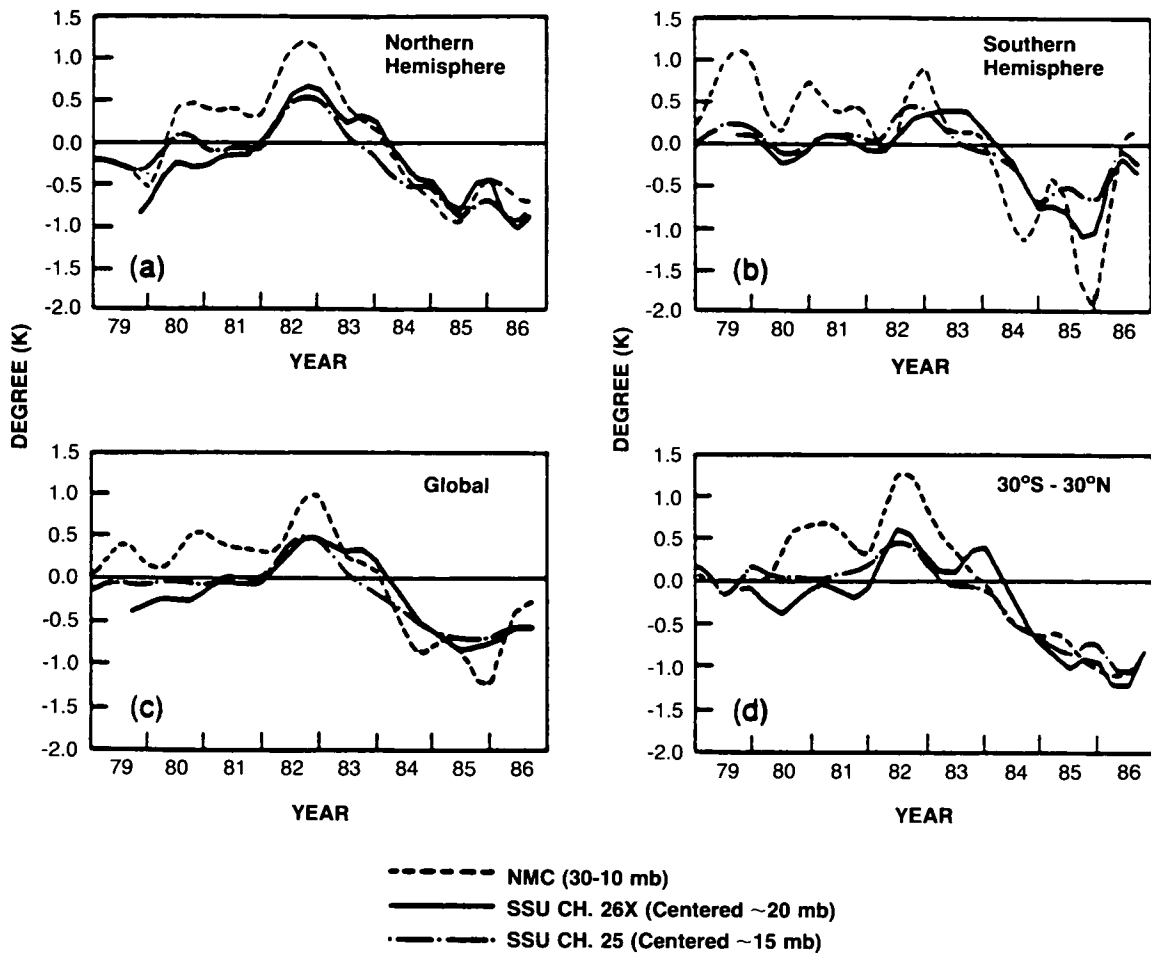


Figure 2.4-1b. Seasonal temperatures with the long-term seasonal averages removed and smoothed 1-2-1 in time: NMC 30-10 mb thickness (dotted); SSU channel 26X centered at approximately 20 mb (solid); and SSU channel 25 centered at approximately 15 mb (three short dashes and a long dash) for (a) Northern Hemisphere average, (b) Southern Hemisphere average, (c) global average, and (d) 30°S-30°N average. Tick marks on the abscissa correspond to the D-J-F seasons.

2.4.4 Influence of Solar Activity

Since the OTP report, a statistical relationship has been established between the temperature, the 11-year solar cycle, and the equatorial QBO (Labitzke, 1987; Labitzke and Van Loon, 1988). The relationship has first been observed in Arctic polar temperatures, when the temperatures are classified between years according to the west and east phases of the QBO. During the west phase, the polar temperatures are correlated with the solar cycle, while in the east phase, the polar temperatures are anti-correlated. The amplitude of this 11-year polar temperature cycle is approximately 10–15 K for either phase of the QBO. The relationship is illustrated in Figure 2.4-4 for the North Pole (from Labitzke and Van Loon, 1988). It has been since extended to other latitudes and altitudes (Labitzke and Chanin, 1988), and to the Southern Hemisphere. At present, no physical mechanism has been found to explain this relationship.

GLOBAL TRENDS

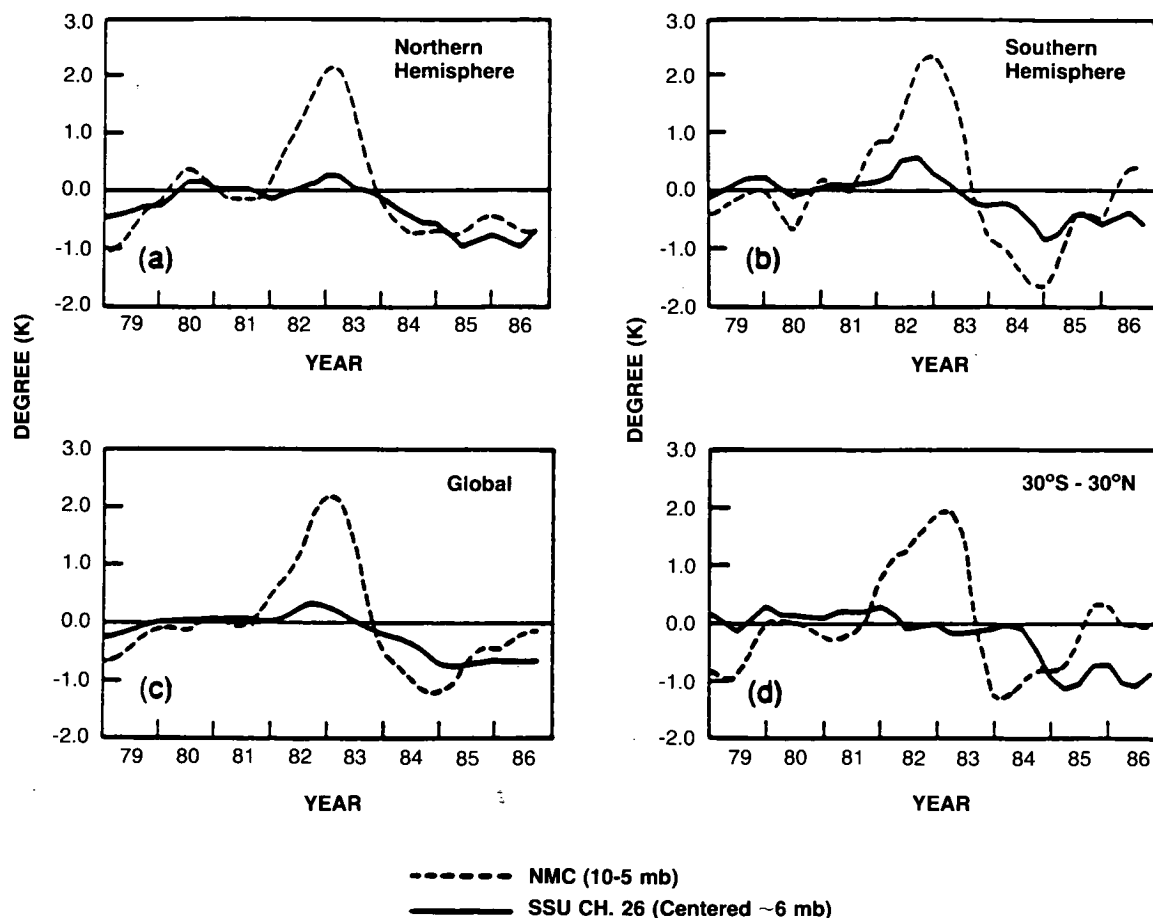


Figure 2.4-1c. Seasonal temperatures with the long-term seasonal averages removed and smoothed 1-2-1 in time: NMC 10-5 mb thickness (dotted); and SSU channel 26 centered at approximately 6 mb (solid), for (a) Northern Hemisphere average, (b) Southern Hemisphere average, (c) global average, and (d) 30°S-30°N average. Tick marks on the abscissa correspond to the D-J-F seasons.

The main consequence of the QBO-solar cycle relationship relevant to the present analysis is that it may be a source of long-term interannual variability. In addition, this relationship is variable with season, latitude, longitude, and height and generally, local data show a significantly larger QBO-solar cycle signal than zonal mean data. One should then be cautious when using local or regional data, unless the record length is large enough to allow the separation of trend and solar induced effects.

2.4.5 Updating of Previously Used Data Sets

Updates of global stratospheric temperature trends have been performed from radiosondes data by Angell (1988) and Labitzke (1989, private communication). Updates of the rocketsonde data have also been provided by Kokin et al. (1989) for the USSR stations of Heiss Island, Volgograd, Thumba, and Molod-zhnaya and by the Japan Meteorological Agency for the Ryori station.

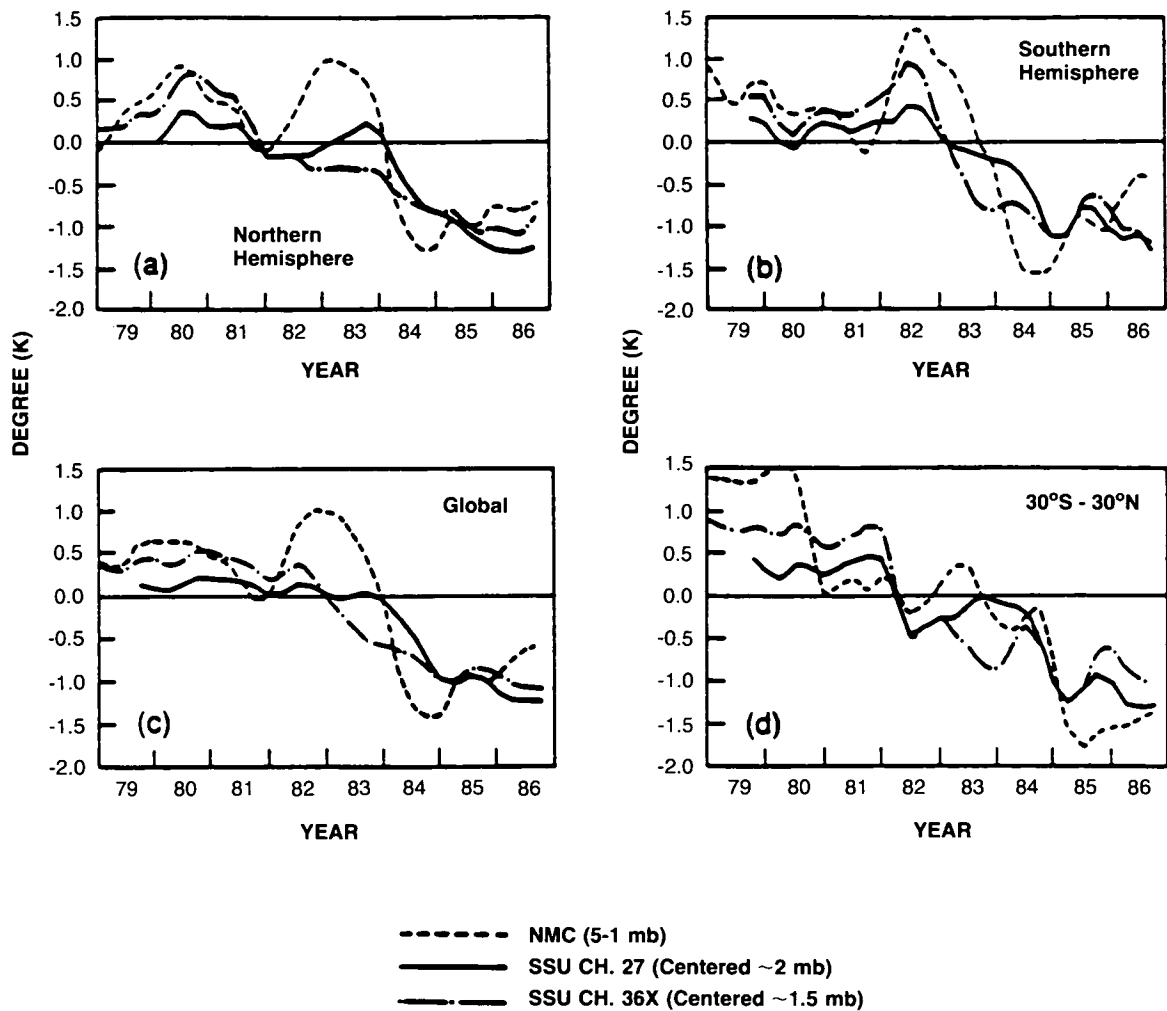


Figure 2.4-1d. Seasonal temperatures with the long-term seasonal averages removed and smoothed 1-2-1 in time: NMC 5-1 mb thickness (dotted); SSU channel 27 centered at approximately 1.5 mb (solid dot) for (a) Northern Hemisphere average, (b) Southern Hemisphere average, (c) global average, and (d) 30°S-30°N average. Tick marks on the abscissa correspond to the D-J-F seasons.

Angell (1988) derives a global cooling of -0.62 K/decade in the 100–50 hPa layer over the period 1973–1987, which mostly results from a strong cooling (-2 K in the Antarctic region). Both Labitzke (1989, private communication) and Angell (1988) conclude on a barely significant warming in the temperate Northern Hemisphere (0.2 K/decade at 50–60°N from Labitzke) at the same altitude level.

At lower latitudes (10–30°N) at the 30 hPa pressure level, Labitzke (1989, private communication) reported no trend in the summer between 1961 and 1981 (excluding the periods during which volcanic aerosols may have warmed the lower stratosphere following the eruptions of Agung [1963] and El Chichon [1982]). Angell (1988) found a 0.4 -K trend for the Western Hemisphere tropics. On the other hand, a mean decrease in temperature of 0.4 K is reported by Labitzke (1989, private communication) at 50–60°N, and a large decrease of 2 K at the polar stations is reported by Kokin et al. (1989) for the last 20 years.

GLOBAL TRENDS

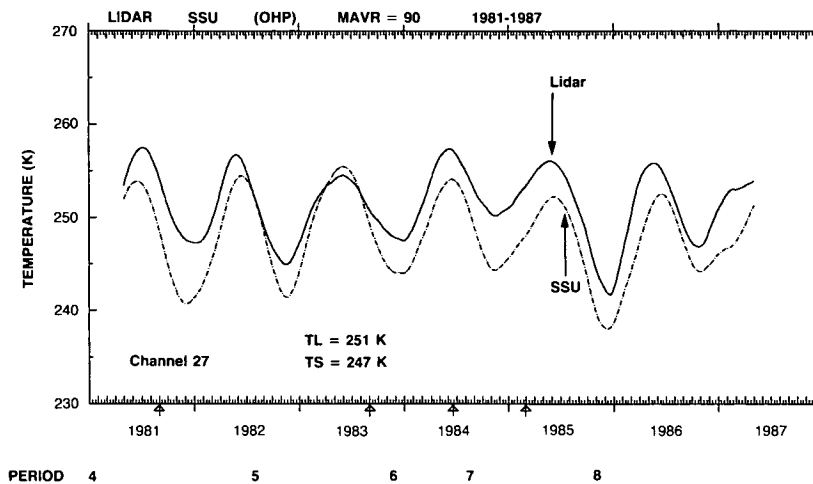


Figure 2.4.2. Lidar temperature and SSU channel 27 brightness temperature from 1981 to 1987 (with a running mean of 90 days).

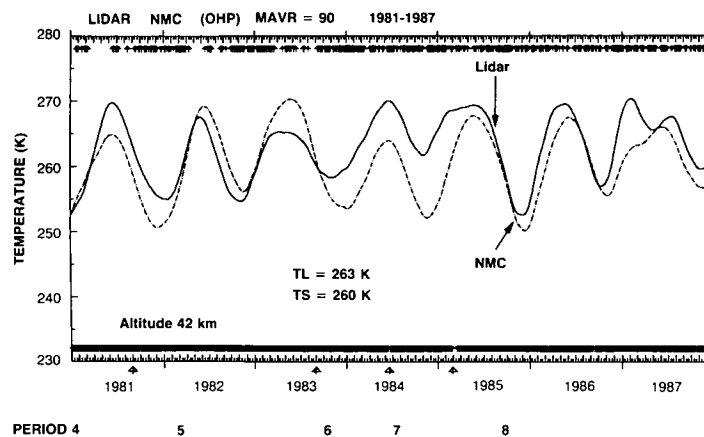


Figure 2.4.3. Lidar and NMC temperature at 42 km (with a running mean of 90 days). The periods corresponding to different NMC analyses are indicated at the bottom.

At the 10-hPa (30 km) pressure level, Labitzke (1989, private communication) reported a -0.5 K/decade trend for the latitude region between $20-50^{\circ}\text{N}$ over the period 1964–1987. Over the same period, Angell (1988) reported a trend of -0.2 K/decade based on radiosonde data. At the same altitude level, the updated rocket data of USSR and Japan led both to a larger trend of -1.5 K/decade, although with a large spatial variability. Using also rocketsonde data, Angell (1988) calculated a trend of -0.8 K/decade at 10 hPa in the Western Hemisphere tropics (1973–1987), and -1 K/decade in the upper stratosphere (5–0.5 hPa). Although the difference between the 10 hPa pressure level radiosonde and the rocketsonde-based trends is within a $\pm 2\sigma$ confidence intervals (Angell, 1988), the OTP reported serious disagreements between edited (see OTP Section 6.2.3) and unedited rocketsonde data. Since the Angell (1988), USSR, and Japan results are from unedited rocketsonde data, caution should be exercised when comparing those data to the rocketsonde data of the OTP. Furthermore, trends at these individual stations might be mainly representative of local evolution.

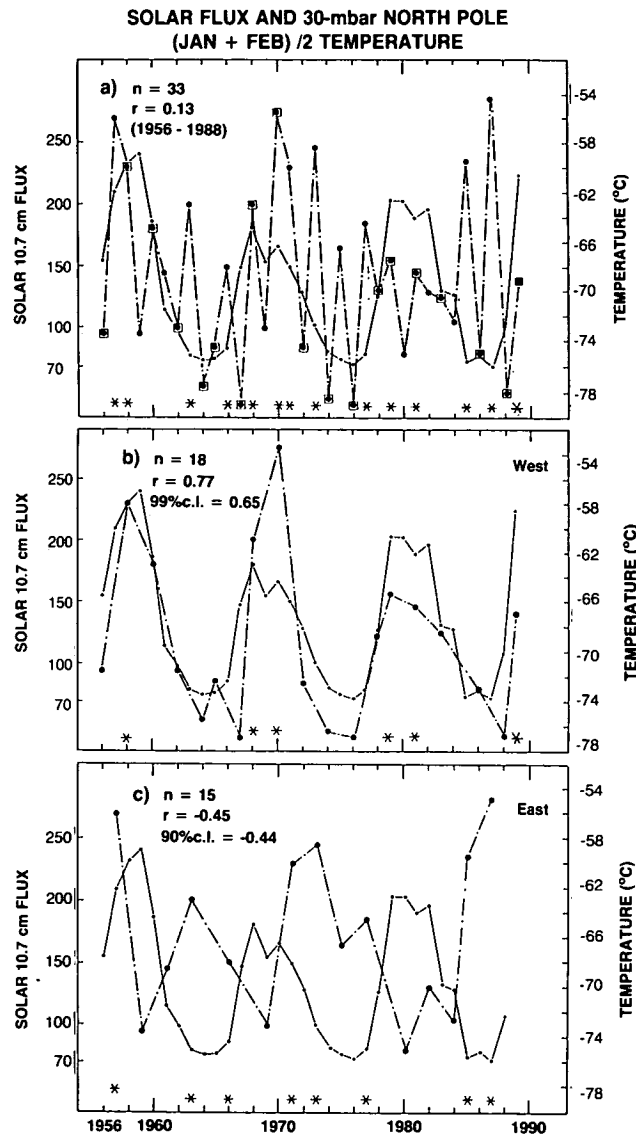


Figure 2.4-4. Comparison of the 10.7 cm solar flux, in $10^{-22}W/(m^2Hz)$ (solid line) and the 30 mb temperature, in degrees Centigrade, at the North Pole, averaged for January and February for (a) all winters, (b) winters in the West phase of the quasi-biennial oscillation (QBO), (c) winters in the East phase of the QBO. Asterisks denote major mid-winter stratospheric warmings (from Labitzke and van Loon, 1988).

As a common conclusion, these studies give some evidence of a generally negative trend, with large spatial variability. The upper limit of the zonally averaged trend is between -0.6 and -0.8 K/decade between the 100 hPa and 10 hPa pressure levels (16–30 km) respectively, with the exception of the Antarctic region. These values are much lower than the local trends derived from rocketsonde data.

2.4.6 Comparison with Trends in Ozone Distribution

The reported SAGE I/SAGE II changes between the 1979–1981 and 1984–1988 periods, in the 20–50 degree latitude bands lead to a maximum decrease of $3\% \pm 2\%$ in ozone concentration at 40 km and a

GLOBAL TRENDS

decrease of -5% at 50 km in the tropics (see Section 2-3-2). These values are very similar to those already reported in the OTP where the SAGE data used were the zonal mean profiles for the latitude band 15°S to 15°N which gave an ozone concentration decrease of -5% peaking at 50 km. Because the predicted temperature change is sensitive to the ozone change above 50 km, two cases were considered: (1) no ozone change outside the 26–50 km altitude range where SAGE measurements are available, (2) a -5% ozone change above 50 km and a -2% change below 26 km. The radiative response showed a temperature decrease of 1K to 1.4 K at 50 km. An additional 0.8-K cooling will occur at the same altitude due to the decrease in the solar flux during the declining phase of the solar cycle. Thus, the expected 50 km temperature was estimated to be of 1.8 to 2.2 K in the tropics. With the updated value of the tropical ozone decrease of 4%, the 50 km change should be 1.4 to 1.8 K.

Changes on global and equatorial temperatures over the period from 1979–1980 to 1984–1985 are shown in Figures 2.4-5 and 2.4-6, reproduced from OTP Figures 6.3.2.1 and 6.3.2.2. The decrease in equatorial temperatures at 48 km from satellite and rocket data over the same period is about $1.75\text{ K} \pm 1\text{ K}$. Global temperatures show a smaller decrease of $1.5\text{ K} \pm 1\text{ K}$. The SAGE ozone changes and the observed equatorial temperature changes appear to be in satisfactory agreement within the $\pm 2\sigma$ confidence interval of the analyses.

2.5 TRENDS IN TROPOSPHERIC GASES AND OZONE

2.5.1 Introduction

The Ozone Trends Panel (OTP) Report presented information on the global trends of a number of tropospheric trace gases that interact with stratospheric ozone, either chemically, as sources of nitrogen,

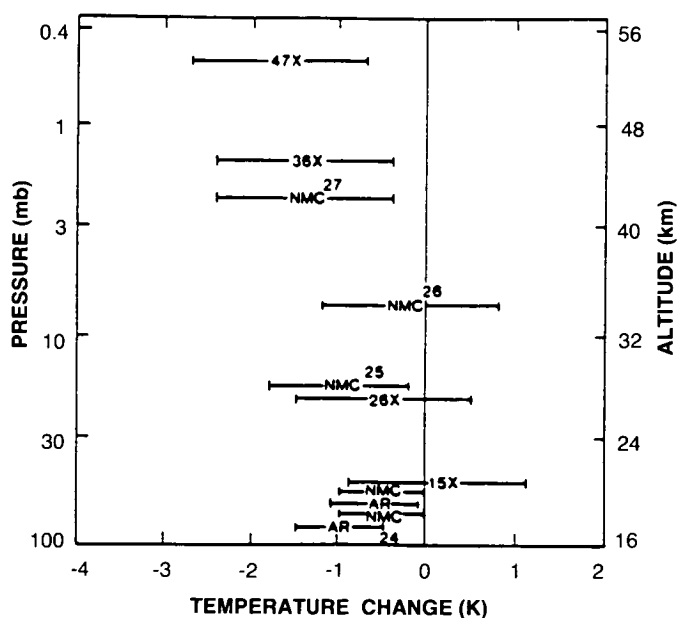


Figure 2.4-5. Summary of global stratospheric temperature differences (1985 and 1986 minus the average of 1979 and 1980). Symbols denote Angell's radiosonde data (AR), NMC data (NMC), and satellite data (channel numbers, see Figure 6.2.2.1 of the OTP Report). Error bars denote uncertainties (see text). Nash and Forrester (1988) estimate their satellite errors as 0.2 K rms (1 K rms for synthesized channels).

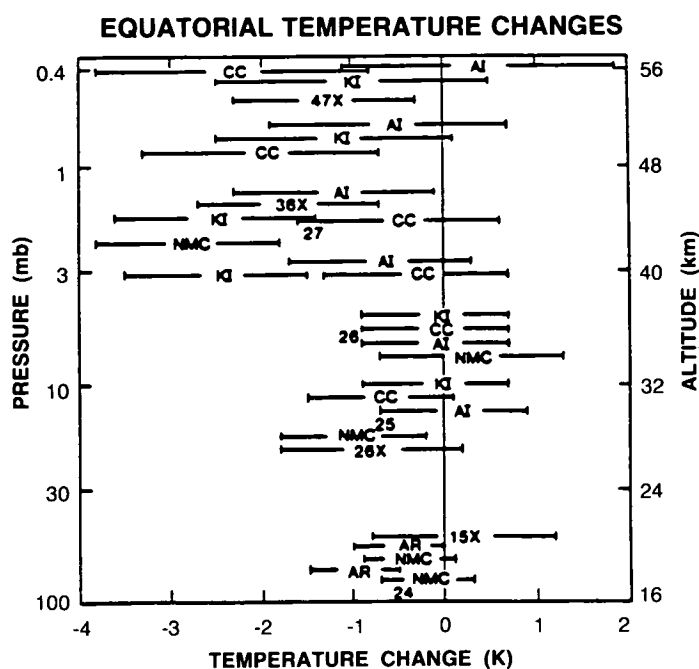


Figure 2.4-6. As in Figure 2.4-4, except for tropics and including rocket stations. Kwajalein Island (KI; 9°N, 168°E), Ascension Island (AI; 9°S, 14°W), and Cape Canaveral (CC; 28°N, 81°W).

hydrogen and halogen catalysts that substantially control ozone destruction, or indirectly by influencing stratospheric temperatures. The OTP Report reviewed available data up to the end of 1986. The purpose of this section is to update the OTP Report with data, where possible, from 1987 and 1988. Section 2.5.2 describes the trends in halocarbons and reviews the progress in the area of trace gas calibration. As shown in the OTP Report, the calibration uncertainties associated with several trace gases are significant, particularly methyl chloroform (CH_3CCl_3), carbon tetrachloride (CCl_4), CFC-113 ($\text{CCl}_2\text{FCClF}_2$), and carbon monoxide (CO). Sections 2.5.3, 2.5.4, and 2.5.5 review the trends observed in atmospheric nitrous oxide (N_2O), methane (CH_4), and carbon monoxide (CO), as these species are of particular importance in determining future stratospheric ozone levels. It would appear in particular that the current rate of CH_4 increase is not constant and this is examined in the available data sets. Also, historical CH_4 data from ice core studies suggest a connection between CH_4 levels and climate. Carbon dioxide (CO_2), a radiatively important trace gas, was not considered in significant detail in the OTP Report. The Section 2.5.6 examines the global rate of increase of CO_2 over the last decade, which shows considerable variability. Finally, the data available on surface and free tropospheric ozone measurements at a number of locations are reviewed in Section 2.5.7 in the light of recent suggestions of large-scale tropospheric increases in the Northern Hemisphere. As an overview, the current trends, concentrations, and lifetimes of trace gases are summarized in Table 2.5-1.

2.5.2 Halocarbons

A variety of anthropogenic and natural halocarbons are present in the global atmosphere. The abundance, sources, and sinks of this group of chemicals have been recently discussed in Gammon et al. (1986) and in the OTP Report (Ehhalt et al., 1989).

GLOBAL TRENDS

Table 2.5-1. Concentrations and global trends of tropospheric gases for 1987. Lifetimes are given, where available (adapted from Ehhalt et al., 1989)

Source Gas	Mixing Ratio	Rate of Increase		Lifetime yr
	pptv	pptv/yr	%/yr	
CCl ₃ F ^a	240 ^h	9.5	4.0	110
CCl ₂ F ₂ ^a	415 ^h	16.5	4.0	75
CH ₃ CCl ₃ ^a	150 ^h	6.0	4.0	7
CCl ₄ ^b	140 ^h	2.0	1.5	40
CCl ₂ FCClF ₂ ^b	45 ⁱ	4-5	10	90
CHClF ₂ ^c	100 ^h	7	7	20
CH ₃ Cl ^d	600			1.5
CHCl ₃ ^c	30 ^h			0.7
CH ₂ Cl ₂ ^c	35 ^j			0.6
CCl ₂ CCl ₂ ^c	30 ^h			0.6
CH ₂ ClCH ₂ Cl ^c	35 ^j			0.6
CClF ₂ CClF ₂ ^c	15 ^j			180
CHClCCl ₂ ^c	10 ^{h,j}			0.1
CClF ₂ CF ₃ ^c	5 ^h			380
CClF ₃ ^c	5 ^h			400
CBrClF ₂ ^d	1.7 ^h	0.2	12	25
CBrF ₃ ^d	2.0 ^h	0.3	15	110
CH ₃ Br ^d	10-15			1.5
CHBr ₃ ^c	2-3			0.4
CH ₃ Br ₃ ^c	2-3			0.5
CH ₃ CH ₃ Br ^c	2-3			
CH ₃ BrCl ^c	1-2			
CHBr ₃ Cl ^c	1			0.6
CH ₃ BrCH ₃ Br ^c	1			0.6
CHBrCl ₃ ^c	1			0.6
N ₂ O ^f	307 ^{k,n}	0.6-0.7 ^{k,m,n}	0.2	150
CH ₄	1680 ^{i,n}	12 ^{f,g,n}	0.7	10
	1680 ^{q,n}	16 ^{q,n}	1.0	
CO ^g	90 ^{i,n}		≈1 (NH) ≈0 (SH)	0.2
CO ₂ ^f	348 ^{f,l,p}	1.6-1.9 ^{f,p}	0.45-0.55 ^f	
O ₃	≈20 ⁿ		≈1 (NH) ≈0 (SH)	

^a GMCC-GAGE data

^b 1987 GAGE data (Cape Grim) and 1986 global distribution (Ehhalt et al., 1989)

^c OGC data at Cape Grim and observed global distribution (Rasmussen and Khalil, 1982)

^d 1986 data (Ehhalt et al., 1989)

^e Gammon et al., 1986

^f GMCC

^g CSIRO

^h OGC calibration

ⁱ NBS calibration

^j SRI calibration (Singh et al., 1979)

^k GMCC calibration

^l WMO calibration

^m SIO data, calibration

ⁿ ppbv

^p ppmv

^q UC data

The halocarbons are the most rapidly increasing species on a percentage basis in the global atmosphere over the last several decades. There is concern about this class of compound because they are sources of stratospheric halogen-free radicals, which catalytically destroy ozone (Rowland and Molina, 1975) and because they absorb in otherwise low opacity infrared wavelength regions of the atmospheric absorption spectrum and thus contribute significantly to the greenhouse effect (Ramanathan et al., 1985). For halocarbons, whose tropospheric lifetimes are much longer than global circulation times, the trends measured at ground level, at sites remote from halocarbon sources, can provide a reasonably accurate determination of global atmospheric trends (Prinn et al., 1983). The global rate of accumulation of halocarbons in the background atmosphere have been recently reviewed (Prinn, 1988a; Ehhalt et al., 1989).

2.5.2.1 CCl₃F, CCl₂F₂, CH₃CCl₃, CCl₄

The global rates of increase of these compounds in 1987 (Table 2.5-1) are similar to those given in the OTP Report. Sources of new observations up to the end of 1987 are the GMCC (Geophysical Monitoring for Climatic Change) program with stations at Barrow, Alaska (71°N); Niwot Ridge, Colorado (40°N); Mauna Loa, Hawaii (20°N); Cape Matatula, Samoa (14°S), and at the South Pole (CCl₃F, CCl₂F₂: Bodhaine and Rosson, 1988). An update of the observations at Cape Point, South Africa (34°S) (CCl₃F, CCl₄: Scheel et al., 1989) and Hokkaido, Japan (45°N) (CCl₃F, CCl₂F₂, CH₃CCl₃ and CCl₄: Makide et al., 1987) is also included.

Global data, additional to that presented in the OTP Report (up to mid-1986), are not available from the GAGE (Global Atmospheric Gases Experiment) program due to an ongoing calibration re-evaluation. Possible revisions to previously presented data (post mid-1985) (Ehhalt et al., 1989) are believed to be small (Prinn, 1989, private communication). The GAGE data collected at Cape Grim, Tasmania, up to the end of 1987 are shown in Figure 2.5-1.

The rate of increase of CH₃CCl₃ at Hokkaido (3.7 ± 0.8 pptv per year [$\pm 2 \sigma$ as for all confidence intervals given hereafter]; Makide et al., 1987) is significantly lower than the global rate of 6.2 ± 0.2 pptv per year deduced from the GAGE program (Prinn et al., 1987). If the low CH₃CCl₃ growth rate measured at Hokkaido is representative of a large area of the Northern Hemisphere, then this implies that the lifetime of CH₃CCl₃ is shorter than that shown in Table 2.5-1. The observed calibration difference of about 20% between the two data sets cannot account for this discrepancy between the observed trends.

As stated in the OTP Report there are considerable uncertainties associated with the absolute calibration of CH₃CCl₃ and CCl₄. For example, the concentrations observed on Hokkaido for these two species are approximately 20% lower than observations reported from the GAGE program for similar latitudes. Analysis of GAGE CCl₄ data suggests that the Makide CCl₄ calibration (Yokata et al., 1985) is consistent with the calculated industrial CCl₄ emissions and an atmospheric lifetime of about 40 years (Simmonds et al., 1988). These calibration uncertainties remain and need to be resolved, as they introduce considerable uncertainty into the deduction of atmospheric lifetimes for these species.

2.5.2.2 Other Chlorocarbons

CCl₂FCClF₂ (CFC-113)

Observations of global background mixing ratios of CCl₂FCClF₂ were summarized in the OTP Report and found to be increasing at about 11% per year in 1986. Further observations at Cape Grim (1984-87) show mean concentrations and increases in 1987 of 33 pptv and 3.4 (± 0.5) pptv per year (Figure 2.5-1).

GLOBAL TRENDS

GROWTH OF HALOCARBONS AND NITROUS OXIDE AT CAPE GRIM

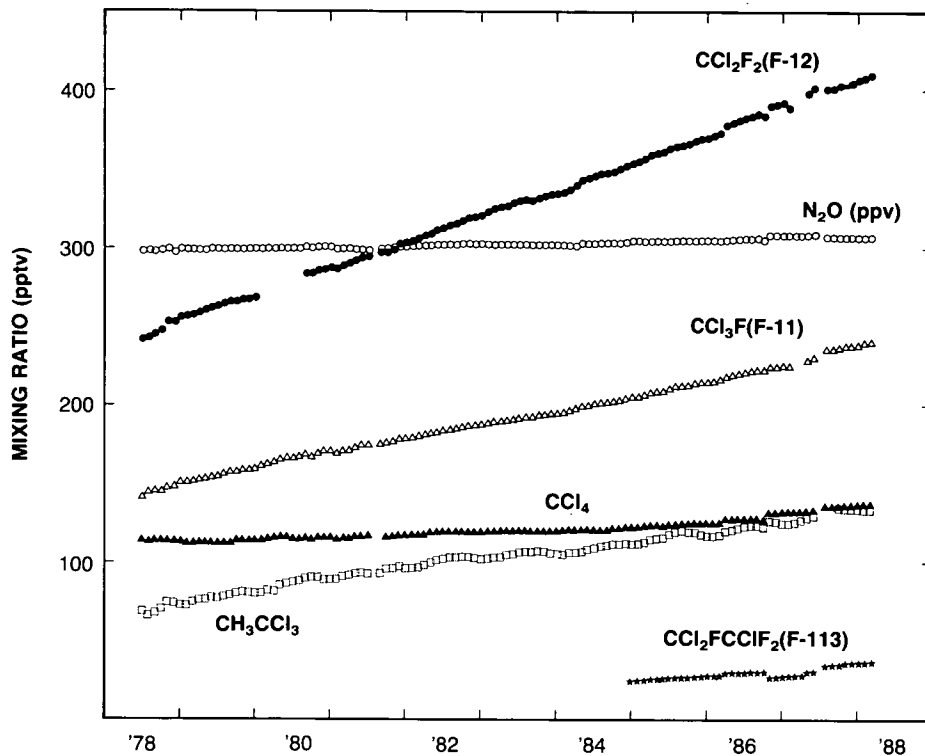


Figure 2.5.1. Halocarbon (pptv) and nitrous oxide (ppbv) observations at Cape Grim, Tasmania, as part of the GAGE program (Fraser and Derek, 1989).

Based on the observed Northern Hemispheric-Southern Hemispheric concentration ratio (Ehhalt et al., 1989), and converting the OGC (Oregon Graduate Center) scale to the NBS scale (NBS/OGC = 1.31, Rasmussen, 1989, private communication), an approximate global mean mixing ratio (45 pptv) and growth rate (10% per year) can be derived. This change in the OGC calibration of $\text{CCl}_2\text{FCClF}_2$, if substantiated, will essentially remove the differences between the GAGE measurements in the Northern Hemisphere and those made on Hokkaido, Japan (for discussion, see OTP Report).

CHClF_2 (HCFC-22)

Recent observations of global background mixing ratios of CHClF_2 have been reviewed (Ehhalt et al., 1989) and found to be increasing at about 7% per year. Further observations at Cape Grim (1984–87) show a mean concentration and increase in 1987 of 91 pptv and $6.5 (\pm 0.3)$ pptv per year (Figure 2.5-2). Based on the previously observed global distribution (Rasmussen and Khalil, 1982) an approximate global average mixing ratio (100 pptv) can be derived (Table 2.5-1).

CH_3Cl

Methyl chloride (CH_3Cl) is the most abundant halocarbon in the atmosphere, and is thought to be largely of natural origin. Observations of global background mixing ratios of CH_3Cl have been reviewed (Ehhalt et al., 1989), suggesting a global background level of 600 pptv. Further observations at Cape Grim (1984–1987) show a 1987 mean level of around 570 pptv and a clear annual cycle (Figure 2.5-3), which has

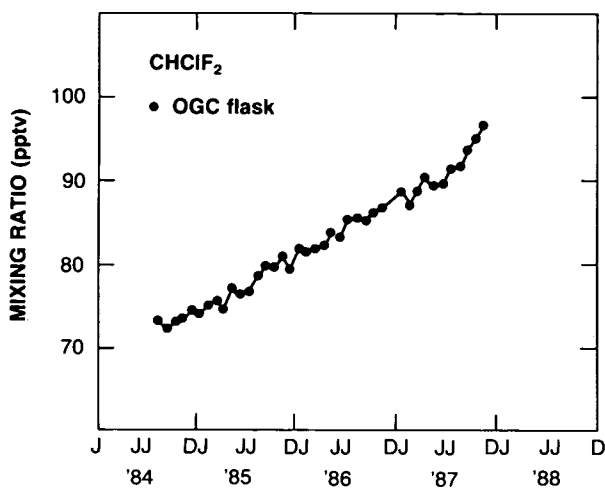


Figure 2.5-2. CHClF_2 (pptv) observations at Cape Grim, Tasmania, from the Oregon Graduate Center flask sampling program (Fraser et al., 1989).

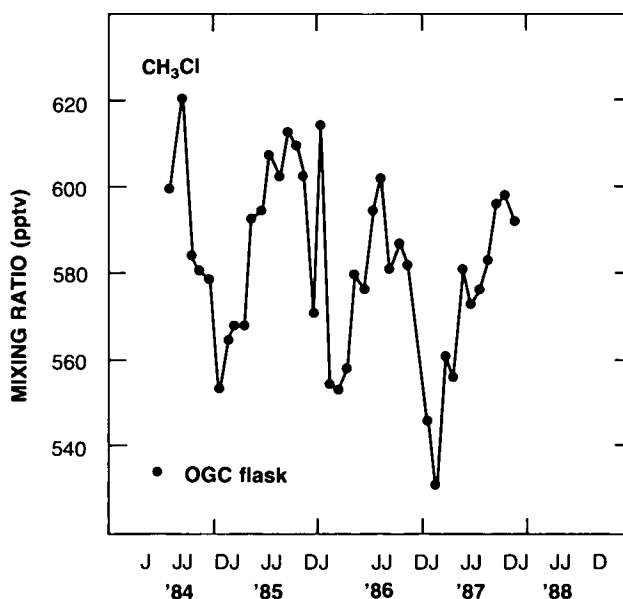


Figure 2.5-3. CH_3Cl (pptv) observations at Cape Grim, Tasmania, from the Oregon Graduate Center flask sampling program (Fraser et al., 1989).

been attributed to seasonal variations in the magnitude of the $\text{CH}_3\text{Cl-OH}$ radical sink (Ehhalt et al., 1989). Cape Grim record is too short to deduce whether there exists a long-term regional trend in CH_3Cl .

CHCl_3

Global background observations of CHCl_3 from the OGC flask-sampling network have been published (Khalil et al., 1983), suggesting a global average mixing ratio of approximately 30 pptv. Further observations

GLOBAL TRENDS

at Cape Grim (1984–87) show a large interannual variability. There is also a suggestion of an annual cycle. The mean level at Cape Grim was about 10 pptv (Fraser et al., 1989; Figure 2.5-4).

2.5.2.3 Bromocarbons

Bromine species are relatively minor components of the stratosphere compared to chlorine species, but are nevertheless important because bromine radicals can very efficiently catalyze ozone destruction (McElroy et al., 1986).

The major sources of stratospheric bromine are the naturally occurring organobromine species such as methyl bromide (CH_3Br), methylene dibromide (CH_2Br_2) and bromoform (CHBr_3), produced by oceanic algae (Rasmussen and Khalil, 1984; Penkett et al., 1985; Khalil and Rasmussen, 1985; Khalil et al., 1987; Cicerone et al., 1988; Class and Ballschmiter, 1988) and the anthropogenic organobromine species, bromodifluoromethane (CBrClF_2 , halon-1211) and bromotrifluoromethane (CBrF_3 , halon-1301), used exclusively as fire fighting agents, and ethylenedibromide ($\text{CH}_2\text{BrCH}_2\text{Br}$), a gasoline additive.

The concentrations of the halons have been growing rapidly in recent years (Lal et al., 1985), and there could be a substantial anthropogenic contribution to the methyl bromide observed in the atmosphere. Penkett et al. (1985) measured average concentrations of 15.4 ± 1.9 pptv and 10.6 ± 0.9 pptv for CH_3Br in the Northern and Southern Hemisphere, respectively, on ship voyages down the Atlantic Ocean from Southampton to Antarctica in 1982 and 1983. They estimated a total source strength of approximately 10^5 tons per year to account for the data, of which 75% could be of anthropogenic origin (Wofsy et al., 1975).

The significance of the growing halon concentrations and a potentially large anthropogenic component in the measured methyl bromide is that these are the predominant forms in which bromine is transferred to the stratosphere, prior to breakdown into Br atoms and BrO radicals.

2.5.3 Nitrous Oxide

Nitrous oxide (N_2O) is an important component of the background atmosphere, being a climatically significant species (Ramanathan et al., 1985), as well as a source of nitrogen oxides in the stratosphere,

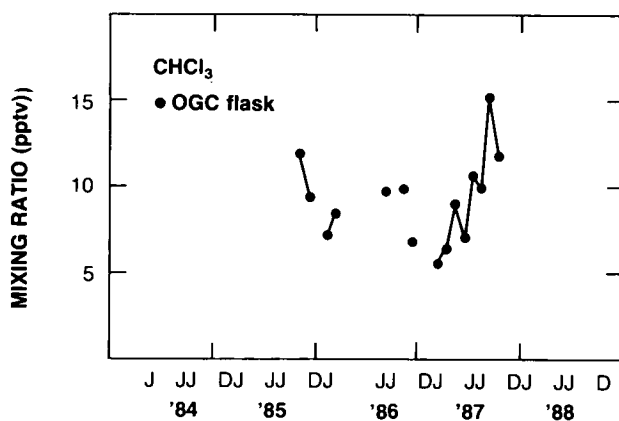


Figure 2.5-4. CHCl_3 (pptv) observations at Cape Grim, Tasmania, from the Oregon Graduate Center flask sampling program (Fraser et al., 1989).

which play a major role in regulating stratospheric ozone levels (Crutzen, 1970). Natural sources of N₂O include microbiological processes on the continents and in the oceans, and anthropogenic sources arise from the combustion of fossil fuels (Weiss and Craig, 1976), biomass burning (Crutzen et al., 1979), and the use of nitrogenous fertilizers (Crutzen and Ehhalt, 1977).

There are several long-term N₂O measurement programs on the background atmosphere at various locations around the globe. Data from the SIO (Scripps Institute for Oceanography) network showed that the global rate of increase in 1986 was 0.63 (± 0.07) ppbv per year (Ehhalt et al., 1989). The Northern Hemispheric data from this program are shown in Figure 2.5-5 (Weiss, 1989), which show an average increase of 0.60 (± 0.06) ppbv per year (Table 2.5-2).

N₂O measurements have been made on air samples collected at the GMCC (Geophysical Monitoring for Climatic Change) sites (Barrow, Niwot Ridge, Mauna Loa, Samoa, and South Pole) since 1977 (Bodhaine and Rosson, 1988). The global average mixing ratio in 1987 was 306.7 ppbv, increasing at 0.73 (± 0.05) ppbv per year (Table 2.5-2). The globally averaged data are also shown in Figure 2.5-5.

A long-term N₂O data record has been collected at Cape Point, South Africa, by scientists from the Fraunhofer Institute for Atmospheric Environmental Research (FIAER), FRG, and CSIR, South Africa, using an *in situ* gas chromatograph (Figure 2.5-5). The 1987 average mixing ratio was 301.2 ppbv, increasing at 0.6 (± 0.2) ppbv per year (Table 2.5-2; Scheel et al., 1988).

A combined OGC-GAGE data analysis showed a global increase of 0.8 ± 0.1 ppbv per year (Ehhalt et al., 1989). Further analysis of the GAGE N₂O data has been delayed by the GAGE calibration re-evaluation. However, the preliminary GAGE N₂O data from Cape Grim in 1987 (Fraser and Derek, 1989) have been analyzed and show an average mixing ratio of 307.8 ppbv increasing at 0.95 (± 0.06) ppbv per year (Table 2.5-2, Figure 2.5-5). The trends deduced from GAGE data are significantly larger than those

Table 2.5-2. N₂O mixing ratios and rates of increase observed in the troposphere

Site	Laboratory	N ₂ O (ppbv) 1987	Rate of Increase		Reference
			ppbv/yr ($\pm 2 \sigma$)	%/yr	
Global Average	GMCC	306.7	0.73 (± 0.05)	0.24	Bodhaine and Rosson (1988)
NH Average	SIO	305.1 ^a	0.60 (± 0.06)		Weiss (1989)
Global Average	SIO	305.1 ^a	0.63 (± 0.07)		Ehhalt et al. (1989)
Cape Point S. Africa	FIAER- CSIR	301.2	0.62 (± 0.20)	0.21	Scheel et al. (1989)
Global Average	OGC	308.2 ^b	0.83 (± 0.05)	0.27	Ehhalt et al. (1989)
Cape Grim Tasmania	CSIRO	307.8	0.95 (± 0.06)	0.31	Fraser and Derek (1989)

^a1986 data

^b1985 data

GLOBAL TRENDS

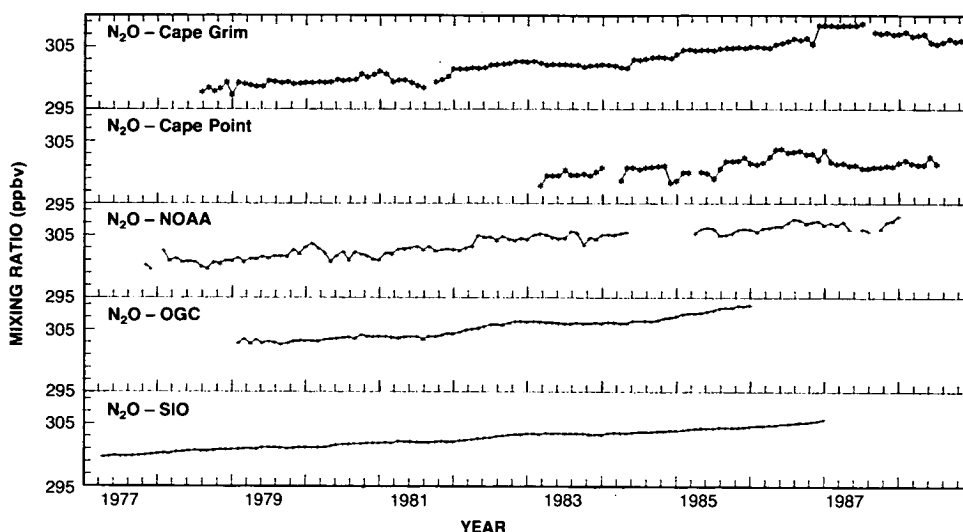


Figure 2.5-5. Long-term trends of N₂O from the GMCC program (average of data from Barrow, Niwot Ridge, Mauna Loa, and Samoa), the SIO program, the OGC-ALE program (average of data from Barrow, Adrigole, Cape Meares, Mauna Loa, Barbados, Samoa and Cape Grim), the FIAER-CSIR program (Cape Point, South Africa) and CSIRO-GAGE data (Cape Grim, Tasmania) (Bodhaine and Rosson, 1988; Weiss, 1989; Ehhalt et al., 1989; Scheel et al., 1988; Fraser and Derek, 1989).

from SIO, GMCC or FIAER-CSIR data (Table 2.5-2), but the significance of these differences cannot be fully assessed until the GAGE re-calibration is completed. The GAGE calibration scale is also significantly higher than those of GMCC and SIO, but this cannot account for the trend differences observed. The globally averaged trends (Table 2.5-1) are based on SIO and GMCC data.

In the OTP Report data were shown on ice core studies of N₂O which, despite a noisy record, showed that N₂O concentrations prior to 1800 were about 280-290 ppbv. Further data have been published (Khalil and Rasmussen, 1988a), that confirm this result with more precise data which show that N₂O levels have risen by about 8% during the last century.

2.5.4 Methane

Methane is an important trace gas because it absorbs infrared radiation, and thus impacts on climate. It affects tropospheric chemistry via hydroxyl radical and ozone budgets, and it impacts on stratospheric chemistry as a source of hydrogen and water vapor and as a sink for stratospheric chlorine.

Recent data from three laboratories making global measurements (GMCC, CSIRO, and UC (University of California)) are summarized in Table 2.5-3. The GMCC and CSIRO programs show significantly lower rates of increase (≈ 12 ppbv per year) than the UC program (16 ppbv per yr). From the GMCC (Steele et al., 1989) and CSIRO (Fraser et al., 1989) programs it would appear that the global rate of CH₄ increase has slowed in recent years. Figure 2.5-6 shows the data from the CSIRO program as well as data collected at Cape Point, South Africa (Scheel et al., 1988), which also show a current low rate of increase (10 ppbv per year). The cause of the recent slowing of the CH₄ increase is not known. Clearly longer data records are necessary to properly define long-term CH₄ variability.

Table 2.5-3. Global average methane mixing ratios and rates of increase observed in the troposphere by various laboratories

Laboratory	Mixing Ratio ppbv	Rate of Increase		Reference
		ppbv/yr ($\pm 2 \sigma$)	%/yr	
GMCC	1674 ^a	12.1 ^a	0.7	Steele et al., 1987, 1989
UC	1680 ^b	16 \pm 1	1.0	Blake and Rowland, 1988
CSIRO	1682 ^c	12 \pm 2	0.7	Fraser et al., 1986b, 1989
FIAER-CSIR	1612 ^d	10.3 \pm 0.4	0.6	Scheel et al., 1988

^a1988 data, OGC calibration
^b1987 data, UC calibration
^c1987 data, NBS calibration
^d1987 data, FIAER calibration

The zonally averaged distribution of methane in the remote marine boundary layer is shown in Figure 2.5-7, from 5 years of data from the GMCC sampling network, comprising 26 globally distributed sites (Steele et al., 1987). The seasonality in the Southern Hemisphere is very repeatable, as is the average latitudinal gradient.

New data have become available on past CH₄ levels. Using infrared solar spectra recorded at the Jungfrauoch Station, Switzerland, in 1951-52 and 1984-87 it has been shown that the total vertical column abundance of CH₄ increased by 0.7(± 0.2)% per year during this period (Zander et al., 1989a). Ice core studies of historic CH₄ levels were reviewed in the OTP Report, which showed that over the past 300 years CH₄ levels have more than doubled. Further studies have been published which extend the CH₄ record back more than 100,000 years. Stauffer et al. (1988) show that the concentration of CH₄ was about 500 ppbv 100,000 years ago and fell to around 350 ppbv near the peak of the last ice age, 18,000 years ago, before rising to a typical Holocene value of about 650 ppbv. Raynaud et al. (1988) have extended the CH₄ record back to 160,000 years before present, and have shown that CH₄ was similarly low at the end of the preceding ice age. These results suggest a relationship between CH₄ levels and climate that may provide further clues in understanding modern CH₄ variability.

2.5.5 Carbon Monoxide

Carbon monoxide is an important trace gas in the troposphere because it plays significant roles in controlling the chemistry of ozone production and hydroxyl radical destruction in the lower atmosphere. It directly affects the oxidizing capacity of the lower atmosphere and can thus influence the concentrations of climatically important gases such as methane, for which oxidation by hydroxyl radical is a major sink.

Because of its short atmospheric residence time (2-3 months) the determination of a secular trend in CO mixing ratio is difficult. Increases are expected because significant CO sources are under human control, such as fossil fuel use, and have been growing (Cicerone, 1988). The available global CO data have

GLOBAL TRENDS

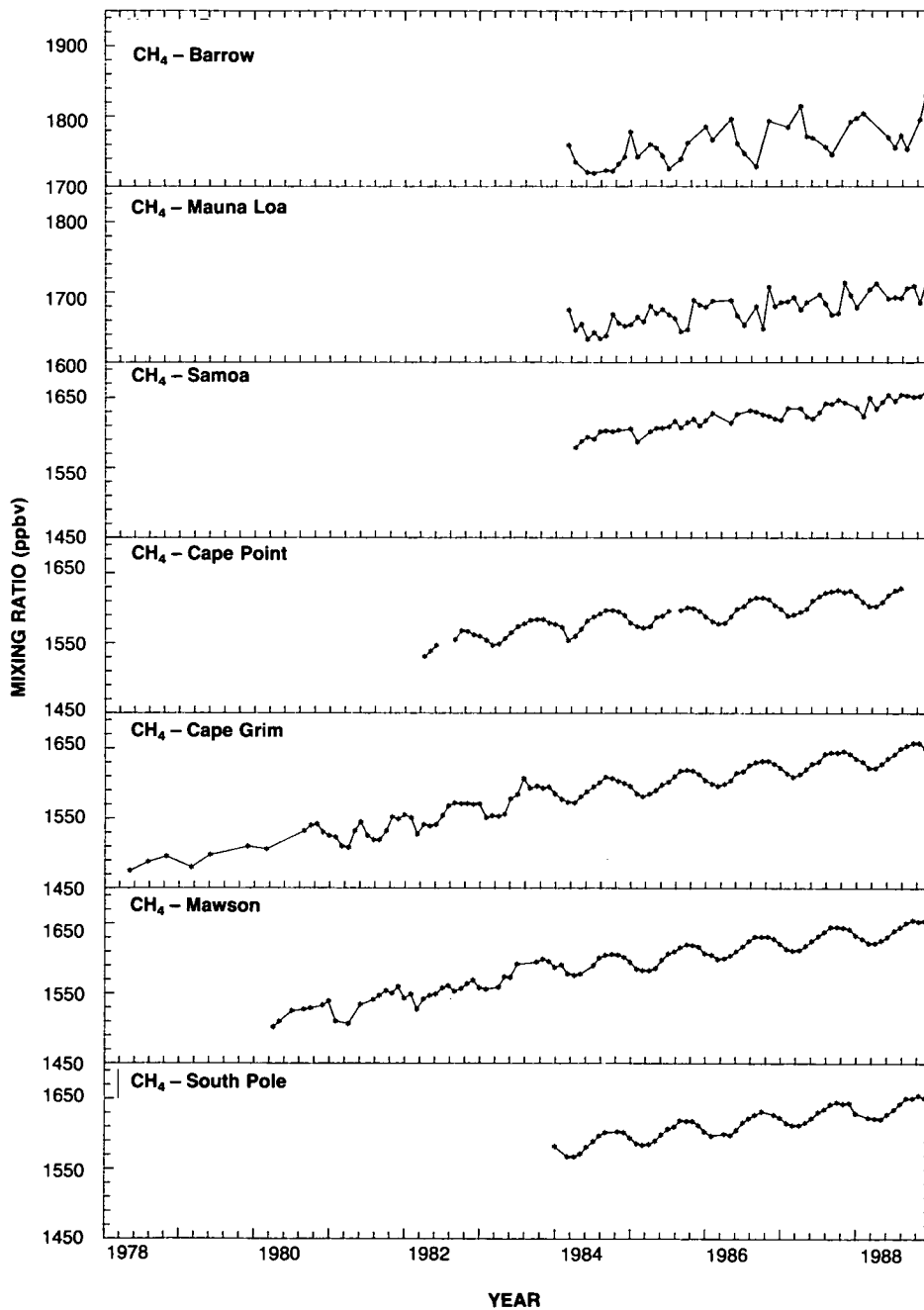


Figure 2.5-6. Long-term trends of CH₄ from the CSIRO global program (Fraser et al., 1986a, 1989) and the FIAER-CSIR program at Cape Point, South Africa (Scheel et al., 1988).

been reviewed (Cicerone, 1988; Ehhalt et al., 1989) suggesting that CO has increased in the Northern Hemisphere over the past 15–30 years, but data from the Southern Hemisphere show no significant or uniform trends. The data have been updated in Table 2.5-4 to include observations from the OGC and CSIRO sampling networks, as well as from Cape Point, South Africa. The CSIRO and FIAER-CSIR data are shown in Fig. 2.5-8.

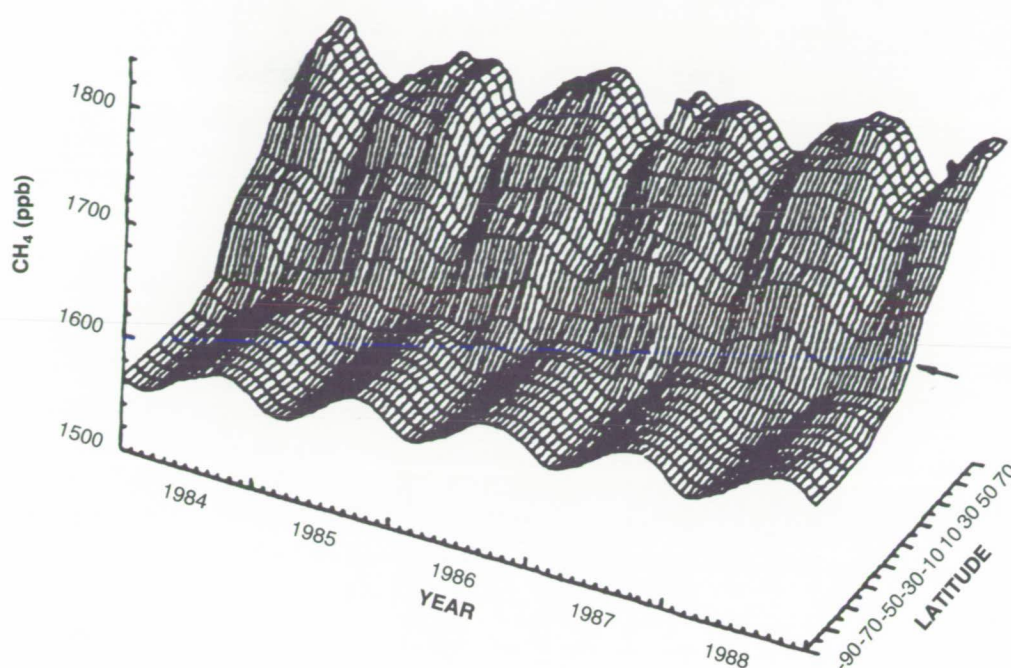


Figure 2.5-7. The global distribution, seasonality, and trend of CH_4 from the GMCC network (Steele et al., 1987 and unpublished data).

All data sets show statistically significant positive CO trends in the Northern Hemisphere of about 1% per year, except the relatively short records collected by CSIRO at Barrow and Mauna Loa, which do not show significant trends. The Southern Hemispheric data do not show consistent trends. The data collected by OGC (Khalil and Rasmussen, 1988b), over the period 1980–87, and CSIRO (1984–88) show a significant, positive trend at Samoa, but not at Cape Grim (CSIRO:1978–88). The relatively long records at Cape Point (1978–88) (Scheel et al., 1988) and Mawson (1980–88) do not show significant trends, whereas the relatively short CSIRO record at the South Pole shows a significant, positive trend. The mid-to-high latitude data from the Southern Hemisphere show remarkably uniform (amplitude and phase) seasonal variations (late summer minimum, winter maximum), which are probably in response to the hydroxyl radical sink (Fraser et al., 1986a,b; Ehhalt et al., 1989).

The secular increase of the total vertical column abundance of CO over Europe has been derived from sets of infrared solar spectra recorded at Jungfraujoch Station, Switzerland, in 1950–51 and in 1985–87. The mean cumulative rate of increase of the total column abundance of CO over this 35-year period was found to be $0.85 (\pm 0.2)\%$ per year (Zander et al., 1989b). As Cicerone (1988) has pointed out, the detection of sustained temporal trends in atmospheric CO is very challenging. Atmospheric CO concentrations are strongly influenced by sources and sinks that vary greatly with season, latitude, and longitude. A successful trend-detection strategy must account for this variability and be capable of dealing with differences between continental and marine regions and between the planetary boundary layer and the free troposphere.

GLOBAL TRENDS

Table 2.5-4. Surface carbon monoxide concentrations and trends

Site	Lat.	Period	Conc. ppbv 1987	Trend %/yr ($\pm 2 \sigma$)	Reference
Moscow	56°N	1952,53– 1970,76		1	Dianov-Klokov & Yurganov, 1981
Northern Hemisphere		1970–82		1.5	Dvoryashina et al., 1984
Jungfraujoch	46°N	1950,51– 1985–87		0.85(± 0.2)	Zander et al., 1989b
New Jersey	40°N	1968–77		positive	Graedel & McRae, 1980
<i>OGC network^a</i>		1980–87			Khalil & Rasmussen, 1988b
Northern Hemisphere			105	0.9(± 0.5)	
Southern Hemisphere			50	1.9(± 0.8)	
Cape Point ^b	34°S	1978–88	60	0.1(± 0.2)	Scheel et al., 1988
<i>CSIRO network^c</i>					
Barrow	71°N	1984–88	155	-1.5(± 2.3)	Fraser et al., 1986a,b
Mauna Loa	20°N	1984–88	90	0.2(± 2.9)	
Samoa	14°S	1984–88	65	3.4(± 2.0)	Fraser, 1989
Cape Grim	41°S	1978–88	60	-0.1(± 0.7)	
Mawson	68°S	1980–88	60	0.2(± 0.9)	
South Pole	90°S	1984–88	55	2.5(± 1.8)	

^aOGC scale
^bFIAER scale
^cNBS scale

2.5.6 Carbon Dioxide

Carbon dioxide (CO₂) is the major greenhouse gas in the atmosphere whose abundance is changing in response to human activities. CO₂ plays a significant role in regulating the temperature of the stratosphere, which in turn influences stratospheric ozone chemistry and abundance. Precise atmospheric measurements of CO₂ have been made since the late 1950s, initially in Antarctica and at Mauna Loa, Hawaii, and presently by an international network of more than 40 sites. The increase of CO₂ in the background atmosphere over the past 15 years has been well documented.

Carbon dioxide data for 1987 from *in situ* analyzers are available from the GMCC network (Bodhaine and Rosson, 1988) and from Cape Grim, Tasmania (Beardsmore and Pearman, 1989). The global average mixing ratio in 1987 deduced from these sites is 348.1 ppmv, with a global average increase of 1.6 ppmv from 1986 to 1987. The long-term trends of CO₂ (1973–1987) from the GMCC sites are shown in Figure 2.5-9. On average, the global increase over this period has remained steady at about 1.5 ppmv per year, but at certain times and sites increases as large 3 ppmv per year and as small 0 ppmv per year have been observed. There are strong correlations between the rates of increase observed at these widely distributed sites.

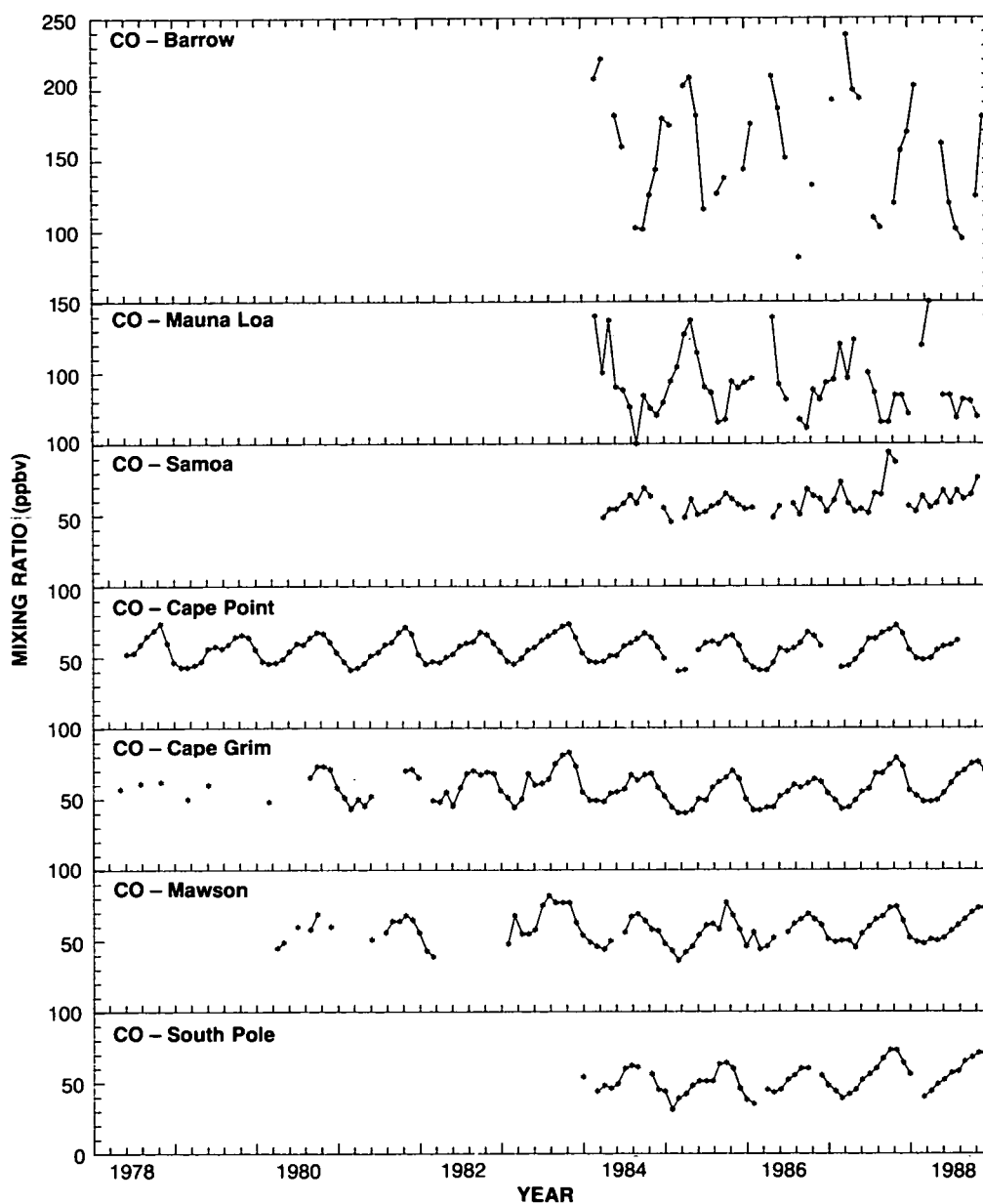


Figure 2.5-8. Long-term trends of CO from the CSIRO network and from Cape Point, South Africa (Fraser et al., 1986a,b, 1988; Fraser and Coram, 1988; Scheel et al., 1988).

Measurements of the global distribution of CO₂ from a network of 26 flask sampling sites (Conway et al., 1988) continued in 1987 (Bodhaine and Rosson, 1988). The global average concentration in 1987 from this network was 348.3 ppmv, and the global average CO₂ increase (1986 to 1987) was 1.9 ppmv.

2.5.7 Tropospheric Ozone

Tropospheric ozone impacts in several important ways on the tropospheric levels of source gases (Levy, 1971). Most notably, it is essential for the photochemical production of the hydroxyl radical, OH,

GLOBAL TRENDS

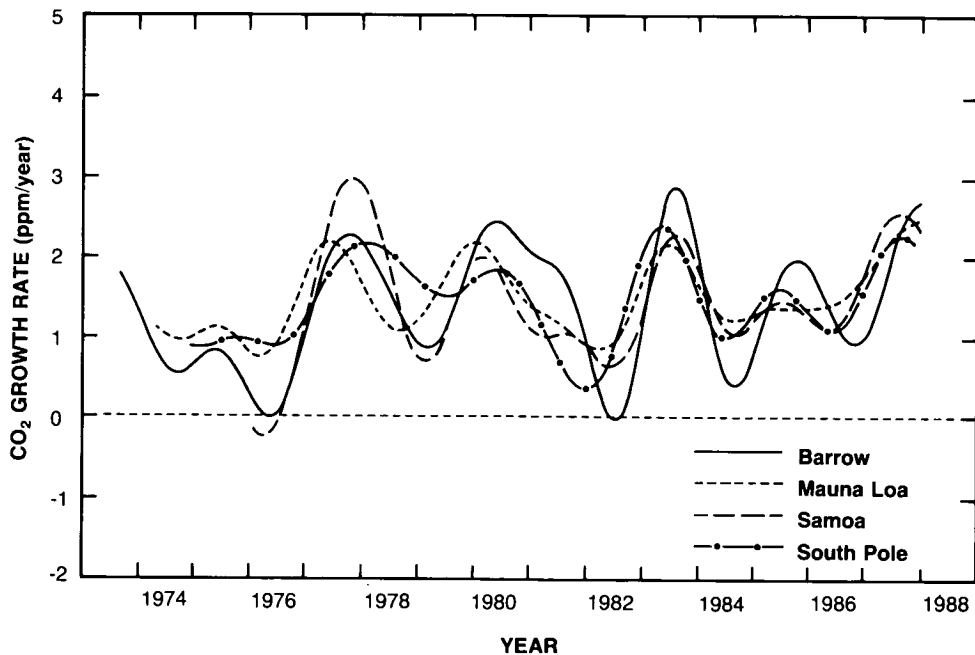


Figure 2.5-9. The temporal behavior of the CO₂ trends observed at the GMCC stations (Bodhaine and Rosson, 1988).

which determines the lifetime of many tropospheric trace gases, and thus also in part determines the ozone depletion potential of the hydrogen-containing source gases. In addition, tropospheric ozone makes a contribution of about 10% to the total ozone column in the atmosphere. Thus, a trend in tropospheric ozone has important consequences for stratospheric ozone concentrations and the detection of stratospheric ozone trends. Tropospheric ozone is also a significant greenhouse gas (Ramanathan et al., 1985).

In fact, a trend in tropospheric ozone, particularly in the Northern Hemisphere, is not unexpected. Ozone is produced photochemically in the troposphere and its precursors, nitrogen oxides, CO, CH₄, and non-methane hydrocarbons are known to have increased, mainly due to anthropogenic emissions (Gammon et al., 1986; Ehhalt et al., 1989).

The evidence for increases in tropospheric ozone has been reviewed (Logan, 1985; Bojkov, 1986, 1988; Penkett, 1988). The available observations on current trends in ozone at or near the Earth's surface are summarized in Table 2.5-5. They seem to support the expected positive trend in regions of the Northern Hemisphere. All seven European sites show statistically significant positive trends. However, all four Canadian sites show negative trends, of which only one is significant. All three Japanese sites show positive trends; two are significant. The Southern Hemispheric sites do not show statistically significant trends, except for the South Pole, which shows a significant negative trend. The central European trends reach as high as 3% per year. It should be noted that these trends fluctuate in time and that some of the European stations have exhibited a slowing down of the positive trends and even a decrease of ozone in recent years.

Only a few of the stations listed in Table 2.5-5 are clean air sites, making semi-continuous surface measurements (at least daily), namely Barrow and Mauna Loa in the Northern Hemisphere and Samoa, Cape Point, Cape Grim (Galbally et al., 1986) and the South Pole in the Southern Hemisphere. These stations are sited to represent large regional air masses. Data from these stations are shown in Figure 2.5-10. Both stations in the Northern Hemisphere show significant positive trends of 0.8% per year, indicating

Table 2.5-5. Surface ozone concentrations and trends deduced from ground based and balloon borne instruments

Site	Latitude	Period	Average Mixing Ratio (ppbv)	Trend %/yr ($\pm 2 \sigma$)
<i>Northern Hemisphere</i>				
Resolute ^a	75°N	1966–85		-0.1(± 0.1)
Barrow	71°N	1973–87	26 ^{b,c}	0.8(± 0.4)
Churchill ^a	59°N	1974–85		-0.7(± 1.3)
Arkona	55°N	1956–84	19 ^d	1.4(± 0.8)
Edmonton ^a	54°N	1973–85		-0.1(± 1.4)
Goose ^a	53°N			-1.1(± 1.0)
Dresden	51°N	1952–84	10 ^d	2.6(± 1.6)
Kaltennordheim	51°N	1955–83	16 ^d	3.1(± 2.1)
Gr.Inselberg	51°N	1972–83	21 ^d	3.1(± 2.4)
Fichtelberg	50°N	1954–84	23 ^d	1.1(± 2.0)
Hohenpeissenberg	48°N	1974–86	31 ^{b,d}	1.1(± 0.3)
Hohenpeissenberg ^a	48°N	1969–86		2.3(± 0.5)
Payerne ^a	47°N	1968–86		2.4(± 0.8)
Sapporo ^a	43°N	1969–86		0.9(± 1.1)
Tateno ^a	36°N	1969–86		1.3(± 0.6)
Kagoshima ^a	32°N	1969–86		2.5(± 1.0)
Mauna Loa	20°N	1973–87	27 ^{b,c}	0.8(± 0.4)
<i>Southern Hemisphere</i>				
Samoa	14°S	1976–87	14 ^{b,c}	-0.3(± 0.7)
Cape Point	34°S	1982–88	20 ^e	0.3(± 2.0)
Cape Grim	41°S	1982–86	24 ^f	0.6(± 0.7)
South Pole	90°S	1975–87	20 ^{b,c}	-0.5(± 0.4)
^a Sonde data ^b nbar ^c Oltmans and Komhyr, 1986; Bodhaine and Rosson, 1988 ^d Feister and Warmbt, 1987 ^e Scheel et al., 1988 ^f Galbally et al., 1986; Elsworth et al., 1988				

that tropospheric ozone increases can be observed in sites remote from industrial emissions (Oltmans and Komhyr, 1986; Bodhaine and Rosson, 1988).

There are nine stations, two in Europe, three in Japan, and four in Canada which provide measurements of ozone in the free troposphere using balloon-borne ozonesondes. The data have been reviewed in Section 2.3-3 and are listed in Table 2.3-4. As indicated above, all European and Japanese stations exhibit positive trends and all Canadian stations exhibit negative trends. The Canadian data might be affected by an instrument change that occurred at all stations in the early 1980s (Bojkov, 1988). A previous analysis of these data (Tiao et al., 1986) showed some evidence for a positive trend of 0.8% per year in the lower troposphere. Averaging over all nine stations the current analysis shows a significant trend in the first three kilometers of 0.8(± 0.5)% per year. Average trends in the troposphere above this altitude were not significant.

GLOBAL TRENDS

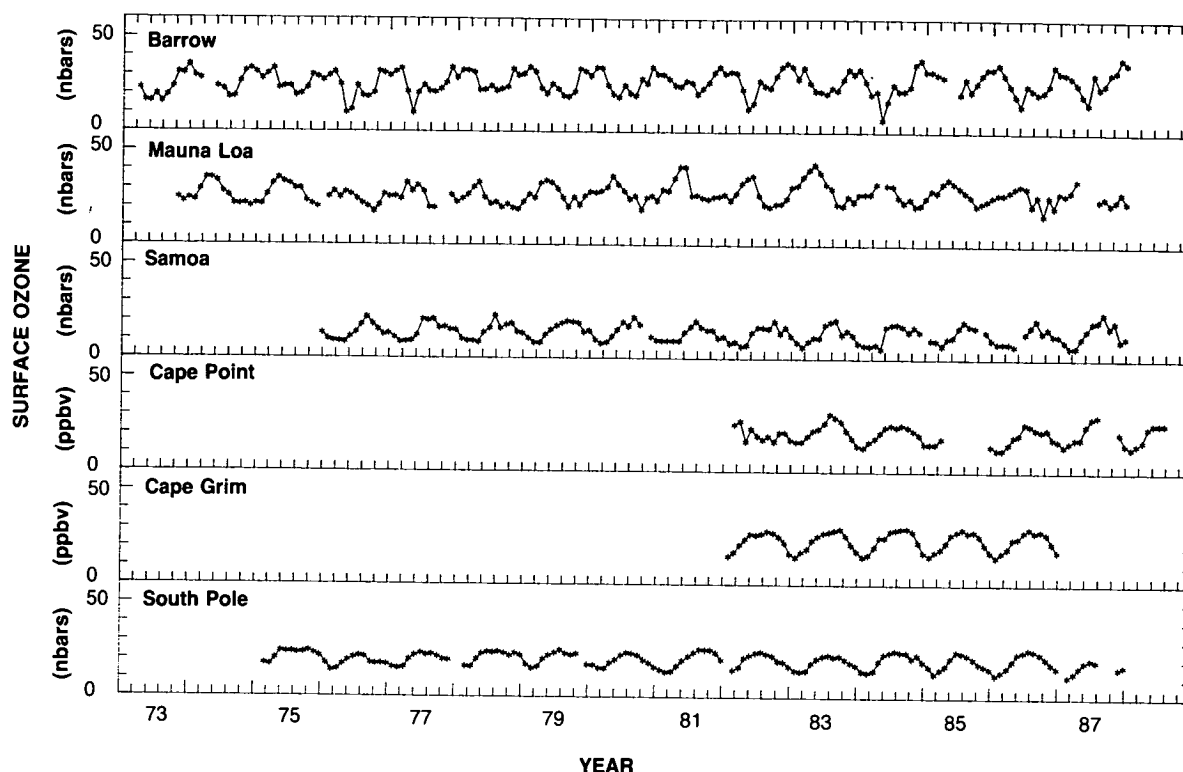


Figure 2.5-10. Surface ozone measurements at the GMCC stations (Olmans and Komhyr, 1986; Bodhaine and Rosson, 1988), at Cape Point, South Africa (Scheel et al., 1988), and at Cape Grim, Tasmania (Galbally et al., 1986; Elsworth et al., 1988).

In addition to the recent tropospheric ozone measurements, there are a few historic records of surface ozone measurements. The most important is a complete series of daily means collected at the Montsouris Observatory in Paris between the years 1876 and 1905. These data were re-analyzed by Bojkov (1986) and Volz and Kley (1988). The annual averages were shown to vary between 5 and 15 ppbv, about a factor of two lower than present ozone levels in a comparable environment.

None of the various pieces of evidence obtained so far and reviewed above provide convincing proof that ozone is increasing on more than a regional scale. When combined, however, they do suggest that ozone has been increasing over a wide scale in the Northern Hemisphere. On the other hand, the few measurements existing in the Southern Hemisphere indicate more or less constant ozone levels, which is not unexpected due to the low levels of ozone precursors observed in the Southern Hemisphere.

It has been suggested that typical tropospheric ozone variability means that the current ozonesonde network, and presumably the network of surface ozone measurement sites, are insufficient to detect a global trend in tropospheric ozone of about 1% per year at the 2σ confidence level, even at stations with records a decade in length (Prinn, 1988b). To detect an ozone trend of 1% per year on a decadal time frame, daily measurements of ozone are required from approximately 40 sites, chosen to represent continental and marine, tropical, temperate, and polar air masses in both hemispheres (Prinn, 1988b). This will require a doubling of the current network. Measurements are particularly lacking from Africa, South America, and Asia. It would appear that similar requirements may be necessary for a suitable global CO network.

2.6 TRENDS IN STRATOSPHERIC AEROSOLS

2.6.1 Introduction

Chapter 10 of the Ozone Trends Panel Report (OTP) presented a detailed description of stratospheric aerosols, their properties, and their possible effects on ozone and ozone observations. The specific objectives of the chapter were: (1) to define the fundamental characteristics of stratospheric aerosols, particularly their morphological, radiative, and chemical properties; (2) to analyze long-term aerosol data bases for possible trends that might influence the identification or interpretation of long-term ozone trends; (3) to assess the transient impacts of volcanically generated aerosols on remote sensing observations such as Umkehr and SBUV measurements over the last two decades, and to consider possible schemes for correcting aerosol errors in these baseline ozone data records; and, (4) to describe polar stratospheric clouds (PSCs) in terms of their frequency, spatial extent duration, and physicochemical properties, on the basis of observational and theoretical studies.

The purpose of this section of the present assessment is to review the findings of the OTP Report, and bring the reader up to date regarding any new or extended aerosol data. Chapter 1 of this assessment on polar ozone described in detail the climatology of PSCs in both polar regions, their physical properties, and heterogeneous phase chemistry involving PSCs. Thus, this section will not include any discussion of PSCs.

2.6.2 Stratospheric Aerosols

With the data available at the time of the OTP Report, no significant trends were detected in the properties of the global background stratospheric aerosol layer. Figure 1.2-30 in Chapter 1 of this document plots the SAM II stratospheric optical depth at a wavelength of 1 μm for the period November 1978 through February 1988 for the Arctic and Antarctic regions. Figure 10.7 in the OTP Report showed the SAM II data record through only 1986. Evident from these figures is the rapid impact of volcanic eruptions and their subsequent slow decay. Over this time period, the strongest impacts were experienced in the Arctic but for the case of El Chichon (17.3°, 93.2°W), which erupted in April 1982, both hemispheres were strongly perturbed.

These enhanced aerosol levels from volcanic eruptions can dramatically and deleteriously impact remote sensors. For example, after the eruption of El Chichon, sea surface temperature retrievals from AVHRR were adversely impacted by as much as a few degrees (Strong, 1984). Similarly, the retrieval of ozone profiles from Umkehr and SBUV measurements were affected, complicating the interpretation of these remote sensing data, especially when used to determine long-term changes or trends. Obviously, as Figure 1.2-30 shows, the El Chichon eruption caused the largest perturbation to stratospheric aerosols experienced over this last decade, but even the impact of smaller eruptions must be understood in order to remove their effects from various data sets. The problem is to determine when the aerosol loading is low enough not to adversely affect the interpretation of the particular sensor's data. The last eruption thought to have caused a level of perturbation similar to that experienced after the eruption of El Chichon was the March 1963 eruption of Agung (8.3°S, 115.5°E).

Routine balloon and lidar aerosol measurements of the stratosphere began in the late 1960s and early 1970s. These long-term measurements have been obtained primarily in the Northern Hemisphere with some short-term data records in the Southern Hemisphere. All these measurements have shown the period of 1978 to 1979 to be lowest on recent record. Therefore, this period has been referred to by most

GLOBAL TRENDS

investigators as a background period for stratospheric aerosols. In the strictest sense, however, with a data record of only 20 years, no one can definitively claim this to be a true background period.

As of this writing, mid-1989, the SAM II record and the lidar record from the NASA Langley Research Center shown in Figure 2.6.1, as well as other similar records, show values that have gradually approached, albeit not yet reached, the values measured in 1978–1979. Since the El Chichon eruption, the only other eruption to significantly perturb the global stratospheric aerosol was the eruption of Ruiz (4.9°N, 75.4°W) in November 1985. The Ruiz enhancement was similar to the enhancement caused by the Mount St. Helens (46.2°N, 122.2°W) eruption of May 1982 and, therefore, most likely has delayed somewhat the recovery from the El Chichon eruption. For example, the present value at Langley for peak backscatter ratio at a laser wavelength of 694 nm, is about 1.2, which represents a 20% enhancement over molecular scattering. In early 1979, this ratio was 1.08 for an 8% enhancement. These are to be compared to the peak backscatter value in late 1982 of 24, which was caused primarily by El Chichon. Integrated backscatter over the stratosphere is also used to describe lidar results. It provides a measure of stratospheric total column loading versus time over the lidar site. Values in 1989 have fallen to $0.8 \times 10^{-4} \text{sr}^{-1}$ from peak values in early 1983 of $27 \times 10^{-4} \text{sr}^{-1}$. Values in early 1979 were only $0.4 \times 10^{-4} \text{sr}^{-1}$. The SAM II results are similar, with lowest Antarctic optical depths measured in October 1979 of 0.5×10^{-3} compared to 1.7×10^{-3} in October 1988, and lowest Arctic optical depths of 1.2×10^{-3} in February 1979 compared to 1.7×10^{-3} in February 1989. Although the 1978–1979 aerosol minimum values have not yet been reached, there is no hard evidence that they will not be reached again, and therefore, there is no evidence that an upward trend in “background” stratospheric aerosols has occurred.

2.6.3 Global Heterogeneous Effects

Recently, Hofmann and Solomon (1989) suggested that stratospheric aerosols, especially during periods enhanced by volcanic eruptions, could possibly cause an ozone depletion through heterogeneous chemistry similar to that occurring on PSCs. They reached this conclusion because recent laboratory studies suggest that the same reactions that occur on PSCs in the cold Antarctic stratosphere, can also

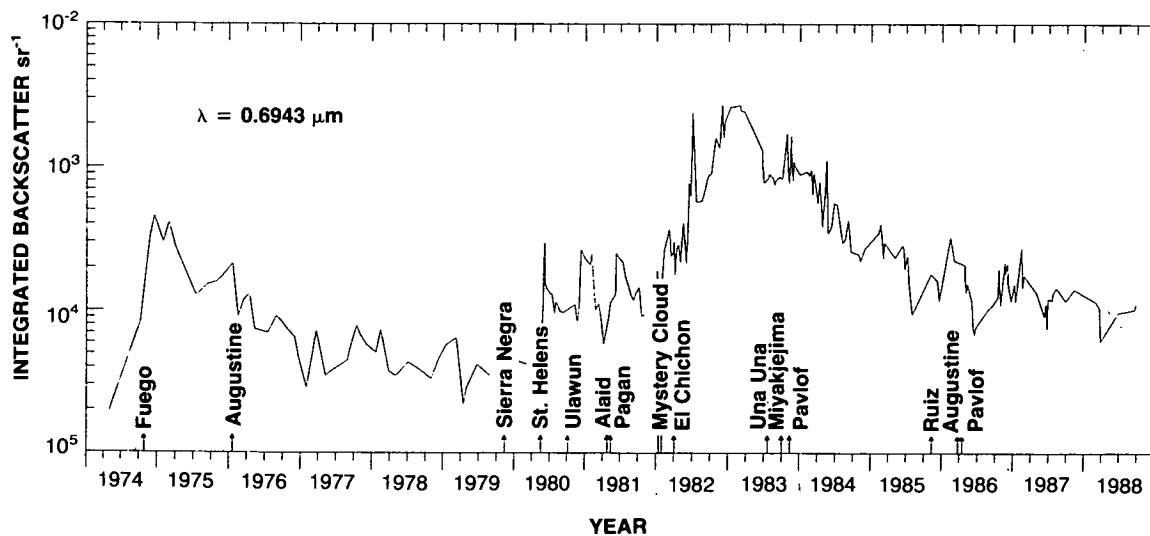


Figure 2.6-1. Aerosol integrated backscatter coefficient over the period 1974-1988 as observed by the NASA Langley Research Center lidar.

take place on sulfuric acid particles present at all latitudes (although at lower rates), and because all the reduction in stratospheric ozone observed at northern mid-latitudes in late 1982 and most of 1983 following the El Chichon eruption cannot be accounted for by considering other known mechanisms. Their model calculations indicate that these reactions will be of greatest potential importance in the middle-to-high latitudes in winter, where the reported total ozone trends (see Section 2.2) are largest and the ozonsonde measurements show record lows after El Chichon. Their results also predict substantial decreases in NO_2 abundances following El Chichon, particularly at middle latitudes in winter. Recall from Chapter 1 that decreases in total odd nitrogen are predicted to be an essential element in Antarctic heterogeneous ozone loss. At Boulder, Colorado (40°N) total column NO_2 measurements showed a pronounced decrease, coincident with the poleward movement of the El Chichon cloud in late 1982. The results from Hofmann and Solomon also show high HNO_3 abundances at mid-to-high latitudes in winter, in agreement with the 1978–79 LIMS HNO_3 measurements but not with current “non-heterogeneous” models.

The possibility of this heterogeneous chemistry extending to the global stratospheric aerosol, especially after a large volcanic eruption, makes it even more urgent that scientists understand these heterogeneous reactions as they apply to ozone depletion.

2.7 SURFACE ULTRAVIOLET RADIATION

2.7.1 Predicted Trends Related To Column Ozone, 1970–1986

Several processes act to attenuate solar ultraviolet radiation as it propagates through the atmosphere. The most important of these is absorption by ozone located in the stratosphere and troposphere. However, scattering by molecules, aerosols, and especially by clouds is significant, while absorption by gaseous air pollutants in the troposphere (NO_2 , SO_2) should be considered at some locations. A long-term change in the abundances of any of the absorbers or scatterers as well as in the surface albedo will lead to a trend in ultraviolet irradiance at the Earth's surface.

The total downward irradiance at any wavelength is the sum of direct and diffuse components, where the latter consists of photons which have been scattered one or more times. The direct irradiance depends on the total column ozone along the path from the sun to the ground and is readily computed from Beer's Law. Calculation of the diffuse component of irradiance requires solution of the radiative transfer equation and must consider the relative importance of scattering and absorption at each altitude. In general, absorption by ozone reduces the surface irradiance to negligible levels at wavelengths shorter than 295 to 300 nm. Backscattering of sunlight to space by clouds reduces the surface irradiance by roughly a constant factor at all wavelengths. To a first approximation the surface ultraviolet irradiance varies linearly with fractional cloud cover, and typical values under a completely cloud covered sky are less than 50% of those for clear skies (Mo and Green, 1974; Ilyas, 1987).

Figure 2.7-1 presents the solar spectral irradiance at the Earth's surface for January and July at latitudes 34.5, 46.0, and 58.5 degrees North computed from the model of Frederick and Lubin (1988). The latitudes correspond to the centers of the bands used by the Ozone Trends Panel (OTP), being 30–39, 40–52, and 53–64 degrees North. All values in Figure 2.7-1 refer to local noon and clear sky conditions. The natural ultraviolet radiation environment at the Earth's surface is characterized by large variations with month and latitude. The sharp decrease in irradiance at wavelengths shorter than 330 nm results from absorption by ozone, and spectral structure between 310 and 330 nm arises from the Huggins bands.

GLOBAL TRENDS

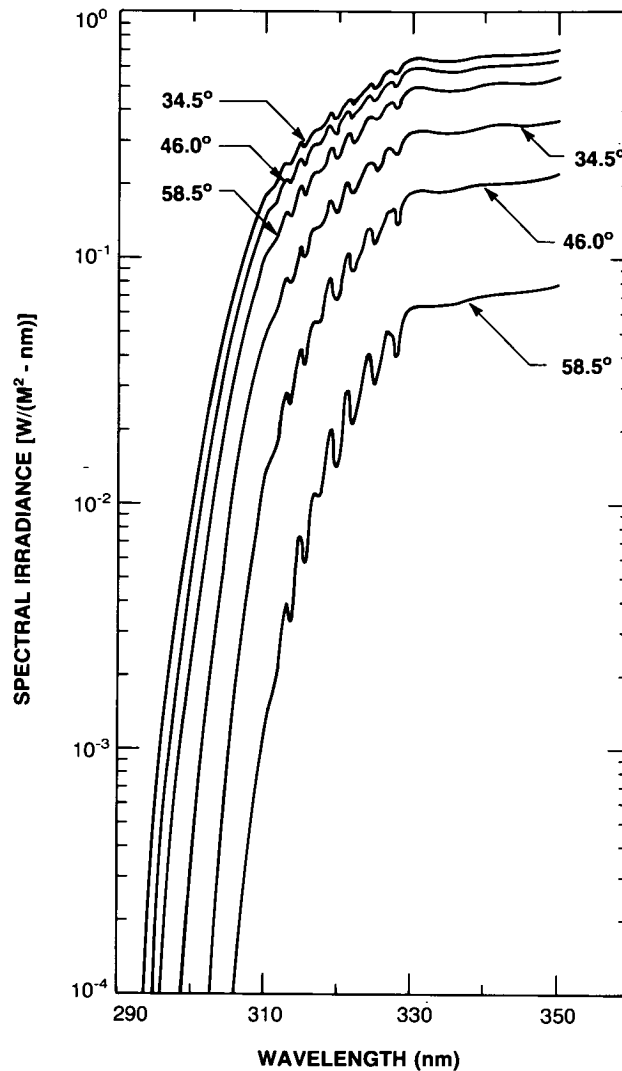


Figure 2.7-1. Solar spectral irradiance incident on the Earth's surface computed for January and July at latitudes 34.5°, 46.0°, and 58.5°N. Calculations refer to clear skies, local noon, and serve as baseline cases appropriate to the year 1970. The top three curves refer to July and the bottom three refer to January.

The Ozone Trends Panel reported a percent change in column ozone for each month of the year over the period 1970 through 1986 in the latitude zones defined above. Table 2.7-1 lists these for the three latitudes represented in Figure 2.7-1 during the months of January, March, and July. Imposed on the long-term trend are variations related to the solar cycle, the QBO, and a random interannual variability. The calculations reported below include only the linear trend component.

Figure 2.7-2 presents the percent changes in noontime surface irradiance attributable to the trend in total ozone between 1970 and 1986. These calculations refer to clear skies, include only the decrease in column ozone, and neglect changes in the profile shape. All curves in Figure 2.7-2 show the expected

Table 2.7-1. Percent Changes in Total Column Ozone, 1970–1986, Used in the Radiative Transfer Calculations*

Month	Latitude Band		
	30–39°N (%)	40–52°N (%)	53–64°N (%)
January	– 2.2	– 2.6	– 8.3
March	– 3.5	– 5.6	– 4.0
July	– 1.3	– 2.2	0.0

*Values from NASA (1988)

increase in percent change as wavelength decreases. In addition, a given percent change in ozone has an increasing impact on surface irradiance as the sun nears the horizon. In general, the largest percent changes occur at wavelengths where the absolute irradiances are small. At wavelengths longer than 330 nm, a trend in total ozone has negligible influence on the surface irradiance.

When the sun is high in the sky, as in summer, it is possible to experience a decrease in ultraviolet irradiance at the ground even with a decline in column ozone. This would arise from a change in the shape of the ozone profile, not included in Figure 2.7-2, and requires an increase in tropospheric ozone, which only partially offsets a reduction in the column at higher altitudes (Bruhl and Crutzen, 1989). The presence of aerosols and clouds leads to efficient scattering of the direct solar beam. This increases the effective path length taken by radiation through the lower atmosphere and consequently enhances absorption by tropospheric ozone (Frederick and Lubin, 1988).

2.7.2 Observed Trends in Surface Ultraviolet Radiation

Scotto et al. (1988) performed a trend analysis of ultraviolet irradiance data collected by a network of eight Robertson-Berger (RB) meters located over the United States from latitudes 30.4 to 46.8 degrees North. The time period covered was 1974 through 1985. The RB meter responds to broadband radiation convolved with an instrument response function which covers the spectral region from the ozone cutoff near 295 nm to approximately 340 nm. The RB data base indicates no increase in irradiance over the 12-year period, and decreases statistically significant to the $\pm 2 \sigma$ confidence level or higher occurred at five of the stations. The discussion below assumes that the derived trend in irradiance is a real atmospheric phenomenon. However, a thorough evaluation of the long-term stability of the RB meter network would be of value.

The numerical analysis of Scotto et al. (1988) was based on the annually integrated RB meter response at each station. The large annual cycle evident in Figure 2.7-1 implies that the annually integrated value receives its greatest contribution from the summer months. This is the season in which Dobson data show little change in total ozone over North America between 1970 and 1988 (see Table 2.2-5). However, Scotto et al. (1988) also examined RB readings by individual months and still found decreases in surface irradiance. The output of the RB meter includes substantial contributions from solar irradiance at wavelengths where absorption by ozone is weak. The meter is therefore not a sensitive indicator of small changes in atmospheric ozone content. With the RB meter response function from Caldwell et al. (1986), the 2.2% decrease in ozone for 40–52 degrees North during July between 1970 and 1986 implies a 1.5–1.6% increase in RB meter response. The 5.6% decrease in ozone during March would appear as a 4.7–4.8% increase in RB output.

GLOBAL TRENDS

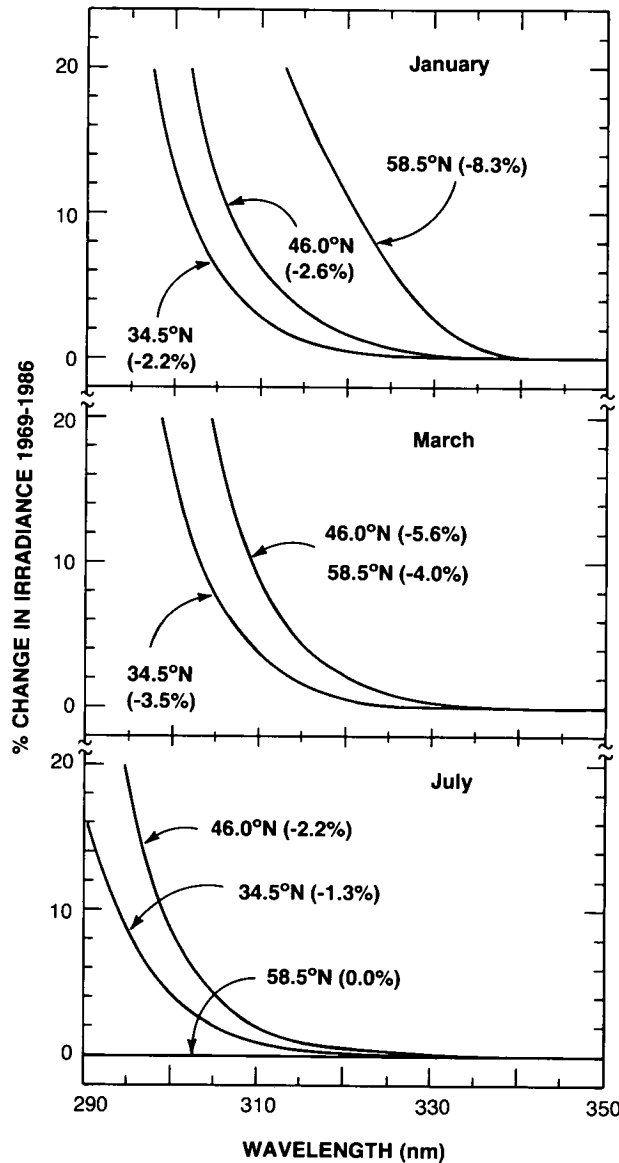


Figure 2.7-2. Percent changes in solar spectral irradiance between 1970 and 1986 computed for January, March, and July at latitudes 34.5°, 46.0°, and 58.5°N. Calculations include only the linear trend in ozone for a given month between 1970 and 1986. The percentage changes in ozone appear in parentheses. Curves for 46.0°N and 58.5°N in March are indistinguishable.

Given that cloud cover, aerosols, localized sources of air pollution, and likely increases in tropospheric ozone influence ground-based radiation measurements, it is not surprising that the RB meter network did not observe an increase in irradiance related to the downward trend in total ozone. The RB results are nonetheless very significant. In particular, they show that a trend in total ozone need not appear as an obvious trend in surface ultraviolet irradiance. The role of cloudiness and other factors that influence the transmission of the troposphere must be considered as well. The major conclusion here is that the results of the RB meters do not contradict the observed downward trend in ozone presented in Section 2.2.

2.8. OUTSTANDING ISSUES

Although a large amount of data has been collected over many years by instruments whose characteristics are reasonably well known, few of these instruments were made for the purpose of determining trends or long-term changes. Taking into account the deficiencies of the present observation system and looking to the future, priority should be given to a system approach based on the complementarity of ground-based and satellite observations. Both total column and vertical distribution satellite measurements of ozone should be checked for instrumental drifts by comparison with a network of carefully calibrated ground-based instruments based on both passive—Dobson, UV, IR, and microwave spectrophotometers—and active-lidar systems. The implementation of such a Network for Detection of Stratospheric Changes requires an internationally coordinated effort with a long-term commitment for scientifically driven operation of the stations. Special attention should be paid to the present dramatic lack of measurements outside of the band from 30 to 60 degrees in the Northern Hemisphere as reflected in particular in the absence of trend determination in the tropical regions. It is therefore of prime importance to establish new sites with an appropriate geographical distribution that takes into account the latitudinal and regional patterns already revealed by the present data analyses. Furthermore, the measurements should not be limited to stratospheric ozone. Data on the vertical distribution of ozone in the troposphere are, for example, required to take into account a possible trend in this atmospheric region. Additional atmospheric variables such as temperature or aerosols have been shown in this report to be of direct influence on the ozone trend. Their measurements will also be complemented by those of selected stratospheric trace gases that are required to quantitatively relate the observed ozone trend to anthropogenic influence. This can be illustrated by the present difficulty in interpreting for example the observed variations of hydrogen chloride (HCl), over the past 15 years.

Based on observed annual changes in CFCs and chemical partitioning arguments, it is expected that HCl should be increasing in the stratosphere at an annual rate of about 3.5%. Insufficient data exist, however, to confirm this important prediction. The longest data records have been collected from aircraft over the period 1978 to 1982 by Mankin and Coffey (1983) and from the Jungfraujoch station over the period 1976 to 1985 by Zander et al. (1987a). Both sets of observations were taken in the solar absorption mode using a high-resolution Fourier transform spectrometer and grating spectrometer, respectively. The Mankin and Coffey (1983) results give an indicated annual increase of 5% in column amount, but the estimated uncertainty in using the data to determine long-term change is 9% (2σ) per year when factors such as frequency of observations, length of data record, and long-term stability of absolute and relative calibration procedures are considered (Prinn, 1988a). The uncertainty estimate is probably conservative. Zander (1989, private communication) reports that the largest increase that can be derived from the ground-based results is 1.5% per year after seasonal effects are removed from his data spanning the 1976 to 1985 time interval. Prinn (1988a) estimates the uncertainty in using these data for detection of long-term changes to $\pm 2\%$ per year (2σ). Similar Jungfraujoch data covering the period 1985 to 1989 indicate a significantly larger trend than the one mentioned above (Zander, 1989, private communication). Tropospheric HCl could make some contribution to the measured total column but, since the Jungfraujoch station is at a 3.5 km altitude, this effect should be relatively small. Both the aircraft and ground-based data sets show an HCl increase with time over the period of their respective data records which is greater than the individual measurements error bars, but they each imply different rates of increase, and their use in quantifying yearly changes leads to uncertainties that preclude verification of the expected annual HCl increase. A much broader space and time sample, combined with the investigations of sporadic potential natural sources of HCl (e.g., volcanic eruptions), is required to address this question. A less definitive, but useful, test of anthropogenic contributions to the stratospheric halogen budget is provided by contemporary measurements of the HCl/HF ratio. Since substantially all of the HF in the present-day stratosphere is of anthro-

GLOBAL TRENDS

pogenic origin, while part of the HCl input is natural, the HCl/HF ratio at any time gives an indication of the anthropogenic input. Measurements covering the period 1977 to 1985 indicate mid-latitude values for this ratio of about 4 to 6 (Zander et al., 1987b), in satisfactory agreement with models and indirectly, therefore, supporting the predicted 3.5% annual change in HCl.

Finally, if technology advances and improvements to old techniques will lead to the implementation of newer and better observing systems, these often require 10 to 15 years before homogeneous data series of at least a decade can be available for trend analyses. It is therefore critically essential that existing measurement programs be maintained and their homogeneity in time be improved. In addition, efforts must be expended to develop a full understanding of the differences between data series from the old and new instruments so that a full-length homogeneous data record can be established to facilitate trend analyses as the newer systems take over from the old ones to provide the mainline data record.

APPENDIX 2.A

2.A.1 Seasonal Trends Model (Total Ozone)

The full statistical model for a monthly ozone series, y_t , $t = 1, 2, \dots, T$, for the multiple trends case is given by:

$$y_t = \sum_{i=1}^{12} \mu_i I_{i,t} + \sum \beta_i I_{i,t} R_t + \gamma_1 Z_{1,t} + \gamma_2 Z_{2,t-k} + \gamma_3 Z_{3,t} + \gamma_4 Z_{4,t} + N_t \quad (A1)$$

where:

- μ_i = ozone mean in month i , $i = 1 \dots 12$,
- $I_{i,t}$ = indicator series for the i^{th} month of the year,
= 1 if month t corresponds to month i of the year
0 otherwise
- β_i = trend in Dobson units per year after 12/69 in month i of the year,
- R_t = linear ramp function beginning in 12/69,
($t - t_0$)/12 if $t > t_0$, where t_0 corresponds to 12/69
0 if $t < t_0$
- $Z_{i,t}$ = solar series minus 120 flux units (minus 120 so that percentage trends will be based on ozone at mid solar cycle),
- $Z_{2,t-k}$ = QBO series lagged k months
- $Z_{3,t}$ = nuclear weapons series
- $Z_{4,t}$ = intervention for calibration shift (some stations, when using the original published data),
1 after the shift
= 0 before the shift
- γ_i = coefficients to be derived for each Z term, $i = 1, 2, 3, 4$
- N_t = residual noise series

There is a month-to-month correlation in ozone values, even after the seasonal and other effects in equation (A1) have been removed, i.e., in the N_t series. This is modeled by allowing N_t to be an autoregressive series of order 1:

$$N_t = \phi N_{t-1} + e_t \quad (\text{A2})$$

where e_t is an uncorrelated series (See Box and Jenkins, 1976; Tsay, 1984).

The noise series N_t is much more variable in winter than in summer. This is accounted for in the statistical model by fitting the above equation with individual months weighted inversely proportional to the monthly variances of the N_t ; for example, all Januarys get the same weight (the UW&C model uses weights applied to the e_t series rather than the N_t series).

Estimated changes in ozone reported in Table 2.2-1 are given as cumulative percent changes over the 17-year period 1970-1986 inclusive, to be comparable to results reported in the OTP summary:

$$\begin{aligned} \omega_i &= \text{17-year change in month } i \text{ in percent} \\ &= \frac{17 \times \beta_i}{\mu_i} \times 100\% \end{aligned} \quad (\text{A3})$$

Percent changes for the winter months (December through March), the summer months (May through August), or the whole year are the average of the percent changes in the corresponding months.

In other tables, trends are given in percent per decade, with 17 years replaced by 10 years in equation (A3).

2.A.2 Uniform Trends Model (Total Ozone)

The uniform trends model is similar to equation (1), except that the coefficient β of the ramp function is the same for all months of the year:

$$y_t = \sum_{i=1}^{12} \mu_i I_{i,t} + \beta R_t + \gamma_1 Z_{1,t} + \gamma_2 Z_{2,t-k} + \gamma_3 Z_{3,t} + \gamma_4 Z_{4,t} + N_t \quad (\text{A4})$$

The percent change over the 17-year period for the uniform model is given by:

$$\begin{aligned} \omega &= \text{17-year change in percent (uniform model)} \\ &= \frac{17 \times \beta}{\text{Ave}_i\{\mu_i\}} \end{aligned} \quad (\text{A5})$$

Trends expressed as percent per decade replace 17 years with 10 years in equation (5).

Monthly weighting is done as described in the previous section.

2.A.3 Regional Models (Total Ozone)

The individual station trend results may be combined within regions (North America, Europe, Japan) to give estimates of regional trends. The methodology, given in Reinsel et al. (1987), calculates the regional trend as a weighted average of the individual station trends. The station weights are functions of the trend uncertainties at each station and the spread among the station trends, with stations with less precisely measured trends (e.g., from shorter records or more variable data) receiving less weight.

GLOBAL TRENDS

The ozone trends in each of the regions are expressed as a random effects model

$$\omega_j = \omega + \theta_j + \epsilon_j \quad (\text{A6})$$

where ω_j is the trend estimate of the j^{th} station (either year-round or by season), θ_j is a random term accounting for station-to-station differences, and ϵ_j represents statistical variation in the trend due to within-station noise.

2.A.4 Regional/Latitudinal Models (Total Ozone)

The regional differences in the trends can be assessed simultaneously with a latitudinal dependence by using the model

$$\omega_{ij} = \delta_0 + \delta_1 (L-45^\circ\text{N}) + \alpha_i + \theta_{ij} + \epsilon_{ij} \quad (\text{A7})$$

where ω_{ij} is the trend estimate at the j^{th} station in the i^{th} region, L is latitude, α_i is a random term representing region-to-region variation in the trends, θ_{ij} is a random term representing station-to-station variation in the trends, and $\delta_0 + \delta_1 (L-45^\circ\text{N})$ provides for a linear relationship between the trend estimates and latitude (L) where δ_0 and δ_1 are the intercept and slope, respectively. Also, ϵ_{ij} is the statistical error in the j^{th} station trend estimate within the i^{th} region.

2.A.5 Empirical Aerosol-Adjustment Model (Umkehr)

In the empirical aerosol-adjustment approach, the models for the Umkehr data are of the following form:

$$y_t = \mu + S_t + \omega x_t + \gamma_1 z_t + \gamma_2 \mu_{t-l} + N_t \quad (\text{A8})$$

where y_t , $t = 1, \dots, T$ denote the monthly averages of Umkehr profile ozone data at a particular layer and a particular station, $\mu_t = e^{-\tau_t} - 1 \approx -\tau_t$ is a transformation of the composite optical thickness series τ_t and is similar to atmospheric transmission values (see Figure 2.3-5). The value l in (A8) is a time shift in the monthly transmission (optical thickness) series over the period; for the period of study, the values of l used were $l = 1$ month for the station Belsk, $l = 0$ for Arosa, Edmonton, and Boulder, $l = -1$ for Lisbon, Sapporo, Tateno, and Kagoshima, and $l = -6$ for New Delhi and Poona. The other terms in the model are S_t , which represents the seasonal annual and semi-annual sinusoidal components, x_t , which represents the $F_{10.7}$ solar flux series, and z_t , which is the hypothesized deterministic linear trend through the period 1977–1987. Thus, this model allows for a linear relation between the Umkehr data and the composite transmission (optical thickness) data during the period 1977–1987 involving the El Chichon volcano to account for errors in the Umkehr data due to volcanic aerosols. For the station Kagoshima, a simple intervention level shift term, starting in January 1986, was also included in the model to account for a possible change in mean level associated with a change of instrument at that time. (The data for Boulder also suggest a possibility of a mean level shift around the early part of 1982, possibly related to a change to the automated Dobson No. 61 instrument at the beginning of 1982. But such an effect has not been considered in the analysis because there is no definite confirmation of such a possible effect). Also, for the station Lisbon, data were not used prior to 1978 because of a level shift in the data before that time due to a calibration change. As there were a substantial number of missing months in the Umkehr data series for most stations, for convenience an autoregressive process only of order one was considered for the noise term N_t ,

$$N_t = \phi N_{t-1} + \epsilon_t, \quad (\text{A9})$$

where the ϵ_t are independent with mean 0 and constant variance σ_t^2 .

2.A.6 Theoretical Aerosol-Adjustment Model (Umkehr)

In the theoretical model approach, the monthly average Umkehr data y_t were first corrected for aerosol errors using the error correction factors supplied by DeLuisi et al. (1989a), which resulted in the corrected Umkehr data series denoted as y_t^* . It is noted that the error correction factors were applied to data at the various stations with the same time shift l as the value used in model (A1). For the corrected data, models of a similar form to (A8), but without the empirical aerosol error adjustment factor $\gamma_2 \mu_{t-l}$, were considered:

$$y_t^* = \mu + S_t + \omega x_t + \gamma_1 z_t + N_t \quad (\text{A10})$$

2.A.7 Trends Model Applied to Ozonesonde Data

For each of the 15 layers at each of the 9 stations the following regression model has been used:

$$y_t = \mu + S_t + \omega x_t + \delta u_t + N_t \quad (\text{A11})$$

where y_t is the average of ozone for month t , μ is a constant term, S_t is a seasonal component consisting of annual and semi-annual sinusoidal terms, ωx_t is a trend term, δu_t is a level shift term and N_t is a noise term. The trend term ωx_t is such that $x_t = 0$, $t < T_0$ and $x_t = (t - T_0)/12$ for $t > T_0$, where T_0 is December, 1969; thus ω is a parameter representing annual rate of change since 1970. The level shift term δu_t , where $u_t = 0$ for $t < T_1$ and $u_t = 1$ for $t > T_1$ with T_1 signifying the time and δ representing the magnitude of the level shift, is used for all layers at the four Canadian stations to account for possible systematic changes in ozone readings due to changes of the sonde instrument from BM to ECC. It is also used for layers 1A-1D at Payerne with $T_1 \approx$ April 1977 for possible effects due to the change of ozonesonde release time. Finally, the errors N_t 's are assumed to be normally and independently distributed with zero means but having different variances for the 12 months of the year.

REFERENCES

- Aimedieu, P., W. A. Matthews, W. Attmanspacher, R. Hartmannsgruber, J. Cisneros, W. Komhyr, and D. E. Robins, Comparison of in situ stratospheric ozone measurements obtained during the MAP/GLOBUS 1983 campaign, *Planet. Space Sci.*, 35, 563-568, 1987.
- Ancellet, G., A. Papayannis, J. Pelon, and G. Megie, Tropospheric ozone lidar measurements, in *NATO Workshop on Tropospheric Ozone*, Lillehammer, Norway, 1987, edited by I. S. Isaksen, D. Reidel, Holland, 1988.
- Angell, J. K., Variations and trends in tropospheric and stratospheric global temperatures, 1958-87, *J. Climate*, 1, 1296-1313, 1988.
- Angell, J. K., and J. Korshover, Global temperature variations in the troposphere and stratosphere, *Mon. Wea. Rev.*, 11, 901-921, 1983.
- Barnes, R. A., Changes in SBUV ozone profiles near Natal, Brazil, from 1979 to 1985, *J. Geophys. Res.*, 93, 1704-1717, 1988.
- Barnes, R. A., and P. G. Simeth, Design of a rocket-borne radiometer for stratospheric ozone measurements, *Rev. Sci. Instrum.*, 57, 544-550, 1986.

GLOBAL TRENDS

- Barnes, R. A., A. R. Bandy, and A. L. Torres, Electrochemical concentration cell ozonesonde accuracy and precision, *J. Geophys. Res.*, *90*, 7881-7887, 1985.
- Barnes, R. A., A. C. Holland, and H. S. Lee, An improved rocket ozonesonde (ROCOZ-A) 2. Preparation of stratospheric ozone profiles, *J. Geophys. Res.*, *91*, 14521-14531, 1986.
- Barnes, R. A., A. C. Holland, and V. W. J. Kirchhoff, Equatorial ozone profiles from the ground to 52 km during the Southern Hemisphere autumn, *J. Geophys. Res.*, *92*, 5573-5583, 1987a.
- Barnes, R. A., D. W. Rusch, and C. L. Parson, A comparison of northern mid-latitude ozone measurements from SME and ROCOZ-A from 1983 to 1985, Paper presented at the fall AGU Meeting, San Francisco, CA, 1987b.
- Barnes, R. A., M. A. Chamberlain, C. L. Parson, and A.C. Holland, An improved rocket ozonesonde (ROCOZ-A) 3. Northern mid-latitude ozone measurements from 1983 to 1985, *J. Geophys. Res.*, *94*, 2239-2254, 1989.
- Barnett, J. J., and M. Corney, Temperature comparisons between Nimbus 7 SAMS, rocket/radiosondes and the NOAA-6 SSU, *J. Geophys. Res.*, *89*, 5294-5302, 1984.
- Bass, A. M., and R. J. Paur, The ultraviolet cross-sections of ozone: I. The measurements, in *Atmospheric Ozone, Proceedings of the Quadrennial Ozone Symposium*, Halkidiki, Greece, edited by C. S. Zerefos and A. Ghazi, pp. 606-610, D. Reidel, Dordrecht, Holland, 1985.
- Beardsmore, D. J., and G. I. Pearman, Baseline carbon dioxide concentrations, in *Baseline 87*, edited by B. W. Forgan, Bureau of Meteorology/CSIRO, in press, 1989.
- Bevilacqua, R. M., and J. J. Olivero, Vertical resolution of middle atmospheric measurements by ground-based microwave radiometry, *J. Geophys. Res.*, *93*, No. D8, 9463, 1988.
- Bhartia, P. K., S. Taylor, and A. J. Fleig, Estimation of errors in the long term change of ozone reported by the SBUV-TOMS instruments—a new way of looking at old data, *Proceedings of the Quadrennial Ozone Symposium 1988*, Gottingen, F.R.G., edited by R. D. Bojkov and P. Fabian, Deepak Publications, Hampton, VA, 1989.
- Blake, D. R., and F. S. Rowland, Continuing worldwide increase in tropospheric methane, 1978 to 1987, *Science*, *239*, 1129-1131, 1988.
- Bloomfield, P., G. Oehbert, M. L. Thompson, and S. Zeger, A frequency domain analysis of trends in Dobson total ozone, *J. Geophys. Res.* *88*, 8512-8522, 1983.
- Bodhaine, B. A., and R. M. Rosson (Eds.), *Geophysical Monitoring for Climatic Change, Summary Report, 1987*, NOAA Air Resources Laboratory, Boulder, Colorado, 1988.
- Bojkov, R. D., Some characteristics of the total ozone deduced from Dobson spectrophotometer and filter-ozone-meter data and their application to a determination of the effectiveness of the ozone network, *Ann. Geophys.*, *25*, 293-299, 1969.
- Bojkov, R. D., Surface ozone during the second half of the nineteenth century, *J. Climate and Applied Meteorology*, *25*, 343-52, 1986.
- Bojkov, R. D., Ozone changes at the surface and in the free troposphere, in *NATO Workshop on Tropospheric Ozone*, Lillehammer Norway, 1987, edited by I. S. Isaksen, Reidel, Holland, 1988.
- Bojkov, R. D., C. L. Mateer, and A. L. Hansson, Comparison of ground-based and total ozone mapping spectrometer measurement, used in assessing the performance of the global ozone observing system, *J. Geophys. Res.*, *93*, 9525-9533, 1988.
- Bojkov, R. D., R. L. Bishop, W. G. Hill, G. C. Reinsel, and G. C. Tiao, Statistical trend analysis of revised Dobson total ozone data over the northern hemisphere, submitted to *J. Geophys. Res.*, 1989.
- Bowman, K. P., and A. J. Krueger, A global climatology of total ozone from the Nimbus-7 Total Ozone Mapping Spectrometer, *J. Geophys. Res.*, *90*, 7967-7976, 1985.
- Box, G. E. P. and G. M. Jenkins, *Time Series Analysis: Forecasting and Control*, Holden-Day, San Francisco, 1976.

- Brewer, A. W., A replacement for the Dobson spectrophotometer?, *Pure Appl. Geophys.*, 106-108, 919-927, 1973.
- Brewer, A. W., and J. R. Milford, The Oxford-Kew ozonesonde, *Proc. Roy. Soc. London, A*, 256, No. 1287, 470-495, 1960.
- Brezgin, N. I., A. F. Chizhov, G. I. Kuznetsov, and O. V. Shtirkov, Rocket observation of atmospheric ozone and aerosol, *Proc. Joint Symposium of Atmospheric Ozone, Berlin, 2*, 47-52, 1977.
- Bruhl, C., and P. J. Crutzen, On the disproportionate role of tropospheric ozone as a filter against solar UV-B radiation, *Geophys. Res. Lett.*, in press, 1989.
- Caldwell, M. M., L. B. Camp, C. W. Warner, and S. D. Flint, Action spectra and their key role in assessing biological consequences of solar UV-B radiation change, in *Stratospheric Ozone Reduction, Solar Ultraviolet Radiation and Plant Life*, edited by R. C. Worrest and M. M. Caldwell, Springer-Verlag, Berlin, pp. 87-111, 1986.
- Cebula, R. P., H. Park, and D. F. Heath, Characterization of the Nimbus-7 SBUV radiometer for the long term monitoring of stratospheric ozone, *J. Atmos. Oceanic Technol.*, 5, 215-227, 1988.
- Chanin, M. L., and A. Hauchecorne, Lidar studies of temperature and density using Rayleigh scattering, *MAP Handbook 13*, 87-99, 1984.
- Chu, W. P., Inversion of SAGE II measurements, *Proceedings of the Sixth Conference on Atmospheric Radiation*, Williamsburg, VA, May 13-16, 1986.
- Chu, W. P., and M. P. McCormick, Inversion of stratospheric aerosol and gaseous constituents from spacecraft solar extinction data in the 0.38-1.0 μ m wavelength region, *Appl. Opt.*, 18, 1404-1413, 1979.
- Cicerone, R. J., How has the atmospheric concentration of CO changed?, in *The Changing Atmosphere*, edited by F. S. Rowland and I. S. A. Isaksen, Wiley-Interscience, New York, pp. 49-61, 1988.
- Cicerone, R. J., L. E. Heidt, and W. H. Pollock, Measurements of atmospheric methyl bromide and bromoform, *J. Geophys. Res.* 93, 3745-49, 1988.
- Class, Th., and K. Ballschmiter, Chemistry of organic traces in air. VIII: Sources and distribution of bromo- and bromochloromethanes in marine air and surface water of the Atlantic ocean, *J. Atmos. Chem.* 6, 35-46, 1988.
- Connor, B. J., J. W. Barrett, A. Parrish, P. M. Solomon, R. L. De Zafra, and M. Jaramillo, Ozone over McMurdo station, Antarctica, austral spring 1986, Altitude profiles for the middle and upper stratosphere, *J. Geophys. Res.*, 92, 13221-13230, 1987.
- Conway, T. J., P. P. Tans, L. S. Waterman, K. W. Thoning, K. A. Masarie, and R. H. Gammon, Atmospheric carbon dioxide measurements in the remote global troposphere, 1981-1984, *Tellus*, 40 B, 81-115, 1988.
- Crutzen, P. J., The influence of nitrogen oxides on the atmospheric ozone content, *J. Roy. Met. Soc.*, 96, 320-325, 1970.
- Crutzen, P. J., and D. H. Ehhalt, Effects of nitrogen fertilizers and combustion on the stratospheric ozone layer, *Ambio*, 6, 112-117, 1977.
- Crutzen, P. J., L. E. Heidt, J. P. Krasnec, W. H. Pollock, and W. Seiler, Biomass burning as a source of atmospheric gases CO, H₂, N₂O, NO, CH₃Cl and COS, *Nature*, 282, 253-256, 1979.
- Cunnold, D. M., F. N. Alyea, and R. G. Prinn, Preliminary calculations concerning the maintenance of the zonal mean ozone distributions in the northern hemisphere, *Pure Appl. Geophys.*, 118, 229-354, 1980.
- Cunnold, D. M., W. P. Chu, R. A. Barnes, M. P. McCormick, and R. Veiga, Validation of SAGE II ozone measurements, *J. Geophys. Res.* 94, 8447-8460, 1989.
- Dave, J. V., J. J. DeLuisi, and C. L. Mateer, Results of a comprehensive theoretical examination of the optical effects of aerosols on the Umkehr measurements, *Spec. Environ. Rep.* 14, 15-22, World Meteorological Organization, Geneva, 1979.

GLOBAL TRENDS

- De la Noe, J., J. Lenoble, and T. Ogawa, Comparison of remote ground-based and satellite ozone profiles at strato-mesospheric altitudes, *Proceedings Int'l Radiation Symposium*, Lille, France, 1988.
- DeLuisi, J. J., Umkehr vertical ozone profiles errors caused by the presence of stratospheric aerosols, *J. Geophys. Res.*, *84*, 1766-1770, 1979.
- DeLuisi, J. J., D. U. Longenecker, C. L. Mateer, and D. J. Wuebbles, An analysis of northern middle-latitude Umkehr measurements corrected for stratospheric aerosols for the years 1979-1986, *J. Geophys. Res.*, in press, 1989a.
- DeLuisi, J. J., D. U. Longenecker, P. K. Bhartia, S. Taylor, and C. L. Mateer, Ozone profiles by Umkehr, SBUV, and ozonesondes: A comparison including the inversion algorithms for Umkehr and SBUV-TOMS instruments—a new way of looking at old data, *Proceedings of the Quadriennial Ozone Symposium 1988*, edited by R. D. Bojkov and P. Fabian, Gottingen, F.R.G., Deepak Publications, Hampton, VA, 1989b.
- DeMore, W. B., and M. Patapoff, Comparison of ozone determinations by ultraviolet photometry and gas-phase titration, *Environ. Sci. Technol.*, *10*, 897-899, 1976.
- Dianov-Klokov, V. I., and L. N. Yurganov, A spectroscopic study of the global spacetime distribution of atmospheric CO, *Tellus*, *33*, 262-273, 1981.
- Dobson, G. M. B., Observers handbook for the ozone spectrophotometer, *Annals of the International Geophysical Year V, Part I*, pp. 46-89, Pergamon Press, New York, 1957.
- Dobson, G. M. B., and C. W. B. Normand, Determination of the constants sets used in the calculation of the amount of ozone from spectrophotometer measurements and of the accuracy of the results, *Annals of the International Geophysical Year XVI, Part II*, pp. 161-191, Pergamon Press, New York, 1962.
- Dvoryashina, E. V., V. I. Diavov-Klokov, and L. N. Yurganov, Variations of the content of carbon monoxide in the atmosphere in the period from 1970 to 1982, *Izvestiya, Akademii Nauk. Phys. Atm. Okeana*, *20*, 27-33, 1984.
- Ehhalt, D. H., P. J. Fraser, D. Albritton, Y. Makide, R. J. Cicerone, F. S. Rowland, M. A. K. Khalil, L. P. Steele, M. Legrand, and R. Zander, Trends in source gases, in *Report of the International Ozone Trends Panel - 1988*, WMO Report Number 18, WMO, Geneva, 1989.
- Elsworth, C. M., I. E. Galbally, and R. Paterson, Ozone in near surface air, in *Baseline 86*, edited by B. W. Forgan and P. J. Fraser, Bureau of Meteorology, CSIRO, 1988.
- Evans, W. F. J. and J. B. Kerr, A comparison of satellite data with Brewer ozone data, *Proceedings of the Quadrennial Ozone Symposium 1988*, Gottingen, F.R.G., edited by R. D. Bojkov and P. Fabian, Deepak Publications, Hampton, VA, 1989.
- Feister, U., and W. Warmbt, Long-term measurements of surface ozone in the German Democratic Republic, *J. Atmos. Chem.* *5*, 1-21, 1987.
- Fisletov, V. E., The total ozone trend in the northern hemisphere, *Meteorologia i Gidzologia*, in press, (in Russian), 1989.
- Fleig, A. J., P. K. Bhartia, and D. S. Silberstein, An assessment of the long term drift in SBUV total ozone data, based on comparison with the Dobson network, *Geophys. Res. Lett.*, *13*, 1359-1362, 1986.
- Fleig, A. J., D. S. Silberstein, C. G. Wellemeyer, P. K. Bhartia, and J. J. DeLuisi, An assessment of the SBUV/TOMS Ozone data quality, based on comparison with external data, *Proceedings of the Quadrennial Ozone Symposium 1988*, Gottingen, F.R.G., edited by R. D. Bojkov and P. Fabian, Deepak Publications, Hampton, VA, 1989a.
- Fleig, A. J., D. S. Silberstein, C. G. Wellemeyer, R. P. Cebula, and P. K. Bhartia, An assessment of the long-term drift in TOMS total ozone data, based on comparison with the Dobson network, *Proceedings of the Quadrennial Ozone Symposium 1988*, Gottingen, F.R.G., edited by R. D. Bojkov and P. Fabian, Deepak Publications, Hampton, VA, 1989b.
- Fraser, P. J., and S. Coram, Atmospheric methane, carbon monoxide and carbon dioxide, 1986, in *Baseline 86*, edited by B.W Forgan and P.J. Fraser, Bureau of Meteorology/CSIRO, 65-66, 1988.

- Fraser, P. J., and N. Derek, Atmospheric halocarbons, nitrous oxide and methane - the GAGE program, 1987, in *Baseline 87*, edited by B. W. Forgan and G. Ayers, Bureau of Meteorology/CSIRO, in press, 1989.
- Fraser, P. J., P. Hyson, R. A. Rasmussen, A. J. Crawford, and M. A. K. Khalil, Methane, carbon monoxide and methylchloroform in the southern hemisphere, *J. Atmos. Chem.* 4, 3-42, 1986a.
- Fraser, P. J., P. Hyson, S. Coram, R. A. Rasmussen, A. J. Crawford and M. A. K. Khalil, Carbon monoxide in the southern hemisphere, *Proc. of the 7th World Clean Air Congress*, 2, 341-52, Sydney, Australia, August 1986b.
- Fraser, P. J., R. J. Francey, J. Mansbridge, and I. E. Enting, The CSIRO global methane program. Presented at the Second Conference on the Scientific Application of Baseline Observations of Atmospheric Composition (SABOAC II), CSIRO, Aspendale, Victoria, Australia, November 14-17, 1988, submitted to *J. Atmos. Chem.*, 1989.
- Frederick, J. E., and D. Lubin, The budget of biologically active ultraviolet radiation in the earth-atmosphere system, *J. Geophys. Res.*, 93, 3825-3832, 1988.
- Galbally, I. E., A. J. Miller, R. D. Hoy, S. Ahmet, R. C. Joynt, and D. Attwood, Surface ozone at rural sites in the Latrobe Valley and Cape Grim, Australia, *Atmos. Environ.* 20, 2403-2422, 1986.
- Gammon, R., S. C. Wofsy, R. J. Cicerone, A. C. Delany, R. T. Harriss, M. A. K. Khalil, J. A. Logan, P. Midgley, and M. Prather, Tropospheric trace species, in *Atmospheric Ozone 1985*, 1, pp. 57-116, WMO Global Ozone Research and Monitoring Project, Report Number 16, 1986.
- Gelman, M. E., A. J. Miller, K. W. Johnson, and R. M. Nagatani, Detection of long-term trends in global stratospheric temperatures from NMC analyses derived from NOAA satellite data, *Adv. Space Res.*, 6, 17-26, 1988.
- Gille, J. C., and J. M. Russell, III, The limb infrared monitor of the stratosphere: Experiment description, performance, and results, *J. Geophys. Res.*, 89, 5125-5140, 1984.
- Godin, S., G. Megie, and J. Pelon, Systematic lidar measurements of the stratospheric ozone vertical distribution, *Geophys. Res. Lett.*, in press, 1989.
- Graedel, T. E., and J. E. McRae, On the possible increase of the atmospheric methane and carbon monoxide concentrations during the last decade, *Geophys. Res. Lett.* 7, 977-979, 1980.
- Griggs, M., Studies of atmospheric ozone, Ph.D. Thesis, University of Oxford, Clarendon Laboratory, Oxford, 1961.
- Gustin, G. P., Universal ozonometer, *Proc. Main Geophys. Obs. Leningrad*, 141, 83-98, 1963.
- Gustin, G. P., On the methodology of total ozone measurements in the global network, *Proc. Main Geophys. Obs. Leningrad*, 406, 63-75, 1978.
- Gustin G. P., and S. A. Sokolenko, Design of optical and electric systems of ozonometer 124, *Proc. Main Geophys. Obs. Leningrad*, 487, 30-36, 1985.
- Hauchecorne, A., and M. L. Chanin, Density and temperature profiles obtained by lidar between 30 and 70 km, *Geophys. Res. Lett.*, 7, 564-568, 1981.
- Heath D. F., A. J. Krueger, H. A. Roeder, and B. H. Henderson, The Solar Backscatter Ultraviolet and Total Ozone Mapping Spectrometer (SBUV/TOMS) for Nimbus G, *Opt. Eng.*, 14, 323-331, 1975.
- Hill, W. G., G. W. Oehlert, and G. C. Reinsel, Trend analysis sensitivity studies of Dobson total ozone data through 1984, *J. Geophys. Res.*, 91, 14515-14520, 1986.
- Hilsenrath, E., W. Attmanspacher, A. Bass, W. Evans, R. Hagemeter, R. A. Barnes, W. Komhyr, K. Maursberger, J. Mentall, M. Proffitt, D. Robins, S. Taylor, A. Torres, and E. Weinstock, Results from the balloon ozone intercomparison campaign (BOIC), *J. Geophys. Res.*, 91, 13137-13152, 1986.
- Hofmann, D. J., and S. Solomon, Ozone destruction through heterogenous chemistry following the eruption of El Chichon, *J. Geophys. Res.*, 94, 5029-5041, 1989.
- Holland, A. A. C., R. A. Barnes, and H. S. Lee, Improved rocket ozonesonde (ROCOZ-A) 1. Demonstration of precision, *Appl. Opt.*, 24, 3286-3295, 1985.

GLOBAL TRENDS

- Ilyas, M., Effect of cloudiness on solar ultraviolet radiation reaching the surface, *Atmos. Environ.* 21, 1483-1484, 1987.
- Kerr, J. B., C. T. McElroy, D. I. Wardle, R. A. Olafson, and W. F. J. Evans, The automated Brewer spectrophotometer, in *Atmospheric Ozone, Proceedings of the Quadrennial Ozone Symposium*, Halkidiki, Greece, edited by C. S. Zerefos and A. Ghazi, pp. 396-410, D. Reidel, Dordrecht, Holland, 1985.
- Kerr, J. B., I. A. Asbridge, and W. F. J. Evans, Intercomparison of total ozone measured by the Brewer and Dobson spectrophotometers at Toronto, *J. Geophys. Res.*, 93, 11129-11140, 1988.
- Kerr, J. B., C. L. Mateer, C. T. McElroy, and W. F. J. Evans, Umkehr measurements made with the Brewer Ozone Spectrophotometer, *Proceedings of the Quadrennial Ozone Symposium 1988*, Göttingen, F.R.G., edited by R. D. Bojkov and P. Fabian, Deepak Publications, Hampton, VA, 1989a.
- Kerr, J. B., I. A. Asbridge, and W. F. J. Evans, Long-term intercomparison between the Brewer and Dobson spectrophotometers at Edmonton, *Proceedings of the Quadrennial Ozone Symposium 1988*, Göttingen F.R.G, edited by R. D. Bojkov and P. Fabian, Deepak Publications, Hampton, VA, 1989b.
- Khalil, M. A. K., and R. A. Rasmussen, The trend of bromochlorodifluoromethane and other bromine containing gases at the South Pole, *Antarctic J. United States*, 19, 206-207, 1985.
- Khalil, M. A. K., and R. A. Rasmussen, Nitrous oxide: Trends and global mass balance over the last 3,000 years, *Ann. Glac.*, 10, 73-79, 1988a.
- Khalil, M. A. K., and R. A. Rasmussen, Carbon monoxide in the Earth's atmosphere: Indications of a global increase, *Nature*, 332, 242-245, 1988b.
- Khalil, M. A. K., R. A. Rasmussen, and R. Gunawardena, Atmospheric bromine in the polar regions, in *Geophysical Monitoring for Climatic Change, Summary Report 1986*, edited by R. S. Schnell and R. M. Rosson, pp. 123-125, 1987.
- Khalil, M. A. K., R. A. Rasmussen, and S. D. Hoyt, Atmospheric chloroform (CHCl₃): Ocean-air exchange and global mass balance, *Tellus*, 35B, 266-274, 1983.
- Kokin, G. A., E. V. Lysenko, and S. Kh. Rosenfeld, Temperature variations in the stratosphere and mesosphere in 1964 to 1988 based on rocket sounding data, *Izvestia Akademii Nauk, Phys. Atm. Okeana*, in press, 1989.
- Komhyr, W. D., A carbon-iodine ozone sensor for atmospheric soundings, *Proceedings of the Ozone Symposium*, W.M.O., Albuquerque, NM, 1964.
- Komhyr, W. D., Electrochemical concentration cells for gas analysis, *Ann. Geophys.*, 25, 203-210, 1969.
- Komhyr, W. D., R. D. Grass, R. D. Evans, R. K. Leonard, and G. M. Semeniuk, Umkehr observations with automated Dobson spectrophotometers, in *Atmospheric Ozone, Proceedings of the Quadrennial Ozone Symposium*, Halkidiki, Greece, pp. 371-375, D. Reidel, Dordrecht, Holland, 1985.
- Komhyr, W. D., R. D. Grass, and R. K. Leonard, Dobson spectrophotometer No. 83: A standard for total ozone measurements, 1962-1987, *Proceedings of the Quadrennial Ozone Symposium 1988*, Göttingen, F.R.G., edited by R.D. Bojkov and P. Fabian, Deepak Publications, Hampton, VA, 1989.
- Konkov V. I., and S. P. Perov, Some preliminary results of chemiluminescent measurements of atmospheric ozone by meteorological rocket, *Proc. of the Joint Symposium on Atmospheric Ozone*, 11, 43-46, 1976.
- Krueger, A. J., and W. R. McBride, Rocket ozonesonde (ROCOZ) design and development, *Navy Weapons Cent. Tech. Publ. 4512*, Navy Weapons Cent., China Lake, Calif., 1968a.
- Krueger, A. J., and W. R. McBride, Sounding rocket -OGO-IV satellite ozone experiment, Rocket ozonesonde measurements, *Navy Weapons Cent. Tech. Publ. 4667*, Navy. Weapons Cent., China Lake, Calif., 1968b.
- Kunzi, K. F., and G. Rubin, The use of microwave sensors in a global ozone monitoring network, Paper presented at Intl. Rad. Symp., Lille, France, Aug. 18-24, 1988.

- Labitzke, K., Sunspots, the QBO and the stratospheric temperature in the north polar region, *Geophys. Res. Lett.*, 14, 535-537, 1987.
- Labitzke, K., J. J. Barnett, and B. Edwards, Draft of a new reference middle atmosphere, *Handbook for MAP, 16*, SCOSTEP Secretariat, Univ. of Illinois, Urbana, 1985.
- Labitzke, K., and M. L. Chanin, Changes in the middle atmosphere in winter related to the 11-year solar cycle, *Ann. Geophys.*, 6, 643-644, 1988.
- Labitzke, K., and H. Van Loon, Association between the 11-year solar cycle, the QBO, and the atmosphere. Part I: The troposphere and stratosphere in the Northern Hemisphere in winter, *J. Atmos. Terr. Phys.*, 50, 197-206, 1988.
- Lal S., R. Borchers, P. Fabian, and B.C. Kruger, Increasing abundance of CF₂ BrCl in the atmosphere, *Nature*, 316, 135-136, 1985.
- Levy II, H., Normal atmosphere: Large radical and formaldehyde concentrations predicted. *Science*, 173, 141-143, 1971.
- Lobsiger, E., Ground-based microwave radiometry to determine stratospheric and mesospheric ozone profiles, *J. Atmos. Terr. Phys.*, 49, 493, 1987.
- Logan, J. A., Tropospheric ozone: Seasonal behavior, trends and anthropogenic influence, *J. Geophys. Res.* 90, 10463-10482, 1985.
- Makide, Y., A. Yokohara, Y. Kubo, and T. Tominaga, Atmospheric concentration of halocarbons in Japan 1979-1986, *Bull. Chem. Soc. Japan*, 60, 571-574, 1987.
- Mankin, W.G., and M.T. Coffey, Latitudinal distribution and temporal changes of stratosphere HCl and HF, *J. Geophys. Res.* 88, 10776-10784, 1983.
- Mateer, C. L., and H. U. Deutsch, Uniform evaluation of Umkehr observations from the World Ozone Network, Part. I. Proposed standard Umkehr evaluation technique. Technical Report, National Center for Atmospheric Research, Boulder, CO, 1964.
- Mateer, C. L., and J. J. DeLuisi, A comparison of ozone profiles derived from Standard Umkehr and Short Umkehr measurements from 15 stations, in *Atmospheric Ozone, Proceedings of the Quadrennial Ozone Symposium*, Halkidiki, Greece, edited by C. S. Zerefos and A. Ghazi, pp. 290-294, Reidel, Dordrecht, Holland, 1985.
- Mateer, C. L., J. B. Kerr, and W. F. J. Evans, Ozone profiles derived from Umkehr observations obtained from the Brewer Ozone Spectrophotometer, in *Atmospheric Ozone, Proceedings of the Quadrennial Ozone Symposium*, Halkidiki, Greece, edited by C. S. Zerefos and A. Ghazi, pp. 407-411, Reidel, Dordrecht, Holland, 1985.
- Mauldin, L. E., III, and W. P. Chu, Optical degradation due to contamination on the SAGE/SAGE II spaceflight instruments, *Proceedings of the Society of Photo-optical Instrumentation Engineers*, 1982.
- Mauldin, L. E., III, N. H. Zuan, M. P. McCormick, J. H. Guy, and W. R. Vaughan, Stratospheric Aerosol and Gas Experiment II instrument: A functional description, *Opt. Eng.*, 24, 307-312, 1985a.
- Mauldin, L. E., III, M. P. McCormick, L. R. McMaster, and W. R. Vaughan, The Stratospheric Aerosol and Gas Experiment II (SAGE II) design and in-orbit performance, *Proceedings of the Society of Photo-optical Instrumentation Engineers, Vol. 589, Instrumentation for Remote Sensing from Space*, pp. 104-111, 1985b.
- McCormick, M. P., P. Hamill, T. J. Pepin, W. P. Chu, T. J. Swisler, and L. R. McMaster, Satellite studies of the Stratospheric Aerosol, and Gas Experiment (SAGE II), *Bull. Am. Met. Soc.*, 60, 1038-1046, 1979.
- McDermid, I. S., and S. Godin, Ground-based laser DIAL system for long-term measurement, *Applied Optics*, in press, 1990.
- McElroy, C. T., C. L. Mateer, J. B. Kerr, and D. I. Wardle, Umkehr observations made with the Brewer ozone spectrophotometer, *Proceedings of the Quadrennial Ozone Symposium 1988*, Gottingen, F.R.G., edited by R. D. Bojkov and P. Fabian, Deepak Publications, Hampton, VA, 1989.

GLOBAL TRENDS

- McElroy, M. B., R. J. Salawitch, S. L. Wofsy, and J. A. Logan, Reductions in Antarctic ozone due to synergistic interactions of chlorine and bromine, *Nature*, 321, 756-762, 1986.
- McKenzie, R. L., and P. V. Johnston, Seasonal variations in stratospheric NO₂ at 45 S, *Geophys. Res. Lett.*, 9, 1255, 1982.
- McPeters, R. D., and W. D. Komhyr, Long-term changes in SBUV-TOMS relative to the world primary standard Dobson instrument, *Proceedings of the Quadrennial Ozone Symposium 1988*, Gottingen, F.R.G, edited by R. D. Bojkov and P. Fabian, Deepak Publications, Hampton, VA, 1989.
- Mégie, G., J. Y. Allain, M. L. Chanin, J. E. Blamont, Vertical profile of stratospheric ozone by lidar sounding from the ground, *Nature*, 270, 5635, 1977.
- Mo, T., and A. E. S. Green, A climatology of solar erythema dose, *Photochem. Photobiol.*, 20, 483-496, 1974.
- Mount, G. H., R. W. Sanders, A. L. Schmeltekopf, and S. Solomon, Visible spectroscopy at McMurdo Station, Antarctica, 1. Overview and daily variations of NO₂ and O₃, austral spring, 1986, *J. Geophys. Res.*, 92, 8320, 1987.
- Nagatani, R. M., A. J. Miller, K. W. Johnson, and M. E. Gelman, *An Eight Year Climatology of Meteorological and SBUV Ozone Data*, NOAA Technical Report NWS 40, 1988
- NASA, *Present State of Knowledge of the Upper Atmosphere: An Assessment Report*, NASA Reference Publication 1208, August 1988.
- Nash, J., and G. F. Forrester, Long-term monitoring of stratospheric temperature trends using radiance measurements obtained by the TIROS-N series of NOAA spacecraft, *Adv. Space. Res.*, 6, 37-43, 1986.
- Nash, J., Extension of explicit radiance observations by the Stratospheric Sounding Unit into the lower stratosphere and lower mesosphere, *Quart. J. Roy. Met. Soc.*, 114, 1153-1171, 1988.
- Newchurch, M. J., G. W. Grams, D. M. Cunnold, and J. J. DeLuise, A comparison of SAGE I, SBUV and Umkehr ozone profiles including a search for Umkehr aerosol effects, *J. Geophys. Res.*, 92, 8382-8390, 1987.
- Noxon, J. F., E. C. Whipple, Jr., and R. S. Hyde, Stratospheric NO₂ 1. Observational method and behavior at mid-latitude, *J. Geophys. Res.*, 84, 5047, 1979.
- Oltmans, S. J., and W. D. Komhyr, Surface ozone distributions and variations from 1973-1984 measurements at the NOAA Geophysical Monitoring for Climatic Change Baseline Observatories, *J. Geophys. Res.*, 91, 5229-5236, 1986.
- Ozone Trends Panel Report-1988, Global ozone research and monitoring project, Report Number 18, edited by R. T. Watson, World Meteorological Organization, Geneva, in press, 1989.
- Pelon, J., and G. Megie, Ozone monitoring in the troposphere and lower stratosphere: Evaluation and operation of a ground-based lidar station, *J. Geophys. Res.*, 87, 4947, 1982.
- Pelon, J., S. Godin, and G. Megie, Upper stratospheric (30-50 km) lidar observations of the ozone vertical distribution, *J. Geophys. Res.*, 91, 8667, 1986.
- Penkett, S. A., Indications and causes of ozone increase in the troposphere, in *The Changing Atmosphere*, edited by F. S. Rowland and I. S. A. Isaksen pp. 91-103, Wiley-Interscience, New York, 1988.
- Penkett, S. A., B. M. R. Jones, M. J. Rycroft, and D. A. Simmons, An interhemispheric comparison of the concentration of bromine compounds in the atmosphere, *Nature*, 318, (6046), 550-553, 1985.
- Perov, S. P., and A. Khrgian, Sovremennye problemy atmosfernogo ozona *L. Hydrometeoizdat*, 1980.
- Perov, S. P., and S. V. Tishin, A rocket gas chemiluminescent technique for measurement of atomic oxygen and ozone concentration in the 15-95 km region, in *Atmospheric ozone, Proceedings of the Quadrennial Ozone Symposium*, Halkidiki, Greece, edited by C. S. Zerefos and A. Ghazi, D. Reidel, Dordrecht, Holland, pp. 527-531, 1985.
- Pommereau, J. P., and F. Goutail, O₃ and NO₂ ground-based measurements by visible spectrometry during Arctic winter and spring 1988, *Geophys. Res. Lett.*, 15, 891, 1988a.

- Pommereau, J. P., and F. Goutail, Stratospheric O₃ and NO₂ observations at the Southern Polar Circle in summer and fall 1988, *Geophys. Res. Lett.* 15, 895, 1988b.
- Prinn, R. G., How have the atmospheric concentrations of the halocarbons changed?, in *The Changing Atmosphere*, edited by F. S. Rowland and I. S. A. Isaksen, pp. 33-48, Wiley-Interscience, New York, 1988a.
- Prinn, R. G., Toward an improved global network for determination of tropospheric ozone climatology and trends, *J. Atmos. Chem.*, 6, 281-298, 1988b.
- Prinn, R. G., P. G. Simmonds, R. A. Rasmussen, R. D. Rosen, F. N. Alyea, C. A. Cardelino, A. J. Crawford, D. M. Cunnold, R. Fraser, and J. E. Lovelock, The Atmospheric Lifetime Experiment: 1. Introduction, instrumentation and overview, *J. Geophys. Res.* 88, 8853-8867, 1983.
- Prinn, R., D. Cunnold, R. Rasmussen, P. Simmonds, F. Alyea, A. Crawford, P. Fraser, and R. Rosen, Atmospheric trends in methylchloroform and the global average for the hydroxyl radical, *Science*, 238, 945-950, 1987.
- Ramanathan, V., R. Cicerone, H. Singh, and J. Kiehl, Trace gas trends and their potential role in climatic change, *J. Geophys. Res.*, 90, 5547-5566, 1985.
- Rasmussen, R. A., and M. A. K. Khalil, Latitudinal distributions of trace gases in and above the boundary layer, *Chemosphere*, 11, 227-235, 1982.
- Rasmussen, R. A., and M. A. K. Khalil, Gaseous bromine in the Arctic and Arctic haze, *Geophys. Res. Letts.* 11, 433-436, 1984.
- Raynaud D., J. Chappellaz, J. M. Barnola, Y. S. Korotkevich, and C. Lorius, Climatic and CH₄ cycle implications of glacial-interglacial CH₄ changes in the Vostok ice core, *Nature*, 333, 655, 1988.
- Regener, V. H., On a sensitive method for the recording of atmospheric ozone, *J. Geophys. Res.*, 65, 3975-3977, 1960.
- Regener, V. H., Measurement of atmospheric ozone with the chemiluminescent method, *J. Geophys. Res.*, 69, 3795-3800, 1964.
- Reinsel, G. C., and G. C. Tiao, Impact of chlorofluoromethanes on stratospheric ozone: A statistical analysis of ozone data for trends, *J. Amer. Stat. Assoc.*, 82, 20-30, 1987.
- Reinsel, G. C., G. C. Tiao, J. J. DeLuisi, C. L. Mateer, A. J. Miller, and J. E. Frederick, An analysis of upper stratospheric Umkehr ozone profile data for trends and the effects of stratospheric aerosols, *J. Geophys. Res.*, 93, 1689-1703, 1984.
- Reinsel, G. C., G. C. Tiao, A. G. Miller, D. J. Wuebble, P. S. Connell, C. L. Mateer and G. G. DeLuisi, Statistical analyses of total ozone and stratospheric Umkehr data for trends and solar cycle relationship, *J. Geophys. Res.*, 92, 2201-2209, 1987.
- Reinsel, G. C., G. C. Tiao, S. K. Ahn, M. Pugh, S. Basu, J. J. DeLuisi, C. L. Mateer, A. J. Miller, P. S. Connell, and D. J. Wuebbles, An analysis of the 7-year record of SBUV satellite ozone data: Global profile features and trends in total ozone, *J. Geophys. Res.*, 93, 1689-1703, 1988.
- Reinsel, G. C., G. C. Tiao, J. J. DeLuisi, S. Basu, and K. Carriere, Trend analysis of aerosol corrected Umkehr profile ozone data through 1987, *J. Geophys. Res.*, in press, 1989.
- Rowland, F. S., and M. Molina, Chlorofluoromethanes in the environment, *Rev. Geophys. Space Phys.*, 13, 1-35, 1975.
- Rusch, D. W., G. H. Mount, C. A. Barth, R. J. Thomas, and M. T. Callan, Solar mesospheric explorer ultraviolet spectrometer: Measurements in the 1.0 to 0.1-mbar region, *J. Geophys. Res.*, 89, 11677-11687, 1984.
- Scheel, H. E., E. G. Brunke, and W. Seiler, Trace gas measurements at the monitoring station Cape Point, South Africa, between 1978 and 1988. (Presented at the Second Conference on the Scientific Application of Baseline Observations of Atmospheric Composition (SABOAC II), CSIRO, Aspendale, Victoria, Australia, November 14-17, 1988). *J. Atmos. Chem.*, 1988.

GLOBAL TRENDS

- Schoeberl, M. R., A. J. Krueger, and P. A. Newman, The morphology of Antarctic total ozone as seen by TOMS, *Geophys. Res. Lett.*, *13*, 1217-1220, 1986.
- Scotto, J., G. Cotton, F. Urbach, D. Berger, and T. Fears, Biologically effective ultraviolet radiation: Surface measurements in the United States, 1974-1985, *Science*, *239*, 762-764, 1988.
- Simmonds, P. G., D. M. Cunnold, F. N. Alyea, C. A. Cardelino, A. J. Crawford, R. G. Prinn, P. J. Fraser, R. A. Rasmussen, and R. D. Rosen, Carbon tetrachloride lifetimes and emissions determined from daily global measurements during 1978-1985, *J. Atmos. Chem.*, *7*, 35-58, 1988.
- Singer, S. F., and R. C. Wentworth, A method for the determination of the vertical ozone distribution from a satellite, *J. Geophys. Res.*, *62*, 299-308, 1957.
- Singh, H. B., L. J. Salas, H. Shigeishi, and E. Sciber, Atmospheric halocarbons, hydrocarbons and sulfur hexafluoride: Global distributions, sources and sinks, *Science*, *203*, 899-903, 1979.
- Somayajulu, Y. V., K. S. Zalpuri, and S. Sampath, Rocket measurement of ozone density distribution in the equatorial stratosphere and mesosphere, *Indian J. Radio Space Phys.*, *10*, 197-200, 1981.
- St. John, D. S., S. P. Bailey, W. H. Fellner, G. M. Minor, and R. D. Snee, Time series search for trend in total ozone measurements, *J. Geophys. Res.*, *86*, 7299-7311, 1981.
- Stauffer, B., E. Lochbronner, H. Oeschgern, and J. Schwander, Methane concentration in the glacial atmosphere was only half of the pre-industrial Holocene, *Nature*, *332*, 812, 1988.
- Steele, L. P., P. J. Fraser, R. A. Rasmussen, M. A. K. Khalil, T. J. Conway, A. J. Crawford, R. H. Gammon, K. A. Masarie, and K. W. Thoning, The global distribution of methane in the troposphere, *J. Atmos. Chem.*, *5*, 125-171, 1987.
- Steele, L. P., P. M. Lang, and R. C. Martin, Atmospheric methane in Antarctica, submitted to *Antarctic J. United States*, 1989.
- Stolarski, R. S., A. J. Krueger, and M. R. Schoeberl, Total ozone trends from TOMS data, *Proceedings of the Quadrennial Ozone Symposium 1988*, Gottingen, F.R.G, edited by R. D. Bojkov and P. Fabian, Deepak Publications, Hampton, VA, 1989.
- Strong, A. E., Monitoring El Chichon aerosol distribution using NOAA-7 satellite AVHRR sea surface temperature, *Geof. Int.*, *23-2*, 129-142, 1984.
- Subbaraya, B. H., and S. Lal, Rocket measurements of ozone concentrations in the stratosphere and mesosphere over Thumba, *Proc. Indian Acad. Sci. (Earth Planet. Sci.)*, *90*, 173-187, 1981.
- Tiao, G. C., G. C. Reinsel, J. H. Pedrick, G. M. Allenby, C. L. Mateer, A. J. Miller, and J. J. DeLuisi, A statistical trend analysis of ozonesonde data, *J. Geophys. Res.*, *91*, 13121-13136, 1986.
- Tiao, G. E., G. C. Reinsel, D. Xu, X. D. Zhu, A. J. Miller, J. J. DeLuisi, C. C. Mateer, and D. J. Wuebbles, Effects of autocorrelation and temporal sampling schemes on estimates of trend and spatial correlation, *J. Geophys. Res.*, in press, 1989.
- Torres, A. L., and A. R. Bandy, Performance characteristic of the electrochemical concentration cell ozonesonde, *J. Geophys. Res.*, *83*, 5501-5504, 1978.
- Tsay, R. S., Regression analysis with time series errors, *J. Am. Stat. Assoc.*, *79*, 118-124, 1984.
- Uchino, O., M. Maeda, J. Kohno, T. Shibata, C. Nagasawa, and M. Hirono, Observation of stratospheric ozone layer by XeCl laser radar, *Appl. Phys. Lett.*, 1978.
- Volz, A., and D. Kley, Ozone measurements in the 19th century: An evaluation of the Mountsouris series, *Nature*, *332*, 240, 1988.
- Wang, P. H., M. P. McCormick, L. R. McMaster, S. Schaffner, and G. E. Woodbury, Time-periodic variations in stratospheric ozone from satellite observations, *Proceedings of the Quadrennial Ozone Symposium 1988*, Gottingen, F.R.G. edited by R. D. Bojkov and P. Fabian, Deepak Publications, Hampton, VA, 1989.
- Wardle, D. I., C. D. Walshaw, and T. W. Wormell, A new instrument for atmospheric ozone, *Nature*, *199*, 1177-1178, 1963.
- Weiss, R. F., Global warming, *Chemical and Engineering News*, March 13, 25-44, 1989.

- Weiss, R. F., and H. Craig, Production of atmospheric nitrous oxide by combustion, *Geophys. Res. Lett.*, **3**, 751-753, 1976.
- Werner, J., K. W. Rothe, and H. Walther, Monitoring of the stratospheric ozone layer by laser radar, *Appl. Phys. B.*, **32**, 113, 1983.
- WMO, World Meteorological Organization, Report of the WMO Meeting of Experts on Assessments of Performance Characteristics of Various Ozone Measuring Systems, *Global Ozone Research and Monitoring Project*, Report 9, WMO, Geneva, 1980.
- WMO, The stratosphere-1981: Theory and measurements, *Global Ozone Research and Monitoring Project*, Report 11, WMO, Geneva, 1981.
- WMO, Sources of errors in detection of ozone trends, *Global Ozone Research and Monitoring Project*, Report 12, WMO, Geneva, 1982.
- WMO, Review of the Dobson spectrophotometer and its accuracy, *Global Ozone Research and Monitoring Project*, Report 13, WMO, Geneva, 1983.
- WMO, Atmospheric ozone 1985: Assessment of our understanding of the processes controlling its present distribution and change, Global Ozone Research and Monitoring Project, WMO, Report 16, sponsored by WMO NASA, NOAA, FAA, UNEP, CEC, and BMFT, Washington, DC, 1986.
- WMO, Report of the NASA/WMO ozone trends panel, 1989, *Global Ozone Research and Monitoring Project*, Report 18, WMO, Geneva, 1989 (cited in text as OTP).
- Wofsy, S. C., M. B., McElroy and Y. L. Yung, The chemistry of atmospheric bromine, *Geophys. Res. Lett.*, **2**, 215-218, 1975.
- Wuebbles, D. J., and D. E. Kinnison, A two-dimensional study of past trends in global ozone, *Proceedings of the Quadrennial Ozone Symposium 1988*, Gottingen, F.R.G., edited by R. D. Bojkov and P. Fabian, Deepak Publications, Hampton, VA, 1989.
- Yokata, A., Y. Makide, and T. Tominaga, A new calibration method for the measurement of CCl_4 concentration at 10^{-10} v/v level and the behavior of CCl_4 in the atmosphere, *Bull. Chem. Soc. Japan*, **58**, 1308-1314, 1985.
- Zander, R., G. Roland, L. Delbouille, A. Savuel, C. B. Farmer, and R. H. Norton, Column abundance and long-term trend of hydrogen chloride (HCl) above the Jungfraujoch station, *J. Atmos. Chem.*, **5**, 395-404, 1987a.
- Zander, R., G. Roland, L. Delbouille, A. Savuel, C. B. Farmer, and R. H. Norton, Monitoring of the integrated column of hydrogen fluoride above the Jungfraujoch station since 1977. The HF/HCl column ratio, *J. Atmos. Chem.*, **5**, 385-394, 1987b.
- Zander, R., Ph. Demoulin, D. H. Ehhalt, and U. Schmidt, 1989a, Secular increase of the vertical abundance of methane derived from IR solar spectra recorded at the Jungfraujoch Station, *J. Geophys. Res.*, in press, 1989a.
- Zander, R., Ph. Demoulin, D. H. Ehhalt, U. Schmidt, and C. P. Rinsland, Secular increase of the total vertical abundance of carbon monoxide above central Europe since 1950, *J. Geophys. Res.*, in press, 1989b.
- Zommerfeld, W., and K. F. Kunzi, Operational ground based ozone sensor (OGOS), *Proceedings of the Quadrennial Ozone Symposium 1988*, Gottingen, F.R.G., edited by R. D. Bojkov and Fabian, Deepak Publications, Hampton, VA, 1989.

N 9 2 - 1 5 4 3 3

509412
122P

THEORETICAL PREDICTIONS

Coordinator

G. Brasseur (Belgium)

Principal Authors and Contributors

B. A. Boville (USA)

G. Brasseur (Belgium)

C. Bruhl (FRG)

M. Caldwell (USA)

P. Connell (USA)

A. De Rudder (Belgium)

A. Douglass (USA)

I. Dyominov (USSR)

D. Fisher (USA)

J. F. Frederick (USA)

R. Garcia (USA)

C. Granier (France)

R. Hennig (FRG)

M. Hitchman (USA)

I. Isaksen (Norway)

C. Jackman (USA)

M. Ko (USA)

S. Madronich (USA)

M. Prather (USA)

R. Rood (USA)

T. Sasaki (Japan)

S. Solomon (USA)

F. Stordal (Norway)

G. Visconti (Italy)

S. Walters (USA)

D. Wuebbles (USA)

A. Zadarozhny (USSR)

E. Zhadin (USSR)

CHAPTER 3

THEORETICAL PREDICTIONS

TABLE OF CONTENTS

3.1	MODEL FORMULATION AND RELIABILITY	283
3.1.1	Introduction	283
3.1.2	Formulation of Stratospheric Models	284
3.1.3	Model-Model Intercomparisons	291
3.1.4	Comparison Between Model Calculations and Observations	301
3.2	MODEL PREDICTIONS	317
3.2.1	Projected Scenarios for Halocarbons and Trace Gases	317
3.2.2	Predicted Response of the Atmosphere for Sample Scenarios	326
3.2.3	Predicted Changes in Surface UV Radiation	383
3.2.4	The Effects of Ozone Changes on Circulation	392
	REFERENCES	395

3.1 MODEL FORMULATION AND RELIABILITY

3.1.1 Introduction

In order to understand the impact of man-made chemicals on the atmospheric ozone layer, it is essential to develop models that can perform long-term predictions of future ozone changes. Such models should make use of current knowledge about atmospheric chemistry, physics, and dynamics and specifically resolve one, two, or three dimensions of the atmosphere. Models that do not resolve all three dimensions must assume a suitable average (or uniformity) over the remaining dimensions. The one-dimensional (1-D) models are strongly limited by their simplified treatment of atmospheric dynamics, based on a crude empirical vertical eddy diffusion formulation. One-dimensional models are usually used to determine global average changes in total ozone column, and in the vertical distribution of ozone density. As the conditions encountered by trace gases are very different as a function of latitude, and because globally averaged models oversimplify the mean atmospheric transport, 1-D model results must be interpreted with caution, subject to verification by more elaborated multidimensional models. The advantages of 1-D models, however, are that a detailed chemistry and the coupling between chemistry and radiation can be treated accurately, and an almost unlimited number of scenarios for future ozone changes can be run on the computers. This has turned out to be useful in connection with abatement strategy for limiting future ozone layer changes.

The advantage of 2-D models is that they can be used to predict latitudinal and seasonal changes in ozone. Current models that are used for long-term predictions of ozone changes have a rather detailed chemistry, and to some extent include radiative and dynamic feedbacks. This has made 2-D models central in the study of future ozone changes. However there are clearly some limitations in their use. The handling of feedback among chemistry, radiation, and dynamics is not straightforward in a 2-D framework. This could be of particular importance in the lower stratosphere, where moderate changes in dynamics could be significant for the ozone distribution and for the exchange of gases between the stratosphere and the troposphere. For studies of the special phenomena connected to polar stratospheric ozone depletion, 2-D models have clear limitations and should be used with care. These phenomena are regional in character and are not latitudinally homogeneous. Furthermore, the chemical processes leading to disturbed chemistry in connection with polar stratospheric clouds contain large uncertainties and are highly non-linear. The treatment of heterogeneous polar chemical processes included in current 2-D models is more uncertain than the treatment of stratospheric gas-phase reactions.

Section 3.1.2 describes the formulation and recent improvements in two-dimensional models, which are used in the present assessment, and describes the three-dimensional models that are currently being developed to better simulate transport of chemically active trace gases, especially in the polar regions. The range in 2-D model calculations is described in Section 3.1.3, which highlights results from a recent intercomparison workshop. Selected fields calculated by these models are compared in Section 3.1.4 with observations. In Section 3.2.1, a number of scenarios have been defined, which encompass possible emission rates of different halocarbons in the future. Because of large uncertainties in the rates for heterogeneous processes, which play an important role in polar regions and possibly at other latitudes, the calculated responses of the models, reported in 3.2.2, include only the effects of homogeneous chemistry. One important distinction among the models is their ability to account for temperature feedbacks on the calculated ozone changes. Predicted changes in biologically damaging surface radiation (UV-B) for selected scenarios included in this assessment are discussed in Section 3.2.3. Finally, the possibility of changes in the atmospheric circulation resulting from substantial ozone depletions in the stratosphere is discussed in Section 3.2.4.

THEORETICAL PREDICTIONS

3.1.2 Formulation of Stratospheric Models

3.1.2.1 Introduction

Differential heating can give rise to a weak meridional circulation in the upper stratosphere and mesosphere, thereby setting up non-zero zonal flows relative to the ground via advection of angular momentum. This meridional circulation is characterized by rising motion in the summer hemisphere, sinking motion in the winter hemisphere, and meridional transport from the summer to the winter hemisphere. Processes generated in the troposphere affect this circulation considerably. These include the extension of the tropospheric meridional circulation into the lower stratosphere and the propagation of waves into the middle atmosphere. The tropospheric meridional circulation is driven partly by convection and by baroclinic waves and is almost always prescribed in current two-dimensional models. *In situ* absorption of planetary-scale and baroclinic Rossby waves accentuates the lower stratospheric meridional circulation, with increased poleward and downward motion. Absorption of gravity wave activity in the mesosphere increases the interhemispheric circulation due to differential heating alone by an order of magnitude. Kelvin, Rossby, and gravity wave absorption give rise to tropical meridional circulations associated with the semiannual and quasi-biennial oscillations. These wave-driven circulations ensure that temperatures are removed from radiative equilibrium, distinctly so in both the mesosphere and winter stratosphere.

Wave-driven circulations advect trace constituents and help control their distribution. In addition, "wave breaking" leads to tracer transport by mechanical turbulence. Wave absorption by radiative damping can also lead to irreversible mixing, provided the photochemical time constant of a tracer is similar to the eddy advective time scale. The propagation and absorption of waves depends on the background dynamical state, which in turn depends on the distribution of radiatively active trace gases. This interaction among wave and mean flow dynamics, photochemistry, and radiation makes the middle atmosphere particularly challenging to model. Middle atmosphere dynamics are thoroughly reviewed in Chapter 6 of WMO (1986). Recent discussions on regimes of dynamical and radiative control are given by Garcia (1987), Snieder and Fels (1988), and Ko et al. (1989).

Chemistry and transport models are the fundamental tool for assessing future ozone depletion. Extensive descriptions of 1-D, 2-D, and 3-D assessment models are given in Chapters 6 and 12 of WMO (1986). There have been significant improvements in most models since then. At present, 2-D models represent the best compromise among computational efficiency, ease of diagnosis, detailed radiation and chemistry, and realistic dynamics. Therefore, 2-D models are the primary assessment tool currently in use. The most useful 2-D model would be one that solves for the time evolution of zonal mean variables using the coupled set of equations governing the atmosphere, where the effects of disturbances on the mean flow and tracers are represented as accurately as possible. Such a model would have a high degree of interaction among wave and mean flow dynamics, photochemistry, and radiation. It would be self-consistent in the sense that the governing equations are mutually satisfied. Subsection 3.1.2.2 addresses self-consistency and degree of interaction in current 2-D models. The usefulness of mechanistic 3-D and general circulation models (GCMs) is discussed in subsection 3.1.2.3. The influence of coupling and feedback on 2-D model scenarios is described at the end of Section 3.2.2. Some recent work on feedbacks in 3-D models is described in Section 3.2.3.

3.1.2.2 2-D Models

Differential radiative heating and rotation account for the zonal flow being stronger and more homogeneous than the meridional or vertical flow. Therefore, it is reasonable to formulate a model in terms of

zonally averaged variables. However, the forced eddies which strongly influence the middle atmosphere are either small-scale or fundamentally three-dimensional. Recently, linear wave theory has been used by 2-D modelers to close the zonal mean dynamical equations for the eddy flux convergence terms. Efforts have focused on determining the meridional circulation and wave driving self-consistently and on capturing the interactive nature of the waves, mean flow, chemistry, and radiation. An international group of 2-D models currently engaged in carrying out scenario calculations is listed in Table 3.1.1. Following a discussion of theory common to 2-D models, the various capabilities of each model will be described.

The Eulerian and transformed Eulerian mean (TEM) equations are described by Andrews and McIntyre (1976), Boyd (1976), and Edmon et al. (1980). Zonal mean isentropic equations are given by Tung (1986, 1987). When all terms are retained, Eulerian, TEM, and isentropic formulations are equally correct. When Rossby waves predominate, both the meridional flux convergence and vertical advection terms are large in the Eulerian mean thermodynamic energy equation. This is true even when the waves are very weakly dissipating, are approximately steady, and the mean flow is only weakly accelerating. It is difficult to interpret the net effect of Rossby wave eddy fluxes on zonal mean dynamical variables in the Eulerian mean system (wave driving), since the meridional heat and momentum fluxes ($\overline{v'\theta'}$ and $\overline{u'v'}$) are large, and zonal mean potential temperature and zonal wind ($\overline{\theta}$ and \overline{u}) are joined through the continuity and thermal wind relations. Therefore, for interpreting the effects of Rossby waves it is useful to employ the TEM equations, with the residual mean meridional circulation defined by

$$\overline{v}^* = \overline{v} - \frac{1}{\rho_o} \frac{\delta}{\delta z} \left[\rho_o \frac{\overline{v'\theta'}}{\overline{\theta}_z} \right] \tag{1a}$$

$$\overline{w}^* = \overline{w} + \frac{1}{\cos\phi} \frac{\delta}{\delta y} \left[\cos\phi \frac{\overline{v'\theta'}}{\overline{\theta}_z} \right], \tag{1b}$$

Table 3.1-1. Capabilities of an international group of 2-D assessment models. The second column indicates whether tracer diffusion coefficients and the meridional circulation are determined simultaneously. The third column indicates how the circulation and diffusion coefficients are determined. The fourth column indicates whether heating rates (δQ), temperatures (δT), or the meridional circulation (δX) is allowed to change.

Model (Representatives)		X/Ks	Interaction	Code
AER1 (Ko, Sze)	No	Observations/Fixed	No	A
Aquila (Visconti, Pitari)	No	Observations/Fixed	No	I
CAO-LI (Jadin, Zvenigorodsky)	No	Observations/Fixed	No	R
DuPont (Fisher)	No	Observations/Fixed	No	
MPI (Brühl)	No	Observations/Fixed	No	M
MRI (Makino)	No	Observations/Fixed	No	J
NSI (Dyominov, Zadorozhny)	No	Observations/Fixed	No	U
Oslo (Isaksen, Stordal)	No	Observations/Fixed	No	O
CalTech (Yung, Zurek)	Yes	Diagnosed	$\delta Q, \delta X$	
GSFC2 (Jackman, Douglass)	Yes	Observations/Fixed	No	G
LLNL (Wuebbles, Connell)	No	Observations/Fixed	$\delta Q, \delta T$	L
Washington (Tung)	Yes	Diagnosed	$\delta Q, \delta X$	
AER2 (Schneider, Ko)	Yes	Raleigh drag	$\delta Q, \delta T, \delta X$	
Cambridge (Gray, Eckman)	No	Gravity		C
NOCAR (Garcia, Solomon)	Yes	Gravity/fixed K_{yy}	$\delta Q, \delta T, \delta X$	N
WisCAR (Brasseur, Hitchman)	Yes	Gravity and Rossby	$\delta Q, \delta T, \delta X$	W

THEORETICAL PREDICTIONS

where $(\bar{\quad})$ and $(\quad)'$ are the zonal mean and deviations therefrom, ρ_0 is basic state density, θ is potential temperature, ϕ is latitude, and v and w are the meridional and vertical wind components. In the TEM framework, the eddy terms in the energy equation are small for Rossby waves, and the chief effect of Rossby waves is expressed as the Eliassen-Palm (EP) flux divergence acting on the zonal momentum equation. Although this aids interpretation of cause and effect for the dynamics, two extra eddy terms complicate the tracer equation (Hitchman and Brasseur, 1988). Moreover, where gravity waves dominate, such as in the mesosphere, meridional fluxes are small, but $\overline{w'\theta'}$ and $\overline{u'w'}$ can both be large. The TEM system then has the same form as the Eulerian equations, and there is again difficulty in interpreting net wave effects. Thus, Eulerian and TEM models are about equally useful.

In solving the zonal mean equations, one must specify the wave driving (flux terms in the dynamical equations) and tracer eddy fluxes. All models make use of the linear perturbation form for tracer μ

$$\mu' = -\eta' \frac{\partial \bar{\mu}}{\partial y} - \zeta' \frac{\partial \bar{\mu}}{\partial z} \quad (2)$$

to obtain

$$\overline{v'\mu'} = -K_{yy} \frac{\partial \bar{\mu}}{\partial y} - K_{yz} \frac{\partial \bar{\mu}}{\partial z} \quad (3a)$$

$$\overline{w'\mu'} = -K_{zy} \frac{\partial \bar{\mu}}{\partial y} - K_{zz} \frac{\partial \bar{\mu}}{\partial z}, \quad (3b)$$

where $K_{yy} = \overline{\eta'v'}$, $K_{yz} = \overline{v'\zeta'}$, $K_{zy} = \overline{w'\eta'}$, and $K_{zz} = \overline{w'\zeta'}$, and η' and ζ' are meridional and vertical parcel displacements.

Often, use is made of the quasi-geostrophic relationship between Rossby wave driving and the meridional flux of quasi-geostrophic potential vorticity, q

$$DF_R = \frac{1}{\rho_0 \alpha \cos \phi} \vec{\nabla} \cdot \vec{F}_R = \overline{v'q'}, \quad (4a)$$

where $\vec{\nabla} \cdot \vec{F}_R$ is the Rossby wave EP flux divergence (Edmon et al., 1980). It is further assumed that relevant disturbances are small in amplitude, so that the flux-gradient relationship

$$\overline{v'q'} = -K_{yy} \bar{q}_y, \quad (4b)$$

holds. Newman et al. (1986) used (4) to determine K_{yy} from observational data. The meridional mixing coefficient obtained under this linearity assumption provides for a self-consistent effect of Rossby waves on tracers and on the mean flow. In isentropic coordinates, when Rossby waves dominate and the flow is nearly adiabatic, analogous relations to (4) apply even in the ageostrophic case (Tung, 1986).

Table 3.1.1 indicates the capabilities of each assessment model. It indicates whether the same information is used to determine tracer diffusion coefficients and the meridional circulation (self-consistency) or whether separate information is used. It lists how the circulation and tracer diffusion coefficients are determined, and the degree of interaction that can occur. Model complexity generally increases

downward. It is tempting to assume that more complex models represent the real atmosphere more faithfully. But feedback capabilities are a recent development. Much more work remains in understanding how they work in each model. All of the models employ a type of TEM formulation, except the classical Eulerian models of MPI and Cambridge. This is rather a small difference compared to the various approximations made in each model.

The strategy in most models in Table 3.1.1, including all of those in the first group, is to specify temperatures and heating rates from observations and to employ constant tracer mixing coefficients (AERI, Aquila, CAO-LI, DuPont, MPI, MRI, NSI, Oslo, GSFC2, LLNL). In this formulation there is usually no allowance for interaction among changing trace gas concentrations, temperatures, and transport. Since ozone concentrations depend on temperature in much of the atmosphere, it is extremely important that temperatures be allowed to change with changing trace gas distributions. In the Oslo model off-line temperature changes are specified from the results of Fels et al. (1980).

Specification of heating rates is tantamount to specifying the mean meridional circulation and, implicitly, the wavedriving, hence the mixing coefficients. For self-consistency, heating rates and mixing coefficients should not be specified independently. The models in the second group in Table 3.1.1 have either self-consistency or an interactive capability. In the GSFC2 model a simultaneous set of satellite observations is employed to determine temperatures, heating rates, the meridional circulation, and, using (4), mixing coefficients. In the LLNL model, perturbed constituent values are allowed to alter temperatures such that the net heating rates do not change. But the circulation and mixing coefficients are fixed and specified separately.

The Washington and California Institute of Technology models employ a different self-consistent approach, described by Tung (1987) and depicted in Figure 3.1.1. Only observed fixed temperatures are required as input. Since observed temperatures implicitly contain information about the effects of wave

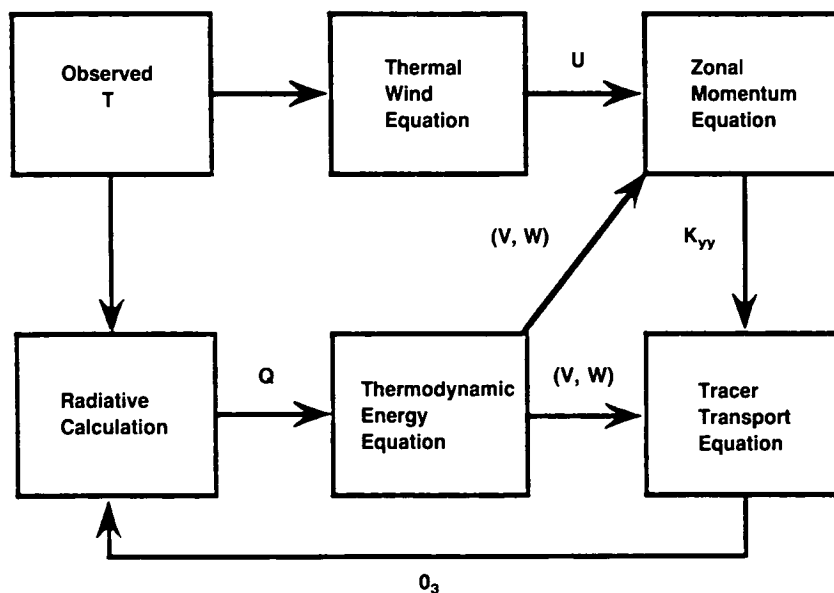


Figure 3.1-1. Schematic diagram showing an algorithm for determining the coupled set of transport parameters with prescribed T as input (adapted from Tung, 1987, Reidel, Inc.).

THEORETICAL PREDICTIONS

driving on the meridional circulation, the distribution of wave driving can be solved for. An ambiguity exists regarding the partitioning of $\bar{\nabla} \cdot \bar{F}$ into gravity, Rossby, and Kelvin wave effects. But in the extratropical winter stratosphere, Rossby waves dominate and (4) can be used. This is a powerful self-consistent technique for analyzing scenarios where temperatures are not expected to be perturbed very far. An interactive determination of simultaneous temperature and constituent changes (time integration) is not possible, although a new temperature field could be extrapolated and the process iterated.

In the last group of models in Table 3.1.1, the effects of one or several wave types are parameterized in an interactive manner. The AER2 model achieves a significant degree of interaction by parameterizing the wave-driving effects of gravity waves as a Rayleigh drag and those of Rossby waves as a diffusion of potential vorticity. Mixing coefficients are held fixed. The GSFC1 model is interactive for temperature, constituents, heating rate, and circulation, and includes a term that causes departures from a smooth annual cycle, but no information about wave physics is included.

The NOCAR, Cambridge, and WisCAR models each include the Lindzen (1981)/Holton (1982) parameterization of breaking gravity waves, which provides the body force, DF_g , due to those waves and the vertical eddy diffusion coefficient, K_{zz} ,

$$DF_g = B (c - \bar{u})^2 \left[(c - \bar{u}) + 3H \frac{\delta \bar{u}}{\delta z} \right] \quad (5a)$$

$$K_{zz} = DF_g \frac{(c - \bar{u})}{N^2} \quad (5b)$$

above the breaking height

$$z_b = 3H \ln \left[\frac{|c - \bar{u}|}{\bar{u}} \right] \quad (5c)$$

and below the critical level where $c = \bar{u}$. Wave driving and vertical diffusivity distributions co-evolve with model zonal winds. In (5) H is scale height, N is buoyancy frequency, B is proportional to the zonal wavenumber, k , and to the portion of a latitude circle occupied by waves, and \bar{u} is a measure of wave amplitude at the forcing level. Suitable values of B and \bar{u} must be specified for discrete values of zonal trace speed c (Garcia and Solomon, 1985; Gray and Pyle, 1987; Brasseur and Hitchman, 1987).

In the Cambridge model constant eddy diffusivities are specified, while planetary Rossby wave momentum fluxes are determined from satellite observations. It has interactive parameterized Kelvin and mixed Rossby-gravity waves, which, together with the gravity wave parameterization, yield realistic semiannual and quasi-biennial oscillations (Gray and Pyle, 1987; 1989). The body force per unit mass due to the absorption of radiatively-damped equatorial waves is given by

$$DF_e = F_o e^{(z-z_o)/H} R(z) e^{-P(z)} e^{-(y/Y_1)} \quad (6a)$$

where F_o is the pseudomomentum flux at the forcing level z_o ,

$$R(z) = \frac{\alpha(z) N}{k(\bar{u} - c)^2} \quad (6b)$$

is an inverse penetration scale given by the damping rate divided by the vertical group velocity,

$$P(z) = \int_{z_0}^z R(z') dz', \quad (6c)$$

α is a radiative damping profile, and Y_L is the meridional half-width about the Equator (Plumb 1977; Dunkerton 1979; Gray and Pyle, 1987). Suitable parameters are chosen for c and F_0 for discrete Kelvin and mixed Rossby-gravity waves, where $Y_L = (2c/\beta)^{1/2}$ for Kelvin waves and $Y_L = (2 - 2ck^2/\beta)^{1/2}$ for mixed Rossby-gravity waves, and β is the northward gradient of planetary vorticity at the Equator.

The WisCAR model does not include equatorial planetary waves, but does include an interactive determination of wave driving and meridional diffusivity due to quasi-stationary planetary Rossby waves. This method, described in Hitchman and Brasseur (1988), makes use of the equation for conservation of Rossby wave activity, A ,

$$\frac{\delta A}{\delta t} + \vec{\nabla} \cdot \vec{F}_R = -\alpha A \quad (7a)$$

$$\vec{\nabla} \cdot \vec{F}_R = \frac{1}{\cos\phi} \frac{\delta}{\delta y} (\cos\phi G_y A) + \frac{\delta}{\delta z} (G_z A), \quad (7b)$$

where \vec{F}_R is the flux of Rossby wave activity. The WKBJ group velocity (G_y , G_z) depends only on model zonal winds. Solving this equation requires specification of the source of wave activity near the tropopause and the damping rate $\alpha(y, z)$. Once Rossby wave driving is obtained from (7) and applied to the meridional circulation, K_{yy} is determined from (4) and applied to all constituents.

Further details of the models may be found in the proceedings of the 2-D model intercomparison workshop held in Virginia Beach in 1988 (cf. Section 3.1.3). It should be emphasized that the strength and distribution of the meridional circulation and mixing coefficients vary a great deal among models. Efforts are being made to establish appropriate magnitudes by comparing model and observed tracer distributions. Schneider et al. (1989) and Jackman et al. (1989a) find that the distribution of total ozone is quite sensitive to the value of these parameters near the tropopause. Other uncertainties in the formulation of 2-D models lie in the applicability of mixing coefficients to individual tracers with differing sources and sinks (Smith et al., 1988) and nonlinearity associated with large amplitude waves.

3.1.2.3 3-D Models

Since the publication of the WMO report "Atmospheric Ozone 1985" (1986) there has been significant development in 3-D stratospheric chemistry models. This development has occurred both with mechanistic dynamical models and GCMs. As the models have evolved, it has become clear, from both theory and data, that some assessment problems are fundamentally three dimensional. It has also become clear that a synergism can exist between 2-D and 3-D models that will improve 2-D models and help to evaluate the impact of the fundamental assumptions of the 2-D formalism. This section describes the role of 3-D models in stratospheric assessment calculations.

Three-dimensional models have had only limited applications in assessment studies because of computational requirements. The computational aspects of stratospheric GCMs with chemistry has recently been discussed in Rood and Kaye (1989). The Goddard 3-D chemistry model, using a 4° latitude by 5° longitude grid with 19 vertical levels, would require approximately 5 hours of CYBER 205 CPU time per

THEORETICAL PREDICTIONS

model day. Therefore, assuming the model could be efficiently fit into core, it would require 76 days on a dedicated computer to model just 1 year. Given that the resolution of this model is known to be inadequate, it is obvious that 3-D assessment applications parallel to the 2-D efforts discussed in this chapter are impossible.

The most valuable assessment activity with 3-D models involves problems that are intrinsically three dimensional, and that can be investigated with time integrations of months. It is precisely such problems that 2-D models cannot properly simulate (e.g., stratospheric warmings). One such problem is the mixing of the Antarctic ozone hole with the rest of the atmosphere during the transition from winter to summer. To model this seasonal transition accurately, Rossby wave activity must be explicitly resolved. Calculations to compute the dilution of the Antarctic ozone hole into the global atmosphere are currently being performed at several laboratories (cf. Section 1.7). It will be required to use a 3-D model to account for the horizontal variation of column ozone change observed over the Northern Hemisphere during the last decade (Figure 2.2-9).

A similar problem exists for the Northern Hemisphere, where it is expected that heterogeneous processes taking place in the polar vortex might be producing enhanced levels of reactive chlorine compounds. In the Antarctic there is much longer isolation of the polar vortex from the rest of the hemisphere and, therefore, localized ozone destruction in the vortex. In the Northern Hemisphere the vortex mixes with the rest of the hemisphere in late winter or early spring, and the chlorine compounds produced within the vortex might deplete ozone more generally in the hemisphere. Once again it is necessary to represent Rossby wave activity accurately to evaluate this potential depletion mechanism.

Quantitatively accurate assessments for the two problems described above can be obtained by using a GCM as an analysis tool to generate wind fields that are representative of actual stratospheric conditions. The use of winds generated by data assimilation using a 3-D model to transport reactive constituents has been described in Rood et al. (1989). These studies suggest that accurate evolution of constituents in a Rossby wave dominated environment (wintertime stratosphere) can be modeled for 60 days or longer. Figure 3.1.2 shows the total ozone field on 28 February 1989 as measured by TOMS and as modeled from a January 1 initial condition. The model captures most of the important features of the Northern Hemisphere total ozone field, and suggests that mixing of high- and low-latitude air is properly represented.

The data assimilation studies also imply that the wintertime polar vortex in the Northern Hemisphere is largely isolated from the rest of the hemisphere, as suggested by Jukes and McIntyre (1987). This implies that studies of polar processes in general are best carried out within the 3-D model formulation. The 2-D model representation communicates nonpolar air with polar air on too short a time scale. Brasseur et al. (personal communication) have already shown the potential application of mechanistic 3-D models to the Antarctic ozone hole. Recent papers by Rose and Brasseur (1985), Grose et al. (1987), and Kaye and Rood (1989) present relatively complete chemical representations in 3-D model studies of the wintertime hemisphere.

The fact that 2-D models have difficulty representing the mixing of middle latitude air with polar air points out another role of 3-D models. Three-dimensional models can be used to quantitatively assess how well 2-D models represent intrinsically three-dimensional processes. Similarly, 3-D models can be used to guide the incorporation of 3-D processes (such as polar heterogeneous chemistry) into 2-D models in an accurate manner. Global or regional 3-D models are expected to contribute not only to polar chemistry processes, but to problems of stratosphere-troposphere exchange, gravity wave mixing, chemical eddy processes, dynamical changes due to ozone decrease and greenhouse gas increase, and any problem where wave propagation and dissipation is of fundamental importance.

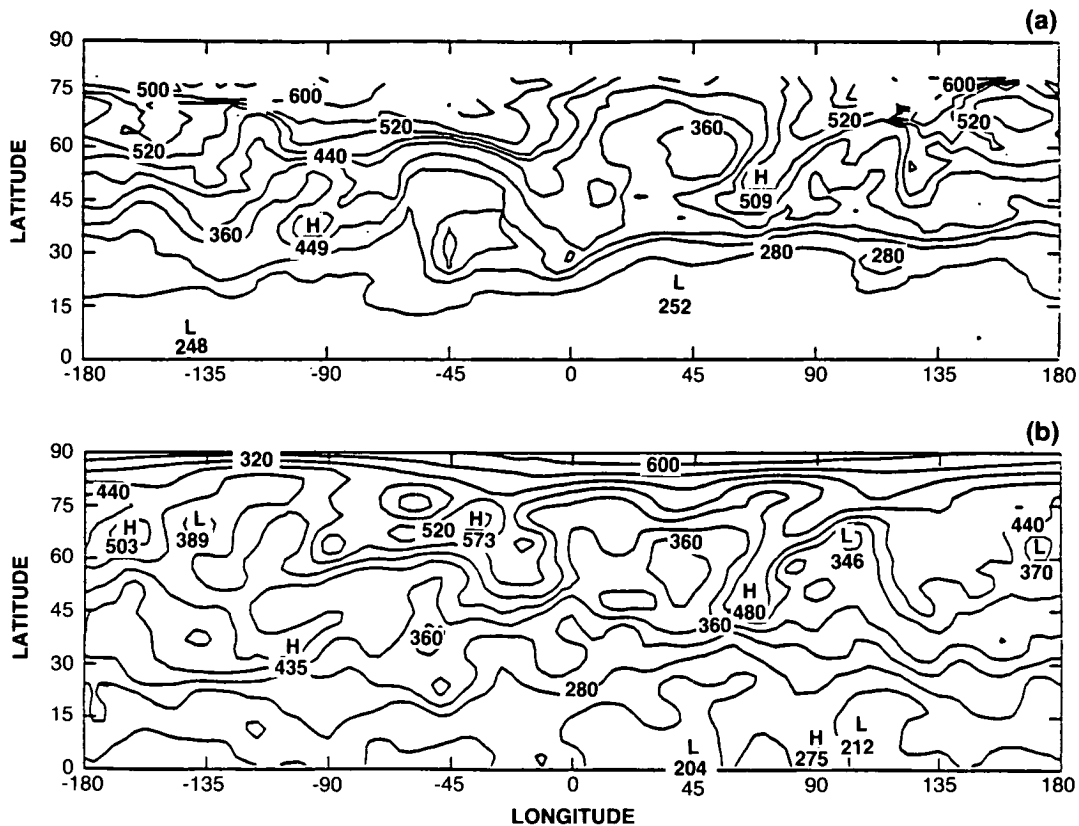


Figure 3.1-2. Total ozone field on 28 February 1989 (a) as measured by TOMS and (b) as modeled from a January 1 initial condition (after Rood et al., 1989).

Even with adequate computer resources, 3-D assessment experiments would not address and solve many of the problems inherent with 2-D assessments. Fundamental problems exist with 3-D simulations of dynamics (WMO, 1986, p. 307), and there is little indication that simply expanding to three dimensions will solve many of the classic problems of atmospheric chemistry (e.g., the 40-km ozone problem). Similar to the 2-D model experience, 3-D dynamics models are controlled to a large extent by the treatment of subscale processes (for instance, Rind et al., 1989). This treatment is necessarily parameterized, and leaves any long-term 3-D assessment with analogous uncertainties to 2-D assessments.

The current state of model development and computational resources limits the applications of 3-D models in assessment studies. Rood and Kaye (1989) estimate that computer speeds must be increased by a factor of 100–1000 (compared to a CYBER 205) for assessment applications similar to those performed by 2-D models. In the meantime, 3-D models will be valuable in limited assessment applications and as complements to 2-D models.

3.1.3 Model—Model Intercomparisons

3.1.3.1 Introduction

The responsibility of making predictions of future ozone levels, as well as the interest of the scientific community in testing and validating models, has led to a series of model intercomparisons. The primary

THEORETICAL PREDICTIONS

objective of these model intercomparisons is to understand the specific, fundamental differences among the stratospheric models and, in particular, their predictions of stratospheric ozone.

Another important objective of the intercomparisons is to promote basic improvements in the treatment of chemistry and transport in all models through the collective scientific effort of the community. The two-dimensional Intercomparison Workshop of September 1988 at Virginia Beach, Virginia was a major effort with international participation. Most of the groups involved in multi-dimensional modeling contributed to the planning and execution of the workshop.

Stratospheric models have become increasingly complex over the last decade, as they have strived to develop more accurate simulations of the radiative transfer in the atmosphere, of the chemical reactions coupling more than two dozen species, and of multi-dimensional transport. The end result of the assessments shown in this chapter, i.e., the perturbations to the ozone distribution at the end of a 100-year simulation, is the consequence of the interaction of the different numerical representations of the chemistry, radiation and atmospheric circulation in the models. In order to understand the difference in calculated ozone perturbations between two models, it is necessary to examine, in greater detail, the detailed components of radiation, chemistry, and transport in each model.

Therefore, the Virginia Beach Workshop (as did previous workshops) defined a set of detailed, but restricted, calculations for the intercomparison that were designed to allow for intercomparison of the individual components, as well as of the integrated model. The participating modeling groups agreed to perform series of specified calculations using the most recent set of photochemical rates (DeMore et al., 1987). The experiments were grouped in order to test several areas of the model simulation of the stratosphere:

- (a) photodissociation and heating rates using the same O_3 and temperature fields in all models;
- (b) transport of synthetic tracers with prescribed chemistry;
- (c) distribution of stratospheric species in the current atmosphere; and
- (d) predictions of perturbations to ozone and temperature for a specified future atmospheric composition.

The Virginia Beach Workshop was the most ambitious in the series of stratospheric model intercomparisons. The agenda was too extensive to be covered in the week-long meeting; and most effort was put into sections (a), (b), and parts of (c) above. A brief summary of the workshop is included here. The complete workshop report (Jackman et al., 1989b) includes over 1400 figures and tables from the participating models and is published as a NASA Conference Proceedings (available from Charles H. Jackman, Code 616, NASA/GSFC, Greenbelt, MD 20771, USA).

3.1.3.2 Photodissociation Rates

The comparison of photodissociation rates (J-values/sec) revealed substantial differences and similarities among the models. In the case of O_2 dissociation, the primary source of stratospheric O_3 , the models fell into two groups. Within each group, agreement was very good over all latitudes and altitudes in the stratosphere, but the two groups disagreed systematically by a factor of 2. Similarly, systematic differences were found in the calculated J-values for CFC-11 and CFC-12. The largest disagreement among the models, up to a factor of 5, occurred for J(NO). Dissociation of NO leads to a sink for odd-nitrogen in the upper

stratosphere and mesosphere. Photolysis of NO occurs in the more opaque part of the Schumann-Runge bands, and the different methods of modeling this J-value have been noted in the previous assessment (WMO, 1986) but have not been resolved since then or in this intercomparison.

A comparison of J-values for species with significant photolysis at near-ultraviolet and visible wavelengths (O_3 , NO_2 , HNO_3 , $ClONO_2$) points to substantial differences in the treatment of scattered light from the troposphere (Rayleigh, clouds, aerosols, and the surface). The importance of scattered light is greatest in the lower stratosphere where photodissociation is dominated by longer wavelengths, the shorter wavelengths being absorbed by ozone in the upper stratosphere. Among the models that included multiple scattering, there are differences in technique and in results; models that did not include scattered light had systematically lower J-values by about 30–50%.

The workshop participants viewed these differences in the modeled J-values as being too large to be explained by the different approaches in modeling (e.g., cross sections, spectral resolution, solar irradiance, diurnal cycles). Consequently, many of the modeling groups are continuing a specific intercomparison not only of J-values, but also of the monochromatic radiative transfer of solar radiation in the stratosphere and troposphere. Key issues involve diurnal averaging, scattering, and atmospheric transmission in the Schumann-Runge bands (175–205 nm).

Validation of the modeled photodissociation rates cannot rely on model intercomparisons alone; a further necessary component is the accurate measurement of the attenuation of sunlight in wavelength regions where O_2 is photodissociated (180–230 nm) and where much of the photolytically active ultraviolet occurs in the lower stratosphere and troposphere (280–340 nm). A limited number of atmospheric measurements and determinations of O_2 transmission are available (Anderson and Hall, 1986; Herman and Mentall, 1982) but have not been fully compared with these models.

3.1.3.3 Heating and Cooling Rates

Stratospheric heating by sunlight is provided almost entirely by absorption by ozone. Agreement between models varies, with some agreement in the lower stratosphere, but differences as large as 35% at the stratopause (about 45 km). Some of the differences in calculated heating rates point to errors in the diurnal averaging or to different treatments of scattered sunlight from the troposphere.

Stratospheric cooling (and on some occasions, heating) is controlled by the transfer of infrared radiation between the ground, clouds, different levels of the atmosphere, and space. The models include what are believed to be the most important species and wavelength intervals: CO_2 bands near 15 μm , O_3 bands near 9.6 μm , and water vapor bands. The calculated net cooling rates agree qualitatively in terms of latitudinal and vertical patterns, but quantitative differences may be large, for example 40% at the stratopause. The tropical lower stratosphere is very cold and presents difficulties in modeling: absorption of 9.6 μm radiation by ozone heats the stratosphere, and the overall effect of the infrared radiation may be a small net heating near the tropopause. As might be expected, the disagreement between models is greatest in this region, with differences even in the sign of the net cooling. The workshop participants are continuing the intercomparison of radiation schemes in a separate, more detailed study.

3.1.3.4 Circulation and Tracer Transport

The distribution of long-lived tracers in the stratosphere (e.g., CFCs, N_2O , CH_4 , O_3 below 30 km) is a balance between photochemistry and transport. Transport in 2-D models is simulated by a combination of

THEORETICAL PREDICTIONS

advection by the mean meridional circulation (i.e., vertical and horizontal winds) and of diffusive mixing (often denoted by K , the diffusion coefficient). The diffusive mixing in 2-D models is intended to simulate tracer transport by those processes that are not explicitly resolved by the zonally and monthly averaged transport in these models (e.g., 3-D or transient eddies). One class of 2-D models specifies the meridional circulation; a more recent class of 2-D models calculates the circulation interactively along with the ozone and temperature fields. See Section 3.1.2 on model formulation for a more detailed discussion.

An intercomparison of the meridional circulation, in terms of residual winds, was made at the workshop. The overall pattern in all models was similar: upwelling in the tropical lower stratosphere and downward transport at mid- and high latitudes. At higher altitudes the pattern is more seasonal with upward motion over the summer pole, meridional transport through the mesosphere, and downward motion over the winter pole. The differences in the meridional wind field, however, cannot be assessed independently of the diffusion used in the models. Unfortunately, the diffusive mixing of the models was difficult to quantify, and thus to compare, because of the different formulations and combinations of vertical, horizontal, and quasi-horizontal mixing. Therefore we continued the intercomparison with a series of synthetic tracer experiments, which used the same specified chemistry in all models, in order to test the "effective" transport of the models.

One of the three synthetic tracers, X, was defined to have a source that would maintain a uniform tropospheric concentration of 1 ppbv below 850 mbar and a sink (similar in magnitude to N_2O) that was defined simply as a function of pressure. The model simulations were carried out to steady-state, and nine of the model results for December are shown here in Figure 3.1-3. Mixing ratios of X at 30 km are similar for all models (0.6–0.8 ppbv at the Equator and 0.1–0.2 ppbv at high latitudes), but by 40 km the values from different models diverge, indicating substantial differences in the strength of the equatorial upwelling in the mid- and upper stratosphere. The global, annually averaged lifetime of X varied from 97 to 127 years, consistent with the range for N_2O reported in Section 3.2.

Two other synthetic tracers were studied: tracer Y, with no atmospheric loss, in which a fixed amount was put initially into the lower troposphere and the rate of transport of a transient emission into the stratosphere was examined; and tracer Z with boundary conditions in the upper stratosphere and lower troposphere meant to resemble that of ozone. The steady-state distribution of the column of tracer Z resembled that of ozone in most models with equatorial minima of order 100 Dobson units (compared with 250 Dobson units for ozone) and a springtime maximum at high latitudes of order 500–600 Dobson units (compared with about 360–460 Dobson units for ozone). The Z experiment tested the seasonal changes in circulation that determine the month-by-month pattern in ozone column and, further, demonstrated the importance of ozone chemistry in the lower stratosphere: production in the tropics balanced by loss at mid- to high latitudes.

3.1.3.5. Current Atmosphere: 1980

The composition of the stratosphere is not uniquely defined by observations; indeed, some overlapping data sets provide conflicting results. Because of the focus and limited amount of time for the Virginia Beach intercomparison, we chose to limit our study to the model-model differences in predictions of the "present-day" atmosphere (defined as 1980 in terms of source gas concentrations). Detailed figures of the model predictions for many chemical species are presented in the conference proceedings and may be compared with available observations.

THEORETICAL PREDICTIONS

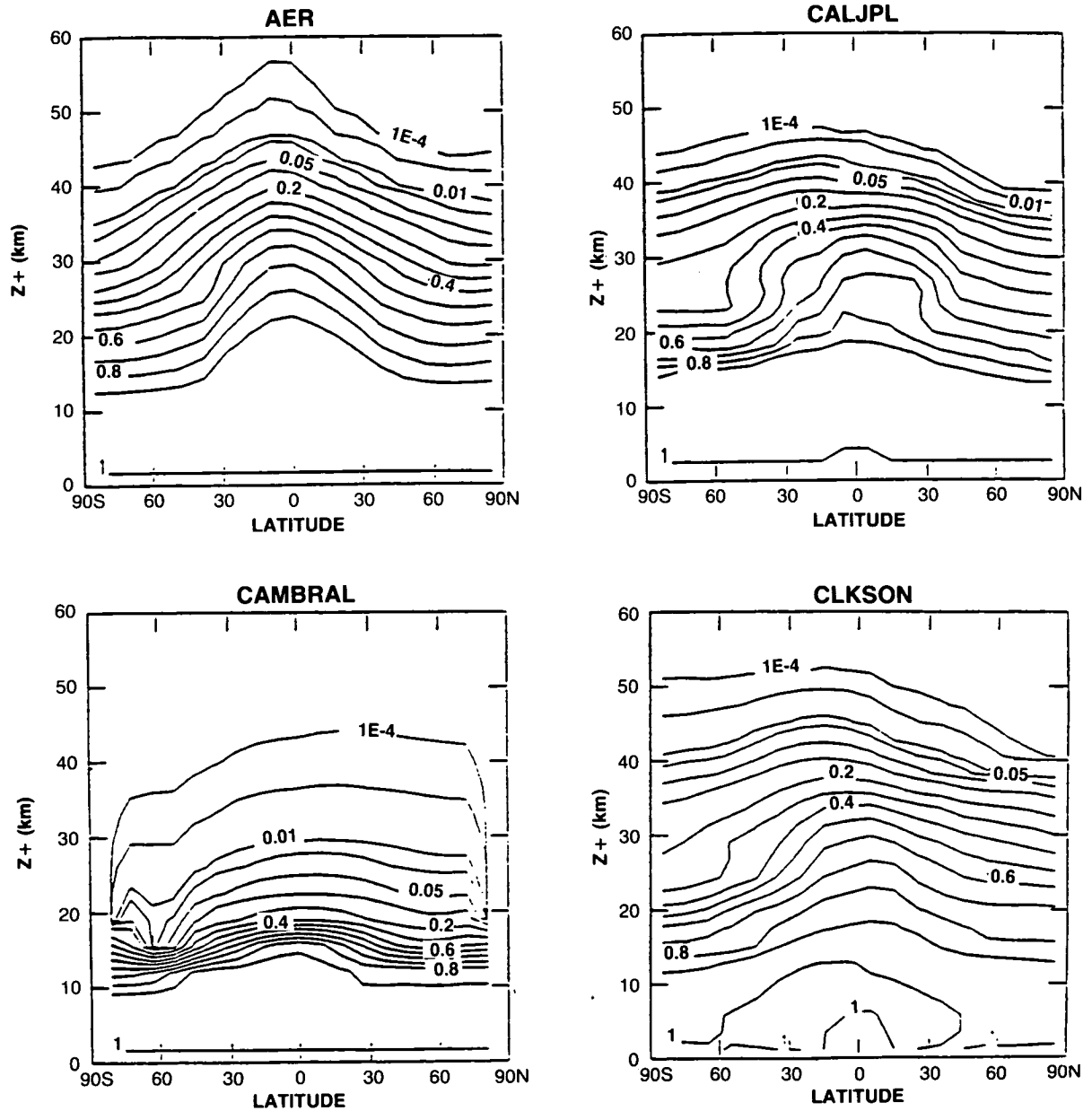


Figure 3.1-3. Two-dimensional distribution of tropospheric source gas X from nine models for the month of December.

THEORETICAL PREDICTIONS

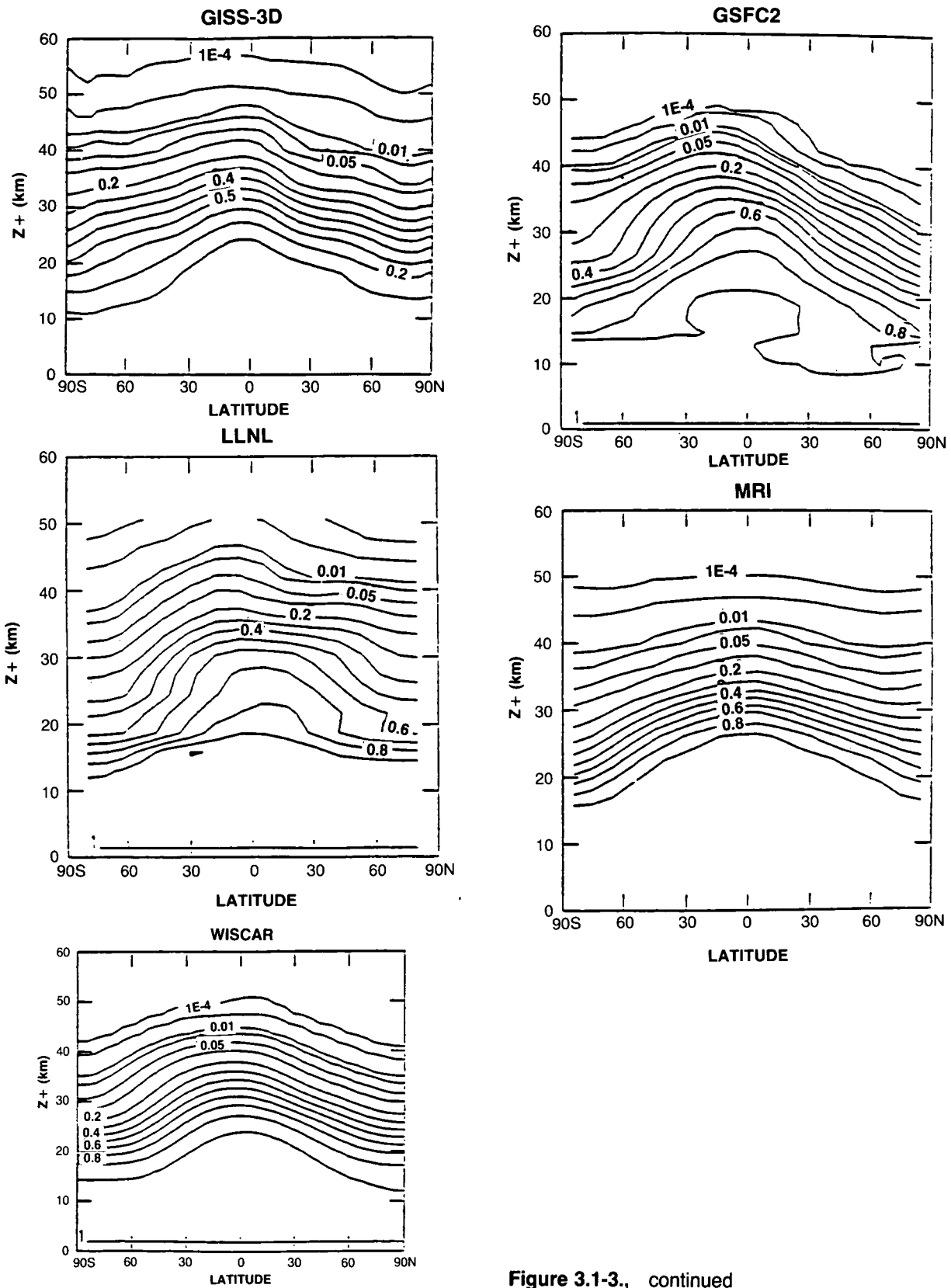


Figure 3.1-3., continued

The classic comparison of model with model and of model with observation is that of ozone column: a minimum in the tropics and a maximum at high latitudes in spring at the pole in the north and offset from the pole (60°S) in the south. In the 2-D models, that quantity is not always useful to intercompare because modelers often use the observed column ozone as a critical test and do not accept a new version of the model (e.g., new chemistry, circulation, diffusion) until it is able to simulate reasonably the observed seasonal and latitudinal patterns in ozone column.

In addition to ozone, the workshop examined the predicted stratospheric column abundances of HNO_3 , HCl , and NO_2 , for which observations of the latitudinal gradients are available. These columns are sensitive to transport and chemistry in the lower stratosphere. For the tropospheric source gases, N_2O , CH_4 , CH_3Cl , CCl_4 , CFCl_3 , and CF_2Cl_2 , we examined their patterns of decrease in the stratosphere which is sensitive to transport and chemistry in the upper and middle stratosphere.

Intercomparison of the faster photochemistry used latitude-by-altitude cross sections of some short-lived radicals (e.g., OH , HO_2 , ClO) and of some ratios (e.g., NO/NO_2 , ClO/HCl). The ratio ClO/HCl is a measure of the fraction of chlorine released from halocarbons that participates in catalytic ozone destruction. It is a result of the balance between several reactions: HCl with OH and subsequently Cl with O_3 to produce ClO , and the reverse sequence transforming ClO to Cl and subsequently Cl with CH_4 to form HCl . The ratio ClO/HCl (noontime or daytime averages for December) is shown in Figure 3.1-4. In the upper stratosphere (30–50 km) the models differ widely, and further examination of the other factors (e.g., OH , O_3 , CH_4 , NO) controlling this ratio is necessary.

The tropospheric simulations of the models were not specifically examined at the workshop. Differences in transport, chemistry, and heterogeneous removal processes within the troposphere are likely to affect some of the stratospheric results and are noted later in this section to introduce uncertainty into the assessment calculations.

A special topic of this intercomparison was the 40-km ozone “problem”: models systematically underpredict the observed abundance by amounts varying from 10 to 50%. The concentration of ozone between 40 and 50 km is expected to be under photochemical control and to involve well-known catalytic loss cycles. As part of the intercomparison, participants contributed detailed tables of photochemical rates for the ozone budget at 3 mbar (Equator in March) from their simulation of the current atmosphere, see Table 3.1.2. The J-value for O_3 determines the ratio O/O_3 and hence the loss rate for odd-oxygen. Reported values varied by as much as 22%, resulting from inherent differences in the calculations of J-values (noted above) and from the different column abundances of ozone above 40 km in the model simulation of the current atmosphere. Production rates for odd-oxygen vary by only 3% across the five participating models; however, the loss rates attributed to individual families (HO_x , NO_x , Cl_x) vary by as much as 50%. Different factors are involved; due to the large variations in background gases (e.g., 50% in NO_y) and in family abundances, the cause of these differences could not be determined at the meeting. A re-examination of the 40-km problem will be part of the next intercomparison.

3.1.3.6 Predictions of Future Ozone

Only a limited number of ozone perturbations using hypothetical scenarios for future atmospheric composition were completed for this workshop. The comparisons focused on changes in ozone, temperature, and stratospheric circulation. A comparison of predicted ozone perturbations (not available for the workshop) is presented in Section 3.2.

THEORETICAL PREDICTIONS

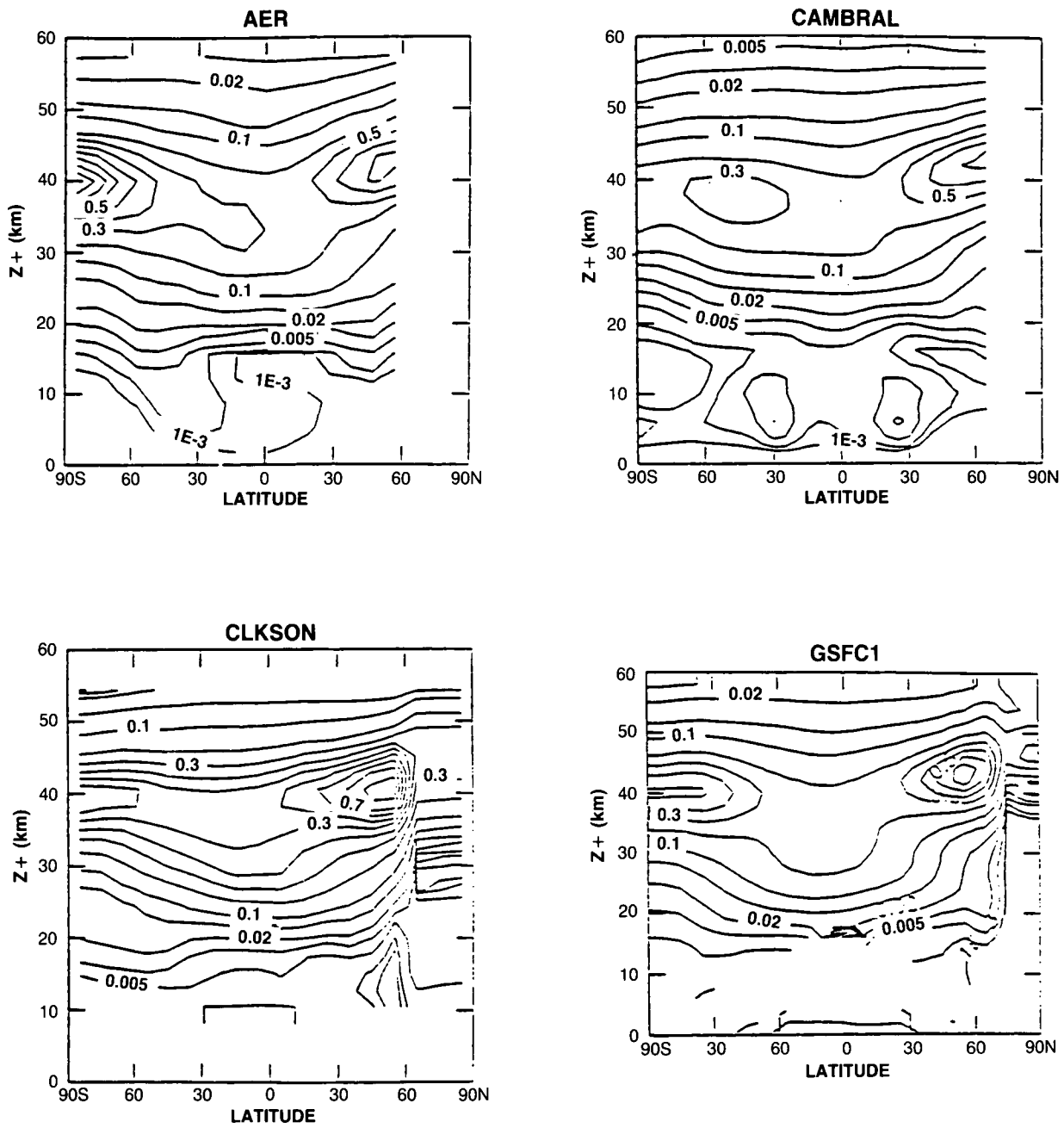


Figure 3.1-4. Two-dimensional distribution of the ClO/HCL ratio from nine models. Eight of the models (AER, CAMBRAL, CLKSON, GSFC2, LARC, MRI, NOCAR, and OSLO) show December values, while one model (GSFC1) shows January values.

THEORETICAL PREDICTIONS

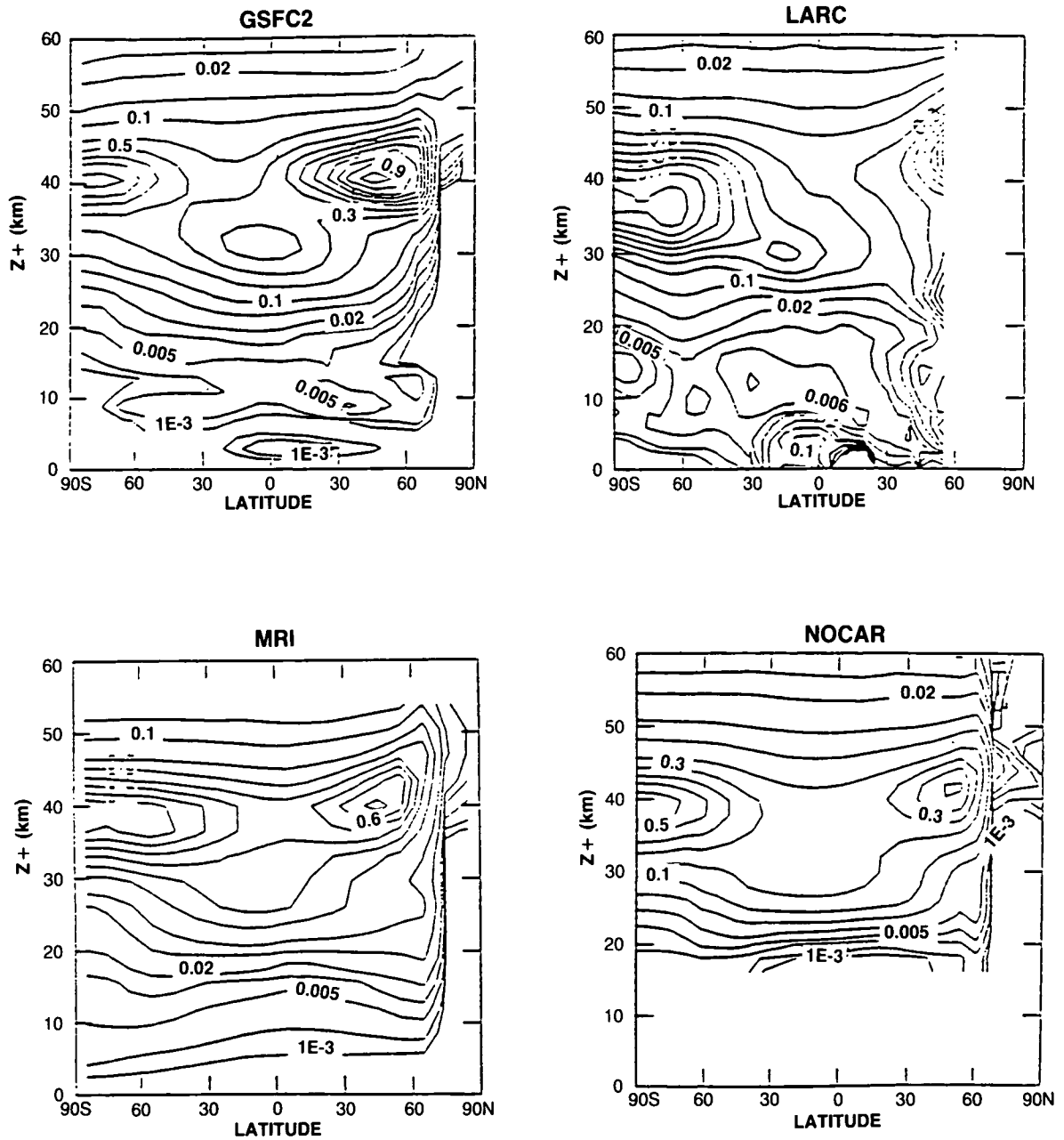


Figure 3.1-4., continued

3.1.3.7 Summary

The recent intercomparison (Jackman, et al., 1989b) overcame many technical obstacles in allowing a direct one-to-one comparison of results from many different models. The modeling community submitted their results in digital form to a central facility operated by Robert Seals at NASA/Langley where the calculations were re-gridded and plotted on a standard grid scale (e.g., Figures 3.1-3 and 3.1-4). The ability

THEORETICAL PREDICTIONS

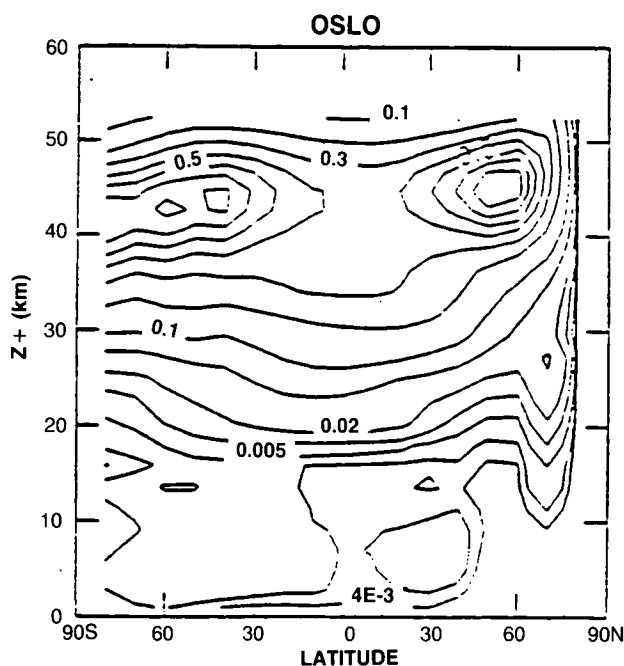


Figure 3.1-4., continued

Table 3.1-2. Comparison of ten rates and species at 3 mb, Equator, in March from five modeling groups

Group	P(tot) cm ⁻³ day ⁻¹	L(O _x) cm ⁻³ day ⁻¹	L(HO _x) cm ⁻³ day ⁻¹	L(NO _x) cm ⁻³ day ⁻¹	L(Cl _x) cm ⁻³ day ⁻¹	J(O ₃ tot) sec ⁻¹	O ₃ ppmv	H ₂ O ppmv	NO _x ppbv	Cl _x ppbv
AER	4.49(11) ^a	8.12(10)	5.85(10)	2.30(11)	7.78(10)	1.00(-3)	5.82	4.50	17.8	2.23
GSFC1	4.72(11)	7.74(10)	6.32(10)	2.49(11)	8.73(10)	9.64(-4)	5.83	4.88	18.9	2.36
GSFC2	4.74(11)	9.14(10)	6.79(10)	2.38(11)	7.82(10)	9.57(-4)	6.04	5.03	18.2	2.01
LLNL	4.52(11)	8.10(10)	6.53(10)	2.20(11)	7.79(10)	1.12(-3)	4.85	4.95	23.0	2.26
MRI	4.61(11)	6.53(10)	7.03(10)	1.80(11)	1.26(11)	1.17(-3)	4.74	5.69	14.8	2.48

^a4.49(11) means 4.49 × 10¹¹

to make such detailed comparisons helped to identify structural differences in model transport and photolysis rates. The meeting has spawned two subgroups with the objective of resolving the differences in the calculation of J-values and heating rates.

The next intercomparison will probably focus on model intercomparisons for the present atmosphere, with emphasis on matching models with observations. One task, for example, will likely be an examination of the transport of long-lived tracers in the winter polar vortex as identified by the recent aircraft campaigns to the Antarctic and Arctic (see Chapter 1 on Polar Ozone).

3.1.4 Comparison Between Model Calculations and Observations

An important prerequisite for the models used in any ozone assessment is that they represent with sufficient accuracy the present distributions of the atmospheric trace gases. The purpose of this section is therefore to examine how well the models reproduce a limited number of observations and to highlight areas of agreements and disagreements between calculated and observed distributions.

Different types of comparisons between models and observed data can be achieved. For example, to validate at the same time the treatment of the transport and the formulation of chemistry in the model, the comparison with data has to be made on the global scale and involve species measured on a continuous basis by space-borne instruments.

In this brief section, we will focus on a comparison between the meridional distributions of trace gases calculated by some of the 2-D models involved in this assessment and the corresponding zonally averaged distributions of these constituents derived from satellite observations (SBUV, LIMS, SAMS). In addition, Dobson maps produced by the different models will be compared with ozone column abundances derived from TOMS data.

In Figure 3.1-5, the distribution of nitrous oxide observed by SAMS is compared to the corresponding distribution calculated by the GSFC2 model. This gas, emitted by the Earth's surface, is transported into the stratosphere, and destroyed by photolysis and reaction with O(¹D). Therefore, the formulation of the chemical processes involved in the budget of this species makes the distribution of this gas relatively

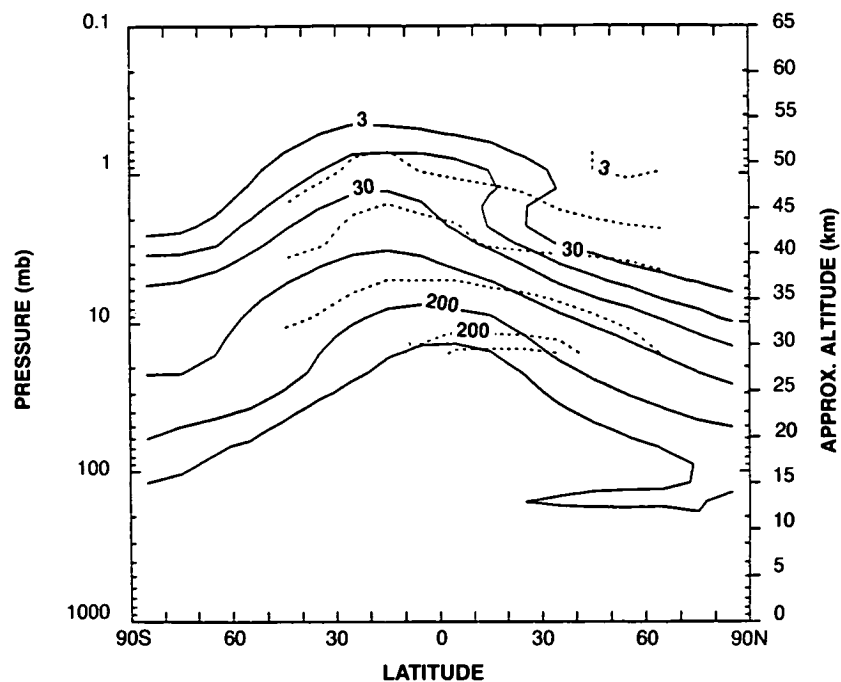


Figure 3.1-5. Zonally and monthly averaged distribution of nitrous oxide (ppbv) observed (dashed lines) in January 1979 by SAMS (on board the Nimbus-7 satellite) and calculated (solid lines) by the GSFC2 two-dimensional model.

THEORETICAL PREDICTIONS

independent of that of other chemical constituents. The SAMS data cover only a limited altitude range (28 to 50 km) over which the mixing ratio varies from about 50 to 3 ppbv. The mixing ratio determined by this model compares relatively well with the observations, at least in qualitative terms. All models involved in the present assessment predict, for a given height, the largest concentrations to be over the tropics. The appearance of a double peak in the mixing ratio isolines, observed for example in April and May, is usually not reproduced by the models. This feature is believed to result from momentum deposition in the tropics by Kelvin and mixed Rossby-gravity waves (Gray and Pyle, 1987).

The same type of conclusions can be drawn for methane. As to nitrous oxide, methane is released in the atmosphere at ground level but, in this case, the destruction of the molecule takes place already in the troposphere as well as in the stratosphere and is due to the action of hydroxyl radicals. The concentration of OH depends on a large number of factors and could therefore be different from model to model. The SAMS values cover an altitude range from about 32 and 57 km over which the mixing ratio varies from 1 to 0.2 ppmv. These observed data are again compared to the GSFC2 model (Figure 3.1-6). Again the agreement is good in January: the mean vertical distribution as well as the latitudinal gradient in the mixing ratio are well reproduced by the model. The problem of the double peak, already mentioned for nitrous oxide, also exists in the case of methane.

Figures 3.1-7(a, I, J, R) present the mixing ratio of nitrogen oxides ($\text{NO} + \text{NO}_2$) from the models developed at MRI and at the University of l'Aquila and at the Central Aerological Observatory and the Leningrad Institute for Meteorology and Hydrology (CAO/LIMH, USSR), as well as the mixing ratio of nighttime NO_2 observed by LIMS (which should be very similar to the 24-hour averaged mixing ratio of $\text{NO} + \text{NO}_2$ because of the rapid chemical conversion of NO into NO_2 after sunset). The observations suggest that the mixing ratio of NO_x reaches its maximum value (16–20 ppbv) over the tropics near 38 km

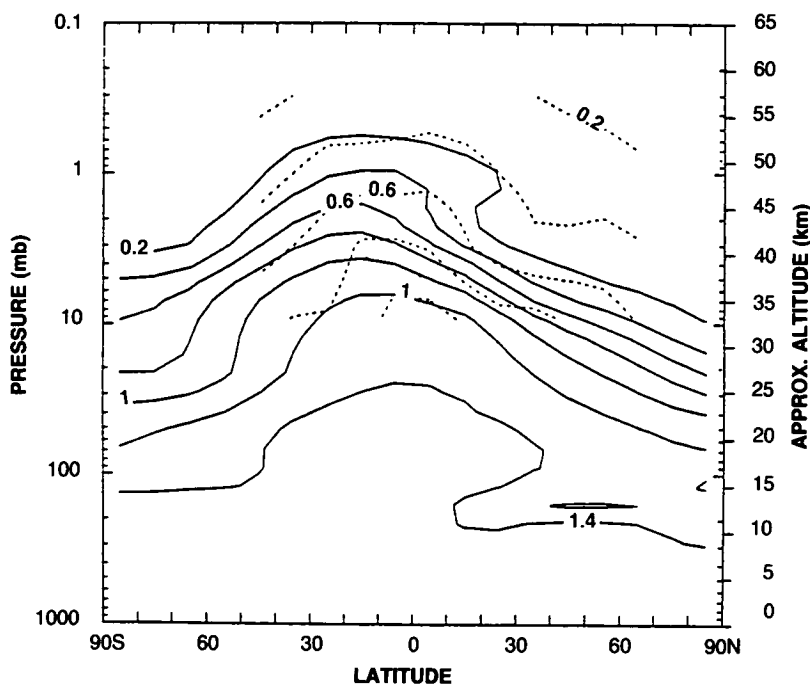


Figure 3.1-6. Same as in Figure 3.1-5 but for methane (ppmv).

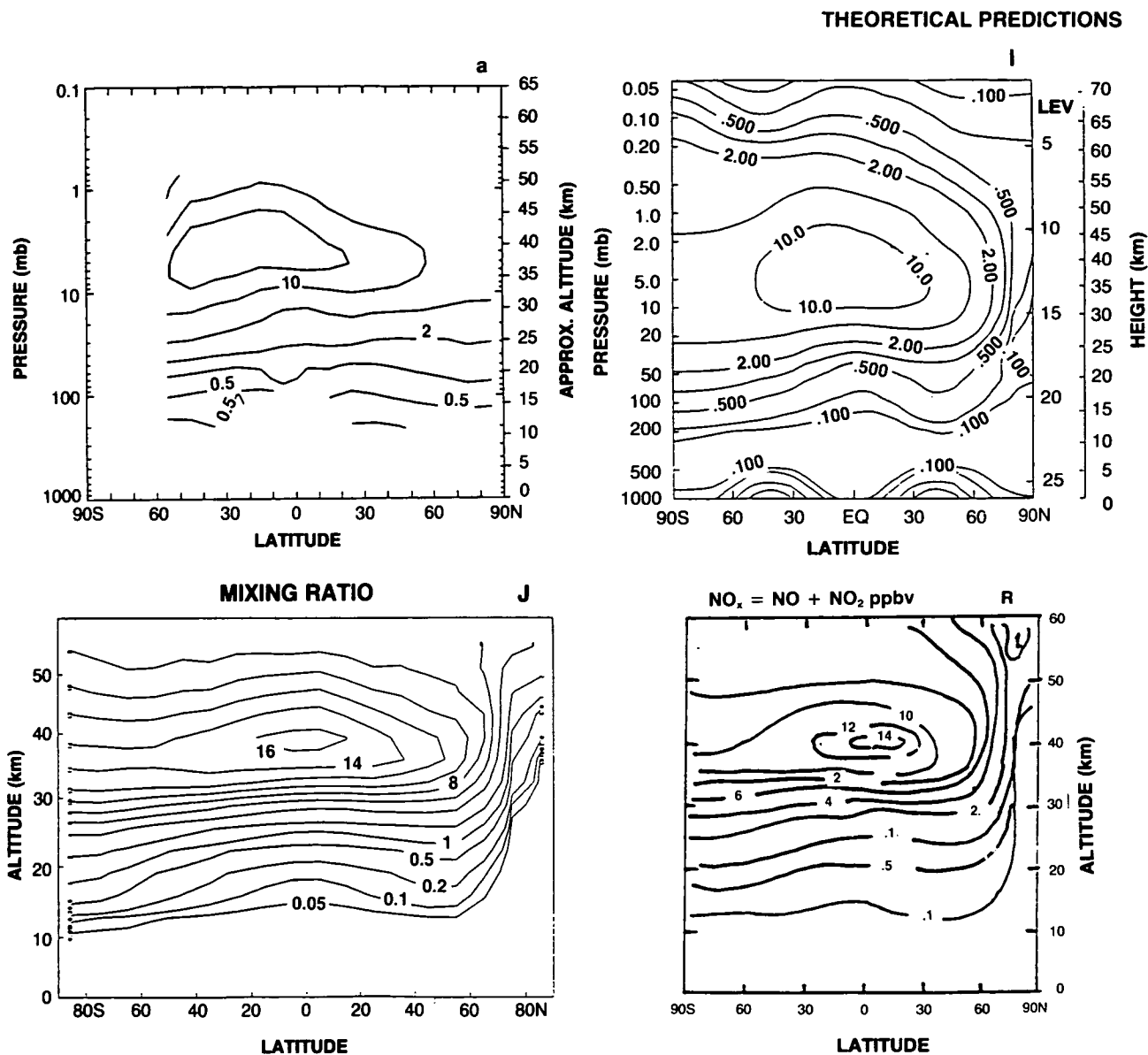


Figure 3.1-7. Zonally and monthly averaged distribution of nighttime NO_2 (ppbv) observed in January 1979 by LIMS (on board the Nimbus-7 satellite) and distributions of $\text{NO}_x = \text{NO} + \text{NO}_2$ derived for January by different two-dimensional models. Note that nighttime densities of NO_2 should be very similar to 24-hour average NO_x densities. Codes for the different models are listed in Table 3.1.1.

altitude. From this height down to the tropopause level, the mixing ratio decreases by more than a factor of 50. The same type of behavior is found in the model. Significant differences however are observed in the lower stratosphere, where the distribution of odd nitrogen is largely determined by the strength of the poorly known sources of NO_x in the upper troposphere and the strength of vertical and meridional transport in the vicinity of the tropopause.

Shown in Figures 3.1-8(a, W) are the distributions of nitric acid observed by LIMS and derived by the WisCAR model. In both cases the maximum mixing ratio near 25 km altitude is of the order of 2 ppbv over the Equator and increases with latitude to values on the order of 5–8 ppbv over the summer pole and

THEORETICAL PREDICTIONS

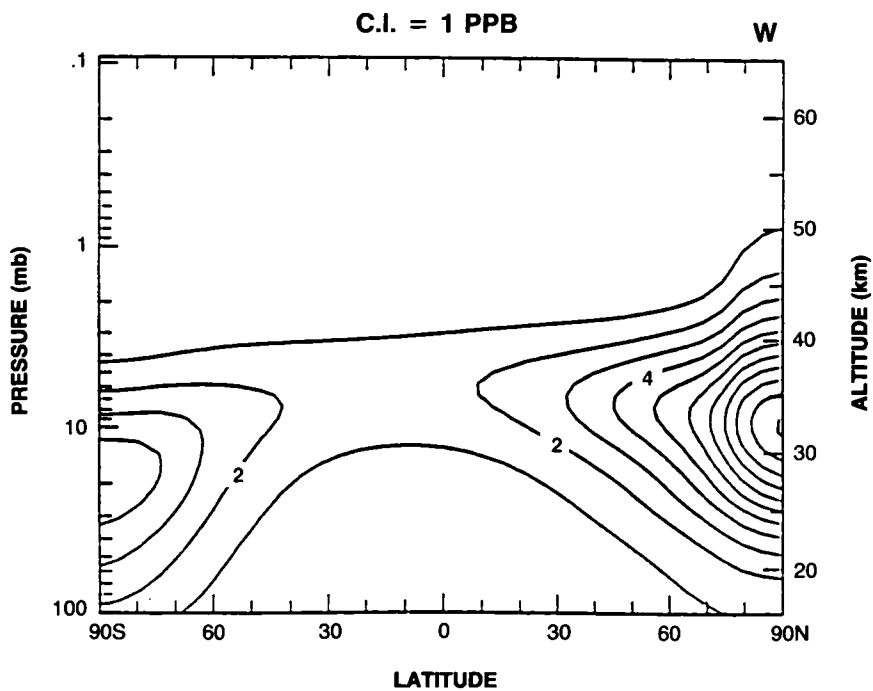
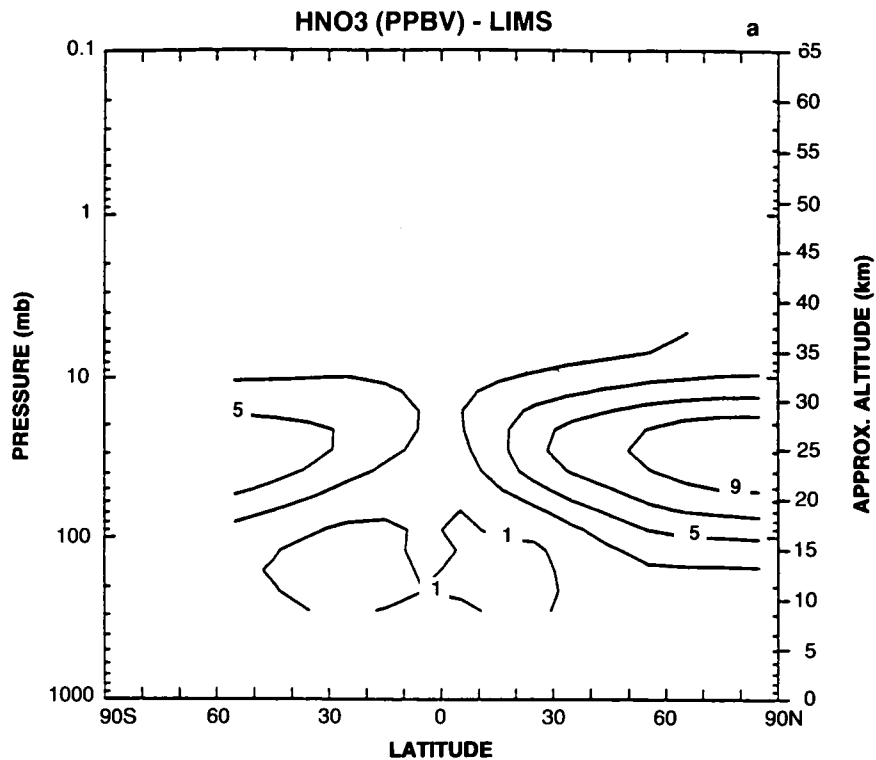


Figure 3.1-8. Same as in Figure 3.1-7 but for nitric acid (ppbv).

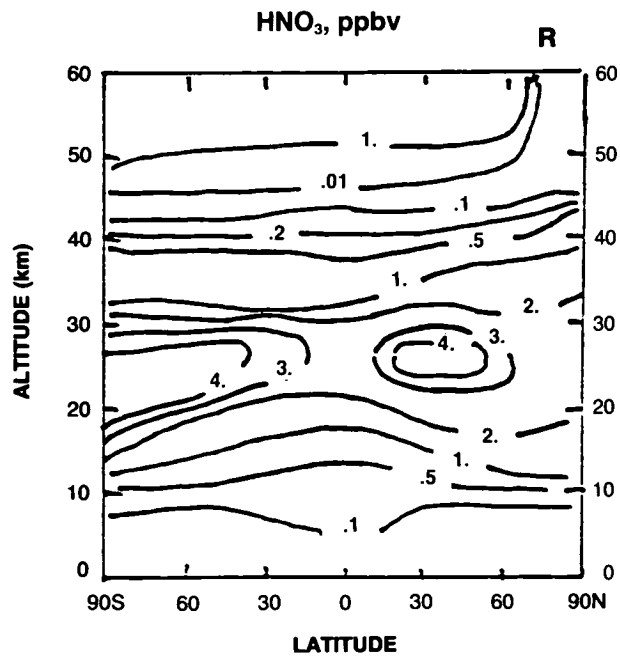
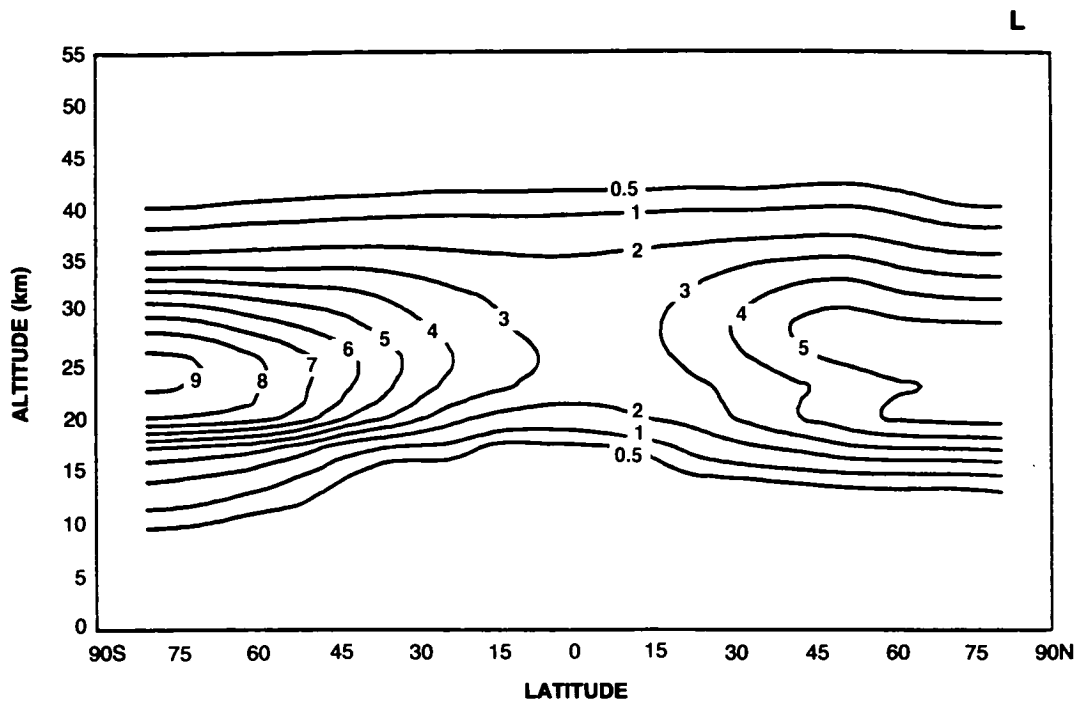


Figure 3.1-8., continued

THEORETICAL PREDICTIONS

10–12 ppbv over the winter polar region. This relatively good agreement is obtained because, in this particular model, a polar night conversion from N_2O_5 into HNO_3 with a time scale of 20 days has been added to the chemical scheme to account for heterogeneous processes occurring on the surface of water particles at high latitudes in winter. Other models such as the LLNL model or the CAO/LIMH model (Figure 3.1-8L and R) when they do not include such a conversion in their chemical scheme, produce the high-latitude maximum HNO_3 mixing ratio in summer rather than in winter.

The distributions of the ozone mixing ratio measured by SBUV and calculated by different models are shown in Figures 3.1-9(a, A, C, I, J, L, O, R, U, W). In general, the agreement between observed and theoretical distributions is fairly good: the maximum mixing ratio located over the Equator near 30–35 km altitude is well represented, the overall meridional distribution of the calculated ozone field is very similar to the observed one. However, most models underestimate the ozone density near 40 km altitude. This long-standing problem has not yet been solved and requires additional work. It should be noted at this point that none of the models discussed here includes the effects of heterogeneous chemistry, so that the “ozone hole” over Antarctica cannot be produced in any model simulation.

Finally, the ozone column displayed as a function of latitude for each month of the year and expressed in Dobson units is shown in Figures 3.1-10(a, A, C, G, I, J, L, O, U, W). The observed values are obtained from the TOMS data. The observations exhibit a minimum column abundance of less than 260 Dobson units in the tropics and the highest values in spring in both hemispheres. In the Northern Hemisphere, this maximum reaches 440 Dobson units and is located over the North Pole. In the Southern Hemisphere, the maximum, located at 60°S is of the order of 380 Dobson units. The models generally show the same type of distributions; differences are largely due to the strength of the meridional transport in the lower stratosphere during the different seasons.

There are hemispheric differences in the wintertime poleward transport. Although in some models there are ad hoc adjustments to transport parameters so that the model behavior will reflect measurements, there are efforts to calculate transport as a consistent representation of circulation and diffusion (see, e.g., Newman et al., 1988; Jackman et al., 1988, 1989; Hitchman and Brasseur, 1988; etc.).

To validate the details of the chemical kinetic scheme used in a given model, it is useful to compare (for a given altitude, latitude, and time of the day) the concentration ratio of species belonging to the same chemical family (e.g., NO_x , Cl_x). In this respect, simultaneous measurements of the concentrations of chemically active trace gases such as those performed by the ATMOS experiment (Raper et al., 1987; Russell et al., 1988) are extremely useful. Figures 3.1-11a and b show, for example, the ATMOS measurements at 30°N between April 30 and May 1, 1985 together with a simulation of the individual odd nitrogen and odd chlorine species made by the Harvard one-dimensional model (McElroy and Salawitch, 1989) for local sunset conditions. The model adopted ATMOS data for O_3 , H_2O , CH_4 and the total amount of odd nitrogen and inorganic chlorine. This work thus provides a test of our understanding of the photochemical processes governing the partitioning between the individual nitrogen and chlorine species. The agreement is rather good for all species measured in the Northern Hemisphere, with the exception of ClONO_2 , for which the model profile falls off much more slowly with height than the observed profile. A recent study by Natarajan and Callis (1989), using the LIMS and ATMOS data to constrain the levels of odd nitrogen and odd chlorine in their model, finds no major discrepancy between calculated and observed ozone (less than 20%) below 52 km.

In conclusion, the 2-D models involved in the present assessment generally reproduce the patterns observed in the ozone column, with a minimum in the tropics and maxima at high latitudes in the spring of

THEORETICAL PREDICTIONS

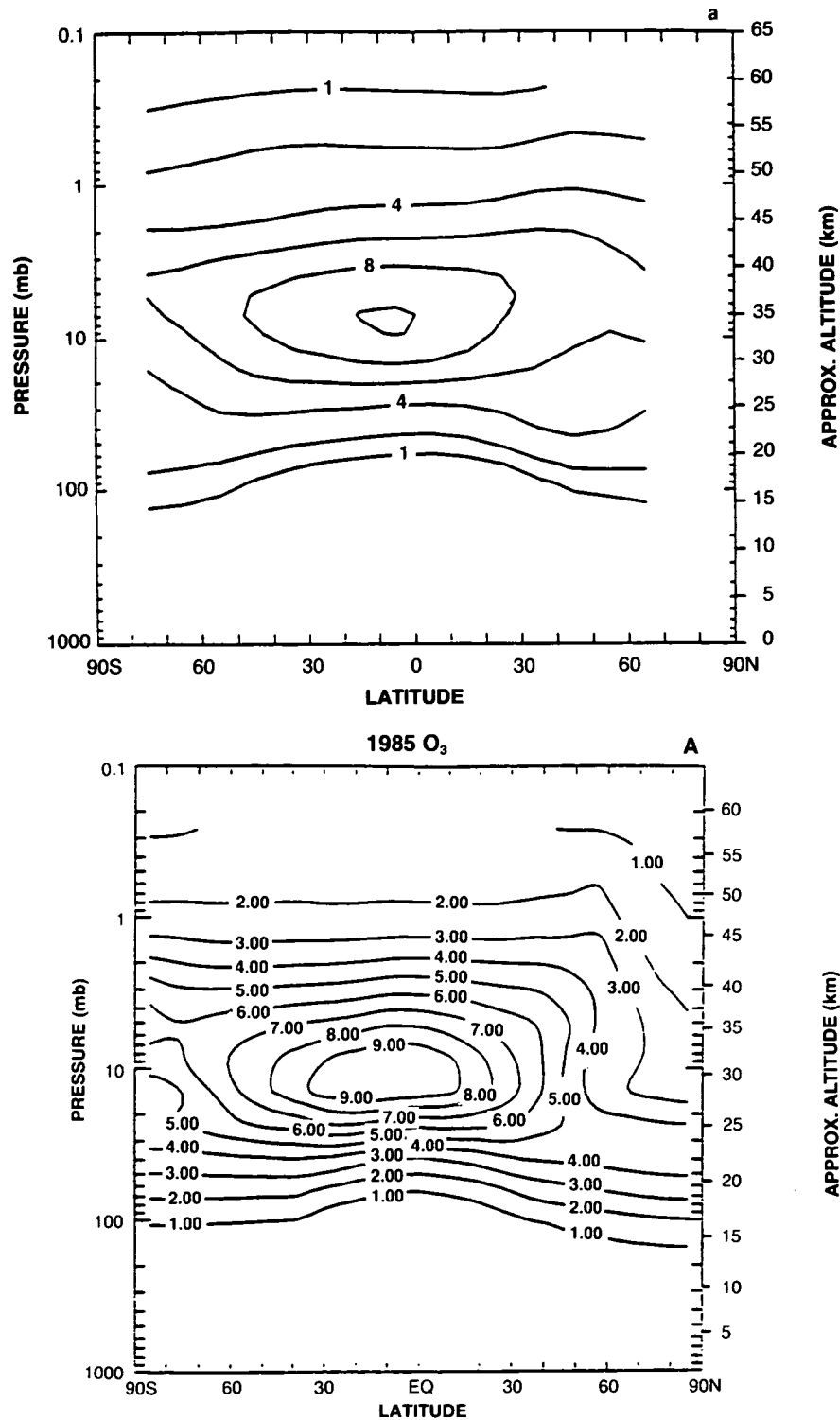
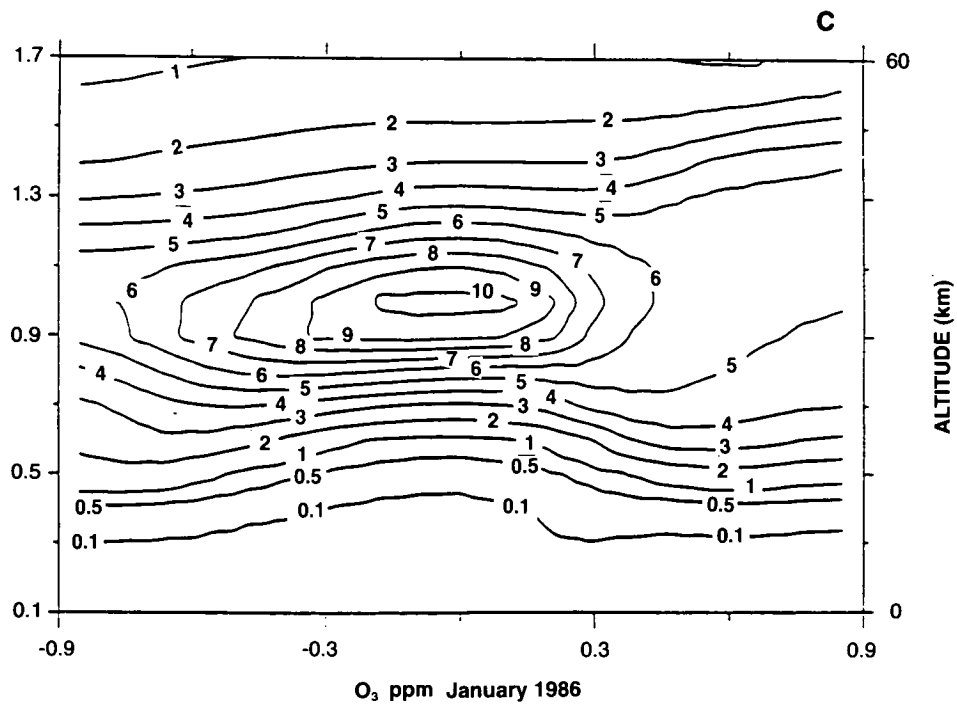


Figure 3.1-9. Zonally and monthly averaged distribution of ozone for January (based on data obtained by SBUV, on board Nimbus-7, in 1979, 1980, and 1981) and distributions of ozone derived for January (or December) by different two-dimensional models. Mixing ratios are expressed in ppmv. Codes of the different models are given in Table 3.1.1. In the case of the NSU model number densities expressed in cm^{-3} are displayed.

THEORETICAL PREDICTIONS



X AXIS • 10² Y AXIS • 10

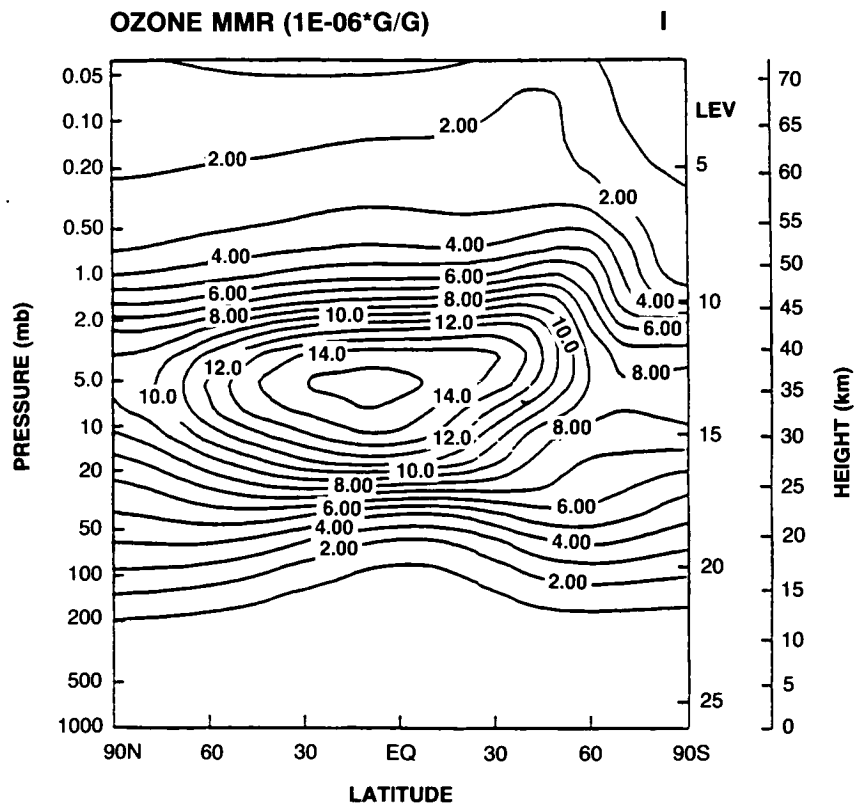


Figure 3.1-9., continued

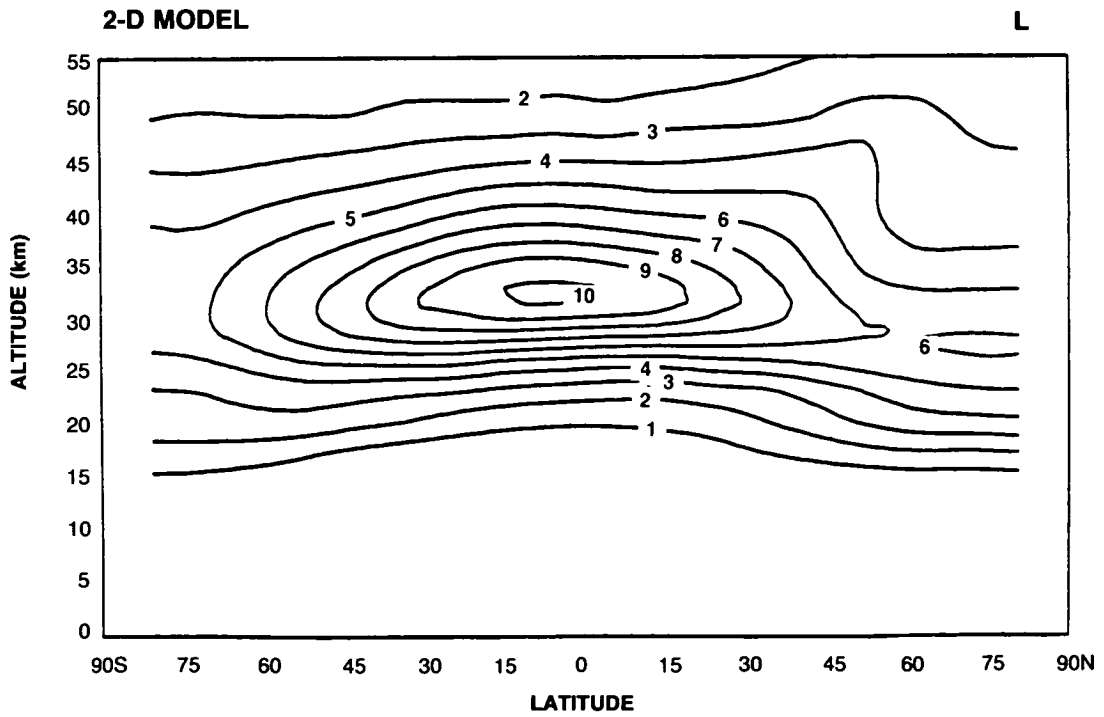
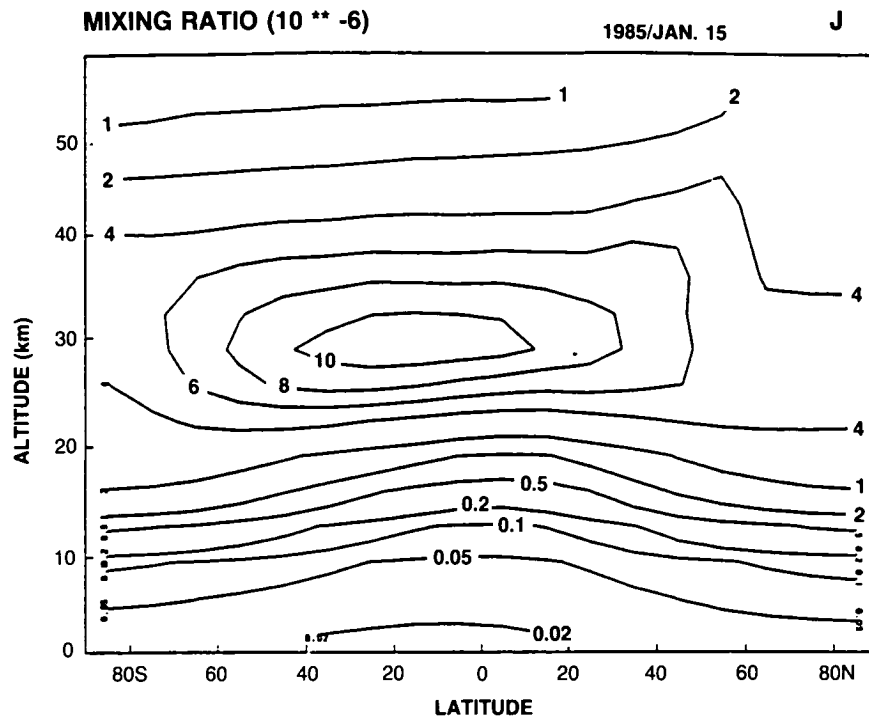


Figure 3.1-9., continued

THEORETICAL PREDICTIONS

O

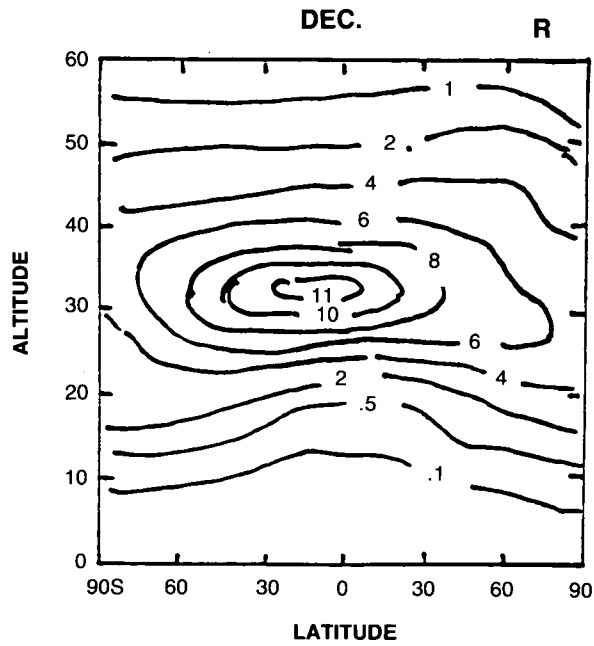
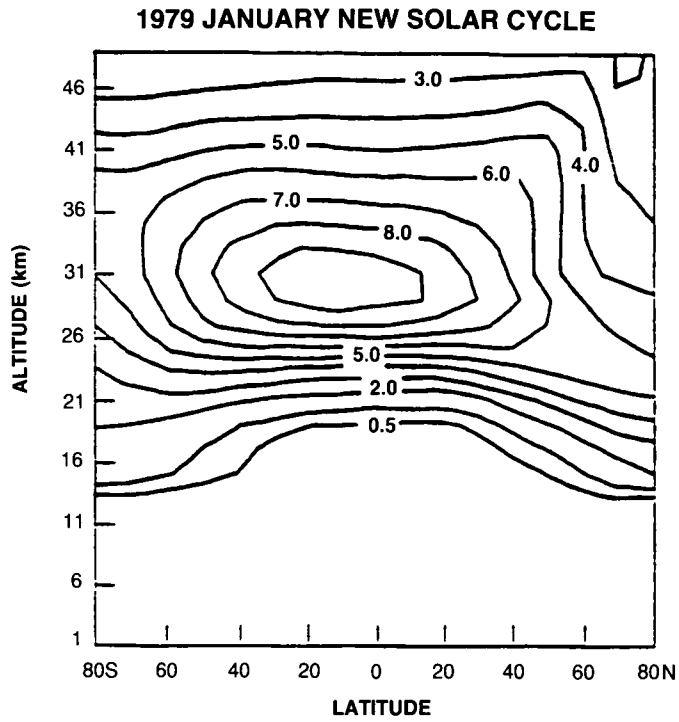


Figure 3.1-9., continued

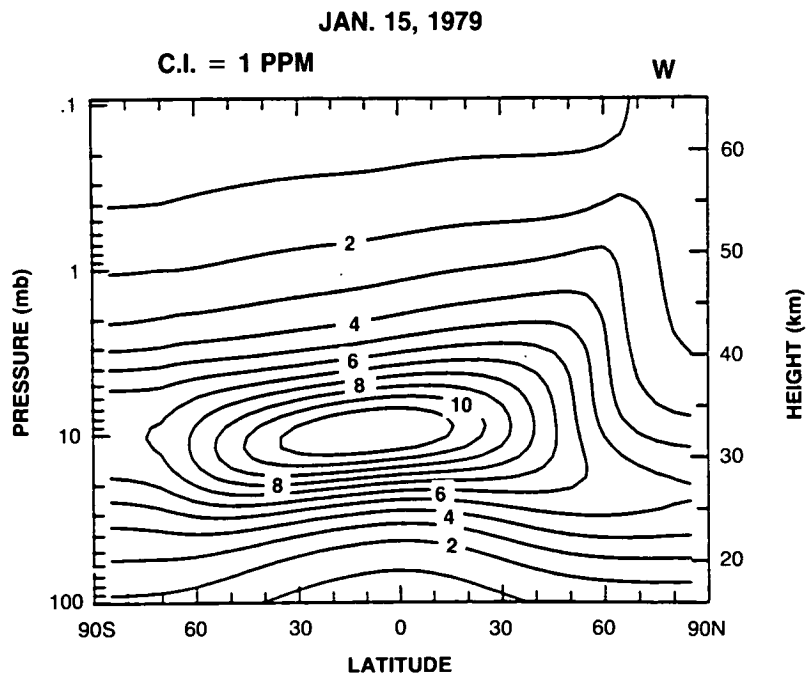
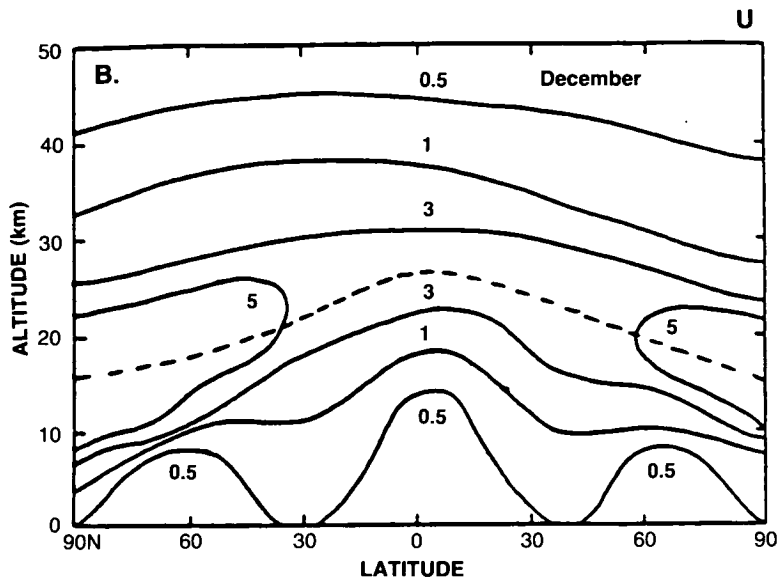


Figure 3.1-9., continued

THEORETICAL PREDICTIONS

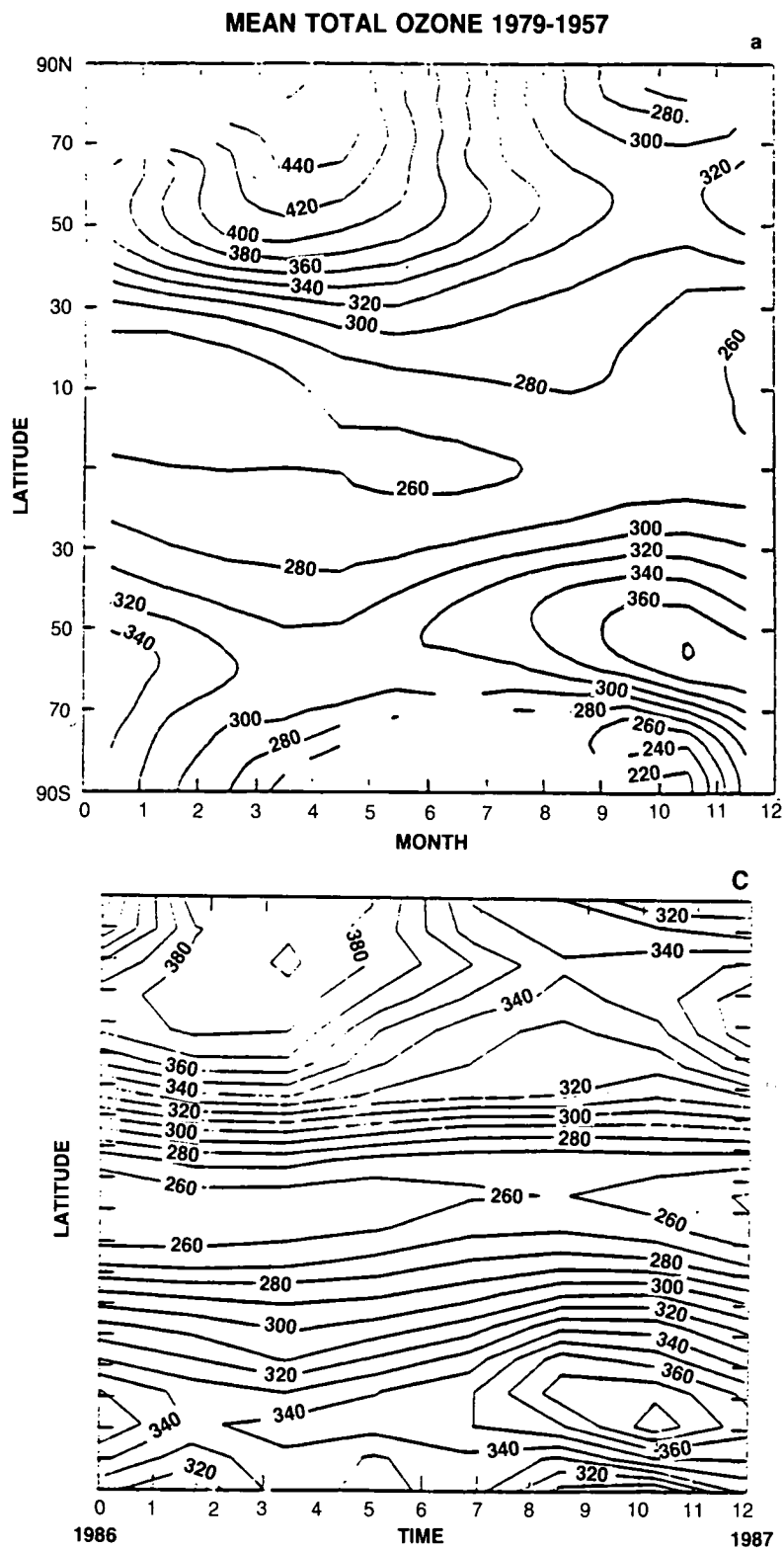
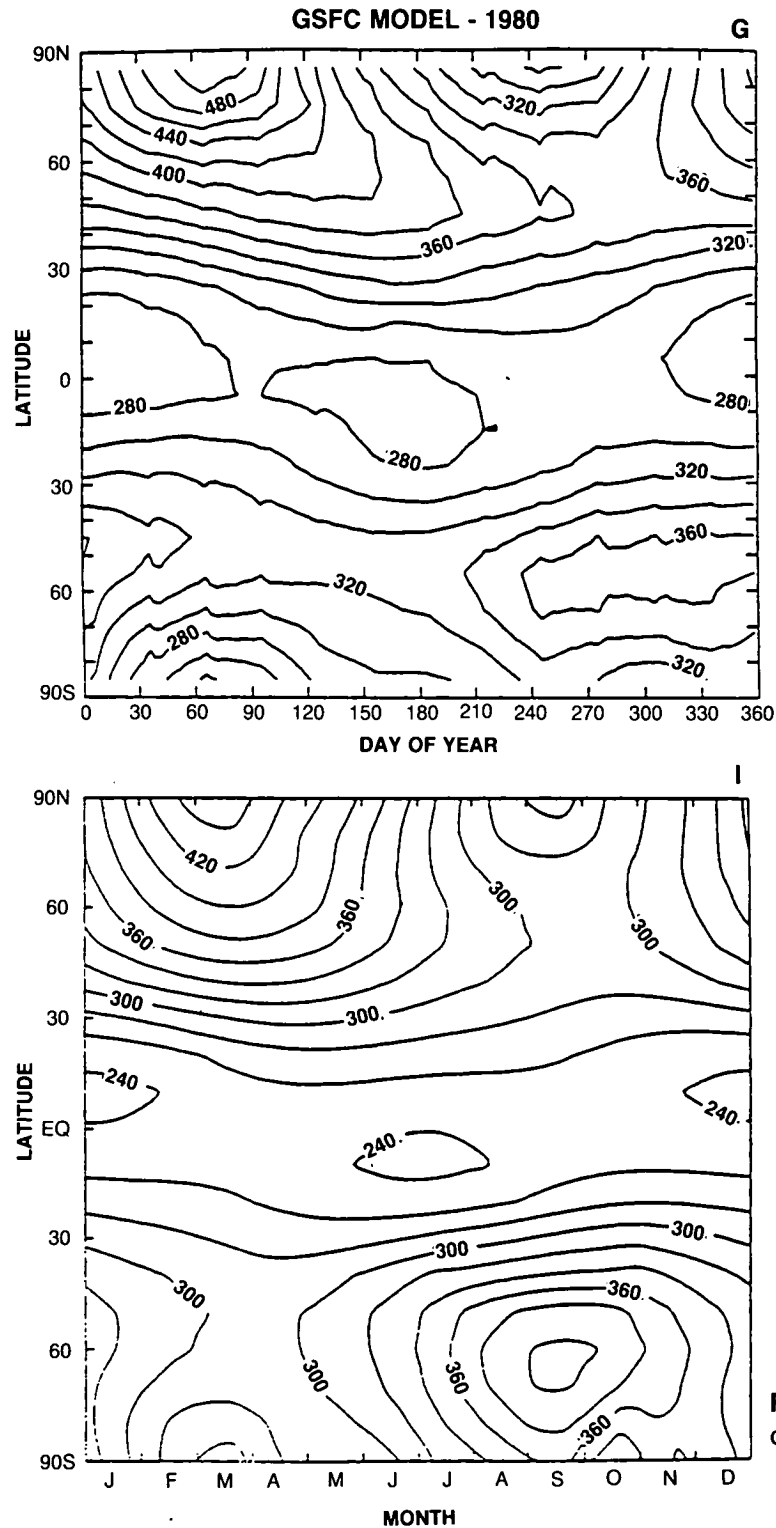


Figure 3.1-10. Latitudinal and seasonal variation of the ozone column abundance (Dobson) based on satellite observations (TOMS) and different model calculations.



both hemispheres. The meridional distribution of ozone is also in good agreement with satellite observations. Discrepancies however are noted; in particular, the models systematically underestimate ozone in the upper stratosphere. Calculated and observed distributions and seasonal variations of species such as nitrous oxide, methane, nitric acid and nitrogen oxides are in qualitative agreement, although substantial

THEORETICAL PREDICTIONS

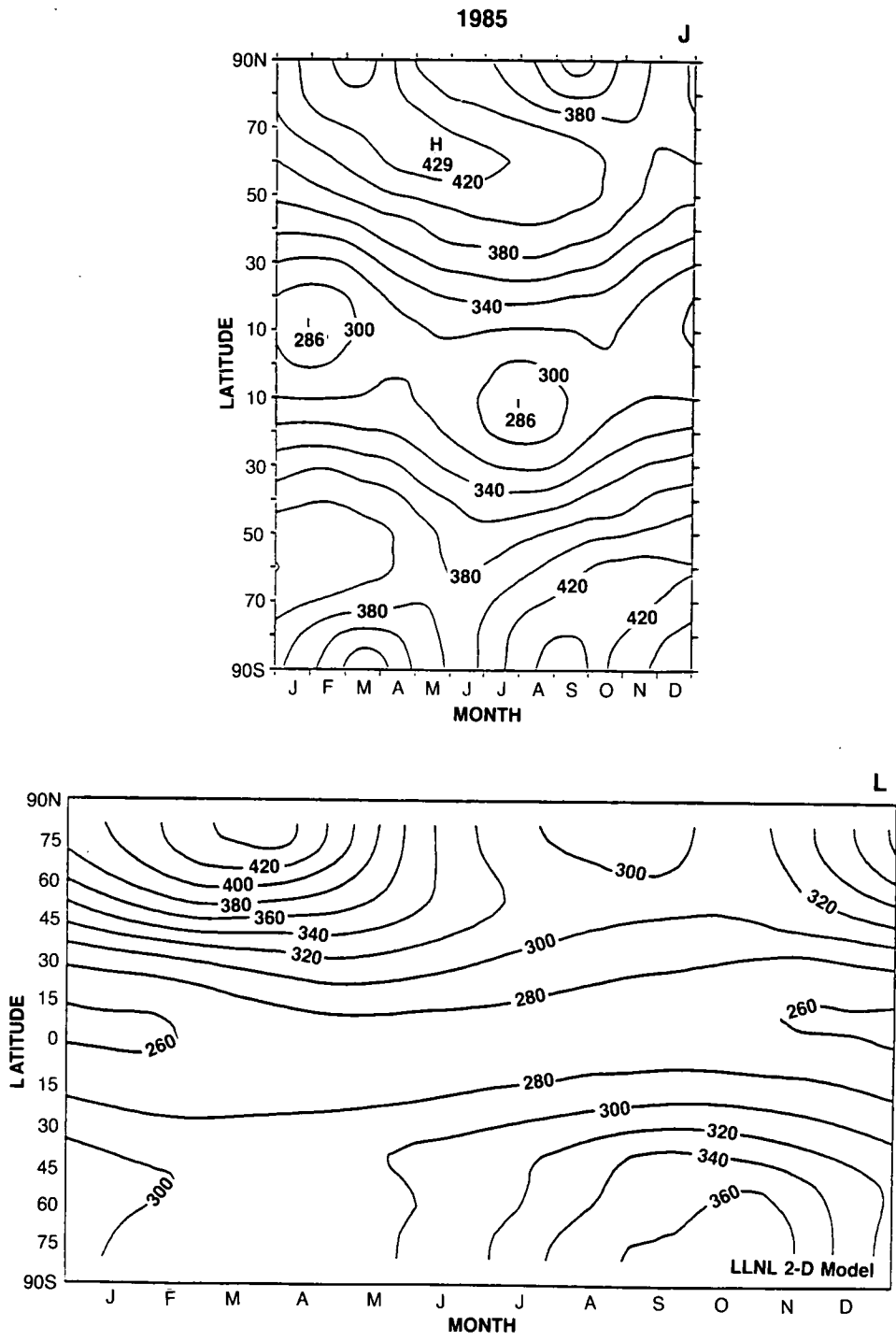


Figure 3.1-10., continued

THEORETICAL PREDICTIONS

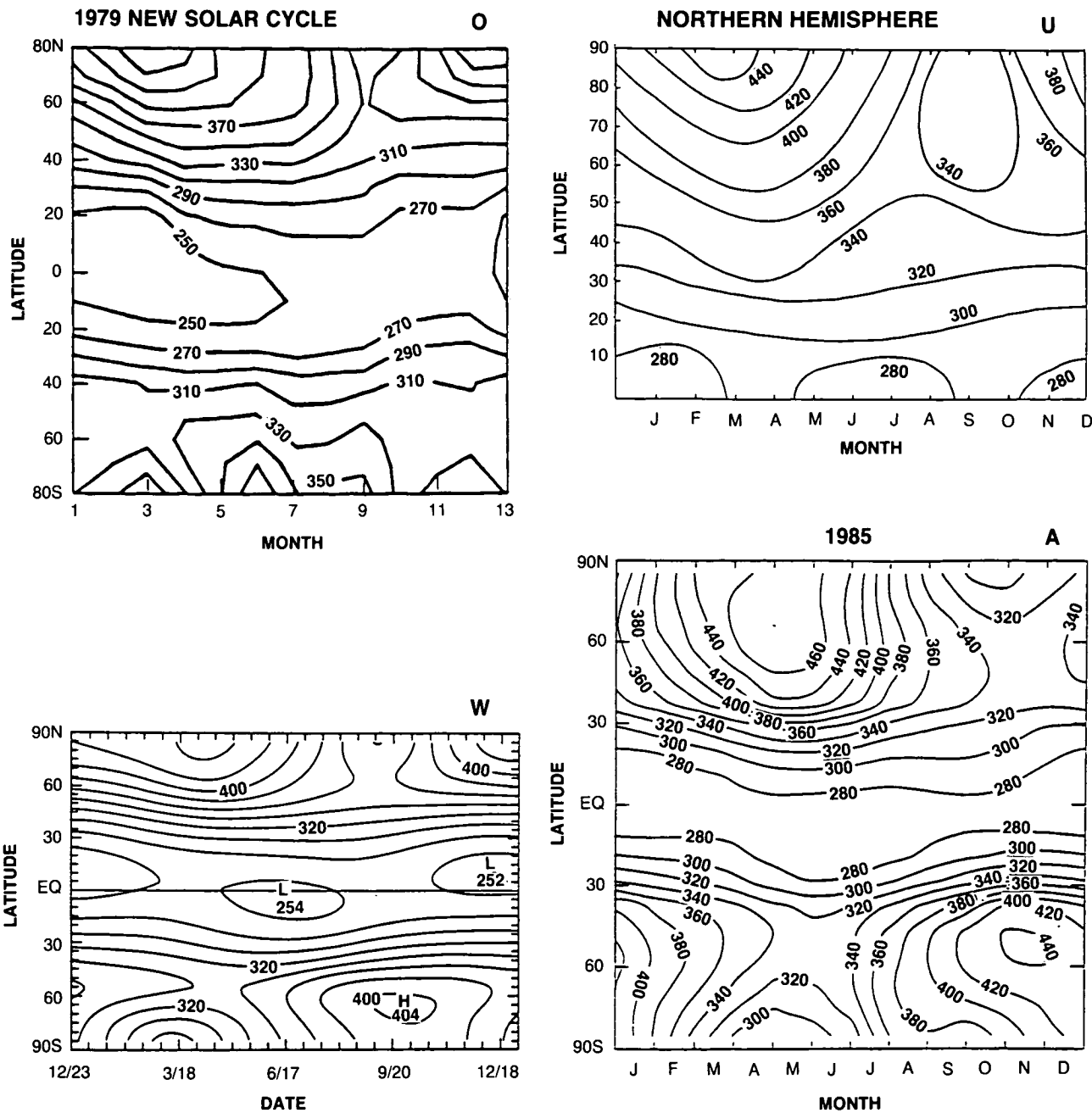


Figure 3.1-10., continued

quantitative differences are found in certain cases. The differences noted between models and observations should be attributed to deficiencies in the chemical scheme, in the radiative transfer codes, or in the transport formulation. Additional work will be performed in the future to improve these models and to validate them with measurements made from space observing systems.

THEORETICAL PREDICTIONS

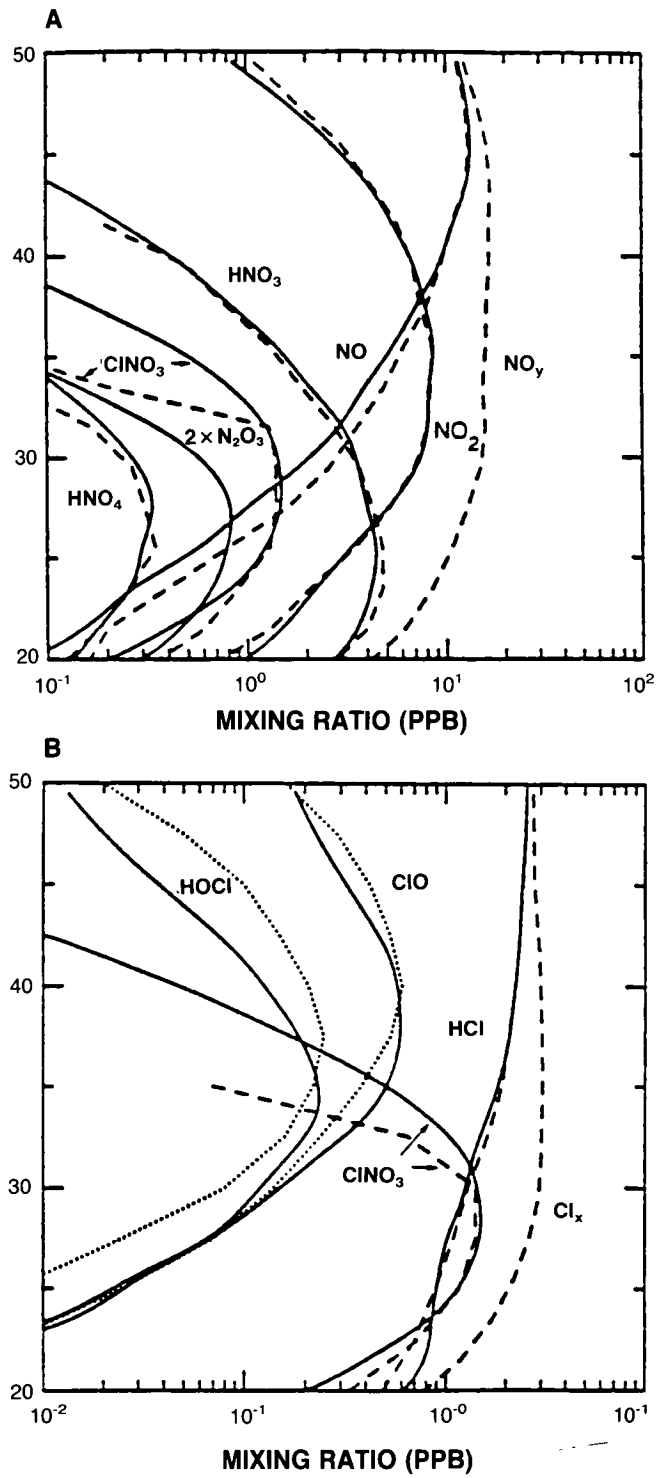


Figure 3.1-11. Comparison between one-dimensional mixing ratio profiles of chemically active trace gases measured by ATMOS at 30°N between April 30 and May 1, 1985, and a model of the odd nitrogen and odd chlorine species in the stratosphere (McElroy and Salawitch, 1989).

3.2 MODEL PREDICTIONS

3.2.1. Projected Scenarios for Halocarbons and Trace Gases

3.2.1.1 Introduction and Definitions

The future composition of the atmosphere will depend on the rate at which we continue to emit some halocarbons and other trace gases. Atmospheric composition will respond also to changes in the global biosphere (i.e., natural sources) and in atmospheric chemistry (i.e., chemical sinks). The calculations presented here examine the impact of global policies that would curtail the use of chlorofluorocarbons controlled under the Montreal Protocol.

We present here a set of projections, or scenarios, for the future atmosphere that focus on halocarbons. These scenarios are not intended to present a formal scientific assessment of future atmospheric composition, but have been chosen to give a spectrum of cases for studying the response of stratospheric ozone to a range of chlorine loading of the atmosphere. The Montreal products are distinguished from other halocarbons, and in these scenarios HCFC-22 acts as a surrogate for all CFC replacement products (except for the halons, which we assume have no brominated replacement). Tropospheric average mixing ratios are specified for all gases except the Montreal products and their replacement (HCFC-22); for these gases projected histories of atmospheric emissions are defined.

The scenarios are designated by letters A through D with a number 1–4 for alternate cases and are defined in Table 3.2-1. The most simply defined scenario, A1, has been designated the Reference Scenario since all other scenarios can be easily defined relative to it. Scenario A1 assumes that currently observed trends in CO₂, CH₄, N₂O, CCl₄, and CH₃CCl₃ will continue and that future emissions of the Montreal products (defined here as CFCs 11, 12, 113, 114, 115, and the halons 1211 and 1301) will remain fixed at the production levels estimated for 1985. We assume steady growth in industrial activity, and with it, a slow but sustained growth in emissions of HCFC-22, CCl₄, and CH₃CCl₃. Increases in CH₄ have been shown in previous assessments to counteract the effect of high chlorine levels on stratospheric ozone; and thus, we consider an alternate scenario A2 in which CH₄ concentrations do not increase after 1985. While this seems unlikely in the immediate future, we have not yet identified the cause of the current CH₄ increases, nor uniquely ascribed them to human activity.

A sequence of three basic scenarios—B, C, and D—examines the impact of a global reduction by the year 2000 in the production/emission of Montreal products by 50% (B1), 85% (C1), and 95% (D1). The history of trace gas mixing ratios for these scenarios is shown in Figure 3.2-1; and the total chlorine and bromine loading of the atmosphere in Figure 3.2-2 and Table 3.2-4. One can see that without draconian reductions in Montreal products (scenarios C and D), it would be difficult to keep chlorine levels from doubling by the middle of the next century. In order to study a scenario in which chlorine returns to 1990 levels, we must impose controls to keep CCl₄ and CH₃CCl₃ fixed (D2), and furthermore, not use a halocarbon like HCFC-22 as a substitute for the Montreal products (D3). Once again, we consider the possibility of CH₄ concentrations remaining fixed at 1985 levels (D4).

None of the standard scenarios (A-D) gives a total atmospheric chlorine content (summed over all halocarbons) that returns by the year 2060 to 1985 levels of about 3 ppbv. It is interesting to note which different combination of halocarbon reductions could possibly yield a chlorine loading of less than 3 ppbv by 2060, and also whether chlorine levels prior to the onset of the Antarctic ozone hole (at most 2 ppbv) could be achieved by 2060 or later in the century with any combination of freezes or cuts in halocarbon

THEORETICAL PREDICTIONS

Table 3.2-1. UNEP Scenarios: 1960 through 2060

For the period 1960 to 1985, all trace gas concentrations are given as mixing ratios based on historical records or approximations thereof. For the period 1985 to 2060 a combination of mixing ratios and fluxes are specified.

A1. Reference Scenario

For the Montreal products (see Table 3.2-2b) we assume constant atmospheric emissions after 1985, using 1986 production as the atmospheric flux. For other trace gases (see Table 3.2-2a) we assume a simple linear rate of change in tropospheric concentration or a compounded growth rate. HCFC-22 uses a regression formula to integrate fluxes into mixing ratios. HCFC-22 has an independent market, is assumed to grow linearly in emissions (see Table 3.2-2b), and in addition is used as a surrogate for all substitutes for the Montreal products.

A2. Reference Scenario with CH₄ fixed at 1600 ppb.

B1. Reference Scenario with 50% reduction in Montreal products

The emission of Montreal products (Table 3.2-2b) is reduced by 10% of their 1995 values for each year from 1996 through 2000 (a total of 50%). Half of the reduction in Montreal products (in kg) is added on top of the reference scenario for HCFC-22 (in kg). There is no halogenated substitute for the halons 1211 and 1301.

C1. Reference Scenario with 85% reduction in Montreal products: same as scenario B1 with 17% reduction per year (total 85%).

D1. Reference Scenario with 95% reduction in Montreal products: same as scenario B1 with 19% reduction per year (total 95%).

D2. Scenario D1 with CCl₄ and CH₃CCl₃ fixed at 1985 levels.

D3. Scenario D1 with CCl₄ and CH₃CCl₃ fixed at 1985 levels and NO replacement of Montreal products with HCFC-22.

D4. Scenario D1 with CH₄, CCl₄, and CH₃CCl₃ fixed at 1985 levels and NO replacement of Montreal products with HCFC-22.

emissions in the year 2000. Therefore, an additional scenario E (options 1–10, described in Table 3.2-7) is used to explore the range of chlorine loading under the assumption that we have the capability by the year 2000 of completely eliminating emissions of all halocarbons, except for CH₃Cl. Only a complete cut in emissions of CFCs, HCFC-22, CCl₄, and CH₃CCl₃ results in chlorine loading less than 2 ppbv by 2060, although a combination of cuts and reductions in emissions (including low levels of CFC emissions) can give values below 3 ppbv. If the time frame is extended to 2090, there is a slightly greater range of emission restrictions that will result in 2 ppbv of atmospheric chlorine and a much greater range that would return chlorine levels to 3 ppbv. Model assessments of these scenarios were not performed, since the ozone perturbations would be dominated by the increases in CH₄, N₂O, and CO₂ rather than the chlorine abundances.

The choice of production/emission levels for 1985 is somewhat uncertain. For example, the emissions of CFC-114 and CFC-115 are based on budgetary estimates using their measured growth in atmospheric

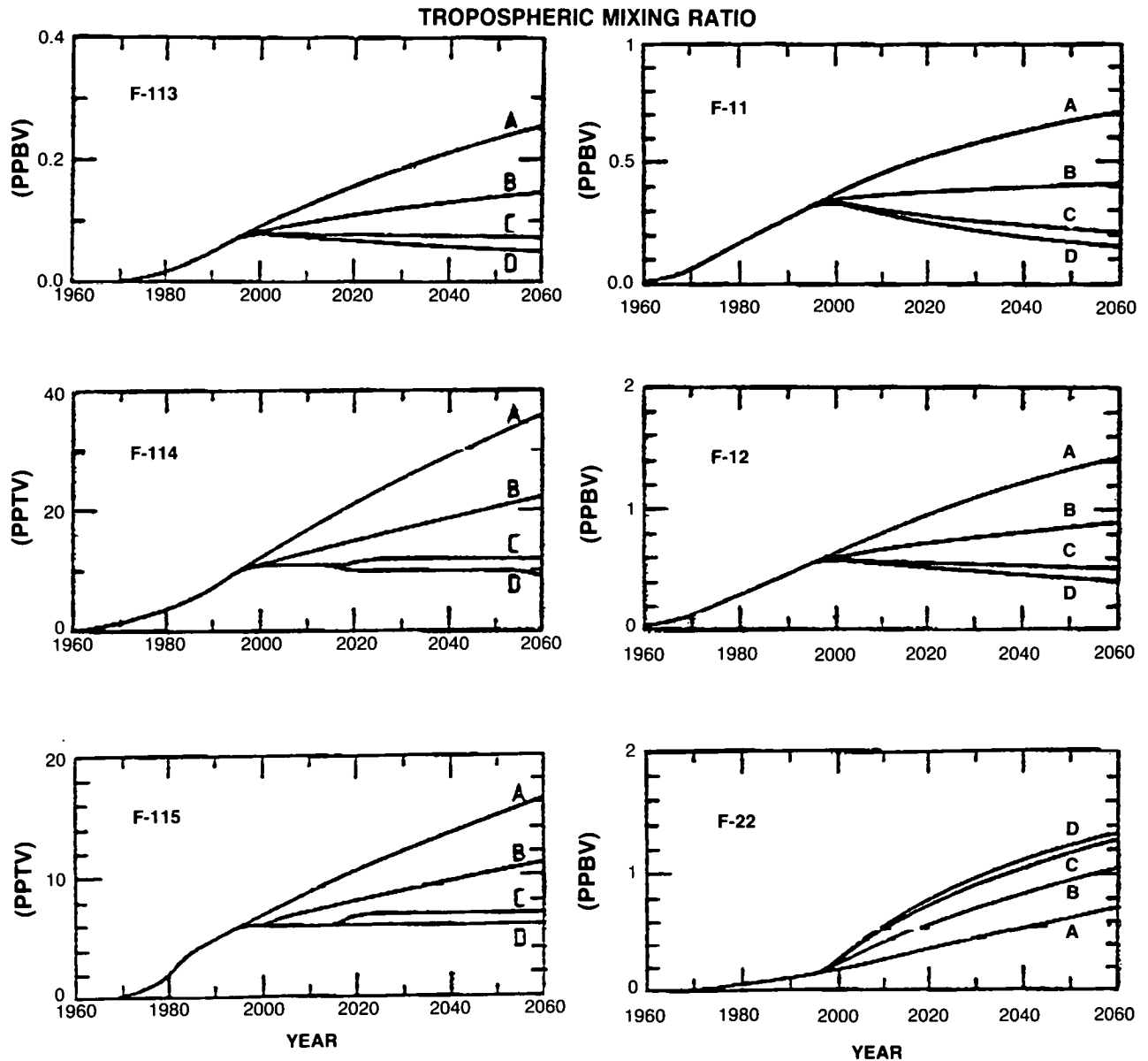


Figure 3.2-1. Time history, 1960-2060, of mean tropospheric concentrations of the trace gases assumed for the different scenarios (see Tables 3.2.2 and 3.2.3).

abundance. There is some uncertainty regarding the absolute calibration of these measurements and, thus also, the corresponding values for emission in Tables 3.2-2a and b. The values for HCFC-11 and -12 do not reflect the *fait accompli* that HCFC production (by reporting companies alone!) has already grown by an average of 14% between 1985 and 1987 (Grant and Thornton: Production, sales and calculated release of CFC-11 and CFC-12, prepared for the Chemical Manufacturers Association, Washington, DC, 1988).

3.2.1.2 Fluxes or Mixing Ratios?

For the convenience of the model calculations we are also including a set of recommended tropospheric mixing ratios that correspond to a given emissions scenario. This conversion is necessary for HCFC-22,

THEORETICAL PREDICTIONS

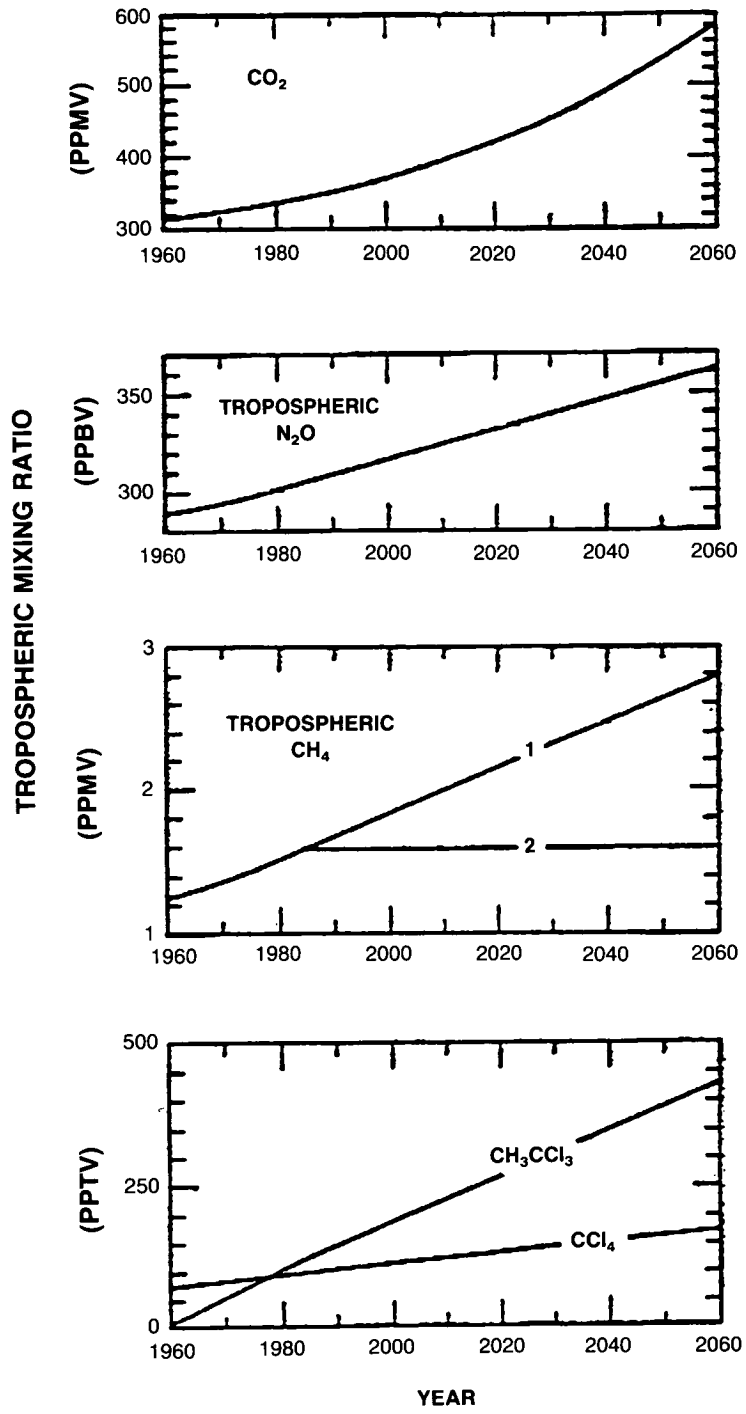


Figure 3.2-1., continued

THEORETICAL PREDICTIONS

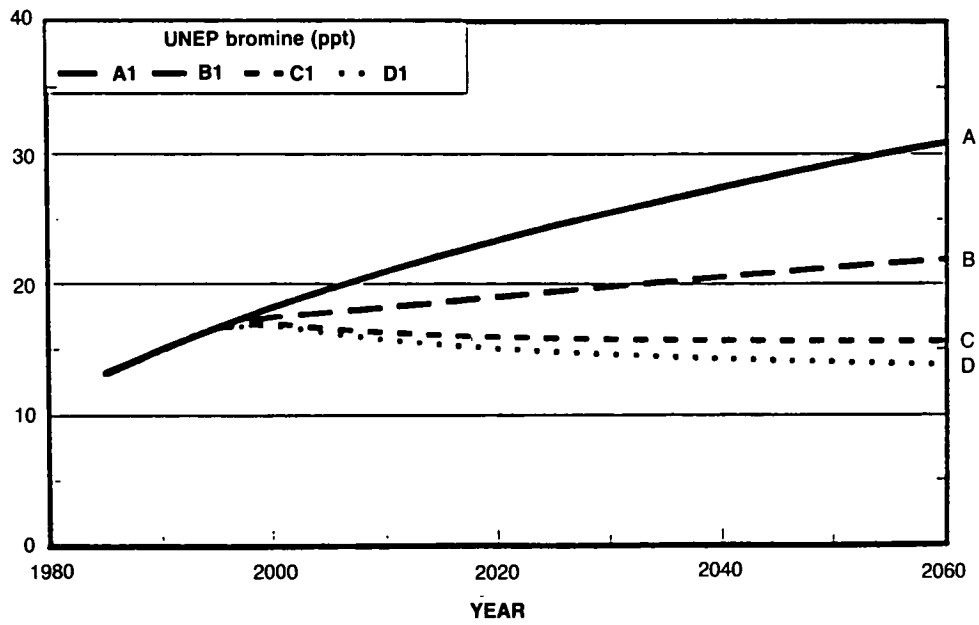
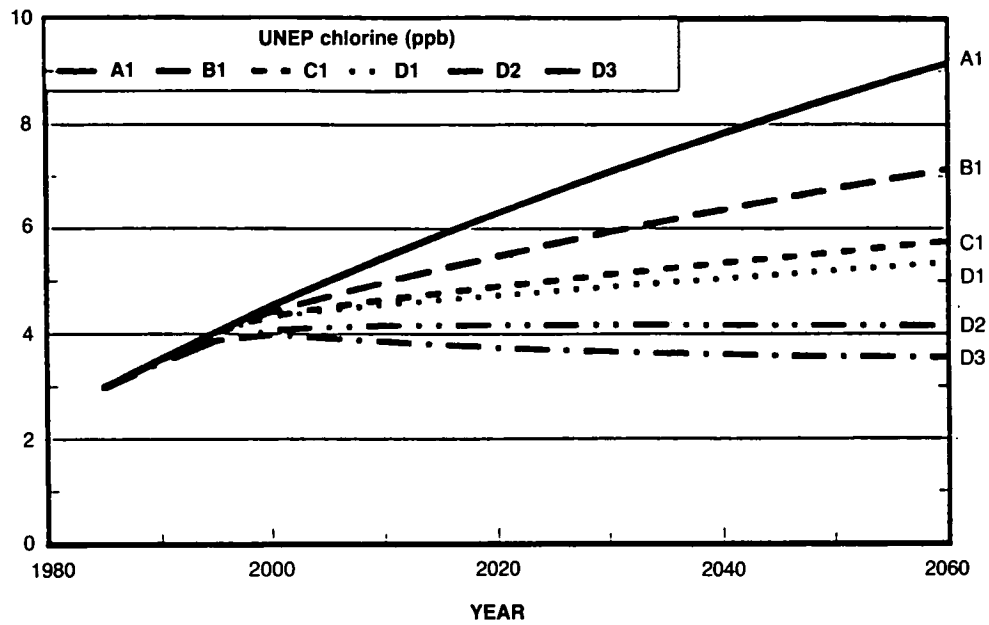


Figure 3.2-2. Time history, 1980–2060, of total atmospheric chlorine and total atmospheric bromine from the different scenarios (see Table 3.2.4).

THEORETICAL PREDICTIONS

Table 3.2-2a. Assumed history of trace gas concentrations: Halocarbons and other gases

Year	CO ₂ ppmv	N ₂ O ppbv	CH ₄ ppbv	CH ₃ Cl pptv	CH ₃ Br pptv	CCl ₄ pptv	CH ₃ CCl ₃ pptv
1960	316	289	1255	600	10	75	5
1965	321	292	1316	600	10	80	30
1970	327	295	1375	600	10	85	55
1975	333	298	1450	600	10	90	80
1980	339	302	1525	600	10	95	105
1985	345	306	1600	600	10	100	130
1986 +	+0.4%	+0.25%	+15	fixed	fixed	+1	+4

Note: The assumed scenario for these gases from 1986 through 2060 involves exponential (i.e., compounded) growth denoted by an increase in %/yr, linear growth denoted by an annual increase in mixing ratio, or fixed concentrations.

Table 3.2-2b. Assumed history of trace gas concentrations: Montreal products and replacements (all pptv)

Year	CFC-11	CFC-12	CFC-113	CFC-114	CFC-115	Halon 1211	Halon 1301	HCFC-22
	CFCl ₃	CF ₂ Cl ₂	C ₂ F ₃ Cl ₃	C ₂ F ₄ Cl ₂	C ₂ F ₅ Cl	CF ₂ BrCl	CF ₃ Br	CHF ₂ Cl
1960	11	33	0.2	0.2	—	—	—	1
1965	27	64	0.8	0.6	—	—	—	4
1970	60	121	2.3	1.4	0.2	0.1	0.1	10
1975	116	207	6.3	2.4	0.8	0.2	0.2	27
1980	173	297	15.3	3.8	2.1	0.5	0.6	54
1985	220	375	30.0	5.0	4.0	1.5	1.7	80
FX (Gg/yr)	350	450	150	15	5	5	8	140 + 7*
LT (yr)	60	120	90	200	400	15	110	20
CC (Gg/pptv)	23.2	20.4	31.6	28.9	26.1	27.9	25.1	14.6

Note: Fluxes (FX) denote emissions in 1985 (Gg = 1E9 g); HCFC-22 emissions* are assumed to grow linearly by an additional 7 Gg/yr for each year after 1985. The Reference Scenario (A) fixes all future emissions of Montreal products at the 1985 level; other scenarios (B, C, D) assume a cutback each year from 1996 to 2000 with part of this reduction (50% by mass) being added to the base scenario for HCFC-22. The conversion factor between emissions and concentration, CC, assumes that the halocarbons are mixed only throughout 95% of the atmosphere with a total dry weight of 5.148E21 g (1.777 10²⁰ moles).

since the lifetime is determined by reactions with tropospheric OH and the current assessment models are not well tested or studied in terms of tropospheric chemistry. For the Montreal products, the predominant loss occurs in the stratosphere and the models should adequately calculate their global loss, but there is significant uncertainty (>25%) in the lifetimes for these gases as seen by the range of values reported by the assessment models in Table 3.2-6.

These calculations of atmospheric concentrations from emissions are simplistic and do not represent the best estimate of future composition (see discussion of uncertainties in lifetimes below). The atmospheric lifetime for each species (LT) is assumed to remain constant throughout the scenario and is given in Table 3.2-2b. The equation used to integrate the globally averaged tropospheric mixing ratios (TM) from the emissions (FX) is given by the following year-to-year regression formula :

$$TM(t+1) = TM(t) * DD + FX(t+1) * (1 - DD) * LT/CC$$

THEORETICAL PREDICTIONS

where $DD = \exp(-1/LT)$ represents the atmospheric decay of the species during one year, and CC is the conversion factor between tropospheric concentration (pptv, assumed to be well mixed) and mass (Gg), see Table 3.2-2b. Slightly greater abundances of these gases are anticipated in the Northern Hemisphere and over source regions, but the latitudinal gradients are not expected to have a significant impact on the stratospheric abundance. The resultant projections for HCFC-22 and the Montreal products are given in Tables 3.2-3(a-d) for scenarios A1-D1, respectively.

Table 3.2-3a. Projected surface mixing ratios for Scenario A: Montreal products and replacements (all pptv)

Year	CFC 11	CFC 12	CFC 113	CFC 114	CFC 115	Halon 1211	Halon 1301	HCFC 22
1985	220	375	30	5	4	1.5	1.7	80
1990	275	468	51	7	5	1.8	3.2	111
1995	325	557	72	10	6	2.1	4.6	146
2000	372	642	91	12	7	2.3	6.0	184
2005	414	724	109	14	8	2.4	7.2	224
2010	453	802	126	17	8	2.5	8.5	266
2015	490	878	143	19	9	2.5	9.7	309
2020	523	950	158	21	10	2.6	10.8	353
2025	553	1019	173	23	11	2.6	11.9	398
2030	582	1085	186	25	12	2.6	12.9	444
2035	607	1149	199	27	13	2.6	13.9	490
2040	631	1210	212	29	13	2.7	14.8	537
2045	653	1269	223	31	14	2.7	15.7	584
2050	673	1325	234	32	15	2.7	16.6	631
2055	692	1379	245	34	16	2.7	17.4	678
2060	709	1431	255	36	16	2.7	18.2	726

Table 3.2-3b. Projected surface mixing ratios for Scenario B: Montreal products and replacements (all pptv)

Year	CFC 11	CFC 12	CFC 113	CFC 114	CFC 115	Halon 1211	Halon 1301	HCFC 22
1985	220	375	30	5	4	1.5	1.7	80
1990	275	468	51	7	5	1.8	3.2	111
1995	325	557	72	10	6	2.1	4.6	146
2000	350	609	84	11	6	2.0	5.5	230
2005	358	639	91	12	7	1.8	6.0	333
2010	365	666	98	13	7	1.7	6.5	424
2015	372	693	104	14	8	1.6	7.0	506
2020	379	719	110	15	8	1.5	7.5	580
2025	385	744	115	16	8	1.5	7.9	649
2030	390	767	121	17	9	1.4	8.4	712
2035	395	790	126	18	9	1.4	8.8	773
2040	400	812	131	19	9	1.4	9.2	830
2045	404	833	135	20	10	1.4	9.5	886
2050	408	853	139	20	10	1.4	9.9	940
2055	411	872	143	21	10	1.4	10.2	992
2060	415	890	147	22	11	1.4	10.5	1044

THEORETICAL PREDICTIONS

Table 3.2-3c. Projected surface mixing ratios for Scenario C: Montreal products and replacements (all pptv)

Year	CFC 11	CFC 12	CFC 113	CFC 114	CFC 115	Halon 1211	Halon 1301	HCFC 22
1985	220	375	30	5	4	1.5	1.7	80
1990	275	468	51	7	5	1.8	3.2	111
1995	325	557	72	10	6	2.1	4.6	146
2000	334	587	79	11	6	1.8	5.2	262
2005	318	579	78	11	6	1.4	5.2	409
2010	304	571	78	11	6	1.1	5.2	535
2015	290	564	77	11	6	0.9	5.2	644
2020	278	557	76	11	6	0.8	5.2	739
2025	267	551	75	11	7	0.7	5.2	824
2030	256	545	75	11	7	0.6	5.2	900
2035	247	539	74	12	7	0.5	5.2	970
2040	238	533	74	12	7	0.5	5.2	1036
2045	230	527	73	12	7	0.5	5.2	1097
2050	222	522	73	12	7	0.5	5.2	1156
2055	215	517	72	12	7	0.4	5.2	1212
2060	209	512	72	12	7	0.4	5.2	1266

Table 3.2-3d. Projected surface mixing ratios for Scenario D:^a Montreal products and replacements (all pptv)

Year	CFC 11	CFC 12	CFC 113	CFC 114	CFC 115	Halon 1211	Halon 1301	HCFC 22
1985	220	375	30	5	4	1.5	1.7	80
1990	275	468	51	7	5	1.8	3.2	111
1995	325	557	72	10	6	2.1	4.6	146
2000	330	580	78	11	6	1.8	5.1	271
2005	307	562	75	11	6	1.3	4.9	431
2010	286	544	72	10	6	1.0	4.8	567
2015	267	527	69	10	6	0.7	4.6	683
2020	249	511	66	10	6	0.6	4.5	784
2025	233	496	64	10	6	0.4	4.4	874
2030	218	481	62	10	6	0.4	4.3	954
2035	204	467	60	10	6	0.3	4.2	1027
2040	191	453	57	10	6	0.2	4.1	1094
2045	180	440	56	10	6	0.2	3.9	1158
2050	169	427	54	9	6	0.2	3.9	1217
2055	159	415	52	9	6	0.2	3.8	1275
2060	150	404	50	9	6	0.2	3.7	1330

^aGiven concentrations apply to all scenarios D1–D4 except for HCFC-22: use values here for scenarios D1 and D2 and from scenario A for D3 and D4.

3.2.1.3 Uncertainties

The historical record of trace gas concentrations back to 1960 is not well known, especially for some of the more exotic CFCs and for global coverage. However, this uncertainty does not introduce any

important source of error in these calculations, since the concentrations must have been small in 1960 and are constrained by the history of production and release over this period. Changes in CO_2 are documented since 1957, and the increases in CH_4 and N_2O are bounded by earlier spectroscopic data and ice core records.

Any scenario for future abundances of the trace gases has obvious uncertainties associated with:

1. the extrapolation of N_2O , CO_2 , CH_4 , and CCl_4 (current sources and sinks are not well quantified, nor predictable in the future);
2. the extrapolation of CH_3CCl_3 and HCFC-22 (even with knowledge of atmospheric emissions, these gases depend on predicting tropospheric OH levels and their changes in a future climate and chemistry);
3. the prediction of stratospheric losses of CFCs (lifetimes are still uncertain at the 20% level with corresponding uncertainty in the abundance of CFCs at steady state); and
4. the prediction of future emissions.

We ignore the uncertainties associated with item (4) by assuming that sources of Montreal products from the chemical industry are controlled, and with item (1) by assuming recent trends in other trace gases can be simply extrapolated. A more rigorous analysis and modeling of these processes is beyond the scope of the current study.

One caveat regarding item (4) concerns the assumption that emission equals production. This assumption holds for end uses in which the CFC is released rapidly into the atmosphere after production (e.g., open cell foams or aerosol propellants), but not for those applications in which the CFC is contained in a closed-cycle system such as refrigeration, certain foams, or fire retardants (i.e., banking). A study has been made for these scenarios (R. Hennig, Mainz) that considers the time lags associated with the current CFC markets. For scenario A, results are only a few percentage points different from those given here; but for scenario D, with large cuts in production, the banking of CFCs extends their emissions, increasing concentrations of CFC-11 and 12 by about 10% over the period 2020–2060.

Tropospheric chemistry (item 2) is expected to respond to changes in climate, stratospheric ozone, and other trace gases; it should be predictable with global models of tropospheric chemistry. The resulting perturbation to OH is likely to change the global mean lifetime of HCFC-22, CH_3CCl_3 , and CH_4 ; and hence, their atmospheric abundances. For further analysis of the atmospheric oxidative capacity see Chapter 4. For CH_4 and CH_3CCl_3 we make no direct assumptions about OH, but for HCFC-22 we have assumed that the lifetime remains constant. If tropospheric OH changes as much as 20% by 2060, then the predicted HCFC-22 concentrations should also change correspondingly.

The lifetimes of the fully halogenated CFCs (item 3) are determined by stratospheric losses and should be calculated accurately with the models used in this assessment. There is, however, disagreement between models regarding the lifetimes of the CFCs: for example, the lifetime of CFC-11 in the current atmosphere is 47 years in the AER model and 60 years in the GSFC2 model (see Table 3.2-6). If the AER lifetime were used in Table 3.2-2, then CFC-11 concentrations in 2060 would be reduced by about a factor of 0.8. We recognize that the contribution of Montreal products to the chlorine and bromine loading of the stratosphere is uncertain at the 20% level.

A further complication is that by 2060 in scenario A1 the lifetimes of most CFCs will decrease by about 5–10% (see Table 3.2-6); the change is due to increased stratospheric losses because there is less

THEORETICAL PREDICTIONS

ozone in the upper stratosphere and more ultraviolet sunlight reaches the middle stratosphere. This effect was not included in the scenarios given in Table 3.2-3, which assumed a fixed lifetime. The model results given in Table 3.2-6 included only direct chemical effects and not any additional impact due to tropospheric climate change or alteration in the stratospheric circulation due to the ozone loss. Thus, predicting the future atmospheric chemical state and dynamical circulation should be an important component of subsequent assessments of CFCs.

Some models (Cambridge and Oslo) ran the assessment simulations with the flux boundary conditions that define the basic scenario (Table 3.2-1); their results will vary in comparison with the other models, in part because the halogen content of the atmosphere differs from the projected histories given in Table 3.2-3. This range in chlorine content, and in the resulting ozone perturbation, is an example of the uncertainty in making these predictions today, but it must not be considered a full estimate of the possible error in current model calculations.

3.2.2 Predicted Response of the Atmosphere for Sample Scenarios

3.2.2.1 Different Models and Different Chemistries

Predictions of stratospheric ozone and temperatures have been made for the standard UNEP scenarios described in Section 3.2.1 and defined by Tables 3.2-1 and 3.2-2. We examine here specific predictions from these scenarios for the recent past—from 1960 to 1980—in which chlorine levels have more than doubled, and for the future—from 1980 to 2020 and to 2060. We shall look at changes in the vertically integrated column of ozone, as well as changes in local ozone concentrations and temperatures throughout the stratosphere. One goal of this section will be to examine model predictions of stratospheric change using different scenarios for chlorine and bromine loading of the atmosphere.

The models used in these calculations are predominantly the standard 2-D stratospheric chemistry models, including also some 1-D climate/chemistry models and 2-D models incorporating heterogeneous chemistry. All models have adopted the same homogeneous gas-phase chemistry from the recent kinetics assessment (DeMore et al., 1987). One-dimensional models are useful for some diagnostic studies, but two-dimensional models are required to simulate ozone over latitudes and seasons, and to compare with observations. The basic predictions presented here were made with the standard 2-D assessment models: we have had the most experience with these models, and a major intercomparison was just completed (see Section 3.1.3).

The appearance of the Antarctic ozone hole revealed significant limitations in our stratospheric modeling and predictive capabilities. The mobilization of the scientific community—including field campaigns, laboratory measurements, and theoretical modeling—has led recently to an understanding of the processes controlling ozone destruction over Antarctica (see Chapter 1, Polar Ozone). The ozone hole has been shown to be related to heterogeneous chemistry occurring on particles in polar stratospheric clouds (PSCs, see Chapter 1). The processing by PSCs occurs irregularly on small spatial scales in the polar stratosphere during winter and is critically dependent on the occurrence of very low temperatures, even if only for brief episodes. Furthermore, during winter the polar regions appear to be chemically isolated from the rest of the lower stratosphere by the circumpolar vortex of high winds. Within the polar stratospheric vortex, extremely low concentrations of source gases (N_2O , CFCs) are observed at 19 km, and can be explained only by descent of photochemically aged air from the middle stratosphere (25–35 km). These chemical and dynamical processes associated with the Antarctic ozone hole are difficult to simulate with the current global models.

THEORETICAL PREDICTIONS

The assessment models used here to predict global ozone change include only gas-phase chemistry. Furthermore, they do not acceptably reproduce the dynamical circulation of the polar vortex that leads to low concentrations of trace gases within the vortex. Accordingly, they do not simulate the Antarctic ozone hole nor make predictions of ozone loss in the lower polar stratosphere for the late spring. The models should, however, provide accurate assessment of large-scale ozone perturbations driven by chlorine-catalyzed chemistry in the middle to upper stratosphere.

Some of the 2-D assessment models have versions that now include a parameterized form of PSC chemistry. These models are now able to predict some form of Antarctic ozone hole, and also to a lesser extent ozone loss that is due to chlorine and bromine catalytic cycles in the Arctic stratosphere. The scientific community has not yet had the opportunity to examine and validate these new forms of chemistry in the 2-D models. Therefore, we do not include their results here as part of the basic predictions, but have put results from the models with heterogeneous chemistry in a special section; with improved treatment of the polar dynamics these models should become part of the standard predictions in subsequent assessments.

We have received calculations for the UNEP scenarios (Tables 3.2-1 and 3.2-2) from several modeling groups and shall examine these in some detail. Only the GSFC2 model was used for all eight scenarios. Other modeling groups have contributed calculations using scenarios that are similar, but not equivalent to any of the UNEP scenarios. We include a brief discussion of these results where applicable.

3.2.2.2 Standard Scenario: 1960–1980

All scenarios are identical through 1985 since they are based on the assumed history of atmospheric composition. We look here at the predicted change over the period 1960 to 1980, a time interval similar to that examined by the International Ozone Trends Panel (OTP, see Watson et al., 1988 for executive summary of Chapter 7). The OTP Report spent significant effort in modeling the solar cycle and atmospheric nuclear tests in addition to the trace gases. Here we consider only the changes caused by increases in the

Table 3.2-4. Chlorine and bromine loading of the atmosphere for the UNEP scenarios

Year	Total Chlorine (ppbv)						Total Bromine (pptv)			
	A1-2	B1	C1	D1	D2	D3-4	A1-2	B1	C1	D1-4
1985	2.98	2.98	2.98	2.98	2.98	2.98	13.2	13.2	13.2	13.2
1990	3.52	3.52	3.52	3.52	3.44	3.44	15.0	15.0	15.0	15.0
1995	4.03	4.03	4.03	4.03	3.87	3.87	16.7	16.7	16.7	16.7
2000	4.52	4.41	4.33	4.31	4.07	3.98	18.2	17.5	17.0	16.9
2005	4.99	4.70	4.50	4.44	4.12	3.91	19.6	17.8	16.6	16.2
2010	5.44	4.97	4.64	4.55	4.15	3.85	21.0	18.2	16.3	15.8
2015	5.88	5.23	4.77	4.64	4.16	3.79	22.2	18.6	16.1	15.4
2020	6.30	5.47	4.90	4.73	4.17	3.74	23.4	19.0	16.0	15.1
2025	6.70	5.71	5.01	4.81	4.17	3.70	24.5	19.4	15.9	14.8
2030	7.09	5.93	5.12	4.89	4.17	3.66	25.5	19.8	15.8	14.6
2035	7.47	6.15	5.23	4.97	4.17	3.63	26.5	20.2	15.7	14.5
2040	7.83	6.36	5.34	5.04	4.16	3.61	27.5	20.6	15.7	14.3
2045	8.18	6.57	5.44	5.12	4.16	3.58	28.4	20.9	15.7	14.2
2050	8.51	6.77	5.54	5.20	4.16	3.57	29.3	21.3	15.7	14.1
2055	8.84	6.96	5.65	5.27	4.15	3.56	30.1	21.6	15.6	13.9
2060	9.16	7.15	5.75	5.35	4.15	3.55	30.9	21.9	15.6	13.8

THEORETICAL PREDICTIONS

trace gases. We specifically did not include the variation in ultraviolet sunlight over the solar cycle: the magnitude of solar change is uncertain and varies from cycle to cycle as noted in the OTP Report; and the 11-year modulation would have made it difficult to compare trends over periods that were not in the same phase of the solar cycle (e.g., 1960–1980 and 1980–2060).

The calculated change in column ozone (%) from 1960 to 1980 in the different 2-D models is plotted in the form of a Dobson map (abscissa = month, ordinate = latitude) in Figures 3.2-3(A,G,J,L,M,O,W). The letter on each figure in this section denotes the model (see Table 3.2-5 for mnemonic codes). The AER, JMRI, GSFC2, and Oslo models predict a latitudinal/seasonal pattern of perturbations to the ozone column that will be seen in many of the calculations shown here: small changes in the tropics (about -0.5 to -1.5%), becoming larger at higher latitudes, peaking at the end of winter (about -2.5 to -3.5%). Among these four models, the patterns are almost identical and the depletions differ globally by up to 1%. The WisCAR model calculates small but varied changes in the tropics extending to mid-latitudes (-1 to $+1\%$) and larger, more typical losses at the poles in late winter (-2 to -3%). The LLNL and Mainz models predict a quite different pattern, with ozone depletion only in the high latitude winter, and increases as large as 1% elsewhere. The Mainz model did not follow the prescribed scenarios (by including tropospheric NO_x increases), and we cannot ascertain whether this factor is the cause of these differences. One major cause of the different predictions for ozone column lies with the large variation in calculating the magnitude of the ozone increases predicted for the lower stratosphere and upper troposphere as discussed next.

The calculated change on local ozone concentrations (%) from 1960 to 1980 is shown in Figures 3.2-4 (A,G,J,L,M,N,O[March],W) for the month of January. Maximum ozone loss occurs in two regions: the winter mid-latitudes between 35 and 45 km and the same altitude range over the summer pole. The AER, JMRI, GSFC2, NOCAR, and Oslo models have a peak change of about -16% at 70°N , and have zero change lines ranging from 26 km to 20 km and below (JMRI). The LLNL and Mainz models have peak ozone loss of only 7 to 12% and, along with the Oslo model, show general increases in tropospheric ozone that are much larger than the other models. (Prediction of increases in tropospheric ozone with these stratospheric models is regarded with much uncertainty by the modeling community, since tropospheric aspects of these models have not been extensively tested and studied; see also discussion of tropospheric ozone chemistry in Chapter 4). The cause of the substantially smaller ozone decreases over the 1960–1980 period by these latter two models needs to be investigated further. It is likely that the changes in temperature (calculated by the LLNL, NOCAR, and Oslo models, but not by the AER, JMRI, GSFC2, and Mainz models) are part of the difference.

In the NOCAR model the largest decreases in temperature over the 1960–1980 period occur near the stratopause (40–58 km) and are typically 2 K, increasing to 4 K over the summer pole (Figure 3.2-4NT). The predicted temperature changes over the past decades from most of the models including temperature feedbacks were not available for this study, should be examined in greater detail, and need to be verified by the research groups through comparison with observations.

In comparing these results with the OTP Report, we note that the scenarios are slightly different and the models have been further developed since those calculations (generally performed in 1987). The OTP results as shown are not directly comparable to these figures; however, from Figure 7–10 of the OTP Report one can see the latitudinal pattern similar to that shown here: annual average decreases in column ozone becoming larger (up to -3%) from 30°N to 60°N in the AER, LLNL, and Oslo models. In the OTP Report, the Cambridge model shows little latitudinal dependence, a result that is also seen here (Figure 3.2-7C) for the longer period 1980–2060 of scenario A1 and that may be due to summer increases in column ozone.

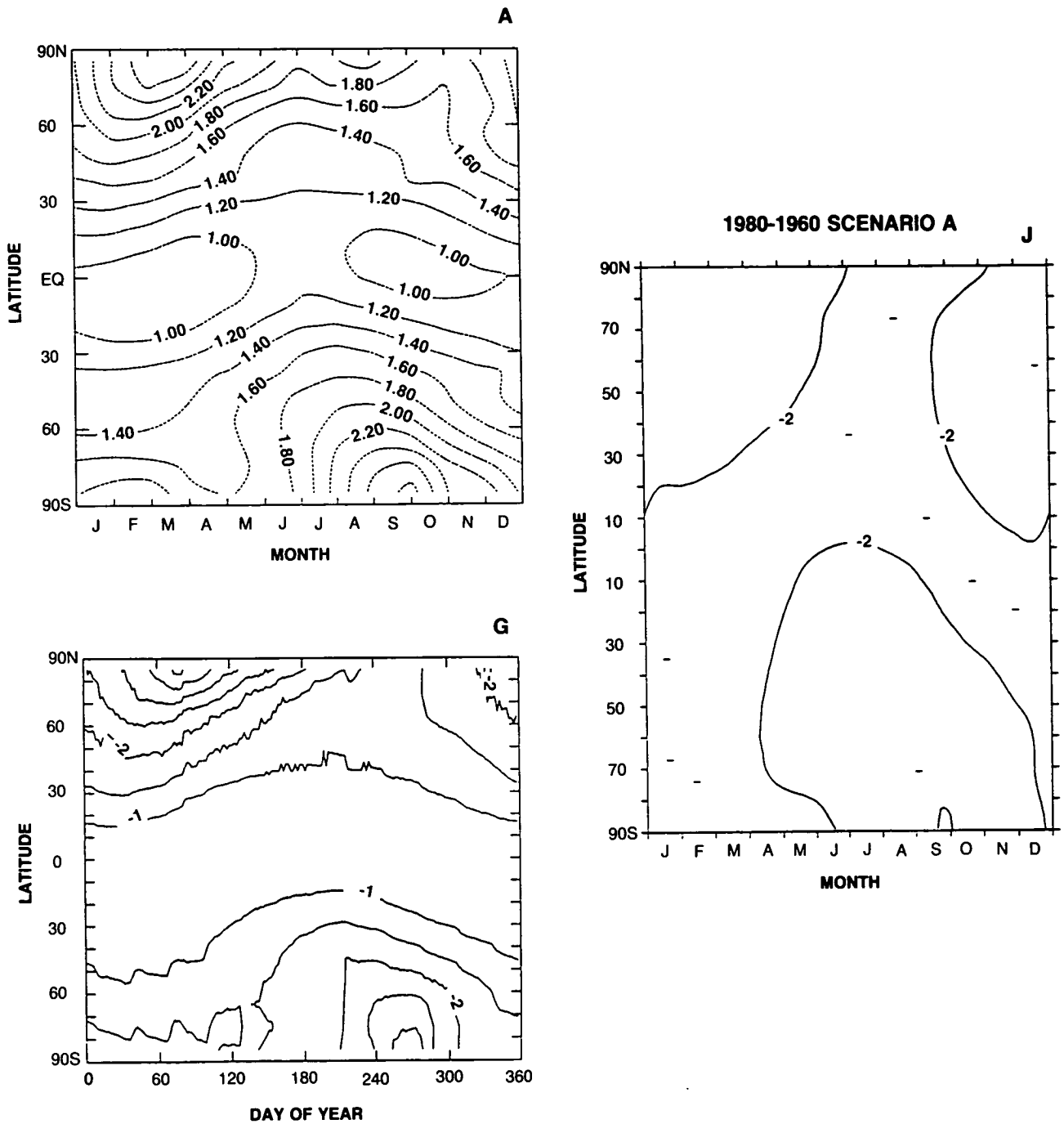


Figure 3.2-3. Dobson map (latitude by month) of percent change in column ozone from 1960 to 1980 using the specified trace-gas scenario. The panels are coded with the model mnemonics (see Table 3.2.5).

The overall changes predicted in ozone from 1960 to 1980 (not including the Antarctic ozone hole and related decreases) are significant and should be detectable, especially if one extends the comparison with observations until 1990. By this time we should be able to test the predictions of the temperature feedback (and correspondingly different ozone perturbations) as well as those of large summertime ozone increases

THEORETICAL PREDICTIONS

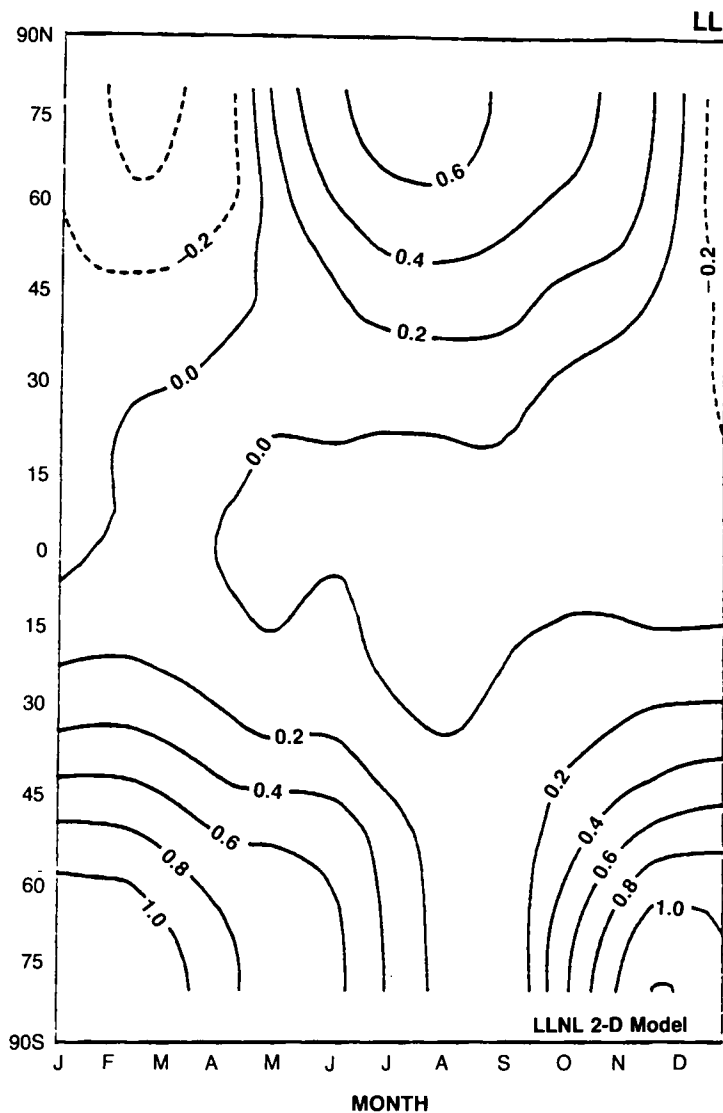


Figure 3.2-3., continued

in the troposphere and lower stratosphere at mid-latitudes. These tests are essential because the different characteristics of the models shown in this 1960–1980 comparison are carried through to the long-term predictions discussed below.

3.2.2.3 Scenario A: 1980–2060

The scenarios A1 and A2 exhibit the most rapid growth in atmospheric chlorine and bromine, and thus produce the largest perturbations among all the scenarios. The impact of large stratospheric abundances of halogens by 2060 (9 ppb of chlorine and 31 ppt of bromine) is offset in part by the rise in methane and carbon dioxide. Methane plays a major role in partitioning of chlorine species (the ratio of HCl to Cl₂) and in ozone production by “smog” chemistry (reactions of CH₃OO and HO₂ with NO). Carbon dioxide is the

THEORETICAL PREDICTIONS

1985 VS 1960

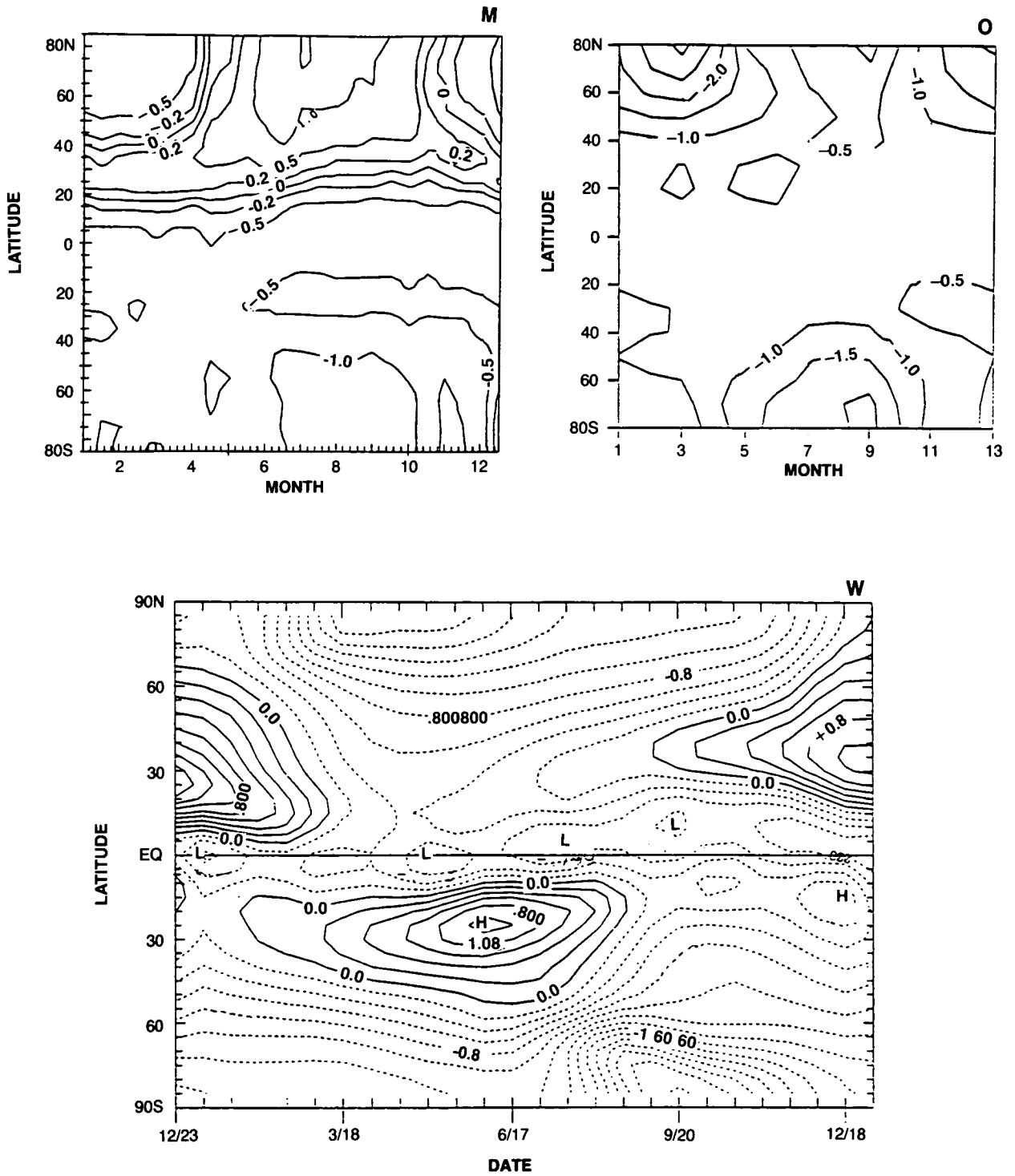


Figure 3.2-3., continued

THEORETICAL PREDICTIONS

Table 3.2-5. Participating assessment models

Name	Code	Scenarios	Institution	Scientists
AER	A	A1, B1, b1*	AER, Inc., MA	Ko, Sze
Camb	C	A1*	U. Camb. & RAL, UK	Pyle
GSFC2	G	A-D all	NASA/Goddard, MD	Jackman, Douglass
Aquila	I	A1	U. Aquila, Italy	Visconti
JMRI	J	A1, B1, D1	Met. Res. Inst., Japan	Sasaki
LLNL	L	A1, A1*, D1	L. Livermore, CA	Wuebbles, Connell
Mainz	M	A1	Max Planck, Mainz	Brühl, Crutzen
NOCAR	N	a1*, d1*	NOAA & NCAR, CO	Solomon, Garcia
Oslo	O	A1*, A2*, D4*	U. Oslo, Norway	Isaksen, Stordal
NSU	U	A1*, D1*	U. Novosibirsk, USSR	Dyominov, Zadorozhny
WisCAR	W	a1*, a2*, d1*	U. Wisc. & NCAR, CO	Hitchman, Brasseur
IASB	(1D)	all	Inst. Sp. Aer., Belgium	De Rudder
MPI	(1D)	all	Max Planck, Mainz	Hennig, Brühl, Crutzen

Note: All models are 2-D unless noted. The lowercase letter means that calculations were performed for a steady-state atmosphere using 1980 and 2060 concentrations. An asterisk (*) denotes a model contribution that also includes feedbacks (CO₂ and O₃ changes) on temperatures. The model codes are used in all figures.

Table 3.2-6. Global mean lifetimes (yr) of the trace gases

Model	CFC 11	CFC 12	CFC 113	CFC 114	CFC 115	Halon 1211	Halon 1301	N ₂ O	CCl ₄
AER									
(1980) ^a	47	99	87	261	399	11	75	113	40
(2060)	43	89	74	230	340	11	62	106	38
GSFC2									
(1980)	60	132	120			13	74	168	52
(2060)	57	124	113			13	70	156	49
JMRI	52	132						151	42
LLNL	60	121	109	240	480			130	52
Oslo	52	102	98	247	522		127	51	
WisCAR									
(1980)	51	130	105					140	36
(2060)	46	123	97					130	32
IASB(1D)	85	166	127					166	67
AER(1D)	60	110	96	~275	~500	11	81	145	53
MPI(1D)	67	135	108	230	455	12	82		58

^aAll results are for contemporary atmosphere (1980) unless otherwise noted; the DuPont model did not do the scenario calculations but is used later in this report.

major infrared-active gas responsible for cooling the stratosphere, and a colder stratosphere generally results in greater ozone abundances. The magnitude of these positive ozone changes (as CH₄ and CO₂ increase) can vary significantly from model to model, and for scenario A1, appear to be the major source of the different results shown here. Scenario A2 (CH₄ fixed) removes some of this sensitivity, and results (from a more limited set of models) show larger and more consistent ozone depletions.

Most of the participating models calculated scenario A1, and results are presented in Figures 3.2-5 through 3.2-8 (same notation for different models as described above). A continuous time-line of the percent

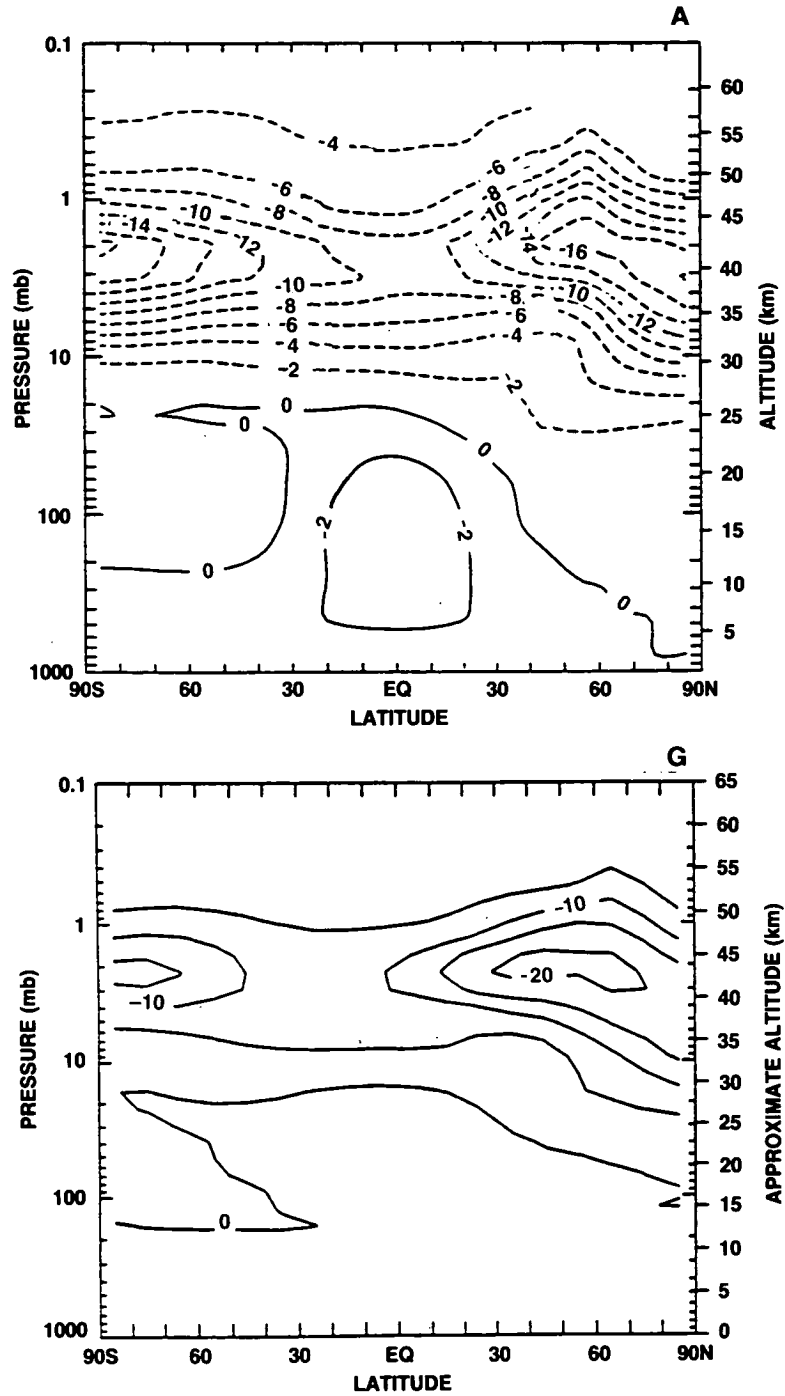
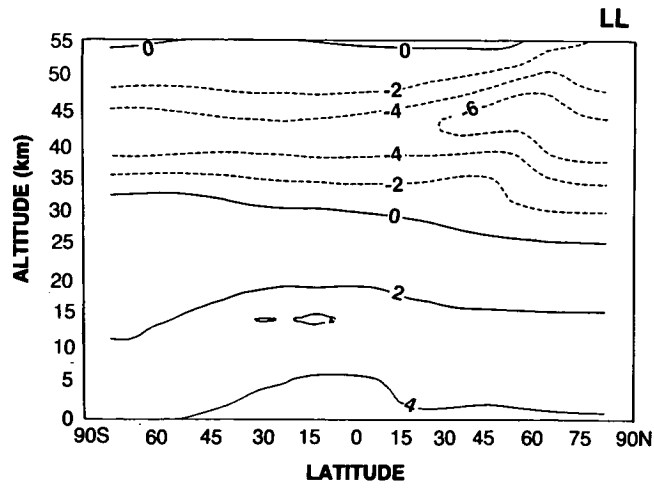
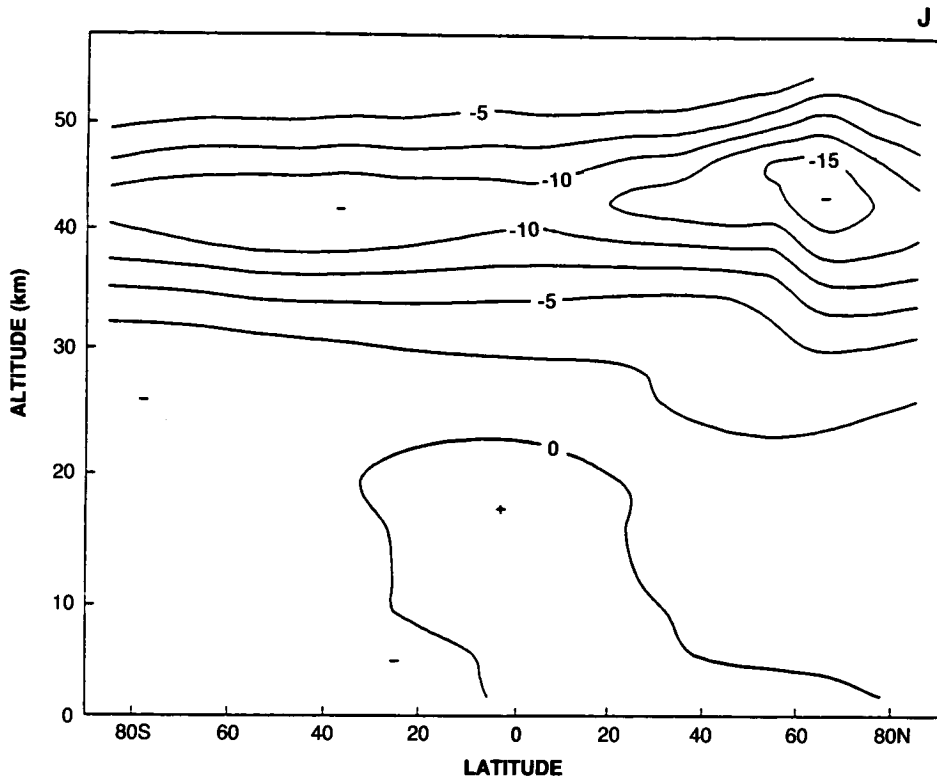


Figure 3.2-4. Latitude-by-altitude (log pressure or height [km]) contour map of the percent change in local ozone concentration from 1960 to 1980 for the specified trace-gas scenario. The panels are coded with the model mnemonics as above. Also included (code NT) is the temperature change (degrees K) from the NOCAR model.

THEORETICAL PREDICTIONS



3.2.4 cont.,

Figure 3.2-4., continued

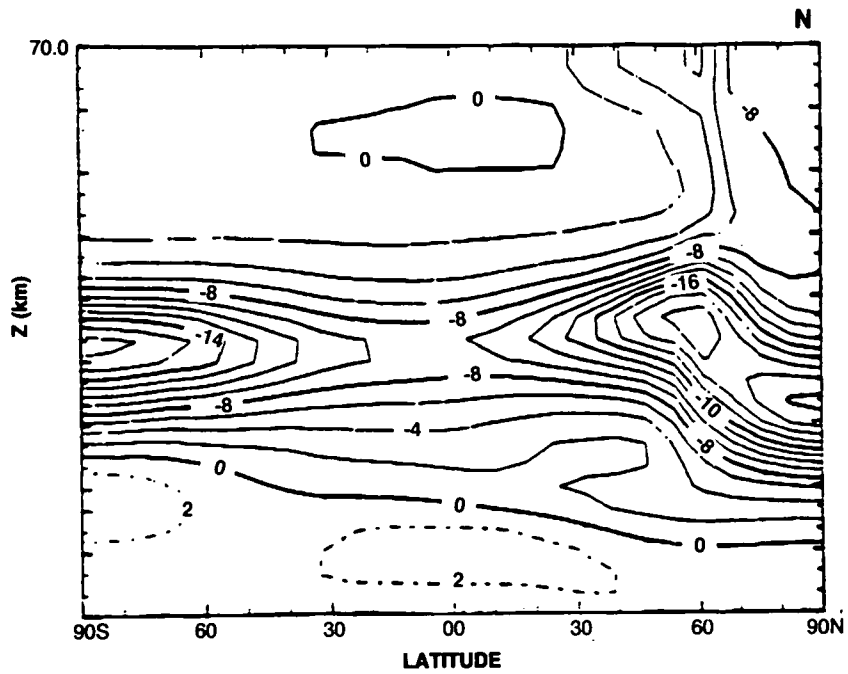
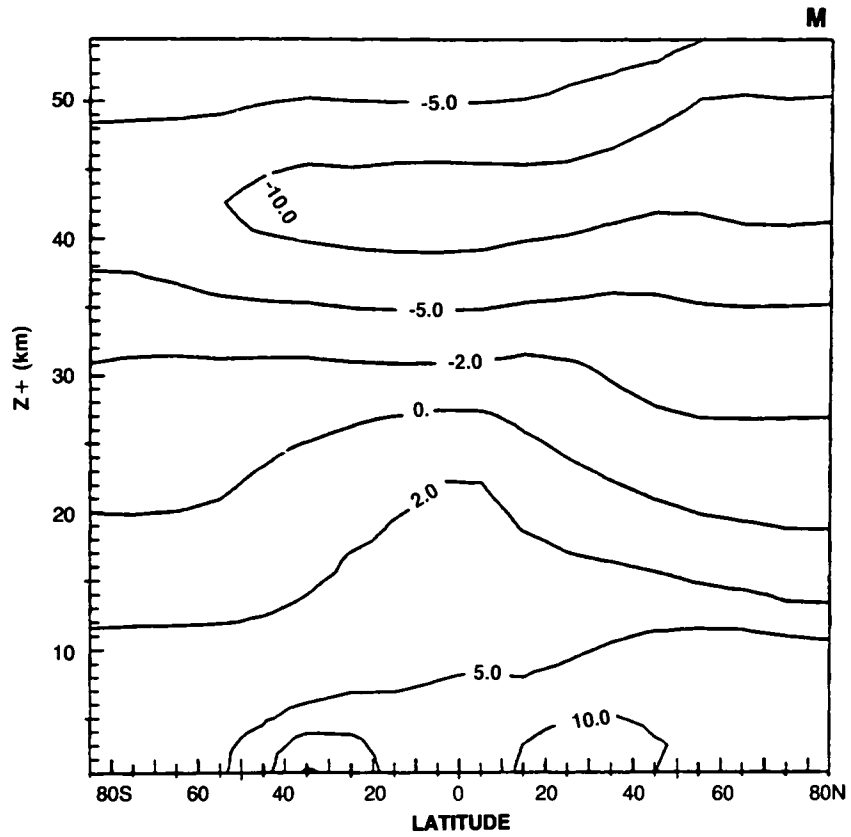


Figure 3.2-4., continued

THEORETICAL PREDICTIONS

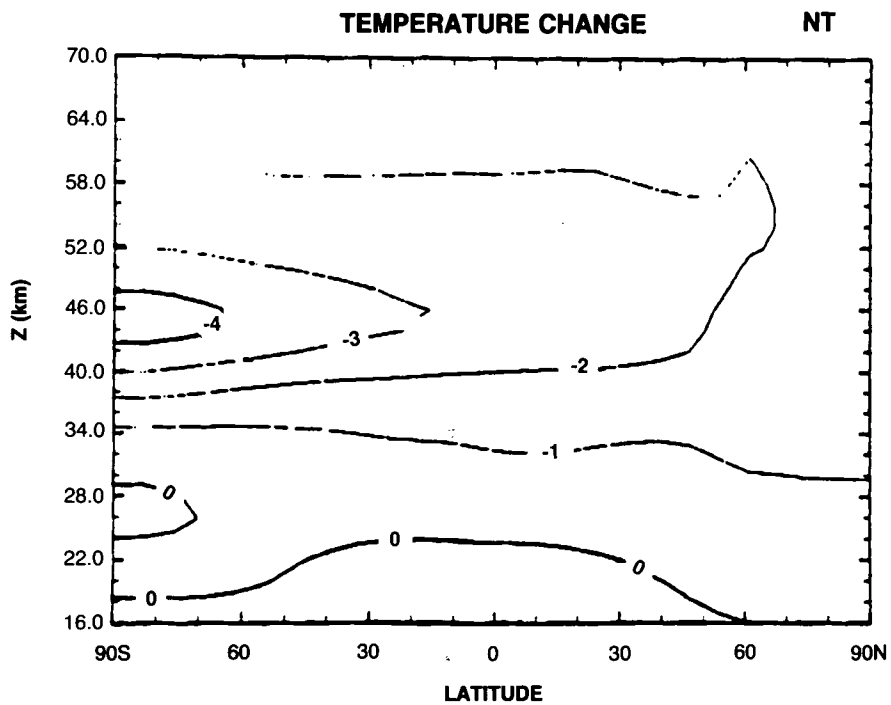
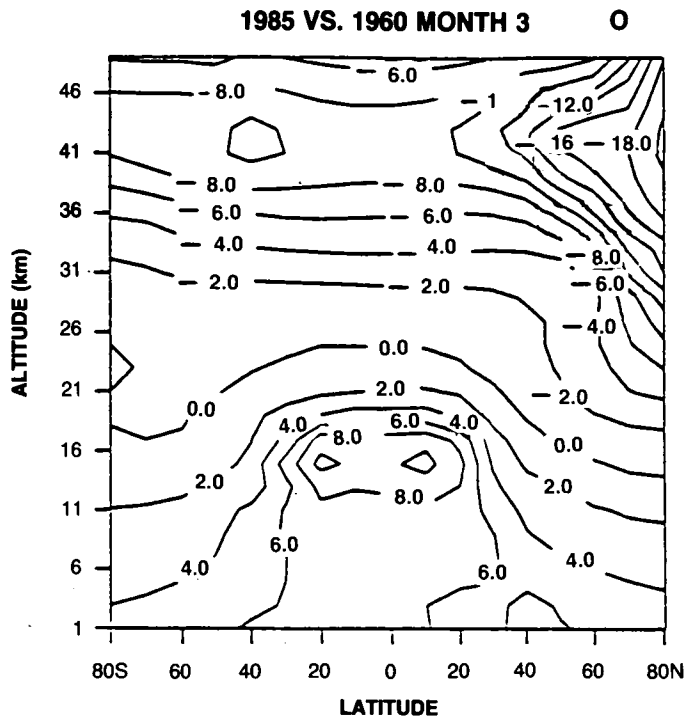


Figure 3.2-4., continued

THEORETICAL PREDICTIONS

change in column ozone relative to March 1980 is shown in Figures 3.2-5(A,G,J,L,M) as a function of latitude for all the months of March from 1980 through 2060. All models show the same pattern: ozone depletions are larger at high latitudes, about 7–10% at 50°N and about 3–8% at 50°S by 2060; tropical losses are always much less, 2–5% by 2060, and lag behind the high latitude regions by at least 40 years. The maximum depletion for all models is asymmetric in these figures because March was chosen as the month for comparison; a reverse pattern would occur if September were selected (see Dobson maps in Figures 3.2-6 and 7).

The Dobson maps of the percent change in ozone column from 1980 to 2020 and from 1980 to 2060 are shown in Figures 3.2-6(A,G,J,L,M) and 3.2-7(A,C,G,I,J,L,LL,M,O,U,W), respectively. By 2020 ozone depletions are typically 1 to 3% in the tropics with maximum losses, usually 6 to 8%, at high latitudes in late winter and early spring. The same latitudinal and seasonal pattern persists at 2060. The largest late winter depletions at high latitudes (poleward of 50 degrees latitude) are greater than 10% in the AER,

Table 3.2-7. Extended scenarios for halocarbon abundances

Code	Scenario Definitions				
	CFC Cut (1996–2000)	Replace as HCFC-22	HCFC-22 Flux	CCl ₄ Growth	CH ₃ CCl ₃ Growth
A1	0%	—	+7 Gg/yr/yr	+1 ppt/yr	+4 ppt/yr
B1	50%	50%	+7 Gg/yr/yr	+1 ppt/yr	+4 ppt/yr
C1	85%	50%	+7 Gg/yr/yr	+1 ppt/yr	+4 ppt/yr
D1	95%	50%	+7 Gg/yr/yr	+1 ppt/yr	+4 ppt/yr
D2	95%	50%	+7 Gg/yr/yr	fix (1985)	fix (1985)
D3	95%	0%	+7 Gg/yr/yr	fix (1985)	fix (1985)
E1	100%	50%	+7 Gg/yr/yr	+1 ppt/yr	+4 ppt/yr
E2	100%	50%	+7 Gg/yr/yr	fix (2000)	fix (2000)
E3	100%	50%	+7 Gg/yr/yr	cut (2000)	fix (2000)
E4	100%	50%	+7 Gg/yr/yr	cut (2000)	cut (2000)
E5	100%	0%	+7 Gg/yr/yr	cut (2000)	cut (2000)
E6	100%	0%	fix (2000)	cut (2000)	cut (2000)
E7	100%	0%	cut (2000)	cut (2000)	cut (2000)
E8	95%	0%	cut (2000)	cut (2000)	cut (2000)
E9	85%	0%	cut (2000)	cut (2000)	cut (2000)
E10	100%	50% cut (2030)	cut (2030)	cut (2000)	cut (2000)

Total Chlorine Abundance (all halocarbons, ppbv)							
Year	A1	B1	C1	D1	D2	D3	
1985	2.98	2.98	2.98	2.98	2.98	2.98	
2000	4.52	4.41	4.33	4.31	4.07	3.98	
2030	7.09	5.93	5.12	4.89	4.17	3.66	
2060	9.16	7.15	5.75	5.35	4.15	3.55	
2090	10.72	8.09	6.25	5.73	4.05	3.42	

Year	E1	E2	E3	E4	E5	E6	E7	E8	E9	E10
1985	2.98	2.98	2.98	2.98	2.98	2.98	2.98	2.98	2.98	2.98
2000	4.30	4.30	4.30	4.30	4.21	4.21	4.21	4.22	4.26	4.30
2030	4.77	4.29	4.09	3.52	2.98	2.84	2.58	2.72	3.01	3.38
2060	5.15	4.19	3.87	3.30	2.67	2.27	1.95	2.18	2.64	2.13
2090	5.47	4.03	3.64	3.07	2.41	1.88	1.55	1.84	2.43	1.59

THEORETICAL PREDICTIONS

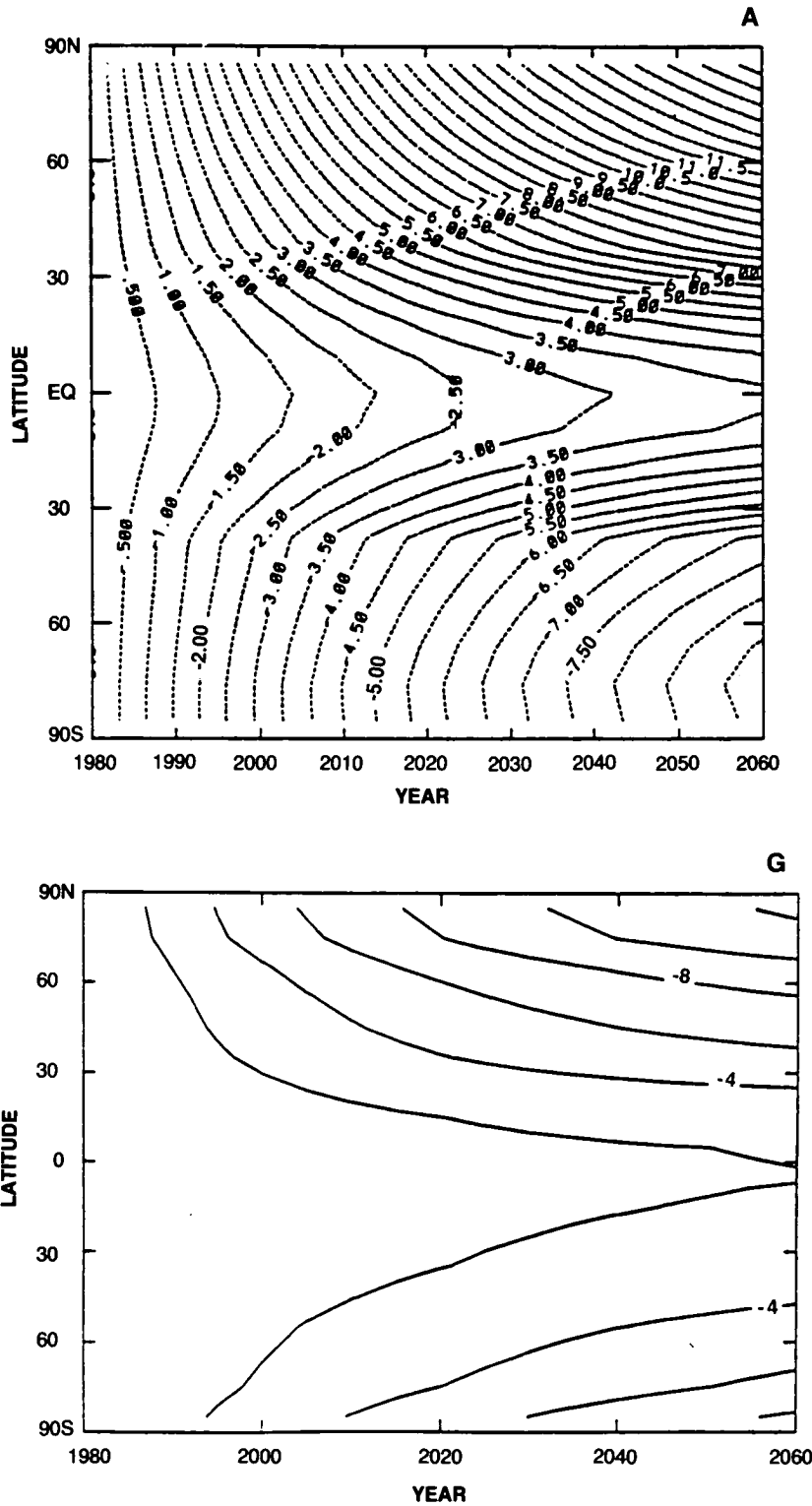


Figure 3.2-5. Time-line of the percent change in column ozone as a function of latitude for the month of March from 1980 through 2060 for scenario A1. (Note the exceptions: the reference year for the JMRI and Mainz plots is 1960 rather than 1980.)

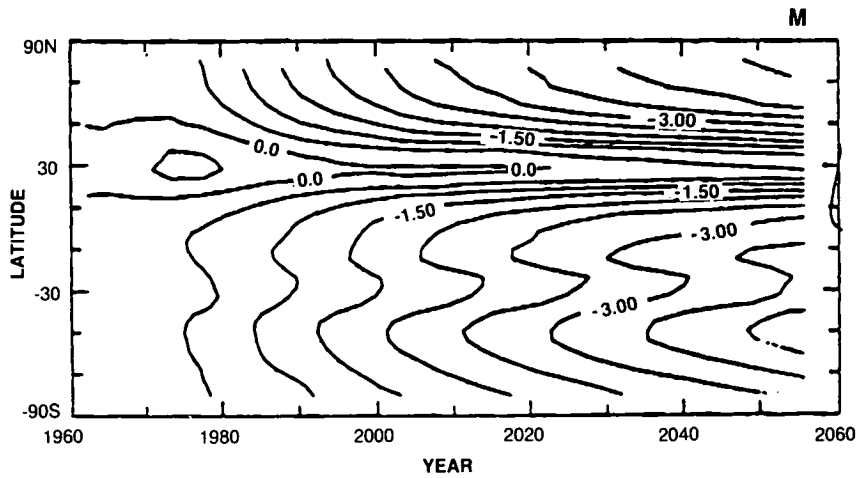
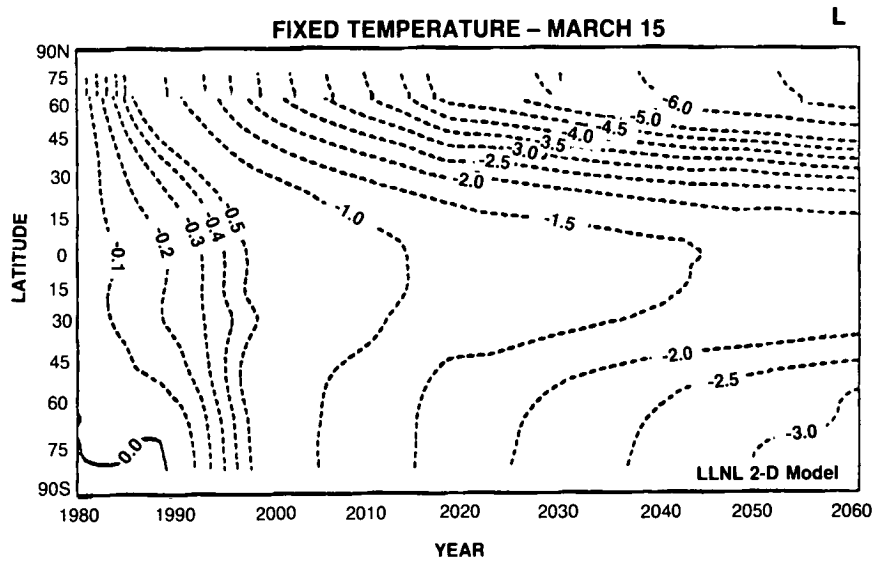
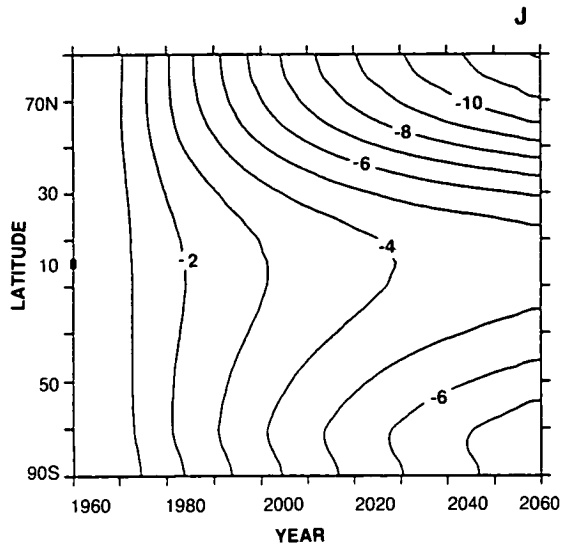


Figure 3.2-5. continued

THEORETICAL PREDICTIONS

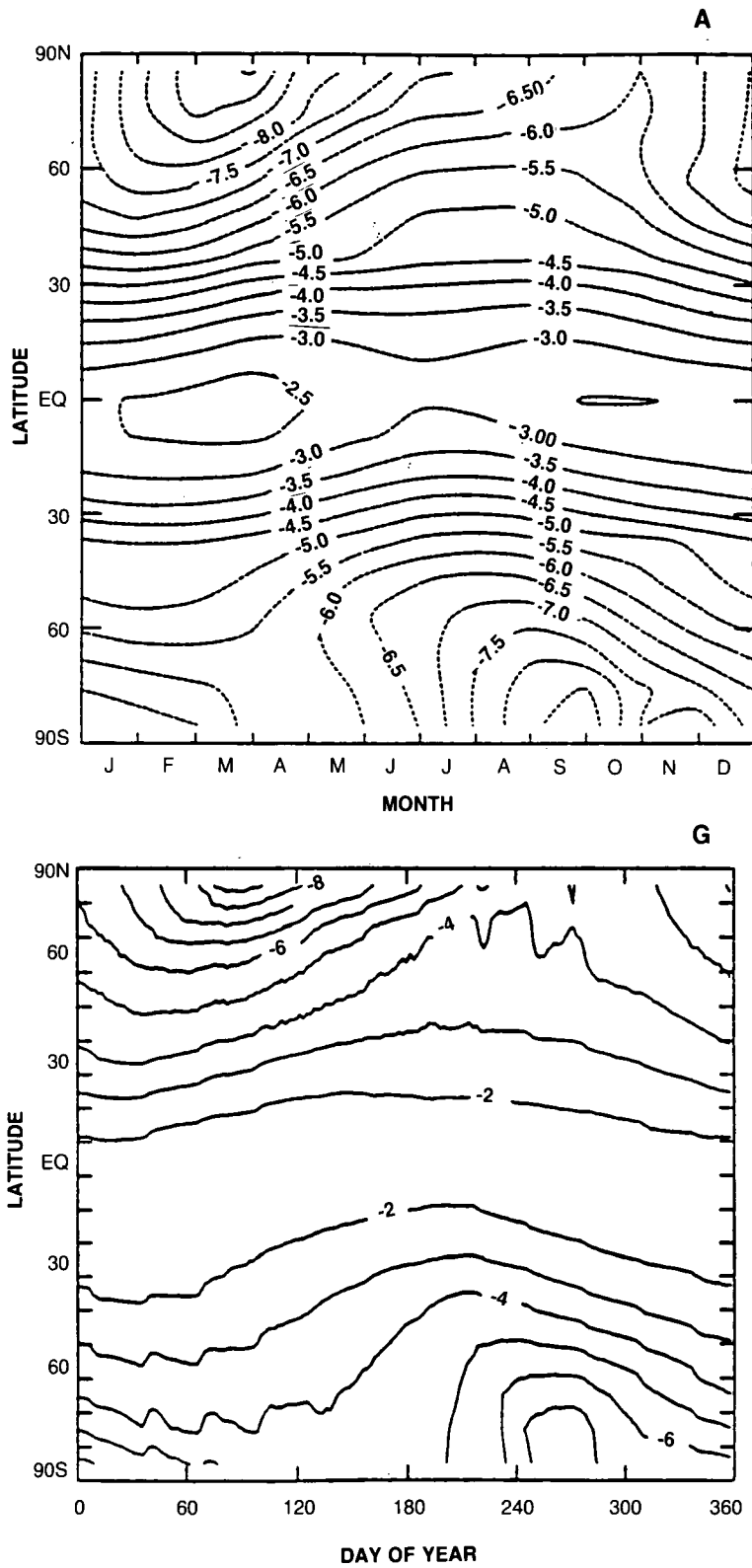


Figure 3.2-6. Dobson map (latitude by month) of percent change in column ozone from 1980 to 2060 using scenario A1.

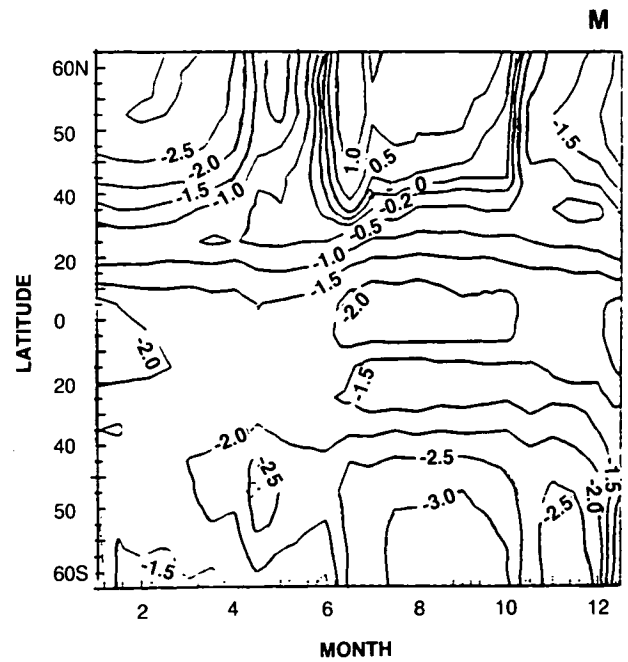
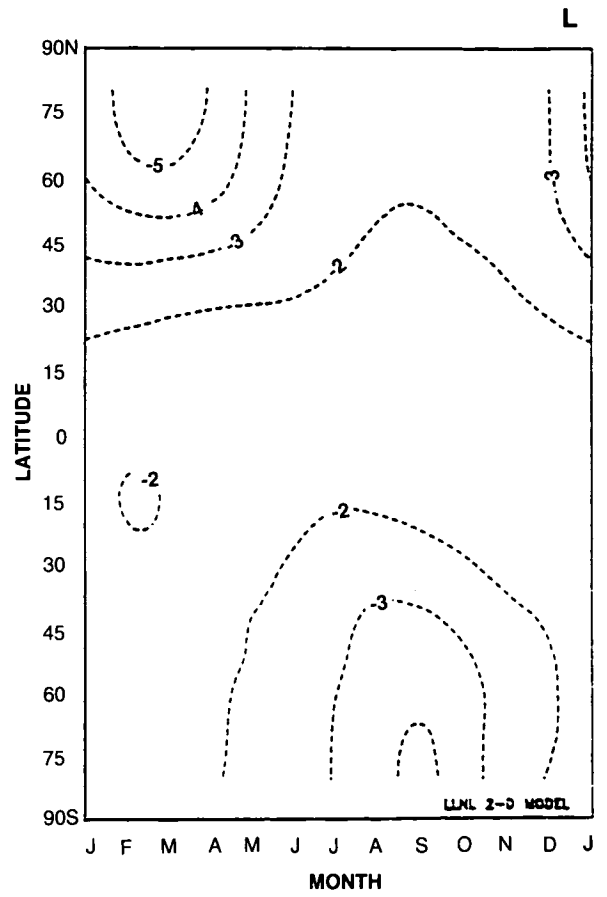
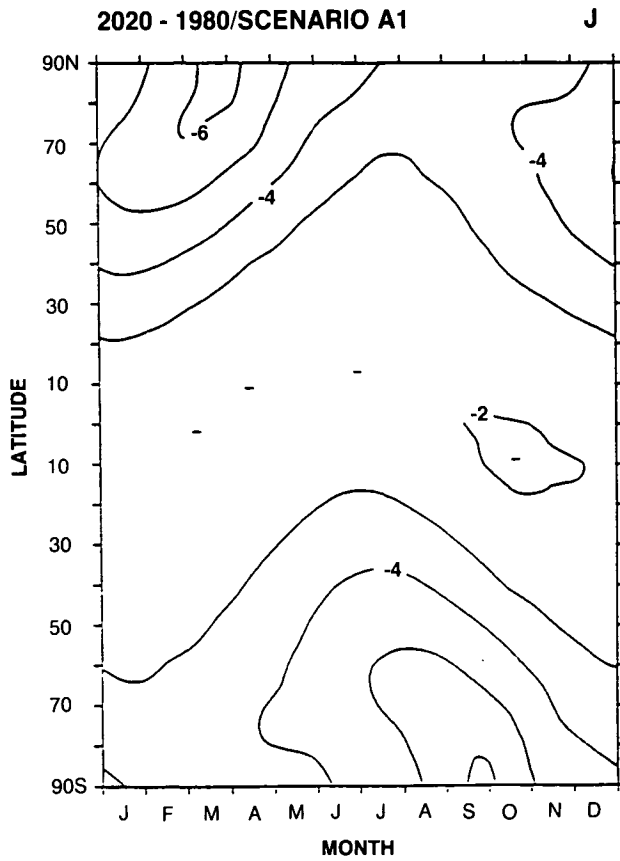


Figure 3.2-6., continued

THEORETICAL PREDICTIONS

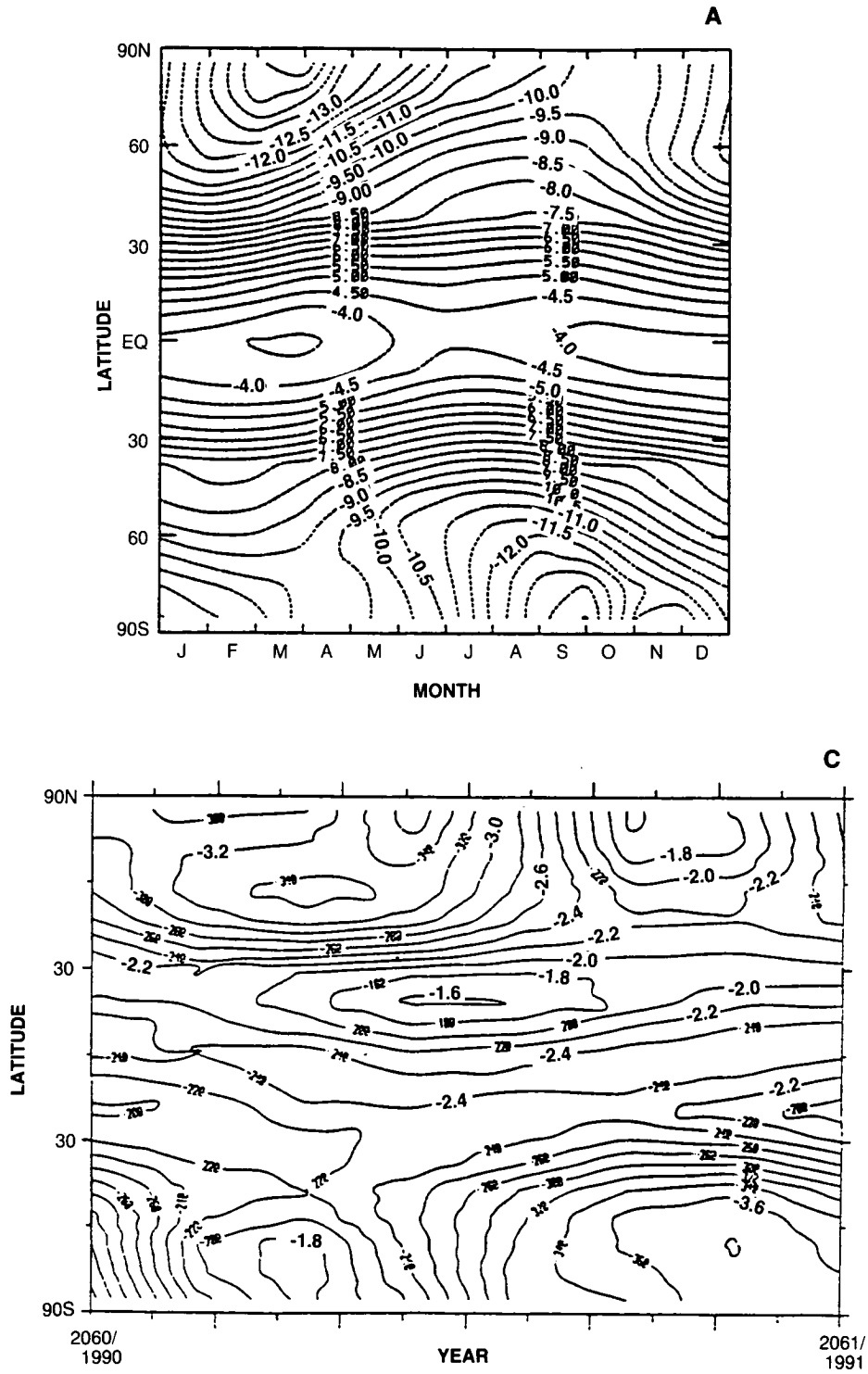


Figure 3.2-7. Dobson map of percent change in column ozone from 1980 to 2060 using scenario A1. (Note the exceptions: Cambridge plots 2060 vs. 1990 beginning with October; the LL plot refers to the LLNL model including temperature feedback; the Oslo model plots 2050 vs. 1985.)

THEORETICAL PREDICTIONS

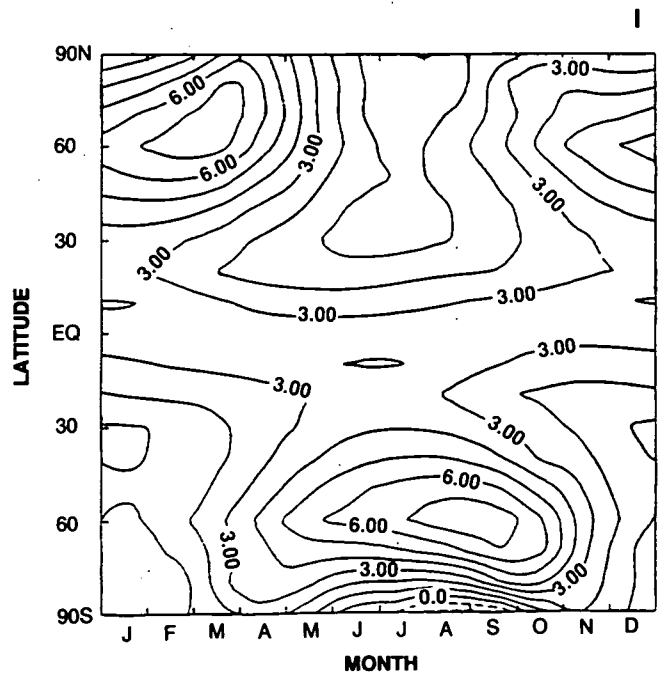
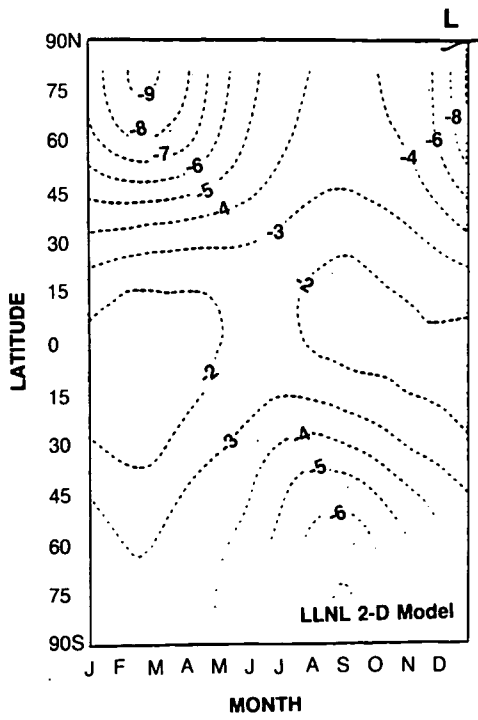
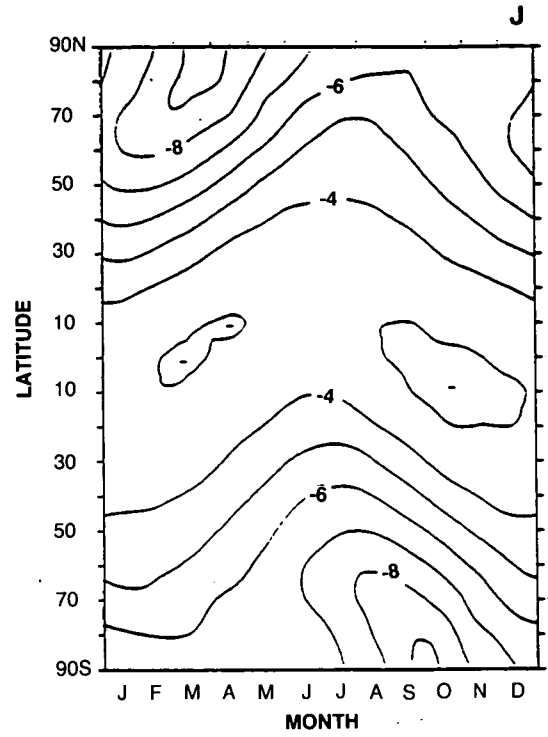
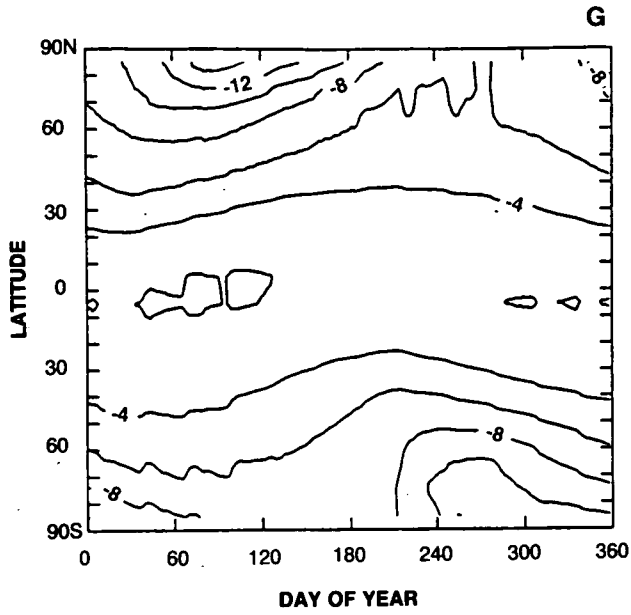


Figure 3.2-7., continued

THEORETICAL PREDICTIONS

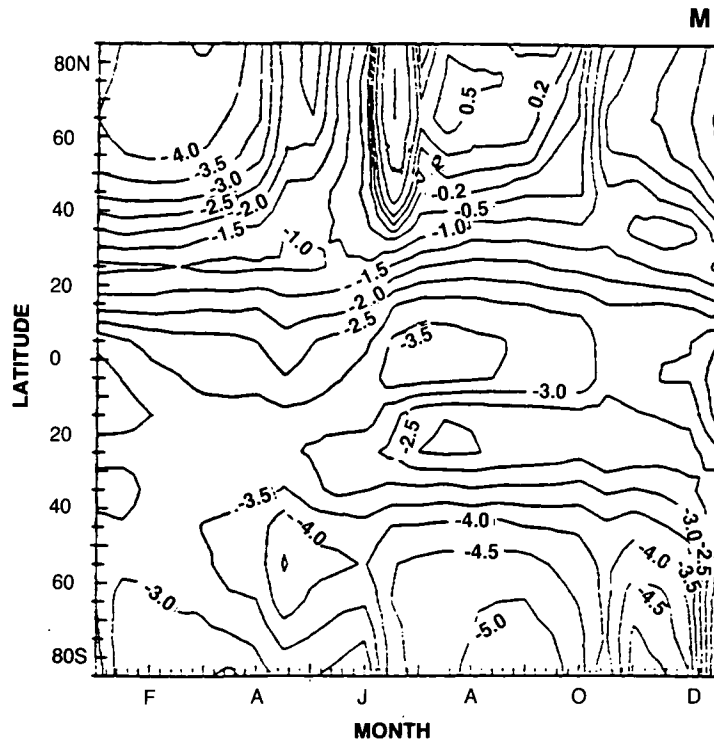
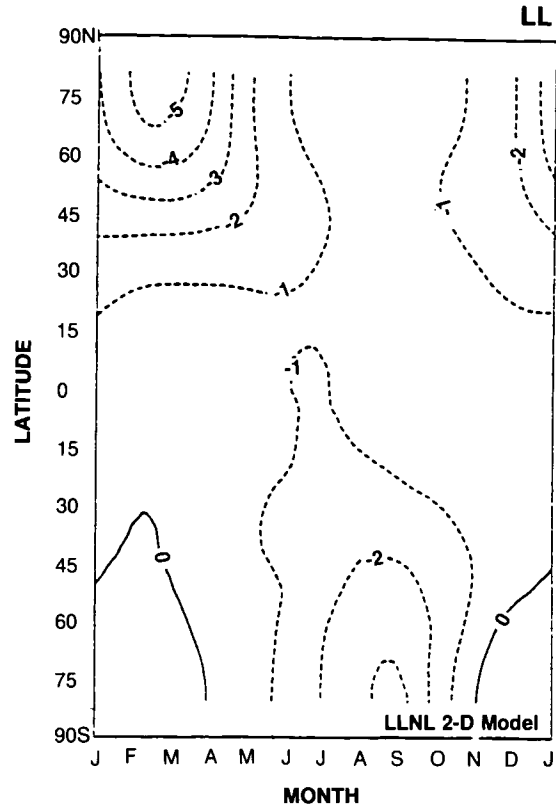
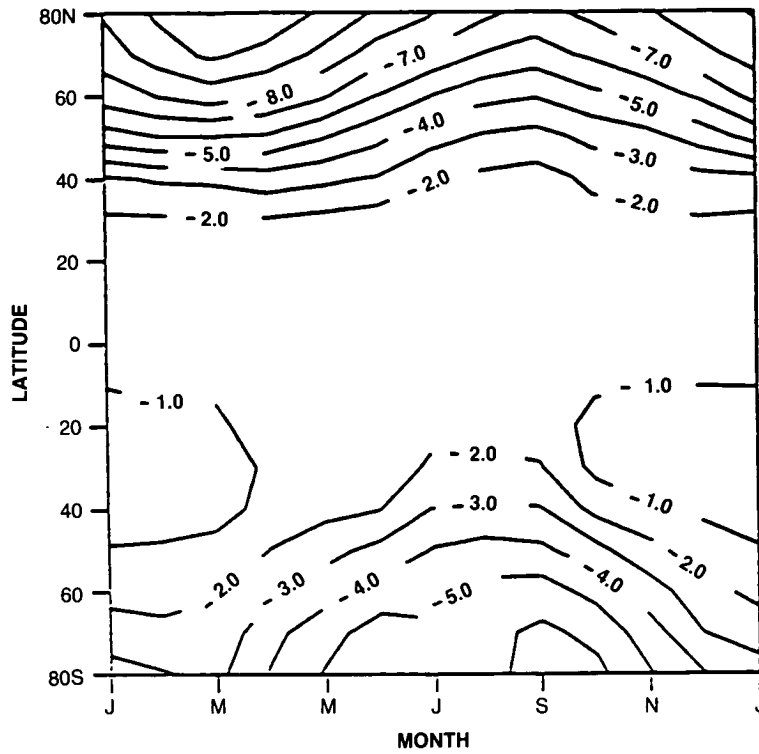


Figure 3.2-7., continued

2050 vs 1985

O



U

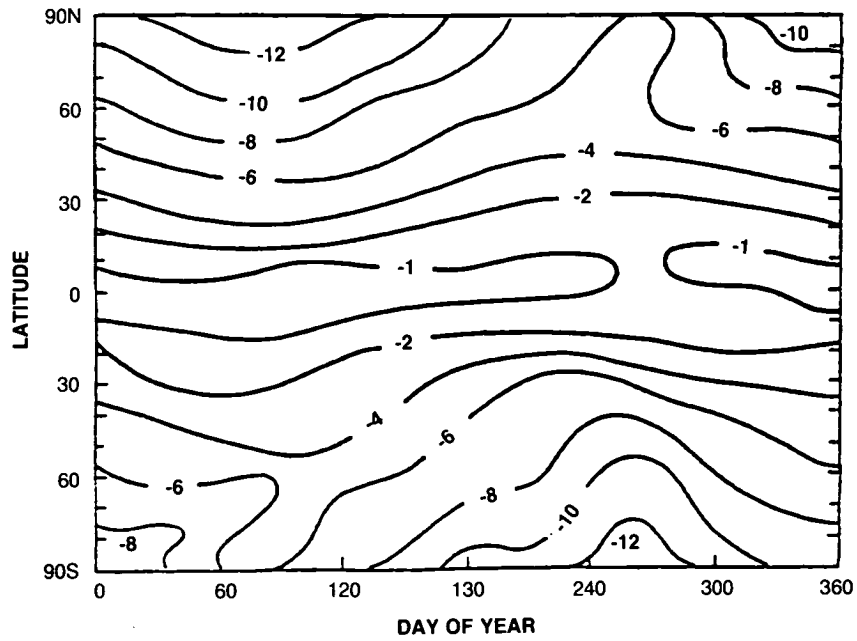


Figure 3.2-7., continued

THEORETICAL PREDICTIONS

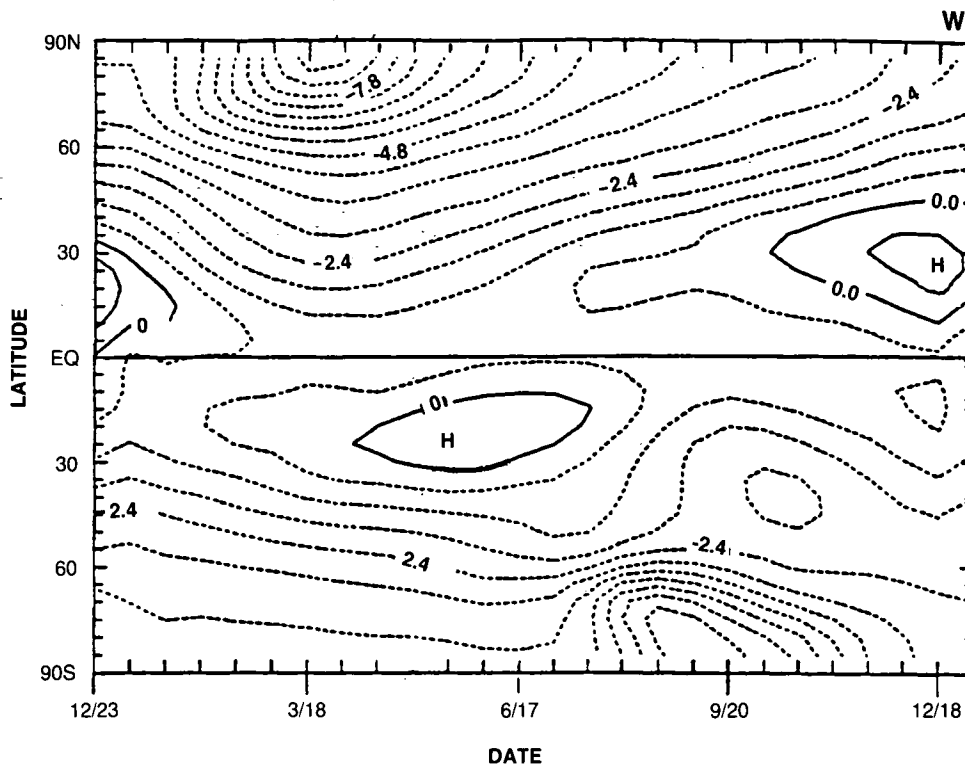


Figure 3.2-7., continued

GSFC2, and NSU models; greater than 7% in the Aquila, JMRI, LLNL, Oslo, and WisCAR models; but only 3–4% in the Cambridge and Mainz models. The LLNL model contributed an additional calculation in which temperature feedbacks were allowed (denoted LL) that resulted in significantly less ozone depletion by 2060, only 4–5% maximum in the northern winter and 2–3% in the southern winter.

One likely cause of this discrepancy among the models is the calculated temperature “feedback” (i.e., decrease in response to O₃ and CO₂ changes) and the photochemical response to it. The temperature of the stratosphere is expected to be lower in the future mainly due to increases in the CO₂ long-wave cooling. The models exhibiting the largest depletions (AER and GSFC2) assume fixed temperatures and circulations; and those with the smallest include temperature feedbacks (generally decreases). This simple explanation does not fit the Oslo and WisCAR models which include temperature feedbacks. The Mainz model is anomalous in predicting significant increases in ozone at mid-latitudes throughout the summer, apparently due to increased production of ozone by methane-related smog chemistry and the inclusion of unprescribed NO_x increases.

The latitude-by-height contours of percent change in the local ozone concentration from January 1980 to January 2060 are shown in Figures 3.2-8 (A,C,G,J,L,LL,M,O,W). The maximum loss in ozone occurs at about 42 km, is greater near the poles, and ranges from 40 to 60%. (The Mainz model is again anomalous, predicting maximum loss in the tropics in addition to high latitude winter). Two models, Cambridge and the LLNL version with temperature feedback (LL), predict similar patterns in ozone depletion with smaller values near the stratopause, 25–40% for Cambridge and 30–35% for LLNL.

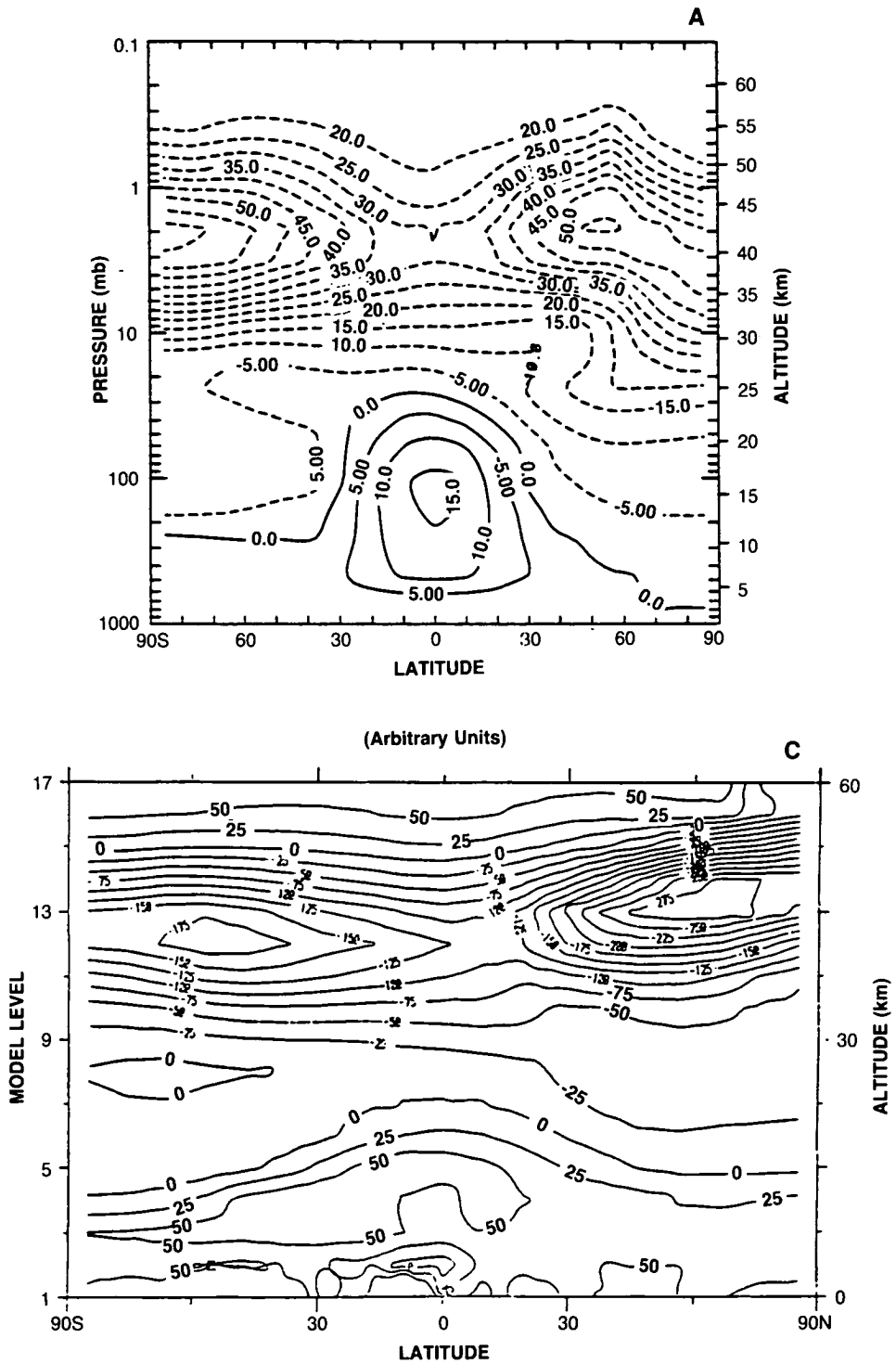


Figure 3.2-8 Latitude-by-altitude (log pressure of height [km]) contour map of the percent change in local ozone concentration from 1980 to 2060 for scenario A1. (The exceptions are noted in 3.2.7.)

THEORETICAL PREDICTIONS

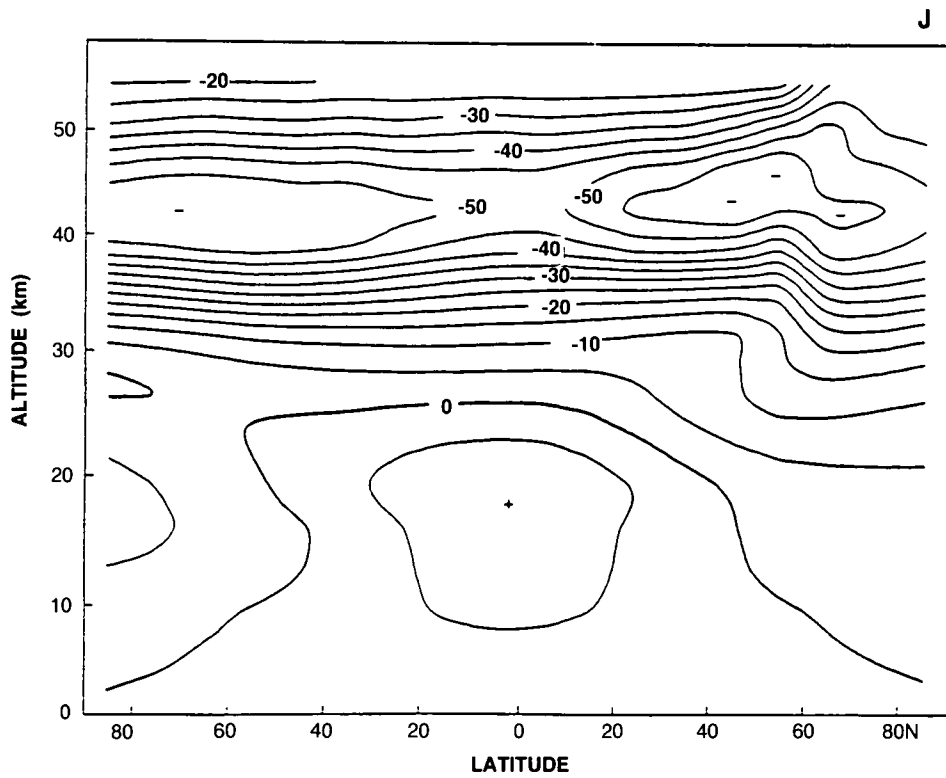
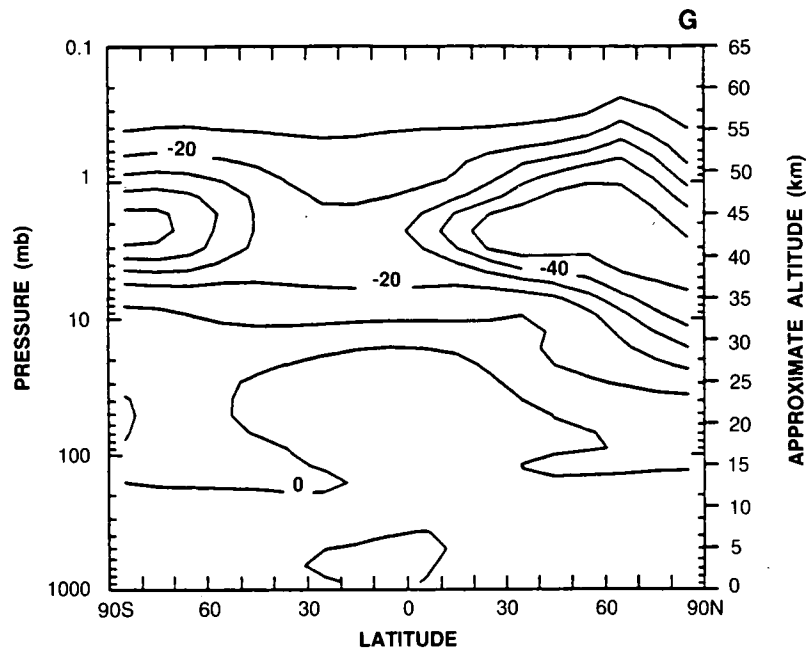


Figure 3.2-8., continued

THEORETICAL PREDICTIONS

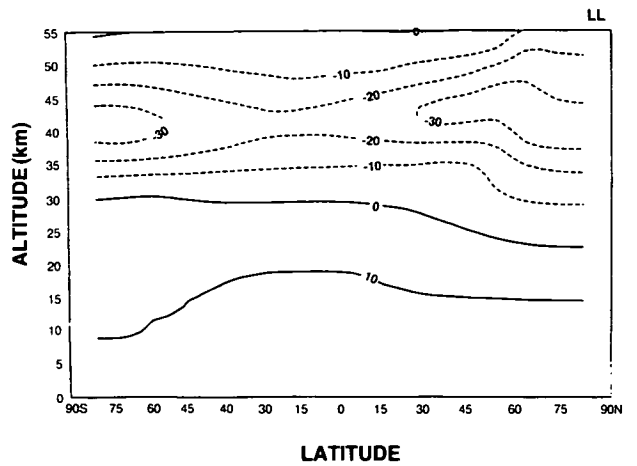
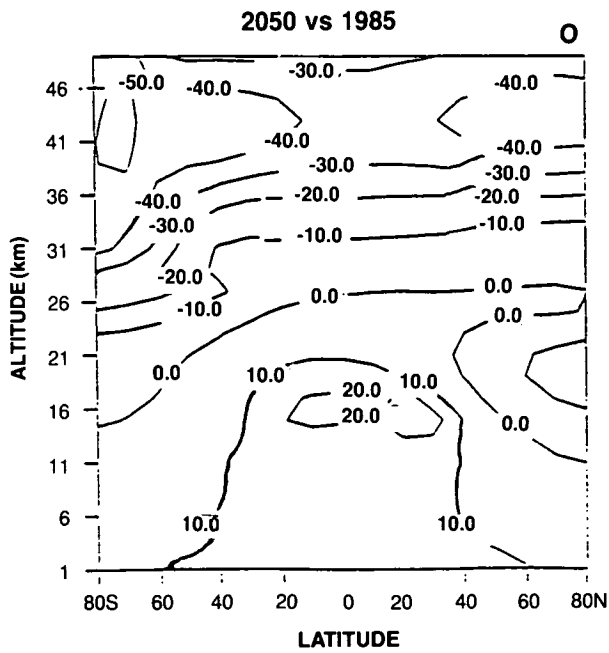
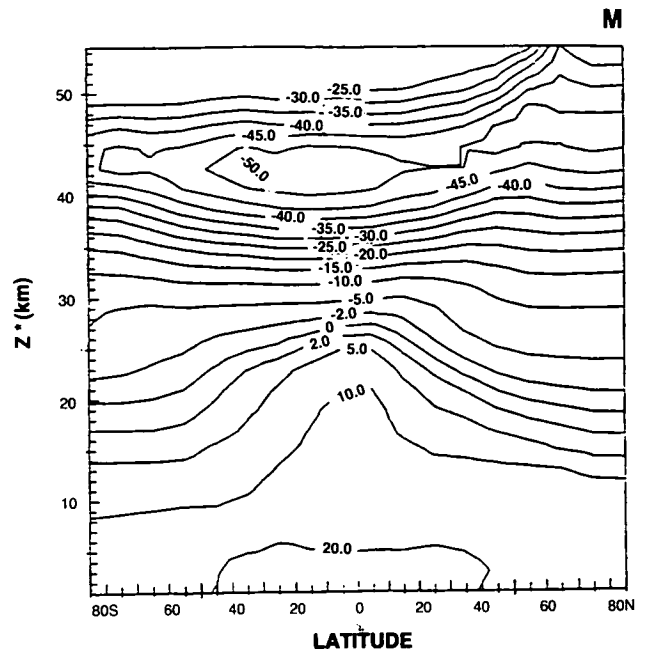
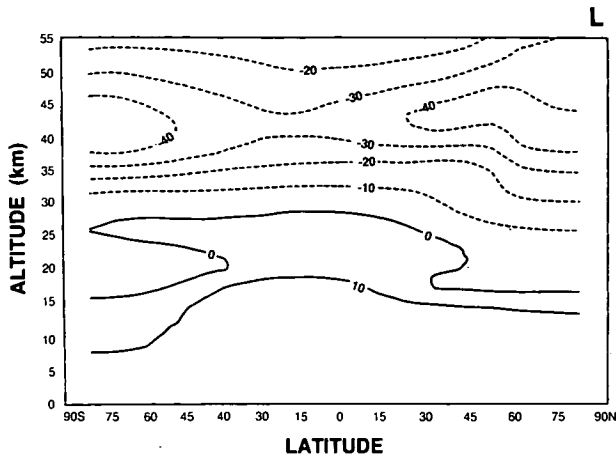


Figure 3.2-8., continued

THEORETICAL PREDICTIONS

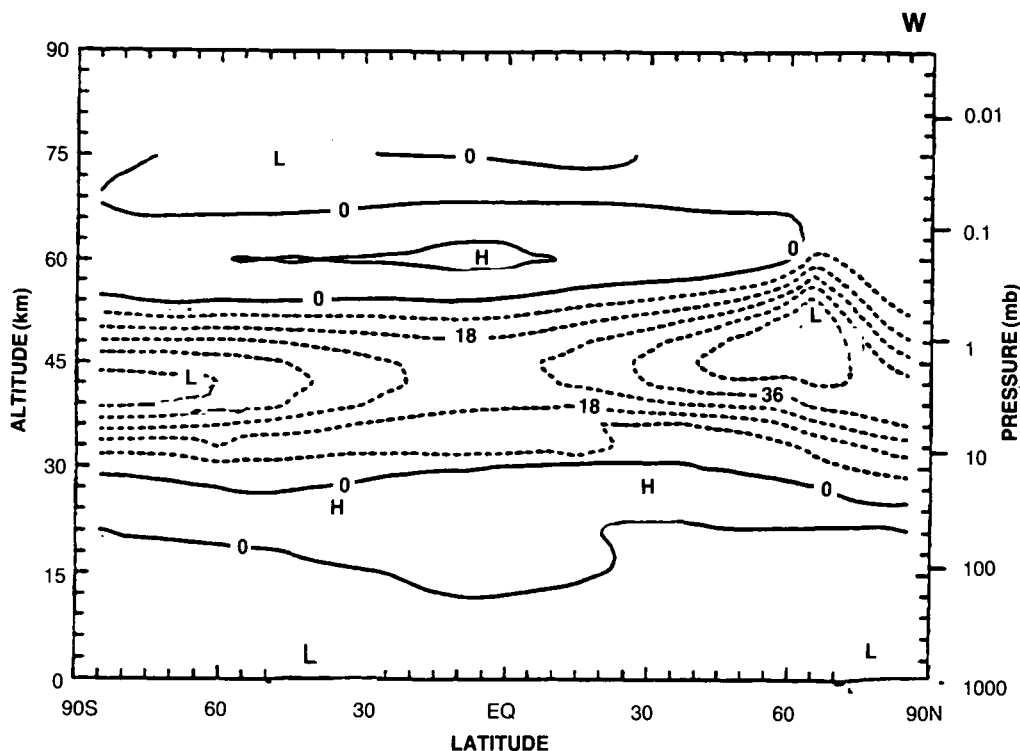


Figure 3.2-8., continued

Overall, the agreement among the models is irregular. All predict some levels of ozone increase in the troposphere and lower stratosphere. The critical difference here is the predicted zero-change contour, which varies considerably from model to model. Much of the calculated change in total column (Figures 3.2-6 and 7) is driven by the small changes in the lower stratosphere. In the upper stratosphere (35–50 km), the predicted ozone depletion is robust among the models if we allow for corrections to values reported from models that do not account for the expected temperature reductions due to decreases in O_3 and increases in CO_2 . In the lower stratosphere (15–25 km) results are more diverse and reflect, among other uncertainties, the difficulty in modeling the temperature change. Note that predictions of perturbations to tropospheric ozone in these calculations are not a robust feature of the models and must be interpreted as having large uncertainty.

Corresponding results for A2 (fixed CH_4) are shown in Figures 3.2-9 through 3.2-11. The continuous time-line of ozone depletion in March (Figure 3.2-9G) shows that when CH_4 does not increase, predicted ozone loss is uniformly greater by about 3% from equator to pole. The Dobson maps of change in column ozone (Figures 3.2-10 [G,O,W]) from the GSFC2, Oslo and WisCAR models show similar results: the seasonal pattern is almost unchanged from A1, but depletions are larger by 3–4% percent for all seasons and latitudes. The change in local ozone concentration (Figures 3.2-11 [G,O,W]) is greater in the region of maximum loss near 42 km by as much as 10%. More importantly, the region of ozone increase occurs at lower altitudes, and much of the lower stratosphere and even troposphere is predicted to experience ozone loss by 2060. Clearly most of the local increases in ozone predicted in A1 are associated with the enhanced methane chemistry in the lower stratosphere and upper troposphere.

The capability to represent the feedback among perturbations in radiatively active trace gases, temperature, and transport is essential if we hope to model the real atmosphere. Ozone reductions should lead to reduced solar heating and consequent changes in the temperature distribution and zonal winds,

hence wave propagation and absorption, and tracer transport. Similarly, “greenhouse” temperature changes may be expected to alter the ozone distribution through photochemical and transport effects. Recently, a few modeling groups have begun to develop the capability to account for these feedbacks. Results for scenario A1 in the AER and WisCAR models are shown in Figures 3.2-12–3.2-15. In both models, increased cooling to space by CO_2 and reduced ultraviolet absorption by O_3 combine to weaken the stratopause markedly (Figure 3.2-12). Due to the temperature dependence of Planck emission to space, cooling is strongest near the summer stratopause. Through the thermal wind relation, this results in weakened summer easterlies near the stratopause (Figure 3.2-13). Similarly, the cold polar winter stratosphere does not cool as much as the tropical stratosphere and leads to slightly reduced westerlies in the polar stratosphere.

The net radiative heating for the 1980 reference atmosphere in December for these two models is shown in Figure 3.2-14. This illustrates how the wave-driven circulation causes departures from radiative equilibrium. The two models agree regarding the dynamically driven descent in the winter hemisphere, which leads to higher temperatures and increased cooling to space, and ascent in the summer hemisphere, which leads to slightly cooler temperatures and net heating. With reduced temperature gradients, weaker zonal winds result in weaker wave driving (Rayleigh drag in the AER model; gravity wave driving in the WisCAR model). This in turn results in a weakened summer to winter interhemispheric flow and reduced summer upwelling and winter downwelling in the upper stratosphere and lower mesosphere, which is reflected in the difference plots for heating rates (Figure 3.2-15). The situation in the lower stratosphere is less clear. Initial results for the WisCAR model, however, suggest that with strengthened westerlies over the south polar lower stratosphere (Figure 3.2-13), Rossby waves would more readily propagate into the region, leading to enhanced upward motion in the summer polar stratosphere, hence stronger net radiative heating, as seen in Figure 3.2-15. Since changes in tropospheric temperature and wave forcing are not included in current 2-D models, these results must be interpreted with caution.

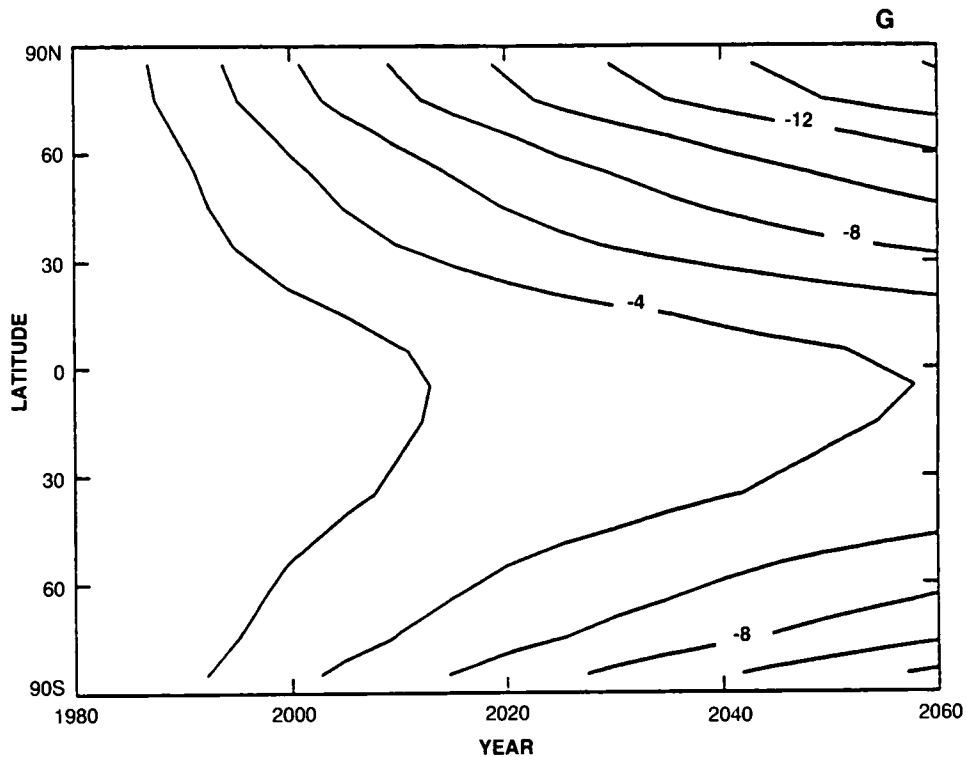


Figure 3.2-9. Time-line vs. latitude of the percent change in column ozone during March from 1980 to 2060 for scenario A2.

THEORETICAL PREDICTIONS

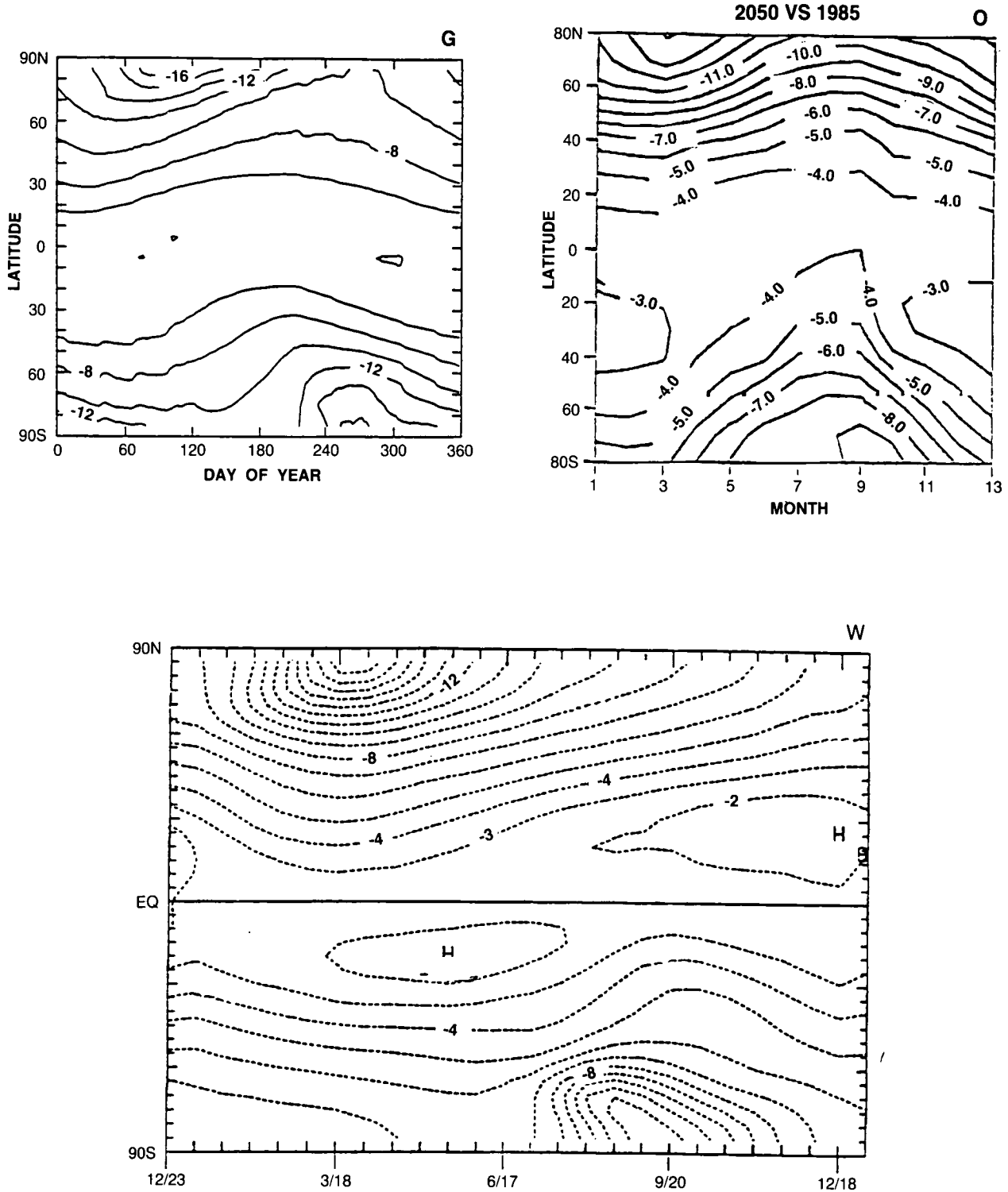


Figure 3.2-10. Dobson map of percent change in column ozone from 1980 to 2060 using scenario A2.

THEORETICAL PREDICTIONS

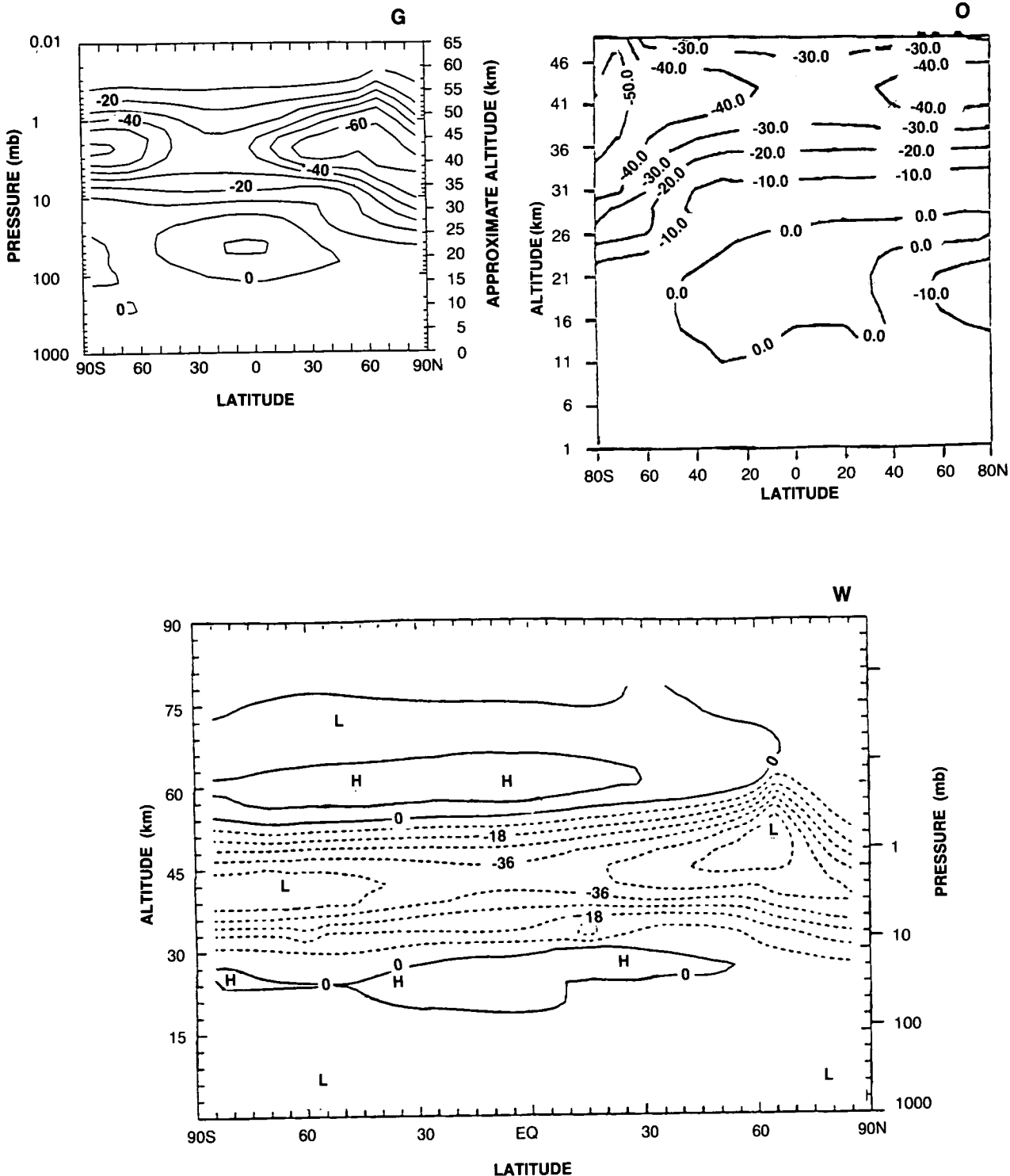


Figure 3.2-11. Latitude-by-altitude map of the percent change in local ozone concentration from 1980 to 2060 for scenario A2.

THEORETICAL PREDICTIONS

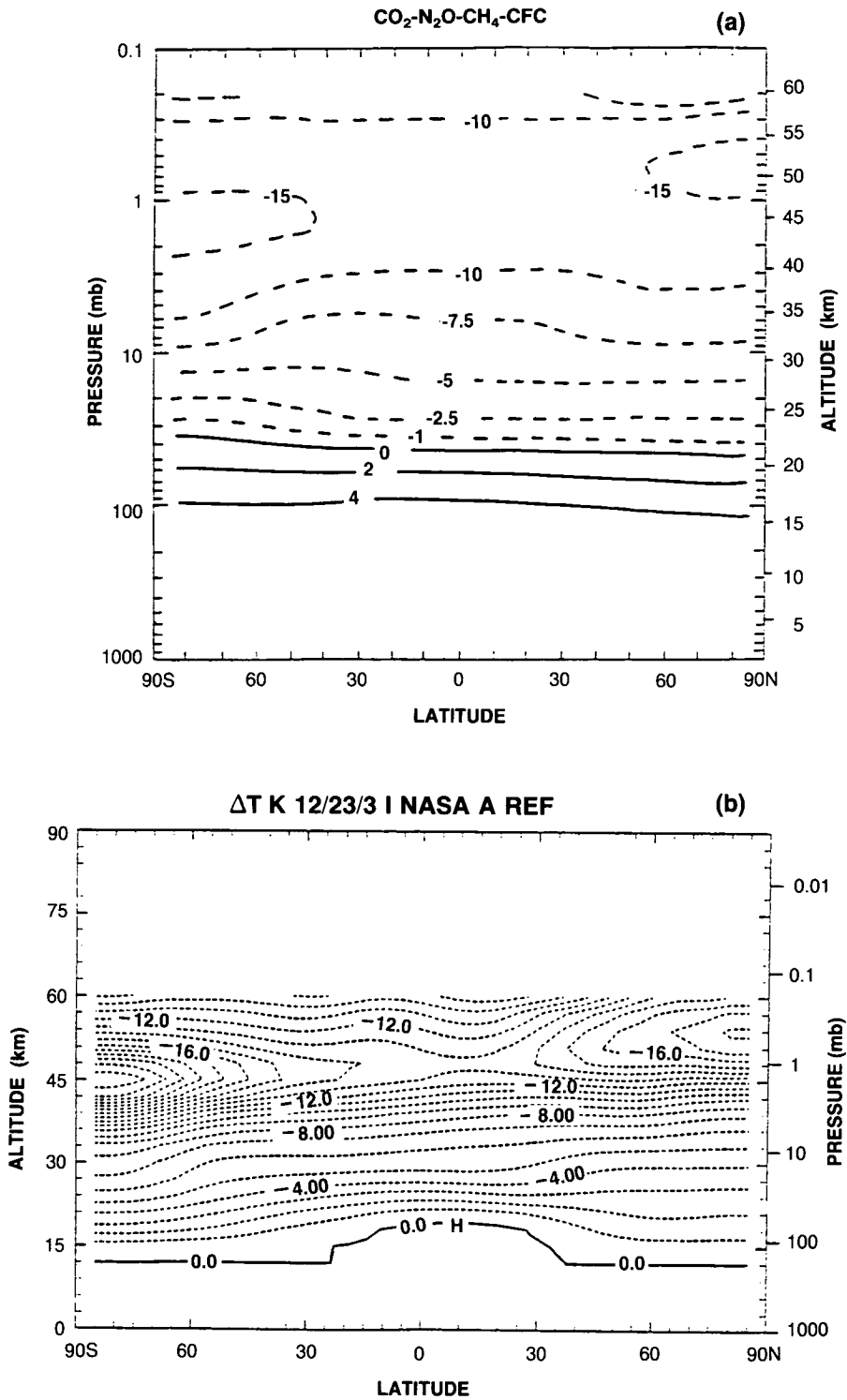


Figure 3.2-12. Temperature change (K) for December (scenario A1: 1980-2060) from the (a) AER and (b) WisCAR models.

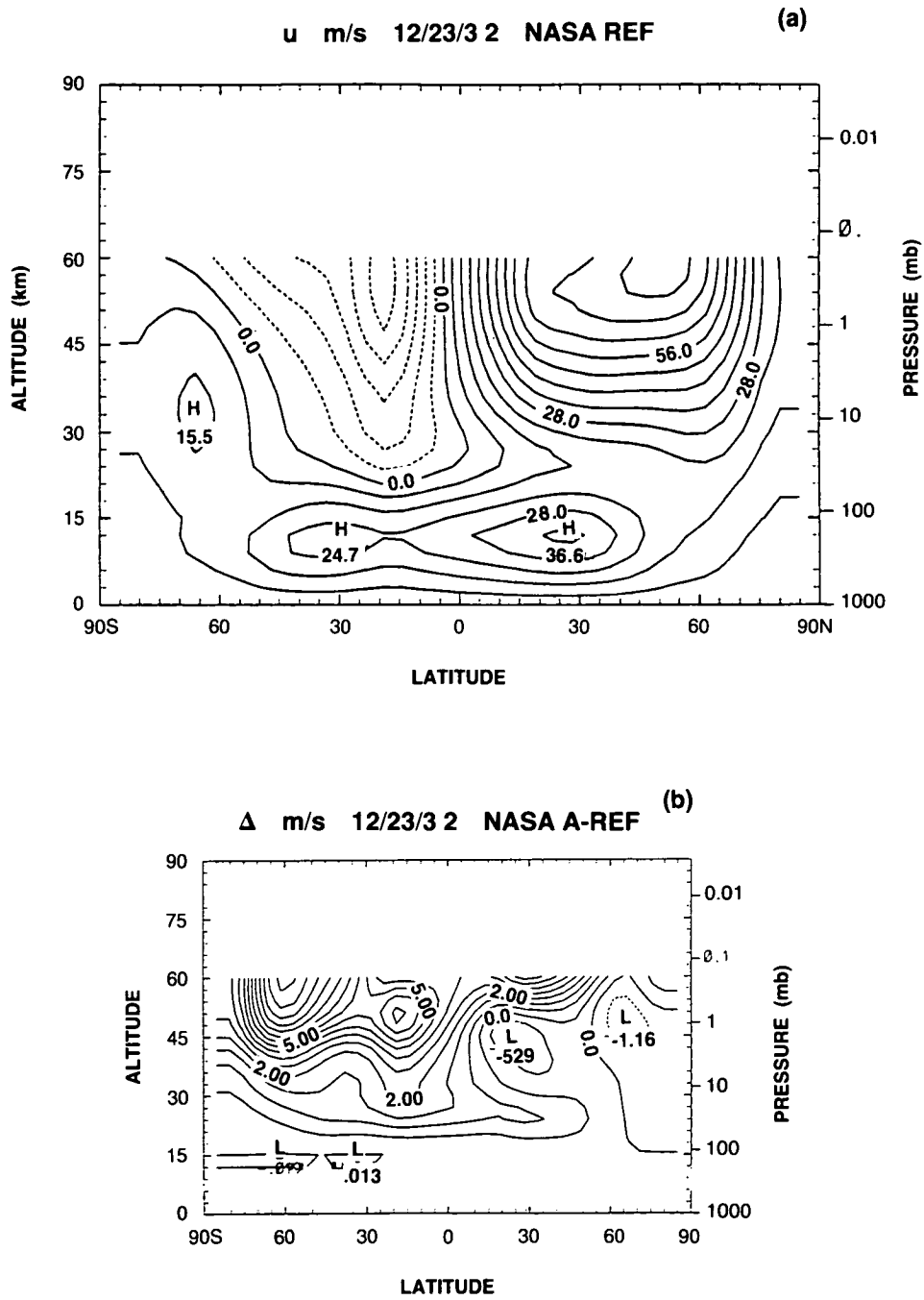


Figure 3.2-13 Zonal wind (a) and zonal wind change from December 1980 to December 2060 (b) for the WisCAR model (scenario A1). Contour intervals are 7 and 0.7 m/s, respectively.

THEORETICAL PREDICTIONS

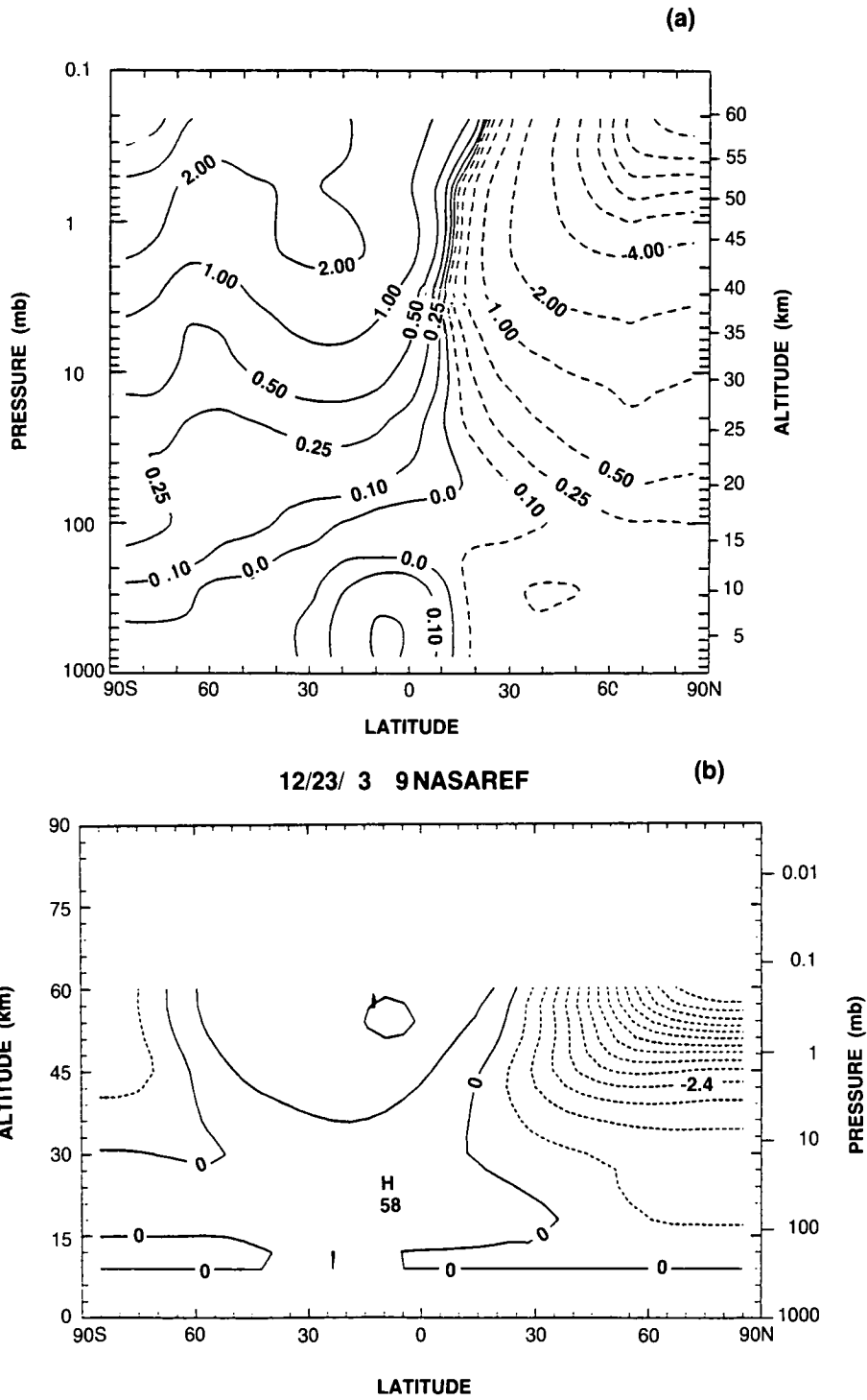


Figure 3.2-14. Net radiative heating (K/day) for December 1980 in the (a) AER and (b) WisCAR models.

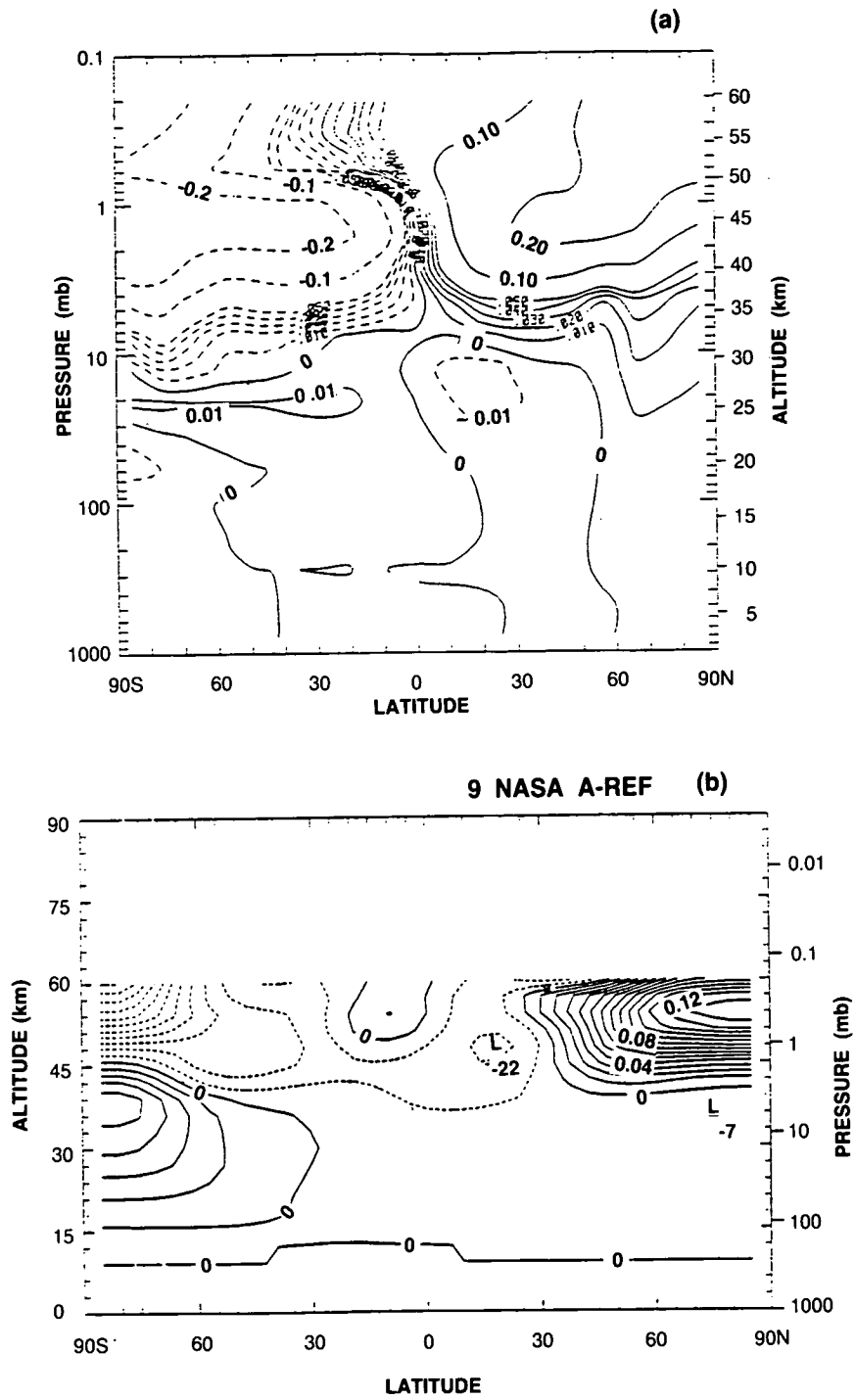


Figure 3.2-15. Change in net radiative heating (K/day) from December 1980 to December 2060 (scenario A1) in the (a) AER and (b) WisCAR models.

THEORETICAL PREDICTIONS

In summary, the chlorine loading of the atmosphere in the reference scenario (A1) increases from 3.0 ppbv in 1985 to 4.5 ppbv in the year 2000, to 7.1 in the year 2030, and to 9.2 in the year 2060. The bromine loading increases from 13 pptv in 1985 (10 pptv CH₃Br constant) to 31 pptv in the year 2060. For models that did not contain the carbon dioxide effect and other temperature feedbacks, reductions in column ozone from 1980 to 2060 ranged from 1% to 4% in the tropics and from 8% to 12% at high latitudes in late winter. For models that included the carbon dioxide effect, the corresponding ozone reductions were less: 0% to 1.5% in the tropics and 4% to 8% in high latitudes in late winter. Ozone reductions at 40 km were about 35–50% in models with no temperature feedback, and about 25–40% in models with temperature feedback, resulting in temperature decreases of 10–20 K. No heterogeneous chemistry was included in these models. When methane increases are suspended in 1985, ozone column reductions are larger in all latitudes and seasons by about 3%. Methane increases reduce the efficiency of the chlorine catalytic cycle and further contribute to the direct production of ozone by “smog chemistry” in the lower stratosphere and troposphere. Many of the differences in the model results occur in the lower stratosphere where it is more difficult to predict the impacts of radiative and chemical forcing.

3.2.2.4 Scenario B: 1980–2060

The scenario B1 corresponds to an idealized simulation of the Montreal Protocol in which production/emissions are cut by 50%. Growth of atmospheric halogens is reduced relative to scenarios A1 and A2: 7 ppb of chlorine and 22 ppt of bromine by 2060. The time-line of column ozone depletion from March 1980 through March 2060 is shown in Figures 3.2-16(A,G,J). Predictions from the AER, GSFC2, and JMRI models are similar, but note that these three models are usually in agreement and that all use fixed temperatures and circulations. The impact of cutting CFC production by 50% is to reduce the ozone depletion by March 2060 at mid-latitudes, relative to scenario A1, by about 2% from approximately 8% to 6%. The Dobson maps of column ozone change from 1980 to 2060, Figures 3.2-17(A,G,J), show similar results: 1–3% in the tropics and 5–8% at high latitudes in late winter. The changes in local ozone concentration over this period (Figures 3.2-18 [A,G,J,N]) are similar to those from A1, with reduced ozone loss in the upper stratosphere (25–40% depletion at 40 km) and a similar enhancement in the lower stratosphere and troposphere that is associated with the increase in methane. The changes in local temperature from the NOCAR model, shown in Figure 3.2-18NT, are largest in the 40–50 km region where ozone loss is greatest and reach a maximum of –13 K over the summer pole.

3.2.2.5 Scenario C: 1980–2060

The scenario C1 (85% cut in CFC production/emissions) further reduces halogen concentrations in 2060 (5.8 ppb of chlorine and 16 ppt of bromine). Results are available only from the GSFC2 model and include the time-line of column ozone depletion from March 1980 through March 2060 (Figure 3.2-19G), the Dobson maps of change in column ozone from 1980 to 2060 (Figure 3.2-20G), and the changes in local January ozone concentrations over this period (Figure 3.2-21G). The impact of further cuts in CFC emissions is seen clearly in the upper stratosphere, and reductions in column ozone are approximately 50% of those calculated in the reference scenario with column ozone losses still as large as 6% at high latitudes in spring.

3.2.2.6 Scenario D: 1980–2060

The scenarios D1, D2, and D3 explore a sequence of reduced chlorine loading to the stratosphere (see Figure 3.2-2). In D2 and D3 the chlorine levels peak and begin to fall by 2030 and 2000, respectively. Scenario D4 reexamines the minimum halogen scenario D3 without the ameliorating effects of methane increases.

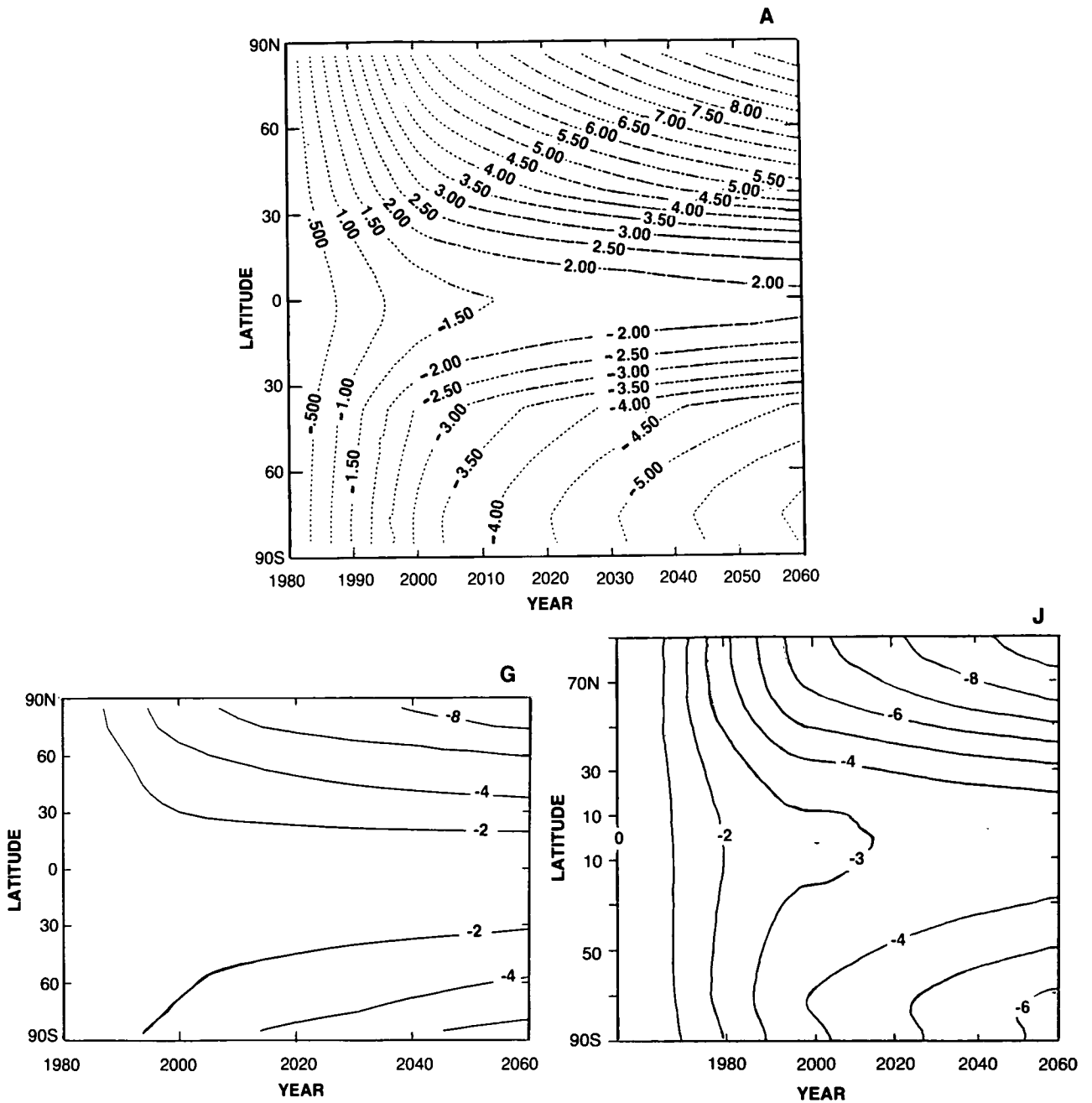


Figure 3.2-16. Time-line vs. latitude of the percent change in column ozone during March from 1980 to 2060 for scenario B1.

The time-line of depletion of column ozone for D1 shown in Figures 3.2-22(G,J,L) displays the familiar latitudinal pattern of greatest losses at high northern latitudes in March. The major difference between this and previous scenarios is that the ozone depletion now reverses at northern mid-latitudes and tends to decline after the year 2000 (although depletion at high southern latitudes continues to rise). The Dobson maps, shown in Figures 3.2-23(G,J,L,U,W), predict the same pattern of ozone depletion as in A1, but

THEORETICAL PREDICTIONS

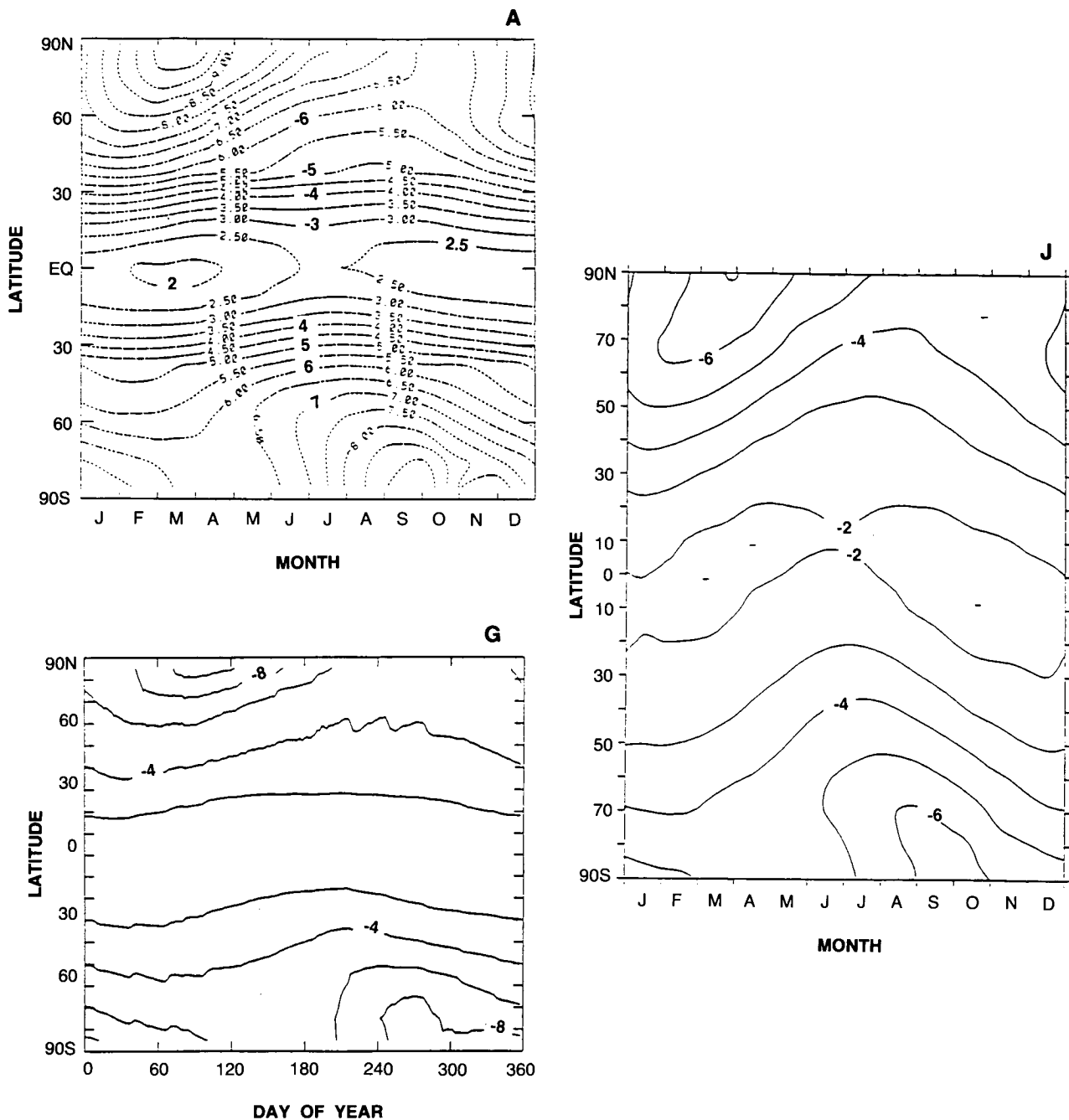


Figure 3.2-17. Dobson map of percent change in column ozone from 1980 to 2060 using scenario B1.

about a factor of 2 smaller at all latitudes. The notable exception being the WisCAR model, which predicts ozone increases of 1–3% everywhere. Local ozone changes (Figures 3.2-24 [G,J,L,W]) in the GSFC2, JMRI, and LLNL models are similar to those predicted for A1, again about a factor of 2 smaller in the upper stratosphere. The WisCAR model predicts ozone loss only in very restricted regions poleward of 30 degrees between 1 and 10 mb. These differences in model predictions for D1 are substantial, associated most likely with model-predicted changes in temperature and circulation, and should be resolved.

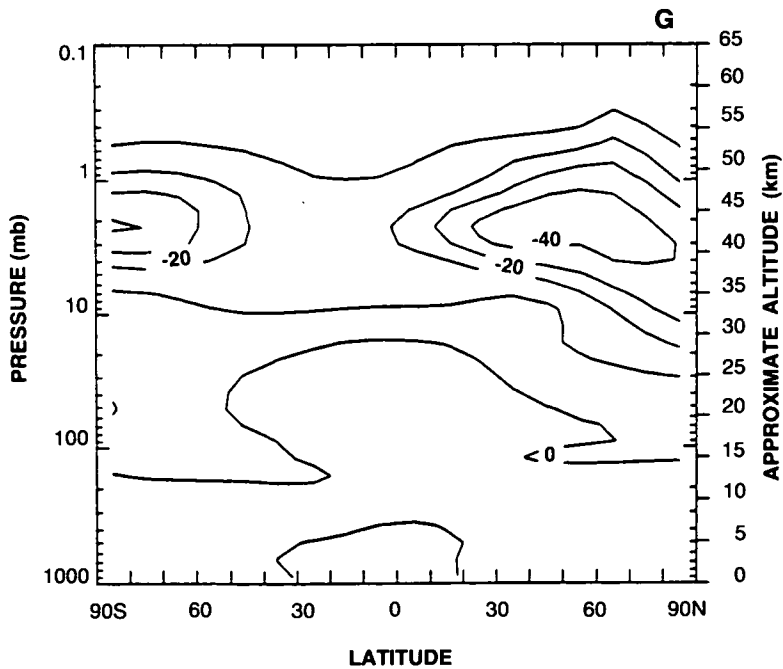
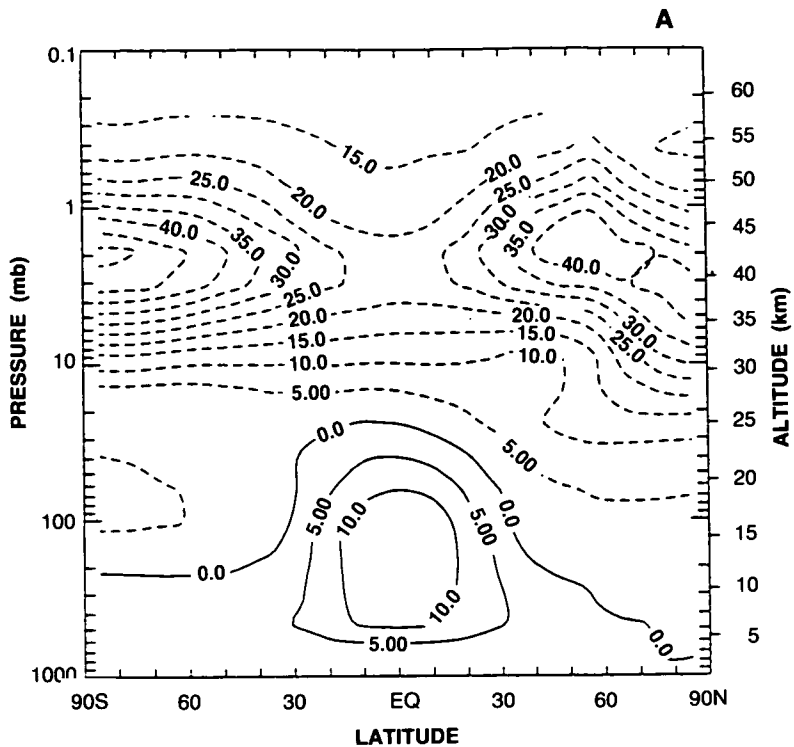


Figure 3.2-18. Latitude-by-altitude map of the percent change in local ozone concentration from 1980 to 2060 for scenario B1.

THEORETICAL PREDICTIONS

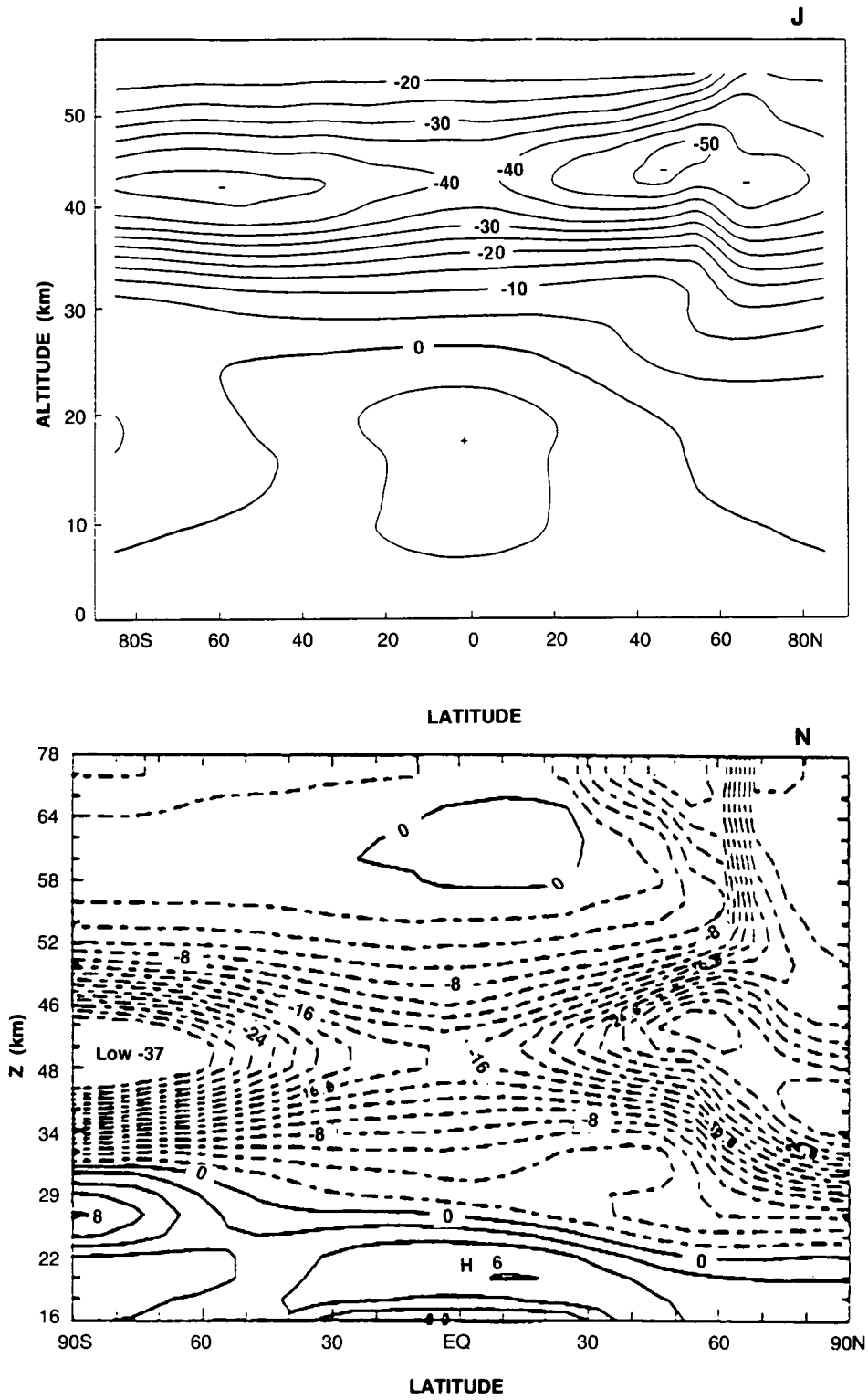


Figure 3.2-18., continued

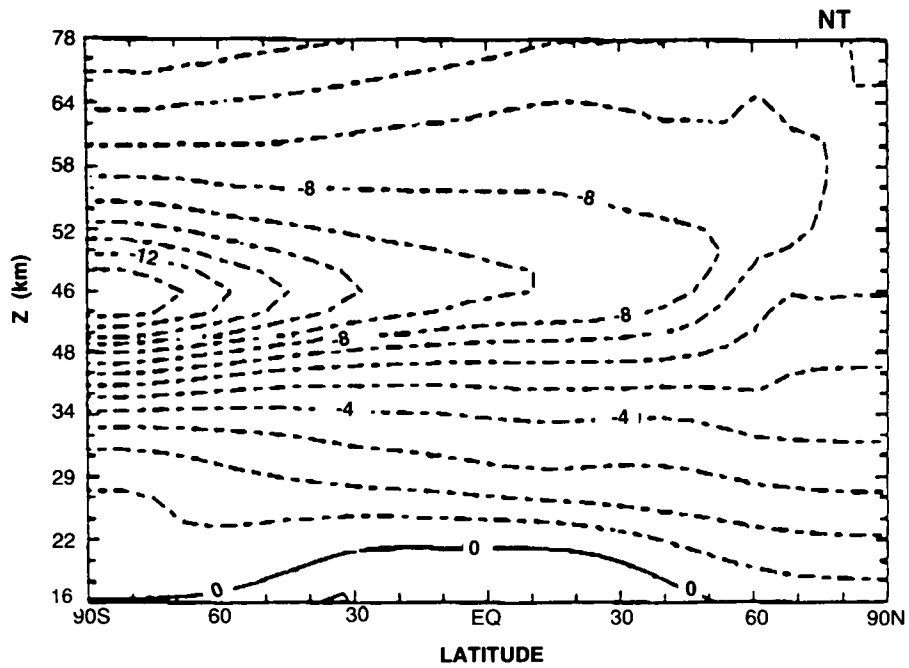


Figure 3.2-18., continued

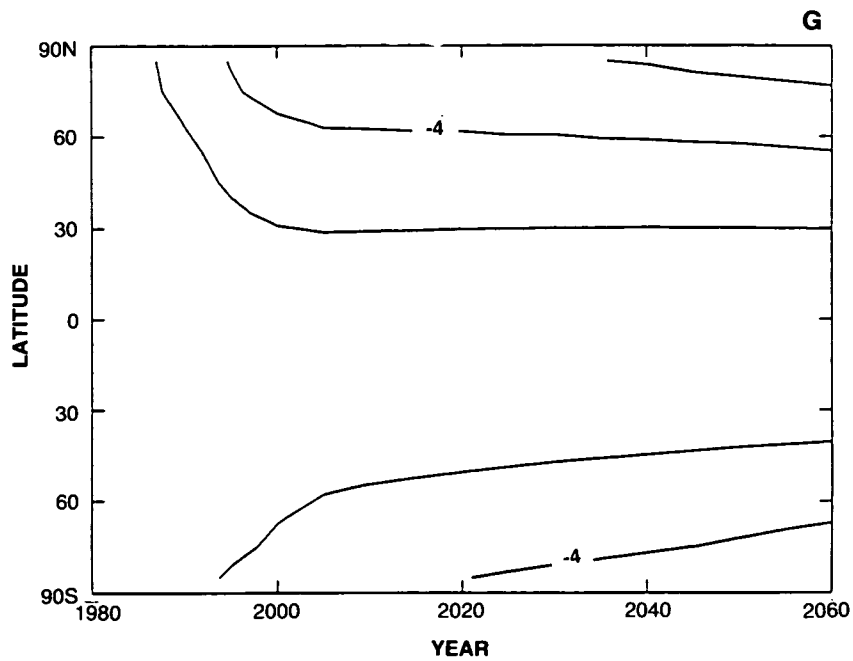


Figure 3.2-19. Time-line vs. latitude of percent change in column ozone during March from 1980 to 2060 for scenario C1.

THEORETICAL PREDICTIONS

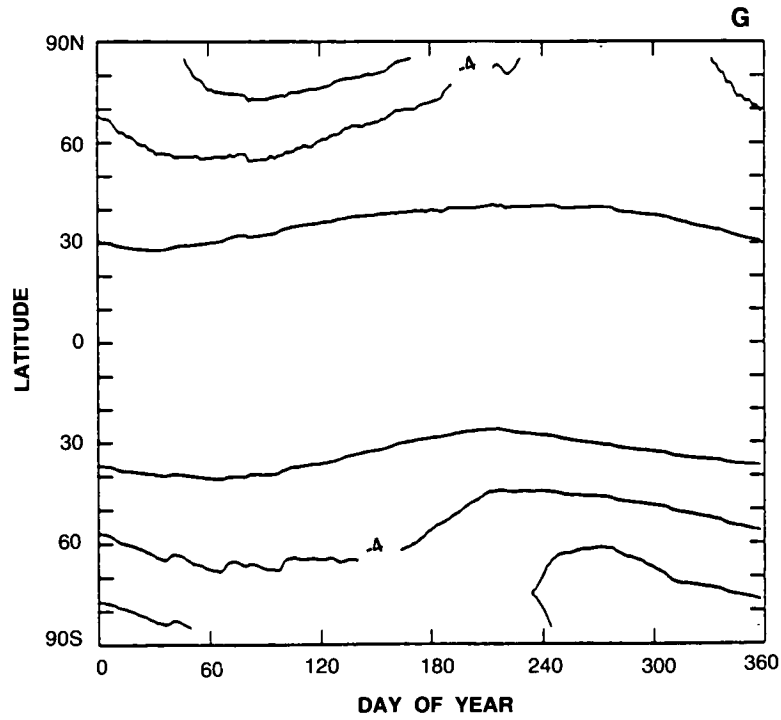


Figure 3.2-20. Dobson map of percent change in column ozone from 1980 to 2060 using scenario C1.

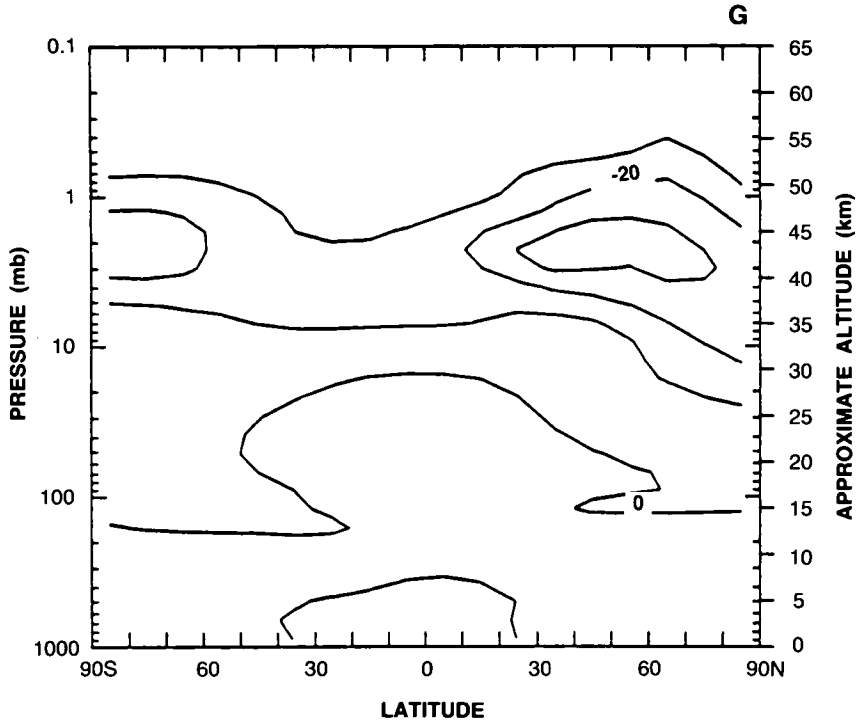


Figure 3.2-21. Latitude-by-altitude map of the percent change in local concentration from 1980 to 2060 for scenario C1.

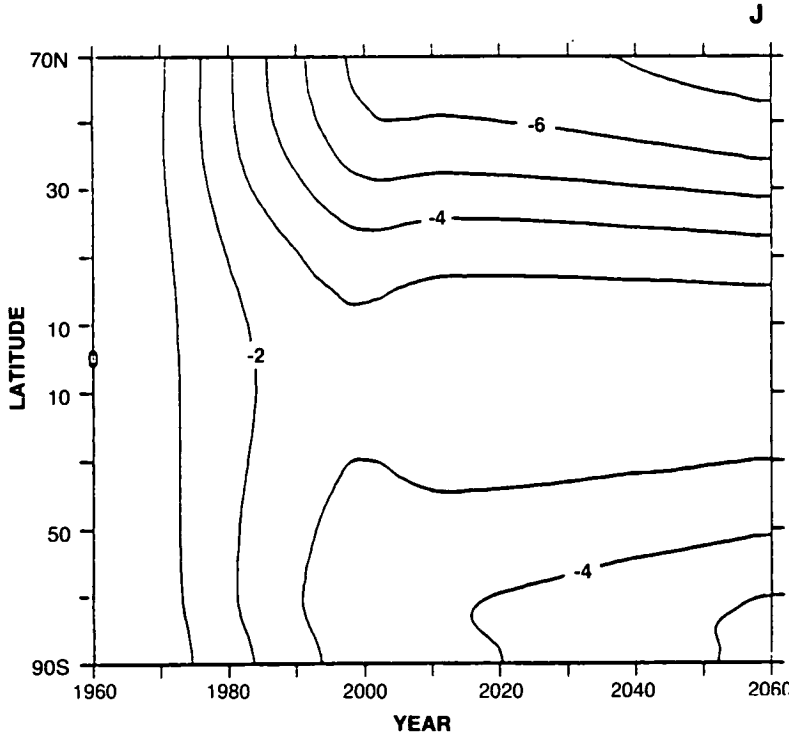
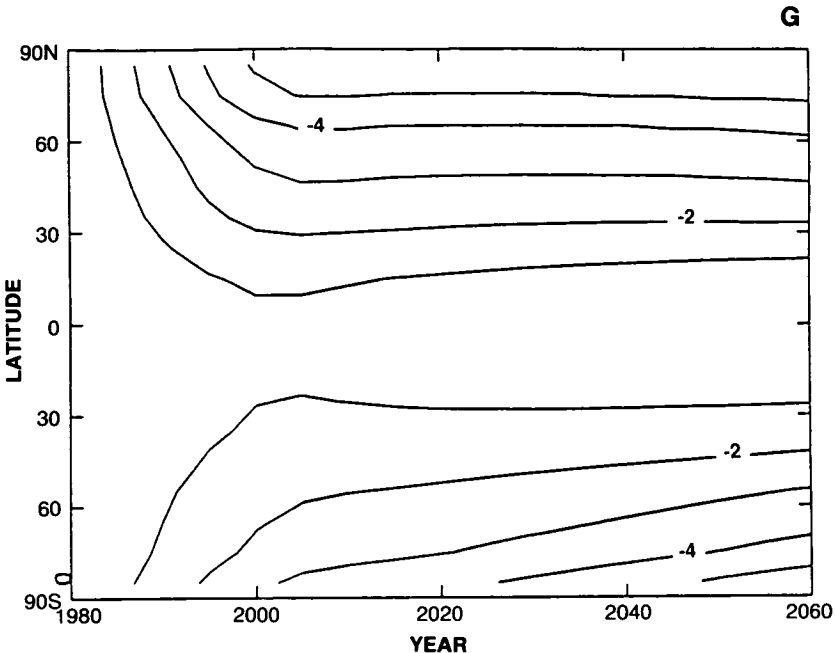


Figure 3.2-22. Time-line vs. latitude of the percent change in column ozone during March from 1980 to 2060 for scenario D1.

THEORETICAL PREDICTIONS

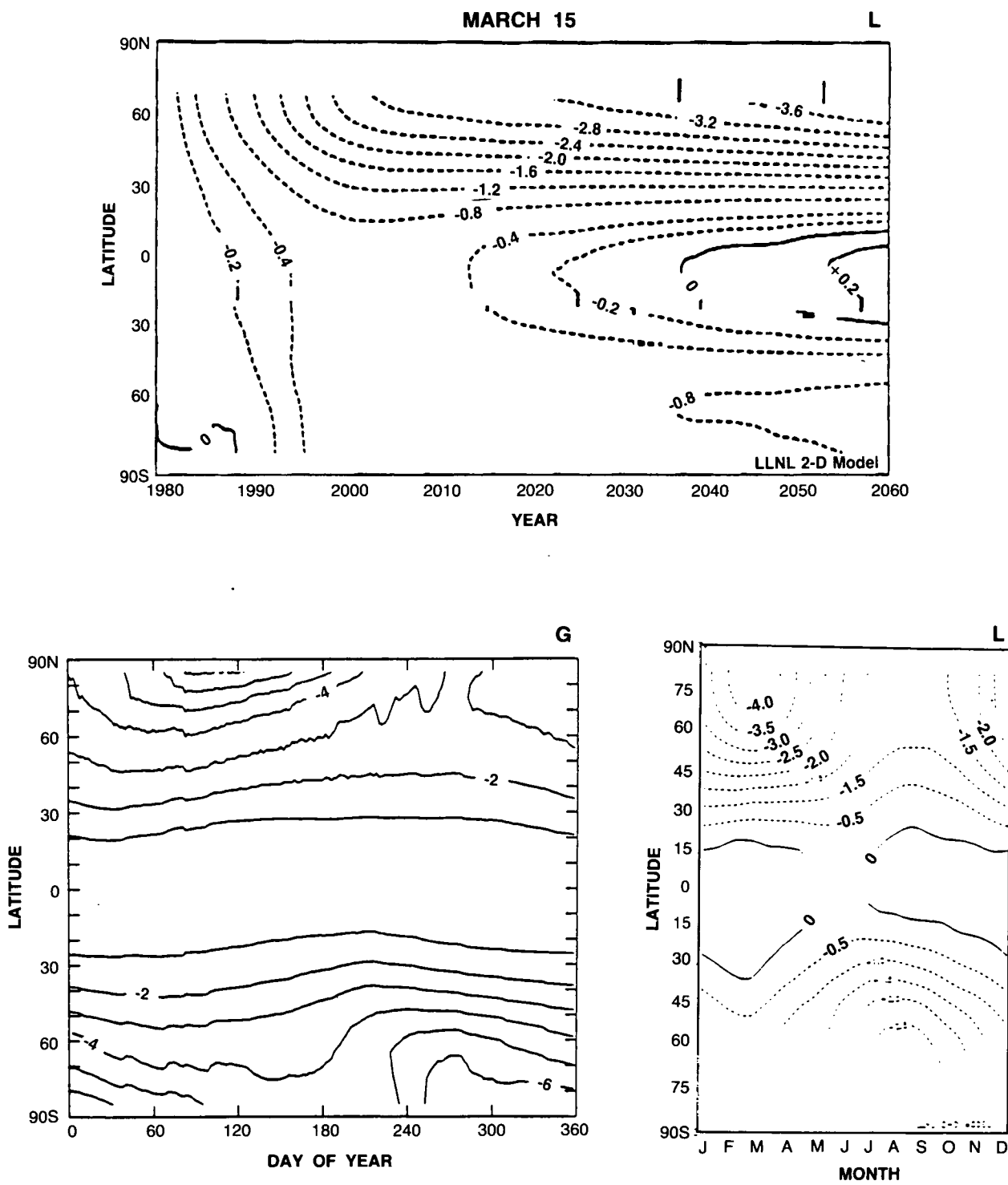


Figure 3.2-23 Dobson map of percent change in column ozone from 1980 to 2060 using scenario D1.

THEORETICAL PREDICTIONS

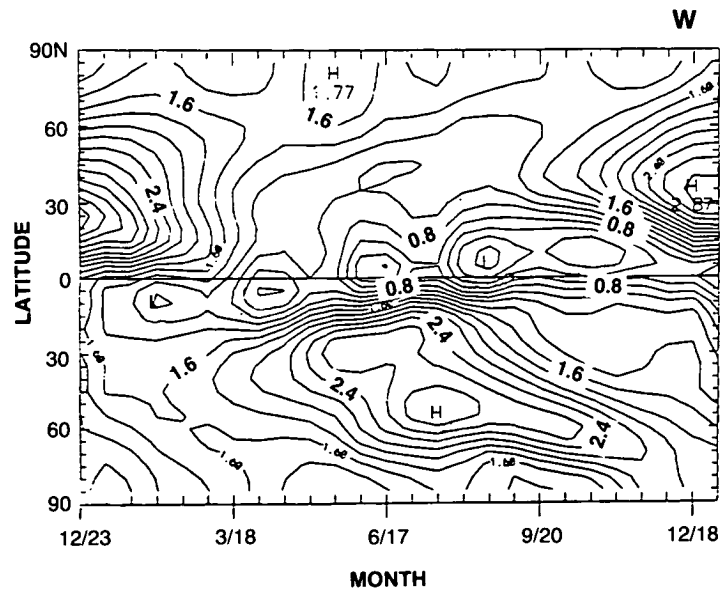
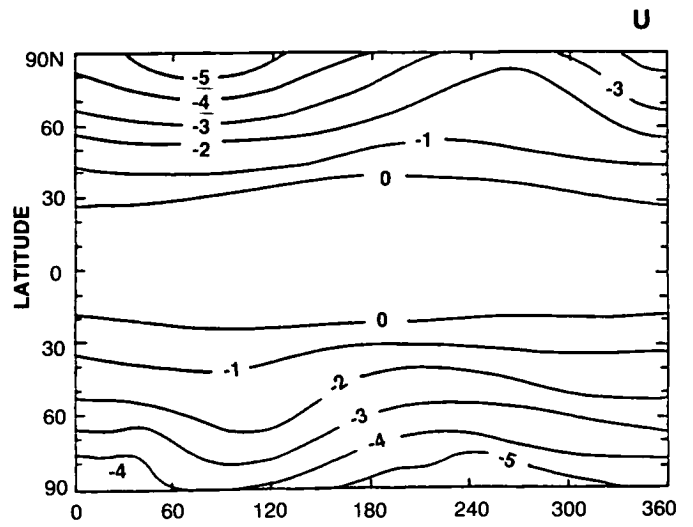
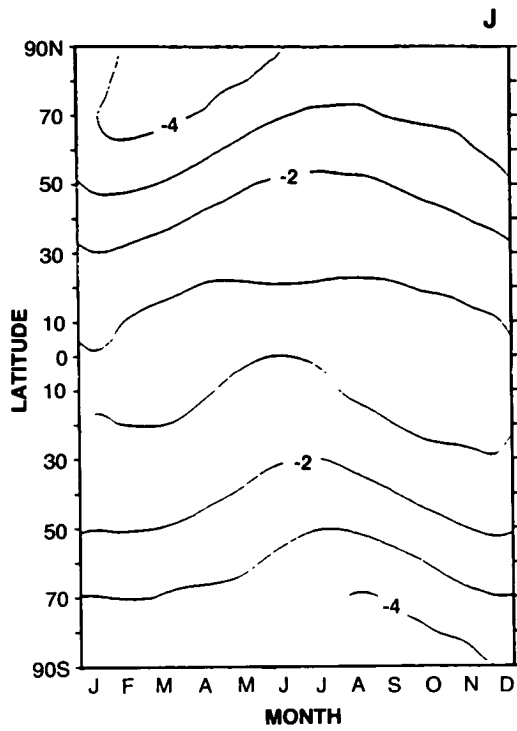


Figure 3.2-23., continued

THEORETICAL PREDICTIONS

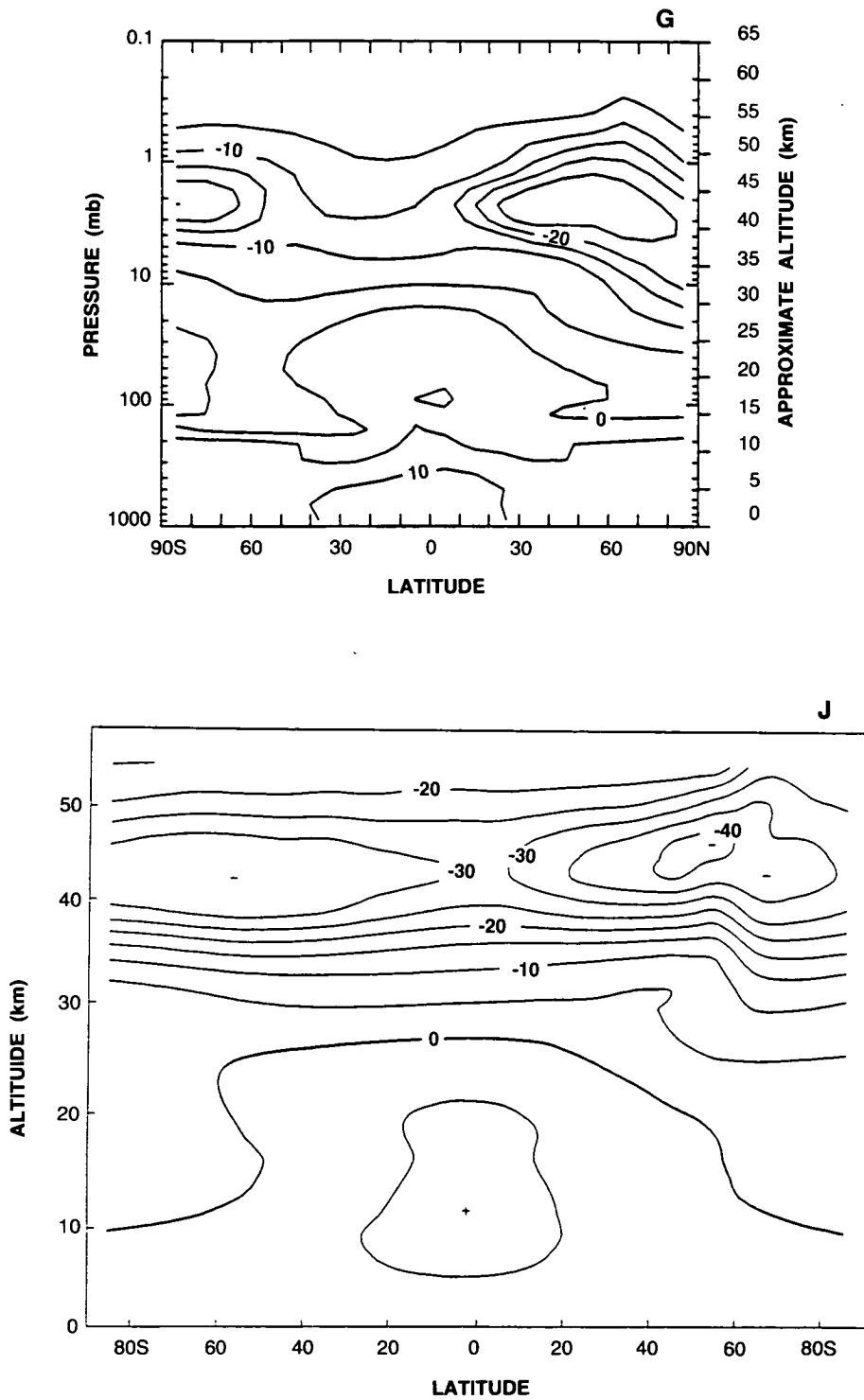


Figure 3.2-24. Latitude-by-altitude map of the percent change in local ozone concentration from 1980 to 2060 for scenario D1.

THEORETICAL PREDICTIONS

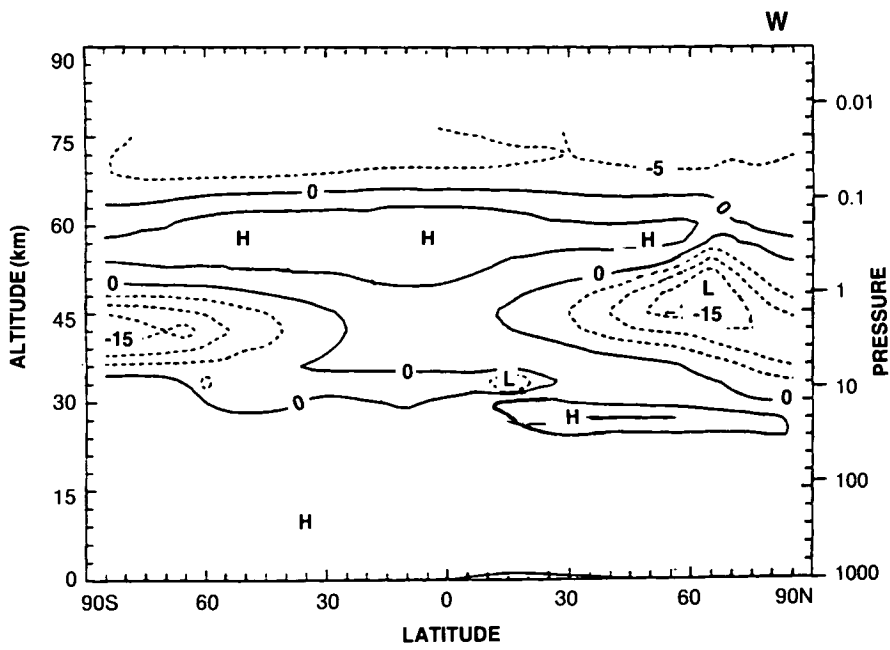
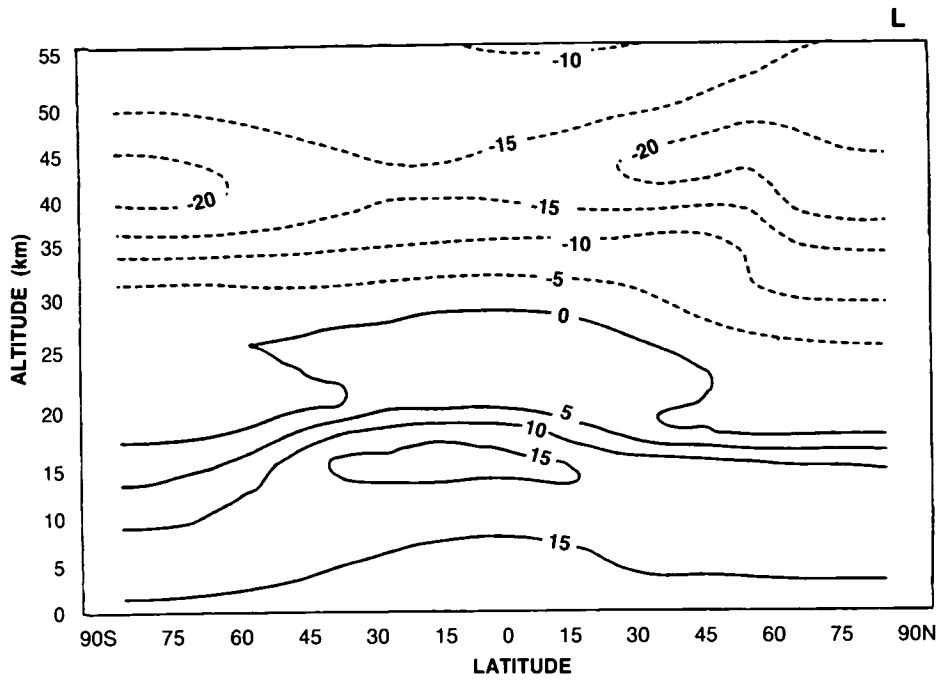


Figure 3.2-24., continued

THEORETICAL PREDICTIONS

Results from scenarios D2 and D3 are shown for the GSFC2 model in Figures 3.2-25 through 3.2-30. The successively lower chlorine loading reduces the ozone depletion and results in more rapid recovery. By 2060 in scenario D3, column ozone depletions are less than 2% everywhere except at high southern latitudes and the north polar spring. If, however, we were to extrapolate the predictions of the WisCAR model (using results from A1 and D1), large ozone increases would be expected.

Scenario D4, without methane increases, shows substantially greater ozone depletion in northern mid-latitudes by 2060: 3% versus 1% in D3 (see Figure 3.2-31G). Furthermore, the recovery of stratospheric ozone seen in D3 is less apparent in D4. The Dobson maps of column ozone change in Figures 3.2-32(G,O) are consistent in overall magnitude; but the GSFC2 model predicts much larger depletions in the Southern Hemisphere, and the Oslo model calculates equally asymmetric depletions in favor of the Northern Hemisphere. Both models predict modest depletions in local ozone concentrations (see Figures 3.2-33 [G,O]), with maximum losses of 10–15% in the high latitude upper stratosphere.

Within the assessment calculations presented here there is apparently larger uncertainty associated with predicting the impact of increasing CH₄ and CO₂ than there is in assessing the impact of additional chlorine and bromine. However, these models do not include the heterogeneous processes assumed to be responsible for the Antarctic ozone hole and possibly some current Arctic ozone loss. The uncertainties associated with predicting the halogen-catalyzed loss of ozone in the lower stratosphere are much greater than indicated by the results presented for scenarios A1 through D4 above. We next consider examples from models that now include some form of heterogeneous chemical processing.

In summary, when the CFC emissions are reduced by 95% (D1), the chlorine and bromine loadings in 2060 are 5.4 ppbv and 14 pptv, respectively. The reductions in column ozone at mid- to high latitudes are less than half of those calculated in the reference scenario: very little change in the tropics and 2–4% at mid-latitudes for models without temperature feedback. Ozone reductions at 40 km are 20–30%. In the one model that included the CO₂ effect, small increases in ozone column, 0–2%, are found at most latitudes. Further reductions in chlorine loading were considered by additionally freezing concentrations of methyl chloroform and carbon tetrachloride (D2), and the chlorine loading at 2060 was reduced to 4.2 ppbv. The reductions in column ozone were about 30% of those in the reference scenario. If the 95% cut in CFC emissions is not compensated for by increased emission of HCFC-22 (D3), the chlorine loading at 2060 is reduced further to 3.6 ppbv, but the calculated ozone columns are not significantly different: little change in the tropics and a decrease of up to 4% at high latitudes. This change in chlorine loading, from 4.2 to 3.6 ppbv, has little effect on column ozone because it is associated with changes in HCFC-22 abundance. In these current assessment models, HCFC-22 does not release a large fraction of its chlorine in the middle stratosphere where chlorine-catalyzed loss of ozone is most important. No heterogeneous chemistry was included in these models.

3.2.2.7 Special Contributions: Heterogeneous Chemistry

The effects of heterogeneous chemistry on ozone have been studied in specialized photochemical models (e.g., non-global, restricted dimensions), but have only recently been incorporated into the global stratospheric models necessary for this assessment. We report here on some preliminary results of this latter research, with the caveat that these models need to be studied, intercompared and further evaluated by the scientific community before we can rely on their predictions. We first present modeling studies of the perturbations to global ozone by heterogeneous reactions on polar stratospheric clouds (PSCs). We then consider the impact of similar heterogeneous mechanisms that may occur on the global sulfate aerosols in the lower stratosphere.

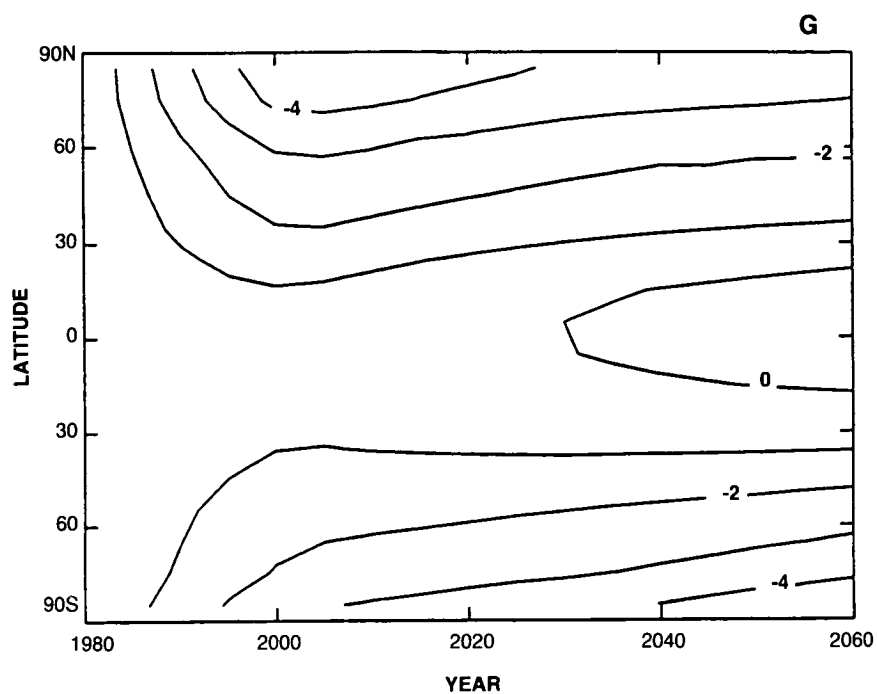


Figure 3.2-25. Time-line vs. latitude of the percent change in column ozone during March from 1980 to 2060 for scenario D2.

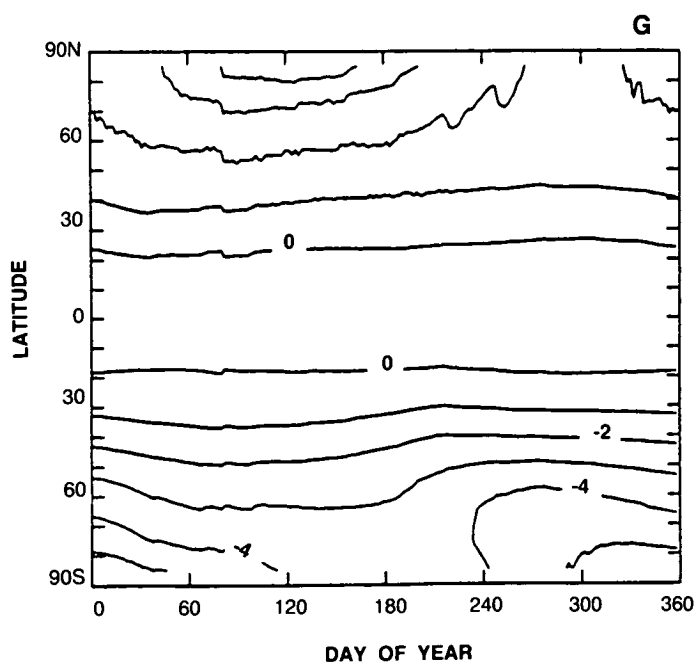


Figure 3.2-26 Dobson map of percent change in column ozone from 1980 to 2060 using scenario D2.

THEORETICAL PREDICTIONS

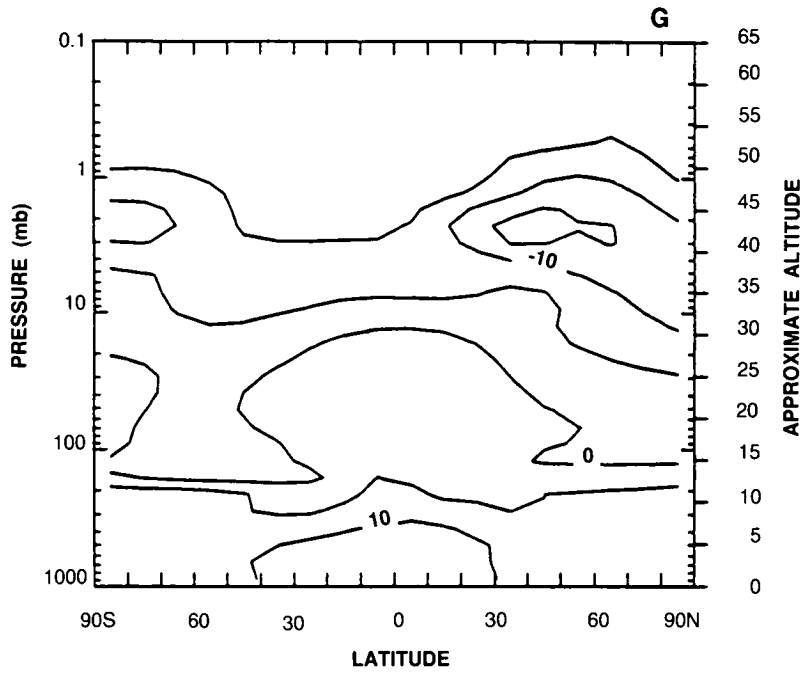


Figure 3.2-27. Latitude-by-altitude map of the percent change in local ozone concentration from 1980 to 2060 for scenario D2.

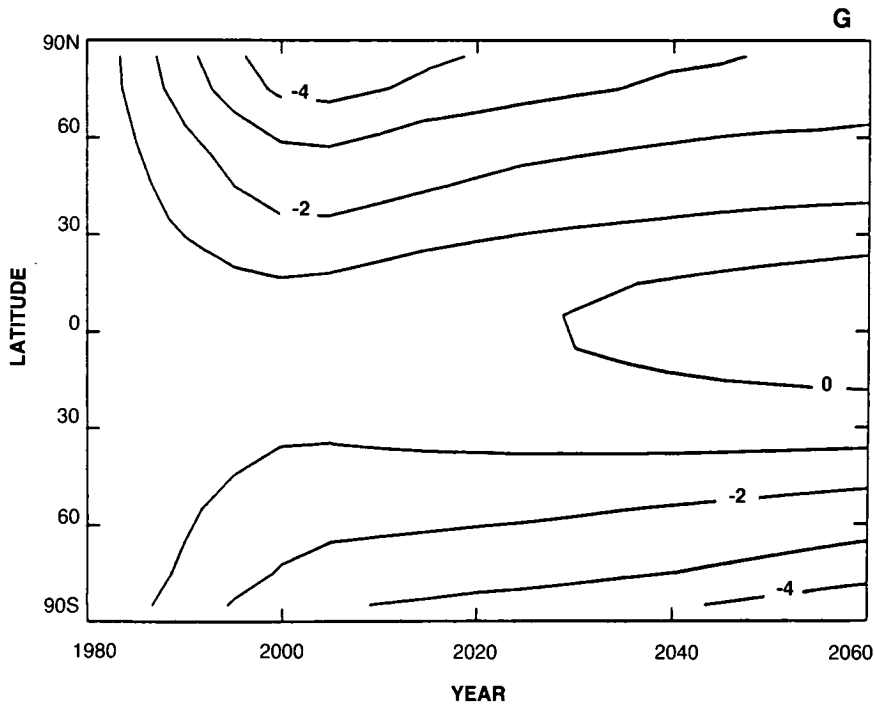


Figure 3.2-28. Time-line vs. latitude of the percent change in column ozone during March from 1980 to 2060 for scenario D3.

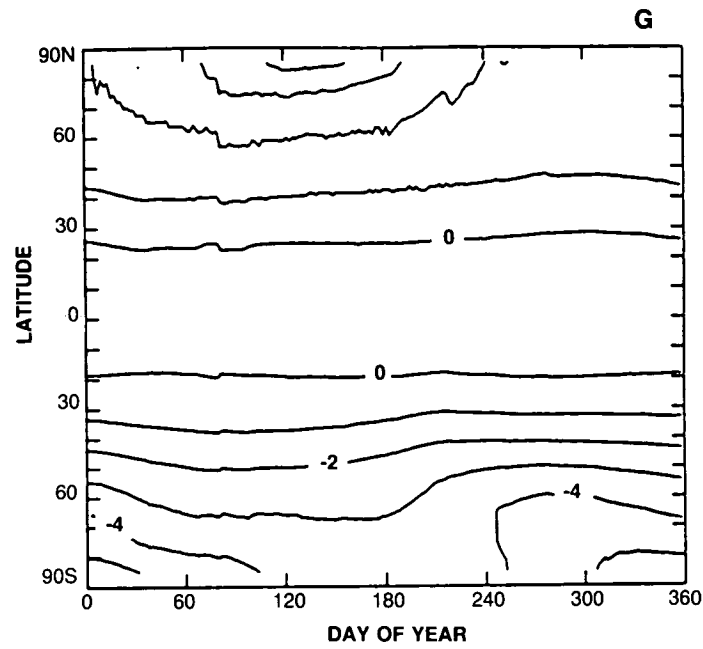


Figure 3.2-29. Dobson map of percent change in column ozone from 1980 to 2060 using scenario D3.

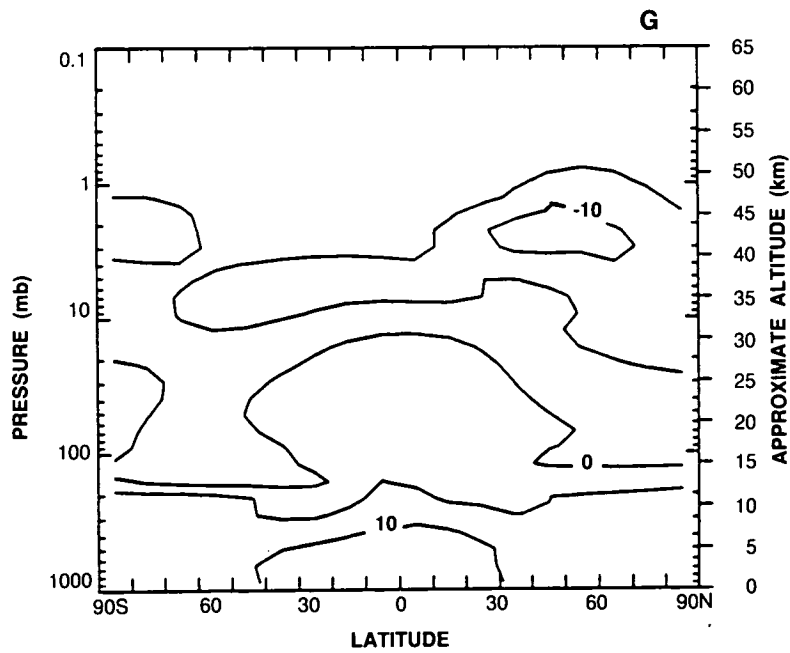


Figure 3.2-30. Latitude-by-altitude map of the percent change in local ozone concentration from 1980 to 2060 for scenario D3.

THEORETICAL PREDICTIONS

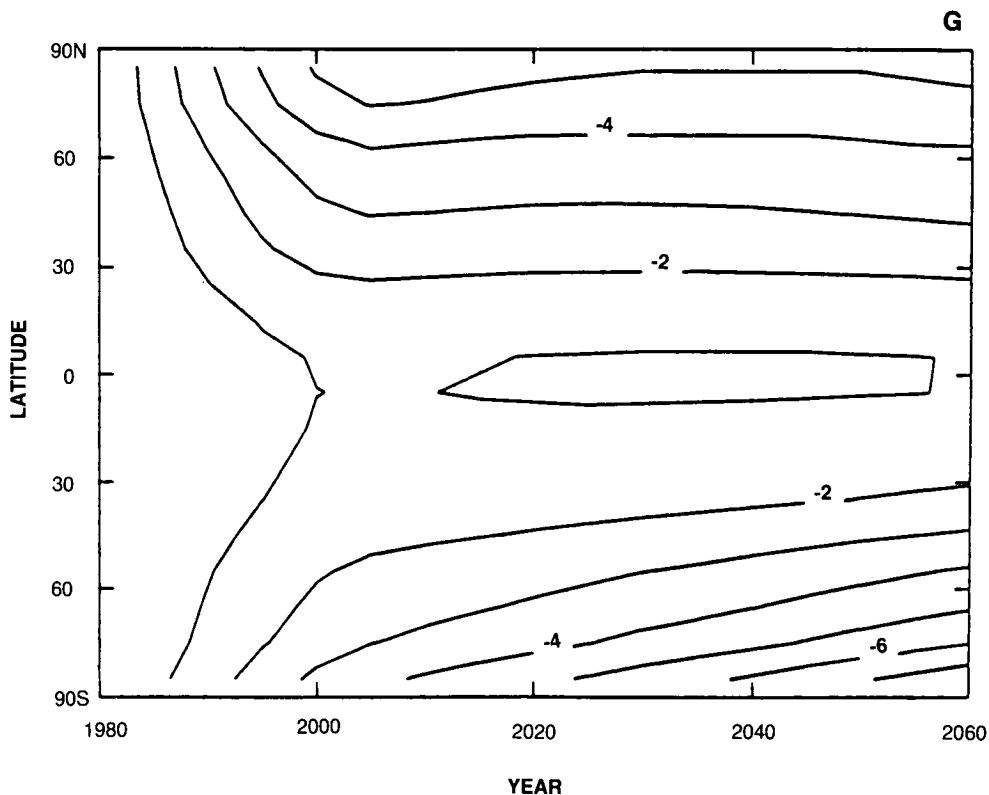
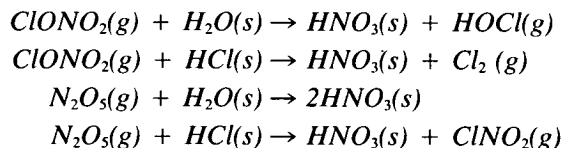


Figure 3.2-31. Time-line vs. latitude of the percent change in column ozone during March from 1980 to 2060 for scenario D4.

Reactions occurring on the surfaces of particles in the stratosphere are now believed to play an important role in the generation of the Antarctic ozone hole every year (See Chapter 1, Polar Ozone). These reactions are believed to take place on PSCs, which occur in at least two forms: nitric acid trihydrate and water ice. The heterogeneous reactions lead to major changes in the partitioning of chlorine species, resulting in enhanced concentrations of ClO; they also reduce concentrations of nitrogen oxides. These net effects, but not the reactions themselves, have been observed in both polar regions. Laboratory measurements of the following heterogeneous reactions have been obtained (Molina et al., 1987; Tolbert et al., 1987, 1988a, 1988b; Leu, 1988a, 1988b; Mozurkewich and Calvert, 1988) :



It should be noted that the treatment of heterogeneous chemistry in these models is highly uncertain due to both the parameterization of PSCs and the uncertainty in the reaction rates.

The Cambridge model studied the potential impact of PSCs on ozone in the Northern Hemisphere by prescribing their presence and properties poleward of 67°N in the lower stratosphere from mid-December

THEORETICAL PREDICTIONS

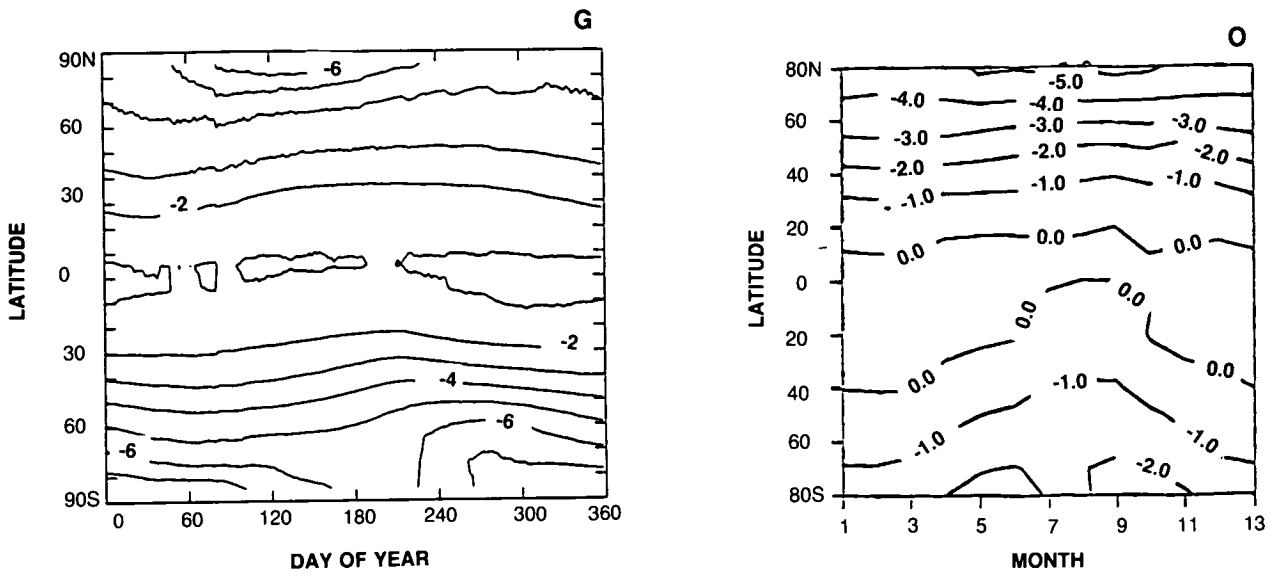


Figure 3.2-32. Dobson map of percent change in column ozone from 1980 to 2060 using scenario D4.

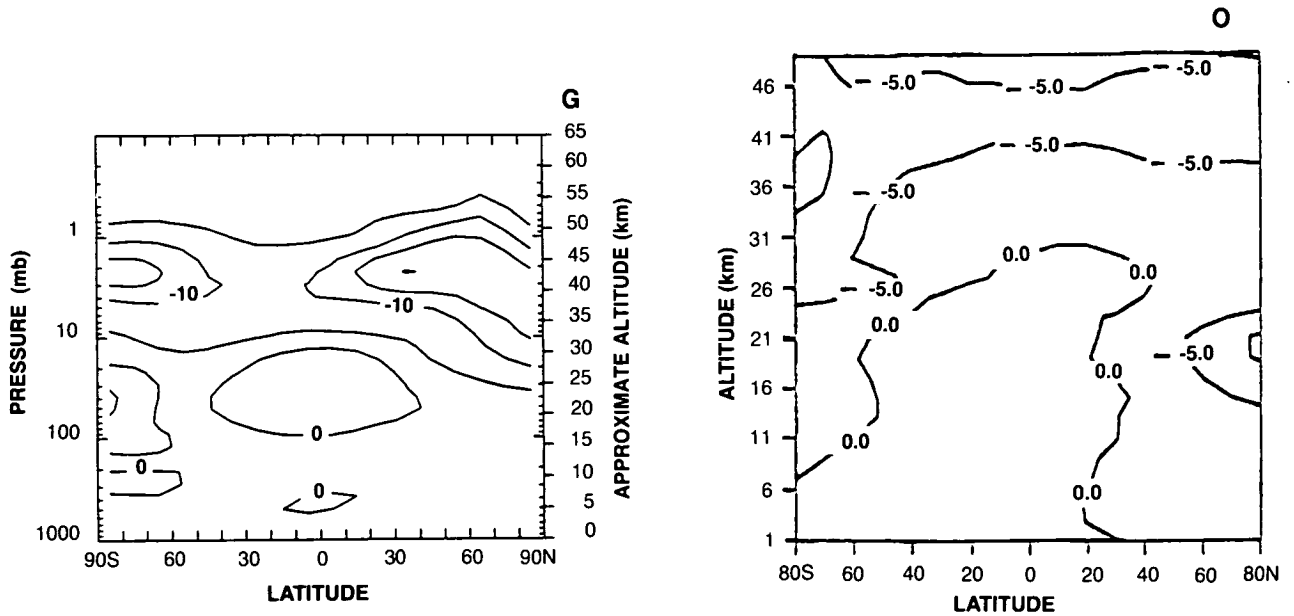


Figure 3.2-33. Latitude-by-altitude map of the percent change in local ozone concentration from 1980 to 2060 for scenario D4.

through mid-March. They used the reactions listed above and examined the ozone depletions at stratospheric chlorine levels (Cl_x) equal to 3 ppbv. Figure 3.2-34 shows the Dobson map of a 2-year sequence of the simulation with PSCs relative to that without. Including the PSCs leads to substantially larger ozone loss (an additional 5–9%) north of 60°N in the early spring. This parameterization should apply also to the Antarctic ozone hole but was not included in this calculation.

THEORETICAL PREDICTIONS

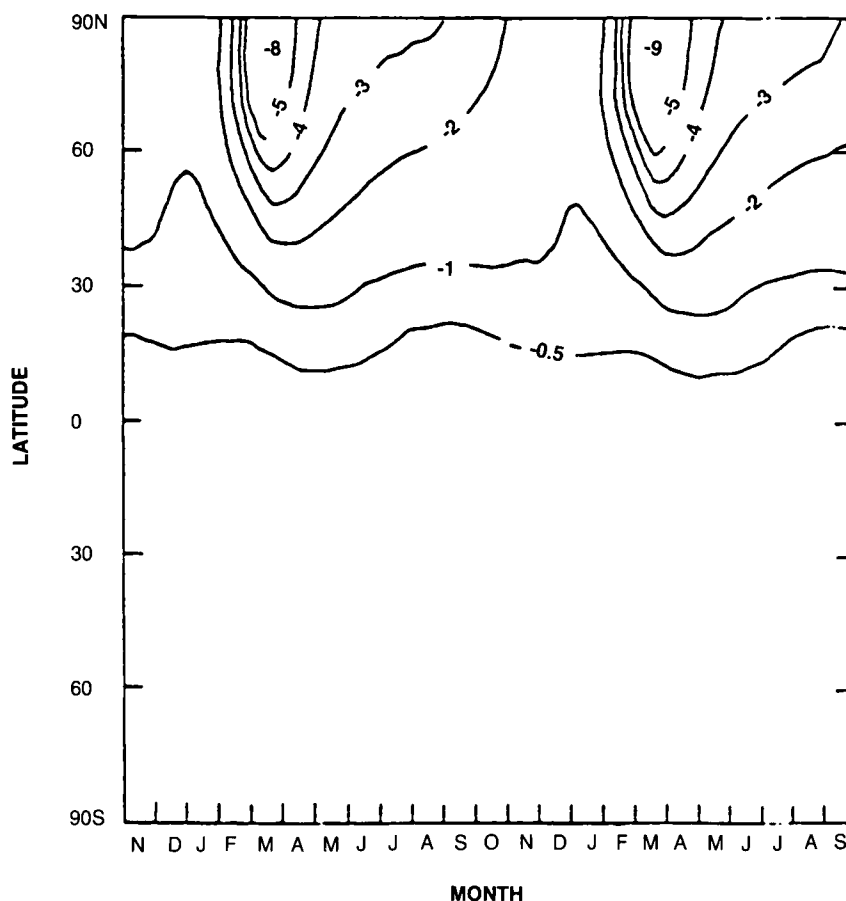


Figure 3.2-34. Two-year sequence of percent change in column ozone from the Cambridge model with PSC chemistry in the Northern Hemisphere. Results are relative to the standard model without PSC chemistry, and models use 3 ppb of free chlorine.

The WisCAR model examined the effects of heterogeneous chemistry by invoking PSC formation when the temperature fell below 195 K. PSCs were assumed to denitrify, dehydrate, and to react ClONO_2 with HCl. Results from calculations of scenario A1, both with and without this polar chemistry, are shown in Figure 3.2-35. The global ozone depletion with this polar chemistry is 6% greater than without; by 2060 depletions in the high latitude springtime exceed 16% in the north and 60% in the south.

The AER model examined the possible impacts of PSC chemistry using a parameterization (second-order rates) of the heterogeneous reactions of ClONO_2 and N_2O_5 with HCl. The calculation was hemispheric, focusing on the Arctic; and reactions are invoked north of 62°N in the wintertime, denitrified lower stratosphere. When compared with the standard AER model for the period 1960–1980 (compare Figure 3.2-36a with 3.2-3A), the ozone depletion doubles at high latitudes ($>45^\circ\text{N}$) for all seasons and increases in the tropics by at most 1%. For the period 1985 to 2060 using scenario B1 (Figure 3.2-36b), depletions of ozone column are substantially larger at high latitudes between February and May than of those from the standard (homogeneous chemistry) calculation for B1 (Figure 3.2-13A), and are generally 1% larger over the rest of the hemisphere.

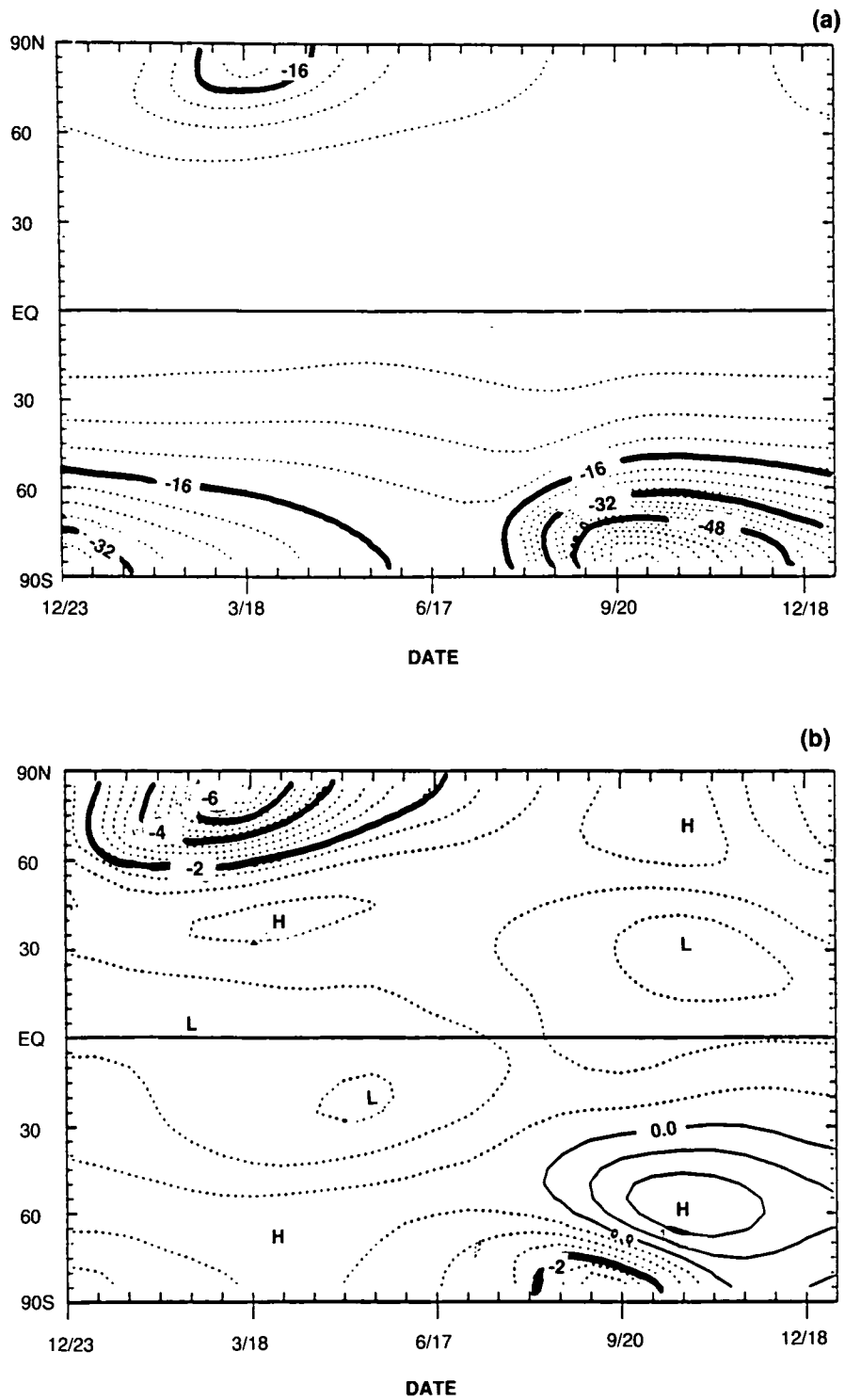


Figure 3.2-35. Dobson maps of percent change in column ozone between 1960 and 2060 from the WisCAR model with (a) and without (b) heterogeneous chemistry on PSCs for scenario A1.

THEORETICAL PREDICTIONS

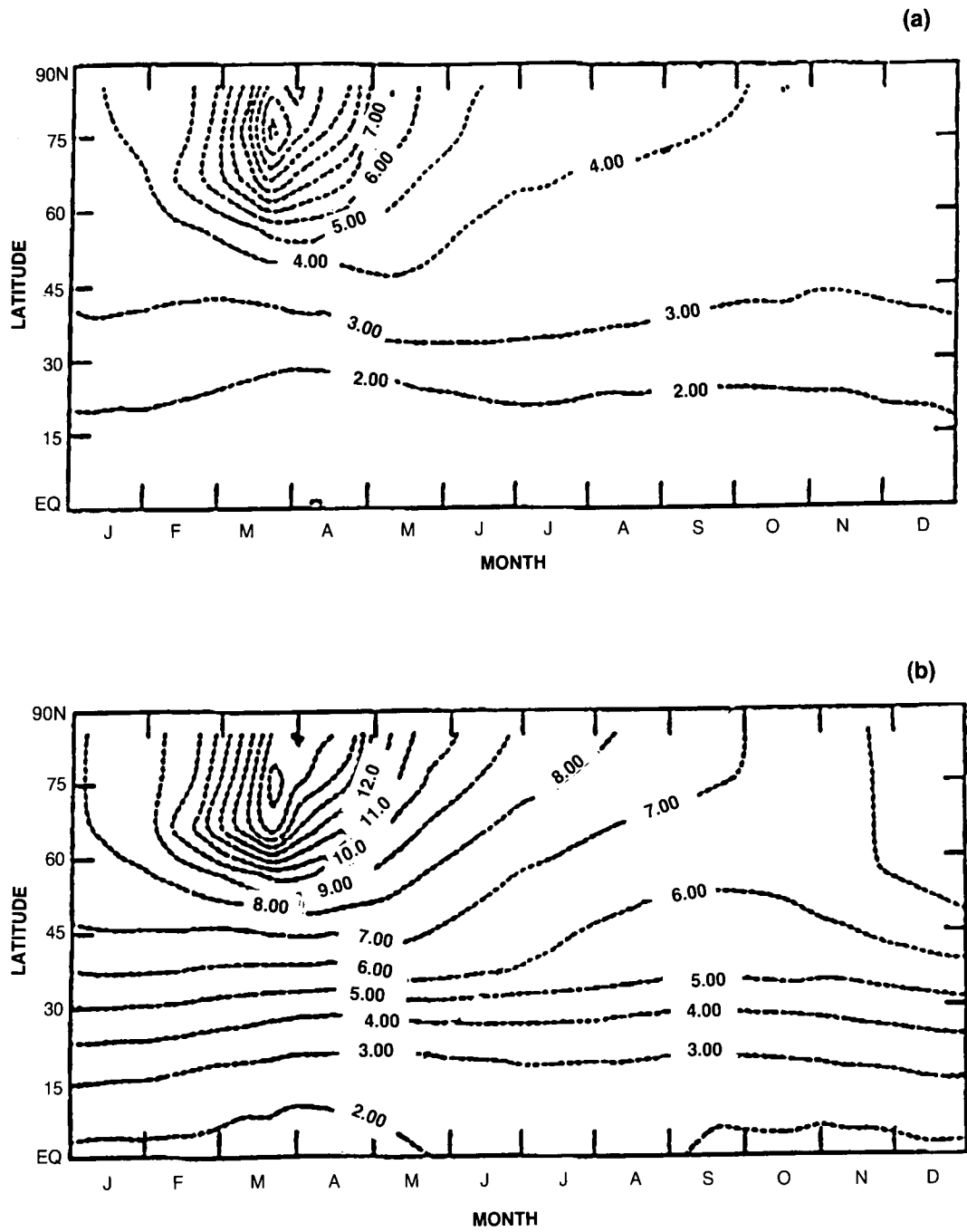


Figure 3.2-36. Dobson maps of percent change in column ozone from 1960 to 1985 (a) and from 1985 to 2060 (b) from the AER model using scenario B1. The model assumed PSC heterogeneous chemistry and denitrification at high northern latitudes in winter.

3.2.2.8 Junge-Layer Chemistry

Recent laboratory studies (Tolbert et al., 1988b) have indicated that reactions similar to those discussed above for PSCs may also occur on water-sulfuric acid solutions, typical of the measured composition of the Junge-layer aerosols. Some uncertainties in modeling the stratospheric chemistry of these reactions include: measurements have been made only for sticking coefficients, not net reaction efficiencies; the sticking coefficients are extremely sensitive to the H₂O content of the solution; in the stratosphere, the sulfuric-acid aerosols absorb water with decreasing temperature and may only be sufficiently reactive at temperatures less than 210 K. Some reactions noted above require sufficient amount of HCl to be dissolved in or adsorbed on the aerosols; however, no data are available on the solubility of HCl in H₂SO₄ /H₂O solutions for stratospheric conditions.

Earlier studies of the effects of Junge-layer chemistry (models by Rodriguez et al., 1988; observations by Brune et al., 1987) pointed out that heterogeneous reactions on the sulfate aerosols, particularly those involving HCl, could have a dramatic impact on the calculated ozone reductions for future years. However, model results showed significant enhancements of ClO below 20 km and thus provided an important observational constraint on the adopted heterogeneous rates. Hofmann and Solomon (1989) also included heterogeneous chemistry to study the impact of enhanced sulfate aerosol concentrations after the El Chichon eruption. Their results showed significant reductions in NO₂ and ozone, the latter being driven by enhanced chlorine chemistry. Because of the uncertainty in the heterogeneous reactions rates, it is clearly important that model simulations of Junge-layer chemistry must be validated by comparison with atmospheric observations, in particular the vertical and latitudinal profiles of ClO and NO₂ in the lower stratosphere.

The Oslo model investigated the impact of heterogeneous Junge-layer chemistry using the chemical model of the sulfate layer from Hofmann and Solomon (1989), except for the reaction of N₂O₅ and HCl. A scenario similar to A1 is calculated and the resultant Dobson maps of percent change in column ozone from 1985 to 2050 are shown for the model with and without the particulate chemistry in Figure 3.2-37. In this model the impact of heterogeneous chemistry enhances the ozone depletion, primarily towards high latitudes. Additional studies with the WisCAR model are similar to those described for the Oslo model and confirm the potential importance of heterogeneous chemistry on the Junge-layer particles, especially at high abundances of chlorine and bromine.

The AER model also examined the global impact of the heterogeneous reaction of HCl with ClONO₂ occurring on the natural sulfate layer. An equivalent second-order rate of $2 \times 10^{-16} \text{ cm}^{-3} \text{ s}^{-1}$ was adopted at 20 km (corresponding to a reaction efficiency of 3×10^{-3} between ClONO₂ and the aerosols), and scaled with the altitude distribution of aerosol surface concentration. The results from scenario B1 with this model are compared with those from the same AER homogeneous chemistry model (Figures 3.2.13A). Ozone depletion is dramatically enhanced by a factor of 3 on average at high latitudes in winter, and a factor of 2 in summer and throughout the tropics (Figure 3.2-38). For the current atmosphere, this model predicts ClO abundances that are higher by factors of 3–4 than the limited set of mid-latitude observations below 20 km; and it may thus overestimate the future ozone depletions. Interestingly, the ozone depletions calculated for the period 1960–1985 (not shown) are similar in magnitude and distribution to those for the PSC simulation from the AER model described above.

A mechanically forced three-dimensional model with heterogeneous chemistry prescribed similarly to the WisCAR model has been developed by Granier and Brasseur (NCAR) (unpublished data). This model is able to generate substantial chemical loss of ozone over Antarctica. Similarly, experiments with

THEORETICAL PREDICTIONS

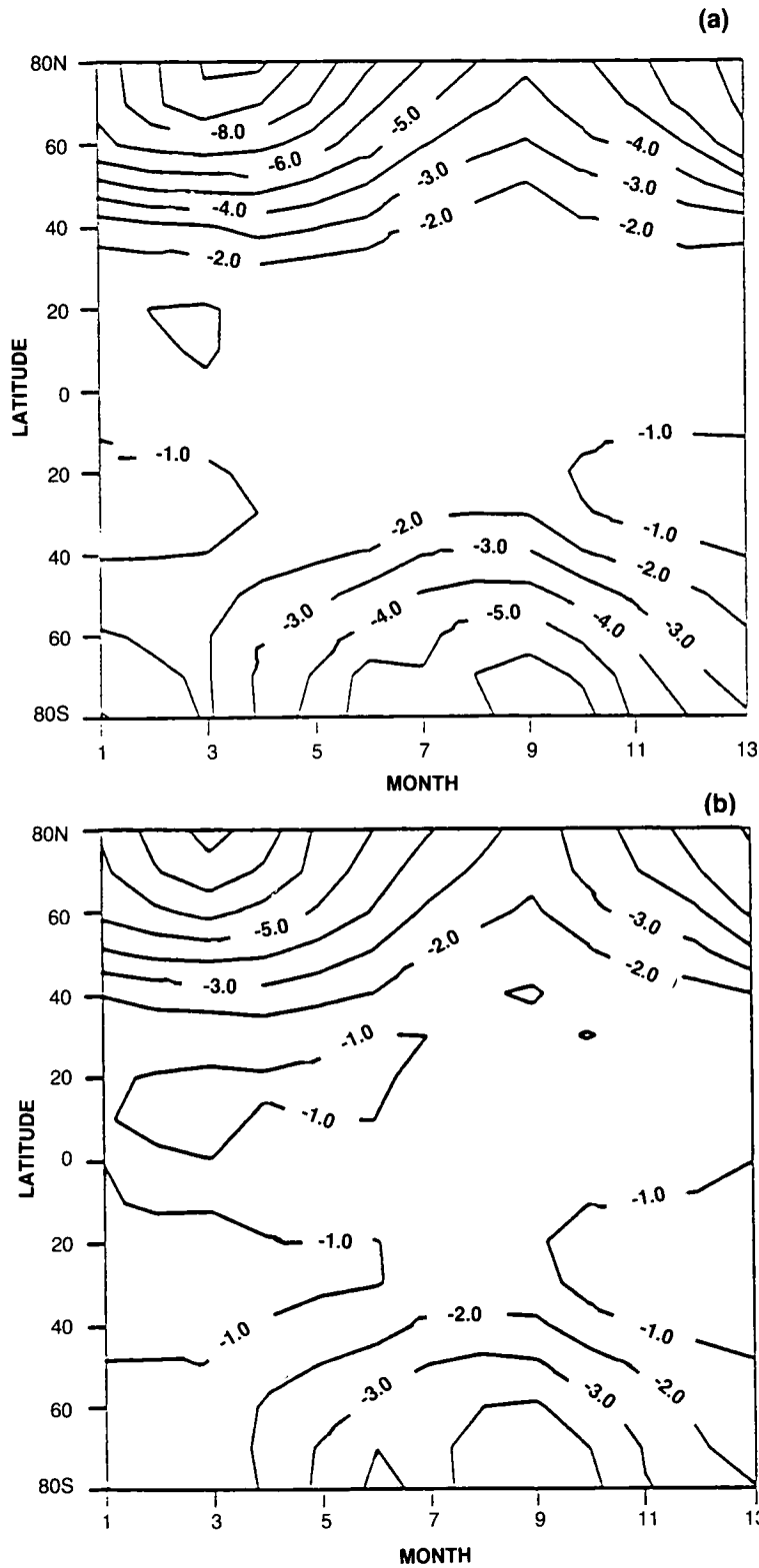


Figure 3.2-37. Dobson maps of percent change in column ozone between 1985 and 2050 from the Oslo model with (a) and without (b) heterogeneous chemistry on the natural sulfate layer. The scenario is similar to A1.

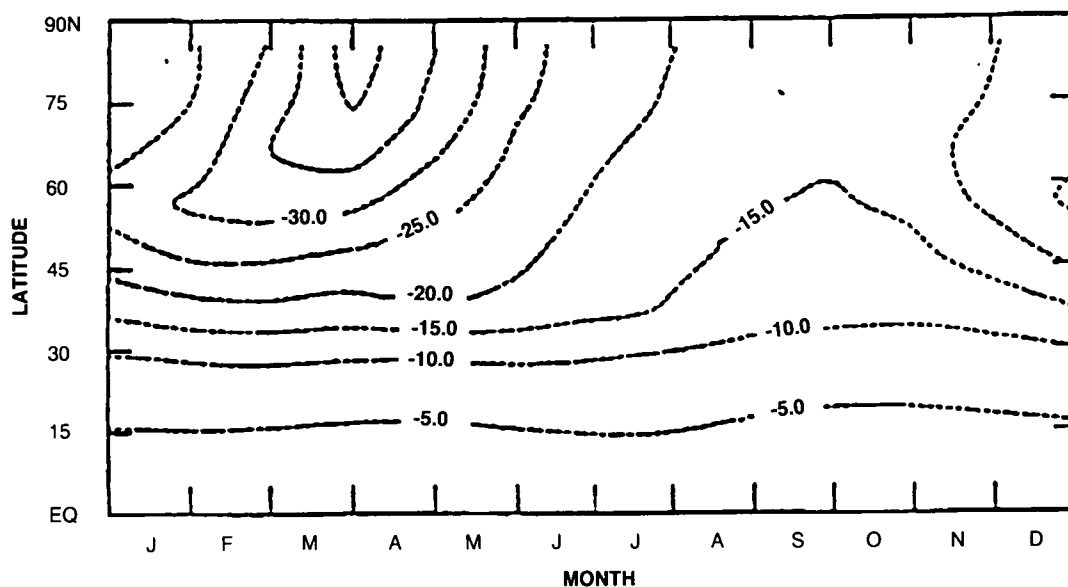


Figure 3.2-38. Dobson maps of percent change in column ozone from 1985 to 2060 from the AER model using scenario B1. The model assumed a Junge-layer heterogeneous chemistry.

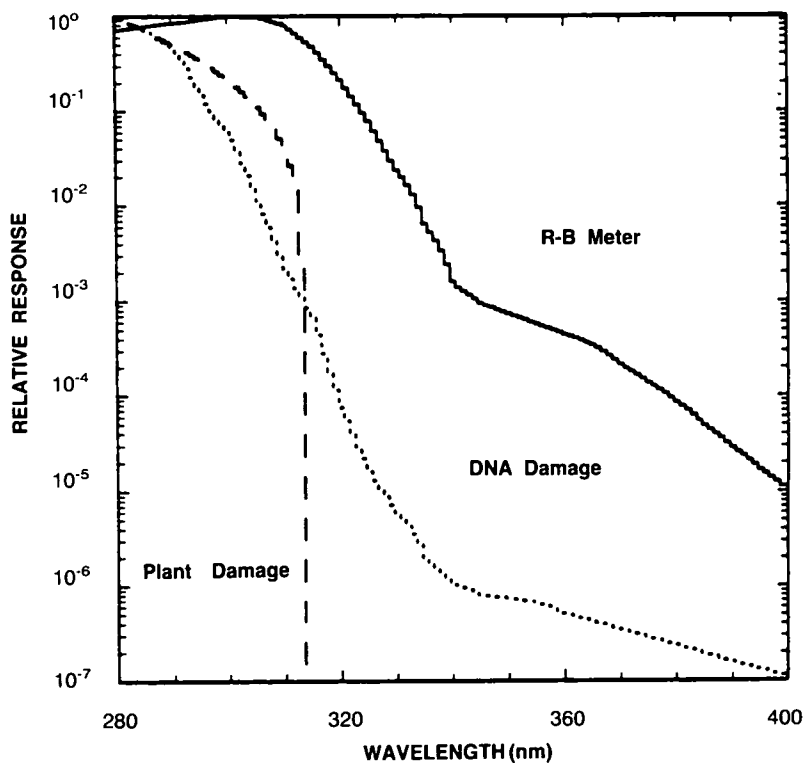


Figure 3.2-39. Action spectra used as weighting functions to calculate biologically effective radiation. All curves are normalized to unity. Values given are relative efficiencies per unit energy.

THEORETICAL PREDICTIONS

a 3-D model developed by Pitari, Verdecchia and Visconti (Aquila) (unpublished data) have been able to induce large ozone depletions over Antarctica using prescribed heterogeneous chemistry. All of these experiments, especially those with 3-D models, are in the early stages of research and must await further development and validation of the models.

3.2.2.9 One-dimensional Models

The application of one-dimensional stratospheric models in recent assessments has been to facilitate the study of many scenarios that would otherwise be too costly to perform with 2-D assessment models. This restriction no longer applies to all of the 2-D models (notably GSFC2 and Oslo), but the 1-D models might still be accurate in assessing changes in the upper stratosphere. Furthermore, they provide a useful forum by enlarging the modeling community that is involved in these assessments. The different approaches and uncertainties in modeling atmospheric photochemistry make it desirable to intercompare as many models as possible.

The perturbations to ozone and temperature at 40 km altitude, mid-latitudes, and during equinox (March or September) in the 2-D models should be comparable to the 40-km changes in the 1-D models (no latitudes or seasons resolved). We choose to compare these changes, 2060 relative to 1980, for some scenarios in Table 3.2-8. The comparison is not extensive, however, and the ozone depletions calculated with the 1-D models are broadly consistent with the 2-D results.

3.2.2.10 Conclusions

Results presented here are based on the standard 2-D stratospheric models that include only the effects of gas-phase chemistry. We have also included some examples of predictions from those same models in which the effects of enhanced chlorine-catalyzed loss of ozone, associated with heterogeneous chemistry on stratospheric aerosols, have been parameterized. Given the new and innovative nature of the modeling of heterogeneous chemistry and the large uncertainties associated with the kinetic data, we cannot yet rely quantitatively on these latter predictions. Nevertheless, in comparing these results it is clear that

Table 3.2-8. Stratopause changes from 1980 to 2060 (40 km or 3 mb, 40°N, March)

Model		Scenario									
		A1	A2	B1	C1	D1	A1	A2	B1	C1	D1
		Ozone Change (%)					Temperature Change (K)				
AER	(2-D)	-42		-31							
Camb	(2-D ^a)	-25					-13				
GSFC2	(2-D)	-43	-54	-32	-23	-20					
LLNL	(2-D)	-40				-20					
	(2-D ^a)	-30					-8				
Mainz	(2-D)	-56									
NSU	(2-D ^a)	-49				-13	-5				
Oslo	(2-D ^a)	-43	-45			-7					
WisCAR	(2-D ^a)	-36					-7				
IASB	(1-D)	-52	-58	-41	-31	-28	-13	-14	-12	-10	-1
MPI	(1-D)	-39	-45				-10	-10			

^aModels with CO₂ and T feedbacks.

predictions of ozone depletion associated with increasing halocarbons (chlorine and bromine) are less in models using gas-phase chemistry than similar predictions in which heterogeneous chemistry has been included in the models.

One clear conclusion from these assessments is that significant depletion of ozone is likely to continue if chlorine and bromine levels are allowed to double (scenarios A and B). Loss of ozone at 40 km is a robust prediction of the models; whereas, depletions of column ozone vary considerably and depend on changes in climate and other trace gases. For the range of scenarios considered here, ozone perturbations are nearly linear in response to additional chlorine. The present combination of models and scenarios does not allow us to separate the impacts of increasing bromine (i.e., halons) relative to the overall increases in chlorinated CFCs.

The increasing atmospheric abundances of CH₄ and CO₂ are a key factor in the predictions of future column ozone. Methane is involved in three major stratospheric cycles: water vapor budget, enhanced ozone production through smog chemistry, and partitioning of the chlorine family between ClO and HCl. Carbon dioxide enhances the radiative cooling of the stratosphere while heating the troposphere and thus possibly changing the overall circulation patterns. In the current scenarios, their individual and combined impacts lead to increased ozone, but there are large differences among the models as to the magnitude of these feedbacks. The effects are not obviously linear and become increasingly more important at low levels of chlorine. For example, the differences between scenarios D1 through D4 cannot be predicted robustly with the current set of assessment models. A major uncertainty with CH₄ and CO₂ is our estimate of future concentrations, since a substantial fraction of their emissions is natural and not under the control of human activities or regulation.

The incomplete treatment of tropospheric chemistry in the current 2-D stratospheric models adds additional uncertainty to the predicted trends in tropospheric ozone, both recent and long-term. This uncertainty affects not only the ozone columns but also tropospheric OH (see Chapter 4) and, hence, the lifetimes and abundances of HCFC-22 and CH₃CCl₃.

Two major questions that have not yet been answered by these predictions for global ozone in the future are: (1) What is the future of the Antarctic ozone hole, will it get deeper or more spatially extensive? and (2) What are the global impacts of polar chemistry, will there be a corresponding Arctic ozone hole? A third major uncertainty in modeling the future atmosphere involves predicting the impact of real climate change to the entire atmosphere, not just the CO₂ cooling in the stratosphere. These difficult questions have been recognized in the most recent assessments (e.g., Watson et al., 1988; SORG, 1988) and unfortunately are not yet answered. Through continued research and model intercomparison, especially testing against the observed changes over the past several decades, we expect to develop atmospheric models that will be able to provide some answers to these questions for the next assessment.

3.2.3 Predicted Changes in Surface UV Radiation

This section discusses the changes in biologically damaging ultraviolet (UV-B) radiation at the Earth's surface that are expected to result from changes in atmospheric ozone concentrations. The calculation is complicated by the fact that the amount of UV radiation reaching the surface is not related to the amount of ozone by a simple inverse proportion. For example, a 1% reduction in the ozone column may not necessarily yield a 1% increase in biologically damaging radiation. Depending on the particular biological system and environment under consideration, the damage may be much larger or much smaller. This complex behavior is a result of several factors, including the strong wavelength dependence of the absorp-

THEORETICAL PREDICTIONS

tion of light by ozone and of the biological response functions, the contribution of diffuse (sky) radiation, and the effect of environmental factors such as the sun angle, the amount of cloud cover and haze, the reflectivity of the ground, and the elevation of the ground above sea level. Detailed models of the propagation of radiation through the atmosphere have been developed previously (Chandrasekhar, 1960; Stamnes, 1986; and references therein), and have been applied with varying degrees of approximation to the problem of estimating biological dose rates related to ozone depletion (Cutchis, 1974; Pyle and Derwent, 1980; Gerstl et al., 1981; Stordal et al., 1982; Frederick and Lubin, 1988a, b; Brühl and Crutzen, 1989). The model used here (and described below) combines a reasonably accurate radiative transfer method with high spectral resolution and good computational efficiency.

3.2.3.1 Model for the Propagation of UV Radiation Through the Atmosphere

The model used in the present work was developed at NCAR for the purpose of photochemical calculations (Madronich, 1987) and was modified somewhat for the calculation of biologically damaging radiation. It includes absorption of light by atmospheric ozone and aerosol particles, and multiple scattering by air molecules (Rayleigh scattering) and by aerosol particles and cloud droplets (Mie scattering). The radiative transfer scheme is based on the delta-Eddington approximation of Shettle and Weinman (1970) and Joseph et al. (1976). The accuracy of this scheme has been discussed by Meadow and Weaver (1980) and King and Harshvardhan (1986), and is sufficient for the present purposes.

The model covers the biologically significant UV wavelength range 280–400 nm. The wavelength grid used in the present calculations is that given by WMO (1986), except that each WMO wavelength interval has been subdivided into five subintervals of equal width to represent more accurately the steep wavelength variation of ozone absorption and biological response spectra. High resolution extraterrestrial irradiance data are from Mentall et al. (1981) (over 280–330 nm) and from Neckel and Labs (1984) (over 330–400 nm). To conform with current recommendations, the irradiance values are scaled to the WMO (1986) values by comparing the integral over each set of five subintervals with the corresponding WMO interval value. Ozone absorption cross sections are from Molina and Molina (1986). These cross sections are somewhat temperature dependent in the UV-B region, so they are re-evaluated for each atmospheric layer of the model using the local temperature. Rayleigh-scattering cross sections are evaluated at the center of each wavelength interval using the expression given by Fröhlich and Shaw (1980). The solar zenith angle and the total ozone column (in Dobson units) must be specified.

To estimate the biological effects of the UV radiation, it is necessary to consider how effective photons of different wavelengths are in inducing biological damage. This is expressed by the action (or response) spectrum. The present calculations consider three different action spectra: a generalized DNA damage spectrum (Setlow, 1974), a generalized plant damage spectrum (Caldwell et al., 1986), and the response spectrum of a UV meter that was designed to approximate the erythema (sunburn) response of Caucasian skin (Robertson-Berger or R-B meter; Robertson, 1975). The R-B meter response is actually somewhat different than the erythema spectrum, but is of interest because of the wide utilization of this instrument in monitoring surface UV radiation (see for example Scotto et al., 1988). Figure 3.2-39 shows the action spectra used in the present work. Note that the spectra were arbitrarily normalized to unity at their maximum, since their absolute magnitudes are not meaningful—only the relative changes with wavelength are of interest here. The biologically effective dose rate is defined as the convolution of the spectral irradiance, $E(\lambda)$, and the action spectrum, $A(\lambda)$,

$$R = \int E(\lambda) A(\lambda) d\lambda = \text{dose rate, Joules } m^{-2} s^{-1}$$

and may be integrated over time to obtain the biologically effective dose, e.g., on a daily, monthly, or annual basis.

A “base” model of the atmosphere was used to perform most of the calculations given below. The base model applies to clear sky (no clouds or aerosols), ground at 0 km above sea level with an albedo of 5%, and a flat horizontal receiver. The altitude profiles of temperature, ozone, and air density are taken from the standard profiles of Nicolet et al. (1982). A detailed comparison of the base model predictions was carried out against the model recently developed by Frederick and Lubin (1988a). Table 3.2.9 shows the results for the R-B meter dose rate, for noon on two different days of the year and a range of latitudes. The two models disagree by no more than 8% over a factor of 40 variation in the irradiance. This 40-fold variation is much larger than the UV changes expected from changes in atmospheric ozone concentrations, so that the models may be considered to be in excellent agreement for the purpose of the present calculations.

3.2.3.2 Surface UV Changes for Different Ozone Change Scenarios

Daily dose rates computed with the NCAR base model are shown in the upper panel of Figure 3.2-40 for the ozone distribution of 1979/1980 (2-year average of TOMS data, R. Stolarski, private communication). The absolute dose values (given in $\text{J m}^{-2} \text{day}^{-1}$) for the DNA damage, plant damage, and the R-B meter cannot be compared directly since the action spectra are relative. However, trends with latitude, time of the year, and local ozone columns are meaningful. The lower panels of Figure 3.2-40 show the radiation

Table 3.2-9. Surface UV irradiance:^a Comparison of model predictions

Latitude	Dobson	Zenith Angle	UC ^b	NCAR ^c
<i>January 16</i>				
60	368.5	81.01	0.0166	0.0179
40	335.6	61.01	0.1798	0.1870
20	247.1	41.01	0.5901	0.5980
0	244.2	21.01	0.9134	0.9160
-20	262.2	1.01	1.0000 ^d	1.0000 ^d
-40	291.2	18.99	0.8377	0.8414
-60	324.8	38.99	0.5180	0.5254
-80	304.2	58.99	0.2238	0.2318
<i>July 16</i>				
80	319.4	58.73	0.2185	0.2265
60	338.8	38.73	0.5115	0.5132
40	307.9	18.73	0.8098	0.8137
20	281.8	1.27	0.9567	0.9566
0	258.1	21.27	0.8794	0.8826
-20	262.1	41.27	0.5622	0.5703
-40	319.1	61.27	0.1844	0.1918
-60	309.0	81.27	0.0191	0.0205

^aWeighted for Robertson-Berger meter response.

^bUniversity of Chicago model (Frederick and Lubin, 1988).

^cNational Center for Atmospheric Research model (Madronich, 1987)—used in this study.

^dNormalization point.

THEORETICAL PREDICTIONS

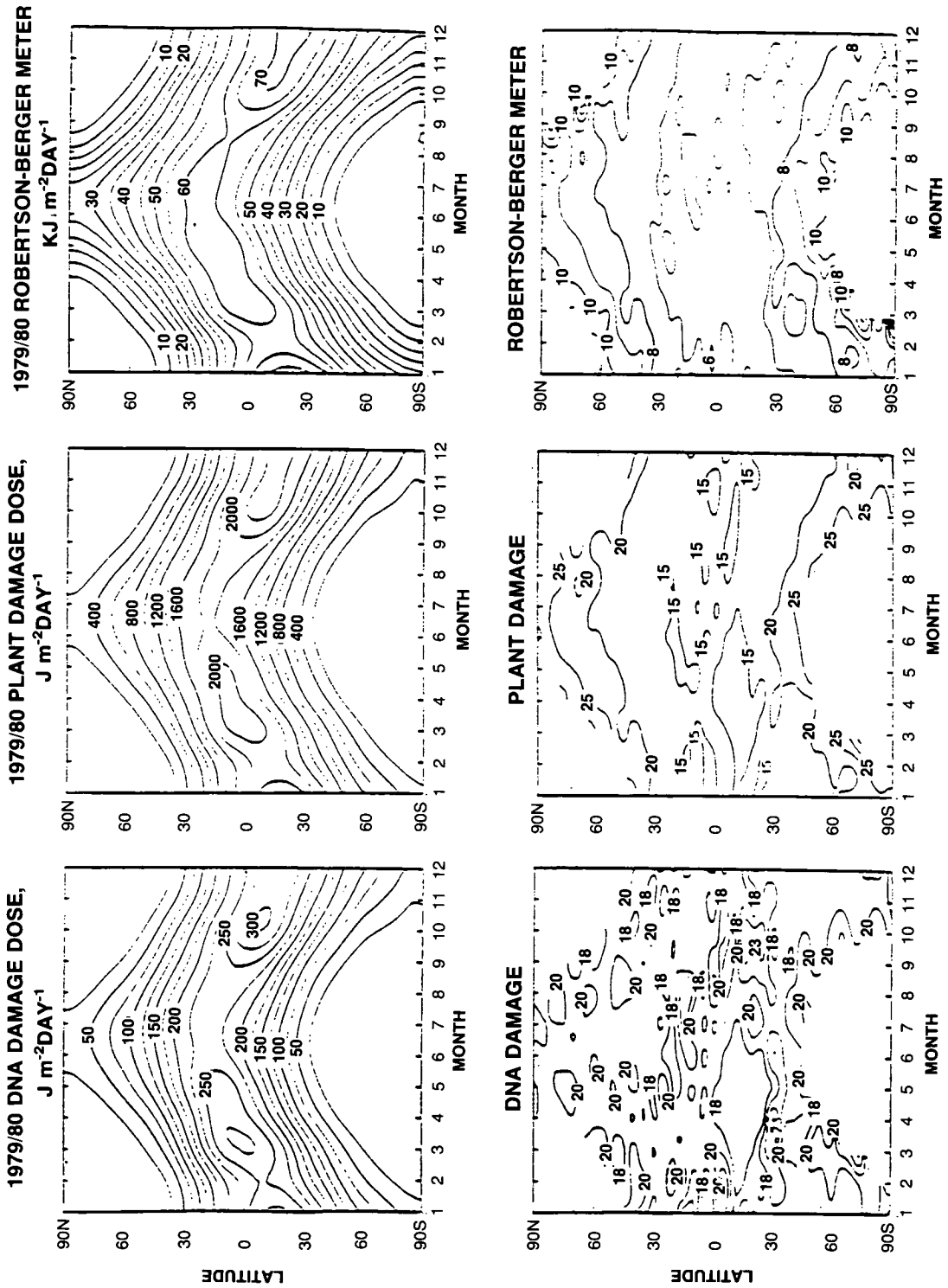


Figure 3.2-40. Daily doses for 1979/80 based on ozone column from TOMS measurements normalized to Dobson. Upper panels show absolute doses for DNA damage, plant damage, and R-B-meter response. Lower panels show radiation amplification factors (RAF) defined as the percent increase in daily dose for a 1% decrease of the local ozone column. RAF values were multiplied by 10.

amplification factors (RAF), defined as the percentage change in dose for a 1% change in the ozone column. These values show the sensitivity of different latitudes and months to changes in the ozone column, and serve to illustrate the non-linear response of UV dose. However, it is important to note that these values are meaningful only for small changes (1%) in the ozone column, since, as was shown by Stordal et al. (1982), RAF values associated with larger changes in ozone may be significantly different.

Changes in surface UV dose may have occurred in the past, as a result of changes in the ozone column abundance. Figure 3.2-41 shows the dose increases computed from measured changes in ozone column over the 8-year period 1979/80–1987/88. The ozone column data used in these plots were estimated from TOMS data normalized with Dobson measurements (R. Stolarski, personal communication). In the Southern Hemisphere, dose increases of 10–50% or more are seen during October and November poleward of 60°S, with smaller increases (2–10%) between 30°S and 60°S. In the Northern Hemisphere, biological dose increases range from 2% to 5%. These changes, attained over an 8-year period, should be compared to the changes predicted over a much longer period by the 2-D models.

Figures 3.2-42–44 show the changes in biologically effective radiation corresponding to the ozone columns calculated with the Goddard Space Flight Center Model2 (GSFC2). Figure 3.2-42 gives the changes in daily doses from 1960 to 1980. For DNA and plant damage, dose increases are calculated to be less than 4% for all locations and times except near the terminator where the absolute amounts of radiation are small. The percent changes for the R-B meter are consistently smaller (about half) than those for plant and DNA damage.

Results for scenario A1 (see Section 3.2.1), which assumes that emissions of the Montreal products will remain constant at 1986 levels, are shown in Figure 3.2-42 (ozone columns calculated with the GSFC2 model). The largest increases in daily doses are predicted to occur in the springtime at mid-latitudes. However, expressed as percent, the largest changes are predicted to occur at high latitudes, with increases in DNA and plant damage near 20–40%. Although these relatively large changes would occur in DNA and plant damage, R-B meters would indicate lesser changes.

Scenario D1 differs from the A1 scenario by assuming that the emissions of Montreal products are reduced by 95%, with the reductions becoming effective over the years 1996–2000. The effects on daily biological doses are shown in Figure 3.2-43 (ozone columns calculated with the GSFC2 model). Compared with the A1 scenario, scenario D1 leads to about half the increases in the doses. The geographical and seasonal distributions of these changes are similar to those predicted for the A1 scenario.

The predicted changes in biologically effective UV are sensitive to the assumptions and parameterizations used in different models and more specifically to the calculated changes in the ozone column by these models. For example, for scenario A1, the WisCAR (University of Wisconsin and NCAR) model predicts only about half of the dose increase predicted by the GSFC2 model.

3.2.3.3 Uncertainties in the Prediction of Surface UV Radiation Changes

The theoretical prediction of surface UV radiation is complicated enormously by the natural variability of the optical characteristics of the atmosphere. For example, it is literally impossible to model all of the natural geometric configurations of partly cloudy skies. Fortunately, and this is an important point, we are mostly interested in the relative changes in surface UV which would result from systematic changes in the concentrations of atmospheric ozone. This assumes implicitly that other environmental factors, such as cloud cover and surface albedo, will on the average remain constant over the period 1960–2060.

THEORETICAL PREDICTIONS

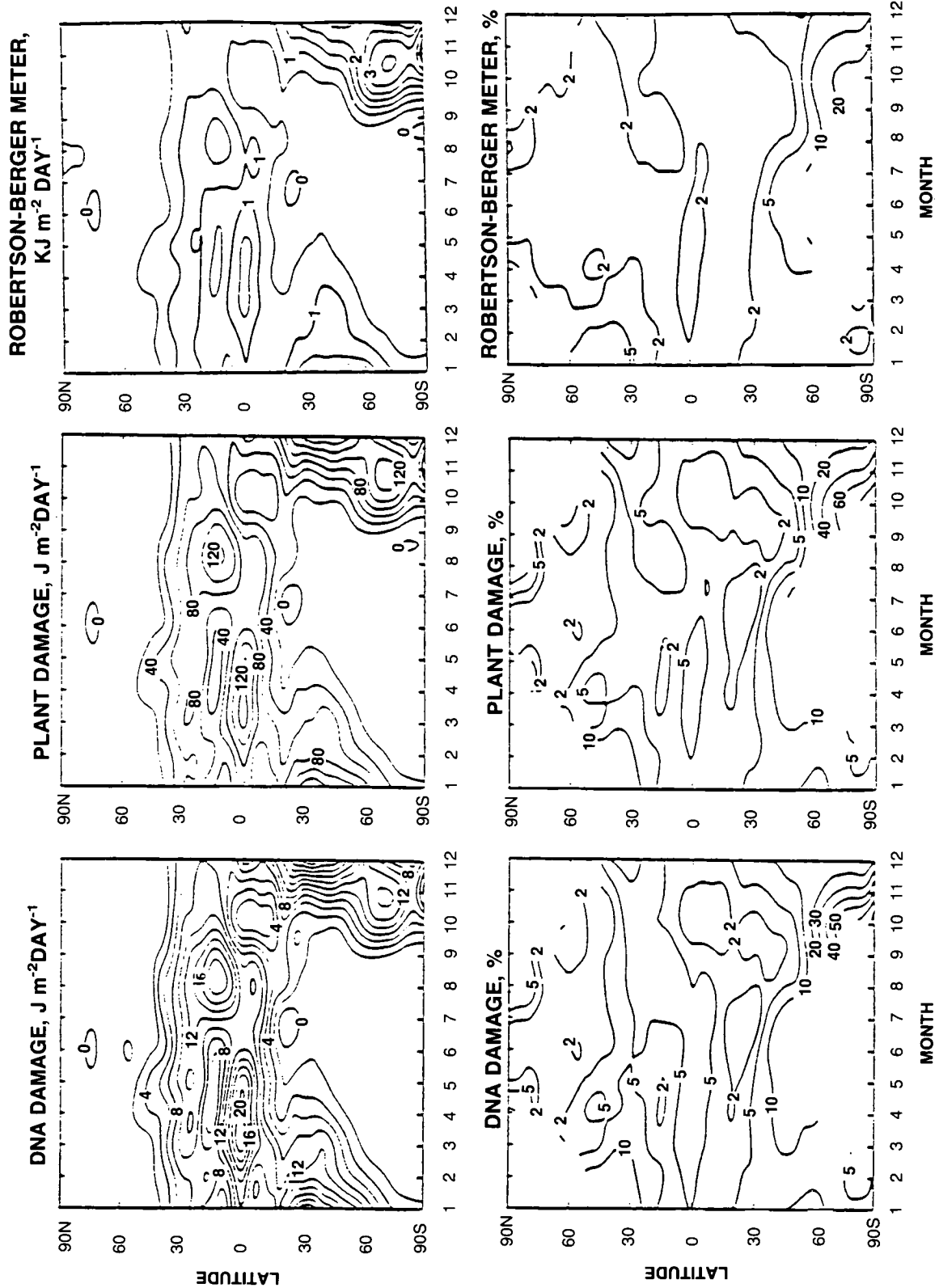


Figure 3.2-41. Daily dose changes from 1960 to 1980, GSFC2 model. Upper panels give absolute dose changes, lower panels give percent changes.

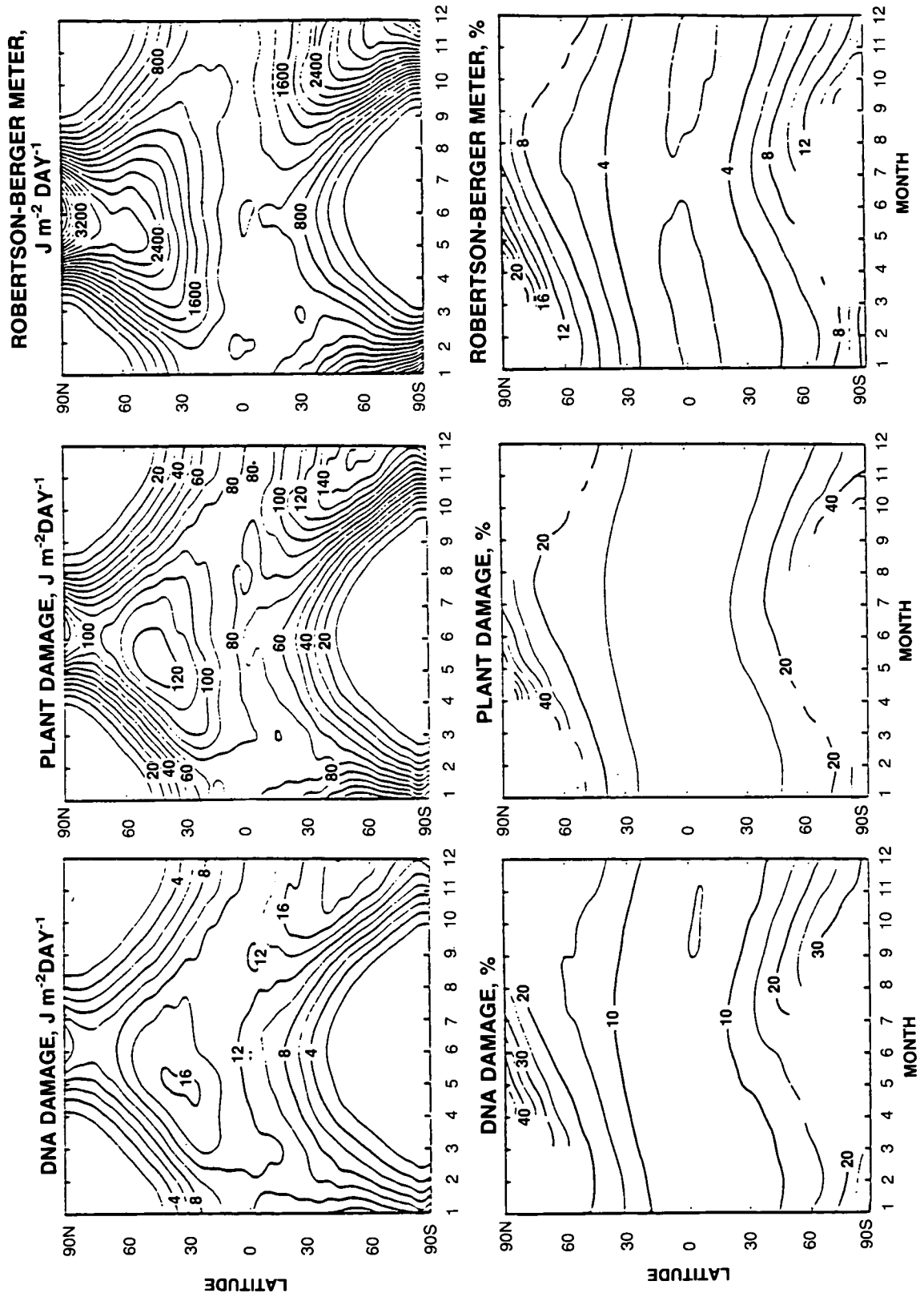


Figure 3.2-42. Daily dose changes from 1960 to 2060, GSFC2 model, scenario A1. Upper panels give absolute dose changes, lower panels give percent changes.

THEORETICAL PREDICTIONS

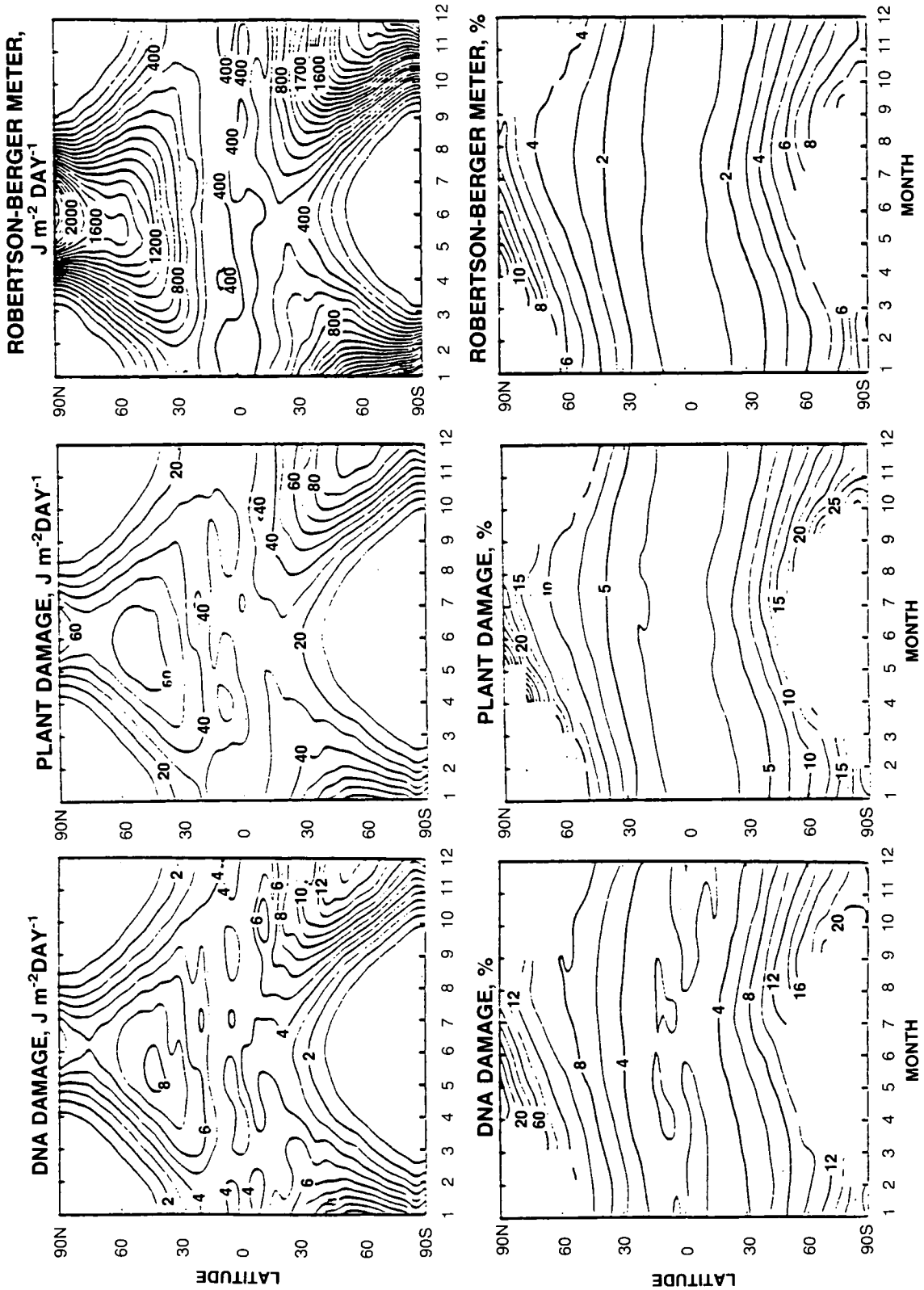


Figure 3.2-43. Daily dose changes from 1960 to 2060, GSFC2 model, scenario D1. Upper panels give absolute dose changes, lower panels give percent changes.

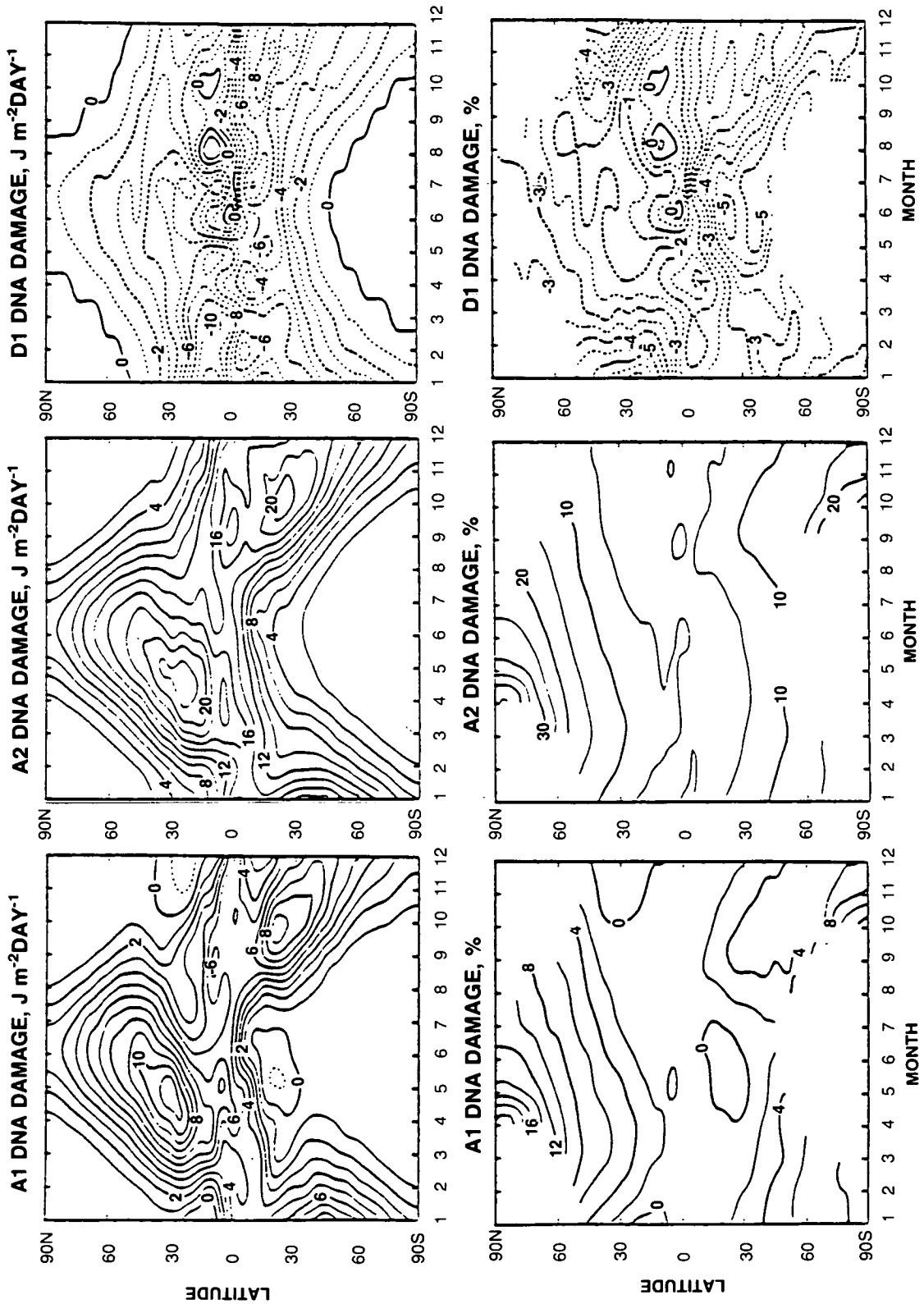


Figure 3.2-44. Daily DNA damage dose changes from 1980 to 2060, WisCAR model scenarios A1, A2, and D1. Upper panels give absolute dose changes, lower panels give percent changes.

THEORETICAL PREDICTIONS

If the assumption of constant environmental factors is valid, the calculation of relative changes in doses is insensitive to the choice of specific environmental factors. This is illustrated in Table 3.2.10, which compares the radiation amplification factor for the DNA damage dose rate calculated with the "base" model to that calculated under different environmental conditions. Clouds, surface albedo, surface elevation, and aerosol haze affect the absolute value of the DNA dose rate, but have a relatively small effect on the RAF and therefore on the sensitivity of the dose rate to future ozone changes. Similarly, the shape and orientation of the receiving surface relative to the incident light is not important in determining the relative dose rate change.

Large errors in the surface UV predictions will result if cloud cover patterns change systematically in the future due to changes in weather patterns associated with the so-called greenhouse effect. Relatively small changes in the average cloud cover may produce large changes in the average surface UV radiation (Frederick and Lubin, 1988b). Changes in the average ground albedo may also be important. At present, these changes are not very predictable.

Another significant uncertainty is the future of tropospheric ozone, which is expected to increase due to human activities. This effectively was included in some of the modeling scenarios discussed in the previous sections. To the extent that the tropospheric ozone contributes to the total ozone column, it was included in the calculations of the surface UV radiation, and tends to cancel the UV enhancements which result from the depletion of the stratospheric ozone. However, this effective shift of ozone from the stratosphere to the troposphere may induce some errors in the calculation of the surface UV. This is because in the stratosphere most of the UV radiation is present in the direct solar beam, while in the troposphere a greater fraction is diffused by Rayleigh and Mie scattering. The effective photon pathlengths through absorbing ozone layers are therefore different for the stratosphere than the troposphere (Brühl and Crutzen, 1989). While this effect is not expected to be large, it contributes to the uncertainty in the prediction of surface UV. More work is needed in the quantification of this effect and especially in reducing the large uncertainties in the prediction of future tropospheric ozone trends.

3.2.4 The Effects of Ozone Changes on Circulation

The dominant processes forcing the circulation of the middle atmosphere are radiative heating by ozone absorption of insolation, radiative cooling by CO₂ longwave emission, and momentum deposition by the dissipation of vertically propagating disturbances (waves) generated in the troposphere. Photochemically driven perturbations in ozone will change the radiative heating of the stratosphere and, consequently,

Table 3.2-10. Environmental effects on DNA radiation amplification factor (RAF)

Model	Solar Zenith Angle			
	0°	60°	75°	85°
Base model ^a	1.88	1.97	2.00	1.99
Surface albedo = 0.50	1.90	1.98	2.02	2.00
Aerosols (Elterman, 1968)	1.89	1.99	2.02	2.01
Cloud, thin	1.90	2.00	2.03	2.01
Cloud, thick	1.93	2.02	2.05	2.03
Hemispherical receiver	1.92	1.98	2.00	2.00
Surface at 3 km above sea level	1.88	1.98	2.01	2.00

^aBase model: surface albedo 0.05, no aerosols, no clouds, horizontal receiver, sea level. RAF computed for ozone column change from 300 to 303 Dobson units.

THEORETICAL PREDICTIONS

the balance among the three dominant forcing processes. Since both the longwave emission and the wave momentum deposition are likely to change in response to substantial radiative heating changes, significant changes in the stratospheric circulation are possible. Stratospheric circulation changes are important because they would affect the transport of ozone and other trace constituents. For example, relatively small changes in the vertical motion within the winter polar vortex would produce substantial changes in the column-integrated ozone abundance at high latitudes.

In addition to photochemically driven perturbations to ozone and stratospheric circulation, we should also consider changes in the concentrations of CO₂ and other greenhouse gases. Increasing greenhouse gas concentrations will act to increase the longwave emission in the upper stratosphere and thus to cool the temperatures. Since reduced radiative heating due to ozone depletion has a similar effect, the two processes will reinforce each other, with the potential for larger changes to the stratospheric circulation. Greenhouse gases also have significant effect on the tropospheric circulation and may change the wave forcing of the stratosphere. The wave momentum deposition is a sensitive function of the wave generation in the troposphere and of the background stratospheric flow, which determines wave propagation and dissipation characteristics.

Unfortunately, very few of the presently available models adequately represent the physical processes important in determining possible circulation changes. This problem is most easily addressed in a 3-D modeling framework where wave generation, propagation, and dissipation processes are explicitly represented, at least for the large-scale waves. Some of the most recent 2-D models include the radiative effects of greenhouse gas increases, and at least one model includes the wave forcing effect through parameterized planetary wave propagation and dissipation (see discussion following scenario A in Section 3.2.2). However, the wave sources must be specified near the tropopause. Two-dimensional models cannot adequately predict changes in tropospheric temperatures and wave forcing of the stratospheric circulation.

Much more work has been done on the transport of trace constituents in 3-D models than on circulation changes resulting from altered ozone and greenhouse gas concentrations. At this time no fully coupled simulations have been performed in 3-D models with the radiative heating determined by a predicted ozone distribution including transport and photochemical effects within the model. There have been a small number of studies that have examined the effects of specified ozone or CO₂ changes. Fels et al. (1980) and Kiehl and Boville (1988) considered the effects of spatially uniform ozone reductions for annual mean conditions and for Northern Hemisphere winter conditions, respectively. For large ozone reductions (>50%), Kiehl and Boville found major differences in the stratospheric circulation with a much weaker polar vortex accompanied by reduced vertical motion (Figure 3.3-45).

The ozone depletions predicted by 2-D models are highly nonuniform, much larger depletions are predicted at high latitudes than at low latitudes and in the upper rather than lower stratosphere. Using a typical ozone depletion scenario, Kiehl and Boville found an increase in the strength of the polar vortex. The changes in the dynamical forcing of the stratosphere were quite modest so that a 2-D model including radiative feedbacks would have predicted similar changes outside of high latitudes in winter. The small vertical velocity changes in high latitudes (Figure 3.3-46) would not be simulated by most 2-D models but could significantly alter the column ozone abundance.

One recent model simulation of doubled CO₂ with a stratospheric GCM predicts noticeable increases in the mean diabatic circulation of the lower stratosphere (Rind et al., 1989). The combination of tropospheric warming and stratospheric cooling leads to an increase in the temperature lapse rate near the tropopause, and also to increased "wave forcing" of the mean diabatic circulation in the lower tropical

THEORETICAL PREDICTIONS

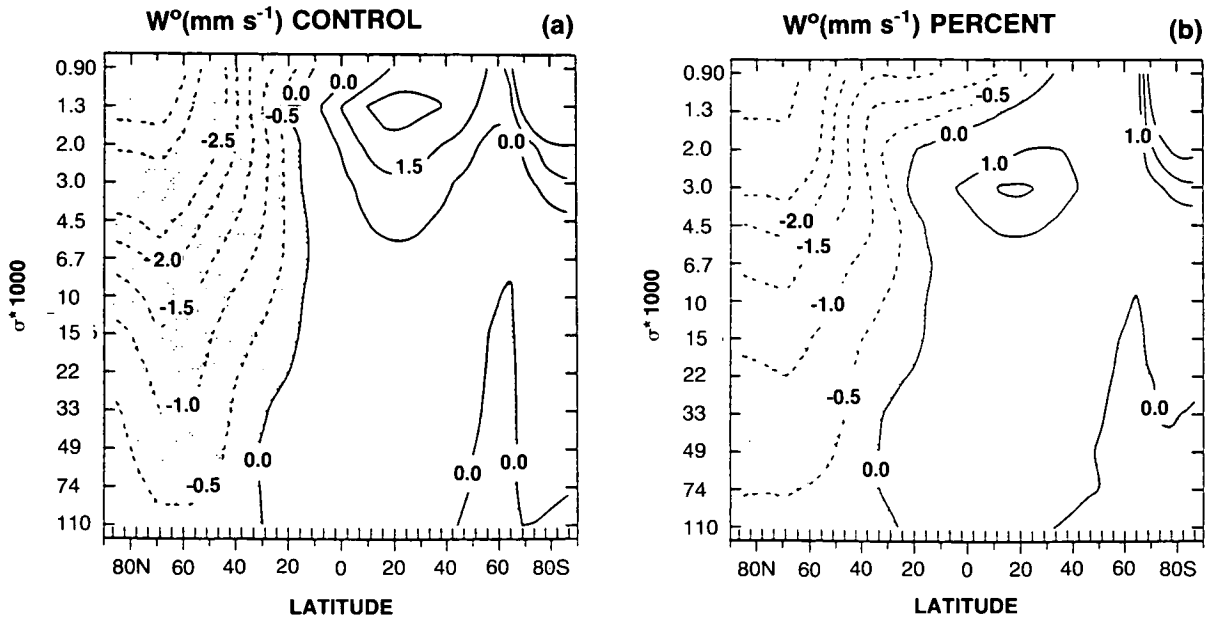


Figure 3.2-45. Transformed Eulerian mean vertical velocity for a 240-day average simulation performed with the NCAR Community Climate Model (Kiehl and Boville, 1988); (a) control case, (b) 75% uniform reduction in the ozone density.

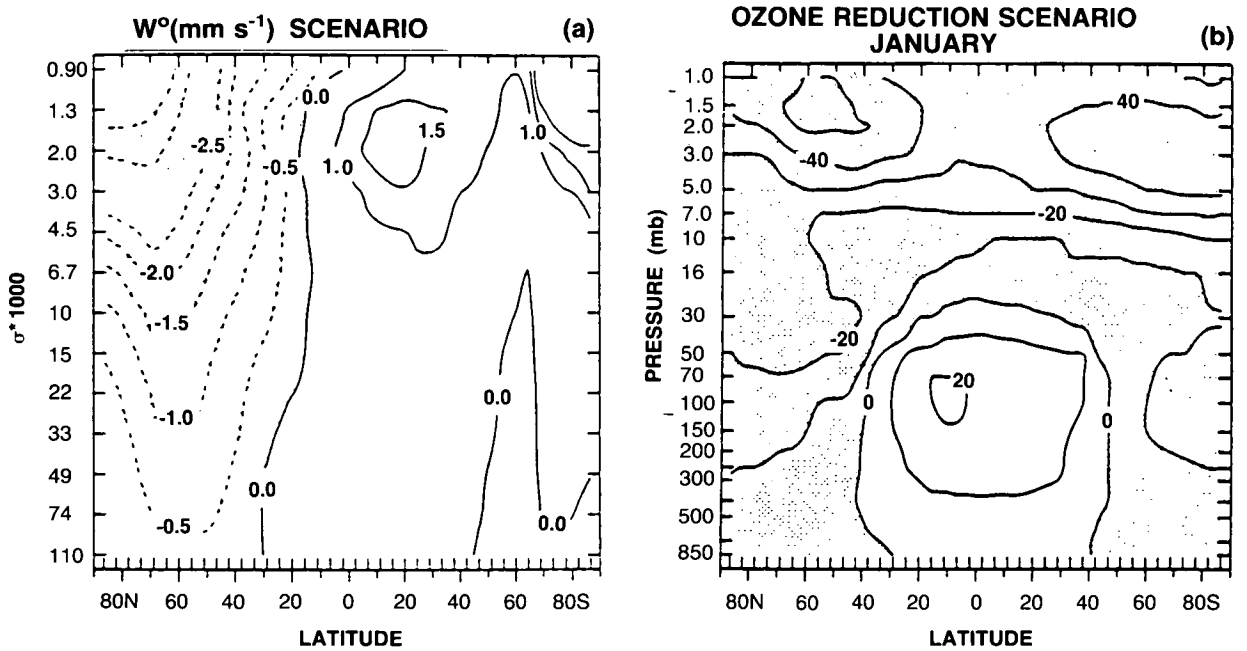


Figure 3.2-46. (a) As in Figure 3.2.40 but for the ozone reduction scenario shown in Figure 3.2.41b; (b) percent change in ozone from the two-dimensional model of Ko et al., 1985.

stratosphere. Another interesting issue for the doubled-CO₂ climate is the altitude at which the temperature change goes from positive (implying consequent ozone reductions) to negative (ozone increases). Results from the GISS model show that this level is sensitive to the tropospheric response, which has been shown in many climate models to vary with latitude and to take several decades to approach a steady state.

So little work has been done on the possible changes in stratospheric circulation that our current understanding of the issues involved and of the possible consequences is minimal. In the next few years we hope that 3-D climate models will examine this problem, diagnosing greenhouse gas-driven changes in the tropospheric climate and resulting stratospheric wave forcing. The response of stratospheric ozone and changes in the lifetimes of CFCs and N₂O should also be predicted within the same 3-D models.

REFERENCES

- Anderson, G. P., and L. A. Hall, Stratospheric determination of O₂ cross sections and photodissociation rate coefficients: 191–215 nm, *J. Geophys. Res.*, *91*, 14509–14515, 1986.
- Andrews, D. G., and M. E. McIntyre, Planetary waves in horizontal and vertical shear: The generalized Eliassen-Palm relation and mean zonal acceleration, *J. Atmos. Sci.*, *33*, 2031–2048, 1976.
- Boyd, J., The noninteraction of waves with the zonally-averaged flow on a spherical earth and the interrelationships of eddy fluxes of energy, heat and momentum, *J. Atmos. Sci.*, *33*, 2285–2291, 1976.
- Brasseur, G., and M. H. Hitchman, The effect of breaking gravity waves on the distribution of trace species in the middle atmosphere, in *Transport Processes in the Middle Atmosphere*, pp. 215–227, Reidel, Dordrecht, Holland, 1987.
- Brühl, C., and P. J. Crutzen, On the disproportionate role of tropospheric ozone as a filter against solar UV-B radiation, submitted to *Geophys. Res. Lett.*, 1989.
- Caldwell, M. M., Plant response to solar ultraviolet radiation, in *Encyclopedia of Plant Physiology, Vol. 12A, Physiological Plant Ecology. I. Responses to the Physical Environment*, edited by O. L. Lange, P. S. Nobel, C. B. Osmond, and H. Ziegler, Springer-Verlag, Berlin, 1981.
- Caldwell, M. M., L. B. Camp, C. W. Warner, and S. D. Flint, Action spectra and their key role in assessing biological consequences of solar UV-B radiation change, in *Stratospheric Ozone Reduction, Solar Ultraviolet Radiation and Plant Life*, edited by R. C. Worrest and M. M. Caldwell, pp. 87–111, Springer-Verlag, Berlin, 1986.
- Chandrasekhar, S., *Radiative Transfer*, Dover, New York, 1960.
- Cutcher, P., Stratospheric ozone depletion and solar ultraviolet radiation on Earth, *Science*, *184*, 13, 1974.
- DeMore, W. B., M. J. Molina, S. P. Sander, D. M. Golden, R. F. Hampson, M. J. Kurylo, C. J. Howard, and A. R. Ravishankara, Chemical kinetics and photochemical data for use in stratospheric modeling, evaluation number 8, JPL Publ. 87-41, 1987.
- Dunkerton, T. J., On the role of the Kelvin wave in the westerly phase of the semiannual zonal wind oscillation, *J. Atmos. Sci.*, *36*, 32–41, 1979.
- Dutsch, H. U., Photochemistry of atmospheric ozone, *Adv. Geophys.*, *15*, 219–232, 1971.
- Edmon, H. J., B. J. Hoskins, and M. E. McIntyre, Eliassen-Palm cross sections for the troposphere, *J. Atmos. Sci.*, *37*, 2600–2616, 1980.
- Elterman L., UV, visible, and IR attenuation for altitudes to 50 km, 1968, *AFCRL-68-0153, No. 285*, Air Force Cambridge Research Laboratories, Bedford, MA., 1968.
- Fels, S. B., J. D. Mahlman, M. D. Schwarzkopf, and R. W. Sinclair, Stratospheric sensitivity to perturbations in ozone and carbon dioxide: Radiative and dynamical response, *J. Atmos. Sci.*, *37*, 2265–2297, 1980.

THEORETICAL PREDICTIONS

- Frederick J. E., and D. Lubin, Possible long-term changes in the biologically active ultra-violet radiation reaching the ground, *Photochem. Photobio.*, 47, 571–578, 1988a.
- Frederick J. E., and D. Lubin, The budget of biologically active ultraviolet radiation in the Earth-atmosphere system, *J. Geophys. Res.*, 93, 3825–3832, 1988b.
- Fröhlich C., and G. E. Shaw, New determination of Rayleigh scattering in the terrestrial atmosphere, *Appl. Opt.*, 19, 1773–1775, 1980.
- Garcia, R. R., On the mean meridional circulation of the middle atmosphere, *J. Atmos. Sci.*, 44, 3599–3609, 1987.
- Garcia, R. R., and S. Solomon, The effect of breaking gravity waves on the dynamics and chemical composition of the mesosphere and lower thermosphere, *J. Geophys. Res.*, 90, D2, 3850–3868, 1985.
- Gerstl, S. A. W., A. Zardecki, and H. L. Wiser, Biologically damaging radiation amplified by ozone depletions, *Nature*, 294, 352–354, 1981.
- Granier, C., and G. Brasseur, Ozone and other trace gases in the Arctic and Antarctic regions: A three-dimensional model, in preparation, 1990.
- Gray, L. J., and J. A. Pyle, Two-dimensional model studies of equatorial dynamics and tracer distributions, *Q. J. Roy. Meteorol. Soc.*, 113, 635–651, 1987.
- Gray, L. J., and J. A. Pyle, A two-dimensional model of the quasi-biennial oscillation of ozone, *J. Atmos. Sci.*, 46, 203–220, 1989.
- Grose, W. L., J. E. Nealy, R. E. Turner, and W. T. Blackshear, Modeling the transport of chemically active constituents in the stratosphere, in *Transport Processes in the Middle Atmosphere*, Reidel, Dordrecht, Holland, 1987.
- Herman, J. R., and J. E. Mentall, O₂ absorption cross sections (187–225 nm) from stratospheric solar flux measurements, *J. Geophys. Res.*, 87, 8967–8975, 1982.
- Hitchman, M. H., and G. Brasseur, Rossby wave activity in a two-dimensional model: Closure for wave driving and meridional eddy diffusivity, *J. Geophys. Res.*, 93, D8, 9405–9417, 1988.
- Hofmann, D. J., and S. Solomon, Ozone destruction through heterogeneous chemistry following the eruption of El Chichon, *J. Geophys. Res.*, 94, 5029, 1989.
- Holton, J. R., Wave propagation and transport in the middle atmosphere. *Phil. Trans Roy. Soc. London*, A296, 73–85, 1980.
- Holton, J. R., The role of gravity wave induced drag and diffusion in the momentum budget of the mesosphere, *J. Atmos. Sci.*, 39, 791–799, 1982.
- Jackman, C. H., P. A. Newman, P. D. Guthrie, and M. R. Schoeberl, Effect of self-consistent horizontal diffusion coefficients on two-dimensional N₂O model distributions, *J. Geophys. Res.*, 93, 5213–5219, 1988.
- Jackman, C. H., A. R. Douglass, P. D. Guthrie, and R. S. Stolarski, The sensitivity of total ozone and ozone perturbation scenarios in a two-dimensional model due to dynamical inputs, *J. Geophys. Res.*, in press, 1989a.
- Jackman, C. H., R. K. Seals, and M. J. Prather (eds.), *Two-Dimensional Intercomparison of Stratospheric Models*, Proceedings of the NASA Workshop held in Virginia Beach, Virginia, September 11–16, 1988, NASA Conference Publication 3042, NASA, 1989b.
- Joseph, J. H., W. J. Wiscombe, and J. A. Weinman, The delta-Eddington approximation for radiative flux transfer, *J. Atmos. Sci.*, 33, 2452–2459, 1976.
- Juckes, M. N., and M. E. McIntyre, A high-resolution one-layer model of breaking planetary waves in the stratosphere, *Nature*, 328, 590–596, 1987.
- Kaye, J. A., and R. B. Rood, Chemistry and transport in a three-dimensional stratospheric model: Chlorine species during a simulated stratospheric warming, *J. Geophys. Res.*, 94, 1057–1083, 1989.

- Kida, H., General circulation of air parcels and transport characteristics derived from a hemispheric GCM. Part I. A determination of advective mass flow in the lower stratosphere, *J. Meteor. Soc. Japan*, *61*, 171–186, 1983.
- Kiehl, J. T., and B. A. Boville, The radiative-dynamical response of a stratospheric-tropospheric general circulation model to changes in ozone, *J. Atmos. Sci.*, *45*, 1798–1817, 1988.
- King, M. D., and Harshvardhan, Comparative accuracy of selected multiple scattering approximations, *J. Atmos. Sci.*, *43*, 784–801, 1986.
- Ko, M. K. W., K. K. Tung, D. K. Weinstein, and N. D. Sze, A zonal-mean model of stratospheric tracer transport in isentropic coordinates: Numerical simulations for nitrous oxide and nitric acid, *J. Geophys. Res.*, *90*, 2313–2329, 1985.
- Ko, M. K. W., N. D. Sze, and D. Weisenstein, The roles of dynamical and chemical processes in determining the stratospheric concentration of ozone in one-dimensional and two-dimensional models, *J. Geophys. Res.*, in press, 1989.
- Leu, M. T., Laboratory studies of sticking coefficients and heterogeneous reactions important in the Antarctic stratosphere, *Geophys. Res. Lett.*, *15*, 17–20, 1988a.
- Leu, M. T., Heterogeneous reactions of N_2O_5 with H_2O and HCl on ice surfaces: Implications for Antarctic ozone depletion, *Geophys. Res. Lett.*, *15*, 855–858, 1988b.
- Lindzen, R. S., Turbulence and stress due to gravity wave and tidal breakdown, *J. Geophys. Res.*, *86*, 9707–9714, 1981.
- Lyjak, L. V., Diffusion coefficients calculated from satellite data, in *Transport Processes in the Middle Atmosphere*, pp. 343–352, Dordrecht, Holland, 1987.
- Madronich S., Photodissociation in the atmosphere: 1. Actinic flux and the effects of ground albedo and clouds, *J. Geophys. Res.*, *92*, 9740–9752, 1987.
- Mahlman, J. D., and L. J. Umscheid, Dynamics of the middle atmosphere: Successes and problems of the GFDL “SKYHI” general circulation model, in *Dynamics of the Middle Atmosphere*, edited by J. R. Holton and T. Matsuno, pp. 501–525, Terrapub, Tokyo, 1984.
- McElroy, M. B., and R. J. Salawitch, Changing composition of the global stratosphere, *Science*, *243*, 763–770, 1989.
- Meadow W. E., and W. R. Weaver, Two-stream approximations to radiative transfer in planetary atmospheres: A unified description of existing methods and a new improvement, *J. Atmos. Sci.*, *37*, 630–643, 1980.
- Mentall J. E., J. E. Frederick, and J. R. Herman, The solar irradiance from 200 to 330 nm, *J. Geophys. Res.*, *86*, 9881–9884, 1981.
- Molina L. T., and M. J. Molina, Absolute absorption cross sections of ozone in the 185- to 350-wavelength range, *J. Geophys. Res.*, *91*, 14501–14508, 1986.
- Molina, M. J., T. L. Tso, L. T. Molina, and F. C. Y. Wang, Antarctic stratospheric chemistry of chlorine nitrate, hydrogen chloride, and ice: Release of active chlorine, *Science*, *238*, 1253–1257, 1987.
- Mozurkewich, M., and J. G. Calvert, Reaction probability on N_2O_5 on aqueous aerosols, *J. Geophys. Res.*, *93*, 15889, 1988.
- Natarajan, M., and L. B. Callis, Examination of stratospheric ozone photochemistry in light of recent data, *Geophys. Res. Lett.*, *16*, 473–476, 1989.
- Neckel H., and D. Labs, The solar radiation between 3300 and 12500 Å, *Solar Physics*, *90*, 205–258, 1984.
- Newman, P. A., M. R. Schoeberl, and R. A. Plumb, Horizontal mixing coefficients for two-dimensional chemical models calculated from National Meteorological Center data, *J. Geophys. Res.*, *91*, D7, 7919–7924, 1986.
- Newman, P. A., M. R. Schoeberl, R. A. Plumb, and J. E. Rosenfield, Mixing rates calculated from potential vorticity, *J. Geophys. Res.*, *93*, 5210–5240, 1988.

THEORETICAL PREDICTIONS

- Nicolet M., R. R. Meier, and D. E. Anderson, Jr., Radiation field in the troposphere and stratosphere-II. Numerical analysis, *Planet. Space Sci.*, 30, 935-983, 1982.
- Pitari G., M. Verdecchia, and G. Visconti, Ozone hole simulation using a prescribed dynamical field, in preparation, 1990.
- Plumb, R. A., The interaction of two internal waves with the mean flow: Implications for the theory of the quasi-biennial oscillation, *J. Atmos. Sci.*, 34, 1847-1858, 1977.
- Plumb, R. A., and J. D. Mahlman, The zonally averaged transport characteristics of the GFDL general circulation/transport model, *J. Atmos. Sci.*, 44, 298-327, 1987.
- Pyle, J. A., and R. G. Derwent, Possible ozone reductions and UV changes at the Earth's surface, *Nature*, 286, 373-375, 1980.
- Raper, O. F., C. B. Farmer, R. Zander, and J. H. Park, Infrared spectroscopic measurements of halogenated sink and reservoir gases in the stratosphere with the ATMOS instrument, *J. Geophys. Res.*, 92, 9851-9858, 1987.
- Reed, R. J., and K. E. German, A contribution to the problem of stratospheric diffusion by large-scale mixing, *Mon. Wea. Rev.*, 93, 313-321, 1965.
- Rind, D., R. Suozzo, and N. K. Balachandran, The GISS global climate-middle atmosphere model. Part II: Model variability due to interactions between planetary waves, the mean circulation and gravity wave drag, *J. Atmos. Sci.*, 45, 371-386, 1989.
- Robertson, D. F., The sunburn unit for comparison of variation of erythemal effectiveness, in *Impacts of Climactic Change on the Biosphere, Part I, Ultraviolet Radiation Effects*, edited by D. S. Nachtwey, M. M. Caldwell, and R. H. Biggs, Monograph 5. Climactic Impact Assessment Program, U.S. Dept. Transportation Report No. DOT-TST-75-55, NTIS, Springfield, Virginia, 1975.
- Rodriguez, J. M., M. K. W. Ko, and N. D. Sze, Antarctic chlorine chemistry: Possible global implications, *Geophys. Res. Lett.*, 15, 257-260, 1988.
- Rood, R. B., and J. A. Kaye, Stratospheric ozone models and supercomputers, to appear in *Proceedings of the Fourth International Conference on Supercomputing*, International Supercomputing Institute, St. Petersburg, Florida, in press, 1989.
- Rood R. B., D. J. Allen, W. E. Baker, D. J. Lamich, and J. A. Kaye, The use of assimilated stratospheric data in constituent transport experiments, *J. Atmos. Sci.*, 46, 687-701, 1989.
- Rose, K., and G. Brasseur, Ozone during a sudden stratospheric warming: A three dimensional simulation, in *Atmospheric Ozone, Proceedings of the Quadrennial Ozone Symposium*, Halkidiki, Greece, edited by C. S. Zerefos and A. Ghazi, D. Reidel, Hingham, Mass., 1985.
- Rose, K., and G. Brasseur, A three-dimensional model of chemically active trace species in the middle atmosphere during disturbed winter conditions, *J. Geophys. Res.*, 94, 16387-16403, 1989.
- Russell III, J. M., C. B. Farmer, C. P. Rinsland, R. Zander, L. Frordevaux, G. C. Toon, B. Gao, J. Shaw, and M. Gunson, Measurements of odd nitrogen compounds in the stratosphere by the ATMOS experiment on Spacelab 3, *J. Geophys. Res.*, 93, 1718-1736, 1988.
- Schneider, H. R., M. E. W. Ko, N. D. Sze, G.-Y. Shi, and W.-C. Wang, The effects of eddy diffusion, drag, and nonlinear terms on the meridional circulation and ozone distributions in an interactive 2-D model, *J. Atmos. Sci.*, in press, 1989.
- Scotto J., G. Cotton, F. Urbach, D. Berger, and T. Ferris, Biologically effective ultraviolet radiation: Surface measurements in the United States, 1974 to 1985, *Science*, 238, 762-764, 1988.
- Setlow, R. B., The wavelengths in sunlight effective in producing skin cancer: A theoretical analysis, *Proc. Natl. Acad. Sci. USA*, 71, 3363-3366, 1974.
- Shettle E. P., and J. A. Weinman, The transfer of solar irradiance through inhomogeneous turbid atmospheres evaluated by Eddington's approximation, *J. Atmos. Sci.*, 27, 1048-1055, 1970.
- Smith, A. K., L. V. Lyjak, and J. C. Gille, The eddy transport of nonconserved trace species derived from satellite data, *J. Geophys. Res.*, 93, D9, 11103-11122, 1988.

THEORETICAL PREDICTIONS

- Snieder, R. K., and S. B. Fels, The flywheel effect in the middle atmosphere, *J. Atmos. Sci.*, 45, 3996–4004, 1988.
- SORG, U. K. Stratospheric Ozone Review Group Report, September 1988, H. M. Stationary, London, ISBN 0 11 752 1485, 1988.
- Stamnes, K., The theory of multiple scattering of radiation in plane parallel atmospheres, *Rev. Geophys.*, 24, 299–310, 1986.
- Stordal, F., O. Hov, and I. S. A. Isaksen, The effect of perturbation of the total ozone column due to CFC on the spectral distribution of UV fluxes and the damaging UV doses at the ocean surface: A model study, in *The Role of Solar Ultraviolet Radiation in Marine Ecosystems*, edited by J. Calkins, Plenum, New York, 1982.
- Tung, K. K., Nongeostrophic theory of zonally averaged circulation. Part I: Formulation, *J. Atmos. Sci.*, 43, 2600–2618, 1986.
- Tung, K. K., A coupled model of zonally averaged dynamics, radiation, and chemistry, in *Transport Processes in the Middle Atmosphere*, pp. 183–198, Reidel, Dordrecht, Holland, 1987.
- Watson, R. T., and Ozone Trends Panel; M. J. Prather and Ad Hoc Theory Panel; and M. J. Kurylo and NASA Panel for Data Evaluation, *Present State of Knowledge of the Upper Atmosphere 1988: An Assessment Report*, NASA Reference Publication 12081, U.S. Govt. Print. Off., Washington, D.C., 1988.
- WMO, Atmospheric Ozone 1985. Assessment of Our Understanding of the Processes Controlling Its Present Distribution and Change, *WMO Report No. 16*, Sponsored by WMO, NASA, NOAA, FAA, UNEP, CEC, and BMFT, Washington, D.C., 1986.

509417

chapter **4**

92p N92-15434

HALOCARBON OZONE DEPLETION AND GLOBAL WARMING POTENTIALS

Coordinators

R. A. Cox (UK) and D. Wuebbles (USA)

Principal Authors and Contributors

R. Atkinson (Australia)
P. Connell (USA)
R. A. Cox (UK)
H. P. Dorn (FRG)
A. De Rudder (Belgium)
R. G. Derwent (UK)
F. C. Fehsenfeld (USA)
D. Fisher (USA)
I. Isaksen (Norway)

M. Ko (USA)
R. Lesclaux (France)
S. C. Liu (USA)
S. A. Penkett (UK)
V. Ramaswamy (USA)
J. Rudolph (FRG)
H. B. Singh (USA)
W.-C. Wang (USA)
D. Wuebbles (USA)

CHAPTER 4

HALOCARBON OZONE DEPLETION AND GLOBAL WARMING POTENTIALS

TABLE OF CONTENTS

4.1	INTRODUCTION	401
4.2	HALOCARBON OXIDATION IN THE ATMOSPHERE	401
4.2.1	Background	401
4.2.2	Tropospheric Chemistry of Halocarbons	402
4.2.3	Hydroxyl Radical Chemistry in the Troposphere	410
4.2.4	Tropospheric Chemistry Influencing OH and Ozone	417
4.2.5	Model Evaluation of Trends in Tropospheric Ozone and OH	422
4.3	OZONE DEPLETION POTENTIALS	424
4.3.1	Background	424
4.3.2	Definition of ODP	424
4.3.3	Model-Calculated ODPs	427
4.3.4	Uncertainties and Sensitivity Studies	431
4.3.5	Summary	450
4.4	HALOCARBON GLOBAL WARMING POTENTIALS	451
4.4.1	Background	451
4.4.2	Definition of Halocarbon GWP	453
4.4.3	Model-Calculated Halocarbon GWPs	455
4.4.4	Uncertainties	459
4.4.5	Summary	461
	REFERENCES	462

4.1 INTRODUCTION

Concern over the global environmental consequences of fully halogenated chlorofluorocarbons (CFCs) has created a need to determine the potential impacts of other halogenated organic compounds on stratospheric ozone and climate. The CFCs, which do not contain an H atom, are not oxidized or photolyzed in the troposphere. These compounds are transported into the stratosphere where they decompose and can lead to chlorine-catalyzed ozone depletion. The hydrochlorofluorocarbons or hydrofluorocarbons (HCFCs or HFCs), in particular those proposed as substitutes for CFCs, contain at least one hydrogen atom in the molecule, which confers on these compounds a much greater sensitivity toward oxidation by hydroxyl radicals in the troposphere, resulting in much shorter atmospheric lifetimes than CFCs, and consequently lower potential for depleting ozone.

The main objective of this chapter is to review the available information relating to the lifetime of those compounds (HCFCs and HFCs) in the troposphere, and to report on up-to-date assessments of the potential relative effects of CFCs, HCFCs, HFCs, and halons on stratospheric ozone and global climate (through "greenhouse" global warming).

The lifetimes of the HCFCs and HFCs are determined by their rate of oxidation by hydroxyl (OH) radicals in the troposphere. Therefore it was necessary to consider the components of tropospheric chemistry affecting the OH radical concentration (i.e., tropospheric ozone, hydrocarbons, and nitrogen oxides) as well as the kinetics and degradation mechanism of the halocarbons. Special attention is also given to the nature of the products of the degradation of the HCFCs and HFCs being considered as possible replacements for CFCs. In parallel with this assessment, an initiative with similar objectives—the Alternative Fluorocarbon Environment Acceptability Study (AFEAS)—was carried out. AFEAS was an in-depth examination by over 50 scientists. The present evaluation has benefited from the availability of this material and the conclusions drawn from it. The AFEAS report, Vol. II, is an Appendix to this report.

The chapter is divided into three main sections. The first section concerns the oxidation of halocarbons in the troposphere. The kinetics and degradation mechanisms of the halocarbons are reviewed and the nature and fate of the degradation products are identified. Estimates of current global OH abundances in the troposphere are discussed and consequent halocarbon lifetimes are provided. The current picture concerning tropospheric ozone and its precursors, as they affect OH, is presented together with a summary of recent model predictions of future changes in tropospheric ozone and OH. The second section concerns the evaluation of potential effects on stratospheric ozone through the determination of relative (to CFC-11) Ozone Depletion Potentials (ODPs), while the third section relates their effects to climate through evaluation of relative halocarbon Global Warming Potentials (GWPs) for these compounds. Discussion in these sections also emphasizes the uncertainties pertinent to calculations of ODPs and halocarbon GWPs.

4.2 HALOCARBON OXIDATION IN THE ATMOSPHERE

4.2.1 Background

The oxidation of atmospheric trace gases containing carbon, hydrogen, nitrogen, sulphur and halogens, emitted by a variety of natural and man-made sources, occurs by chemical reactions initiated directly or indirectly by solar radiation. These chemical processes yield either non-reactive long-lived products such as CO₂ or water vapor, or acidic species such as HNO₃, H₂SO₄, HF, or HCl which are removed from

OZONE DEPLETION POTENTIALS

the atmosphere by physical processes. The oxidation processes occur mainly in the troposphere, and they prevent the build-up of excessive concentrations of these trace substances in the atmosphere. Moreover, in the context of the topic of stratospheric ozone depletion, tropospheric oxidation acts as a filter preventing the injection into the stratosphere of the source gases for radicals in the NO_x , ClO_x , and BrO_x families, which can catalytically destroy ozone.

The chemical oxidation processes generally, but not exclusively, take place in the gas phase. For volatile organic compounds including halogenated hydrocarbons, the major oxidizing species is the hydroxyl radical OH, which reacts to abstract hydrogen atoms or adds to unsaturated linkages, thus initiating a free radical degradation mechanism. The fully halogenated chlorofluoroalkanes do not contain these reactive sites and consequently cannot be degraded in this way.

The OH radicals are generated photochemically and are maintained at a steady-state concentration in the sunlit atmosphere. The average concentration of OH, together with its rate coefficient for reaction with a particular compound, determines the atmospheric lifetime of that compound. For a given emission rate, the amount of any compound that can build up in the troposphere will be in proportion to its lifetime, and it follows that the amount that reaches the stratosphere by transport from the troposphere will be heavily influenced by its rate of tropospheric oxidation. Current and future changes in the oxidizing efficiency of the troposphere, as measured by the average OH concentration, are clearly of high importance in assessing the suitability of hydrochlorofluorocarbons as substitutes for the CFCs.

The oxidation mechanisms in the troposphere are caused by the presence of ozone, since photolysis of ozone in the ultraviolet region leads to the formation of the hydroxyl radical. Moreover, approximately 10% of the total ozone column is present in the troposphere, and therefore, changes in ozone concentration in this altitude range need to be considered as part of the assessment of overall column changes. Tropospheric ozone also adds significantly to the total greenhouse warming by virtue of its pressure-broadened infrared absorption in the atmospheric window, and also by its influence through chemistry on other radiative active trace gases (e.g., CH_4).

In recent years there has been a major initiative to understand the budgets and life cycle of tropospheric ozone. It is now clear that earlier theories, advocating a purely dynamical description with injection of ozone from the stratosphere and removal by surface deposition, are inadequate. *In situ* chemical production and loss of ozone, first suggested in the mid 1970s, clearly plays a role in determining the global tropospheric ozone budget and has probably led to increases in O_3 over large parts of the Northern Hemisphere. The reactions controlling ozone production and loss in the troposphere are photochemically initiated and involve a variety of trace species including nitrogen oxides, volatile organics, and free radicals in the HO_x family (OH and HO_2).

There are other oxidizing species present in the troposphere which help to maintain stable composition in the atmosphere. These include peroxy radicals, nitrate radicals (NO_3), halogen atoms, and ozone. These species are generally much less important than OH for tropospheric oxidation. Other oxidizing reactions can occur in the aqueous phase in cloud and rain, where hydrogen peroxide (H_2O_2) plays an important role. These are not important for oxidation of halocarbons.

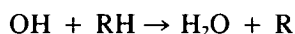
4.2.2 Tropospheric Chemistry of Halocarbons

As discussed in Section 4.2.1 above, most organic compounds including halocarbons are degraded in the troposphere primarily by reaction with the OH radical. The chemical reactivity of halocarbons is

reviewed in this section, considering the dominant atmospheric removal pathways, i.e. gas phase reaction with the OH radical and photolysis. Reactions with O₃ and with the NO₃ radical are of negligible importance as an atmospheric removal pathway. In addition, the specific reaction pathways of the halocarbon degradation processes prevailing in the troposphere are examined and the principal halogenated degradation products are identified. The final fate of these degradation products in the troposphere is discussed by considering both their homogeneous gas phase chemistry and their physical removal pathways. The reactions of HCFCs and HFCs with O(¹D) atoms are unimportant in the troposphere but may be important in producing active chlorine or OH in the stratosphere.

4.2.2.1 OH Radical Reactions

The reaction of OH with HFCs and HCFCs involves abstraction of a hydrogen atom to form water and a haloalkyl radical (R):



The rate constants for the reactions of OH with many HFCs and HCFCs have been evaluated as part of the AFEAS assessment (see Vol. II, Appendix). Recommendations are given for the five HCFCs and three HFCs specified by AFEAS as primary alternatives as well as for all other isomers of C₁ and C₂ HCFCs and HFCs where rate data exist. In addition, recommendations are included for CH₃CCl₃, CH₂Cl₂, and CH₄. The recommended rate constants from this evaluation are given in Table 4.2-1.

The format used for the presentation of the recommended rate constant data is the same as that used by the NASA Panel for Data Evaluation (see DeMore et al., 1987). The rate constant tabulation is given in Arrhenius form $k(T) = A \exp(-E/RT)$, and contains the following information:

1. Reaction stoichiometry.
2. Arrhenius A factor (in units of cm³ molecule⁻¹ s⁻¹).
3. Temperature dependence ("activation temperature," E/R) and associated uncertainty ($\Delta E/R$).
4. Rate constant at 298 K (in units of cm³ molecule⁻¹ s⁻¹).
5. Uncertainty factor at 298 K.

All of the uncertainties are one standard deviation, 1σ . Hence, 95% confidence limits are given by 2σ . The uncertainty (1σ) at any temperature can be calculated from the expression:

$$f(T) = f(298) \exp\{\Delta E/R(1/T - 1/298)\}$$

The rate constants are well defined and significant uncertainties only appear when the Arrhenius expressions in Table 4.2.1 are used for extrapolations over a wide temperature range. In particular, at temperatures around 277 K, which corresponds to the region of the troposphere where most of the degradation of these molecules occurs, the rate coefficients are accurate to within ~20%.

4.2.2.2 Photolysis

Photolysis is a potential atmospheric loss process for those haloalkanes containing multiple Cl and/or Br atoms. The absorption spectra are unstructured and continuous, and may extend out to 300 nm,

OZONE DEPLETION POTENTIALS

Table 4.2-1. Recommended rate constants and uncertainties for reactions of OH with selected HFCs and HCFCs

Reaction	Fluorocarbon Number	A ^a	E/R ± E/R ^b	k ₂₉₈ ^a	f(298)
OH + CHFCl ₂	HCFC-21	1.2(-12)	1100 ± 150	3.0(-14)	1.1
OH + CHF ₂ Cl	HCFC-22	1.2(-12)	1650 ± 150	4.7(-15)	1.1
OH + CHF ₃	HFC-23	7.4(-13)	2350 ± 400	2.1(-16)	1.5
OH + CH ₂ Cl ₂	30	5.8(-12)	1100 ± 150	1.4(-13)	1.2
OH + CH ₂ FCl	HCFC-31	3.0(-12)	1250 ± 150	4.5(-14)	1.15
OH + CH ₂ F ₂	HFC-32	2.5(-12)	1650 ± 200	1.0(-14)	1.2
OH + CH ₃ F	HFC-41	5.4(-12)	1700 ± 300	1.8(-14)	1.2
OH + CH ₄	50	2.3(-12)	1700 ± 200	7.7(-15)	1.2
OH + CHCl ₂ CF ₃	HCFC-123	6.4(-13)	850 ± 150	3.7(-14)	1.2
OH + CHFClCF ₃	HCFC-124	6.6(-13)	1250 ± 300	1.0(-14)	1.2
OH + CHF ₂ CF ₃	HFC-125	3.8(-13)	1500 ± 500	2.5(-15)	2.0
OH + CH ₂ ClCF ₂ Cl	HCFC-132b	3.6(-12)	1600 ± 400	1.7(-14)	2.0
OH + CH ₂ ClCF ₃	HCFC-133a	5.2(-13)	1100 ± 300	1.3(-14)	1.3
OH + CHF ₂ CHF ₂	HFC-134	8.7(-13)	1500 ± 500	5.7(-15)	2.0
OH + CH ₂ FCF ₃	HFC-134a	1.7(-12)	1750 ± 300	4.8(-15)	1.2
OH + CH ₃ CCl ₃	140a	5.0(-12)	1800 ± 300	1.2(-14)	1.3
OH + CH ₃ CFCl ₂	HCFC-141b	2.7(-13)	1050 ± 200	7.5(-15)	1.3
OH + CH ₃ CF ₂ Cl	HCFC-142b	9.6(-13)	1650 ± 150	3.8(-15)	1.2
OH + CH ₂ FCHF ₂	HFC-143	2.8(-12)	1500 ± 500	1.8(-14)	2.0
OH + CH ₃ CF ₃	HFC-143a	2.6(-13)	1500 ± 500	1.7(-15)	2.0
OH + CH ₂ FCH ₂ F	HFC-152	1.7(-11)	1500 ± 500	1.1(-13)	2.0
OH + CH ₃ CHF ₂	HFC-152a	1.5(-12)	1100 ± 200	3.7(-14)	1.1
OH + CH ₃ CH ₂ F	HFC-161	1.3(-11)	1200 ± 300	2.3(-13)	2.0

^aUnits are cm³ molecule⁻¹s⁻¹.

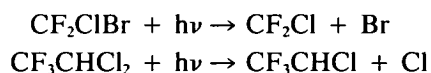
^bUnits are K.

which could result in photodissociation in the troposphere. However, the cross sections are very low in the long wavelength region, resulting in very low photolysis rates in the troposphere for fluorochloroalkanes and brominated compounds such as CF₃Br. Only for haloalkanes containing one Br and one or more Cl atoms (CF₂ClBr, CHCl₂Br, and CH₂ClBr) or two or more Br atoms (CF₂Br₂, CH₂Br₂, CHClBr₂, and CHBr₂) does photolysis in the troposphere become significant.

Solar photolysis is likely to contribute significantly to the stratospheric destruction of the alternative fluorocarbons which have two or more chlorine atoms bonded to the same carbon atom.

The absorption cross sections for several HFCs and HCFCs have been reviewed as part of the AFEAS assessment. Two of the eight HCFCs considered in the review, namely HCFC-123 and HCFC-141b, have significant stratospheric photolysis. For these two species there is good agreement among the various measurements of the ultraviolet cross sections in the wavelength region which is important for atmospheric photodissociation, that is, around 200 nm. There is also good agreement for HCFC-124, HCFC-22, and HCFC-142b; these three species contain only one chlorine atom per molecule and OH reaction is the dominant loss process in both the stratosphere and the troposphere.

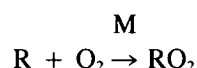
Photodissociation occurs with quantum yields which are expected to be unity, and results in the detachment of a Br atom for bromine-containing haloalkanes, or a chlorine atom from HCFCs, e.g.,



The subsequent reactions of the haloalkyl radicals formed are discussed below.

4.2.2.3 Reactions of the Haloalkyl (R) Radicals

Under tropospheric conditions, the only reaction of the haloalkyl radicals, R, is with O₂.



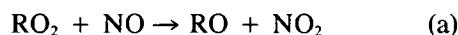
For the halomethyl radicals CF₃, CFCl₂, and CCl₃, these additional reactions are in the fall-off region between second- and third-order kinetics at the temperatures and pressures encountered in the troposphere. However, the bimolecular rate constants are estimated to be within a factor of ~2 of the limiting high pressure rate constants throughout the troposphere, with

$$k(\text{R} + \text{O}_2) \cong 10^{-12} \text{ cm}^3 \text{ molecule}^{-1} \text{ s}^{-1}$$

leading to a lifetime of the haloalkyl radicals in the troposphere of <10⁻⁶s.

4.2.2.4 Reactions of the Haloalkyl Peroxy (RO₂) Radicals

At the expected tropospheric concentrations of NO, NO₂, the HO₂ radical, and other organic peroxy radicals, the dominant reactions of the haloalkyl peroxy radicals will be with NO, NO₂, and the HO₂ radical, i.e., these reactions proceed by



M



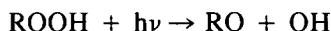
leading to the formation of haloalkoxy radicals, RO, halogenated peroxy nitrates (ROONO₂) and hydroperoxides (ROOH). Based upon kinetic data reported for reactions (a) and (b) of the chlorofluoromethyl peroxy radicals (NASA, 1987; IUPAC, 1989), it appears that $k_a \sim 1.6 \times 10^{-11} (\text{T}/300)^{-1.2} \text{ cm}^3 \text{ molecule}^{-1} \text{ s}^{-1}$ and $k_b \sim 1 \times 10^{-11} \text{ cm}^3 \text{ molecule}^{-1} \text{ s}^{-1}$ for tropospheric conditions.

No data are available for the reactions of haloalkyl peroxy radicals with the HO₂ radical. Based upon the absolute rate constant data for the reactions of the HO₂ radical with CH₃O₂ and C₂H₅O₂, the rate constant for the reactions of alkyl peroxy radicals with HO₂ is $\sim 3.4 \times 10^{-13} e^{800/\text{T}} \text{ cm}^3 \text{ molecule}^{-1} \text{ s}^{-1}$, and in the absence of experimental data for the haloalkyl peroxy radicals this expression may be assumed to apply for reaction (c) above.

OZONE DEPLETION POTENTIALS

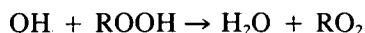
4.2.2.5 Reactions of the Hydroperoxides (ROOH)

The gas-phase loss processes of the hydroperoxides are expected to be photolysis and reaction with the OH radical. The absorption cross sections for CH₃OOH have been measured, and photolysis



is estimated to lead to a lifetime of CH₃OOH and other ROOH species of a few days in the lower troposphere.

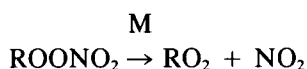
Reaction of the haloalkyl hydroperoxides, ROOH, with the OH radical will proceed by H atom abstraction to reform the RO₂ radical



Abstraction of an H atom from the haloalkyl (R) group, even if possible, is estimated to be of minor or negligible importance. Based upon the available kinetic data for (CH₃)₃COOH and CH₃OOH, the rate constant for the reaction of the OH radical with ROOH to form RO₂ + HO₂ is $1.7 \times 10^{-12} e^{220/T} \text{ cm}^3 \text{ molecule}^{-1} \text{ s}^{-1}$. This OH radical reaction is then of comparable importance to the photolysis of the ROOH species. However, since the estimated lifetime of the ROOH species due to photolysis and reaction with the OH radical is ~2–3 days in the lower troposphere, wet deposition and/or incorporation of ROOH into cloud, rain and fog water must also be expected to be of importance as a tropospheric sink for these hydroperoxides.

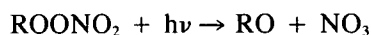
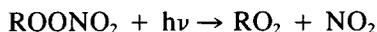
4.2.2.6 Reactions of the Haloalkyl Peroxynitrates (ROONO₂)

The peroxynitrates undergo thermal decomposition and photolysis. Thermal decomposition



is expected to be the dominant loss process for these compounds in the lower troposphere. Consistent with the reverse formation reaction, the decomposition rate constants for the halomethyl peroxynitrates are in the fall-off region at the temperatures and pressures of the troposphere, but are within a factor of ~2 of the high-pressure rate constants (IUPAC, 1989). For the peroxynitrates CF₂ClOONO₂, CFCI₂OONO₂, and CCl₃OONO₂, the limiting high-pressure decomposition rate constant is $\sim 1 \times 10^{15} e^{-11000/T} \text{ s}^{-1}$.

The absorption cross sections of CFCI₂OONO₂ and CCl₃OONO₂ have been measured over the wavelength range 210–280 nm (Morel et al., 1980) and the cross sections for these ROONO₂ species are generally similar to those for HOONO₂ and CH₃OONO₂. Photolysis is expected to proceed by



with an overall quantum yield of unity. The individual quantum yields for these photolysis pathways are not known.

The tropospheric reactions of the haloalkyl peroxy radicals lead ultimately to the corresponding alkoxy radicals, RO.

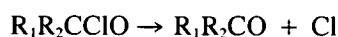
4.2.2.7 Reactions of the Haloalkoxy (RO) Radicals

Haloalkoxy radicals undergo three types of reactions under the conditions of the troposphere:

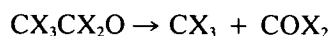
- (1) reaction with O₂ for those radicals containing an α-H atom



- (2) Cl atom elimination for those radicals containing an α-chlorine atom



- (3) C-C bond dissociation for $\geq C_2$ radicals,



where X is an H or halogen atom.

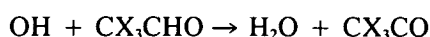
All of these RO radical reactions yield carbonyl compounds. Experimental studies of haloalkane oxidation mechanisms and thermochemical considerations allow the preferred reaction pathway(s) to be predicted with a reasonable degree of confidence for each particular RO radical. The tropospheric reactions of CF₃O are not well understood, since F atom elimination is too slow to be of any significance. However, it is assumed that CF₃O will form COF₂ under tropospheric conditions.

The principal carbonyl compounds expected to be formed during the tropospheric degradation reactions of the haloalkanes are HCOF, HCOCl, HCOBr, COF₂, COFCl, COCl₂, CF₃COF, CF₃COCl, and other CX₃COY compounds (X being H and/or halogen and Y a halogen atom). A complete list of the products expected from the degradation of the HCFCs and HFCs selected for the AFEAS assessment are summarized in Table 4.2-2.

4.2.2.8 Reactions of Carbonyl Halides, Acetyl Halides, and Halogen-Substituted Acetaldehyde

Reactions of the carbonyl halides COX₂ and acetyl halides CX₃C(O)Y (X = H and/or halogen; Y = halogen) with OH radicals and other reactive tropospheric species are expected to be too slow to be of any significance. Furthermore, photolysis is expected to be very slow for these species.

The halogen-substituted acetaldehydes, CX₃CHO (X = F, H, Cl), can, however, react with the OH radical

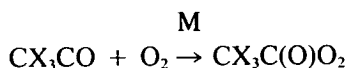


to form an acyl radical. As for the acetyl radical (IUPAC, 1989), these CX₃CO radicals will rapidly add O₂ (with a rate constant of $\sim 10^{-12}$ cm³ molecule⁻¹ s⁻¹ under tropospheric conditions)

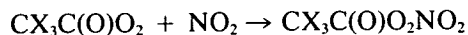
OZONE DEPLETION POTENTIALS

Table 4.2-2. Fluorine-containing products in the atmospheric degradation of selected fluorocarbons

Compound	Formula	Atom & Radical	Carbonyl	Acid	Hydroxide	Nitrate
HCFC-123	HCCl ₂ CF ₃	CF ₃ CCl ₂ OO	CF ₃ CClO		CF ₃ CCl ₂ OOH	CF ₃ CCl ₂ OONO ₂
		CF ₃ CCl ₂ O				
		CF ₃ OO			CF ₃ OOH	CF ₃ OONO ₂
		CF ₃ O			CF ₃ OH	CF ₃ ONO ₂
HCFC-141b	CCl ₂ FCH ₃	CCl ₂ FCH ₂ OO	CCl ₂ FCHO		CCl ₂ FCH ₂ OOH	CCl ₂ FCH ₂ OONO ₂
		CCl ₂ FCH ₂ O				
		CCl ₂ FOO			CCl ₂ FOOH	CCl ₂ FOONO ₂
		CCl ₂ FO	CClFO			
		CCl ₂ FC(O)OO	CCl ₂ FC(O)OOH		CCl ₂ FC(O)OONO ₂	
			CCl ₂ FC(O)OH			
HCFC-142b	CClF ₂ CH ₃	CClF ₂ CH ₂ OO	CClF ₂ CHO		CClF ₂ CH ₂ OOH	CClF ₂ CH ₂ OONO ₂
		CClF ₂ CH ₂ O				
		CClF ₂ OO	CF ₂ O		CClF ₂ OOH	CClF ₂ OONO ₂
		CClF ₂ O			CClF ₂ C(O)OOH	CClF ₂ C(O)OONO ₂
		CClF ₂ C(O)OO				
CClF ₂ C(O)OH						
HCFC-22	CHClF ₂	CClF ₂ OO	CF ₂ O		CClF ₂ OOH	CClF ₂ OONO ₂
		CClF ₂ O				
HCFC-124	CHCl- FCF ₃	CF ₃ CClFOO	CF ₃ CFO		CF ₃ CClFOOH	CF ₃ CClFOONO ₂
		CF ₃ CClFO				
		CF ₃ OO			CF ₃ OOH	CF ₃ OONO ₂
		CF ₃ O			CF ₃ OH	CF ₃ ONO ₂
HFC-134a	CH ₂ FCF ₃	CF ₃ CHFOO	CHFO CF ₃ CFO		CF ₃ CHFOOH	CF ₃ CHFOONO ₂
		CF ₃ CHFO				
		CF ₃ OO	CF ₂ O		CF ₃ OOH	CF ₃ OONO ₂
		CF ₃ O			CF ₃ OH	CF ₃ ONO ₂
		CFO			CF(O)OOH	CF(O)OONO ₂
HFC-152a	CHF ₂ CH ₃	CH ₃ CF ₂ OO	CF ₂ O		CH ₃ CF ₂ OOH	CH ₃ CF ₂ OONO ₂
		CH ₃ CF ₂ O				
		CHF ₂ CH ₂ OO	CHF ₂ CHO		CHF ₂ CH ₂ OOH	CHF ₂ CH ₂ OONO ₂
		CHF ₂ CH ₂ O				
		CHF ₂ OO			CHF ₂ OOH	CHF ₂ OONO ₂
		CHF ₂ O	CHFO			
		CHF ₂ C(O)OO	CHF ₂ C(O)OOH		CHF ₂ C(O)OONO ₂	
	CHF ₂ C(O)OH					
CFO	CF(O)OOH	CF(O)OONO ₂				
HFC-125	CHF ₂ CF ₃	CF ₃ CF ₂ OO	CF ₂ O CF ₃ CFO		CF ₃ CF ₂ OOH	CF ₃ CF ₂ OONO ₂
		CF ₃ CF ₂ O				
		CF ₃ OO	CF ₃ OOH		CF ₃ OONO ₂	
		CF ₃ O	CF ₃ OH		CF ₃ ONO ₂	



to form acyl peroxy radicals. These radicals are expected to degrade ultimately to the carbonyl halides and carbon dioxide. However, the $\text{CX}_3\text{C(O)O}_2$ radicals are expected to form peroxy nitrates by reaction with NO_2 :



The peroxy nitrate products are similar to the well-known peroxyacetyl nitrate (PAN) and are expected to be thermally stable in the troposphere. In addition, photolysis of these halogenated peroxy nitrates is expected to be very slow and their residence time due to gas phase degradation could be long.

4.2.2.9 Physical Loss Processes

The low gas phase reactivity of many of the halogenated carbonyl compounds produced in the degradation of HCFCs and HFCs leads to a potentially important role for physical loss process from the atmosphere, i.e., incorporation into rain or clouds, or sea water, with subsequent hydrolysis. Although handicapped by the total absence of Henry's law solubility data for any of the compounds of interest and the limited availability of relevant kinetic data, an assessment of the rates and mechanisms of aqueous phase removal of the gas phase degradation products has been carried out, as part of the AFEAS assessment.

The species X_2CO , HXCO , CH_3CXO , CF_3OH , CX_3OONO_2 , and ROOH ($\text{X} = \text{F}$ or Cl , $\text{R} =$ halo-substituted methyl or acetyl) are all expected to be removed from the atmosphere on time scales limited by transport to cloudy regions or the marine boundary layer (i.e., about 1 month). Some support for this comes from the recent measurements of COCl_2 by Wilson et al. (1988) in the troposphere and lower stratosphere, which are consistent with a tropospheric physical loss process. Aqueous phase reactions of these species result in the formation of chloride, fluoride, and carbon dioxide, as well as formic, acetic, and oxalic acids. The species CX_3CXO , $\text{CX}_3\text{CX}_2\text{OOH}$, $\text{CX}_3\text{CX}_2\text{OONO}_2$, $\text{CX}_3\text{C(O)OONO}_2$, and $\text{CX}_3\text{C(O)OOH}$ are also expected to be removed from the atmosphere rapidly, and their aqueous phase reactions result in the formation of halo-substituted acetates, $\text{CX}_3\text{C(O)O}$.

The species $\text{CX}_3\text{C(O)OH}$ are very acidic and, as a result, are highly soluble in cloud water. These acids are expected to be rapidly removed from the atmosphere by rainout. However, the aqueous phase species $\text{CX}_3\text{C(O)O}^-$ are expected to be resistant to chemical degradation. Trichloroacetate can thermally decompose on a time scale of 2–10 years to yield carbon dioxide and chloroform. In freshwater, the reaction of $\text{CCl}_3\text{C(O)O}^-$, $\text{CF}_2\text{ClC(O)O}^-$ may have very long aqueous phase lifetimes. The longest-lived species, $\text{CF}_3\text{C(O)O}^-$, could have a lifetime in natural waters as long as several hundred years. Processes which could possibly degrade $\text{CF}_n\text{Cl}_{3-n}\text{C(O)O}^-$ on shorter time scales than suggested above, but whose rates cannot be estimated with any degree of confidence at this time, include oxidation by photochemically generated valence band holes in semiconductor particles and hydrolysis catalyzed by enzymes in microorganisms and plants; further research aimed at characterizing these processes is needed.

One possible gas phase degradation product about which very little is known is CF_3ONO_2 . This compound has never been observed, and may be thermally unstable. If CF_3ONO_2 is thermally stable, then it may have a long lifetime toward aqueous phase removal. Henry's law solubility data and hydrolysis kinetics data for CF_3ONO_2 are needed before its aqueous phase removal rate can be assessed with any degree of confidence.

OZONE DEPLETION POTENTIALS

4.2.2.10 Summary of Halocarbon Oxidation Chemistry

The following main conclusions concerning possible CFC substitutes can be drawn from the discussion of halocarbon processes contained in this chapter and in the more detailed AFEAS assessment contained in the Appendix to this report.

Tropospheric reaction with the OH radical is the major and rate determining loss process for the HFCs and HCFCs in the atmosphere. The rate coefficients for the OH reactions are well defined at the temperatures appropriate for tropospheric reaction. There are virtually no experimental data available concerning the subsequent reactions occurring in the atmospheric degradation of these molecules. By consideration of data for degradation of alkanes and chloroalkanes, it is possible to postulate the reaction mechanism and products formed in the troposphere from HCFCs and HFCs. However, the results are subject to large qualitative and quantitative uncertainty, and may even be incorrect.

A large variety of chlorine- and fluorine-containing intermediate products such as hydroperoxides, peroxy nitrates, carbonyl halides, aldehydes, and acids can be expected from the degradation of the proposed CFC substitutes. Based on the available knowledge of gas phase chemistry, only four of these products appear to be potentially significant carriers of chlorine to the stratosphere. These are CClFO , CF_3CClO , $\text{CClF}_2\text{CO}_3\text{NO}_2$, and $\text{CCl}_2\text{FCO}_3\text{NO}_2$. However, physical removal processes may reduce this potential. In addition, the possibility of pathways and products not predicted by the arguments-by-analogy are a cause for concern.

A large part of the uncertainty of the mechanistic details of the HCFC oxidation arises from an insufficient knowledge of the thermal stability and reactivity of halogenated alkoxy radicals. In particular, the mechanism of oxidation of the CF_3O radical, which is assumed to produce CF_2O , is not known for atmospheric conditions and needs further study. Particular attention should also be paid to obtaining data on the photochemistry, gas phase reactivity, and solubility of the carbonyl, acetyl, and formyl halides in order to assess their removal rates and mechanisms.

Based on current knowledge, the products identified are unlikely to cause significant changes to the effective greenhouse warming potential of the proposed CFC substitutes. This conclusion would be modified if long-lived products such as CF_3H were formed by unidentified pathways.

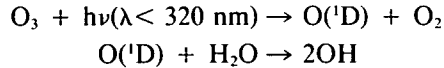
It would be prudent to carry out comprehensive laboratory tests and atmospheric measurements to ascertain the validity of the proposed degradation mechanisms for HCFCs and HFCs, before large amounts of these substances are released to the environment.

4.2.3 Hydroxyl Radical Chemistry in the Troposphere

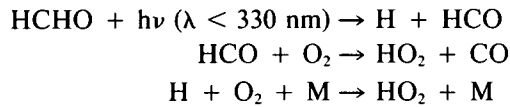
4.2.3.1 Processes Governing OH Concentration in the Troposphere

Following Weinstock's (1969) suggestion that reaction with OH radicals provides a major sink for atmospheric CO and CH_4 , Levy (1971) was the first to propose that relatively high steady-state concentrations of OH and other radicals might be present in the troposphere, as a result of photochemical reactions involving ozone and other trace gases. Since that time, a comprehensive and relatively consistent theory has been developed concerning the sources, chemical cycles, and sinks which control the OH concentration in the troposphere.

The essential chemistry in the theory of tropospheric OH is illustrated in Figure 4.2-1. The steady-state concentration of OH is determined by a balance between production and loss processes for free radicals, and the fast interconversion reactions coupling OH with the hydroperoxy radical (HO₂). The main production route results from the photolysis of ozone at λ < 320 nm to produce excited O(¹D) atoms. The O(¹D) atoms are mainly quenched to the ground state, but a significant fraction reacts with water vapor to produce OH:



It follows that the rate of OH production is proportional to the water vapor mixing ratio. In addition, the photolysis of H₂O₂ organic hydroperoxides provide minor secondary sources of OH in the troposphere. Because the hydroperoxyl radical, HO₂, is rapidly converted to OH by reacting with NO and O₃, photochemical reactions leading to formation of HO₂ provide a further, indirect source of OH. The most important contribution of this type comes from the UV photolysis of formaldehyde, HCHO, which is present in the troposphere as a result of the oxidation of CH₄ and other volatile organic compounds:



Because CH₄ oxidation is a chain reaction initiated by OH attack (see Figure 4.2-1), the organic oxidation chemistry provides an amplification of the primary OH production resulting from ozone photolysis, as emphasized by Warneck (1975).

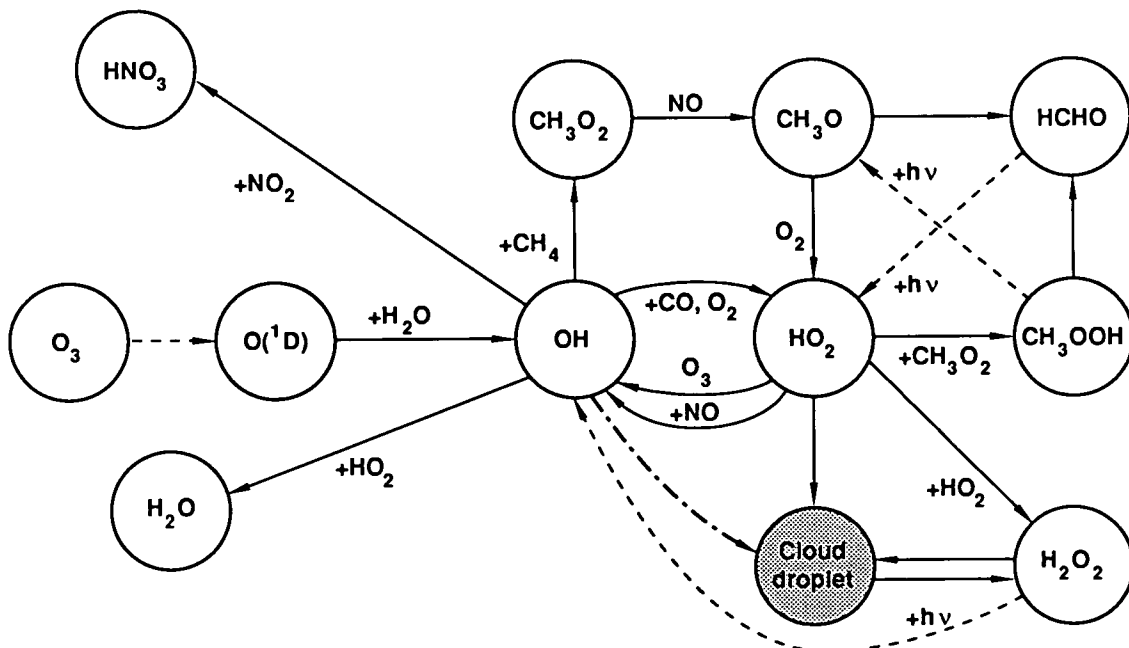


Figure 4.2-1. Reactions governing concentrations of OH and HO₂.

OZONE DEPLETION POTENTIALS

The loss processes involve combination reactions of the OH and HO₂ radicals with each other and also with NO₂ to form stable, non-radical products, e.g., H₂O, H₂O₂, HNO₃, and HO₂NO₂. The more rapid reactions of OH with CO and CH₄ do not lead to overall loss of radicals since HO₂ is formed, which is cycled back to OH. Nevertheless, the steady-state concentration of OH is influenced by the concentrations of reactive trace gases such as CH₄, CO, O₃, and NO since these determine, through the fast interconversion reactions, the partitioning of the total radical pool between OH and HO₂.

The possible influence of cloud droplets and aerosol particles in providing heterogeneous loss mechanisms for HO_x free radicals has been considered by Warneck (1974). Aerosol loadings in the clean troposphere are too low to provide significant sinks; but in the polluted boundary layer and in fogs and clouds, heterogeneous loss of HO₂, which has a longer chemical lifetime than OH, can be an important factor in reducing the radical concentration. These factors combined with the dependence of OH on local trace gas concentration lead to an expected large local variability in the concentrations of OH.

Since the dominant primary source of OH is the UV photolysis of ozone, a large seasonal, diurnal, and latitudinal variation in the production rate is implied. Moreover, water vapor mixing ratio and cloudiness will also influence OH production. These factors were discussed by Warneck (1975) and have subsequently been investigated in detail in photochemical models of the troposphere, used to calculate globally averaged tropospheric OH concentration (Crutzen and Fishman, 1977; Derwent and Curtis, 1977; Logan et al., 1981). The models predict highest OH concentrations in the lower tropical troposphere with very low values in polar regions.

At nighttime, there are no photochemical sources of OH. Nighttime free radical chemistry does occur, however, as a result of initiation by attack of nitrate radicals on organic molecules, but OH steady-state concentrations are much lower than in the sunlit atmosphere.

4.2.3.2 Validation of OH Photochemistry

In contrast to the well-developed theory of tropospheric OH, experimental measurements of OH concentrations and verification of the theory have provided a challenge which has not yet been satisfactorily overcome.

Three techniques for the time-resolved measurement of local OH concentrations have been developed over a number of years, these being the ¹⁴C-tracer method, laser-induced fluorescence (LIF), and long-path absorption spectroscopy (LPAS). Both the ¹⁴C-tracer method and the LIF technique are subject to a number of potentially severe interferences, and the results of even the most recent measurements using these techniques must be treated with caution. To date the UV LPAS technique appears to give the most reliable measurements. The most recently developed high resolution instrument (Dorn et al., 1988; Platt et al., 1988) overcomes interference problems by detecting a spectral range covering several OH absorption features. This method gives absolute OH concentrations and does not require calibration. The only information needed for data analysis is the oscillator strength for OH which is known to be better than 5%.

The daytime OH measurements published over the last four years using all three techniques vary between approximately 0.4 and 9×10^6 OH radicals per cm³, which is broadly consistent with current model predictions. Validation of a time-dependent model, however, requires not only the measurement of OH itself, but also the simultaneous determination of all input parameters that control the local OH chemistry. In the recent LPAS measurements, sufficient supporting data were obtained to allow full model

calculation of the expected local OH concentrations (Perner et al., 1987). Comparison of these recent experimental results with the model calculations leads to the following conclusions:

1. In the presence of high NO₂ concentrations (>2 ppbv), the steady-state OH concentration is controlled only by the primary source term (ozone photolysis and subsequent reaction of O(¹D) atoms with water vapor) and one main loss reaction (OH + NO₂ forming nitric acid). Thus the calculation of OH concentrations needs only measurements of O₃, J(O¹D), H₂O, and NO₂, with the most critical being the correct determination of J(O¹D). In this case the measurements agree with the calculated OH concentrations to within ~50%.
2. In relatively clean air (NO₂ < 1 ppbv), the OH concentration calculated using a detailed model with the supporting measurements as input parameters exceeded the measured concentrations by about a factor of two. This implies an inadequate description of the HO_x losses in the model.

Further development of techniques for OH measurements are clearly necessary and confidence in the measurements would be aided by a successful intercomparison of more than one system. Also, there is a need for measurements at different characteristic locations, in particular at high altitudes remote from local terrestrial sources of gases and particles.

4.2.3.3 Indirect Determination of Global Hydroxyl Radical

Indirect methods for determining the OH abundance from trace gas budget considerations have provided the best test for global models of OH distribution. In principle, any molecule can be used provided that the following conditions are satisfied.

- Its removal occurs by reaction with OH alone and the rate of this removal is accurately known both as a function of temperature and pressure.
- Its atmospheric abundance is accurately known.
- The source strength and distribution in time and space is accurately known.

While many chemicals (e.g., CO, non-methane hydrocarbons [NMHC]) are nearly exclusively removed by OH radicals, it has not been possible to use them because their sources are diverse and often unknown. However, in two cases the above conditions are met to varying degrees: man-made halocarbons and naturally occurring ¹⁴CO. In recent decades synthetic halogenated chemicals have been injected into the environment in such significant amounts that a measurable global background is present. Because of the exclusive man-made source of halocarbons, the major uncertainties associated with the source term can, in principle, be eliminated. A select group of these halocarbons are also removed from the atmosphere nearly exclusively by reaction with OH. Similarly, ¹⁴CO has a well-defined cosmic ray source and its atmospheric abundance can be related to OH. In the following paragraphs previous attempts to evaluate OH abundance in this way are summarized and a recent assessment of the global OH concentrations and resultant halocarbon lifetimes conducted within AFEAS is presented.

Methyl chloroform and the hydroxyl radical

A first demonstration of this technique was presented by Singh (1977a, b) and Lovelock (1977), who selected methyl chloroform (CH₃CCl₃) as the currently most suitable OH-tracer fulfilling the above criteria.

OZONE DEPLETION POTENTIALS

Analysis of CH_3CCl_3 data have been performed by numerous investigators during the last decade. In most cases, box models of various kinds have been used to estimate its lifetime. Table 4.2-3 summarizes the global average lifetime of CH_3CCl_3 derived in a variety of published studies. The first emission inventory reported by Neely and Plonka (1978) has been widely used. Subsequent emissions data have been estimated from production figures assuming that the production-to-emission ratio of Neely and Plonka (1978) has not changed significantly. Only 3 to 4% of the emissions are thought to occur in the Southern Hemisphere. Prinn et al. (1987) estimate that the CH_3CCl_3 global emission data are probably known to be $\sim 5\%$. A recent analysis of methyl chloroform emissions by Midgely (1989) confirms this.

A bulk of the uncertainty in CH_3CCl_3 lifetime reported in Table 4.2-3 comes from the determination of the atmospheric burden of CH_3CCl_3 . Over the years the estimates of the global average CH_3CCl_3 lifetime cover the range 6–12 years. The most recent ALE/GAGE data after correction (see Table 4.2-3) result in a mean CH_3CCl_3 lifetime of 6 to 7 years.

The CH_3CCl_3 mean lifetime estimate can be compared to that predicted by a global model with a well-defined OH field. It is convenient to define an equivalent average OH concentration that is consistent with the CH_3CCl_3 global lifetime. Such an estimate of OH must take into account the fact that $\text{OH} + \text{CH}_3\text{CCl}_3$ reaction rate is a function of temperature and also must assume that other removal processes are negligible. With these assumptions a mean OH concentration of $5\text{--}7 \times 10^5$ molecule cm^{-3} fits the data best. The hemispheric asymmetry in the CH_3CCl_3 lifetime (Table 4.2-3) also implies that the OH levels in the SH are somewhat higher than the NH values.

Table 4.2-3. Atmospheric lifetime of methyl chloroform and estimates of equivalent OH concentrations

Global average CH_3CCl_3 Lifetime (years)	Mean OH (10^5 molecule cm^{-3}) ^a	Comments	Reference
7 ± 1	3–6		Singh (1977a)
5–10	5–10		Lovelock (1977)
8–11	4	$\tau_{\text{NH}} \sim 1.5 \tau_{\text{SH}}$	Singh (1977b)
3	10	$\tau_{\text{NH}} \sim 3 \tau_{\text{SH}}$	Neely and Plonka (1978)
8	6		McConnell and Schiff (1978)
7 ± 1	—		Makide and Rowland (1981)
5 ± 2	7 ± 2		Derwent and Eggleton (1981)
9 ± 2	6 ± 1		Singh et al. (1983)
$10(+5/-3)^b$	5 ± 2		Prinn et al. (1983)
6 ± 1.5^c	8		Khalil and Rasmussen (1984)
6 ± 1^c	7 ± 2		Fraser et al. (1986)
12^b	—		Golombek and Prinn (1986)
6 ± 1^c	8 ± 1	$\tau_{\text{NH}} \sim 1.15 \tau_{\text{SH}}$	Prinn et al. (1987)
6.5 ± 1	—	$\tau_{\text{NH}} \sim 1.2 \tau_{\text{SH}}$	Blake and Rowland (1988)

^aUsing model results it is reasonable to assume that the OH abundance between 0–30° latitude is nearly twice as large as between 30–90° latitude. Thus, a global OH average (molecule cm^{-3}) of 7.5×10^5 would correspond to OH values of 10×10^5 and 5×10^5 at 0–30° and 30–90° latitudes, respectively.

^bUncorrected ALE/GAGE CH_3CCl_3 data.

^cCorrected ALE/GAGE CH_3CCl_3 data. All atmospheric measurements multiplied by 0.8. The actual derived lifetime is 6.3 years.

Other halocarbons have been used in a similar manner to estimate OH, for example, dichloromethane, 1,2 dichloroethane and tetrachloroethene (Singh et al., 1983). A two-box model shows that removal rates of these molecules are consistent with average OH concentrations of 4 to 5×10^5 molecules cm^{-3} . Because of their relatively short lifetimes (several months) compared to CH_3CCl_3 , these chemicals could potentially reveal OH latitudinal and seasonal gradients with greater sensitivity. However, their source strengths are not as well defined as that of CH_3CCl_3 . In addition, these analyses are sensitive to the seasonal variations in emissions which are poorly known.

^{14}CO and the hydroxyl radical

The first attempts to calculate the global mean tropospheric hydroxyl concentration from isotopic distribution in atmospheric carbon monoxide were made by Weinstock (1969) and by Weinstock and Niki (1972). They used the three available ^{14}CO measurements by McKay et al. (1963), an estimate of the global source strength for ^{14}CO from the well-known cosmic ray bombardment of atmospheric nitrogen molecules, and the $\text{OH} + \text{CO}$ rate coefficient to derive an estimate for the atmospheric turnover time for ^{12}CO of the order of 1 month. Furthermore, they suggested that OH radicals were responsible for the CO removal and obtained an estimate of the global mean OH abundance.

The ^{14}CO concentrations in the troposphere are extremely small with a winter maximum of 20 molecule cm^{-3} and a summer minimum of about 10 molecule cm^{-3} . Volz et al. (1981) improved the methodology based on four refinements, viz:

- additional measurements of ^{14}CO in the lower troposphere,
- evaluated chemical kinetic data for the $\text{OH} + \text{CO}$ reaction, and
- a global two-dimensional time-dependent model to investigate the coupled $\text{CH}_4\text{-H}_2\text{-CO-NO}_x\text{-O}_3$ life cycles, replacing the box model approach.

These analyses led Volz et al. (1981) to obtain a mean tropospheric OH concentration of $6.5^{+3}_{-2} \times 10^5$ molecule cm^{-3} . No additional data on ^{14}CO have been collected in the intervening years and no Southern Hemispheric data are available. Derwent and Volz-Thomas (1989) in a re-evaluation of this technique conclude that the average OH derived by this method remains unchanged.

4.2.3.4 Recent Assessment of Tropospheric OH Abundance and Halocarbon Lifetimes

The above summary shows that an overall volume-averaged OH concentration of $6 (\pm 2) \times 10^5$ molecule cm^{-3} best represents all of the available information on the CH_3CCl_3 and ^{14}CO budgets. However, the usefulness of a global mean OH concentration for determination of overall reaction rates and lifetimes of HCFCs derived in this fashion is questionable. This arises because of the non-uniformity of the OH abundance and of the distribution of the molecules with which it reacts, and also because of the different temperature dependencies of the reaction rates in the troposphere. In the recent AFEAS assessment these factors were considered at some depth. Prather (1989) used 3-dimensional tropospheric OH fields that were calculated from a climatology of sunlight, temperature, and trace gas mixing ratios. These OH fields were then used to study the methyl chloroform budget by calculating the integrated loss of this molecule in a 3-D chemical transport model of the troposphere and to test the accuracy of scaling the HCFC lifetimes to an assumed methyl chloroform lifetime.

OZONE DEPLETION POTENTIALS

In the AFEAS assessment, the lifetimes of HCFCs and HFCs were determined by three separate approaches:

1. 2-D chemical transport model with semi-empirical fit to ^{14}CO ;
2. Photochemical calculation of 3-D OH fields and integrated loss;
3. Scaling of the inferred CH_3CCl_3 lifetime by rate coefficients.

Resulting lifetimes from all three independent approaches generally agree within 15%, as shown in Table 4.2-4. The integrated losses calculated from the global OH fields in the models (1 and 2) are constrained by modeling of the observations and budgets for ^{14}CO and CH_3CCl_3 , respectively. Method (3) may be expressed simply as

$$\text{lifetime}(\text{HCFC}) = 6.3 \text{ yr} \times k(\text{CH}_3\text{CCl}_3 \text{ at } T = 277 \text{ K}) / k(\text{HCFC at } T = 277 \text{ K}),$$

where the current estimate of the lifetime for methyl chloroform (6.3 yr) is based on the ALE/GAGE analysis (Prinn et al., 1987). Some of the errors associated with this scaling and the choice of the temperature of 277 K for scaling the reaction rates have been tested with the 3-D OH fields from method (2). Based on the sensitivity studies from methods (1) and (2), method (3) should be reliable for calculating HCFC lifetimes in the range 1 to 30 years. Method (2) shows that the middle tropical troposphere (2–6 km) dominates the atmospheric loss and would be an important region in which to make observations of OH.

Table 4.2-4. Atmospheric lifetimes for HCFCs and HFCs, based on Derwent and Volz-Thomas (1989) and Prather (1989)

HCFC	$k(\text{cm}^3 \text{ molec}^{-1} \text{ s}^{-1})$	Lifetime (yr) for method ^a		
		(1)	(2)	(3)
CH_3CCl_3 (range)	$5.0 \times 10^{-12} \exp(-1800/T)$	5.0 (3–7)	5.4 (4–7)	6.3 (5.4–7.5)
CH_3F	$5.4 \times 10^{-12} \exp(-1700/T)$	3.3	3.8	4.1
CH_2F_2	$2.5 \times 10^{-12} \exp(-1650/T)$	6.0	6.8	7.3
CHF_3	$7.4 \times 10^{-13} \exp(-2530/T)$	635.0	289.0	310.0
CH_2FCl	$3.0 \times 10^{-12} \exp(-1250/T)$	1.26	1.33	1.44
CHFCl_2	$1.2 \times 10^{-12} \exp(-1100/T)$	1.80	1.89	2.10
CHF_2C (22)	$1.2 \times 10^{-12} \exp(-1650/T)$	13.0	14.2	15.3
$\text{CH}_3\text{CH}_2\text{F}$	$1.3 \times 10^{-11} \exp(-1200/T)$	0.31	0.25	0.28
$\text{CH}_2\text{FCH}_2\text{F}$	$1.7 \times 10^{-11} \exp(-1500/T)$	0.60	0.58	0.63
CH_3CHF_2 (152a)	$1.5 \times 10^{-12} \exp(-1100/T)$	1.46	1.53	1.68
CH_2FCHF_2	$2.8 \times 10^{-12} \exp(-1500/T)$	3.2	3.5	3.8
CH_3CF_3	$2.6 \times 10^{-13} \exp(-1500/T)$	40.0	38.0	41.0
CHF_2CHF_2	$8.7 \times 10^{-13} \exp(-1500/T)$	10.4	11.4	12.3
CH_2FCF_3 (134a)	$1.7 \times 10^{-12} \exp(-1750/T)$	13.1	14.4	15.5
CHF_2CF_3 (125)	$3.8 \times 10^{-13} \exp(-1500/T)$	25.9	26.1	28.1
CH_3CFCl_2 (141b)	$2.7 \times 10^{-13} \exp(-1050/T)$	6.7	6.7	7.8
$\text{CH}_3\text{CF}_2\text{Cl}$ (142b)	$9.6 \times 10^{-13} \exp(-1650/T)$	16.6	17.8	19.1
$\text{CH}_2\text{ClCF}_2\text{Cl}$	$3.6 \times 10^{-12} \exp(-1600/T)$	3.5	4.0	4.2
CH_2ClCF_3	$5.2 \times 10^{-13} \exp(-1100/T)$	4.1	4.4	4.8
CHCl_2CF_3 (123)	$6.4 \times 10^{-13} \exp(-850/T)$	1.40	1.42	1.59
CHFClCF_3 (124)	$6.6 \times 10^{-13} \exp(-1250/T)$	5.5	6.0	6.6

^aLifetimes from Method (1) do not include stratospheric loss; those from Method (2) include small additional stratospheric loss. Method (3) is based on scaling the methyl chloroform lifetime of 6.3 yr (Prinn et al. 1987) by the ratio of the rate coefficients at 277 K.

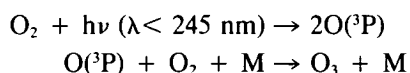
Estimated uncertainties in the HCFC and HFC lifetimes between 1 and 30 years are $\pm 50\%$ for (1) and $\pm 40\%$ for (3) and (2). These ranges include the uncertainty in the rate constants for the OH reactions. Global OH values that give lifetimes outside of these ranges of uncertainty are inconsistent with detailed analyses of the observed distributions for ^{14}CO and CH_3CCl_3 . The expected spatial and seasonal variations in the global distribution of HCFCs with lifetimes of 1 to 30 years have been examined with methods (1) and (2) and found to have insignificant effect on the calculated lifetimes. Larger uncertainties apply to gases with lifetimes shorter than one year; however, for these species our concern is for destruction on a regional scale rather than global accumulation.

Clearly any changes in the concentrations of ozone and other trace gases in the troposphere, which affect OH abundance, will have an impact on HCFC lifetimes and in the following section we review the relevant tropospheric chemistry and current perception of future atmospheric behavior in this context.

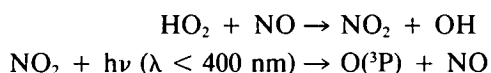
4.2.4 Tropospheric Chemistry Influencing OH and Ozone

4.2.4.1 Processes Controlling Tropospheric Ozone

Tropospheric ozone may be produced by *in situ* chemistry (Crutzen, 1973; Chameides and Walker, 1973; Fishman and Crutzen, 1978) or by transfer from the stratosphere, where O_3 is generated by the photodissociation of molecular oxygen at altitudes above 25 km, followed by combination of the ground state oxygen atoms with O_2 :



The *in situ* source of tropospheric ozone is the reaction of HO_2 or organic peroxy radicals with NO followed by the photodissociation of the nitrogen dioxide produced and the $\text{O}({}^3\text{P}) + \text{O}_2$ reaction.

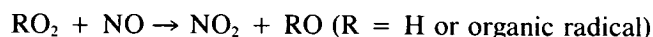


Although NO and NO_2 concentrations are very low throughout most of the troposphere, the effect of this reaction sequence can provide a significant O_3 source.

Ozone is also consumed in the troposphere as a result of photodissociation in the ultraviolet region. Most of the excited $\text{O}({}^1\text{D})$ atoms are quenched by N_2 and O_2 to the ground state, $\text{O}({}^3\text{P})$, which reform ozone, but that fraction which reacts with other trace molecules (e.g., with water to produce OH), represents a net loss of ozone. Photolysis of ozone in the near UV (Huggins bands) and visible (Chappuis bands) does not lead to net ozone loss. There is also an *in situ* loss of ozone through reaction with NO_2 (to give NO_3), HO_2 and unsaturated hydrocarbons. Model calculations (e.g., Levy et al., 1985) point to an approximate balance between *in situ* sources and sinks for tropospheric ozone, averaged over the globe. This is consistent with estimates of the magnitude of the surface sink for ozone, which averaged over the globe, is approximately equal to the stratospheric injection. However, analysis of observations and regional budgets (Logan, 1985; Bojkov, 1986; Penkett, 1988) show a clear indication that Northern Hemisphere tropospheric ozone is increasing. Changes in the seasonal modulation of ozone concentration, and in the man-made emissions and concentration of trace gases which affect ozone, suggest that the increase is due to a shift in the balance between *in situ* production and loss (Penkett, 1988). This balance essentially depends on the amount of

OZONE DEPLETION POTENTIALS

NO_x present in the background atmosphere together with the concentration of peroxy radicals derived from oxidation of CO, CH₄ and non-methane hydrocarbons, which controls the flux through the reactions in which NO is oxidized to NO₂.



The amount of tropospheric ozone is clearly central to the problem of the oxidizing efficiency of the troposphere, since O₃ photolysis is the primary source of OH radicals as well as being an oxidizing species itself. It follows that the future trends of oxidizing capacity will be tied to the future tropospheric burden of CO, CH₄, non-methane hydrocarbons and other organics, as well as nitrogen oxides. We now summarize the current picture of the distribution of ozone precursors in the troposphere. The distribution of ozone itself in the troposphere is covered in the assessment of global ozone concentrations in Chapter 2.

4.2.4.2 Tropospheric Distribution of Reactive Nitrogen Species

The tropospheric lifetime of NO_x (NO + NO₂) is rather short and consequently it is not possible to define an average, representative NO_x mixing ratio on a hemispheric or global scale.

The NO_x levels in urban and industrial areas are determined largely by anthropogenic sources. This leads to near surface NO_x mixing ratios in rural areas of the eastern United States and Western Europe typically in the range between 1 ppbv and 10 ppbv. In less populated and coastal regions, the NO_x levels depend on the prevailing meteorology and the proximity and distribution of urban sources. In these locations the NO_x mixing ratios typically range between 0.1 and 1 ppbv.

Surface measurements at remote locations reflect the influence of natural sources, such as soil emissions and lightning, which are principally terrestrial sources that are seasonal. These sources may provide surface concentrations of NO_x that typically range between 0.02 ppbv and 0.1 ppbv (Fehsenfeld et al., 1988). It should be noted that at most locations on land, particularly in the mid-latitudes, the NO_x levels in ambient air are influenced by anthropogenic activities. In remote maritime air and in the polar regions that are not influenced by anthropogenic activities, the NO_x concentrations are exceedingly small, typically 0.001 ppbv to 0.01 ppbv, and are associated with the downward mixing of NO_x from NO_x reservoirs in the upper troposphere.

The free tropospheric burden of NO_x is also strongly influenced by anthropogenic NO_x, particularly from combustion sources in the Northern Hemisphere. Variability in the atmospheric transport and photochemical lifetimes, together with the contribution of aircraft emissions of NO_x and natural sources such as lightning and stratospheric subsidence, increases the variability of NO_x concentration in the free troposphere. Here the NO_x mixing ratios may vary from 0.02 ppbv in remote regions to 5 ppbv over populated areas. In general, throughout the free troposphere the NO_x mixing ratio increases with height, as illustrated by the NO distribution shown in Figure 4.2-2.

The distribution of NO_y (NO_y: sum of all oxidized nitrogen species except N₂O = NO + NO₂ + NO₃ + 2 × N₂O₅ + HNO₃ + PAN + HO₂NO₂ + organic nitrates) is very similar to that of the source compound NO_x. Near the sources the majority of NO_y is in the form of NO_x. However, the NO_x will be rapidly converted to PAN, HNO₃, or other NO_y compounds. For example, during periods of maximum insolation the photochemical lifetime of NO_x is less than one day. Thus, in the remote free troposphere NO_x accounts for only a small fraction (approximately 10%) of the NO_y. For this reason, NO_y is a more

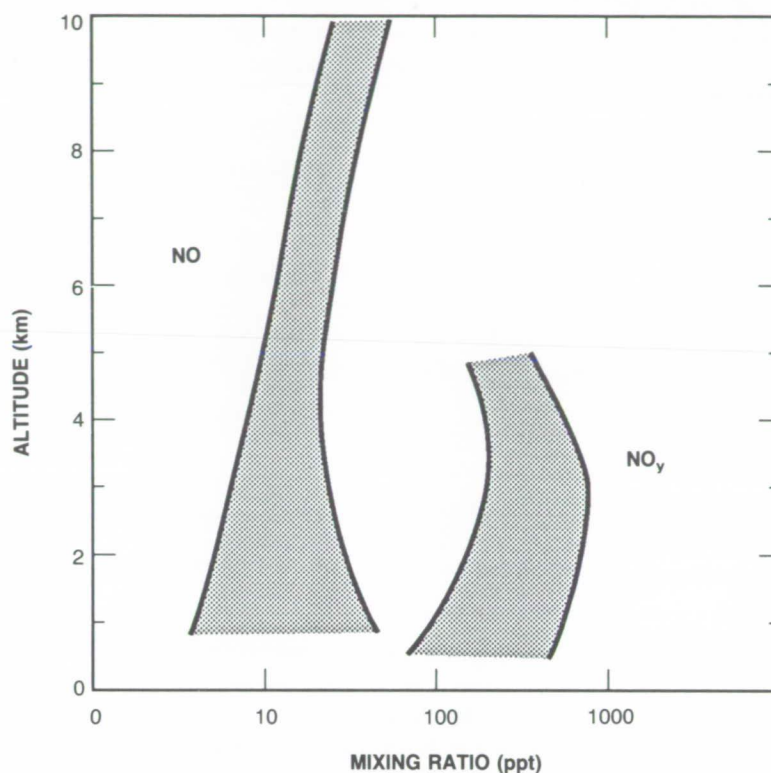


Figure 4.2-2. Schematic presentation of the measured vertical distribution of NO and NO_y over midlatitude oceanic and coastal regions.

conserved compound and the variation in the concentration of NO_y will be less than that of its short-lived precursor, NO_x.

In the remote troposphere the main fraction of the total NO_y often consists of HNO₃ and PAN (Fahey et al., 1986). HNO₃ can be quite effectively removed from the atmosphere by wet and dry deposition, whereas PAN is reasonably quickly thermally decomposed back into peroxyacetyl radicals and NO₂ at temperatures representative of the atmospheric boundary layer at low latitudes and at mid-latitudes in summer. Due to its stability at lower temperature, sometimes PAN levels of several hundred pptv can be observed in the free troposphere at mid- and high northern latitudes (Singh et al., 1986). Thus PAN and possibly other organic nitrates can serve as a potential reservoir and transport medium for the rather short-lived NO_x. However, up to now no quantitative estimate of the possible magnitude of such an effect has been made.

There is evidence from analysis of ice cores from Greenland and the Alps of a substantial increase in the concentration of nitrate ions, formed from NO₂ oxidation, over a similar period (1895–1978) (Neftel et al., 1985). This points to an increasing concentration of NO_x in parts of the Northern Hemisphere troposphere. Because of their short lifetimes, any increases in nitrogen oxides are expected to be confined to the continental source areas and nearby regions. The influence of nitrogen oxides may be spreading, however, due to a widening of source areas associated with increasing economic activity in the developing

OZONE DEPLETION POTENTIALS

world and due to reservoir species such as peroxyacetyl nitrate (PAN), which are formed in NMHC-NO_x interactions and which have relatively long atmospheric lifetimes and can dissociate to produce NO₂ far from source regions.

4.2.4.3 Tropospheric Distribution of Hydrocarbons and CO

The most important and abundant atmospheric hydrocarbon is methane. Its global distribution is well established and it exhibits only a relatively small variability in the background troposphere. The Northern Hemispheric CH₄ mixing ratios are about 1.7 ppm, the Southern Hemispheric levels are slightly lower, about 1.6 ppm.

CO has a considerably lower tropospheric abundance, but due to its higher reactivity towards OH radicals it is very important for the oxidizing efficiency of the atmosphere. The tropospheric distribution of CO is reasonably well known and there is a significant interhemispheric gradient. CO mixing ratios in the Southern Hemisphere are around 50–70 ppbv, and roughly a factor 2–3 higher in the Northern Hemisphere. A distinct seasonal variation in CO levels in both hemispheres has been identified. However, global coverage of CO distribution is still inadequate.

The current picture of the distribution of non-methane hydrocarbons (NMHC) in the troposphere is still far from complete due in part to the limited number of investigations, and there is large variability in the background concentrations. This variability results from the relatively short average atmospheric residence times, which range from a few hours to a few months. Also, the different NMHCs have various sources with different geographical distributions. The most important sources are listed in Table 4.2-5.

Large-scale distributions of NMHC in the remote troposphere have been published by several investigators (Singh and Kasting, 1988; Rudolph, 1988). Most of these studies focused on the latitudinal variability of NMHC, but there are also a few studies which present data on the vertical distribution of NMHC.

Table 4.2-5. Estimates of global hydrocarbon emissions into the atmosphere^a

Source	C ₂ H ₆	C ₃ H ₈	C ₄ H ₁₀	C ₂ H ₂	C ₆ H ₆	C ₂ H ₄	C ₃ H ₆	C ₅ H ₁₂	C ₇ H ₈	C ₈ H ₁₀	C ₅ H ₈	C ₁₀ H ₁₆
Engine exhaust	+	+	+	++	++	++	+	+	++	++		
Evaporation losses			++		+			++	+	+		
Natural gas leakage	++	++	++									
Oil + coal burning												
Chemical industry	+					+			+			
Solvent use									++	+		
Biomass burning	++	++		+	+	++	++		+	+	+++	+++
Foliage emissions	+					+					+++	+++
Microbial production	+					++	+					
Ocean emissions	++	++	++			+++	+++	++				

^aData from Ehhalt and Rudolph, 1984.

Note: + = Moderate source

++ = Strong source

+++ = Very strong source

The distribution of the longer-lived NMHC ($\tau > 1$ week) show some systematic features which can be ascribed to a representative latitudinal profile. On the average the highest mixing ratios are observed at mid- to high northern latitudes, roughly 1–3 ppbv of ethane, 0.2–0.6 ppbv of propane and n-butane, 0.1–0.5 ppbv of acetylene, 0.05–0.25 ppbv of benzene, and 0.02–0.1 ppbv of i-butane. In general, all these species show a considerable decrease towards lower latitudes and this gradient is more pronounced for the shorter-lived of these NMHC. This reflects both the source distribution with high emissions in the industrialized zone of the Northern Hemisphere and the faster removal at low latitudes due to the higher OH radical concentrations at tropical latitudes. Average Southern Hemisphere mixing ratios are roughly 0.15–0.4 ppbv ethane, 0.03–0.1 ppbv propane, 0.01–0.05 ppbv n-butane, 0.01–0.05 ppbv acetylene, 0.01–0.03 ppbv benzene, and 0.005–0.03 ppbv i-butane. There is a clear seasonal cycle in the troposphere mixing ratios of the light aliphatic hydrocarbons, with substantially higher values in the winter months. The cycle is consistent with predominant removal of these hydrocarbons by reaction with OH.

There seems to be a slight but systematic decrease from low southern latitudes towards mid southern latitudes. For ethane and probably the other hydrocarbons, there seems to be a significant and systematic seasonal cycle. In both hemispheres the minima are in the respective late summer, maxima in late winter.

For more reactive NMHC with average atmospheric residence times of less than one week, it is no longer justified to consider their distributions as being systematic with latitude. These atmospheric concentrations are determined by emissions, removal reactions, and transport on a local or regional scale (up to several hundred km). The most important NMHC in this category ($1 \text{ week} > \tau > 0.5 \text{ days}$) are C_2 – C_5 alkenes and, to a lesser extent, $< C_5$ alkanes and alkylbenzenes. Since the sources of C_2 – C_5 alkenes include biomass burning, emissions from vegetation, and emissions from oceans, substantial concentrations in the range from 0.1 to a few ppbv of ethene and propane have been observed over nonindustrialized continental regions and the oceans.

The extremely reactive terpenes and isoprene in general show a very strong decrease with increasing altitude and can generally only be observed near their sources within the atmospheric boundary layer. Over areas with dense vegetation, isoprene mixing ratios around 0.5–2 ppbv and monoterpene mixing ratios approaching 1 ppbv are frequently observed (Rasmussen and Khalil, 1988; Zimmerman et al., 1988). The emissions of many biogenic NMHC strongly depend on temperature, relative humidity, and light intensity. The types of emitted compounds also depend on the type of vegetation, e.g., isoprene is primarily emitted from deciduous plants whereas coniferous trees mainly act as terpene sources. The estimated global emission rate of isoprene is about $480 \times 10^{12} \text{ g yr}^{-1}$ (Rasmussen and Khalil, 1988). Comparable emission rates have been estimated for the other terpenoid compounds.

The global source strength of all NMHCs, but not including isoprene and the terpenes, is estimated to be about 100 – $130 \times 10^{12} \text{ g yr}^{-1}$. Since these NMHC emission estimates are highly uncertain and probably underestimated, we cannot yet make any quantitative estimates on the contribution of NMHC to the tropospheric O_3 and OH concentrations. Also, the atmospheric oxidation of NMHC leads to the *in situ* production of CO, which has a longer residence time than the NMHC and could extend their influence over a wider spatial regime. A comparison with the global CH_4 emission rate of about $400 \times 10^{12} \text{ g yr}^{-1}$ shows that the possible contribution of NMHC (not including isoprene and terpenes) can be quite substantial. The influence of isoprene and the terpenes on O_3 and OH may also be very substantial but, as yet, this effect has not been quantified.

The available measurements of non-methane hydrocarbons in the troposphere do not allow a systematic long-term trend to be recognized. Moreover, the observed variability of NMHC will prevent easy

OZONE DEPLETION POTENTIALS

recognition of any global trend in the near future. It appears more promising to estimate future (and past) changes of atmospheric NMHC concentrations from possible changes in their main sources. The fossil fuel activities have led to large increases in the emissions of non-methane hydrocarbons (NMHCs), but as yet these are on a smaller scale than methane itself and again the magnitude of the sources is in dispute. The question of the influence of the breakdown of halogenated organic molecules such as the HCFCs and HFCs on tropospheric ozone production has been reviewed in the AFEAS assessment (Niki, 1989). It is concluded that these molecules are such a small fraction of the total budget of organic compounds oxidized that their effect will be trivial.

4.2.5 Model Evaluation of Trends in Tropospheric Ozone and OH

As shown in Chapter 2, there is now observational evidence that changes are taking place in the concentration of tropospheric ozone and its precursor gases such as CH₄, CO, and possibly NO_x. The hydroxyl radical concentration is controlled by fast gas phase reactions. Simple model analysis of the photochemistry (Cox and Derwent, 1981; Liu, 1988) shows that increases in CH₄ and CO tend to decrease OH concentration whereas increases in NO_x and O₃ tend to increase OH. Changes in the solar UV due to depletion of stratospheric ozone could potentially lead to an increase in the oxidizing efficiency through direct effects on the ozone and OH photochemistry. Increases in water vapor concentration due to global warming will also lead to an increase in OH production. Observational data are totally inadequate for establishment of any changes in OH concentration and assessment of such changes must rely on model calculations.

There have been a number of model evaluations of the impact of man's activities on tropospheric ozone and OH concentrations through increased emissions of methane, CO, NO_x, and non-methane hydrocarbons. Initially, models with limited spatial resolution were employed, but increasingly one-, two-, and three-dimensional models have been developed to study both the chemical and dynamical aspects of tropospheric ozone (Crutzen, 1974; Fishman and Crutzen, 1978; Derwent and Curtis, 1977; Isaksen, 1981; Levy, Mahlman and Moxim, 1980; Logan et al., 1981; Crutzen and Bruhl, 1989). Attention given to tropospheric modeling in previous ozone layer depletion evaluations has not been as detailed as that given to stratospheric modeling. Nevertheless, considerable progress has been made in theoretical studies towards resolving many of the issues relevant to an understanding of tropospheric sinks for alternative halocarbons and increased tropospheric ozone concentrations.

The major conclusions of these studies can be summarized as follows:

- The increased availability of NO_x due to man's activities can change the Northern Hemisphere photochemistry from a net sink for ozone into a net source.
- The Northern Hemisphere ozone budget is now dominated by man-made sources, particularly in the lower troposphere.
- There may well have been a small decrease in the mean tropospheric OH concentration in the Southern Hemisphere since the pre-industrial era. The magnitude and direction of any change in the Northern Hemisphere is not clear.

The accuracy with which any of these statements based on tropospheric modeling reflect what has actually happened in the real world depends on the adequacy and completeness of the model formulations together with their input assumptions. Significant progress in basic understanding has been achieved

towards the goal of predicting the extent and direction of man's influence on the oxidizing capacity of the troposphere.

However, significant problems still remain. Potential sources of error or uncertainty in current one- and two-dimensional models arise principally through the following inadequacies of formulation:

- the non-linear relationship between ozone production and precursor molecule concentrations, which creates difficulties in spatial averaging;
- the short lifetime of NO_x and its close coupling to a surface wet and dry deposition sink, which creates difficulties with large-scale transport modeling;
- uncertainties in the latitudinal and seasonal distributions of the source strengths of methane, CO, NO_x , and non-methane hydrocarbons;
- uncertainties in the representation of tropospheric chemistry, including the representation of peroxy radical reactions, photodissociation processes (including the representation of clouds and aerosol scattering), nighttime chemistry and heterogeneous chemistry (including the removal of peroxy radicals on clouds, droplets and aerosols); and
- inadequate observational data to test the models.

In particular, the consideration of the first two areas listed above suggests that current models may overestimate tropospheric ozone production from man-made sources. On the other hand, some modeling studies have demonstrated an important role for convective lifting of NO_x from the boundary layer to the free troposphere with increased O_3 production. Despite these considerable uncertainties, current models are able to account for the observed trends in tropospheric ozone concentrations in the Northern Hemisphere from pre-industrial times through to the present day. This requires a simultaneous and consistent treatment of man's influence on the life cycles of methane, CO, NO_x , and the non-methane hydrocarbons. Many of the relevant factors are poorly understood. However, there is no reason to anticipate that man's influence on these trace gas life cycles will diminish over the next decade or so. It is pertinent to extrapolate current trends of these trace gas concentrations into the near future and to explore with the current models the influence of the changes on the oxidizing capacity of the troposphere in terms of OH and ozone.

As worldwide industrial development continues in mid-latitudes and spreads to lower latitudes of the Northern Hemisphere, ozone concentrations are anticipated to grow throughout the Northern Hemisphere as a result of increased emissions of the precursors (Crutzen, 1988). The magnitude of any change in OH or ozone will be strongly scenario dependent and will be related directly to the pattern of change in the methane, CO, NO_x , and non-methane hydrocarbon source terms (Isaksen and Hov, 1987; Thompson et al., 1989). Based on current perceptions of trends in trace gas concentrations, tropospheric ozone could increase by as much as 50% and the tropospheric mean OH concentration could decrease by as much as 25% by the middle of the next century.

The evaluation of future changes in tropospheric ozone and OH with current one- and two-dimensional models are subject to similar errors and uncertainties as those described above in the context of changes from the pre-industrial to the present-day atmosphere. Again, the non-linearities involved in relating OH and ozone to NO_x concentrations give rise to concern. Models incorporating a more realistic description of the transport processes may indicate less sensitivity of tropospheric ozone and OH to changes in trace gas concentrations.

OZONE DEPLETION POTENTIALS

So far attention has been given to the direct influences on the oxidizing capacity of the troposphere and they can only be crudely represented in current one- and two-dimensional models. Several potentially important indirect influences have been proposed. These include:

- increased UV-B penetration due to ozone depletion will increase tropospheric ozone photolysis rates, and consequently increase the mean OH source term (Liu and Trainer, 1987);
- increased tropospheric temperatures may decompose methane clathrates and stimulate tundra methane emissions and biogenic hydrocarbon emissions (Ehhalt, 1988); and
- increased water vapor mixing ratios may increase tropospheric OH concentrations.

Understanding is growing steadily such that it should be possible in the near future to generate some consistent trace gas scenarios to aid in evaluating the influence of mankind on future tropospheric ozone and OH concentrations.

4.3 OZONE DEPLETION POTENTIALS

4.3.1 Background

Recent consideration of international regulatory actions on the production of chlorofluorocarbons (CFCs) and other halogenated species has prompted significant interest in determination of the relative potential from such industrially produced compounds to affect stratospheric ozone and, more recently, global climate. The concept of relative Ozone Depletion Potentials (ODPs), introduced by Wuebbles (1981), has been adopted as a guideline or quick reference for estimating the relative potential for CFCs and other halocarbons to destroy stratospheric ozone. Several past papers have determined ODPs for selected chlorinated constituents (Wuebbles, 1983; Hammitt et al., 1987; Rognerud et al., 1989). This concept plays an important role in the implementation of the regulatory policies for fully halogenated CFCs adopted in the Montreal Protocol (UNEP, 1987).

Several atmospheric modeling groups have recently reevaluated the ODPs for the relevant CFCs, the potential replacements (particularly several HCFCs and HFCs), and other industrially produced chlorinated and brominated compounds of interest being considered. The 1-D and 2-D global atmospheric models used in these evaluations incorporate the most recently available laboratory data on the chemical kinetics and radiative parameters of the species being examined. The discussion that follows primarily focuses on the recent studies by Fisher et al. (1989a, b), Connell and Wuebbles (1989), and Gillotay et al. (1989). Most of the calculations presented here are also contained, generally in greater detail, in the Fisher et al. (1989b) paper published in the AFEAS Report (Vol. II Appendix to this report). The Fisher et al. (1989a, b) papers are the result of a cooperative study among four modeling groups: Atmospheric and Environmental Research, Inc. (AER); E.I. du Pont de Nemours and Company (DuPont); Lawrence Livermore National Laboratory (LLNL); and the University of Oslo. The Belgian Institute for Space Aeronomy (BISA) also contributed some 1-D model results to this report; these results were done separately and have not been as carefully compared as were the results of the other four groups.

4.3.2 Definition of ODP

Ozone Depletion Potential (ODP) has traditionally been defined as the steady-state ozone reduction calculated for each unit mass of a gas emitted per year (as a continuous release) into the atmosphere relative

to that for a unit mass emission of CFC-11. This definition provides a single-valued relative measure of the maximum calculated effect on ozone of a given compound compared to the effect calculated for CFC-11.

Figure 4.3-1, taken from Fisher et al. (1989a), shows the resulting reduction in total ozone from the DuPont 1-D model for 5×10^9 kg of halocarbon emitted into the atmosphere during the first year, with no emission in subsequent years. As seen from the table insert in Figure 4.3-1, the time-integrated effects of the initial 5×10^9 kg emissions agree closely to the normal steady-state determined ODPs. This confirms that ODP is a valid measure of the relative, cumulative effect on stratospheric ozone for each mass unit emitted into the atmosphere.

It is also important to recognize the limitations in the ODP concept as defined above. As an example, ODP is defined in terms of the steady-state ozone change; it is, therefore, not representative of the relative transient effects expected for shorter-lived compounds during the early years of emission. During these early years, shorter-lived compounds may have changes in ozone much closer to the changes in ozone determined for longer-lived gases, such as CFC-11, than would be expected based on their relative ODP values.

Figure 4.3-2 shows the tropospheric concentration of two compounds following the onset of a constant emission level of each. One of the compounds has a 100-year lifetime (comparable to lifetimes of CFCs) and the other compound has a 5-year lifetime (comparable to lifetimes of hydrohalocarbons). We see that the ratio of the relative atmosphere concentration ratio does not approach steady-state until after about

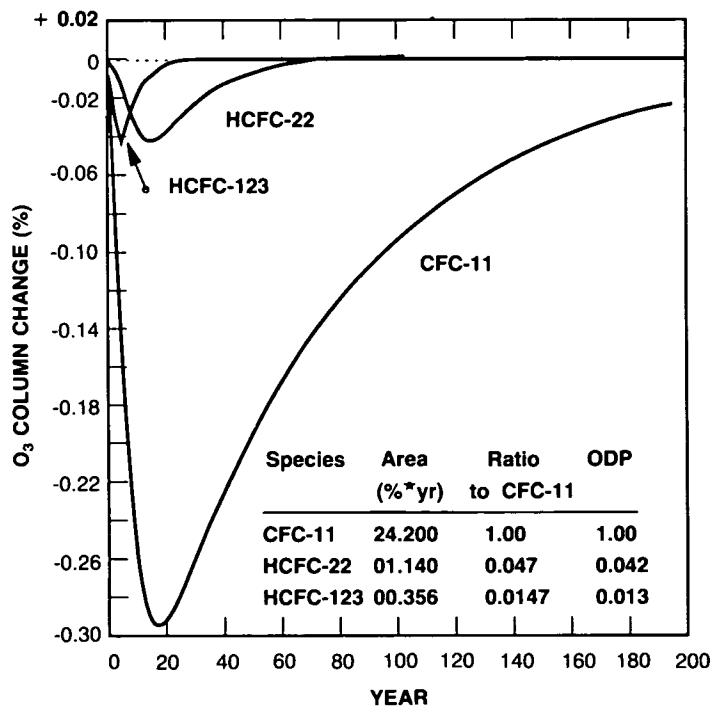


Figure 4.3-1. Calculated column ozone change in the DuPont 1-D model following a pulsed input (for one year) of 5.0×10^9 kg (Fisher et al., 1989 b) of specified gas.

OZONE DEPLETION POTENTIALS

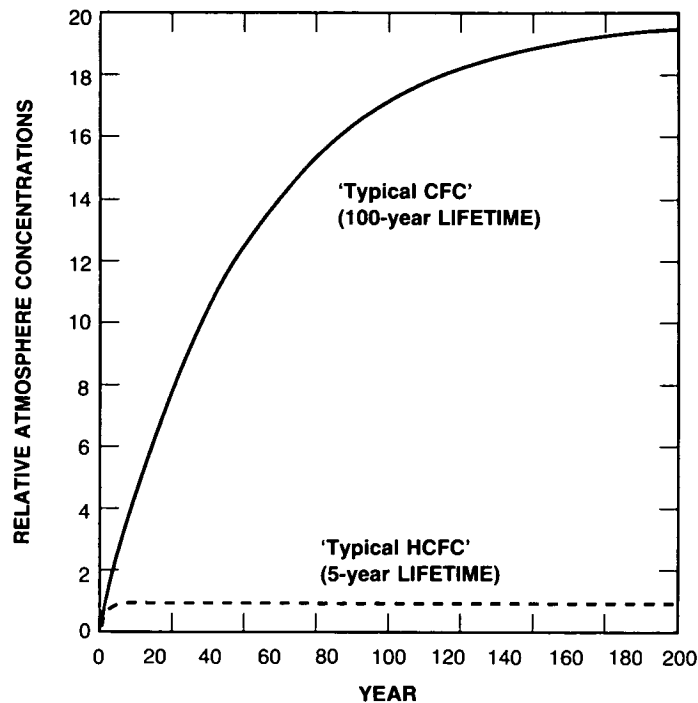


Figure 4.3-2. Atmospheric concentrations of halocarbons with 5- and 100-year lifetimes following onset of a constant emission of each compound.

400 years. Since the ODPs are based on steady-state relative effects which are (nearly) proportional to CFC concentrations, the calculated relative effects for short-lived compounds during the approach to steady-state can be larger than indicated by the ODP value. This is simply because the effect from the short-lived species has reached its full strength, whereas the effect from the long-lived species is still short of its steady-state value.

Other uncertainties and limitations associated with the concept of and determination of Ozone Depletion Potentials will be discussed later. Included is further evaluation of time-dependent relative ozone depletion.

In order to make the ODP definition consistent among models and at the same time have a conservative estimate of relative effects, the following criteria were selected for the model calculations included:

1. Depletion level—the calculations are based on emission rates of each compound required to give a modeled ozone depletion of approximately 1%. This value of depletion was selected in order to yield results large enough to avoid the noise level inherent with numerical models, yet small enough to remain in the linear perturbation region.
2. Trace gas levels—changing concentrations of other trace gases affect calculated tropospheric OH levels (Sze [1977] and Chameides et al. [1977]) and future depletions. However, we chose to base the calculations on current levels of CO₂, CH₄, CO, and N₂O due to the uncertainties in

future concentrations. The constant concentration assumption was chosen for clarity and simplicity.

3. Chlorine levels—since the long-lived CFCs are present in today's atmosphere and will affect chlorine chemistry over the time scales that hydrohalocarbons might be used, background halocarbon concentrations were assumed constant at current levels (yielding an asymptotic chlorine concentration of ~3 ppbv, with the exception of U. Oslo, who used 5.2 ppbv).
4. Bromine chemistry—current levels of bromine compounds were included in the model chemistry where appropriate.

Using the above provisions, the ODP for species x was then calculated as:

$$\text{ODP}(x) = \delta\text{O}_3(x) / \delta\text{O}_3(\text{CFC-11})$$

where $\delta\text{O}_3(x)$ is the change in total ozone at steady-state per unit mass emission rate. CFC-11 is used as the reference gas.

4.3.3 Model-Calculated ODPs

Each compound considered enters the atmosphere at ground level and, in general, is removed by a combination of chemical processes: reaction with hydroxyl (OH) in the troposphere and the stratosphere, reaction with excited-state oxygen in the stratosphere, and photolytic breakdown by ultraviolet light in the stratosphere. Laboratory measurements indicate that CFCs (e.g., CFC-11, -12, -113, -114, and -115) are primarily destroyed by ultraviolet light in the stratosphere and, to a lesser degree, by reaction with excited atomic oxygen; reaction with hydroxyl radical for these gases is unimportant. Hydrohalocarbons are removed by all three processes, but the predominant mechanism is reaction with OH in the troposphere. The reaction of the hydrohalocarbons with hydroxyl radicals leads to appreciably shorter atmospheric lifetimes compared to the CFCs.

Reaction rate constants and photolysis cross sections required as model input were obtained consistently from a number of sources for most of the calculations presented here. Whenever possible, recommendations from the most recent evaluation by the NASA panel (DeMore et al., 1987) were used. Rate data for several key reactions have been reevaluated by Hampson et al. (1989), and Molina (1989); these were used when available. Some reaction rate parameters were obtained from the open literature (Davidson et al. [1978], Hubrich and Stuhl [1980]), while some data were only available from unpublished sources (Magid, private communication, 1988). Finally, for some HFCs, no photolysis measurements could be found; since photolysis is of little importance for these species, neglecting this destruction mechanism has little impact on the derived lifetimes. Table 4.3-1 lists references and, when possible, the assumed reaction rates for destruction of each CFC, HCFC, and HFC. Several halons (namely, halon -1301, -1211, -1202, and -2402) are also considered in this report. The photolysis data needed for the halon species are based primarily on Molina et al. (1982). All models utilize their "best" representations for transport and radiation processes.

Both one- and two-dimensional models have been used for these evaluations. One-dimensional models calculate the global-averaged altitudinal variation of the relevant atmospheric chemical processes. These models all share the advantage that they are easy to operate and evaluate. Two-dimensional (2-D) models allow examination of calculated effects over the full range of latitudes and seasons. As such, their added complexity is offset by better representation of nonlinear characteristics of global stratospheric transport

OZONE DEPLETION POTENTIALS

Table 4.3-1. Chemical rate data used in ODP calculations

Species	Photolysis Ref.	OH Reactions			O(¹ D) Reactions		
		Reaction Rate ^a		Ref.	Reaction Rate ^b	Branching Ratio ^c	Ref.
		A	E/R				
CFC-11	a	—	—	—	2.3(−10)	0.75	a
CFC-12	a	—	—	—	1.4(−10)	0.86	a
CFC-113	b	—	—	—	2.0(−10)	0.80	c
CFC-114	b	—	—	—	1.6(−10)	0.80	c
CFC-115	b	—	—	—	8.9(−11)	0.80	c
HCFC-22	a	1.2(−12)	1650	f	1.0(−10)	1.0	f
HCFC-123	d	6.4(−13)	850	f	2.3(−10)	1.0	f
HCFC-124	d	6.6(−13)	1250	f	1.0(−10)	1.0	f
HFC-125	—	3.8(−13)	1500	f	0.5(−10)	1.0	f
HFC-134a	e	1.7(−12)	1750	f	0.5(−10)	1.0	f
HCFC-141b	d	2.7(−13)	1050	f	1.5(−10)	1.0	f
HCFC-142b	d	9.6(−13)	1650	f	1.4(−10)	1.0	f
HFC-143a	—	2.6(−13)	1500	f	0.6(−10)	1.0	f
HFC-152a	e	1.5(−12)	1100	f	1.0(−10)	1.0	f
CCl ₄	a	—	—	—	3.3(−10)	0.86	a
CH ₃ CCl ₃	a	5.0(−12)	1800	a	3.18(−10)	0.80	c

^aReaction rate constant of form: $k = A \exp[-E/(RT)]$, where A and k have the units of $\text{cm}^3/(\text{molecule sec})$.

^bReaction rate constant with units $\text{cm}^3/(\text{molecule sec})$.

^cFraction of O(¹D) disappearances proceeding through reaction channel, remainder pass through quenching channel to O(³P) and no reaction with the halocarbon.

Reference Key:

- a DeMore et al. (1987)
- b Hubrich and Stuhl (1980)
- c Davidson et al. (1978)
- d Molina (1989)
- e Magid (private communication, 1988)
- f Hampson, Kurylo, and Sander (1989)

and radiative processes. Ozone changes calculated by 2-D models are averaged with respect to both latitude and seasons before calculation of ODPs.

The calculated atmospheric lifetime of each gas species provides a key comparison of modeled results. Table 4.3-2 shows a comparison of lifetime values (of the CFCs, HCFCs, and HFCs) calculated by the models. In general, the calculated lifetimes for CFC-11 and CFC-12 are consistent with the lifetimes determined from the ALE-GAGE observations (Cunnold et al., 1986; Watson et al., 1988). However, the CFC-11 lifetimes from the 2-D models are on the low side of the uncertainty range, while 1-D results for the CFC-12 lifetime tend to be on the high side. The calculated HCFC and HFC lifetimes from all of the models are within the uncertainty range of those reported in section 4.2 as determined by Prather (1989) and Derwent and Volz-Thomas (1989) in the AFEAS Report (see Vol. II, Appendix).

The Ozone Depletion Potentials calculated by eight models (from five research groups) for each of these species is given in Table 4.3-3. For each of the hydrogen-containing compounds, the calculated ODPs have been scaled by the ratio of the inferred lifetime for methyl chloroform (~6.3 years; see section 4.2) to the lifetime derived by each model. This scaling is an attempt to indirectly account for the different global tropospheric amounts of OH between models. The reaction with OH is a primary sink for the

OZONE DEPLETION POTENTIALS

Table 4.3-2. Atmospheric lifetimes (in years) calculated with one-dimensional and two-dimensional models^a

Species	Chemical Formula	1-D Model Results				2-D Model Results			
		LLNL	AER	DuPont	BISA	Oslo	LLNL	AER	DuPont
CFC-11	CFCl ₃	80.0	60.0	71.0	85	60.0	52.0	47.0	46.0
CFC-12	CF ₂ Cl ₂	154.0	125.0	154.0	166	105.0	101.0	95.0	118.0
CFC-113	CFCl ₂ CF ₂ Cl	96.0	96.0	117.0	113	101.0	79.0	—	—
CFC-114	CF ₂ CICF ₂ Cl	209.0	260.0	319.0		236.0	197.0	—	—
CFC-115	CF ₂ CICF ₃	680.0	690.0	548.0		522.0	393.0	399.0	—
HCFC-22	CHClF ₂	20.0	20.0	16.0		17.2	15.0	24.0	12.7
HCFC-123	CF ₃ CHCl ₂	1.9	2.1	1.6		1.7	1.5	2.4	1.2
HCFC-124	CF ₃ CHClF	8.4	8.8	6.9		7.4	6.4	10.0	5.3
HFC-125	CF ₃ CHF ₂	37.0	37.0	25.0		—	27.0	43.0	19.0
HFC-134a	CF ₃ CH ₂ F	21.0	21.0	16.0		—	15.0	24.0	12.5
HCFC-141b	CCl ₂ FCH ₃	8.9	9.4	7.8		8.0	6.9	11.0	5.8
HCFC-142b	CClF ₂ CH ₃	25.0	25.0	19.0		20.9	19.0	28.0	18.1
HFC-143a	CF ₃ CH ₃	54.0	52.0	42.0		—	40.0	—	—
HFC-152a	CHF ₂ CH ₃	2.1	2.3	1.7		—	1.5	2.7	1.3
Carbon Tetrachloride	CCl ₄	73.0	53.0	61.0	64	52.2	47.0	40.0	40.0
Methyl Chloroform	CH ₃ CCl ₃	7.4	7.4	6.0		6.3	5.8	7.8	4.7

^aThe results of the LLNL, AER, DuPont, and Oslo groups have been published by Fisher et al. (1989a, b).

Table 4.3-3. Ozone Depletion Potentials (ODP) calculated with one-dimensional and two-dimensional models, assuming scaling for HCFC ODPs by methyl chloroform inferred lifetime^a

Species	Chemical Formula	1-D Model Results				2-D Model Results			
		LLNL	AER	DuPont	BISA	Oslo	LLNL	AER	DuPont
CFC-11	CFCl ₃	1.0	1.0	1.0	1.0	1.0	1.0	1.0	1.0
CFC-12	CF ₂ Cl ₂	1.0	0.9	1.0	0.9	0.9	0.9	0.9	0.9
CFC-113	CFCl ₂ CF ₂ Cl	0.8	0.8	0.9	0.9	0.9	0.8	—	—
CFC-114	CF ₂ CICF ₂ Cl	0.8	0.6	0.8	0.8	0.6	0.6	—	—
CFC-115	CF ₂ CICF ₃	0.4	0.4	0.5	0.4	0.4	0.3	0.4	—
HCFC-22	CHClF ₂	0.05	0.05	0.04	0.05	0.04	0.05	0.06	0.04
HCFC-123	CF ₃ CHCl ₂	0.13	0.16	0.13	0.01 ^b	0.013	0.017	0.022	0.017
HCFC-124	CF ₃ CHClF	0.016	0.018	0.017	—	0.018	0.019	0.024	0.017
HFC-125	CF ₃ CHF ₂	0.0	0.0	0.0	0.0	0.0	0.0	0.0	0.0
HFC-134a	CF ₃ CH ₂ F	0.0	0.0	0.0	0.0	0.0	0.0	0.0	0.0
HCFC-141b	CCl ₂ FCH ₃	0.07	0.08	0.07	0.1 ^b	0.09	0.09	0.11	0.09
HCFC-142b	CClF ₂ CH ₃	0.05	0.05	0.05	0.06 ^b	0.06	0.05	0.06	0.05
HFC-143a	CF ₃ CH ₃	0.0	0.0	0.0	0.0	0.0	0.0	0.0	0.0
HFC-152a	CHF ₂ CH ₃	0.0	0.0	0.0	0.0	0.0	0.0	0.0	0.0
Carbon Tetrachloride	CCl ₄	1.1	1.2	1.1	1.0	1.2	1.1	1.0	1.2
Methyl Chloroform	CHCCl ₃	0.10	0.12	0.10	—	0.14	0.13	0.16	0.15

^aScaling assumes CH₃CCl₃ lifetime of 6.3 years, based on discussion in Section 4.2.

^bBased on Gillotay et al. (1989).

OZONE DEPLETION POTENTIALS

hydrogen-containing species; differences in calculated tropospheric OH concentrations account for much of the model differences in chemical lifetimes for these gases. Therefore, amounts of OH account for much of the variation in ODPs derived between models. However, as noted by Fisher et al. (1989a, b), using globally averaged OH deduced from CH_3CCl_3 to calculate lifetimes for other HCFCs may not necessarily be accurate, particularly for those HCFCs with lifetimes substantially different from methyl chloroform.

As seen in Table 4.3-3, the ODPs for each hydrogen-containing species, including the suggested replacement compounds, are much smaller than those for the CFCs. This difference largely reflects the reactivity of these species with OH, resulting in shorter chemical lifetime for the HCFCs compared to the CFCs. Several compounds, such as HFC-134a and HCF-152a, have ODPs of zero because they do not contain chlorine.

In general, the ODPs derived using the different models compare extremely well with each other. However, significant differences between modeled ODPs still exist. The variation between models in the ODP for CH_3CCl_3 , for example, is likely related to differences in the calculated distribution of OH with altitude and latitude between models. Although the two-dimensional models generally have a sounder physical basis for their formulation than existing one-dimensional models, there are no significant differences between the 1-D and 2-D model results.

Table 4.3-4 gives the ODPs determined by three groups (AER and LLNL 1-D models and U. Oslo 2-D model) for several brominated halocarbons. Although the ODPs for these compounds are shown relative to CFC-11 for historical reasons, the ODPs for bromine-containing compounds should in reality be compared relative to each other because of the strong dependence to background chlorine levels in determining bromine effects on ozone. Therefore, in Table 4.3-4, Bromine Ozone Depletion Potentials (BODPs) are used for relative comparisons with halon-1301, the compound with the longest lifetime and largest ODP, as the reference. The major ozone destruction due to the halons comes from coupled chlorine-bromine chemistry in the lower stratosphere. Because of interactions between chlorine and bromine chemistry, the traditional ODPs are critically dependent on chlorine levels in the background atmosphere. Also, because current models underestimate the ClO concentrations in the lower stratosphere at high latitudes in early spring, the traditional ODP definition (relative to CFC-11) may underestimate the true ozone depletion potential for these compounds.

Table 4.3-4. Ozone depletions (ODPs) for brominated compounds as calculated in the AER and LLNL 1-D models and the U. Oslo 2-D model

Common Name	Atmospheric Lifetime (yrs)			ODP ^a			BODP ^b		
	AER	LLNL	Oslo	AER	LLNL	Oslo	AER	LLNL	Oslo
halon-1301	81	107.0	72	16.0	13.2	7.8	1.0	1.0	1.0
halon-1211	12	15.0	18	3.5	2.2	3.0	0.22	0.17	0.38
halon-1202		1.5			0.3			0.02	
halon-2402		28.0	23		6.2	5.0		0.5	0.64

^aRelative to CFC-11, shown for historical purposes. Values will be underestimates if they account for effects at polar latitudes.

Assumed upper stratospheric Cl_x mixing ratio is 3 ppbv in the LLNL and AER models and 4.5 ppbv in the Oslo model.

^bBromine Ozone Depletion Potentials (BODPs) defined relative to halon-1301, the longest brominated gas.

4.3.4 Uncertainties and Sensitivity Studies

The above globally averaged ODP values are derived from model calculations based on present-day atmospheric conditions using current representations of chemical and transport processes. Although the ODPs agree reasonably well among the models, many uncertainties still exist. Establishing a strict criterion for estimating the overall uncertainty in the calculated ODPs is not a straightforward task. There are still many uncertainties associated with the treatment of atmospheric chemical, radiative, and dynamical processes in current models. Perhaps the single largest uncertainty is that none of the models used for calculating ODPs includes the chemical and dynamical processes causing the seasonal ozone losses associated with the ozone hole over Antarctica. The possible impact of this uncertainty is discussed below.

Additional calculations have been carried out to test the sensitivity of the relative ODP effects to (1) levels of other trace gases, (2) seasonal and latitudinal dependencies and (3) assumed stratospheric transport processes. The relative time-dependent effects of different gases on total ozone is also examined.

4.3.4.1 Ozone Hole Effects

None of the ODP calculations consider the potential effect of heterogeneous chemistry in the lower stratosphere, particularly within the circulation vortex occurring at either pole during late winter and early springtime. Currently, inclusion of such effects in ODP calculations is premature since modeling of heterogeneous chemistry in general, and the polar phenomena in particular, are still in the early stages.

Because of the apparent special chlorine processing and dynamics within the winter polar vortex, local Antarctic ODPs are expected to be larger than those shown in Table 4.3-3. Insofar as the observed long-lived tracer distributions, such as those for CFC-11 in the polar vortex, suggest that much of the total chlorine may be available there, then an upper limit on Antarctic ODPs can be determined by calculating the relative amounts of chlorine transported through the tropopause by the different gases. It can be argued, within existing uncertainties, that active chlorine at all altitudes within the stratosphere, and perhaps into the mesosphere, may be available for affecting ozone within the polar vortex.

Values from four 2-D models (AER, LLNL, Oslo, DuPont) for the maximum relative chlorine loading into the stratosphere, termed Chlorine Loading Potentials (CLPs), are given in Table 4.3-5 based on the model calculated lifetimes. CLP, defined as the chlorine transported through the tropopause per mass emitted relative to CFC-11, is proportional to the relative number of chlorine atoms per molecule and the atmospheric lifetime and is inversely proportional to the molecular weight. A set of reference lifetimes, based on the estimates used in scenario development in Chapter 3, section 3.2.1 for the CFCs and from the analysis in Section 4.2 for the HCFCs and HFCs, is given in Table 4.3-6 along with the corresponding CLP values. These values are as much as a factor of two to three larger than the derived ODP values.

The reader may wonder why the values of the chlorine loading potential CLP are often larger than the ODPs for the same species. If all sources of stratospheric chlorine were equivalent in the photochemical reactivity sense once they reached the stratosphere, CLP values would be identical to the ODP values. Two major reasons account for the chlorine loading potential values being larger than the ODPs for many of the species. First, several of the CFCs and HCFCs, such as HCFC-22 and HCFC-142b, are incompletely dissociated within the stratosphere. Second, differences in the dissociation reactivity produce different chlorine distribution for the various gases.

OZONE DEPLETION POTENTIALS

Table 4.3-5. Chlorine Loading Potentials (CLPs) from 2-D models for CFCs, HCFCs, and HFCs, scaled by lifetime of CH₃CCl₃ (= 6.3 yr)

Species	Oslo CLP	LLNL CLP	AER CLP	DuPont CLP
CFC-11	1.0	1.0	1.0	1.0
CFC-12	1.3	1.5	1.5	1.9
CFC-113	1.2	1.1		
CFC-114	2.1	2.0		
CFC-115	2.6	2.2	2.5	
HCFC-22	0.15	0.17	0.22	0.20
HCFC-123	0.017	0.01	0.03	0.02
HCFC-124	0.04	0.04	0.06	0.05
HFC-125	0.0	0.0	0.0	0.0
HFC-134a	0.0	0.0	0.0	0.0
HCFC-141b	0.10	0.11	0.15	0.13
HCFC-142b	0.16	0.18	0.22	0.20
HFC-143a	0.0	0.0	0.0	0.0
HFC-152A	0.0	0.0	0.0	0.0
CCl ₄	1.0	1.1	1.0	1.0
CH ₃ CCl ₃	0.11	0.12	0.14	0.14

Table 4.3-6. Maximum relative Chlorine Loading Potential (CLP) for examined CFCs, HCFCs, HFCs, and other chlorinated halocarbons based on reference species lifetimes chosen to be compatible with available atmospheric measurements and modeling studies

Species	Reference ^a Lifetime (yrs)	Chlorine Loading Potentials ^b
CFC-11	60.0	1.0
CFC-12	120.0	1.5
CFC-113	90.0	1.11
CFC-114	200.0	1.8
CFC-115	400.0	2.0
HCFC-22	15.3	0.14
HCFC-123	1.6	0.016
HCFC-124	6.6	0.04
HFC-125	28.1	0.0
HFC-134a	15.5	0.0
HCFC-141b	7.8	0.10
HCFC-142b	19.1	0.14
HFC-143a	41.0	0.0
HFC-152a	1.7	0.0
CCl ₄	50.0	1.0
CH ₃ CCl ₃	6.3	0.11

^aLifetimes (e-folding time) are on estimates used in scenario development in Chapter 3, section 3.2.1 for the CFCs and from the analysis in Section 4.2 for the HCFCs and HFCs.

^bChlorine Loading Potential is defined as the maximum chlorine transported across the tropopause per mass emitted relative to the same for CFC-11; it is proportional to lifetime and the number of chlorine atoms per molecule, and is inversely proportional to molecular weight.

At this time, until model studies of heterogeneous chemistry and validation of transport parameterization have been completed, it is difficult to put definite limits on the uncertainties of the model-calculated ODP values. The answer to this question depends on the extent of the influence that polar springtime ozone destruction will have on global ozone, and on the extent of the downward transport within the Antarctic and Arctic polar vortex. The preliminary results reported in Fisher et al. (1989b) indicate that comparison of model-simulated trace gas distributions with available observation may be useful to limit the uncertainties. The CLP values (i.e., Table 4.3.6) provide an upper limit on ODP value within the Antarctic (and perhaps, the Arctic) region, while dilution effects, after breakup of the vortex, may extend higher ODP values to other latitudes. At this time, the ramifications of polar ozone depletion on the globally determined concept of ODPs are not clear.

4.3.4.2 Sensitivity of ODPs to Other Trace Gas Levels

ODP values have all been based on calculated ozone changes in a modeled atmosphere, assuming present-day levels of CFCs, CO₂, CH₄, CO, N₂O, Br_x, and other trace gases. Because it is important to quantify the effects of possible changes in the future trace gas concentrations on ODPs, we will present calculations of the sensitivity of the ODPs to trace gas concentrations that may occur within the next century if current concentration trends continue.

Trace gas concentrations were varied from current concentrations as shown in Table 4.3-7. These concentrations were changed both individually and as an ensemble in the sensitivity calculations. Calculated changes in ozone for tested CFCs and HCFCs are relative to an atmosphere including the assumed trace gas perturbation. Two models were used to determine the sensitivity of atmospheric lifetimes and ODPs to trace gas concentrations. Calculations with the AER 1-D model assumed a background stratospheric chlorine content of 3 ppbv. Calculations with the Oslo 2-D model used a background chlorine amount of 5.2 ppbv. Prior calculations with the Oslo model indicate little effect on the derived ODPs from the assumed chlorine background amount.

Table 4.3-8 shows the calculated changes in atmospheric lifetimes of CFC-11, CFC-12, HCFC-22, and HCFC-123 for the various sensitivity calculations. The largest effects are evident for the HCFCs in the cases where CH₄ and CO concentrations are perturbed. Both CH₄ and CO strongly influence tropospheric HO_x chemistry; therefore the concentration of OH, and consequently the primary destruction of the HCFCs, is affected, resulting in the determined impact on atmospheric lifetimes. The relatively minor changes in lifetime of the CFCs are primarily a result of increased photolysis rates for the trace gas perturbed atmospheres.

Table 4.3-7. Change in ground level trace gas concentrations assumed in sensitivity studies

Trace Gas	Background Atmosphere	Perturbed Atmosphere
CO ₂	340.0 ppmv	680.0 ppmv
CH ₄	1.6 ppmv	3.2 ppmv
CO	100.0 ppbv	200.0 ppbv
N ₂ O	300.0 ppbv	360.0 ppbv
Br _x	20.0 pptv	40.0 pptv

OZONE DEPLETION POTENTIALS

Table 4.3-8. Sensitivity of calculated lifetimes to changes in trace gas values (based on AER 1-D results)

	Lifetimes (years)			
	CFC-11	CFC-12	HCFC-22	HCFC-123
Present-day atmosphere	60	125	20	2.1
CO ₂ (350 → 680 ppmv)	61	128	20	2.1
CH ₄ (1.6 → 3.2 ppmv)	60	126	23	2.5
CO (100 → 200 ppbv)	60	125	25	2.7
N ₂ O (300 → 360 ppbv)	59	123	20	2.1
CH ₃ Br (20 → 40 pptv)	59	125	20	2.1
All changes combined	60	127	26	2.9

Table 4.3-9 presents ODPs resulting from these calculations. For both the AER 1-D model and the Oslo 2-D model, the largest sensitivity in the ODP for CFC-12 occurs for the assumed concentration change in N₂O. As expected, ODPs for the HCFCs are affected most by change in CH₄ and CO levels.

The calculated sensitivities to background trace gas concentrations can be explained as follows. First, changes in atmospheric lifetimes will affect the ODP in that, as the lifetime increases/decreases, more/less of the CFC or HCFC is accumulated in the atmosphere at steady state for the same mass emitted. Secondly, the response of ozone to increases in chlorine can be different in the future atmosphere. However, this change in response will only affect the ODP estimates if the response of the individual CFCs or HCFCs is different from that of CFC-11. An example of this involves the increased N₂O case: although the absolute changes in ozone for each of the CFCs and HCFCs were determined to be less than half of the ozone changes determined for the present atmosphere calculations, sensitivity of the derived ODPs is much

Table 4.3-9. Sensitivity of ozone potentials to changes in trace gas values

1. AER 1-D Model				
	CFC-12	HCFC-22	HCFC-123	
Present-day atmosphere	0.92	0.057	0.019	
CO ₂ (340 → 680 ppmv)	0.93	0.051	0.018	
CH ₄ (1.6 → 3.2 ppmv)	0.93	0.069	0.023	
CO (100 → 200 ppbv)	0.93	0.070	0.024	
N ₂ O (300 → 360 ppbv)	1.01	0.071	0.019	
CH ₃ Br (20 → 40 pptv)	0.92	0.055	0.019	
All changes combined	0.95	0.076	0.026	
2. Oslo 2-D Model (all calculations with 5.2 ppbv Cl _y)				
	CFC-12	HCFC-22	HCFC-123	HCFC-124
Present-day atmosphere	0.92	0.046	0.013	0.018
CO ₂ (340 → 600 ppmv)	0.94	0.049	0.016	
CH ₄ (1.6 → 3.2 ppmv)	0.93	0.058	0.016	
N ₂ O (300 → 360 ppbv)	0.97	0.042	0.015	
Br _x (18 → 33 pptv)	0.91	0.051	0.016	0.020
All changes combined	0.96	0.062	0.018	

smaller. The increase in NO_y will moderate the impact of increased chlorine by tying up a larger portion of the chlorine in the form of chlorine nitrate, ClONO_2 . This effect is most noticeable in the lower stratosphere where ClONO_2 is more stable. The compensating effect should be more efficient for CFC-11 where more of the odd chlorine is found in the lower stratosphere. This accounts for the high ODP of CFC-22 in the increased N_2O case in the AER model; the Oslo 2-D model does not show this effect.

In conclusion, both lifetimes and derived ODPs are moderately sensitive to significant changes in background trace gas concentrations. However, for the scenarios examined, the range in sensitivity of the ODPs is well within the overall uncertainty range for model-determined ODP values. Possible systematic errors, perhaps due to missing chemistry or other processes, may provide a much more significant impact on the derived ODP values.

4.3.4.3 Variation in ODPs with Latitude and Season

Another manifestation of the effect of differences between species on the chlorine distribution is the variations of the ODP values as a function of latitude and season. Several of the compounds show strong variations in their ODPs as a function of latitude and season.

Figure 4.3-3, based on calculations with the LLNL two-dimensional model (Connell and Wuebbles, 1989; Fisher et al., 1989b), shows the calculated change in total ozone as a function of latitude and season for CFC-11. A constant emission rate of CFC-11 was assumed sufficient to give a steady-state global

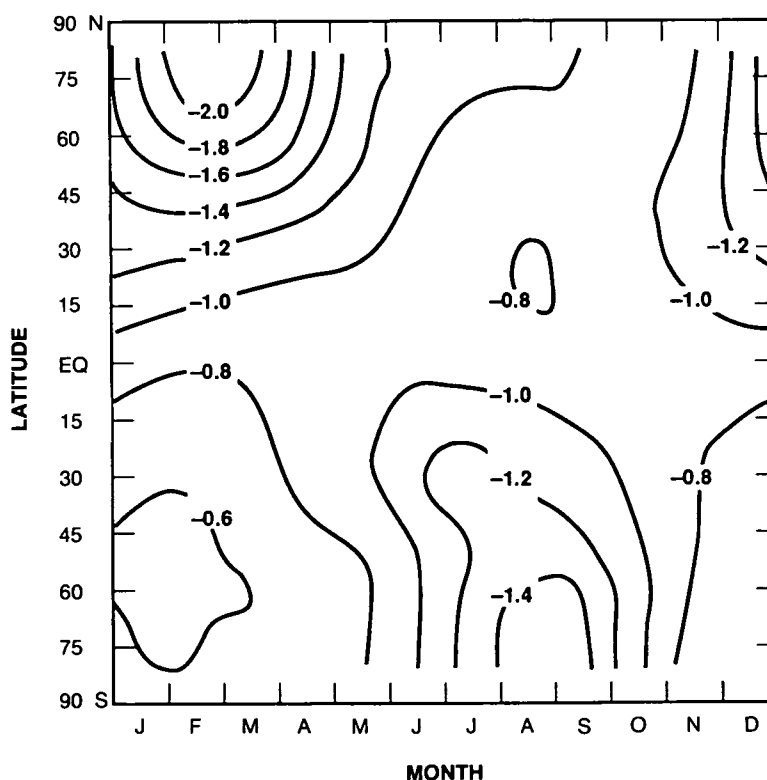


Figure 4.3-3. Calculated latitudinal and seasonal steady-state ozone change from emission of CFC-11 necessary for global 1% change in total ozone (LLNL 2-D model).

OZONE DEPLETION POTENTIALS

decrease in total ozone of about one percent. As expected from previous 2-D analyses of CFC effects on ozone (e.g., WMO, 1985), the largest changes in ozone occur at the poles in late winter to early spring. Once the calculated changes are compared relative to CFC-11 and adjusted for differences in assumed emission rates, the resulting values indicate a generally variable dependency on latitude and generally weaker seasonal variations. In particular, the ODPs for CFC-12, HCFC-22, HCFC-124, and HCFC-142b have strong latitudinal variations, with the ODP increasing from lower tropical values to higher polar values by as much as a factor of three. The changes in total ozone at steady state from the LLNL model, and the derived ODPs from the LLNL, AER, Oslo, and DuPont 2-D models, for CFC-12 and HCFC-22 are shown in Figures 4.3-4 and 4.3-5, respectively. There are significant variations (more than a factor of two) with latitude and season in the ODPs derived for these two compounds. In both cases, the ODPs are smallest in the tropics and largest at the poles in late summer. The results from the models are in good general agreement regarding this pattern, although the LLNL model shows slightly more seasonal response for some species than the other models, particularly at high latitudes in the Southern Hemisphere. Other species, such as HCFC-123, HCFC-141b, and CH_3CCl_3 show little variation with latitude or season (see Fisher et al. (1989b) and Connell and Wuebbles (1989) for figures and further discussion).

The strong latitudinal ODP variation of some species (in contrast to the weak variation determined for others) warrants further discussion. The distinguishing difference between the species categories is based on the difference in the distribution of chlorine atoms which, in turn, depends on the altitudes for destruction of the respective species. Compounds that do not survive transport to the upper stratosphere for dissociation, and are therefore similar to CFC-11, show very little variation in their ODP with latitude

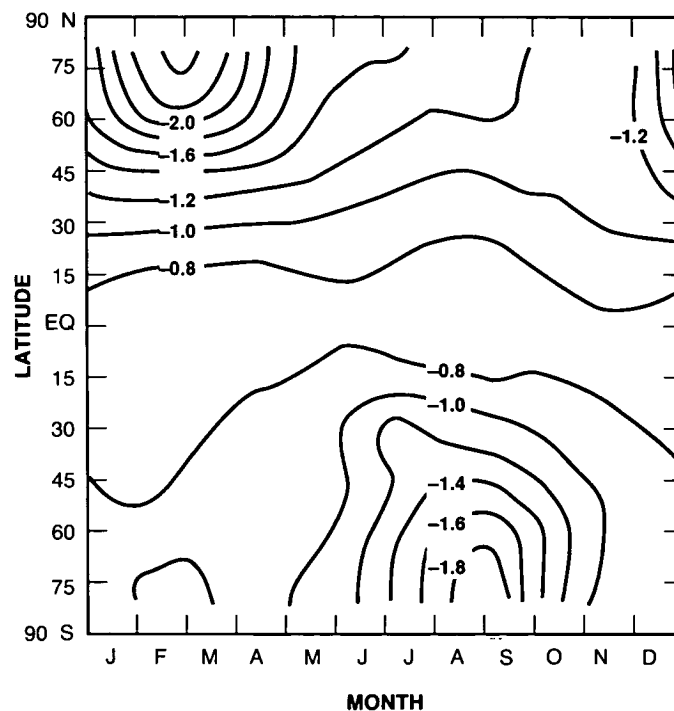


Figure 4.3-4a. Calculated latitudinal and seasonal steady-state ozone change from emission of CFC-12 necessary to give 1% change in total ozone (LLNL 2-D model).

OZONE DEPLETION POTENTIALS

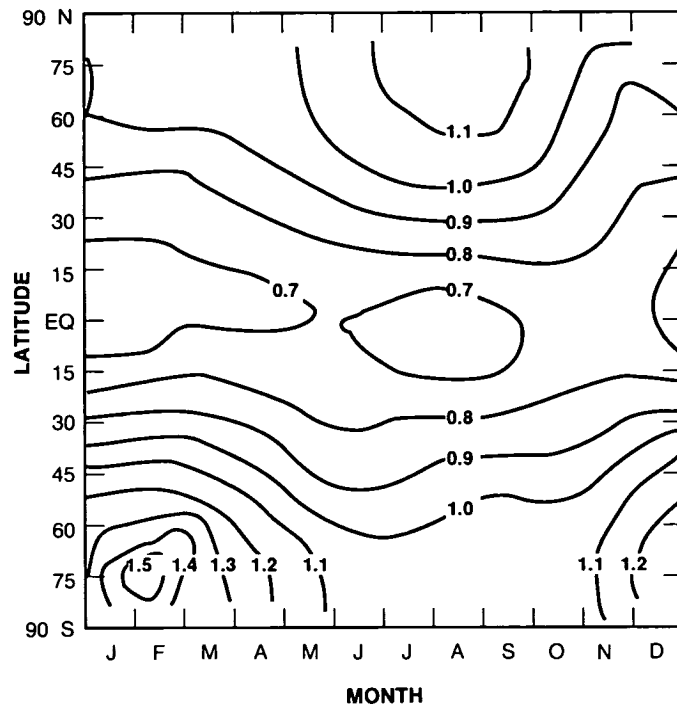


Figure 4.3-4b. Calculated latitudinal and seasonal relative ozone depletion of CFC-12 (LLNL 2-D model).

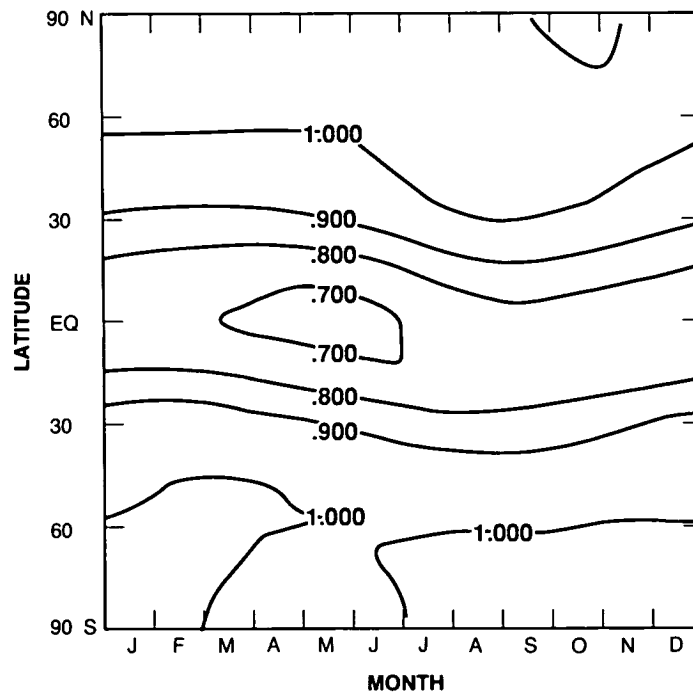


Figure 4.3-4c. Calculated latitudinal and seasonal relative ozone depletion of CFC-12 (AER 2-D model).

OZONE DEPLETION POTENTIALS

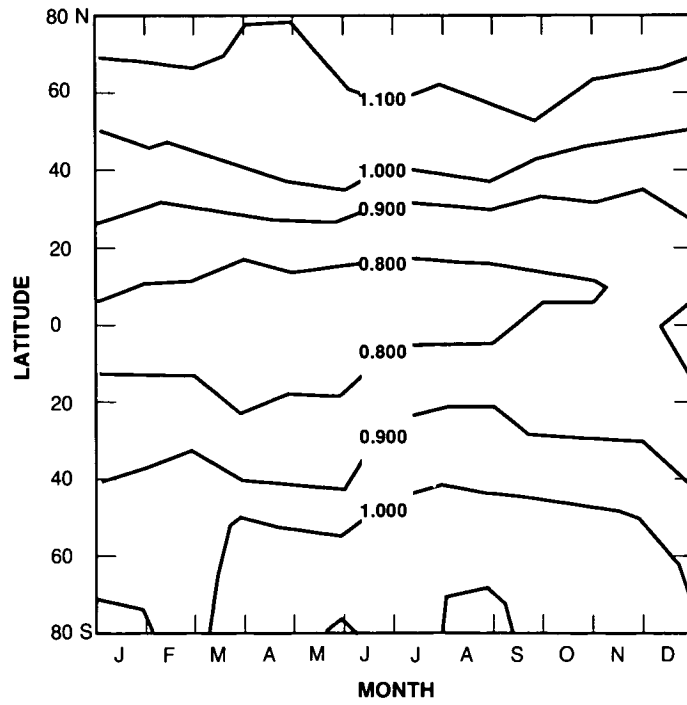


Figure 4.3-4d. Calculated latitudinal and seasonal relative ozone depletion of CFC-12 (Oslo 2-D model).

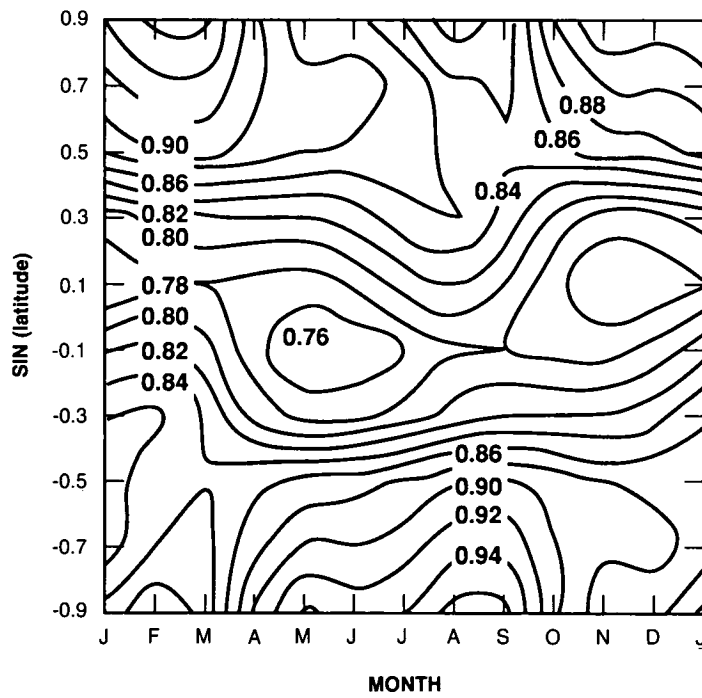


Figure 4.3-4e. Calculated latitudinal and seasonal relative ozone depletion of CFC-12 (DuPont 2-D model).

OZONE DEPLETION POTENTIALS

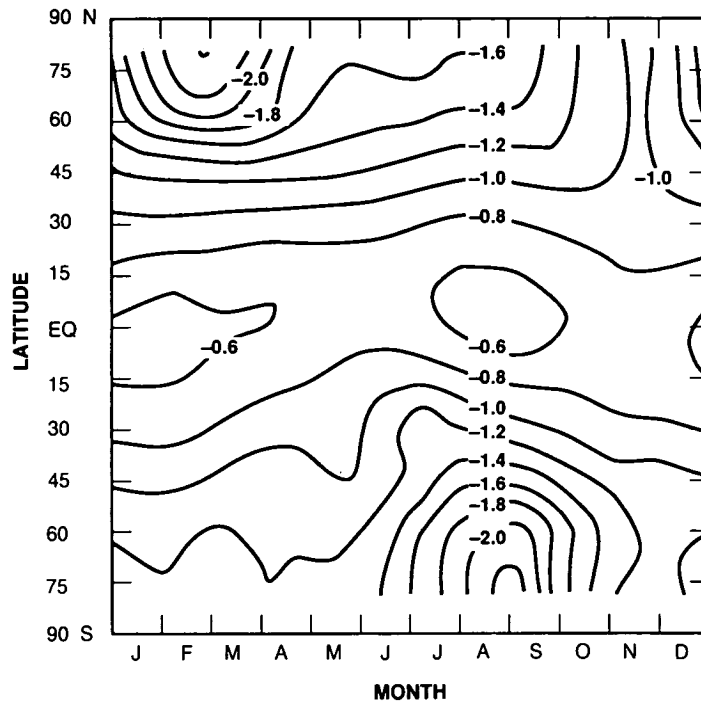


Figure 4.3-5a. Calculated latitudinal and seasonal steady-state ozone change necessary to give 1% change in total ozone from emission of HCFC-22 (LLNL 2-D model).

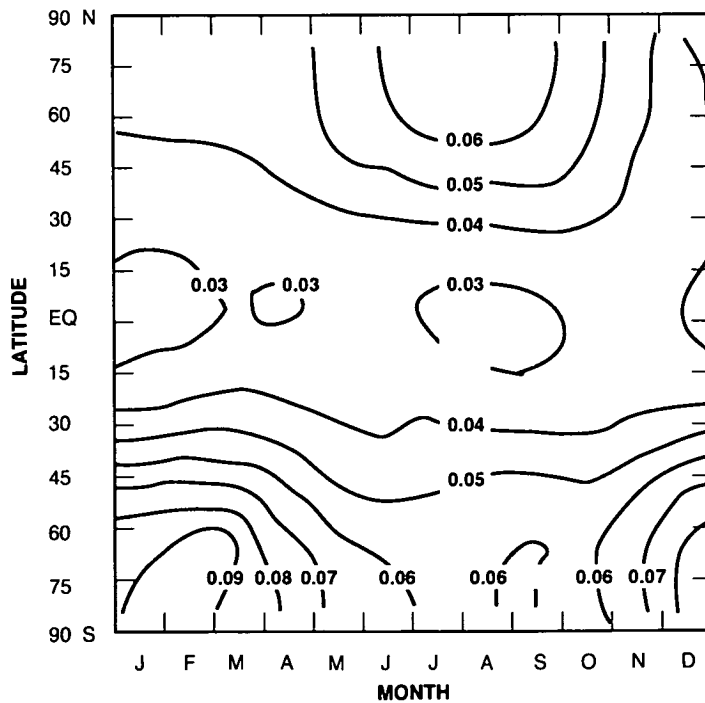


Figure 4.3-5b. Calculated latitudinal and seasonal relative ozone depletion of CFC-22 (LLNL 2-D model).

OZONE DEPLETION POTENTIALS

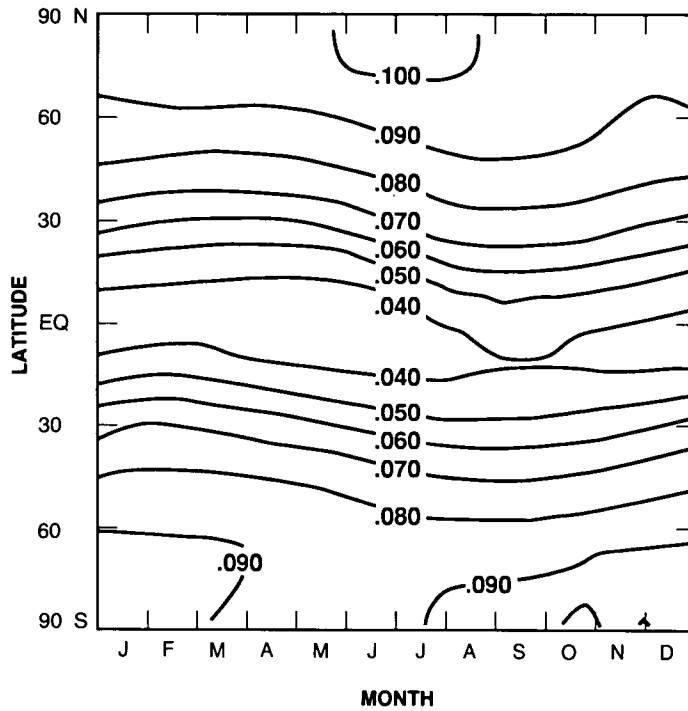


Figure 4.3-5c. Calculated latitudinal and seasonal relative ozone depletion from emission of HCFC-22 (AER 2-D model).

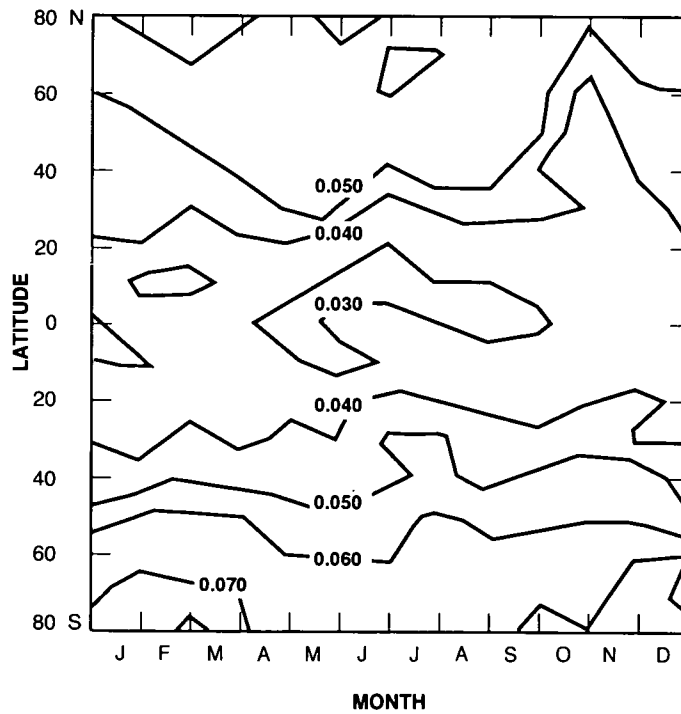


Figure 4.3-5d. Calculated latitudinal and seasonal relative ozone depletion from emission of HCFC-22 (Oslo 2-D model).

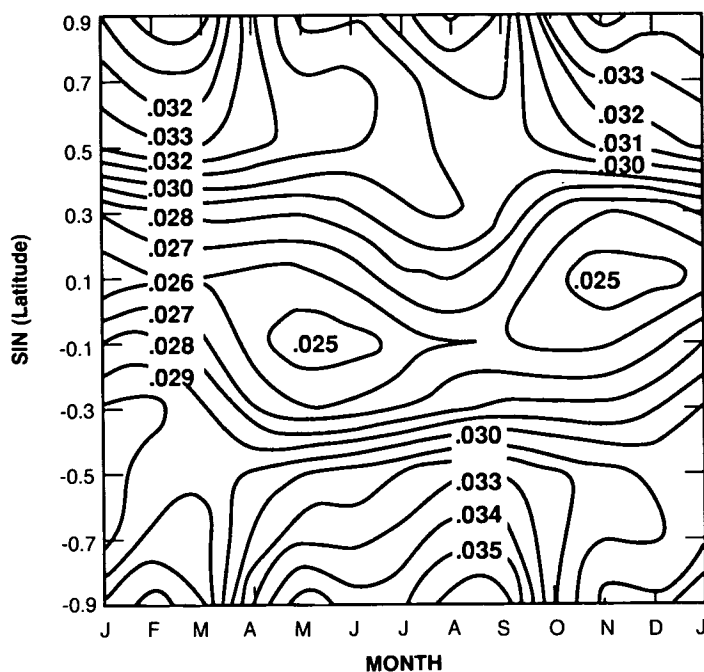


Figure 4.3-5e. Calculated latitudinal and seasonal relative ozone depletion from emission of HCFC-22 (DuPont 2-D model).

and season. HCFC-123 is an example of such a species. On the other hand, species that persist into the upper stratosphere (even if the dominant removal is at lower altitudes) show strong latitudinal dependencies. CFC-12 and HCFC-22 are two examples that show a significant latitudinal dependency. CFC-12 is primarily dissociated at higher altitudes than CFC-11. HCFC-22, on the other hand, is primarily destroyed in the troposphere and lower stratosphere by reaction with OH radical, yet models and observations indicate that a significant fraction survives transport to the upper stratosphere.

The resulting strong variations of ODPs with latitude occur in response to latitudinal differences in upper stratospheric chemistry on ozone destruction and the resultant effects of transport on both the ClO_x produced and on the ozone being destroyed. The extent of these variations depends on the treatment and the strength of the modeled transport. It is not surprising, therefore, to find some differences in the ODP variations with latitude and season between models. The effects of heterogeneous chemistry and polar dynamical effects, not included in the calculations here, would lead to some modifications of these findings but should not qualitatively change the response.

4.3.4.4 Sensitivity of ODP to Modeled Transport

The question can next be raised as to the sensitivity of ODP values to model parameters—primarily transport processes. The treatment of transport processes is a source of significant uncertainty in 2-D models. Changing the model transport parameters would affect the ODP directly in three ways. First, the ODP values can change because of changes in lifetimes. The lifetime for CFC-11 is sensitive to the strength of the circulation in the stratosphere while the lifetime of HCFC-22, which is dominated by removal in the

OZONE DEPLETION POTENTIALS

troposphere, is less sensitive. Second, changing transport parameters would affect the distribution of chlorine atoms in the stratosphere. The responses of each species differ according to where the chlorine atoms are released. Finally, change in transport can also affect the response of ozone to chemical perturbations.

Four sets of calculations were performed using different circulations and K_{yy} (latitudinal eddy diffusivity) values to examine the sensitivity to variations in transport within the AER 2-D model. Calculated effects of CFC-11 and HCFC-22 emissions were determined in each case. These cases are designated by:

Case 1	standard	standard ($3 \times 10^9 \text{ cm}^2 \text{ s}^{-1}$)
Case 2	standard	small ($1 \times 10^8 \text{ cm}^2 \text{ s}^{-1}$)
Case 3	weak	standard ($3 \times 10^9 \text{ cm}^2 \text{ s}^{-1}$)
Case 4	weak	small ($1 \times 10^8 \text{ cm}^2 \text{ s}^{-1}$)

The weak circulation for cases 3 and 4 is chosen to test the response of ODP for HCFC-22 if a larger portion of the HCFC-22 is dissociated in the upper stratosphere. The circulation is adjusted so that the HCFC-22 molecules spend more time in the upper stratosphere, resulting in 90% dissociation of the molecules. Adopting smaller K_{yy} values for cases 2 and 4 represents an attempt to obtain lower concentrations for species such as N_2O , CFC-11, and CFC-12 in the polar lower stratosphere more in line with the observations obtained in the polar vortices during the Antarctic Airborne Ozone Experiment (AAOE) campaign. For simplicity, the smaller value was adopted globally and year round. Clearly, if the smaller values are restricted to the high latitudes and limited to certain seasons, the response could be somewhat different.

Figure 4.3-6 shows calculated profiles of CFC-11 from the four cases for August at 75°S compared to the AAOE measurements. The profiles at equinox for the Equator are shown in Figure 4.3-7. The cases with small K_{yy} predict CFC-11 profiles that are in better agreement with observations at polar latitudes. At the same time, the concentration at the Equator calculated under case 2 is large compared to case 1. Corresponding graphs for HCFC-22 are shown in Figures 4.3-8. Figure 4.3-9 shows the calculated column abundances of O_3 for the four cases. The results from cases 2 and 4 are distinctly different from observations with high columns predicted at high latitudes. Table 4.3-10 summarizes the calculated lifetimes and ODP values from the four cases. The calculated lifetime of CFC-11 is sensitive to the transport field, whereas the lifetime of HCFC-22 is less dependent. The ODP values for HCFC-22 for these cases reflect the impact of transport on the CFC-11 destruction process. Figure 4.3-10a shows that while there is an increase in ODP values at high latitudes for case 2 relative to case 1 (Figure 4.3-5c), the decrease at the tropics more than compensates for it in the global ODP value. Corresponding results for cases 3 and 4 are shown in Figures 4.3-10b and 4.3-10c.

In summary, the analysis presented here represents an attempt to quantify the sensitivity of the calculated ODP to model parameterization of transport. It is difficult to draw a definitive conclusion based on these limited number of simulations. The attempts to increase the ODP at high latitudes by using smaller K_{yy} lead to much smaller ODPs at the tropics because of decreased eddy transport. It is possible that there may be other combinations of circulation and K_{yy} that would change the ODP results significantly. These results did show that the same change in circulation would also have significant effects on the model-simulated ozone and other trace gas profiles. Comparison of these simulated results with available observations would provide a way to validate the ODP values.

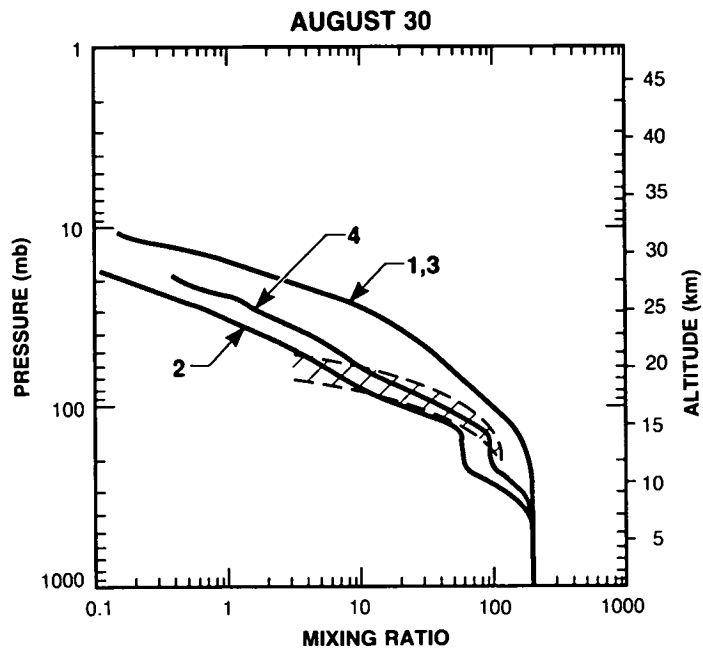


Figure 4.3-6. Calculated CFC-11 profiles from transport sensitivity study at 75° south at equinox (AER 2-D model). AAOE measurements indicated by cross hatch area.

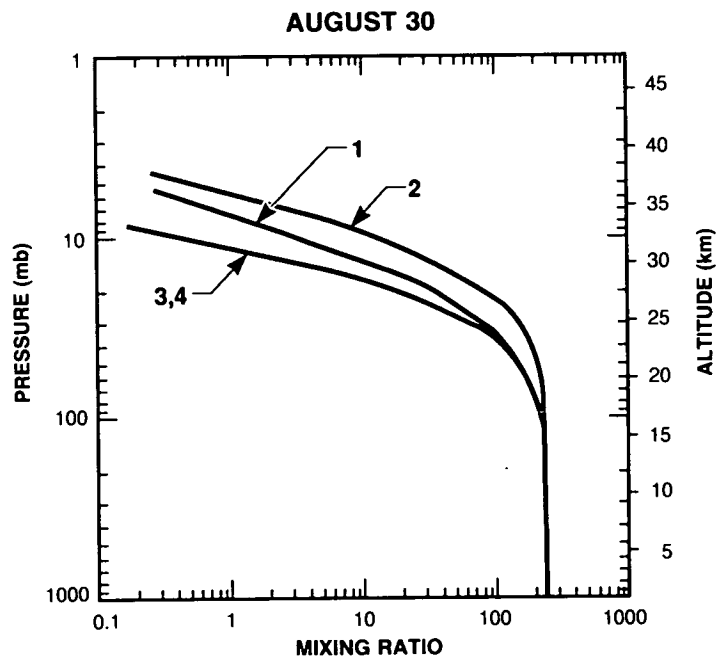


Figure 4.3-7. Calculated CFC-11 profiles from transport sensitivity study at Equator at equinox (AER 2-D model).

OZONE DEPLETION POTENTIALS

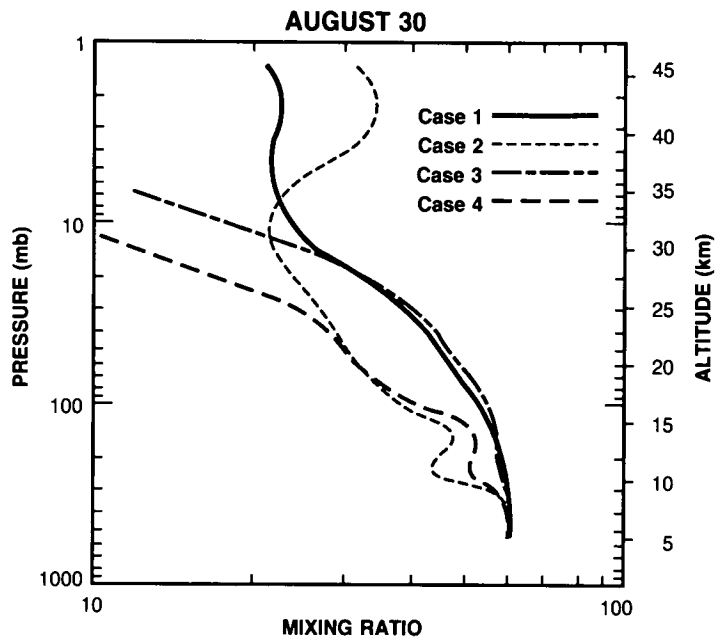


Figure 4.3-8a. Calculated HCFC-22 profiles from transport sensitivity study at 75° south equinox (AER 2-D model).

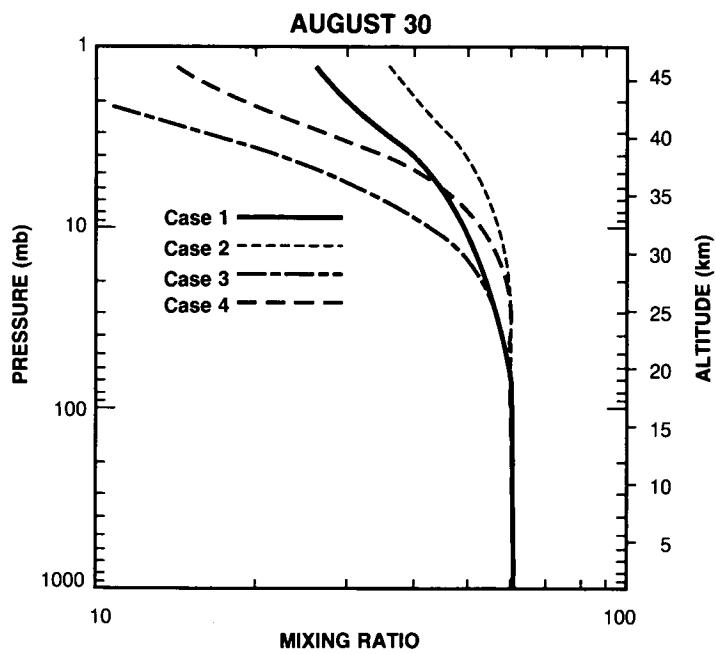


Figure 4.3-8b. Calculated HCFC-22 profiles from transport sensitivity study at the Equator at equinox (AER 2-D model).

OZONE DEPLETION POTENTIALS

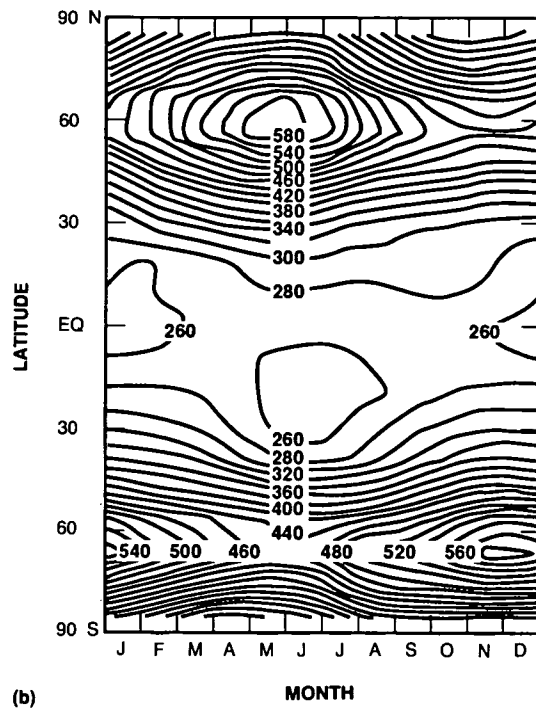
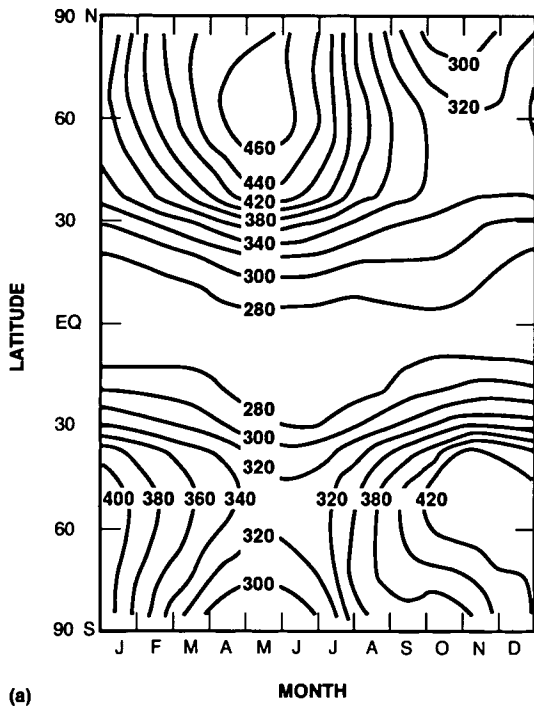


Figure 4.3-9a. i(a) Calculated total ozone abundance (Dobson Units) from transport sensitivity studies [case 1 of transport sensitivity study] (AER 2-D model). (b) Calculated total ozone abundance (Dobson Units) from transport sensitivity studies [case 2 of transport sensitivity study] (AER 2-D model).

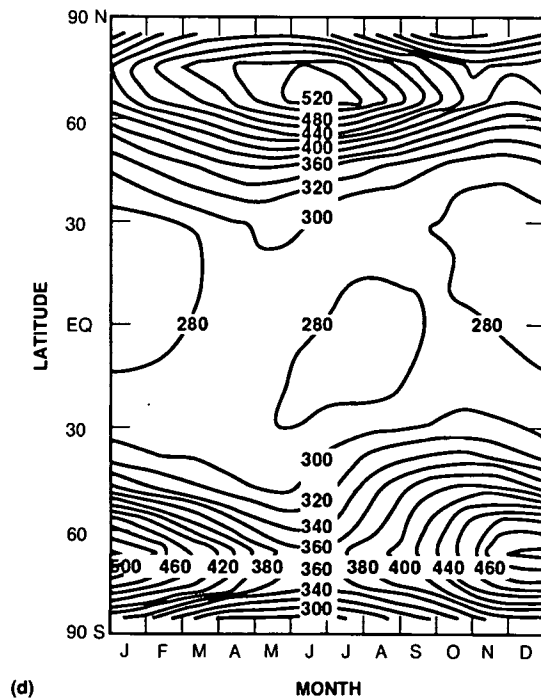
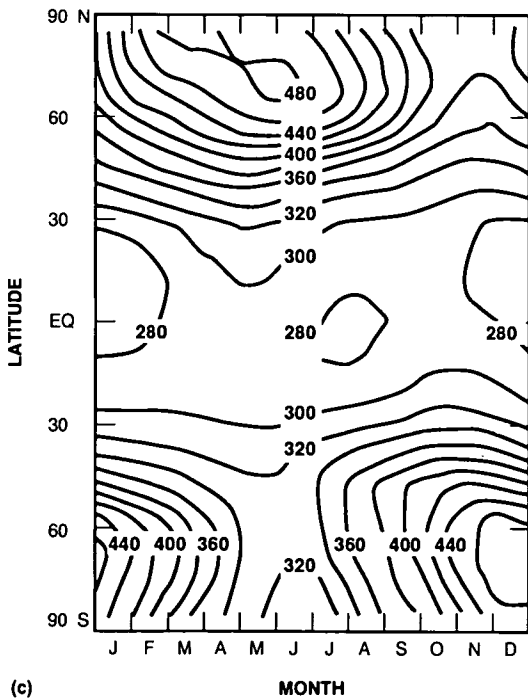


Figure 4.3.9b. ii(c) Calculated total ozone abundance (Dobson Units) from transport sensitivity studies [case 3 of transport sensitivity studies] (AER 2-D model). (d) Calculated total ozone abundance (Dobson Units) from transport sensitivity studies [case 4 of transport sensitivity study] (AER 2-D model).

OZONE DEPLETION POTENTIALS

Table 4.3-10. Results of transport sensitivity study (AER 2-D Model) on ODP and CLP for HCFC-22^a

	Case 1	Case 2	Case 3	Case 4
CFC-11 lifetime	47 years	34 years	51 years	44 years
HCFC-22 lifetime	24 years	22 years	24 years	23 years
ODP	0.07	0.035	0.055	0.034
CLP	0.27	0.35	0.25	0.28

^aThese calculations do not include the CH₃CCl₃ lifetime scaling included in Table 4.3-3.

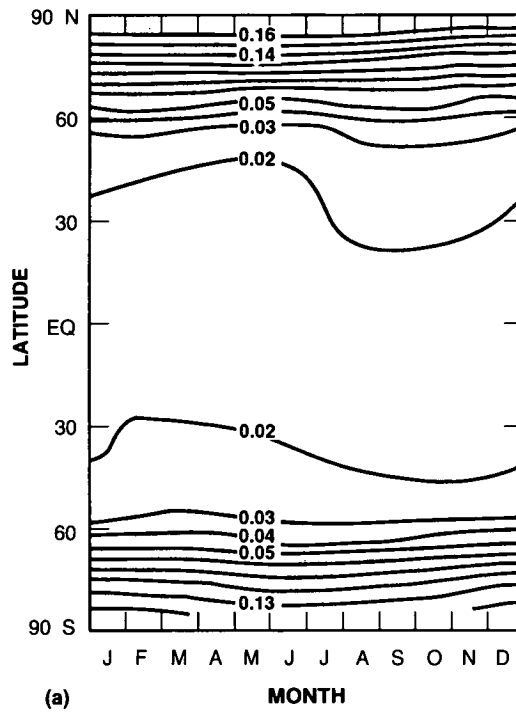


Figure 4.3-10a. Calculated latitudinal and seasonal relative ozone depletion from emission of HCFC-22 [case 2 of transport sensitivity study] (AER 2-D model).

OZONE DEPLETION POTENTIALS

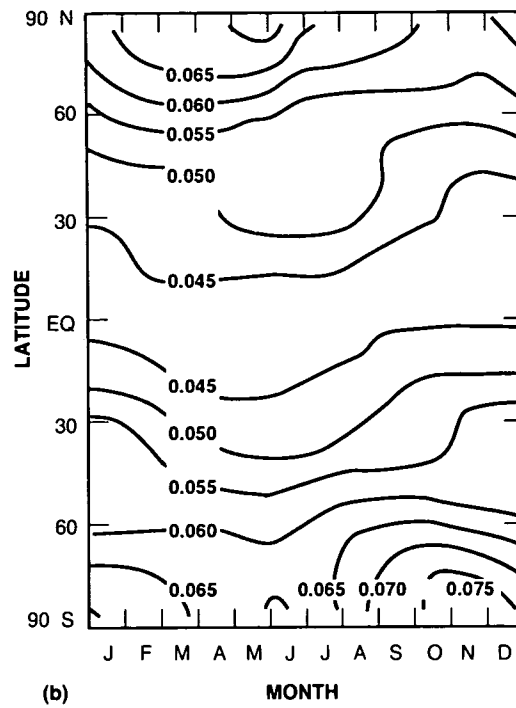


Figure 4.3-10b. Calculated latitudinal and seasonal relative ozone depletion from emission of HCFC-22 [case 3 of transport sensitivity study] (AER 2-D model).

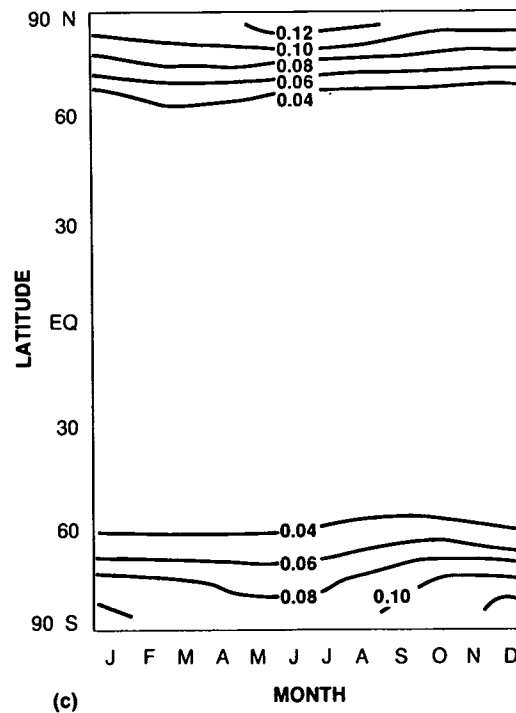


Figure 4.3-10c. Calculated latitudinal and seasonal relative ozone depletion from emission of HCFC-22 [case 4 of the transport sensitivity study] (AER 2-D model).

OZONE DEPLETION POTENTIALS

4.3.4.5 Time-Dependent Relative Ozone Depletion—Transient Effects

One of the limitations associated with the ODP parameter is that it is based on steady-state perturbations; it does not consider the relative time-dependent effects of different constituents on ozone. While we have shown that ODP is equivalently a measure of the cumulative chronic effects of unit-emitted mass of a gas over its life cycle in the atmosphere, we are also interested in the transient response at a constant emission level.

As mentioned earlier, ODP values determined at steady-state may not be representative of the relative transient effects expected for shorter-lived compounds during the early years of emission. During these early years, before one to two equivalent species lifetimes have passed, the ozone depletion per unit mass relative to CFC-11 can be much larger than the steady-state ODP value for some of the short-lived constituents. We note, however, that the changes in ozone occurring during the first few years after emissions are also relatively small compared to the steady-state ozone change. Relative time-dependent ozone depletions for several HCFCs and CFCs from the LLNL 1-D model are shown in Figure 4.3-11 and from the DuPont 1-D model in Figure 4.3-12. Results for the first few years are not shown because the derived changes in ozone were too small to be numerically accurate.

The transient values for relative ozone depletion and the time it takes to approach the steady-state values depend on the time-dependent behavior of the calculated O_3 decrease for the species examined and for the reference gas CFC-11. Since the atmospheric lifetimes of the HCFCs examined in this study are shorter than that of CFC-11, the time constant for exponential decay to the ODP asymptote is determined

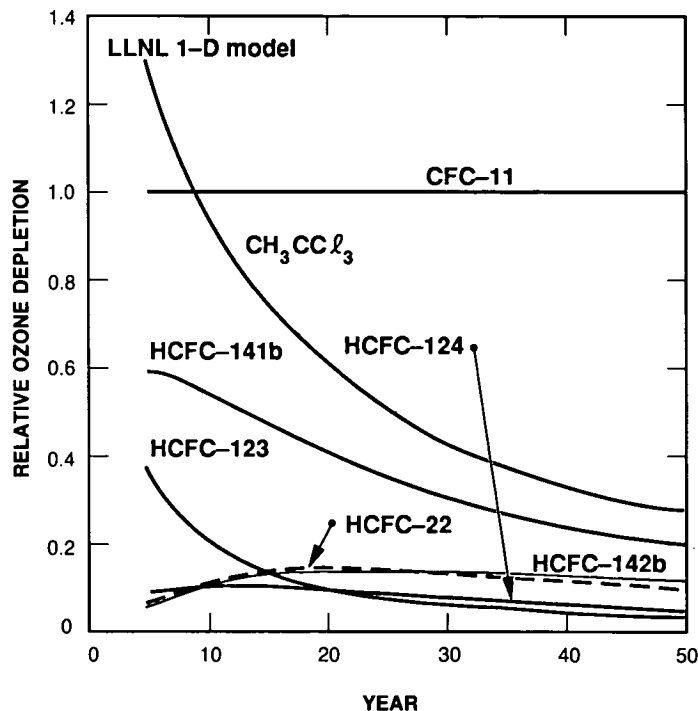


Figure 4.3-11. Calculated time-dependent change in relative ozone column depletion following a step change in emission of the tested halocarbons (LLNL 1-D model).

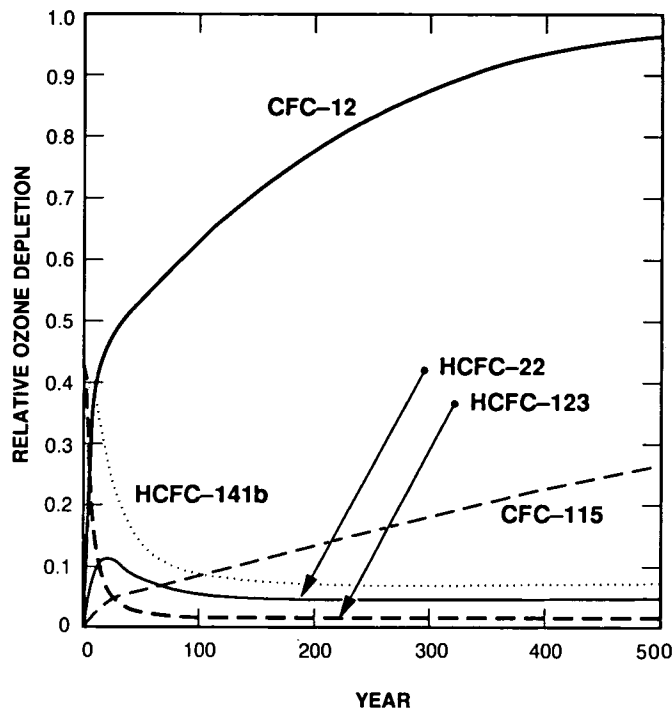


Figure 4.3-12. Calculated time-dependent change in relative ozone column depletion following a step change in emission of the tested halocarbons (DuPont 1-D model).

by the CFC-11 lifetime. The magnitude of the transient relative ozone depletion depends on the stratospheric lifetimes and how rapidly the chlorine atoms are released after transport into the stratosphere.

Several of the HCFCs, namely HCFC-123, HCFC-141b, and CH_3CCl_3 , have much larger relative ozone depletions at early times compared to the ODP values. Each of these gases has relatively short reaction-time constants within the stratosphere—compared to CFC-11. As a result, chlorine atoms are quickly released by these gases and the full effect on ozone is reached much sooner than CFC-11. At longer times, the relative ozone depletions asymptotically approach the ODP value.

Other species, such as HCFC-22, HCFC-124, and HCFC-142b, have long reactive time constants in the stratosphere. The time-dependent relative ozone depletions have much different behavior for these species. The relative ozone depletion builds gradually to a maximum value for these species, reflective of their long stratospheric time constants and the amount of time needed to build up stratospheric concentrations. After the first 20–40 years, the relative ozone depletion for these species gradually decays to the ODP value.

For gases with longer lifetimes than the reference gas, no maximum in relative ozone depletion is noted. This can be seen by examining the results for CFC-12 and CFC-115 in Figure 4.3-12.

Figure 4.3-13 shows the relative time-dependent behavior of chlorine being transported through the tropopause for these same gases (taken relative to CFC-11). In all the cases, the time-dependent strato-

OZONE DEPLETION POTENTIALS

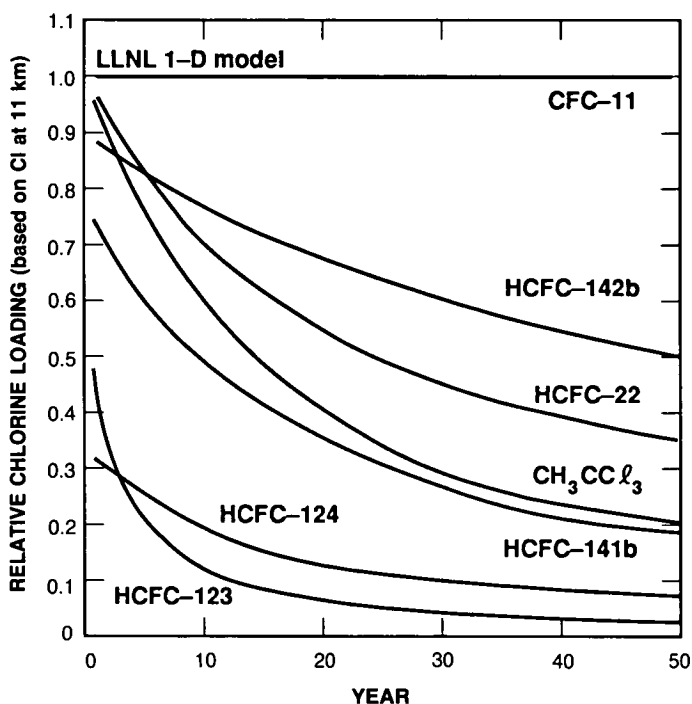


Figure 4.3-13. Calculated time-dependent relative chlorine loading following a step change in emission of the tested halocarbons (LLNL 1-D model).

spheric chlorine loading is much larger initially compared with the eventual steady-state relative Chlorine Loading Potential (CLP) value (given previously in Table 4.3-6) if the lifetime of the species is less than the reference gas.

In summary, time-dependent ozone depletion and chlorine loading values for the HCFCs are generally larger for the first 50 years than the ODP and CLP values defined at steady state. This, in part, arises from the longer atmospheric lifetime of the reference gas (CFC-11). Time-dependent relative ozone depletions for CFCs with lifetimes longer than CFC-11 show a monotonic increase to the steady-state ODP value.

4.3.5 Summary

One-dimensional and two-dimensional global atmospheric models have determined ODPs for a number of halocarbons, including CFCs, other chlorinated compounds, several potential replacement hydrohalocarbons, and several brominated compounds. Although 2-D models have generally a sounder physical basis, there are no real differences between 1-D and 2-D results. In general, the ODPs for fully halogenated compounds, such as the CFCs, are much larger than those for the hydrogenated halocarbons, which include the potential replacement compounds considered.

Brominated compounds should be compared with each other, because of the strong dependence of bromine effects on ozone to background chlorine levels. Bromine Ozone Depletion Potentials (BODPs)

are used for relative comparisons with Halon-1301, which has the longest lifetime and largest ODP, as the reference.

Although the calculated ODPs agree reasonably well among models, many uncertainties still exist. None of the models used for calculating ODPs include the chemical and dynamical processes causing the seasonal ozone losses over Antarctica. Another uncertainty lies in the model-calculated OH, which is a major source of uncertainty for both lifetimes and ODPs of the HCFCs.

Because of the apparent special chlorine processing and dynamics within the winter polar vortex, local Antarctic ODPs are expected to be larger than those derived. Insofar as the observed long-lived tracer distributions, such as CFC-11 in the polar vortex, suggest that much of the total chlorine may be available there, then an upper limit on Antarctic ODPs can be determined by calculating the relative amounts of chlorine transported through the tropopause by the different gases. These CLPs determined using assumed reference lifetimes (which generally agree with those in the models used here) can be as large as a factor of two to three times the derived ODP values. The ramifications of polar ozone depletion for global ODPs are not currently clear.

The time-dependent relative ozone depletion values differ from the steady-state ODP values. The time-dependent values depend on the atmospheric lifetime and the transport time to the region of destruction of the gas. The shorter the stratospheric lifetime, the sooner the gas will impact stratospheric ozone and hence the higher the transient relative ozone depletion. For example, HCFC-123 has a shorter lifetime than CFC-11; its relative ozone depletion is largest soon after emission. Other gases in this category include HCFC-141b and CH_3CCl_3 . Species such as HCFC-22, HCFC-124, and HCFC-142b have somewhat longer time constants in the stratosphere. Their relative ozone depletions build slowly to values (based on their time constants) as large as 0.2 and then decay slowly with time to the derived steady-state ODP value. Relative ozone depletion values for HCFCs are greater than ODP values even after 30 to 50 years. Time-dependent relative ozone depletions for CFCs with lifetimes longer than CFC-11 show a monotonic increase to the ODP value. The ODP is the cumulative response; as discussed above, the transient response of relative ozone depletion may be larger than the ODP value at early times after emission.

Several of the halocarbons indicate a strong latitude dependence in their ODP values and a generally weaker seasonal variation. In particular, ODPs for species such as CFC-12, HCFC-22, HCFC-124, and HCFC-142b, which have stratospheric loss patterns very different from CFC-11, produce strong latitudinal gradients in ODPs, with the largest ODPs near summer poles and smallest values in the tropics. The effects of heterogeneous chemistry and polar dynamical effects could modify these findings.

Sensitivity analyses indicate that ODPs are affected to only a minor degree ($\leq 20\%$) by assumed variations in background levels of N_2O , CH_4 , CO_2 , CO , total stratospheric chlorine, and total stratospheric bromine.

4.4 HALOCARBON GLOBAL WARMING POTENTIALS

4.4.1 Background

The radiative perturbations and potential climatic effects due to the infrared absorption properties of chlorofluorocarbons (CFC-11 and CFC-12) have been assessed in WMO (1985). That assessment and those from accompanying studies (Wang and Molnar, 1985; Owens et al., 1985; Ramanathan et al., 1985, 1987;

OZONE DEPLETION POTENTIALS

Fisher et al., 1989c) demonstrated that the direct radiative forcing (i.e., one in which all parameters are held fixed while the concentration of any CFCs is increased from 0 to 1 ppbv), consists of an increase in the downward longwave flux at the surface (surface radiative forcing) and a decrease in the net upward flux at the tropopause (surface-troposphere net radiative forcing). This imbalance results in a net increase in the amount of longwave radiation trapped within the Earth's atmosphere system, thereby potentially enhancing the greenhouse effect.

Since the 1985 reports, infrared spectral absorption data of several halogenated compounds have become available (Magid, private communication, 1988 and Gehring, private communication, 1988) which not only include CFCs, but also include HFCs and HCFCs. Interest in the latter two classes of compounds stems from their role as potential replacement compounds for CFCs. Laboratory measurements show that all the halogenated compounds possess significant absorption in the 500–1400 cm^{-1} ("window") region. The absorption spectrum for any of these species typically is one of individual lines spaced very closely together in an arbitrary frequency interval giving the appearance of a continuum structure. The absorption cross sections of the HFCs and HCFCs also occur at similar frequencies in the "window" region and are comparable in magnitude to those for CFCs.

Because the absorption bands of all replacement halogenated compounds fall in the infrared "window" region, the potential greenhouse effects need to be assessed. This need is emphasized by the fact that the clear portions of the Earth's atmosphere have virtually no other constituents (excepting aerosols) with major absorption bands in the "window" region. In overcast conditions, clouds also have absorption bands in this region. Furthermore, the Earth's outward-going radiation is at a maximum near the "window" region for the Earth's surface temperatures. Therefore, the presence of halogenated compounds could play an important part in determining the radiation balance in the clear portion of the atmosphere and a non-negligible role in the overcast portions.

Besides the influence on the infrared radiative fluxes, there is yet another aspect of the perturbations by the halogenated compounds, as pointed out in WMO (1985). This is the heating perturbations induced in the upper troposphere and lower stratosphere which, owing to the large radiative time constant of those regions of the atmosphere, have the potential to increase the temperatures there. Any change in the temperatures near the tropopause region is of potential significance for the tropospheric-stratospheric exchange of water vapor.

The effectiveness of greenhouse gases is accentuated by their lifetimes and in large part by their corresponding atmospheric abundances.

In this report, we consider the most recently available laboratory spectral data of the halogenated compounds and assess the following:

- the direct radiative forcing due to the halogenated compounds, as evaluated by both line-by-line (GFDL) and band models (AER, DuPont),
- the changes in the surface temperature, as evaluated by the one-dimensional radiative-convective models (AER, DuPont), and
- the relative changes in the surface temperatures taking into account the chemical lifetimes of the compounds expressed as Greenhouse Warming Potentials.

The GFDL line-by-line radiative transfer model has been developed from that described in Schwarzkopf and Fels (1989). The band models employed in the AER and DuPont algorithms have been described earlier (Wang and Molnar, 1985; Owens et al., 1985). The absorption cross sections of the halogenated compounds are incorporated in a manner similar to the water vapor continuum. It should be noted that in the absence of a temperature-dependent dataset, none of these algorithms incorporate temperature dependence in calculated radiative effects.

No attempt is made to calculate Greenhouse Warming Potentials for non-halocarbon gases such as carbon dioxide and methane. Due to their current atmospheric concentrations and the spectral locations of their infrared absorption bands, calculated global warming is not proportional to atmospheric concentration changes of these gases. In contrast, calculated warmings are linearly proportional to halocarbon concentrations.

4.4.2 Definition of Halocarbon GWP

Halocarbon Global Warming Potential (Halocarbon GWP) is defined parallel to the Ozone Depletion Potential. It is defined as the ratio of steady-state calculated warming for each unit mass of a gas emitted into the atmosphere (as indicated by the change in infrared flux at the tropopause) relative to the calculated warming for a mass unit of reference gas CFC-11. This definition was chosen as a representative measure of the potential of a compound to effect global warming, since:

1. It provides a measure of the cumulative effect on the radiative balance over its chemical lifetime for each unit released into the atmosphere (see below).
2. The Halocarbon GWP yields a single value for each compound rather than a time-varying multitude of values.
3. It provides a measure of the maximum calculated effect of a compound compared to the maximum calculated effect of CFC-11 on an equal mass basis.

The first reason is perhaps the most important in that it estimates the cumulative effect on potential global warming of each unit released. An illustrative test was performed which quantified the chronic effect from a single pulsed release of test gas into the atmosphere. This particular test used the DuPont model to calculate cumulative global warmings over a 500-year time period following emissions of HCFC-123, HCFC-22, and CFC-11.

The calculated cumulative warmings are shown in Figure 4.4-1. For each case, the modeled warming is maximum very soon after the release and exponentially decays with a time constant equal to the atmospheric lifetime of the species. As seen in the insert table, the time-integrated warmings echo the relative values of the Halocarbon GWP calculated from steady-state figures.

In order to make the definition of Halocarbon GWP consistent between models as well as a conservative estimate of relative effects, the following criteria have been selected:

1. Trace gas levels—Changing the concentration of other trace gases could affect the calculated future equilibrium temperature rise from gases under evaluation here for two reasons. First, if there is overlap of absorption spectra, certain frequency bands would have less effect. Secondly, chemistry and therefore lifetime can be affected by perturbation of these chemicals. Current levels of CO₂, CH₄, N₂O, O₃, and stratospheric H₂O were used in model calculations.

OZONE DEPLETION POTENTIALS

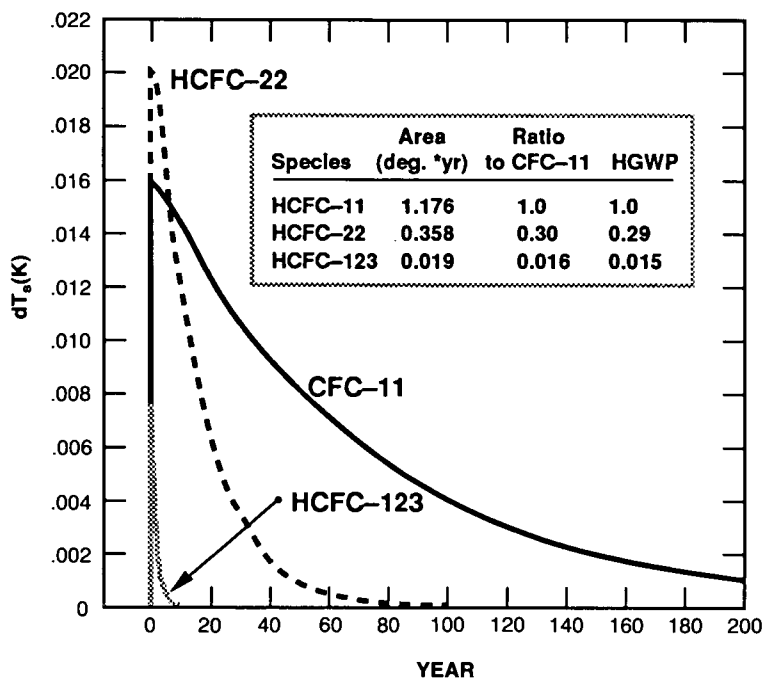


Figure 4.4-1. Calculated change in surface temperature following a pulsed emission of 5×10^9 kg of specified gas.

2. Radiative forcing level—The calculations are based on gas concentrations that yield modeled responses large enough to avoid the “noise levels” of the numerical models, yet small enough to be in the linear response region.
3. Reference gas—CFC-11 has been chosen as the reference compound for Halocarbon GWP calculations in order to have a reference material consistent for both Halocarbon GWP and ODP.

Furthermore, additional parameters are useful in order to facilitate discussion:

4. Net initial IR flux perturbation at the tropopause will be symbolically represented as dF (per unit mixing ratio in the troposphere).
5. Specific Surface Temperature Change—The calculated surface temperature increase for a one part per billion (by volume) surface increase of any gas is defined as the specific surface temperature change, or symbolically dT_s .
6. The climate feedback factor (Dickinson, 1982), represented by λ , is the ratio of the model-calculated surface temperature change to a perturbation in the net radiative forcing (discussion follows).

The response of the Earth’s surface atmosphere to a radiative forcing exerted by the presence of the halogenated compounds involves several feedback mechanisms and can be expressed as:

$$dT_s = \lambda dF$$

where dT_s is a measure of the climate response. The factor λ depends on mechanisms not all of which are quantitatively understood. Nevertheless, as stated in WMO (1985), λ can be expected to be in the range of $0.25-1 \text{ K/W m}^{-2}$. Studies surveyed by Ramanathan et al. (1985) have two values ranging from 0.47–0.53, while the DuPont and AER models have a λ of 0.64, and 0.81, respectively. It must be realized that the range in λ stated above is not a rigid bracketing. Two important aspects of climate modeling severely restrict our present ability to better quantify λ precisely. One is the lack of understanding of the response of the ocean circulation and the ensuing effects on the atmosphere. The second is the lack of knowledge of the changes in the cloud amounts and cloud properties due to changes in the halocarbon radiative forcing. Our knowledge in both the areas needs to improve substantially in order to better quantify λ .

The Halocarbon GWP definition resembles the ODP definition. For any gas, the general definition is:

$$\text{Halocarbon GWP} = \frac{\text{Calculated IR forcing due to compound X} / \text{Emission rate (steady state) of compound X}}{\text{Calculated IR forcing due to CFC-11} / \text{Emission rate (steady state) of CFC-11}}$$

Note, since lifetimes are proportional to the ratio of atmospheric abundance to (molecular weight * emission rate), an equivalent form of this definition is:

$$\text{Halocarbon GWP} = \frac{[dF(x) * \text{Lifetime}(x) / \text{Molecular weight}(x)]}{[dF(\text{CFC-11}) * \text{Lifetime}(\text{CFC-11}) / \text{Molecular weight}(\text{CFC-11})]}$$

(This formula has been used to calculate Halocarbon GWP from the line-by-line radiative model results.)

Since radiative-convective models calculate a change in surface temperature, it is useful to express an equivalent form of the Halocarbon GWP, assuming the same value of λ for all gases, as:

$$\text{Halocarbon GWP} = \frac{[dT_s(x) * \text{Lifetime}(x) / \text{Molecular weight}(x)]}{[dT_s(\text{CFC-11}) * \text{Lifetime}(\text{CFC-11}) / \text{Molecular weight}(\text{CFC-11})]}$$

Note also, many of these gases have the potential of affecting heating rates indirectly as well, since they can chemically influence the distribution of ozone. Examination of model results indicates that this is a second order effect, at least two orders of magnitude below the IR effect and well below the sensitivity of these calculations (Wang et al., 1989).

4.4.3 Model-Calculated Halocarbon GWPs

A primary input to these radiative calculations are the altitudinal steady-state concentration profiles which are calculated using appropriate chemistry models.

After the concentration profile is determined, the effect of each gas is calculated using a radiative model. This calculation accounts for the amount of energy absorbed by each IR gas over the radiation spectrum and accounts for the spectral overlap with other IR active gases. Quantitative infrared data for this input are available (see Fisher et al., 1989c).

Table 4.4-1 shows the net IR radiative flux at the tropopause ($\cong 12 \text{ km}$) for a 1 ppbv tropospheric mixing ratio, as calculated by each of the three models. Note that each of the model's calculations was

OZONE DEPLETION POTENTIALS

Table 4.4-1. Net IR radiative flux at the tropopause (at 12 km) [Wm^{-2}] for 1 ppbv tropospheric mixing ratio of each gas

Species	AER ^a	DuPont ^b	GFDL ^c
CFC-11	0.175	0.133	0.35 (0.22) ^d , (0.30) ^e
CFC-12	0.248	0.158	0.42
CFC-113	0.223	0.163	0.42
CFC-114	0.258	0.181	
CFC-115	0.204	0.164	0.44
HCFC-22	0.151	0.107	0.29
HCFC-123	0.140	0.092	0.28
HCFC-124	0.153	0.108	
HFC-125	0.189	0.119	
HFC-134a	0.135	0.095	0.26
HCFC-141b	0.109	0.076	0.22
HCFC-142b	0.144	0.101	0.27
HFC-143a	0.111	0.087	
HFC-152a	0.092	0.059	0.17
CCl ₄	0.080	0.063	
CH ₃ CCl ₃	0.038	0.033	
[2 × CO ₂]	4.41	3.87	5.68

Note difference in base assumptions:

^aAER calculations based on

—global mean conditions

—48.5% cloud cover

—cloud with spectral optical thickness at 0.55 μm of 8.9. (cloud albedo = 0.54)

^bDuPont calculations based on

—global mean conditions

—50% cloud cover

—cloud albedo = 0.5

^cGFDL calculations based on

—mid-latitude, summer atmosphere

—clear sky conditions

—uniform gas mixing ratio

^dCFC-11 only in troposphere

^eCFC-11 only in troposphere, with 50% black cloud cover at ~4 km

based on different cloud assumptions (GFDL used a clear sky, DuPont used 50% cloud cover [albedo = 0.5], and the AER was based on control climate cloud field with 48.5% cloud cover). Note also that the GFDL model assumed mid-latitude summer radiative conditions, whereas both AER and DuPont models are based on globally and annually averaged radiation.

Specific surface warmings are calculated using the AER and DuPont radiative convective models and are shown in Table 4.4-2 for each of these gases. Again differences in the λ factors between these models yield a systematic difference in the response of surface warming to net radiative flux changes for each compound. Note that HCFCs and HFCs on the average have lower specific surface warming values than

OZONE DEPLETION POTENTIALS

Table 4.4-2. Specific surface temperature (dT_s) increases and lambda (λ) values resulting from 1 ppbv of each gas

Species	dT _s (°K/ppbv)		λ (°K/ppbv/Wm ⁻²)	
	AER	Du Pont	AER	Du Pont
CFC-11	0.135	0.084	0.771	0.632
CFC-12	0.202	0.102	0.815	0.647
CFC-113	0.174	0.103	0.780	0.632
CFC-114	0.208	0.115	0.806	0.635
CFC-115	0.170	0.107	0.833	0.652
HCFC-22	0.124	0.070	0.821	0.650
HCFC-123	0.111	0.059	0.793	0.644
HCFC-124	0.126	0.070	0.824	0.645
HFC-125	0.160	0.078	0.847	0.654
HFC-134a	0.114	0.061	0.844	0.647
HCFC-141b	0.086	0.048	0.789	0.637
HCFC-142b	0.120	0.066	0.833	0.651
HFC-143a	0.092	0.054	0.829	0.625
HFC-152a	0.076	0.038	0.826	0.649
CCl ₄	0.062	0.040	0.775	0.628
CH ₃ CCl ₃	0.027	0.020	0.710	0.618
[2 × CO ₂]	[3.08]	[1.651]		

CFCs by approximately 40%. (Net dF values are also lower by ~40%.) Although total absorptances are about equivalent for each class of compounds, overlap with absorptance bands of other infrared active gases diminishes the efficiencies of these gases as greenhouse gases. Most of the hydrogenated halocarbons have bands that overlap the bands of both CH₄ and N₂O as well as water vapor above 1250 cm⁻¹.

Table 4.4-3 shows the Halocarbon GWP values calculated by each of the three models. Reference lifetimes are based on the estimates used in scenarios developed in Section 3.3.1 for CFCs and from the analysis in Section 4.2 for HCFCs and HFCs.

Halocarbon GWPs for fully halogenated compounds are larger than those for the hydrogenated halocarbons. Fully halogenated CFCs have Halocarbon GWP values ranging from 1.0 to 7.5, whereas HCFCs and HFCs range from 0.02 to 0.7.

Halocarbon GWP values differ between species due to differences in infrared absorbances and differences in lifetimes. The range of absorbances is approximately 4, while the lifetimes range by a factor of 250. Thus, the range of 400 among the Halocarbon GWP values is primarily a result of differences in lifetimes. Additionally, the Halocarbon GWP for halon-1301 has been calculated based on specific surface warmings reported in WMO 1985 and a relative lifetime (to CFC-11) of 1.3 (from LLNL 1-D and Oslo 2-D models). This Halocarbon GWP value is 1.4.

OZONE DEPLETION POTENTIALS

Table 4.4-3. Halocarbon global warming potentials

Species	Reference ^a Lifetime (Yrs)	AER ^b	DuPont ^b	GFDL ^b
CFC-11	60.0	1.0	1.0	1.0
CFC-12	120.0	3.4	2.8	2.7
CFC-113	90.0	1.4	1.4	1.3
CFC-114	200.0	4.1	3.7	
CFC-115	400.0	7.5	7.6	7.5
HCFC-22	15.3	0.37	0.34	0.34
HCFC-123	1.6	0.02	0.017	0.019
HCFC-124	6.6	0.10	0.092	
HFC-125	28.1	0.65	0.51	
HFC-134a	15.5	0.29	0.25	0.26
HCFC-141b	7.8	0.097	0.087	0.096
HCFC-142b	19.1	0.39	0.34	0.34
HFC-143a	41.0	0.76	0.72	
HFC-152a	1.7	0.033	0.026	0.029
CCl ₄	50.0	0.34	0.35	
CH ₃ CCl ₃	6.3	0.022	0.026	

^aLifetimes are based on estimates used in scenario development (Chapter 3, Section 3.2.1) for CFCs and from the analysis in Section 4.2 for HCFCs and HFCs.

^bAER and DuPont results are based on surface temperature perturbations calculated using radiative-convective models; GFDL results are based on line-by-line determined radiative forcing.

4.4.3.1 Sensitivity to Trace Gas Levels

The Halocarbon GWP values have all been based on calculations that assume present-day values for concentrations of trace gases of CO₂, CH₄, CO, N₂O, and CFCs. Because the Halocarbon GWP values are for consideration with future atmospheres different from today, we have examined the sensitivity of these parameters to changes in CO₂ and CH₄ at levels that might be achieved if current trends continue.

Trace gas changes and the resulting calculated changes in lifetimes, surface temperature rises, and Halocarbon GWP values (from the AER model) are shown in Table 4.4-4. Calculated changes in surface temperature for tested CFCs and HCFCs were compared to a reference atmosphere including the assumed gas perturbation (note the Halocarbon GWP values are different than listed above, since they are based on model-calculated lifetimes rather than reference lifetime values).

As seen in Table 4.4-4, trace gas changes have little effect on Halocarbon GWP values. CO₂ has the greatest effect on CFC radiative forcing because the albedo feedback is weaker in the warmer atmosphere. As a result, the radiative forcing for CFC-11 and -12 is somewhat weakened. Methane affects the chemical lifetimes of the HCFCs, resulting in slightly greater Halocarbon GWP values for these compounds. Nevertheless, these relatively major perturbations in trace gas levels have only minor effect on calculated Halocarbon GWP values, indicating that the GWP formalism is robust over the range of trace gases projected for the next century.

Table 4.4-4. Sensitivity study—variation in trace gas levels and impact on halocarbon GWP values (AER 1-D model)

	Atmosphere	Species			
		CFC-11	CFC-12	HCFC-22	HCFC-123
Lifetime (yrs)	Present Day	60	125	20	2.1
	CH ₄ (1.6 → 3.2 ppbv)	60	126	23	2.5
	CO ₂ (340 → 680 ppm)	61	128	20	2.1
dT _s (°K/ppbv)	Present Day	0.14	0.20	0.12	0.11
	CH ₄ (1.6 → 3.2 ppbv)	0.14	0.20	0.12	0.11
	CO ₂ (340 → 680 ppm)	0.12	0.17	0.12	0.11
GWP	Present Day	1.0	3.5	0.49	0.026
	CH ₄ (1.6 → 3.2 ppbv)	1.0	3.5	0.56	0.031
	CO ₂ (340 → 680 ppm)	1.0	3.4	0.49	0.027

4.4.3.2 Time Dependency of Relative Global Warming

Since the Halocarbon GWP parameter is based on steady-state effects, it does not describe the relative time-dependent effects of constituents on warming. Even though the Halocarbon GWP is an equivalent measure of the cumulative warming during its lifetime for each unit mass emitted, the transient response to a constant emission level is also of interest.

The calculated warmings for a number of halocarbons are shown in Figure 4.4-2. As seen, the calculated warming reaches an asymptote rapidly for the HCFCs, but requires longer periods to approach steady-state for CFCs. These response patterns echo the respective patterns for increases in atmospheric abundances for each species, seen in Figure 4.4-3.

Relative warmings are shown in Figure 4.4-4. For HCFCs, the relative effects are at a maximum at very short times. One can easily show (using L'Hospital's rule) that the initial relative value is the ratio of the value of the specific surface temperature increase ([°K/ppbv] / molecular weight—relative to the same ratio for CFC-11). Thus initially, while the individual effects are small, the relative effects are on the order unity. However, as atmospheric concentrations build and chemistry differences affect the relative amount in the atmosphere, the relative effects either grow or decrease depending on whether the lifetimes are longer or shorter than that of CFC-11. As seen in Figure 4.4-4, the HCFCs have lifetimes shorter than the lifetime of the reference gas and have relative effects that asymptotically approach the Halocarbon GWP value with a time constant equal to the lifetime of CFC-11. Longer-lived species have relative effects that grow with time, asymptotically approaching their Halocarbon GWP value with time constant for their own lifetime.

4.4.4 Uncertainties

Uncertainties in the effectiveness of gases to produce global warming fall into two general classes—those that are generalized for the entire greenhouse effect and those that are specific to individual species.

OZONE DEPLETION POTENTIALS

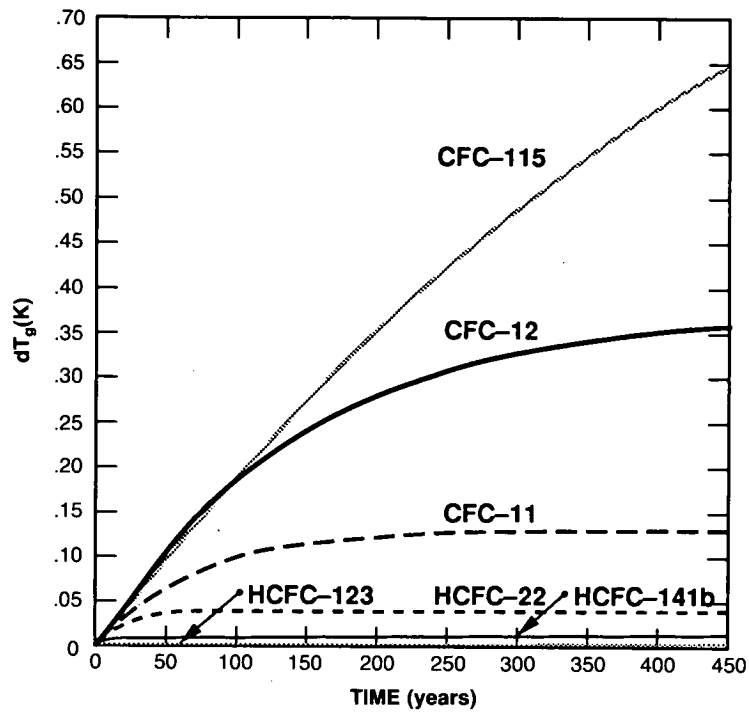


Figure 4.4-2. Change of calculated warming following a step change of emission of specified gas at 5×10^8 kg/yr (DuPont 1-D model).

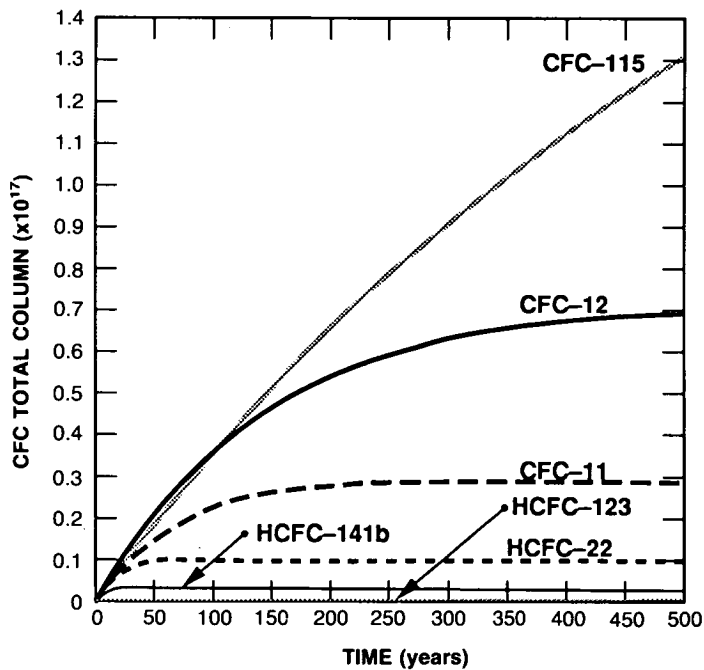


Figure 4.4-3. Column of (hydro) chlorofluorocarbons following a step change of emission of specified gas at 5×10^8 kg/yr (DuPont 1-D model).

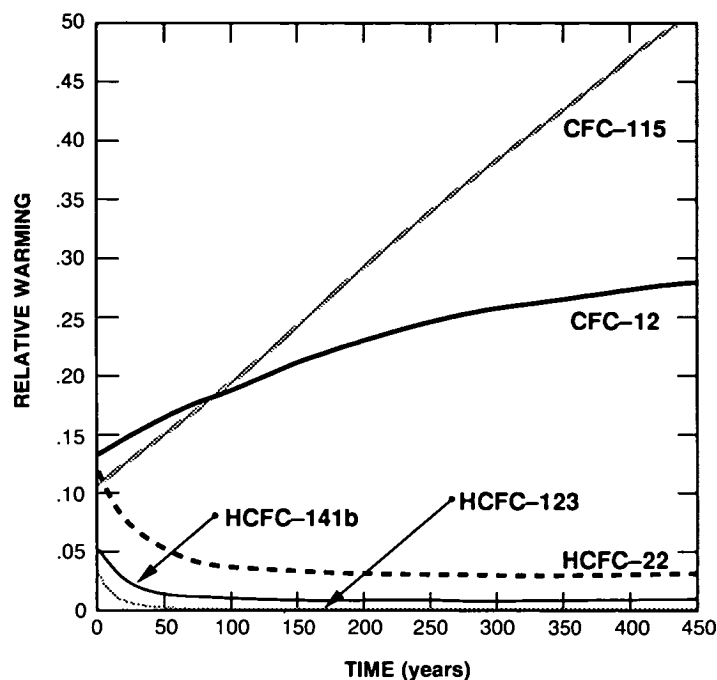


Figure 4.4-4. Calculated relative warmings following a step change of emission of specified gas [CFC-11 reference] (DuPont 1-D model).

There are a number of uncertainties in the modeling of greenhouse warming. These concern the radiative properties of the Earth's surface-atmosphere system, such as changes in the surface and ice cover albedos, and changes in cloud cover and composition. Changes in the temperature structure of the atmosphere will affect the convective patterns and chemistry of the stratosphere. The coupling of oceans (as heat reservoirs) and ocean currents to surface temperature changes will also affect the timing and location of the warming. Research is being carried out to understand these questions, which apply to all gases that affect the future radiative balance of the Earth.

Uncertainties also exist regarding the individual species and their influence on the radiative balance. Temperature dependence of the absorptances of individual species need to be resolved and modeled. The chemical processes affecting both lifetimes and atmospheric profiles are also the subject of continuing research. Resolution of questions related to the general greenhouse warming modeling will directly affect timing and magnitude of global warming, whereas resolution of the radiative and chemical parameterizations for halocarbons will have a direct impact on the Halocarbon GWP values for these species.

4.4.5 Summary

Halocarbon Global Warming Potentials have been defined and calculated in order to allow estimates of the relative environmental effects of halocarbons. The results presented here indicate that the Halocarbon GWPs depend primarily on the atmospheric lifetime of the compounds and to a lesser degree on the molecular IR absorption characteristics.

OZONE DEPLETION POTENTIALS

The reduction in Halocarbon GWP that might be expected due to use replacement of a CFC by a hydrohalocarbon can be estimated by taking the ratio of the Halocarbon GWP of the hydrohalocarbon to the Halocarbon GWP of the CFC it would replace. For example, the reduction in Halocarbon GWP in replacing uses of CFC-12 by HCFC-134a is $(0.26 \pm 0.030)/(3.07) = 0.085 \pm 0.01$. Of course, the relative quantities of the compound required in the use application must also be taken into account.

Although the Halocarbon GWP values reported here agree reasonably well among models, uncertainties in the values still exist because of the uncertainties in modeled chemistry and dynamics and their direct effect on the chemical lifetimes of these compounds.

Halocarbon GWP values appear to be reasonably robust parameters since their calculated values are nearly insensitive to assumed concentrations of other radiative gases. The minor shifting of the Halocarbon GWP values is primarily influenced by the changes in calculated lifetimes and therefore the abundance in the atmosphere.

Calculated time-dependent relative global warmings for Halocarbons are initially on order unity but decrease or increase depending on whether their lifetimes are shorter or longer than that of the reference gas. At longer times, the relative global warmings asymptotically approach the Halocarbon GWP values.

REFERENCES

- Blake, D. R., and F. S. Rowland, Continuing worldwide increase in tropospheric methane, 1978 to 1987, *Science*, 239, 1129–1131, 1988.
- Bojkov, R. D., Surface ozone during the second half of the nineteenth century, *J. Climate and Appl. Meteor.*, 25, 343–352, 1986.
- Chameides, W. L., and J. C. G. Walker, A photochemical theory of tropospheric ozone, *J. Geophys. Res.*, 78, 8751–8760, 1973.
- Chameides, W. L., S. C. Liu, and R. C. Cicerone, Possible variations in atmospheric methane, *J. Geophys. Res.*, 82, 1795–1798, 1977.
- Connell, P. S., and D. J. Wuebbles, "Evaluating CFC Alternatives From the Atmospheric Viewpoint," Air and Waste Management Association paper 89-5.7, 1989; also Lawrence Livermore National Laboratory report UCRL-99927 Rev.1, 1989.
- Cox, R. A., and R. G. Derwent, Gas phase chemistry of the minor constituents of the troposphere, in *Specialist Periodic Report Gas Kinetics and Energy Transfer*, Vol. 4, The Royal Society of Chemistry, London, pp. 189–232, 1981.
- Crutzen, P. J., A discussion of the chemistry of some minor constituents of the stratosphere and troposphere, *Pure and Applied Geophys.*, 106–108, 1385–1399, 1973.
- Crutzen, P. J., Photochemical reactions initiated by and influencing ozone in unpolluted tropospheric air, *Tellus*, 26, 47–57, 1974.
- Crutzen, P. J., Tropospheric ozone: An overview, in *Tropospheric Ozone: Regional and Global Scale Interactions*, edited by I. S. A. Isaksen, NATO ASI Series C, D. Reidel, Dordrecht, 1988.
- Crutzen, P. J., and C. Bruhl, The impact of observed changes in atmospheric chemistry and climate, in *The Environmental Record in Glaciers and Ice Sheets*, edited by H. Oeschger and C. C. Langway, Jr., Wiley, New York, pp. 249–266, 1989.
- Crutzen, P. J., and J. Fishman, Average concentrations of OH in the troposphere, and the budgets of CH₄, CO, CH₃CCl₃, *Geophys. Res. Lett.*, 4, 321–324, 1977.

- Cunnold, D. M., R. G. Prinn, R. A. Rasmussen, P. G. Simmonds, F. N. Alyea, C. A. Cardelino, A. J. Crawford, P. J. Fraser, and R. D. Rosen, Atmospheric lifetime and annual release estimates for CCl_3F and CCl_2F_2 from five years for ALE data, *J. Geophys. Res.*, *91*, 10797–10817, 1986.
- Davidson, J. A., H. I. Schiff, T. J. Brown, and C. J. Howard, Temperature dependence of the rate constants for reactions of O(¹D) atoms with a number of halocarbons, *J. Chem. Phys.*, *69*, 4277–4279, 1978.
- DeMore, W. B., M. J. Molina, S. P. Sander, D. M. Golden, R. F. Hampson, M. J. Kurylo, C. J. Howard, and A. R. Ravishankara, *Chemical Kinetics and Photochemical Data for Use in Stratospheric Modeling*, JPL Publication 87–41, pp. 196, Jet Propulsion Laboratory, Pasadena, CA, 1987.
- Derwent, R. G., and A. R. Curtis, "Two-Dimensional Model Studies of Some Trace Gases and Free Radicals in the Troposphere," AERE report R8853, H.M. Stationery Office, London, 1977.
- Derwent, R. G., and A. E. J. Eggleton, Two-dimensional model studies of methyl chloroform in the troposphere, *Quart. J. Roy. Met. Soc.*, *107*, 231–242, 1981.
- Derwent, R., and A. Volz-Thomas, The tropospheric lifetime of halocarbons and their reactions with OH radicals: an assessment based on the concentration of ¹⁴CO, in *Alternative Fluorocarbons Environmental Acceptability Study (AFEAS)*, Vol. II, Appendix, this report (1990), 1989.
- Dickinson, R. E., Modeling climatic changes due to carbon dioxide increases, in *Carbon Dioxide Review*, edited by W.C. Clark, pp. 101–133, Clarendon Press, New York, 1982.
- Dorn, H. P., J. Callies, U. Platt, and D. H. Ehhalt, Measurement of tropospheric OH concentrations by laser long-path absorption spectroscopy, *Tellus*, *40B*, 437–445, 1988.
- Ehhalt, D. H., How has the atmospheric concentration of CH_4 changed? in *The Changing Atmosphere*, edited by F. S. Rowland and I. S. A. Isaksen, Wiley-Interscience, New York, pp. 25–32, 1988.
- Ehhalt, D. H., and J. Rudolph, On the importance of light hydrocarbons in multiphase atmospheric systems, Ber. Kernforschungsanlage, Julich, West Germany, JUL-1942, pp. 1–43, 1984.
- Fahey, D. W., G. Hubler, D. D. Parrish, E. J. Williams, R. B. Norton, B. A. Ridley, H. C. Singh, S. C. Liu, and F. C. Fehsenfeld, Reactive nitrogen species in the troposphere: Measurements of NO , NO_2 , HNO_3 , particulate nitrate, peroxyacetyl nitrate (PAN), O_3 , and total reactive odd nitrogen (NO_x) at Niwot Ridge, Colorado, *J. Geophys. Res.*, *91*, 9781–9793, 1986.
- Fehsenfeld, F. C., D. D. Parrish, and D. W. Fahey, The measurement of NO_x in the non-urban troposphere, in *Tropospheric Ozone: Regional and Global Scale Interactions*, edited by I. S. A. Isaksen, NATO ASI Series C, D. Reidel, Dordrecht, 1988.
- Fisher, D. A., C. H. Hales, D. L. Filkin, M. K. W. Ko, D. N. Sze, P. S. Connell, D. J. Wuebbles, I. S. A. Isaksen, and F. Stordal, Ozone depletion potentials for CFCs and possible replacements, submitted to *Nature*, 1989a.
- Fisher, D. A., C. H. Hales, D. L. Filkin, M. K. W. Ko, N. D. Sze, P. S. Connell, D. J. Wuebbles, I. S. A. Isaksen, and F. Stordal, Relative effects on stratospheric ozone of halogenated methanes and ethanes of social and industrial interest, in *Alternative Fluorocarbons Environmental Acceptability Study (AFEAS)*, Vol. II, Appendix, this report (1990), 1989b.
- Fisher, D. A., C. H. Hales, W. C. Wang, K. W. Ko, and N. D. Sze, Relative effects of global warming of halogenated methanes and ethanes of social and industrial interest, in *Alternative Fluorocarbons Environmental Acceptability Study (AFEAS)*, Vol. II, Appendix, this report (1990), 1989c.
- Fishman, J., and P. J. Crutzen, The origin of ozone in the troposphere, *Nature*, *274*, 855–858, 1978.
- Fraser, P. J., P. Hyson, R. A. Rasmussen, A. J. Crawford, and M. A. K. Khalil, Methane, carbon monoxide and methyl chloroform in the southern hemisphere, *J. Atmos. Chem.*, *4*, 3–42, 1986.
- Gillotay, G., P. C. Simon, and G. Brasseur, Absorption cross section of alternative chlorofluoroethanes and potential effects on the ozone layer, *Planet Space Sci.*, in press 1989.
- Golombek, A., and R. G. Prinn, A global three-dimensional model of the circulation and chemistry of CFCl_3 , CF_3Cl_2 , CH_3CCl_3 , CCl_4 and N_2O , *J. Geophys. Res.*, *91*, 3985–4001, 1986.

OZONE DEPLETION POTENTIALS

- Hampson, R. F., Kurylo, M. J., and Sander, S. P., Evaluated rate constants for selected HCFC's and HFC's with OH and O(¹D), in *Alternative Fluorocarbons Environmental Acceptability Study (AFEAS)*, Vol. II, Appendix, this report (1990), 1989.
- Hammit, J. K., F. Camm, P. S. Connell, W. E. Mooz, K. A. Wolf, D. J. Wuebbles, and A. Bemazai, Future emission scenarios for chemicals that may deplete stratospheric ozone, *Nature*, **330**, 711-716, 1987.
- Hubrich, C., and F. Stuhl, The ultraviolet absorption of some halogenated methanes and ethanes for atmospheric interest, *J. Photochem.*, **12**, 93-107, 1980.
- Isaksen, I. S. A., Tropospheric ozone budget and possible man-made effects, in *Quadrennial International Ozone Symposium*, Vol. II, edited by J. London, pp. 845-852, IAMAP, NCAR, Boulder, Colorado, 1981.
- Isaksen, I. S. A., and O. Hov, Calculation of trends in the tropospheric concentrations of O₃, OH, CO, CH₄ and NO, *Tellus*, **39B**, 271-285, 1987.
- IUPAC:R. Atkinson, D. L. Baulch, R. A. Cox, R. F. Hampson Jr., J. A. Kerr, and J. Troe, Evaluated kinetic and photochemical data for atmospheric chemistry, Suppl. III, *J. Phys. Chem. Ref. Data*, 1989.
- Khalil, M. A. K., and R. A. Rasmussen, The atmospheric lifetime of methyl chloroform, *Tellus*, **36B**, 317-332, 1984.
- Levy II, H., Normal atmosphere: Large radical and formaldehyde concentrations predicted, *Science*, **173**, 141-143, 1971.
- Levy II, H., J. D. Mahlman, and W. J. Moxim, A stratospheric source of reactive nitrogen in the unpolluted troposphere, *Geophys. Res. Lett.*, **7**, 441-444, 1980.
- Levy II, H., J. D. Mahlman, W. J. Moxim, and S. C. Liu, Tropospheric ozone: The role of transport., *J. Geophys. Res.*, **90**, 3753-3772, 1985.
- Liu, S. C., Group report on oxidizing capacity of the atmosphere, in *The Changing Atmosphere*, edited by F. S. Rowland and I. S. A. Isaksen, Wiley Interscience, New York, pp. 219-232, 1988.
- Liu, S. C., and M. Trainer, Tropospheric ozone response to column ozone change, *J. Atmos. Chem.*, **6**, 221-223, 1987.
- Logan, J. A., Tropospheric ozone: Seasonal behavior, trends and anthropogenic influence. *J. Geophys. Res.*, **90**, 10463-10482, 1985.
- Logan, J. A., M. J. Prather, S. C. Wofsy, and M. B. McElroy, Tropospheric chemistry: A global perspective, *J. Geophys. Res.*, **86**, 7210-7254, 1981.
- Lovelock, J. E., Methyl chloroform in the troposphere as an indicator of OH radical abundance, *Nature*, **267**, 32-33, 1977.
- Makide, Y., and F. S. Rowland, Tropospheric concentrations of methyl chloroform, CH₃CCl₃, in January 1978 and estimates of atmospheric residence times for hydrocarbons, *Proc. Natl. Acad. Sci., USA*, **59**, 5933-5937, 1981.
- McConnell, J. C., and H. I. Schiff, Methyl chloroform: Impact on stratospheric ozone, *Science*, **199**, 174-177, 1978.
- McKay, C., M. Pandow, and R. Wolfgang, On the chemistry of natural radio-carbon, *J. Geophys. Res.*, **68**, 3829-3931, 1963.
- Midgeley, P. N., The production and release to the atmosphere of 1,1,1-trichloroethane (methyl chloroform), *Atm. Env.*, in press, 1989.
- Molina, M. J., Review of ultraviolet absorption cross sections of a series of alternative fluorocarbons, in *Alternative Fluorocarbons Environmental Acceptability Study (AFEAS)*, Vol. II, Appendix, this report (1990), 1989.
- Molina, L. T., M. J. Molina, and F. S. Rowland, Ultraviolet absorption cross sections of several brominated methanes and ethanes of atmospheric interest, *J. Phys. Chem.*, **86**, 2672-2675, 1982.

- Morel, O., R. Simonaitis, and J. Heicklen, Ultraviolet absorption spectra of HO_2NO_2 , $\text{CCl}_3\text{O}_2\text{NO}_2$, $\text{CCl}_2\text{FO}_2\text{NO}_2$ and $\text{CH}_3\text{O}_2\text{NO}_2$, *Chem. Phys. Lett.*, *73*, 38–42, 1980.
- NASA:W. B. DeMore, S. P. Sander, M. J. Molina, D. M. Golden, R. F. Hampson, M. J. Kurylo, C. J. Howard, and A. R. Ravishankara, *Chemical Kinetics and Photochemical Data for Use in Stratospheric Modeling*, NASA Panel for Data Evaluation, Evaluation No. 8, JPL, Publication 87-41, Jet Propulsion Laboratory, Pasadena, CA, 1987.
- Neely, W., and J. Plonka, Estimation of time-averaged hydroxyl radical concentrations in the troposphere, *Environ. Sci. Tech.*, *12*, 317–321, 1978.
- Neftel, A., J. Beer, H. Oeschger, and F. Zurcher, Sulphate and nitrate concentrations in snow from south Greenland, *Nature*, *314*, 611–613, 1985.
- Niki, H., An assessment of potential impact of alternative fluorocarbons on tropospheric ozone, in *Alternative Fluorocarbons Environmental Acceptability Study (AFEAS)*, Vol. II, Appendix, this report (1990), 1989.
- Owens, A. J., C. H. Hales, D. L. Filkin, C. Miller, J. M. Steed, and J. P. Jesson, A coupled one-dimensional radiative-convective, chemistry transport model of the atmosphere, *J. Geophys. Res.*, *90*, 2283–2311, 1985.
- Perner, D., U. Platt, M. Trainer, G. Huebler, J. W. Drummond, W. Junkermann, J. Rudolph, B. Schubert, A. Volz, D. H. Ehhalt, K. J. Rumpel, and G. Helas, Tropospheric OH concentrations: A comparison of field data with model predictions, *J. Atmos. Chem.*, *5*, 185–216, 1987.
- Platt, U., M. Rateike, W. Junkermann, J. Rudolph, and D. H. Ehhalt, New tropospheric OH measurements, *J. Geophys. Res.*, *93*, 5159–5166, 1988.
- Prather, M. J., Tropospheric hydroxyl concentrations and the lifetimes of hydrochlorofluorocarbons (HCFCs), in *Alternative Fluorocarbons Environmental Acceptability Study (AFEAS)*, Vol. II, Appendix, this report (1990), 1989.
- Prinn, R. G., R. A. Rasmussen, P. G. Simmonds, F. N. Alyea, D. M. Cunnold, B. C. Lane, C. A. Cardelino, and A. J. Crawford, The atmospheric lifetime experiments, 5, results for CH_2Cl_2 based on three years of data, *J. Geophys. Res.*, *88*, 8415–8426, 1983.
- Prinn, R. G., D. Cunnold, R. A. Rasmussen, P. Simmonds, F. Alyea, A. J. Crawford, P. Fraser, and R. Rosen, Atmospheric trends in methyl chloroform and the global average for the hydroxyl radical, *Science*, *238*, 945–950, 1987.
- Ramanathan, V., R. J. Cicerone, H. B. Singh, and J. T. Kiehl, Trace gas trends and their potential role in climate change, *J. Geophys. Res.*, *90*, 5547–5566, 1985.
- Ramanathan, V., L. Callis, R. Cess, J. Hansen, I. Isaksen, W. Huhn, A. Lacis, F. Luther, J. Mahlman, R. Reck, and M. Schlesinger, Climate-chemical interactions and effects of changing atmospheric trace gases, *Rev. Geophys.*, *25*, 1441–1482, 1987.
- Rasmussen, R. A., and M. A. K. Khalil, Isoprene over the Amazon basin, *J. Geophys. Res.*, *93*, 1417–1421, 1988.
- Rognerud, B., I. S. A. Isaksen, and F. Stordal, Model studies of stratospheric ozone depletion, *Proceedings of the Quadrennial Ozone Symposium*, Gottingen, F.R.G., edited by R. D. Bojkov and P. Fabian, Deepak Publications, Hampton, VA., 1988.
- Rudolph, J., Two-dimensional distribution of light hydrocarbons: Results from the STRATOZ III experiment, *J. Geophys. Res.*, *93*, 8367–8377, 1988.
- Schwarzkopf, M. D., and S. B. Fels, The simplified exchange method revised: An accurate rapid method for computation of IR cooling rates, *J. Geophys. Res.*, in press, 1989.
- Singh, H. B., Atmospheric halocarbons: Evidence in favour of reducing average hydroxyl radical concentration in the troposphere, *Geophys. Res. Lett.*, *4*, 101–104, 1977a.
- Singh, H. B., Preliminary estimates of average tropospheric OH concentrations in the northern and southern hemispheres, *Geophys. Res. Lett.*, *4*, 453–456, 1977b.

OZONE DEPLETION POTENTIALS

- Singh, H. B., and J. F. Kasting, Chlorine-hydrocarbon photochemistry in the marine troposphere and lower stratosphere, *J. Atmos. Chem.*, 7, 261–285, 1988.
- Singh, H. B., L. J. Salas, and R. E. Stiles, Selected man-made halogenated chemicals in the air and oceanic environment, *J. Geophys. Res.*, 88, 3675–3683, 1983.
- Singh, H. B., L. J. Salas, and W. Viezee, The global distribution of peroxyacetyl nitrate, *Nature*, 321, 588–591, 1986.
- Sze, N. D., Anthropogenic CO emissions: Implications for the atmospheric CO-OH-CH₄ cycle, *Science*, 195, 673, 1977.
- Thompson A. M., R. W. Stewart, M. A. Owens, and J. A. Heruche, Sensitivity of tropospheric oxidants to global chemical and climate change, *Atmos. Environ.*, 23, 519–532, 1989.
- United Nations Environment Programme., *Montreal Protocol on Substances that Deplete the Ozone Layer—Final Act.*, UNEP, Nairobi, Kenya, 1987.
- Volz, A., D. H. Ehhalt, and R. G. Derwent, Seasonal and latitudinal variation in ¹⁴CO and the tropospheric concentration of hydroxyl radicals, *J. Geophys. Res.*, 86, 5163–5171, 1981.
- Wang, W.-C., and G. Molnar, A model study of the greenhouse effects due to increasing CH₄, N₂O, CF₂Cl₂ and CFC₁₃, *J. Geophys. Res.*, 90, 12971–12980, 1985.
- Wang, W.-C., G. Molnar, M. K. W. Ko, S. Goldenberg, and N. D. Sze, Atmospheric trace gas and global climate: A seasonal study, *Tellus*, in press, 1989.
- Warneck, P., On the role of OH and HO₂ radicals in the troposphere, *Tellus*, 26, 39–46, 1974.
- Warneck, P., Production rates of OH in the troposphere, *Planet. Space Sci.*, 23, 1507–1518, 1975.
- Watson, R. T. and Ozone Trends Panel, Prather, M. J. and Ad Hoc Theory Panel, and Kurylo, M. J. and NASA Panel for Data Evaluation, *Present State of Knowledge of the Upper Atmosphere 1988: An Assessment Report*, NASA Reference Publication 1208, U.S. Govt. Print. Off., Washington D.C., 1988.
- Weinstock, B. The residence time of carbon monoxide in the atmosphere, *Science*, 166, 224–225, 1969.
- Weinstock, B., and H. Niki, Carbon monoxide balance in nature, *Science*, 176, 290–292, 1972.
- Wilson, S. R., P. J. Crutzen, G. Schuster, D. W. T. Griffith, and G. Helas, Phosgene measurements in the upper troposphere and lower stratosphere, *Nature*, 334, 689–691, 1988.
- WMO, *Atmospheric Ozone 1985*, WMO Global Ozone Research and Monitoring Project, WMO Report No. 16, Sponsored by WMO, NASA, NOAA, FAA, UNEP, CEC, and BMFT, Washington, D.C., 1986.
- Wuebbles, D. J., "The Relative Efficiency of a Number of Halocarbons for Destroying Stratospheric Ozone," Rep. UCID-18924, Lawrence Livermore National Laboratory, Livermore, CA, 1981.
- Wuebbles, D. J., Chlorocarbon emission scenarios: Potential impact on stratospheric ozone, *J. Geophys. Res.*, 88, 1433–1443, 1983.
- Zimmerman, P. R., J. P. Greenberg, and C. E. Westberg, Measurements of atmospheric hydrocarbons and biogenic emissions fluxes in the Amazon boundary layer, *J. Geophys. Res.* 93, 1407–1416, 1988.

Appendix A
Contributors and Reviewers

Appendix B
List of Figures and Tables

APPENDIX A

CONTRIBUTORS AND REVIEWERS

STEERING COMMITTEE

Chairmen

R.T. Watson	NASA Headquarters	USA
D.L. Albritton	NOAA Aeronomy Laboratory	USA

Members

F. Arnold	Max-Planck-Institut fur Kernphysik	FRG
R.D. Bojkov	World Meteorological Organization	Switzerland
D. Ehhalt	Kernforschungsanlage Julich	FRG
P. Fraser	CSIRO	Australia
I. Isaksen	University of Oslo	Norway
V. Khattatov	State Committee for Hydrometeorology	USSR
C. Mateer	Atmospheric Environment Service (Retired)	Canada
T. Matsuno	University of Tokyo	Japan
M. Prendez	Universidad de Chile	Chile
J.A. Pyle	University of Cambridge	UK
B.H. Subbaraya	Physical Research Laboratory	India
P. Usher	United Nations Environment Programme	Kenya

AUTHORS

Chapter 1. Polar Ozone

Coordinator

S. Solomon	NOAA Aeronomy Laboratory	USA
------------	--------------------------	-----

Principal Authors

W.L. Grose	NASA Langley Research Center	USA
R.L. Jones	Meteorological Office	UK
M.P. McCormick	NASA Langley Research Center	USA
M.J. Molina*	Jet Propulsion Laboratory	USA
A. O'Neill	Meteorological Office	UK
L.R. Poole	NASA Langley Research Center	USA
K.P. Shine	University of Reading	UK
S. Solomon	NOAA Aeronomy Laboratory	USA

*Dr. Molina has been at MIT since Fall 1989.

CONTRIBUTORS

Other Contributors

R.A. Plumb	Massachusetts Institute of Technology	USA
U. Schmidt	Kernforschungsanlage Julich	FRG
V. Pope	Meteorological Office	UK

Chapter 2. Global Trends

Coordinator

G. Megie	Service d'Aeronomie du CNRS	France
----------	-----------------------------	--------

Principal Authors

M.-L. Chanin	Service d'Aeronomie du CNRS	France
D. Ehhalt	Kernforschungsanlage Julich	FRG
P. Fraser	CSIRO	Australia
J.F. Frederick	University of Chicago	USA
J.C. Gille	National Center for Atmospheric Research	USA
M.P. McCormick	NASA Langley Research Center	USA
G. Megie	Service d'Aeronomie du CNRS	France
M. Schoeberl	NASA Goddard Space Flight Center	USA

Other Contributors

L. Bishop	Allied-Signal, Inc.	USA
R.D. Bojkov	World Meteorological Organization	Switzerland
W. Chu	NASA Langley Research Center	USA
J.J. DeLuisi	NOAA Air Resources Laboratory	USA
J.F. Frederick	University of Chicago	USA
M. Geller*	NASA Goddard Space Flight Center	USA
S. Godin	Service d'Aeronomie du CNRS	France
N.R.P. Harris	University of California, Irvine	USA
W.J. Hill	Allied-Signal, Inc.	USA
R.D. Hudson	NASA Goddard Space Flight Center	USA
J.B. Kerr	Atmospheric Environment Service	Canada
W.D. Komhyr	NOAA Air Resources Laboratory	USA
K. Kunzi	University of Bremen	FRG
K. Labitzke	Freie Universitat, Berlin	FRG
C. Mateer	Atmospheric Environment Service (Retired)	Canada
R.D. McPeters	NASA Goddard Space Flight Center	USA
A.J. Miller	NOAA Climate Analysis Center	USA
R.M. Nagatani	NOAA Climate Analysis Center	USA
G.C. Reinsel	University of Wisconsin, Madison	USA
G.C. Tiao	University of Chicago	USA

*Dr. Geller is now with SUNY Stony Brook.

Chapter 3. Theoretical Predictions

Coordinator

G. Brasseur	National Center for Atmospheric Research	Belgium
-------------	--	---------

Principal Authors and Contributors

B.A. Boville	National Center for Atmospheric Research	USA
G. Brasseur	National Center for Atmospheric Research	Belgium
C. Bruhl	Max-Planck-Institut fur Chemie	FRG
M. Caldwell	Utah State University	USA
P. Connell	Lawrence Livermore National Laboratory	USA
A. De Rudder	Belgium Institute for Space Aeronomy	Belgium
A. Douglass	NASA Goddard Space Flight Center	USA
I. Dyominov	Novosibirsk State University	USSR
D. Fisher	E.I. DuPont de Nemours and Co., Inc.	USA
J.F. Frederick	University of Chicago	USA
R. Garcia	National Center for Atmospheric Research	USA
C. Granier	Service d'Aeronomie du CNRS	France
R. Hennig	Max-Planck-Institut fur Chemie	FRG
M. Hitchman	University of Wisconsin	USA
I. Isaksen	University of Oslo	Norway
C. Jackman	NASA Goddard Space Flight Center	USA
M. Ko	Atmospheric and Environmental Research, Inc.	USA
S. Madronich	National Center for Atmospheric Research	USA
M. Prather	NASA Goddard Institute for Space Studies	USA
R. Rood	NASA Goddard Space Flight Center	USA
S. Solomon	NOAA Aeronomy Laboratory	USA
F. Stordal	University of Oslo	Norway
T. Sasaki	Meteorological Research Institute	Japan
G. Visconti	University de l'Aquila	Italy
S. Walters	National Center for Atmospheric Research	USA
D. Wuebbles	Lawrence Livermore National Laboratory	USA
A. Zadarozhny	Novosibirsk State University	USSR
E. Zhadin	Central Aerological Observatory	USSR

Chapter 4. Halocarbon Ozone Depletion and Global Warming Potentials

Coordinators

R.A. Cox	Harwell Laboratory	UK
D.J. Wuebbles	Lawrence Livermore National Laboratory	USA

CONTRIBUTORS

Principal Authors and Contributors

R. Atkinson	California Statewide Air Pollution Center	USA
P. Connell	Lawrence Livermore National Laboratory	USA
H.P. Dorn	Kernforschungsanlage Julich	FRG
A. De Rudder	Belgium Institute for Space Aeronomy	Belgium
R.G. Derwent	Harwell Laboratory	UK
F.C. Fehsenfeld	NOAA Aeronomy Laboratory	USA
D. Fisher	E. I. DuPont de Nemours and Co., Inc.	USA
I. Isaksen	University of Oslo	Norway
M. Ko	Atmospheric and Environmental Research, Inc.	USA
R. Lesclaux	Universite de Bordeaux	France
S.C. Liu	NOAA Aeronomy Laboratory	USA
S.A. Penkett	University of East Anglia	UK
V. Ramaswamy	NOAA Geophysical Fluid Dynamics Laboratory	USA
J. Rudolph	Kernforschungsanlage Julich	FRG
H.B. Singh	NASA Ames Research Center	USA
W.-C. Wang	Atmospheric and Environmental Research, Inc.	USA

Reviewers

Attendees: Review Meeting, 10-14 July 1989,
Les Diablerets, Switzerland

D.L. Albritton	NOAA Aeronomy Laboratory	USA
R.D. Bojkov	World Meteorological Organization	Switzerland
G. Brasseur	National Center for Atmospheric Research	Belgium
D. Cariolle	Meteorologie Nationale EERM/CNRM	France
G.D. Cartwright	NOAA National Weather Service/WMO	USA
M.-L. Chanin	Service d'Aeronomie du CNRS	France
A. Charnikov	Central Aerological Observatory	USSR
R.A. Cox	Harwell Laboratory	UK
D.H. Ehhalt	Kernforschungsanlage Julich	FRG
J.C. Farman	British Antarctic Survey	UK
D. Fisher	E.I. DuPont de Nemours and Co., Inc.	USA
P.J. Fraser	CSIRO	Australia
J.F. Frederick	University of Chicago	USA
J.C. Gille	National Center for Atmospheric Research	USA
W.J. Hill	Allied-Signal, Inc.	USA
M. Hitchman	University of Wisconsin	USA
A.M.A. Ibrahim	Egyptian Meteorological Authority	Egypt
M. Ilyas	University of Science of Malaysia	Malaysia
J.B. Kerr	Atmospheric Environment Service	Canada
M.J. Kurylo	NASA Headquarters	USA
C. Mateer	Atmospheric Environment Service (Retired)	Canada
T. Matsuno	University of Tokyo	Japan

CONTRIBUTORS

M.P. McCormick	NASA Langley Research Center	USA
M. McFarland	E. I. DuPont de Nemours and Co., Inc.	USA
G. Megie	Service d'Aeronomie du CNRS	France
M.J. Molina	Jet Propulsion Laboratory	USA
A. O'Neill	Meteorological Office	UK
A. Owino	Kenya Meteorological Department	Kenya
S.A. Penkett	University of East Anglia	UK
M. Prather	NASA Goddard Institute for Space Studies	USA
M. Prendez	Universidad de Chile	Chile
J.A. Pyle	University of Cambridge	UK
V. Ramaswamy	NOAA Geophysical Fluid Dynamics Laboratory	USA
J.M. Rodriguez	Atmospheric and Environment Research, Inc.	USA
J.M. Russell	NASA Langley Research Center	USA
S. Solomon	NOAA Aeronomy Laboratory	USA
R. Stolarski	NASA Goddard Space Flight Center	USA
B.H. Subbaraya	Physical Research Laboratory	India
A.F. Tuck	NOAA Aeronomy Laboratory	USA
P. Usher	United Nations Environment Programme	Kenya
R.T. Watson	NASA Headquarters	USA
D.J. Wuebbles	Lawrence Livermore National Laboratory	USA

Mail Reviewers

J.G. Anderson	Harvard University	USA
J.K. Angell	NOAA Air Resources Laboratory	USA
R. Atkinson	Bureau of Meteorology	Australia
G. Betteridge	Physics and Engineering Laboratory, DSIR	New Zealand
J.P. Burrows	Max-Planck-Institut fur Chemie	FRG
B. Carli	IROF-CNR	Italy
S. Chubachi	Meteorological Research Laboratory	Japan
T.S. Clarkson	Meteorological Service	New Zealand
P. Crutzen	Max-Planck-Institut fur Chemie	FRG
D.W. Fahey	NOAA Aeronomy Laboratory	USA
G. Fiocco	University la Sapieuza	Italy
A. Ghazi	Commission of the European Communities	Belgium
L. Gray	Rutherford - Appleton Laboratories	UK
J.S. Hoffman	Environmental Protection Agency	USA
Y. Iwasaka	Nagoya University	Japan
P. Johnson	Physics and Engineering Laboratory, DSIR	New Zealand
P. S. Jovanovic	Association of Scientific Unions	Yugoslavia
J.G. Keys	Physics and Engineering Laboratory, DSIR	New Zealand
V. Kirchoff	INPE	Brazil
D. Kley	Kernforschungsanlage Julich	FRG
Y.-P. Lee	National Tsing Hua University	Taiwan
W.A. Matthews	Physics and Engineering Laboratory, DSIR	New Zealand
R. McKenzie	Physics and Engineering Laboratory, DSIR	New Zealand
A.P. Mitra	Department of Science and Industrial Research	India

CONTRIBUTORS

J. L. Moyers	National Science Foundation	USA
L.P. Prahm	Danish Meteorological Institute	Denmark
M. H. Proffitt	NOAA Aeronomy Laboratory	USA
L. X. Qui	Academia Sinica	PRC
F. S. Rowland	University of California, Irvine	USA
P. C. Simon	Institut d'Aeronomie Spatiale	Belgium
Y. Sasano	National Institute for Environmental Studies	Japan
J. Swager	Air Directorate	Netherlands
D.W. Wei	Institute of Atmospheric Physics, NEPA	PRC
R. Zellner	University of Gottingen	FRG
C.S. Zerefos	University of Thessaloniki	Greece

Logistical Support

R. D. Bojkov	World Meteorological Organization	Switzerland
M. -C. Charrierts	World Meteorological Organization	Switzerland
F. M. Ormond	ARC Professional Services Group	USA
J. Waters	NOAA Aeronomy Laboratory	USA

APPENDIX B

LIST OF FIGURES and TABLES*

FIGURES

	Page
Introduction	
Figure 1.1	Calculated time-dependent change in relative ozone depletion following a step change in emission of halocarbons xxx
Figure 1.2	Calculated column ozone change following a pulsed input of 5×10^9 xxxi
Chapter 1—Polar Ozone	
Figure 1.1.2-1	Logarithm of the computed lifetime of the odd oxygen family in Northern Hemisphere winter versus latitude and height 3
Figure 1.1.2-2	The first three years of ozone data from the Dobson instrument at Halley Bay, Antarctica compared to Spitzbergen 4
Figure 1.1.2-3	Observed global variation of total ozone with latitude and season 5
Figure 1.1.2-4	Seasonal cycles of total ozone and 50 mb temperatures at 60°N (Jan.-Dec.) and 60°S (July-June) 6
Figure 1.1.2-5	As in Figure 1.1.2-4, but for 80°N (Jan.-Dec.) and 80°S (July-June) 6
Figure 1.1.3-1	Observed long-term trends in total ozone from the ground-based Antarctic stations at Syowa, Halley Bay, and the South Pole 8
Figure 1.1.3-2	TOMS October monthly mean minimum total ozone measurements along with equatorial zonal wind speed 9
Figure 1.1.3-3	Seasonal decline in total ozone above McMurdo Station in 1986 as deduced by visible, UV, and IR spectroscopy, as well as from ozonesonde observations 10
Figure 1.1.3-4	(A) Same as Figure 1.1.3-3, but for 1987; (B) Seasonal decline in the daily TOMS ozone minimum during 1987 11
Figure 1.1.3-5	Contour plot of the ozone decrease obtained from 1978-1988; derived from a TOMS linear trend analysis 12
Figure 1.1.3-6	SAGE II total column ozone above 100 mb for all measurement events from day 270 through 293 (Sept. 27- Oct., 20 1985, 1986, and 1987; September 26-October 19, 1988) 13
Figure 1.1.3-7	False color images of SAGE II total column ozone above 100 mb for 1985 through 1988 14
Figure 1.1.5-1	Observations of the change in the vertical profile of ozone as measured by ozonesondes. At Syowa, the South Pole, Halley Bay, McMurdo, Molodezhnaya, and Dakshin Gangotri 18
Figure 1.1.5-2	(A) Average vertical profiles of summertime ozone from February 1-10 (SAGE II). (B) The most severely depleted profiles observed (SAGE I [1981] and SAGE II [1985-1988]) 19

*Titles have been shortened to economize on space.

FIGURES

Page

Figure 1.1.5-3	Trend in total ozone at 18 km observed from ozonesondes at McMurdo Station in 1986 and 1987	20
Figure 1.2.1-1	(Left) Vertical profiles of cloud particles observed during balloon soundings at McMurdo Station in September, 1988. (Right) Particle size distributions at various altitudes	25
Figure 1.2.2-1	Observations of PSC sightings (per week) from SAM II during 1979, 1980, 1981, 1982, and 1984 for May through October in the Southern Hemisphere vortex ...	28
Figure 1.2.2-2	As in Figure 1.2.2-1, but for 20, 22, and 24 km	29
Figure 1.2.2-3	As in Figure 1.2.2-1, but for 1985 through 1988	29
Figure 1.2.2-4	As in Figure 1.2.2-3, but for 20, 22, and 24 km	30
Figure 1.2.2-5	As in Figure 1.2.2-1, but for November through April in the Northern Hemisphere vortex for the 1978-1979 through 1983-1984 winter seasons	31
Figure 1.2.2-6	As in Figure 1.2.2-5, but for 20, 22, and 24 km	31
Figure 1.2.2-7	As in Figure 1.2.2-5, but for 1984-1985 through 1988-1989	32
Figure 1.2.2-8	As in Figure 1.2.2-7, but for 20, 22, and 24 km	32
Figure 1.2.3-1	SAM II optical depth integrated from 2 km above the tropopause to 30 km, for the Northern and Southern Hemispheres	33
Figure 1.2.3-2	Observations of SAM II PSC sightings for Antarctica from 1979 through 1988 at 14, 16, and 18 km, during the month of October	34
Figure 1.2.3-3	As in Figure 1.2.3-2, but for September	35
Figure 1.2.4-1	Changes in net heating caused by mountain PSCs with and without cirrus	38
Figure 1.3.2-1	Plot of the flight track data for the encounter with a PSC event on August 17, 1987	41
Figure 1.3.2-2	Observations of the percent of total observed nitrate in the particulate phase as a function of time for September 4, 1987	42
Figure 1.5.1-1	ClO dimer thermal decomposition and photolysis rates	47
Figure 1.5.1-2	Calculated time behavior of ClO and ClONO ₂ during Arctic spring for three different cases	50
Figure 1.5.2-1	Absorption cross sections of ClOOCl	51
Figure 1.5.2-2	Rate constants for the ClO + ClO + M → Cl ₂ O ₂ + M reaction, with N ₂ as the third body M	52
Figure 1.5.2-3	Photolysis rates for Cl ₂ O ₂ , HOCl, Cl ₂ , HNO ₃ , and O ₂ at 70°S at noon as a function of day, at the 50 mb level	53
Figure 1.6.1-1	Observed ClO mixing ratio latitude gradients on the 425 and 450 K potential temperature surfaces averaged over the AAOE mission period	56
Figure 1.6.1-2	The vertical profile of ClO mixing ratio within the southern polar vortex, from ground-based microwave measurements and in situ measurements	56
Figure 1.6.1-3	Diurnal variation of the column abundance of ClO below about 25 km at McMurdo Station, Antarctica	57
Figure 1.6.1-4	Diurnal variation of the column abundance of OClO above McMurdo Station September 18-19, 1986	58
Figure 1.6.1-5	Daily measurements of the sunset OClO column abundances above McMurdo Station in 1986 and 1987	59
Figure 1.6.1-6	Observed distribution of the ClONO ₂ column abundance, a function of latitude relative to the edge of the vortex in August and September, 1987	60
Figure 1.6.1-7	Observed latitude gradients of HCl and HF on the 24th of September and 2nd of October, 1987	61

	Page
Figure 1.6.2-1	Observations of the latitude gradient of column NO ₂ in the Southern Hemisphere 63
Figure 1.6.2-2	Observations of the seasonal trend in morning and evening twilight slant column NO ₂ abundances from three Antarctic sites 64
Figure 1.6.2-3	Total NO ₂ (a), total O ₃ (b), and 50 mb temperature (c) at Molodezhnaya in 1987 and Mirny in 1988 65
Figure 1.6.2-4	Cross section of NO ₂ vs. latitude and pressure for the period September 27 to October 7, 1987, from SAGE II observations 66
Figure 1.6.2-5	Observed column of HNO ₃ plotted as a function of latitude relative to the edge of the polar vortex in August and September, 1987 66
Figure 1.6.2-6	Measurements of total reactive nitrogen (NO _y) versus N ₂ O obtained from aircraft observations 67
Figure 1.6.2-7	Observed total reactive nitrogen profile as a function of potential temperature .. 69
Figure 1.6.2-8	Observed NO mixing ratios versus latitude relative to the chemically perturbed region 70
Figure 1.6.3-1	Observed latitude gradient of H ₂ O on September 22, 1987 near 450 K surface ... 70
Figure 1.6.3-2	Cross section of H ₂ O vs. latitude and pressure for the period September 27 to October 7, 1987, measured by SAGE II 71
Figure 1.6.3-3	BrO mixing ratios versus latitude for nine flights from about 54° and 72°S, taken between August 28 and September 22, 1987 72
Figure 1.6.3-4	Variation of the BrO mixing ratio with potential temperature 73
Figure 1.6.3-5	Diurnal variation of the BrO slant column at McMurdo Station 74
Figure 1.6.4-1	Calculated and observed ClO mixing ratios on the 428 K surface, 4-12 September, 1987 76
Figure 1.6.4-2	Calculated and observed ClO mixing ratio profiles at 72°S, 4th/9th September, 1987 77
Figure 1.6.4-3	Observed NO and ClO mixing ratios from an aircraft flight on August 28, 1987
Figure 1.6.4-4	Observed and calculated rates of ozone decline for different ClO dimer formation rates as a function of potential temperature 79
Figure 1.6.4-5	Observed October mean total ozone abundance over Halley Bay, Antarctica ... 81
Figure 1.7.1-1	The range, near 90 mb, of minimum brightness temperatures poleward of latitude 20, computed daily for winter and spring from 1980 to 1988 83
Figure 1.7.1-2	Comparison of N ₂ O vertical profiles during austral winter-spring, austral summer, and austral winter 84
Figure 1.7.1-3	Vertical distributions of the total amount of chlorine bonded in the five most abundant anthropogenic halocarbons 85
Figure 1.7.1-4	(i) Monthly mean perspectives during June 1982 of the three-dimensional structure of the westerly vortex in the Southern Hemisphere 86
Figure 1.7.1-4	(ii) As for Figure 1.7.1(i), but for September 87
Figure 1.7.1-4	(iii) As for Figure 1.7.1(i), but for October 87
Figure 1.7.1-5	Time of the reversal of the zonal wind at latitude 60°, and of the temperature difference between 60° and 85° for the Northern and Southern Hemispheres 88
Figure 1.7.1-6	Evolution of zonal-mean total ozone (Dobson units) derived from the TOMS instruments, 1987 and 1988 90
Figure 1.7.1-7	Minimum brightness temperature near 90 mb (Channel 24 of the MSU) in the Southern Hemisphere during 1987 91

FIGURES

	Page
Figure 1.7.1-8	The fractional area of the Southern Hemisphere over which minimum temperatures near 90 mb in 1987 fell below 193 K 91
Figure 1.7.1-9	As for Figure 1.7.1-7 but for 1988 92
Figure 1.7.1-10	As for Figure 1.7.1-8 but for 1988 92
Figure 1.7.1-11	Isentropic maps of Ertel's potential vorticity and winds on the 500 K isentropic surface in the Southern Hemisphere on 1 August 1987 93
Figure 1.7.1-12	As for Figure 1.7.1-11, but for 31 October 1987 94
Figure 1.7.1-13	As for Figure 1.7.1-11, but on 1 August 1988 94
Figure 1.7.1-14	As for Figure 1.7.1-11, but on 20 October 1988 95
Figure 1.7.1-15	As for Figure 1.7.1-11, but for the Northern Hemisphere on 18 January 1989 96
Figure 1.7.1-16	As for Figure 1.7.1-11, but for the Northern Hemisphere on 20 February 1989 .. 97
Figure 1.7.1-17	Minimum brightness temperature derived from channel 24 of the MSU in the Northern Hemisphere for December through May 98
Figure 1.7.1-18	The total ozone fields (in Dobson units) from November 1978 to October 1987 with annual cycle removed 99
Figure 1.7.1-19	As for Figure 1.7.1-18, but after application of a broad-band filter 100
Figure 1.7.1-20	Variation in October mean total ozone and 70 mb temperature over the South Pole 101
Figure 1.7.1-21	As for Figure 1.7.1-20, but for the April mean in the Northern Hemisphere 101
Figure 1.7.1-22	Correlation of August-September winds over Singapore at 30 mb with the total ozone decline rate in September 102
Figure 1.7.1-23	Ozone mixing ratio variation at the maximum of the 11-year solar cycle 103
Figure 1.7.2-1	An example of a mini-hole over the Antarctic Peninsula on 5 September 1987 ... 105
Figure 1.7.2-2	(i) Longitude/pressure cross sections on 5 September 1987 at latitude 65°S from 90°W to 30°W, and from 250 to 30 mb 106
Figure 1.7.2-2	(ii) As for Figure 1.7.2-2 (i) 107
Figure 1.7.2-3	A sequence of potential vorticity distributions on the 428 K surface of potential temperature 108
Figure 1.7.4-1	Ertel's potential vorticity on the 600 K isentropic surface 111
Figure 1.7.4-2	TOMS total ozone. Monthly variation of difference between 1987-1988 average and 1979-1980 average as a function of latitude 112
Figure 1.7.4-3	Percent change in the simulated steady-state seasonal and latitudinal distribution of zonal-mean column ozone 113
Figure 1.7.4-4	Percent difference in zonal-mean column ozone for Antarctic ozone hole 114
Figure 1.7.4-5	Percent difference in the integrated global and hemispheric column ozone for Antarctic ozone hole 116
Figure 1.7.4-6	TOMS total ozone for the Southern Hemisphere 117
Figure 1.7.4-7	Difference between Ertel's potential vorticity (500 K isentropic surface) for 8 December and 14 December 1987 118
Figure 1.8.1-1	Linear trends calculated from NMC data for the period 1979-1986, for August, September, November, and December 119
Figure 1.8.2-1	Deviations of temperatures 1958-1988 (°C) for Angell's (1988b) six south polar stations 120
Figure 1.8.2-2	Monthly mean temperatures at 100 mbar for Halley Bay, 1958-1988 121
Figure 1.8.2-3	Temperatures at 100 mbar as a function of month from Halley Bay 122
Figure 1.8.2-4	Deviation of NMC zonal mean temperatures for 1987 from the 1979-1986 mean for September to December 123

	Page
Figure 1.8.3-1	2-D model temperatures at 39 mb and 76°S with and without an imposed ozone hole 125
Figure 1.8.3-2	Deviation of zonal mean temperature for a calculation with an imposed ozone hole from a control run without the hole, using the NCAR Community Climate Model 126
Figure 1.9-1	Ratio of biologically effective downward radiation computed for a range of ozone values at McMurdo 127
Figure 1.9-2	Computed time history of erythemal irradiance for local noon and clear skies over Palmer Station 129
Figure 1.9-3	Spectra of UV solar irradiance measured from Palmer Station at local noon 130
Figure 1.9-4	Ratio of noontime irradiance for 295-305 nm to that for 335-345 nm, for the period 19 September and 21 December 1988 131
Figure 1.10.1-1	Observation of the Noxon cliff 131
Figure 1.10.1-2	The mean annual cycle of NO ₂ at 71°N (Point Barrow, Alaska) 132
Figure 1.10.1-3	Variation of total NO ₂ column abundance over Point Barrow, Alaska (71°N) in three different winter-spring seasons 133
Figure 1.10.1-4	NO _x (NO + NO ₂) mixing ratio profiles observed on balloon flights using a chemiluminescent detector 134
Figure 1.10.1-5	Zonally and monthly averaged HNO ₃ mixing ratio distributions for November, December, and January from LIMS observations 136
Figure 1.10.1-6	Latitude gradients of HCl and HF in the Northern Hemisphere 137
Figure 1.10.1-7	Observations of the nighttime abundance of OClO versus lunar zenith angle at various locations 138
Figure 1.10.2-1	Ozone partial pressure and mixing ratio profiles measured at Kiruna, Sweden, on 23 January, 1989 140
Figure 1.10.2-2	NMC temperatures at 30 mb for the 1988-1989 Northern Hemisphere winter-spring season 141
Figure 1.10.2-3	NMC temperatures at 30 mb for the 1975-1976 Northern Hemisphere winter-spring season 142
 Chapter 2—Global Trends	
Figure 2.1-1	Time-lines of measurements available for use in ozone trend analyses at the present time 164
Figure 2.1-2	Location of Dobson and M-83 stations 166
Figure 2.1-3	Time-lines for ozone-measuring systems that are projected to be operating over the next decade 175
Figure 2.1-4a	Comparison between archived TOMS total ozone data and Dobson data 182
Figure 2.1-4b	Comparison between TOMS total ozone data where diffuser plate degradation was corrected by the “pair justification” method and Dobson data 183
Figure 2.1-5	Samples of profile pairs measured by ozonesondes and the SAGE I instrument and the mean percentage difference between the ozonesondes and the SAGE I ozone 186
Figure 2.1-6	Samples of profile pairs measured by ozonesondes and the SAGE II instrument and the mean percentage difference between the ozonesondes and the SAGE II ozone 187
Figure 2.1-7	Mean differences between SAGE I and ozonesondes and SAGE II and ozonesondes 188

FIGURES

	Page
Figure 2.2-1	Monthly and zonally averaged Dobson total ozone values versus time after removal of seasonal, QBO, solar cycle, and nuclear test effects 197
Figure 2.2-2a	Regional plots of Dobson total ozone after removal of seasonal, solar, QBO, and nuclear test effects for North America, Europe, and Japan 198
Figure 2.2-2b	Same as 2.2-2a for winter months (December-March) 199
Figure 2.2-2c	Same as 2.2-2a for summer months (May-August) 200
Figure 2.2-3	Plots of Dobson total ozone monthly averages combined into time series for each latitudinal zone 201
Figure 2.2-4	Individual trend estimates for the period 1970-1986 using the AS2 model 203
Figure 2.2-5	Same as Figure 2.2-4 except trends are fitted only through October 1982 205
Figure 2.2-6	Same as Figure 2.2-4 except trends are fitted using updated data into 1988 208
Figure 2.2-7	Differences between estimated trends into 1988 versus trends through 1986 210
Figure 2.2-8	Solar coefficient computed for 25 Northern Hemisphere stations from the AS2 model 211
Figure 2.2-9a	Geographic structure in total ozone changes based on TOMS 212
Figure 2.2-9b	Same as Figure 2.2-9a for Southern Hemisphere 213
Figure 2.2-10	Geographic pattern of change in total ozone derived from SBUV for the Northern Hemisphere winter and summer 215
Figure 2.2-11	Geographic pattern of change in total ozone derived from SBUV for the Southern Hemisphere winter and summer 215
Figure 2.2-12	Changes in total ozone based on eight-year data sets from the SBUV and TOMS instruments 217
Figure 2.2-13	Changes in total ozone derived from Dobson data for the eight-year period over which SBUV measurements are available 218
Figure 2.3-1	Latitudes of the SAGE I and SAGE II sampling locations for sunset 222
Figure 2.3-2	Zonal mean ozone number density at 30 km for SAGE I during the period 2/79-11/81 and SAGE II during the period 10/84-11/87 for five latitude bands 223
Figure 2.3-3	Daily mean ozone number density at 35 km for SAGE II for twelve latitude bands 224
Figure 2.3-4	Mean percentage difference between SAGE II and SAGE I versus altitude computed from the intersection of SAGE I with SAGE II 225
Figure 2.3-5	Deseasonalized Umkehr data at Arosa for layers 4-9, unadjusted for aerosols, for the period January 1977 through December 1987 227
Figure 2.3-6	Stratospheric aerosol optical thickness derived from lidar data for the period 1977-1987 228
Figure 2.3-7	Umkehr data trend estimates from 10 individual Umkehr stations for layers 4-9, for the period January 1977 through December 1987 229
Figure 2.3-8	Trend estimates derived from ozonesondes measurements at 9 stations for 15 fractional Umkehr layers 233
Figure 2.4-1a	Seasonal temperatures with the long-term seasonal averages removed and smoothed 1-2-1 in time for Angell, Berlin, NMC, MSU, SSU 238
Figure 2.4-1b	Seasonal temperatures with the long-term seasonal averages removed and smoothed 1-2-1 in time: NMC; SSU Channels 25 and 26 × 239
Figure 2.4-1c	Seasonal temperatures with the long-term seasonal averages removed and smoothed 1-2-1 in time: NMC; SSU Channel 26 240
Figure 2.4-1d	Seasonal temperatures with the long-term seasonal averages removed and smoothed 1-2-1 in time: NMC 5-1 mb; SSU Channels 27 and 36 X 241

	Page
Figure 2.4-2	Lidar temperature and SSU channel 27 brightness temperature from 1981 to 1987 242
Figure 2.4-3	Lidar and NMC temperature at 42 km 242
Figure 2.4-4	Comparison of the 10.7 cm solar flux, in 10^{-22} W/(m ² Hz), and the 30-mb temperature, in °C, at the North Pole 243
Figure 2.4-5	Summary of global stratospheric temperature differences (1985 and 1986 minus the average of 1979 and 1980) 244
Figure 2.4-6	As in Figure 2.4-4, except for Tropics and including rocket stations 245
Figure 2.5-1	Halocarbon (pptv) and nitrous oxide (ppbv) observations at Cape Grim, Tasmania, as part of the GAGE program 248
Figure 2.5-2	CHClF ₂ (pptv) observations at Cape Grim, Tasmania, from the Oregon Graduate Center flask sampling program 249
Figure 2.5-3	CH ₃ Cl (pptv) observations at Cape Grim, Tasmania, from the Oregon Graduate Center flask sampling program 249
Figure 2.5-4	CHCl ₃ (pptv) observations at Cape Grim, Tasmania, from the Oregon Graduate Center flask sampling program 250
Figure 2.5-5	Long-term trends of N ₂ O from the GMCC program, the SIO program, the OGC-ALE program, the FIAER-CSIR program, and CSIRO-GAGE data 252
Figure 2.5-6	Long-term trends of CH ₄ from the CSIRO global program and the FIAER-CSIR program at Cape Point, South Africa 254
Figure 2.5-7	The global distribution, seasonality, and trend of CH ₄ from the GMCC network 255
Figure 2.5-8	Long-term trends of CO from the CSIRO network and from Cape Point, South Africa 257
Figure 2.5-9	The temporal behavior of the CO ₂ trends observed at the GMCC stations 258
Figure 2.5-10	Surface ozone measurements at the GMCC stations, at Cape Point, South Africa, and at Cape Grim, Tasmania 260
Figure 2.6-1	Aerosol integrated backscatter coefficient over the period 1974-88 262
Figure 2.7-1	Solar spectral irradiance incident on the Earth's surface computer for January and July at latitudes 34.5°, 46.0°, and 58.5°N 264
Figure 2.7-2	Percent changes in solar spectral irradiance between 1970 and 1986 computed for January, March, and July at latitudes 34.5°, 46.0°, and 58.5°N 266

Chapter 3—Theoretical Predictions

Figure 3.1-1	Schematic diagram showing an algorithm for determining the coupled set of transport parameters with prescribed T as input 287
Figure 3.1-2	Total ozone field on 28 February 1989 as measured by TOMS and as modeled from a January 1 initial condition 291
Figure 3.1-3	Two-dimensional distribution of tropospheric source gas X from nine models for the month of December 295
Figure 3.1-4	Two-dimensional distribution of the ClO/HCl ratio from nine models 298
Figure 3.1-5	Zonally and monthly averaged distribution of nitrous oxide observed in January 1979 by SAMS and calculated by GSFC model 301
Figure 3.1-6	Same as in Figure 3.1-5 but for methane 302
Figure 3.1-7	Zonally and monthly averaged distribution of nighttime NO ₂ observed in January 1979 by LLMS 303

FIGURES

	Page
Figure 3.1-8	Same as in Figure 3.1-7 but for nitric acid 304
Figure 3.1-9	Zonally and monthly averaged distribution of ozone for January based on data obtained by SBUV and distribution by different two-dimensional models 307
Figure 3.1-10	Latitudinal and seasonal variation of the ozone column abundance based on satellite observations (TOMS) and different model calculations 312
Figure 3.1-11	Comparison between one-dimensional mixing ratio profiles of chemically active trace gases measured by ATMOS 316
Figure 3.2-1	Time history, 1960-2060, of mean tropospheric concentrations of the trace gases assumed for the different scenarios 319
Figure 3.2-2	Time history, 1980-2060, of total atmospheric chlorine and total atmospheric bromine from the different scenarios 321
Figure 3.2-3	Dobson map of percent change in column ozone from 1960 to 1980 using the specified trace-gas scenario 329
Figure 3.2-4	Latitude-by-altitude contour map of the percent change in local ozone concentration from 1960 to 1980 for the specified trace-gas scenario 333
Figure 3.2-5	Time-line of the percent change in column ozone as a function of latitude for the months of March from 1980 through 2060 for scenario A1 338
Figure 3.2-6	Dobson map of percent change in column ozone from 1980 to 2020 using scenario A1 340
Figure 3.2-7	Dobson map of percent change in column ozone from 1980 to 2060 using scenario A1 342
Figure 3.2-8	Latitude-by-altitude contour map of the percent change in local ozone concentration from 1980 to 2060 for scenario A1 347
Figure 3.2-9	Time-line vs. latitude of the percent change in column ozone during March from 1980 to 2060 for scenario A2 351
Figure 3.2-10	Dobson map of percent change in column ozone from 1980 to 2060 using scenario A2 352
Figure 3.2-11	Latitude-by-altitude map of the percent change in local ozone concentration from 1980 to 2060 for scenario A2 353
Figure 3.2-12	Temperature change (K) for December (scenario A1: 1980-2060) from the AER and WisCAR models 354
Figure 3.2-13	Zonal wind and zonal wind change from December 1980 to December 2060 for the WisCAR model (scenario A1) 355
Figure 3.2-14	Net radiative heating (K/day) for December 1980 in the AER and WisCAR models 356
Figure 3.2-15	Change in net radiative heating (K/day) from December 1980 to December 2060 (scenario A1) in the AER and WisCAR models 357
Figure 3.2-16	Time-line vs. latitude of the percent change in column ozone during March from 1980 to 2060 for scenario A1 359
Figure 3.2-17	Dobson map of percent change in column ozone from 1980 to 2060 using scenario B1 360
Figure 3.2-18	Latitude-by-altitude map of the percent change in local ozone concentration from 1980 to 2060 for scenario B1 361
Figure 3.2-19	Time-line vs. latitude of the percent change in column ozone during March from 1980 to 2060 for scenario C1 363
Figure 3.2-20	Dobson map of percent change in column ozone from 1980 to 2060 using scenario C1 364

	Page
Figure 3.2-21	Latitude-by-altitude map of the percent change in local ozone concentration from 1980 to 2060 for scenario C1 364
Figure 3.2-22	Time-line vs. latitude of the percent change in column ozone during March from 1980 to 2060 for scenario D1 365
Figure 3.2-23	Dobson map of percent change in column ozone from 1980 to 2060 using scenario D1 366
Figure 3.2-24	Latitude-by-altitude map of the percent change in local ozone concentration from 1980 to 2060 for scenario D1 368
Figure 3.2-25	Time-line vs. latitude of the percent change in column ozone during March from 1980 to 2060 for scenario D2 371
Figure 3.2-26	Dobson map of percent change in column ozone from 1980 to 2060 using scenario D2 371
Figure 3.2-27	Latitude-by-altitude map of the percent change in local ozone concentration from 1980 to 2060 for scenario D2 372
Figure 3.2-28	Time-line vs. latitude of the percent change in column ozone during March from 1980 to 2060 for scenario D3 372
Figure 3.2-29	Dobson map of percent change in column ozone from 1980 to 2060 using scenario D3 373
Figure 3.2-30	Latitude-by-altitude map of the percent change in local ozone concentration from 1980 to 2060 for scenario D3 373
Figure 3.2-31	Time-line vs. latitude of the percent change in column ozone during March from 1980 to 2060 for scenario D4 374
Figure 3.2-32	Dobson map of percent change in column ozone from 1980 to 2060 using scenario D4 375
Figure 3.2-33	Latitude-by-altitude map of the percent change in local ozone concentration from 1980 to 2060 for scenario D4 375
Figure 3.2-34	Two-year sequence of percent change in column ozone from the Cambridge model with PSC chemistry in the Northern Hemisphere 376
Figure 3.2-35	Dobson maps of percent change in column ozone from 1960 to 2060 from the WisCAR model with and without heterogeneous chemistry on PSCs for scenario A1 377
Figure 3.2-36	Dobson maps of percent change in column ozone from 1960 to 1985 and from 1985 to 2060 from the AER model using scenario B1 378
Figure 3.2-37	Dobson maps of percent change in column ozone from 1985 to 2050 from the Oslo model with and without heterogeneous chemistry on the natural sulfate layer 380
Figure 3.2-38	Dobson maps of percent change in column ozone from 1985 to 2060 from the AER model using scenario B1 381
Figure 3.2-39	Action spectra used as weighting functions to calculate biologically effective radiation 381
Figure 3.2-40	Daily doses for 1979/80 based on ozone column from TOMS measurements normalized to Dobson 386
Figure 3.2-41	Daily dose changes from 1960 to 1980, GSFC2 model 388
Figure 3.2-42	Daily dose changes from 1960 to 2060, GSFC2 model, scenario A1 389
Figure 3.2-43	Daily dose changes from 1960 to 2060, GSFC2 model, scenario D1 390
Figure 3.2-44	Daily DNA damage dose changes from 1980 to 2060, WisCAR model, scenarios A1, A2, and D1 391

FIGURES

	Page
Figure 3.2-45	Transformed Eulerian mean vertical velocity for a 240-day average simulation performed with the NCAR Community Climate Model 394
Figure 3.2-46	As in Figure 3.3-40 but for the ozone reduction scenario shown in Figure 3.3.41b; percentage change in ozone from the two-dimensional model of Ko et al., 1985 394
 Chapter 4—Halocarbon Ozone Depletion Potentials and Global Warming Potentials	
Figure 4.2-1	Reactions governing concentrations of OH and HO ₂ 411
Figure 4.2-2	Schematic presentation of the measured vertical distribution of NO and NO _y over midlatitude oceanic and coastal regions 419
Figure 4.3-1	Calculated column ozone change in the DuPont 1-D model following a pulsed input of 5.0×10^9 kg of specified gas 425
Figure 4.3-2	Atmospheric concentrations of halocarbons with 5- and 100-year lifetimes following onset of a constant emission of each compound 426
Figure 4.3-3	Calculated latitudinal and seasonal steady-state ozone change from emission of CFC-11 necessary for global 1% change in total ozone (LLNL 2-D model) 435
Figure 4.3-4a	Calculated latitudinal and seasonal steady-state ozone change from emission of CFC-12 necessary to give 1% change in total ozone (LLNL 2-D model) 436
Figure 4.3-4b	Calculated latitudinal and seasonal relative ozone depletion of CFC-12 (LLNL 2-D model) 437
Figure 4.3-4c	Calculated latitudinal and seasonal relative ozone depletion of CFC-12 (AER 2-D model) 437
Figure 4.3-4d	Calculated latitudinal and seasonal relative ozone depletion of CFC-12 (Oslo 2-D model) 438
Figure 4.3-4e	Calculated latitudinal and seasonal relative ozone depletion of CFC-12 (DuPont 2-D model) 438
Figure 4.3-5a	Calculated latitudinal and seasonal steady-state ozone change necessary to give 1% change in total ozone from emission of HCFC-22 (LLNL 2-D model) 439
Figure 4.3-5b	Calculated latitudinal and seasonal relative ozone depletion of CFC-22 (LLNL 2-D model) 439
Figure 4.3-5c	Calculated latitudinal and seasonal relative ozone depletion from emission of HCFC-22 (AER 2-D model) 440
Figure 4.3-5d	Calculated latitudinal and seasonal relative ozone depletion from emission of HCFC-22 (Oslo 2-D model) 440
Figure 4.3-5e	Calculated latitudinal and seasonal relative ozone depletion from emission of HCFC-22 (DuPont 2-D model) 441
Figure 4.3-6	Calculated CFC-11 profiles from transport sensitivity study at 75°S at equinox (AER 2-D model) 443
Figure 4.3-7	Calculated CFC-11 profiles from transport sensitivity study at Equator at equinox (AER 2-D model) 443
Figure 4.3-8a	Calculated HCFC-22 profiles from transport sensitivity study at 75°S at equinox (AER 2-D model) 444
Figure 4.3-8b	Calculated HCFC-22 profiles from transport sensitivity study at Equator at equinox (AER 2-D model) 444
Figure 4.3-9a	Calculated total ozone abundance (Dobson units) from transport sensitivity studies (case 1 and case 2) 445

FIGURES

	Page
Figure 4.3-9b	Calculated total ozone abundance (Dobson units) from transport sensitivity studies (case 3 and case 4) 445
Figure 4.3-10a	Calculated latitudinal and seasonal relative ozone depletion from emission of HCFC-22 (case 2) 446
Figure 4.3-10b	Calculated latitudinal and seasonal relative ozone depletion from emission of HCFC-22 (case 3) 447
Figure 4.3-10c	Calculated latitudinal and seasonal relative ozone depletion from emission of HCFC-22 (case 4) 447
Figure 4.3-11	Calculated time-dependent change in relative ozone column depletion following a step change in emission of the tested halocarbons (LLNL 1-D model) 448
Figure 4.3-12	Calculated time-dependent change in relative ozone column depletion following a step change in emission of the tested halocarbons (DuPont 1-D model) 449
Figure 4.3-13	Calculated time-dependent relative chlorine loading following a step change in emission of the tested halocarbons (LLNL 1-D model) 450
Figure 4.4-1	Calculated change in surface temperature following a pulsed emission of 5×10^9 kg of specified gas 454
Figure 4.4-2	Change of calculated warming following a step change of emission of specified gas at 5×10^8 kg/yr 460
Figure 4.4-3	Column of chlorofluorocarbons following step change of emission of specified gas at 5×10^8 kg/yr 460
Figure 4.4-4	Calculated relative warmings following a step change of emission of specified gas (CFC-11 reference) 461

TABLES

	Page
Introduction	
Table 1	Range of Ozone Depletion Potentials (ODPs) and halocarbon Global Warming Potentials (GWPs) determined by one-dimensional and two-dimensional models xi
Table 2	Scenarios for halocarbon abundances xxiv
Table 3	Range of Ozone Depletion Potentials (ODPs) determined by one-dimensional and two-dimensional models xxviii
Table 4	Ozone Depletion Potentials for brominated compounds as calculated in the LLNL one-dimensional model and the University of Oslo two-dimensional model xxix
Table 5	Maximum relative Chlorine Loading Potential (CLP) for examined CFCs, HCFCs, HFCs xxix
Table 6	Halocarbon Global Warming Potentials (Halocarbon GWPs) scaled relative to reference set of halocarbon lifetimes xxxii
 Chapter 1—Polar Ozone	
Table 1.1.6-1	Changes in average total ozone abundances, as measured at individual Dobson stations over the 22-year period, 1965-1986 21
Table 1.1.6-2	Coefficients of multiple regression statistical analysis of re-analyzed Dobson measurements of total ozone concentrations collected into latitudinal band averages 22
Table 1.1.6-3	Percentage changes in total column ozone 23
Table 1.4-1	Reaction probabilities on water-ice 44
Table 1.6-1	Potential temperatures and approximate geometric altitude and pressure equivalents for late winter and early spring for the Antarctic region 55
Table 1.6.4-1	Assumed chlorine tracer concentrations and inorganic chlorine content as a function of potential temperature at 72°S 75
Table 1.9-1	Comparison of noontime irradiances computed for McMurdo during October with values for the summer solstice 128
 Chapter 2—Global Trends	
Table 2.1-1	Estimated overall percentage differences of the calculated zonal mean ozone layer amount of SBUV, SAGE, and LIMS with respect to the average of these three instruments 184
Table 2.1-2	Summary of Ozone Trend Estimates (in % per year) in total ozone and associated standard error 191
Table 2.2-1	Comparison of trend results by season and latitude 195
Table 2.2-2	List of Dobson total ozone stations at latitudes between 26°N and 64°N 202
Table 2.2-3	Summary of sensitivity analysis (% per decade effect on trends) 204
Table 2.2-4	Regional sensitivity analysis comparing trends from the “provisionally revised” Dobson data set with the original published data 206
Table 2.2-5	Trends in total ozone derived from Dobson data updated into 1988 compared with trends derived through 1986 209

TABLES

	Page
Table 2.2-6	Trends in total ozone derived by region based on data through 1986 and data updated through October 1988 211
Table 2.2-7	Latitudes and longitudes of the 14 grid points selected for comparison of changes in ozone derived from SBUV and TOMS 216
Table 2.2-8	Changes in total ozone derived from the Dobson network for periods coincident with the SBUV and TOMS data sets 219
Table 2.3-1	Overall trend estimates (in % per year) from 10 Umkehr stations for the period 1977-1987 with associated standard errors ($\pm 2\sigma$) 230
Table 2.3-2	Ozonesonde stations, data spans, and measurement methods 231
Table 2.3-3	Fractional Umkehr layers 231
Table 2.3-4	Trend estimates for nine stations (in % per year; data through December 1986 when available) 232
Table 2.3-5	Summary of averages of trend estimates (% per year) and standard errors (S.E. $\pm 2\sigma$) 234
Table 2.5-1	Concentrations and global trends of tropospheric gases for 1987 246
Table 2.5-2	N ₂ O mixing ratios and rates of increase observed in the troposphere 251
Table 2.5-3	Global average methane mixing ratios and rates of increase observed in the troposphere by various laboratories 253
Table 2.5-4	Surface carbon monoxide concentrations and trends 256
Table 2.5-5	Surface ozone concentrations and trends deduced from ground-based and balloon-borne instruments 259
Table 2.7-1	Percent changes in total column ozone, 1970-1986, used in the radiative transfer calculations 265
 Chapter 3—Theoretical Predictions	
Table 3.1-1	Capabilities of an international group of 2-D assessment models 285
Table 3.1-2	Comparison of ten rates and species at 3 mb, Equator, in March from five modeling groups 300
Table 3.2-1	UNEP Scenarios: 1960 through 2060 318
Table 3.2-2a	Assumed history of trace gas concentrations: Halocarbons and other gases 322
Table 3.2-2b	Assumed history of trace gas concentrations: Montreal products and replacements 322
Table 3.2-3a	Projected surface mixing ratios for Scenario A: Montreal products and replacements 323
Table 3.2-3b	Projected surface mixing ratios for Scenario B: Montreal products and replacements 323
Table 3.2-3c	Projected surface mixing ratios for Scenario C: Montreal products and replacements 324
Table 3.2-3d	Projected surface mixing ratios for Scenario D: Montreal products and replacements 324
Table 3.2-4	Chlorine and bromine loading of the atmosphere for the UNEP scenarios 327
Table 3.2-5	Participating assessment models 332
Table 3.2-6	Global mean lifetimes (yr.) of the trace gases 332
Table 3.2-7	Extended scenarios for halocarbon abundances 337
Table 3.2-8	Stratopause changes from 1980 to 2060 382
Table 3.2-9	Surface UV irradiance ^a : Comparison of model predictions 385
Table 3.2-10	Environmental effects on DNA radiation amplification factor (RAF) 392

TABLES

Page

Chapter 4—Halocarbon Ozone Depletion Potentials and Global Warming Potentials

Table 4.2-1	Recommended rate constants and uncertainties for reactions of OH with selected HFCs and HCFCs	404
Table 4.2-2	Fluorine-containing products in the atmospheric degradation of selected fluorocarbons	408
Table 4.2-3	Atmospheric lifetime of methyl chloroform and estimates of equivalent OH concentrations	414
Table 4.2-4	Atmospheric lifetimes for HCFCs and HFCs	416
Table 4.2-5	Estimates of global hydrocarbon emissions into the atmosphere	420
Table 4.3-1	Chemical rate data used in ODP calculations	428
Table 4.3-2	Atmospheric lifetimes (in years) calculated with one-dimensional and two-dimensional models	429
Table 4.3-3	Ozone Depletion Potentials (ODPs) calculated with one-dimensional and two-dimensional models, assuming scaling for HCFC ODPs by methyl chloroform inferred lifetime	429
Table 4.3-4	Ozone Depletion Potentials (ODPs) for brominated compounds as calculated in the AER and LLNL 1-D models and the U. Oslo 2-D model	430
Table 4.3-5	Chlorine Loading Potentials (CLPs) from 2-D models for CFCs, HCFCs, and HFCs, scaled by lifetime of CH ₃ CCl ₃ (=6.3 yr.)	432
Table 4.3-6	Maximum relative Chlorine Loading Potential (CLP) for examined CFCs, HCFCs, HFCs and other chlorinated halocarbons	432
Table 4.3-7	Change in ground level trace gas concentrations assumed in sensitivity studies ...	433
Table 4.3-8	Sensitivity of calculated lifetimes to changes in trace gas values, based on AER 1-D results	434
Table 4.3-9	Sensitivity of ozone potentials to changes in trace gas values	434
Table 4.3-10	Results of transport sensitivity study (AER 2-D Model) on ODP and CLP for HCFC-22	446
Table 4.4-1	Net IR radiative flux at the tropopause (@ 12 km) [Wm ⁻²] for 1 ppbv tropospheric mixing ratio of each gas	456
Table 4.4-2	Specific surface temperature (dT _s) increases and lambda (λ) values resulting from 1 ppbv of each gas	457
Table 4.4-3	Halocarbon Global Warming Potentials (GWPs)	458
Table 4.4-4	Sensitivity study—variation in trace gas levels and impact on halocarbon GWP values (AER D-1 model)	459